FVAmuc/Ulrike Rorneis

13 – 17 June · Künstlerhaus · Munich · Germany

Proceedings of the XIV International Conference on Hadron Spectroscopy

Hadron 2011

B. Grube, S. Paul, N. Brambilla (Eds.)

Proceedings of the

XIV International Conference on Hadron Spectroscopy

hadron2011

13–17 June 2011
Künstlerhaus, Munich, Germany

Editors: B. Grube, S. Paul, and N. Brambilla
Munich (Germany), 2011

How to Cite an Article

These proceedings are published electronically in the Electronic Conference Proceedings Archive (eConf) at `http://www.slac.stanford.edu/econf/C110613/`. To cite an article please use the following template:

> [Author name], *in Proceedings of the XIV International Conference on Hadron Spectroscopy (hadron2011)*, Munich, 2011, edited by B. Grube, S. Paul, and N. Brambilla, eConf C110613 (2011) [arXiv number].

Imprint

Proceedings of the XIV International Conference on Hadron Spectroscopy

Conference Homepage
`http://www.hadron2011.de`

Online Proceedings
`http://www.slac.stanford.edu/econf/C110613/`

Editors:	B. Grube, S. Paul, and N. Brambilla (Technische Universität München)
Cover Design:	Ulrike Ollinger (Cluster of Excellence "Origin and Structure of the Universe")
Cover Photo:	© FVAmuc/Ulrike Rorneis, courtesy of Tourist Office Munich (Press and Media Service)
Photos on pages vii and 896:	Wenzel Schürmann (Technische Universität München)

December 2011

Foreword

During the week of 13–17 June, over 230 physicists gathered in the Künstlerhaus, in the heart of Munich, to attend the biennial international hadron physics conference.

Hadron2011, the 14th International Conference on Hadron Spectroscopy, was the latest in a long series that started 1985 in Maryland. Originally conceived as a conference on light-meson spectroscopy it now covers all aspects of hadron physics, though spectroscopy and hadron production are still the topics that characterize the meeting. As many as 37 plenary talks, 128 presentations in parallel sessions and 37 posters offered ample possibilities to find out about the latest developments and results, from hypernuclear physics to meson and quarkonium spectroscopy, from nucleon structure and meson-baryon interaction to heavy-ion physics.

The topics included were

- Spectroscopy of light- and heavy-quark mesons
- Baryons
- Quarkonia
- Glueballs, hybrids, and multiquarks
- Phenomenological models
- Effective field theories
- QCD on the lattice
- Hadron structure
- Hadrons in matter
- Heavy-ion collisions
- Future facilities

The conference began by looking at issues related to light mesons, with a summary of recent theoretical progress and experimental tests in chiral dynamics and low-energy scattering phenomena. There are new results on light-meson spectroscopy from the BESIII experiment in Beijing and COMPASS at CERN. While COMPASS impressively confirms previous findings on the $\pi_1(1600)$, an exotic meson seen in high-energy diffraction, new structures have been observed in radiative J/ψ decays pointing towards new and narrow meson states between 1.8 and 2.5 GeV/c^2, the details and nature of which have still to be unraveled.

Even after many years of precision experiments, the size of the proton is still a hot topic. New findings in laser spectroscopy of muonic hydrogen, which give a proton radius more than 6σ smaller than previously determined, have opened the hunt for new explanations, although theory cannot offer effects large enough to solve the puzzle.

Research in nucleon structure has for many years shifted to spin degrees of freedom. After precision measurements on the helicity contribution of quarks in polarized nucleons, COMPASS has also set new limits on spin effects resulting from polarized gluons. These

findings are confirmed by spin experiments at the Relativistic Heavy Ion Collider (RHIC) at Brookhaven. With this, the focus now turns towards transverse-spin degrees of freedom (transversity). Non-collinear treatment of partons inside the nucleon offers a large number of new observables, which can link to quark angular momenta. Both COMPASS and RHIC have new physics programs on transverse polarization effects; measurements of Drell-Yan processes using polarized targets are also on the way. Hopes are high that the unexpected single spin asymmetries that have been observed in pion production at RHIC may finally be understood.

On the low-Q^2 side, big efforts at various laboratories, such as Bonn, Mainz, Jefferson Lab etc., are offering real- or virtual-photon beams. These allow a coherent set of (double-)polarized scattering and production experiments, also with many-body final states. Using the complete set of polarized measurements, the puzzle of baryon resonances, their identification and quantum numbers seems now to be in reach via new and sophisticated partial-wave analyses.

Quarkonium spectroscopy and the hunt for further quarkonium-like states that seem not to fit the $q\bar{q}$ picture of the meson have been and still are highlights in hadron physics. Precision experiments finally allowed the BELLE and BaBar experiments at KEK and SLAC, respectively, to observe missing quarkonium states such as $h_b(1S)$, $h_b(2S)$ as well as η_c and $\eta_c(2S)$. More precise determination of masses and widths as well as unexpected decay patterns were revealed also by BESIII, which has observed about 10^9 J/ψ decays. The puzzle of the mass and width of the $D(D_s)$ meson states seems to be solved with their spin assignments being resolved. The conference also heard of the remarkable progress in achieving a comprehensive and unified theory description of quarkonium properties at zero and finite temperature in an effective field theory framework.

The biggest current puzzle in hadron physics concerns the large number of exotic quarkonium-like states with narrow widths and high excitation energies as compared to the open-flavor meson channel. New work was reported on the $X(3872)$ and other, partly new states. Theoretical investigations offer a rich choice of possibilities. The $X(3872)$ has a good chance of just being the radial excitation of the χ_c state, but there is also a beautiful effective field theory description in the molecular interpretation case. However, further stunning observations were reported from the beauty sector. Two charged quarkonium-like states found by BELLE lie close in mass to the open b-threshold and have been dubbed Z_b in analogy to the charm sector.

Lattice calculations have shown huge progress with new algorithms allowing the extraction of excited baryon and meson state energies. A report from the Flavianet Lattice Averaging Group presented lattice results for kaon and pion physics with the aim of making them easily accessible to the community. There are also new calculations of hadron structure, the baryon and meson form-factors and the $g-2$ factor.

First and impressive results were reported from all of the LHC experiments. In particular, CMS and LHCb, offering the best mass resolutions, have confirmed the potential of hadron

machines in this field. In addition to the usual quarkonium states, exotic states have also been observed and the elusive B_c mesons have already been seen. At this stage, the focus on the production cross-section of heavy quarkonia, which can now be understood at LHC energies, assuming color octet contributions and next-to-leading order (NLO) processes to be relevant. The descriptions follow data up to transverse momenta as high as 20 GeV/c. The largest uncertainties come from unknown polarization effects that influence acceptance calculations. On the theoretical side, huge progress has been achieved with the full NLO calculation of the J/ψ cross section in non-relativistic QCD (NRQCD) and a combined global data analysis of all existing experiments that hints at the universality of the long-distance NRQCD matrix elements.

Hadron machines are unique in the production of b-baryons and Fermilab's Tevatron has so far been leading this field. The CDF collaboration reported on recent progress with the observation of excited Σ_b states and a radially excited Λ_c. CDF and DØ also presented new precision measurements of mass and width of other charmed baryons.

A thermal medium, of the type generated in heavy-ion collisions at the LHC, can modify hadron properties, especially in the case of heavy quarks and quarkonia. The theory of such modifications was reviewed and first results of lead-lead collisions at the LHC presented. Results from ATLAS and CMS show the striking effects of jet-quenching and also the melting of the excited Y states as compared to the ground-state partner. At lower energies, mass shifts and absorption cross-sections of vector mesons have been studied in the medium. Mass shifts — a long-standing issue, where many predictions have stimulated experimental efforts — have not been observed but small effects have been reported by the HADES experiment at GSI, Darmstadt, on the width of mesons in nuclei.

Recent and impressive progress in light-meson and quarkonium spectroscopy is in good part a result of recent high-luminosity experiments, which offer 10-100 times the statistical sample of their predecessors. Heavy-meson physics, for long the domain of lepton colliders, is now seeing LHC experiments starting to compete in an impressive way and using their low-luminosity data from 2010 to catch up with the Tevatron experiments. An interesting future lies ahead with even further increases in luminosity and precision being offered by future experiments such as BELLE II, the SuperB facility and the PANDA experiment at the Facility for Antiproton and Ion Research (FAIR).

Two impressive summary talks concluded the conference. Stefano Bianco of Frascati/INFN reviewed the experimental situation, a challenging task in view of the large number of new results presented. On the theoretical side, Chris Quigg of Fermilab gave a very inspiring outlook on hadron physics. He recognized the enormous diversity and reach of experimental programs, which offer insights from unexpected quarters, while remarkable progress has been achieved in theory with the emergence of lattice QCD. However, many puzzles remain, leaving ample opportunities with much work to do, as there are still "simple" questions that the field cannot answer.

Participants enjoyed the coffee breaks in the sun-covered courtyard of the Künstlerhaus, a

building erected for artists to meet and enjoy social events more than 100 years ago. Long and intense discussions also offered vital scientific exchange around the poster session, making this event a pleasant ending to the day. Long hours of sitting were compensated on Wednesday afternoon by a bicycle tour through the old town of Munich and the English garden with refreshing drinks in the beer garden. Last but not least, the conference enjoyed a guest talk on neutrino physics by Thierry Lasserre of Saclay, who discussed the mass determination from flavor oscillation and reported fresh results from T2K on hints of $\nu_\mu \to \nu_e$ oscillation.

In order to promote young scientists an international jury was set up to select the best young-scientist talks from both, experimental and theoretical physics. The prizes were awarded to **Sebastian Neubert** (TU-München) for his overview talk on "Light-Meson Spectroscopy" and **Andreas Jüttner** (CERN) for his "Review on Recent Results of the FLAG Working Group". The very lively poster session also was acknowledged with two similar prizes for the best posters presented by **Jenifer Nebrada** (Univ. Computense Madrid): "Quark mass dependence of meson-meson resonances and phase shifts within standard and unitarized ChPT" and **Michael Kunkel** (Old Dominion University): "Dalitz Decay of Pseudoscalar Mesons from Photoproduction on Hydrogen Target with CLAS". We thank the selection committees for their thorough work.

For all the speakers and their contributions see the conference web site: www.hadron2011.de

Thanks

It is with great pleasure that we thank for the large support we have obtained from the German Science Foundation (DFG), the Excellence Cluster "Universe" in Garching, the Helmholtz Association, the Virtual Institute on "Spin and Strong QCD" (VIQCD), and sponsorship obtained from CAEN GmbH, Springer Science and Media, ISEG Spezialelektronik GmbH and W-IE-NE-R Plein & Baus GmbH. Without this help, the conference could not have been organized.

For the organizers (TU-München)

Stephan Paul
Nora Brambilla
Boris Grube

December 2011

A history of hadron conferences. From right: A. Zaytsev (Protvino 2001), S.-U. Chung (Brookhaven 1999), A. Reis (Rio de Janeiro 2005), S. Bianco (Frascati 2007), S. Paul (Munich 2011) and P. Eugenio (Tallahasse 2009).

Harry Lipkin, left, of the Weizmann Institute, who turned 90 on 16 June, receives a birthday gift from hadron2011.

Conference Organization

International Advisory Committee

C. Amsler	Zürich	S. Nagamiya	KEK
T. Barnes	ORNL/U. Tenn.	M. Nakao	KEK
E. Berger	Argonne	E. Oset	València
S. Bianco	INFN-Frascati	S. Paul	München (*Chair*)
N. Brambilla	München (*Vice-Chair*)	K. Peters	GSI
T. Bressani	Torino	A. Reis	CBPF-Rio de Janeiro
V. Burkert	JLAB	I. Shipsey	Purdue
S. Chung	Brookhaven	A. Skrinsky	Novosibirsk
F. Close	Oxford	U. Thoma	Bonn
M. Davier	Orsay	A. Thomas	Adelaide
P. Eugenio	Florida State	Y. Wang	Beijing
A. Golutvin	London	U. Wiedner	Bochum
H. Lipkin	Weizmann	H. Wittig	Mainz
G. Mallot	CERN	A. Zaitsev	Protvino
B. Meadows	Cincinnati	B. Zou	Beijing

Local Organizing Committee

Technische Universität München

N. Brambilla (*Vice-Chair*)	F. Haas
S. U. Chung	B. Ketzer
L. Fabbietti	U. Ollinger
K. Frank	S. Paul (*Chair*)
J. Friedrich	S. Uhl
B. Grube	

Sponsors

Deutsche Forschungsgemeinschaft

Virtual Institute on “Spin and Strong QCD”

Helmholtz Gemeinschaft

Cluster of Excellence “Origin and Structure of the Universe”

Contents

Plenary Session

Plenary Session

Session Chairs

Suh-Urk	Chung	TU München/BNL
Martin	Faessler	LMU München
Marek	Karliner	Tel Aviv University
Claude	Amsler	Universität Zürich
Hartmut	Wittig	Universität Mainz
Volker	Metag	Universität Gießen
Kamal K.	Seth	Northwestern University
Eulogio	Oset	University of Valencia
Alexander M.	Zaitsev	IHEP Protvino
Harry	Lipkin	Weizmann Institute of Science

Contents

Chiral Symmetry and Low-Energy Pion-Photon Reactions

Norbert Kaiser[1]
Physik-Department T39
Technische Universität München
D-85747 Garching, GERMANY

This talk reviews the description of low-energy pion Compton scattering $\pi^-\gamma \to \pi^-\gamma$ and (neutral/charged) pion-pair production $\pi^-\gamma \to \pi^-\pi^0\pi^0/\pi^+\pi^-\pi^-$ at next-to-leading order in chiral perturbation theory. The first process allows one to extract the pion electric and magnetic polarizabilities (α_π and β_π), while the second reaction is governed by the chiral pion-pion interaction. In addition to the strong interaction effects from chiral loops and counterterms, the QED radiative corrections to these processes are also studied. The predictions of chiral perturbation theory will be tested by the COMPASS experiment at CERN. In case of the total cross section for $\pi^-\gamma \to \pi^+\pi^-\pi^-$ in the near threshold region $\sqrt{s} < 5m_\pi$ a recent analysis of the COMPASS data nicely confirms the prediction of chiral perturbation theory.

1 Introduction and summary

The pions (π^+, π^0, π^-) are the Goldstone bosons of spontaneous chiral symmetry breaking in QCD: $SU(2)_L \times SU(2)_R \to SU(2)_V$. Their low-energy dynamics can therefore be calculated systematically (and accurately) with chiral perturbation theory in form of a loop-expansion based on an effective chiral Lagrangian. The accurate two-loop prediction [1] for the isospin-zero S-wave $\pi\pi$-scattering length $a_0 = (0.220 \pm 0.005)m_\pi^{-1}$ has been confirmed in the E865 [2] and NA48/2 [3] experiments by analyzing the $\pi^+\pi^-$ invariant mass distribution of the rare kaon decay mode $K^+ \to \pi^+\pi^-e^+\nu_e$. One particular implication of that good agreement between theory and experiment is that the quark condensate $\langle 0|\bar{q}q|0\rangle$ constitutes the dominant order parameter [4] of spontaneous chiral symmetry breaking (considering the two-flavor sector of QCD). Likewise, the DIRAC experiment [5] has been proposed to determine the difference of the isospin-zero and isospin-two S-wave $\pi\pi$-scattering lengths $a_0 - a_2$ by measuring the life time ($\tau \simeq 3\,\text{fs}$) of pionium (i.e. $\pi^+\pi^-$ bound electromagnetically and decaying into $\pi^0\pi^0$). In the meantime the NA48/2 experiment [6] has accumulated very high statistics for the charged kaon decay modes $K^\pm \to \pi^\pm\pi^0\pi^0$, which allowed to

[1] nkaiser@ph.tum.de

extract the value $a_0 - a_2 = (0.257 \pm 0.006) m_\pi^{-1}$ for the $\pi\pi$-scattering length difference from the cusp effect in the $\pi^0\pi^0$ mass spectrum at the $\pi^+\pi^-$ threshold. This experimental result is again in very good agreement with the two-loop prediction $a_0 - a_2 = (0.265 \pm 0.004) m_\pi^{-1}$ of chiral perturbation theory [1]. For a discussion of isospin breaking corrections which have to be included in a meaningful comparison between theory and experiment, see ref. [7]. Clearly, these remarkable confirmations give confidence that chiral perturbation theory is the correct framework to calculate reliably and accurately the strong interaction dynamics of the pions at low energies.

Electromagnetic processes offer further possibilities to probe the internal structure of the pion. For example, pion Compton scattering $\pi^-\gamma \to \pi^-\gamma$ at low energies allows one to extract the electric and magnetic polarizabilities (α_π and β_π) of the charged pion. Chiral perturbation theory at two-loop order gives for the dominant pion polarizability difference the firm prediction $\alpha_\pi - \beta_\pi = (5.7 \pm 1.0) \cdot 10^{-4}\,\mathrm{fm}^3$ [8]. It is however in conflict with the existing experimental results from Serpukhov $\alpha_\pi - \beta_\pi = (15.6 \pm 7.8) \cdot 10^{-4}\,\mathrm{fm}^3$ [9] and MAMI $\alpha_\pi - \beta_\pi = (11.6 \pm 3.4) \cdot 10^{-4}\,\mathrm{fm}^3$ [10] which amount to values more than twice as large. Certainly, these existing experimental determinations of $\alpha_\pi - \beta_\pi$ raise doubts about their correctness since they violate the chiral low-energy theorem notably by a factor 2. The chiral low-energy theorem relates $\alpha_\pi - \beta_\pi = \alpha(\bar{\ell}_6 - \bar{\ell}_5)/(24\pi^2 f_\pi^2 m_\pi) + \mathcal{O}(m_\pi)$ to the axial-vector-to-vector form factor ratio $h_A/h_V = 0.443 \pm 0.015 = (\bar{\ell}_6 - \bar{\ell}_5)/6 + \mathcal{O}(m_\pi^2)$ measured in the PIBETA experiment [11] via the radiative pion decay $\pi^+ \to e^+\nu_e\gamma$. The two-loop calculations of refs. [8, 12, 13] assure that the $\mathcal{O}(m_\pi)$ corrections to $\alpha_\pi - \beta_\pi$ are in fact small. It is worth to note that a recent dispersive analysis [14] of the Belle data for $\gamma\gamma \to \pi^+\pi^-$ gives the fit value $\alpha_\pi - \beta_\pi = 4.7 \cdot 10^{-4}\,\mathrm{fm}^3$, compatible with the prediction of chiral perturbation theory. In a similar work by Hoferichter et al. [15] the complete system of Roy-Steiner equations for $\gamma\gamma \to \pi\pi$ and the crossed channel $\gamma\pi \to \gamma\pi$ has been solved. These integral equations fully respect analyticity, unitarity and crossing symmetry of the scattering amplitudes.

In that controversial situation, it is promising that the ongoing COMPASS experiment at CERN aims at measuring the pion polarizabilities, α_π and β_π, with high statistics using the Primakoff effect. The scattering of high-energy negative pions in the Coulomb field of a heavy nucleus (of charge Z) gives access to cross sections for $\pi^-\gamma$ reactions through the equivalent photon method:

$$\frac{d\sigma}{ds\,dQ^2} = \frac{Z^2\alpha}{\pi(s-m_\pi^2)}\,\frac{Q^2 - Q^2_{\min}}{Q^4}\,\sigma_{\pi^-\gamma}(s)\,, \qquad Q_{\min} = \frac{s-m_\pi^2}{2E_{\mathrm{beam}}}\,. \tag{1}$$

Here, Q denotes the momentum transferred by the virtual photon to the heavy nucleus of charge Z, and one aims at isolating the Coulomb peak $Q \to 0$ from the strong interaction background. The last factor $\sigma_{\pi^-\gamma}(s)$ is the total cross section for a $\pi^-\gamma$ reaction induced by real photons with $\sqrt{s}$ the corresponding $\pi^-\gamma$ center-of-mass energy. Note that eq.(1) applies in the same form to differential cross sections on both sides. The COMPASS experiment is set up to detect simultaneously various (multi-particle) hadronic final states which are

produced in the Primakoff scattering process of high-energy pions. In addition to pion Compton scattering $\pi^-\gamma \to \pi^-\gamma$ (which is of primary interest for determining the pion polarizabilities α_π and β_π) the reaction $\pi^-\gamma \to \pi^-\pi^0$ serves as a test of the QCD chiral anomaly (i.e. the anomalous $VAAA$ rectangle quark diagram) by measuring the $\gamma 3\pi$ coupling constant $F_{\gamma 3\pi} = e/(4\pi^2 f_\pi^3) = 9.72\,\mathrm{GeV}^{-3}$. For the two-body process $\pi^-\gamma \to \pi^-\pi^0$ the one-loop [16, 17] and two-loop corrections [18] of chiral perturbation theory as well as QED radiative corrections [19] have been worked out. Thus an accurate theoretical framework is available to analyze the upcoming data. The consistent theoretical framework to extract the pion polarizabilities from the measured cross sections for (low-energy) pion-Compton scattering $\pi^-\gamma \to \pi^-\gamma$ or the primary pion-nucleus bremsstrahlung process $\pi^- Z \to \pi^- Z\gamma$ has been described (in one-loop approximation) in refs. [17, 20]. It has been stressed that at the same order as the pion polarizability difference $\alpha_\pi - \beta_\pi$ there exists a further (partly compensating) pion structure effect in form of a unique pion-loop correction (interpretable as photon scattering off the "pion-cloud around the pion"). In addition to these strong interaction effects, the QED radiative corrections to real and virtual pion Compton scattering $\pi^-\gamma^{(*)} \to \pi^-\gamma$ have been calculated in refs. [20, 21]. The relative smallness of the pion structure effects in low-energy pion Compton scattering makes it necessary to include these higher order electromagnetic corrections.

The $\pi^-\gamma$ reaction with three charged pions in the final state is used by the COMPASS collaboration in the energy range $1\,\mathrm{GeV} < \sqrt{s} < 2.5\,\mathrm{GeV}$ to study the spectroscopy of non-strange meson resonances ($a_1(1260)$, $a_2(1320)$, $\pi_2(1670)$, etc.) and to search for so-called exotic meson resonances [22] (e.g. $\pi_1(1600)$) with quantum numbers different from simple (constituent) quark-antiquark bound states. The statistics of the COMPASS experiment is actually so high that the event rates with three pions in the final state can even be continued downward to the threshold. The cross sections (and other more exclusive observables) of the $\pi^-\gamma \to 3\pi$ reactions in the low-energy region $\sqrt{s} < 1\,\mathrm{GeV}$ offer new possibilities to test the strong interaction dynamics of pions as predicted by chiral perturbation theory. The total cross sections for the processes $\pi^-\gamma \to \pi^-\pi^0\pi^0$ and $\pi^-\gamma \to \pi^+\pi^-\pi^-$ have been calculated in ref. [17] at tree-level. Both reactions are governed (at leading order) by the chiral pion-pion interaction in combination with the electromagnetic photon-pion coupling. Clearly, in order to sharpen the predictions for $\pi^-\gamma \to 3\pi$ complete next-to-leading order calculations with inclusion of all corrections from pion-loops and chiral-invariant counterterms are necessary. In the neutral channel $\pi^-\gamma \to \pi^-\pi^0\pi^0$ it is found that the total cross sections (and two-pion mass spectra) get enhanced by a factor $1.5 - 1.8$ by the next-to-leading order corrections [23]. By contrast the cross sections for charged pion-pair production remain almost unchanged in comparison to their tree-level results. This different behavior can be understood from the varying influence of the chiral corrections on the pion-pion final-state interaction ($\pi^+\pi^- \to \pi^0\pi^0$ versus $\pi^-\pi^- \to \pi^-\pi^-$). In case of the cross sections for $\pi^-\gamma \to \pi^+\pi^-\pi^-$ in the near threshold region $\sqrt{s} < 5m_\pi$, a recent analysis of the COMPASS data nicely confirms the prediction of chiral perturbation theory (see herefore the contributions of S. Neubert and S. Grabmüller to these proceedings).

2 Charged Pion-Compton Scattering

Let us start with defining the invariant amplitudes for the pion Compton scattering process: $\pi^-(p_1)+\gamma(k_1,\epsilon_1)\to\pi^-(p_2)+\gamma(k_2,\epsilon_2)$. The corresponding T-matrix in the center-of-mass frame has (in Coulomb gauge $\epsilon^0_{1,2}=0$) the form:

$$T_{\pi\gamma}=8\pi\alpha\Big\{-\vec{\epsilon}_1\cdot\vec{\epsilon}_2^{\,*}\,A(s,t)+\vec{\epsilon}_1\cdot\vec{k}_2\,\vec{\epsilon}_2^{\,*}\cdot\vec{k}_1\,\frac{2}{t}\Big[A(s,t)+B(s,t)\Big]\Big\}\,, \tag{2}$$

with $\alpha=1/137.036$ the fine-structure constant, and $s=(p_1+k_1)^2>m_\pi^2$ and $t=(k_1-k_2)^2<0$ the independent Mandelstam variables. $m_\pi=139.57\,\mathrm{MeV}$ denotes the charged pion mass. Performing the sums over transversal photon polarizations and applying the flux and phase space factors, the resulting differential cross section reads:

$$\frac{d\sigma}{d\Omega_{\rm cm}}=\frac{\alpha^2}{2s}\Big\{|A(s,t)|^2+|A(s,t)+(1+z)B(s,t)|^2\Big\}\,, \tag{3}$$

with $t=(s-m_\pi^2)^2(z-1)/2s$, where $z=\cos\theta_{\rm cm}=\hat{k}_1\cdot\hat{k}_2$ is the cosine of the cms scattering angle. The amplitudes at tree level coincide with those of scalar quantum electrodynamics:

$$A(s,t)^{(\rm tree)}=1,\qquad\qquad B(s,t)^{(\rm tree)}=\frac{s-m_\pi^2}{m_\pi^2-s-t}\,. \tag{4}$$

The one-pion loop diagrams of chiral perturbation theory generate, after renormalization of the pion mass, the following (finite) contribution to the Compton amplitude $A(s,t)$:

$$A(s,t)^{(\rm loop)}=\frac{1}{(4\pi f_\pi)^2}\left\{-\frac{t}{2}-2m_\pi^2\ln^2\frac{\sqrt{4m_\pi^2-t}+\sqrt{-t}}{2m_\pi}\right\}, \tag{5}$$

where $f_\pi=92.4\,\mathrm{MeV}$ denotes the pion decay constant. This term can be interpreted as the (leading) correction arising from photon scattering off the "pion cloud around the pion". The internal structure of the pion enters through its electric and magnetic polarizabilities, which obey at one-loop order the constraint $\alpha_\pi+\beta_\pi=0$. The pertinent $\gamma\gamma\pi\pi$ contact vertex from the chiral Lagrangian $\mathcal{L}^{(4)}_{\pi\pi}$ gives rise to the contribution

$$A(s,t)^{(\rm pola)}=-\frac{\beta_\pi m_\pi t}{2\alpha}<0\,,\qquad \alpha_\pi-\beta_\pi=\frac{\alpha(\bar{\ell}_6-\bar{\ell}_5)}{24\pi^2 f_\pi^2 m_\pi}\,. \tag{6}$$

The combination of low-energy constants can be extracted from the axial-vector-to-vector form factor ratio $h_A/h_V=0.443\pm0.015=(\bar{\ell}_6-\bar{\ell}_5)/6+\mathcal{O}(m_\pi^2)$ measured in the PIBETA experiment [11] at PSI via the radiative pion decay $\pi^+\to e^+\nu_e\gamma$. The two-loop analysis of ref. [13] yields the value $\bar{\ell}_6-\bar{\ell}_5=3.0\pm0.3$, implying pion polarizabilities of magnitude $\alpha_\pi=-\beta_\pi\simeq 3.0\cdot10^{-4}\,\mathrm{fm}^3$.

The effects of the pion structure on the differential Compton cross section are shown in Fig. 1. The reduction of $d\sigma/d\Omega_{\rm cm}$ in backward directions ($z\simeq-1$) caused by the polarizability difference $\alpha_\pi-\beta_\pi$ gets in fact partly compensated by the pion-loop correction

$A(s,t)^{(\mathrm{loop})} \sim t^2 > 0$ written in eq.(5). In order to visualize more directly the effect of the pion polarizabilities, we show in Fig. 2 the ratio $d\sigma/d\sigma_0$ between the differential cross sections in backward direction, $z = -1$, calculated with finite, $\alpha_\pi = -\beta_\pi = 3.0 \cdot 10^{-4}\,\mathrm{fm}^3$, and with zero pion polarizabilities. At $\sqrt{s} = 4m_\pi$ the effect becomes now quite sizeable, where it amounts to almost a 20% reduction of the backward differential cross section. Let us also mention that these results receive only small corrections in a full two-loop description of pion Compton scattering [8]. At this order the predictions for the pion polarizability difference and sum are: $\alpha_\pi - \beta_\pi = (5.7 \pm 1.0) \cdot 10^{-4}\,\mathrm{fm}^3$ and $\alpha_\pi + \beta_\pi = (0.16 \pm 0.1) \cdot 10^{-4}\,\mathrm{fm}^3$. Isospin breaking corrections to pion Compton scattering arising from the mass difference of the charged and neutral pion (which is mainly of electromagnetic origin) have been considered in ref. [24]. The effects on the Compton cross section turn out to be negligibly small, i.e. they are of the order of just a few permille.

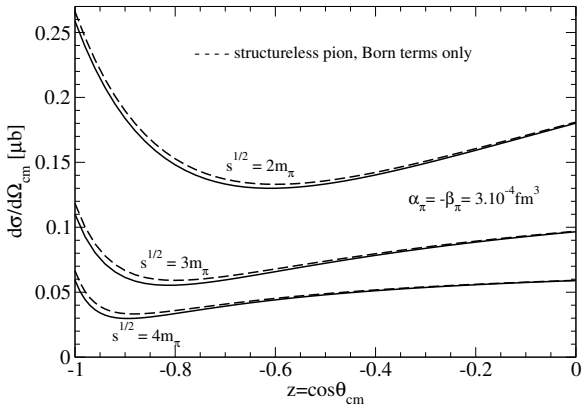

Figure 1: Differential cross section for pion Compton scattering.

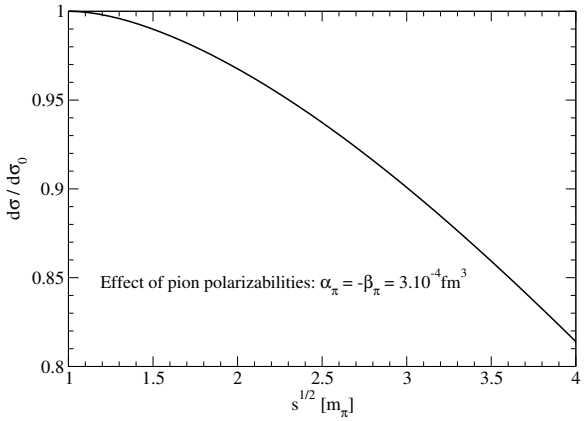

Figure 2: Ratio $d\sigma/d\sigma_0$ between differential cross sections in backward direction ($z = -1$) calculated with finite, $\alpha_\pi = -\beta_\pi = 3.0 \cdot 10^{-4}\,\mathrm{fm}^3$, and with zero pion polarizabilities.

3 Radiative Corrections

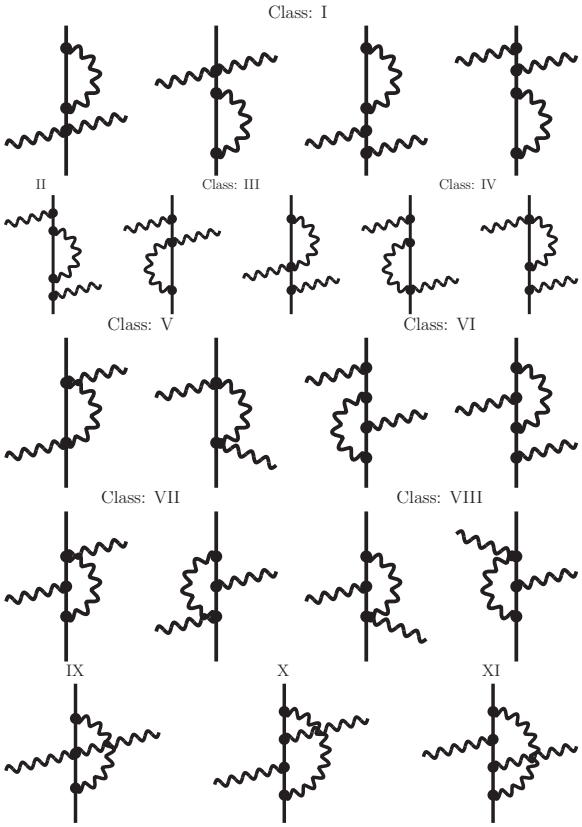

Figure 3: One-photon loop diagrams for pion Compton scattering

The relative smallness of the pion structure effects in Compton scattering makes it necessary to consider also higher order electromagnetic corrections arising from photon loops and soft photon bremsstrahlung. The pertinent one-photon loop diagrams are shown in Fig. 3. The analytical expressions for the loop amplitudes $A(s,t)$ and $B(s,t)$ of order α are given in section 3 of ref. [20]. Since scalar QED is a renormalizable quantum field theory ultraviolet divergent terms drop out in the total sum of all diagrams. Infrared finiteness of the virtual radiative corrections is achieved (in the standard way) by including soft radiation below an energy cut-off λ. In its final effect, the (single) soft photon radiation off the in- or out-going pion multiplies the tree-level differential cross section $d\sigma/d\Omega$ by a factor:

$$\delta_{\rm soft} = \alpha\mu \int\limits_{|\vec{l}|<\lambda} \frac{d^{d-1}l}{(2\pi)^{d-2}l_0} \left\{ \frac{2m_\pi^2 - t}{p_1\cdot l\, p_2\cdot l} - \frac{m_\pi^2}{(p_1\cdot l)^2} - \frac{m_\pi^2}{(p_2\cdot l)^2} \right\}, \tag{7}$$

which exactly cancels the infrared divergent terms generated by the photon loops (proportional to $\xi_{\rm IR} = 1/(d-4) + (\gamma_E - \ln 4\pi)/2 + \ln(m_\pi/\mu)$ in dimensional regularization).

The sum of virtual and real radiative corrections to pion Compton scattering is shown in Fig. 4 at selected center-of-mass energies $\sqrt{s} = (2,3,4,5)m_\pi$ as a function of $z = \cos\theta_{\rm cm}$. The detection threshold for soft photons has been set to the value $\lambda = 5\,\mathrm{MeV}$. One observes that the radiative corrections grow with the center-of-mass energy and that they become maximal in backward directions $z \simeq -1$, reaching values up to -2.4% at $\sqrt{s} = 4m_\pi$. With such an angular dependence the pure QED radiative corrections have the same kinematical signature as the effects from the pion's low-energy structure (i.e. pion polarizability difference plus pion-loop correction). In magnitude they are still suppressed by a factor $5-10$. A proper inclusion of radiative corrections is therefore essential if one wants to extract the pion polarizabilities with good accuracy. In the calculation of radiative corrections the leading pion structure can be accounted for by interpreting one of the two-photon contact vertices in the photon-loop diagrams as the polarizability vertex proportional to $\beta_\pi m_\pi$. As one can see from Fig. 5 such an improved description leaves the size and angular dependence of the radiative corrections practically unchanged.

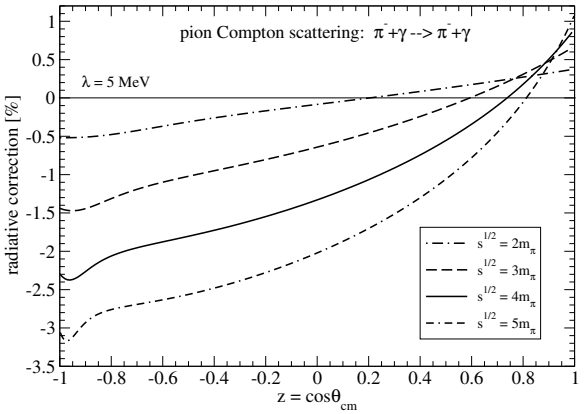

Figure 4: Radiative corrections to pion Compton scattering. The pion is treated as a structureless spin-0 boson.

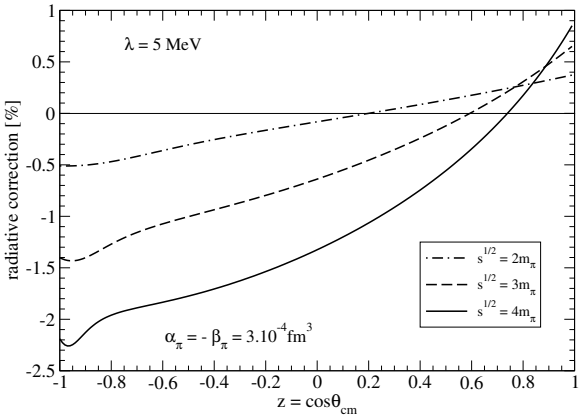

Figure 5: Radiative corrections to pion Compton scattering taking into account the polarizability difference $\alpha_\pi - \beta_\pi \simeq 6.0 \cdot 10^{-4}\,\mathrm{fm}^3$.

4 Neutral Pion-Pair Production

In this section we treat the neutral pion-pair production process $\pi^-(p_1) + \gamma(k,\epsilon\,) \to \pi^-(p_2) + \pi^0(q_1) + \pi^0(q_2)$. The general form of the T-matrix reads (in Coulomb-gauge):

$$T = \frac{2e}{f_\pi^2}\Big[\vec{\epsilon}\cdot\vec{q}_1\, A_1 + \vec{\epsilon}\cdot\vec{q}_2\, A_2\Big]\,. \tag{8}$$

In this decomposition A_1 and A_2 are two dimensionless production amplitudes which depend on $s = (p_1+k)^2$ and four other independent Lorentz-invariant variables:

$$s_1 = (p_2+q_1)^2\,, \quad s_2 = (p_2+q_2)^2\,, \quad t_1 = (q_1-k)^2\,, \quad t_2 = (q_2-k)^2\,. \tag{9}$$

This set is very convenient for describing the permutation of the two identical neutral pions in the final state via $(s_1 \leftrightarrow s_2,\, t_1 \leftrightarrow t_2)$. The tree diagrams of chiral perturbation theory for the processes $\pi^-\gamma \to 3\pi$ are shown in Fig. 6. In the case of neutral pion-pair production only the left diagram contributes. In terms of the kinematical variables introduced in eq.(9) the tree-level amplitudes read:

$$A_1^{(\mathrm{tree})} = A_2^{(\mathrm{tree})} = \frac{2m_\pi^2 + s - s_1 - s_2}{3m_\pi^2 - s - t_1 - t_2}\,. \tag{10}$$

In this expression the numerator comes from the chiral $\pi^+\pi^- \to \pi^0\pi^0$ interaction and the denominator from the propagator of outgoing π^- to which the (real) photon couples.

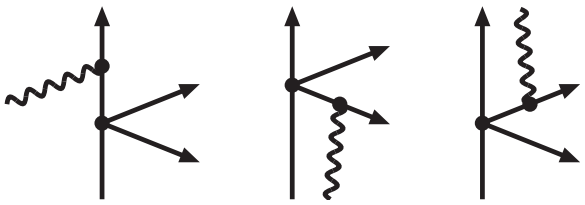

Figure 6: Tree diagrams for $\pi^-\gamma \to \pi^-\pi^0\pi^0$ and $\pi^+\pi^-\pi^-$. Arrows indicate outgoing pions. Only the left diagram contributes to $2\pi^0$-production.

The next-to-leading order corrections arise from pion-loop diagrams and chiral-invariant counterterms involving the low-energy constants $\bar{\ell}_1$, $\bar{\ell}_2$, $\bar{\ell}_3$ and $\bar{\ell}_4$. The analytical expressions for the pertinent production amplitudes A_1 and A_2 are given for individual diagrams in section 2.1 of ref. [23]. The total cross section is obtained by integrating the squared (transversal) T-matrix over the three-pion phase space:

$$\sigma_{\mathrm{tot}}(s) = \frac{\alpha}{32\pi^3 f_\pi^4 (s-m_\pi^2)} \iint\limits_{z^2<1} d\omega_1 d\omega_2 \int_{-1}^{1} dx \int_0^\pi d\phi \,\Big|\hat{k}\times(\vec{q}_1 A_1 + \vec{q}_2 A_2)\Big|^2\,. \tag{11}$$

Fig. 7 shows the total cross section $\sigma_{\rm tot}(s)$ for the reaction $\pi^-\gamma \to \pi^-\pi^0\pi^0$ in the low-energy region from threshold $\sqrt{s} = 3m_\pi$ up to $\sqrt{s} = 7m_\pi$. The dashed line corresponds to the tree approximation and the full line includes in addition the next-to-leading order corrections from chiral loops and counterterms. We use for the low-energy constants $\bar{\ell}_j$ the values: $\bar{\ell}_1 = -0.4 \pm 0.6$, $\bar{\ell}_2 = 4.3 \pm 0.1$, $\bar{\ell}_3 = 2.9 \pm 2.4$, $\bar{\ell}_4 = 4.4 \pm 0.2$, as determined (with improved empirical input) in ref. [1] from $\pi\pi$-scattering data. One observes that the total cross section gets enhanced sizeably (by a factor of $1.5 - 1.8$) after the inclusion of the next-to-leading order chiral corrections. Although the dynamics of the whole process is much richer this feature can be understood (in an approximate way) from the $\pi^+\pi^- \to \pi^0\pi^0$ final state interaction. The $\pi^+\pi^- \to \pi^0\pi^0$ interaction strength at threshold is determined by the difference of the isospin-zero and isospin-two S-wave $\pi\pi$-scattering lengths. Considering the corresponding one-loop expression

$$\frac{1}{3}(a_0 - a_2) = \frac{3m_\pi}{32\pi f_\pi^2}\left[1 + \frac{m_\pi^2}{36\pi^2 f_\pi^2}\left(\bar{\ell}_1 + 2\bar{\ell}_2 - \frac{3\bar{\ell}_3}{8} + \frac{9\bar{\ell}_4}{2} + \frac{33}{8}\right)\right], \tag{12}$$

one finds that the correction to 1 inside the square bracket amounts to about 0.20 (inserting the central values of $\bar{\ell}_j$). The square of this number is in fact close to the enhancement factor of the total cross section. It is also important to investigate the uncertainties induced by the present errorbars of the low-energy constants $\bar{\ell}_j$. Taking the total cross section at $\sqrt{s} = 6m_\pi$ as a measure one finds a relative uncertainty of about $\pm 5.4\%$ which is mainly connected with the errorbar of $\bar{\ell}_1 = -0.4 \pm 0.6$. It is comforting that the badly known low-energy constant $\bar{\ell}_3 = 2.9 \pm 2.4$ has very little influence on the observables considered here. Altogether this amounts to a fairly accurate prediction which presumably can be trusted up to center-of-mass energies of $\sqrt{s} \simeq 6m_\pi$.

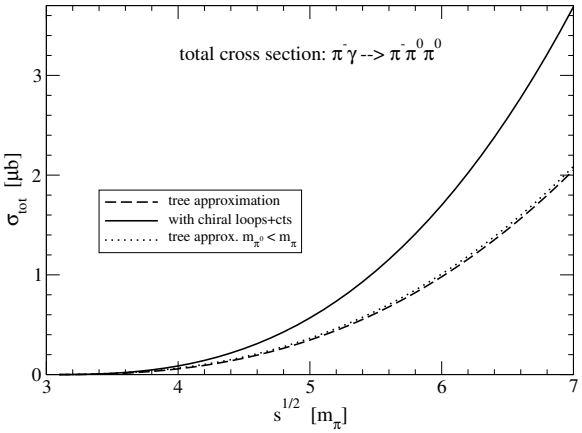

Figure 7: Total cross sections for neutral pion-pair production.

The radiative corrections to the process $\pi^-\gamma \to \pi^-\pi^0\pi^0$ have been calculated recently in ref. [25]. In this case only about a dozen photon-loop diagrams contribute and the radiative corrections can be represented by an overall correction factor, $R \sim \alpha/2\pi$, which multiplies the tree-level amplitude. The various contributions from photon-loops and soft photon

bremsstrahlung to the total cross section are shown in Fig. 8. From threshold up to cms energies of $\sqrt{s} = 7m_\pi$ these radiative corrections are small and vary from $+1.6\%$ to -1.6%.

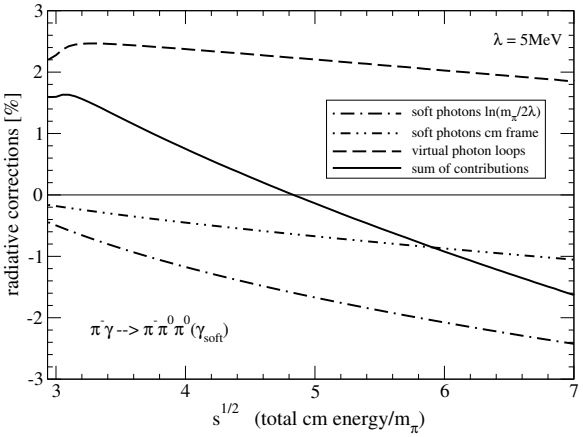

Figure 8: Radiative corrections to neutral pion-pair production.

5 Charged Pion-Pair Production

Finally, we discuss the charged pion-pair production process $\pi^-(p_1) + \gamma(k,\epsilon\,) \to \pi^+(p_2) + \pi^-(q_1) + \pi^-(q_2)$. By assigning the four-momentum p_2 to the out-going positively charged pion $\pi^+(p_2)$ one can exploit the complete equivalence to the $\pi^-\gamma \to \pi^-\pi^0\pi^0$ reaction concerning its kinematical description. The T-matrix (in Coulomb-gauge) and the Mandelstam variables are the same as defined in eqs.(8,9). The three non-vanishing tree diagrams shown in Fig. 6 lead to the following tree-level amplitudes:

$$A_1^{(\mathrm{tree})} = \frac{s + m_\pi^2 - s_1 - s_2}{3m_\pi^2 - s - t_1 - t_2} + \frac{s - s_1 - s_2 + t_2}{t_1 - m_\pi^2} - 1\,, \tag{13}$$

$$A_2^{(\mathrm{tree})} = \frac{s + m_\pi^2 - s_1 - s_2}{3m_\pi^2 - s - t_1 - t_2} + \frac{s - s_1 - s_2 + t_1}{t_2 - m_\pi^2} - 1\,. \tag{14}$$

Beyond leading order the dynamical content of charged pion-pair production $\pi^-\gamma \to \pi^+\pi^-\pi^-$ is considerably more extensive than that of neutral pion-pair production $\pi^-\gamma \to \pi^-\pi^0\pi^0$ because the photon can now couple to all three out-going (charged) pions. Many more diagrams with pion-loops and chiral counterterms do contribute. These diagrams have all been evaluated in section 3.1 of ref. [23]. Using consistently the same values of the low-energy constants $\bar{\ell}_1$, $\bar{\ell}_2$, $\bar{\ell}_3$ and $\bar{\ell}_4$ the result for the total cross section (computed via eq.(11)) follows as shown in Fig. 9. As a striking feature one observes that the total cross section for $\pi^-\gamma \to \pi^+\pi^-\pi^-$ remains almost unchanged in the region $\sqrt{s} < 6m_\pi$ after inclusion of the next-to-leading order chiral corrections. Although the dynamics of the whole process is much richer this can be understood (in a suggestive way) from the

$\pi^-\pi^- \to \pi^-\pi^-$ final state interaction. By considering the one-loop expression for the isospin-two S-wave $\pi\pi$-scattering length

$$a_2 = -\frac{m_\pi}{16\pi f_\pi^2}\left[1 - \frac{m_\pi^2}{12\pi^2 f_\pi^2}\left(\bar{\ell}_1 + 2\bar{\ell}_2 - \frac{3\bar{\ell}_3}{8} - \frac{3\bar{\ell}_4}{2} + \frac{3}{8}\right)\right], \tag{15}$$

one deduces that the correction to 1 inside the square bracket amounts to a very small number. Chiral corrections (even at two-loop order [1]) affect the isospin-two $\pi\pi$-interaction only very weakly and this feature seems to be reflected by $\sigma_{\rm tot}(s)$ in Fig. 9. A recent analysis of the COMPASS data in the region $\sqrt{s} < 5m_\pi$ confirms the prediction of chiral perturbation theory (see the contributions of S. Neubert and S. Grabmüller to these proceedings).

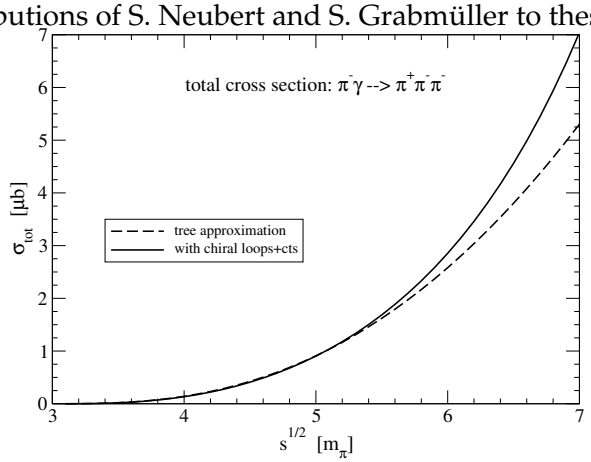

Figure 9: Total cross sections for charged pion-pair production.

The $\pi^+\pi^-$ mass spectra in Fig. 10 also show some interesting structures. The dip at intermediate $\pi^+\pi^-$ masses is a manifestation of chiral pion-loop dynamics. It is expected that the high-statistics data of the COMPASS experiment can reveal such dynamical details.

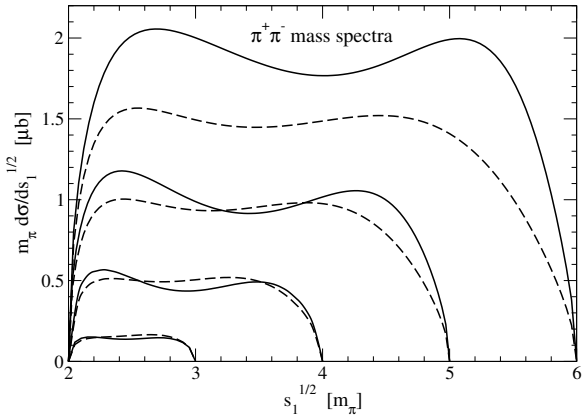

Figure 10: $\pi^+\pi^-$ mass spectra for the reaction $\pi^-\gamma \to \pi^+\pi^-\pi^-$.

Acknowledgments

I thank the organizers for invitation to the conference HADRON2011. I thank Jan Friedrich for many informative discussions and fruitful collaboration over the past years.

Bibliography

[1] G. Colangelo, J. Gasser, and H. Leutwyler, *Nucl. Phys.* **B603**, 125 (2001).
[2] S. Pislak et al., *Phys. Rev.* **D67**, 072004 (2003).
[3] J.R. Batley et al., *Eur. Phys. J.* **C54**, 411 (2008).
[4] G. Colangelo, J. Gasser, and H. Leutwyler, *Phys. Rev. Lett.* **86**, 5008 (2001).
[5] B. Adeva et al., *J. Phys.* **G30**, 1929 (2004).
[6] J.R. Batley et al., *Eur. Phys. J.* **C64**, 589 (2009).
[7] M. Bissegger, A. Fuhrer, J. Gasser, B. Kubis, and A. Rusetsky, *Nucl. Phys.* **B 806**, 178 (2009); G. Colangelo, J. Gasser, and A. Rusetsky, *Eur. Phys. J.* **C59**, 777 (2009).
[8] J. Gasser, M.A. Ivanov, and M.E. Sainio, *Nucl. Phys.* **B745**, 84 (2006); and private communications.
[9] Y.M. Antipov et al., *Phys. Lett.* **B121**, 445 (1983); *Z. Phys.* **C26**, 495 (1985).
[10] J. Ahrens et al., *Eur. Phys. J.* **A23**, 113 (2005).
[11] E. Frlez et al., *Phys. Rev. Lett.* **93**, 181804 (2004); E. Frlez, *Nucl. Phys. Proc. Suppl.* **162**, 148 (2006).
[12] U. Bürgi, *Phys. Lett.* **B377**, 147 (1996); *Nucl. Phys.* **B479**, 392 (1996).
[13] J. Bijnens and P. Talavera, *Nucl. Phys.* **B489**, 387 (1997);
C.Q. Geng, I.L. Ho, and T.H. Wu, *Nucl. Phys.* **B684**, 2815 (2004).
[14] R. Garcia-Martin and B. Moussallam, *Eur. Phys. J.* **C70** 155 (2010).
[15] M. Hoferichter, D.R. Philips, and C. Schat, hep-ph/1106.4147.
[16] J. Bijnens, A. Bramon, and F. Cornet, *Phys. Lett.* **B237**, 488 (1990);
J. Bijnens, *Int. J. Mod. Phys.* **A8**, 3045 (1993).
[17] N. Kaiser and J.M. Friedrich, *Eur. Phys. J.* **A36**, 181 (2008).
[18] T. Hannah, *Nucl. Phys.* **B593**, 577 (2001).
[19] L. Ametller, M. Knecht, and P. Talavera, *Phys. Rev.* **D64**, 094009 (2001).
[20] N. Kaiser and J.M. Friedrich, *Nucl. Phys.* **A812**, 186 (2008).
[21] N. Kaiser and J.M. Friedrich, *Eur. Phys. J.* **A39**, 71 (2008).
[22] COMPASS collaboration: M.G. Alekseev et al., *Phys. Rev. Lett.* **104**, 241803 (2010).
[23] N. Kaiser, *Nucl. Phys.* **A848**, 198 (2010).
[24] N. Kaiser, *Eur. Phys. J.* **A47**, 15 (2011).
[25] N. Kaiser, *Eur. Phys. J.* **A46**, 373 (2010).

Latest Developments in Heavy Meson Spectroscopy

Fulvia De Fazio
Istituto Nazionale di Fisica Nucleare, Sezione di Bari
Via Orabona 4, I-70126 Bari, ITALY

I discuss developments in heavy meson spectroscopy. In particular, I consider the system of $c\bar{s}$ mesons and the puzzling state X(3872), with focus on the strategies for their classification.

1 Introduction

In the last decade, many new charm and beauty hadrons have been discovered. Some of them fit the quark model scheme, others still need to be properly classified. Here I focus on $c\bar{s}$ mesons and, to introduce the topic, I describe the properties of mesons with a single heavy quark in the infinite heavy quark mass limit. Then, I turn to the state X(3872) observed in the hidden charm spectrum.

Before the B-factory era, the $c\bar{s}$ spectrum consisted of the pseudoscalar $D_s(1968)$ and vector $D_s^*(2112)$ mesons, s-wave states of the quark model, and of the axial-vector $D_{s1}(2536)$ and tensor $D_{s2}(2573)$ mesons, p-wave states. In 2003, two narrow resonances were discovered: $D_{sJ}(2317)$ and $D_{sJ}^*(2460)$ with $J^P = 0^+, 1^+$ [1, 2]. Their identification as $c\bar{s}$ states was debated [3]; however, they have the right quantum numbers to complete the p-wave multiplet, and their radiative decays occur accordingly, so that their interpretation as ordinary $c\bar{s}$ mesons seems natural and now widely accepted [3–5]. Afterwards, two other $c\bar{s}$ mesons decaying to DK were observed: $D_{sJ}(2860)$ [6] and $D_{sJ}(2700)$ [7], the latter with $J^P = 1^-$. Later, in [8] it was found that $D_{sJ}(2700)$ is likely the first radial excitation of D_s^*. In [8] also another state was observed: $D_{sJ}(3040)$. As discussed in Section 3, the predictions for the decays of $D_{sJ}(2860)$, $D_{sJ}(2700)$ and $D_{sJ}(3040)$ following from different identifications can be used for the classification [9, 10].

In Section 4, after briefly recalling some of the latest news in the spectroscopy of hidden charm and beauty mesons, I survey the properties of X(3872) and study a few radiative decay modes which are useful to shed light on its structure.

2 Hadrons containing a single heavy quark Q

The description of mesons with a single heavy quark Q is simplified in QCD in the heavy quark $m_Q \to \infty$ limit, when the spin s_Q of the heavy quark and the angular momentum

s_ℓ of the light degrees of freedom: $s_\ell = s_{\bar q} + \ell$ ($s_{\bar q}$ being the light antiquark spin and ℓ the orbital angular momentum of the light degrees of freedom relative to Q) are decoupled. Hence spin-parity s_ℓ^P of the light degrees of freedom is conserved in strong interactions [11] and mesons can be classified as doublets of s_ℓ^P. Two states with $J^P = (0^-, 1^-)$, denoted as (P, P^*), correspond to $\ell = 0$ (the *fundamental* doublet). The four states corresponding to $\ell = 1$ can be collected in two doublets, (P_0^*, P_1') with $s_\ell^P = \frac{1}{2}^+$ and $J^P = (0^+, 1^+)$, (P_1, P_2) with $s_\ell^P = \frac{3}{2}^+$ and $J^P = (1^+, 2^+)$. For $\ell = 2$ the doublets have $s_\ell^P = \frac{3}{2}^-$, consisting of states with $J^P = (1^-, 2^-)$, or $s_\ell^P = \frac{5}{2}^-$ with $J^P = (2^-, 3^-)$ states. And so on. For each doublet, one can consider a tower of similar states corresponding to their radial excitations.

One can predict whether these states are narrow or broad. For example, strong decays of the members of the $J_{s_\ell}^P = (1^+, 2^+)_{3/2}$ doublet to the fundamental doublet plus a light pseudoscalar meson occur in d-wave. Since the rate for this process is proportional to $|\vec p|^5$ (in general, to $|\vec p|^{2\ell+1}$, p being the light pseudoscalar momentum and ℓ the angular momentum transferred in the decay), these states are expected to be narrow. On the contrary, the members of the $J_{s_\ell}^P = (0^+, 1^+)_{1/2}$ doublet decay in s-wave, hence they should be broad.

$D_s(1968)$, $D_s^*(2112)$ belong to the lowest $s_\ell^P = \frac{1}{2}^-$ doublet. $D_{s1}(2536)$, $D_{s2}(2573)$ correspond to the doublet with $J_{s_\ell}^P = (1^+, 2^+)_{3/2}$, $D_{sJ}(2317)$, $D_{sJ}^*(2460)$, to that with $J_{s_\ell}^P = (0^+, 1^+)_{1/2}$. Mixing between the two 1^+ states is allowed at $O(1/m_Q)$; however, for non-strange charm mesons such a mixing was found to be small [12, 13].

In the heavy quark limit, the various doublets are represented by effective fields: H_a for $s_\ell^P = \frac{1}{2}^-$ ($a = u, d, s$ is a light flavour index), S_a and T_a for $s_\ell^P = \frac{1}{2}^+$ and $s_\ell^P = \frac{3}{2}^+$, respectively; X_a and X_a' for $s_\ell^P = \frac{3}{2}^-$ and $s_\ell^P = \frac{5}{2}^-$, respectively:

$$
\begin{aligned}
H_a &= \frac{1+\not v}{2}[P^*_{a\mu}\gamma^\mu - P_a\gamma_5] \\
S_a &= \frac{1+\not v}{2}\left[P'^\mu_{1a}\gamma_\mu\gamma_5 - P^*_{0a}\right] \\
T_a^\mu &= \frac{1+\not v}{2}\left\{P^{\mu\nu}_{2a}\gamma_\nu - P_{1a\nu}\sqrt{\frac{3}{2}}\gamma_5\left[g^{\mu\nu} - \frac{1}{3}\gamma^\nu(\gamma^\mu - v^\mu)\right]\right\} \\
X_a^\mu &= \frac{1+\not v}{2}\left\{P^{*\mu\nu}_{2a}\gamma_5\gamma_\nu - P^{*\prime}_{1a\nu}\sqrt{\frac{3}{2}}\left[g^{\mu\nu} - \frac{1}{3}\gamma^\nu(\gamma^\mu - v^\mu)\right]\right\} \\
X'^{\mu\nu}_a &= \frac{1+\not v}{2}\left\{P^{\mu\nu\sigma}_{3a}\gamma_\sigma - P^{*\prime\alpha\beta}_{2a}\sqrt{\frac{5}{3}}\gamma_5\left[g^\mu_\alpha g^\nu_\beta - \frac{1}{5}\gamma_\alpha g^\nu_\beta(\gamma^\mu - v^\mu) - \frac{1}{5}\gamma_\beta g^\mu_\alpha(\gamma^\nu - v^\nu)\right]\right\};
\end{aligned}
\tag{1}
$$

the various operators annihilate mesons of four-velocity v (conserved in strong interactions) and contain a factor $\sqrt{m_P}$. At the leading order in the heavy quark mass and light meson momentum expansion the decays $F \to HM$ ($F = H, S, T, X, X'$ and M a light pseudoscalar meson) can be described by the Lagrangian interaction terms (invariant under chiral and

heavy-quark spin-flavour transformations) [14, 15]:

$$
\begin{aligned}
\mathcal{L}_H &= g\, Tr[\overline{H}_a H_b \gamma_\mu \gamma_5 \mathcal{A}^\mu_{ba}] \\
\mathcal{L}_S &= h\, Tr[\overline{H}_a S_b \gamma_\mu \gamma_5 \mathcal{A}^\mu_{ba}] \; + \; h.c.\,, \\
\mathcal{L}_T &= \frac{h'}{\Lambda_\chi} Tr[\overline{H}_a T^\mu_b (iD_\mu \not{\mathcal{A}} + i \not{D}\, \mathcal{A}_\mu)_{ba} \gamma_5] + h.c. \\
\mathcal{L}_X &= \frac{k'}{\Lambda_\chi} Tr[\overline{H}_a X^\mu_b (iD_\mu \not{\mathcal{A}} + i \not{D}\, \mathcal{A}_\mu)_{ba} \gamma_5] + h.c. \\
\mathcal{L}_{X'} &= \frac{1}{{\Lambda_\chi}^2} Tr[\overline{H}_a X'^{\mu\nu}_b [k_1 \{D_\mu, D_\nu\} \mathcal{A}_\lambda + k_2 (D_\mu D_\nu \mathcal{A}_\lambda + D_\nu D_\lambda \mathcal{A}_\mu)]_{ba} \gamma^\lambda \gamma_5] + h.c.
\end{aligned}
\tag{2}
$$

where $D_{\mu ba} = -\delta_{ba}\partial_\mu + \frac{1}{2}\left(\xi^\dagger \partial_\mu \xi + \xi \partial_\mu \xi^\dagger\right)_{ba}$, $\mathcal{A}_{\mu ba} = \frac{i}{2}\left(\xi^\dagger \partial_\mu \xi - \xi \partial_\mu \xi^\dagger\right)_{ba}$ and $\xi = e^{\frac{i\mathcal{M}}{f_\pi}}$. $\mathcal{M}$ is a matrix containing the light pseudoscalar meson fields ($f_\pi = 132$ MeV), $\Lambda_\chi \simeq 1$ GeV the chiral symmetry-breaking scale. $\mathcal{L}_S$, $\mathcal{L}_T$ describe decays of positive parity heavy mesons with the emission of light pseudoscalar mesons in s- and d- wave, respectively, g, h and h' representing effective coupling constants. $\mathcal{L}_X$, $\mathcal{L}_{X'}$ describe the decays of negative parity mesons with the emission of light pseudoscalar mesons in p- and f- wave with couplings k', k_1 and k_2. The structure of the Lagrangian terms for radial excitations of the doublets is the same, but the couplings $g, h, \ldots$ have to be substituted by $\tilde{g}, \tilde{h}, \ldots$.

3 $c\bar{s}$ mesons: The case of $D_{sJ}(2860)$, $D_{sJ}(2700)$ and $D_{sJ}(3040)$

In 2006, BaBar observed a heavy $c\bar{s}$ meson, $D_{sJ}(2860)$, decaying to D^0K^+ and D^+K_S, with mass $M = 2856.6 \pm 1.5 \pm 5.0$ MeV and width $\Gamma = 47 \pm 7 \pm 10$ [6]. Shortly after, analysing the D^0K^+ invariant mass distribution in $B^+ \to \overline{D}^0 D^0 K^+$ Belle Collaboration [7] found a $J^P = 1^-$ resonance, $D_{sJ}(2710)$, with $M = 2708 \pm 9^{+11}_{-10}$ MeV and $\Gamma = 108 \pm 23^{+36}_{-31}$ MeV.

In order to classify $D_{sJ}(2860)$ and $D_{sJ}(2710)$, their strong decays were studied in [9], comparing the predictions which follow from different quantum number assignments. I summarize here the main results, starting with $D_{sJ}(2860)$. A new $c\bar{s}$ meson decaying to DK can be either the $J^P = 1^-$ state of the $s^P_\ell = \frac{3}{2}^-$ doublet, or the $J^P = 3^-$ state of the $s^P_\ell = \frac{5}{2}^-$ one, in both cases with lowest radial quantum number. Otherwise $D_{sJ}(2860)$ could be a radial excitation of already observed $c\bar{s}$ mesons: the first radial excitation of D_s^* ($J^P = 1^-$ $s^P_\ell = \frac{1}{2}^-$) or of $D_{sJ}(2317)$ ($J^P = 0^+$ $s^P_\ell = \frac{1}{2}^+$) or of $D^*_{s2}(2573)$ ($J^P = 2^+$ $s^P_\ell = \frac{3}{2}^+$). As for $D_{sJ}(2710)$, having $J^P = 1^-$, it could be either the first radial excitation belonging to the $s^P_\ell = \frac{1}{2}^-$ doublet ($D_s^{*\prime}$) or the low lying state with $s^P_\ell = \frac{3}{2}^-$ (D^*_{s1}).

For both mesons the ratios of decay rates $R_1 = \frac{\Gamma(D_{sJ} \to D^*K)}{\Gamma(D_{sJ} \to DK)}$ $R_2 = \frac{\Gamma(D_{sJ} \to D_s\eta)}{\Gamma(D_{sJ} \to DK)}$ ($D^{(*)}K = D^{(*)+}K_S + D^{(*)0}K^+$), obtained using eqs. (1) and (2), are useful to discriminate among the various assignments [9]. Table 1 reports such ratios in the various cases; it is interesting that they do not depend on the coupling constants, but only on the quantum numbers.

$D_{sJ}(2860)$	R_1	R_2
$s_\ell^p = \frac{1}{2}^-$, $J^P = 1^-$, $n = 2$	1.23	0.27
$s_\ell^p = \frac{1}{2}^+$, $J^P = 0^+$, $n = 2$	0	0.34
$s_\ell^p = \frac{3}{2}^+$, $J^P = 2^+$, $n = 2$	0.63	0.19
$s_\ell^p = \frac{3}{2}^-$, $J^P = 1^-$, $n = 1$	0.06	0.23
$s_\ell^p = \frac{5}{2}^-$, $J^P = 3^-$, $n = 1$	0.39	0.13
$D_{sJ}(2710)$	R_1	R_2
$s_\ell^p = \frac{1}{2}^-$, $J^P = 1^-$, $n = 2$	0.91	0.20
$s_\ell^p = \frac{3}{2}^-$, $J^P = 1^-$, $n = 1$	0.043	0.163

Table 1: Predicted ratios R_1 and R_2 (see text for definitions) for the various assignment of quantum numbers to $D_{sJ}(2860)$ and $D_{sJ}(2710)$.

I first consider $D_{sJ}(2860)$. The case $s_\ell^p = \frac{3}{2}^-$, $J^P = 1^-$, $n = 1$ can be excluded since, using $k' \simeq h' \simeq 0.45 \pm 0.05$ [13], would give a width incompatible with the measurement. In the assignment $s_\ell^p = \frac{1}{2}^+$, $J^P = 0^+$, $n = 2$ the decay to D^*K is forbidden. However, in this case $D_{sJ}(2860)$ should have a spin partner with $J^P = 1^+$ decaying to D^*K with a small width and mass around 2860 MeV. To explain the absence of such a signal one should invoke a mechanism favoring the production of the 0^+ $n = 2$ state and inhibiting that of 1^+ $n = 2$ state, which is difficult to imagine.

Among the remaining possibilities, the assignment $s_\ell^p = \frac{5}{2}^-$, $J^P = 3^-$, $n = 1$ seems the most likely one. In this case the small DK width is due to the kaon momentum suppression factor: $\Gamma(D_{sJ} \to DK) \propto q_K^7$. The spin partner, D_{s2}^*, has $s_\ell^p = \frac{5}{2}^-$, $J^P = 2^-$, decaying to D^*K and not to DK. It would also be narrow in the $m_Q \to \infty$ limit, where the transition $D_{s2}^* \to D^*K$ occurs in f-wave. As an effect of $1/m_Q$ corrections this decay can occur in p-wave, so that D_{s2}^* could be broader; hence, it is not necessary to invoke a mechanism inhibiting the production of this state with respect to $J^P = 3^-$. If $D_{sJ}(2860)$ has $J^P = 3^-$, it is not expected to be produced in non leptonic B decays such as $B \to DD_{sJ}(2860)$. Actually, in the Dalitz plot analysis of $B^+ \to \overline{D}^0 D^0 K^+$ no signal of $D_{sJ}(2860)$ was found [7].

In the latest BaBar analysis [8] $D_{sJ}(2860)$ has been observed decaying to DK and D^*K final states, hence excluding the assignment $J^P = 0^+$. However, the measurement [8]

$$\frac{BR(D_{sJ}(2860) \to D^*K)}{BR(D_{sJ}(2860) \to DK)} = 1.10 \pm 0.15_{stat} \pm 0.19_{syst}$$

leaves the identification of $D_{sJ}(2860)$ still an open issue. A confirmation that $D_{sJ}(2860)$ is a $J^P = 3^-$ state could be the detection of its non-strange partner D_3, also expected to be narrow, that can be produced in semileptonic and in non leptonic B decays [16].

Let us now look at $D_{sJ}(2710)$. As Table 1 shows, R_1 is very different if $D_{sJ}(2710)$ is $D_s^{*\prime}$ or

D^*_{s1}. Comparing the results in that Table with the BaBar measurement [8]:

$$\frac{BR(D_{sJ}(2710) \to D^*K)}{BR(D_{sJ}(2710) \to DK)} = 0.91 \pm 0.13_{stat} \pm 0.12_{syst}$$

allows to conclude that $D_{sJ}(2710)$ is most likely $D^{*\prime}_s$, the first radial excitation of $D^*_s(2112)$.

From the computed widths, assuming that $\Gamma(D_{sJ}(2710))$ is saturated by the considered modes and identifying $D_{sJ}(2710)$ with $D^{*\prime}_s$, the coupling $\tilde{g}$, analogous to g in (2) when H is the doublet of the $n = 2$ radial excitations, can be determined $\tilde{g} = 0.26 \pm 0.05$, a value similar to those obtained for analogous effective couplings [17]. This result for $\tilde{g}$ can provide information about D'_s, the spin partner of $D_{sJ}(2710)$ having $J^P = 0^-$; it is the first radial excitation of D_s and can decay to $D^{*0}K^+$, $D^{*+}K^0_{S(L)}$, $D^*_s\eta$. In the heavy quark limit, these partners are degenerate. Using the result for $\tilde{g}$ one predicts $\Gamma(D'_s) = (70 \pm 30)$ MeV.

Identifying $D_{sJ}(2700)$ with $D^{*\prime}_s$, its charmed non strange partners are $D^{*\prime +}$ and $D^{*\prime 0}$, the radial excitations of $D^{*+,0}$. Their masses can be fixed to 2600 ± 50 MeV assuming that $D_{sJ}(2700)$ is heavier by an amount of the size of the strange quark mass. $D^{*\prime}$ can decay to $D^{*\prime} \to D\pi$, D_sK, $D\eta$, $D^*\pi$, $D^*\eta$ so that the previous result for $\tilde{g}$ gives $\Gamma(D^{*\prime +(0)}) = (128 \pm 61)$ MeV. Noticeably, studying $D^+\pi^-$, $D^0\pi^+$, $D^{*+}\pi^-$ systems, BaBar found four new charmed non strange mesons [18] and, among these, the state $D^*(2600)$ likely to be identified with $D^{*\prime}$ (the non strange partner of $D_{sJ}(2700)$), and the state $D(2550)^0$ likely to be the spin partner of $D^*(2600)$, corresponding to the first radial excitation of the D meson. Comparison of the measured widths $\Gamma(D^*(2600)) = 93 \pm 6 \pm 13$ MeV, $\Gamma(D(2550)) = 130 \pm 12 \pm 13$ MeV with the prediction for $\Gamma(D^{*\prime +(0)})$ supports the proposed identification.

In [8] another broad structure was observed, $D_{sJ}(3040)$, with $M = 3044 \pm 8_{stat}(^{+30}_{-5})_{syst}$ MeV and $\Gamma = 239 \pm 35_{stat}(^{+46}_{-42})_{syst}$ MeV. $D_{sJ}(3040)$ decays to D^*K and not to DK, hence it has unnatural parity: $J^P = 1^+, 2^-, 3^+, \cdots$. The lightest not yet observed states with such quantum numbers are the two $J^P = 2^-$ states belonging to the doublets with $s_\ell = 3/2$ and $s_\ell = 5/2$ denoted as D_{s2} and $D^{\prime *}_{s2}$, respectively. The identification with the radial excitations with $n = 2$, $J^P = 1^+$, and $s_\ell = 1/2$ (the meson $\tilde{D}'_{s1}$) or $s_\ell = 3/2$ (the meson $\tilde{D}_{s1}$) is also possible. Notice that, if the identification of $D_{sJ}(2860)$ as the $J^P_{s_\ell} = 3^-_{5/2}$ meson were experimentally confirmed, this would disfavor the assignment of $D_{sJ}(3040)$ to its spin partner $D^{*\prime}_{s2}$ with $J^P_{s_\ell} = 2^-_{5/2}$, since a mass inversion in a spin doublet seems unlikely. For a similar reason, one would also disfavor the identification of $D_{sJ}(3040)$ with D_{s2}, although in that case the two mesons would belong to different doublets. The strong decays of $D_{sJ}(3040)$ to a charmed meson and a light pseudoscalar one can be evaluated using the effective Lagrangians in Eq.(2). In particular, one can compute the ratio $R_1 = \frac{\Gamma(D_{sJ}(3040) \to D^*_s\eta)}{\Gamma(D_{sJ}(3040) \to D^*K)}$ ($D^*K = D^{*0}K^+ + D^{*+}K^0_S$), with results collected in Table 2 [10]. The spread among them is useful to discriminate among the assignments, in particular between $\tilde{D}'_{s1}$ and $D^{*\prime}_{s2}$.

The mass of $D_{sJ}(3040)$ is large enough to allow decays to $(D^*_0, D'_1)K$, $(D_1, D^*_2)K$ and $D^*_{s0}\eta$, with different features in the four cases. Other allowed modes are into DK^* or $D_s\phi$ which can be described using an approach based on effective Lagrangian terms [19]. The results

decay modes	$\tilde{D}'_{s1}$ (n=2) $(J^P_{s_\ell} = 1^+_{1/2})$	$\tilde{D}_{s1}$ (n=2) $(J^P_{s_\ell} = 1^+_{3/2})$	D_{s2} (n=1) $(J^P_{s_\ell} = 2^-_{3/2})$	$D^{*\prime}_{s2}$ (n=1) $(J^P_{s_\ell} = 2^-_{5/2})$
D^*K, $D^*_s\eta$	$s-$ wave	$d-$ wave	$p-$ wave	$f-$ wave
R_1	0.34	0.20	0.245	0.143
D^*_0K, $D^*_{s0}\eta$, D'_1K	$p-$ wave	$p-$ wave	$d-$ wave	$d-$ wave
D_1K	$p-$ wave	$p-$ wave	-	$d-$ wave
D^*_2K	$p-$ wave	$p-$ wave	$s-$ wave	$d-$ wave
DK^*, $D_s\phi$	$s-$ wave	$s-$ wave	$p-$ wave	$p-$ wave
	$\Gamma \simeq 140$ MeV	$\Gamma \simeq 20$ MeV	negligible	negligible

Table 2: Features of the decay modes of $D_{sJ}(3040)$ for the four proposed assignments.

obtained in the four possible identifications are collected in Table 2 [10], from which some conclusions can be drawn. The determination of the wave in which a particular decay proceeds is useful to predict a hierarchy among the widths of the states in the four cases. Consequently, the two $J^P = 1^+$ are expected to be broader than the two $J^P = 2^+$ states, hence it is likely that $D_{sJ}(3040)$ should be identified with one of such two axial-vector mesons. These can be distinguished since the widths to the DK^* and $D_s\phi$ decay modes are larger for $\tilde{D}'_{s1}$ than for $\tilde{D}_{s1}$. Finally, although less probable, the identification with D_{s2} can be discarded/confirmed studying the D^*_2K $s-$wave final state.

4 Heavy quarkonium and the intriguing case of X(3872)

Besides the new charmed mesons, new heavy quarkonium or quarkonium-like states were observed. Some have been classified as standard quarkonia: the charmonia h_c [20], $\eta_c(2S)$ [21], $\chi_{c2}(2P)$ [22], and, in the beauty case, the $\eta_b(1S)$ [23], $h_b(1P)$ [24, 25] and $h_b(2P)$ [25]. Others are still awaiting for the right interpretation, since not only their quantum numbers are not established, but even their $Q\overline{Q}$ structure is questioned [26]. Among these, the charged $Z(4430)^-$ state seen by Belle Collaboration in $B \to Z^-K$, decaying to $\psi(2S)\pi^-$, $\chi_{c1}\pi^-$ [27]. The minimal quark content of this state would be $c\bar{c}u\bar{d}$, identifying it necessarily as an exotic state. Search for Z^- was performed by BaBar, but no signal was found [28]. Later on, Belle found other charmonium-like charged Z states [29] and, more recently, also bottomonium-like $Z_b(10610)$ and $Z_b(10650)$ states decaying to $\Upsilon(nS)\pi^\pm$ (n=1,2,3) and $h_b(mP)\pi^\pm$ (m=1,2) [30]. These states require confirmation, too.

Here I focus on the state $X(3872)$, discovered in 2003 by Belle Collaboration in $B^\pm \to K^\pm X \to K^\pm J/\psi\pi^+\pi^-$ decays [31] and confirmed by BaBar [32], CDF [33] and D0 [34] Collaborations. The PDG resonance parameters are: $M(X) = 3871.57 \pm 0.25$ MeV and $\Gamma(X) < 2.3$ MeV (90/% C.L.) [35]. Looking at the $J/\psi\pi^\pm\pi^0$ channel, no charged partners were found [36]. The mode $X \to J/\psi\gamma$ allows to fix charge conjugation of X to $C = +1$. Moreover, a $D^0\overline{D}^0\pi^0$

enhancement in $B \to D^0\overline{D}^0\pi^0 K$ decay was reported [37] with $\frac{B(X\to D^0\overline{D}^0\pi^0)}{B(X\to J/\psi\pi^+\pi^-)} = 9 \pm 4$, hence X mainly decays into final states with open charm mesons.

These measurements, though not fully consistent with the charmonium interpretation (as far as the mass of X is concerned), do not contradict it. However, the observation of $X \to J/\psi\pi^+\pi^-\pi^0$ with the measurement $\frac{B(X\to J/\psi\pi^+\pi^-\pi^0)}{B(X\to J/\psi\pi^+\pi^-)} = 1.0 \pm 0.4 \pm 0.3$ [38] implies, considering the two modes as induced by ρ^0 and ω intermediate states, isospin violation.

The three pion decay is also important to fix the spin-parity of X. While the angular analysis in $X \to J/\psi\pi^+\pi^-$ favours $J^P = 1^+$, studies of the three pion distribution in $X \to J/\psi\omega \to J/\psi\pi\pi\pi$ are more favourable to $J^P = 2^-$ [39]. Hence, if X is a $c\bar{c}$ state it can be either the first radial excitation of χ_{c1}, χ'_{c1}, or the state η_{c2} having $J^{PC} = 2^{-+}$.

On the other hand, the peculiar features of X suggested the conjecture that it is not a charmonium state. In particular, the coincidence between its mass and the $D^{*0}\overline{D}^0$ mass: $M(D^{*0}\overline{D}^0) = 3871.2 \pm 1.0$ MeV, inspired the proposal that $X(3872)$ could be a molecule [40], a bound state of D^{*0} and $\overline{D}^0$ with small binding energy [41], an interpretation that would account for a few properties of $X(3872)$. For example, if the wave function of $X(3872)$ has various hadronic components [42] one could explain why this state seems not to have definite isospin. However, the molecular binding mechanism still needs to be clearly identified, while the description of X(3872) as a charmonium state presents alternative arguments to the molecular description [43, 44]. Concerning the isospin violation, to correctly interpret the large ratio $\frac{B(X\to J/\psi\pi^+\pi^-\pi^0)}{B(X\to J/\psi\pi^+\pi^-)}$ one has to consider that phase space effects in two and three pion modes are very different and it turns out that the isospin violating amplitude is 20% of the isospin conserving one [45]: $\frac{B(X\to J/\psi\rho^0)}{B(X\to J/\psi\omega)} \simeq 0.2$.

I focus on two studies of X decays. The first one [46] compares the charmonium versus the molecular interpretation, discussing the argument that, if X(3872) is a DD^* molecule the decay $X \to D^0\overline{D}^0\gamma$ should be dominant with respect to $X \to D^+D^-\gamma$, such decays being mainly due to the decays of its meson components [42]. In order to discuss whether this is true, in [46] the ratio $R = \frac{\Gamma(X\to D^+D^-\gamma)}{\Gamma(X\to D^0\overline{D}^0\gamma)}$ has been computed assuming that X(3872) is an ordinary $J^{PC} = 1^{++}$ charmonium state.

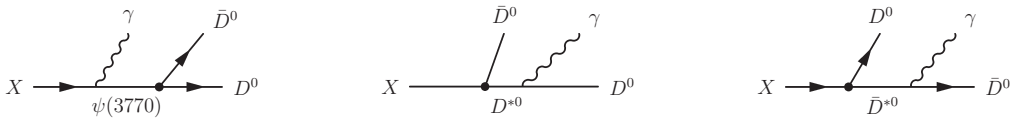

Figure 1: Diagrams describing the radiative modes $X \to D\overline{D}\gamma$.

The transition $X(3872) \to D\overline{D}\gamma$ can be studied assuming that the radiative decay amplitude is dominated by polar diagrams with D^* and the $\psi(3770)$ mesons as intermediate states nearest to their mass shell (fig.1). These amplitudes can be expressed in terms of

two unknown quantities: the coupling constant $\hat{g}_1$ governing the $X\overline{D}D^*(D\overline{D}^*)$ matrix elements, and the one appearing in the $X\psi(3770)\gamma$ matrix element. For the matrix element $X\overline{D}D^*(D\overline{D}^*)$ one can use a formalism suitable to describe the interaction of the heavy charmonium with the doublet H in (1) [47]. In the multiplet:

$$P^{(Q\overline{Q})\mu} = \left(\frac{1+\not{v}}{2}\right)\left(\chi_2^{\mu\alpha}\gamma_\alpha + \frac{1}{\sqrt{2}}\epsilon^{\mu\alpha\beta\gamma}v_\alpha\gamma_\beta\chi_{1\gamma} + \frac{1}{\sqrt{3}}(\gamma^\mu - v^\mu)\chi_0 + h_1^\mu\gamma_5\right)\left(\frac{1-\not{v}}{2}\right) \tag{3}$$

the fields χ_2, χ_1, χ_0 correspond to the spin triplet with $J^{PC} = 2^{++}, 1^{++}, 0^{++}$, respectively, while the spin singlet h_1 has $J^{PC} = 1^{+-}$. If $X(3872) = \chi'_{c1}$, it is described by χ_1. The strong interaction with the D and D^* mesons can be described by the effective Lagrangian [48]

$$\mathcal{L}_1 = ig_1 Tr\left[P^{(Q\overline{Q})\mu}\overline{H}_{1a}\gamma_\mu\overline{H}_{2a}\right] + h.c.\ . \tag{4}$$

Using (4) the couplings XDD^* which enter in the second and the third diagrams in fig.1, can be expressed in terms of the dimensionless coupling constant $\hat{g}_1 = g_1\sqrt{m_D}$. Notice that, due to isospin symmetry, the couplings of the meson X to charged and neutral D are equal, at odds with the molecular description where X mainly couples to neutral D.

The matrix element $< D(k_1)\gamma(k,\tilde{\epsilon})|D^*(p_1,\xi) >= i\,e\,c'\,\epsilon^{\alpha\beta\tau\theta}\,\tilde{\epsilon}^*_\alpha\,\xi_\beta\,p_{1\tau}\,k_\theta$ is also required. The parameter c' accounts for the coupling of the photon to both the charm and the light quark and can be fixed from data on radiative D^{*+} decays [35].

To compute the first diagram in fig.1 the matrix element $< \psi_{(3770)}(q,\eta)\gamma(k,\tilde{\epsilon})|X(p,\epsilon) >= i\,e\,c\,\epsilon^{\alpha\beta\mu\nu}\,\tilde{\epsilon}^*_\alpha\,\epsilon_\beta\,\eta^*_\mu\,k_\nu$ is needed; c is an unknown parameter. On the other hand, the coupling $\psi(3770)D\overline{D}$ can be fixed from experiment to $g_{\psi D\overline{D}} = 25.7 \pm 1.5$.

Putting all the ingredients together one obtains the ratio $R = \frac{\Gamma(X\to D^+D^-\gamma)}{\Gamma(X\to D^0\overline{D}^0\gamma)}$, plotted in fig.2 [46] versus $\frac{c}{\hat{g}_1}$, showing that the radiative X decay into charged D mesons is always suppressed with respect to the mode with neutral D and in any case $R < 0.7$. Moreover, for small values of $\frac{c}{\hat{g}_1}$ the ratio R is tiny, so that this is not peculiar of a molecular structure of $X(3872)$.

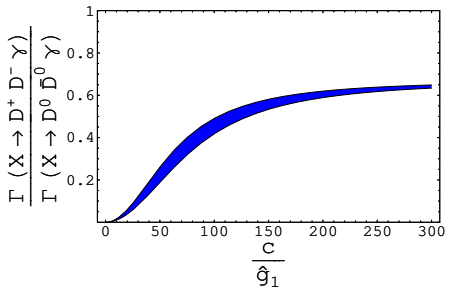

Figure 2: Ratio of $X \to D^+D^-\gamma$ to $X \to D^0\overline{D}^0\gamma$ decay widths versus the ratio of parameters $c/\hat{g}_1$.

$\hat{g}_1$ enters also in the mode $X(3872) \to D^0\overline{D}^0\pi^0$ that can be considered as induced by intermediate D^* states. The amplitude depends on the coupling constant $D^*D\pi$, proportional to the constant g in eq. (2). Using data on D^{*+} decays to $D\pi$ [35], one can derive $g = 0.64 \pm 0.07$. This allows to constrain $\hat{g}_1 < 4.5$ from the upper bound $\Gamma(X \to D^0\overline{D}^0\pi^0) < \Gamma(X(3872)) < 2.3$ MeV. Hence, a value of $\hat{g}_1$ of the typical size of the hadronic couplings can reproduce the small width of $X(3872)$.

The second analysis that I discuss also aims at shedding light on the structure of X(3872) through the calculation of its radiative decay rates to $J/\psi\gamma$ and $\psi(2S)\gamma$ assuming that it is the state χ'_{c1} [49] and using an effective Lagrangian approach which exploits spin symmetry for heavy $Q\overline{Q}$ states [50]. Unlike the heavy-light $Q\bar{q}$ mesons, in heavy quarkonia there is no heavy flavour symmetry [51], hence it would not be possible to exploit data on charmonium to obtain quantitative information on bottomonium or viceversa. However, at a qualitative level, bottomonium system can help in understanding charmonium.

A heavy $Q\overline{Q}$ state ($Q = c,\, b$) can be identified by $n^{2s+1}L_J$ as a meson with parity $P = (-1)^{L+1}$ and charge-conjugation $C = (-1)^{L+s}$: n is the radial quantum number, L the orbital angular momentum, s the spin and J the total angular momentum. Radiative transitions between states belonging to the same nL multiplet to states belonging to another $n'L'$ one are described in terms of a single coupling constant $\delta^{nLn'L'}$.

I introduce the effective fields for the states involved in the decays $X \to J/\psi\gamma$ and $X \to \psi(2S)\gamma$. Identifying X with the state χ'_{c1}, it belongs to the multiplet with $L = 1$ introduced in (3). J/ψ and $\psi(2S)$ are described by the $J^P = 1^-$ H_1 component of the doublet:

$$J = \frac{1+\not{v}}{2}\left[H_1^\mu\gamma_\mu - H_0\gamma_5\right]\frac{1-\not{v}}{2}\,. \tag{5}$$

The effective Lagrangian describing radiative transitions among members of the P wave and of the S wave multiplets has been derived in [50]:

$$\mathcal{L}_{nP\leftrightarrow mS} = \delta_Q^{nPmS}\,Tr\left[\overline{J}(mS)J_\mu(nP)\right]v_\nu F^{\mu\nu} + \text{h.c.}\,. \tag{6}$$

$F^{\mu\nu}$ the electromagnetic field strength tensor. Hence, a single constant δ_Q^{nPmS} describes all the transitions among the members of the nP multiplet and those of the mS one.

I consider the ratios $R_J^{(b)} = \frac{\Gamma(\chi_{bJ}(2P)\to\Upsilon(2S)\,\gamma)}{\Gamma(\chi_{bJ}(2P)\to\Upsilon(1S)\,\gamma)}$, proportional to $R_\delta^{(b)} = \frac{\delta_b^{2P1S}}{\delta_b^{2P2S}}$ ($J = 0, 1, 2$). From the measured branching ratios of $\chi_{bJ}(2P) \to \Upsilon(1S)\,\gamma\,, \Upsilon(2S)\,\gamma$ [35], the average value can be obtained: $R_\delta^{(b)} = 8.8 \pm 0.7$. It is reasonable that, even though the couplings might be different in the beauty and the charm cases, their ratios stay stable. Therefore, using the result for $R_\delta^{(b)}$ in the case of χ'_{c1} decays, I get:

$$R_1^{(c)} = \frac{\Gamma(\chi_{c1}(2P) \to \psi(2S)\,\gamma)}{\Gamma(\chi_{c1}(2P) \to \psi(1S)\,\gamma)} = 1.64 \pm 0.25\,. \tag{7}$$

In [52] the following ratio has been measured [1]:

$$R_X = \frac{\Gamma(X(3872) \to \psi(2S)\,\gamma)}{\Gamma(X(3872) \to \psi(1S)\,\gamma)} = 3.5 \pm 1.4\,. \tag{8}$$

In view of the underlying approximation, one can conclude that the experimental value in (8) and the theoretical prediction (7) are close enough to consider plausible the identification $X(3872) = \chi_{c1}(2P)$, in contrast to the composite scenarios, in which the mode $X(3872) \to \psi(2S)\,\gamma$ is suppressed compared to $X(3872) \to \psi(1S)\,\gamma$ [43,54].

5 Conclusions

In the last decade, many predicted charm and beauty mesons have been discovered, along with many unexpected ones. In the case of D_{sJ} mesons, the analysis of their decay modes allows to classify them as ordinary $c\bar{s}$ states, although the identification of $D_{sJ}(2860)$ is still under scrutiny.

The case of hidden charm and beauty mesons is more complicated. As for $X(3872)$, two analyses of the radiative decays of X show that the charmonium interpretation seems to be a likely one, although experimentally it is still unclear whether its spin-parity is $J^P = 1^+$ or $J^P = 2^-$.

Acknowledgments

I thank P. Colangelo, R. Ferrandes, S. Nicotri, A. Ozpineci and M. Rizzi for collaboration.

Bibliography

[1] B. Aubert *et al.*, Phys. Rev. Lett. **90**, 242001 (2003).

[2] D. Besson *et al.*, Phys. Rev. **D68**, 032002 (2003) [Erratum-ibid. **D75**, 119908 (2007)].

[3] P. Colangelo, F. De Fazio and R. Ferrandes, Mod. Phys. Lett. **A19**, 2083 (2004).

[4] P. Colangelo and F. De Fazio, Phys. Lett. **B570**, 180 (2003).

[5] P. Colangelo, F. De Fazio and A. Ozpineci, Phys. Rev. **D72**, 074004 (2005).

[6] B.Aubert *et al.*, Phys. Rev. Lett. **97**, 222001 (2006).

[7] J. Brodzicka *et al.*, Phys. Rev. Lett. **100**, 092001 (2008).

[1] Belle Collaboration has recently provided an upper limit for the Ratio $R_X < 2.1$ (at 90% C.L.) [53].

[8] B. Aubert *et al.*[BABAR Collaboration], Phys. Rev. **D80**, 092003 (2009).

[9] P. Colangelo *et al.*, Phys. Lett. **B642**, 48 (2006); Phys. Rev. **D77**, 014012 (2008).

[10] P. Colangelo and F. De Fazio, Phys. Rev. **D81**, 094001 (2010).

[11] For a review see: M. Neubert, Phys. Rept. **245**, 259 (1994).

[12] K. Abe *et al.*[Belle Collaboration], Phys. Rev. **D69**, 112002 (2004).

[13] P. Colangelo, F. De Fazio and R. Ferrandes, Phys. Lett. **B634**, 235 (2006).

[14] M.B.Wise, Phys. Rev. **D45**, R2188 (1992); G. Burdman *et al.*, Phys. Lett. **B280**, 287 (1992); P. Cho, Phys. Lett. **B285** 145 (1992); H.Y. Cheng *et al.,* Phys. Rev. **D46**, 1148 (1992).

[15] R. Casalbuoni *et al.*, Phys. Lett. **B299**, 139 (1993).

[16] P. Colangelo, F. De Fazio and G. Nardulli, Phys. Lett. **B478**, 408 (2000).

[17] V. M. Belyaev *et al.*, Phys. Rev. **D51**, 6177 (1995); P. Colangelo *et al.*, Phys. Lett. **B334**, 175 (1994); Phys. Lett. **B339**, 151 (1994); Phys. Rev. **D52**, 6422 (1995); Eur. Phys. J. **C4**, 503 (1998); Phys. Lett. **B532**, 193 (2002).

[18] P. del Amo Sanchez *et al.*[The BABAR Collaboration], Phys. Rev. **D82**, 111101 (2010).

[19] R. Casalbuoni *et al.*, Phys. Lett. B **292**, 371 (1992).

[20] J. L. Rosner *et al.*[CLEO Collaboration], Phys. Rev. Lett. **95**, 102003 (2005).

[21] S. K. Choi *et al.*[BELLE collaboration], Phys. Rev. Lett. **89**, 102001 (2002) [Erratum-ibid. **89**, 129901 (2002)]; B. Aubert *et al.*[BABAR Collaboration], Phys. Rev. Lett. **92**, 142002 (2004); D. M. Asner *et al.*[CLEO Collaboration], Phys. Rev. Lett. **92**, 142001 (2004).

[22] S. Uehara *et al.*[Belle Collaboration], Phys. Rev. Lett. **96**, 082003 (2006).

[23] B. Aubert *et al.*[BABAR Collaboration], Phys. Rev. Lett. **101**, 071801 (2008).

[24] J. P. Lees [The BABAR Collaboration], arXiv:1102.4565 [hep-ex].

[25] I. Adachi *et al.*[Belle Collaboration], arXiv:1103.3419 [hep-ex].

[26] For a review: N. Brambilla *et al.*, Eur. Phys. J. **C71**, 1534 (2011).

[27] S. K. Choi *et al.*[BELLE Collaboration], Phys. Rev. Lett. **100**, 142001 (2008).

[28] B. Aubert *et al.*[BABAR Collaboration], Phys. Rev. D **79**, 112001 (2009).

[29] R. Mizuk *et al.*[Belle Collaboration], Phys. Rev. D **78**, 072004 (2008).

[30] Belle Collaboration, arXiv:1105.4583 [hep-ex].

[31] S. K. Choi *et al.*[Belle Collaboration], Phys. Rev. Lett. **91**, 262001 (2003).

[32] B. Aubert *et al.*[BABAR Collaboration], Phys. Rev. **D71**, 071103 (2005).

[33] D. Acosta *et al.*[CDF II Collaboration], Phys. Rev. Lett. **93**, 072001 (2004).

[34] V. M. Abazov *et al.*[D0 Collaboration], Phys. Rev. Lett. **93**, 162002 (2004).

[35] K. Nakamura *et al.*(Particle Data Group), J. Phys. **G 37**, 075021 (2010).

[36] B. Aubert *et al.*[BaBar Collaboration], Phys. Rev. **D71**, 031501 (2005).

[37] G. Gokhroo *et al.*, Phys. Rev. Lett. **97**, 162002 (2006).

[38] K. Abe *et al.*[Belle Collaboration], Phys. Rev. Lett. **94**, 182002 (2005).

[39] P. del Amo Sanchez *et al.*[BABAR Collaboration], Phys. Rev. D **82**, 011101 (2010).

[40] M. B. Voloshin and L. B. Okun, JETP Lett. **23**, 333 (1976).

[41] See M. B. Voloshin, Prog. Part. Nucl. Phys. **61**, 455 (2008) and references therein.

[42] M. B. Voloshin, Int. J. Mod. Phys. **A21**, 1239 (2006).

[43] T. Barnes and S. Godfrey, Phys. Rev. **D69**, 054008 (2004).

[44] T. Barnes *et al.*, Phys. Rev. **D72**, 054026 (2005); E. J. Eichten *et al.*, Phys. Rev. **D69**, 094019 (2004); Phys. Rev. **D73**, 014014 (2006) [Erratum-ibid. **D73**, 079903 (2006)].

[45] M. Suzuki, Phys. Rev. **D72**, 114013 (2005).

[46] P. Colangelo, F. De Fazio and S. Nicotri, Phys. Lett. **B650**, 166 (2007).

[47] R. Casalbuoni *et al.*, Phys. Rept. **281**, 145 (1997).

[48] P. Colangelo, F. De Fazio and T. N. Pham, Phys. Rev. **D69**, 054023 (2004).

[49] F. De Fazio, Phys. Rev. **D79**, 054015 (2009) [Erratum-ibid. **D83**, 099901 (2011)].

[50] R. Casalbuoni *et al.*, Phys. Lett. **B302**, 95 (1993).

[51] B. A. Thacker and G. P. Lepage, Phys. Rev. **D43**, 196 (1991).

[52] B. Aubert *et al.*[BABAR Collaboration], Phys. Rev. Lett. **102**, 132001 (2009).

[53] V. Bhardwaj *et al.*[Belle Collaboration], arXiv:1105.0177 [hep-ex].

[54] E. S. Swanson, Phys. Rept. **429**, 243 (2006).

Brief review of the theory of the muonic hydrogen Lamb shift and the proton radius

Antonio Pineda
Grup de Física Teòrica, Universitat Autònoma de Barcelona, E-08193 Bellaterra, Barcelona, Spain

Recently the muonic hydrogen lamb shift has been measured with unprecedented accuracy, allowing for a precise determination of the proton radius. This determination is 5 sigma away from the previous CODATA value obtained from (mainly) the hydrogen lamb shift and the electron-proton scattering. Within an effective field theory formalism, I will define the proton radius and briefly review some aspects of the theoretical prediction for the muonic hydrogen lamb shift, studying both the pure QED-like computation and the hadronic effects.

1 Introduction

The recent measurement of the muonic hydrogen Lamb shift, $E(2P_{3/2}(F=2)) - E(2S_{1/2}(F=1))$,

$$E_{exp} = 206.2949(32)\text{meV}$$

and the associated determination of the electromagnetic proton radius [1]:

$$r_p = 0.84184(67)\text{fm}\,. \tag{1}$$

has led to a lot of controversy. The reason is that this number is 5 sigma away from the CODATA value, $r_p = 0.8768(69)$ fm [2]. If instead one uses this value in the theoretical expression of the muonic Hydrogen Lamb shift one gets the following discrepancy:

$$E_{exp} - E_{th} = 0.311 \text{ meV} \tag{2}$$

between theory and experiment. Two main options are clearly at hand: either the theoretical determination is not correct (or not as precise as claimed), or previous determinations of the proton radius were incorrect (or not as precise as claimed). Here we would like to study the theoretical expression of the muonic Hydrogen Lamb shift within an effective field theory perspective. We do it partially, and only focus on some few aspects, as a full analysis would require much more space. In particular spin effects will not be considered. We believe that the use of effective field theories helps in organizing the computation by providing with power counting rules to asses the importance of the different contributions. This will be even more important once higher order effects are included. For the present

discussion a $\mathcal{O}(m_r\alpha^5)$ precision is enough to visualize the discrepancy. Higher order effects are way smaller than the discrepancy found in Eq. (2). Moreover $\mathcal{O}(m_r\alpha^5)$ is the only thing completely known at present[1].

The dynamics of the muonic hydrogen is characterized by several scales:
$m_p \sim \Lambda_\chi$,
$m_\mu \sim m_\pi \sim m_r = \frac{m_\mu m_p}{m_p+m_\mu}$,
$m_r\alpha \sim m_e$.
By considering ratios between them the main expansion parameters are obtained:
$\frac{m_\pi}{m_p} \sim \frac{m_\mu}{m_p} \sim \frac{1}{9}$,
$\frac{m_r\alpha}{m_r} \sim \frac{m_r\alpha^2}{m_r\alpha} \sim \alpha \sim \frac{1}{137}$.

We use the effective field theory Potential Non-Relativistic QED (pNRQED) [3]. Specially relevant for us is Ref. [4], which contains much more detailed information on the application of pNRQED to the muonic hydrogen, and we refer to it for details (see also [5–7]). pNRQED profits from the hierarchy $m_\mu \gg m_\mu\alpha \gg m_\mu\alpha^2$ and the Lagrangian reads

$$L_{pNRQED} = \int d^3\mathbf{r}d^3\mathbf{R}dtS^\dagger(\mathbf{r},\mathbf{R},t)\Big\{i\partial_0 - \frac{\mathbf{p}^2}{2m_r} - V(\mathbf{r},\mathbf{p},\sigma_1,\sigma_2) + e\mathbf{r}\cdot\mathbf{E}(\mathbf{R},t)\Big\}S(\mathbf{r},\mathbf{R},t) - \int d^3\mathbf{r}\frac{1}{4}F_{\mu\nu}F^{\mu\nu}\,, \tag{3}$$

where S is the field representing the muonic hydrogen, $\mathbf{R}$ the center of mass coordinate and $\mathbf{r}$ the relative distance.

V stands for the potential and admits an expansion in powers of $1/m_\mu$:

$$V(\mathbf{r},\mathbf{p},\sigma_1,\sigma_2) = V^{(0)}(r) + \frac{V^{(1)}(r)}{m_\mu} + \frac{V^{(2)}(r)}{m_\mu^2} + \cdots\,. \tag{4}$$

The potential is obtained through matching to the underlying theory. Since pNRQED describes degrees of freedom with $E \sim m_\mu\alpha^2$, any other degree of freedom with larger energy is integrated out. This implies treating the proton and muon in a non-relativistic fashion and integrating out pions. This is the step of going from Heavy Baryon Effective Theory (HBET) to NRQCD. By integrating out the scale $m_\mu\alpha$, pNRQED is obtained and the potentials appear. Schematically the path followed is the following:

$$HBET(m_\pi/m_\mu) \to NRQED(m_\mu\alpha) \to pNRQED\,.$$

[1]This is also the precision presently reached in heavy quarkonium spectrum computations. This made provide with some cross checks between both systems.

2 Pure QED contributions

We first focus on the pure QED contributions. We mostly follow Pachucki's work [8–10], as it mainly follows an strict order by order in α computation, trying to accommodate their results in our formalism. See however [1] (or [11, 12]) for more complete list of references.

The static potential can be written in the following way in momentum space

$$\tilde{V}^{(0)} \equiv -4\pi Z_\mu Z_p \alpha_V(k) \frac{1}{\mathbf{k}^2}, \tag{5}$$

$$\alpha_{eff}(k) = \alpha \frac{1}{1+\Pi(-\mathbf{k}^2)}\,, \tag{6}$$

where $\Pi(k^2)$ is the vacuum polarization due to electrons and can be computed order by order in α:

$$\Pi(k^2) = \alpha\Pi^{(1)}(k^2) + \alpha^2\Pi^{(2)}(k^2) + \alpha^3\Pi^{(3)}(k^2) + ...$$

$$\alpha_V(k) = \alpha_{eff}(k) + \sum_{\substack{n,m=0 \\ n+m=even>0}} Z_\mu^n Z_p^m \alpha_{eff}^{(n,m)}(k) = \alpha_{eff}(k) + \delta\alpha(k)\,, \qquad \delta\alpha(k) = \mathcal{O}(\alpha^4). \tag{7}$$

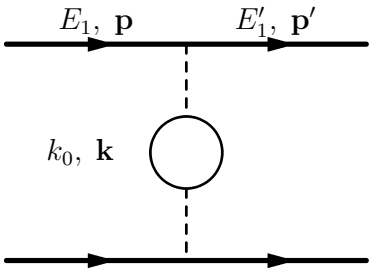

Figure 1: *Leading correction to the Coulomb potential due to the electron vacuum polarization.* $\mathbf{k} = \mathbf{p} - \mathbf{p}'$ *and* $k_0 = E_1 - E_1'$.

The leading order contribution to the lamb shift comes from the one-loop vacuum polarization correction to the static potential (see Fig. 1)

$$E_{LO} = \langle n|\delta V|n\rangle = 205.0074 \text{ mev} = \mathcal{O}(m_r\alpha^3)\,.$$

The $\mathcal{O}(m_r\alpha^4)$ contribution to the lamb shift comes from the two-loop static potential and from the iteration of the one-loop potential in quantum mechanics perturbation theory. The latter yields $\Delta E = 0.151$ meV. The former is purely due to vacuum polarization corrections (see Fig. 2) and yields $\Delta E = 1.5079$ meV.

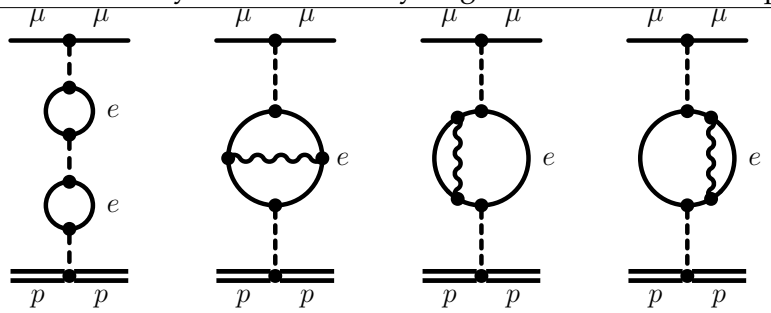

Figure 2: *The static potential at two loops.*

The three-loop static potential contribution due to the vacuum polarization (and the associated iterations from perturbation theory were computed in Ref. [13] (see also [14] for an small correction). The result was quite small $\Delta E = 0.0076$ meV $= \mathcal{O}(m_r\alpha^5)$.

All previous contributions were due to the vacuum polarization. The only contribution from the static potential that is not due to the vacuum polarization at $\mathcal{O}(m_r\alpha^5)$ comes from $\delta\alpha$. It is a light-by-light (Wichmann-Kroll and Delbrück) contribution and very small [15]

$$\Delta E \simeq -0.0009 \text{ meV}\,.$$

It should be mentioned that the limit $m_e \to 0$ of the static potential is known at three loops from QCD [16, 17], which could be used as a check. It is also reasonable to think that the result with finite m_e could also be obtained from these results (albeit numerically) with a finite amount of work.

There are no corrections due to the $1/m_\mu$ potential at $\mathcal{O}(m_r\alpha^5)$. From the $1/m_\mu^2$ potential (see [4] for its expression in pNRQED) there are the tree level relativistic corrections, which give $\Delta E = 0.0575$ meV $= \mathcal{O}(m\alpha^4)$. The incorporation of the one-loop vacuum polarization to the relativistic $1/m_\mu^2$ tree-level potential gives the following result $\Delta E = 0.0169$ meV $= \mathcal{O}(m\alpha^5)$ [10].

In order to complete the pure QED $\mathcal{O}(m\alpha^5)$ corrections one has to include the interaction with the ultrasoft photons (see Fig. 3). They yield the result (taken from [8])

$$\Delta E = -0.6677 \text{ meV} = \mathcal{O}(m\alpha^5)\,.$$

The $\frac{m_\mu}{m_p}$ ultrasoft effects contribute

$$\Delta E = -0.045 \text{ meV} = \mathcal{O}(m\alpha^5\frac{m_\mu}{m_p})\,.$$

In pNRQED these results would not come from the interaction with the ultrasoft photons only, as it would be factorization scale dependent, they also include effects due to the NRQED matching coefficients encoded in the $1/m_\mu^2$ potentials. The procedure is pretty much the same the one used for positronium in Ref. [5]. The details for muonic hydrogen will be worked out elsewhere.

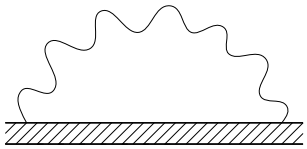

Figure 3: *self-energy correction to the muonic hydrogen energy due to the interaction with ultrasoft photons.*

At $\mathcal{O}(m\alpha^5\frac{m_\mu^2}{m_p^2})$ one starts to have overlap with hadronic effects, which we discuss in the next section.

3 Hadronic Contributions

In the previous section we have considered the proton to be point-like. We now incorporate the finite-size effects due to the hadronic structure of the proton. These effects are encoded in the coefficient multiplying the delta potential (note that the combination of NRQED matching coefficients that appears in the potential is always the same).

$$\delta V^{(2)}_{had}(r) \equiv \frac{1}{m_p^2} D_d^{had} \delta^3(\mathbf{r}) \to \Delta E = \frac{1}{m_p^2} D_d^{had} \frac{1}{\pi} (\frac{m_r \alpha}{n})^3 \delta_{l0} \tag{8}$$

where

$$D_d^{had} = -c_3^{had} - 16\pi\alpha d_2^{had} + \frac{\pi\alpha}{2} c_D^{had}\,. \tag{9}$$

We define $c_3 = c_3^{point-like} + c_3^{had}$, $d_2 = d_2^{point-like} + d_2^{had}$ $c_D = c_D^{point-like} + c_D^{had.}$,so that c_3^{had}, d_2^{had}, c_D^{had} are the left-over of the matching coefficients of NRQED Lagrangian

$$\delta\mathcal{L} = \cdots \frac{d_2}{m_p^2} F_{\mu\nu} D^2 F^{\mu\nu} + \cdots - e\frac{c_D}{m_p^2} N_p^\dagger \boldsymbol{\nabla}\cdot\mathbf{E} N_p + \cdots + \frac{c_3}{m_p^2} N_p^\dagger N_p \mu^\dagger \mu \tag{10}$$

after subtraction of the point-like contributions. We do in this way because traditionally the point-like contributions are already included in the "pure" QED corrections described in the previous section[2]. I more extended discussion can be found in Refs. [4, 6].

d_2^{had} encodes the hadronic vacuum polarization effect. Its contribution to the Lamb shift is tiny, $\Delta E = 0.011$ meV, and not much subject to uncertainty as it can be determined with enough precision from dispersion relations.

[2]Note though, that for an strict effective theory point of view, at scales of the order of m_p, it is not a good approximation to consider the proton point like. Therefore, in a way, we are introducing an "spurious" contribution in the hadronic matching coefficients.

More subject to discussion are the hadronic corrections associated to c_3^{had}. They are usually split into two terms (see the discussion in Refs. [4, 6]): $c_3^{had} = c_{3,Zemach}^{had} + c_{3,*206*pol}^{had}$. We symbolically draw them in Figs. 4 and 5, and discuss them in the next subsections. A common feature of both of them is that they are power-like chiral enhanced: $\sim \frac{m_\mu}{m_\pi}$. This is very important, as it allows chiral perturbation theory to predict the leading order term without introducing any extra parameter. The resulting correction to the Lamb shift is of $\mathcal{O}(m_\mu \alpha^5 \times \frac{m_\mu^2}{\Lambda_\chi^2} \times \frac{m_\mu}{m_\pi})$.

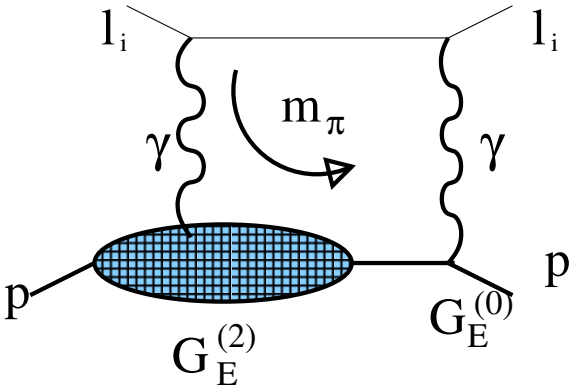

Figure 4: *Symbolic representation (plus permutations) of the Zemach $\langle r^3 \rangle$ correction, Eq. (11).*

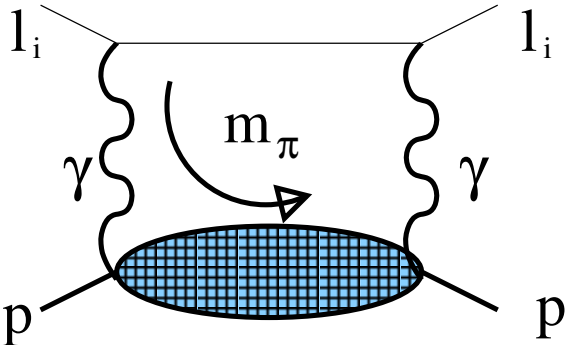

Figure 5: *Symbolic representation of Eq. (17).*

3.1 Zemach correction, $\langle r^3 \rangle$

It is the one analogous to the Zemach correction defined in the hyperfine splitting [18]. It is also common to rewrite it in terms of a coefficient $\langle r_p^3 \rangle$

$$c_{3,Zemach}^{had} = \frac{\pi}{3}\alpha^2 m_p^2 m_\mu \langle r_p^3 \rangle, \qquad \frac{\langle r_p^3 \rangle}{\text{fm}^3} = \frac{96}{\pi}\int d^{D-1}k \frac{1}{\mathbf{k}^6} G_E^{(0)} G_E^{(2)}\,, \tag{11}$$

where $G_E^{(n)}$ is the electric Sachs form factor to order n in the chiral counting ($G_E^{(0)}=1$). We also use dimensional regularization ($D=4+2\epsilon$). This gets rid of power-like divergences which are then automatically set to zero (no need for counterterms as one would with cutoff regularization). The final result is finite and it is possible to obtain an analytic expression for the leading term in the chiral and large N_c expansion (by including the Δ particle contribution). It reads [4]

$$c_{3,Zemach}^{had} = 2(\pi\alpha)^2\left(\frac{m_p}{4\pi F_0}\right)^2\frac{m_\mu}{m_\pi}\left\{\frac{3}{4}g_A^2+\frac{1}{8}+\frac{2}{\pi}g_{\pi N\Delta}^2\frac{m_\pi}{\Delta}\sum_{r=0}^{\infty}C_r\left(\frac{m_\pi}{\Delta}\right)^{2r}+g_{\pi N\Delta}^2\sum_{r=1}^{\infty}H_r\left(\frac{m_\pi}{\Delta}\right)^{2r}\right\}, \tag{12}$$

where ($\Delta=M_\Delta-M_p\sim 300$ MeV)

$$C_r=\frac{(-1)^r\Gamma(-3/2)}{\Gamma(r+1)\Gamma(-3/2-r)}\left\{B_{6+2r}-\frac{2(r+2)}{3+2r}B_{4+2r}\right\}, \qquad r\geqslant 0\,, \tag{13}$$

$$B_n\equiv\int_0^\infty dt\frac{t^{2-n}}{\sqrt{1-t^2}}\ln\left[\frac{1}{t}+\sqrt{\frac{1}{t^2}-1}\right] \qquad H_n\equiv\frac{n!(2n-1)!!\Gamma[-3/2]}{2(2n)!!\Gamma[1/2+n]}\,. \tag{14}$$

This expression produces the following number for $\langle r_p^3\rangle$ and the associated energy shift:

$$\frac{\langle r_p^3\rangle|_{\chi PT}}{\text{fm}^3}=1.9\ \text{(Pineda)}\rightarrow\Delta E=0.010\frac{\langle r_p^3\rangle}{\text{fm}^3}=0.019\ \text{meV} \tag{15}$$

This number can be compared with some recent determinations of $\langle r_p^3\rangle$ using dispersion relations [19–22]

$$\frac{\langle r_p^3\rangle|_{"exp"}}{\text{fm}^3}=\left\{\begin{array}{l}2.71(13)\ \text{Friar}-\text{Sick}\\ 2.85(8)\ \text{Bernauer}-\text{Arrington}\end{array}\right\}\rightarrow\Delta E=0.027-0.029$$

In principle the difference between these two determinations comes from different fit functions and data, which may give a first estimate of the associated uncertainty of the dispersion relation analysis. We find quite reassuring that the difference with the chiral computation is around 40 %, which could be easily accommodated with higher order corrections. Much more difficult to accommodate would be the value advocated in Ref. [23], $\langle r_p^3\rangle\sim 36.5$, from a direct fit to the muonic hydrogen Lamb shift using the CODATA value for the proton value. This would require that higher order corrections in the chiral computation to be a factor 15 larger than the leading order result. We believe this is at odds with chiral symmetry, even more so taking into account that one of the motivations of such proposal was the lack of experimental data at low momentum, but it is precisely in this region where chiral perturbation theory should work better.

3.2 Polarizability correction

The determination of the polarizability correction from experiment is on more shaky grounds than for the Zemach correction, producing the larger uncertainty in the theoretical expression for the Lamb shift. The reason is that dispersion relations do not fix the result completely. The final number used in [1] was taken from the average in Ref. [24] $\Delta E = 0.015 \pm 0.004$ using the results from, [9] $\Delta E = 0.012 \pm 0.002$ meV, [25] $\Delta E = 0.017 \pm 0.004$ meV, and [26] $\Delta E = 0.016$ meV. For a recent discussion see Ref. [27].

Here again chiral computations may turn out to be crucial to asses the size of this correction. The reason, as before, is that the polarizability correction is power-like chiral enhanced. Therefore, chiral perturbation theory can predict the leading order term with no new parameter. This is the attitude followed in Ref. [7], where a chiral computation using dispersion relations yielded

$$c_{3,pol}^{had} = -e^4 m_p m_\mu \int \frac{d^4k_E}{(2\pi)^4}\frac{1}{k_E^4}\frac{1}{k_E^4+4m_\mu^2 k_{0,E}^2}\left\{(3k_{0,E}^2+\mathbf{k}^2)S_1(ik_{0,E},-k_E^2)-\mathbf{k}^2 S_2(ik_{0,E},-k_E^2)\right\}$$

where

$$T^{\mu\nu} = i\int d^4x\, e^{iq\cdot x}\langle p,s|TJ^\mu(x)J^\nu(0)|p,s\rangle\,,$$

which has the following structure ($\rho = q\cdot p/m$):

$$\begin{aligned} T^{\mu\nu} &= \left(-g^{\mu\nu}+\frac{q^\mu q^\nu}{q^2}\right)S_1(\rho,q^2)+\frac{1}{m_p^2}\left(p^\mu-\frac{m_p\rho}{q^2}q^\mu\right)\left(p^\nu-\frac{m_p\rho}{q^2}q^\nu\right)S_2(\rho,q^2) \\ &\quad -\frac{i}{m_p}\epsilon^{\mu\nu\rho\sigma}q_\rho s_\sigma A_1(\rho,q^2)-\frac{i}{m_p^3}\epsilon^{\mu\nu\rho\sigma}q_\rho\big((m_p\rho)s_\sigma-(q\cdot s)p_\sigma\big)A_2(\rho,q^2) \end{aligned} \tag{16}$$

After introducing the chiral expressions for the structure factors from the diagrams in Fig. 6, one obtains

$$\begin{aligned} c_{3,pol}^{had} &= -e^4 m_p^2\frac{m_\mu}{m_\pi}\left(\frac{g_A}{f_\pi}\right)^2\int\frac{d^{D-1}k_E}{(2\pi)^{D-1}}\frac{1}{(1+\mathbf{k}^2)^4}\int_0^\infty\frac{dw}{\pi}w^{D-5}\frac{1}{w^2+4\frac{m_\mu^2}{m_\pi^2}\frac{1}{(1+\mathbf{k}^2)^2}} \\ &\quad\times\left\{(2+(1+\mathbf{k}^2)^2)A_E(w^2,\mathbf{k}^2)+(1+\mathbf{k}^2)^2\mathbf{k}^2w^2B_E(w^2,\mathbf{k}^2)\right\} \end{aligned} \tag{17}$$

where (for $D=4$)

$$A_E = -\frac{1}{4\pi}\left[-\frac{3}{2}+\sqrt{1+w^2}+\int_0^1 dx\frac{1-x}{\sqrt{1+x^2w^2+x(1-x)w^2\mathbf{k}^2}}\right], \tag{18}$$

$$B_E = \frac{1}{8\pi}\left[\int_0^1 dx\frac{1-2x}{\sqrt{1+x^2w^2+x(1-x)w^2\mathbf{k}^2}}-\frac{1}{2}\int_0^1 dx\frac{(1-x)(1-2x)^2}{(1+x^2w^2+x(1-x)w^2\mathbf{k}^2)^{\frac{3}{2}}}\right].$$

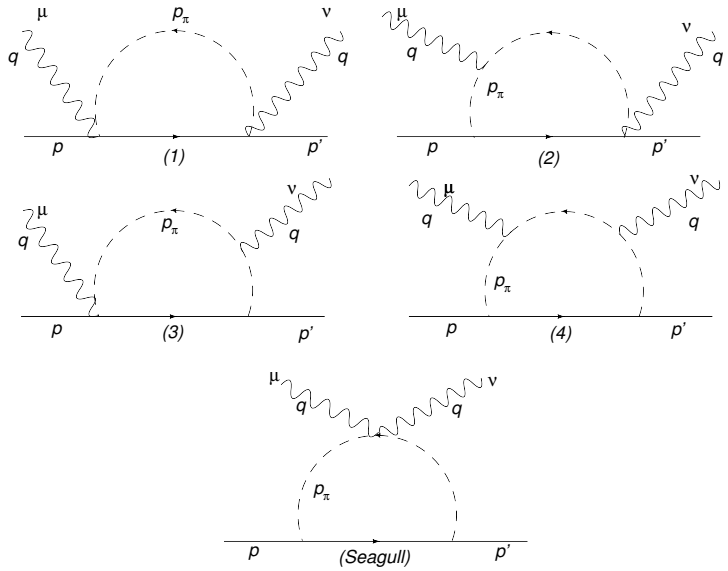

Figure 6: Diagrams contributing to T^{ij}. Crossed diagrams are not explicitly shown but calculated.

This gives the number

$$\Delta E|_{\chi PT}(pions) = 0.018 \text{ meV}\,. \tag{19}$$

We consider a more through chiral study of this object, in particular including the Δ particle, compulsory. The introduction of the Δ particle produced a large effect in the case of the Zemach correction, something similar may happen here. Whereas we can (and should, see Ref. [28] for a recent discussion) further analyze the error associated to the polarizability correction, we would like to emphasize that in order to explain Eq. (2), the corrections to the leading order chiral computation should be a factor 15 larger than the number obtained in Eq. (19).

3.3 Definition of the proton radius

From the effective theory point of view, the proton radius corresponds to an specific combination of the Wilson coefficients of the effective theory. Let us see how this relation appears. One first considers the following matrix element

$$\langle p', s|J^\mu|p, s\rangle = \overline{u}(p')\left[F_1(q^2)\gamma^\mu + iF_2(q^2)\frac{\sigma^{\mu\nu}q_\nu}{2m_p}\right]u(p)\,. \tag{20}$$

We are interested in the low energy limit of the form factors

$$F_i(q^2) = F_i + \frac{q^2}{m_p^2}F_i' + ... \tag{21}$$

or more precisely of the Sachs form factors

$$G_E(q^2) = F_1(q^2) + \frac{q^2}{4m_p^2}F_2(q^2), \qquad G_M(q^2) = F_1(q^2) + F_2(q^2). \tag{22}$$

The proton radius is usually defined as the derivative of the Electric Sachs form factor at zero momentum:

$$r_p^2(\nu) = 6\frac{d}{dq^2}G_{E,p}(q^2)|_{q^2=0} = \frac{3}{4}\frac{1}{m_p^2}\left(c_D^{(p)}(\nu) - 1\right) \tag{23}$$

$$c_D = 1 + 2F_2 + 8F_1' = 1 + 8m_p^2 \left.\frac{dG_{p,E}(q^2)}{d\,q^2}\right|_{q^2=0}, \tag{24}$$

This set of equations allows to visualize the relation between the proton radius and the matching coefficients of the effective theory [4]. They also highlight the problem of defining the proton radius through the derivative of the Electric Sachs form factor at zero momentum, as this object is infrared divergent. Then, what is the definition of the proton radius used to obtain Eq. (1)? It corresponds to subtract the point-like effect of c_D:

$$r_p^2 = \frac{3}{4}\frac{1}{m_p^2}\left(c_D(\nu) - c_{D,point-like}(\nu)\right)$$

where, in the $\overline{\rm MS}$ scheme,

$$c_{D,point-like} = 1 + \frac{\alpha}{\pi}\left(\frac{4}{3}\ln\frac{m_p^2}{\nu^2}\right).$$

4 Conclusions

We have briefly reviewed the theoretical determination of the spin-independent corrections to the Lamb shift that contribute at $\mathcal{O}(m_r\alpha^5)$. We believe that it is important to have a model independent and efficient approach to the problem. Effective Field Theories are suitable for this task. The use of effective theories highlights that the proton radius is a matching coefficient of the effective theory and, in general, an scheme/scale dependent object. In principle, this is not a problem as far as one knows the definition one is using.

The pure QED computation appears to be solid, not to say extremely reliable. Yet it could be interesting to reanalyze some parts of the computation from an effective theory perspective. We also remark that the correction coming from the three-loop static potential has only been computed by one group. On the other hand, the analogous QCD static potential has been obtained by two groups. We believe that with a reasonable amount of effort, such computations may yield cross checks of the QED computation for muonic hydrogen.

For the hadronic corrections there are precise determinations of the effects associated to the Zemach correction, $\langle r^3 \rangle$, using dispersion relations. Chiral perturbation theory provides with a highly non-trivial double check of the magnitude of this correction. The reason is that the chiral computation is power-like chiral enhanced. It actually linearly diverges in the chiral limit. Therefore, the leading order computation in chiral perturbation theory is a pure prediction, with no free parameter. This rules out much larger values of $\langle r^3 \rangle$ than those obtained from experiment, as such values would be in tension with the chiral perturbation theory prediction.

The polarizability correction is the major source of uncertainty. The reason is that dispersion relations alone are not able to fully determine this quantity, suffering from some ambiguity in the parameterization. Therefore, the chiral perturbation theory result may turn out to be crucial here to determine the size of this correction. Again the chiral computation is power-like chiral enhanced and linearly diverges in the chiral limit. Thus, the leading order computation in chiral perturbation theory is a pure prediction, with no free parameter. At present there is room for improvement over the result obtained in Ref. [7] using chiral perturbation theory with dispersion relations. In particular, it does not include the contribution due to the Δ particle, which, in the case of the Zemach term, turned out to be quite important. It will then be very important to compute it to really asses the size of this correction. Obviously any eventual determination from lattice of this quantity would be most welcome.

Acknowledgments

This work was partially supported by the spanish grants FPA2007-60275 and FPA2010-16963, and by the catalan grant SGR2009-00894.

Bibliography

[1] R. Pohl *et al.*, Nature **466** (2010) 213.

[2] P. J. Mohr, B. N. Taylor and D. B. Newell, Rev. Mod. Phys. **80**, 633 (2008) [arXiv:0801.0028 [physics.atom-ph]].

[3] A. Pineda and J. Soto, Nucl. Phys. Proc. Suppl. **64**, 428 (1998) [arXiv:hep-ph/9707481].

[4] A. Pineda, Phys. Rev. C **71**, 065205 (2005) [arXiv:hep-ph/0412142].

[5] A. Pineda and J. Soto, Phys. Rev. D **59**, 016005 (1999) [arXiv:hep-ph/9805424].

[6] A. Pineda, Phys. Rev. C **67**, 025201 (2003) [arXiv:hep-ph/0210210].

[7] D. Nevado and A. Pineda, Phys. Rev. C **77**, 035202 (2008) [arXiv:0712.1294 [hep-ph]].

[8] K. Pachucki, Phys. Rev. **A53**, 2092 (1996).

[9] K. Pachucki, Phys. Rev. **A60**, 3593 (1999).

[10] A. Veitia and K. Pachucki, Phys. Rev. **A69**, 042501 (2004).

[11] E. Borie, arXiv:1103.1772.

[12] U. D. Jentschura, Annals Phys. **326**, 500 (2011) [arXiv:1011.5275 [hep-ph]].

[13] T. Kinoshita and M. Nio, Phys. Rev. Lett. **82**, 3240 (1999) [Erratum-ibid. **103**, 079901 (2009)] [arXiv:hep-ph/9812442].

[14] V. G. Ivanov, E. Y. Korzinin and S. G. Karshenboim, arXiv:0905.4471 [physics.atom-ph].

[15] S. G. Karshenboim, E. Y. Korzinin, V. G. Ivanov and V. A. Shelyuto, JETP Lett. **92**, 8 (2010) [arXiv:1005.4880 [physics.atom-ph]].

[16] C. Anzai, Y. Kiyo and Y. Sumino, Phys. Rev. Lett. **104**, 112003 (2010) [arXiv:0911.4335 [hep-ph]].

[17] A. V. Smirnov, V. A. Smirnov and M. Steinhauser, Phys. Rev. Lett. **104**, 112002 (2010) [arXiv:0911.4742 [hep-ph]].

[18] A. C. Zemach, Phys. Rev. **104**, 1771 (1956).

[19] J. L. Friar and I. Sick, arXiv:nucl-th/0508025.

[20] M. O. Distler, J. C. Bernauer and T. Walcher, Phys. Lett. B **696**, 343 (2011) [arXiv:1011.1861 [nucl-th]].

[21] J. C. Bernauer *et al.* [A1 Collaboration], Phys. Rev. Lett. **105**, 242001 (2010) [arXiv:1007.5076 [nucl-ex]].

[22] J. Arrington, W. Melnitchouk and J. A. Tjon, Phys. Rev. C **76**, 035205 (2007) [arXiv:0707.1861 [nucl-ex]].

[23] A. De Rujula, Phys. Lett. B **693** (2010) 555 [arXiv:1008.3861 [hep-ph]].

[24] E. Borie, arXiv:physics/0410051.

[25] R. Rosenfelder, Phys. Lett. B **463**, 317 (1999) [arXiv:hep-ph/9903352].

[26] R.N. Faustov and A.P. Martynenko, AIP Conf. Proc. **564**, 277 (2001).

[27] C. E. Carlson and M. Vanderhaeghen, arXiv:1101.5965 [hep-ph].

[28] R. J. Hill and G. Paz, arXiv:1103.4617 [hep-ph].

Nucleon Spin Structure and Parton Distribution Functions

Jörg Pretz[1] on behalf of the *COMPASS* Collaboration
Physikalisches Institut
Universität Bonn
D-53115 Bonn, GERMANY

This article gives an overview over recent results on quark and gluon helicity distributions obtained in deep inelastic lepton nucleon scattering and proton proton interactions. Future experimental programs to study the nucleon structure will be discussed as well.

1 Introduction

In the Quark Parton Model, the nucleon is successfully described in terms of parton distribution functions (PDFs). Whereas unpolarized parton distributions like $q(x)$ and $g(x)$ interpreted as number densities of quarks and gluons at a given longitudinal momentum fraction x in the nucleon are relatively well known, distributions involving polarization degrees of freedom are less well known. The most prominent ones, related to the nucleon spin problem, are the helicity distributions $\Delta q(x)$, $\Delta g(x)$ and the transversity distributions $\Delta q_T(x)$.

This paper focuses on the helicity distributions. Effects occurring when considering transverse momenta and transverse polarizations are discussed in the contribution of M. Anselmino [3]. Section 2 gives a short summary of the nucleon spin puzzle and its connection to helicity distributions of quarks and gluons. Section 3 discusses various experimental methods to access the helicity distributions. Recent results are presented in Section 4. Future experimental programs are discussed in Section 5.

2 The nucleon spin puzzle

The spin of the nucleon can be decomposed in helicity ($\Delta\Sigma$ & ΔG) and orbital angular momentum contributions (L_q & L_g) of quarks and gluons

$$\frac{1}{2} = \frac{1}{2}\Delta\Sigma + \Delta G + L_q + L_g \ .$$

[1]jorg.pretz@cern.ch

For a recent discussion on ambiguities in this decomposition see [1]. Whereas the static quark model predicts $\Delta\Sigma = 1$ and zero contribution from ΔG, L_q and L_g, relativistic quark models predict a helicity contribution of quarks, $\Delta\Sigma$ of the order of 60% [2]. Results from polarized deep inelastic scattering indicate a much smaller value: $\Delta\Sigma \approx 25\%$, allowing thus for large contributions of ΔG, L_q and L_g. In recent years mainly the measurement of ΔG was in the focus of research because a large contribution $\Delta G \approx 2-3$ could explain the small value of $\Delta\Sigma$ measured in deep inelastic scattering via the mechanism of axial anomaly [4]. While a contribution of 400 – 600 % (corresponding to $\Delta G = 2-3$) of the gluon helicity to the nucleon spin may sound strange, one should keep in mind that although perturbative QCD is not able to predict ΔG, it can predict its scale dependence. It is given by $\Delta G(\mu)\alpha_s(\mu) = \text{const.}$ in next-to-leading order (NLO) QCD, i.e. with increasing scale μ, ΔG must increase because the strong coupling constant α_s decreases.

The helicity contributions of quarks, $\Delta\Sigma$ can be further decomposed in the contributions of different quark flavors depending on the momentum fraction x carried by the quarks:

$$\Delta\Sigma = \int_0^1 \sum_q \Delta q(x)\mathrm{dx}$$

where the sum runs over all light quark flavors $q = u, d, s, \overline{u}, \overline{d}, \overline{s}$. The helicity distribution is defined as $\Delta q(x) = q^{\uparrow}(x) - q^{\downarrow}(x)$, the unpolarized distributions are given by $q(x) = q^{\uparrow}(x) + q^{\downarrow}(x)$. Similar to the unpolarized quark distributions $q^{\uparrow}(x)(q^{\downarrow}(x))$ are number densities of quarks with spin parallel (anti-parallel) to the nucleon spin.

In a similar way the first moment of the gluon distribution is given by the integral over the gluon helicity distribution

$$\Delta G = \int_0^1 \Delta g(x)\mathrm{d}x\,.$$

As mentioned above, presently we know that $\Delta\Sigma$ is of the order of 25%. Open questions addressed in this article are the distribution of these 25% among the different quark flavors and new results on the gluon helicity distribution $\Delta g(x)$.

3 Accessing the helicity distributions

Helicity distributions can be accessed in deep inelastic scattering and proton-proton scattering. The most simple case of inclusive polarized deep inelastic scattering

$$\vec{\ell} + \vec{N} \to \ell' + X$$

will be discussed in more detail. In all reactions mentioned X stands for unobserved final state particles. A polarized lepton creates a polarized photon. By changing the relative spin orientation of lepton and nucleon the two situations shown in Fig. 1 are obtained. In the

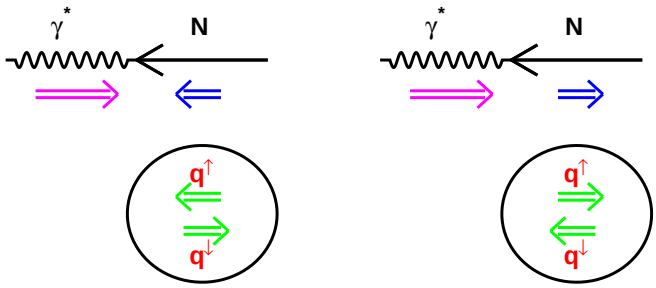

Figure 1: Accessing the helicity distributions in polarized deep inelastic scattering. Double arrows indicate the spin direction.

left diagram photon and nucleon spins are antiparallel. In this case the photon can only be absorbed by a quark having its spin aligned with the nucleon spin ($q^{\uparrow}$). The absorption of the photon by the quark having its spin anti-aligned with the nucleon spin would result in quark with $J_z = 3/2$ in the final state and is thus forbidden. In a similar way, if photon and nucleon spin are aligned (Fig. 1, right) the photon can only be absorbed by a quark having its spin anti-aligned with the nucleon spin ($q^{\downarrow}$).

The photon-nucleon cross section asymmetry denoted by A_1 is thus given by

$$A_1(x) = \frac{\sigma^{\uparrow\downarrow}_{\gamma^* N} - \sigma^{\uparrow\uparrow}_{\gamma^* N}}{\sigma^{\uparrow\downarrow}_{\gamma^* N} + \sigma^{\uparrow\uparrow}_{\gamma^* N}} = \frac{\sum_q e_q^2(\Delta q(x) + \Delta\bar{q}(x))}{\sum_q e_q^2(q(x) + \bar{q}(x))}, \tag{1}$$

e_q being electric charge of the quark $q = u, d, s$.

Selecting specific hadronic final states, h, in semi-inclusive deep inelastic scattering

$$\vec{\ell} + \vec{N} \to \ell' + h + X$$

allows to get more detailed information on the quark helicity distributions. The corresponding photon-nucleon asymmetry reads

$$A_1^h(x,z) = \frac{\sum_q e_q^2 \left(\Delta q(x) D_q^h(z) + \Delta\bar{q}(x) D_{\bar{q}}^h(z)\right)}{\sum_q e_q^2 \left(q(x) D_q^h(z) + \bar{q}(x) D_{\bar{q}}^h(z)\right)}. \tag{2}$$

The fragmentation functions $D_q^h(z)$ describe the probability that a quark q fragments into a hadron h carrying an energy fraction z of the virtual photon energy ν in the target rest frame. Semi-inclusive deep inelastic scattering allows to separate contributions from quarks and anti-quarks because in general the corresponding fragmentation functions differ ($D_q^h \neq D_{\bar{q}}^h$). Moreover, by selecting strange hadrons (K^+ and K^-) one can for example enhance the contribution of the strange quarks.

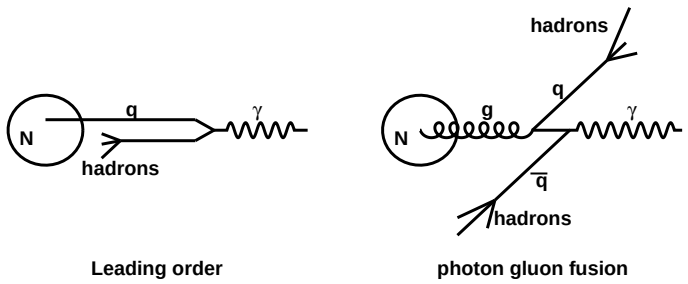

Figure 2: Leading Order (LO) and photon-gluon-fusion (PGF) process in deep inelastic scattering.

Another possibility to measure the quark helicity distributions is polarized pp scattering. Single spin asymmetries of the process

$$\vec{p} + p \to W^{\pm} + \cdots \to e^{\pm} + \ldots$$

give access to quark helicity distributions with the advantage that no knowledge on fragmentation functions is needed. These single spin asymmetries are related to the helicity distributions in the following way

$$A_L^{W^+} = \frac{\Delta\overline{d}(x_1)u(x_2) - \Delta u(x_1)\overline{d}(x_2)}{u(x_1)\overline{d}(x_2) + \overline{d}(x_1)u(x_2)}, \quad A_L^{W^-} = \frac{\Delta\overline{u}(x_1)d(x_2) - \Delta d(x_1)\overline{u}(x_2)}{d(x_1)\overline{u}(x_2) + \overline{u}(x_1)d(x_2)}.$$

Accessing the gluon helicity distribution is more difficult. It can for example be done by a next-to-leading order (NLO) analysis of spin asymmetries where the leading order (LO) expression given in Eqs. (1) and (2) are modified and receive contributions involving $\Delta g(x)$. Another possibility is to look for hadronic final states tagging the participation of gluons in the scattering process. This can be done by selecting for example hadrons with large transverse momentum with respect to the virtual photon axis or charmed mesons. This is illustrated in Fig. 2. In a leading order process where the photon is absorbed by one of the quarks, hadrons are essentially produced along the axis of the virtual photon (Fig. 2 left). If a gluon participates in the partonic sub-process, hadrons can be produced at larger p_T (Fig. 2 right). A particular clean tag of the gluon in the partonic subprocess is the detection of a charmed meson D^0 or D^* in the final state, because these are almost exclusively produced via the process $\gamma + g \to c + \bar{c}$.

In polarized pp scattering double spin asymmetries for various final states gives access to gluon helicity contribution. These asymmetries depend on the product of parton helicity distributions Δq^2, Δg^2 and $\Delta q \times \Delta g$.

4 Results

4.1 Quark Helicity distributions

Figure 3 shows the inclusive asymmetry A_1^p obtained from several experiments in deep inelastic scattering of polarized electrons or muons on polarized protons vs. the Bjorken variable x, which equals in LO the parton momentum fraction, for a momentum transfer $Q^2 > 1\text{GeV}^2$. Note that due to the different center of mass energies data points at a given x may have different values of Q^2.

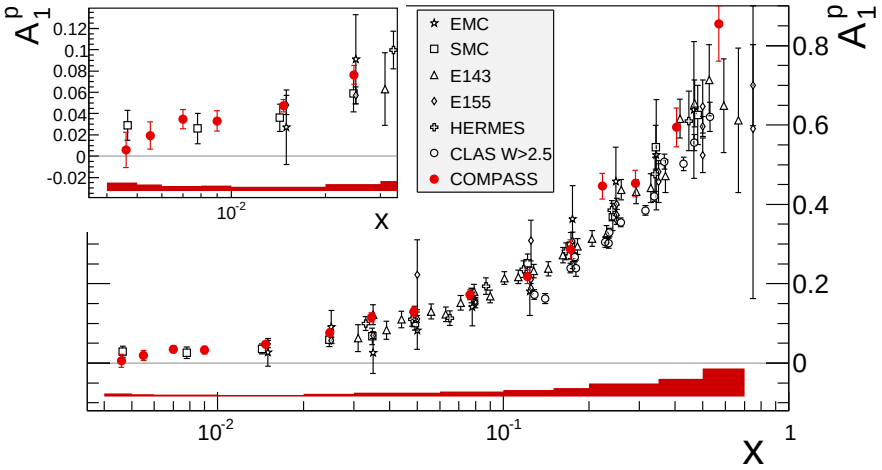

Figure 3: Results for the inclusive asymmetry A_1^p [5].

Using these asymmetries together with the corresponding asymmetries for neutron and deuteron and information from the neutron and hyperon decay constants results in the values for the first moments of the quark distributions given in Table 1. The most right column shows results from Lattice QCD calculations which are in remarkable agreement with the results obtained from experiment.

As discussed in Section 3 inclusive deep inelastic scattering gives only access to the sum quark and anti-quark contributions because $e_q^2 = e_{\bar{q}}^2$, whereas semi-inclusive deep inelastic scattering allows to separate contribution from quarks and anti-quarks. Figure 4 shows semi-inclusive asymmetries measured on a proton target together with the inclusive asymmetry from the COMPASS and HERMES experiment.

From these asymmetries together with asymmetries measured on the deuteron target the quark helicity distributions are determined. The analysis is done in leading order QCD where the measured asymmetries are related to the helicity distribution via the following

Table 1: First moments of the polarized quark distributions at $Q^2 = 10\text{GeV}^2$. Note that the error for the result on the global analysis does not include an uncertainty for the unmeasured region 0<x<0.001.

		global analysis [6]	lattice QCD [8]
$\Delta\Sigma$	=	0.25 ± 0.05	
$\Delta u + \Delta\overline{u}$	=	0.81 ± 0.03	0.82 ± 0.04
$\Delta d + \Delta\overline{d}$	=	-0.46 ± 0.03	-0.41 ± 0.04
$\Delta s + \Delta\overline{s}$	=	-0.11 ± 0.06	

matrix equation:

$$\begin{aligned} \vec{A}(x) &= B\left(q(x), \int D_q^h(z)\mathrm{d}z\right) \Delta\vec{q}(x) \quad \text{with} \\ \vec{A} &= (A_{1,p}, A_{1,p}^{\pi^+}, A_{1,p}^{\pi^-}, A_{1,p}^{K^+}, A_{1,p}^{K^-}, A_{1,d}, A_{1,d}^{\pi^+}, A_{1,d}^{\pi^-}, A_{1,d}^{K^+}, A_{1,d}^{K^-}) \\ \Delta\vec{q} &= (\Delta u, \Delta d, \Delta s, \Delta\overline{u}, \Delta\overline{d}, \Delta\overline{s}) \end{aligned} \tag{3}$$

The matrix B connecting the asymmetries with the helicity distributions depends on the unpolarized quark distributions and the fragmentation functions. Systematic errors originating form the choice of fragmentation functions are discussed in the contribution of N. Makke [9].

Figure 5 shows the results assuming $\Delta s = \Delta\overline{s}$ published in Ref. [10]. Dropping this assumption, no difference was observed between Δs and $\Delta\overline{s}$. It only led to an increase in statistical error for the other helicity distributions. Δu is positive and Δd is negative mainly at large x. The sea quark distributions are all close to zero over the whole measured range $0.004 < x < 0.3$. For the strange quark one finds $\int_{0.004}^{0.3} \Delta s(x)\mathrm{d}x = -0.01 \pm 0.01 \pm 0.01$. The large negative value in Table. 1 comes mainly from the unmeasured low x region and is constrained from the neutron and hyperon decay constants. The truncated first moment $\int_{0.004}^{0.3} \Delta\overline{u}(x) - \Delta\overline{d}(x)\mathrm{d}x = 0.06 \pm 0.04(\text{stat}) \pm 0.02(\text{syst})$ is slightly positive and disfavors models with $\Delta\overline{u}(x) - \Delta\overline{d}(x) < 0$.

First results on single spin asymmetries via the exchange of a $W^\pm$ measured by the PHENIX and STAR collaborations at $\sqrt{s} = 500$ GeV at RHIC/BNL are shown in Fig. 6. The measured asymmetries have the expected sign, as can be seen by comparing them to the curves in the Figure which result from various global analyses. To compete with the results from deep inelastic scattering more data are needed.

4.2 Gluon helicity distribution

Figure 7 (left) shows the result on $\Delta g/g$ from direct measurements from deep inelastic scattering using double spin asymmetries of high p_T hadrons and open charm production.

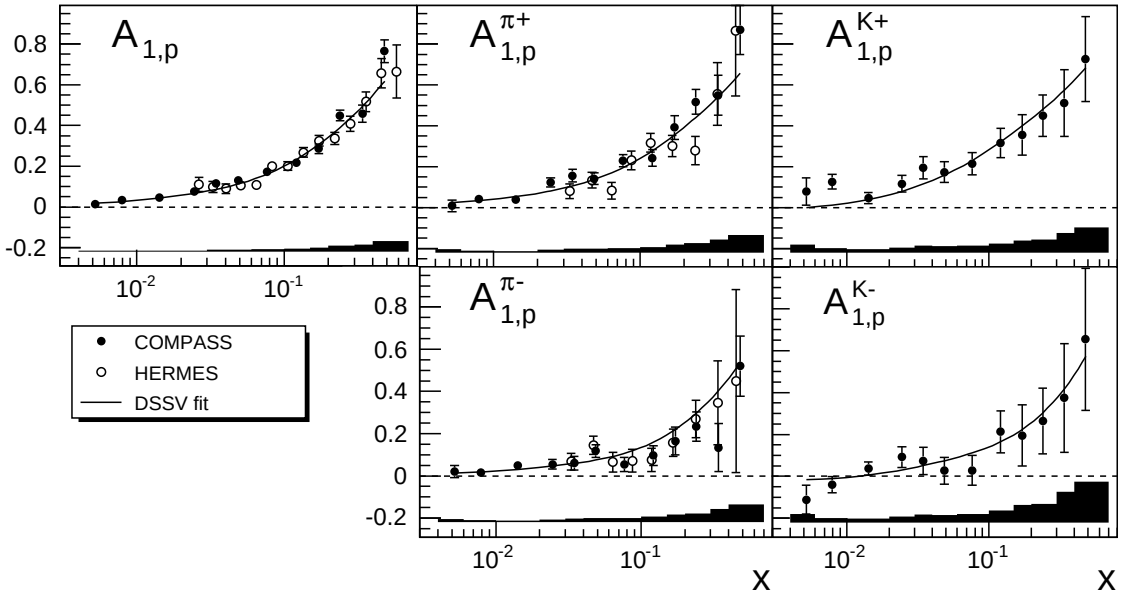

Figure 4: The inclusive and semi-inclusive asymmetry for π^+, π^-, K^+ and K^- for the proton target vs. x from the COMPASS and the HERMES experiment.

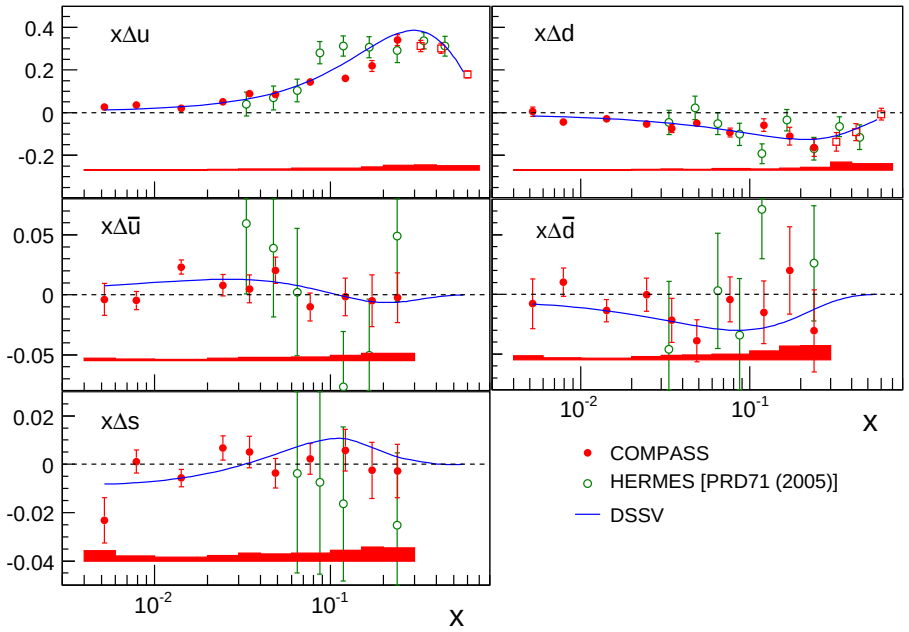

Figure 5: The quark helicity distributions determined from inclusive and semi-inclusive asymmetries.

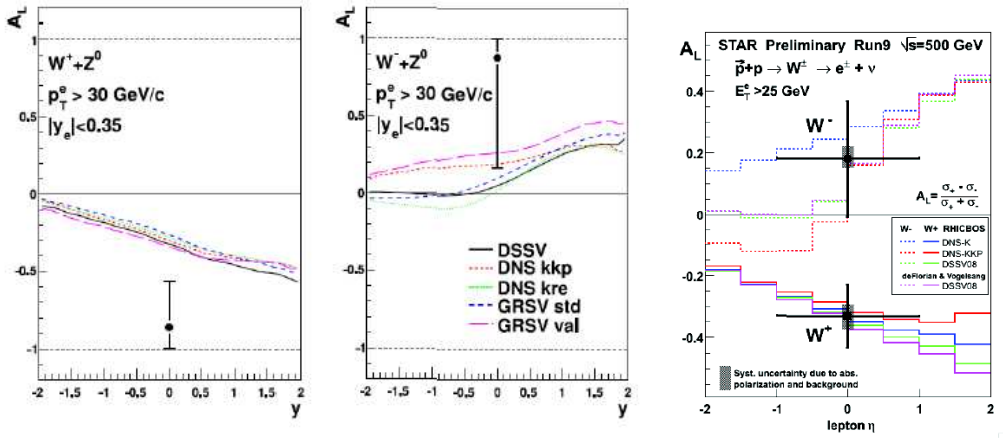

Figure 6: The single spin asymmetry $A_L^{W^+}$ (left) and $A_L^{W^-}$ (right) from the PHENIX [11] experiment and the $A_L^{W^\pm}$ (right) from the STAR [12] experiment as a function of the lepton rapidity compared to results from global analyses of deep inelastic scattering data.

The measured asymmetries are directly related to the polarizations of gluons $\Delta g/g$:

$$A \propto \frac{\Delta g}{g} + A_{\text{bgd}} \,.$$

All results indicate that $\Delta g/g$ is small in the measured region $x_g \approx 0.1$ certainly excluding large values $\Delta G = 2 - 3$. Here the data where analyzed in LO QCD [2]. For the open charm data also a NLO analysis is available. The result is shown in Fig. 7 (right) together with results of various global analyses. Note that the vertical error bars indicate statistical and systematic error, whereas the horizontal error bars indicate the x_g range covered by the data.

Double spin asymmetries in pp scattering from π^0 production (PHENIX) and jet production (STAR) are shown in Fig. 8. Comparing these asymmetries measured as a function of the transverse momentum p_T with parameterizations gives information on $\Delta g(x)$. More results on $\Delta g(x)$ from the pp scattering at the RHIC experiments are discussed in the contribution of E. Aschenauer [7].

Results from a global NLO QCD analysis including inclusive, semi-inclusive asymmetries as well as asymmetries from pp scattering are shown in Fig. 9 [6]. Note that the newest COMPASS semi-inclusive results and most recent RHIC results are not yet included in this analysis, but they will not change the overall picture [14].

The results on $\Delta u + \Delta\overline{u}$ and $\Delta d + \Delta\overline{d}$ are driven by the inclusive asymmetries, whereas the sea quark contributions are mainly determined by the semi-inclusive asymmetries. The

[2] The LO process in this context is the lowest order diagram involving a gluon, thus the PGF-diagram shown in Fig. 2 (right)

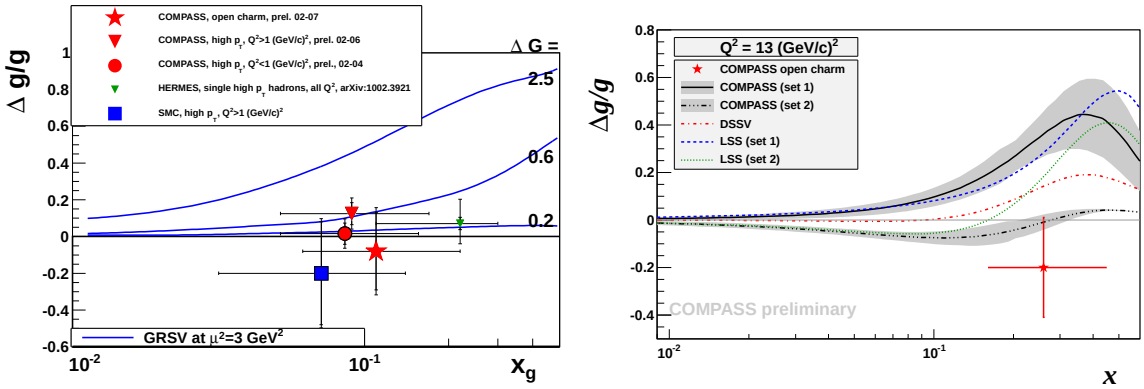

Figure 7: Left: Results from direct measurements of $\Delta g/g$ using a LO QCD analysis. The three blue lines are parameterization corresponding to three different first moments of ΔG.
Right: NLO result from the COMPASS open charm data together with three analyses: COMPASS: global analysis of inclusive asymmetries and the open charm measurement, LSS: global analysis of inclusive and semi-inclusive asymmetries [13], DSSV: global analysis discussed below [6].

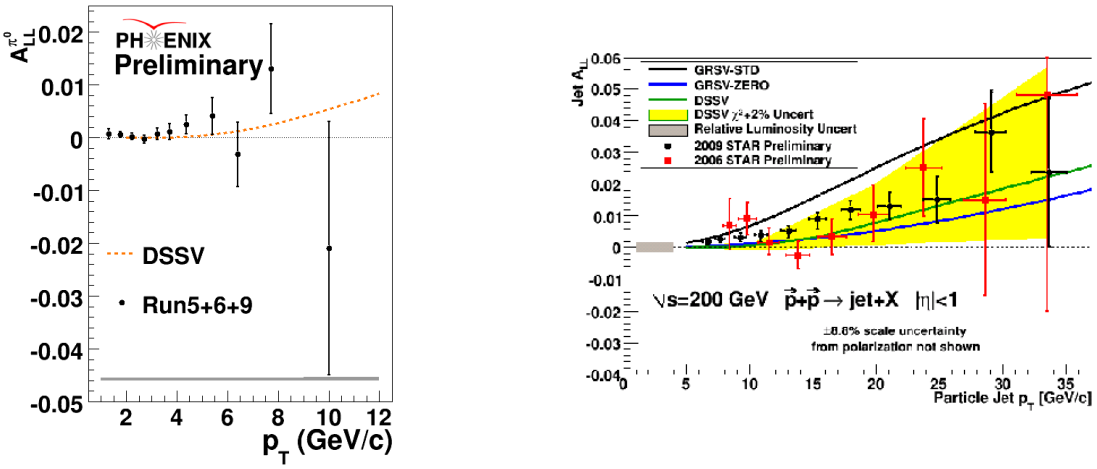

Figure 8: Double spin asymmetries in pp scattering from π^0 production (PHENIX) and jet production (STAR).

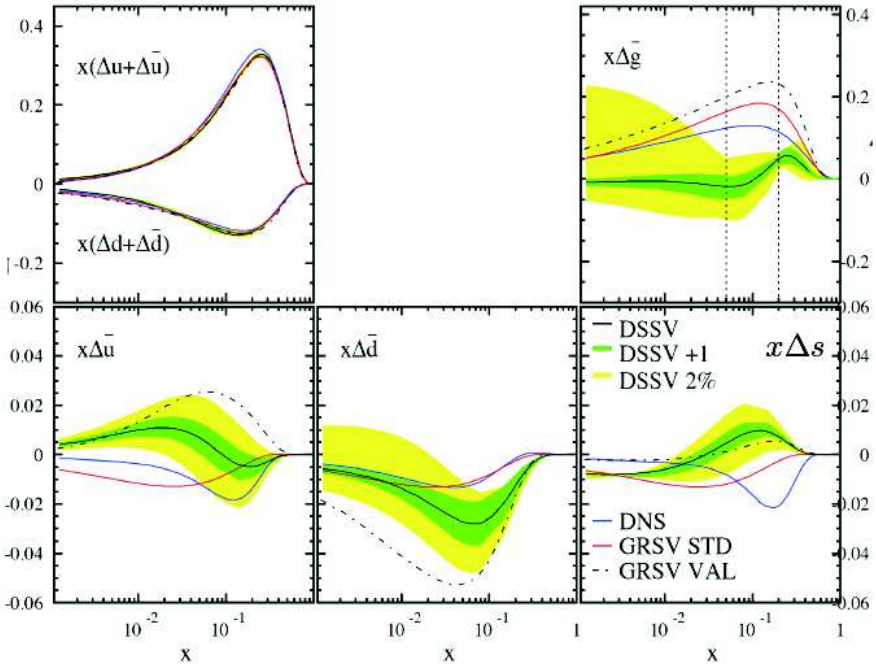

Figure 9: Results on helicity distributions from a global analysis [6].

largest influence on $\Delta g(x)$ comes from the pp data at RHIC. For the truncated first moment one finds

$$\int_{0.001}^{1} \Delta g(x) \mathrm{dx} = 0.013^{+0.702}_{-0.314}\,.$$

Note that the direct measurements from deep inelastic scattering are not yet included in this global analysis because for some channels a NLO QCD description is not yet available. Their inclusion will in the near future further constrain $\Delta g(x)$.

5 Future experimental programs

Table 2 gives an overview over some important parameter of past, present and future experiments in polarized deep inelastic scattering. In the near future experiments at JLAB, CERN, and BNL will continue to take data. Recently a new COMPASS proposal was accepted to study so called Generalized Parton Distributions in Deep Inelastic Virtual Compton Scattering (DVCS) and Hard Exclusive Meson Production (HEMP) as well as Transverse Momentum Dependent distributions (TMDs) in Drell-Yan processes [15, 16]. Similar programs are foreseen at JLAB and BNL.

Table 2 lists also projects for the far future. The electron ion collider (EIC) projects in the US are discussed in the contribution of J. Lee [17]. The project discussed in Europe at GSI, a

Table 2: Parameters of experiments to study deep inelastic scattering.

Experiment	JLab (12 GeV)	HERMES @DESY	ENC @FAIR/GSI	COMPASS @CERN	EIC @BNL/JLab
s/GeV^2	23	50	180	300	10000
$x_{bj,min} = \frac{1\text{GeV}^2}{ys}$ for $y = 0.9$ and $Q^2 > 1\text{GeV}^2$	$5 \cdot 10^{-2}$	$2 \cdot 10^{-2}$	$6 \cdot 10^{-3}$	$4 \cdot 10^{-3}$	10^{-4}
$\mathcal{L}/(1/\text{cm}^2/\text{s})$	$\approx 10^{38}$	$\approx 10^{32}$	$\approx 10^{32-33}$	$\approx 10^{32}$	$\approx 10^{33-34}$
$(P_T P_B f)^2$	0.026	0.16	0.41	0.026	0.24

3 GeV electron beam colliding with a 15 GeV proton beam has a center of mass energy and a luminosity comparable to the one of the running COMPASS experiment. The last line of the table gives the product squared of target, beam polarization and the target dilution factor. This quantity is of particular interest for double polarization experiments. Multiplied with the luminosity it gives an effective luminosity which is proportional to the figure of merit (= inverse squared of the statistical error) of the measured asymmetry. In this quantity one would gain a factor $0.41/0.026 \approx 16$. For the collider a polarization of 80% for both beams is assumed. In addition to this factor a large gain in hadron reconstruction is expected. In the case of a collider one does not suffer from hadron interactions in a solid state target. Such a collider, even at center of mass energies of already running experiments, would thus offer great opportunities for studies of the spin structure of the nucleon.

6 Summary & Outlook

It is well established since several years that the helicity contribution of quarks to the nucleon spin is only about $\Delta\Sigma = 25\%$ in contrast to a value of about 60% expected in relativistic quark models.

New data, mainly from semi-inclusive double spin asymmetries from the COMPASS experiment allowed to determine the contributions of the different quark flavors as a function of the Bjorken variable x to $\Delta\Sigma$. More data will decide whether the difference in the contribution of the light sea quarks $\Delta\overline{u}$ and $\Delta\overline{d}$ is only a statistical deviation. The RHIC experiment published first data on single spin asymmetries giving a direct access to the helicity distributions.

Concerning the gluon helicity distribution, the results indicate that the gluon distribution is small, but it should be kept in mind the error on the first moment is still on the order of 1/2, i.e. the gluon could still account for 100% of the nucleon spin.

New experimental programs at JLAB, CERN and BNL will continue in the near future measurements of the nucleon structure, where the interest will be enlarged to measurements of Generalized Parton Distributions (GPDs) and Transverse Momentum Dependent distributions (TMDs) giving also access to orbital angular momentum contributions. In the far future new facilities, like a polarized electron nucleon collider would offer great potential to study the spin structure of the nucleon at a much deeper level.

Bibliography

[1] E. Leader, Phys. Rev. D **83** (2011) 096012, [arXiv:1101.5956 [hep-ph]]

[2] S. Bass, The spin structure of the proton, World Scientific, 2008

[3] M. Anselmino, these proceedings

[4] R. D. Carlitz, J. C. Collins and A. H. Mueller, Phys. Lett. B **214** (1988) 229

[5] M. G. Alekseev *et al.* [COMPASS Collaboration], Phys. Lett. **B690** (2010) 466-472, [arXiv:1001.4654 [hep-ex]]

[6] D. de Florian, R. Sassot, M. Stratmann and W. Vogelsang, Phys. Rev. D **80** (2009) 034030

[7] E. Aschenauer, these proceedings

[8] J. D. Bratt *et al.* [LHPC Collaboration], Phys. Rev. D **82** (2010) 094502, [arXiv:1001.3620 [hep-lat]]

[9] N. Makke, these proceedings

[10] M. G. Alekseev *et al.* [COMPASS Collaboration], Phys. Lett. B **693** (2010) 227 [arXiv:1007.4061 [hep-ex]]

[11] J. S. Haggerty [PHENIX Collaboration], PoS **ICHEP2010** (2010) 149

[12] J. Balewski, APS meeting April 2010

[13] E. Leader, A. V. Sidorov, D. B. Stamenov, [arXiv:1012.5033 [hep-ph]]

[14] M. Stratmann, DIS 2010, Newport News, USA

[15] E.-M. Kabuß, these proceedings

[16] COMPASS II proposal
`http://wwwcompass.cern.ch/compass/proposal/compass-II_proposal/compass-II_proposal.pdf`

[17] J. Lee, these proceedings

Recent developments in quarkonium and open flavour production calculations

Mathias Butenschön[1]
II. Institut für Theoretische Physik, Universität Hamburg
Luruper Chaussee 149, 22761 Hamburg, Germany

This report reviews recent theory progress in the field of heavy quarkonium and open heavy flavour production calculations.

1 Heavy Quarkonium Production

1.1 Introduction

Heavy quarkonia are bound states of a heavy quark and its antiquark. There are charmonia and bottomonia. According to the factorization theorem of nonrelativistic QCD (NRQCD) [1], the cross section to produce a heavy quarkonium H factorizes according to

$$\sigma(ab \to H + X) = \sum_n \sigma(ab \to c\bar{c}[n] + X)\langle \mathcal{O}^H[n] \rangle, \tag{1}$$

where the $\sigma(ab \to c\bar{c}[n] + X)$ are perturbatively calculated short distance cross sections describing the production of a heavy quark pair (here $c\bar{c}$) in an intermediate Fock state n, which does not have to be color neutral. The $\langle \mathcal{O}^H[n] \rangle$ are nonperturbative long distance matrix elements (LDMEs) extracted from experiment and describing the transition of that intermediate $c\bar{c}$ state into the physical H via soft gluon radiation. NRQCD predicts each of the LDMEs to scale with a definite power of the relative heavy quark velocity $v \ll 1$, which serves as an additional expansion parameter besides α_s: In case of $H = J/\psi$, the leading order contribution in the v expansion stems from $n = {}^3S_1^{[1]}$ and equals the traditional color singlet model (CSM) prediction, while the leading relativistic corrections are made up by the ${}^1S_0^{[8]}$, ${}^3S_1^{[8]}$, and ${}^3P_J^{[8]}$ states. The upper index "8" stands for color octet (CO), and these contributions are usually just called *the* color octet contributions. The CSM alone is theoretically incomplete due to uncancelled infrared divergences in the case of p wave quarkonia. On the other hand, however, the validity of the NRQCD factorization and the universality of the LDMEs are still not proven and subject to dispute. Most of the work reviewed in the following therefore just aims at testing them.

[1] mathias.butenschoen@desy.de

1.2 NLO calculations of color octet contributions

The calculation of next-to-leading order (NLO) corrections to the short distance cross sections of the intermediate CO states, especially to the ${}^3P_J^{[8]}$ states, have proven challenging. But as for unpolarized J/ψ production, up to now they have been calculated for all relevant collision processes. The $2 \to 1$ processes for photo- and hadroproduction have already been calculated in 1998 [2]. Inclusive production in direct two photon collisions followed in 2005 [3], in direct photoproduction [4] and electron-positron scattering neglecting the small ${}^3S_1^{[8]}$ contribution [5] in 2009. The hadroproduction calculations [6] were still missing the ${}^3P_J^{[8]}$ contributions. Full calculations involving all CO states followed in 2010 with two independent works [7, 8]. The missing pieces of single and double resolved two photon scattering, resolved photoproduction and the ${}^3S_1^{[8]}$ contributions of electron-positron scattering were finally presented in 2011 [9].

The two hadroproduction works [7,8] initially stirred some confusion, because the extracted CO LDMEs seem incompatible although the short distance cross sections agree within the expected numerical uncertainties. That difference is mainly due to the fact that in [8] a combined fit to the transverse momentum p_T distributions in H1 HERA photoproduction and CDF Tevatron hadroproduction data was performed, while in [7] a Tevatron-only fit was performed. When fitting to hadroproduction data alone, the fit is unconstrained, so only two linear combinations of the CO LDMEs can be extracted in [7], and the fit results depend strongly on parameters like the lower cut on p_T. But when both groups perform the fit in the same way, meaning doing a three-parameter fit neglecting feed-down contributions like in [8], but fitting only the seven data points from the CDF Tevatron run 2 measurement [10] with $p_T > 7$ GeV like in [7], the fit results do agree within the fit errors. So there is no obvious inconsistency between the two works.

1.3 Global fit of J/ψ CO LDMEs to unpolarized production data

In [9] a global NLO fit of the CO LDMEs to 194 data points of inclusive unpolarized J/ψ production from 10 different experiments has been performed, see figure 1 and table 1. This extends the previous fit [8] mentioned in the last section by including a lot more photoproduction and hadroproduction data and additionally including data from two-photon collisions measured by DELPHI [16] and electron-positron collisions measured by BELLE [13]. The new ingredients do not alter the fit values much, but the fit errors are strongly reduced. The reason is that in order to constrain the fit, input from basically just one photoproduction and one hadroproduction experiment is needed, and that input was already present in [8].

The global fit shows that at NLO all considered processes except perhaps the two-photon collisions can be described well when including the CO contributions. As explained in more detail in [9], the distribution in the inelasticity variable z of photoproduction at HERA

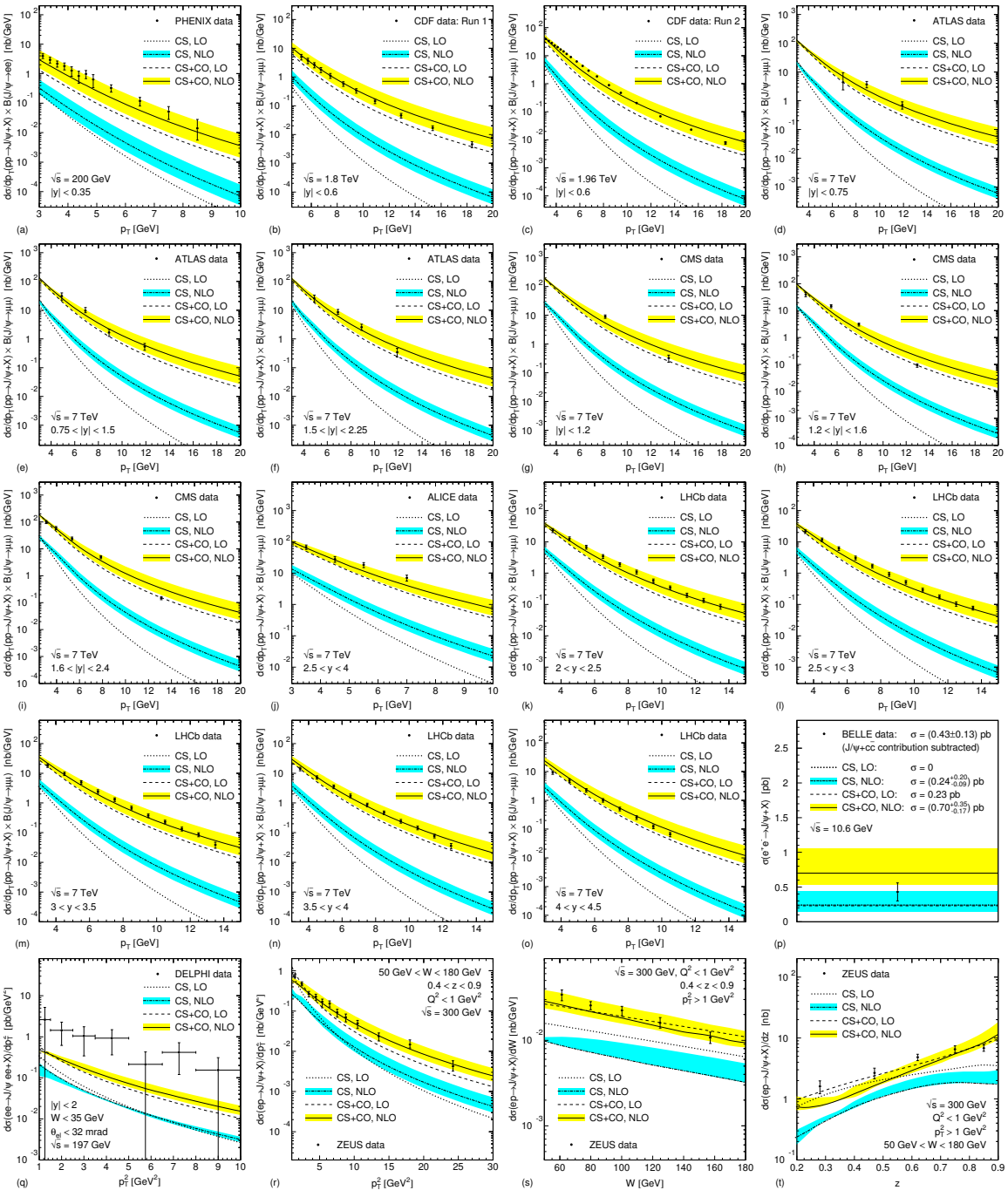

Figure 1: Plots a-t: Results of global fit [9] compared to ALICE [11], ATLAS [12], BELLE [13], CDF [10, 14], CMS [15], DELPHI [16], LHCb [17], PHENIX [18], and ZEUS [19] data. The blue bands are the color singlet model predictions, the yellow bands include the color octet contributions.

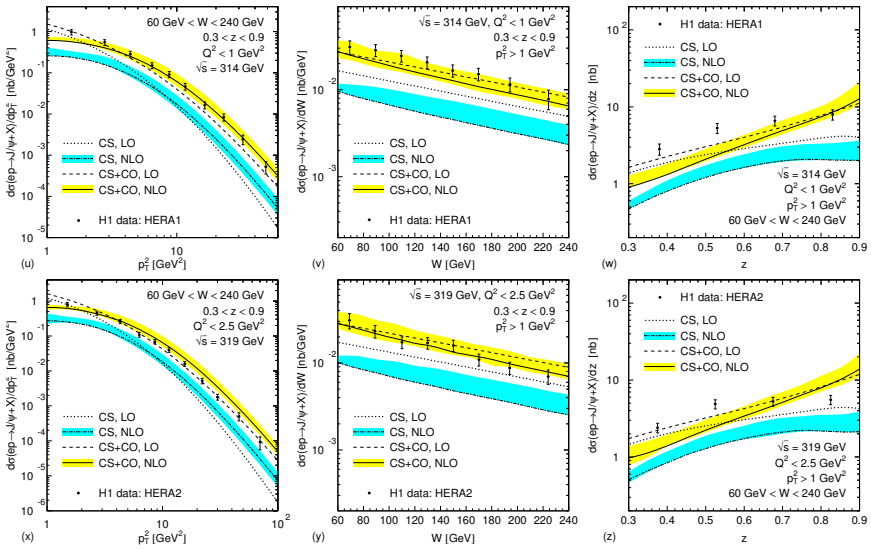

Figure 1: Plots u-z (continuation): Results of global fit [9] compared to H1 [20, 21] data. The blue bands are the color singlet model predictions, the yellow bands include the color octet contributions.

	Set A: Do not mind feed-downs	Set B: Subtract feed-downs first
$\langle \mathcal{O}^{J/\psi}(^1S_0^{[8]}) \rangle$	$(4.97 \pm 0.44) \times 10^{-2}$ GeV^3	$(3.04 \pm 0.35) \times 10^{-2}$ GeV^3
$\langle \mathcal{O}^{J/\psi}(^3S_1^{[8]}) \rangle$	$(2.24 \pm 0.59) \times 10^{-3}$ GeV^3	$(1.68 \pm 0.46) \times 10^{-3}$ GeV^3
$\langle \mathcal{O}^{J/\psi}(^3P_0^{[8]}) \rangle$	$(-1.61 \pm 0.20) \times 10^{-2}$ GeV^5	$(-9.08 \pm 1.61) \times 10^{-3}$ GeV^5

Table 1: Results of global fit [9] for the J/ψ CO LDMEs. Set A corresponds to the main fit shown in figure 1. In set B, estimated feed-down contributions from higher charmonium states were subtracted from the prompt data prior to fitting (hadroproduction: 36%, photoproduction: 15%, $\gamma\gamma$ scattering: 9%, e^+e^- annihilation: 26%).

is now well described even at high z (see figures 1t, w and z), where the older Born analyses predicted a steep rise in the cross section not found in the data. The fact that the DELPHI data overshoots the NRQCD prediction is not worrying since the experimental errors are huge with just 16 events entering the data of figure 1q. The CS contributions alone are on the other hand shown to fall clearly short of the data everywhere except for the BELLE total e^+e^- cross section, see figure 1p.

1.4 Polarization observables

Polarized NLO J/ψ production cross sections have been evaluated within the CSM, for direct photoproduction [22] and hadroproduction [23], and for the $^1S_0^{[8]}$ and $^3S_1^{[8]}$ intermediate states in hadroproduction [6]. Recently, for the first time, polarized NLO cross sections including all CO contributions have been calculated, namely for direct photoproduction

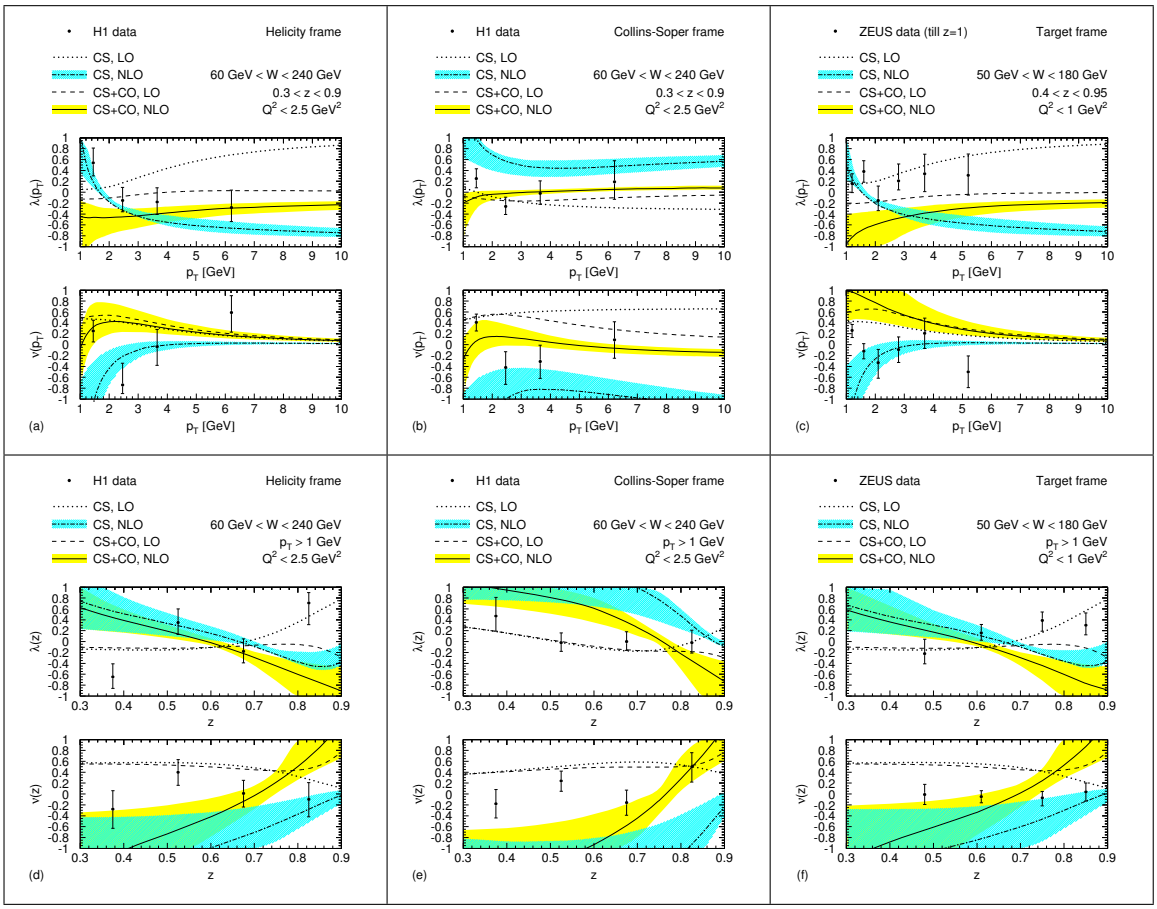

Figure 2: Polarization parameters λ and ν for direct photoproduction at HERA using CO LDME set B of table 1, compared to H1 [21] and ZEUS [25] data. Blue bands: Uncertainties of NLO CS curve due to scale variations. Yellow bands: Uncertainties of NLO CS+CO curve due to scale variations and uncertainties of the CO LDMEs. From [24].

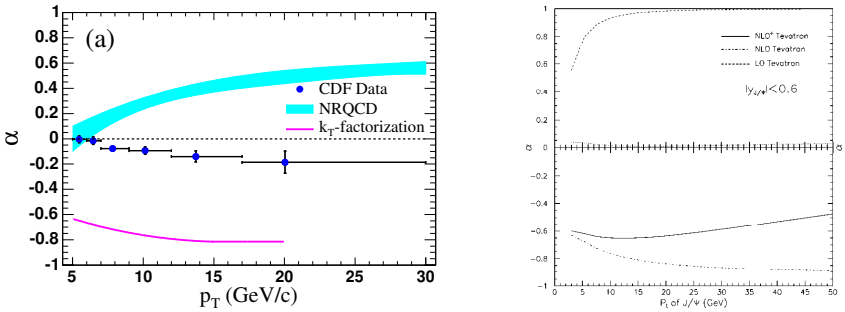

Figure 3: Polarization parameter α in the helicity frame at the Tevatron [27], compared to a LO NRQCD prediction and the CSM k_T factorization prediction [28] (left) and the LO and NLO CSM prediction in collinear factorization [23] (right). From [27] (left) and [23] (right).

at HERA [24]. In figure 2, the predictions for the polarization parameters λ and ν are compared to data. They are defined by the angular momentum distribution of the decay muons via

$$\frac{d\sigma(J/\psi \to \mu^+\mu^-)}{d\cos\theta\, d\phi} \propto 1 + \lambda\cos^2\theta + \mu\sin 2\theta\cos\phi + \frac{\nu}{2}\sin^2\theta\cos 2\phi, \tag{2}$$

where θ and ϕ are the polar and azimuthal angles of the μ^+ in the J/ψ rest frame for specific choices of the coordinate axes. $\lambda = 0$ corresponds to unpolarized J/ψ, whereas $\lambda = +1$ (-1) stands for fully transversely (longitudinally) polarized J/ψ. Unfortunately, the H1 [21] and ZEUS [25] data do not yet allow to distinguish the production mechanisms clearly, but kinematical regions can be identified, in which a distinction could be possible in a future more precise ep collider experiment: At higher p_T, NRQCD predicts the J/ψ to be largely unpolarized in contrast to the CSM predictions. In the z distributions, however, the scale uncertainties are sizeable and the error bands of the CSM and NRQCD largely overlap. The LO calculation corresponding to that NLO analysis has first been performed in [26].

As for hadroproduction at the Tevatron, the CDF [27] measurement shows that the J/ψ's are largely unpolarized, whereas the NLO CSM calculation [23] predicts largely longitudinally polarized J/ψ, see figure 3. The parameter α equals λ in the definition (2). Predictions including all the CO contributions have so far only been made at LO [29].

1.5 Improving the Color Singlet Model: k_T factorization

In heavy quarkonium production, the hard scattering scales are typically much lower than the collision energies, and the tested longitudinal momentum fractions x of the partons inside the protons are so small that the partons' transverse momenta k_T are of the same order as the longitudinal momenta and should hence not be neglected. That is the basic idea behind using the k_T factorization approach [30] in quarkonium production calculations. The initial gluons are therefore off-shell in this formalism. The partonic cross sections, which are so far only evaluated at LO in α_s, are then convoluted with unintegrated, k_T dependent gluon parton distribution functions (PDFs), which are derived from the usual gluon PDFs either in a DGLAP [31], a BFKL [32] or a so called CCFM [33] approach. This derivation of the unintegrated PDFs is certainly the most subtle point here. Usually, only CS contributions are considered. The k_T factorization method gives very good descriptions of the J/ψ photo- and electroproduction at HERA [34, 35], and has also been applied for hadroproduction of J/ψ, χ_c and Y at Tevatron [28, 35, 36] and RHIC [37]. The Monte Carlo program CASCADE [38] also successfully simulates initial gluon radiation within the k_T factorization approach applying the CCFM [33] evolution equation.

1.6 Improving the Color Singlet Model: "NNLO*"

The CSM could describe the hadroproduction data better if the next-to-next-to-leading-order (NNLO) corrections had a large K factor like the NLO corrections. NNLO corrections

consist of three parts: Two-loop contributions, one-loop times tree-level contributions and pure real corrections. Only the sum of the three parts is infrared finite and gives the physical result. Unfortunately, to date only the real corrections are calculated. In [39], a "NNLO*" correction was defined. It consists only of the real corrections, which are made finite by cutting off phase space parts around the singularities in which $k_i \cdot k_j < x_{\text{cut}}$, with k_i and k_j being momenta of external light QCD partons. The "NNLO*" band is computed by shifting this cutoff parameter x_{cut}. This band reminds us that the NNLO cross sections can be expected to have a flatter p_T dependence than the NLO ones, and it is possible that the NNLO corrections may indeed be large and positive, like the "NNLO*" ones.

2 Open heavy flavour production

2.1 Theory frameworks

Heavy flavoured hadrons are hadrons consisting of one heavy quark and one or two light quarks. Examples are the D mesons (charm plus one light quark) and the B mesons (bottom plus one light quark). The production of these particles is described by the fragmentation of outgoing heavy or light QCD partons into the heavy flavoured hadrons. The partonic cross sections are thus folded not only with the PDFs but also with nonperturbative fragmentation functions (FFs), whose exact definition and theoretical interpretation depend on the calculational scheme used. There are two main traditional schemes, which are valid in complementary kinematical regions: The fixed-flavour-number scheme (FFNS), which was also applied in all the heavy quarkonium calculations of section 1, and the zero-mass variable-flavour-number scheme (ZM-VFNS). Let us for simplicity assume charm c as the heavy quark. In the FFNS, we then have only the light quarks u, d, s and gluons as incoming particles, the heavy quark c only appears as a final state particle, and the heavy quark mass m_c is kept finite. Here, we have two kinematical scales: m_c and the typical scale Q, which could be the hadron's transverse momentum. This scheme is valid only at $m_c^2 \lessapprox Q^2$, because at very large Q^2, large logarithms $\log(Q^2/m_c^2)$ spoil the convergence of the perturbative expansion. On the other hand, the ZM-VFNS is the classic parton model. Here, the charm is treated massless like a light quark, and it appears both as an incoming and an outgoing parton. Instead of the quasi-collinear logarithms $\log(Q^2/m_c^2)$, genuinely collinear divergent terms appear, which are factorized into the charm quark PDFs and FFs. Since any m_c dependent terms are missing, the ZM-VFNS is a good approximation only in the limit $m_c^2 \ll Q^2$. Although the FFNS alone can already describe the data well in the currently accessed kinematical regions, one would like to have a combined scheme, which interpolates between the FFNS and the ZM-VFNS, and is by itself valid at all scales Q^2. There are currently two of these interpolating schemes on the market: The general-mass variable-flavour-number scheme (GM-VFNS) [40] and the fixed-order NLL scheme (FONLL) [41].

The GM-VFNS is an extension of the ZM-VFNS in such a way that in Feynman diagrams

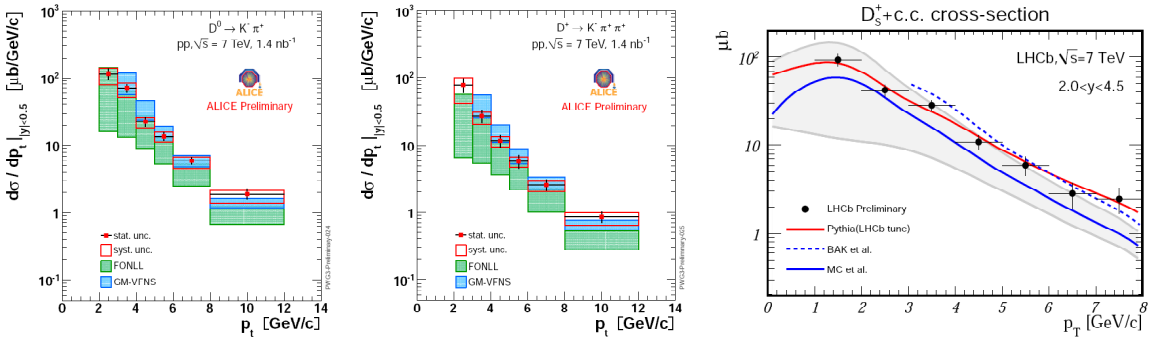

Figure 4: D^0, D^+ and D_s^+ hadroproduction at the LHC. GM-VFNS (BAK et al.) and FONLL (MC et al.) predictions are compared to preliminary data measured by the ALICE [52] and LHCb [53] collaborations. From [52] (left and middle) and [53] (right).

where c appears only as an outgoing parton, we do now consider a nonzero heavy quark mass m_c, while when it does also/only appear as an incoming particle, the heavy quark mass is still kept zero like in the original ZM-VFNS. The bulk of the heavy mass dependence is now taken into account, and the applicability of the ZM-VFNS is lowered down to scales of about a few times the heavy quark mass. The large $\log(Q^2/m_c^2)$ terms now appearing are factorized into the heavy quark PDFs and FFs and resummed using the DGLAP [31] evolution equation according to the QCD factorization theorems, which are proven to hold also in the case of these quasi-collinear logarithms [42].

In the FONLL scheme the predictions of the FFNS and the ZM-VFNS are overlaid by using a $Q = p_T$ dependent weight function, such that the FFNS and ZM-VFNS are recovered in the respective p_T limits. Additionally, the heavy quark FFs contain perturbative pieces at the starting scale $\mu_0 = m_c$, such that the ZM-VFNS result matches the FFNS one at NLO.

2.2 Applications

Predictions at NLO accuracy have been made within the GM-VFNS for $D^{*\pm}$ production in two photon-collisions [43] and photoproduction [44], for hadroproduction of D^0, $D^{*\pm}$, $D^\pm$, $D_s^\pm$ and $\Lambda_c^\pm$ [40,45] and B meson hadroproduction [46]. NLO predictions in the FONLL scheme have been calculated for D meson photoproduction [47], D^0, $D^{*\pm}$, $D^\pm$, $D_s^\pm$ and $\Lambda_c^\pm$ production at the Tevatron [41], B meson production at the Tevatron [48] as well as D and B meson production at RHIC [49]. An important input for all these calculations are the nonperturbative FFs, which are extracted from fits to scaled energy or momentum distributions of heavy flavour production in electron-positron collisions. In the GM-VFNS framework, these have been extracted in [50] and in the FONLL framework in [48,51].

In figure 4 GM-VFNS and FONLL predictions for hadroproduction of D^0, D^+ and D_s^+ mesons are compared to recent preliminary data by ALICE [52] and LHCb [53]. The predictions of both models agree with the data.

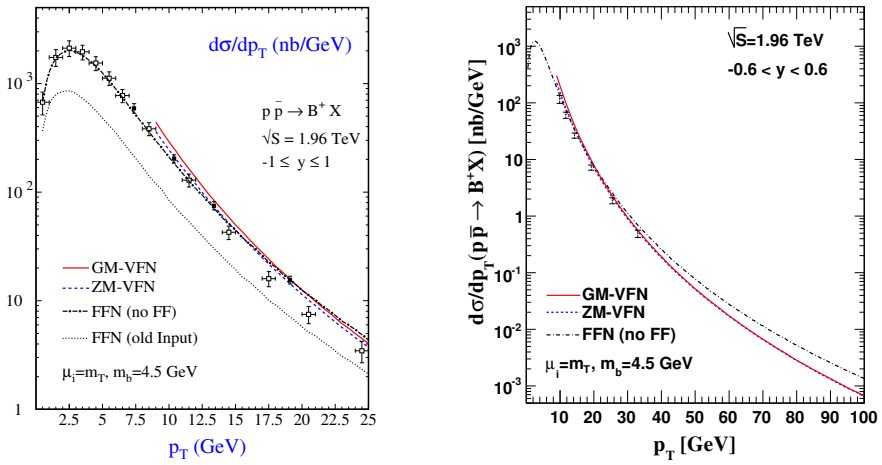

Figure 5: Hadroproduction of B^+ mesons at the Tevatron. FFNS, ZM-VFNS and GM-VFNS predictions are compared to data measured by the CDF collaboration [54]. The "FFN (old input)" line is an older prediction of the FFNS evaluated with outdated input parameters. From [46].

In figure 5 predictions for B^+ hadroproduction at the Tevatron [54] are compared with predictions of the FFNS, ZM-VFNS and GM-VFNS [46]. We see that all three predictions are compatible with the data in their respective regions of applicability. At very high p_T we see the difference between the FFNS on the one hand and the ZM-VFNS and the GM-VFNS on the other hand. At high p_T the latter two agree by construction, while we start to see differences between them at moderate values of p_T.

Acknowledgments

The author would like to thank Bernd Kniehl for collaboration on our common work about J/ψ production and Bernd Kniehl and Gustav Kramer for advice on the part about open heavy flavour production, which is based on the recent review [55].

Bibliography

[1] G. T. Bodwin, E. Braaten and G. P. Lepage, Phys. Rev. D **51**, 1125 (1995) [Erratum-ibid. D **55**, 5853 (1997)].

[2] A. Petrelli, M. Cacciari, M. Greco, F. Maltoni, and M. L. Mangano, Nucl. Phys. B **514**, 245 (1998); F. Maltoni, M. L. Mangano and A. Petrelli, Nucl. Phys. B **519**, 361 (1998).

[3] M. Klasen, B. A. Kniehl, L. N. Mihaila and M. Steinhauser, Phys. Rev. D **71**, 014016 (2005).

[4] M. Butenschoen and B. A. Kniehl, Phys. Rev. Lett. **104**, 072001 (2010).

[5] Y.-J. Zhang, Y.-Q. Ma, K. Wang, and K.-T. Chao, Phys. Rev. D **81**, 034015 (2010).

[6] B. Gong, X. Q. Li and J. X. Wang, Phys. Lett. B **673**, 197 (2009) [Erratum-ibid. **693**, 612 (2010)]; B. Gong, J. X. Wang and H. F. Zhang, Phys. Rev. D **83**, 114021 (2011).

[7] Y.-Q. Ma, K. Wang, and K.-T. Chao, Phys. Rev. Lett. **106**, 042002 (2011).

[8] M. Butenschoen and B. A. Kniehl, Phys. Rev. Lett. **106**, 022003 (2011).

[9] M. Butenschoen and B. A. Kniehl, Phys. Rev. D **84**, 051501(R) (2011) [arXiv:1105.0820 [hep-ph]].

[10] D. Acosta *et al.* [CDF Collaboration], Phys. Rev. D **71**, 032001 (2005).

[11] E. Scomparin for the ALICE collaboration, Nucl. Phys. B (Proc. Suppl.) **214**, 56 (2011).

[12] G. Aad *et al.* [ATLAS Collaboration], ATLAS-CONF-2010-062 (2010).

[13] P. Pakhlov *et al.* [Belle Collaboration], Phys. Rev. D **79**, 071101 (2009).

[14] F. Abe *et al.* [CDF Collaboration], Phys. Rev. Lett. **79**, 572 (1997); F. Abe *et al.* [CDF Collaboration], Phys. Rev. Lett. **79**, 578 (1997).

[15] V. Khachatryan *et al.* [CMS Collaboration], Eur. Phys. J. C **71**, 1575 (2011).

[16] J. Abdallah *et al.* [DELPHI Collaboration], Phys. Lett. B **565**, 76 (2003).

[17] R. Aaij *et al.* [LHCb Collaboration], Eur. Phys. J. C **71**, 1645 (2011).

[18] A. Adare *et al.* [PHENIX Collaboration], Phys. Rev. D **82**, 012001 (2010).

[19] S. Chekanov *et al.* [ZEUS Collaboration], Eur. Phys. J. C **27**, 173 (2003).

[20] C. Adloff *et al.* [H1 Collaboration], Eur. Phys. J. C **25**, 25 (2002).

[21] F. D. Aaron *et al.* [H1 Collaboration], Eur. Phys. J. C **68**, 401 (2010).

[22] P. Artoisenet, J. Campbell, F. Maltoni, and F. Tramontano, Phys. Rev. Lett. **102**, 142001 (2009); C. H. Chang, R. Li, and J. X. Wang, Phys. Rev. D **80**, 034020 (2009).

[23] B. Gong and J. X. Wang, Phys. Rev. Lett. **100**, 232001 (2008); B. Gong and J. X. Wang, Phys. Rev. D **78**, 074011 (2008).

[24] M. Butenschoen and B. A. Kniehl, arXiv:1109.1476 [hep-ph].

[25] S. Chekanov *et al.* [ZEUS Collaboration], JHEP **0912**, 007 (2009).

[26] M. Beneke, M. Krämer and M. Vänttinen, Phys. Rev. D **57**, 4258 (1998).

[27] A. Abulencia *et al.* [CDF Collaboration], Phys. Rev. Lett. **99**, 132001 (2007).

[28] S. P. Baranov, Phys. Rev. D **66**, 114003 (2002).

[29] P. L. Cho and M. B. Wise, Phys. Lett. B **346**, 129 (1995); M. Beneke and M. Krämer, Phys. Rev. D **55**, 5269 (1997); E. Braaten, B. A. Kniehl and J. Lee, Phys. Rev. D **62**, 094005 (2000).

[30] L. V. Gribov, E. M. Levin and M. G. Ryskin, Phys. Rept. **100**, 1 (1983); E. M. Levin and M. G. Ryskin, Phys. Rept. **189**, 267 (1990); S. Catani, M. Ciafaloni and F. Hautmann, Phys. Lett. B **242**, 97 (1990); S. Catani, M. Ciafaloni and F. Hautmann, Nucl. Phys. B **366**, 135 (1991); J. C. Collins and R. K. Ellis, Nucl. Phys. B **360**, 3 (1991).

[31] V. N. Gribov and L. N. Lipatov, Sov. J. Nucl. Phys. **15**, 438 (1972); G. Altarelli and G. Parisi, Nucl. Phys. B **126**, 298 (1977); Y. L. Dokshitzer, Sov. Phys. JETP **46**, 641 (1977).

[32] E. A. Kuraev, L. N. Lipatov and V. S. Fadin, Sov. Phys. JETP **45**, 199 (1977); I. I. Balitsky and L. N. Lipatov, Sov. J. Nucl. Phys. **28**, 822 (1978) [Yad. Fiz. **28**, 1597 (1978)].

[33] M. Ciafaloni, Nucl. Phys. B **296**, 49 (1988); S. Catani, F. Fiorani and G. Marchesini, Phys. Lett. B **234**, 339 (1990); S. Catani, F. Fiorani and G. Marchesini, Nucl. Phys. B **336**, 18 (1990); G. Marchesini, Nucl. Phys. B **445**, 49 (1995).

[34] A. V. Lipatov and N. P. Zotov, Eur. Phys. J. C **27**, 87 (2003); S. P. Baranov and N. P. Zotov, J. Phys. G **29**, 1395 (2003); S. P. Baranov, A. V. Lipatov and N. P. Zotov, Eur. Phys. J. C **71**, 1631 (2011).

[35] B. A. Kniehl, D. V. Vasin and V. A. Saleev, Phys. Rev. D **73**, 074022 (2006).

[36] B. A. Kniehl, V. A. Saleev and D. V. Vasin, Phys. Rev. D **74**, 014024 (2006).

[37] S. P. Baranov and A. Szczurek, Phys. Rev. D **77**, 054016 (2008).

[38] H. Jung and G. P. Salam, Eur. Phys. J. C **19**, 351 (2001); H. Jung, Comput. Phys. Commun. **143**, 100 (2002).

[39] P. Artoisenet, J. M. Campbell, J. P. Lansberg, F. Maltoni and F. Tramontano, Phys. Rev. Lett. **101**, 152001 (2008); J. P. Lansberg, Eur. Phys. J. C **61**, 693 (2009).

[40] B. A. Kniehl, G. Kramer, I. Schienbein and H. Spiesberger, Phys. Rev. D **71**, 014018 (2005); B. A. Kniehl, G. Kramer, I. Schienbein and H. Spiesberger, Eur. Phys. J. C **41**, 199 (2005).

[41] M. Cacciari, M. Greco and P. Nason, JHEP **9805**, 007 (1998).

[42] J. C. Collins, Phys. Rev. D **58**, 094002 (1998).

[43] G. Kramer and H. Spiesberger, Eur. Phys. J. C **22**, 289 (2001); G. Kramer and H. Spiesberger, Eur. Phys. J. C **28**, 495 (2003).

[44] G. Kramer and H. Spiesberger, Eur. Phys. J. C **38**, 309 (2004); B. A. Kniehl, G. Kramer, I. Schienbein and H. Spiesberger, Eur. Phys. J. C **62**, 365 (2009).

[45] B. A. Kniehl, G. Kramer, I. Schienbein and H. Spiesberger, Phys. Rev. Lett. **96**, 012001 (2006); B. A. Kniehl, G. Kramer, I. Schienbein and H. Spiesberger, Phys. Rev. D **79**, 094009 (2009).

[46] B. A. Kniehl, G. Kramer, I. Schienbein and H. Spiesberger, Phys. Rev. D **77**, 014011 (2008).

[47] M. Cacciari, S. Frixione and P. Nason, JHEP **0103**, 006 (2001).

[48] M. Cacciari and P. Nason, Phys. Rev. Lett. **89**, 122003 (2002); M. Cacciari, S. Frixione, M. L. Mangano, P. Nason and G. Ridolfi, JHEP **0407**, 033 (2004).

[49] M. Cacciari, P. Nason and R. Vogt, Phys. Rev. Lett. **95**, 122001 (2005).

[50] J. Binnewies, B. A. Kniehl and G. Kramer, Phys. Rev. D **58**, 014014 (1998); J. Binnewies, B. A. Kniehl and G. Kramer, Phys. Rev. D **58**, 034016 (1998); B. A. Kniehl and G. Kramer, Phys. Rev. D **71**, 094013 (2005); B. A. Kniehl and G. Kramer, Phys. Rev. D **74**, 037502 (2006); T. Kneesch, B. A. Kniehl, G. Kramer and I. Schienbein, Nucl. Phys. B **799**, 34 (2008).

[51] M. Cacciari and P. Nason, JHEP **0309**, 006 (2003); M. Cacciari, P. Nason and C. Oleari, JHEP **0604**, 006 (2006).

[52] A. Dainese, presented at the LHC physics day "Charm and bottom quark production at the LHC", 3 December 2010, CERN.

[53] P. Urquijo for the LHCb collaboration, LHCb-CONF-2010-013 (2010).

[54] T. Aaltonen *et al.* [CDF Collaboration], Phys. Rev. D **79**, 092003 (2009).

[55] G. Kramer, Nucl. Phys. Proc. Suppl. **214**, 123 (2011).

News on hadrons in a hot medium

Mikko Laine[1]
Faculty of Physics, University of Bielefeld, D-33501 Bielefeld, Germany

Some of the modifications that a thermal medium, of the type generated in heavy ion collision experiments at the LHC, may impose on the properties of hadrons, are reviewed. The focus is on hadrons containing at least one heavy quark (charm or bottom or their antiparticles).

1 Introduction

The title that I was given is quite broad, so I chose to interpret it in a particular way. Denoting by T the temperature and by μ the baryonic chemical potential, the part "hot medium" will be taken to indicate the temperature range 50 MeV $\ll T \ll$ 1000 MeV, perhaps reachable in the current generation of heavy ion collision experiments; the medium is also assumed *not* to be "dense", meaning that the chemical potential is small, $|\mu| \ll \pi T$. The most drastic cut concerns "hadrons": in this talk only those which more or less maintain their identity in the temperature range considered are discussed, meaning that at least one heavy quark with a mass $M \gg \pi T$ should be present. The final cut is related to the word "news": I will try to concentrate on recent works from 2010/2011, not tracing literature any further back than to 2004 (with one exception).

With these excuses, the outline is that I will start by reviewing "open c, b", i.e. the fate of D and B mesons in a hot medium. Subsequently recent developments concerning quarkonium physics, or "bound $c\bar{c}, b\bar{b}$", i.e. J/ψ and Y mesons, are discussed. A final short section concerns what I refer to as "thermal $c\bar{c}, b\bar{b}$", standing for quark-antiquark pairs generated from thermal fluctuations. I would like to apologize once more for the exclusion of lighter hadrons, on which many new insights have been reported at this conference and elsewhere and but on which I possess no expertise.

2 Open c, b

Jets forming around energetic single heavy quarks are among the basic events in a hadronic collision, and the gluon-fusion amplitude that is responsible for them, illustrated at leading

[1]laine@physik.uni-bielefeld.de

order as

(1) 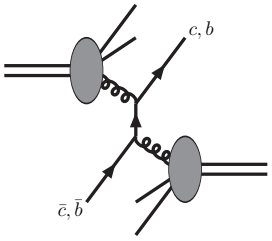

is theoretically relatively well understood [1]. For thermal physics, the interesting question is what happens after the initial production. The idea is that apart from the heavy quarks, a lot of "soft stuff" gets generated as well, which could rapidly reach a state of thermal equilibrium. Then the heavy quarks need to propagate through this "medium" (shown with yellow below), a process that can be sketched as

(2)  .

What is illustrated here is that the heavy quark jets tend to get slowed down and eventually stopped, by bremsstrahlung as well as by elastic scatterings. In the latter case some gluons can be off-shell and soft, and this can lead to large infrared effects from processes like

(3)  .

Therefore we may expect, with some hindsight already folded in, that despite their large inertia the heavy quarks do interact strongly with the medium. In fact, experimentally, charm quark jets get "quenched" practically as effectively as light jets; this is shown in fig. 1, and is among the reasons that the medium generated in heavy ion collisions is nowadays conceived to constitute a "strongly interacting quark-gluon plasma", or sQGP.

It is a challenge for the theoretical finite-temperature community to quantitatively explain, starting from the basic rules of QCD and statistical physics, the experimentally observed strong interactions felt by the heavy quarks. (Although inspiring, AdS/CFT-based studies for analogous theories are not discussed here for lack of space.) Indeed many different lines of research have been pursued in this vain. For instance, a parameter that characterizes the strength of interactions felt by the heavy quarks, called the "momentum diffusion coefficient", has been computed at leading [3] and next-to-leading [4,5] order in the weak-coupling expansion. Given that the weak-coupling expansion shows questionable convergence, various model studies at $T \gg 200$ MeV also appear well-motivated as an intermediate stage [6–8]. In the end, though, it is important to come up with a non-perturbative first-principles formulation within QCD [9,10] and move towards a numerical lattice determination of the quantities in question [11–13]. (For charm this is also being attempted

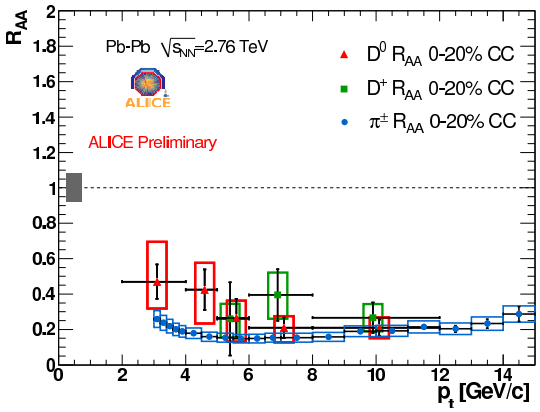

Figure 1: The "nuclear modification factor", R_{AA}, as a function of the transverse momentum, from recent ALICE data [2]. The fact that $R_{AA} < 1$ indicates that jets get quenched, and the data show that D-mesons stop about as effectively as pions despite their much larger inertia. In fact even B-mesons appear to interact strongly with the medium [2].

through a "brute force" approach [14].) Another line is that at low temperatures, $T \ll 200$ MeV, the same physics can be addressed analytically through the use of chiral effective theories or extensions thereof [15–18]. There are also many works in continuous progress, with a basic philosophy that can be traced back to ref. [3], that aim to implement theoretical results of the type mentioned in a combined hydrodynamics and Langevin simulation, in order to obtain results that can be directly compared with experiment.

Let me highlight a couple of these developments in a bit more detail. A perhaps most economical non-perturbative formulation of the problem, valid at least for the bottom case, is to make use of Heavy Quark Effective Theory in order to remove the heavy quark mass scale from the problem, leaving over a purely gluonic correlator [10]:

$$G_E(\tau) \equiv -\frac{1}{3}\sum_{i=1}^{3} \frac{\Big\langle \mathrm{Re\,Tr}\Big[U_{\beta;\tau}\, gE_i(\tau,\mathbf{0})\, U_{\tau;0}\, gE_i(0,\mathbf{0})\Big]\Big\rangle}{\Big\langle \mathrm{Re\,Tr}[U_{\beta;0}]\Big\rangle}\,, \tag{4}$$

where gE_i stands for the (bare) colour-electric field and $U_{\tau_2;\tau_1}$ is a straight timelike Wilson line in Euclidean signature. The "transport coefficient" corresponding to this correlator yields the momentum diffusion coefficient alluded to above, often denoted by κ. In fig. 2 results are shown from the direct next-to-leading order perturbative computation of κ and from a measurement of the correlator defined in eq. (4). It should become clear how large corrections (left) could be pretty much hidden on the Euclidean lattice (right), whose results at first sight follow closely a next-to-leading order prediction. This indicates that a very high resolution is needed in the lattice measurement; therefore no final results are available to date, but the problem appears (relatively) well-posed, and work continues.

As another highlight, consider the hadronic phase, $T \ll 200$ MeV. The momentum diffusion coefficient mentioned above can be related (in the limit $M \gg \pi T$) to the "usual" diffusion

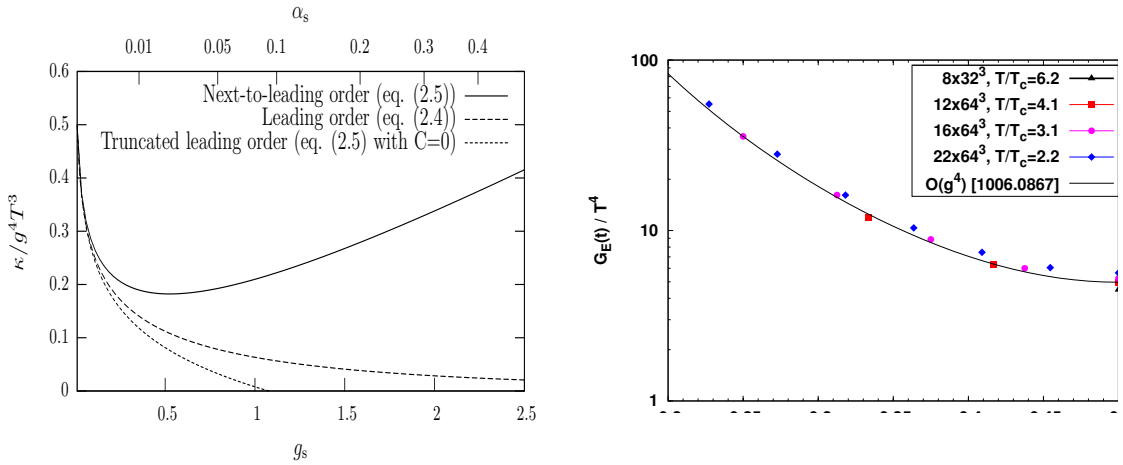

Figure 2: Left: Leading and next-to-leading order results for the heavy-quark momentum diffusion coefficient, κ, as a function of a renormalized gauge coupling (from ref. [5]). Right: Lattice results for the corresponding Euclidean correlator (from ref. [12]), compared with a next-to-leading order determination of the same quantity (from ref. [11]).

coefficient, let us denote it by D, through the Einstein relation, $D = 2T^2/\kappa$. If interactions are strong, then κ is large (cf. fig. 2 left) and therefore D is small. In fig. 3, results are shown from various works, concentrating particularly on the hadronic phase; the results have been obtained by making use of Heavy Meson Chiral Perturbation Theory, hadronic models, or some "intermediate" framework. The main observations are that, first of all, various works differ signficantly from each other so that they probably contain non-negligible systematic uncertainties; but that, second, it seems conceivable that strong interactions are *not* immediately switched off in the hadronic phase. This might play a role in the analysis of heavy ion collision data as well.

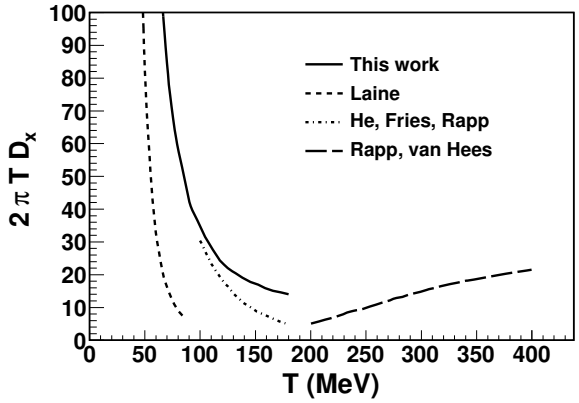

Figure 3: The charm quark diffusion coefficient from ref. [18], with results from refs. [6, 15, 16] also shown for comparison.

3 Bound $c\bar{c}, b\bar{b}$

Although quarkonium physics is in some sense a more traditional and popular probe for quark-gluon plasma formation than the physics related to heavy quark jets discussed in the previous section, it is also clear that this is a more challenging topic, both theoretically and experimentally. The difficulty becomes apparent already by drawing a simple example for an initial hard process in which quarkonium can get generated:

(5) 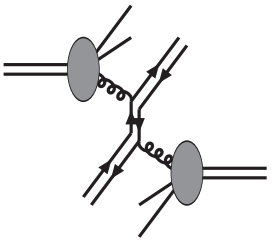 .

Clearly the cross section must be smaller than that in eq. (1), and furthermore the corresponding rate is more difficult to compute reliably. On a more positive note, the final signal is simple, given that quarkonium can decay into a dilepton pair, say $\mu^+\mu^-$, which is easily identified and whose invariant mass can be measured with a relatively good resolution:

(6) 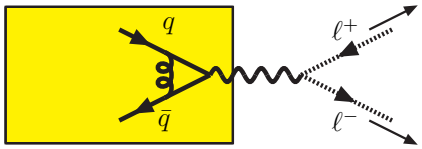

.

Indeed a possible thermal modification of the bottomonium spectral shape, illustrated in fig. 4, is among the most spectacular early results from the LHC heavy ion program.

Apart from experimental news, there has also been some theoretical progress on thermal quarkonium physics in recent years. I would like to imagine that a slight paradigm shift is taking place: whereas it was originally envisaged that quarkonium remains a coherent quantum-mechanical bound state in a thermal medium, with only the potential that binds it together getting modified by Debye screening [23], a process that could perhaps be illustrated as

(7) 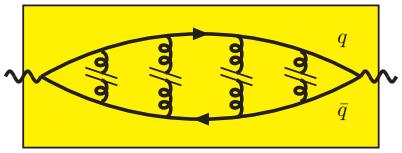

,

a "modern" view is that there might be an additional effect also taking place: coherence may be (partly) lost due to random kicks from a heat bath. Technically, this implies that a suitably defined static potential may develop an imaginary part. The corresponding physics could be thought of for instance in terms of the following diagram, obtained from eq. (7) by

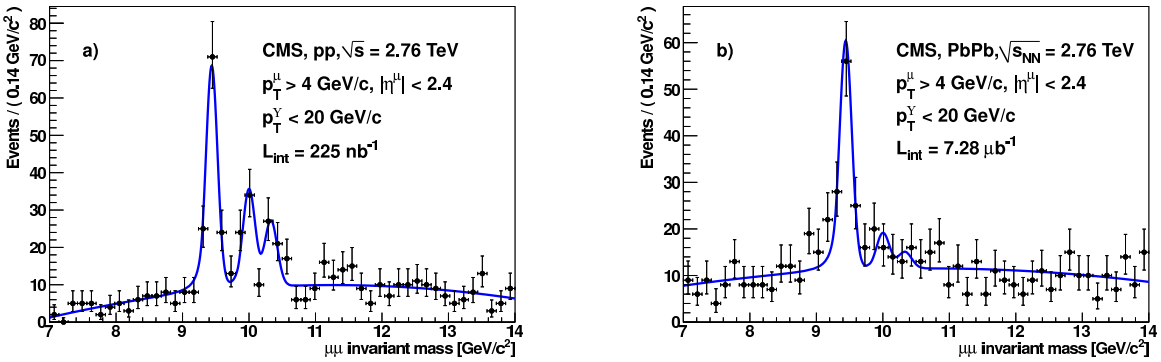

Figure 4: The disappearance of spectral features from bottomonium resonances when going from *pp* to *PbPb* collisions, according to CMS (from ref. [19]). Qualitatively the pattern appears to be in accordance with a classic "sequential suppression" scenario [20] (see also ref. [21]); a quantitative interpretation has been put forward in ref. [22].

twisting two of the gluon lines outwards:

(8) 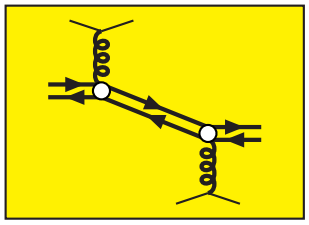 .

The full body of literature concerning quarkonium at high temperatures is too vast to fit in this review, so I restrict to mentioning representative theoretical works that contain elements in this "modern" direction. Various computations resulting in a complex real-time static potential have been reported e.g. in refs. [24–34] (actually many inequivalent definitions of a "static potential" are being used). These results can be given a systematic role at least in the weak-coupling regime where a number of momentum scales can be identified and, if there is a hierarchy between them, a full-fledged effective field theory approach can be formulated (termed "PNRQCD$_{\rm HTL}$" in a particular regime) [35–38]. On the side of applications, at high temperatures where quarkonium "melts" the quantities that can still be defined are the spectral function and the thermal part of the dilepton production rate, $\mathrm{d}N_{\mu^-\mu^+}/\mathrm{d}^4x\,\mathrm{d}^4Q$ [8, 39–45]. On the other hand, if we stay below the melting temperature, which may be phenomenologically relevant particularly for some of the bottomonium resonances (cf. fig. 4), then it is meaningful to speak of the "binding energy" of a bound state as well as of its "width"; these are simpler objects than the complete spectral function, and can be computed in rather explicit form [46], including even their velocity dependence [47] (see also ref. [48]). Ultimately, of course, a lattice investigation is needed [49–52], but even those might preferably be formulated within a non-relativistic effective theory approach [53–55], particularly in the bottomonium case.

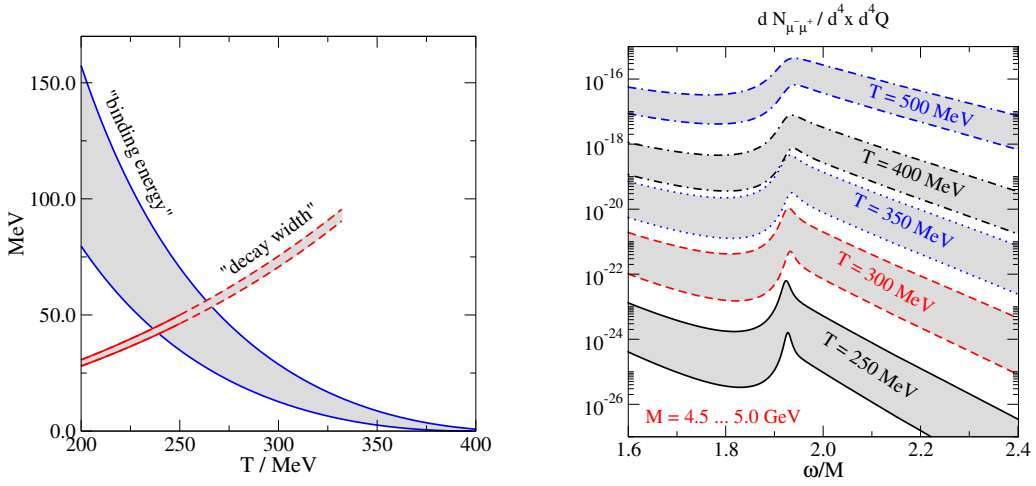

Figure 5: Left: A thermal "decay width" that decoherence due to random kicks from the heat bath could bestow upon a quantum-mechanical bound state (from ref. [24]). Right: A thermal component in the dilepton production rate, with a resonance peak at low temperatures going over into a smooth threshold at high temperatures (from ref. [43]).

Let me again highlight a couple of these developments in a bit more detail. The conceptual change from an "on-off" melting picture towards a gradual evolution of the spectral shape of a quarkonium resonance is illustrated on the qualitative level in fig. 5, for the bottomonium case. More quantitatively, at low temperatures, far below "melting" ($T \ll 250$ MeV in terms of a situation illustrated in fig. 5(left)), the width shows a specific T-dependence [46] and, as mentioned, its velocity-dependence is also computable [47].

As a second highlight, let me mention lattice computations within effective theories. For lattice QCD, a "scale hierarchy" (say, between m_π and m_B) is always a serious challenge, because for a reliable representation of continuum physics the lattice spacing should be shorter than the smallest physical length scale of the system, whereas for an exclusion of finite-volume effects the lattice extent should exceed the largest physical length scale; these complementary requirements easily lead to a prohibitively large number of lattice sites. On the other hand, for effective field theories, the existence of a clear scale hierarchy is a blessing. This suggests the idea of combining the two approaches; indeed a study of the bottomonium system within the so-called NRQCD approach has recently been launched [55] (there are well-known issues related to the existence of a continuum limit but these should be no worse than at zero temperature). Another direction is to directly determine a real-time static potential, perhaps to be used within a "PNRQCD$_{\rm HTL}$"-type framework, through a spectral analysis of an imaginary-time Wilson loop [53, 54], as sketched in fig. 6.

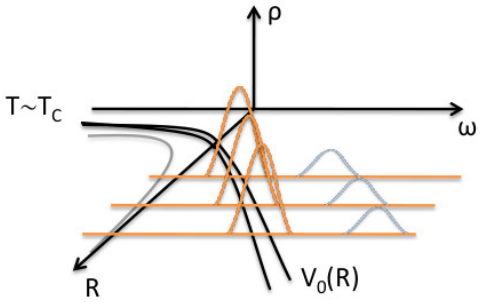

Figure 6: A sketch for how a spectral analysis of an imaginary-time Wilson loop could reveal a real part of a static potential, from the position of a peak, and an imaginary part, from its width (from a talk by A. Rothkopf, illustrating the work reported in refs. [53, 54]).

4 $c\bar{c}, b\bar{b}$ from thermal fluctuations

It is interesting to ask under which conditions heavy quarks or mesons can "chemically equilibrate", i.e. be part of the heat bath with an entropy density determined by T, rather than by some non-thermal initial process such as those illustrated in eqs. (1), (5). Naively, one would think that this is the case only for $T \gg 2M$, so that there is no Boltzmann suppression, $\exp(-\frac{2M}{T})$, hindering the rate of pair creation of a quark-antiquark pair. However, trying to be more quantitative, one may ask e.g. how the heavy quark mass M should be interpreted; say, as an $\overline{\rm MS}$ scheme mass, $M \to m_c^{\overline{\rm MS}}(3\,{\rm GeV}) \approx 1$ GeV; as a more "physical" pole mass, $M \to m_c^{\rm pole} \sim (1.5-2.0)$ GeV; or as something else? Furthermore, the Boltzmann weight comes with a prefactor which might partially compensate for the exponential suppression, and in fact anyone familiar with the "imaginary-time" formalism of thermal field theory would from the outset suggest a comparison of $2M$ with $2\pi T$ rather than T, which is a significant difference. All in all, it seems that the issue is non-trivial.

In any case, sample results from computations of how chemically equilibrated charm quarks would contribute to thermodynamic observables are shown in fig. 7, both from the weak-coupling expansion and from the lattice. It seems that there could be effects visible at surprisingly low temperatures; this might be relevant for the initial stages of hydrodynamics at the LHC, where current phenomenological studies tend to ignore charm quarks altogether. (For another argument in a related direction, see ref. [60].)

5 Conclusions

In heavy ion collisions at the LHC, heavy-quark related observables are becoming increasingly important: the existence of the heavy mass scale makes experimental signals clearly identifiable, and also facilitates theoretical analyses by allowing for the use of modern effective theory methods. That said, much further work is needed for quantitative conclusions.

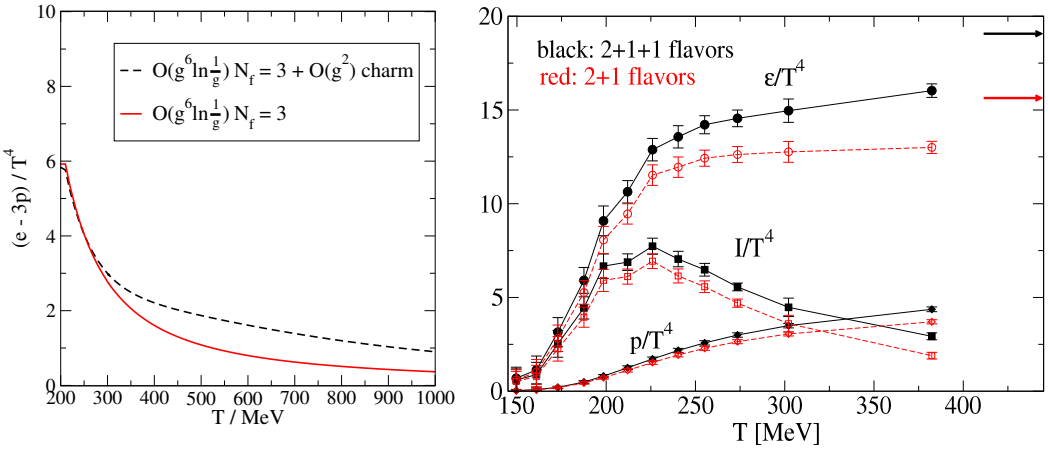

Figure 7: Left: Perturbative results for the "trace anomaly", with and without charm quarks (from ref. [56]). Right: Lattice estimates for the same quantity, denoted here by I (from ref. [57]; see refs. [58, 59] for similar works by other groups).

Acknowledgments

This work was partly supported by the BMBF under project *Heavy Quarks as a Bridge between Heavy Ion Collisions and QCD*.

Bibliography

[1] M. Cacciari, P. Nason and R. Vogt, *QCD predictions for charm and bottom production at RHIC*, Phys. Rev. Lett. 95 (2005) 122001 [hep-ph/0502203].

[2] A. Dainese [ALICE Collaboration], *Heavy-flavour production in Pb-Pb collisions at the LHC, measured with the ALICE detector*, 1106.4042.

[3] G.D. Moore and D. Teaney, *How much do heavy quarks thermalize in a heavy ion collision?*, Phys. Rev. C 71 (2005) 064904 [hep-ph/0412346].

[4] S. Caron-Huot and G.D. Moore, *Heavy quark diffusion in perturbative QCD at next-to-leading order*, Phys. Rev. Lett. 100 (2008) 052301 [0708.4232].

[5] S. Caron-Huot and G.D. Moore, *Heavy quark diffusion in QCD and $\mathcal{N} = 4$ SYM at next-to-leading order*, JHEP 02 (2008) 081 [0801.2173].

[6] H. van Hees, M. Mannarelli, V. Greco and R. Rapp, *Nonperturbative heavy-quark diffusion in the quark-gluon plasma*, Phys. Rev. Lett. 100 (2008) 192301 [0709.2884].

[7] M. Laine *et al*, *Heavy Quark Thermalization in Classical Lattice Gauge Theory: Lessons for Strongly-Coupled QCD*, JHEP 05 (2009) 014 [0902.2856].

[8] F. Riek and R. Rapp, *Quarkonia and Heavy-Quark Relaxation Times in the Quark-Gluon Plasma*, Phys. Rev. C 82 (2010) 035201 [1005.0769].

[9] J. Casalderrey-Solana and D. Teaney, *Heavy quark diffusion in strongly coupled $\mathcal{N} = 4$ Yang-Mills*, Phys. Rev. D 74 (2006) 085012 [hep-ph/0605199].

[10] S. Caron-Huot, M. Laine and G.D. Moore, *A Way to estimate the heavy quark thermalization rate from the lattice*, JHEP 04 (2009) 053 [0901.1195].

[11] Y. Burnier, M. Laine, J. Langelage and L. Mether, *Colour-electric spectral function at next-to-leading order*, JHEP 08 (2010) 094 [1006.0867].

[12] H.B. Meyer, *The errant life of a heavy quark in the quark-gluon plasma*, New J. Phys. 13 (2011) 035008 [1012.0234].

[13] Y. Burnier, M. Laine and L. Mether, *A Test on analytic continuation of thermal imaginary-time data*, Eur. Phys. J. C 71 (2011) 1619 [1101.5534].

[14] H.T. Ding *et al*, *Heavy Quark diffusion from lattice QCD spectral functions*, 1107.0311.

[15] M. Laine, *Heavy flavour kinetic equilibration in the confined phase*, JHEP 04 (2011) 124 [1103.0372].

[16] M. He, R.J. Fries and R. Rapp, *Thermal Relaxation of Charm in Hadronic Matter*, Phys. Lett. B 701 (2011) 445 [1103.6279].

[17] S. Ghosh, S.K. Das, S. Sarkar and J.-e. Alam, *Dragging D mesons by hot hadrons*, Phys. Rev. D 84 (2011) 011503 [1104.0163].

[18] L. Abreu, D. Cabrera, F.J. Llanes-Estrada and J.M. Torres-Rincon, *Charm diffusion in a pion gas implementing unitarity, chiral and heavy quark symmetries*, 1104.3815.

[19] S. Chatrchyan *et al.* [CMS Collaboration], *Suppression of excited* Y *states in PbPb collisions at $\sqrt{s_{NN}}$ = 2.76 TeV*, 1105.4894.

[20] F. Karsch, D. Kharzeev and H. Satz, *Sequential charmonium dissociation*, Phys. Lett. B 637 (2006) 75 [hep-ph/0512239].

[21] N. Borghini and C. Gombeaud, *Dynamical evolution of heavy quarkonia in a deconfined medium*, 1103.2945.

[22] M. Strickland, *Thermal* Y*(1s) and χ_{b1} suppression in $\sqrt{s_{NN}}$=2.76 TeV Pb-Pb collisions at LHC*, 1106.2571.

[23] T. Matsui and H. Satz, *J/ψ Suppression by Quark-Gluon Plasma Formation*, Phys. Lett. B 178 (1986) 416.

[24] M. Laine, O. Philipsen, P. Romatschke and M. Tassler, *Real-time static potential in hot QCD*, JHEP 03 (2007) 054 [hep-ph/0611300].

[25] M. Laine, O. Philipsen and M. Tassler, *Thermal imaginary part of a real-time static potential from classical lattice gauge theory simulations*, JHEP 09 (2007) 066 [0707.2458].

[26] A. Beraudo, J.P. Blaizot and C. Ratti, *Real and imaginary-time $Q\overline{Q}$ correlators in a thermal medium*, Nucl. Phys. A 806 (2008) 312 [0712.4394].

[27] J.L. Albacete, Y.V. Kovchegov and A. Taliotis, *Heavy Quark Potential at Finite Temperature in AdS/CFT Revisited*, Phys. Rev. D 78 (2008) 115007 [0807.4747].

[28] Y. Burnier, M. Laine and M. Vepsäläinen, *Quarkonium dissociation in the presence of a small momentum space anisotropy*, Phys. Lett. B 678 (2009) 86 [0903.3467].

[29] A. Dumitru, Y. Guo and M. Strickland, *The Imaginary part of the static gluon propagator in an anisotropic (viscous) QCD plasma*, Phys. Rev. D 79 (2009) 114003 [0903.4703].

[30] J. Noronha and A. Dumitru, *Thermal Width of the* Υ *at Large 't Hooft Coupling*, Phys. Rev. Lett. 103 (2009) 152304 [0907.3062].

[31] O. Philipsen and M. Tassler, *On Quarkonium in an anisotropic quark gluon plasma*, 0908.1746.

[32] A. Beraudo, J.P. Blaizot, P. Faccioli and G. Garberoglio, *A path integral for heavy-quarks in a hot plasma*, Nucl. Phys. A 846 (2010) 104 [1005.1245].

[33] V. Chandra and V. Ravishankar, *Quarkonia in anisotropic hot QCD medium in a quasi-particle model*, Nucl. Phys. A 848 (2010) 330 [1006.3995].

[34] M. Margotta, K. McCarty, C. McGahan, M. Strickland and D. Yager-Elorriaga, *Quarkonium states in a complex-valued potential*, Phys. Rev. D 83 (2011) 105019 [1101.4651].

[35] M.A. Escobedo and J. Soto, *Non-relativistic bound states at finite temperature: the hydrogen atom*, Phys. Rev. A 78 (2008) 032520 [0804.0691].

[36] N. Brambilla, J. Ghiglieri, A. Vairo and P. Petreczky, *Static quark-antiquark pairs at finite temperature*, Phys. Rev. D 78 (2008) 014017 [0804.0993].

[37] M.A. Escobedo and J. Soto, *Non-relativistic bound states at finite temperature (II): the muonic hydrogen*, Phys. Rev. A 82 (2010) 042506 [1008.0254].

[38] N. Brambilla, M.A. Escobedo, J. Ghiglieri and A. Vairo, *The spin-orbit potential and Poincaré invariance in finite temperature pNRQCD*, JHEP 07 (2011) 096 [1105.4807].

[39] C. Hoyos, K. Landsteiner and S. Montero, *Holographic meson melting*, JHEP 04 (2007) 031 [hep-th/0612169].

[40] M. Laine, *A Resummed perturbative estimate for the quarkonium spectral function in hot QCD*, JHEP 05 (2007) 028 [0704.1720].

[41] Y. Burnier, M. Laine and M. Vepsäläinen, *Heavy quarkonium in any channel in resummed hot QCD*, JHEP 01 (2008) 043 [0711.1743].

[42] M. Laine, *How to compute the thermal quarkonium spectral function from first principles?*, Nucl. Phys. A 820 (2009) 25c [0810.1112].

[43] Y. Burnier, M. Laine and M. Vepsäläinen, *Heavy quark medium polarization at next-to-leading order*, JHEP 02 (2009) 008 [0812.2105].

[44] H.R. Grigoryan, P.M. Hohler and M.A. Stephanov, *Towards the Gravity Dual of Quarkonium in the Strongly Coupled QCD Plasma*, Phys. Rev. D 82 (2010) 026005 [1003.1138].

[45] P. Petreczky, C. Miao and A. Mocsy, *Quarkonium spectral functions with complex potential*, Nucl. Phys. A 855 (2011) 125 [1012.4433].

[46] N. Brambilla *et al*, *Heavy Quarkonium in a weakly-coupled quark-gluon plasma below the melting temperature*, JHEP 09 (2010) 038 [1007.4156].

[47] M.A. Escobedo, M. Mannarelli and J. Soto, *Non-relativistic bound states in a moving thermal bath*, Phys. Rev. D 84 (2011) 016008 [1105.1249].

[48] F. Dominguez and B. Wu, *On dissociation of heavy mesons in a hot quark-gluon plasma*, Nucl. Phys. A 818 (2009) 246 [0811.1058].

[49] A. Jakovac, P. Petreczky, K. Petrov and A. Velytsky, *Quarkonium correlators and spectral functions at zero and finite temperature*, Phys. Rev. D 75 (2007) 014506 [hep-lat/0611017].

[50] G. Aarts, C. Allton, M.B. Oktay, M. Peardon and J.-I. Skullerud, *Charmonium at high temperature in two-flavor QCD*, Phys. Rev. D 76 (2007) 094513 [0705.2198].

[51] H.T. Ding *et al*, *Charmonium correlation and spectral functions at finite temperature*, PoS LATTICE2010 (2010) 180 [1011.0695].

[52] H. Ohno *et al*, *Charmonium spectral functions with the variational method in zero and finite temperature lattice QCD*, 1104.3384.

[53] A. Rothkopf, T. Hatsuda and S. Sasaki, *Proper heavy-quark potential from a spectral decomposition of the thermal Wilson loop*, PoS LAT2009 (2009) 162 [0910.2321].

[54] A. Rothkopf, T. Hatsuda and S. Sasaki, *Complex heavy-quark potential at finite temperature from lattice QCD*, 1108.1579.

[55] G. Aarts *et al*, *Bottomonium above deconfinement in lattice nonrelativistic QCD,* Phys. Rev. Lett. 106 (2011) 061602 [1010.3725].

[56] M. Laine and Y. Schröder, *Quark mass thresholds in QCD thermodynamics,* Phys. Rev. D 73 (2006) 085009 [hep-ph/0603048].

[57] C. DeTar *et al*, *QCD thermodynamics with nonzero chemical potential at $N_t = 6$ and effects from heavy quarks,* Phys. Rev. D 81 (2010) 114504 [1003.5682].

[58] M. Cheng [RBC-Bielefeld Collaboration], *Charm Quarks and the QCD Equation of State,* PoS LAT2007 (2007) 173 [0710.4357].

[59] S. Borsanyi *et al.*, *The QCD equation of state with dynamical quarks,* JHEP 11 (2010) 077 [1007.2580].

[60] G. Torrieri and J. Noronha, *Flavoring the Quark-Gluon Plasma with Charm,* Phys. Lett. B 690 (2010) 477 [1004.0237].

Recent experimental results from the relativistic heavy-ion collisions at LHC and RHIC

Ilya Selyuzhenkov[1]
Research Division and ExtreMe Matter Institute EMMI,
GSI Helmholtzzentrum für Schwerionenforschung
Planckstraße 1 64291 Darmstadt, Germany

A new era has started in the field of relativistic heavy-ion physics with lead beams delivered by the Large Hadron Collider (LHC) in November 2010. In this proceedings I highlight the main results from experimental measurements with Pb–Pb collisions at the incident energy of 2.76 TeV/nucleon recorded by the LHC experiments. Recent experimental developments from the Relativistic Heavy Ion Collider (RHIC) at the GeV incident energy scale are also discussed. All together LHC and RHIC measurements provide new insights on the properties and features of the new hot and dense form of matter created in the course of the relativistic heavy-ion collision.

1 Introduction

The main goal of the more than a ten years of operation of the Relativistic Heavy Ion Collider (RHIC), and of the heavy-ion program recently launch at the Large Hadron Collider (LHC) is to study the properties of the hot and dense matter, the so called quark-gluon plasma (QGP), which is believed to have existed a few microseconds after the big bang. By colliding heavy nuclei at relativistic energies we heat up the normal cold matter and transfer it from the hadronic phase to fireball of deconfined quarks and gluons, which allows us to probe the QGP properties in the laboratory.

Theoretically the time evolution of the system created in the course of heavy-ion collisions is described by a sequence of several stages. It starts from the initial pre-equilibrium state when hard parton scattering occurs and gluonic fields are formed. The next stage is the formation and then expantion of a thermalized state of matter, the quark-gluon plasma, which is conventionally described by hydrodynamics. Consequently, the quarks and gluons are coupled (hadronize) into hadrons, which ends with the phase of chemical and then kinetic freeze out (all interactions are ceased at this moment). The only data which directly accessible for experimentalist is the information on this last hadronic stage. Evidently, it

[1]ilya.selyuzhenkov@gmail.com

is not possible to constrain theoretical models which pretend to describe the evolution of the heavy-ion collision and identify the one which most precisely reflects the nature of the collision with a single measurement, and so it is necessary to study many experimental observables to pin down the properties of the QGP.

In this proceedings I highlight the new results from the ALICE, CMS, and ATLAS Collaborations from the first heavy-ion run at LHC in November 2010, as well as recent experimental developments by the STAR and PHENIX Collaborations at RHIC. I start with a discussion of global properties of the collisions at LHC energies, such as charged hadrons multiplicity, particle yields, and a measurement of the collision freeze out volume from the Bose-Einstein correlations of identical pions. I then briefly review the results for anisotropic flow which reflect collectivity in particles production and allows us to experimentally constrain the possible initial conditions of the collision and the QGP viscosity. Switching to hard probes, I present the main results on the suppression of particle production at high transverse momenta in heavy-ion collision. I continue the discussion with a few highlights from the beam energy scan program at RHIC aimed to probe the properties of the phase boundary and search for the critical point in the QCD phase diagram. I complete my proceedings with a few remarks on probes of local parity violation in the strong interaction which shows the potential to go beyond the scope of the QGP physics with the heavy-ion programs at RHIC and LHC.

2 Particle yields

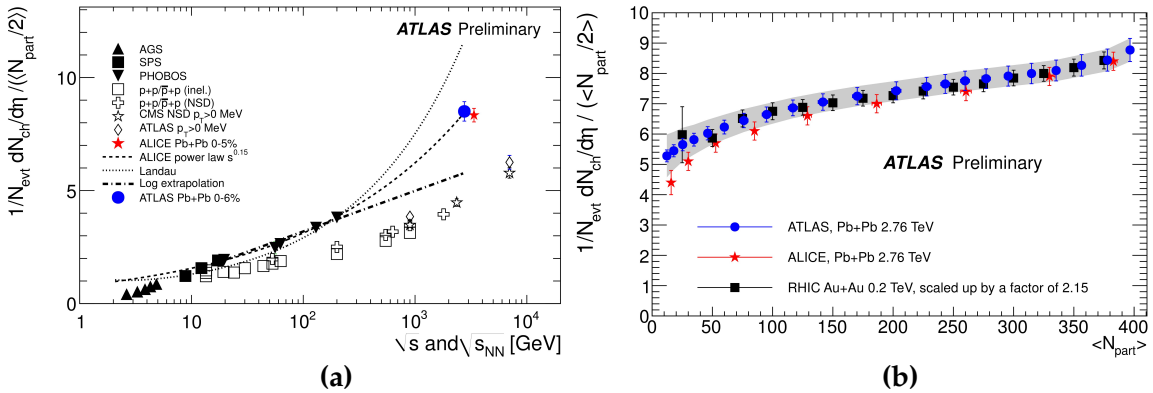

Figure 1: (a) Charged particle multiplicity per participant pair measured for Pb–Pb collisions by the ALICE and ATLAS Collaborations at LHC, and compared to results for proton-proton and heavy-ion collisions at lower energies. (b) Centrality dependence of the multiplicity per participant pair measured by the ALICE and ATLAS Collaborations at the LHC, and the STAR Collaboration at RHIC. Figures taken from [1].

Figure 1(a) shows a compilation of the results for charged particle multiplicity density

measured for heavy-ion collisions at the LHC and lower energies at RHIC, SPS, and AGS, as well as for proton-proton collisions. The charged particle multiplicity density in central Pb–Pb collisions at 2.76 TeV/nucleon is measured to be $\mathrm{d}N_{\mathrm{ch}}/\mathrm{d}\eta \approx 1600$, what is larger by a factor of 2.15 than that at top RHIC energy. Compared to pp collisions at the same energy the charge density is increased by a factor of 1.9. The measured multiplicity and spectra correspond to an increase by 2.5-3 times in energy density from RHIC to LHC, which for central Pb–Pb collisions at LHC is measured to be $dE_t/d\eta \sim 2$ TeV per unit of rapidity [2]. As it can be seen from Fig. 1(b) the shape of the charged particle production per participant pair versus centrality is almost identical for RHIC and LHC energies, what may indicate that saturation effects do not significantly change despite shifting toward smaller Feynman x_f at LHC.

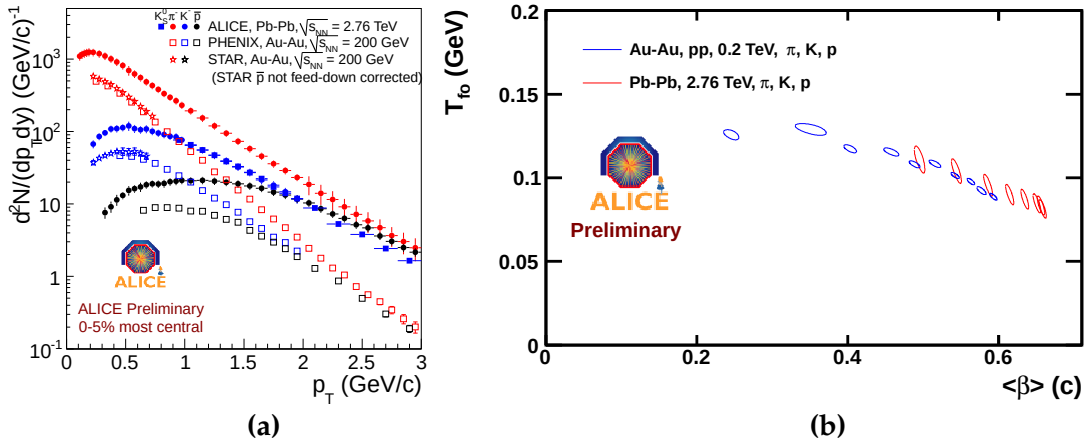

Figure 2: (a) Identified charged particle spectra measured by the ALICE Collaboration for heavy-ion collisions at the LHC in comparison with results for top RHIC energy. (b) Freeze-out temperature, T_{f0}, and radial velocity, $\langle\beta_t\rangle$, extracted from the blast wave fits to the identified charged particle spectra measured at RHIC and LHC. Figures taken from [3].

Figure 2(a) shows the transverse momentum spectra of identified particle measured by the ALICE Collaboration for the 0-5% most central Pb–Pb collisions at 2.76 TeV/nucleon. The spectra slopes change dramatically compared to RHIC data (open symbols in Fig. 2(a)), especially for protons. This reflects a significantly stronger radial flow. The radial flow velocity reaches about 60% of the speed of light with a simultaneous reduction of the kinetic freeze-out temperature down to 80 MeV (Fig. 2(b)).

3 Bose-Einstein correlations

Figure 3 shows the decoupling time and the size of the freeze-out (homogeneity) region of the fireball created in Pb–Pb collisions at LHC and at lower energies. The volume and the

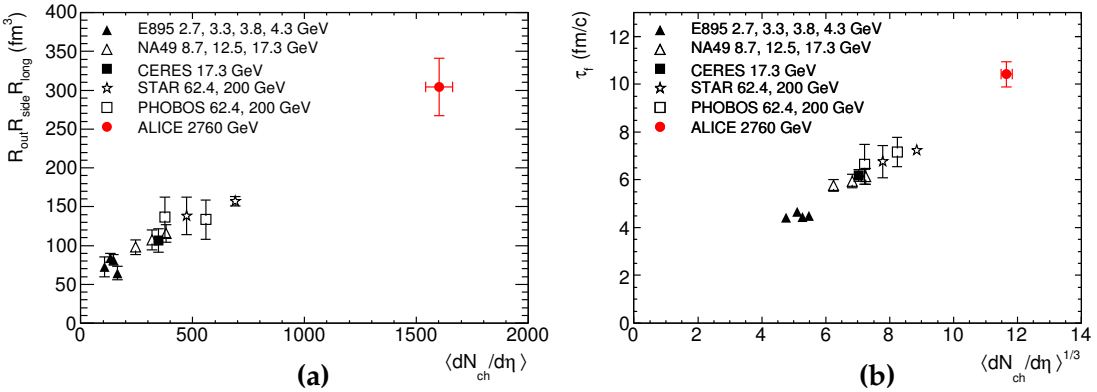

Figure 3: (a) The homogeneity volume (triple product of the pion HBT radii which is proportional to the system volume via $(2\pi)^{\frac{3}{2}}$ coefficient). (b) The decoupling time of the system created in the heavy-ion collision. Results are for Pb–Pb collisions at 2.76 TeV/nucleon measured by the ALICE Collaboration, and for central Au–Au and Pb–Pb collisions for lower AGS and RHIC energies. Figures taken from [4].

system lifetime are deduced from the Hanbury-Brown-Twiss (HBT) momentum-space two-particle correlations of identical pions. The HBT homogeneity region, which is connected to the HBT out- long- and side- radii via $(2\pi)^{\frac{3}{2}} R_{\rm out} R_{\rm side} R_{\rm long}$, increases by a factor 2 (Fig. 3(a)) compared to the top RHIC energy of 0.2 TeV/nucleon pair. The system lifetime also increases by more than 30% (Fig. 3(b)). These trends are consistent with hydrodynamical model calculations for LHC energies using parameters tuned to reproduce the RHIC data.

4 Anisotropic transverse flow

Azimuthal anisotropic flow is a key observable indicating collectivity among particles produced in relativistic heavy-ion collisions. Figure 4 shows the integrated (a) and p_t differential (b) elliptic flow, v_2, measured in Pb–Pb collisions at 2.76 TeV/nucleon. The immediate conclusion to be drawn from the comparison of v_2 results measured at LHC by the ALICE, ATLAS, and CMS Collaborations to that at lower RHIC energies is that the integrated v_2 increases by 30%, see Fig. 4(a). Figure 4(b) shows the differential flow results as a function of charged particle's transverse momentum, $p_{\rm t}$. The results from RHIC and the LHC are similar in both magnitude and the shape of $p_{\rm t}$ dependence. This behavior is a consequence of a stronger radial flow at the LHC as was already discussed in Sec. 2 above. The strong particle collectivity reflected by large v_2 at LHC shows that the system

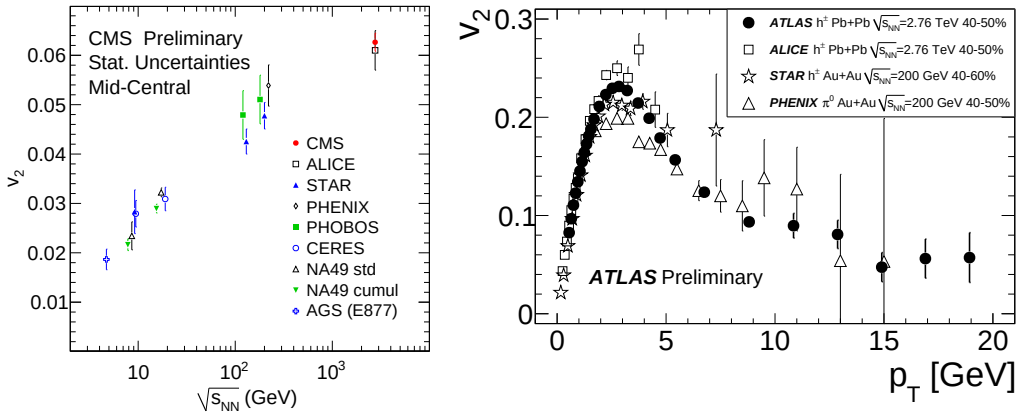

Figure 4: (a) Integrated elliptic flow v_2 as a function of the collisions energy. (b) v_2 as a function of transverse momentum for the 40-50% centrality range measured in heavy-ion collisions at RHIC and LHC. Figure (a) taken from [2], figure (b) from [1].

created in heavy-ion collision at TeV energy scale behaves as a strongly interacting, close to be a perfect fluid - similar to the properties of the QGP observed at RHIC. All this speaks towards applicability of the hydrodynamic model description of the heavy-ion collisions at LHC energies.

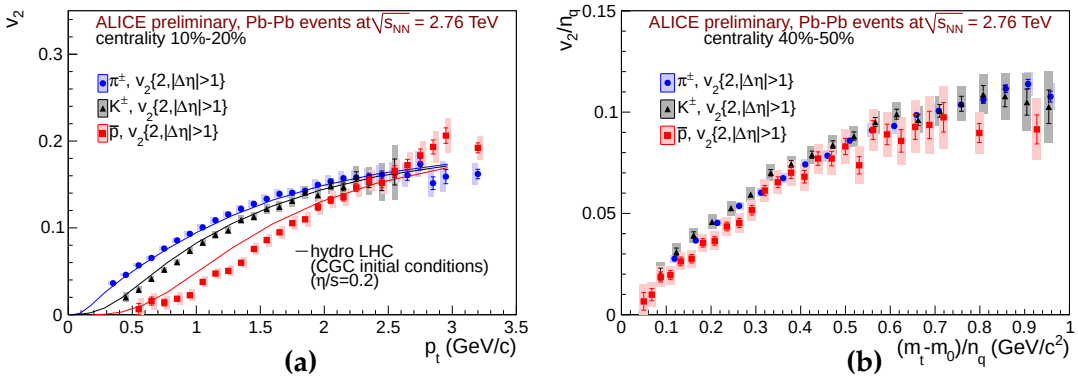

Figure 5: (a) Elliptic flow of pions, kaons and anti-protons vs. transverse momentum for the 10-20% centrality range. The lines are hydrodynamical model calculations. (b) Elliptic flow versus transverse kinetic energy are both scaled with the number of constituent quarks for the 40-50% centrality range. Figures taken from [5].

Qualitatively the validity of the hydrodynamic description for LHC and effects of stronger radial flow can be tested with the anisotropic flow measurement of identified particles and its dependence on the mass of different species. Figure 5 shows the p_t differential elliptic flow of charged pions, kaons, and protons measured by the ALICE Collaboration in Pb–Pb

collisions at 2.76 TeV/nucleon. The observed larger than at RHIC mass splitting of v_2 agrees well with a picture of increased radial flow and follows viscous hydrodynamic predictions (solid lines in Fig. 5(a)) except for anti-protons in the most central collisions. Anti-protons also fall out of the universal scaling with number of quarks seen at RHIC energies.

One of the main highlights of recent anisotropic flow results from both RHIC and LHC experiments is establishing the connection between the measured event anisotropy in the momentum space (anisotropic flow) and the fluctuations of the energy density in the initial state of the heavy-ion collisions.

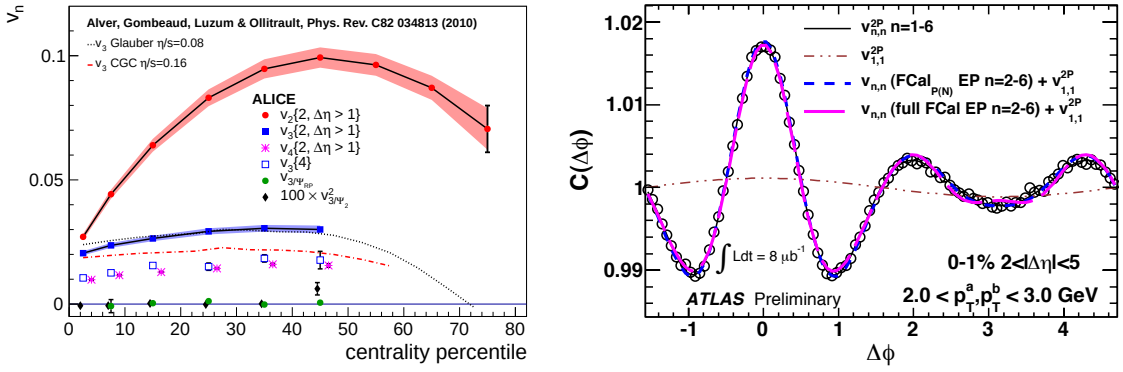

Figure 6: (a) Integrated elliptic (v_2), triangular (v_3), and quadrangular (v_4) flow measured for Pb–Pb collisions at 2.76 TeV/nucleon by the ALICE Collaboration. (b) Two-particle correlation function measured for 1% most central collisions by the ATLAS Collaboration. The measured 2-particle correlations are reproduced well by the combination of the Fourier coefficients from the anisotropic flow measurement (solid lines). Figure (a) taken from [5], figure (b) from [1].

Figure 6(a) shows higher order harmonics of anisotropic flow (v_3, v_4) together with the largest v_2 component for Pb–Pb collisions at 2.76 TeV/nucleon measured by the ALICE Collaboration. The geometrical origin of the v_3 component is established by comparison of the vanishing triangular flow, v_3, when measured with respect to the collision reaction plane (green symbols in Fig. 6(a)), vs. non-zero v_3 measured with respect to the participant plane - the plane determined by the event-by-event fluctuating shape of the initial energy density (blue squares in Fig. 6(a)). Triangular and higher order harmonic flow also explains the double hump structure seen originally at RHIC in the two-particle azimuthal correlations and often referred to as the Mach Cone effect. Figure 6(b) shows that for the most central Pb–Pb collisions at 2.76 TeV/nucleon the whole shape of the two particle azimuthal correlations is driven by the interplay between various anisotropic flow components, mainly v_2 and v_3.

5 Particle production at large transverse momenta

Production of particles with very large transverse momentum, p_t, in heavy-ion collisions happens very early in the collision history and therefore these particles have to propagate through the hot and dense medium created in the collision. Consequently, the modification of high p_t particle production compared to the production without medium (e.g. in proton-proton collisions) carries information about the medium properties such as the energy loss mechanism and its dependence on the path length. Quantitatively the modification of particle production is described by the nuclear modification factor, R_{AA}, which presents the ratio of the particle yields in heavy-ion collision to that of the proton-proton collisions scaled by the corresponding number of binary collisions. Figure 7(a) shows the charged particle

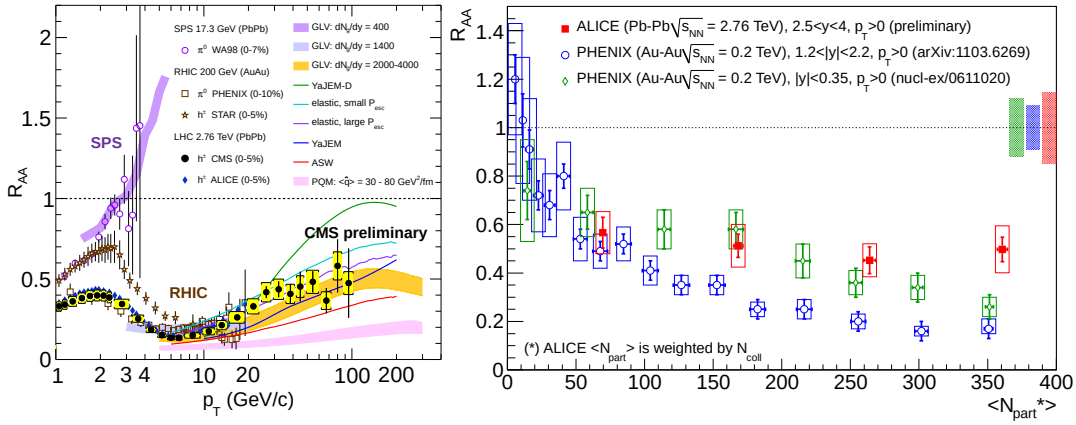

Figure 7: (a) Nuclear modification factor, R_{AA}, as a function of transverse momentum for neutral pions and charged hadrons for the most central heavy-ion collisions. (b) R_{AA} of J/ψ as a function of the number of participants measured at RHIC and LHC. Figure (a) taken from [2], figure (b) from [8].

nuclear modification factor, R_{AA}, for Pb–Pb collisions at 2.76 TeV/nucleon measured by the ALICE and CMS Collaborations compared to results for charged and identified neutral pions from RHIC and SPS experiments. The deviation of R_{AA} from unity reflects the effect of medium modification, and reveals strong suppression ($R_{AA} << 1$) of particle production in heavy-ion collisions compared to that in proton-proton interactions. As a function of transverse momentum, R_{AA} shows a minimum around 5-7 GeV/c, and then rises significantly towards higher transverse momentum but even at $p_t \sim 100$ GeV/c the particle production is largely suppressed ($R_{AA} \sim 0.5$). Compared to different model calculations (color lines in Fig. 7(a)) these new results provide strong constrains on models with different parton energy loss. Figure 7(b) shows that even heavy quark (J/ψ) production is strongly suppressed at RHIC and LHC, though at LHC the suppression is reduced in accord with the expectations from the statistical model [9].

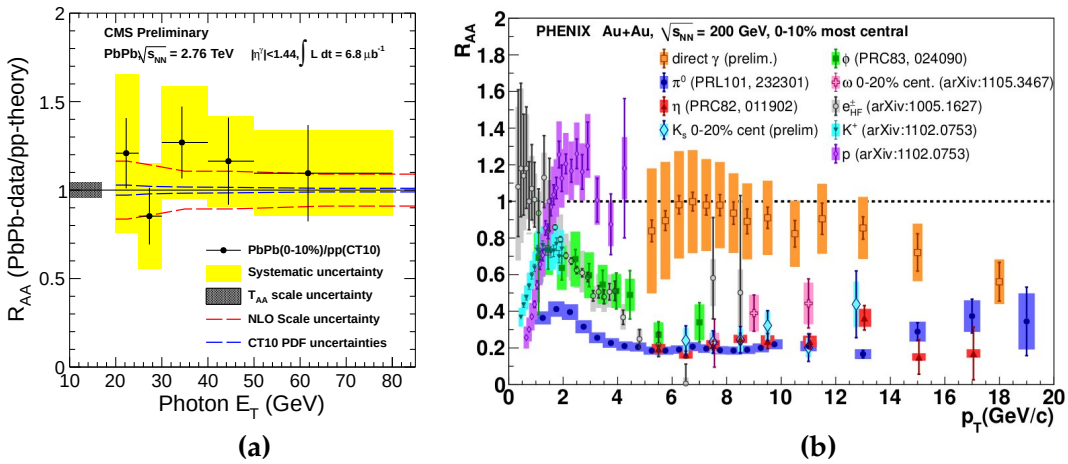

Figure 8: (a) Nuclear modification factor, $R_{\rm AA}$, of isolated photons as a function of transverse momentum for 0-10% central events measured by the CMS Collaboration. (b) Results by the PHENIX Collaboration for $R_{\rm AA}$ of several mesons and direct photons for the 0-10% central Au–Au collisions. Figure (a) taken from [2], figure (b) from [7].

Important probes of the nuclear parton densities created in heavy-ion collision are the colorless objects such as prompt photon and Z boson, since they are produced directly from hard parton interactions and propagate through the medium of quarks and gluons without modification. Figure 8(a) shows the $R_{\rm AA}$ of direct photons as a function of the photon transverse energy for the most central Pb–Pb collisions measured by the CMS Collaboration. Photon R_{AA} measured at LHC is consistent with unity (no modification), which is similar to the recent results for prompt photons by the PHENIX Collaboration (orange points in Fig. 8(b)). The $R_{\rm AA}$ of another colorless probe, the Z boson, is also measured by the CMS Collaboration and found to be consistent with no medium modification: $R^{(Z)}_{\rm AA} = 1.2 \pm 0.29({\rm stat.}) \pm 0.16({\rm syst.})$ [10].

6 RHIC beam energy scan and the search for the critical point

Another frontier of the heavy-ion physics program, which complements the study of the QGP properties at RHIC and LHC, is to determine the nature of the phase transition between confined (hadrons) and deconfined (quark-gluon plasma) matter with a search for the critical point on the QCD phase diagram. These two objectives are the main goals of the Beam Energy Scan program at the RHIC facility. The features of the phase transition and proximity of the critical point can be studied by looking at irregular changes in the degrees of freedom of the system created in heavy-ion collisions. Experimentally this should be reflected in non-monotonic behavior of the sensitive physics observables. Examples of sensitive observables are particle collectivity such as anisotropic flow or HBT correlations,

or fluctuations in the system (e.g. fluctuations of the conserved quantities such as baryon number or strangeness).

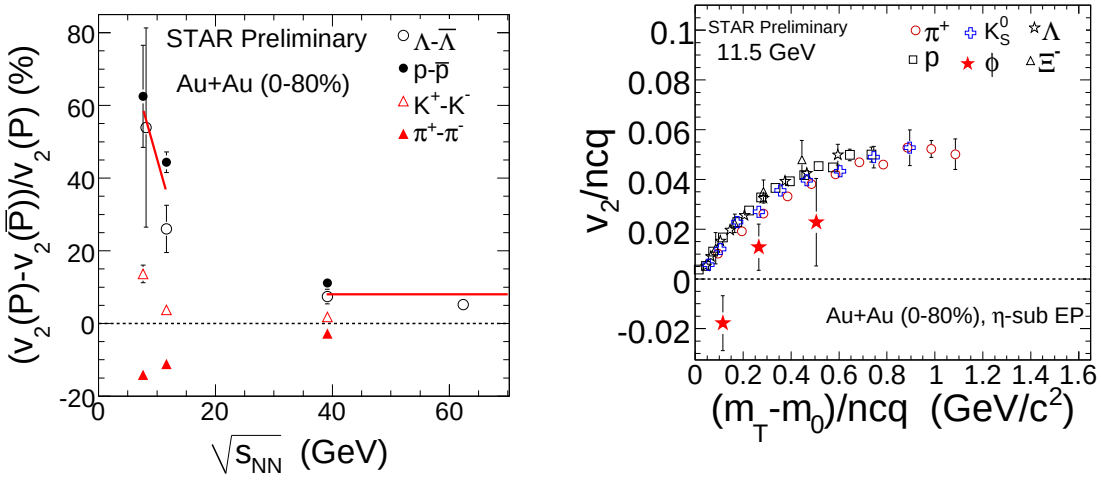

(a) **(b)**

Figure 9: (a) Fractional difference between elliptic flow of particles and anti-particles for 0-80% Au–Au collisions plotted vs. collision energy. (b) Elliptic flow of identified particles for Au–Au collisions at 11.5 GeV/nucleon versus transverse kinetic energy both scaled by the number of constituent quarks. Figures taken from [11].

Figure 9(a) shows the relative variation in the identified particle and anti-particle elliptic flow measured by the STAR Collaboration for different collision energies ranging from 11.5 GeV/nucleon up to the top RHIC energy of 200 GeV/nucleon. With decreasing collision energy the baryon and anti-baryon elliptic flow difference increases dramatically compared to that for mesons. Another change in the elliptic flow patter at lower energies is the breaking of the constituent quark scaling for the elliptic flow which seems to hold at top RHIC energy. Figure 9(b) shows number of constituent quark scaled elliptic flow of identified particles for Au–Au collisions at 11.5 GeV/nucleon. Despite the large statistical errors, results for the ϕ-meson (which carries the information about the strange quark production) deviates significantly from the overall scaling of other particles, which probably indicate the breaking of the quark collectivity at lower energies and change in the degrees of freedom in the system.

Figure 10(a) shows results for the higher order moments (the skewness, S, and kurtosis, κ) of the net proton number. Small deviation of the conserved quantity, the baryon number, from the Hadron Gas Resonance (HGR) model below 39 GeV/nucleon may suggest a hint of proximity to the critical point. Figure 10(b) shows the charged particle R_{AA} down to

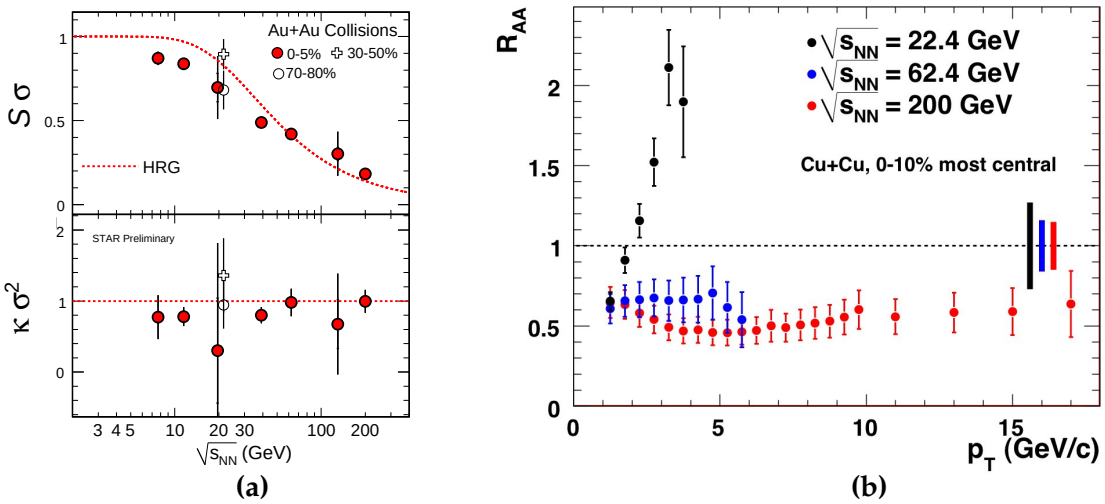

Figure 10: (a) Higher order moments of the net proton number vs. collision energy. (b) The nuclear modification factor of neutral pions as a function of transverse momentum for Cu–Cu collisions at three different energies. Figure (a) taken from [11] and figure (b) taken from [12].

an energy of 22.4 GeV/nucleon and it illustrates the significant change in pattern of the particle suppression at lower energy compare to the top RHIC energy. Overall, there are some hints from the Beam Energy Scan program at RHIC on the possible critical point between energies of 7 and 20 GeV/nucleon. Hopefully the upcoming measurements from RHIC energy scan will allow us to make a conclusive statement about existence of the QCD critical point.

7 Probes of local parity violation in strong interactions

The strong magnetic field created in the interaction zone of non-central relativistic heavy-ion collisions may interact with the topologically non-trivial gluonic field configurations of QCD such as instantons and sphalerons. It is predicted [13] that experimentally this may lead to charge separation of hadrons produced in the collision along the magnetic field, which itself is aligned perpendicular to the reaction plane of the collision. Since instanton and sphaleron configurations breaks the parity symmetry of QCD, the measurement of charge separation provides a unique experimental test of how well the parity symmetry is preserved by the strong interaction [14].

Experimentally the effects of charge separation can be quantified by the charge dependent azimuthal correlations with respect to the reaction plane. Figure 11 shows the experimental results for the $\langle \cos(\phi_\alpha + \phi_\beta - 2\Psi_{RP}) \rangle$ correlator, which is the parity even observable but

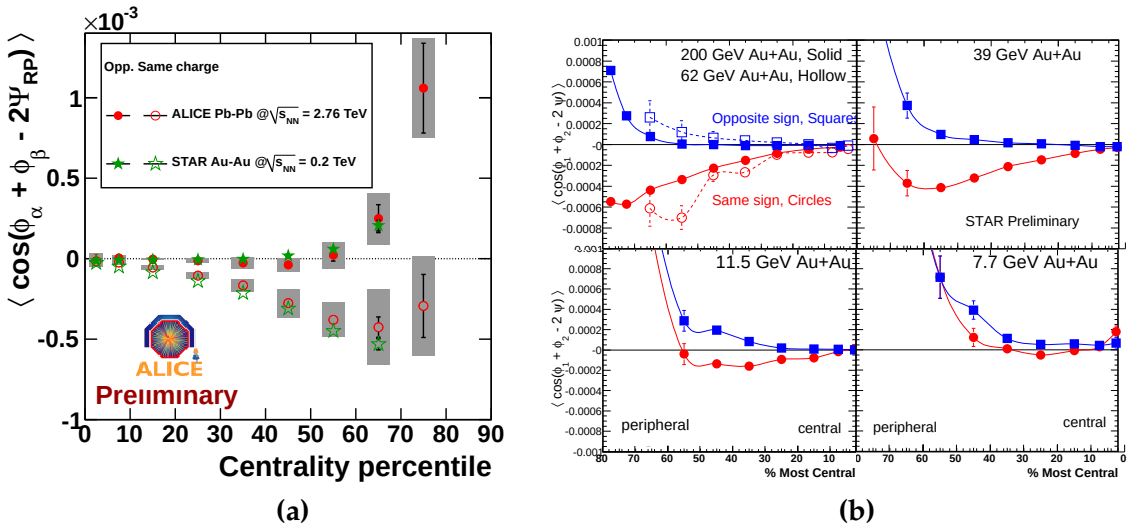

(a) (b)

Figure 11: Charged dependent azimuthal correlations with respect to the reaction plane of heavy-ion collision vs. centrality: (a) comparison between results for Pb–Pb collisions at 2.76 TeV/nucleon vs. the measurement for Au–Au at 200 GeV/nucleon, (b) results for Au–Au collisions for 5 different collision energies in the range of 7.7 - 200 GeV/nucleon. Note the inverted centrality scale in figures (a) and (b). Figure (a) taken from [15] and figure (b) from [11].

directly sensitive to the event-by-event charge fluctuations, and thus to the possible local parity violation in strong interactions. The STAR and PHENIX Experiments at RHIC, and now the ALICE Collaboration at LHC [15] observe a significant charge separation at higher collision energies (Fig. 11(a)), which seems to disappears between 11.5 and 7.7 GeV energies (lower panel in Fig. 11(a)). The experimental situation is significantly complicated by the presence of the parity conserving background correlations which may contribute to the measured charge dependent azimuthal correlations at RHIC and LHC. Recent progress in understanding the possible parity even backgrounds, such as identifying the large flow fluctuations in the first harmonic flow helps to better understand background contributions, but there is still a long way to go before we will be able to conclude whether the observed charge separation is indeed connected to the effects of local parity violation, or it is just a complicated interplay of yet unidentified background sources.

8 Summary

The results by the ALICE, ATLAS, and CMS Collaborations from the first heavy-ion run at the Large Hadron Collider in November 2010 opened a new era of experimental studies of the quark-gluon plasma in the laboratory. Together with the new high statistics data collected during the past few years by the STAR and PHENIX Experiments at the Relativistic

Heavy Ion Collider this provides an extremely rich experimental data set which allows us to study the properties of the quark-gluon plasma in the great detail, and let us to learn more about the features of the universe a few microseconds just after the Big Bang. I am looking forward to further experimental developments and more exciting results from the LHC and RHIC scientific communities!

Bibliography

[1] P. Steinberg [ATLAS Collaboration], arXiv:1107.2182 [nucl-ex].

[2] B. Wyslouch [CMS Collaboration], arXiv:1107.2895 [nucl-ex].

[3] M. Floris [ALICE Collaboration], arXiv:1108.3257 [hep-ex].

[4] K. Aamodt *et al.* [ALICE Collaboration], Phys. Lett. **B696** (2011) 328-337.

[5] R. Snellings [ALICE Collaboration], arXiv:1106.6284 [nucl-ex].

[6] A. Adare *et al.* [PHENIX Collaboration], arXiv:1105.3928 [nucl-ex].

[7] D. Sharma [PHENIX Collaboration], Proceeding of Quark Matter 2011 Conference: `http://www.phenix.bnl.gov/phenix/WWW/publish/deepali/qm2011/proceedings.pdf`.

[8] G. Martinez Garcia [ALICE Collaboration], arXiv:1106.5889 [nucl-ex].

[9] A. Andronic, P. Braun-Munzinger, K. Redlich, J. Stachel, arXiv:1106.6321 [nucl-th].

[10] Y. -J. Lee [CMS Collaboration], arXiv:1107.2131 [hep-ex].

[11] B. Mohanty [STAR Collaboration], arXiv:1106.5902 [nucl-ex].

[12] M. L. Purschke [PHENIX Collaboration], Proceeding of Quark Matter 2011 Conference: `http://www.phenix.bnl.gov/phenix/WWW/publish/purschke/qm2011/purschke_proc_vers3.pdf`.

[13] D. E. Kharzeev, L. D. McLerran and H. J. Warringa, Nucl. Phys. A **803**, 227 (2008).

[14] S. A. Voloshin, Phys. Rev. **C70**, 057901 (2004).

[15] P. Christakoglou [ALICE Collaboration], arXiv:1106.2826 [nucl-ex].

Review: The FLAG working group

Andreas Jüttner[1] on behalf of the FLAG Collaboration
speakers affiliation:
CERN, Physics Department, TH Unit
CH-1211 Geneva 23, Switzerland

The FLAG working group reviews lattice results relevant for pion and kaon physics with the aim of making them easily accessible to the particle physics phenomenology community. The set of quantities considered so far comprises light quark masses, kaon and pion form factors, the kaon mixing parameter, and low energy constants of $SU(2)_L \times SU(2)_R$ and $SU(3)_L \times SU(3)_R$ chiral perturbation theory.

1 Introduction

Strong claims like

- "We find a (2-3)σ tension in the unitarity triangle" [1]
- "... confirming CKM unitarity at the permille level" [2]
- "... we find evidence of new physics in both B_d and B_s systems" [3]
- "Possible evidence for the breakdown of the CKM-paradigm of CP-violation" [4] ,

have recently been made based on lattice QCD results. This illustrates the role lattice QCD predictions are playing for the phenomenology of the Standard Model (SM). To this end the FLAG working group has formed with the aim of allowing also to an outsider a judgement of the quality and *state-of-the-art-fulness* of lattice results.

The quantities FLAG is currently considering comprise the light quark masses m_u, m_d, m_s, the ratio of the leptonic kaon and pion decay constant, f_K/f_π, the semi-leptonic $K \to \pi$ form factor at vanishing momentum transfer $f_+(0)$, the kaon mixing parameter B_K and a number of low energy constants of $SU(2)_L \times SU(2)_R$ and $SU(3)_L \times SU(3)_R$ chiral perturbation theory.

The FLAG report provides all relevant formulae and notation, a detailed quality assessment of every computation, where FLAG considers appropriate an average or recommended range and a lattice dictionary for non-experts and details of every single lattice simulation. After having made a start FLAG is currently discussing extending the set of quantities (e.g. charm and beauty). Periodic updates of the results are planned. Note also the similar effort by [1].

[1] juettner@mail.cern.ch

2 Lattice QCD

While perturbation theory is an invaluable tool at weak coupling it cannot make predictions for bound state observables like the proton mass or the properties of hadron decays. While potential models and sum rules clearly allow for studying these properties, only lattice QCD has the potential to make systematically improvable predictions.

QCD is a theory with three colour charges, six quarks in the fundamental representation with broken iso-spin in an infinite space-time continuum with the charged pion mass being 139.6MeV. In order to regularise the theory and make it accessible to simulations by means of a Monte-Carlo integration of its defining path integral, in lattice QCD one reduces its dynamical flavour content to $N_f = 2$ (degenerate up- and down-quark), 2+1 (plus a strange quark) or 2+1+1 (plus a charm quark), keeps the iso-spin symmetry exact, varies the pion mass ideally close to the physical point, considers only a finite volume of around 3-4fm and discretises space time with a lattice spacing of typically down to 0.05fm.

Clearly lattice QCD is thus affected by a number of systematic effects which need to be understood theoretically and controlled in the numerical simulation. For each of the major systematic effects FLAG has laid our quality criteria which are explained in detail in the document. In order to allow the reader a rough screening of available results, summaries are provided in terms of a colour coding:

- ★ when the systematic error has been estimated in a satisfactory manner and convincingly shown to be under control;
- ● when a reasonable attempt at estimating the systematic error has been made, although this could be improved;
- ■ when no or a clearly unsatisfactory attempt at estimating the systematic error has been made.

This colour coding has been set up for judging the quality of the chiral extrapolation, the continuum extrapolation, finite size effects, renormalisation, renormalisation scale running and the publication status. Where applicable, results only enter averages if they carry no red tag for any of the criteria. This also applies to the publication status - only published and peer-reviewed results (or simple updates of previously published data and analyses) qualify for inclusion into any average. FLAG treats results with different flavour content N_f separately.

3 FLAG summaries

In this section a selection of results of the FLAG document with a focus on the determination of the CKM-matrix element V_{us} are highlighted. Note that the summaries are based on the FLAG document [2]. Results that have appeared in the meantime will be included in future updates of the document.

3.1 CKM first-row unitarity - $|V_{us}|$

The determination of $|V_{us}|$ proceeds as follows: On the one hand, one experimentally measures the rate of a flavour changing process $s \to u$, where s is the strange quark and u the up quark. On the other hand one computes the SM prediction for the same process whose amplitude is proportional to the CKM-matrix element $|V_{us}|$ and which receives contributions from the electromagnetic, the weak and the strong interactions. While the former two are treated in perturbation theory for the processes considered here, the contribution from the latter needs to be computed in lattice QCD. Eventually, $|V_{us}|$ is determined by equating the experimental result with the SM-prediction.
For kaon/pion leptonic decays the relation between experiment and theory in the SM was computed by Marciano [5] and using the latest analysis of experimental results [6] it yields the correlation

$$\left|\frac{V_{us} f_K}{V_{ud} f_\pi}\right| = 0.2758(5)\,. \tag{1}$$

Since lattice QCD can provide f_K/f_π one obtains a prediction for $|V_{us}/V_{ud}|$. For semi-leptonic kaon decays the latest summary of experimental results together with SM-contributions yields [6]

$$|V_{us}| f_+(0) = 0.2163(5)\,, \tag{2}$$

and $|V_{us}|$ is readily extracted provided a prediction of $f_+(0)$.
Figure 1 exemplifies FLAG's compilation of results showing the lattice data with 2, 2+1 and 2+1+1 flavours of dynamical fermions for both $f_+(0)$ and f_K/f_π. As an example we show the underlying data for $f_+(0)$ together with the FLAG assessment in table 1. The results for f_K/f_π and for $f_+(0)$ for $N_f = 2$, $N_f = 2+1$ and $N_f = 2+1+1$, respectively, are all mutually compatible. The observation that the simulation and analysis techniques that lead to all these results differ significantly amongst the quoted collaborations causes confidence in the approach. The effect of adding the dynamical strange quark (and the charm quark) does not lead to any visible effects beyond the current level of precision.
The following averages/recommended values are explained in detail in the FLAG document: $f_K/f_\pi|_{N_f=2+1} = 1.193(5)$ (average over BMW, MILC and HPQCD/UKQCD), $f_K/f_\pi|_{N_f=2} = 1.210(18)$ (ETM) and, $f_+(0)|_{N_f=2+1} = 0.959(5)$ (RBC+UKQCD) and $f_+(0)|_{N_f=2} = 0.956(8)$ (ETM).
On the one hand these results can be used for making predictions for $|V_{ud}|$, $|V_{us}|$, $f_+(0)$ and f_K/f_π based on the experimental results (1) and (2) and on the assumption of CKM first row unitarity $|V_{ud}|^2 + |V_{us}|^2 + |V_{ub}|^2 = 1$ (at the current level of precision $|V_{ub}|$ is too small to play any significant role). On the other hand, when using only the experimental result as input the first row unitarity can be tested. This is summarised in the plot in figure 2.
Given that KLOE-2 is aiming at reducing the uncertainty in their experimental determination for $|V_{us}| f_+(0)$ by a factor of about two in the near future [36,37] it is fair to ask about prospects on the theory side. Recent progress for $f_+(0)$ [7,8,38] has allowed to remove

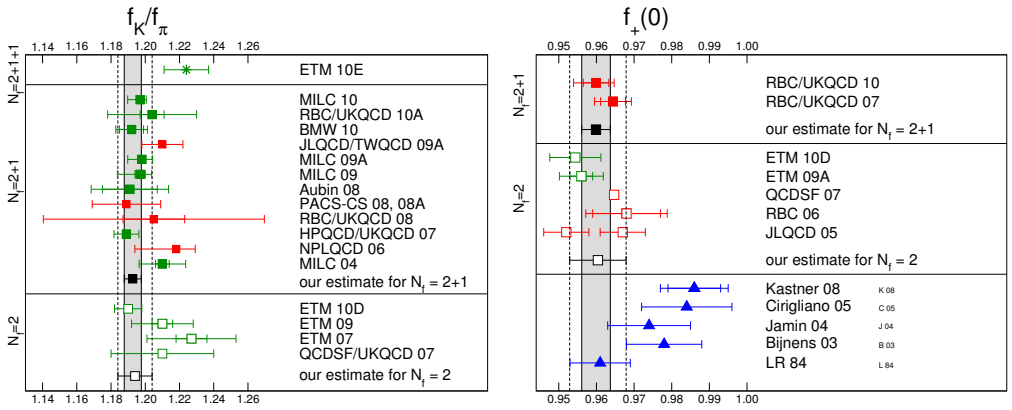

Figure 1: Scatter plots of the lattice data on the ratio of leptonic decay constants f_K/f_π and the semi-leptonic $K \to \pi$ vector form factor at vanishing momentum transfer, $f_+(0)$. Green symbols identify results that are free of *red tags* according to FLAG's assessment. The vertical bands correspond to FLAG's average/recommended range for $N_f = 2$ and $N_f = 2 + 1$, respectively.

Collaboration	N_f	publication status	chiral extrapolation	continuum extrapolation	finite volume errors	$f_+(0)$
RBC/UKQCD 10	2+1	A	●	■	★	$0.9599(34)(^{+31}_{-47})(14)$
RBC/UKQCD 07	2+1	A	●	■	★	0.9644(33)(34)(14)
ETM 10D	2	C	●	★	●	$0.9544(68)_{stat}$
ETM 09A	2	A	●	●	●	0.9560(57)(62)
QCDSF 07	2	C	■	■	★	$0.9647(15)_{stat}$
RBC 06	2	A	■	■	★	0.968(9)(6)
JLQCD 05	2	C	■	■	★	0.967(6), 0.952(6)

Table 1: Quality assessment of the semi-leptonic $K \to \pi$ vector form factor at vanishing momentum transfer, $f_+(0)$. FLAG classifies the publication status as `A` published or plain update of published results, `P` preprint or `C` conference contribution.

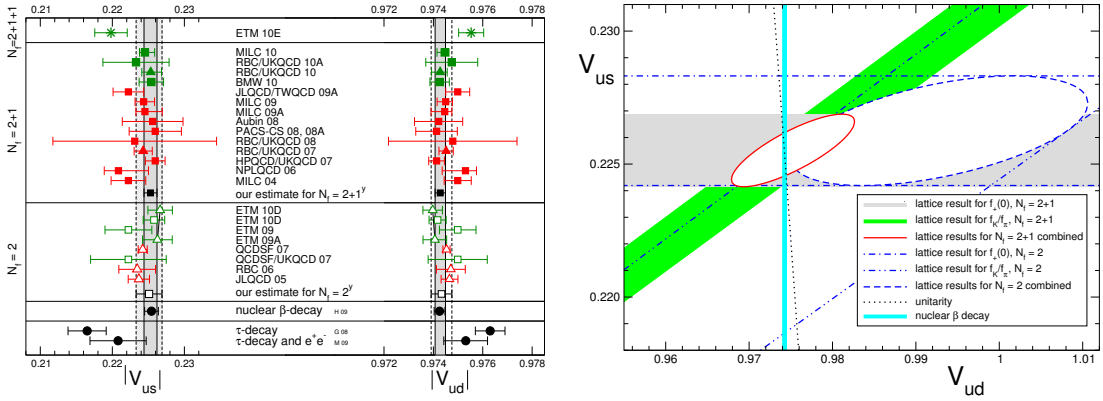

Figure 2: Left: Lattice predictions for $|V_{us}|$ and $|V_{ud}|$ assuming SM unitarity. Right: FLAG's illustration of lattice results in the $|V_{us}|$-$|V_{ud}|$-plane [2]. The ellipse represent the combined unitarity analysis for $N_f = 2+1$ flavours (solid red) and $N_f = 2$ flavours (dashed blue) while the black dashed line represents SM-unitarity. According to this analysis all results are compatible with first row unitarity.

one of the two most dominant uncertainties (momentum resolution in lattice simulations). The remaining dominant uncertainty is the one due to the chiral extrapolation which will disappear once results appear for physical pion masses. Cut-off effects in this observable will remain a sub-dominant uncertainty for a while: flavour symmetry implies that if the average light quark mass m_q is set equal to the strange quark mass m_s, the lattice data yield $f_+(0) = 1$, irrespective of the lattice spacing or the size of the box and for any value of m_s. Cut-off effects can therefore only affect the difference $1 - f_+(0)$, which turns out to be about 0.04. For f_K/f_π the error due to the chiral extrapolation will also disappear once all collaborations simulate directly at the physical point. The statistical error can be reduced by simulating longer (naively it reduces with $1/\sqrt{N}$ where N is proportional to the Monte Carlo time).

3.2 Neutral Kaon mixing

The mixing of neutral pseudoscalar mesons plays an important role in the understanding of the physics of CP-violation. Here we present the summary of lattice data for neutral kaon mixing which provides a probe for indirect CP-violation. The plot in figure 3 shows the status of lattice computations for $\hat{B}_K$. There has been tremendous progress over the last, say, five years. In particular the utilisation of chirally symmetric lattice fermion formulations [39, 40] has allowed to circumvent the problem of operator mixing of the 4-fermion operator. This reduces systematic effects considerably. The FLAG recommended values for the renormalisation group independent B-parameter which are indicated by the vertical bands in the plot in figure 3 are $\hat{B}_K = 0.738(20)$ ($N_f = 2+1$, Aubin 09, RBC/UKQCD 10B) and $\hat{B}_K = 0.792(25)(17)$ ($N_f = 2$, ETM 09D).

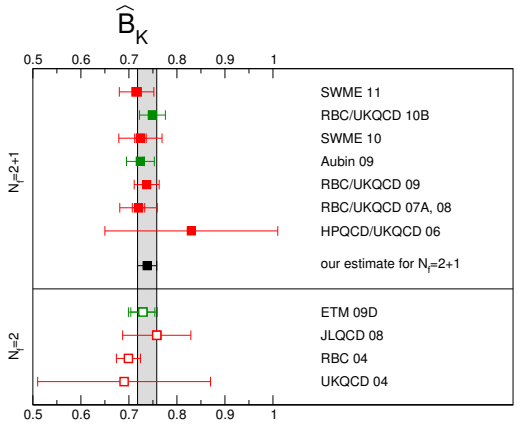

Figure 3: Scatter plot for $N_f = 2$ and $N_f = 2+1$ results for the neutral kaon mixing parameter $\hat{B}_K$.

3.3 Quark masses

The bare parameters of the $N_f = 2(2+1)$ Lagrangian are the gauge coupling and the up- and down- (and strange) quark masses. Since lattice QCD is simulated in the iso-spin limit, it is sufficient to provide two (three) hadronic quantities from experiment to tune the parameters of the Lagrangian to their physical values. There exist well defined procedures for how to determine renormalised quark masses in a second step. Various collaborations have carried out programmes to determine the light quark masses and the scatter plot in figure 4 gives an impression for the precision which can by now be achieved in lattice QCD. The FLAVIA recommended values indicated by the vertical bands in the plots are $m_{ud} = 3.43(11)$MeV, $m_s = 94(3)$MeV for $N_f = 2+1$ (MILC 09A, RBC/UKQCD 10A and HPQCD 10) and $m_{ud} = 3.6(2)$MeV, $m_s = 95(6)$MeV for $N_f = 2$ (ETM 10B). In fact, the precision is so good that QCD and QED iso-spin breaking effects play a significant role and need to be taken into account in any reliable estimate of the systematic uncertainties. The combined statistical and systematic errors in the FLAG average for $N_f = 2+1$ are around 3% for both the average up- and down-quark mass and the strange quark mass. FLAG also provides estimates of the individual up- and down-quark masses and found, based on phenomenological estimates of the quark's electro-magnetic self-energies that the up-quark mass to be different from zero by 15 standard deviations.

3.4 Low energy constants

On the one hand lattice practitioners are putting a lot of effort into improving algorithms and computers in order to be able to simulate QCD for physical quark masses, in this way avoiding systematic-affected extrapolations to the physical point. That this is now possible has been demonstrated only recently [72]. However, many simulations are carried out with

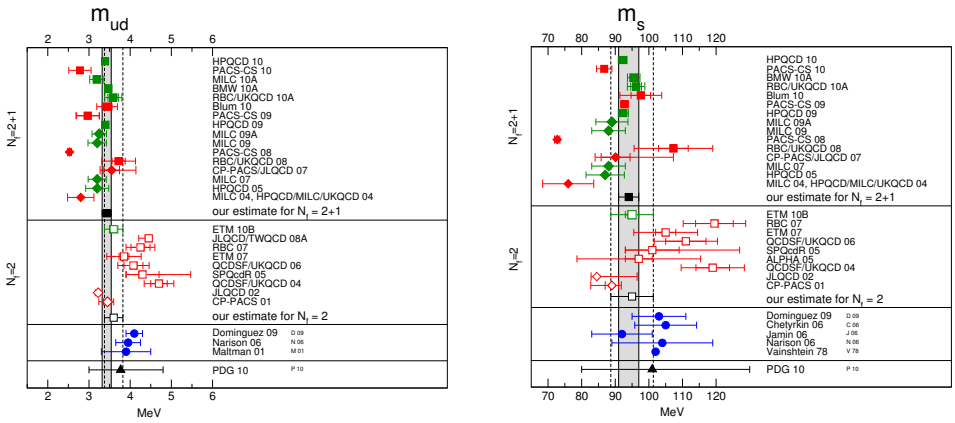

Figure 4: Scatter plot for the average up- and down-quark masses and the strange quark mass.

heavier than physical quark masses and chiral perturbation theory is employed to provide ansätze for the mass dependence of the observable under consideration. The low-energy constants of chiral perturbation theory can be determined from fits of these ansätze to the lattice data. The FLAG document also presents an overview and analysis over the status of determinations of these low-energy constants.

4 Outlook

FLAG has set out to provide the (Beyond) Standard Model phenomenologist with predictions for low-energy parameters and observables of QCD. The aim is to screen and judge all available lattice data from a specialist's point of view and to provide a summary of the status and a quality assessment of each single result for the non-specialist and where appropriate also an average or recommended range.

FLAG is envisaging regular updates of the summary table and scatter plots and also of the averages. In addition FLAG is working on extending the set of data considered so far towards observables and parameters related to charm and bottom quarks.

Acknowledgments

Many thanks to all involved in organising this interesting conference and for inviting FLAG. The speaker would also like to thank the prize-committee for choosing his talk!

Bibliography

[1] J. Laiho, E. Lunghi, and R. S. Van de Water, *Phys. Rev.* **D81**, 034503 (2010), arXiv:0910.2928.

[2] G. Colangelo, S. Dürr, A. Jüttner, L. Lellouch, H. Leutwyler, et al. (2010), arXiv:1011.4408, arXiv:1011.4408.

[3] A. Lenz, U. Nierste, J. Charles, S. Descotes-Genon, A. Jantsch, et al., *Phys.Rev.* **D83**, 036004 (2011), arXiv:1008.1593.

[4] E. Lunghi, and A. Soni, *Phys.Lett.* **B697**, 323–328 (2011), arXiv:1010.6069.

[5] W. J. Marciano, *Phys. Rev. Lett.* **93**, 231803 (2004), hep-ph/0402299.

[6] M. Antonelli, et al., *Eur. Phys. J.* **C69**, 399–424 (2010), arXiv:1005.2323.

[7] [RBC/UKQCD 10], P. A. Boyle, et al., *Eur. Phys. J.* **C69**, 159–167 (2010), arXiv:1004.0886.

[8] [RBC/UKQCD 07], P. A. Boyle, et al., *Phys. Rev. Lett.* **100**, 141601 (2008), arXiv:0710.5136.

[9] [ETM 10D], V. Lubicz, F. Mescia, L. Orifici, S. Simula, and C. Tarantino, *PoS* **LAT2010**, 316 (2010), arXiv:1012.3573.

[10] [ETM 09A], V. Lubicz, F. Mescia, S. Simula, and C. Tarantino, *Phys. Rev.* **D80**, 111502 (2009), arXiv:0906.4728.

[11] [QCDSF 07], D. Brömmel, et al., *PoS* **LAT2007**, 364 (2007), arXiv:0710.2100.

[12] [RBC 06], C. Dawson, T. Izubuchi, T. Kaneko, S. Sasaki, and A. Soni, *Phys. Rev.* **D74**, 114502 (2006), hep-ph/0607162.

[13] [JLQCD 05], N. Tsutsui, et al., *PoS* **LAT2005**, 357 (2006), hep-lat/0510068.

[14] [ETM 10E], F. Farchioni, G. Herdoiza, K. Jansen, M. Petschlies, C. Urbach, et al., *PoS* **LAT2010**, 128 (2010), arXiv:1012.0200.

[15] [MILC 10], A. Bazavov, et al., *PoS* **LAT2010**, 074 (2010), arXiv:1012.0868.

[16] [RBC/UKQCD 10A], Y. Aoki, et al. (2010), arXiv:1011.0892.

[17] [BMW 10], S. Dürr, et al., *Phys. Rev.* **D81**, 054507 (2010), arXiv:1001.4692.

[18] [JLQCD/TWQCD 09A], J. Noaki, et al., *PoS* **LAT2009**, 096 (2009), arXiv:0910.5532.

[19] [MILC 09A], A. Bazavov, et al., *PoS* **CD09**, 007 (2009), arXiv:0910.2966.

[20] [MILC 09], A. Bazavov, et al., *Rev. Mod. Phys.* **82**, 1349–1417 (2010), arXiv:0903.3598.

[21] [Aubin 08], C. Aubin, J. Laiho, and R. S. Van de Water, *PoS* **LAT2008**, 105 (2008), arXiv:0810.4328.

[22] [PACS-CS 08], S. Aoki, et al., *Phys. Rev.* **D79**, 034503 (2009), arXiv:0807.1661.

[23] [PACS-CS 08A], and Y. Kuramashi, *PoS* **LAT2008**, 018 (2008), arXiv:0811.2630.

[24] [RBC/UKQCD 08], C. Allton, et al., *Phys. Rev.* **D78**, 114509 (2008), arXiv:0804.0473.

[25] [HPQCD/UKQCD 07], E. Follana, C. T. H. Davies, G. P. Lepage, and J. Shigemitsu, *Phys. Rev. Lett.* **100**, 062002 (2008), arXiv:0706.1726.

[26] [NPLQCD 06], S. R. Beane, P. F. Bedaque, K. Orginos, and M. J. Savage, *Phys. Rev.* **D75**, 094501 (2007), hep-lat/0606023.

[27] [MILC 04], C. Aubin, et al., *Phys. Rev.* **D70**, 114501 (2004), hep-lat/0407028.

[28] [ETM 09], B. Blossier, et al., *JHEP* **07**, 043 (2009a), arXiv:0904.0954.

[29] (2007), [QCDSF/UKQCD 07], G. Schierholz et al., *Probing the chiral limit with clover fermions I: The meson sector, talk given at Lattice 2007, Regensburg, Germany*, PoS **LAT2007**, 133, http://www.physik.uni-regensburg.de/lat07/hevea/schierholz.pdf.

[30] [LR 84], H. Leutwyler, and M. Roos, *Z. Phys.* **C25**, 91 (1984).

[31] P. Post, and K. Schilcher, *Eur. Phys. J.* **C25**, 427–443 (2002), hep-ph/0112352.

[32] J. Bijnens, and P. Talavera, *Nucl. Phys.* **B669**, 341–362 (2003), hep-ph/0303103.

[33] M. Jamin, J. A. Oller, and A. Pich, *JHEP* **02**, 047 (2004), hep-ph/0401080.

[34] V. Cirigliano, et al., *JHEP* **04**, 006 (2005), hep-ph/0503108.

[35] A. Kastner, and H. Neufeld, *Eur. Phys. J.* **C57**, 541–556 (2008), arXiv:0805.2222.

[36] D. Babusci, C. Bini, F. Bossi, G. Isidori, D. Moricciani, et al. (2010), arXiv:1007.5219.

[37] E. De Lucia (2010), talk at CKM2010 - 6th International Workshop on the CKM Unitarity Triangle, Warwick, UK.

[38] P. Boyle, J. Flynn, A. Juttner, C. Sachrajda, and J. Zanotti, *JHEP* **0705**, 016 (2007), * Temporary entry *, hep-lat/0703005.

[39] [Aubin 09], C. Aubin, J. Laiho, and R. S. Van de Water, *Phys. Rev.* **D81**, 014507 (2010), arXiv:0905.3947.

[40] [RBC/UKQCD 10B], Y. Aoki, et al. (2010), arXiv:1012.4178.

[41] [SWME 11], J. Kim, C. Jung, H.-J. Kim, W. Lee, and S. R. Sharpe (2011), arXiv:1101.2685.

[42] [SWME 10], T. Bae, et al., *Phys. Rev.* **D82**, 114509 (2010), arXiv:1008.5179.

[43] [RBC/UKQCD 09], C. Kelly, P. A. Boyle, and C. T. Sachrajda, *PoS* **LAT2009**, 087 (2009), arXiv:0911.1309.

[44] [RBC/UKQCD 07A], D. J. Antonio, et al., *Phys. Rev. Lett.* **100**, 032001 (2008), hep-ph/0702042.

[45] [HPQCD/UKQCD 06], E. Gamiz, et al., *Phys. Rev.* **D73**, 114502 (2006), hep-lat/0603023.

[46] [ETM 09D], V. Bertone, et al., *PoS* **LAT2009**, 258 (2009), arXiv:0910.4838.

[47] [JLQCD 08], S. Aoki, et al., *Phys. Rev.* **D77**, 094503 (2008), arXiv:0801.4186.

[48] [RBC 04], Y. Aoki, et al., *Phys. Rev.* **D72**, 114505 (2005), hep-lat/0411006.

[49] [UKQCD 04], J. M. Flynn, F. Mescia, and A. S. B. Tariq, *JHEP* **11**, 049 (2004), hep-lat/0406013.

[50] [RBC/UKQCD 10C], C. Albertus, Y. Aoki, P. Boyle, N. Christ, T. Dumitrescu, et al., *Phys.Rev.* **D82**, 014505 (2010), arXiv:1001.2023.

[51] [FNAL-MILC 09], C. Bernard, C. DeTar, M. Di Pierro, A. El-Khadra, R. Evans, et al., *PoS* **LATTICE2008**, 278 (2008), arXiv:0904.1895.

[52] [ETM 09], B. Blossier, et al., *PoS* **LAT2009**, 151 (2009b), arXiv:0911.3757.

[53] [JLQCD 03], S. Aoki, et al., *Phys.Rev.Lett.* **91**, 212001 (2003), hep-ph/0307039.

[54] [MILC 02], C. Bernard, et al., *Phys.Rev.* **D66**, 094501 (2002), hep-lat/0206016.

[55] [CP-PACS 01], A. Ali Khan, et al., *Phys.Rev.* **D64**, 054504 (2001), hep-lat/0103020.

[56] [HPQCD 06], E. Dalgic, A. Gray, E. Gamiz, C. T. Davies, G. Lepage, et al., *Phys.Rev.* **D76**, 011501 (2007), hep-lat/0610104.

[57] [FNAL-MILC 10], J. Simone, et al., *PoS* **LATTICE2010**, 317 (2010).

[58] [ETM 10B], B. Blossier, et al., *Phys. Rev.* **D82**, 114513 (2010), arXiv:1010.3659.

[59] [JLQCD/TWQCD 08A], J. Noaki, et al., *Phys. Rev. Lett.* **101**, 202004 (2008), arXiv:0806.0894.

[60] [RBC 07], T. Blum, T. Doi, M. Hayakawa, T. Izubuchi, and N. Yamada, *Phys. Rev.* **D76**, 114508 (2007), arXiv:0708.0484.

[61] [ETM 07], B. Blossier, et al., *JHEP* **04**, 020 (2008), arXiv:0709.4574.

[62] [QCDSF/UKQCD 06], M. Göckeler, et al., *Phys. Rev.* **D73**, 054508 (2006), hep-lat/0601004.

[63] [SPQcdR 05], D. Becirevic, et al., *Nucl. Phys.* **B734**, 138–155 (2006), hep-lat/0510014.

[64] [ALPHA 05], M. Della Morte, et al., *Nucl. Phys.* **B729**, 117–134 (2005), hep-lat/0507035.

[65] [QCDSF/UKQCD 04], M. Göckeler, et al., *Phys. Lett.* **B639**, 307–311 (2006), hep-ph/0409312.

[66] [JLQCD 02], S. Aoki, et al., *Phys. Rev.* **D68**, 054502 (2003), hep-lat/0212039.

[67] [CP-PACS 01], A. Ali Khan, et al., *Phys. Rev.* **D65**, 054505 (2002), Erratum: *Phys. Rev.* **D66** (2003) 059901, hep-lat/0105015.

[68] [PACS-CS 10], S. Aoki, et al., *JHEP* **08**, 101 (2010), arXiv:1006.1164.

[69] [MILC 10A], A. Bazavov, et al., *PoS* **LAT2010**, 083 (2010), arXiv:1011.1792.

[70] [HPQCD 10], C. McNeile, C. T. H. Davies, E. Follana, K. Hornbostel, and G. P. Lepage, *Phys. Rev.* **D82**, 034512 (2010), arXiv:1004.4285.

[71] [BMW 10A], S. Dürr, et al. (2010), arXiv:1011.2403.

[72] [BMW 10B], S. Dürr, et al. (2010), arXiv:1011.2711.

[73] [Blum 10], T. Blum, et al., *Phys. Rev.* **D82**, 094508 (2010), arXiv:1006.1311.

[74] [PACS-CS 09], S. Aoki, et al., *Phys. Rev.* **D81**, 074503 (2010), arXiv:0911.2561.

[75] [HPQCD 09], C. T. H. Davies, et al., *Phys. Rev. Lett.* **104**, 132003 (2010), arXiv:0910.3102.

[76] [CP-PACS/JLQCD 07], T. Ishikawa, et al., *Phys. Rev.* **D78**, 011502 (2008), arXiv:0704.1937.

[77] [HPQCD 05], Q. Mason, H. D. Trottier, R. Horgan, C. T. H. Davies, and G. P. Lepage, *Phys. Rev.* **D73**, 114501 (2006), hep-ph/0511160.

[78] [HPQCD/MILC/UKQCD 04], C. Aubin, et al., *Phys. Rev.* **D70**, 031504 (2004), hep-lat/0405022.

[79] K. Nakamura, et al., *J.Phys.G* **G37**, 075021 (2010).

[80] S. Narison, *Phys. Rev.* **D74**, 034013 (2006), hep-ph/0510108.

[81] K. Maltman, and J. Kambor, *Phys. Lett.* **B517**, 332–338 (2001), hep-ph/0107060.

[82] C. A. Dominguez, N. F. Nasrallah, R. Röntsch, and K. Schilcher, *Nucl. Phys. Proc. Suppl.* **186**, 133–136 (2009), arXiv:0808.3909.

Effective Field Theories for Quarkonium and Dipole Transitions

Antonio Vairo[1]
Physik-Department
Technische Universität München
James-Franck-Str. 1, 85748 Garching, Germany

Effective field theories for quarkonium at zero and finite temperature provide an unifying description for a wide class of phenomena. As an example, we discuss physical effects induced by dipole transitions.

1 Hierarchies

Quarkonia, i.e. heavy quark-antiquark bound states, are systems characterized by hierarchies of energy scales [1]. They follow from the quark mass, M, being the largest scale in the system, which, in particular, means that $M \gg p$, the typical momentum transfer in the system, $M \gg \Lambda_{\rm QCD}$, the hadronic scale, and $M \gg \pi T \gg$ other thermal scales, where T is the temperature of the medium. These hierarchies allow systematic studies through the construction of suitable effective field theories (EFTs).

(i) The non-relativistic expansion
$M \gg p$ implies that quarkonia are non-relativistic and characterized by the hierarchy of scales typical of a non-relativistic bound state: $p \sim 1/r \sim Mv$ and $E \sim Mv^2$, where r is the typical radius, E the typical binding energy and $v \ll 1$ the heavy-quark velocity in the centre-of-mass frame. Note that the hierarchy of non-relativistic scales makes the very difference of quarkonia with heavy-light mesons, which are characterized just by the two scales M and $\Lambda_{\rm QCD}$.

Systematic expansions in the small heavy-quark velocity v may be implemented at the Lagrangian level by constructing suitable non-relativistic effective field theories (EFTs) [2].

(ii) The perturbative expansion
$M \gg \Lambda_{\rm QCD}$ implies $\alpha_{\rm s}(M) \ll 1$: phenomena happening at the scale M may be treated perturbatively. We may further have small couplings if $Mv \gg \Lambda_{\rm QCD}$ and $Mv^2 \gg \Lambda_{\rm QCD}$, in which case $\alpha_{\rm s}(Mv) \ll 1$ and $\alpha_{\rm s}(Mv^2) \ll 1$ respectively. Moreover, we have $v \sim \alpha_{\rm s}(Mv)$. This

[1]antonio.vairo@ph.tum.de

is likely to happen only for the lowest charmonium and bottomonium states, which may be described by weakly-coupled Coulombic bound states, while excited quarkonia probe the transition from Coulombic to confined bound states.

(iii) The thermal expansion
If the temperature of the medium in heavy-ion collisions is such that $M \gg \pi T$, which is the case for most present days colliders, this implies that the quarkonium remains a non-relativistic bound state also in the thermal bath induced by the medium. However, the temperature will, in general, interfere with the other scales of the bound state. As a consequence, bound state observables like masses, lifetimes, decay widths etc. will be modified by the medium. In particular, it is expected that at sufficiently high temperatures the interference of the medium will be such to dissociate the quarkonium. Since different quarkonia have different radii and different binding energies, different quarkonia are expected to dissociate in the medium at different temperatures, providing a thermometer for the plasma [3], see also [4]. $\pi T \gg$ other thermal scales implies a hierarchy also in the thermal scales.

2 Effective field theories

The hierarchies of EFTs for quarkonium at zero and finite temperature are shown in Fig. 1. In the following, we will consider systems for which $Mv \gg T$, so that both the scale M and the scale Mv may be integrated out ignoring medium effects (third column of Fig. 1).

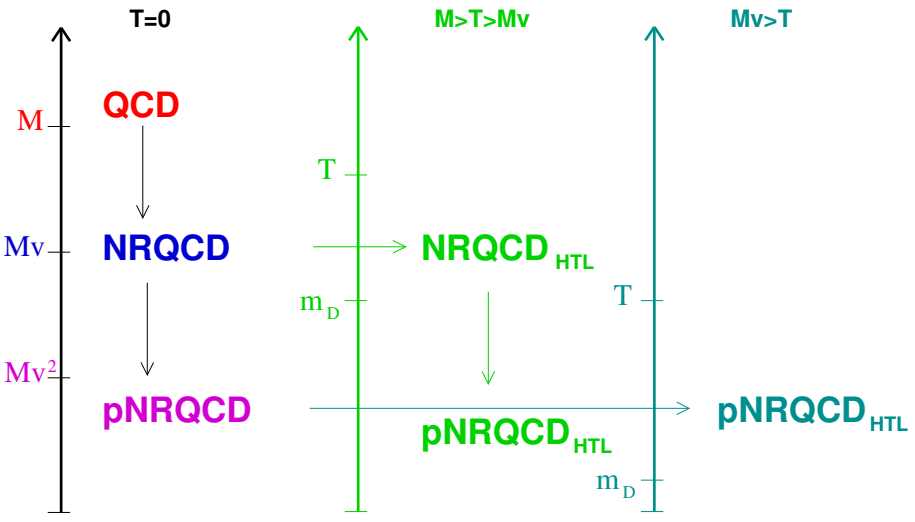

Figure 1: Hierarchies of EFTs for quarkonium at zero temperature [2] and at finite temperature [5–9].

Heavy quark-antiquark annihilation and production happen at the scale M. The suitable EFT is NRQCD [10, 11]. The effective Lagrangian is organized as an expansion in $1/M$ and

$\alpha_{\rm s}(M)$:

$$\mathcal{L}_{\rm NRQCD} = \sum_n \frac{c_n(\alpha_{\rm s}(M),\mu)}{M^n} \times O_n(\mu)\,, \tag{1}$$

where O_n are NRQCD operators of dimension $4+n$ and c_n are NRQCD matching coefficients. For quarkonium production in NRQCD, see also [12].

The heavy quark and antiquark in quarkonium cannot be resolved at scales lower than Mv. The suitable EFT is pNRQCD [13, 14]. The effective Lagrangian is organized as an expansion in $1/M$, $\alpha_{\rm s}(M)$ and r:

$$\mathcal{L}_{\rm pNRQCD} = \int d^3r \sum_n \sum_k \frac{c_n(\alpha_{\rm s}(M),\mu)}{M^n} \times V_{n,k}(r,\mu',\mu)\, r^k \times O_{n,k}(\mu')\,, \tag{2}$$

where $O_{n,k}$ are pNRQCD operators and $V_{n,k}$ are the pNRQCD matching coefficients. The matching coefficients of the four-fermion, dimension six, operators may be interpreted as the potentials of the bound-state Schrödinger equation, while the matching coefficients of the higher-dimension operators describe the couplings of the heavy quarks to the low-energy degrees of freedom.

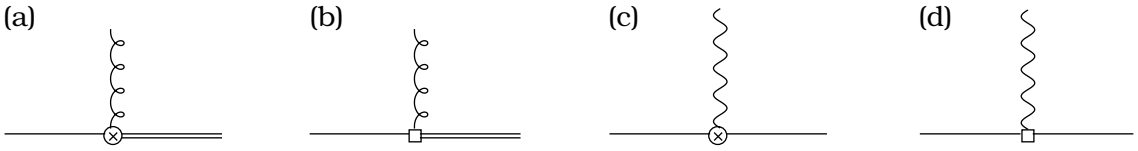

Figure 2: Chromoelectric (a), chromomagnetic (b), electric (c) and magnetic (d) dipole interaction vertices. The single line stands for a colour-singlet quark-antiquark propagator, while the double line for a colour-octet quark-antiquark propagator.

To list the low-energy degrees of freedom and to write explicitly the Lagrangian of pNRQCD we need to specify our system. In the following, we will concentrate on the physics of the quarkonium ground states in the presence of a medium whose temperature is much lower than the typical moment transfer in the bound state (this situation includes the vacuum). For a recent review, also on the physics of the quarkonium ground states, we refer to [15]. The suitable EFT for the quarkonium ground states is weakly coupled pNRQCD, since for those systems $Mv \sim M\alpha_{\rm s} \gg Mv^2 \sim M\alpha_{\rm s}^2 \gtrsim \Lambda_{\rm QCD}$. The degrees of freedom are quark-antiquark states (colour singlet, S, colour octet, O), low-energy gluons and photons, and n_f light quarks (q_i). The Lagrangian reads

$$\begin{aligned}\mathcal{L}_{\rm pNRQCD} &= \int d^3r\, {\rm Tr}\left\{ {\rm S}^\dagger \left(i\partial_0 - \frac{\mathbf{p}^2}{M} + \cdots - V_s \right) {\rm S} + {\rm O}^\dagger \left(iD_0 - \frac{\mathbf{p}^2}{M} + \cdots - V_o \right) {\rm O} \right\} \\ &\quad -\frac{1}{4} F^a_{\mu\nu} F^{\mu\nu\, a} - \frac{1}{4} F_{\mu\nu} F^{\mu\nu} + \sum_{i=1}^{n_f} \bar{q}_i\, i\not{D} q_i + \Delta\mathcal{L}\,.\end{aligned} \tag{3}$$

At leading order in the power counting, the singlet field S satisfies a Schrödinger equation with potential V_s. Higher-order terms are in $\Delta\mathcal{L}$, which describes the interaction with the low-energy degrees of freedom. The leading interactions are (chromo)electric and (chromo)magnetic dipole interactions (ee_Q is the electric charge of the heavy flavour Q):

$$\begin{aligned}\Delta\mathcal{L} &= \int d^3r\ \mathrm{Tr}\Bigg\{ V_A \mathrm{O}^\dagger \mathbf{r}\cdot g\mathbf{E}\,\mathrm{S} + \cdots + \frac{1}{2M}\,V_1\,\left\{\mathrm{S}^\dagger, \boldsymbol{\sigma}\cdot g\mathbf{B}\right\}\mathrm{O} + \cdots \\ &\quad + V_A^{\mathrm{em}}\,\mathrm{S}^\dagger \mathbf{r}\cdot ee_Q\mathbf{E}^{\mathrm{em}}\mathrm{S} + \cdots + \frac{1}{2M}\,V_1^{\mathrm{em}}\,\left\{\mathrm{S}^\dagger, \boldsymbol{\sigma}\cdot ee_Q\mathbf{B}^{\mathrm{em}}\right\}\mathrm{S} + \ldots \Bigg\}. \qquad (4)\end{aligned}$$

The corresponding Feynman diagram vertices are shown in Fig. 2. The matching coefficients V_A, V_1, V_A^{em} and V_1^{em} are one at leading order in the coupling.

In the following, we will consider the effect of the self-energy correction to the singlet propagator induced by the dipole vertices (4) in three different observables: the quark-antiquark static energy at zero temperature in perturbation theory, the photon line shape in the $J/\psi \to X\,\gamma$ radiative decay for 0 MeV $\leqslant E_\gamma \lesssim$ 500 MeV and the $\Upsilon(1S)$ width induced by a medium whose temperature is about twice the critical temperature.

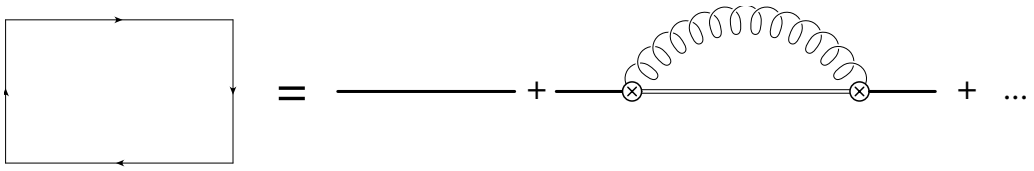

Figure 3: The Wilson loop in the large time limit (left side) in terms of the pNRQCD singlet propagator (right side).

3 The perturbative potential and static energy at $T = 0$

The quark-antiquark static energy, E_0, is given by the large-time exponential fall off of the static Wilson loop [16]. In pNRQCD, the large-time Wilson loop is matched by the singlet propagator, see Fig. 3. Hence, the static energy is given by the singlet static potential $V_s^{(0)}$ plus corrections due to the coupling of the singlet to low-energy gluons and light quarks. The one-loop correction is shown in the right side of Fig. 3: the low-energy gluon is coupled to the singlet through the chromoelectric dipole vertex of Fig.2(a). Explicitly the static energy is given by

$$E_0(r) = V_s^{(0)}(r,\mu) - i\frac{g^2}{3}V_A^2\int_0^\infty dt\, e^{-it(V_o^{(0)}-V_s^{(0)})}\,\langle \mathrm{Tr}\{\mathbf{r}\cdot\mathbf{E}(t)\,\mathbf{r}\cdot\mathbf{E}(0)\}\rangle(\mu) + \ldots\,, \qquad (5)$$

where the chromoelectric correlator $\langle \mathrm{Tr}\{\mathbf{r}\cdot\mathbf{E}(t)\,\mathbf{r}\cdot\mathbf{E}(0)\}\rangle$ comes from the two chromoelectric dipole vertices. The factorization scale, μ, dependence cancels between the two terms in the right-hand side, therefore, the μ dependence of the singlet static potential, $V_s^{(0)} \sim \ln r\mu, \ln^2 r\mu$, ..., may be deduced from the μ dependence of the one loop correction in pNRQCD $\sim \ln(V_o^{(0)} - V_s^{(0)})/\mu, \ln^2(V_o^{(0)} - V_s^{(0)})/\mu, \ldots \ln r\mu, \ln^2 r\mu, \ldots$.

Since the static Wilson loop is known up to N^{3}LO [17–20], the octet potential, $V_o^{(0)}$, is known up to NNLO [21,22], $V_A = 1 + \mathcal{O}(\alpha_s^2)$ [23] and the chromoelectric correlator $\langle \mathrm{Tr}\{\mathbf{r}\cdot\mathbf{E}(t)\,\mathbf{r}\cdot\mathbf{E}(0)\}\rangle$ is known up to NLO [24], from (5) it follows that up to N^{4}LO (in the scheme of [23])

$$
\begin{aligned}
V_s^{(0)}(r,\mu) \;=\; & -\frac{4}{3}\frac{\alpha_s(1/r)}{r}\left[1 + \tilde{a}_1\frac{\alpha_s(1/r)}{4\pi} + \tilde{a}_{2\,s}\left(\frac{\alpha_s(1/r)}{4\pi}\right)^2\right. \\
& + \left(144\,\pi^2\,\ln r\mu + \tilde{a}_{3\,s}\right)\left(\frac{\alpha_s(1/r)}{4\pi}\right)^3 \\
& \left. + \left(a_4^{L2}\ln^2 r\mu + \left(a_4^{L} + 48\pi^2\,\beta_0(-5+6\ln 2)\right)\ln r\mu + \tilde{a}_{4\,s}\right)\left(\frac{\alpha_s(1/r)}{4\pi}\right)^4\right], \qquad (6)
\end{aligned}
$$

where the coefficient $\tilde{a}_1$ may be read from [25, 26], $\tilde{a}_{2\,s}$ from [17], $\tilde{a}_{3\,s}$ from [19, 20], a_4^{L2} and a_4^{L} from [23], while $\tilde{a}_{4\,*200*s}$ is unknown. The potentially large logarithms, $\ln r\mu$, may be resummed by solving the corresponding renormalization group equations; the static potential at N^{3}LL then reads [27,28]:

$$
\begin{aligned}
V_s^{(0)}(r,\mu) \;=\; & V_s^{(0)}(r,1/r) + \frac{8}{9}r^2\left[V_o^{(0)}(r,1/r) - V_s^{(0)}(r,1/r)\right]^3 \\
& \times\left(\frac{2}{\beta_0}\ln\frac{\alpha_s(\mu)}{\alpha_s(1/r)} + \eta_0\left[\alpha_s(\mu) - \alpha_s(1/r)\right]\right), \qquad (7)
\end{aligned}
$$

$$
\eta_0 \;\equiv\; \frac{1}{\pi}\left[-\frac{\beta_1}{2\beta_0^2} + \frac{12}{\beta_0}\left(\frac{-5n_f + 18\pi^2 + 141}{108}\right)\right], \qquad (8)
$$

where β_i are the coefficients of the beta function.

Finally, summing back the low-energy contributions in (5), we obtain the static quark-antiquark energy at N^{3}LL [28], which may be compared with lattice data (see Fig. 4). The conclusion is that perturbation theory, supplemented by a suitable renormalon subtraction scheme, describes well the static quark-antiquark energy at short distances, i.e. up to distances of about 0.25 fm ($r_0 \approx 0.5$ fm in physical units). Indeed, one can use this to extract $\Lambda_{\overline{\mathrm{MS}}}^{n_f=0} r_0 = 0.622^{+0.019}_{-0.015}$ and, in perspective, r_0, once high-precision unquenched lattice data will be available [29].

4 The photon line shape in $J/\psi \to X\,\gamma$ for 0 MeV $\leqslant E_\gamma \lesssim$ 500 MeV

We consider the radiative decay $J/\psi \to X\,\gamma$ for 0 MeV $\leqslant E_\gamma \lesssim$ 500 MeV. The relevant scales are: $p \sim 1/r \sim M_c v \sim 700$ MeV - 1 GeV $> \Lambda_{\mathrm{QCD}}$, $E_{J/\psi} \equiv M_{J/\psi} - 2M_c \sim M_c v^2 \sim 400$ MeV -

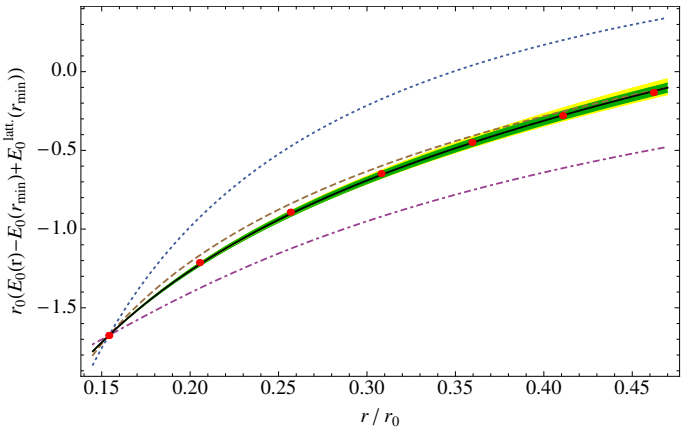

Figure 4: The static quark-antiquark energy at N^{3}LL taken from [29] plotted against the quenched lattice data from [30]. r_0 stands for a lattice scale of dimension -1.

600 MeV and 0 MeV $\leqslant E_\gamma \lesssim$ 500 MeV, which is smaller than $M_c v$. It follows that the system is *(i)* non-relativistic, *(ii)* weakly-coupled at the scale $M_c v$: $v \sim \alpha_s$, and *(iii)* that we may multipole expand in the external photon energy [31].

Three main processes contribute to $J/\psi \to X\,\gamma$ for 0 MeV $\leqslant E_\gamma \lesssim$ 500 MeV.

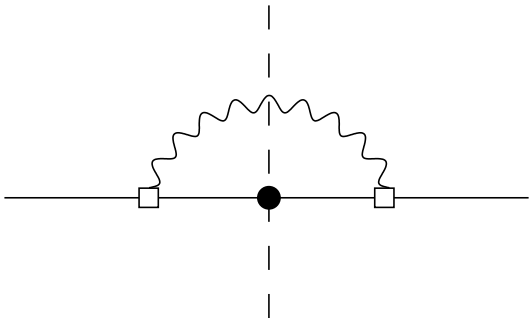

Figure 5: Magnetic dipole transition induced by the vertex of Fig. 2(d). The black dot stands for the imaginary part of V_s, which is responsible for the decay of the η_c.

(i) Magnetic dipole transition $J/\psi \to \eta_c\,\gamma \to X\,\gamma$
The J/ψ may decay through an intermediate magnetic dipole transition to an η_c and a photon. This process is shown by the cut diagram in Fig. 5. The differential width reads

$$\frac{d\Gamma_{\rm mag}}{dE_\gamma} = \frac{64}{27}\frac{\alpha}{\pi}\frac{E_\gamma}{M_{J/\psi}^2}\frac{\Gamma_{\eta_c}}{2}\frac{E_\gamma^2}{(M_{J/\psi}-M_{\eta_c}-E_\gamma)^2+\Gamma_{\eta_c}^2/4}\,. \tag{9}$$

$\Gamma_{\eta_c} \sim M_c\alpha_s^5$ is the η_c width; for $\Gamma_{\eta_c} \to 0$ one recovers $\Gamma(J/\psi \to \eta_c\,\gamma) = \dfrac{64}{27}\alpha\dfrac{E_\gamma^3}{M_{J/\psi}^2}$. We

observe that the non-relativistic Breit–Wigner distribution goes like:

$$\frac{E_\gamma^2}{(M_{J/\psi}-M_{\eta_c}-E_\gamma)^2+\Gamma_{\eta_c}^2/4} = \begin{cases} 1 & \text{for } E_\gamma \gg M_c\alpha_{\rm s}^4 \sim M_{J/\psi}-M_{\eta_c} \\ \frac{E_\gamma^2}{(M_{J/\psi}-M_{\eta_c})^2} & \text{for } E_\gamma \ll M_c\alpha_{\rm s}^4 \sim M_{J/\psi}-M_{\eta_c} \end{cases} . \tag{10}$$

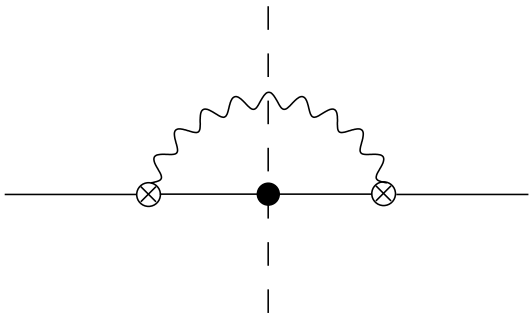

Figure 6: Electric dipole transition induced by the vertex of Fig. 2(c). The black dot stands for the imaginary part of V_s, which is responsible for the decay of the $\chi_{c0,2}(1P)$.

(ii) Electric dipole transition $J/\psi \to \chi_{c0,2}(1P)\,\gamma \to X\,\gamma$
The J/ψ may decay through an intermediate electric dipole transition to a $\chi_{c0,2}$ and a photon. This process is shown by the cut diagram in Fig. 6. The differential width reads [32]

$$\begin{aligned} \frac{d\Gamma_{\rm ele}}{dE_\gamma} &= \frac{7168}{6561}\frac{\alpha}{\pi}\frac{E_\gamma}{M_{J/\psi}}\alpha_{\rm s}^5\,|a(E_\gamma)|^2\,, \\ a(E_\gamma) &\equiv \frac{(1-\nu)(3+5\nu)}{3(1+\nu)^2} \\ &\quad + \frac{8\nu^2(1-\nu)}{3(2-\nu)(1+\nu)^3}\,{}_2F_1(2-\nu,1;3-\nu;-(1-\nu)/(1+\nu))\,, \\ \nu &\equiv \sqrt{-E_{J/\psi}/(E_\gamma-E_{J/\psi})}\,. \end{aligned} \tag{11}$$

Since

$$|a(E_\gamma)|^2 = \begin{cases} 1 & \text{for } E_\gamma \gg M_c\alpha_{\rm s}^2 \sim E_{J/\psi} \\ E_\gamma^2/(2E_{J/\psi})^2 & \text{for } E_\gamma \ll M_c\alpha_{\rm s}^2 \sim E_{J/\psi} \end{cases} , \tag{12}$$

$d\Gamma_{\rm mag}/dE_\gamma$ and $d\Gamma_{\rm ele}/dE_\gamma$ are of equal order for $M_c\alpha_{\rm s} \gg E_\gamma \gg M_c\alpha_{\rm s}^2 \sim -E_{J/\psi}$; the magnetic contribution dominates for $-E_{J/\psi} \sim M_c\alpha_{\rm s}^2 \gg E_\gamma \gg M_c\alpha_{\rm s}^4 \sim M_{J/\psi}-M_{\eta_c}$; it also dominates by a factor $E_{J/\psi}^2/(M_{J/\psi}-M_{\eta_c})^2 \sim 1/\alpha_{\rm s}^4$ for $E_\gamma \ll M_c\alpha_{\rm s}^4 \sim M_{J/\psi}-M_{\eta_c}$. In practice, since $|a(E_{J/\psi})|^2 \approx 0.075$, the magnetic dipole transition $J/\psi \to \eta_c\,\gamma \to X\,\gamma$ is the dominant process over the whole range 0 MeV $\leqslant E_\gamma \lesssim$ 500 MeV.

(iii) Fragmentation
Fragmentation and other background processes are typically modeled and fitted to the data.

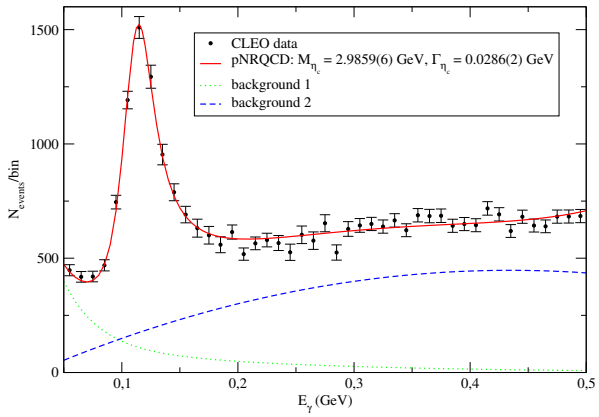

Figure 7: Fit of $d(\Gamma_{\rm mag}+\Gamma_{\rm ele})/dE_\gamma$ plus background [33] on the CLEO data of [34].

Fitting (9) plus (11) plus background on the CLEO data of [34], we get Fig. 7 [33]. The line-shape parameters are

$$M_{\eta_c} = 2985.9 \pm 0.6\,(\text{fit})\,\text{MeV}\,, \qquad \Gamma_{\eta_c} = 28.6 \pm 0.2\,(\text{fit})\,\text{MeV}\,, \tag{13}$$

where theoretical errors have not been included. Besides M_{η_c} and Γ_{η_c} the fitting parameters are the overall normalization, the signal normalization, and (three) background parameters.

A study of electric transition in quarkonium in pNRQCD has been presented in [35].

5 $\Upsilon(1S)$ thermal width for $T \lesssim 2T_c$

The bottomonium vector ground state, $\Upsilon(1S)$, produced in heavy-ion collisions at the LHC may possibly realize the hierarchy [36] (see also [37])

$$M_b \approx 5\,\text{GeV} \;>\; M_b\alpha_{\rm s} \approx 1.5\,\text{GeV} \;>\; \pi T \approx 1\,\text{GeV} \;>\; M_b\alpha_{\rm s}^2 \approx 0.5\,\text{GeV} \;\gtrsim\; m_D, \Lambda_{\rm QCD}\,,$$

where T is the temperature of the QCD plasma created by the collisions. A temperature T, such that πT is of the order of 1 GeV, is about twice the critical temperature of the quark-gluon plasma formation, T_c; m_D stands for the next-relevant thermal scale: the Debye mass. Studies of the $\Upsilon(1S)$ properties and, in particular, of its width in the above conditions are very timely because signals of bottomonium dissociation have just been seen by the CMS experiment [38].

According to the above hierarchy, the bound state is weakly coupled, the temperature is lower than $M_b\alpha_{\rm s}$, implying that the bound state is mainly Coulombic, and the effects due to the scale $\Lambda_{\rm QCD}$ and to the other thermodynamical scales may be neglected.

Integrating out T from pNRQCD modifies pNRQCD into pNRQCD$_{\rm HTL}$ (see Fig. 1), whose Yang–Mills Lagrangian gets an additional hard thermal loop (HTL) part [39] and potentials

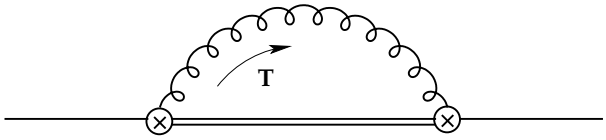

Figure 8: Leading thermal contribution to the singlet propagator from the scale T.

get additional thermal corrections. One effect of the HTL part is to give a mass, m_D, to the temporal gluons. The leading thermal contribution to the potential is encoded in the diagram of Fig. 8, where thermal gluons couple to the singlet through chromoelectric dipole vertices (the difference with the diagram in Fig. 3 is in the gluon propagator). The loop momentum region is taken to be $k_0 \sim T$ and $k \sim T$.

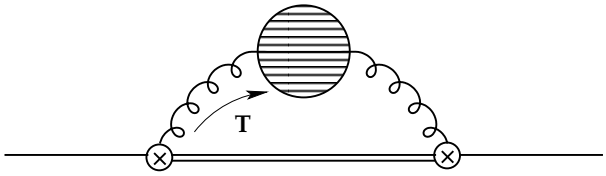

Figure 9: Gluon self-energy correction to the diagram of Fig. 8.

The gluon self-energy correction to the diagram in Fig. 8 is shown in Fig. 9. This diagram has an imaginary part that contributes to the thermal width of the state:

$$\Gamma_{1S}^{(T)} = \left[-\frac{4}{3}\alpha_s T m_D^2 \left(-\frac{2}{\epsilon} + \gamma_E + \ln\pi - \ln\frac{T^2}{\mu^2} + \frac{2}{3} - 4\ln 2 - 2\frac{\zeta'(2)}{\zeta(2)}\right) - \frac{32\pi}{3}\,\alpha_s^2\, T^3\, \ln 2\right] a_0^2\,, \tag{14}$$

where $a_0 = \dfrac{3}{2M_b\alpha_s}$. The width is infrared (IR) divergent; the divergence has been regularized in dimensional regularization ($D = 4 + \epsilon$).

The origin of this thermal width may be traced back to the Landau-damping phenomenon, i.e. the scattering of heavy quarks with hard space-like particles in the medium (see Fig. 10). The Landau-damping phenomenon plays a crucial role in quarkonium dissociation [40]. It is when $\mathrm{Im}\, V_s(r)|_{\mathrm{Landau-damping}} \sim \mathrm{Re}\, V_s(r) \sim \alpha_s/r$ that the quarkonium dissociates. The dissociation temperature is parametrically given by $\pi T_{\mathrm{dissociation}} \sim M_b g^{4/3}$. Note that the interaction is screened when $1/r \sim m_D$ and that in the weak coupling ($m_D \sim gT$) $\pi T_{\mathrm{screening}} \sim M_b g \gg \pi T_{\mathrm{dissociation}}$. The typical dissociation temperature, $T_{\mathrm{dissociation}}$, for the $\Upsilon(1S)$ is about 450 MeV [9], which implies that a temperature, T, such that πT is about 1 GeV, is below the dissociation temperature.

Integrating out the energy scale E from pNRQCD$_{\mathrm{HTL}}$ provides corrections to the mass and width of the quarkonium in the thermal bath. The leading diagram is shown in Fig. 11,

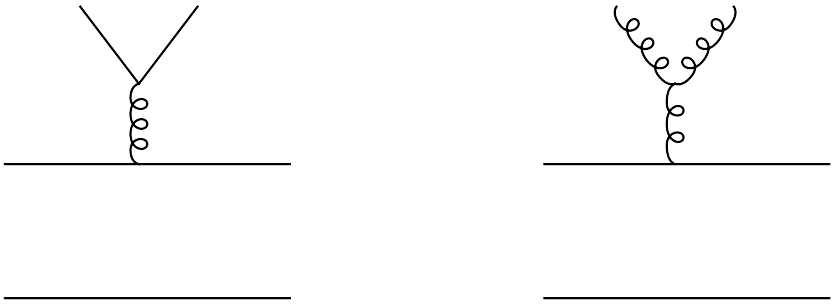

Figure 10: Landau-damping scatterings.

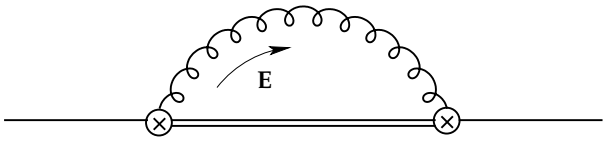

Figure 11: Leading thermal contribution to the singlet propagator from the scale E. Gluons are HTL gluons.

where HTL gluons couple to the singlet through chromoelectric dipole vertices. The loop momentum region is taken to be $k_0 \sim E$ and $k \sim E$. For $E \gg m_D, \Lambda_{\rm QCD}$, the contribution to the thermal width of the $\Upsilon(1S)$ is given by

$$\begin{aligned}\Gamma_{1S}^{(E)} &= 4\alpha_{\rm s}^3 T - \frac{64}{9M_b}\alpha_{\rm s} T E_1 + \frac{32}{3}\alpha_{\rm s}^2 T \frac{1}{M_b a_0} + \frac{7225}{162}E_1\alpha_{\rm s}^3 \\ &\quad -\frac{4\alpha_{\rm s} T m_D^2}{3}\left(\frac{2}{\epsilon} + \ln\frac{E_1^2}{\mu^2} + \gamma_E - \frac{11}{3} - \ln\pi + \ln 4\right) a_0^2 + \frac{128\alpha_{\rm s} T m_D^2}{81}\frac{\alpha_{\rm s}^2}{E_1^2} I_{1,0}\,, \end{aligned} \tag{15}$$

where $E_1 = -\dfrac{4M_b\alpha_{\rm s}^2}{9}$ and $I_{1,0} = -0.49673$ (similar to the Bethe logarithm). The width is ultraviolet (UV) divergent. Note that the UV divergence of (15) cancels against the IR divergence of (14).

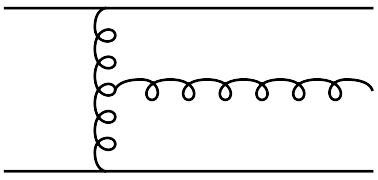

Figure 12: Singlet-to-octet break up diagram.

The thermal width $\Gamma_{1S}^{(E)}$, which is of order $\alpha_{\rm s}^3 T$, is generated by the break up of a quark-antiquark colour-singlet state into an unbound quark-antiquark colour-octet state (see e.g.

Fig. 12): a process that is kinematically allowed only in a medium. The singlet to octet break up is, therefore, a different phenomenon with respect to the Landau damping. In the situation $M_b\alpha_s^2 \gg m_D$, the first dominates over the second by a factor $(M_b\alpha_s^2/m_D)^2$ [5].

The complete thermal width up to $\mathcal{O}(m\alpha_s^5)$ is [8]:

$$\begin{aligned}\Gamma_{1S}^{(\text{thermal})} &= \Gamma_{1S}^{(T)} + \Gamma_{1S}^{(E)} = \frac{1156}{81}\alpha_s^3 T + \frac{7225}{162}E_1\alpha_s^3 + \frac{32}{9}\alpha_s\, T m_D^2\, a_0^2\, I_{1,0} \\ &\quad - \left[\frac{4}{3}\alpha_s T m_D^2\left(\ln\frac{E_1^2}{T^2} + 2\gamma_E - 3 - \ln 4 - 2\frac{\zeta'(2)}{\zeta(2)}\right) + \frac{32\pi}{3}\,\alpha_s^2\, T^3\,\ln 2\right] a_0^2\,. \end{aligned} \tag{16}$$

The width is an observable, therefore, finite and scheme independent. The logarithm, $\ln E_1^2/T^2$, is a relic of the cancellation between the IR divergence at the scale T and the UV divergence at the scale E.

6 Conclusions

Our understanding of the theory of quarkonium has dramatically improved over the last fifteen years. An unified picture has emerged that is able to describe large classes of observables for quarkonium in the vacuum and in a medium. For the ground state, precision physics is possible and lattice data provide often a crucial complement. In the case of quarkonium in a hot medium, systematic treatments have disclosed new phenomena that may eventually be responsible for the quarkonium suppression observed in heavy-ion collisions.

Acknowledgments

I acknowledge financial support from the DFG cluster of excellence "Origin and structure of the universe" (www.universe-cluster.de) and from the DFG project BR4058/1-1 "Effective field theories for strong interactions with heavy quarks".

Bibliography

[1] N. Brambilla *et al.*, Heavy quarkonium physics, CERN-2005-005, (CERN, Geneva, 2005) [arXiv:hep-ph/0412158].

[2] N. Brambilla, A. Pineda, J. Soto and A. Vairo, Rev. Mod. Phys. **77**, 1423 (2005) [arXiv:hep-ph/0410047].

[3] T. Matsui and H. Satz, Phys. Lett. B **178**, 416 (1986).

[4] Talk by M. Laine at this conference, arXiv:1108.5965 [hep-ph].

[5] N. Brambilla, J. Ghiglieri, A. Vairo and P. Petreczky, Phys. Rev. D **78**, 014017 (2008) [arXiv:0804.0993 [hep-ph]].

[6] M. A. Escobedo and J. Soto, Phys. Rev. A **78**, 032520 (2008) [arXiv:0804.0691 [hep-ph]].

[7] A. Vairo, PoS **CONFINEMENT8**, 002 (2008) [arXiv:0901.3495 [hep-ph]].

[8] N. Brambilla, M. A. Escobedo, J. Ghiglieri, J. Soto and A. Vairo, JHEP **1009**, 038 (2010) [arXiv:1007.4156 [hep-ph]].

[9] M. A. Escobedo and J. Soto, Phys. Rev. A **82**, 042506 (2010) [arXiv:1008.0254 [hep-ph]].

[10] W. E. Caswell and G. P. Lepage, Phys. Lett. B **167**, 437 (1986).

[11] G. T. Bodwin, E. Braaten and G. P. Lepage, Phys. Rev. D **51**, 1125 (1995) [Erratum-ibid. D **55**, 5853 (1997)].

[12] Talk by M. Butenschön at this conference, arXiv:1109.1740 [hep-ph].

[13] A. Pineda and J. Soto, Nucl. Phys. Proc. Suppl. **64**, 428 (1998) [arXiv:hep-ph/9707481].

[14] N. Brambilla, A. Pineda, J. Soto and A. Vairo, Nucl. Phys. B **566**, 275 (2000) [arXiv:hep-ph/9907240].

[15] N. Brambilla *et al.*, Eur. Phys. J. C **71**, 1534 (2011) [arXiv:1010.5827 [hep-ph]].

[16] L. Susskind, In Les Houches 1976, Proceedings, Weak and Electromagnetic Interactions At High Energies, 207-308 (Amsterdam, 1977).

[17] Y. Schröder, Phys. Lett. B **447**, 321 (1999) [arXiv:hep-ph/9812205].

[18] N. Brambilla, A. Pineda, J. Soto and A. Vairo, Phys. Rev. D **60**, 091502 (1999).

[19] C. Anzai, Y. Kiyo and Y. Sumino, Phys. Rev. Lett. **104**, 112003 (2010).

[20] A. V. Smirnov, V. A. Smirnov and M. Steinhauser, Phys. Rev. Lett. **104**, 112002 (2010).

[21] B. A. Kniehl, A. A. Penin, Y. Schröder, V. A. Smirnov and M. Steinhauser, Phys. Lett. B **607**, 96 (2005) [arXiv:hep-ph/0412083].

[22] N. Brambilla, J. Ghiglieri, P. Petreczky, A. Vairo, Phys. Rev. **D82**, 074019 (2010). [arXiv:1007.5172 [hep-ph]].

[23] N. Brambilla, X. Garcia i Tormo, J. Soto and A. Vairo, Phys. Lett. B **647**, 185 (2007).

[24] M. Eidemüller and M. Jamin, Phys. Lett. B **416**, 415 (1998) [arXiv:hep-ph/9709419].

[25] W. Fischler, Nucl. Phys. B **129**, 157 (1977).

[26] A. Billoire, Phys. Lett. B **92**, 343 (1980).

[27] A. Pineda and J. Soto, Phys. Lett. B **495**, 323 (2000).

[28] N. Brambilla, X. Garcia i Tormo, J. Soto and A. Vairo, Phys. Rev. D **80**, 034016 (2009) [arXiv:0906.1390 [hep-ph]].

[29] N. Brambilla, X. Garcia i Tormo, J. Soto and A. Vairo, Phys. Rev. Lett. **105**, 212001 (2010) [arXiv:1006.2066 [hep-ph]].

[30] S. Necco and R. Sommer, Nucl. Phys. B **622**, 328 (2002).

[31] N. Brambilla, Y. Jia and A. Vairo, Phys. Rev. D **73**, 054005 (2006) [arXiv:hep-ph/0512369].

[32] M. B. Voloshin, Mod. Phys. Lett. A **19**, 181 (2004).

[33] N. Brambilla, P. Roig and A. Vairo, AIP Conf. Proc. **1343**, 418 (2011) [arXiv:1012.0773 [hep-ph]]; TUM-EFT 26/11, in preparation.

[34] R. E. Mitchell *et al.* [CLEO Collaboration], Phys. Rev. Lett. **102**, 011801 (2009) [Erratum-ibid. **106**, 159903 (2011)] [arXiv:0805.0252 [hep-ex]].

[35] Talk by P. Pietrulewicz at this conference, TUM-EFT 24/11; N. Brambilla, P. Pietrulewicz and A. Vairo, TUM-EFT 25/11, in preparation.

[36] A. Vairo, AIP Conf. Proc. **1317**, 241 (2011) [arXiv:1009.6137 [hep-ph]].

[37] Talk by J. Ghiglieri at this conference, arXiv:1108.5875 [hep-ph].

[38] C. Silvestre for the CMS collaboration, arXiv:1108.5077 [hep-ex].

[39] E. Braaten and R. D. Pisarski, Phys. Rev. D **45**, 1827 (1992).

[40] M. Laine, O. Philipsen, P. Romatschke and M. Tassler, JHEP **0703**, 054 (2007) [arXiv:hep-ph/0611300].

Highlights from BESIII experiment

Hai-Bo Li[1] on behalf of the BESIII Collaboration
Institute of High Energy Physics
Bejing 100049, China

BESIII had collected large data samples on J/ψ and ψ' peaks during the first run in 2009. From 2010 to 2011, about 2.9 fb^{-1} integrated luminosity were obtained on the peak of $\psi(3770)$ for open charm physics. We review recent results on charmonium decays and hadron spectroscopy. The prospects on open charm physics are also discussed.

1 Introduction

The newly built BEPCII/BESIII is an upgrade to the previous BEPC/BES [1]. The BEPCII is a double ring collider with a design luminosity of $1 \times 10^{33}\text{cm}^{-2}\text{s}^{-1}$ at a center-of-mass energy of 3.78 GeV, which luminosity is one order of higher than that at CESR-c. It is operating between 2.0 and 4.6 GeV in the center of mass. The BESIII experiment is used to study the charm and τ physics. It is foreseen to collect on the order of 10 billion J/ψ events or 3 billion $\psi(2S)$ events per year according to the designed luminosity. About 32 million $D\overline{D}$ pairs and 2.0 million $D_S\overline{D}_S$ at threshold will be collected per year [1]. In last run, the peak luminosity of BEPCII has reached $6.4 \times 10^{32}\text{cm}^{-2}\text{s}^{-1}$.

The BESIII detector [1] consists of the following main components: 1) a main draft chamber (MDC) equipped with about 6500 signal wires and 23000 field wires arranged as small cells with 43 layers. The designed single wire resolution is 130 μm and the momentum resolution 0.5% at 1 GeV; 2) an electromagnetic calorimeter(EMC) made of 6240 CsI(Tl) crystals. The designed energy resolution is 2.5%@1.0 GeV and position resolution 6mm@1.0 GeV; 3) a particle identification system using Time-Of-Flight counters made of 2.4 m long plastic scintillators. The designed resolution is 80 ps for two layers, corresponding to a K/π separation (2σ level) up to 0.8 GeV; 4)a superconducting magnet with a field of 1 tesla; 5) a muon chamber system made of Resistive Plate Chambers(RPC).

In 2009, the BESIII had collected about 225 M and 106M data set on the J/ψ and ψ' peaks, respectively. About 2.9 fb^{-1} integrated luminosity on the $\psi(3770)$ peak had been accumulated for open charm physics, and the data size is about 3.5 times of that at CLEO-c. The results in this paper is based above data set.

[1] lihb@ihep.ac.cn

2 Highlights from BESIII

The BESIII collaboration has published so-far a variety of papers with many new results in the field of light hadron and charmonium spectroscopy, as well as charmonium decays [2–11]. A number of new hadronic states were discovered or confirmed, and various decay properties were measured for the first time. In addition, many data analyses are in an advanced stage and will lead to a rich set of new publications in the near future. Here, we show recent highlights from the BESIII, thereby, illustrating the potential of the BESIII experiment. In this paper, for the reported experimental results, the first error and second error will be statistical and systematic, respectively, if they are not specified.

2.1 $\eta_c(1S)$ resonance via $\psi' \to \gamma\eta_c$ decay

Precise measurement of M1 transition of ψ' is important for us to understand the QCD in the relativistic and nonperturbative regimes. The $\psi' \to \gamma\eta_c$ transition is also a source of information on the η_c mass and width. There is currently a 3.3 σ inconsistency in previous η_c mass measurements from J/ψ and $\psi' \to \gamma\eta_c$ (averaging 2977.3 ± 1.3 MeV/c^2) compared to $\gamma\gamma$ or $p\overline{p}$ production (averaging 2982.6 ± 1.0 MeV/c^2) [12]. The width measurements also spread from 15 to 30 MeV, it is around 10 MeV in the earlier days of experiments using J/ψ radiative transition [13, 14], while the recent experiments, including photon-photon fusion and B decays, gave higher mass and much wider width [15–18]. The most recent study by the CLEO-c experiment [19], using both ψ' and J/$\psi \to \gamma\eta_c$ decays, and pointed out there was a distortion of the η_c line shape. CLEO-c attributed the η_c line-shape distortion to the energy-dependence of the M1 transition matrix element. In the $J/\psi \to \gamma\eta_c$ from CLEO-c, the distorted η_c lineshape can be described by the relativistic Breit-Wigner (BW) distribution modified by a factor of E_γ^3 together with a dumping factor to suppress the tail on the higher photon energies. KEDR Collaboration did the same thing but tried different dumping factor [20].

Based on the data sample of 106 M ψ' events collected with BESIII detector, the η_c mass and width are measured from the radiative transition $\psi' \to \gamma\eta_c$. The η_c candidates are reconstructed from six exclusive decay modes: $K_sK\pi$, $K^+K^-\pi^0$, $\eta\pi^+\pi^-$, $K_sK^+\pi^-\pi^+\pi^-$, $K^+K^-\pi^+\pi^-\pi^0$, and $3(\pi^+\pi^-)$, where K_s is reconstructed in $\pi^+\pi^-$ mode, η and π^0 from $\gamma\gamma$ final states. For a hindered M1 transition the matrix element acquires terms proportional to E_γ^2, which, when combined with the usual E_γ^3 term for the allowed transitions, lead to contributions in the radiative width proportional to E_γ^7. Thus, the η_c lineshape is described by a BW modified by E_γ^7 convoluted with a resolution function. It is important to point out that the interference between η_c and non-resonance in the signal region is also considered. The statistical significance of the interference is 15 σ. This affects the η_c resonant parameters significantly. Assuming an universal relative phase between the two amplitudes, we obtain η_c mass and width, $M = 2984.2 \pm 0.6 \pm 0.5$ MeV/c^2 and $\Gamma = 31.4 \pm 1.2 \pm 0.6$ MeV, respectively, as well as the relative phase $\phi = 2.41 \pm 0.06 \pm 0.04$ rad. Figure 1 shows the

fit results in the six η_c decay modes. With precise measurement of the η_c mass, one can obtain the hyperfine splitting, $\Delta M_{hf}(1S)_{c\bar{c}} \equiv= M(J/\psi) - M(\eta_c) = 112.5 \pm 0.8$ MeV, which agrees with the quark model prediction [21], and will be helpful for understanding the spin-dependent interactions in hidden quarkonium states.

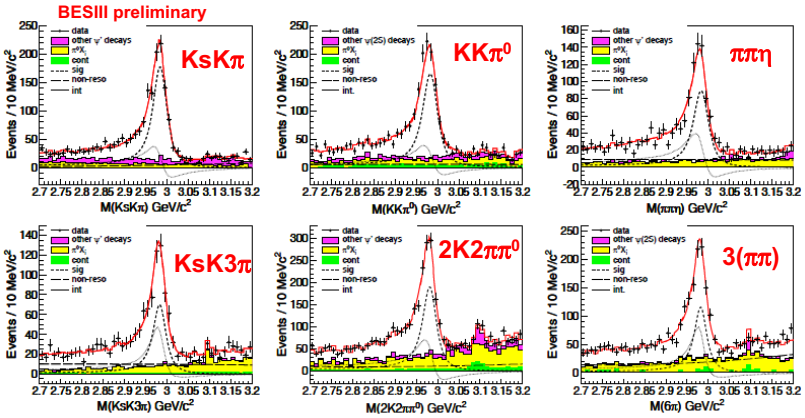

Figure 1: The invariant mass distributions for the decays $K_sK\pi$, $K^+K^-\pi^0$, $\eta\pi^+\pi^-$, $K_sK^+\pi^-\pi^+\pi^-$, $K^+K^-\pi^+\pi^-\pi^0$, and $3(\pi^+\pi^-)$, respectively. Solid curves show the fitting results; the fitting components (η_c signal/non-resonance/interference) are shown as (dashed/long-dashed/dotted) curves. Points with error bar are data, shaded histograms are (in green/yellow/magenta) for (continuum/other η_c decays/other ψ' decays) backgrounds.

2.2 Observation of $\psi' \to \gamma\eta_c(2S)$

The first radially excited S-wave spin singlet state in the charmonium system, $\eta_c(2S)$, was observed by the Belle Collaboration in the decay process $B^\pm \to K^\pm\eta_c(2S)$, $\eta_c(2S) \to K_sK^\pm\pi^\mp$ [22]. It was confirmed by the CLEO [23] and BABAR [24] Collaborations in the two-photon fusion process $e^+e^- \to e^+e^-(\gamma\gamma), \gamma\gamma \to \eta_c(2S) \to K_sK^\pm\pi^\mp$ and by the BABAR Collaboration in the double-charmonium production process $e^+e^- \to J/\psi(c\bar{c})$ [25]. The only evidence for $\eta_c(2S)$ in the $\psi' \to \gamma\eta_c(2S)$ decay was from Crystal Ball Collaboration [26] by looking at the radiative photon spectrum. Recently, CLEO-c Collaboration searched for the $\psi' \to \gamma\eta_c(2S)$ signal with $\eta_c(2S)$ exclusive decay into 11 modes by using 25.9 M ψ' events, and no evidence found. Product branching fraction upper limits are determined as a function of $\Gamma(\eta_c(2S))$ for the 11 individual modes [27].

Using the largest ψ' data sample in the world which was collected by the BESIII, we searched for the M1 transition $\psi' \to \gamma\eta_c(2S)$ through the hadronic final states $K_sK^\pm\pi^\mp$. A bump is observed around 3635 MeV on the mass spectrum as shown in Fig. 2. In order to determine the background and mass resolution using data, the mass spectrum range is enlarged ($3.47 \sim 3.72$ GeV/c^2) to include χ_{c1} and χ_{c2} events. The resonances χ_{c1} and χ_{c2}

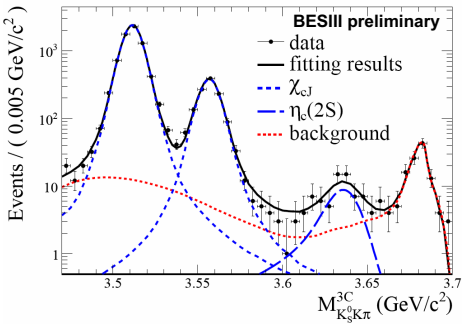

Figure 2: Fitting of the mass spectrum for $\eta_c(2S) \to K_s K^{\pm}\pi^{\mp}$.

are described by the corresponding Monte Carlo (MC) shape convolved a Gaussian which takes account the small difference on the mass shift and resolution between data and MC. So the mass resolution for the $\eta_c(2S)$ in the fitting is fixed to the linear extrapolation of the mass resolutions from the χ_{c1} and χ_{c2} signals in data. The line shape for $\eta_c(2S)$ produced by such the M1 transition is described by $(E_\gamma^3 \times BW(m) \times damping(E_\gamma)) \otimes Gauss(0,\sigma)$ where m is the invariant mass of $K_s K^{\pm}\pi^{\mp}$, $E_\gamma = \frac{m^2_{\psi'}-m^2}{2m^2_{\psi'}}$ is the energy of the transition photon in the rest frame of ψ', $damping(E_\gamma)$ is the function to damp the diverging tail raised by E_γ^3 and $Gauss(0,\sigma)$ is the Gaussian function describing the detector resolution. The possible form of the damping function is somewhat arbitrary, and one suitable function used by KEDR for a similar process is [20]

$$\frac{E_0^2}{E_\gamma E_0 + (E_\gamma E_0 - E_0)^2}$$

where $E_0 = \frac{m^2_{\psi'}-m^2_{\eta_c(2S)}}{2m^2_{\psi'}}$ is the peaking energy of the transition photon. In the fit, the width of $\eta_c(2S)$ is fixed to PDG value. From the fit to the data, a signal with a statistical significance of 6.5 standard deviation is observed which is the first observation of the M1 transition $\psi' \to \gamma\eta_c(2S)$. The measured mass for $\eta_c(2S)$ is $3638.5 \pm 2.3 \pm 1.0$ MeV/c^2. The measured branching ratio is $BR(\psi' \to \gamma\eta_c(2S)) \times BR(\eta_c(2S) \to K_s K^{\pm}\pi^{\mp}) = (2.98 \pm 0.57 \pm 0.48) \times 10^{-6}$. Together with the BABAR result $BR(\eta_c(2S) \to K\overline{K}\pi) = (1.9 \pm 0.4 \pm 1.1)\%$ [28], the M1 transition rate for $\psi' \to \gamma\eta_c(2S)$ is derived as $BR(\psi' \to \gamma\eta_c(2S)) = (4.7 \pm 0.9 \pm 3.0) \times 10^{-4}$.

Most recently, the Belle Collaboration measured $\eta_c(1S)$ and $\eta_c(2S)$ resonant parameters in the decay of $B^{\pm} \to K^{\pm}(K_s K\pi)^0$ by considering the interference between $\eta_c(1S)/\eta_c(2S)$ decay and non-resonant in the $B^{\pm}$ decay [30]. Meanwhile, the BABAR Collaboration also updated the analysis of $e^+e^- \to e^+e^-(\gamma\gamma), \gamma\gamma \to \eta_c(1S)/\eta_c(2S) \to (K_s K\pi)^0$ and $K^+K^-\pi^+\pi^-\pi^0$ modes [31]. Table 1 shows the summary of the typical production processes (ψ' radiative decays, $\gamma\gamma$ fusion and B decays) for $\eta_c(1S)/\eta_c(2S)$ and corresponding resonant parameter measurements. These results indicate that the $\eta_c(1S)$ parameters agree well from different

	BESIII [29] $\psi' \to \gamma\eta_c/\eta_c(2S)$	Belle [30] B decays	BABAR [31] $\gamma\gamma$ fusion	PDG 2010 [12]
$M(\eta_c(1S))$ MeV/c^2	$2984.4 \pm 0.5 \pm 0.6$	$2985.4 \pm 1.5^{+0.2}_{-2.0}$	$2982.2 \pm 0.4 \pm 1.4$	2980.3 ± 1.2
$\Gamma(\eta_c(1S))$ MeV	$30.5 \pm 1.0 \pm 0.9$	$35.1 \pm 3.1^{+1.0}_{-1.6}$	$32.1 \pm 1.1 \pm 1.3$	28.6 ± 2.2
$M(\eta_c(2S))$ MeV/c^2	$3638.5 \pm 2.3 \pm 1.0$	$3636.1^{+3.9+0.5}_{-1.5-2.0}$	$3638.5 \pm 1.5 \pm 0.8$	3637 ± 4
$\Gamma(\eta_c(2S))$ MeV	12 (fixed)	$6.6^{+8.4+2.6}_{-5.1-0.9}$	$13.4 \pm 4.6 \pm 3.2$	14 ± 7

Table 1: Comparison of the mass and width for $\eta_c(1S)/\eta_c(2S)$ in different production processes, $\psi' \to \gamma\eta_c(1S)/\eta_c(2S)$, $B^{\pm} \to K^{\pm}\eta_c(1S)/\eta_c(2S)$ and $\gamma\gamma$ fusion, from different experiments. The PDG values are only world average from earlier results. . For the time being, the most precise measurements for $\eta_c(1S)$ resonance are from BESIII, while these for $\eta_c(2S)$ resonant parameters are from BABAR in $\gamma\gamma$ fusion.

production processes.

2.3 $h_c(1P)$ properties

The BESIII Collaboration reported the results on the production and decay of the h_c using 106M of ψ' decay events in 2010 [2], where we studied the distributions of mass recoiling against a detected π^0 to measure $\psi' \to \pi^0 h_c$ both inclusively (E1-untagged) and in events tagged as $h_c \to \gamma\eta_c$ (E1-tagged) by detection of the E1 transition photon. In 2011, 16 specific decay modes of η_c are used to reconstruct η_c candidates in the decay mode of $h_c \to \gamma\eta_c$. Figure 3 shows the π^0 recoiling mass for individual η_c decay modes in the decay chain of $\psi' \to \pi^0 h_c$, $h_c \to \gamma\eta_c$, while Fig. 4 is the sum of the 16 decay modes. We fit the 16 π^0 recoil-mass spectra simultaneously that yields $M(h_c) = 3525.31 \pm 0.11(stat.) \pm 0.15(syst.)$ MeV/c^2 and $\Gamma(h_c) = 0.70 \pm 0.28(stat.) \pm 0.25(syst.)$ MeV/c^2. These preliminary results are consistent with the previous BESIII inclusive results and CLEO-c exclusive results.

The centroid of the ^3P_J states (χ_{c0},χ_{c1},χ_{c2}) is known to be $\langle M(^3P_J)\rangle = [5M(^3P_2) + 3M(^3P_1) + M(^3P_0)] = 3525.30 \pm 0.04$ MeV [12]. If the ^3P_J states centroid mass $\langle M(^3P_J)\rangle$ is identified as the mass of $M(^3P)$, then BESIII observes the hyperfine splitting as $\Delta M_{hf}(1P)_{cc} = -0.01 \pm 0.11(stat.) \pm 0.14(syst.)$ MeV which agrees with zero.

We also look at the $\eta_c(1S)$ mass distributions in the exclusive decay modes. Figure 5 shows the distribution of invariant mass distribution from exclusive hadronic decays of $\eta_c(1S)$, the shape of the η_c is symmetric in $h_c(1P) \to \gamma\eta_c(1S)$ radiative transition and no distortion observed as in $J/\psi/\psi'$ radiative decays. The analysis is still on going for the resonant parameters.

2.4 The radiative decays $\psi' \to \gamma P$ with $P = \{\pi^0, \eta, \eta'\}$

The radiative decay of the ψ' to a pseudo-scalar meson, such as the π^0, η, and η', is of interest since it can be used to study the two-gluon coupling to $c\bar{c}$ states, to study the

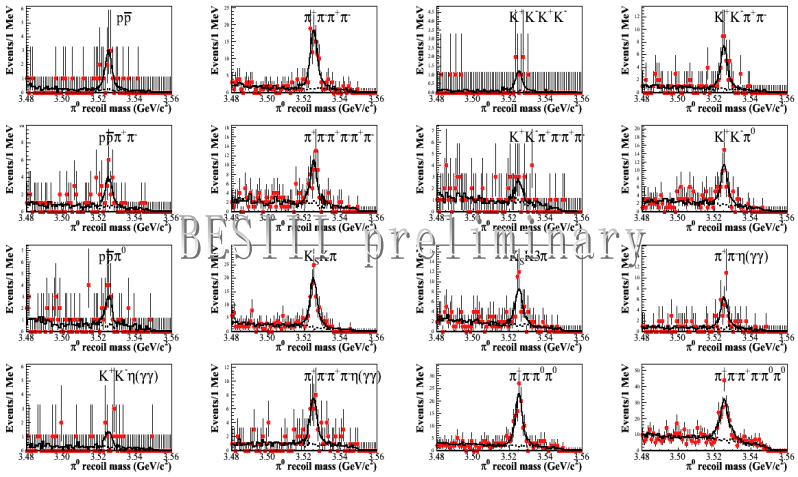

Figure 3: The π^0 recoiling mass for 16 η_c decay modes.

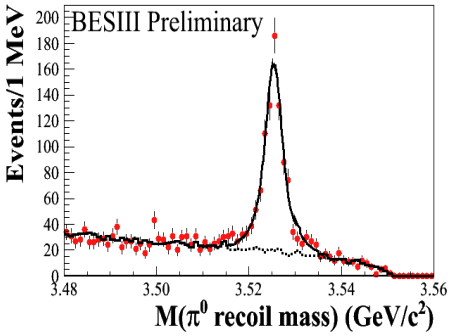

Figure 4: The π^0 recoiling mass for the sum of 16 η_c decay modes.

$\eta - \eta'$ mixing angle, and to probe the π° form factor in the time-like region. Recently, the CLEO-c Collaboration reported measurements for the decays of J/ψ, ψ', and ψ'' to γP [32], and no evidence for $\psi' \to \gamma\eta$ or $\gamma\pi^0$ was found. With 106M ψ' data sample at BESIII, the processes $\psi' \to \gamma\pi^0$ and $\psi' \to \gamma\eta$ are observed for the first time with signal significances of 4.6σ and 4.3σ, respectively, and with branching fractions of $B(\psi' \to \gamma\pi^0) = (1.58 \pm 0.40 \pm 0.13) \times 10^{-6}$ and $B(\psi' \to \gamma\eta) = (1.38 \pm 0.48 \pm 0.09) \times 10^{-6}$. With a measured branching fraction, $B(\psi' \to \gamma\eta') = (126 \pm 3 \pm 8) \times 10^{-6}$. The mass distributions of the pseudo-scalar meson candidates can be found in Fig. 6 the BESIII Collaboration determined for the first time the ratio of the η and η' production rates from ψ' decays, $R_{\psi'} \equiv B(\psi' \to \gamma\eta)/B(\psi' \to \gamma\eta') = (1.10 \pm 0.38 \pm 0.07)\%$. This ratio is below the 90% C.L. upper bound determined by the CLEO-c Collaboration and, in contradiction to predictions of leading-order perturbative-QCD, one order of magnitude smaller than the corresponding ratio for the J/ψ decays, $R_{J/\psi} = (21.1 \pm 0.9)\%$. More details on the data analysis can be found

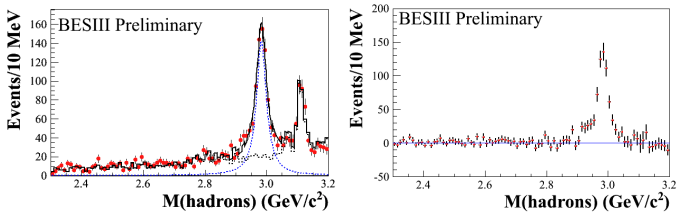

Figure 5: The invariant mass distributions for the sum of 16 η_c decay modes. Right is background subtracted.

in Ref. [3]. These observations are interpreted in the framework of vector meson dominance (VMD) in association with the $\eta_c - \eta(\eta')$ mixings due to the axial gluonic anomaly [33].

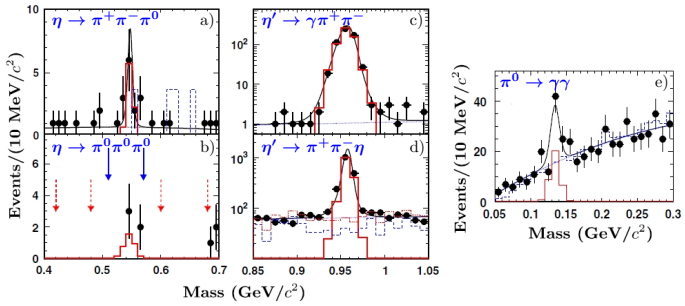

Figure 6: Mass distributions of the pseudo-scalar meson candidates for $\psi' \to \gamma P$: a) $P = \eta(\to \pi^+\pi^-\pi^0)$; b) $P = \eta(\to 3\pi^0)$; c) $P = \eta'(\to \gamma\pi^+\pi^-)$; d) $P = \eta'(\to \pi^+\pi^-\eta(\to \gamma\gamma))$; d) $P = \pi^\circ(\to \gamma\gamma)$. For more details, we refer to Ref. [3].

2.5 Measurements of $J/\psi \to N\overline{N}$ branching fractions

The expected three main contributions to the decay $J/\psi \to N\overline{N}$ are shown in Fig. 7. This decay mode should be a very good test of PQCD, because of the 3 gluons in the OZI violating J/ψ strong decay just matching the 3 $(q\bar{q})$ pairs (as in Fig. 7(a)). The ratio between $BR(J/\psi \to n\overline{n})$ and $BR(J/\psi \to p\overline{p})$ strongly depends on the phase between the strong and the electromagnetic (e.m.) contributions as shown in Fig. 7 [34]. According to PDG values, $BR(J/\psi \to n\overline{n})$ is very similar to $BR(J/\psi \to p\overline{p})$, which gives a clear indication that strong and e.m. contributions do not interfere and have to be added in quadrature. An estimate for the relative phase ϕ on the basis of previous experimental results is $\phi = 89^o \pm 15^o$ [34]. However, the current experimental uncertainty on $BR(J/\psi \to n\overline{n})$ is still large $[(2.2 \pm 0.4) \times 10^{-3}]$, which is main contribution to the uncertainty on the phase determination. Therefore, it motivates the BESIII experiment to measure $J/\psi \to n\overline{n}$ decay rate with high statistical J/ψ sample.

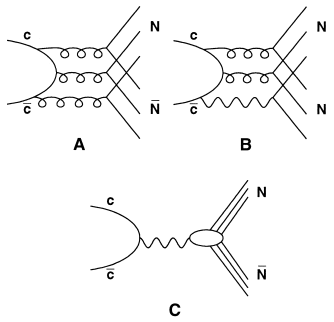

Figure 7: Feynman diagrams of the three main contributions to the J/ψ decay in nucleon-antinucleon. A) purely strong amplitude, B) strong-electromagnetic amplitude and C) purely electromagnetic amplitude. These plots are from reference [34]

Based on 225M J/ψ events collected at BESIII, the anti-neutron is identified by shower energy deposition and hit information in EMC, with constraints of known center-of-mass energy and back-to-back between neutron and anti-neutron, the branching ratio is determined to be $BR(J/\psi \to n\bar{n}) = (2.07 \pm 0.01 \pm 0.17) \times 10^{-3}$. At the same time, the branching ratio for $J/\psi \to p\bar{p}$ is determined to be $BR(J/\psi \to p\bar{p}) = (2.112 \pm 0.004 \pm 0.027) \times 10^{-3}$. These result improve by a large factor comparing to the previous measurements and strongly support the orthogonal phase of strong and e.m. amplitudes.

2.6 η' and $\eta(1405)$ in J/$\psi \to \gamma\pi\pi\pi$ decays

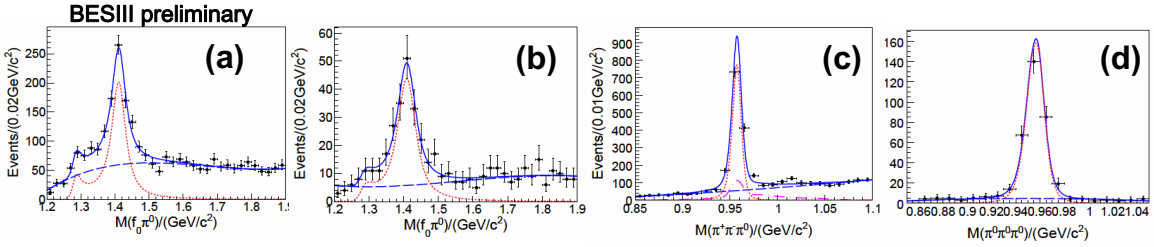

Figure 8: The invariant mass distributions: (a) invariant mass of $f_0(980)\pi^0$ from J/$\psi \to \gamma\pi^+\pi^-\pi^0$; (b) invariant mass of $f_0(980)\pi^0$ mass from J/$\psi \to \gamma\pi^0\pi^0\pi^0$; (c) the invariant mass of $\eta' \to 3\pi$s in J/$\psi \to \gamma\pi^+\pi^-\pi^0$, (d) mass of $\eta' \to 3\pi$s from J/$\psi \to \gamma\pi^0\pi^0\pi^0$, respectively.

The spectrum of radial excitation states of isoscalar η and η' is still not well known. An important issue is about the nature of $\eta(1405)$ and $\eta(1475)$ states, which are not well established. BESIII measured the decays of J/$\psi \to \gamma\pi^+\pi^-\pi^0$ and $\gamma\pi^0\pi^0\pi^0$. In the two decay modes, clear $f_0(980)$ signals are observed on both $\pi^+\pi^-$ and $\pi^0\pi^0$ spectra,

the width of observed $f_0(980)$ is much narrower ($\sim$ 10 MeV) than that in other processes [12]. By taking events in the window of $f_0(980)$ on the $\pi\pi$ mass spectrum, we observed evidence of $f_1(1285)$ in the low mass region of $f_0(980)\pi^0$ as shown in Fig. 8 (a) and (b), which corresponding to significance of about 4.8 σ for $f_1(1285) \to f_0(980)\pi^0$ in $f_0(980) \to \pi^+\pi^-$ mode (1.4 σ in $f_0(980) \to \pi^0\pi^0$). It is interesting that clear peak around 1400 MeV is also observed on the mass of $f_0(980)\pi^0$ (see Fig. 8 (a) and (b)). Preliminary angular analysis indicates that the peak on 1400 MeV is from $\eta(1405) \to f_0(980)\pi^0$ decay. BESIII measured the combined branching fraction of $\eta(1405)$ production to be $BR(J/\psi \to \gamma\eta(1405)) \times BR(\eta(1405) \to f_0(980)\pi^0) \times BR(f_0(980) \to \pi^+\pi^-) = (1.48 \pm 0.13 \pm 0.17) \times 10^{-5}$ and $BR(J/\psi \to \gamma\eta(1405)) \times BR(\eta(1405) \to f_0(980)\pi^0) \times BR(f_0(980) \to \pi^0\pi^0) = (6.99 \pm 0.93 \pm 0.95) \times 10^{-6}$, respectively. It is the first time that we observe anomalously large isospin violation in the strong decay of $\eta(1405) \to f_0(980)\pi^0$.

Following BESIII measurements, in reference [35], the authors interpret this puzzle as an intermediate on-shell $K\overline{K^*} + c.c.$ rescattering to the isospin violating $f_0(980)\pi^0$ by exchanging on-shell kaon. Further experimental study on the $\eta(1405)$ parameters and identification of quantum number are needed at BESIII.

By looking at the invariant mass of $\pi\pi\pi$ in $J/\psi \to \gamma 3\pi$s decays as shown in Fig. 8 (c) and (d), we observe signals for $\eta' \to \pi^+\pi^-\pi^0$ and $\pi^0\pi^0\pi^0$ decays, respectively, and determine the decay rates to be $BR(\eta' \to \pi^+\pi^-\pi^0) = (3.83 \pm 0.15 \pm 0.39) \times 10^{-3}$ and $BR(\eta' \to \pi^0\pi^0\pi^0) = (3.56 \pm 0.22 \pm 0.34) \times 10^{-3}$, respectively. For $\eta' \to \pi^+\pi^-\pi^0$ decay, it is consistent with CLEO-c's measurements and precision is improved by a factor of 4. In contrast , for $\eta' \to \pi^0\pi^0\pi^0$ decay, it is two times larger than that in the PDG value [12].

2.7 Observation of resonances above 2.0 GeV in $J/\psi \to \gamma\eta'\pi^+\pi^-$ decay

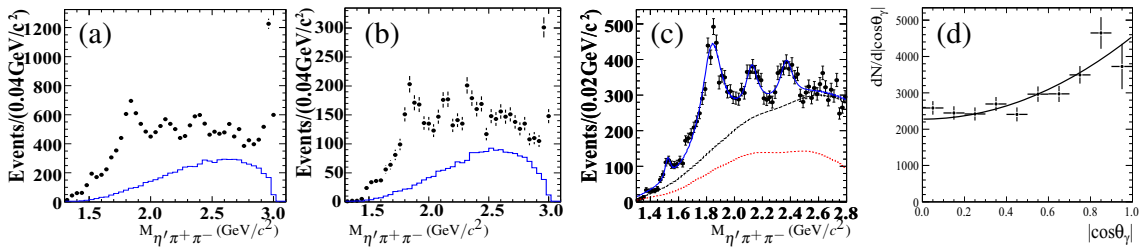

Figure 9: The invariant mass distributions of $\eta'\pi^+\pi^-$ with (a) $\eta' \to \gamma\rho$ (b) $\eta' \to \eta\pi^+\pi^-$, and (c) the combined plot for (a) and (b), and fitting results. (d) is for the $\cos(\theta_\gamma)$ distribution, where θ_γ is the pole angle of the radiative photon. The points with error bar are data. The histograms are from $J/\psi \to \gamma\eta'\pi^+\pi^-$ phase space MC.

The $X(1835)$ was firstly observed at the BESII with a statistical significance of 7.7σ [36]. The possible interpretations of the $X(1835)$ include a $p\overline{p}$ bound state [37,38], a glueball [39], a

radial excitation of the η' meson [40], etc. We report a study of $J/\psi \to \gamma\eta'\pi^+\pi^-$ that used two η' decay modes, $\eta' \to \gamma\rho$ and $\eta' \to \pi^+\pi^-\eta$. Figure 9 (a) and (b) show the $\eta'\pi^+\pi^-$ invariant mass spectrum in $J/\psi \to \gamma\eta'\pi^+\pi^-$ with $\eta' \to \gamma\rho$ and $\eta' \to \pi^+\pi^-\eta$ decay modes, respectively. The $X(1835)$ resonance is clearly seen. Additional peaks are observed around 2.1 and 2.3 GeV/c^2, denoted as $X(2120)$ and $X(2370)$, as well as the $f_1(1510)$ in the low mass region and the distinct $\eta_c(1S)$ signal in the high mass region.

Fits to the mass spectra have been made using four efficiency-corrected Breit-Wigner functions convolved with a Gaussian mass resolution plus a nonresonant $\pi^+\pi^-\eta'$ contribution and background representations. The fitting result of the combined mass spectrum is shown in Fig. 9(c). The mass and width of X(1835) are measured to be $M = 1836.5 \pm 3.0^{+5.6}_{-2.1}$ MeV/c^2 and $\Gamma = 190 \pm 9^{+38}-36$ MeV with a significance larger than 20σ. The masse and width for $X(2120)$ ($X(2370)$) is determined to be $M = 2122.4 \pm 6.7^{+4.7}_{-2.7}$ MeV/c^2 ($M = 2376.3 \pm 8.7^{+3.2}_{-4.3}$ MeV/c^2) and $\Gamma = 83 \pm 16^{+31}_{-11}$ MeV ($\Gamma = 83 \pm 17^{+44}_{-6}$ MeV) with significance $7.2\sigma(6.4\sigma)$. For $X(1835)$, the $cos\theta_\gamma$ distribution is shown in Fig. 9, where θ_γ is the polar angle of the radiative photon in the J/ψ center of mass system. It agrees with $(1 + cos^2\theta_\gamma)$, which is expected for a pseudoscalar.

2.8 Observation of $X(1870) \to a_0^\pm\pi^\mp$ in $J/\psi \to \omega\eta\pi^+\pi^-$ decay

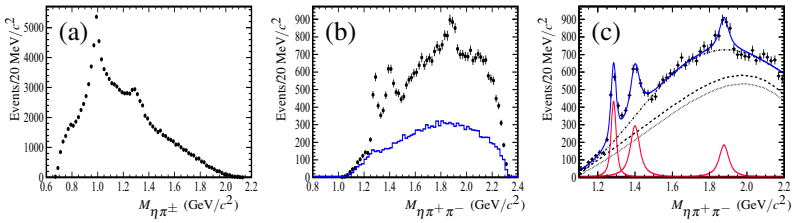

Figure 10: The invariant mass distributions of (a) $\eta\pi^\pm$, (b) $\eta\pi^+\pi^-$ with events in $a_0(980)$ mass window; (c): fitting results; In (b), the histograms are from $J/\psi \to \omega\eta\pi^+\pi^-$ phase space MC.

Experimentally, the study of the production mechanism of the $X(1835)$ and $\eta1405)$, e.g. searches for them in $\eta\pi\pi$ final states with other accompanying particles (ϕ, ω etc.), are useful for clarifying their nature. In particular, the measurements of the production width of these two states in hadronic decays of the J/ψ and a comparison with corresponding measurements in J/ψ radiative decay would provide important information about the glueball possibility. We present results of a study of $J/\psi \to \omega\eta\pi^+\pi^-$, in which the ω decays to $\pi^+\pi^-\pi^0$ and the η/π^0 decays to a pair of photons. In the mass spectrum of $\eta\pi^p m$, as shown in Fig. 10 (a), the $a_0^\pm(980)$ peak is clearly seen. The mass spectrum of $\eta\pi^+\pi^-$ with events in the $a_0(980)$ mass window is shown in Fig. 10 (b). Both $f_1(1285)$ and $\eta(1405)$ are observed significantly. A clear peak around 1800 MeV, denoted as $X(1870)$ is also seen for the first time in the decay of $J/\psi \to \omega\eta\pi^+\pi^-$. A fit with three resonances with simple BW

formula yields a mass $M = 1877.3 \pm 6.3^{+3.4}_{-7.4}$ MeV/c^2 and a width $\Gamma = 57 \pm 12^{+19}_{-4}$ MeV for the $X(1870)$ structure with s statistical significance of 7.2σ. Whether the resonant structure of $X(1870)$ is due to the $X(1835)$, the $\eta_2(1870)$, or a new resonance still needs further study such as a partial wave analysis that will be possible with the larger J/ψ data sample. For the $\eta(1405)$, the product branching ratio of its hadronic production is measured to be smaller than that for its production in the radiative J/ψ decays [12]. For detail about this analysis, one can find more in reference [41].

2.9 Open charm physics

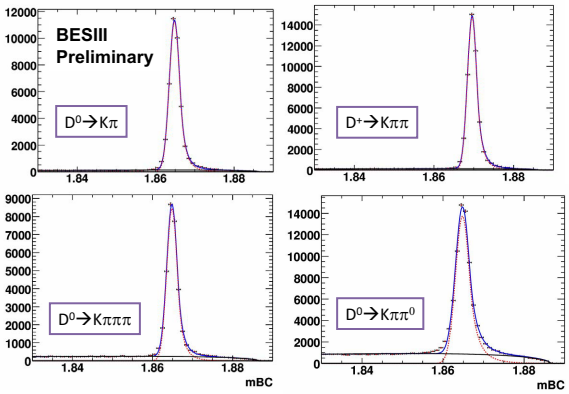

Figure 11: Beam constraint mass distributions.

As of May, 2011, the BESIII has accumulated integrated luminosity of 2.9 fb^{-f} on $\psi(3770)$ peak for open charm physics, which is about 3.5 times the previous largest $\psi(3770)$ data set taken by the CLEO-c Experiment. Taking advantage of the high luminosity provided by the BEPCII collider, BESIII is expected to take much more data at both 3770 MeV and higher energies. Many high precision measurements, including CKM matrix elements related to charm weak decays, decay constants f_D and f_{Ds}, form factors from D semileptonic decays, Dalitz decays, searches for CP violation, and absolute decay branching fractions, will be accomplished in the near future.

There are many advantages of doing charm physics at experiments with e^+e^- collider at threshold. With e^+e^- colliding, the initial energy and quantum numbers are known. For $\psi(3770) \rightarrow D\overline{D}$, both D daughter mesons can be fully reconstructed, allowing absolute measurements, namely, the so called double-tag technique. The continuum background is greatly suppressed by doing this, and kinematic constraints can be applied to infer missing particles on the other side D meson. To demonstrate the cleanliness of the D tags, in Fig. 11, we show a beam-constrained mass plots for some od the fully reconstructed $D^0/D^{\pm}$ decay modes, from part of data. The beam-constrained mass $m_{BC} = \sqrt{E^2_{beam} - p^2_D}$, where E_{beam} is the beam energy and p_D is the candidate momentum, is obtained by substituting the

reconstructed D energy with the beam energy. With this technique, the neutrino can be reconstructed in the leptonic and semileptonic D decays, so that decay constants and form factor/CKM matrix elements can be precisely measured. Thus, these precise measurements could be used to test and calibrate the theoretical tools such as lattice QCD, which are critical for dealing with B decays.

3 Summary

The BESIII experiment addresses a wide range of topics in the field of QCD and searches for new physics beyond the standard model. At present the BESIII collaboration has collected a record on statistics on J/ψ, ψ', and $\psi(3770)$ charmonium states. These data are being exploited to provide precision measurements with a high discovery potential in light hadron and charmonium spectroscopy, charmonium decays, and open charm productions. Most recent highlights from BESIII are reviewed in this paper.

Since very recently, data about 470 pb^{-1} luminosity have been taken at a center-of-mass energy of 4010 GeV, which could give new insights in our understanding of the recently discovered XYZ states and which will allow to explore the field of D_s physics.

Acknowledgments

We would like to thank the accelerator people at BEPCII for their hard work which makes our high luminosity possible. We would also like to thank the great computational and software support of the IHEP staff. This work is supported in part by the Ministry of Science and Technology of China under Contract No. 2009CB825200; 100 Talents Program of CAS.

Bibliography

[1] M. Ablikim *et al.* (BESIII Collaboration), *Design andconstructionoftheBESIIIdetector*,Nucl. Instrum. Meth. **A614**, 345(2009).

[2] M. Ablikim *et al.* (BESIII Collaboration), *Measurements of $h_c(^1P_1)$ in ψ' Decays*, Phys. Rev. Lett. **104**, 132002 (2010) [hep-ex/1002.0501].

[3] M. Ablikim *et al.* (BESIII Collaboration), *Evidence for ψ' decays into $\gamma\pi^0$ and $\gamma\eta$*, Phys. Rev. Lett. **105**, 261801 (2010) [hep-ex/1011.0885].

[4] M. Ablikim *et al.* (BESIII Collaboration), *Branching fraction measurements of χ_{c0} and χ_{c2} to $\pi^0\pi^0$ and $\eta\eta$*, Phys. Rev. D **81**, 052005 (2010) [hep-ex/1001.5360].

[5] M. Ablikim *et al.* (BESIII Collaboration), *Observation of a $p\overline{p}$ mass threshold enhancement in $\psi' \to \pi^+\pi^- J/\psi(J/\psi \to \gamma p\overline{p})$ decay*, Chin. Phys. C **34**, 4 (2010) [hep-ex/1001.5328].

[6] M. Ablikim *et al.* (BESIII Collaboration), *Confirmation of the $X(1835)$ and observation of the resonances $X(2120)$ and $X(2370)$ in $J/\psi \to \gamma\pi^+\pi^-\eta'$*, Phys. Rev. Lett. **106**, 072002 (2011) [hep-ex/1012.3510].

[7] M. Ablikim *et al.* (BESIII Collaboration), *Measurement of the Matrix Element for the Decay $\eta' \to \eta\pi^+\pi^-$*, Phys. Rev. D **83**, 012003 (2011) [hep-ex/1012.1117].

[8] M. Ablikim *et al.* (BESIII Collaboration), *First Observation of the Decays $\chi_{cJ} \to \pi^0\pi^0\pi^0\pi^0$*, Phys. Rev. D **83**, 012006 (2011) [hep-ex/1011.6556].

[9] M. Ablikim *et al.* (BESIII Collaboration), *Study of $a_0^0(980) - f_0(980)$ mixing*, Phys. Rev. D **83**, 032003 (2011) [hep-ex/1012.5131].

[10] M. Ablikim *et al.* (BESIII Collaboration), *Study of χ_{cJ} radiative decays into a vector meson*, Phys. Rev. D **83**, 112005 (2011) [hep-ex/1103.5564].

[11] M. Ablikim *et al.* (BESIII Collaboration), *Observation of χ_{c1} Decays into Vector Meson Pairs $\phi\phi$, $\omega\omega$, and $\omega\phi$*, Phys. Rev. Lett. **107**, 092001 (2011).

[12] PDG 2010: Particle Data Group, *Review of Particle Physics*, Journal of Physics **G 37**, 075021 (2010).

[13] R. M. Baltrusaitis *et al.* (Mark-III Collaboration), Phys. Rev. **D 33**, 629 (1986).

[14] J. Z. Bai *et al.* (BES Collaboration), Phys. Lett. **B 555**, 174 (2003).

[15] D. M. Asner *et al.* (CLEO Collaboration), Phys. Rev. Lett. **92**, 142001 (2004).

[16] B. Aubert *et al.* (BABAR Collaboration), Phys. Rev. Lett. **92**, 142002 (2004).

[17] S. Uehara *et al.* (Belle Collaboration), Eur. Phys. J. **C 53**, 1 (2008).

[18] A. Vinokurova *et al.* (Belle Collaboration), arXiv:1105.0978 [hep-ex].

[19] R. E. Mitchell *et al.* (CLEO Collaboration), Phys. Rev. Lett. **102**, 011801 (2009).

[20] V. V. Anashin *et al.* (KEDR Collaboration), arXiv:1012.1694.

[21] E. Eichten, K. Gottfried, T. Kinoshita, K. D. Lane and T.-M. Yan, Phys. Rev. **D17**, 3090 (1978).

[22] S.-K. Choi *et al.* (Belle Collaboration), Phys. Rev. Lett. **89**, 102001 (2002).

[23] D. M. Asner *et al.* (CLEO Collaboration), Phys. Rev. Lett. **92**, 142001 (2004).

[24] B. Aubert *et al.* (BABAR Collaboration), Phys. Rev. Lett. **92**, 142002 (2004).

[25] B. Aubert *et al.* (BABAR Collaboration), Phys. Rev. **D 72**, 031101 (2005).

[26] C. Edwards *et al.* (Crystal Ball Collaboration), Phys. Rev. Lett. **48**, 70 (1982).

[27] D. Cronin-Hennessy *et al.* (CLEO Collaboration), Phys. Rev. **D 81**, 052002 (2010).

[28] B. Aubert *et al.* (Babar Collaboration), Phys. Rev. **D 78**, 012006 (2008).

[29] L. L. Wang, for the BESIII Collaboration, this conference (preliminary results).

[30] A. Vinokurova *et al.* (Belle Collaboration), arXiv:1105.0978.

[31] P. del Amo Sanchez *et al.* (BABAR Collaboration), Phys. Rev. **D 84**, 012004 (2011).

[32] T. K. Pedlar *et al.* (CLEO Collaboration), Phys. Rev. D **79**, 111101 (2009).

[33] Q. Zhao, Phys. Lett. **B697**, 52(2011).

[34] R. Baldini *et al.* (FENICE Collaboration), Phys. Lett. **B 444**, 111 (1998).

[35] J.-J. Wu, X.-H. Liu, Q. Zhao and B.-S. Zou, arXiv: 1108.3772.

[36] M. Ablikim *et al.* (BESII Collaboration) Phys. Rev. Lett. **95**, 262001 (2005).

[37] G. J. Ding and M. L. Yan, Phys. Rev. **C 72**, 015208 (2005).

[38] G. J. Ding and M. L. Yan, Eur. Phys. J. **A 28**, 351 (2006).

[39] B. A. Li, Phys. Rev. D 74, 034019 (2006).

[40] T. Huang and S. L. Zhu, Phys. Rev. D 73, 014023 (2006).

[41] M. Ablikim *et al.* (BESIII Collaboration),arXiv:1107.1806.

Highlights from J-PARC Hadron Facility

Toshiyuki Takahashi[1] on behalf of J-PARC E19 Collaboration
Institute of Particle and Nuclear Studies (IPNS),
High-Energy Accelerator Organization (KEK)
Tsukuba, 305-0801, Japan

Starting with the first beam to Hadron Facility on January 23, 2009, four secondary beam lines, K1.8, K1.8BR, KL and K1.1BR, were in operation in November 2011. The first physics run for E19, penta-quark search via the $p(\pi^-, K^-)X$ reaction, was carried out at K1.8 beam line using SKS spectrometer. No peak structure was observed on the missing mass spectrum in the region of 1.51 – 1.55 GeV/c^2 at P_π=1.92 GeV/c with the sensitivity of $\sim$0.3 μb/sr. The beam operation to Hadron Facility in April was cancelled due to the big Earthquake on March 11. Fortunately there was no grave damage on J-PARC. All the staff and users are now working toward the beam recovery and user beam in JFY 2011.

1 Overview of J-PARC Accelerators and Hadron Facility

The Japan Accelerator Research Complex (J-PARC) comprises three accelerators of 400 MeV LINAC, 3 GeV Rapid Cycle Synchrotron (RCS), and 50 GeV Main Ring (MR), and three experimental facilities, At present the beam energy is limited to 181 MeV at LINAC and 30 GeV at MR. The most characteristic feature of J-PARC accelerators is its high beam power. The designed beam power of RCS and MR are 1 MW and 750 kW, respectively [1]. Another feature is multi-purpose accelerator. High energy proton beam can generate many kinds of secondary particles such as kaons, neutrinos, muons, and neutrons etc. Using these variety of beams with high-intensity, experimental researches from basic science to the industrial applications will be performed. At the Material and Life Science Facility (MLF), neutron and muon beams are produced from 3 GeV proton beam for material physics, life science etc. The fast extracted beam from MR to Neutrino Beam Line generates neutrino beam to Super-Kamiokande for T2K experiment. The Hadron Experimental Facility is another facility which uses MR beam, where nuclear and particle physics experiments are performed using the secondary meson beams as well as the primary proton beam.

The layout of the Hadron Experimental Hall is shown in Fig.1. The slow extracted beam is transported along the 250 m long Switch Yard and hits a production target at the almost upstream of the Hall (T1), and is finally absorbed by a beam dump. The produced secondary

[1] toshiyuki.takahashi@kek.jp

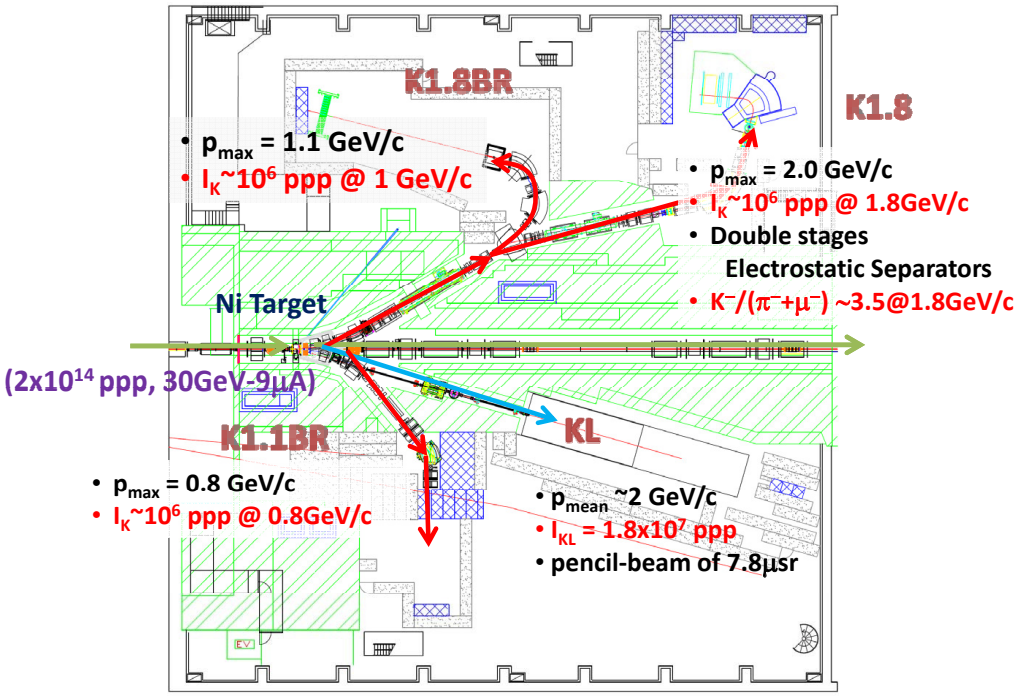

Figure 1: The layout of the Hadron Experimental Hall. Three are 4 secondary beam lines at present. The expected kaon intensities when the primary beam of 2×10^{14} ppp (270 kW) is achieved are displayed in the figure.

particles are delivered along the secondary beam lines to the experimental areas. Four beam lines are available at present. K1.8, K1.8BR, and K1.1BR can deliver the mass-separated charged particles, while KL is a neutral beam line for $K_L \to \pi^0\nu\bar{\nu}$ rare decay experiment [2]

The K1.8 beam line of 2.0 GeV/c maximum was constructed for studies of strangeness $S = -2$ system, especially for spectroscopy experiments. Due to double stages of the electrostatic separators (ESS) with the designed field of 75 kV/cm and 6 m length, high purity kaons of $K^-/(\pi^- + \mu^-)$=~3.5 can be obtained. A high resolution beam spectrometer with the designed resolution of $\Delta p/p$ =3.3×10^{-4} (FWHM) and SKS spectrometer with a solid angle of 100 msr and 0.1% resolution [3] for scattered particles are equipped at K1.8. K1.8BR beam line is branched at the D3 magnet of K1.8 with single ESS. The maximum momentum is 1.1 GeV/c. K1.1BR is a low momentum (~0.8 GeV/c) beam line with a 2 m length ESS.

2 History of the Construction and Beam Operations

The construction of J-PARC started in April 2001. After the complete of Hadron Switch Yard in March 2006 and Hadron Hall in July 2007, construction of the primary and secondary

beam lines for Hadron Facility started. The beam was successfully accelerated at LINAC on January 24 2007, at RCS on October 31 2008. The 3 GeV beam was injected into MR on May 22 2008 and accelerated up to 30 GeV on December 23 2008.

Hadron primary beam line and one secondary beam line, K1.8BR, had been constructed by the end of 2008 and were ready to accept the MR beam in January 2009. On January 23 2009, protons were accelerated up to 30 GeV again and then successfully extracted into Hadron Hall to the beam dump. The production target was installed on February 12 and the secondary beam was confirmed at K1.8BR. Protons and pions were identified online in the time of flight spectrum, while kaons were confirmed later by the detailed offline analysis.

Neutrino beam commissioning started on April 23 2009. In the Hadron Facility, construction of new beam lines, K1.8 and KL as well as SKS spectrometer system were underway. Spill feed-back devices for slow extraction were installed at MR in summer. The beam operation to the Hadron Facility started on October 22. Although most of the time was allocated for the accelerator commissioning, the secondary beam tuning and SKS spectrometer commissioning were carried out at K1.8 using 1kW MR beam.

In JFY2011, the operation of slow extraction was allocated from October 12 to November 16. In addition to the start of K1.1BR operation, a lot of progress has been seen. The first and the most important one is improvement of the extraction efficiency. By the careful alignment of the electrostatic and magnetic septa and dynamic control of the bump orbit, the extraction efficiency of 99.6%, which is the world record, has been achieved. This is promising for the increase of the beam power, since the beam extraction loss is one of the major factors to limit the beam power. Thus the stable operation of 3.6 kW (4.5×10^{12} protons/spill, where 6 sec. duration with $\sim$2.2 sec. extraction time) was realized for user time. Secondary, the first physics run for E19 has been successfully carried out at K1.8.

In spite of the efforts of the accelerator group, however, the time structure of the extracted beam was not good due to the large ripple of the power supplies. The duty factor which is defined as a ratio of the beam on time to the extraction time window (not synchrotron cycle) is less 1% without the spill feed-back control. It improved to $\sim$17% by the operation of spill feed-back control with the optimum parameters. Further improvement was observed by applying the transverse-RF in the flat-top period. But it could not operated for a long time because of the pressurization.

3 The First Results of E19, Penta-quark Experiment, at K1.8

As described the previous section, the first physics run for E19 was carried out last autumn.

E19 aims to search for penta-quark, Θ^+, via the $p(\pi^-, K^-)X$ reaction with high missing mass resolution. Since the first report from LEPS Collaboration [4], a lot of positive and negative results have been reported. The situation is still controversial. For example,

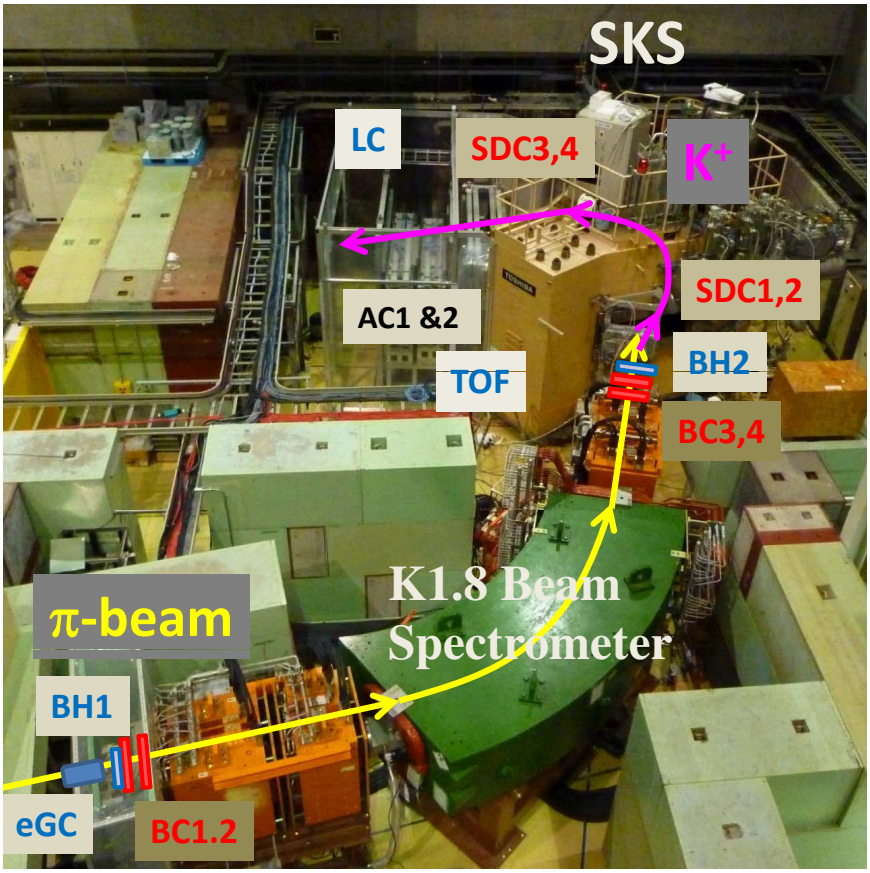

Figure 2: Beam and SKS spectrometers at K1.8 beam line.

negative result is given from $\gamma d \to pK^-K^+(n)$ reaction at CLAS [5], while new LEPS data on γC$\to K^+K^-(n)$ [6] gives positive one. However these results are not inconsistent with each other, since the measured kinematics such as incident energy and angular range are different. Strong energy or angular dependence may exist in this channel. Thus, reaction mechanism may be a key to resolve the present situation and the experimental selection to and limitation on the reaction mechanism are very important. The K^* exchange mechanism is unlikely by the two negative results of $\gamma p \to K^0_s K^+ n$ from CLAS [7] and $K^+ p \to \pi^+ X$ at KEK-PS [8].

The positive result with the best significance so far is $\gamma p \to \pi^+ K^- K^+ n$ from CLAS [9], where Θ^+ is thought be produced $\pi^- p \to K^- \Theta^+$ via the $N^*(2420)$. In addition, the cross section of this s-channel reaction via the neutron intermediate state is directly related to the width of Θ^+. Therefore the pion-induced reaction channel is worth studying.

This reaction was previously studied at K2 beam line of KEK 12GeV-PS (E522) using KURAMA spectrometer and polyethylene target [10]. The 7×10^9 pions were irradiated

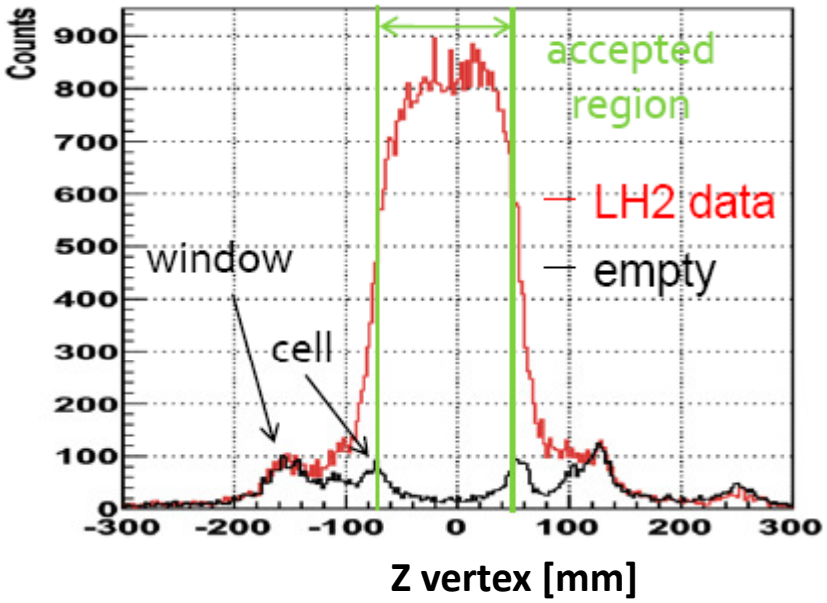

Figure 3: Reaction vertex distribution along the beam direction.

with two incident momenta of 1.87 and 1.92 GeV/c. A bump structure was observed in the missing mass spectrum at 1.53 GeV/c^2 only at 1.92 GeV/c data. If this bump is a true signal, the production cross section is estimated to be 1.9 μb/sr in laboratory system. However the S/N is only 2.5σ, thus, the upper limit was set to 2.9 μb/sr.

In E19, we are going to study the $p(\pi^-, K^-)\Theta^+$ channel at 1.87, 1.92 and 1.97 GeV/c with much improved performances; a resolution of ~2.5 MeV(FWHM) by using SKS spectrometer, good S/N by using a liquid H_2 target instead of CH_2, and high statistics of 4.8×10^{11} pions on target for each momentum. The expected sensitivity is 75 nb/sr.

Last autumn, we took step-1 data at 1.92 GeV/c. Figure 2 shows K1.8 beam spectrometer and SKS. Beam pions were analyzed by the K1.8 beam spectrometer, which comprises $QQDQQ$ magnetic system, trackers, and trigger counters. Gas Cerenkov counter to reject electrons/positions (eGC), 11-segmented plastic hodoscope counter (BH1) and two sets of 1mm spacing MWPC's (BC1 and 2) are installed upstream of the $QQDQQ$, while two sets of drift chambers with anode spacing of 3mm and 5mm (BC3 and 4) and 9-segmented hodoscope counter (BH2) are installed downstream of the $QQDQQ$.

Scattered kaons were analyzed by the SKS spectrometer. Two sets of drift chambers (SDC1 and 2) with similar structure with the BC3 and 4 and two sets of the large-size drift chambers (SDC3 and 4) are installed as trackers upstream and downstream of the superconducting magnet, respectively. Time of flight wall counter (TOF) as well as PID counters of Aerogel Cerenkov counters (AC1 and AC2) and Lucite Cerenkov counter (LC) are located after SDC4. In the momentum calculation, we have to use the calculated field map instead of the

Table 1: Summary for the calibration and production runs.

Reaction	P_{beam} (GeV/c)	SKS Field (T)	number of pions
$p(\pi^-, p)\pi^-$	-0.5	$+2.45$	2.0×10^8
$p(\pi^-, K^+)\Sigma^-$	-1.37	$+2.45$	1.2×10^{10}
$p(\pi^+, K^+)\Sigma^+$	$+1.37$	$+2.45$	3.0×10^9
$p(\pi^-, K^-)X$	$+1.92$	-2.45	7.8×10^{10}

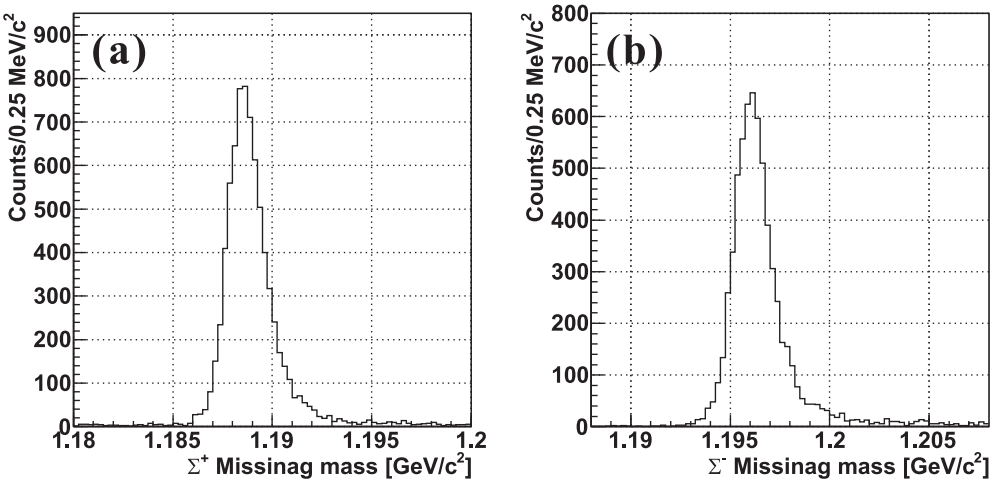

Figure 4: Missing mass spectra for $p(\pi^+, K^+)\Sigma^+$ (a) and $p(\pi^-, K^+)\Sigma^-$ (b) at 1.37 GeV/c.

measured one, since 1/6 of the coil was electrically removed because of the earth fault of the coil when the cooling system was modified. Thus, the calibration of the spectrometers and confirmation of the resolution were very important. $\Sigma^\pm$ productions were measured by the $p(\pi^\pm, K^+)$ reactions at 1.37 GeV/c for this purpose.

The liquid H_2 target adopts a continuous flow of liquid helium in the cooling system without refrigerators. The target cell is a cylinder of ϕ=67.8 mm and 120 mm long, which is made of polyethylene terephthalate (PET) of 0.30 mm thick for the cylinder part, and Mylar of 0.25 μm thick for the end cap. The temperature and the density of the liquid H_2 were very stable within 10^{-5} during the data-taking. A reaction vertex distribution along the beam direction for (π^-, π^-) events is shown in Fig.3. Windows of the target cell and vacuum chamber are clearly seen in the empty target data. The background contamination is estimated to be less than 3%.

Due to the bad time structure of the beam as described before, pion beam intensity was limited to 1.1M/spill. The irradiated numbers of pions for calibration and production runs are summarized in Table.1. In the present analysis, we used only the events in which the

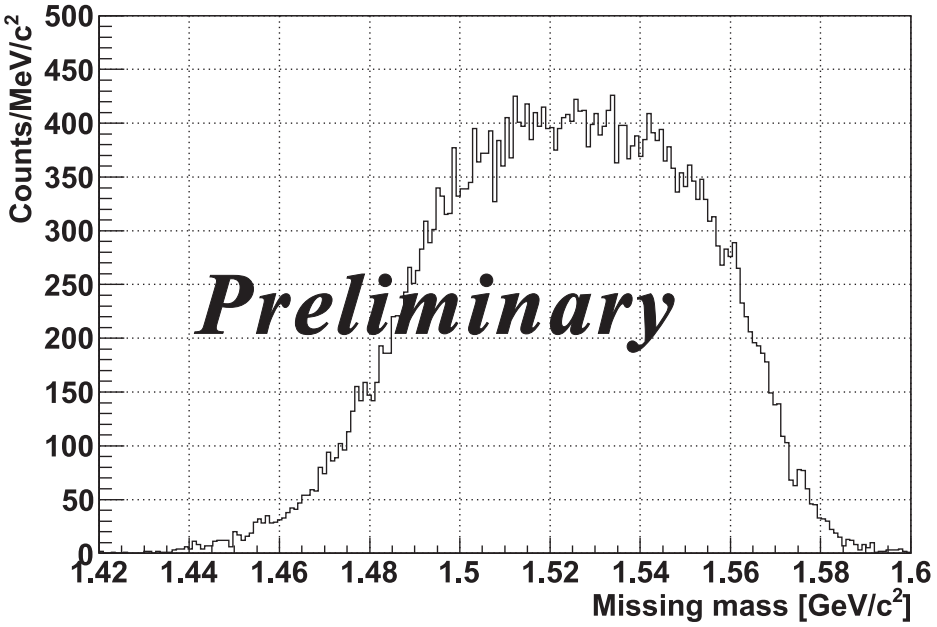

Figure 5: The missing mass spectrum for $p(\pi^-, K^-)X$ at 1.92 GeV/c.

track multiplicity of the beam spectrometer part is only one. About 15% of the events were lost by this selection.

Although magnetic fields of the beam and SKS spectrometers were monitored by Hall probe and NMR, respectively, the absolute central momentum and offset of the beam spectrometer, and absolute value of the SKS magnetic field were adjusted so that the measured $\Sigma^{\pm}$ masses reproduce the PDG values. The missing mass spectra for $\Sigma^{\pm}$ are shown in Fig.4. The resolution of Σ peak was 1.9 ± 0.1 MeV/c^2 in FWHM, thus the missing mass resolution for $\Theta^+(1530\ \mathrm{MeV}/c^2)$ production kinematics is estimated to be 1.5 MeV/c^2 in FWHM.

The missing mass spectrum for $p(\pi^-, K^-)X$ is shown in Fig.5. No peak structure was observed. The present upper limit with 90% confidence level in the mass region of 1.51 to 1.55 GeV/c^2 is estimated to be $\sim$0.3 μb/sr in laboratory frame, which is averaged over from 2 to 15°. Assumed isotropic distribution in center-of-mass frame, it corresponds to $\sim$0.3 μb. Theoretical model based on the low-energy theorem of chiral symmetry predicts that Θ^- production cross section in the present reaction is 5 – 10 μb for J^P=1/2$^+$ case and 0.1 – 0.2 μb for 1/2$^-$ case, depending on the choice of the form factor, when 1 MeV width is assumed [11]. The obtained upper limit in the present data is comparable with the theoretical prediction with 1 MeV width. If the sensitivity of 75 nb as expected in the proposal is achieved, we may restrict the width of Θ^+ and the production mechanism.

New analysis to increase the statistics is underway. By combining the trajectories and BH

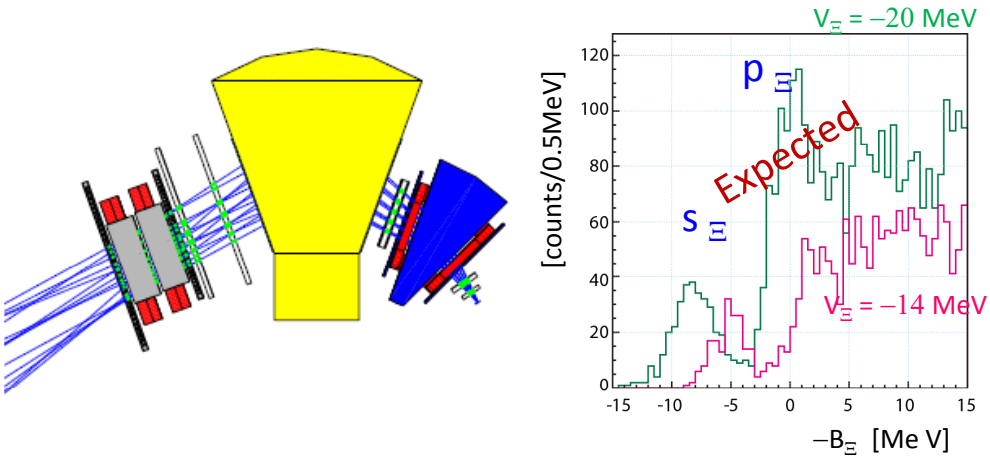

Figure 6: SksPlus spectrometer for E05 (left). The expected missing mass spectrum for one month data-taking with $1.6 \times 10^6 K^-$/spill beam (right). If Woods-Saxon potential depth is -20 MeV, two bound states where Ξ^- in s- and p- states, are expected, whereas one bound state is expected for the -14 MeV potential depth.

hits, narrower time gate can be applied for the trajectory analysis. Data-taking at 2.0 GeV/c was planned in April 2011. However the beam time was cancelled due to the big earthquake on March 11. We would like to start the data-taking soon after the recovery of the J-PARC beam.

4 Spectroscopy of Ξ-Hypernuclei by the (K^-, K^+) Reaction

Hypernuclear physics is one of the major subjects at J-PARC. Seven experiments on hypernuclear physics have been approved at K1.8 beam line[2]. Among those experiments Ξ-hypernuclear spectroscopy by the (K^-, K^+) reaction (E05) [12] has the first priority.

Ξ-hypernuclei are not experimentally established so far. The (K^-, K^+) missing mass spectroscopy on carbon target was previously carried out [13, 14]. Due to the poor experimental resolution and statistics, however, Ξ-hypernuclear state was not observed as a clear peak although some yields were observed in the bound region. The depth of the Ξ-nucleus potential was deduced to be $-$(14–20) MeV from the spectrum shape analysis. Therefore the observation of Ξ-hypernuclear states with a good resolution and statistics is the most important in order to establish Ξ hypernuclei and determine the strength of the Ξ-nucleus and the underlying ΞN interaction from them.

E05 aims to observe Ξ-hypernuclear states, for the first time, via the $^{12}\mathrm{C}(K^-, K^+)^{12}_{\Xi}\mathrm{Be}$

[2] A new experimental proposal on ΣN scattering was approved at the 12th PAC meeting on July 8–10, 2011.

reaction with good resolution and high statistics. High intensity K^- beam at 1.8 GeV/c with 1.6×10^6/spill will be analyzed by K1.8 beam spectrometer while scattered K^+ will be measured by SksPlus spectrometer as shown in Fig.6 (left), in which an dipole magnet is added in front of the SKS to keep the acceptance in 1.1–1.3 GeV/c region with good resolution. The 3 MeV (FWHM) resolution is expected using 5.4 g/cm^2 target. With one month data-taking, $\sim$100 bound states will be expected as shown in Fig.6 (right).

5 The Effect of the Earthquake on March 11

On March 11 2011 a big earthquake occurred, and big Tsunamis attacked to the wide area of the coast in north-east of Japan. Fortunately there was no injured or dead person and no Tsunami effect in J-PARC. There were no significant damage in all buildings although the land around the buildings sank and many roads around J-PARC were severely damaged. The serious damages were found in RCS, where power substation and cooling water were damaged. All of the elements of the accelerators moved, therefore alignments are necessary for the recovery.

In the Hadron Facility, the alignment of the primary and secondary beam lines as well as the rearrangement of the shielding structure are necessary, which is very time-consuming work due to large number of the elements. No serious damage was found on the detectors of the beam spectrometer and SKS, although the SKS magnet and the shielding structure moved at K1.8. At K1.8BR, one wire chamber located at the beam line was broken because the last dipole magnet (K1.8BRD5) moved.

According to the J-PARC recovery plan announced on May 20 [15], the facility recovery will be confirmed by an beam injection and acceleration in December and user operation will start from January 2012. Now all of the staffs and users at J-PARC are working hard to achieve the recovery as planned. I hope that the beam will be back in December and we can restart experiments soon.

Acknowledgments

The author acknowledges the members of J-PARC Hadron Beam-Line group and K1.8 Experimental group which he belongs to. He wishes to thank the supporting staffs of the Accelerator, Beam-Line, Experimental-Floor, and Cryogenics groups for their efforts of the beam operation and supports to the experiments. Most of the detectors and their readout system at K1.8 beam spectrometer and SKS were constructed with the support from a Grant-In-Aid for Scientific Research on Priority Areas, Multi-Quark Systems with Strangeness.

Bibliography

[1] Accelerator technical design report for J-PARC, Accelerator Group JAERI/KEK Project Team, March 2003, http://hadron.kek.jp/~accelerator/TDA/tdr2003/index2.html.

[2] J-PARC Proposal P14, http://j-parc.jp/NuclPart/pac_0606/pdf/p14-Yamanaka.pdf.

[3] T. Fukuda *et al,* Nucl. Inst. Meth. A361,485 (1995).

[4] T. Nakano *et al.*, Phys. Rev. Lett. **91**, 012002 (2003).

[5] CLAS Collaboration, B. McKinnon *et al.*, Phys. Rev. Lett. **96**, 212001 (2006).

[6] T. Nakano *et al.*, Phys. Rev. C**79**, 025210 (2009).

[7] CLAS Collaboration, M. Battaglieri *et al.*, Phys. Rev. Lett. **96** 042001 (2006).

[8] K. Miwa *et al.*, Phys. Rev. C **77**, 045203 (2008).

[9] CLAS Collaboration, V. Kubarovsky *et al.*, Phys. Rev. Lett. **92**, 032001 (2004).

[10] K. Miwa *et al.*, Phys. Lett. B **635**, 72 (2006).

[11] T. Hyodo, private communication.

[12] J-PARC Proposal P05, http://j-parc.jp/NuclPart/pac_0606/pdf/p05-Nagae.pdf.

[13] T. Fukuda *et al.*, Phys. Rev. C **58**, 1306 (1998).

[14] P. Khaustov *et al.*, Phys. Rev. C **61**, 054603 (2000).

[15] http://www.j-parc.jp/picture/2011/05/J-PARC-Recovery_schedule.pdf. The latest status of J-PARC can be found at http://www.j-parc.jp/en/topics/2011/en.html.

Production and Spectroscopy of Heavy Hadrons at the LHC

Harold Evans[1] on behalf of the ALICE, ATLAS, CMS, and LHCb Collaborations
Physics Department
Indiana University
Bloomington, IN, 47405-7105
USA

Measurements of heavy flavor production and decay have featured prominently in the early results from the four large LHC experiments: ALICE, ATLAS, CMS, and LHCb. These results provide tests of QCD models in a new energy region and point the way toward future measurements of CP violation and searches for new physics. An overview of open heavy flavor studies is presented here, focusing on how the new measurements extend our knowledge of this area of physics. Heavy quarkonia states at the LHC are summarized in other proceedings of this conference. I also discuss briefly how heavy flavor measurements are likely to evolve as LHC luminosities increase.

1 Introduction

Heavy hadron production and spectroscopy are not primary focuses of any of the four large LHC experiments. Nevertheless, each of the collaborations have produced interesting and important results in this area. In fact, more than 50 heavy flavor results were available from ALICE, ATLAS, CMS, and LHCb at the time of this conference. Clearly, I will not be able to cover them all in this brief review. Rather, I'll attempt to concentrate on large themes in the field and discuss how recent results from the LHC have contributed to our understanding in these areas. Necessarily, I will be forced to gloss over many interesting details of the measurements I mention. More information on theses measurements can be found in the numerous and excellent parallel talks by LHC speakers at Hadron2011. Results from the LHC in the related topics of charmonium [1] and bottomonium [2] can be found in two separate plenary talks. However, some important heavy flavor measurements will be skipped, not because of lack of interest, but simply because of lack of space. These include: measurements of many heavy flavor states that have been observed previously; studies of CP-violation and other electro-weak topics; the search for rare B and D decays; and all of top-quark physics.

[1]hgevans@indiana.edu

2 Experimental Issues

The wealth of results presented here was made possible, in large part, by the excellent performance of the LHC machine. Results discussed in these proceedings were obtained with up to 40 pb^{-1} data taken in 2010 where maximum peak luminosities of 2×10^{32} $cm^{-2}\cdot s^{-1}$ were observed. Already, at the time of this conference in June 2011, LHC peak luminosity had been increased by an order of magnitude and more than 1 fb^{-1} had been delivered to ATLAS and CMS. Approximately a third of that was seen by LHCb, which limits instantaneous luminosity to protect its delicate vertex detectors. As we will see, this rapidly increasing luminosity has important consequences for the heavy flavor production and spectroscopy programs at the four experiments, particularly ALICE, ATLAS, and CMS.

Another important factor in obtaining the results that I will discuss is the excellent performance of the detectors. All of them recorded collisions from the LHC with more than 90% efficiency in 2010. The detectors themselves are described in detail in references [3–6]. Their most important attributes for the study of heavy flavors are: angular acceptance, triggering, tracking, and particle identification. In order to understand the results produced by the experiments, it's useful to compare their approaches in each of these areas.

An extremely important feature of the experiments for heavy flavor related measurements is the range that they cover in $\eta \equiv -\ln[\tan(\theta/2)]$. Heavy quarks are produced predominantly in the forward region ($|\eta| \gtrsim 1.5$) in proton-proton collisions at LHC energies. However backgrounds also peak in this area making the extraction of signals more difficult. ATLAS and CMS are "central" detectors, with muon coverage of $|\eta| < 2.7$ and $|\eta| < 2.4$, respectively. ALICE also has central coverage for electrons, $|\eta| < 0.9$, but detects muons in the forward direction, $-4.0 < \eta < -2.5$. Finally, LHCb has only forward coverage: $1.9 < \eta < 4.9$. These acceptances are summarized in Fig. 1.

Of all the elements of the LHC detectors, trigger systems are perhaps the most critical in constraining the heavy flavor capabilities of the experiments. To deal with the challenge of selecting ~200 Hz of interesting events from the 40 MHz rate of bunch crossings, the experiments have constructed complicated, multi-level trigger systems. Even with state-of-the-art triggers, though, heavy flavors present many difficulties. Heavy flavor events tend to have lower p_T scales than most electro-weak or new physics processes. Thus, their properties overlap much more strongly with the overwhelming background of light quark production than do, for example, those of W, Z, or Higgs events. This problem is exacerbated as luminosities go up and the average number of proton-proton collisions per bunch crossing increases.

The experiments deal with these problems in a variety of ways. For those analyses that need inclusive event selections, "minimum-bias" or low p_T jet triggers must be used, but these gave acceptable rates only during very early LHC running when luminosities were orders of magnitude lower than present values. Hence, inclusive analyses tend to be constrained to only a tiny fraction of the total LHC running period. Since heavy hadrons

decay semi-leptonically with branching ratios of $\mathcal{O}(10\%)$, triggers that are sensitive to leptons (particularly muons) can be very effective at selecting events containing B- and D-hadrons – but only those decaying to muons. Additionally, trigger rates for the relatively low p_T muons (<10 GeV) that tend to be produced in B and D decays quickly become untenable as luminosities increase. So the most effective single-muon triggers for heavy flavor physics were eliminated fairly early in the 2010 run. Only low p_T dimuon triggers remain active, and even those are seeing their thresholds gradually creep up. Finally, LHCb takes advantage of its unique capabilities to construct displaced vertex triggers at its lowest trigger level (the other experiments employ displaced vertex triggers at higher levels). These triggers remain unprescaled to the highest luminosity allowed by LHCb and give it access to fully hadronic decays of heavy hadrons.

Once events are accepted by the trigger system, offline reconstruction of their properties becomes the most important consideration. Tracking and particle identification are particularly critical for heavy hadrons. In the area of tracking two issues often arise in heavy flavor analyses: mass reconstruction and secondary vertex finding. The accuracy of the first of these depends primarily on precise measurements of track momenta, while the second is driven by the spatial (hit) resolution achievable by individual tracking elements and by the position of the inner-most tracking element. The vertexing performance of all four detectors is fairly similar. As an example, each achieves an impact parameter resolution of $\sim$30 μm for tracks in the 5–10 GeV range. Larger differences are seen in mass resolution, as illustrated in Fig. 2, with LHCb having the clear advantage here.

Finally, particle identification is an important part of most heavy flavor analyses. All four of the experiments have excellent capabilities to identify leptons, and each has some handles on $\pi/K/p$ separation. However, LHCb makes the most extensive use of hadron identification in the results presented here. Their RICH detectors allow them to tag $\sim$95% of charged kaons with a pion contamination of only 7%.

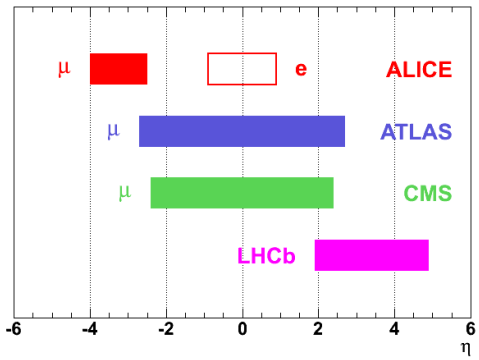

Figure 1: Angular acceptances of the four large LHC experiments.

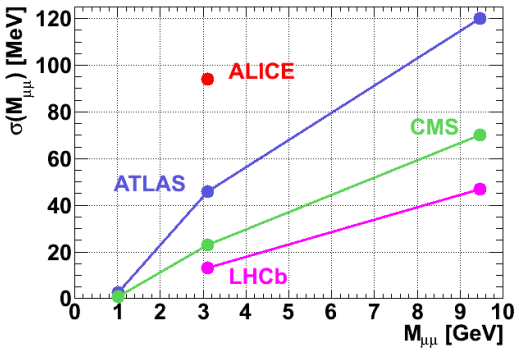

Figure 2: Dimuon mass resolution vs invariant mass for the four large LHC experiments.

3 Heavy Flavor Production

The study of beauty and charm production at colliders has a long and interesting history. Because of the relatively high b and c quark masses, perturbative calculations of their production were expected to converge rather quickly. However, until the early 2000's, measurements of b production at the Tevatron and HERA were generally factors of 2–3 higher than Next to Leading Order (NLO) predictions. The shape of the b-production spectrum and charm production were much better described. For a more detailed review of the situation see reference [7]. This problem was largely resolved (see reference [8] for a review) by a combination of experimental and theoretical improvements. On the theoretical side, problems due to large $\ln(p_T/m_b)$ terms at high b-quark p_T were ameliorated by the use of Fixed Order Next to Leading Log (FONLL) resummation; and consistent, FONLL, treatment of fragmentation functions in the calculations was achieved. Experimentally, collaborations made use of these consistent calculations, took more care in reporting observations that were less sensitive to fragmentation/hadronization uncertainties (B-hadron and b-jet cross-sections), and used updated values of Parton Density Functions and α_s.

The result of these improvements was generally excellent agreement between measurement and NLO prediction [8]. However, it is important to verify that this agreement is maintained at the high energies of LHC collisions. At the present time, our NLO understanding has been incorporated into the standard, Leading Order (LO) event generators, `PYTHIA` [9] and `HERWIG` [10] through a variety of interfaces (`MC@NLO` [11], `POWHEG` [12], FONLL [13] are used in the analyses presented here) all implementing the calculations in slightly different ways. Additionally, intermediate implementations of beyond-LO calculations also exist (for example, MadGraph/MadEvent [15] and CASCADE [14]) that allow specific features of those calculations to be probed. All of these can be used to create detailed predictions that can be compared directly to experimental data.

3.1 Inclusive Heavy Flavor Production

Preliminary, inclusive measurements of heavy flavor production in pp collisions at $\sqrt{s}$ = 7 TeV have been made by the ALICE and ATLAS collaborations. Inclusive samples of electrons and muons are selected by both experiments. ALICE considers electrons in the central region ($|\ y\ |<0.8$) in 2.6 nb^{-1} of data and subtracts a mix of "photonic" background from γ conversions, π^0, and other Dalitz decays based on the measured π^0 cross-section. They measure muons in the forward region ($-4< \eta < -2.5$) using a 16.5 pb^{-1} data set. These samples are dominated by b and c decays to leptons. Both measurements agree quite well with FONLL predictions, as shown (for the electron case) in Fig. 3.

The ATLAS analysis [16] uses 1.3–1.4 pb^{-1} of data selected with single electron and muon triggers of varying thresholds. Theoretical predictions for Drell-Yan $W/Z/\gamma^*$ are subtracted resulting in spectra that are dominated by heavy flavor decays. The collaboration reports

differential cross-sections for electrons in the kinematic range, $7 < p_T < 26$ GeV and $|\eta| < 2.0$; and for muons in the range, $4 < p_T < 100$ GeV and $|\eta| < 2.5$. These measurements are compared to predictions using FONLL, POWHEG+PYTHIA, and POWHEG+HERWIG. Figure 4 shows the muon result. Good agreement is observed between both measurements and the FONLL prediction. The generators, POWHEG+PYTHIA and POWHEG+HERWIG, also do a reasonably good job although the HERWIG version predicts a significantly lower cross-section. Interestingly, the ATLAS muon data now has enough reach in p_T to be sensitive to the deviation between the pure NLO and the FONLL calculations that becomes significant for $p_T > 35$ GeV. The data indicates clearly the need for an NLL resummation at high p_T.

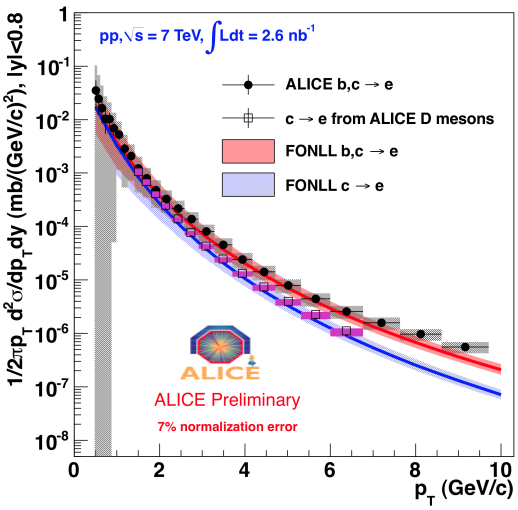

Figure 3: The differential $pp \to eX$ cross-section at $\sqrt{s} = 7$ TeV measured by ALICE in $|y| < 0.8$.

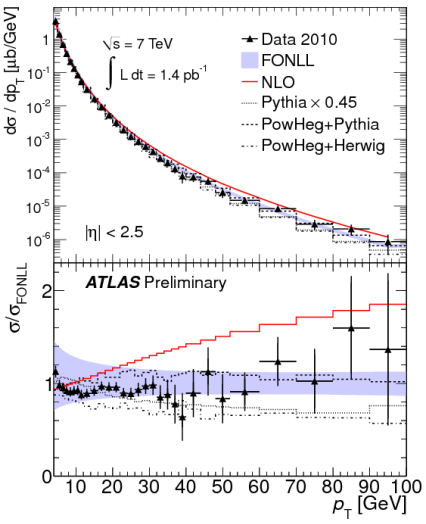

Figure 4: The differential $pp \to \mu X$ cross-section at $\sqrt{s} = 7$ TeV measured by ATLAS in $|\eta| < 2.5$.

3.2 Charm Production

ALICE, ATLAS, and LHCb have all made preliminary measurements of charm production using samples of D mesons collected using micro- or minimum-bias triggers. The ALICE result is based on samples of $D^0 \to K^-\pi^+$, $D^+ \to K^-\pi^+\pi^+$, and $D^{*+} \to D^0(K^-\pi^+)\pi^+$ (and charge conjugate) decays selected from 1.6 nb^{-1}, about 20% of the 2010 data. They measure differential cross-sections in the range $2 < p_T < 12$ GeV in different rapidity ranges that are then adjusted to $|y| < 0.5$. ATLAS uses $D^+ \to K^-\pi^+\pi^+$, $D^{*+} \to D^0(K^-\pi^+)\pi^+$, and $D_s^+ \to \phi(K^+K^-)$ (and charge conjugate) decays in 1.1 nb^{-1} of data taken during early 2010 running to measure differential cross-sections in the kinematic range, $p_T > 3.5$ GeV (extending to ~40 GeV) and $|\eta| < 2.1$ [17]. These data contain contributions from both c- and b-quark production. However, charm production dominates by approximately a factor

of 20. Finally, LHCb reconstructs all of the above decay modes using 1.18 nb^{-1} of early data taken with a micro-bias trigger in the kinematic region, $0 < p_T < 8$ Gev. They present differential cross-sections in several rapidity region in $2 < y < 4.5$ [18]. Charm and beauty components to this data sample are separated using a fit to the D meson impact parameter distribution.

All differential cross-section results are good agreement with NLO predictions in a variety of different implementations. However, uncertainties on these predictions are quite large and measurements are now limited by systematics.

3.3 Beauty Production

Beauty production at the LHC is measured using a wide variety of different methods. ATLAS [19] and CMS [20] separate b-production from lighter quark events using the momenta of muons transverse to a nearby jet's direction (p_T^{rel}) as a discriminant that is sensitive to the underlying parton's mass. In samples of 4.8 pb^{-1} collected with low p_T muon+jet triggers (ATLAS), and 85 nb^{-1} of low p_T single-muon triggers (CMS) the collaborations measure differential cross-sections as a function of b-jet p_T (ATLAS) and muon p_T (CMS). Another inclusive method employed by ATLAS [21] and CMS [22] selects b-quark events using jets containing reconstructed secondary vertices in 3.0 pb^{-1} and 60 nb^{-1}, respectively, of data taken using a mixture of minimum-bias and jet triggers. This method allows sensitivity to higher values of jet p_T (up to 260 GeV) than the p_T^{rel} technique. The substantial B-hadron lifetime also provides a handle on B-hadron production in several partially inclusive results. LHCb uses the D^0 impact parameter distribution of $pp \to \mu D^0 X$ candidates in 2.9 nb^{-1} of micro-bias, and 12.1 nb^{-1} of single-muon trigger data to measure the $pp \to H_b X$ cross-section in several bins between $2 < \eta < 6$ [23]. ATLAS [24], CMS [25], and LHCb [26] all use a pseudo-proper time variable in their J/ψ analyses to measure the $b \to J/\psi X$ differential cross-section as well. Finally, CMS has made B-hadron differential cross-section measurements using the exclusive decay modes $B^+ \to J/\psi(\mu^+\mu^-)K^+$ [27], $B_d \to J/\psi(\mu^+\mu^-)K^0_S$ [28], and $B_s \to J/\psi(\mu^+\mu^-)\phi(K^+K^-)$ [29] (and conjugates) collected using their dimuon triggers. These measurements all agree quite well with a variety of NLO calculations, with the possible exception the exclusive mode cross-sections where the NLO predictions are consistently lower than the measurements. But again the uncertainties on the experimental results are generally dominated by systematic effects even with the small amounts of integrated luminosity used.

To probe the calculations more deeply, correlations between the produced b and $\bar{b}$ need to be used. First results in this area are now available from ATLAS and CMS. ATLAS uses its secondary vertexing analysis [21] to select events with two identified b-jets. The dijet invariant mass that they observe is shown in Fig. 5. Agreement with `POWHEG+PYTHIA` predictions is good across a wide range of dijet masses. CMS, on the other hand, probes correlations between the b and $\bar{b}$ using angular variables. Their analysis [30], which uses 3.1 nb^{-1} of single-jet trigger data, searches for events with two reconstructed secondary vertices

from which they reconstruct the opening angle between the two B-hadrons responsible for the vertices. This technique allows access to the events with very small $B\overline{B}$ opening angles that are particularly sensitive to NLO effects. An example of their results is shown in Fig. 6, where the angular separation, $\Delta R = \sqrt{\Delta\phi^2 + \Delta\eta^2}$, between the $B\overline{B}$ pair observed in CMS data and predicted by various beyond LO calculations is plotted compared to the LO PYTHIA prediction. None of the higher order predictions do a good job describing the data in the low ΔR region where higher order effects are expected to dominate.

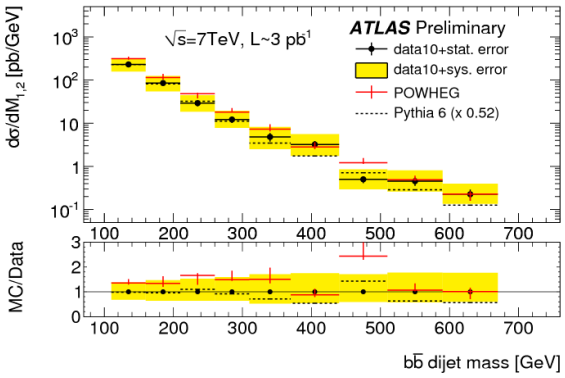

Figure 5: The differential $pp \to b\bar{b}$ cross-section as a function of $b\bar{b}$ dijet invariant mass measured for b-jets with p_T>40 GeV and $|y|$<2.1 at ATLAS.

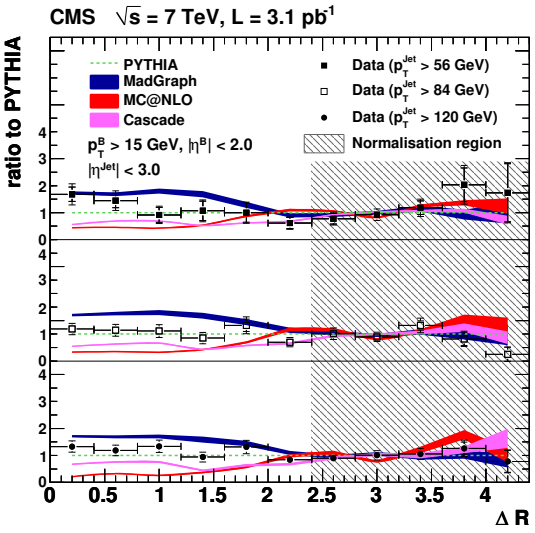

Figure 6: Ratios of differential $B\overline{B}$ cross-sections as a function of ΔR measured by CMS compared to various predictions.

3.4 Heavy Flavor Fragmentation

Another important component in our understanding of heavy flavor production is the process of fragmentation of b- and c-quarks into beauty and charm hadrons of various flavors. The ATLAS and LHCb collaborations have produced new measurements in these areas. The ATLAS study of $D^{(*)}$ meson production [17] allows the measurement of several charm fragmentation related parameters after subtracting predicted B-hadron decay contributions from their measured $D^{(*)}$ meson cross-sections and extrapolating these $c\bar{c}$ measurements to the full kinematic phase space. ATLAS derives a strangeness suppression factor, $\gamma_{s/d}$, which corresponds to the ratio of the total $D_s^{\pm}$ production cross section from $c\bar{c}$, $\sigma_{c\bar{c}}^{tot}(D_s^{\pm})$, to the sum of $\sigma_{c\bar{c}}^{tot}(D^{*\pm})$ and the part of $\sigma_{c\bar{c}}^{tot}(D^{\pm})$ that does not arise from $D^{*\pm}$ decays. ATLAS also measures the fraction of D mesons produced in the vector state, P_V, as the ratio of $D^{*\pm}$ to the sum of $D^{*\pm}$ and $D^{\pm}$ production. Both measurements are in good agreement with averages of LEP results [17,31] as shown in Fig. 7.

LHCb fragmentation measurements concentrate on the b-quark sector. They have determined the ratio of b-quarks fragmenting to hadrons containing s- and d-quarks, f_s/f_d, using $B^0 \to D^- \pi^+$, $B^0 \to D^- K^+$ and $B_s \to D_s^- \pi^+$ decays in 35 nb^{-1} of data [32]. They have also determined the strange quark fraction, $f_s/(f_u + f_d)$ and the Λ_b baryon fraction, $f_{\Lambda_b}/(f_u + f_d)$ in b-quark fragmentation using 3 pb^{-1} samples of semi-muonic decays of B-hadrons [33]. They observe no dependence of the strange quark fraction on p_T or η, but do see evidence of a linear dependence of the Λ_b fraction on p_T in all η regions they consider. As can be seen in Fig. 7, their results are consistent with [2], but more precise than, the current world averages [34] and individual results from CDF [35] and LEP [34].

Finally, LHCb has observed a clear signal of 43 $\pm$ 13 events, in 32.5 pb^{-1} of data, for the decay $B_c^\pm \to J/\psi \pi^\pm$ [36]. Comparing this to the production of $B^\pm \to J/\psi K^\pm$ yields a ratio, $\sigma(B_c^+) \times B(B_c^+ \to J/\psi \pi^+) / \sigma(B^+) \times B(B^+ \to J/\psi K^+) = (2.2 \pm 0.8 \pm 0.2)\%$, in good agreement with a prediction made using the BcVegPy generator [37], $(1.4 \pm 0.4 \pm 0.1)\%$.

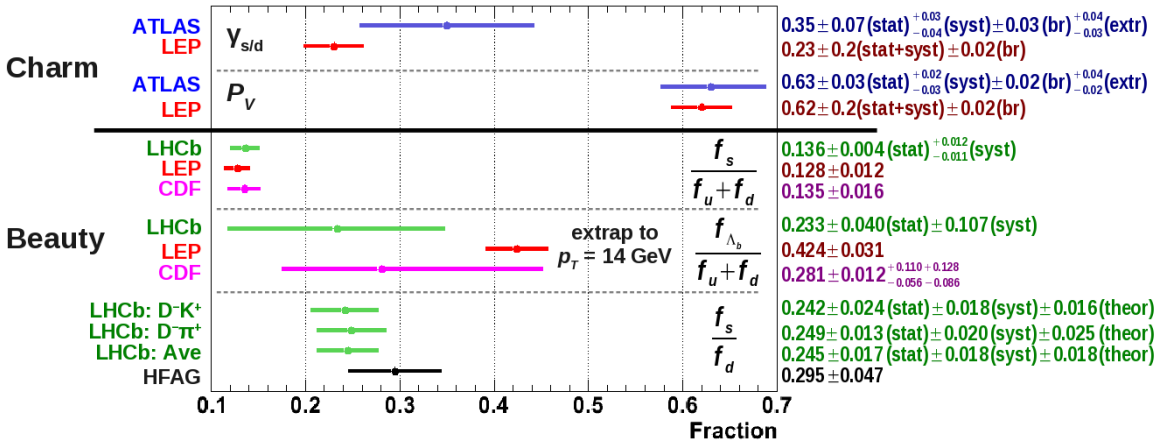

Figure 7: A summary of beauty and charm hadron fragmentation fraction measurements. Note: to allow a consistent comparison, the f_{Λ_b} results are extrapolated to p_T = 14 GeV using LHCb's parametrization [33].

4 Spectroscopy and Exclusive Final States

All heavy flavor hadrons are produced copiously at the LHC and each of the large experiments have reconstructed sizable samples of most of the low-lying states. However, exclusive reconstruction of beauty and charm hadrons is an area where LHCb is taking a leading role. Their ability to trigger on hadronic decays and their efficient $\pi/K/p$ identification capabilities, as well as other detector optimizations, make exclusive final state reconstruction one of their strengths.

[2] In the case of the Λ_b fraction, all results have been adjusted to an average p_T of 14 GeV.

LHCb takes advantage of this strength is several ways. In the areas of hadron properties, they have been able to identify several new hadronic decays of B_s mesons with the data they have taken to date. They are also using exclusively reconstructed decays as a tool to study electro-weak symmetry breaking and to search for new physics through measurements of parameters of the CKM matrix. Of particular interest here are measurements of the angles $\gamma \equiv arg(-V_{ub}^* V_{ud}/v_{cb}^* V_{cd})$ and $\beta_s \equiv arg(-V_{tb}^* V_{ts}/v_{cb}^* V_{cs})$, which are currently the most poorly measured of the "unitarity triangle" quantities.

LHCb has observed several new decay modes of the B_s meson. They have studied B_s decays to excited $c\bar{s}$ states: $B_s \to \mu D_{s1} X$ and $B_s \to \mu D_{s2}^* X$ with $D_{s1}^+, D_{s2}^{*+} \to D^0(K^-\pi^+)K^+$ [38]. Measurements of the relative fractions of these states allow sensitive tests of QCD models. Using data samples of 20 and 3 pb^{-1}, LHCb finds $\mathcal{B}(\overline{B_s^0} \to D_{s2}^{*+} X\mu^-\overline{\nu})$ / $\mathcal{B}(\overline{B_s^0} \to X\mu^-\overline{\nu})$ = (3.3 $\pm$ 1.0 $\pm$ 0.4)% and $\mathcal{B}(\overline{B_s^0} \to D_{s1}^+ X\mu^-\overline{\nu})$ / $\mathcal{B}(\overline{B_s^0} \to X\mu^-\overline{\nu})$ = (5.4 $\pm$ 1.2 $\pm$ 0.4)%. The D_{s1} result is in good agreement with a previous measurement by the D0 collaboration [39], but this is the first observation of the D_{s2}^* decay mode. These measurements are in general agreement with predictions of 3.2% and 5.7% respectively from the ISGW2 model [40] but slightly higher than quark model expectations of 1.8% and 2% [41].

LHCb has also made a first observation of the decay mode $B_s^0 \to K^{*0}\overline{K^{*0}}$, which proceeds solely through loop $b \to s$ diagrams in the Standard Model, and can be used in the extraction of γ and β_s. Using 35 fb^{-1} of data they observe a signal with 7σ significance, as shown in Fig. 8, and measure $\mathcal{B}(B_s^0 \to K^{*0}\overline{K^{*0}})$ = [1.95 $\pm$ 0.47(stat) $\pm$ 0.51(syst) $\pm$ 0.29(f_d/f_s)]$\times 10^{-5}$ [42] in reasonable agreement with the prediction of $(0.79^{+0.43}_{-0.39})\times 10^{-5}$ based on QCD factorization [43].

Measurement of the angle γ to date have relied primarily on $B^- \to D^{(*)}K^{(*)-}$ decays. However, many other modes also have the potential to contribute. These include $B^0 \to D^0 K^{*0}$, $B^- \to D^0 K^-\pi^+\pi^-$, $\overline{B^0} \to D^+\pi^-\pi^+\pi^-$, and $B_s^0 \to D_s^+ K^-\pi^+\pi^-$. LHCb has taken first steps toward widening the scope of γ measurements by observing several of these decays or closely related final states. They measure

Mode	**Events**	**Branching Ratio ($\times 10^4$)**	**Ref.**
$\overline{B_s^0} \to D^0 K^{(*0)}$	34.5 $\pm$ 6.9	4.44 $\pm$ 1.00(stat) $\pm$ 0.55(syst) $\pm$ 0.56(f_s/f_d) $\pm$ 0.69($B \to D\rho$)	[44]
$\overline{B^0} \to D^+\pi^-\pi^+\pi^-$	1151 $\pm$ 45	61.6 $\pm$ 2.6 $\pm$ 6.9	[45]
$B^- \to D^0\pi^-\pi^+\pi^-$	973 $\pm$ 45	59.6 $\pm$ 2.9 $\pm$ 6.1	[45]
$\overline{B_s^0} \to D_s^+\pi^-\pi^+\pi^-$	139 $\pm$ 24	62.8 $\pm$ 11.0 $\pm$ 12.1	[45]
$\Lambda_b^0 \to \Lambda_c^+\pi^-\pi^+\pi^-$	165 $\pm$ 18	122 $\pm$ 14 $\pm$ 46	[45]

which represent either first observations of these final states (the first and last measurements listed above) or significant improvements over current world averages.

Finally, LHCb was the first to observe the decay $B_s \to J/\psi[\mu^+\mu^-]f_0(980)[\pi^+\pi^-]$ [46]. As shown in Fig. 9 they see a clear peak in the $J/\psi\pi^+\pi^-$ distribution at the B_s mass in 33

pb^{-1} of data. They measure $\Gamma[B_s^0 \to J/\psi f_0(\pi^+\pi^-)]/\Gamma[B_s^0 \to J/\psi\phi(K^+K^-)] = 0.252^{+0.046\,+0.027}_{-0.032\,-0.033}$ in good agreement with the later D0 measurement of $0.210 \pm 0.032 \pm 0.036$ [47]. This decay is similar to $B_s \to J/\psi\phi$, which is commonly used to determine the angle β_s. However, since the $J/\psi f_0$ mode consists of a single CP-odd eigenstate, it can be used to extract β_s without having to rely on the complicated angular analysis necessary to disentangle the CP states in the $J/\psi\phi$ mode.

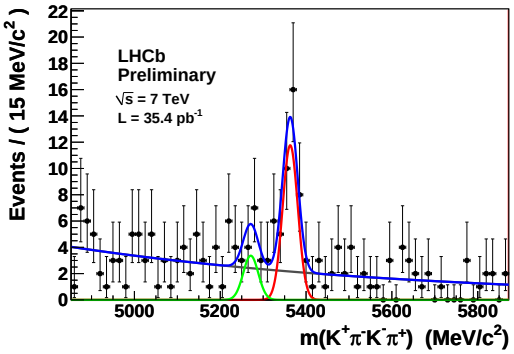

Figure 8: The $K^+\pi^-K^-\pi^+$ invariant mass distribution measured by LHCb in their $B_s \to K^{*0}\overline{K^{*0}}$ analysis [42]

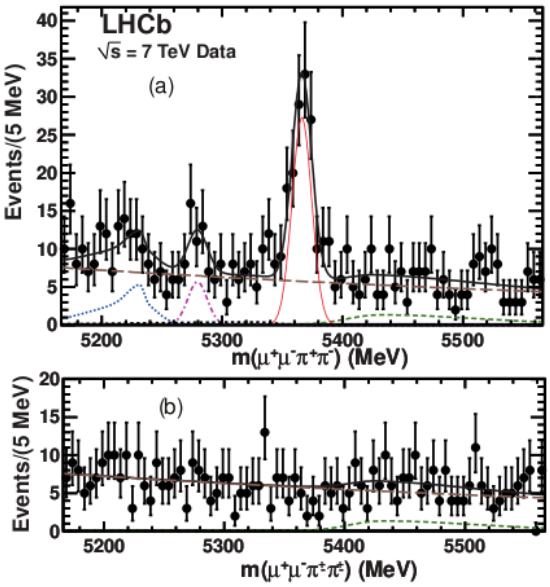

Figure 9: The $J/\psi\pi^+\pi^-$ invariant mass distribution measured by LHCb in their $B_s \to J/\psi f_0$ analysis [46] for right sign (top) and wrong sign $\pi\pi$ combinations, where the $\pi\pi$ mass is required to lie within 90 MeV of the $f_0(980)$ mass.

5 Conclusions

The first year of LHC running has produced a wealth of results in the heavy flavor sector from ALICE, ATLAS, CMS, and LHCb. Each of the experiments has made measurements of open beauty and charm production. In general, the good agreement between data and NLO QCD predictions that was observed at the Tevatron continues to hold at higher LHC energies although most measurements are already systematics limited. Upon considering those measurements that are particularly sensitive to the details of the calculations, though, some areas of disagreement seem to be appearing. These are most evident in exclusive b production and in the angular correlations observed between b and $\overline{b}$ jets. Unfortunately (for these measurements), the rapidly increasing LHC luminosity requires all the experiments

to move away from the inclusive, low p_T triggers that have provided the bulk of the data for production studies. In the future, these studies will need to shift focus, primarily to rely on those final states that are accessible using dimuon triggers (for example, $\Lambda_b \to J/\psi\Lambda$). Even for these, muon p_T thresholds will steadily increase. Clearly, the next round of heavy flavor measurements will have to use different techniques than those described here.

Trigger considerations also affect the areas of exclusive final states and spectroscopy for ATLAS and CMS. However, the LHCb collaboration is truly starting to hit its stride here. They have already made several first observations of heavy flavor decay modes and are now beginning to have enough data to probe CP violation using a wide variety of techniques.

The next few years will be challenging ones for the heavy flavor efforts of the four large LHC experiments. Overcoming the difficulties posed by increasing luminosity and the demands of ever higher precision will require both perseverance and cleverness. The excellent results presented here, though, show that ALICE, ATLAS, CMS, and LHCb are up to the task. Look forward to even more interesting heavy flavor results from the LHC at the next meeting of this conference!

Acknowledgments

I am grateful to my colleagues on ALICE, ATLAS, CMS, and LHCb for their helpful input to this article. Thanks also to the local organizers for an interesting and enjoyable conference.

Bibliography

[1] Y. Gao, these proceedings.

[2] N. Leonardo, these proceedings.

[3] K. Aamodt *et al.* [ALICE Collaboration], JINST **3**, S08002 (2008).

[4] G. Aad *et al.* [ATLAS Collaboration], JINST **3**, S08003 (2008).

[5] R. Adolphi *et al.* [CMS Collaboration], JINST **3**, S08004 (2008).

[6] A. A. Alves *et al.* [LHCb Collaboration], JINST **3**, S08005 (2008).

[7] M. Cacciari, `arXiv:hep-ph/0407187`.

[8] M. Mangano, `arXiv:hep-ph/0411020`.

[9] T. Sjostrand, S. Mrenna, P. Z. Skands, JHEP **05**, 026 (2006), `arXiv:hep-ph/0603175`.

[10] G. Corcella *et al.*, JHEP **01**, 010 (2001), `arXiv:hep-ph/0011363`.

[11] S. Frixione, B. R. Webber, JHEP **06**, 029 (2002), arXiv:hep-ph/0204244.
S. Frixione, P. Nason, B. R. Webber, JHEP **08**, 007 (2003), arXiv:hep-ph/0305252.

[12] P. Nason, JHEP **11**, 040 (2004), arXiv:hep-ph/0409146.
S. Frixione, P. Nason, G. Ridolfi, JHEP **09**, 126 (2007), arXiv:0707.3088[hep-ph].
S. Frixione, P. Nason, C. Oleari, JHEP **11**, 070 (2007), arXiv:0709.2092[hep-ph].
S. Alioli, P. Nason, C. Oleari, E. Re, JHEP **06**, 043 (2010), arXiv:1002.2581[hep-ph].

[13] M. Cacciari, P. Nason, C. Oleari, JHEP **04**, 006 (2006), arXiv:hep-ph/0510032.

[14] H. Jung, G. P. Salam, Eur. Phys. J. **C19**, 351 (2001), arXiv:hep-ph/0012143.

[15] J. Alwall, M. Herquet, F. Maltoni, O. Mattelaer, T. Stelzer, JHEP **06**, 128 (2011), arXiv:1106.0522[hep-ph].

[16] G. Aad *et al.* [ATLAS Collaboration], arXiv:1109.0525[hep-ex].

[17] The ATLAS Collaboration, ATLAS-CONF-2011-017.

[18] The LHCb Collaboration, LHCb-CONF-2010-013.

[19] The ATLAS Collaboration, ATLAS-CONF-2011-057

[20] V. Khachatryan *et al.* [CMS Collaboration], JHEP **1103**, 090 (2011), arXiv:1101.3512[hep-ex].

[21] The ATLAS Collaboration, ATLAS-CONF-2011-056.

[22] The CMS Collaboration, CMS-PAS-BPH-10-009.

[23] R. Aaij *et al.* [LHCb Collaboration], Phys. Lett. **B694**, 209 (2010), arXiv:1009.2731[hep-ex].

[24] G. Aad *et al.* [ATLAS Collaboration], Nucl. Phys. **B850**, 387 (2011), arXiv:1104.3038[hep-ex].

[25] V. Khachatryan *et al.* [CMS Collaboration], Eur. Phys. J. **C71**, 1575 (2011), arXiv:1011.4193[hep-ex].

[26] R. Aaij *et al.* [LHCb Collaboration], Eur. Phys. J. **C71**, 1645 (2011), arXiv:1103.0423[hep-ex].

[27] V. Khachatryan *et al.* [CMS Collaboration], Phys. Rev. Lett. **106**, 112001 (2011), arXiv:1101.0131[hep-ex].

[28] S. Chatrchyan *et al.* [CMS Collaboration], Phys. Rev. Lett. **106**, 252001 (2011), arXiv:1104.2892[hep-ex].

[29] S. Chatrchyan *et al.* [CMS Collaboration], Phys. Rev. **D84**, 052008 (2011), arXiv:1106.4048[hep-ex].

[30] V. Khachatryan *et al.* [CMS Collaboration], JHEP **1103**, 136 (2011), arXiv:1102.3194[hep-ex].

[31] L. Gladilin, arXiv:hep-ex/9912064.

[32] The LHCb Collaboration, LHCb-CONF-2011-013.

[33] The LHCb Collaboration, LHCb-CONF-2011-028.

[34] D. Asner *et al.* [Heavy Flavor Averaging Group], arXiv:1010.1589[hep-ex].

[35] T. Aaltonen *et al.* [CDF Collaboration], Phys. Rev. **D77**, 072003 (2008), arXiv:0801.4375[hep-ex].

[36] The LHCb Collaboration, LHCb-CONF-2011-017.

[37] C. -H. Chang, C. Driouichi, P. Eerola, X. G. Wu, Comp. Phys. Commun. **159**, 192 (2004), arXiv:hep-ph/0309120. C. -H. Chang, J. -X. Wang, X. -G. Wu, Comp. Phys. Commun. **175**, 624 (2006), arXiv:hep-ph/0604238.

[38] R. Aaij *et al.* [LHCb Collaboration], Phys. Lett. **B698**, 14 (2011), arXiv:1102.0348[hep-ex].

[39] V. M. Abazov *et al.* [D0 Collaboration], Phys. Rev. Lett. **102**, 051801 (2009), arXiv:0712.3789[hep-ex].

[40] D. Scora, N. Isgur, Phys. Rev. **D52**, 2783 (1995), arXiv:hep-ph/9503486.

[41] H. B. Mayorga, A. Moreno Briceno, J. H. Munoz, J. Phys. **G29**, 2059 (2003), arXiv:hep-ph/0209032.

[42] The LHCb Collaboration, LHCb-CONF-2011-019.

[43] M. Beneke, J. Rohrer, D. Yang, Nucl. Phys. **B774**, 64 (2007), arXiv:hep-ph/0612290.

[44] The LHCb Collaboration, LHCb-CONF-2011-008.

[45] The LHCb Collaboration, LHCb-CONF-2011-007.

[46] R. Aaij *et al.* [LHCb Collaboration], Phys. Lett. **B698**, 115 (2011), arXiv:1102.0206[hep-ex].

[47] The D0 Collaboration, D0 Note 6152 (2011).

Meson-baryon interactions and baryon resonances

Tetsuo Hyodo[1]
Department of Physics, Tokyo Institute of Technology, Meguro, Tokyo 152-8551, Japan

Meson-baryon interactions are the fundamental building blocks to study the structures of baryon resonances and meson properties in few-body nuclear systems. We review the recent progress in the investigation of the meson-baryon interaction in the strangeness $S = -1$ sector and the structure of the $\Lambda(1405)$ resonance. In particular, we present an attempt to construct a realistic $\overline{K}N$-$\pi\Sigma$ interaction in chiral SU(3) dynamics in response to the precise measurement of the kaonic hydrogen, and discuss the subthreshold extrapolation of the $\overline{K}N$ interaction with the information of the $\pi\Sigma$ channel.

1 Introduction

Hadrons are the asymptotic degrees of freedom of QCD at low energy due to color confinement, and the interactions among hadrons exhibit rich phenomena in the nonperturbative regime of the strong interaction. For instance, hadronic interactions in some sectors are so strong that two-body resonances are generated by hadronic dynamics [1]. Such hadronic molecular states can also be found in the heavy quark sector, in which many new exotic mesons have been recently observed [2]. The study of the hadron interactions and possible composite structures will elucidate a novel construction of hadrons and will open a new perspective in hadron spectroscopy.

Hadronic interactions have been studied in various approaches. A traditional method for the hadron-hadron interaction is the meson-exchange picture [3]. One of the recent achievements is the extraction of the inter-hadron forces from lattice QCD [4, 5]. For scattering systems including the Nambu-Goldstone bosons, on the other hand, chiral symmetry serves as a guiding principle to construct hadron interactions. A series of works based on chiral dynamics [6–8] has demonstrated that the combination of the chiral low energy interaction with the unitarity condition of the scattering amplitude provides a unique tool to study the hadron interactions and resonances.

Here we consider meson-baryon scatterings with baryon resonances based on chiral SU(3) dynamics. Among others, we focus on the recent active discussions on the negative parity $\Lambda(1405)$ resonance with strangeness $S = -1$ and isospin $I = 0$. There have been a long-standing debate on its structure; a three-quark state in the constituent quark model

[1]hyodo@th.phys.titech.ac.jp

picture [9] vs. a $\overline{K}N$ bound state in the $\pi\Sigma$ continuum in the meson-baryon picture [10]. When the $\Lambda(1405)$ resonance is regarded as a $\overline{K}N$ bound state, the interaction between $\overline{K}$ and N is attractive enough to generate a bound state below the threshold. This picture motivates the study of the antikaon bound states in nuclei, the $\overline{K}$-nuclei [11]. In this way, the study of the $\Lambda(1405)$ resonance has large impact on various fields of the strangeness sector of the nonperturbative QCD. In section 2 we introduce the formulation of chiral SU(3) dynamics, and discuss the structure of the $\Lambda(1405)$ resonance from various aspects. In section 3, we summarize the current status of the experimental investigations of the $\overline{K}N$-$\pi\Sigma$ amplitude and show possible future directions to be pursued for the construction of a realistic $\overline{K}N$-$\pi\Sigma$ interaction.

2 $\Lambda(1405)$ in meson-baryon scattering

In this section we overview the framework of the chiral SU(3) dynamics for the meson-baryon scattering [6, 7] in which the low energy chiral interaction is combined with the unitarity of the scattering amplitude. A detailed formulation of the model is given in Ref. [8]. We then discuss the structure of the $\Lambda(1405)$ resonance in this approach, paying attention to the pole structure in the complex energy plane.

2.1 Chiral SU(3) dynamics

Regarding the light pseudoscalar mesons (π, K, and η) as the Nambu-Goldstone (NG) bosons associated with the spontaneous breaking of chiral $\mathrm{SU}(3)_R \times \mathrm{SU}(3)_L$ symmetry, we can describe the low energy dynamics of the NG bosons in chiral perturbation theory [12], which is an effective field theory based on the low energy expansion of the QCD Green's function. The chiral low energy theorems in current algebra are concisely encoded as the leading order results of the perturbative expansion.

In chiral perturbation theory for meson-baryon systems, the covariant derivative of the baryon kinetic term provides the meson-baryon four-point vertex as

$$\mathcal{L}^{\mathrm{WT}} = \frac{1}{4f^2}\mathrm{Tr}\left(\overline{B}i\gamma^\mu[\Phi\partial_\mu\Phi - (\partial_\mu\Phi)\Phi, B]\right),$$

where Φ (B) is the octet meson (baryon) field and f is the meson decay constant. From this interaction Lagrangian, we obtain the meson-baryon contact interaction called Weinberg-Tomozawa (WT) term, which takes on the following form after the s-wave projection:

$$V_{ij}^{\mathrm{WT}}(W) = -\frac{C_{ij}}{4f^2}(2W - M_i - M_j)\sqrt{\frac{M_i + E_i}{2M_i}}\sqrt{\frac{M_j + E_j}{2M_j}}, \tag{1}$$

where W is the total energy of the center-of-mass frame, i labels the meson-baryon channel, and M_i (E_i) is the mass (energy) of the baryon in channel i. The coupling strength C_{ij} is

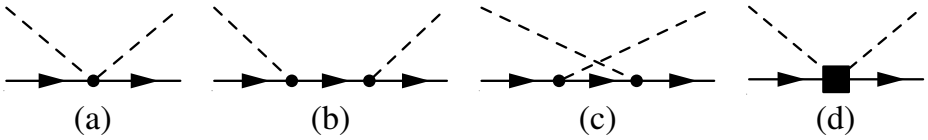

Figure 1: Feynman diagrams for the meson-baryon interactions in chiral perturbation theory. (a) Weinberg-Tomozawa interaction, (b) s-channel Born term, (c) u-channel Born term, and (d) Next-to-leading-order (NLO) interaction. The dots represent the $\mathcal{O}(p)$ vertices while the square denotes the $\mathcal{O}(p^2)$ vertex.

determined by the flavor structure of the meson-baryon channel and the group theoretical argument [13]. Equation (1) provides the meson-baryon scattering length in accordance with the chiral low energy theorem [14].

In addition to the WT term, there are Born terms at $\mathcal{O}(p)$ and contact terms at $\mathcal{O}(p^2)$ [15], so the amplitude in chiral perturbation theory at next-to-leading order is given by

$$V(W) = V^{\mathrm{WT}}(W) + V^{\mathrm{Born}}(W) + V^{\mathrm{NLO}}(W).$$

They are systematically calculated by the diagrams shown in Figure 1. The Born terms mainly contribute to the p-wave amplitude and their s-wave component is in the higher order in the nonrelativistic expansion than the WT term. The next-to-leading-order (NLO) terms contain seven low energy constants which are not determined by the symmetry argument. Thus, for a qualitative discussion on the structure of the $\Lambda(1405)$ resonance, it is sufficient to adopt the WT interaction as the main component. In section 2.2, we consider the structure of the $\Lambda(1405)$ resonance using the model with only the WT term. We will include the Born and the NLO terms in section 3.1 for the quantitative discussion to construct a realistic $\overline{K}N$-$\pi\Sigma$ scattering amplitude.

Chiral perturbation theory well describes the low energy meson-baryon scattering, but the unitarity condition is not always guaranteed because the amplitude is proportional to the meson momentum. To recover the unitarity, we make use of the dispersion relation. The unitarity condition leads to the optical theorem for the forward scattering amplitude $T(s)$:

$$\mathrm{Im}\, T^{-1}(s) = \frac{\rho(s)}{2} \quad \text{for } s \geqslant s_+, \tag{2}$$

where $s = W^2$ is the Mandelstam variable and the two-body phase space factor is given by $\rho(s) = M\sqrt{(s-s_-)(s-s_+)}/(4\pi s)$ with $s_\pm = (M \pm m)^2$. Since the scattering amplitude is analytic in the complex energy plane except for possible poles (CDD poles), we can write the inverse scattering amplitude using dispersion relation as

$$T^{-1}(W) = \sum_n \frac{R_n}{W - W_n} + \tilde{a}(s_0) + \frac{s - s_0}{2\pi} \int_{s_+}^{\infty} ds' \frac{\rho(s')}{(s'-s)(s'-s_0)},$$

which is consistent with the optical theorem (2). Single subtraction is performed at the subtraction point s_0 with the subtraction constant $\tilde{a}(s_0)$ to tame the divergence. W_n and R_n represent the position and the residue of the CDD poles, which cannot be determined within the scattering theory. Noting that the dispersion integral on the unitarity cut can be regarded as (the finite part of) the meson-baryon loop function $G(W)$, we can write the general form of the scattering amplitude as

$$T(W) = [\mathcal{T}^{-1}(W) - G(W)]^{-1}, \tag{3}$$

where $\mathcal{T}^{-1}(W)$ expresses the CDD pole contributions. The explicit form of the loop function is given by a diagonal matrix as

$$\begin{aligned} G_k(W) =& \frac{1}{(4\pi)^2}\Big\{ a_k(\mu) + \ln\frac{M_k^2}{\mu^2} + \frac{m_k^2 - M_k^2 + W^2}{2W^2}\ln\frac{m_k^2}{M_k^2} \\ &+ \frac{\overline{q}_k}{W}[\ln(W^2 - (M_k^2 - m_k^2) + 2W\overline{q}_k) + \ln(W^2 + (M_k^2 - m_k^2) + 2W\overline{q}_k) \\ &- \ln(-W^2 + (M_k^2 - m_k^2) + 2W\overline{q}_k) - \ln(-W^2 - (M_k^2 - m_k^2) + 2W\overline{q}_k)]\Big\}, \end{aligned}$$

with $\overline{q} = \sqrt{(s - s_-)(s - s_+)}/(2\sqrt{s})$. $a_k(\mu)$ represents the subtraction constant which plays a role of the ultraviolet cutoff. To determine $\mathcal{T}(W)$, we match the loop expansion of the general form of the amplitude (3) with that in chiral perturbation theory [7]. Since the meson-baryon loop contribute as $\mathcal{O}(p^3)$ in chiral perturbation theory, we can identify the $\mathcal{T}(W)$ function as the tree-level amplitude up to $\mathcal{O}(p^2)$:

$$\mathcal{T}(W) = V^{\mathrm{WT}}(W) + V^{\mathrm{Born}}(W) + V^{\mathrm{NLO}}(W) + \dots.$$

where ellipsis denotes the higher order contributions. In this way, we can construct the scattering amplitude which is consistent with the unitarity condition and exhibits the correct low energy behavior required by chiral symmetry.

This form of the amplitude can be regarded as the solution of the scattering equation with the interaction kernel derived in chiral perturbation theory. In other words, we regard the meson-baryon tree-level amplitude as an interaction kernel of the scattering equation, and the meson-baryon amplitude is obtained by solving the scattering equation $T = V + VGT$ as illustrated in Figure 2.

2.2 The structure of the $\Lambda(1405)$ resonance

We have constructed the framework of chiral SU(3) dynamics. In this section, we apply this framework to the strangeness $S = -1$ and isospin $I = 0$ meson-baryon scattering, and study the property of the $\Lambda(1405)$ resonance. In this sector, four channels ($\overline{K}N$, $\pi\Sigma$, $\eta\Lambda$, and $K\Xi$) participate in the coupled-channel scattering. For the clarity of the mechanism, we adopt the simplest model with the WT interaction. It is shown that this model successfully

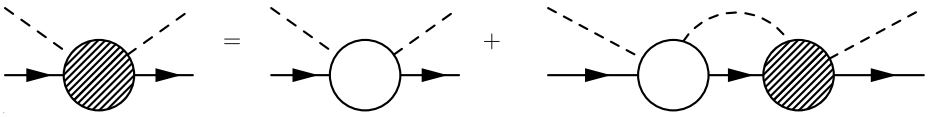

Figure 2: Schematic illustration of the scattering equation. The shaded (empty) blob represents the T-matrix (potential V). The loop function G is expressed by the intermediate meson-baryon loop.

reproduces the observables in the $K^- p$ scattering and the mass spectrum of the $\Lambda(1405)$ resonance [8].

In the meson-baryon scattering amplitude, baryon resonances are expressed as pole singularities in the second Riemann sheet of the complex energy plane. Close to the resonance energy region, the scattering amplitude can be written as the Breit-Wigner term plus a slowly varying background term:

$$T_{ij}(W) = \frac{g_i g_j}{W - M_R + i\Gamma_R/2} + T_{ij}^{\mathrm{BG}}(W),$$

where M_R and Γ_R are the mass and width of the resonance state, respectively, and g_i stands for the coupling strength to the channel i. In this way, the properties of resonances can be read off from the pole structure of the amplitude.

In the study of $\Lambda(1405)$, it is found that there are two poles in the resonance energy region [16]. This is illustrated in Figure 3 by plotting the absolute value of the scattering amplitude in the complex energy plane. We observe one bump structure on the real axis, which is influenced by two independent poles in the complex plane. By calculating the residues of the poles, it is shown that the higher energy pole strongly couples to the $\overline{K}N$ channel while the lower energy pole has larger coupling strength to the $\pi\Sigma$ channel. Because of the different coupling strengths, the scattering amplitude of $\overline{K}N \to \pi\Sigma$ and that of $\pi\Sigma \to \pi\Sigma$ are affected by two poles with different weights. As a consequence, the resonance shape of the $\Lambda(1405)$ resonance in the $\pi\Sigma$ mass spectrum may depend on the reaction process [16].

The physical origin of the double-pole structure can be traced back to the two attractive components of the chiral interaction [17]. The explicit form of the C_{ij} coefficients of the WT interaction (1) for $S = -1$ and $I = 0$ channel is

$$C_{ij} = \begin{pmatrix} 3 & -\sqrt{\frac{3}{2}} & \frac{3}{\sqrt{2}} & 0 \\ & 4 & 0 & \sqrt{\frac{3}{2}} \\ & & 0 & -\frac{3}{\sqrt{2}} \\ & & & 3 \end{pmatrix} \begin{matrix} \overline{K}N \\ \pi\Sigma \\ \eta\Lambda \\ K\Xi \end{matrix}.$$

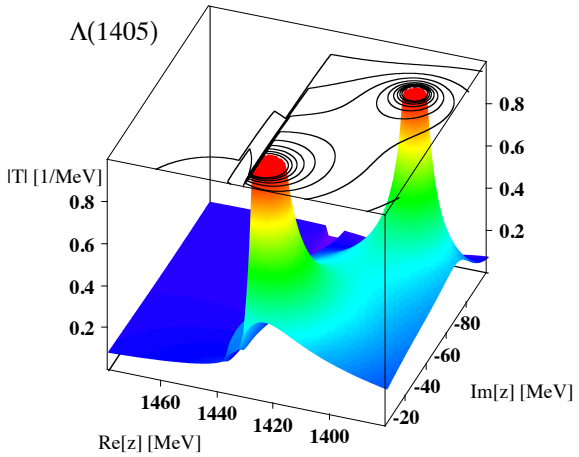

Figure 3: The absolute value of the scattering amplitude around the $\Lambda(1405)$ energy region in the complex plane.

A positive value corresponds to the attractive interaction, so we find from the diagonal components that both the $\overline{K}N$ and $\pi\Sigma$ channels are attractive. When we solve the scattering equation by eliminating the off-diagonal components, the $\overline{K}N$ channel develops one bound state below the threshold, and the $\pi\Sigma$ channel generates a resonance above the threshold. This is illustrated in Fig. 4 by plotting these pole positions together with those in the full coupled-channel model. It is clear from the figure that the higher energy pole originates in the $\overline{K}N$ bound state and the lower energy pole is evolved from the $\pi\Sigma$ resonance. Identifying the origin of the poles as a $\overline{K}N$ bound state and a $\pi\Sigma$ resonance is reasonable from the strong coupling of the higher (lower) energy pole to the $\overline{K}N$ ($\pi\Sigma$) channel. This analysis suggests that the $\Lambda(1405)$ resonance is realized as a Feshbach resonance in the resonating open channel [18]

Given the different nature of the coupling strengths, we notice that the pole structure of $\Lambda(1405)$ has an important phenomenological consequence in the $\overline{K}N$ interaction [17]. We find that the $\overline{K}N$ interaction generates a quasi-bound state around 1420 MeV, rather than the nominal resonance position of 1405 MeV, and the physical $\Lambda(1405)$ is formed cooperatively with the attraction in the $\pi\Sigma$ channel. Thus, the strength of the $\overline{K}N$ interaction is closely related to the precise pole position(s) of the $\Lambda(1405)$ resonance. This issue will be further discussed in section 3, in relation with the quantitative refinements of the $\overline{K}N$-$\pi\Sigma$ interaction.

Before closing this section, let us mention several recent studies on the internal structure of the $\Lambda(1405)$ resonance. The origin of resonances is studied in Ref. [19] through the renormalization procedure. As explained in section 2.1, the CDD pole contribution should be included in the interaction kernel V, but certain choice of the subtraction constants in the loop function may introduce a seed of resonance in the loop function. To eliminate

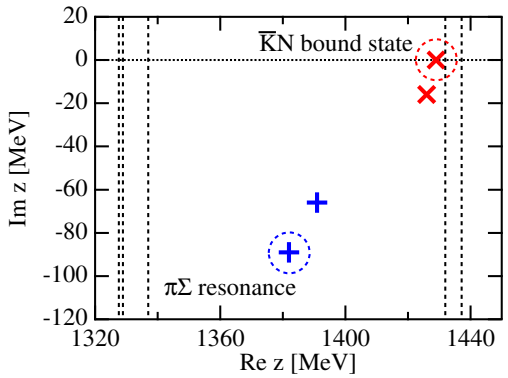

Figure 4: Pole positions of the scattering amplitude for $\Lambda(1405)$ in the complex energy plane. Crosses enclosed by circles represent poles obtained by switching off the transition couplings. Vertical dashed lines indicate the meson-baryon threshold energies.

the CDD pole contribution from the loop function, the natural renormalization scheme is introduced (the meaning of this scheme is further discussed from the viewpoint of the compositeness [20]). Using the phenomenological fitting and the natural renormalization scheme, it is shown that the $\Lambda(1405)$ is dominated by the meson-baryon molecular structure.

This picture is further confirmed from different aspects. The study of the N_c scaling shows that the three-quark component in the $\Lambda(1405)$ resonance is small [21]. Through the evaluation of the electromagnetic properties [22], the spatial size of the $\Lambda(1405)$ is found to be much larger than the ground state hadrons which are presumably dominated by the three-quark structure. All these studies consistently indicate the dominance of the meson-baryon molecular structure of the $\Lambda(1405)$ resonance.

3 Toward a realistic meson-baryon interaction

We have been discussing the structure of the $\Lambda(1405)$ resonance from the viewpoint of hadron spectroscopy. One of the central issues in the strangeness nuclear physics is the exploration of the kaonic nuclei. Since the $\Lambda(1405)$ resonance is located just below the $\overline{K}N$ threshold, its structure is closely related with the $\overline{K}N$ interaction [17]. There are several theoretical studies on the $\overline{K}NN$ system [23]. The results of these studies show that the $\overline{K}NN$ three-body system will develop a quasi-bound state below the threshold with a large width. On the other hand, quantitative estimation of the binding energy does not converge with each other.

To illustrate the current situation of the $\overline{K}N$ interaction, here we list the present experimental database which can be used to constrain the theoretical models:

- *above* the $\overline{K}N$ threshold: total cross sections of K^-p scattering into K^-p, $\overline{K}^0n$, $\pi^0\Sigma^0$, $\pi^+\Sigma^-$, $\pi^-\Sigma^+$, and $\pi^0\Lambda$ channels.
- *at* the $\overline{K}N$ threshold: threshold branching ratios and the $\overline{K}N$ scattering lengths.
- *below* the $\overline{K}N$ threshold: $\pi\Sigma$ invariant mass spectra.

At this point, it should be noted that the relevant energy region of the study of the bound antikaon in nuclei is below the $\overline{K}N$ threshold. Thus, the main reason of the discrepancy in the predictions of the $\overline{K}NN$ bound state can be attributed to the lack of the experimental information, especially in the region below the $\overline{K}N$ threshold. To increase the precision of the model calculation, we should accumulate 1) the $\overline{K}N$ data at the threshold and 2) the $\pi\Sigma$ data below the $\overline{K}N$ threshold, as we explain below.

The $\overline{K}N$ data at the threshold is the direct information of the $\overline{K}N$ channel with the lowest possible energy. At present, threshold branching ratios are measured with good accuracy [24]. In addition to that, the K^-p scattering length is very important to constrain the $\overline{K}N$ interaction. Recent experimental efforts enable us to extract the precise value of this scattering length [25].

Below the threshold, there is no direct information of the $\overline{K}N$ channel, and this region should be constrained indirectly through the data in the $\pi\Sigma$ channel. Many recent experiments report the $\pi\Sigma$ mass spectra for the $\Lambda(1405)$ energy region. Although they are important subthreshold informations of the $\overline{K}N$ interaction, usually the normalization of the spectrum is not known and several interference effects in experiments may modify the relevant structure [8]. Instead, it is pointed out that the $\pi\Sigma$ threshold observables (scattering length and effective range) are also useful to constrain the subthreshold extrapolation of the $\overline{K}N$ interaction [26]. The scattering length is given as a number at fixed energy, so it is unambiguously incorporated in the extrapolation procedure.

In this circumstance, it is of great relevance to construct a realistic $\overline{K}N$-$\pi\Sigma$ interaction using new experimental information, and to provide future directions of the study of meson-baryon interaction. We present a comprehensive analysis with the next-to-leading order chiral interaction in section 3.1, by use of the new precise measurement of the kaonic hydrogen. In section 3.2, we discuss the possibility of determining the $\pi\Sigma$ scattering lengths through the analysis of the hadronic decays of Λ_c.

3.1 Improved constraints from new $\overline{K}N$ threshold data

Very recently, SIDDHARTA collaboration has reported a precise measurement of the 1s level of the kaonic hydrogen [25]. The reported values of the energy shift ΔE and width Γ are

$$\Delta E = 283 \pm 36(stat) \pm 6(syst)\ \text{eV}, \quad \Gamma = 541 \pm 89(stat) \pm 22(syst)\ \text{eV}. \tag{4}$$

Model	WT	WTB	NLO	Experiment [25]
ΔE [eV]	373	377	306	283 ± 42
Γ [eV]	495	514	591	541 ± 111
χ^2/d.o.f	1.12	1.15	0.96	
pole positions [MeV]	$1422 - 16i$	$1421 - 17i$	$1424 - 26i$	
	$1384 - 90i$	$1385 - 105i$	$1381 - 81i$	

Table 1: Results of the systematic χ^2 analysis by chiral SU(3) dynamics for the $S = -1$ meson-baryon scattering [28]. Shown are the energy shift and width of the 1s state of the kaonic hydrogen (ΔE and Γ), χ^2/d.o.f of the fitting, and the pole positions of the isospin $I = 0$ amplitude in the $\overline{K}N$-$\pi\Sigma$ region.

The error bars are significantly reduced from previous measurements. These values are related to the (complex) $K^- p$ scattering length through the improved Deser-Trueman formula [27]. Thus, this new information can be used to constrain the real and imaginary parts of the $K^- p$ scattering amplitude at the $\overline{K}N$ threshold.

A systematic χ^2 analysis with these new constraints is performed in the framework of chiral SU(3) dynamics including NLO terms [28]. Three models with different interaction kernels are examined: WT model (with the Weinberg-Tomozawa term $V = V^{\mathrm{WT}}$), WTB model (with the Weinberg-Tomozawa and Born terms $V = V^{\mathrm{WT}} + V^{\mathrm{Born}}$), and NLO model (all the terms $V = V^{\mathrm{WT}} + V^{\mathrm{Born}} + V^{\mathrm{NLO}}$). The subtraction constants (and the low energy constants in the NLO model) are fitted to the new data of the kaonic hydrogen (4), the threshold branching ratios, and the $K^- p$ total cross sections.

The results of the fitting are summarized in Table 1. Reasonable agreement with data is obtained in all cases, but in the WT and WTB models, some of the subtraction constants deviate from the natural value [19]. The NLO model gives the best fit (χ^2/d.o.f.< 1) and well reproduces the SIDDHARTA result (4), with natural-size subtraction constants [28]. Since the total cross section data is included in the χ^2 analysis, the new result (4) is shown to be consistent with the cross section data (see Refs. [15] for the comparison with previous measurements of the kaonic hydrogen).

The pole positions of the amplitude are shown in Table 1. All three models provide two poles in the energy region of the $\Lambda(1405)$ as discussed in section 2.2 and the double-pole structure of the $\Lambda(1405)$ resonance is confirmed. The uncertainty analysis, along the same line with Ref. [29], is also performed to check the stability of the fitting [28].

3.2 Information of $\pi\Sigma$ channel

As demonstrated in Ref. [26], the subthreshold extrapolation of the $\overline{K}N$ amplitude should not be discussed separately from the dynamics of the $\pi\Sigma$ channel. Although it is desirable to impose a constraint at the $\pi\Sigma$ threshold, so far no experimental information is available.

Determination of the $\pi\Sigma$ scattering lengths in the Λ_c decays is discussed in Ref. [30], in the same strategy with the method developed for the $\pi\pi$ scattering length [31]. Because of the isospin breaking in the masses of π and Σ, there is about 10 MeV mass difference in the transitions of $\pi^+\Sigma^- \to \pi^-\Sigma^+$, $\pi^+\Sigma^- \to \pi^0\Sigma^0$, and $\pi^+\Sigma^0 \to \pi^0\Sigma^+$. In the weak decays of the Λ_c into $\pi\pi\Sigma$ channels, cusp structure appears at the energy of the former $\pi\Sigma$ channel in the spectrum of the latter $\pi\Sigma$ channel. This cusp structure reflects the transition amplitude between $\pi\Sigma$ channels at the threshold, which is nothing but the (off-diagonal) $\pi\Sigma$ scattering length. The value of the scattering length can be extracted from the expansion of the $\pi\Sigma$ spectrum around the threshold. It is shown that the substantial cusp effect should be observed in the spectrum, when the $\pi\Sigma$ interaction in $I = 0$ is strongly attractive to generate a pole singularity around the threshold [30].

This method can be applied to three different modes in the Λ_c decays. Isospin decomposition of these channels reads

$$a^{-+} = \frac{1}{3}a^0 - \frac{1}{2}a^1 + \frac{1}{6}a^2 + \ldots, \quad a^{00} = \frac{1}{3}a^0 - \frac{1}{3}a^2 + \ldots, \quad a^{0+} = -\frac{1}{2}a^1 + \frac{1}{2}a^2 + \ldots,$$

where a^I is the scattering length with isospin I and ellipses represent the isospin breaking corrections. Since these three channels are not linearly independent as $a^{-+} - a^{00} = a^{0+} + \ldots$, this method alone is not sufficient to determine all the isospin components, even if we extract the scattering lengths in all three channels. The last piece of the information may be completed by Lattice QCD [5,32] which can determine the $\pi\Sigma$ scattering length in the $I = 2$ channel.

4 Summary

We have studied the $\overline{K}N$-$\pi\Sigma$ interaction and the $\Lambda(1405)$ resonance based on chiral SU(3) symmetry and unitarity. It is shown that the chiral symmetry constrains the dynamics of the Nambu-Goldstone boson with hadrons at low energy, and the unitarity of the scattering amplitude enables us to construct the dynamical approach to the hadron scattering amplitude. We show that the $\Lambda(1405)$ resonance and the $S = -1$ meson-baryon scattering are well described in the framework of chiral SU(3) dynamics. The $\Lambda(1405)$ resonance exhibits a peculiar pole structure which is driven by the two attractive components of the chiral interaction in the $\overline{K}N$ and $\pi\Sigma$ channels.

The precise measurement of the kaonic hydrogen provides new constraints on the $\overline{K}N$-$\pi\Sigma$ amplitude. The chiral SU(3) dynamics at next-to-leading order is capable of accommodating this new information consistently with the total cross section data. The $\pi\Sigma$ scattering length can be an alternative observable to further constrain the $\overline{K}N$ interaction in the lower energy region. These activity will bring us a deep understanding of the $\Lambda(1405)$ resonance and will provide a baseline of the application of the $\overline{K}N$ interaction to the strangeness nuclear physics.

Acknowledgments

The author is grateful to Yoichi Ikeda, Daisuke Jido, Makoto Oka, and Wolfram Weise for many stimulating discussions and fruitful collaborations. He thanks the support from the Global Center of Excellence Program by MEXT, Japan through the Nanoscience and Quantum Physics Project of the Tokyo Institute of Technology. This work was partly supported by the Grant-in-Aid for Scientific Research from MEXT and JSPS (No. 21840026).

Bibliography

[1] R. H. Dalitz, S. F. Tuan, Phys. Rev. Lett. **2**, 425 (1959); J. D. Weinstein, N. Isgur, Phys. Rev. D **27**, 588 (1983).

[2] E. S. Swanson, Phys. Rept. **429**, 243 (2006).

[3] R. Machleidt, K. Holinde, C. Elster, Phys. Rept. **149**, 1 (1987); A. Mueller- Groeling, K. Holinde, J. Speth, Nucl. Phys. A **513**, 557 (1990).

[4] N. Ishii, S. Aoki, T. Hatsuda, Phys. Rev. Lett. **99**, 022001 (2007).

[5] A. Torok *et al.*, Phys. Rev. D **81**, 074506 (2010).

[6] N. Kaiser, P. B. Siegel, W. Weise, Nucl. Phys. A **594**, 325 (1995); E. Oset, A. Ramos, Nucl. Phys. A **635**, 99 (1998); M. F. M. Lutz, E. E. Kolomeitsev, Nucl. Phys. A **700**, 193 (2002).

[7] J. A. Oller, U. G. Meißner, Phys. Lett. B **500**, 263 (2001).

[8] T. Hyodo, D. Jido, Prog. Part. Nucl. Phys. (2011), doi:10.1016/j.ppnp.2011.07.002, arXiv:1104.4474 [nucl-th].

[9] N. Isgur, G. Karl, Phys. Rev. D **18**, 4187 (1978).

[10] R. H. Dalitz, T. C. Wong, G. Rajasekaran, Phys. Rev. **153**, 1617 (1967).

[11] Y. Akaishi, T. Yamazaki, Phys. Rev. C **65**, 044005 (2002).

[12] J. Gasser, H. Leutwyler, Nucl. Phys. B **250**, 465 (1985); V. Bernard, N. Kaiser, U. G. Meißner, Int. J. Mod. Phys. E **4**, 193 (1995).

[13] T. Hyodo, D. Jido, A. Hosaka, Phys. Rev. Lett. **97**, 192002 (2006); Phys. Rev. D **75**, 034002 (2007).

[14] S. Weinberg, Phys. Rev. Lett. **17**, 616 (1966); Y. Tomozawa, Nuovo Cim. A **46**, 707 (1966).

[15] B. Borasoy, R. Nißler, W. Weise, Phys. Rev. Lett. **94**, 213401 (2005); Eur. Phys. J. A **25**, 79 (2005).

[16] D. Jido, J. A. Oller, E. Oset, A. Ramos, U. G. Meißner, Nucl. Phys. A **725**, 181 (2003).

[17] T. Hyodo, W. Weise, Phys. Rev. C **77**, 035204 (2008).

[18] B. Marcelis, *et al.*, Phys. Rev. A **70**, 012701 (2004).

[19] T. Hyodo, D. Jido, A. Hosaka, Phys. Rev. C **78**, 025203 (2008).

[20] T. Hyodo, D. Jido, A. Hosaka, arXiv:1108.5524 [nucl-th].

[21] T. Hyodo, D. Jido, L. Roca, Phys. Rev. D **77**, 056010 (2008); L. Roca, T. Hyodo, D. Jido, Nucl. Phys. A **809**, 65 (2008).

[22] T. Sekihara, T. Hyodo, D. Jido, Phys. Lett. B **669**, 133 (2008); Phys. Rev. C **83**, 055202 (2011).

[23] N. V. Shevchenko, A. Gal, J. Mares, Phys. Rev. Lett. **98**, 082301 (2007); N. V. Shevchenko, A. Gal, J. Mares, J. Revai, Phys. Rev. C**76**, 044004 (2007); T. Yamazaki, Y. Akaishi, Phys. Rev. C **76**, 045201 (2007). Y. Ikeda, T. Sato, Phys. Rev. C**76**, 035203 (2007); Phys. Rev. C**79**, 035201 (2009); A. Dote, T. Hyodo, W. Weise, Nucl. Phys. A**804**, 197 (2008); Phys. Rev. C **79**, 014003 (2009); Y. Ikeda, H. Kamano, T. Sato, Prog. Theor. Phys. **124**, 533 (2010); T. Uchino, T. Hyodo, M. Oka, arXiv:1106.0095 [nucl-th], to appear in Nucl. Phys. A.

[24] D. N. Tovee *et al.*, Nucl. Phys. B **33**, 493 (1971); R. J. Nowak *et al.*, Nucl. Phys. B **139**, 61 (1978).

[25] M. Bazzi *et al.*, arXiv:1105.3090 [nucl-ex].

[26] Y. Ikeda, T. Hyodo, D. Jido, H. Kamano, T. Sato, K. Yazaki, Prog. Theor. Phys. **124**, 1205-1224 (2011).

[27] U. G. Meißner, U. Raha, A. Rusetsky, Eur. Phys. J. C **35**, 349 (2004).

[28] Y. Ikeda, T. Hyodo, W. Weise, in preparation.

[29] B. Borasoy, U. G. Meißner, R. Nißler, Phys. Rev. C **74**, 055201 (2006).

[30] T. Hyodo, M. Oka, arXiv:1105.5494 [nucl-th], to appear in Phys. Rev. C.

[31] N. Cabibbo, Phys. Rev. Lett. **93**, 121801 (2004).

[32] Y. Ikeda *et al.*, in preparation.

An Overview of Recent Results from CLAS

Kenneth H. Hicks[1] on behalf of the CLAS Collaboration
Department of Physics and Astronomy, Ohio University
Athens, Ohio 45701, USA

The unique capabilities of the CLAS detector to measure exclusive meson electroproduction off protons, with almost complete coverage of the final hadron phase space, has extended our knowledge of excited baryon structure. Consistent results from $N\pi$ and $N\pi\pi$ final states provide convincing evidence for reliable extraction of N^* electrocouplings. Theoretical analyses of these results, using self-consistent dynamical calculations using an internal quark core and an external meson-baryon cloud suggest that meson-baryon dressing amplitudes need to be included. The meson-baryon dressing was already shown to be necessary to get agreement between calculations and data on the Δ resonance transition magnetic moment at low Q^2. Similarly, a new measurement of the transition magnetic moment for strange baryons also disagrees with quark models, suggesting the need for meson-baryon dressings. In the near future, the CLAS detector will be replaced with CLAS12, providing new high-precision data.

1 Introduction

With the goal of understanding the resonance structure of the nucleon, the CLAS Detector [1] has measured a variety of electron and photon scattering reactions off a proton target. The resulting data provide a wealth of information about the electrocouplings of nucleon resonances at photon four-momentum transfers ranging up to $Q^2 < 5\,\mathrm{GeV}^2$. In addition, the electromagnetic decay of baryon resonances having strangeness, such as the Σ^* resonance at mass 1385 $\mathrm{GeV/c^2}$, have been measured for the first time due to the high luminosity and large acceptance of the CLAS experiments. Both of these phenomena point toward the active role of a meson-baryon cloud as part of the wave-function describing baryon resonances. Theoretical progress made by the Excited Baryon Analysis Center (EBAC) at Jefferson Lab provides calculations that allow interpretation of the experimental data using a dynamical coupled channels model [2–4] that includes a bare N^* core and its fluctuation into a meson-baryon cloud. Superposition of the amplitues from the meson-baryon cloud and the quark core predicts measureable effects in the N^* electrocouplings. With the advent of high precision data from CLAS and other facilities around the world, these theoretical ideas can be tested and have led to a better understanding of baryon resonances.

[1] hicks@ohio.edu

One of the major breakthroughs of recent years in the understanding of QCD is the non-perturbative calculations using the Dyson-Schwinger equation (DSE) [5]. Shown in Fig. 1 is the quark mass as a function of the momentum variable q of the dressed quark propagator. When the quark is hit hard, giving the propagator a momentum greater than about 1 GeV, the effective quark mass becomes very small, while for soft interactions, the quark becomes "dressed" with a gluon cloud, attaining an effective mass (even in the chiral limit) of about 1/3 of the nucleon mass. Fig. 1 also shows data from lattice gauge calculations for light quark masses, which agrees with the curves from the DSE approach with the same input quark mass. The lesson to take away is that 97% of the dressed quark mass comes from the gluon dressing of the bare (core) quark in the regime of large quark-gluon coupling. Hence quarks should not be assigned a fixed mass (as is done in the non-relativistic constituent quark model), especially when probing high momentum transfer reactions. Furthermore, because gluons couple to quark-antiquark loops, the gluon cloud also has virtual meson components.

Non-perturbative interactions of dressed quarks and gluons create a quark core of both ground and excited states of the proton. On top of that, we have the contribution from an external meson-baryon cloud, required by the general unitarity condition for meson-baryon interaction amplitudes [4].

An example of the importance of meson-baryon effects is shown in Fig. 2, where data on the magnetic dipole transition form factor, $G_M(Q^2)$, for $\gamma^* N \rightarrow \Delta$ transitions is shown as a function of the virtual photon 4-momentum, Q^2. At low Q^2, the solid (dashed) curve calculated with (without) the baryon dressing show a significant contribution of the meson-baryon cloud to this observable [6]. In the non-relativistic quark model, the value of $G_M(0)$ is directly proportional to the proton magnetic moment, and the value of G_M extrapolate to $Q^2 = 0$ can only be explained in that model if the experimental magnetic moment is lowered by about 30%. Without the meson-baryon cloud effects, this simple theoretical model is in direct contradiction with experimental facts. Hence there is a need for dynamical meon-baryon amplitudes to explain the electrocoupling to the best known nucleon resonance, the Δ. It should not be a surprise if dynamical meson-baryon effects are also necessary to explain electrocouplings to other baryon resonances.

In the following sections, experimental results from CLAS using virtual photons, including both single and double pion-production reactions, are compared with theoretical models and the magnitude of the meson-baryon dressing amplitudes. Next, the electromagnetic decay of baryons with strangeness are described, showing strong evidence for effects from the meson-baryon cloud. A short recap of the search for exotic mesons and glueball-mixing at CLAS is provided, followed by a description of the planned upgrade to 12 GeV beam energies and the new CLAS12 detector at Jefferson Lab.

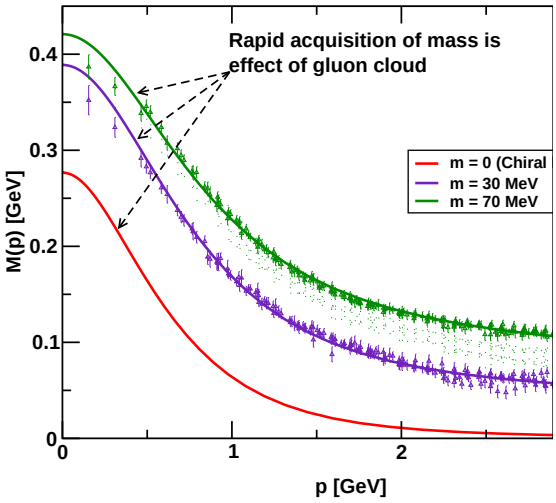

Figure 1: Calculations of the quark effective mass as a function of the quark momentum using the Dyson-Schwinger equation, from Ref. [5].

2 Experimental Description and Results

The measurements reported here were done using the high intensity electron beam with energies up to 6 GeV with 100% duty cycle from the Continuous Electron Beam Accelerator Facility (CEBAF), located at the Thomas Jefferson National Accelerator Facility in the USA. CEBAF has the shape of a racetrack, with two superconducting RF-linacs along the straight sections and groups of normal conducting magnets along the recirculation arcs. The electron beam can be circulate around the linacs up to five times, gaining approximately 1.2 GeV on each pass (a distance of about 1.4 km). The beam can be sent simultaneously to three experimental halls: A, B and C.

The CEBAF Large Acceptance Spectrometer (CLAS), housed in Hall B, is shown in Fig. 3. Both electron and tagged photon beams can be directed onto the target, shown in the center of the cutaway region of the figure. Surrounding the target is a toroidal magnetic field generated by six superconducting coils spaced uniformly in angle about the beamline axis. Within each of the six sectors, there are multiple layers of drift chambers, spaced radially outward from the target, to track the outgoing particles. For photon beam experiments, a segmented scintillator called the start counter surrounds the target, providing timing

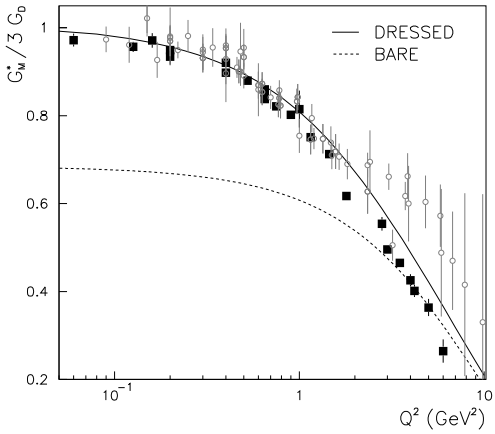

Figure 2: The transition magnetic moment G_M, in units of the proton dipole form factor as a function of Q^2 for the $\gamma^* N \rightarrow \Delta$ electromagnetic transition, from Ref. [6].

information for charged particles and forms part of the trigger in coincidence with the tagged electron. Outside of the three regions of drift chambers, a gas Cerenkov counter identifies electrons and helps to discriminate pions from electrons. The whole system is surrounded by a layer of plastic scintillator bars to record the time-of-flight (TOF) of particles from the target. At the outermost layer, shown by the triangular sections in Fig. 3, is the electromagnetic calorimeter, made from alternating layers of plastic scintillator and thin lead sheets, used for detection of electrons, photons and (for some experiments) neutrons.

For all data presented below, the target was a liquid hydrogen cell. A typical luminosity for electron running was about $10^{34}/\mathrm{cm}^2/\mathrm{s}$ and for photon experiments, the rate on a typical 40 cm target was about 10^7 photons/sec, integrated from 10% to 95% of the electron beam energy, in a classic bremsstrahlung distribution. Both beams and target can be polarized, which provides additional information for partial wave analysis of scattering reactions. Complete sets of polarization measurements are the next step in a series of results coming from CLAS data, with the goal of isolating spin-dependent amplitudes in production of baryon resonances.

Fig. 4 shows the electrocoupling of the $P_{11}(1440)$ resonance. Using a total of about 12000

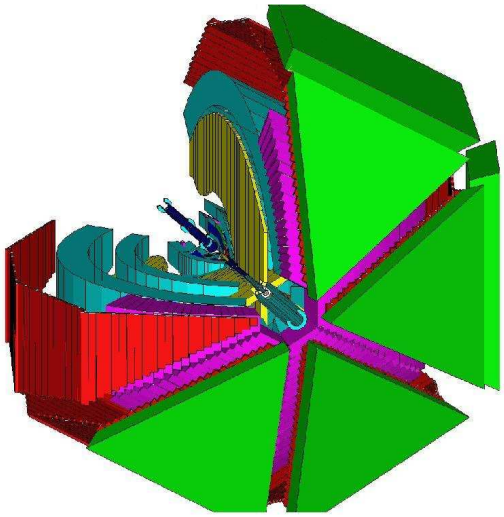

Figure 3: Schematic diagram of CLAS detector, with one region cut away to show the inner structure of detectors.

data points on differential cross sections, from experiments using both unpolarized beams or longitudinal polarization of beam and/or target, CLAS has the most complete coverage of the kinematics corresponding to the Roper resonance, centered at 1440 MeV with a width of several hundred MeV. More information on the data set, including electrocouplings to the $S_{11}(1535)$ resonance, can be found in Ref. [7]. The data shown in Fig. 4 are for the $A_{1/2}$ amplitude, scaled up by a factor of 1000, where the open symbols for $Q^2 > 0$ are from single pion electroproduction data (both $\pi^+ n$ and $\pi^0 p$) and the closed symbols [8] are from two-pion electroproduction ($\pi^+\pi^- p$) data [9]. Points at $Q^2 = 0$ are from high-precision single-pion photoproduction data [10].

Consistent results on electrocouplings of the $P_{11}(1440)$ and $D_{13}(1530)$ resonances obtained in independent analyses of two major meson electroproduction channels ($N\pi$ and $N\pi\pi$) with different non-resonant contributions clearly show the reliable extraction of these fundamental quantities. Furthermore, the reaction models [7] for extraction of N^* electrocouplings from independent analyses of $N\pi$ and $p\pi^+\pi^-$ channels allows a determination of electrocouplings of all resonances that decay preferentially to these final state. Preliminary results on electrocouplings of $S_{31}(1620)$, $S_{11}(1650)$, $F_{15}(1685)$, $D_{33}(1700)$ and $P_{13}(1720)$ states were obtained [7] from the CLAS data on $p\pi^+\pi^-$ electroproduction data within the theoretical

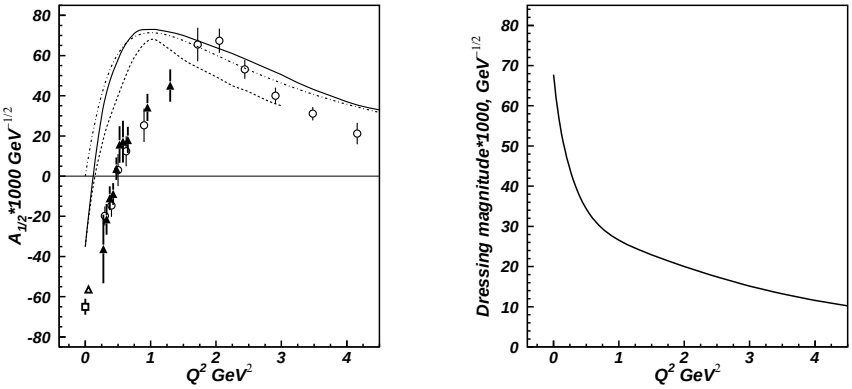

Figure 4: Left: Electrocoupling of the $P_{11}(1440)$ resonance; right: calculated magnitude of the meson-baryon dressing amplitudes for the same resonance. See text for discussion of symbols and curves.

framework discussed in Ref. [11].

The curves in the left panel of Fig. 4 are from light-front quark models [12,13] (solid and dashed) and from a diquark model [14] (dot-dashed). These curves all follow the general trend of the data, but fail to predict the data at low Q^2. One explanation may be that the curves in the left panel do not include meson-baryon dressing, which is calculated within the dynamical coupled-channels model [3], with its magnitude shown in the right panel of Fig. 4. As shown in the previous figure, the meson-baryon dressing has a substantial effect on theoretical calculations of Δ-resonance transition magnetic moments, and a similarly large effect of the dressing is calculated for the Roper resonance shown in Fig. 4.

Further evidence for the importance of the meson-baryon cloud comes from electromagnetic decay of excited strange baryons. Recent analysis of CLAS data for the reaction $\gamma p \to K\Sigma^*$ provides high statistics for the Σ^* resonance, a decuplet baryon with strangeness -1. The Σ^* can decay via the strong force to $\Sigma\pi^0$ or via electromagnetic (EM) decay to $\Sigma\gamma$. The latter is expected to have a branching ratio of about 1%, and hence is difficult to measure. Just like the Δ transition magnetic moment discussed above, the EM decay of the Σ^* holds information on the effect of the meson-baryon cloud. Previously reported CLAS data for the EM decay $\Sigma^{*0} \to \Lambda\gamma$ has already shown that this is an important effect [15].

The missing mass for $\gamma p \to K^0\Sigma^+ X$ is shown [16] in Fig. 5 where the upper histogram is for all data (after cuts to isolate the given final state) with a prominant peak at the mass of the π^0

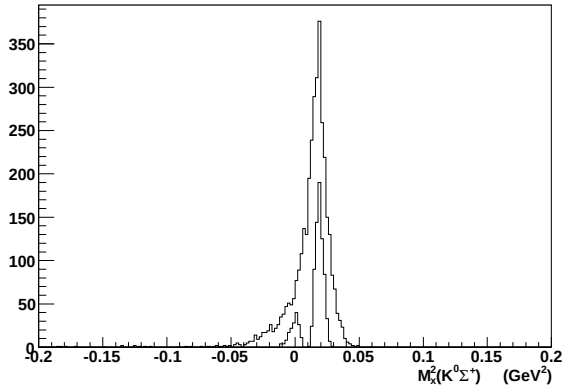

Figure 5: Missing mass of the reaction $\gamma p \to K^0\Sigma^+ X$ from CLAS data [16].

and a “shoulder" at zero mass corresponding to γ decay. By use of a sophisticated kinematic fit, which can be shown to be robust in its ability to extract the ratio of EM to strong decay of the Σ^{*+}, the lower histograms in Fig. 5 are the result, showing a clean separation of these two decays. This is the world’s first extraction of the EM decay branching ratio for the Σ^{*+}, which provides a test of the meson-baryon cloud for baryons with strangeness. The results are shown in Table 1, where the experimentally extracted transition magnetic moments ($Q^2 = 0$) are compared with the first-order $1/N_c$ expansion of Jenkins and Manohar [17] and the naive quark model [18]. Both theoretical models substantially underpredict the experimentally measured values, similar to the case of the Δ transition magnetic moment [6].

While CLAS has provided world-class data, resulting in the world’s best extractions of electrocouplings and transition magnetic moments, this detector will be dismantled in 2012 and replaced with a new detector, CLAS12, for operation with the energy upgrade of CEBAF to 12 GeV. A computer drawing of the CLAS12 detector is shown in Fig. 6. The main features of CLAS12 is its ability to take data at luminosities higher by an order of

Transitions	$1/N_c$ Model	Quark Model	Experiment
$\mu_{\Sigma\Sigma^{*+}}$	2.17±0.30	2.33	3.22±0.35
$\mu_{\Lambda\Sigma^{*0}}$	2.28±0.32	2.28	2.75±0.23

Table 1: Transition magnetic monemts of the $\Sigma(1385)$ from the $1/N_c$ and naive quark model compared with the CLAS experimental results.

magnitude than the present CLAS detector. In addition, CLAS12 has improved particle identification, along with tracking at angles as small as 5° in the laboratory frame.

There are two major parts to the CLAS12 detector: the Central Detector, which includes a superconducting solenoid (shown in the left part of Fig. 6) and the Forward Detector, which includes a six-sector toroidal magnetic field (shown in the middle of Fig. 6). Inside the solenoid will be a silicon vertex tracker (SVT) and central time-of-flight detectors (CTOF). At forward angles will be a high-threshold and a low-threshold Cerenkov detector (HTCC and LTCC), 3 regions of drift chambers (DC), forward time-of-flight scintillators (FTOF), a pre-shower calorimeter (PCAL) and an electromagnetic calorimeter (EC). Not visible is a low-angle inner calorimeter (IC) for detection of high-energy photons.

The primary physics goals of CLAS12 is to measure: Generalized Parton Distributions (GPDs), Transverse Momentum Distributions (TMDs), hadronization in Deep Inelastic Scattering (DIS), meson spectroscopy and studies of N^* structure at photon virtualities of $Q^2 > 5.0$ GeV^2. Each of these topic will be discussed briefly below.

GPDs were introduced about a decade ago, using a theoretical approximation valid for hard-quark scattering that has proven to be extremely efficient at describing experimental data. Leading order Feynmann diagrams for GPDs (also called “handbag" diagrams) describe the correlations between the helicity, longitudinal momentum and transverse position of quarks in the nucleon. Two spin-independent GPDs (H and E) and two spin-dependent GPDs ($\tilde{H}$ and $\tilde{E}$) are accessible through exclusive hard reactions such as Deeply Virtual Compton Scattering (DVCS) measurements using the CLAS12 detector.

TMDs can be accessed via semi-inclusive deep inelastic scattering (SIDIS) where a meson is detected along with a scattered electron. Using polarized beams and polarized targets, TMDs such as the Sivers and Boer-Mulders functions provide information about the momentum distribution of the quarks transverse to the beam direction. Non-zero values for these functions are related to the orbital angular momentum of the quarks, which contribute to the overall nucleon spin. The future CLAS12 data will provide unprecidented precision of the TMDs, resulting in better knowledge of the quark momentum distributions in the nucleon.

Studies of nucleon resonances at the largest photon virtualities ever achieved, from Q^2 of 5 to 12 GeV^2, will allow us for the first time to access almost directly the quark degrees of freedom in N^* structure. It will also allow us to explore the origin of the dynamical

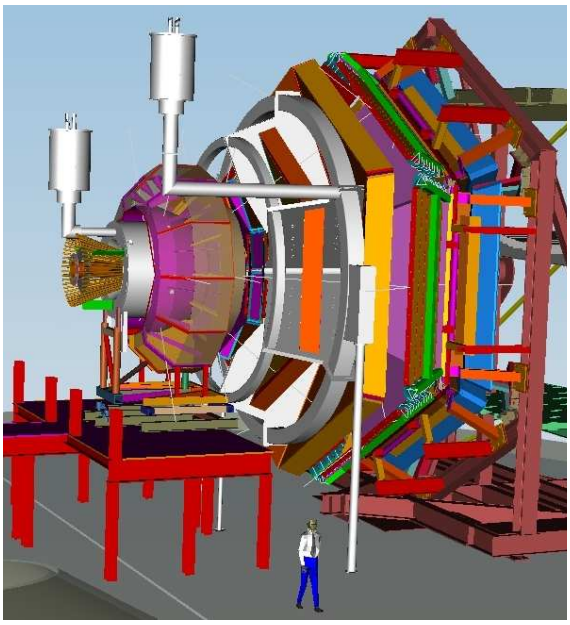

Figure 6: Schematic drawing of the CLAS12 detector, which will soon be installed in Hall B, replacing the CLAS detector.

mass and structure of dressed quarks, along with the non-perturbative strong interactions coming from QCD that are responsible for nucleon structure [19].

3 Summary

Effects of the meson-baryon clould are now evident from the analysis of high-precision data from CLAS. Such effects are expected theoretically from calculations using the Dyson-Schwinger equation, where the effective quark mass changes with Q^2. Experimentally, data from electroproduction of nucleon resonances, such as the Δ and Roper resonances, show clear deviations from calculations with no meson-baryon cloud. For the Δ, agreement is again achieved for dynamical calculations that include the meson-baryon cloud. For the $P_{11}(1440)$, the magnitude of the meson-baryon cloud effects are consistent with the difference between measured electrocouplings and light-front quark models. Decuplet-octet transition magnetic moments of the strange baryons also disagree with quark model calculations, pointint to the need for dynamical coupled-channels calculations that include the meson-baryon cloud.

Future measurements with the CLAS12 detector, which will replace the CLAS detector for the planned 12 GeV energy upgrade at Jefferson Lab, open new possibilities to measure GPDs and TMDs using polarized beams and polarized targets. These data will provide new information on, amoung other things, the orbital angular momentum of quarks inside the nucleon and correlations between momentum and position of these quarks. A rich physics program awaits the measurements that will be done with CLAS12.

Acknowledgments

I am grateful to members of the CLAS Collaboration who contribued to the physics results and the detector technology presented in this talk. This work was supported in part by the National Science Foundation, the U.S. Department of Energy, the French Commisariat à l'Energie Atomique, the Italian Instituto Nazionale di Fisica Nucleare, the Korea Research Foundation, and a research grant of the Russian Federation.

Bibliography

[1] B. Mecking *et al.*, NIM A **503**, 513 (2003).

[2] A. Matsuyama, T. Sato, and T.-S.H. Lee, Phys. Rep. **439** 193 (2007).

[3] B. Julia-Diaz *et al.*, Phys. Rev. C **77**, 045205 (2008).

[4] N. Suzuki *et al.*, Phys. Rev. C **82**, 045206 (2010).

[5] M.S. Bhagwat, I.C. Cloët and C.D. Roberts, in *Exclusive Reactions at High Momentum Transfer*, A. Radyushkin and P. Stoler, eds. (World Scientific, Singapore, 2008), pp. 112-120.

[6] B. Julia-Diaz, T.-S.H. Lee, A. Matsuyama and L.C. Smith Phys. Rev. C **77**, 045205 (2008).

[7] I.G. Aznauryan *et al.*, Phys. Rev. C **80**, 055203 (2009).

[8] I.G. Aznauryan, V.D. Burkert, V.I. Mokeev, arXiv:1108.1125.

[9] G.V. Fedotov *et al.*, Phys. Rev. C **79**, 015204 (2009).

[10] M. Dugger *et al.*, Phys. Rev. C **79**, 065206 (2009).

[11] V.I. Mokeev *et al.*, Phys. Rev. C **80**, 045212 (2009).

[12] I.G. Aznauryan, Phys. Rev. C **76**, 025212 (2007).

[13] S. Capstick and B.D. Keister, Phys. Rev. D **51**, 3598 (1995).

[14] G. Ramalho and K. Tsushima, Phys. Rev. D **81**, 074020 (2010).

[15] D. Keller, *et al.*, Phys. Rev. D **83**, 072004 (2011).

[16] D. Keller, *et al.*, submitted to Phys. Rev. D.

[17] E. Jenkins and A.V. Manohar, Phys. Lett. B **335**,452 (1994).

[18] R. Dhir and R.C. Verma, Eur. Phy. J. A **42**, 243-249 (2010).

[19] I.G. Aznauryan *et al.*, arXiv:0907.1901.

Heavy Flavor Baryons at the Tevatron

Thomas Kuhr[1] on behalf of the CDF and D0 Collaborations
Karlsruhe Institute of Technology
Institut für Experimentelle Kernphysik
Wolfgang-Gaede-Str. 1
D-76131 Karlsruhe, GERMANY

The Tevatron experiments CDF and D0 have filled many empty spots in the spectrum of heavy baryons over the last few years. The most recent results are described in this article: The first direct observation of the Ξ_b^0, improved measurements of Σ_b properties, a new measurement of the $\Lambda_b \to J/\psi\Lambda$ branching ratio, and a high-statistics study of charm baryons.

1 Introduction

The Λ_b baryon, with quark content $|udb\rangle$, is known since about 20 years. But only recently considerable progress could be made on the other components of the b-baryon family by the Tevatron experiments CDF and D0. The charged Σ_b baryons ($|uub\rangle$ and $|ddb\rangle$) were observed in the decay to $\Lambda_b\pi^\pm$ by CDF in 2007 [1]. In the same year the charged Ξ_b state ($|dsb\rangle$) was directly observed by D0 [2] and CDF [3] in the decay to $J/\psi\Xi^-$. Until then only indirect observations of the Ξ_b via an excess in $\Xi^-\ell^-$ events were reported by the ALEPH [4] and DELPHI [5] experiments. In 2008 the Ω_b^- ($|ssb\rangle$) was discovered by D0 in the decay to $J/\psi\Omega^-$ [6]. CDF observed the Ω_b^- briefly afterwards [7], but measured a mass that is incompatible with the value quoted by D0. In the last year the Tevatron experiments continued to improve the knowledge about heavy baryons by further measurements, which are presented in this article.

The progress on the field of heavy baryons has been possible because of the large dataset delivered by the Tevatron $p\overline{p}$ collider running at a center of mass energy of $\sqrt{s} = 1.96$ TeV. During the Run II period, both experiments, CDF and D0, collected about 10 fb^{-1} of data. The Tevatron is well suited for heavy baryon studies, e.g. compared to B factories, because all kinds of heavy hadrons are produced with significant cross section. On the other hand the high combinatorial background and the huge inelastic cross section are a challenge. To be able to record the interesting events with heavy flavor hadrons, highly selective and

[1] Thomas.Kuhr@kit.edu

efficient triggers are essential [8]. Both experiments can trigger on dimuon pairs so that heavy baryon decays to J/ψ mesons can be studied. While D0 has an efficient single muon trigger, CDF is able to trigger on hadronic decays of heavy hadrons identified by tracks displaced from the primary vertex.

2 Ξ_b^0 Observation

The Ξ_b^- was directly observed by D0 and CDF in the decay to $J/\psi\Xi^-$. The events were triggered by the dimuon decay of the J/ψ and the Ξ^- was reconstructed via $\Xi^- \to \Lambda\pi^-$. Since the corresponding decay of the neutral isospin partner, Ξ_b^0 ($|usb\rangle$) $\to J/\psi\Xi^0$ with $\Xi^0 \to \Lambda\pi^0$, involves a neutral pion which cannot be detected efficiently, a search for the Ξ_b^0 requires a trigger on a hadronic decay. CDF reported the first observation of the Ξ_b^0 [9] in the decay chain $\Xi_b^0 \to \Xi_c^+\pi^-$, $\Xi_c^+ \to \Xi^-\pi^+\pi^+$, and $\Xi^- \to \Lambda\pi^-$ briefly after the Hadron2011 conference and therefore this result is included in this article although it was not shown at the conference. In the same analysis of 4.2 fb^{-1} of data, CDF also confirms the observation of the Ξ_b^- baryon, reconstructed for the first time in its hadronic final state $\Xi_c^0\pi^-$ with $\Xi_c^0 \to \Xi^-\pi^+$.

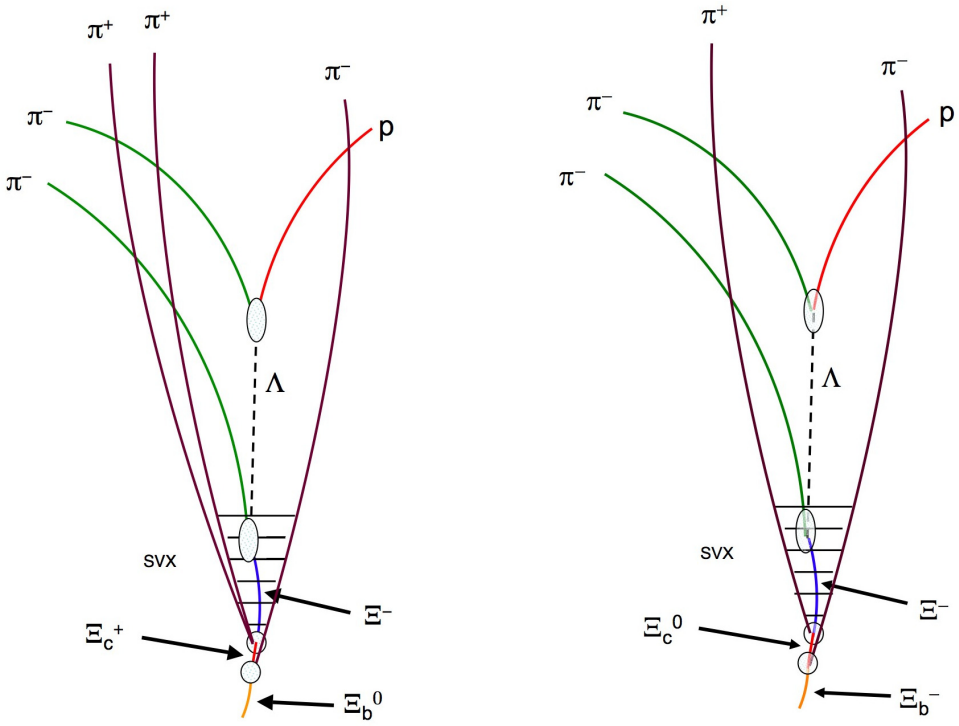

Figure 1: Illustration of the Ξ_b^0 (left) and Ξ_b^- (right) decay topology.

The reconstruction starts with the selection of Λ candidates from $p\pi^-$ pairs. Ξ^- candidates are constructed from $\Lambda\pi^-$ pairs which are then combined with one or two π^+ tracks to form Ξ_c^0 or Ξ_c^+ candidates, respectively. The addition of a further π^- track to the Ξ_c baryons yields the Ξ_b candidates. A schematic illustration of the reconstructed decay chain is shown in Fig. 1.

The long lifetime of hyperons and charm baryons is exploited by requirements on the reconstructed flight lengths, decay times, or impact parameters. The Ξ^- candidate is required to be identified by hits in the silicon vertex detector (SVX) which significantly reduces background as illustrated in Fig. 2. A simultaneous vertex fit of all tracks with mass constraints for the Λ, Ξ^-, and Ξ_c is performed to improve the momentum resolution of the Ξ_b. The reconstructed invariant mass spectra of Ξ_b candidates are shown in Fig. 3.

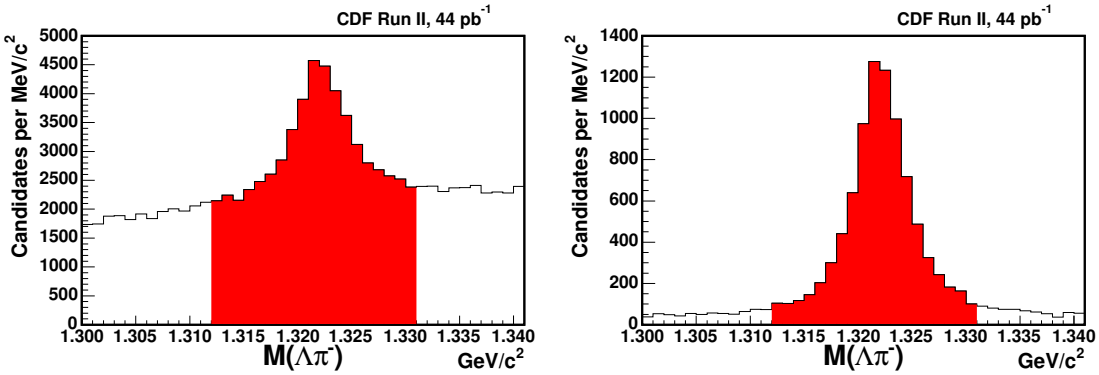

Figure 2: The invariant mass distributions of Ξ^- candidates without (left) and with (right) the requirement of SVX hits.

A clear signal is evident for the Ξ_b^- and Ξ_b^0. To determine the significance and to measure the mass of the states, an unbinned likelihood fit is performed. The signal is described by a Gaussian and the background by a linear function. The width of the Gaussian is given by the reconstructed mass resolution of each candidate multiplied with a common scale factor which is fitted to a value consistent with 1. The significance is determined from a likelihood ratio to be at least 6.8σ. The yields are $25.8^{+5.5}_{-5.2}$ Ξ_b^- and $25.3^{+5.6}_{-5.4}$ Ξ_b^0 baryons. Their masses are measured to be $m(\Xi_b^-) = (5796.7 \pm 5.1 \pm 1.4)$ GeV/c^2 and $m(\Xi_b^0) = (5787.8 \pm 5.0 \pm 1.3)$ GeV/c^2. The systematic uncertainties are given by the absolute mass scale, the mass resolution scale, and the world average Ξ_c masses. The Ξ_b^- mass is well consistent with the one measured in the $J/\psi\Xi^-$ decay channel [3].

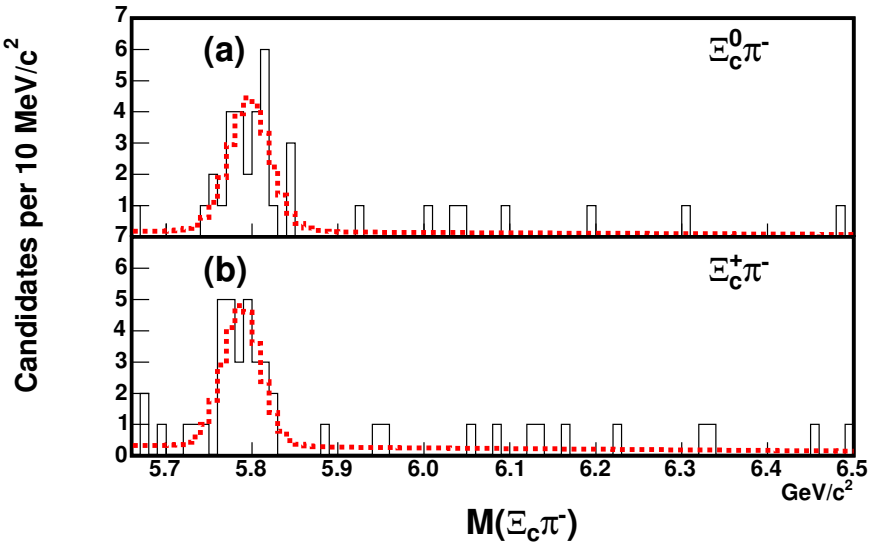

Figure 3: The $\Xi_c^0\pi^-$ (a) and $\Xi_c^+\pi^-$ (b) mass distributions with fit projection as dashed line.

3 $\Sigma_b^{(*)}$ Masses and Widths

$\Sigma_b^{(*)}$ baryons form an isospin triplet and have a flavor symmetric light di-quark with spin 1. This couples with the heavy quark spin to two possible spin states, $J^P = \frac{1}{2}^+$ and $J^P = \frac{3}{2}^+$, referred to as Σ_b and Σ_b^*, respectively. The $\Sigma_b^{(*)}$ baryons decay strongly to the Λ_b ground state via the emission of a pion. Figure 4 illustrates the spectrum of baryons consisting of u, d, and one b quark.

The decays of the charged $\Sigma_b^{(*)}$ states were first observed by CDF in 2007 [1]. In a data sample of 1.1 fb^{-1}, the significance of each of the four states was about 3σ. Assuming the same hyperfine splitting between Σ_b^* and Σ_b for both charged states, the masses were measured. Now CDF presented an updated analysis of 6 fb^{-1} of data with improved significances, unconstrained mass measurements, and first measurements of the $\Sigma_b^{(*)}$ natural widths [10].

The Λ_b baryons from the $\Sigma_b^{(*)} \to \Lambda_b\pi^\pm$ decay are reconstructed in the decay to $\Lambda_c^+\pi^-$ with $\Lambda_c^+ \to pK^-\pi^+$. The tracks of the final state particles from the Λ_c^+ and Λ_b decay are usually displaced from the primary vertex so that these decays are selected by the hadronic trigger. The selection requirements on lifetime and kinematic variables are optimized on the significance of the Λ_b signal. The reconstructed Λ_b invariant mass distribution is shown in Fig. 5. The selected sample contains 16 000 Λ_b baryons with a signal to background ratio

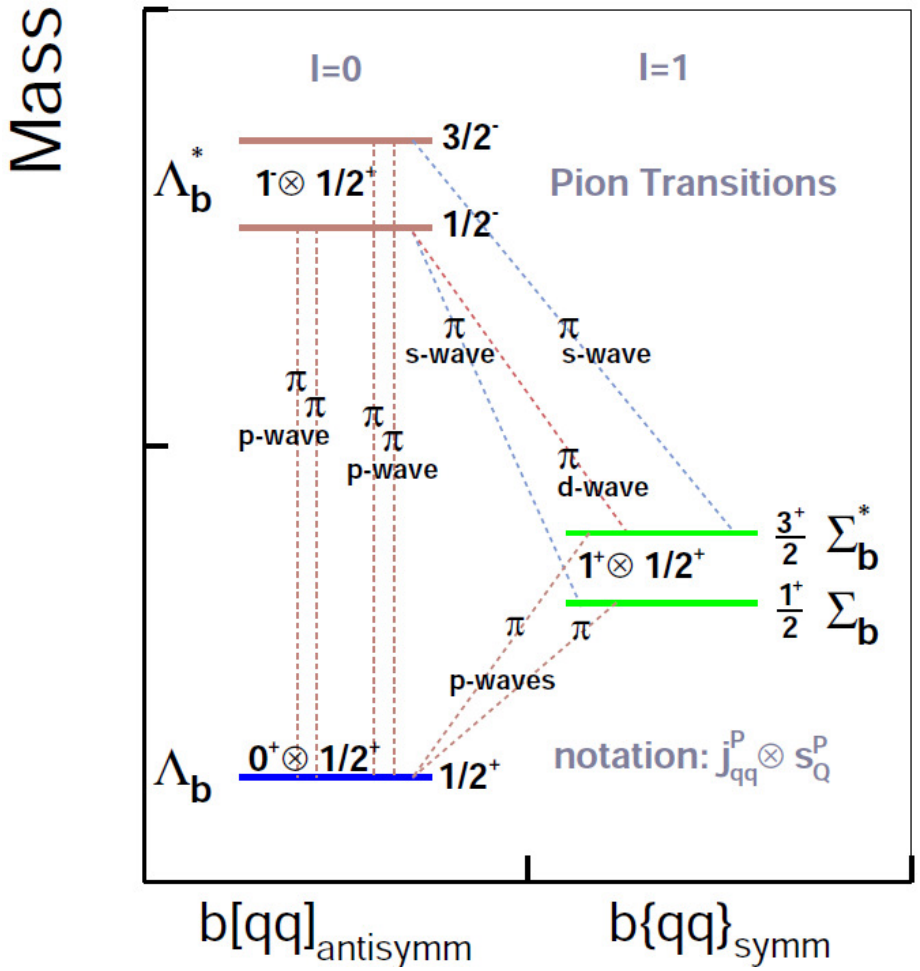

Figure 4: Spectrum and decays of b baryons with no strangeness.

of about 1.8. Thus the main background to the $\Sigma_b^{(*)}$ signals in $\Lambda_b\pi^\pm$ combinations are real Λ_b with a random pion.

To measure masses and width, the Q value distribution is fitted, where Q is the difference between the reconstructed $\Lambda_b\pi^\pm$ mass and the sum of Λ_b and pion masses. The background is described by an empirical function consisting of a second order polynomial times a square root function to describe the threshold behavior. Compared to the previous analysis, the background description does not rely on simulation any more. Each of the four signal peaks is parametrized by a non-relativistic Breit-Wigner. To account for the p wave decay, a variable width is used which scales with p_π^3 where p_π is the pion momentum in the $\Sigma_b^{(*)}$ rest frame. The natural line shape is convolved with a double Gaussian resolution function whose parameters are determined from simulation. Projections of the fit are shown in Fig. 6.

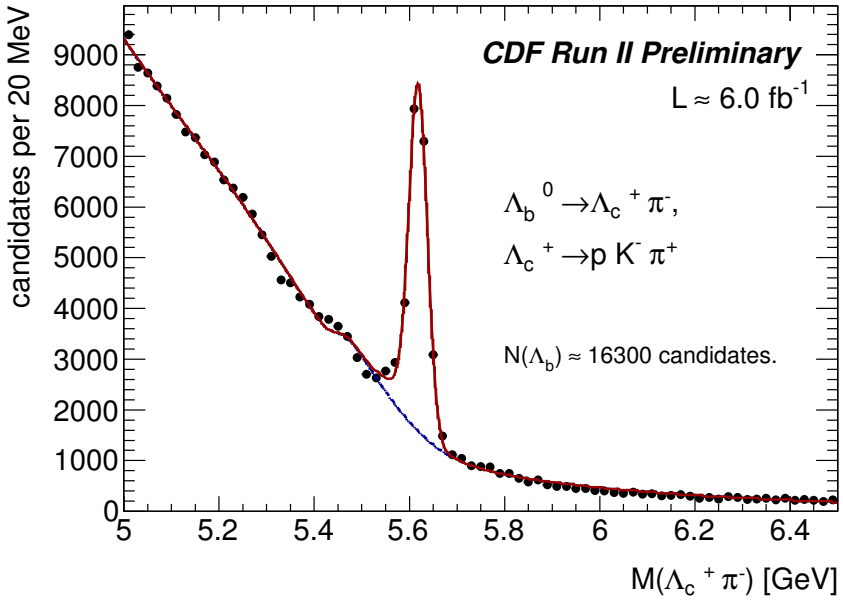

Figure 5: Invariant mass distribution of Λ_b candidates.

The hypotheses of having two, one, or no signal peaks are compared using a likelihood ratio. For both isospin states the hypothesis of two peaks is favored by more than 7σ over any of the other hypotheses, meaning that each peak has a significance above 7σ.

The measured masses and width are quoted in Tab. 1. The dominant systematic uncertainty for the Q values is the uncertainty on the momentum scale which is estimated from the comparison of reconstructed Σ_c^{++}, Σ_c^0, Λ_c^{*+}, and D^{*+} masses with world average values. The systematic uncertainty of the widths is dominated by the uncertainty on the resolution model estimated from $D^{*+} \to D^0\pi^+$ decays. Further considered sources of systematic uncertainties are the background model and a fit bias. When absolute masses are calculated from the Q values the systematic uncertainty is limited by the knowledge of the Λ_b mass.

Compared with the previous analysis, the mass measurements are improved in precision by at least a factor two. The isospin splittings and the natural widths are measured for the first time.

4 $\Lambda_b \to J/\psi\Lambda$ Branching Ratio

The quark level transition $b \to s$ is a flavor changing neutral current process and thus forbidden at tree level in the standard model and therefore considered a sensitive probe for new physics. While such processes are well studied for B mesons, little is known about

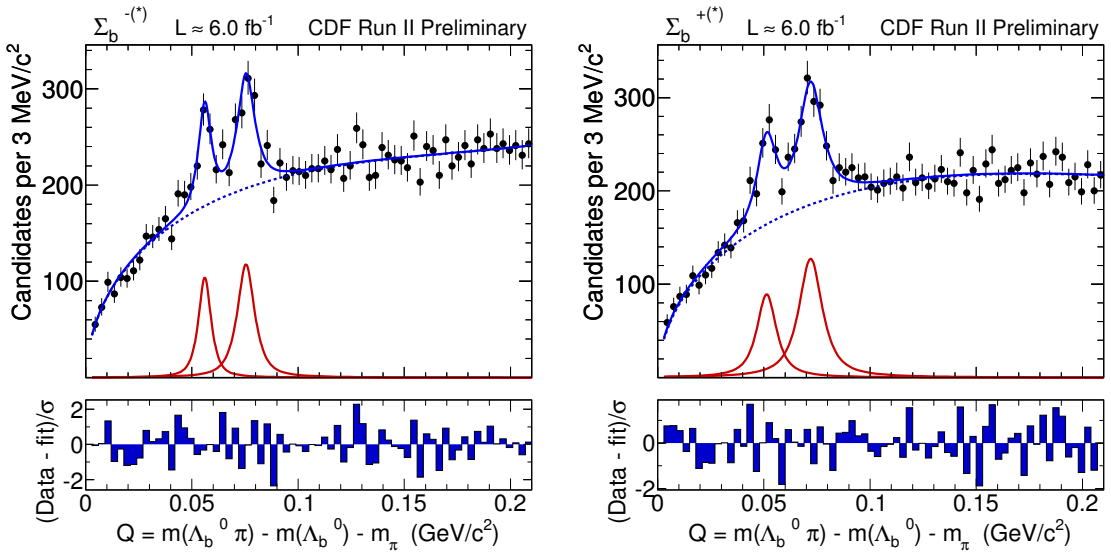

Figure 6: Q value distribution of $\Sigma_b^{(*)+}$ (left) and $\Sigma_b^{(*)-}$ (right) candidates.

$b \to s$ transitions in baryons. The decay $\Lambda_b \to J/\psi\Lambda$ is kinematically very similar to the flavor changing neutral current decay $\Lambda_b \to \mu^+\mu^-\Lambda$ and was first observed by CDF in Run I [11]. However, the measured value of the Λ_b production fraction times branching ratio, $f(b \to \Lambda_b)\mathcal{B}(\Lambda_b \to J/\psi\Lambda) = (4.7 \pm 2.3\,(\text{stat.}) \pm 0.2\,(\text{syst.})) \times 10^{-5}$ has large uncertainties.

The D0 experiment presented a new measurement of this quantity using a data sample of 6.1 fb^{-1} selected by a dimuon trigger [12]. The Λ and Λ_b daughter particles are fitted to a vertex, respectively, and requirements on momenta, impact parameters and decay times are imposed that are optimized on the signal significance as estimated from simulation and data sidebands. Cascade decays like $\Sigma \to \Lambda\gamma$ or $\Xi^0 \to \Lambda\pi^0$ are suppressed by requiring that the direction from the primary to the Λ decay vertex coincides with the Λ momentum direction.

Kinematically very similar $B^0 \to J/\psi K_S^0$ decays with $K_S^0 \to \pi^+\pi^-$ are used as normalization channel. Figure 7 shows the invariant mass distributions of Λ_b and B^0 candidates with a fit of a double Gaussian for signal and a second order polynomial for background.

Taking the relative efficiency from simulation, the following relative cross section is measured:

$$\sigma_{rel} = \frac{f(b \to \Lambda_b)\mathcal{B}(\Lambda_b \to J/\psi\Lambda)}{f(b \to B^0)\mathcal{B}(B^0 \to J/\psi K_S^0)} = 0.345 \pm 0.034\,(\text{stat.}) \pm 0.033\,(\text{syst.}) \pm 0.003\,(\text{PDG}).$$

The dominant systematic uncertainty comes from the unknown Λ_b polarization, followed by the uncertainty due to the fit model. The uncertainties on the relative efficiency and the cross-feed fractions have no significant influence. Several cross checks were performed to

State	Q value [MeV/c^2]	Mass [MeV/c^2]	Width [MeV/c^2]	Yield
Σ_b^+	$52.0^{+0.9\ +0.09}_{-0.8\ -0.4}$	$5811.2^{+0.9}_{-0.8} \pm 1.7$	$9.2^{+3.8\ +1.0}_{-2.9\ -1.1}$	$468^{+110\ +18}_{-95\ -15}$
Σ_b^-	$56.2^{+0.6\ +0.07}_{-0.5\ -0.4}$	$5815.5^{+0.6}_{-0.5} \pm 1.7$	$4.3^{+3.1\ +1.0}_{-2.1\ -1.1}$	$333^{+93}_{-73} \pm 35$
Σ_b^{*+}	$72.7 \pm 0.7^{+0.12}_{-0.6}$	$5832.0 \pm 0.7 \pm 1.8$	$10.4^{+2.7\ +0.8}_{-2.2\ -1.2}$	$782^{+114\ +25}_{-103\ -27}$
Σ_b^{*-}	$75.7 \pm 0.6^{+0.08}_{-0.6}$	$5835.0 \pm 0.6 \pm 1.8$	$6.4^{+2.2\ +0.7}_{-1.8\ -1.1}$	$522^{+85}_{-76} \pm 29$

	Isospin splitting [MeV/c^2]
$m(\Sigma_b^+) - m(\Sigma_b^-)$	$-4.2^{+1.1\ +0.07}_{-0.9\ -0.09}$
$m(\Sigma_b^{*+}) - m(\Sigma_b^{*-})$	$-3.0 \pm 0.9^{+0.12}_{-0.13}$

Table 1: Measurements of $\Sigma_b^{(*)}$ properties. The first uncertainties are statistical, the second uncertainties systematic.

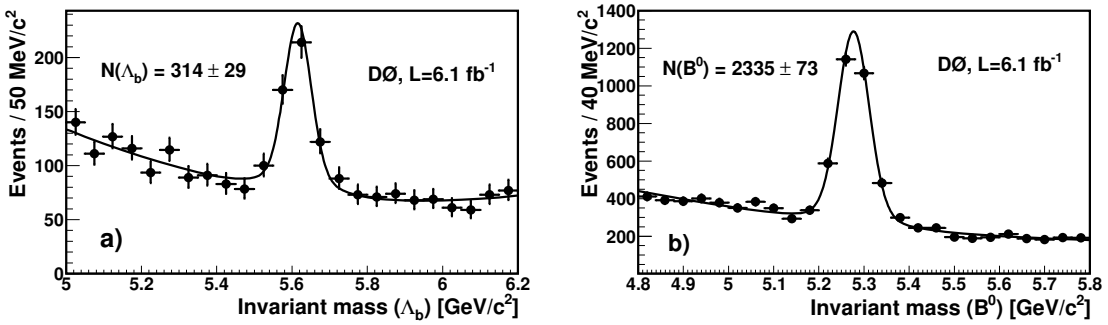

Figure 7: Invariant mass distributions of Λ_b (left) and B^0 (right) candidates.

verify the stability of the result. Using the world average values for the B^0 production and decay fractions, a result of $f(b \to \Lambda_b)\mathcal{B}(\Lambda_b \to J/\psi\Lambda) = (6.01 \pm 0.60\ (\text{stat.}) \pm 0.58\ (\text{syst.}) \pm 0.28\ (\text{PDG})) \times 10^{-5} = (6.01 \pm 0.88) \times 10^{-5}$ is obtained which is about three times more precise than the CDF Run I measurement.

5 Charm Baryons

The Tevatron experiments have not only provided significant contributions on the b baryon sector, but have also collected large samples of charm baryon decays which allow studies at unprecedented precision. The spectrum and decay modes of the $\Sigma_c^{(*)}$ and Λ_c^{*+} states studied by CDF [13] are the same as the ones shown in Fig. 4, but for the charm instead of the b baryon sector.

In a data sample of 5.2 fb^{-1}, $\Lambda_c^+ \to pK^-\pi^+$ decays are selected by a trigger on displaced tracks. Since charm hadrons have a shorter lifetime than b hadrons, about half of the

triggered Λ_c^+ particles come from b baryon decays. Λ_c^+ candidates are combined with one or two pion tracks to form $\Sigma_c^{(*)}$ or Λ_c^{*+} candidates, respectively. Neural networks are used for the selection of Λ_c^+, $\Sigma_c^{(*)}$, and Λ_c^{*+} candidates. The networks are trained with data only using the ${}_sPlot$ technique.

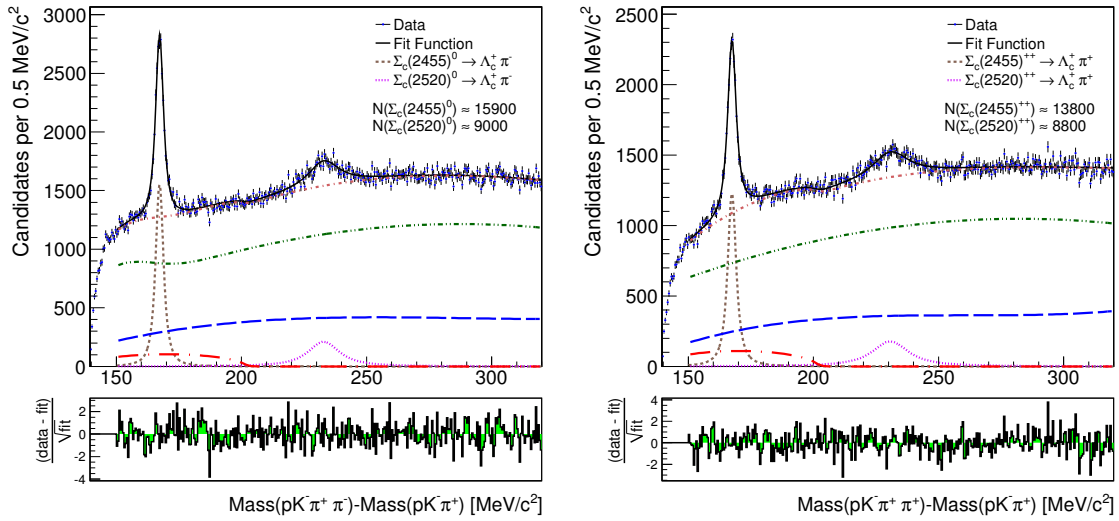

Figure 8: Mass difference distributions of $\Sigma_c^{(*)0}$ (left) and $\Sigma_c^{(*)++}$ (right) candidates.

Distributions of mass differences relative to the reconstructed Λ_c^+ mass are fitted to measure mean masses and widths. The distributions for the $\Sigma_c^{(*)}$ states are shown in Fig. 8. The signals are described by a nonrelativistic Breit-Wigner convolved with a triple Gaussian resolution function. The combinatorial background (green dash-dot-dotted line) is described by a second order polynomial with parameters determined from Λ_c^+ sidebands. In the case of the neutral Σ_c states an additional component from D^* reflections has to be taken into account which is parametrized by a Gaussian. Real Λ_c^+ with a random pion (blue dashed line) are parametrized by a third order polynomial with all parameters free in the fit. The third background component comes from $\Lambda_c^+(2625) \to \Lambda_c^+ \pi^+ \pi^-$ decays (red dash-dotted line). It is determined using the $\Lambda_c^+(2625)$ yield measured in data. $\Lambda_c^+(2595)$ particles decay mainly resonantly and thus contribute to the signal.

The fit to the mass difference distribution of Λ_c^{*+} candidates is shown in Fig. 9 (right). Signals and backgrounds are treated in the same way as in the fits to the $\Sigma_c^{(*)}$ distributions, except that the cross-feed background now comes from $\Sigma_c^{(*)}$ decays and the threshold effect of $\Lambda_c^{*+}(2595) \to \Sigma_c \pi$ has to be taken into account. This is done by using a mass dependent width as illustrated in Fig. 9 (left). The parameter determining the width of the lineshape is the pion coupling constant h_2. CDF has shown that a mass independent width, as used in previous analyses, does not describe the data. Because of the low signal yield in previous

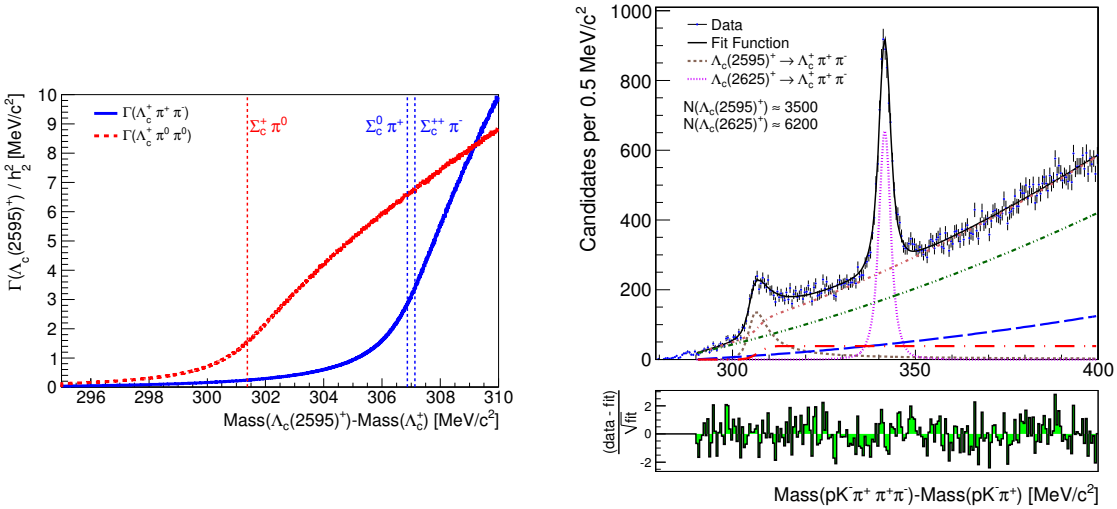

Figure 9: Mass dependent $\Lambda_c^{*+}(2595)$ partial decay widths (left) and mass difference distribution of Λ_c^{*+} candidates (right).

experiments of up to 112 ± 17 events [14], the threshold effect was not observable so far. As a consequence of the threshold effect, the mean $\Lambda_c^{*+}(2595)$ mass is significantly shifted towards lower values.

Numerical results of the measured masses and widths are given in Tab. 2. The $\Sigma_c^{(*)}$ results agree well with the world average values and are of comparable precision. A significant improvement in precision of the Λ_c^{*+} propertied and observation of the threshold effect in the $\Lambda_c^{*+}(2595)$ line shape as predicted in Ref. [15] are achieved as illustrated in Fig. 10.

State	Δm [MeV/c^2]	Γ [MeV/c^2]
$\Sigma_c(2455)^{++}$	$167.44 \pm 0.04 \pm 0.12$	$2.34 \pm 0.13 \pm 0.45$
$\Sigma_c(2455)^{0}$	$167.28 \pm 0.03 \pm 0.12$	$1.65 \pm 0.11 \pm 0.49$
$\Sigma_c(2520)^{++}$	$230.73 \pm 0.56 \pm 0.16$	$15.03 \pm 2.12 \pm 1.36$
$\Sigma_c(2520)^{0}$	$232.88 \pm 0.43 \pm 0.16$	$12.51 \pm 1.82 \pm 1.37$
$\Lambda_c(2595)^{+}$	$305.79 \pm 0.14 \pm 0.20$	$h_2^2 = 0.36 \pm 0.04 \pm 0.07$
$\Lambda_c(2625)^{+}$	$341.65 \pm 0.04 \pm 0.12$	< 0.97 at 90% CL

Table 2: Charm baryon properties. The first uncertainties are statistical and the second systematic.

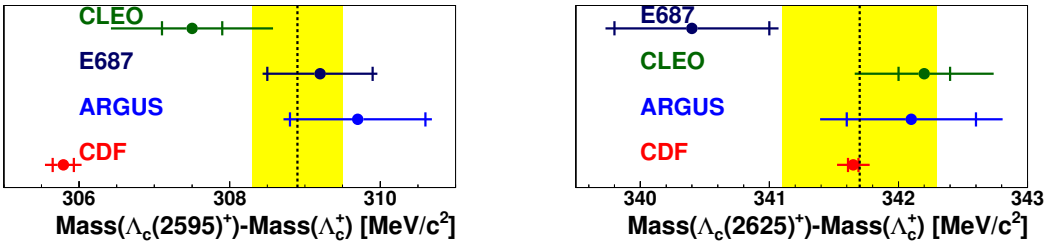

Figure 10: Comparison of Λ_c^{*+} mass difference measurements by CLEO [14], Fermilab E687 [16, 17], ARGUS [18], CDF and the world average without the CDF result (yellow band).

6 Conclusions

So far our knowledge about baryons containing a b quark fits on one page in the PDG particle list table [19]. Thus the observation of new states and improved or even first measurements of heavy baryon properties are very welcome to improve the phenomenological models of strongly bound states and to advance on the way to a deeper understanding of low energy QCD. The Tevatron experiments CDF and D0 have been very active in the last few years and contributed significantly to our knowledge of heavy baryons. With the good performance of the Tevatron both experiments could continue to present new and updated results on this sector as shown in this article.

Bibliography

[1] T. Aaltonen *et al.* (CDF Collaboration), Phys. Rev. Lett. **99**, 202001 (2007).

[2] V. M. Abazov *et al.* (D0 Collaboration), Phys. Rev. Lett. **99**, 052001 (2007).

[3] T. Aaltonen *et al.* (CDF Collaboration), Phys. Rev. Lett. **99**, 052002 (2007).

[4] D. Buskulic *et al.* (ALEPH Collaboration), Phys. Lett. B **384**, 449 (1996).

[5] P. Abreu *et al.* (DELPHI Collaboration), Z. Phys. C **68**, 541 (1995).

[6] V. M. Abazov *et al.* (D0 Collaboration), Phys. Rev. Lett. **101**, 232002 (2008).

[7] T. Aaltonen *et al.* (CDF Collaboration), Phys. Rev. D **80**, 072003 (2009).

[8] L. Ristori, G. Punz, Annu. Rev. Nucl. Part. Sci. **60**, 595 (2010).

[9] T. Aaltonen *et al.* (CDF Collaboration), arXiv:1107.4015 [hep-ex].

[10] CDF Collaboration, CDF note 10286.

[11] F. Abe *et al.* (CDF Collaboration), Phys. Rev. **D 55**, 1142-1152 (1997).

[12] V. M. Abazov *et al.* (D0 Collaboration), Phys. Rev. **D 84**, 031102 (2011).

[13] T. Aaltonen *et al.* (CDF Collaboration), Phys. Rev. **D 84**, 012003 (2011).

[14] K. W. Edwards *et al.* (CLEO Collaboration), Phys. Rev. Lett. **74**, 3331-3335 (1995).

[15] A. E. Blechman, A. F. Falk, D. Pirjol, J. M. Yelton, Phys. Rev. **D 67**, 074033 (2003).

[16] P. L. Frabetti *et al.* (E687 Collaboration), Phys. Rev. Lett. **72**, 961-964 (1994).

[17] P. L. Frabetti *et al.* (E687 Collaboration), Phys. Lett. **B365**, 461-469 (1996).

[18] H. Albrecht *et al.* (ARGUS Collaboration), Phys. Lett. **B402**, 207-212 (1997).

[19] K. Nakamura *et al.* (Particle Data Group Collaboration), J. Phys. G **37**, 075021 (2010).

Baryon Spectroscopy and Resonances

Robert G. Edwards[1]
Jefferson Laboratory
12000 Jefferson Avenue
Newport News, Virginia 23606, USA

A short review of current efforts to determine the highly excited state spectrum of QCD, and in particular baryons, using lattice QCD techniques is presented.

The determination of the highly excited spectrum of QCD is a major theoretical and experimental challenge. The experimental investigation of the excited baryon spectrum has been a long-standing element of the hadronic-physics program, an important component of which is the search for so-called "missing resonances", baryonic states predicted by the quark model based on three constituent quarks but which have not yet been observed experimentally. Should such states not be found, it may indicate that the baryon spectrum can be modeled with fewer effective degrees of freedom, such as in quark-diquark models. In the past decade, there has been an extensive program to collect data on electromagnetic production of one and two mesons at Jefferson Lab, MIT-Bates, LEGS, MAMI, ELSA, and GRAAL. To analyze these data, and thereby refine our knowledge of the baryon spectrum, a variety of physics analysis models have been developed at Bonn, George Washington University, Jefferson Laboratory and Mainz.

To provide a theoretical determination and interpretation of the spectrum, *ab initio* computations within lattice QCD have been used. Historically, the calculation of the masses of the lowest-lying states, for both baryons and mesons, has been a benchmark calculation of this discretized, finite-volume computational approach, where the aim is well-understood control over the various systematic errors that enter into a calculation; for a recent review, see [1]. However, there is now increasing effort aimed at calculating the excited states of the theory, with several groups presenting investigations of the low-lying excited baryon spectrum, using a variety of discretizations, numbers of quark flavors, interpolating operators, and fitting methodologies (Refs. [2–5]). Some aspects of these calculations remain unresolved and are the subject of intense effort, notably the ordering of the Roper resonance in the low-lying Nucleon spectrum.

Considerable progress towards the computation of the highly excited spectrum of QCD has been made within recent years through the development and employment of new (and old) theoretical techniques. The energies of excited states are determined from the exponential

[1] edwards@jlab.org

fall-off of two-point (Euclidean) correlation functions. The variational method (Refs. [6–8]), familiar as the Rayleigh-Ritz method in quantum mechanics, uses the time dependence of the eigenvalues of a matrix of such correlation functions to project optimally onto the excited levels. For the success of such a technique, a basis of interpolating operators is required that sufficiently spans the space. This basis of operators must respect the symmetries of the restricted cubic box used in lattice calculations. Here is where some knowledge of the underlying physics is valuable. Namely, QCD appears to prefer excited states with the quarks distributed non-locally within space. This in turn suggests an operator construction where the interpolating fields are also non-local in space and transform according to continuum symmetries like total angular momentum, parity, etc. These operators are then projected into forms that transform suitably on the cubic lattice.

The program outlined above has been underway for a few years now utilizing "anisotropic" lattices, with a finer temporal than spatial resolution, enabling the hadron correlation functions to be observed at short temporal distances and hence many energy levels to be extracted [9, 10]. Calculations have been carried out in quenched [11–13], with two dynamical quark flavors [14], and now two light and one dynamical strange quark flavors [15] where a recent calculation showed a glimpse of the excited Nucleon, Δ and Ω excited-state spectrum. Crucial to the success of this program has been the development of the "distillation" method which enables the efficient computation of correlators involving the non-local operators [16].

The development of new operator constructions that follow from continuum symmetry constructions has allowed, for the first time, the reliable identification of the spin and masses of the single particle spectrum at a statistical precision at or below about 1%. In particular, the excited spectrum of isovector as well as isoscalar mesons (Refs. [17–19]) shows a pattern of states, some of which are very familiar from the $q\overline{q}$ constituent quark model, with up to total spin $J = 4$ and arranged into corresponding multiplets. In addition, there are indications of a rich spectrum of exotic J^{PC} states, as well as a pattern of states interpretable as non-exotic hybrids [20]. The pattern of these multiplets of states, as well as their relative separation in energy, suggest a phenomenology of constituent quarks coupled with effective gluonic degrees of freedom. In particular, the pattern of these exotic and non-exotic hybrid states appears to be consistent with a bag-model description and inconsistent with a flux-tube model [20].

Recently, this lattice program has been extended into the baryon spectrum, revealing for the first time, the excited-state single-particle spectrum of Nucleons and Deltas along with their total spin up to $J = \frac{7}{2}$ in both positive and negative parity [21]. There was found a high multiplicity of levels spanning across J^P which is consistent with $SU(6) \otimes O(3)$ multiplet counting, and hence with that of the non-relativistic qqq constituent quark model. In particular, the counting of levels in the low lying negative parity sectors are consistent with the non-relativistic quark model and with the observed experimental states [22]. The spectrum observed in the first excited positive parity sector is also consistent in counting with the quark model, but the comparison with experiment is less clear with the quark

model predicting more states than are observed experimentally, spurring phenomenological investigations to explain the discrepancies (e.g., see Refs. [22–28]).

In addition, it was found that each of the operators in the basis features prominently in some energy level, and there is significant mixing among each of the allowed multiplets, including the **20**-plet that is present in the non-relativistic qqq quark model, but does not appear in quark-diquark models [25], and in particular Ref. [29]. These results lend credence to the assertion that there is no "freezing" of degrees of freedom with respect to those of the non-relativistic quark model. These qualitative features of the calculated spectrum extend across all three of the quark-mass ensembles studied. Furthermore, no evidence was found for the emergence of parity-doubling in the spectrum [30].

It was argued that the extracted N and Δ spectrum can be interpreted in terms of single-hadron states, and based on investigations in the meson sector [18] and initial investigations of the baryon sector at a larger volume [21], little evidence was found for multi-hadron states. To study multi-particle states, and hence the resonant nature of excited states, operator constructions with a larger number of fermion fields are needed. Such constructions are in progress, and it is believed that the addition of these operators will lead to a denser spectrum of states. With suitable understanding of the discrete energy spectrum of the system, the Lüscher formalism [31] and its inelastic extensions [32] can be used to extract the energy dependent phase shift for a resonant system, such as has been performed for the $I = 1$ ρ system [33]. The energy of the resonant state is determined from the energy dependence of the phase shift. It is this resonant energy that is suitable for chiral extrapolations.

The extraction and identification of a highly excited, spin identified single-hadron spectrum, represents an important step towards a determination of the excited baryon spectrum. The calculation of the single-baryon spectrum including strange quarks is ongoing. Combining the methods developed paper with finite volume techniques for the extraction of phase shifts, future work will focus on the determination of hadronic resonances within QCD.

Acknowledgments

Support is from U.S. Department of Energy contract DE-AC05-06OR23177, under which Jefferson Science Associates, LLC, manages and operates Jefferson Laboratory.

Bibliography

[1] C. Hoelbling, PoS **LATTICE2010**, 011 (2010) [arXiv:1102.0410 [hep-lat]].

[2] M. S. Mahbub, W. Kamleh, D. B. Leinweber, A. O Cais and A. G. Williams, Phys. Lett. B **693**, 351 (2010) [arXiv:1007.4871 [hep-lat]].

[3] M. S. Mahbub, A. O. Cais, W. Kamleh, D. B. Leinweber and A. G. Williams, Phys. Rev. D **82**, 094504 (2010) [arXiv:1004.5455 [hep-lat]].

[4] G. P. Engel, C. B. Lang, M. Limmer, D. Mohler and A. Schafer [BGR [Bern- Graz-Regensburg] Collaboration], Phys. Rev. D **82**, 034505 (2010) [arXiv:1005.1748 [hep-lat]].

[5] N. Mathur *et al.*, Phys. Lett. B **605**, 137 (2005) [arXiv:hep-ph/0306199].

[6] C. Michael, Nucl. Phys. B **259**, 58 (1985).

[7] M. Luscher and U. Wolff, Nucl. Phys. B **339**, 222 (1990).

[8] B. Blossier, M. Della Morte, G. von Hippel, T. Mendes and R. Sommer, JHEP **0904**, 094 (2009) [arXiv:0902.1265 [hep-lat]].

[9] R. G. Edwards, B. Joo and H. W. Lin, Phys. Rev. D **78**, 054501 (2008) [arXiv:0803.3960 [hep-lat]].

[10] H. W. Lin *et al.* [Hadron Spectrum Collaboration], Phys. Rev. D **79**, 034502 (2009) [arXiv:0810.3588 [hep-lat]].

[11] S. Basak *et al.* [Lattice Hadron Physics Collaboration (LHPC)], Phys. Rev. D **72**, 074501 (2005) [arXiv:hep-lat/0508018].

[12] S. Basak *et al.*, Phys. Rev. D **72**, 094506 (2005) [arXiv:hep-lat/0506029].

[13] S. Basak *et al.*, Phys. Rev. D **76**, 074504 (2007) [arXiv:0709.0008 [hep-lat]].

[14] J. M. Bulava *et al.*, Phys. Rev. D **79**, 034505 (2009) [arXiv:0901.0027 [hep-lat]].

[15] J. Bulava *et al.*, Phys. Rev. D **82**, 014507 (2010) [arXiv:1004.5072 [hep-lat]].

[16] M. Peardon *et al.* [Hadron Spectrum Collaboration], Phys. Rev. D **80**, 054506 (2009) [arXiv:0905.2160 [hep-lat]].

[17] J. J. Dudek, R. G. Edwards, M. J. Peardon, D. G. Richards and C. E. Thomas, Phys. Rev. Lett. **103**, 262001 (2009) [arXiv:0909.0200 [hep-ph]].

[18] J. J. Dudek, R. G. Edwards, M. J. Peardon, D. G. Richards and C. E. Thomas, Phys. Rev. D **82**, 034508 (2010) [arXiv:1004.4930 [hep-ph]].

[19] J. J. Dudek, R. G. Edwards, B. Joo, M. J. Peardon, D. G. Richards and C. E. Thomas, Phys. Rev. D **83**, 111502 (2011) [arXiv:1102.4299 [hep-lat]].

[20] J. J. Dudek, arXiv:1106.5515 [hep-ph].

[21] R. G. Edwards, J. J. Dudek, D. G. Richards and S. J. Wallace, arXiv:1104.5152 [hep-ph].

[22] K. Nakamura *et al.* [Particle Data Group], J. Phys. G **37**, 075021 (2010).

[23] N. Isgur and G. Karl, Phys. Rev. D **19**, 2653 (1979) [Erratum-ibid. D **23**, 817 (1981)].

[24] S. Capstick and N. Isgur, Phys. Rev. D **34**, 2809 (1986).

[25] M. Anselmino, E. Predazzi, S. Ekelin, S. Fredriksson and D. B. Lichtenberg, Rev. Mod. Phys. **65**, 1199 (1993).

[26] L. Y. Glozman and D. O. Riska, Phys. Rept. **268**, 263 (1996) [arXiv:hep-ph/9505422].

[27] S. Capstick and W. Roberts, Prog. Part. Nucl. Phys. **45**, S241 (2000) [arXiv:nucl-th/0008028].

[28] J. L. Goity, C. Schat and N. N. Scoccola, Phys. Lett. B **564**, 83 (2003) [arXiv:hep-ph/0304167].

[29] D. B. Lichtenberg and L. J. Tassie, Phys. Rev. **155**, 1601 (1967).

[30] L. Y. Glozman, Phys. Lett. B **475**, 329 (2000) [arXiv:hep-ph/9908207].

[31] M. Luscher, Nucl. Phys. B **364**, 237 (1991).

[32] M. Lage, U. G. Meissner and A. Rusetsky, Phys. Lett. B **681**, 439 (2009) [arXiv:0905.0069 [hep-lat]].

[33] X. Feng, K. Jansen and D. B. Renner, Phys. Rev. D **83**, 094505 (2011) [arXiv:1011.5288 [hep-lat]].

In-medium hadron properties: Experimental overview

Piotr Salabura[1]
M. Smoluchowski Institute of Physics
Jagiellonian University
PL-30-052 Kraków, Poland

Hadron modifications in nuclear matter are discussed in connection to chiral symmetry restoration and/or hadronic many body effects. Experiments with photon, proton and heavy ion beams are used to probe properties of hadrons embedded in nuclear matter at different temperatures and densities. Most of the information has been gathered for the light vector mesons ρ, ω and ϕ which, due to their short life time, decay to large extent inside the medium. Decay channels involving dileptons, photons and hadrons have been selected to measure meson line shape and/or nuclear transparency in cold nuclear matter. Measurements of dileptons from heavy ion collisions allow to separate contribution from dense phase and to characterize its properties. A review of recent experimental results, focused on low energy domain, is presented.

1 Introduction

Sizable mass modifications have been predicted by various theoretical models for hadrons embedded into cold or hot and dense nuclear matter. In this respect, most attention has been focused on the light vector mesons ρ, ω, and ϕ) (for review see [1] and contribution of B.Kämpfer to this conference). Early work based on QCD sum rules suggested a direct link between changes of the meson masses and QCD vacuum properties, characterized by a reduction of the expectation value of the two-quark condensate [2, 4]. More recent work shows however that, while such a link indeed should exist, it is much more complicated and offers rather limited predictive power [1]. On the experimental side, a lot of activities have been carried out over the last years. The E325 experiment at KEK reported [3] a mass drop of the ρ meson in nucleus according to the Brown-Rho scaling [4]. This observation triggered further experimental investigations conducted at JLAB, ELSA, and MAMI using photon beams, as well as at COSY and GSI using proton beams. In heavy-ion collisions a search for vector meson mass modifications via dilepton spectroscopy was pioneered by the CERES [5] and HELIOS [6] collaborations at the CERN SPS and the DLS experiment [7] at Bevalac. A low-mass pair excess, below the ρ/ω pole, was reported and was widely discussed in many theoretical papers. However, the limited statistics of these experiments did not allow to derive firm conclusions. The breakthrough in this field was achieved with

[1] salabura@if.uj.edu.pl

the high-statistics NA60 data set, which allowed, for the first time, to extract a spectral function of the ρ meson in hot and dense nuclear matter at SPS energies [8]. Likewise, the HADES experiment at GSI has recently provided high precision data in the low energy regime [9].

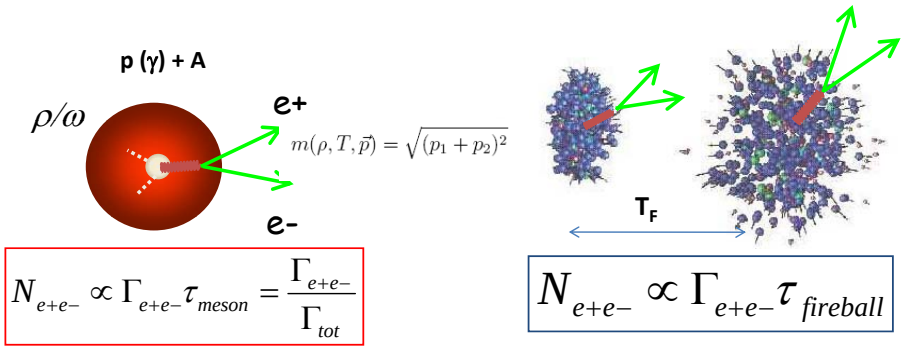

Meson	Mass [MeV/c²]	Γ [MeV/c²]	cτ [fm/c]	BR(V→e+e-)	BR in hadrons
ρ^0	770	150	1.3	4.4×10^{-5}	$\pi^+\pi^-$ (~100%)
ω	782	8.4	23.4	7.1×10^{-5}	$\pi^0\gamma$ (8%)
ϕ	1020	4.4	44.4	3.1×10^{-5}	K^+K^- (50%)
				NO FSI !	FSI !

Figure 1: Schematic view of ρ/ω meson decays in $p + A$ and HI collisions. The e^+e^- yield in $p + A$ is proportional to the inverse in-medium meson width whereas in HI collisions is proportional to the life time of the fireball. The table below summarizes the vector meson properties

There are two experimental approaches to measure in-medium mass modifications of the vector mesons: (i) via the reconstruction of their invariant mass from the detected decay products and (ii) by quantifying the meson absorption from the production yields. The best suited final state are dileptons (or possibly photons), void of strong final-state interactions (FSI) with the nuclear matter but one has to cope with the small branching ratios. (see Fig.1). Notice also that there is a clear difference between experiments investigating the meson production off the nucleus and those using HI collisions. Whereas in the first case the measured yield is directly proportional to the "in-medium" branching ratio, in the second case, because mesons can be regenerated in the rather long-lived fireball of rapidly changing density and temperature, connecting yields and medium effects is more complicated. Figure 1 illustrates both situations schematically. On the other hand, the density and temperature reached in HI collisions is of course higher and larger effects can be expected. Finally, in order to access the true in-medium radiation one has to subtract the contributions of meson decaying in the late state of the HI collision, that is after the so

called "freeze-out" where all interactions between the produced particles have ceased.

2 Cold nuclear matter

The standard experimental technique to measure a width of meson embedded in cold nuclear matter is based on the so-called transparency ratio (T_A), defined as the ratio of the meson production cross section in a given photon (or proton) -nucleus reaction to the cross section for this reaction on the nucleon scaled with the nuclear mass A. More insight into the transparency ratio can be obtained with a Glauber model [10,11] which relates the nuclear cross section $\sigma_{\gamma A}$ to the elementary cross section $\sigma_{\gamma N}$ and the meson absorption, expressed in terms of the imaginary part of the meson self-energy $\Pi(q,\rho(r))$, itself directly related to the meson in-medium width in the nucleus rest frame $\Gamma_{coll}(q,\rho(r))$. Both quantities, $\Pi(q,\rho(r))$ and $\Gamma_{coll}(q,\rho(r))$, depend on the meson momentum q and the local density $\rho(r)$. The in-medium increase of width ($\Gamma_{coll} > \Gamma_{vac}$) is commonly called collision broadening.

$$\sigma_{\gamma A} = \int d\Omega \int d^3r \rho(\overrightarrow{r}) \frac{d\sigma_{\gamma N}}{d\Omega} exp(\frac{1}{q}\int_0^{\delta\overrightarrow{r'}} dl\, Im\Pi(q,\rho(\overrightarrow{r'})))P(\overrightarrow{r}+\delta\overrightarrow{r'})$$

where

$\Gamma_{coll(q)} = -\frac{Im\Pi(q)}{\omega}$, ($\omega$ is energy)

and $\overrightarrow{r'} = \overrightarrow{r} + l\frac{\overrightarrow{r}}{r}$ with $\delta\overrightarrow{r'} = \frac{v\gamma}{\Gamma_{vac}}\frac{\overrightarrow{q}}{q}$

One should keep in mind the importance of nuclear effects which have to be considered in a calculation of the meson production off the nucleus. The latter is indeed affected by initial-state interactions (not for photons) of the beam particle, shadowing and Pauli blocking. A further complication arises from two-step meson production processes, that are those who involve intermediate hadrons produced in first-chance collisions (for example pions) and are obviously not present in reactions on the nucleon. In order to reduce these effects, the transparency ratio is therefore usually defined w.r.t. a reference measurement on the carbon nucleus. But even this, as it it will be shown later, does not completely guarantee full elimination of the effects related to two-step production. On the other hand, for a non-leptonic exit channel, FSI of the decay products with the medium must be taken into account by means of an absorption factor $P(r)$.

Figure 2 shows two examples of signal extraction for the ω meson from photo-production using e^+e^- (CLAS at JLab) [12], and $\pi^0\gamma$ (CBELSA/TAPS) [13] final states and photon beams in a similar energy range ($1.1-3.8$ GeV for CLAS, $1.1-2.2$ GeV for CBELSA/TAPS). In the latter case, the ρ meson contribution is not present and the π^0 FSI is reduced by means of a cut on the reconstructed pion kinetic energy $E_K > 150$ MeV. A further advantage of the dielectron measurement is its well controlled combinatorial background subtraction based on like sign-pairs measured in the same run, but a clear limitation is its lower statistics.

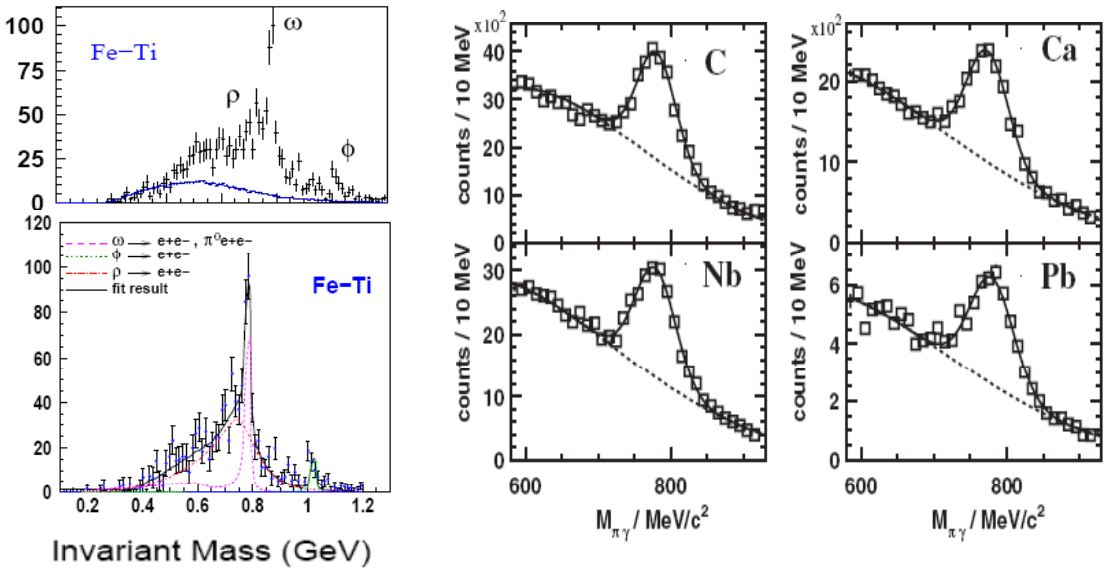

Figure 2: Left: invariant e^+e^- mass distributions from $\gamma + A$ reactions obtained by CLAS [12]. Upper part: total and combinatorial background and lower part: signal distribution compared to a fit composed of main dielectron sources. Right: invariant mass distribution of $\pi^0\gamma$ measured by CBELSA/TAPS [13] together with background fits.

The T_A obtained for the ω meson by CBELSA/TAPS and CLAS are presented in Fig. 3 (left) together with the model calculations done by the Giessen [14] and Valencia [15] theory groups. The extracted in-medium ω width $\Gamma^{\omega}_{\in-medium} \simeq 210$ MeV (in the ω rest frame) is significantly larger as compared to the vacuum value given in Fig. 1. The e^+e^- measurement [16] seems to show even slightly larger suppression, but the large error bars do not allow to derive final conclusions. In fact, the experimental point obtained on lead is an upper limit since no statistical significant ω signal could be observed there. One should also mention that both experiments measured ω decays at slightly different average momenta ($p^{CLAS}_{\omega} \simeq 1800$, $p^{CBELSA/TAPS}_{\omega} \simeq 1000$ MeV/c). Hence a more differential inspection of T_A as a function of the momentum is necessary. The respective momentum dependency of T_A is shown in the right panel of Fig. 3 for the CBELSA/TAPS data; it exhibits no strong effect. Assuming a low density approximation, also an in-medium $\omega - N$ cross section σ^*_{VN} could be estimated from the relation $\Gamma_{in-medium} \simeq v\rho\sigma^*_{VN}$. It has been found to be a factor $3-4$ larger than the typical "free" $\omega - N$ cross sections [13]. This may indicate the important role of many-particle interactions and questions the applicability of the approximation.

The impact of two-step processes on the T_A of ω, η and η' mesons has been investigated by CBELSA/TAPS by applying a condition on the kinetic energy of the outgoing meson: $E_K > 1/2(E_\gamma - m_M)$. This is discussed in more detail in the contribution of M. Nanova. The main conclusions are as follows: The measured T_A for the ω and η' exhibit no dependence

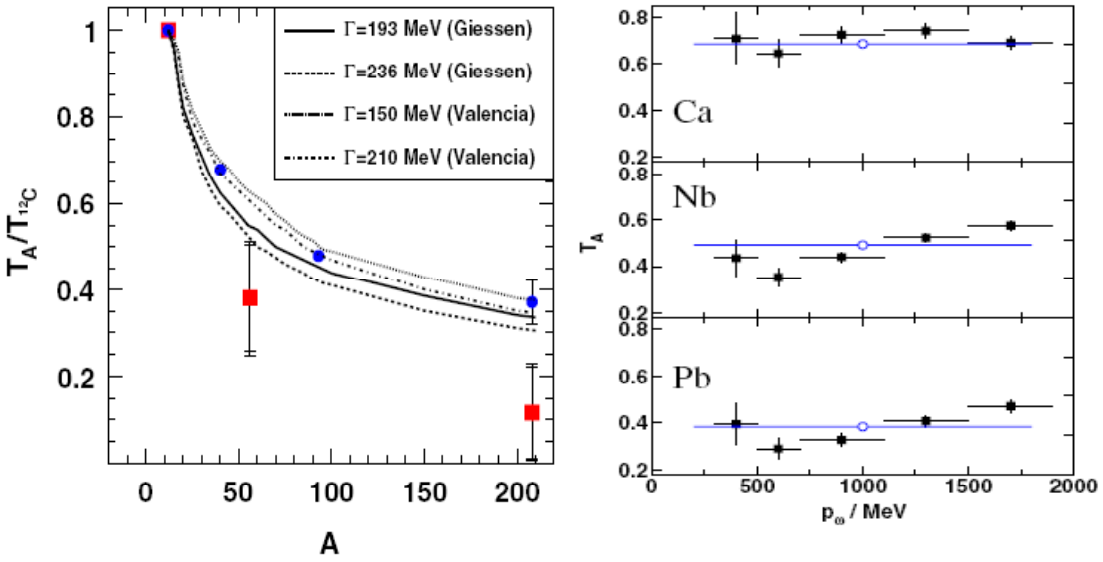

Figure 3: Left: Transparency ratios T_A measured for the ω meson by CBELSA/TAPS (blue points) and CLAS (red) as a function of mass number A [16]. Solid lines shows model predictions for the various in-medium meson widths from Valencia and Giessen groups. Right: Transparency ratio as a function of the ω momentum measured by CBELSA/TAPS for various nuclei [13]. Blue points are averaged values.

on the kinetic energy of the outgoing meson. In contrast, for the lighter η meson there is a clear reduction of T_A for the fast mesons. This can be explained by a strong reduction of two-step processes and the dominant role of the direct $\gamma - N$ reaction in the production of fast η mesons. On the other hand, the production of slow η is affected by the secondary $\pi - N$ reactions. The absence of such an effect in case of the ω and η' can be explained by the meson mass differences and hence different production threshold for the secondary productions. This conclusion is corroborated by the observed nuclear cross section scaling $\sigma_{\gamma A} \sim A^{\alpha}$ with $\alpha \simeq 2/3$ for the ω, and fast η mesons. Indeed, such a scaling is expected for surface production.

ϕ meson absorption in nuclear matter was measured in photon (CLAS [16], Spring8 [17]) and proton (ANKE [18]) induced reactions for an average meson momentum $< p_{\phi} > \simeq 1.7$ and 1.1 GeV/c, respectively. The measured T_A are, within error bars, consistent with each other, but the errors of the photo-production experiment are large. A recent high-statistics measurements from ANKE is presented in the contribution by A. Polyanskiy. The comparison with the model calculations of the Valencia, Moscow and Dresden groups indicate a ϕ-meson in-medium width of $\Gamma^{\phi}_{in-medium} \simeq 30 - 50$ MeV/c. However, the momentum distribution of the produced ϕ mesons off the nucleus indicates an enhancement over the model predictions at low momenta and calls for further investigations.

A new analysis of the ω line shape has been presented at this conference by A2 collaboration by M.Thiel. No statistically significant difference with respect to the ω vacuum spectral function is observed. Also, transport calculations done with GiBUU incorporating collisional broadening are consistent with the measured T_A (shown in Fig. 3) and demonstrate that there is almost no sensitivity of the meson line shape to in-medium ω modifications. This is due to the fact that the observed significant increase of the in-medium ω width leads to a strong suppression of the in-medium decays, as $1/\rho^2$, and hamper its observation via a line shape analysis with the presently available statistics. A similar conclusions holds also for the other long-lived mesons (η, η', and ϕ), but not for the short lived ρ meson, for which in-medium modifications should be directly visible in invariant e^+e^- mass measurements. Unfortunately, the situation concerning in-medium modifications of the ρ meson in cold nuclear matter is controversial. As it was already mentioned, the E325 experiment at KEK claims the observation of a ρ meson mass drop. On the other hand, the detailed analysis of the ρ meson invariant-mass distribution measured by CLAS [12] (see Fig. 2, lower left) reveals no mass shift, but only a slight broadening ($\Gamma^{\rho}_{in-medium} \simeq 217$ GeV). These contradicting statements might be explained by the background subtraction procedure applied to the KEK data which did not use like-sign pair background for the normalization, but a fit procedure. As discussed in [1], this could lead to an overestimation of the background in the mass region above the ρ peak, resulting in an apparent downward shift of the meson mass distribution.

New results from proton-induced reactions at a beam energy of 3.5 GeV have recently been obtained by the HADES collaboration. The large acceptance of the detector and the low beam energy allow for detection of e^+e^- pairs from π^0, η (via Dalitz decays) and the ρ, ω down to low momenta ($p_{e^+e^-} < 1.0$ GeV/c) and low invariant masses not covered by the CLAS and E325 experiments. Differential e^+e^- production cross sections as function of the e^+e^- invariant mass, momentum and rapidity have been measured for the $p + p$ and $p + Nb$ reactions and are discussed in contribution of M Weber. The direct comparison of both distributions to the yields expected from the known hadronic sources (from a Pythia calculation) reveals important unexplained strength below the vector meson pole which becomes even more pronounced in proton-nucleus collisions and low momentum dielectrons. Such increase at low $p_{e^+e^-}$ in $p + A$ reactions might be interpreted as a fingerprint of the contribution of two-step processes to meson production. It is well known that ρ couple strongly to low-lying nucleon resonances, as for example $N*(1520), \Delta(1720), ..$, which can be excited by secondary pions. On the other hand, it has also been suggested that such couplings strongly modify the in-medium ρ meson spectral function. Therefore, a more detailed comparison to model calculations for both $p + A$ and $\gamma + A$ reactions incorporating both processes are needed to derive final conclusions.

3 Heavy Ion reactions

Before we discuss new results on dilepton production in low-energy HI reactions we shall first recall results from the SPS at $\sqrt{s} = 17.3$ GeV. The CERES and NA60 experiments measured a significant low-mass (below the ρ/ω pole) pair excess above the contribution expected from the freeze-out decays. A full characterization of this excess as a function of the pair invariant mass, transverse momentum and virtual photon polarization has been established thanks to the high-quality dimuon data from NA60 [8, 19]. The excess represents radiation from the hot and dense phase of the collision and has been extracted by a model-independent subtraction of the freeze-out contribution (the so-called "hadronic cocktail") from the total measured dimuon signal.

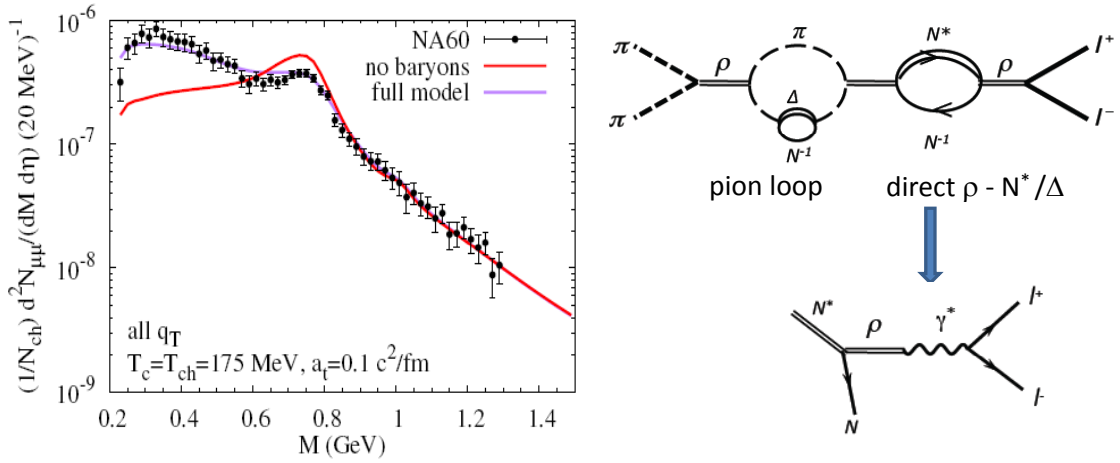

Figure 4: Left: Acceptance-corrected $\mu^+ + \mu^-$ excess as a function of the invariant mass for $In + In$ at 158 AGeV extracted by NA60 [19] compared to the model predictions of [20]. Right: schematic diagram of main contributions to the ρ meson spectral function responsible for the in-medium meson modifications. Effect of the second diagram related to baryons is visualized comparison of two lines: red (no baryons) and violet (full model).

Figure 4 shows the acceptance-corrected dimuon invariant-mass distribution of the excess obtained by the NA60 collaboration [19]. From comparisons to many model calculations one concludes that the excess is related to pions annihilating into the ρ meson and is very sensitive to the ρ in-medium spectral function. The solid lines in Fig. 4 show results from the model calculations of Rapp and Hees [20]. The spectral function of the ρ appears to be strongly affected by two main in-medium effects, schematically depicted in the right side of Fig. 4: (i) modification of the pion loop in the ρ meson selfenergy and (ii) direct rho-meson couplings to the resonance-hole excitations. It appears that the second mechanism plays the bigger role in the melting of the ρ meson visible in Fig. 4 (compare red and violet lines).

The right diagram is also directly related to an elementary process of the baryon resonance (N*, Delta) Dalitz decay into the nucleon and a virtual photon. A strong coupling to the intermediate vector meson, as also predicted by Vector Meson Dominance (VMD), should be reflected in the respective transition form-factor. Indeed, such a coupling is known for the meson Dalitz decays and is well described by VMD in case of π^0 and η, but fails for the ω Dalitz decays. On the baryon Dalitz decays there are no data yet. Hence, it is very interesting to investigate such decays at lower energy, where baryons, as we will see below, are also relevant sources for pair production.

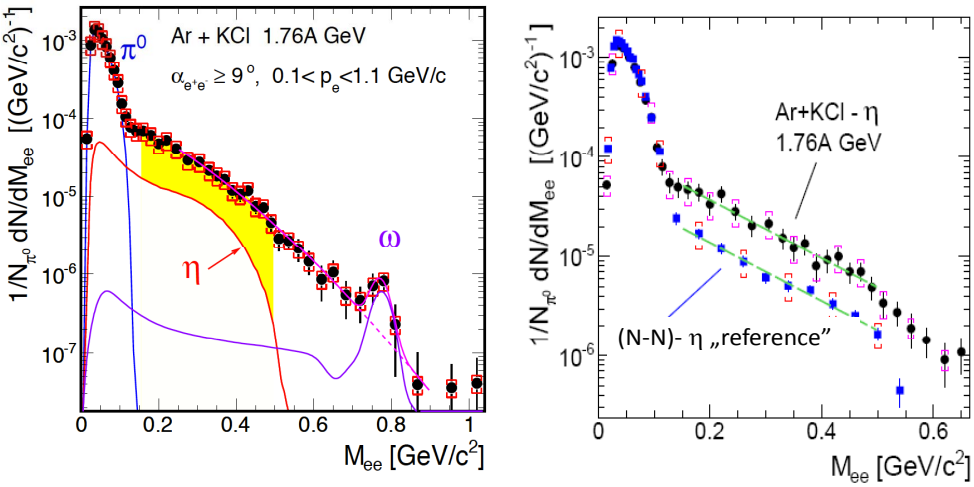

Figure 5: e^+e^- invariant mass distributions from $Ar + KCl$ collisions at 1.756 AGeV measured by HADES [9]. Left: Comparison to the expected mesonic e^+e^- sources after freeze-out. Both distributions are normalized to the π^0 yield as measured in HADES via charged pions (solid line). Right: e^+e^- invariant mass distributions from $Ar + KCl$ collisions with the subtracted η meson contribution compared to the distributions extracted from $N + N$ collisions

Indeed, in the $1 - 2$ AGeV energy range, particle production in heavy-ion collisions is dominated by pion production which originates mainly from the $\Delta(1232)$ resonance. Multiplicities of heavier mesons, like the η (related to the $N^*(1535)$), are already very low (of order $1 - 2\%$). Production multiplicities for both mesons are known from their decay into real photons from former TAPS measurements [21]. The dielectron invariant-mass distribution measured with HADES in the medium-heavy system $Ar + KCl$ at 1.756 AGeV is shown in Fig. 5, left [9]. It is compared to the expected mesonic e^+e^- sources from the π^0, η Dalitz decays, according to the measured multiplicities, and from the ω extrapolated from m_T scaling. One should note, that the ω signal is seen for the first time at such a low energy in HI collisions (below its free $N - N$ threshold). As one can see, these mesonic contributions do not explain the measured yield and leave room (yellow band) for the expected baryonic sources: resonance (here mainly $\Delta(1232)$) Dalitz decays and nucleon-nucleon

bremsstrahlung, which also plays a role at these low energies.

Since the relevant baryonic contributions are not experimentally known and various model calculations differ in predictions, the cross sections for pair production have been measured in separate $p+p$ and $n+p$ runs below the η production threshold (at 1.25 GeV) with the HADES detector [22]. The averaged pair multiplicities ($1/2(M_{pp}^{e^+e^-} + M_{pn}^{ee})$) are displayed as a function of the invariant e^+e^- mass on the right-hand side of Fig. 5 (blue points) together with the corresponding distribution from the $Ar+KCl$ system, all with their respective η Dalitz contribution subtracted. The normalization was done to the mean of the charged pion (π^+, π^-) multiplicity, measured independently by HADES, which at this energy is a good measure of neutral pion multiplicity. The normalization to the pion yield takes care about dependency of particle production on system-size via scaling with an average number of participants A_{part} [22]. As one can see, a significant excess with respect to the $N-N$ reference is visible above the π^0 mass, signaling an additional contribution from the dense phase of the HI collision. On the other hand, it has been shown that the comparison of this $N-N$ reference with the e^+e^- spectrum measured in the smaller $C+C$ system at 1 and 2 AGeV shows no such overshoot [9]. This means that going to the larger $Ar+KCl$ collision system, with $A_{part} \simeq 40$, a stronger than linear scaling of the pair production with A_{part} is observed.

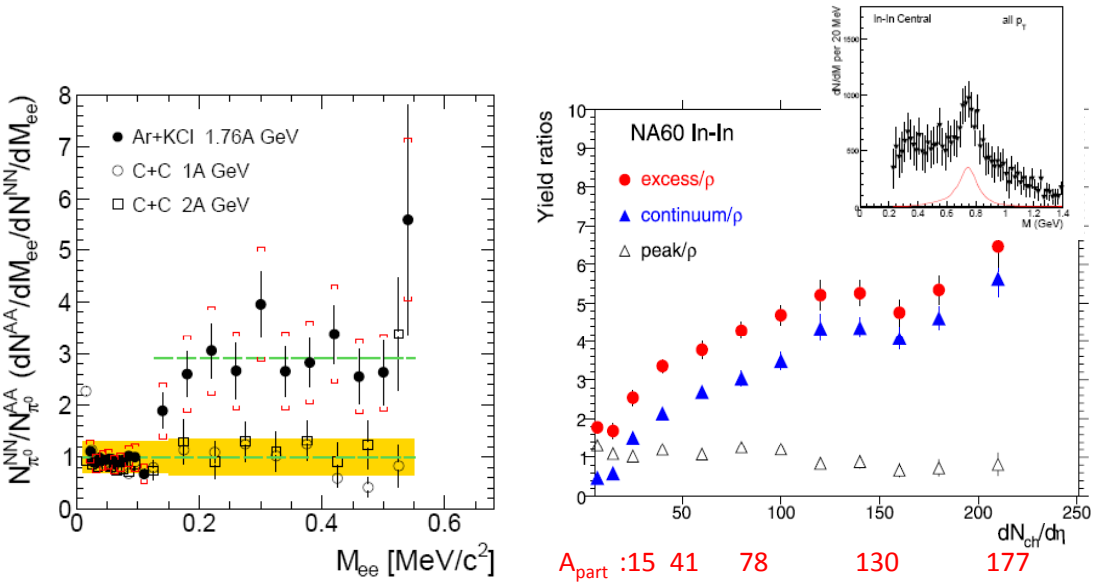

Figure 6: Left: Ratio of e^+e^- yields measured in $Ar+KCl$ and $C+C$ collisions at $1-2$ AGeV to the one measured in $N-N$ reactions as a function of the invariant mass, normalized to the respective π^0 yields [9]. Right: Ratios of the dimuon excess measured in $In+In$ collisions at 158 AGeV to the ρ meson yield from the freeze-out [19] as a function of centrality. The excess (shown in the insert) has been decomposed into 3 parts: total (red points), continuum (blue), peak(black).

This scaling indicates the important role of the regeneration process inside the hot and dense nuclear matter which can be observed via dilepton spectroscopy due to their unique, highly penetrating nature. A very nice example of such a behavior is the observation made by NA60 for the ρ meson, described as a "rho clock" [19]. This effect is shown on the right-hand side of Fig. 6, which presents ratios of the total excess, ρ "peak" and the "continuum" part of the excess w.r.t. the "cocktail rho" (ρ from the freeze-out defined as the ρ with the vacuum spectral function and intensity bound to the measured ω peak) as a function of centrality. From the extracted excess evolution NA60 concluded that up to 6 ρ generations are created inside the fireball in $In-In$ collisions. Following this idea, the HADES excess, shown on the left side of Fig. 6 as a function of the e^+e^- invariant mass, can be quantified to be around 3 w.r.t. the $N-N$ reference and interpreted in a way that on average 3 Δ generations are created in $Ar+KCl$ during the fireball life time. Thus an even larger increase can be expected for heavier system that will be investigated in forthcoming experiments with the $Au+Au$ collision system.

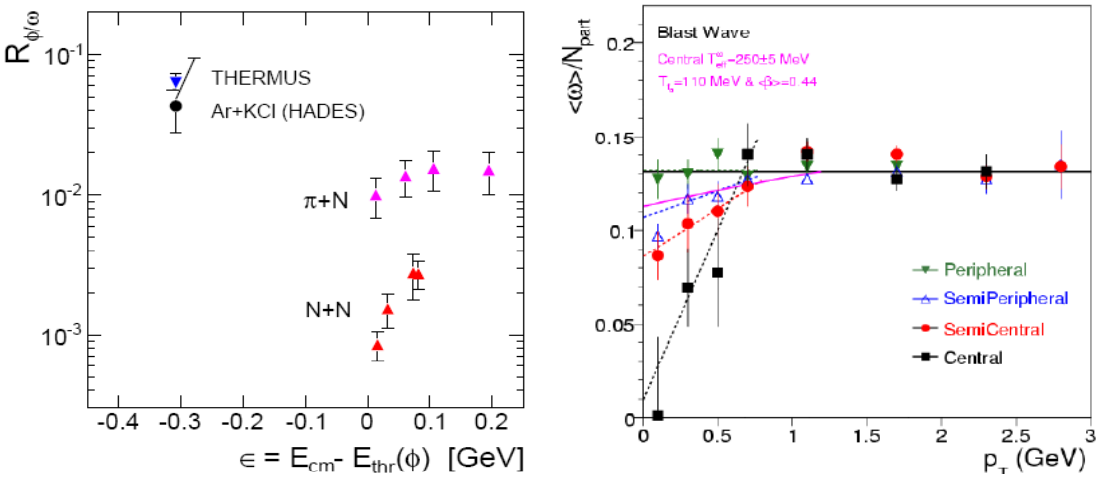

Figure 7: Left: ϕ to ω production ratio in $A+A$ [9] and $\pi+N$, $N+N$ as a function of the excess energy above the production threshold for ϕ in elementary reactions [9]. Right: ω multiplicity per participant for various centralities as a function of transverse momentum measured in $In+In$ at 158 AGeV [19]

Interesting new results on ϕ and ω production in HI collisions at energies below the nucleon-nucleon production threshold have been obtained by HADES as well. Figure 7 shows the ratio of the ϕ to ω multiplicities, $R_{\phi/\omega}$, measured in $Ar+KCl$ collisions at 1.756 AGeV, together with predictions of the statistical model THERMUS (blue circle) and results from elementary $p+p$ and $\pi+N$ reactions [9]. The data points are all plotted as a function of the excess energy for the exclusive ϕ production in $p+p$ and $\pi+N$ reactions, respectively.

One can see from this comparison that in the heavy-ion reaction $R_{\phi/\omega}$ is more than one order of magnitude larger than in $N+N$ collisions and also at least a factor $3-5$ larger than in pion-induced processes. On the other hand, the ratio is consistent with the thermal model assuming full thermalization and no OZI suppression. This can indicate that the ϕ meson is produced in multi-step, processes involving short-lived resonances. It could of course also be influenced by different absorption of both mesons in nuclear matter. Indeed, the results from cold matter experiments, discussed in section 2, indicate larger absorption of the ω meson as compared to the ϕ that can enhance the in-medium $R_{\phi/\omega}$.

The effect of ω absorption and the absence of such effect on the ϕ have been observed by NA60 in $In+In$ collisions at 158 AGeV [19,23]. In search for possible medium effects, NA60 studied the yield in the ω and ϕ peaks as a function of the transverse momentum of these mesons. Figure 7 displays the ω multiplicity per participant as a function of the transverse momentum for various centrality conditions. In the most central collisions one can observed a clear drop of the multiplicity at low transverse momenta. This can be explained by ω absorption, since due to the short life time of the fireball at this beam energy in-medium effects can only be expected for low-momentum mesons. A similar analysis performed for the ϕ meson does not show any such effect. Furthermore, a direct analysis of the ϕ meson line shape does not reveal any changes with respect to its vacuum shape.

4 Conclusions

Significant increase of the ω, ϕ meson widths in cold nuclear matter have been concluded from the transparency ratios measured in photon and proton induced reactions. In-medium inelastic meson-nucleon cross sections derived by means of low density approximation provide much larger values as compared to the one known from elementary reactions and can indicate important role of many-body interactions. Observed dependence of the transparency ratio on the meson momentum appears to be important observable to quantify role of secondary processes in the meson production.

Dilepton production in heavy reactions allows for the extraction of the radiation from the hot and dense phase of the collision. At SPS energies it is connected to pion annihilation and allows for the measurement of the in-medium ρ meson spectral functions. It appears to be strongly modified (broadenning) by many-body interactions with the surrounding hadron gas with dominant role of baryons. From the yield analysis of the radiation one can conclude that the mesons are regenerated inside hot and dense nuclear matter. A similar excess has also been observed at lower energies (1-2 AGeV) and can be connected to radiation from baryonic (mainly $\Delta(1232)$) resonances. It has been argued that both processes can be linked together by underlying elementary process of the Dalitz decay of baryonic resonances. In contrast to the ρ meson no changes in the ω or ϕ meson line shapes have been observed in HI collisions. However, analysis of the meson production yields as a function of the centrality and the meson transverse momentum indicate significant

absorption of the ω meson, in agreement with cold matter experiments.

Acknowledgments

Author would like to thank C. Djalali, M. Hartmann, V. Metag, M. Nanova, J. Weil R. Holzmann and HADES collaboration for preparation of this contribution. This work was also supported by GSI and grant NN202198639 (Poland)

Bibliography

[1] S. Leupold, V. Metag and U. Mosel *et al.*, Int. J. Mod. Phys. E **19**, 147 (2010).

[2] T. Hatsuda and S. H. Lee, Phys. Rev. C **46** 34 (1992).

[3] M. Naruki et al., Phys. Rev. Lett. **96** 092301 (2006).

[4] G. E. Brown and M. Rho, Phys. Rev. Lett. **66** 2720 (1991).

[5] G. Agakishiev et al. [CERES Collaboration], Phys. Rev. Lett. **75** 1272 (1995).

[6] M. Masera [HELIOS Collaboration], Nucl. Phys. A **590** 93C (1995).

[7] R. J. Porter et al. [DLS Collaboration], Phys. Rev. Lett. **79** 1229 (1997).

[8] R. Arnaldi et al. [NA60 Collaboration], Phys. Rev. Lett. **96** 162302 (2006).

[9] G. Agakishiev et al. [HADES Collaboration], Phys.Rev. C **84** 014902 (2011).

[10] D. Cabrera et al., Nucl. Phys. A **733** 130 (2004)

[11] P. Muehlich and U. Mosel, Nucl. Phys. A bf 765 188 (2006)

[12] R. Nasseripour et al. [CLAS Collaboration], Phys. Rev. Lett. **99** 262302 (2007)

[13] M. Kotulla et al. [CBELSA/TAPS Collaboration], Phys. Rev. Lett. **100** 192302 (2008)

[14] P. Muehlich et al., Nucl. Phys. A **780** 187 (2006)

[15] M. Kaskulov, E. Hernandez and E. Oset, Eur. Phys. J. A **31** 245 (2007)

[16] M. H. Wood et al. [CLAS Collaboration], Phys. Rev. Lett. **105** 112301 (2010)

[17] T. Ishikawa et al., Phys. Lett. B **608** 215 (2005)

[18] A. Polyanskiy et al. [ANKE Collaboration] Phys. Lett. B **695** 74 (2011).

[19] R. Arnaldi et al. [NA60 Collaboration], Eur. Phys. J. C **61** 711 (2009)

[20] H. van Hees and R. Rapp, Nucl. Phys. A **806** 339 (2008).

[21] R. Averbeck, et al., TAPS Collaboration, Z. Phys. A 359 (1997) 65.

[22] G. Agakishiev et al. [HADES Collaboration], Phys. Lett. B **690** 118 (2010).

[23] R. Arnaldi et al. [NA60 Collaboration], Eur. Phys. J. C **64** 1 (2009)

The BELLE II project

Boris A. Shwartz[1]
Budker Institute of Nuclear Physics of SB RAS
Lavrentiev av., 11, 630090 Novosibirsk, Russia

This talk describes the SuperKEKB/Belle II project with a brief survey of other flavor factories projects.

1 Introduction

In the last ten years a lot of physics results came from two B-factories – KEKB [1] and PEP-II [2]. Experiments had been conducted at these B-factories with the Belle [3] (KEKB) and BaBar [4] (PEP-II) detectors in the energy range of the Y meson family. Both detectors are forward/backward asymmetric detectors with high vertex resolution, magnetic spectrometry, excellent calorimetry and sophisticated particle identification ability. Integrated luminosity collected by both detectors exceeded 1500 fb^{-1}. Now both B-factories completed operation. At present one new super B-factory is under construction, another one is at the beginning stage and the Super-C-tau project is at the R&D stage in Novosibirsk. This report concentrates on the SuperKEKB/Belle II project with a brief survey of other projects.

At the end of June 2010, the Belle detector completed its operation after 10 years of experiments and collection of more than 1000 fb^{-1} of integrated luminosity at the KEKB asymmetric-energy e^+e^- collider. The world highest luminosity of the collider, $2.1 \times 10^{34}\text{cm}^{-2}\text{s}^{-1}$, as well as high quality and performance of the Belle detector provided a basis to obtain numerous results in several fields of particle physics. Although the most known Belle achievements concern the CP symmetry violation in the quark sector, very important results were also obtained in the heavy quarkonium spectroscopy, tau lepton decays and two-photon physics.

Motivated by the success of the KEKB/Belle experiment, the new advanced project, KEKB II/Belle II, was accepted. The KEKB II luminosity will exceed the previous one by about 40 times. In many aspects, Belle II will have considerably better performance than Belle. This upgrade will open exciting possibilities in a search and study of new physics phenomena in the heavy quarkonia, lepton flavour violation in tau decays as well as in other particle physics fields.

[1] shwartz@inp.nsk.su

2 Main results from previous B-factories and physics at 50 ab^{-1}

The main goal of the previous generation of B-factories was a study of the CP symmetry violation in B meson decays. This goal was achieved successfully. In 2001, the presence of CP violation in the B meson system was established by the Belle and BaBar collaborations [5] which observed time-dependent asymmetry in the decay process $B^0 \to J/\Psi K^0_S$. Later the CP violation including direct CP violation was observed in many other decay modes. In general, in these experiments Standard Model (SM) was confirmed with the Kobayashi-Maskawa mechanism of CP violation.

In case of CP asymmetry the time dependence of the decay probability is expressed as:

$$p(\Delta t) = \frac{e^{|\Delta t|/\tau_{B_0}}}{4\tau_{B_0}}\{1 \pm [S_{f_{CP}} \sin(\Delta m_d \Delta t) + A_{f_{CP}} \cos(\Delta m_d \Delta t)]\}, \quad (1)$$

where $S_{f_{CP}} = -\xi_{f_{CP}} \sin(2\phi_1)$ – corresponds to indirect CP violation; $A_{f_{CP}}$ – direct CP violation; $\xi_{f_{CP}}$ is CP eigenvalue of the state. The preliminary result of Belle on the CP asymmetry based on the 711 fb^{-1} sample (772M BB pairs) is [6]: $S = 0.668 \pm 0.023 \pm 0.013$ (syst.), $A = 0.007 \pm 0.016 \pm 0.013$ (syst.). The measured asymmetry in $B^0 \to J/\Psi K^0_S$ decays is shown in Fig. 1. In experiments at the super B-factories the accuracy of $\sin(2\varphi_1)$ will be improved by more than twice.

Direct CP violation was also observed at B-factories in $B^0 \to \pi^+\pi^-$ and $B^0 \to K^+\pi^-$ decays. The angle ϕ_2 has been measured with $B^0 \to \pi\pi$, $\rho\pi$ and $\rho\rho$ systems using isospin symmetries. The angle ϕ_3 has also been measured through the processes $B \to D(^*)K(^*)$ and the evidence of direct CP violation in $B \to DK$ decays was obtained.

Magnitudes of the CKM matrix elements have been measured by the Belle and BaBar much more precisely than before. At 50 ab^{-1}, which should be reached with new generation of B-factories, uncertainties in the ϕ_2 and ϕ_3 angles will be improved to about 1.5°. The $\overline{\rho}$ and $\overline{\eta}$ parameters of the unitarity triangle will be determined with 6-8 times better accuracy than now.

Another very important goal of the experiments at B factories is a search for the New Physics, i.e. phenomena which are not described by the SM.

The value of time-dependent CP violation (TDCPV) measured in the decay $B^0 \to \phi K_S$ determines $\sin 2\phi_1$. Now the difference of this value measured in the $B^0 \to \phi K_S$ and in the $B \to J/\psi K_S$ modes is $\Delta S \equiv \sin 2\phi_1^{\phi K_S} - \sin 2\phi_1^{J/\psi K^0} = 0.22 \pm 0.17$, while the SM prediction is about 0.03. A confirmation of this difference would be a serious indication of a New Physics. With the Belle II detector the accuracy of this quantity can be better than the SM theoretical prediction.

In the SM the CP violation in the b quark radiative decays is suppressed. For example the decay time-dependent CP asymmetry in the $B^0 \to K_S\pi^0\gamma$ decay is estimated to be $S \approx -2(m_s/m_b)\sin 2\phi_1 \approx -0.04$. On the other hand, in L-R symmetric models, the asymmetry

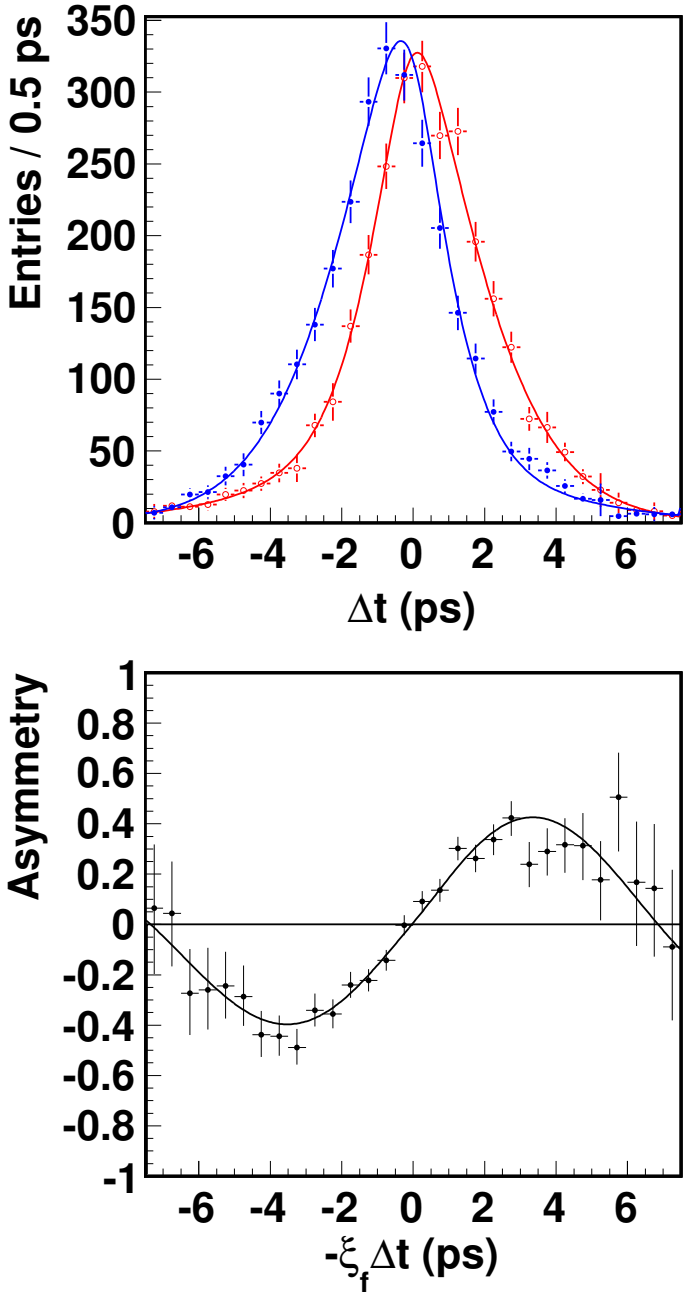

Figure 1: The measured asymmetry in $B^0 \to J/\Psi K^0_S$ decays.

can be as large as $S \approx 0.67 \cos 2\phi_1 \approx 0.5$. The expected accuracy of $S(K_S\pi^0\gamma)$ with 50 ab^{-1} will reach the SM value and thus cover the whole range of NP predictions.

The process sensitive to the new physics with charged Higgs boson is a decay $B^+ \to \tau^+\nu_\tau$. The branching ratio of this decay was measured by Belle with $657{\cdot}10^6$ $B\overline{B}$ events is [8]:

$$B(B^+ \to \tau^+\nu) = (1.54^{+0.38}_{-0.37}(stat.)^{+0.29}_{-0.31}(syst.)) \times 10^{-4}.$$

BaBar result on this value based on $468{\cdot}10^6$ $B\overline{B}$ events [9] is:

$$B(B^+ \to \tau^+\nu) = (1.7 \pm 0.8(stat.) \pm 0.2(syst.)) \times 10^{-4}.$$

The averaging performed by HFAG results in the value $(1.64 \pm 0.39) \times 10^{-4}$ which is higher than the SM prediction based on the CKM fit $(0.763^{+0.114}_{-0.061}) \times 10^{-4}$.

Excellent performance of the electromagnetic calorimeter is crucial for the this measurement. The Belle II calorimeter maintains this performance even with more severe backgrounds expected at SuperKEKB. With much higher statistics this will provide an improvement of the accuracy of the ratio Γ/Γ_{SM} to about 0.08 including uncertainties from theory (on V_{ub} and f_B), while a purely experimental uncertainty will reach 0.04.

Charged lepton flavour violation (LFV) would be a very clear manifestation of the new physics since in the Standard Model the lepton flavour violation decays are extremely rare. For example, $Br(\tau \to l\gamma) \sim 10^{-54}$ and $Br(\tau \to 3leptons) \sim 10^{-14}$. At Belle and BaBar 44 different LFV modes were searched for. The most stringent limit is $B(\tau \to \mu^+e^-e^-) < 1.5 \times 10^{-8}$ [7]. The sensitivity for different modes is limited by background suppression or statistics. In general, the improvement in upper limits on the LFV decays achieved by studies at the B-factories is ~ 100 compared to CLEO.

With 50 ab^{-1} of integrated luminosity the sensitivity to the considered processes will be: for $\tau \to l\gamma$ – $Br \sim O(10^{-8-9})$; for $\tau \to lll, l + meson$ – $Br \sim O(10^{-9-10})$, which reaches the range of predictions in some NP models.

A lot of results were obtained by Belle and BaBar on the hadron spectroscopy. The latest example from the bottomonium family is the observation of the h_b mesons as well as the new unexpected Z_b states. Details can be found in the report of A.Kuzmin at this conference [10].

Earlier, several new states (XYZ states) were found in the charm sector. The detailed report about these results was presented at this conference by S.Eidelman [11].

In the last years a lot of new data on the spectroscopy of light hadrons were obtained at the B- and ϕ-factories, at the BaBar, Belle and KLOE detectors, using initial state radiation (ISR) processes [13]. The status report of this research is given by E.Solodov at this conference [12]. With 50 times high statistics expected at superB-factories the amount and accuracy of physics results provided by this approach will be drastically widen. These results will be competitive and complementary to the data from conventional low energy e^+e^- colliders.

3 SuperKEKB and Belle II

The SuperKEKB collider will be the upgraded KEKB using the same tunnel and some elements of the previous B-factory. The new project is based on the so called "Nano-Beam" scheme, first proposed in [14]. The main features of this project are the following:

- reuse of the KEKB components as much as possible;
- to keep the present cells in HER.
- replacement of the dipole magnets in LER, reusing other main magnets in the LER arcs.
- no option for polarization is considered at present.

The fundamental parameters of the new collider are listed in Table 1

	KEKB (achieved)	SuperKEKB
Energy, GeV (e^+/e^-)	3.5/8.0	4.0/7.0
Beam current, A	1.64/1.19	3.6/2.6
Vertical β function at IP, mm	5.9/5.9	0.27/0.30
Beam-beam parameter, ξ_y	0.129/0.090	0.09/0.081
Luminosity, $10^{34}\text{cm}^{-2}\text{s}^{-1}$	2.11	80

Table 1: Comparison of the main parameters of SuperKEKB and previous KEKB colliders

SuperKEKB/Belle II project is approved and the commissioning of the collider is planned to the second half of 2014 FY. The goal is to collect the integrated luminosity of 50 ab^{-1} by the end of 2021.

The Belle II detector project is described in the Technical Design Report [15]. Demands on the detector are defined first of all by the rates from various physics processes at the luminosity of $8 \times 10^{34}\text{cm}^{-2}\text{s}^{-1}$ as listed in Table 2.

The schematic view of the Belle II detector (top half) in comparison to the previous Belle detector (bottom half) is presented in Fig. 2.

Vertex detection at the Belle II detector will be implemented via the Pixel Detector (PXD) and Silicon Vertex Detector (SVD). The PXD is based on DEPFET technology which allows to produce very thin (down to 50 μm) sensors. Two layers of PXD with the pixel size of 50×75 μm will be arranged around the interaction region.

The SVD consists of four layers of double-sided silicon strip detectors (DSSD). To increase radial coverage the slanted sensors are used in the forward region. The rectangular and wedge shape DSSDs with the strip pitch from 160/50 μm to 240/75 μm are used in SVD. The configuration of PXD and SVD in comparison with the Belle detector is presented in

Physics process	Cross section, nb	Rate, Hz
$\Upsilon(4S) \to B\overline{B}$	1.2	960
Continuum e^+e^- →hadrons	2.8	2200
$e^+e^- \to \mu^+\mu^-$	0.8	640
$e^+e^- \to \tau^+\tau^-$	0.8	640
Bhabha ($\theta_{lab} > 17^\circ$)	44	350*
$e^+e^- \to \gamma\gamma$ ($\theta_{lab} > 17^\circ$)	2.4	19*
2γ-processes, ($\theta_{lab} > 17^\circ, p_t > 0.1\text{GeV}/c$)	80	15000
Total	130	20000

Table 2: Total cross section and trigger rates with $L = 8 \times 10^{34}\text{cm}^{-2}\text{s}^{-1}$ from various physics processes at $\Upsilon(4S)$.
(*) - rate is prescaled by a factor of 1/100.

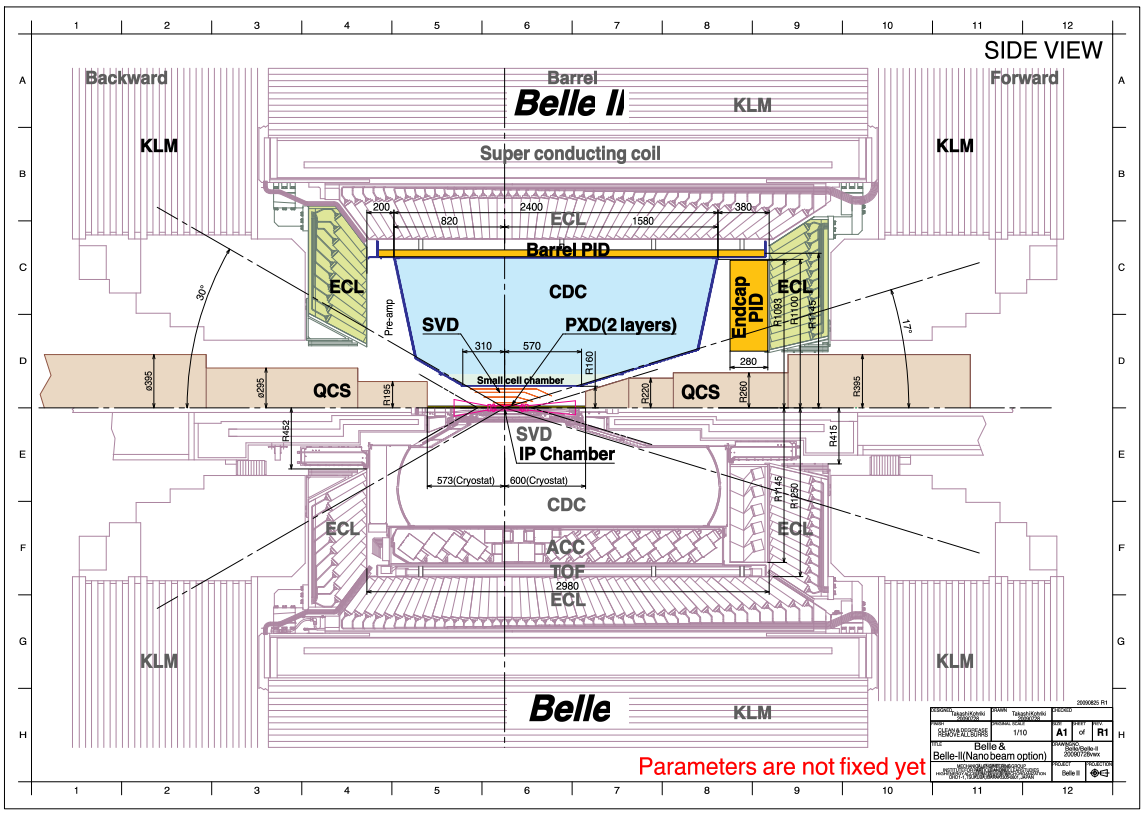

Figure 2: Schematic view of the Belle II detector (top half) in comparison to the previous Belle detector (bottom half).

	Belle II	Belle
Beam Pipe r, mm	10	15
DEPFET		
Layer 1 r, mm	14	
Layer 2 r, mm	22	
DSSD		
Layer 3 r, mm	38	20
Layer 4 r, mm	80	43.5
Layer 5 r, mm	115	70
Layer 6 r, mm	140	88

Table 3: SVD configuration.

Table 3. The PXD and SVD together should provide impact parameter resolution of about 20 μm.

The central drift chamber (CDC) of the Belle II detector is intended for three basic functions: track reconstruction and its precise momentum measurement; a measurement of the ionization losses of the charged particles for the identification purposes; a generation of the signals for the trigger system. The Belle II CDC follows the global structure of its predecessor in the Belle detector, for the material of the major parts, the superlayer wire configuration, the cell structure, the wire material and the gas mixture.

The radii of inner and outer cylinders changed from 77 to 160 mm and from 880 to 1130 mm, respectively. The number of layers increases slightly, from 50 to 56 while the number of the sense wires changed from 8400 to 14336. The momentum resolution of Belle II with CDC and SVD is:

$$\sigma_{p_t}/p_t = 0.1\% \cdot p_t[\mathrm{GeV/c}] \oplus 0.3\%/\beta.$$

The expected dE/dx resolution is about 5%.

The particle identification system in the barrel part of the Belle II detector is based on the time-of-propagation (TOP) counters [16]. The basic idea is to detect simultaneously the direction and arrival time of the Cherenkov photons propagating in the quartz radiator. Photons are detected by the Hamamatsu 16 channel MCP-PMTs which have excellent timing and gain performance. This system will provide a good pion-kaon separation in the momentum range up to 3.5 GeV/c.

Identification of charged particles in the forward endcap region will be performed by the proximity-focusing aerogel ring-imaging Cherenkov detector (ARICH). Cherenkov photons emitted in the 2 cm thick aerogel radiator with the refraction index $n \approx 1.05$ pass 20 cm expansion gap and are detected by the array of position sensitive hybrid avalanche photodetectors (HAPD). This system allows to obtain 99% of kaon identification efficiency at 1% of pion misidentification for particles with 4 GeV/c momentum.

The first priority of the electromagnetic crystal calorimeter (ECL) upgrade is the calorimeter electronics modification following the general strategy of the Belle upgrade. The main idea is to shorten the shaping time and to use a pipe-line readout with waveform analysis. A radical way to improve the characteristics of ECL is a replacement of the slow CsI(Tl) in the endcap part where the background rate is extremely high. The baseline for such an option is to use pure CsI crystals instead crystals doped by Tl. The light readout is made with vacuum photopenthodes. The existing mechanical structure is kept. This option has been developing for the last five years and is now well prepared for construction.

A superconducting solenoid providing a magnetic field of 1.5 T as well as an iron yoke will be reused from the Belle detector.

At Belle the KL&Muon detector consisted of the glass-electrode resistive plate chambers (RPC). The upgrade plan implies keeping the RPC system in the barrel part of the Belle II and replacement of the endcap parts to the system based on the plastic scintillators. The endcap KL&Muon detectors consist of the polisterene scintillator bars with implemented WLS fibers for light collection. To detect the reemitted light delivered by fibers, MPPCs of 1.3×1.3 mm area will be used.

The trigger system of the Belle II detector should satisfy the following requirements:

- high efficiency for hadronic events;
- maximum average trigger rate of 30 kHz;
- fixed latency of about 5 μs;
- timing precision of less than 10 ns;
- minimum two-event separation of 200 ns;
- trigger configuration that is flexible and robust.

To meet these requirements, the Belle triggering scheme with new technologies was adopted.

The data acquisition (DAQ) system of the Belle II detector has to cope with a high data flow which will reach 600 MB/sec at full luminosity. The system transfers the data from the front-end electronics through several steps of data processing, and finally to the storage system. The main components of the data flow are the unified data link called the Belle2Link, the common readout platform called COPPER, the event builder system, and the high level trigger (HLT) system.

The detector front-end boards with digitizers are placed near or inside the detector structure and the digitized signals are transferred into COPPER systems through long optical fibers using the Belle2Link. A simple data reduction is performed on each front-end electronics board or on the receiver module of COPPER, while the data formatting and module-level event building is done on COPPER using the on-board CPU. The further event building

and reduction are done on the readout PCs and the event builder, and finally processed by the HLT farms for the software event selection.

4 SuperB in Italy

Another project of the SuperB-factory, SuperB, was developed to be constructed in Italy [17].

SuperB is a two-ring, asymmetric-energy ($E^- = 4.18$ GeV, $E^+ = 6.7$ GeV) collider with:

- large Piwinski angle and "crab waist" (LPA & CW) collision scheme;
- ultralow emittance lattices;
- an option of the longitudinally polarized electron beam is possible;
- target luminosity of $10^{36}\text{cm}^{-2}\text{s}^{-1}$ at the $\Upsilon(4S)$;
- possibility to run at τ/charm threshold with $L = 10^{35}\text{cm}^{-2}\text{s}^{-1}$.

The circumference of the rings is 1258 m, the number of bunches will be from 978 to 1956 for different modes providing the electron (positron) current from 1.9(1.5) to 4.0(3.1) A.

This collider was designed taking into account the following criteria:

- minimizing building costs;
- minimizing running costs;
- reuse of some PEP-II B-Factory hardware (magnets, RF).

The SuperB detector is based on the BaBar detector experience and some elements [18]. The detector contains the silicon vertex tracker based on the silicon pixel and silicon strip detectors, drift chamber, modified DIRK system for particle identification. The barrel calorimeter and superconducting solenoid of the BaBar detector will be used in the new project. Forward and backward regions are still under discussions and study. Two crystal options are studied for forward endcap calorimeter: LYSO or pure CsI crystals.

5 BINP Super-Tau-charm factory project

A Super $c - \tau$-factory (CTF) is a symmetric electron-positron collider operating in the range of center-of-mass (c.m.) energies from 2 to 5 GeV with a high luminosity of about $10^{35}\text{cm}^{-2}\text{s}^{-1}$ [19]. The main goal of experiments at CTF is a study of the processes with c quarks and τ leptons in the final state using data samples that are 3-4 orders of magnitude higher than available today.

The following most important tasks should be listed:

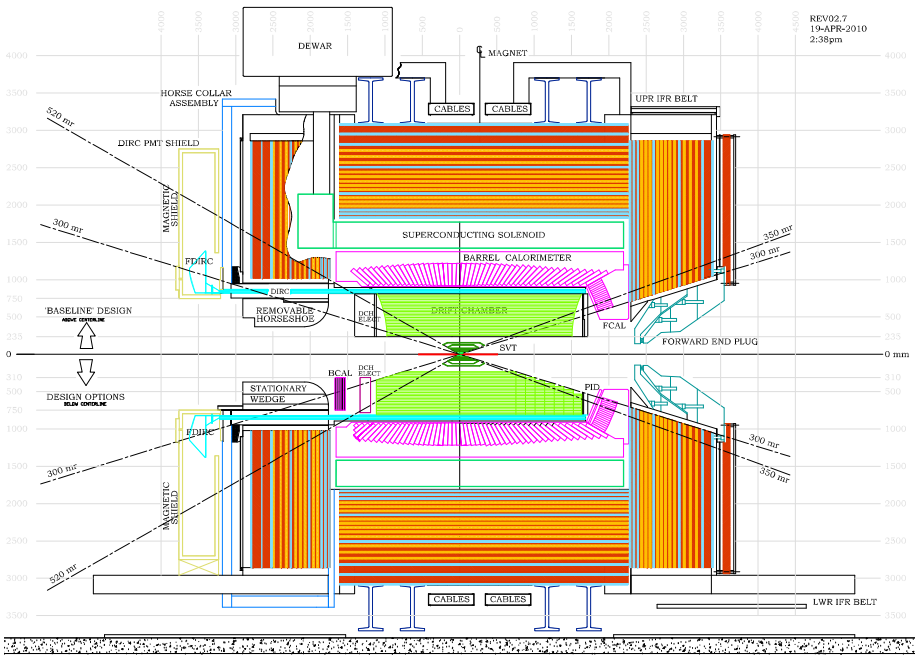

Figure 3: Schematic view of the SuperB detector.

- Precise charm physics:
  - Precise measurement of the charm hadron parameters which are crucial for the high-precision CKM matrix (strong phases, f_D, f_{D_s}, form factors).
  - Study of D^0 mixing, search for CPV in mixing, strong phases for ϕ_3 measurements at SuperB and LHC using C-tau-factory as a unique source of coherent $D^0/\overline{D}^0$ states.
- High-precision τ-lepton physics with polarized beams:
  - Tests of the charged lepton universality, study of the Lorentz structure of τ-decays.
  - Search for CP and T violation in τ-decays.
  - Search for LFV decays ($\tau \to \mu\gamma$).
  - Search for second class currents (using kinematical constraints at threshold).
- High-statistics hadron spectroscopy and search for exotics:
  - Precise charmonium spectroscopy.
  - Spectroscopy of the highly excited charmonium states (complementary to Bottomonium).

– Light hadron spectroscopy in charmonium decays.

The collider of this project implies two rings with a Crab Waist collision scheme and single interaction point with sub-millimeter β_y at IP. The beam energy of each ring is from 1.0 to 2.5 GeV. To keep damping parameters in the whole energy range to optimize the luminosity, four superconducting wigglers are included. A possibility of experiments with the longitudinally polarized electrons in the whole energy range is provided by a special source of polarized electrons and five siberian snakes in the ring. The collider will be equipped by an on-line energy monitoring system based on back Compton scattering of the laser photons which provides an accuracy of $5 \div 10 \cdot 10^{-5}$.

The detector for the BINP C-tau-factory should have ultimate hermeticity; ability of $e/\mu/\pi/K$ separation up to 2 GeV/c; good momentum resolution for charged particles; high efficiency to low p_T tracks, excellent energy resolution of electromagnetic calorimeter including high efficiency to low energy ($\sim$20 MeV) photons. The detector design is now under development.

6 Conclusion

The last decade demonstrated the fruitfulness and efficiency of the flavor "factories" in particle physics. The huge amount of results was obtained at the B-factories, but many new questions arose and the broad field of research will be opened by the superB-factories. It is clear that the superB-factories will produce the information complementary to the LHC. At present, the superKEKB/Belle II project is under construction and other B- and c-tau-factories projects are at a design stage. We can hope for new exciting results in the next decade.

Acknowledgments

I would like to thank organisers for the kind invitation to this impressive Conference as well as for their help and hospitality in Munich. My participation in this Conference was supported by the grant RFBR 11-02-08128.

Bibliography

[1] S. Kurokawa *et al.*, Nucl. Instr. and Meth., **A499**, 1 (2003).

[2] PEP-II Conceptual Design Report, SLAC-372, LBL-PUB-5303, CALT-68-1715, UCRL-ID-106426, UC-IIRPA-91-01 (1991).

[3] A. Abashian *et al.*, Nucl. Instr. and Meth., **A479**, 117 (2002).

[4] B. Aubert *et al.*, Nucl. Instr. and Meth., **A479**, 1 (2002).

[5] A. Abashian *et al.*, (Belle Collaboration), Phys. Rev. Lett. **86**, 2509 (2001);
B. Aubert *et al.*, (BABAR Collaboration), Phys. Rev. Lett. **86**, 2515 (2001).

[6] A.Poluektov, Recent EW results from Belle, talk given at Morion EW conference, 2011.

[7] Y. Miyazaki *et al.*, Phys. Lett. B **660** 154 (2008).

[8] K. Hara *et al.*(Belle Collaboration), Phys. Rev. **D82**, 071101 (2010).

[9] B. Aubert *et al.*(BABAR Collaboration), Phys. Rev. **D81**, 051101(2010).

[10] A.Kuzmin, Bottomonium results at Belle, talk at this conference.

[11] S.Eidelman, Status of X, Y, Z states, talk at this conference.

[12] E.Solodov, Recent results on hadrons via Initial State radiation at BABAR, talk at this conference.

[13] V.N. Baier, V.A.Khoze, Sov. Phys. JETP **21** 1145 (1965);
S. Binner, H.J. Kuhn, K. Melnikov, Phys. Lett.B **459** 279 (1999);
M.Benayoun *et al.*, Mod. Phys. Lett. A **14** 2605 (1999).

[14] P. Raimondi, Talk, given at the 2d SuperB workshop, Frascati, http://www.lnf.infn.it/conference/superb06/talks/raimondi1.ppt, 2006.

[15] T. Abe *et al.*, Belle II technical design report, KEK Report 2010-1 (2010).

[16] K. Inami *et al.*, Nucl. Instr. and Meth. **A595**, 96 (2008).

[17] M.E. Biagini *et al.*, http://arxiv.org/abs/1009.6178, 2010;
M. Biagini, talk at XVII SuperB Workshop and Kick-off Meeting, Elba, May 29-June 1, 2011.

[18] E. Grauges *et al.*, INFN/AE 10/4, LAL 10-115, SLAC-R-954, arXiv:1007.4241v1 (2010).

[19] E. Levichev, The project of a Tau-Charm factory with crab waist in Novosibirsk, Phys. Part. Nucl. Lett., **5**, 554(2008);
A. Blinov *et al.*, The Project of Tau-charm factory with crab waist in Novosibirsk. ICFA Beam Dyn. Newslett., **48**, 268 (2009).

The Future of Hadrons: The Nexus of Subatomic Physics

Chris Quigg[1]
Theoretical Physics Department
Fermi National Accelerator Laboratory
P.O. Box 500, Batavia, Illinois 60510 USA

I offer brief observations on matters discussed at the XIV International Conference on Hadron Spectroscopy and explore prospects for hadron physics.

1 Impressions and Musings

The organizers of *Hadron 2011* have asked me to offer some perspectives on the state and prospects of hadron physics, stimulated by the presentations at this meeting and by some themes in the recent literature. I must begin by noting the enormous diversity and reach of experimental programs reported here in Munich, along with quite remarkable progress in theory, including the emergence of lattice QCD as a versatile and reliable tool. The coherence provided by quantum chromodynamics means that insights may arise from unexpected quarters [1]. It is more than ever advisable to take a broad view that integrates across hadronic physics and to connect with the rest of subatomic physics. Connections work both ways: *You* may answer questions that seem far afield! It also seems important to look beyond nuclear and particle physics for insights into scattering and bound-state problems, to seek new ways to address hadronic questions, and to ask, "How are we prisoners of conventional thinking?" Part of the pleasant challenge of the moment is that recent advances leave us with many puzzles and opportunities, including "simple" questions that we cannot yet answer.

In contrast to biological evolution, lines in theoretical physics that do not win are not extinguished, never to rise again. We are free to borrow potent ideas from the past and to apply them in new settings, to powerful effect. A recent example is the application of S-matrix style unitarity to the evaluation of multiparton amplitudes [2]. Tools that organized the exploratory particle-production data in the 1970s, such as triple-Regge analysis [3], may offer ways to understand the far more comprehensive measurements now becoming available. If the old ways do not explain every feature of the new data, they should at least show us which results are surprising, and which should be expected.

[1] quigg@fnal.gov

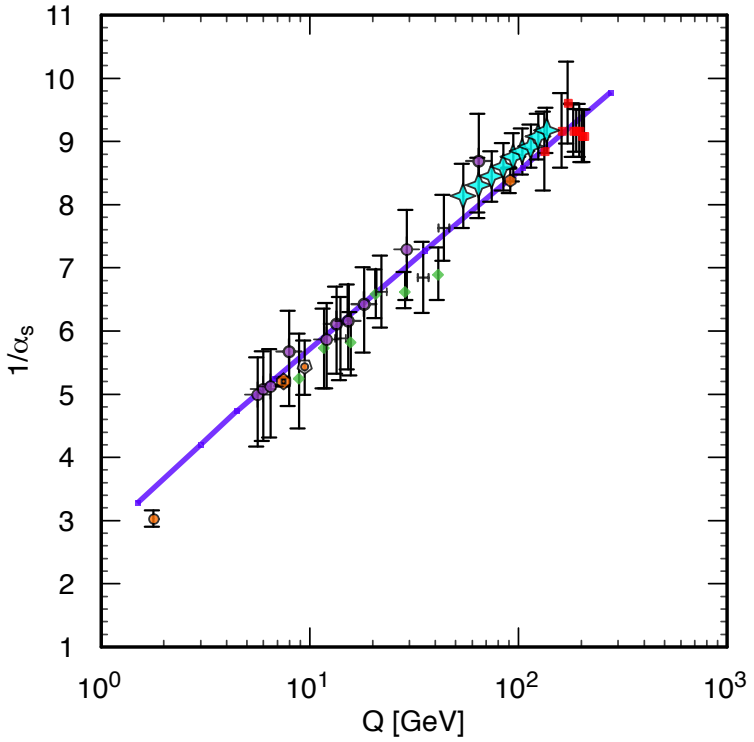

Figure 1: Measurements of the strong coupling $1/\alpha_s(Q)$ as a function of the energy scale $\ln Q$. The curve shows the QCD prediction at four loops, using 3-loop threshold matching at the heavy-quark pole masses $m_c = 1.5$ GeV, $m_b = 4.7$ GeV. From Ref. [4].

2 QCD: the basis of hadronic physics

Our picture of matter is built on a set of pointlike ($r \lesssim 10^{18}$ m) constituents: the quark and lepton families. The fundamental fermions interact through forces derived from $\mathrm{SU(3)_c} \otimes \mathrm{SU(2)_L} \otimes \mathrm{U(1)}_Y$ gauge symmetries. Quarks are influenced by the strong interaction, and so carry color, the strong-interaction charge, whereas leptons do not feel the strong interaction, and are colorless.

We have accumulated persuasive evidence—both theoretical and experiments—that quantum chromodynamics underlies all strong-interaction phenomena [4]. The defining attribute of QCD is that it is an asymptotically free theory, by which we understand that the coupling strength, or effective charge, diminishes at short distances or high momentum transfers. Determinations of α_s in a variety of experimental settings confirm the evolution predicted by QCD: the compilation in Figure 1 shows that, to excellent approximation, $\alpha_s(Q)$ varies linearly with $\ln Q$, as expected at leading order in perturbation theory.

Over a few decades in the scale Q, α_s decreases from a value at which perturbation theory is

a questionable tool to values for which perturbative calculations appear eminently plausible. At still lower scales than those depicted in Figure 1, nonperturbative analysis is required. At high scales and small values of α_s, quarks and gluons, the *fundamental fields* of QCD, are manifest, as we see in high-resolution, hard-scattering studies of proton structure, in phenomena involving matter at high density, and in the formulation of lattice calculations. At lower scales, it is more efficient to deal with *effective* degrees of freedom such as constituent quarks and Goldstone bosons, to formulate effective field theories, and to construct informed approximations such as isobar (resonance) models and semiphenomenological descriptions of nuclei and nuclear structure.

From the variation of $\alpha_s(Q)$, we see how a theory based on an interaction Lagrangian that contains no dimensionful parameters can be characterized by a scale Λ, with dimensions of energy, by means of *dimensional transmutation.* The identification

$$1/\alpha_{\mathsf{s}}(2m_c) \equiv \frac{27}{6\pi} \ln\left(\frac{2m_c}{\Lambda}\right) \tag{1}$$

sets the value of Λ appropriate for three active quark flavors. The coefficient of $\ln Q$ in the evolution of $1/\alpha_s$ decreases by $2/6\pi$ at each successive quark threshold.

Lattice QCD including dynamical quarks allows us to evaluate the proton mass according to Einstein's first formulation of his famous equation, which identifies mass with rest energy: $M_p = E_0/c^2$. To excellent approximation, the proton mass is given by a calculable constant times Λ, plus small corrections [5]. Indeed, the quark masses contribute but a few percent of the proton mass: $3(m_u + m_d)/2 \approx 10 \pm 2$ MeV [6]. Hadrons are a thus new kind of matter, whose masses are not given by the sum of the masses of the parts. Instead, the rest energy of a hadron is determined mainly by confinement energy stored up in the gluon field or the kinetic energy of the quarks [7].

Since the slope of $1/\alpha_s(Q)$ changes when new colored objects come into play, we should be alert for slope changes more pronounced than those implied by a new flavor of color-triplet quark. A provocative possibility arises in a simplified view of a supersymmetric world in which an entire family of superpartners becomes active at 1 TeV. The resulting slope change is dramatic: from $7/2\pi$ below the SUSY threshold to $3/2\pi$ above. It is important to contemplate how the LHC experiments might extend α_s determinations to much higher scales (perhaps by measuring W + jets ?) and what calculational advances will be needed to enable precise determinations.

3 Connections and Controlled Approximations

The essence of doing science consists in *making connections* that lead us beyond independent explanations for distinct phenoma toward a coherent understanding of many phenomena. A network of understanding helps us see how different observations fit together and—very important—helps us to recognize when something *doesn't fit.*

Connections among experiments or observations are not the only important ones. Whenever possible, we need to make connections between our models and the QCD Lagrangian—either directly, or through effective field theories, lattice field theory, or a controlled approximation to full QCD. I would also stress the potential value of reaching toward connections with our knowledge of nuclear forces, with the behavior of nuclear matter under unusual conditions, and with phenomena such as Feshbach resonances [8] encountered in the study of many-body systems [9].

Under different circumstances, various approximations to QCD emerge as controlled expansions in small parameters. Nonrelativistic QCD applies to heavy-heavy ($Q_1\overline{Q}_2$) mesons, for which the quark masses greatly exceed the QCD scale parameter, $m_{Q_i} \gg \Lambda_{\rm QCD}$ [10]. NRQCD takes as its expansion parameter the heavy-quark velocity divided by the speed of light. Heavy-quark effective theory (HQET) applies usefully to heavy-light ($Q\overline{q}$) systems, for which $m_Q \gg \Lambda_{\rm QCD}$ [11]. In first approximation, the spin of the heavy quark is static, so the "light-quark spin" $\vec{\jmath}_q = \vec{L} + \vec{s}_q$ is a good quantum number and the relevant expansion parameter is $\Lambda_{\rm QCD}/m_Q$. Chiral symmetry is a valuable starting point for light quark systems ($q_1\overline{q}_2$) [12]. In this case, the expansion parameter compares the current-quark mass to the scale of chiral-symmetry breaking, and is generally taken as $m_q/4\pi f_\pi$, where f_π is the pion decay constant.

4 What Is a Proton?

4.1 Beyond the parton-model idealization

For hard-scattering phenomena, we have learned to regard the proton as a broadband, unseparated beam of quarks, antiquarks, gluons, and perhaps other constituents, characterized by parton densities $f_i^{(a)}(x_a, Q^2)$, the number density of species i with momentum fraction x_a seen by a probe with resolving power Q^2. The Q^2-evolution of the parton densities is given by QCD perturbation theory, but the low-scale distributions $f_i^{(a)}(x_a, Q_0^2)$ have a nonperturbative origin. Historically, the parton distributions were idealized as free of correlations, and depending only on longitudinal degrees of freedom. Remarkably, this truncated version of reality has served us extraordinarily well for more that forty years.

Intense experimental and theoretical activity on generalized parton distributions [13], transverse momentum distributions [14], and the three-dimensional structure of the proton [15] represents an important step beyond the traditional idealization. Bjorken [16] has suggested that by studying event structure in high-energy collisions we might be able to see signs of correlations among the partons, perhaps by observing diquark–diquark collisions. I would like to underline the importance of looking at both events and distributions for lightly triggered events. At lower energies, the bulk of particle production came from soft collisions—diffraction plus short-range order—as we learned from systematic studies

inspired by Ken Wilson [17]. I think it is highly likely that novel structures, and perhaps new classes of processes, will reveal themselves in lightly triggered events at the LHC [18].

4.2 Seeking the relevant degrees of freedom: diquarks?

Much of our insight into how hadrons behave follows from the idealization that mesons are quark–antiquark states, baryons are three-quark states, and that the quarks have only essential correlations. In the case of baryons, this reasoning leads us to the plausible starting point of SU(6) (flavor-spin) wave functions, which indeed offer a useful framework for discussing magnetic moments and other static properties. Some long-standing observations, however, show us the limitations of the zeroth-order guess. If we examine deeply inelastic scattering in the limit as $x \to 1$, spin asymmetries indicate that the SU(6) wave functions are inadequate [19], and the ratio F_2^n/F_2^p is far from the uncorrelated expectation of $\frac{2}{3}$ [20].

When we try to account for correlations, it may be fruitful to consider diquarks as physical objects. Color algebra tells us that the $\mathbf{3} \otimes \mathbf{3}$ quark–quark combination is attractive in the $\mathbf{3}^*$ representation that corresponds to an antisymmetric diquark structure. A simple analysis suggests that the attraction of $[qq]_{\mathbf{3}^*}$ is half as strong as that of the $[q\bar{q}]_{\mathbf{1}}$ ($\mathbf{3} \otimes \mathbf{3}^* \to \mathbf{1}$) channel. The suggestion [21] to regard members of the scalar nonet as $qq\bar{q}\bar{q}$ states organized as $[[qq]_{\mathbf{3}^*}[\bar{q}\bar{q}]_{\mathbf{3}}]_{\mathbf{1}}$ is well known. A few years ago, Selem and Wilczek revisited the Chew–Frautschi systematics of N and Δ resonances [22], and found it plausible to view even low-spin, light baryons as $q[qq]_{\mathbf{3}^*}$ configurations. But now Edwards, *et al.* [23], using lattice techniques with dynamical fermions to investigate excited-state baryon spectroscopy, find N^* and Δ level structures that do not support a dominant quark–diquark configuration. It is interesting to inquire how the quark–diquark picture might square with intuition from the $1/N_c$ expansion [24].

It is worth examining the $q[qq]_{\mathbf{3}^*}$ proposal by considering its implications for doubly heavy (QQq) baryons. The comparison with heavy-light ($Q\bar{q}$) mesons offers a chance to calibrate the attractive forces in the $\mathbf{3}^*$ and color-singlet channels. Similarly, extending studies of the systematics of $qq \cdot \bar{q}\bar{q}$ states to $Qq \cdot \bar{Q}\bar{q}$ states could develop and challenge the way we think about diquarks and test color-spin symmetry as an organizing principle. Finally, in heavy-ion collisions, we should be alert for tests of the utility of diquarks in color–flavor locking, color superconductivity, and other novel phenomena.

4.3 What are the appropriate degrees of freedom at long distances?

As its momentum decreases, the current quark of perturbative QCD evolves into a constituent quark, as illustrated in Figure 2 [25]. The constituent-quark mass arises from the cloud of low-momentum gluons winking in and out of existence through quantum fluctuations around the current quark. Dynamical chiral symmetry breaking is an inherently nonperturbative effect that spontaneously generates a quark mass, even in the chiral

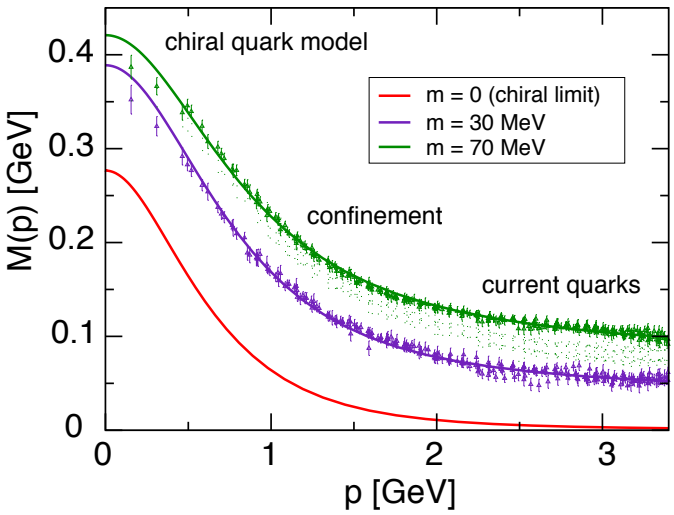

Figure 2: The dressed-quark mass function $M(p)$, computed by Dyson–Schwinger techniques, compared with numerical simulations of lattice-QCD for several values of the current-quark mass m (adapted from [25]).

limit $m \to 0$. This evidence gives a quantitative basis for the highly useful chiral-quark model [26], in which constituent quarks and Goldstone bosons are taken as the apt degrees of freedom at low scales.

The chiral quark model presents an intuitive picture of how quasistatic properties of the nucleon might arise. Perturbative evolution of the parton distributions treats symmetrically quarks and antiquarks, and up and down flavors. Any differences between quark and antiquark distributions, or the distributions of up and down quarks, must therefore be set at low scales. An interesting challenge is presented by the Gottfried sum rule,

$$\begin{aligned} I_{\rm G}(Q^2) &\equiv \int_0^1 dx \frac{F_2^p(x,Q^2) - F_2^n(x,Q^2)}{x} \\ &= \int_0^1 dx \sum_i e_i^2 \left[q_i^{(p)}(x,Q^2) + \overline{q}_i^{(p)}(x,Q^2) q_i^{(n)}(x,Q^2) + \overline{q}_i^{(n)}(x,Q^2) \right], \end{aligned} \tag{2}$$

for which the New Muon Collaboration long ago found [27] the value 0.240 ± 0.016, below the expectation of $\frac{1}{3}$ in the quark-parton model with a flavor-symmetric light-quark sea. To see how an asymmetry could come about, imagine that a constituent quark fluctuates into a current quark plus a Nambu–Goldstone boson, as illustrated in Figure 3 [28]. The resulting pion cloud changes the parton distributions for protons and neutrons, but doesn't enter the difference $F_2^p - F_2^n$ because $F_2^{\pi^+} = F_2^{\pi^-}$. The Gottfried sum rule defect arises from the asymmetry of the left-behind quarks, which arises from the (uud) vs. (udd) composition of valence quarks in the proton and neutron. The pion cloud also doesn't affect the spin budget of the nucleon, because the pion is spinless. However, the γ_5 coupling flips the helicity

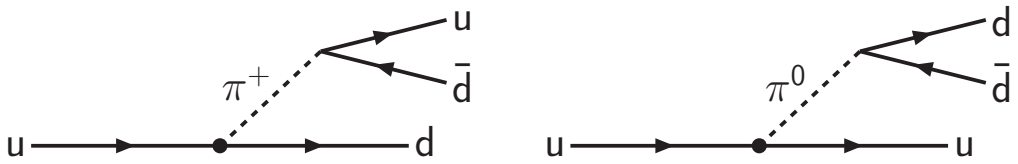

Figure 3: Example fluctuations of a valence up-quark in the chiral quark model.

of the left-behind quark. Consequently, we should expect spin contributions $\Delta d, \Delta s < 0$, $\Delta\bar{d}, \Delta\bar{s} = 0$, which set interesting targets for experiment.

Even at low scales, where the strong interactions are *a priori* strong, we know cases in which partonic arguments yield results in agreement with experimental observations. One example is the surprising success of the simple picture of hadron masses put forward by De Rujula, Georgi, and Glashow [29]. An analytic hadronization model for event shapes by Dokshitzer, Marchesini and Webber derives the structure of power corrections from perturbative QCD [30]. The model assumes that the strong coupling remains finite at low energy scales where simple perturbative calculations break down. A mean value at low scales,

$$\alpha_0(\mu_I) \equiv (1/\mu_I) \int_0^{\mu_I} dQ\, \alpha_{\mathbf{s}}(Q), \quad \mu_I = 2\,\mathrm{GeV} \tag{3}$$

has been extracted from several observables [31]. These are consistent with the idea that the effective coupling freezes at low scales, with $\alpha_0(2\,\mathrm{GeV}) \approx 0.5$. If that is indeed the case, it is plausible to consider quarks and gluons as apt long-distance degrees of freedom. It may also clarify such noteworthy simplicities as the unimportance of nonvalence components for hadron properties, Bloom–Gilman duality, precocious scaling, and the perturbative approach to bound states [32].

4.4 Could chiral symmetry and confinement coexist?

Confinement and the spontaneous breaking of chiral symmetry for light quarks go hand in hand [33]. In the case of heavy–light $(Q\bar{q})$ mesons and doubly heavy (QQq) baryons, it is interesting to inquire whether a vestige of the chiral symmetry of the tethered light quark might be revealed in parity-doubled bound states transforming as linear representations of the light-quark chiral symmetry [34]. For the heavy–light mesons D, D_s, B, B_s, we should then expect chiral supermultiplets linking states with adjacent values of the orbital angular momentum, $(L, L+1)$, but with the same value of the light-quark spin, j_q, that we

encountered in §3. In particular, the chiral symmetry should link the levels

$$\begin{aligned} j_q = \tfrac{1}{2}: &\quad 1\mathrm{S}(0^-, 1^-) \text{ and } 1\mathrm{P}(0^+, 1^+) \\ j_q = \tfrac{3}{2}: &\quad 1\mathrm{P}(1^+, 2^+) \text{ and } 1\mathrm{D}(1^-, 2^-) \\ &\ddots \end{aligned}$$

This association of parity doublets implies that the hyperfine splitting should be the same for partner levels: $M_{1^+} - M_{0^+} = M_{1^-} - M_{0^-}$, etc. It will be very interesting to extend observations to the doubly heavy baryons and to establish for a range hadrons with tethered light quarks how far QCD is from the conjecture described here.

4.5 Proton structure and dark matter searches

The search for cold dark matter as weakly interacting massive particles (WIMPs) is advancing on many fronts [35]. Passive experiments that seek direct detection by registering collisions of passing WIMPs with the detector material provide limits or signals expressed in terms of the WIMP mass and the cross section for spin-dependent or spin-independent scattering. There is high interest in confronting observations with the expectations of hypotheses about the nature of the dark-matter particles [36]. That is where hadronic physics enters. For popular forms of neutralino dark matter, the dominant contribution to the spin-independent cross section plausibly arises from Higgs-boson exchange between the WIMP and the target nucleon. How does the Higgs boson interact with the nucleon? Surely not by coupling to the nucleon mass, because QCD has taught us that the nucleon mass is generated to very high approximation by the strong interactions. Higgs couplings to the up and down quarks are small, in proportion to their tiny current-quark masses, so it is likely that the major contribution arises from Higgs couplings to the minority "hidden" constituents of the nucleon, strange quarks and beyond. The role of $(\bar{s}s)$ [37] and heavier condensates and details of the gluon condensate are incompletely understood, and this gives rise to an uncertainty in the spin-independent cross section of up to an order of magnitude [38]. We can certainly hope to address the narrow question of heavy-flavor presence in the nucleon both experimentally and theoretically. Perhaps now is the time to ask whether a theoretical reconception is called for.

4.6 Nucleon structure at a neutrino factory?

If a millimole of muons produced in hadron reactions can be captured, cooled, and accelerated to some tens of GeV, it may be possible to construct a neutrino factory, for which the instability of the stored muons is a virtue [39]. The intense neutrino beams would be ideal for the study of neutrino oscillations over long baselines, but the possibilities of close-in experimentation are also quite remarkable. With a flux of 10^{20} neutrinos per year, we could contemplate ν scattering on thin targets, *e.g.*, hydrogen or deuterium, ν scattering on active

semiconductor targets to study heavy-flavor production, and even ν scattering on polarized targets. Preliminary studies indicate that it would be possible to determine flavor by flavor the valence and sea-quark distribution functions with very small statistical errors [40] and to extract detailed information on polarized structure functions [41]. A modern critical evaluation of these conclusions would be very enlightening.

5 Spectroscopy of states containing heavy quarks

We have extensive knowledge of baryons containing a single c or b quark, but no established observations of doubly heavy baryons. Searching for QQq states is an important goal for the LHC experiments. Let us review the essential expectations. In the heavy-quark limit, there are parallels between $[QQ^{(\prime)}]_{\mathbf{3}*}q$ baryons and $Q\overline{q}$ mesons as heavy–light systems. At the level of one-gluon-exchange,

$$V_{[QQ^{(\prime)}]_{\mathbf{3}*}}(r) = \tfrac{1}{2}V_{(Q\overline{q})_{\mathbf{1}}}(r). \tag{4}$$

How faithfully does this simple estimate reflect reality? In addition to the meson-like excitations of the tethered light quark, the doubly heavy baryons should exhibit excitations of the core, from which we may learn about $[QQ^{(\prime)}]_{\mathbf{3}*}$ dynamics. If we are able to explore bcq baryons, the unequal masses of the heavy quarks might give us a window on shortcomings of intuition drawn from nonrelativistic potential models, just as we hope for the B_c mesons.

Weak decays of doubly heavy baryons entail a rich set of heavy-heavy and heavy-light transitions that isolate different pieces of the effective Hamiltonian for charged-current interactions. Strong and electromagnetic cascades from excited states will involve two length scales, $r_{\rm H} = \langle r^2_{(QQ^{(\prime)})}\rangle^{\frac{1}{2}}$ and $r_\ell = \langle r^2_{(QQ^{(\prime)}q)}\rangle^{\frac{1}{2}}$. The core excitations in particular should reveal some extremely narrow states. Studies of production dynamics should also stretch our understanding, both by extending fragmentation models to new regimes and through the comparison with quarkonium production dynamics.

For the B_c meson family, I will be very brief. We need to elaborate the experimental systematics of decays, including the $\tau\nu_\tau$ annihilation channel, b decays, and c decays. It would also be highly informative to reconstruct part of the excitation spectrum in $\pi^+\pi^-$ or γ cascades.

Finally, a few words on the ordinary quarkonium states of the ψ and Y families and the new states associated with quarkonium. For the ordinary states, we should aim for a comprehensive understanding of the decays to $\pi^+\pi^-(Q\overline{Q})$. There are enough inconsistencies and puzzling effects that it is time to rethink our reliance on the color multipole expansion. This has implications for some of the extraordinary states as well—those that have mysteriously large branching fractions to $\pi^+\pi^-(Q\overline{Q})$.

The many new states associated with charmonium raise many new questions and opportunities. A few [$\chi_{c2}(2P)(3927)$, for example] look like simple $c\bar{c}$ levels. Most new states

are not simple quarkonium, and indeed we should expect most states above the flavor threshold to have multiple personalities. Not all the expected charmonium levels have yet been observed. In addition to the $\eta_{c2}(1^1\mathrm{D}_2)$ and $\psi_2(1^3\mathrm{D}_2)$, the narrow states $1^3\mathrm{D}_3$, $2^3\mathrm{P}_2$, and $1^3\mathrm{F}_4$ remain at large. The rich harvest of states, including candidate charged states that do not fit the standard $Q\overline{Q}$ body plan, shows the virtue of making all possible few-particle combinations.

On the theory side, we need to better understand the role of thresholds in shaping the states associated with quarkonium on their own, near would-be quarkonium levels, and in the company of attractive s-wave amplitudes. Close scrutiny of the similarities and differences of the new states associated with $(c\bar{c})$ and $(b\bar{b})$ should be very informative.

6 A New Era of Heavy-Ion Physics

The 2010 heavy-ion run of the LHC, devoted to Pb-Pb collisions at $\sqrt{s_{NN}} = 2.76\,\mathrm{TeV}$, has begun to realize the great potential of experimentation in the new energy regime to illuminate a broad array of topics in hadronic physics. Effects long sought, or teased out of the data with great difficulty at lower energies, show themselves readily at the LHC. The new challenge is to develop the new observations into robust and quantitative tools. I give two illustrations.

If a hard-scattering event occurs within a quark-gluon plasma, the outgoing partons will lose energy through collisions with the hot stuff of their environment [42]. Should one of the partons traverse a longer path in the hot matter, it would suffer a greater energy loss than its partner; the ensuing jet of hadrons would be degraded, or even extinguished. Both ATLAS [43] and CMS [44] have observed, and begun to characterize, just such an effect.

A quark-gluon plasma is expected to screen the potential that binds heavy quark-antiquark pairs and so to melt quarkonium states—the lightly bound excited states first [45]. The CMS Collaboration reports the double ratio [46]

$$\frac{\mathrm{Y(2S+3S)/Y(1S)}|_{[\mathrm{Pb\,Pb}]}}{\mathrm{Y(2S+3S)/Y(1S)}|_{[pp]}} = 0.31^{+0.19}_{-0.15}\ (\mathrm{stat.}) \pm 0.03\ (\mathrm{syst.}). \tag{5}$$

Analysis of the sequential-melting scenario is complicated by the fact that a significant fraction of the observed yield of the deeply bound $J/\psi(1\mathrm{S})$ and $\mathrm{Y}(1\mathrm{S})$ states is due to decays of excited states. It would therefore be of great interest to investigate directly the melting of χ states, and to compare the behavior of the J/ψ and Y families. The energy dependence of the phenomenon should provide insight into the nature of the hot medium. Studies of quarkonium melting in the B_c system should also be enlightening, once excited states have been observed.

We can expect much more from ALICE, ATLAS, and CMS in the next heavy-ion run.

7 Concluding Remarks

QCD has been validated as a new law of nature. It is internally consistent up to very high energies, and so could be a complete theory of the strong interactions. Whether QCD is the final answer for the strong interactions is a subject for continuing experimental tests, which are being extended in experimentation at the Large Hadron Collider. Beyond the comparison of perturbative calculations with experiment, it remains critically important to test the confinement hypothesis by searching for free quarks, or for signatures of unconfined color. Sensitive negative searches for quarks continue to be interesting, and the definitive observation of free quarks would be revolutionary. Breakdowns of factorization would compromise the utility of perturbative QCD. Other discoveries that would require small or large revisions to QCD include the observation of new kinds of colored matter beyond quarks and gluons, the discovery that quarks are composite, or evidence that $\mathrm{SU}(3)_c$ gauge symmetry is the vestige of a larger, spontaneously broken, color symmetry.

While probing our underlying theory for weakness or new openings, we have plenty to do to apply QCD to myriad experimental settings, to learn its implications for matter under unusual conditions, and to become more adept at calculating its consequences. New experimental tools provide the means for progress on a very broad front.

Acknowledgments

It is a pleasure to express heartfelt thanks to the International Advisory Committee and the Local Organizing Committee, and especially to Stephan Paul and Karin Frank, for preparing a superb program and a stimulating week in the inspiring surroundings of the Künstlerhaus. I am grateful to the Excellence Cluster *«Origin and Structure of the Universe»* for generous support. I thank Eric Laenen and the NIKHEF Theory Group for warm hospitality during the preparation of this manuscript. I salute the contributors and participants for excellent presentations and enlightening discussions. Fermilab is operated by the Fermi Research Alliance under contract no. DE-AC02-07CH11359 with the U.S. Department of Energy.

Bibliography

[1] For examples from gauge-string duality and the AdS/CFT correspondence, see S. S. Gubser and A. Karch, Ann. Rev. Nucl. Part. Sci. **59,** 145 (2009); D. T. Son and A. O. Starinets, ibid. **57,** 95 (2007).

[2] For a review of on-shell methods for evaluating multiparton amplitudes, see C. F. Berger and D. Forde, Ann. Rev. Nucl. Part. Sci. **60,** 181 (2010). A comprehensive guide to one-loop calculations is given by R. K. Ellis, *et al.,* "One-loop calculations in quantum field theory: from Feynman diagrams to unitarity cuts," arXiv:1105.4319.

[3] The approach is outlined in C. E. DeTar, *et al.*, Phys. Rev. Lett. **26**, 675 (1971). An influential early application is R. D. Field and G. C. Fox, Nucl. Phys. **B80**, 367 (1974).

[4] For a pedagogical survey, see A. S. Kronfeld and C. Quigg, Am. J. Phys. **78**, 1081 (2010).

[5] This is illustrated for the light-hadron masses in S. Durr, *et al.*, Science **322**, 1224 (2008).

[6] T. Ishikawa, *et al.* [CP-PACS and JLQCD Collaborations], *Phys. Rev. D***78,** 011502 (2008)

[7] I developed these ideas further in C. Quigg, Rept. Prog. Phys. **70**, 1019 (2007).

[8] H. Feshbach, Ann. Phys. (N.Y.) **5,** 357 (1958).

[9] For examples, see E. Braaten and H. W. Hammer, Phys. Rept. **428**, 259 (2006).

[10] W. E. Caswell and G. P. Lepage, Phys. Lett. **167B,** 437 (1986); G. T. Bodwin, E. Braaten, and G. P. Lepage, Phys. Rev. D**51,** 1125 (1995). For an effective theory for quarkonium, see N. Brambilla, A. Pineda, J. Soto, and A. Vairo, Nucl. Phys. **B566,** 275 (2000).

[11] For a wide-ranging textbook treatment, see A. V. Manohar and M. B. Wise, *Heavy Quark Physics* (Cambridge University Press, Cambridge, 2000).

[12] See, for example, B. W. Lee, *Chiral Dynamics* (Gordon & Breach, New York, 1972).

[13] Among reviews see M. Diehl, Phys. Rept. **388,** 41 (2003); X. Ji, Ann. Rev. Nucl. Part. Sci. **54,** 413 (2004); A. V. Belitsky and A. V. Radyushkin, Phys. Rept. **418,** 1 (2005).

[14] For an overview, see J. C. Collins, *Foundations of Perturbative QCD* (Cambridge University Press, Cambridge, 2011).

[15] D. Boer, *et al.*, "Gluons and the quark sea at high energies: Distributions, polarization, tomography," A report on the joint BNL/INT/Jlab program on the science case for an Electron-Ion Collider arXiv:1108.1713.

[16] J. Bjorken, "The Parton Model: 2010," talk at the Rockefeller Spring Workshop on Electron-Nucleus Collider Physics, http://j.mp/q1fkVA.

[17] K. G. Wilson, "Some Experiments in Multiple Production," Cornell Report CLNS-131 (1970) [http://j.mp/nzNH4D].

[18] C. Quigg, "Learning to See at the Large Hadron Collider," arXiv:1001.2025; "Looking into Particle Production at the Large Hadron Collider," Nuovo Cim. **33C,** 327 (2011).

[19] V. W. Hughes and J. Kuti, Ann. Rev. Nucl. Part. Sci. **33**, 611 (1983).

[20] W. Melnitchouk and A. W. Thomas, Phys. Lett. **B377**, 11 (1996).

[21] R. L. Jaffe, Phys. Rev. **D15**, 267 (1977).

[22] A. Selem and F. Wilczek, "Hadron systematics and emergent diquarks," hep-ph/0602128.

[23] R. G. Edwards, *et al.*, "Excited state baryon spectroscopy from lattice QCD," arXiv:1104.5152.

[24] R. F. Dashen, E. E. Jenkins, and A. V. Manohar, Phys. Rev. **D49**, 4713 (1994).

[25] M. S. Bhagwat, I. C. Cloet, and C. D. Roberts, "Covariance, Dynamics and Symmetries, and Hadron Form Factors," arXiv:0710.2059. See also L. Chang and C. D. Roberts, "Hadron Physics: The Essence of Matter," arXiv:1003.5006.

[26] A. Manohar and H. Georgi, *Nucl. Phys.* **B234,** 189 (1984).

[27] P. Amaudruz, *et al.* [New Muon Collaboration], Phys. Rev. Lett. **66**, 2712 (1991). For reviews, see P. L. McGaughey, J. M. Moss, and J. C. Peng, Ann. Rev. Nucl. Part. Sci. **49,** 217 (1999); S. Kumano, Phys. Rept. **303,** 183 (1998).

[28] E. J. Eichten, I. Hinchliffe, and C. Quigg, Phys. Rev. **D45**, 2269 (1992).

[29] A. De Rujula, H. Georgi, and S. L. Glashow, Phys. Rev. **D12**, 147 (1975).

[30] Y. L. Dokshitzer, G. Marchesini, and B. R. Webber, Nucl. Phys. **B469**, 93 (1996); Y. L. Dokshitzer and B. R. Webber, Phys. Lett. **B404**, 321 (1997).

[31] P. A. Movilla Fernandez, *et al.*, Eur. Phys. J. **C22**, 1 (2001).

[32] P. Hoyer, "Introduction to QCD - a bound state perspective," arXiv:1106.1420.

[33] For evidence from lattice QCD, see M. Cheng, *et al.*, Phys. Rev. **D77**, 014511 (2008); A. Bazavov, *et al.* [HotQCD Collaboration], *ibid.* **80**, 014504 (2009).

[34] W. A. Bardeen, E. J. Eichten, and C. T. Hill, Phys. Rev. **D68**, 054024 (2003).

[35] For a snapshot, see the dark-matter talks at the 2011 conferences on Topics in Astroparticle and Underground Physics, http://taup2011.mpp.mpg.de.

[36] J. L. Feng and D. Sanford, JCAP **1105**, 018 (2011).

[37] A recent contribution is R. Babich, *et al.*, "Exploring strange nucleon form factors on the lattice," arXiv:1012.0562.

[38] J. Giedt, A. W. Thomas and R. D. Young, Phys. Rev. Lett. **103**, 201802 (2009); R. D. Young, AIP Conf. Proc. **1354**, 19 (2011); R. D. Young and A. W. Thomas, Phys. Rev. D**81**, 014503 (2010).

[39] Study of a Very Low Energy Neutrino Factory, http://j.mp/qk09Ik.

[40] R. D. Ball, D. A. Harris, and K. S. McFarland, "Flavor decomposition of nucleon structure at a neutrino factory," [hep-ph/0009223].

[41] S. Forte, "Polarized structure functions with neutrino beams," [hep-ph/0501020].

[42] J. D. Bjorken, "Energy Loss of Energetic Partons in Quark-Gluon Plasma: Possible Extinction of High-p_t Jets in Hadron-Hadron Collisions," http://j.mp/fHADsk.

[43] G. Aad, *et al.* [ATLAS Collaboration], Phys. Rev. Lett. **105**, 252303 (2010).

[44] S. Chatrchyan, *et al.* [CMS Collaboration], Phys. Rev. C**84,** 024906 (2011).

[45] T. Matsui and H. Satz, Phys. Lett. **B178**, 416 (1986).

[46] S. Chatrchyan, *et al.* [CMS Collaboration], Phys. Rev. Lett. **107**, 052302 (2011).

light mesons

Light Mesons

Light Mesons

Conveners

Paul	Eugenio	Florida State University (*Chair*)
Hartmut	Wittig	Universität Mainz
Alexander M.	Zaitsev	IHEP Protvino
Claude	Amsler	Universität Zürich
Yifang	Wang	IHEP Beijing
Suh-Urk	Chung	TU München/BNL

Session Chairs

Wolfgang	Ochs	MPI für Physik
Wolfgang	Dünnweber	LMU München
Dennis	Weygand	Jefferson Lab
Volker	Crede	Florida State University
Paul	Eugenio	Florida State University
Claude	Marchand	CEA IRFU/SPhN Saclay

Contents

Nature of the lightest scalar meson, its N_c behaviour and semi-local duality

Jose R. Pelaez[a], M.R. Pennington[b], J. Ruiz de Elvira[a], and D.J. Wilson[c]
[a]*Dept. de Física Teórica II, Facultad de Ciencias Físicas, Universidad Complutense de Madrid, E-28040, Madrid, Spain*
[b]*Theory Center, Thomas Jefferson National Accelerator Facility, 12000 Jefferson Av., Newport News, VA 23606, U.S.A*
[c]*Physics Division, Argonne National Laboratory, Argonne, Illinois 60439, U.S.A.*

One-loop unitarized Chiral Perturbation Theory (UChPT) calculations, suggest a different N_c behaviour for the σ or $f_0(600)$ and $\rho(770)$ mesons: while the ρ meson becomes narrower with N_c, as expected for a $\bar{q}q$ meson, the $f_0(600)$ contribution to the total cross section below 1 GeV becomes less and less important. Here we review our recent work [1] where we have shown, by means of finite energy sum rules, that a different N_c behaviour for these resonances may lead to a conflict with semi-local duality for large N_c, since local duality requires a cancellation between the $f_0(600)$ and $\rho(770)$ amplitudes. However, UChPT calculations also suggest a subdominant $\bar{q}q$ component for the $f_0(600)$ with a mass above 1 GeV and this can restore semi-local duality, as we show.

1 Introduction

QCD perturbative calculations are not applicable to the longstanding [2] controversy on the non-$\bar{q}q$ nature of light scalar mesons. However, the QCD $1/N_c$ expansion [3] allows for a clear identification of a $\bar{q}q$ resonance, since it becomes a bound state, whose width behaves O($1/N_c$), and its mass as O(1). In addition, in this low energy region one can use Chiral Perturbation Theory (ChPT) [4,5] to obtain a model independent description of the dynamics of pions, kaons and etas, which are the pseudo-Goldstone Bosons of the QCD spontaneous breaking of Chiral Symmetry. Lately, by combining the $1/N_c$ expansion of ChPT with dispersion theory, it has been possible to study the nature of light resonances thus generated in meson-meson scattering [7,8].

Let us recall that the ChPT Lagrangian is built as a low energy expansion respecting all QCD symmetries, and using only pseudo-Goldstone boson fields. The small masses of the three lightest quarks can be treated perturbatively and thus ChPT becomes a series in momenta and meson masses, generically $O(p^2/\Lambda^2)$. Apart from these masses and f_π —the pion decay constant, which sets the scale $\Lambda \equiv 4\pi f_\pi$ —there are no free parameters at leading order. The chiral expansion is renormalized order by order by absorbing loop divergences in the

coefficients of higher order counterterms, called low energy constants (LECs), whose values depend on the underlying QCD dynamics, and have to be determined from experiment. However, the leading $1/N_c$ dependence of the LECs is known and model independent [5], thus allowing us to study the N_c dependence of low energy hadronic observables.

1.1 Unitarization and dispersion theory

Unitarity implies that, for physical values of s, partial waves t^{IJ} of definite isospin I and angular momenta J for *elastic* meson-meson scattering satisfy:

$$\text{Im}\, t^{IJ} = \sigma |t^{IJ}|^2 \quad \Rightarrow \quad \text{Im}\frac{1}{t^{IJ}} = -\sigma \tag{1}$$

where $\sigma = 2p/\sqrt{s}$, and p is the CM momentum. Note that unitarity implies that $|t^{IJ}| \leqslant 1/\sigma$, and typically elastic resonances are characterized by the saturation of this bound. However, ChPT partial waves are a low energy expansion $t \simeq t_2 + t_4 + t_6 + \cdots$, (we will drop the IJ indices for simplicity.) where $t_{2k} \equiv O(p/(4\pi f_\pi))^{2k}$, and thus they cannot satisfy unitarity exactly, but just perturbatively, i.e: $\text{Im}\, t_2 = 0, \quad \text{Im}\, t_4 = \sigma t_2^2, \quad etc\,...$

The elastic Inverse Amplitude Method (IAM) [9,10] uses ChPT to evaluate the subtraction constants and the left cut of a dispersion relation for the inverse of the partial wave. The elastic right cut is calculated exactly with Eq.(1)—thus ensuring elastic unitarity. Note that the IAM is derived only from elastic unitarity, analyticity in the form of a dispersion relation, and ChPT, which is only used at low energies. Remarkably, the IAM can be rewritten as a simple algebraic formula in terms of ChPT amplitudes, but it satisfies exact elastic unitarity, at low energies recovers the chiral expansion up to the initially given order, and reproduces meson-meson scattering data up to energies ~ 1 GeV. This is done with values of the LECs which are fairly compatible with the values obtained within standard ChPT. Since it is derived from a dispersion relation, it can be analytically continued into the second Riemann sheet where, within the SU(2) ChPT formalism that we use here, we find the poles associated to the $\rho(770)$ and $f_0(600)$ resonances. Hence, we can study, without any *a priori* assumption, the nature of the $\rho(770)$ and $f_0(600)$ from first principles and QCD.

1.2 The $1/N_c$ expansion

For our purposes [1], the relevant observation is that the leading $1/N_c$ behaviour of the ChPT LECs is known. Thus, in order to obtain the leading N_c behaviour of the resonances generated with the IAM, we just have to rescale $f_\pi \to f_\pi\sqrt{N_c/3}$, the one-loop LECs as $l_i^r \to l_i^r N_c/3$ and the two loop ones as $r_i \to r_i (N_c/3)^2$.

This procedure [7] was first applied to the one-loop SU(3) ChPT amplitudes, and the result was that the light vector resonances, as for example the $\rho(770)$, followed the expected behaviour of $\bar{q}q$ states remarkably well, as we show in the left panel of Fig.1. In contrast,

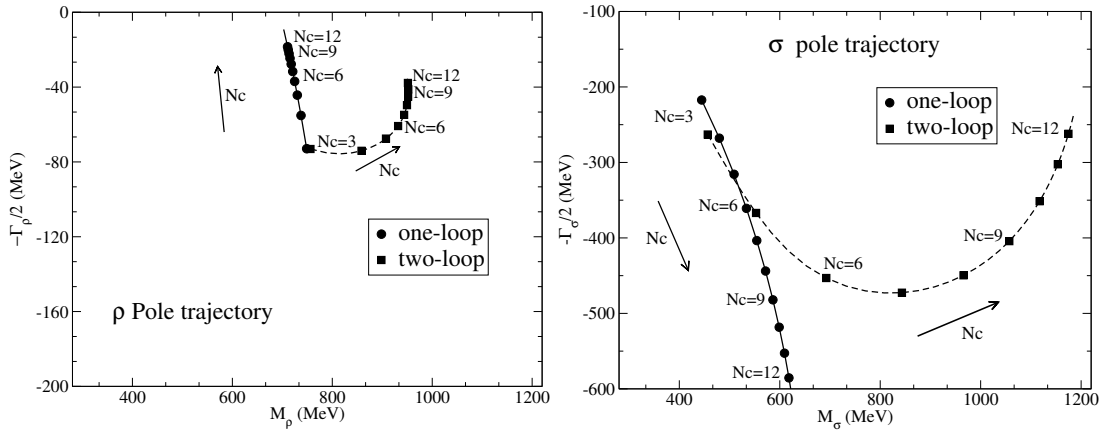

Figure 1: Left, the ρ meson behaves as a $\bar{q}q$ state. Center: At O(p^4) the σ does not. Right: At O(p^6) emerges a subleading $\bar{q}q$ component at 1.2 GeV

as seen on the right panel of Fig.1 the $f_0(600)$ behavior is at odds with that of $\bar{q}q$ states. It follows that the dominant component of the $f_0(600)$ (and the other members of the lightest scalar nonet) does not have a $\bar{q}q$ nature.

Of course, these results have some uncertainty, particularly on the renormalization scale where the N_c scale is to be applied, which was studied also in [7]. However, the general conclusions are rather robust: whereas vector mesons behave predominantly as a $\bar{q}q$, the scalar ones do not, at least for N_c not far from 3, which is where the IAM can be applied (not at $N_c \to \infty$, see [11])

The two-loop SU(2) ChPT amplitude analysis [8] showed that when the $\rho(770)$ is to follow its expected $\bar{q}q$ behaviour, the $f_0(600)$ still did not follow a $\bar{q}q$ behavior at first, and its pole moved away from the 400-600 MeV region of the real axis. However, for $N_c \sim 8$, the $f_0(600)$ started behaving as a $\bar{q}q$, see Fig. 1 (Right). In conclusion, the two-loop IAM confirms once again that the $f_0(600)$ does not behave predominantly as a $\bar{q}q$ state, but suggests the existence of a subdominant $\bar{q}q$ component that originates at a mass of $\simeq 1.2$ GeV, which is approximately twice that of the physical σ at $N_c = 3$. This seems to support models like [12] that have indeed suggested a non-$\bar{q}q$ nonet below 1 GeV and an additional $\bar{q}q$ one above.

2 Semi-local duality

A well known feature of the real world (N_c = 3) is that of "local duality". At low energies the scattering amplitude is well represented by a sum of resonances (with a background), but as the energy increases the resonances (having more phase space for decay) become wider and increasingly overlap. This overlap generates a smooth Regge behaviour described by a small number of crossed channel Regge exchanges. Indeed, detailed studies of meson-baryon scattering show that the sum of resonance contributions at all energies "averages" the

higher energy Regge behaviour. Thus, s-channel resonances are related to Regge exchanges in the t-channel and are "dual" to each other: one uses one or the other.

Regge exchanges are also built from $\bar{q}q$ and multi-quark contributions. However, in the isospin 2 $\pi\pi$ scattering channel there are no $\bar{q}q$ resonances, and so the Regge exchanges with these quantum number must involve multi-quark components. Data teach us that even at $N_c = 3$ these components are suppressed compared to the dominant $\bar{q}q$ exchanges. hence, semi-local duality means that in $\pi^+\pi^- \to \pi^-\pi^+$, which is an isospin 2 process, the low energy resonances must have contributions to the cross-section that "on the average" cancel. In particular, using the crossing relations the I=2 t-channel amplitude can be recast as a function of s-channel amplitudes:

$$\text{Im}\, A^{t2}(s,t) = \frac{1}{3}\text{Im}\, A^{s0}(s,t) - \frac{1}{2}\text{Im}\, A^{s1}(s,t) + \frac{1}{6}\text{Im}\, A^{s2}(s,t), \tag{2}$$

but since A^{s2} is repulsive and small, the strong cancellation occurs between A^{s0} and A^{s1}. However, these channels are saturated at low energies by the $f_0(600)$ and $\rho(770)$ resonances, respectively. Hence, semi-local duality requires the contribution of these two resonances to cancel "on average" in keeping with I = 2 exchange in the t-channel. This "on the average cancellation" is properly defined via Finite Energy Sum Rules:

$$F(t)_n^{21} = \frac{\int_{\nu_{th}}^{\nu_{\max}} d\nu\ \text{Im}\, A^{t2}(s,t)/\nu^n}{\int_{\nu_{th}}^{\nu_{\max}} d\nu\ \text{Im}\, A^{t1}(s,t)/\nu^n}, \quad \nu = (s-u)/2. \tag{3}$$

Semi-local duality between Regge and resonance contributions teaches us that on the "average" and at least over one resonance tower, we have:

$$\int_{\nu_{\text{th}}}^{\nu_{\max}} d\nu\ \nu^{-n}\text{Im}\, A^{t2}(s,t)_{\text{Data}} \sim \int_{\nu_{\text{th}}}^{\nu_{\max}} d\nu\ \nu^{-n}\text{Im}\, A^{t2}(s,t)_{\text{Regge}} \tag{4}$$

where Regge amplitudes are given as usual for $\alpha'\nu \gg 1$ by

$$\text{Im}A^{tI}(\nu,t) \simeq \sum_R \beta_R(t)\,[\alpha'\,\nu]^{\alpha_R(t)} \tag{5}$$

(see [1] for its low energy extrapolation), and where $\alpha_R(t)$ denote the Regge trajectories with the appropriate t-channel quantum numbers, $\beta_R(t)$ their Regge couplings and α' is the universal slope of the $q\bar{q}$ meson trajectories (~ 0.9 GeV^{-2}). For the $I = 0$ exchange the dominant trajectories are the Pomeron and the f_2 with intercepts close to 1 and 0.5 respectively, while the $I = 1$ ρ exchange is degenerate with the f_2. For the exotic $I = 2$ channel with its leading Regge exchange being a $\rho - \rho$ cut, we expect its intercept to be much smaller than that of the ρ, and its couplings to be correspondingly smaller. Therefore using Eqs.(4) and (5), local duality implies that $|F(t)_n^{21}| \ll 1$.

We can now use the IAM to check the N_c dependence of $\pi\pi$ scattering amplitudes. In particular the I=2 s-channel amplitude remains repulsive with N_c, and still there is no

ν_{max}	400 GeV^2	2.5 GeV^2	2 GeV^2	1 GeV^2
F_1^{21}	0.021 ± 0.016	0.180 ± 0.066	0.199 ± 0.089	-0.320 ± 0.007
F_2^{21}	0.057 ± 0.024	0.068 ± 0.024	0.063 ± 0.025	-0.115 ± 0.013
F_3^{21}	0.249 ± 0.021	0.257 ± 0.022	0.259 ± 0.022	0.221 ± 0.021

Table 1: Values of the ratio F_n^{21} using the KPY parametrization and different cutoffs. All F_n^{21} ratios for a 20 GeV cutoff turn out very small, of the order 1:50 or 1:15 . However, we see that they are only 1:4 or 1:5 when s_{max} is still $\sim$2 GeV^2

ν_{max}=1 GeV^2			
	KPY08	1 loop UChPT	2 loop UChPT
F_1^{21}	-0.350 ± 0.083	-0.355 ± 0.061	-0.351
F_2^{21}	-0.131 ± 0.042	-0.157 ± 0.097	-0.172
F_3^{21}	0.215 ± 0.027	0.175 ± 0.138	0.145

Table 2: Comparison between the F_n^{21} at $t = 4M_\pi^2$, using only S and P waves with a *cutoff* of 1 GeV^2, calculated with data parametrizations or our IAM amplitudes.

resonance exchange. Therefore semi-local duality implies that the t-channel $I = 2$ Regge exchange should continue to be suppressed as N_c increases. Since the Regge trajectories do not depend on N_c, still $|F(t)_n^{21}| \ll 1$ when increasing N_c due to a strong cancellation between the $\rho(770)$ and the $f_0(600)$ which would not occur if the $f_0(600)$ disappeared completely from the spectrum.

3 Results

Using the IAM we can study the behaviour of Eq. (3) with N_c [1], and then check if $|F(t)_n^{21}| \ll 1$ when increasing the number of colors. However, the IAM is only valid in the low energy region, and we have to check the influence of the high energy part on this cancellation. For this reason, in Table 1 we first calculate the value of the FESR for different *cutoffs* using the $\pi\pi$ KPY [15] data parametrization as input. We thus check that local duality is satisfied for N_c=3 since $|F(t)_n^{21}| \ll 1$, and at least for n=2,3, the main contribution to the FESR suppression occurs below 1 GeV, where we can apply the IAM. Therefore, we can use the IAM to study local duality, and check the FESR suppression with N_c. In evaluating the amplitudes ImA^{sI}, we represent these by a sum of s-channel partial waves, so that:

$$\text{Im}\, A^{sI}(s,t) = \sum_J (2J+1)\text{Im}\, t^{IJ}(s) P_J(\cos(\theta_s)). \tag{6}$$

However, using the IAM only S0, P and S2 waves can be described. It it is necessary to check the effect of those waves in Eq. (3). In Table 2 we show how the influence of higher waves is around 10%, and that the IAM predicts correctly the FESR suppression.

Let us now increase N_c: if the $\rho(770)$ mass remains constant and its width becomes narrower, but the $f_0(600)$ contribution to the total cross section below 1 GeV becomes less and less important, then the ratios $|F(t)_n^{21}|$ grow and there is a conflict with semi-local duality. This is shown in the thin lines of Figure 2 (Note the gray area above $N_c = 30$, where we consider the IAM merely qualitative). Note however, that this is a generic problem for any model where the $f_0(600)$ contribution vanishes, not just the IAM. However if there is a subdominant $\bar{q}q$ component for the $f_0(600)$ with a mass somewhat above 1 GeV, as occurs naturally within the two-loop IAM—but also in a part of the one-loop parameter space—this is enough to ensure the cancellation with the $\rho(770)$ contribution. The effect is shown by the thick lines of Figure 2.

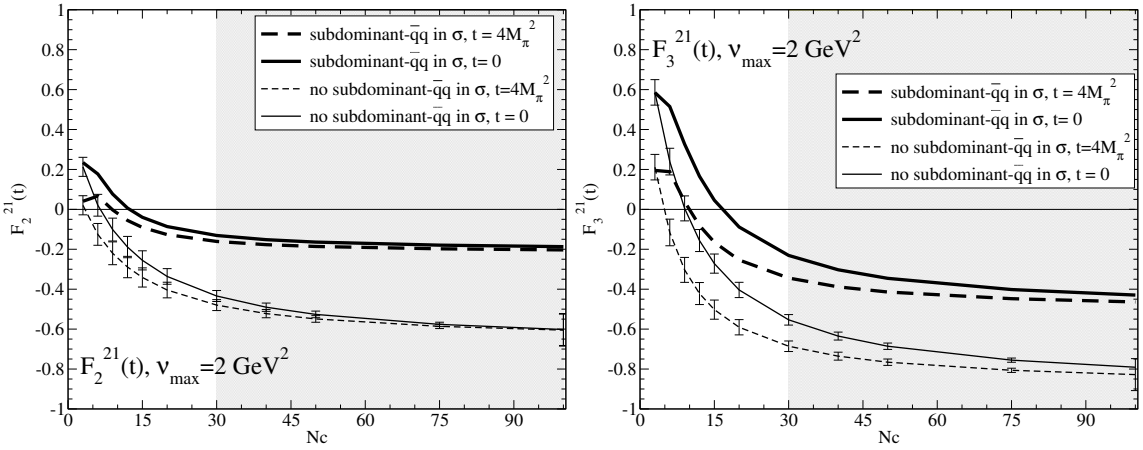

Figure 2: At O(p^4), solid line, there is no FESR suppression and local duality fails as N_c grows. However, at O(p^6), dashed line, the σ subleading $\bar{q}q$ component ensures local duality even when increasing N_c

4 Conclusions

The $1/N_c$ expansion of ChPT unitarized using the IAM shows that the $f_0(600)$ meson is not predominantly a $\bar{q}q$ state, since the σ amplitude becomes smaller and smaller below 1 GeV as N_c increases. This different behavior from that of a $q\bar{q}$ state as the $\rho(770)$, leads to a potential conflict with semi-local duality. However, unitarized ChPT calculations also suggest a subdominant $\bar{q}q$ state that emerges somewhat above 1 GeV. This subdominant component ensures that semi-local duality is still satisfied as N_c increases.

Acknowledgments

J.R.P. thanks the organicers of Hadron 2011 for support and for creating such a stimulating

conference. Work partially supported by Spanish Ministerio de Educación y Ciencia research contracts: FPA2007-29115-E, FPA2008-00592 and FIS2006-03438, U. Complutense/ Banco Santander grant PR34/07-15875-BSCH and UCM-BSCH GR58/08 910309. We acknowledge the support of the European Community-Research Infrastructure Integrating Activity "Study of Strongly Interacting Matter" (acronym HadronPhysics2, Grant Agreement n. 227431) under the Seventh Framework Programme of EU. This paper has in part been authored by Jefferson Science Associates, LLC under U.S. DOE contract No. DE-AC05-06OR23177 and supported by the U.S. DOE, Office of Nuclear Physics, Contract No. DE-AC02-06CH11357.

Bibliography

[1] J. Ruiz de Elvira, J. R. Pelaez, M. R. Pennington, D. J. Wilson, [arXiv:1009.6204 [hep-ph]].

[2] R. L. Jaffe, Phys. Rev. **D15**, 267 (1977).

[3] G. 't Hooft, *Nucl. Phys. B* **72**, 461 (1974). E. Witten, *Annals Phys.* **128**, 363 (1980).

[4] S. Weinberg, *Physica A* **96**, 327 (1979).

[5] J. Gasser and H. Leutwyler, *Annals Phys.* **158**, 142 (1984).

[6] Nucl. Phys. **B250**, 465 (1985).

[7] J. R. Pelaez, *Phys. Rev. Lett.* **92**, 102001 (2004). *Mod. Phys. Lett.* A **19**, 2879 (2004)

[8] J. R. Pelaez and G. Rios, *Phys. Rev. Lett.* **97**, 242002 (2006)

[9] T. N. Truong, *Phys. Rev. Lett.* **61**, 2526 (1988). A. Dobado, M. J. Herrero and T. N. Truong, *Phys. Lett. B* **235**, 134 (1990).

[10] A. Dobado and J. R. Pelaez, *Phys. Rev. D* **47**, 4883 (1993). *Phys. Rev. D* **56**, 3057 (1997).

[11] J. R. Pelaez, J. Nebreda, G. Rios, Prog. Theor. Phys. Suppl. **186**, 113-123 (2010).

[12] E. van Beveren, T. A. Rijken, K. Metzger, C. Dullemond, G. Rupp and J. E. Ribeiro, *Z. Phys. C* **30**, 615 (1986). E. van Beveren and G. Rupp, *Eur. Phys. J. C* **22**, 493 (2001). J. A. Oller, E. Oset and J. R. Pelaez, *Phys. Rev. D* **59**, 074001 (1999). [Erratum-ibid. D **60**, 099906 (1999 ERRAT,D75,099903.2007)]. F. E. Close and N. A. Tornqvist, *J. Phys. G* **28**, R249 (2002).

[13] C. Amsler *et al.* (Particle Data Group), Phys. Lett. **B667**, 1 (2008).

[14] A. Donnachie and P. V. Landshoff, Nucl. Phys. B **267**, 690 (1986).

[15] R. Kaminski, J. R. Pelaez and F. J. Yndurain, *Phys. Rev. D* **77**, 054015 (2008).

Central Meson Production in ALICE

Rainer Schicker on behalf of the ALICE Collaboration
Phys. Inst.
Philosophenweg 12
D-69120 Heidelberg, GERMANY

The ALICE experiment at the Large Hadron Collider (LHC) at CERN consists of a central barrel, a muon spectrometer and of additional detectors for trigger and event classification purposes. The low transverse momentum threshold of the central barrel gives ALICE a unique opportunity to study the low mass sector of central production at the LHC. I will report on first analysis results of meson production in double gap events in proton-proton collisions at $\sqrt{s}$ = 7 TeV and in PbPb collisions at $\sqrt{s_{NN}}$ = 2.76 TeV.

1 Introduction

The ALICE experiment consists of a central barrel and of a forward muon spectrometer [1]. Additional detectors for trigger purposes and for event classification exist outside of the central barrel. Such a geometry allows the investigation of many topics of diffractive reactions at hadron colliders, for example the measurement of single and double diffractive dissociation cross sections and the study of central diffraction. The ALICE physics program foresees data taking in pp and PbPb collisions at nominal luminosities $\mathcal{L} = 5 \times 10^{30} cm^{-2} s^{-1}$ and $\mathcal{L} = 10^{27} cm^{-2} s^{-1}$, respectively. An asymmetric system pPb will be measured soon with a first test expected this year.

2 The ALICE Experiment

In the ALICE central barrel, momentum reconstruction and particle identification are achieved in the pseudorapidity range $-1.4 < \eta < 1.4$ combining the information from the Inner Tracking System (ITS) and the Time Projection Chamber (TPC). In the pseudorapidity range $-0.9 < \eta < 0.9$, the information from the Transition Radiation Detector (TRD) and the Time of Flight (TOF) system is in addition available. A muon spectrometer covers the range $-4.0 < \eta < -2.5$. At very forward angles, the energy flow is measured by Zero Degree Calorimeters (ZDC) [2]. Detectors for event classification and trigger purposes are located on both sides of the ALICE central barrel. First, the scintillator arrays V0A and V0C cover the pseudorapidity range $2.8 < \eta < 5.1$ and $-3.7 < \eta < -1.7$, respectively. The four- and eightfold segmentation in pseudorapidity and azimuth result in 32 individual

counters in each array. Second, a Forward Multiplicity Detector (FMD) based on silicon strip technology covers the pseudorapidity range $1.7 < \eta < 5.1$ and $-3.4 < \eta < -1.7$, respectively. Third, two arrays of Cherenkov radiators T0A and T0C deliver accurate timing for measuring the time of collisions. Figure 1 shows the pseudorapidity coverage of these detector systems.

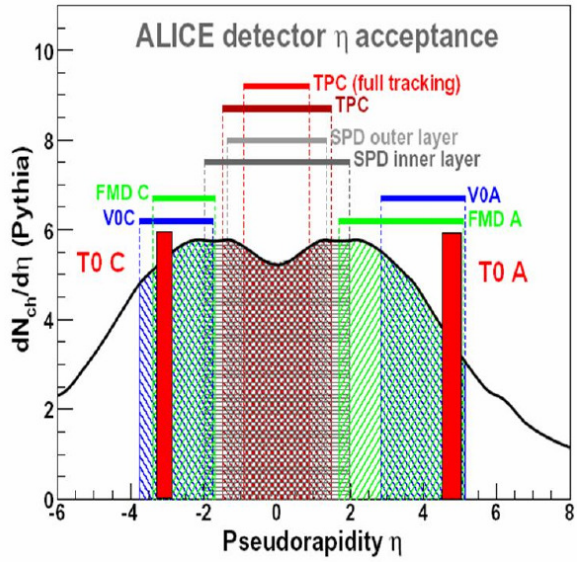

Figure 1: Pseudorapidity coverage of the ALICE detectors.

3 Central diffraction in ALICE

Central diffractive events are experimentally defined by activity in the central barrel and by no activity outside the central barrel. This condition can be implemented in the trigger at level zero (L0) by defining barrel activity as hits in the ITS pixel detector, or the TOF system. The gap condition is realized by the absence of V0 signals, hence a gap of two units on either barrel side can be defined at L0. In the offline analysis, the information from the V0, T0, FMD, SPD and TPC detectors define the gaps spanning the range $0.9 < \eta < 5.1$ and $-3.7 < \eta < -0.9$. Events with and without detector signals in these two ranges are defined to be no-gap and double gap events, respectively.

A rapidity gap can be due either to Pomeron, Reggeon or photon exchange. A double gap signature can therefore be induced by a combination of these exchanges. Pomeron-Pomeron events result in centrally produced states with quantum numbers C = +1 (C = C-parity) and I = 0 (I = isospin). The corresponding quantum numbers in photon-Pomeron induced events are C = -1 and I = 0 or I = 1 [3].

4 Central meson production in pp-collisions

In the years 2010-2011, ALICE recorded zero bias and mimimum bias data in pp-collisions at a center-of-mass energy of $\sqrt{s} = 7$ TeV. The zero bias trigger was defined by beam bunches crossing at the ALICE interaction point, while the minimum bias trigger was derived by minimum activity in either the ITS pixel or the V0 detector. Events with double gap topology as described above are contained in this minimum bias trigger, hence central diffractive events were analyzed from the minimum bias data sample.

For the results presented below, a sample of 3.5×10^8 minimum bias events was analyzed. First, the fraction of events satisfying the gap condition described above was calculated. This fraction was found to be about 2×10^{-4}. Only runs where this fraction was calculated to be within 3 σ of the average value of the corresponding distribution were further analyzed. This procedure resulted in about 7×10^4 double gap events. As a next step, the track multiplicity in the pseudorapidity range $-0.9 < \eta < 0.9$ was evaluated .

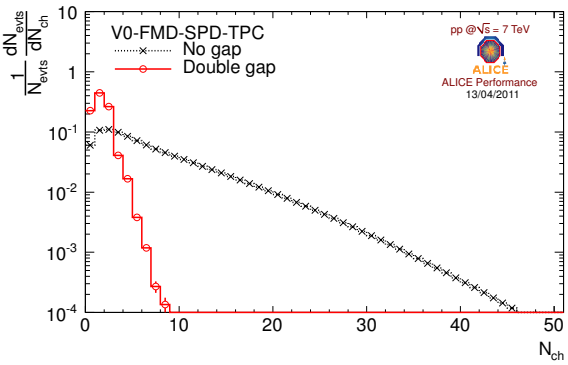

Figure 2: Track multiplicity within pseudorapidity range -0.9 < η < 0.9 for no-gap and double gap events.

Figure 2 shows the track multiplicity in the pseudorapidity range $-0.9 < \eta < 0.9$ for double and no-gap events. Very low transverse momentum tracks never reach the TPC which results in events with track multiplicity zero. The multiplicity distributions of the double and no-gap events clearly show different behaviors as demonstrated in Figure 2.

The specific energy loss dE/dx as measured by the TPC in combination with the TOF detector information identifies pions with transverse momenta $p_T \geqslant 300$ MeV/c. The events with exactly two pions are selected, and the invariant mass of the pion pairs is shown in Figure 3. These pion pairs can be of like or unlike sign charge. Like sign pion pairs can arise from two pion pair production with loss of one pion of same charge in each pair, either due to the low p_T cutoff described above, or due to the finite pseudorapidity coverage of the detectors used for defining the rapidity gap. For charge symmetric detector acceptances, the unlike sign pairs contain the signal plus background, whereas the like

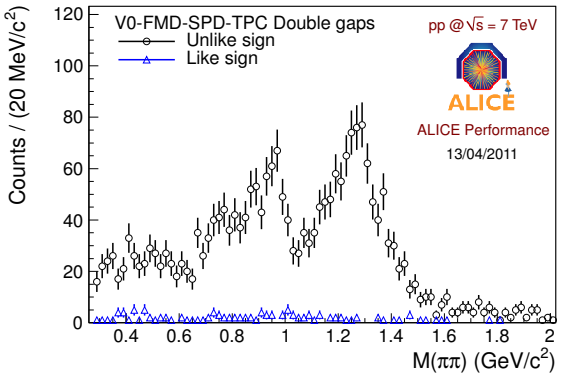

Figure 3: Invariant mass distribution of like and unlike sign pion pairs.

sign pairs represent the background. From the two distributions shown in Figure 3, the background is estimated to be less than 5%.

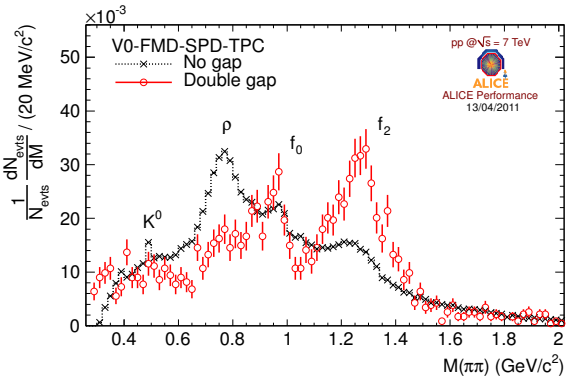

Figure 4: Pion pair invariant mass distribution for double and for no-gap events.

Figure 4 displays the normalized background corrected pion pair mass for double and no-gap events. The particle identification by the TOF detector requires the single track transverse momentum p_T to be larger than about 300 MeV/c. This single track p_T cut introduces a significant acceptance reduction for pair masses $M(\pi\pi) \leqslant 0.8\ GeV/c^2$ at low pair p_T. The distributions shown are not acceptance corrected. In the no-gap events, structures are seen from K^0_s and ρ^0-decays. Two additional structures are associated with $f_0(980)$ and $f_2(1270)$ decays. In the double gap distribution, the K^0_s and ρ^0 are highly suppressed while the $f_0(980)$ and $f_2(1270)$ with quantum numbers $J^{PC} = (0, 2)^{++}$ are much enhanced. This enhancement of $J^{PC} = J^{++}$ states is evidence that the double gap condition used for analysing the minimum bias data sample selects events dominated by double Pomeron exchange.

5 Central meson production in PbPb-collisions

Diffractive and electromagnetic processes in PbPb-collisions show a variety of intriguing features [4, 5]. First, photoabsorption can lead to giant dipole resonance excitation with subsequent neutron decay. In such decays, the charge to mass ratio is modified. In addition, bound-free pair production also leads to a modified charge to mass ratio of one or both of the nuclei involved. Both processes contribute to the beam life time. Second, photon-photon processes result in electromagnetic production of pseudoscalars π^0, η, η' and of pairs of bosons $\pi^+\pi^-, K^+K^-$ and fermions $e^+e^-, \mu^+\mu^-, \tau^+\tau^-$. Third, photon-Pomeron processes can, for example, result in diffractive photoproduction of vector mesons $\rho^0, \phi, J/\Psi, \Upsilon$.

The first heavy ion run at the LHC took place in Nov-Dec 2010. In this period, about 12×10^6 minimum bias PbPb-collisions were recorded with the ALICE detectors. In addition to the minimum bias trigger, data were taken with two dedicated triggers for investigating meson production in the ALICE central barrel. First, a trigger OM2 based on number of TOF hits $\geqslant 2$ was running. Second, a trigger CCUP2 defined by the logic combination: (TOF hits $\geqslant 2$) AND (ITS pixel) AND (double gap condition) was defined.

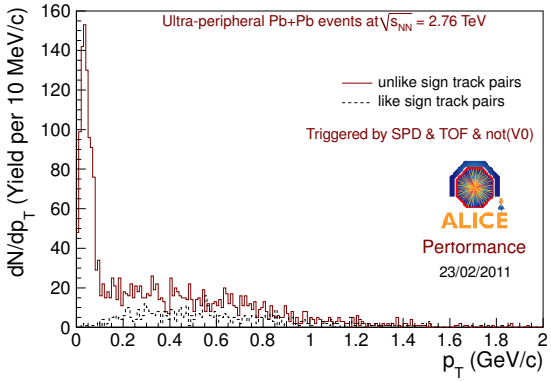

Figure 5: Transverse momentum of unlike and like sign CCUP2 triggered pairs in PbPb-collisions at $\sqrt{s_{NN}}$ = 2.76 TeV.

The OM2 and CCUP2 triggered events with exactly two tracks in the central barrel were selected, and the pair transverse momentum was calculated. Both of these triggers result in similar pair p_T distributions. The pair p_T of CCUP2 triggered events is shown in Figure 5 for like and unlike sign pairs. The unlike sign distribution clearly shows a strong peak at $p_T \leqslant 100$ MeV/c consistent with coherent production off a Pb nucleus.

Figure 6 shows the invariant mass for the unlike sign CCUP2 triggered pairs with pair $p_T \leqslant 150$ MeV/c. This distribution is not corrected for finite detector acceptance and for detector resolution. The shape of the distribution shown in Figure 6 is consistent with production of the ρ^0-meson with $J^{PC} = 1^{--}$. As for the p_T-distribution, the OM2 and CCUP2 triggers result in similar pair invariant mass distributions. Hence these results indicate that

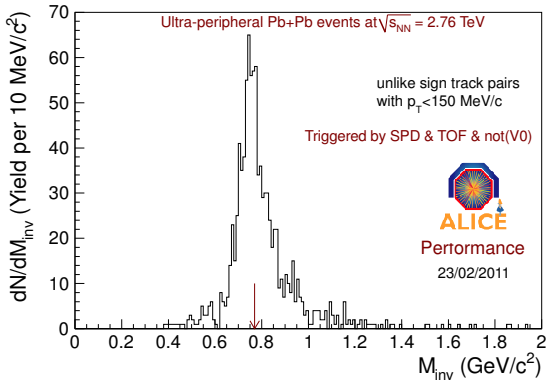

Figure 6: Invariant mass of unlike sign pairs with $p_T \leqslant 150$ MeV/c for CCUP2 triggered pairs in PbPb collisions at $\sqrt{s_{NN}}$ = 2.76 TeV.

double gap events in PbPb collisions are not dominated by Pomeron-Pomeron events as is the case in proton-proton collisions.

6 Conclusions and Outlook

First analysis results show that central meson production in double gap events at LHC energies is consistent with the hypothesis of Pomeron-Pomeron and photon-Pomeron exchange in pp and PbPb-collisions, respectively. The next step in the study of these events will be a quantitative analysis of the results.

Acknowledgments

This work is supported in part by German BMBF under project 06HD197D and by WP8 of the hadron physics program of the 7^{th} EU program period.

Bibliography

[1] K. Aamodt *et al.*, ALICE Collaboration, JINST **3** (2008) S08002

[2] R. Arnaldi *et al.*, Nucl. Instr. and Meth. A **564** (2006) 235

[3] O. Nachtmann, Annals of Physics, **209** (1991) 436, and references therein

[4] G. Baur *et al.*, Phys. Rep. **364** (2002) 359

[5] A.J. Baltz *et al.*, Phys. Rep. **458** (2008) 1

Glueballs from gluon jets at the LHC

Wolfgang Ochs[a] and Peter Minkowski[b]
[a]*Max-Planck-Institut für Physik, D-80805 Munich, GERMANY*
[b]*University of Bern, CH - 3012 Bern, SWITZERLAND*

The existence of glueballs within QCD is uncontroversial but their experimental verification is still in doubt. We discuss the new possibilities for a search of glueballs as the leading object in gluon jets at the LHC. We summarize previous results from LEP which demonstrate a significant excess rate of electrically neutral leading clusters in comparison with MC models.

1 QCD expectations and search for glueballs

According to an early prediction of QCD the self-interacting gluons are able to bind themselves and to give rise to a new spectroscopy of gluonic matter or glueballs; specific scenarios for glueball phenomenology go back to 1975 [1], for recent reviews, see [2]. Today, quantitative predictions are derived from lattice QCD and from QCD sum rules. The lightest glueball is found to be a scalar with $J^{PC} = 0^{++}$ and a mass of 1.0-1.7 GeV.

There have been considerable efforts to identify glueballs experimentally. The aim is at first to establish the lightest $q\bar{q}$ nonets in the spectrum; then, the appearence of extra states could hint towards a glueball. More directly, one looks for an enhanced production of a glueball candidate in "gluon rich" processes but a suppression in $\gamma\gamma$ reactions [2].

Studies of production and decay of resonances along these lines have led to various scenarios for classification of the lightest scalar states

$$f_0(600),\ f_0(980),\ f_0(1370),\ f_0(1500),\ f_0(1710).$$

According to one approach (e.g. [3]), the glueball could be mixed into the three states above 1 GeV together with two members of the $q\bar{q}$ nonet. Alternatively, the glueball could be related to the broad $f_0(600)$ (e.g. [4,5]). A problem in constructing multiplets is the status of $f_0(1370)$ which is not seen in phase shift analyses of $\pi^+\pi^- \to \pi^+\pi^-, \pi^0\pi^0$ [6].

The production of resonances has been studied in a number of gluon-rich processes: "central production" $pp \to p\ gb\ p$ by double Pomeron exchange, $J/\psi \to \gamma\ gb$, $p\overline{p} \to \pi\ gb$, $B \to K\ gb$ (through $b \to sg$) and, finally, forward fragmentation of a gluon into glueballs.

Only in the last reaction involving a high energy gluon jet the gluon can be identified as a source, in the other processes the overall energy is low of Ø (few GeV) and the role of gluons

is not obvious anymore. An interesting result on central production has been presented at this conference by ALICE at LHC [7]: in the double gap events the isoscalar states $f_0(980)$ and $f_2(1270)$ are enhanced in comparison to no-gap events. The enhanced production of the well known $q\bar{q}$ state $f_2(1270)$ demonstrates that the double Pomeron mechanism does not enhance exclusively glueballs. We also note that the Pomeron structure has been investigated at HERA [8]. Present results suggest a dominant fracton ($\sim 70\%$) of momentum to be carried by gluons, but the ratio $G(x)/S(x)$ of gluon over singlet quark densities at large momentum fractions $x \sim 1$ varies between $G/S \sim 0$ for ZEUS data according to [9] and $G/S \sim 1-2$ for H1. Then, the production of $q\bar{q}$ states in double Pomeron scattering could be a reflection of the sizable quark valence component of the Pomeron.

2 Leading particle systems in gluon jets

According to the well known concept of quark fragmentation the leading particles at large Feynman x are those which carry the initial quark of the jet as a valence quark

$$q \to \text{Meson}\ (q\bar{q}') + X,$$

for example, leading particles in a u-quark jet are a $\pi^+(u\bar{d})$ or a $\pi^0(\{u\bar{u} + d\bar{d}\}/\sqrt{2})$ with half strength, whereas $\pi^-(d\bar{u})$ is suppressed at large x. In analogy, one can consider the fragmentation of a gluon and suppose that the leading particle in the jet is the one with a gluonic valence component

$$g \to \text{Meson}\ (gg) + X.$$

Models of this kind with leading glueballs, but also with leading isoscalars like η, η', ω at large x have been suggested already long ago [10], for x-distributions, see also [11].

Studies of gluon jets at LEP did not establish a clear support of the model for isoscalar $q\bar{q}$ mesons [12]. While the L3 collaboration found for the jet of lowest momentum in $e^+e^- \to 3$ jets a considerable enhancement of η production by factor 2-3 beyond MC calculations for $x_p > 0.06$, where $x_p = p/p_{beam}$, ALEPH later reported agreement between data and revised MC versions (similarly also for η', but with low statistics). OPAL found an excess η rate over MC's at the higher momenta but did not separate quark and gluon jets in this range. No other isoscalar particles have been studied separately for quark and gluon jets.

The distributions of charge and mass of the leading cluster Q_{lead} and M_{lead} in gluon jets beyond a rapidity gap reflect the colour neutralisation mechanism [13]. In particular, the "color octet neutralisation" is a precondition for glueball production. In that case, two gluons, if separated beyond the confinement radius R_c, will create two other gluons to form colour neutral sub-systems. Alternatively, colour triplet neutralisation is possible with creation of two $q\bar{q}$ pairs, or both mechanisms with probablilities P_8 and P_3. For large rapidity gaps one expects the charge distribution to approach a limiting behaviour with charge $Q_{lead} = 0$ with P_8 and charges $Q_{lead} = 0, \pm 1$ with P_3,

		p_T	x_T	g in di-jet	q in γ+ jet
TEVATRON	1.8 TeV	50	0.056	60%	75 %
LHC	7 TeV	200	0.057	60%	80 %
		50	0.014	75%	90 %
		800	0.229	25%	75%

Table 1: Rates for gluon and quark jets at TEVATRON [15] and LHC [16].

Results from LEP on leading clusters have been obtained from OPAL, DELPHI and ALEPH [14]. All experiments agree upon a significantly enhanced rate for neutral clusters ($Q_{lead} = 0$) beyond a rapidity gap in gluon jets by 10-40% as compared to the JETSET MC, depending on the selection and purity of the jets. On the other hand, the corresponding distributions for quark jets or for gluon jets without gap agree well with MC's. In addition, DELPHI and OPAL find the excess of gluon jets with $Q_{lead} = 0$ with typically lower masses $M_{lead} \lesssim 2.5$ GeV. A natural explanation would be a leading gluonic system or glueball.

3 Proposal for LHC studies of gluonic systems

Studies of leading particle systems can be performed at the LHC with some advantages. Most importantly, gluon jets can be selected with higher energies in comparison to LEP and they are more copiously produced with good statistics. It is possible to compare quark and gluon jets with similar energies from different processes.
1. leading order processes to be calculated from $pdf's$ and parton-parton cross sections:
Quark jets can be obtained from final states $pp \to \gamma + jet + X$ with subprocess $qg \to \gamma q$ dominating at the lower p_T. Gluon jets are found among di-jet events, also at low p_T. Examples are presented in Tab. 1.
A good purity of quark jets can be obtained in this way, but gluon jets with their steeper fragmentation need higher purity to reduce background.
2. gluon bremsstrahlung:
Using a trigger on total transverse energy one selects 3-jet events. Similar to the case at $e^+e^- \to 3\ jets$ the lowest momentum jet is most likely a gluon jet from QCD bremsstrahlung (qqg, qgg or ggg). The fraction of gluon jets can be derived within the DGLAP approximation for low k_T. For example, at small x_g one finds, given the ratio of gluon to quark production rate $R_g = \sigma_g/\sigma_q$ the fraction $F_g(x_g) = \frac{1}{1+4x_g/(8+18R_g)}$ which yields for $R_g = 1$, as example,

$$F_g \approx 95\% \text{ at } x_g = 0.2, \qquad F_g \approx 85\% \text{ at } x_g = 0.5.$$

Studies at LHC could be useful in two directions:
1. Leading clusters with larger rapidity gaps.
The new possibilities at LHC follow from the gluon jet energies larger by an order of magnitude as compareed to LEP (typically < 25 GeV). This allows for a better separation

of the leading cluster. The rapidity gaps could extend up to $\Delta y \sim 4$ (add $\ln 10 \approx 2.3$ to $\Delta y \approx 1.7$). With increasing rapidity gaps the leading charges should be closer to their asymptotic distribution with values $Q = 0, \pm 1$ allowing for a better estimate of probabilities P_3 and P_8.
2. Direct study of resonances in mass distributions.
The spectra of the invariant mass of leading particles beyond the gap are generally found quite smooth. There is some evidence in gluon jets for $f_0(980)$ in the $\pi\pi$ (DELPHI [14]) and for $f_0(1500)$ in the 4π spectrum (OPAL [14]). The rapidity gap cuts affect the angular decay distribution of the cluster and could reduce the resonance signal. This is avoided if the mass spectra are constructed first and then their x distribution is studied. Such resonance x spectra have not yet been determined for quark and gluon jets separately.

The distinguishing feature for identifying a glueball is its x distribution in comparison with the reference spectrum of a well defined $q\bar{q}$ resonance (examples $\rho,\ f_2(1270),\ \phi(1020)$) of comparable mass in the quark and gluon jet resp. The glueball should be "suppressed" in a quark jet and should be "leading" in a gluon jet, i.e. above a $q\bar{q}$ reference resonance, according to the following scheme (for scalar f_0's):

meson	quark jet	gluon jet	
		triplet neutr.	octet neutr.
$q\bar{q} : f_0\ [ref : \rho, f_2, \phi \ldots]$	leading	suppressed	suppressed
$gb : f_0\ [ref : \rho, f_2 \ldots]$	suppressed	suppressed	leading
$q\bar{q} : f_0$, strongly mixed	leading	suppressed	leading (?)
$4q : f_0(600)/\sigma, f_0(980)$ (?)	suppressed	suppressed	suppressed

Table 2: Identifying glueballs through reference spectra in quark and gluon jets.

The last line in the table relies on the validity of particular models, here we refer to the quark counting approach [17]. To the extent, that the x-distribution of $f_0(980)$ almost coincides with the one of $f_2(1270)$ [18], there is no evidence for structure beyond $q\bar{q}$ of $f_0(980)$.

In principle, also mixed $gb - q\bar{q}$ states could be recognized by comparing with the appropriate superposition of two reference distributions. Gluonic components could appear in the spectra of $(\pi\pi)^0$ ($f_0(600)/"\sigma",\ f_0(980),\ f_0(1500)$), of $(4\pi)^0$ (($f_0(1370)(?),\ f_0(1500)$) and $(K\overline{K})^0$, ($f_0(980),\ f_0(1500),\ f_0(1710)$).

4 Summary

1. The existence of glueballs is predicted since long, the clear evidence is still missing.

2. Lesson from LEP: evidence for a new fragmentation component:
excess of neutral clusters by up to 40% beyond expectation from MC's.
Gluon jets may not be built up from quark strings only.

3. There is a new chance of finding glueballs in gluon jets at LHC:
excess of neutral leading clusters with increasing gap size;
resonance x-spectra in quark and gluon jets in comparison with reference spectra.

Bibliography

[1] H. Fritzsch, P. Minkowski, Nuovo Cim. **A30** (1975) 393.

[2] E. Klempt, A. Zaitsev, Phys. Rept. **454** (2007) 1;
V. Crede, C. A. Meyer, Prog. Part. Nucl. Phys. **63** (2009) 74.

[3] C. Amsler, F. E. Close, Phys. Lett. **B353** (1995) 385.

[4] P. Minkowski, W. Ochs, Eur. Phys. J. **C9** (1999) 283.

[5] S. Narison, Nucl. Phys. B 509 (1998) 312.

[6] W. Ochs, AIP Conf. Proc. **1257** (2010) 252.

[7] R. Schicker [ALICE Collaboration], this conference.

[8] S. Chekanov *et al.* [ZEUS Collaboration], Nucl. Phys. **B713** (2005) 3;
A. Aktas *et al.* [H1 Collaboration], Eur. Phys. J. **C48** (2006) 715.

[9] C. Royon *et al.*, Nucl. Phys. **B781** (2007) 1.

[10] P. Roy, T. F. Walsh, Phys. Lett. **B78** (1978) 62;
C. Peterson, T. F. Walsh, Phys. Lett. **B91** (1980) 455.

[11] P. Roy, K. Sridhar, JHEP **9907** (1999) 013;
H. Spiesberger, P. M. Zerwas, Phys. Lett. **B481** (2000) 236.

[12] M. Acciarri *et al.* [L3 Collaboration], Phys. Lett. **B371** (1996) 126;
R. Barate *et al.* [ALEPH Collaboration], Eur. Phys. J. **C16** (2000) 613;
G. Abbiendi *et al.* [OPAL Collaboration], Eur. Phys. J. **C17** (2000) 373.

[13] P. Minkowski, W. Ochs, Phys. Lett. **B485** (2000) 139.

[14] G. Abbiendi *et al.* [OPAL Collaboration], Eur. Phys. J. **C35** (2004) 293.
J. Abdallah *et al.* [DELPHI Collaboration], Phys. Lett. **B643** (2006) 147.
S. Schael *et al.* [ALEPH Collaboration], Eur. Phys. J. **C48** (2006) 685.

[15] D. E. Acosta *et al.* [CDF Collaboration], Phys. Rev. Lett. **94** (2005) 171802.

[16] J. Gallicchio, M. D. Schwartz, [arXiv:1104.1175 [hep-ph]].

[17] S. J. Brodsky, G. R. Farrar, Phys. Rev. Lett. **31** (1973) 1153.

[18] K. Ackerstaff *et al.* [OPAL Collaboration], Eur. Phys. J. **C4** (1998) 19.

Structure of scalar mesons and the Higgs sector of strong interaction

Martin Schumacher[1]
Zweites Physikalisches Institut
der Universität Göttingen
D-37077 Göttingen, Germany

The σ meson may be considered as the Higgs boson of strong interaction. While the observation of the electroweak Higgs boson is the primary goal in ongoing experiments at the LHC, the σ meson is by now well studied both as an on-shell particle and as a virtual particle while being part of the constituent quark. This makes it timely to give an overview of the present status of the Higgs sector of strong interaction which includes the scalar mesons $\sigma(600)$, $\kappa(800)$, $f_0(980)$ and $a_0(980)$ together with the pseudo Goldstone bosons π, K and η.

1 Introduction

Scalar mesons below 1 GeV together with the pseudo Goldstone bosons π, K and η may be considered as the Higgs sector of strong interaction. While the EW Higgs boson up to now appears to escape experimental observation in the ongoing LHC experiments [1] the strong counterpart, the σ meson is by now well studied both as on-shell particle and as a virtual particle while being part of the constituent quark. The latter observation has been facilitated through Compton scattering by the proton in an experiment carried out at MAMI (Mainz) published in 2001 [2, 3]. In this experiment it has been shown that the scalar t-channel makes a strong contribution to the Compton scattering amplitude, being successfully represented in terms of a t-channel pole located at m_σ^2 where m_σ is the bare mass of the σ meson, determined in this experiment to be $\sim$ 600 MeV. Inspite of this great success the physical interpretation of the experiment remained uncertain because an explicit σ meson is a strongly unwanted particle in chiral perturbation theory. This led to an unnecessary delay, because a detailed theoretical investigation was required extending until 2010, when it was shown that the t-channel pole at m_σ^2 is a well founded concept and that the related t-channel amplitude may be understood as being due to Compton scattering by the σ meson while being part of the constituent quark [4]. The findings in [4] were extended to include the whole scalar nonet below 1 GeV in [5]. The present work is in part based on this latter publication where more details may be found.

[1] mschuma3@gwdg.de

2 The doorway model and the structure of scalar mesons

The scalar nonet below 1 GeV cannot be understood in terms of flavor structures as provided by $SU(3)_f$ [6] because of the ordering of the meson masses. This problem was solved by introducing tetraquarks $(q\overline{q})^2$ [6]. The tetraquark model implies the possibility of a dissociation of the kind $(q\overline{q})^2 \rightleftarrows (q\overline{q} + q\overline{q})$, leading to $q\overline{q}$ as a small structure component. In [5] this small $q\overline{q}$ structure component was interpreted in terms of a doorway state which serves as the entrance channel in a two-photon fusion reaction and is in agreement with the experimental two-photon widths of the mesons:

$$\sigma(600): \quad \gamma\gamma \to \frac{u\overline{u} + d\overline{d}}{\sqrt{2}} \to u\overline{u}d\overline{d} \to \pi\pi, \tag{1}$$

$$f_0(980): \quad \gamma\gamma \to \frac{1}{\sqrt{2}}\left(\frac{u\overline{u} + d\overline{d}}{\sqrt{2}} - s\overline{s}\right) \to \frac{s\overline{s}(u\overline{u} + d\overline{d})}{\sqrt{2}} \to \pi\pi, K\overline{K}, \tag{2}$$

$$a_0(980): \quad \gamma\gamma \to \frac{1}{\sqrt{2}}\left(\frac{-u\overline{u} + d\overline{d}}{\sqrt{2}} + s\overline{s}\right) \to \frac{s\overline{s}(u\overline{u} - d\overline{d})}{\sqrt{2}} \to \eta\pi, K\overline{K}. \tag{3}$$

The $q\overline{q}$ configuration of the $a_0(980)$ meson violates isospin conservation. This is of no problem because we consider the $q\overline{q}$ configuration only as a small structure component.

In t-channel nucleon Compton scattering the reaction chain

$$\gamma\gamma \to \{\sigma(600), f_0(980), a_0(980)\} \to N\overline{N} \tag{4}$$

is considered where the excitation of the $N\overline{N}$ pair is virtual. This leads to the consequence that the masses of the scalar mesons entering into (4) are the bare masses, i.e. the masses for the case of zero particle decay width. The validity of this concept has been shown in [7] where quantitative predictions of electromagnetic polarizabilities of the nucleon led to excellent agreement with experimental data.

3 Mass prediction for scalar mesons in terms of spontaneous, dynamical and explicit symmetry breaking

In case of pseudoscalar and scalar mesons the following phenomena contribute to the generation of the masses of the mesons:
(i) The $U(1)_A$ anomaly,
(ii) spontaneous or dynamical symmetry breaking,
(iii) explicit symmetry breaking leading to non-zero current-quark masses.
The $U(1)_A$ anomaly is a gluonic (instanton [8]) effect which works on $SU(3)_f$ flavor states which are completely symmetric in the chiral limit. For pseudoscalar and scalar mesons this is only the case for the η_0 flavor state and has the consequence that η_0 has a mass

in the chiral limit whereas all the other pseudoscalar mesons are massless. These latter pseudoscalar mesons form the octet of Goldstone bosons as depicted in the left panels of Figures 1 and 2. The left panel of Figure 1 shows the mexican-hat potential where the

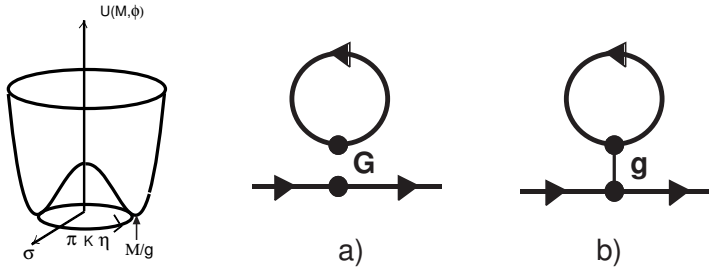

Figure 1: Left panel: Spontaneous symmetry breaking in the chiral limit (cl) illustrated by the LσM: In the $SU(2)$ sector there is one "strong Higgs boson", the σ meson having a mass of $m_\sigma^{\rm cl} = 652$ MeV taking part in spontaneous symmetry breaking, accompanied by an isotriplet of massless π mesons serving as Goldstone bosons. In the $SU(3)$ sector there are 8 massless Goldstone bosons π, K, η, and nine scalar mesons σ, κ, f_0 and a_0, all of them having the same mass as the σ meson in the chiral limit. The mass degeneracy is removed by explicit symmetry breaking. Right panel: Tadpole graphs of dynamical symmetry breaking. a) Four fermion version of the Nambu-Jona–Lasinio (NJL) model, b) bosonized NJL model.

Goldstone bosons correspond to the minimum of the potential. The mexican-hat potential describes spontaneous symmetry breaking in terms of a mass parameter μ and a self-coupling parameter λ. Since these parameters are unknown no quantitative prediction of the masses of the constituent quark and of the scalar mesons is possible. This is different in the quark-level linear σ model (QLLσM) where the graphs shown in Figure 1 a) and b) are taken into account. In this way the Delbourgo-Scadron relation [9]

$$M = g\, f_0 \tag{5}$$

is obtained with $g = 2\pi/\sqrt{3}$ being the σ-quark coupling constant and $f_0 = 89.8$ MeV the pion decay constant in the chiral limit. Eq. (5) leads to $m^{\rm cl} = 2M = 652$ MeV as given in the caption of Figure 2. Explicit symmetry breaking is described by generalizing the mass formula valid for the σ meson

$$m_\sigma^2 = \frac{16\pi^2}{3} f_\pi^2 + m_\pi^2 \tag{6}$$

by taking into account the larger fraction of strange quarks in the $\kappa(800)$ and the $(f_0(980), a_0(980))$ mesons in their tetraquark structures. This leads to

$$m_\kappa^2 = \frac{16\pi^2}{3}\frac{1}{2}(f_\pi^2 + f_K^2) + \frac{1}{2}(m_\pi^2 + m_K^2) \tag{7}$$

$$m_{a_0,f_0}^2 = \frac{16\pi^2}{3} f_K^2 + m_\eta^2 \tag{8}$$

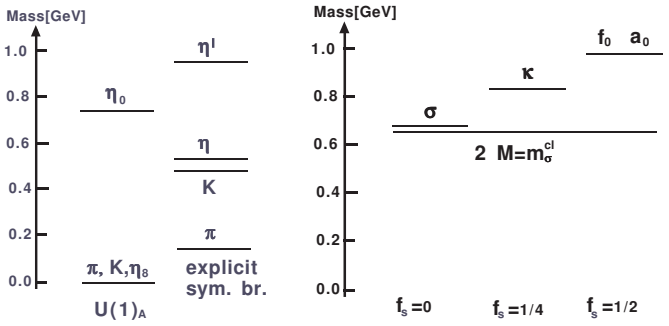

Figure 2: Left panel: Pseudoscalar mesons after U(1)$_A$ symmetry breaking (left column) and after additional explicit symmetry breaking (right column). Right panel: Masses of the members of the scalar nonet. In the chiral limit all the scalar mesons have the same mass amounting to $2M = m_\sigma^{\rm cl} = 652$ MeV, where M is the mass of the constituent quark in the chiral limit and $m_\sigma^{\rm cl}$ the mass of the σ mesons in the chiral limit (cl). Explicit symmetry breaking shifts the masses upward with the fraction f_s of strange quarks in the tetraquark structure being the parameter determining the size of the shift.

where $f_\pi = 92.42 \pm 0.26$ MeV and $f_K = 113.0 \pm 1.0$ MeV. The masses predicted in this way are $m_\sigma = 685$ MeV, $m_\kappa = 834$ MeV and $m_{a_0,f_0} = 986$ MeV in close agreement with the experimental data.

Bibliography

[1] Markus Schumacher, for the ATLAS collaboration, arXiv:1106.2496 [hep-ex].
[2] G. Galler, et al., Phys. Lett. B 501 (2011) 245.
[3] S. Wolf, et al., Eur. Phys. J. A 12 (2001) 231.
[4] Martin Schumacher, Eur. Phys. J. C 67 (2010) 283, arXiv:1001.0500 [hep-ph]
[5] Martin Schumacher, J. Phys. G: Nucl. Part. Phys. 38 (2011) 083001, arXiv:1106.1015 [hep-ph].
[6] R.L. Jaffe, K. Johnson, Phys. Lett. B 60 (1976) 201, R.J. Jaffe, Phys. Rev. D 15 (1977) 267, *ibid.* 281, *ibid.* 17 (1978) 1444.
[7] Martin Schumacher, Nucl. Phys. A 826 (2009) 131, arXiv:0905.4363 [hep-ph].
[8] G. 't Hooft, Phys. Rep. 142 (1986) 357.
[9] R. Delbourgo, M.D. Scadron, Mod. Phys. Lett. A 10 (1995) 251, arXiv:hep-ph/9910242; Int. J. Mod. Phys. A 13 (1998) 657, arXiv:hep-ph/9807504.

Chiral unitary theory of scalar mesons in a finite volume

Eulogio Oset[a], M. Döring[b], U.-G. Meißner[b,c], and A. Rusetsky[b]
[a]*Departamento de Física Teórica and IFIC, Centro Mixto Universidad de Valencia-CSIC, Institutos de Investigación de Paterna, Aptdo. 22085, 46071 Valencia, Spain*
[b]*Helmholtz-Institut für Strahlen- und Kernphysik (Theorie) and Bethe Center for Theoretical Physics, Universität Bonn, Nußallee 14-16, D-53115 Bonn, Germany*
[c]*JCHP, IAS-4, IKP-3, Forschungszentrum Jülich, D-52425 Jülich, Germany*

We develop a scheme for the extraction of the properties of the scalar mesons $f_0(600)$, $f_0(980)$, and $a_0(980)$ from lattice QCD data. This scheme is based on a two-channel chiral unitary approach with fully relativistic propagators in a finite volume. In order to discuss the feasibility of finding the mass and width of the scalar resonances, we analyze synthetic lattice data with a fixed error assigned, and show that the framework can be indeed used for an accurate determination of resonance pole positions in the multi-channel scattering.

1 Introduction

We present a method to calculate energy levels for $\pi\pi$ and $K\overline{K}$ in a finite volume using for this purpose the chiral unitary approach that produces the $f_0(600)$, $f_0(980)$, and $a_0(980)$ resonances as dynamically generated in the continuum. After this we face the inverse problem: assuming that the levels obtained in the finite box are lattice data we determine the phase shifts in the continuum and extract the resonance properties [1].

2 The formalism

In the chiral unitary approach we obtain the T-matrix for the $\pi\pi$ and $K\overline{K}$ coupled channels by means of the Bethe Salpeter equation

$$T = [1 - VG]^{-1}V \tag{1}$$

where V is the 2x2 matrix of the transition potential and G, a diagonal matrix is the loop function of the two meson propagators

$$G_j = \int^{|\vec{q}|<q_{\max}} \frac{d^3\vec{q}}{(2\pi)^3} \frac{1}{2\omega_1(\vec{q})\,\omega_2(\vec{q})} \frac{\omega_1(\vec{q})+\omega_2(\vec{q})}{E^2-(\omega_1(\vec{q})+\omega_2(\vec{q}))^2+i\epsilon},$$

$$\omega_{1,2}(\vec{q}) = \sqrt{m_{1,2}^2+\vec{q}^2}\,. \tag{2}$$

In a box of length L the energy levels are given by the poles of the T matrix of eq. (1) substituting G by $\tilde{G}$ given by

$$\tilde{G}_j = \frac{1}{L^3} \sum_{\vec{q}}^{|\vec{q}|<q_{\max}} \frac{1}{2\omega_1(\vec{q})\,\omega_2(\vec{q})} \frac{\omega_1(\vec{q})+\omega_2(\vec{q})}{E^2-(\omega_1(\vec{q})+\omega_2(\vec{q}))^2},$$

$$\vec{q} = \frac{2\pi}{L}\vec{n}, \quad \vec{n}\in\mathbb{Z}^3\,. \tag{3}$$

As we can see, all we have done is to replace the integral by a discrete sum over the free eigenvalues of the box given by the periodic boundary conditions.

In one channel, the poles of T in the box are obtained when

$$V^{-1}(E)-\tilde{G}(E)=0\,. \tag{4}$$

Then the T matrix in the continuum for the energies eigenvalues of the box can be obtained by means of

$$T(E)=\Big(V^{-1}(E)-G(E)\Big)^{-1}=\big(\tilde{G}(E)-G(E)\big)^{-1}\,. \tag{5}$$

By changing the value of L one can achieve that different energies appear as eigenvalues of the box and then obtain the T matrix in the continuum for any desired energy, via eq. (5). As shown in [1] this equation is nothing else than Lüscher's formula [2]. However, for smaller values of L, differences emerge which are due to the presence of the relativistic propagators in the loops (see Ref. [1] for a detailed discussion on this issue).

The main purpose of [1] was to extend the idea of Lüscher to two channels, following the lines of [3]. For this purpose we propose several methods in [1], but we will outline only one here, which is practical and at reach by present lattice calculations.

Let us assume that we have the lattice data of fig. 1, which have been obtained from the chiral unitary approach in the finite box, and we want to obtain the $\pi\pi$ and $K\overline{K}$ phase shifts in the continuum from these data. For this purpose we take the levels 2 and 3 of Fig. 1 and a few energies from them, associating an error of 10 MeV to these energies. Then we

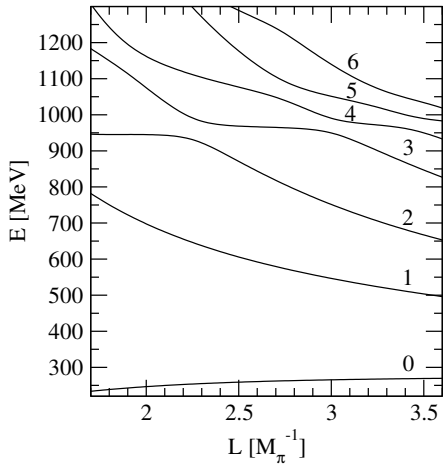

Figure 1: Energy levels as functions of the cubic box size L, derived from the chiral unitary approach of Ref. [4] and using $\tilde{G}$ from Eq. (3).

make a fit to these data assuming that we have a potential, suggested by the chiral unitary approach, of the type

$$V_{ij} = a_{ij} + b_{ij}(s - 4M_K^2)\,. \tag{6}$$

The levels in the box with two channels are obtained from the poles of the T matrix which come from the condition that the determinant of $(1 - VG)$ is zero,

$$\det(\mathbb{1} - V\tilde{G}) = 1 - V_{11}\tilde{G}_1 - V_{22}\tilde{G}_2 + (V_{11}V_{22} - V_{12}^2)\tilde{G}_1\tilde{G}_2 = 0\,. \tag{7}$$

As one can see in fig. 2, the method shows that one can reconstruct the phase shifts in the continuum with an acceptable accuracy and from there the $f_0(980)$ resonance. The same can be done for the $a_0(980)$ and the $f_0(600)$. As lessons that one draws from the work we can say that the two channel method is necessary for the description of the $f_0(980)$ and $a_0(980)$ resonances, the analysis with only the $\pi\pi$ channel leading to inaccurate results and incorrect conclusions. Another lesson learned is that the flattening of a level in the box as a funtion of L is not a guarantee that this energy corresponds to a resonance. The flattening can occur around the threshold of a new channel without it corresponding to a resonance in the continuum. The method developed in [1] should be very helpful in the analysis of future lattice data for groups looking for hadron spectra from lattice QCD [5].

Bibliography

[1] M. Döring, U. -G. Meißner, E. Oset, A. Rusetsky, [arXiv:1107.3988 [hep-lat]].

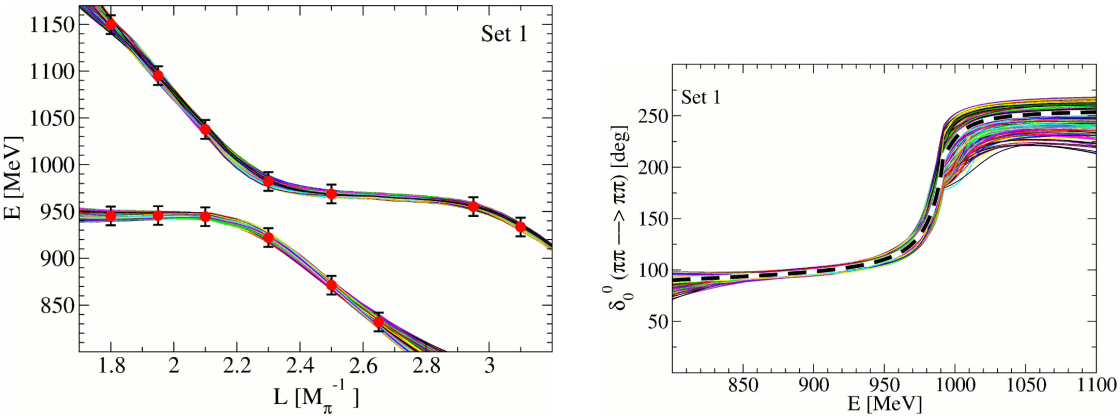

Figure 2: Left: Generated data points (10 MeV error, 13 points) with periodic b.c.; Fits that fulfill the $\chi^2_{\rm best}+1$ criterion are also shown (bands). Right: Extracted phase shifts corresponding to the set shown in the figure to the left. Dashed line: The calculated phase shifts by using the approach of Ref. [4]; Bands: Reconstruction of these phase shift.

[2] M. Lüscher, Commun. Math. Phys. **105** (1986) 153 (1986).

[3] V. Bernard, M. Lage, U.-G. Meißner and A. Rusetsky, JHEP **1101** (2011) 019.

[4] J. A. Oller, E. Oset, Nucl. Phys. **A620**, 438-456 (1997).

[5] Y. Nakahara, M. Asakawa, T. Hatsuda, Phys. Rev. **D60** (1999) 091503; K. Sasaki, S. Sasaki and T. Hatsuda, Phys. Lett. B **623** (2005) 208; N. Mathur, A. Alexandru, Y. Chen *et al.*, Phys. Rev. **D76** (2007) 114505; S. Basak, R. G. Edwards, G. T. Fleming *et al.*, Phys. Rev. **D76** (2007) 074504; J. Bulava, R. G. Edwards, E. Engelson *et al.*, Phys. Rev. **D82** (2010) 014507; C. Morningstar, A. Bell, J. Bulava *et al.*, AIP Conf. Proc. **1257** (2010) 779; J. Foley, J. Bulava, K. J. Juge *et al.*, AIP Conf. Proc. **1257** (2010) 789; M. G. Alford and R. L. Jaffe, Nucl. Phys. B **578** (2000) 367; T. Kunihiro, S. Muroya, A. Nakamura, C. Nonaka, M. Sekiguchi and H. Wada [SCALAR Collaboration], Phys. Rev. D **70** (2004) 034504; H. Suganuma, K. Tsumura, N. Ishii and F. Okiharu, PoS **LAT2005** (2006) 070; Prog. Theor. Phys. Suppl. **168** (2007) 168; C. McNeile and C. Michael [UKQCD Collaboration], Phys. Rev. D **74** (2006) 014508; A. Hart, C. McNeile, C. Michael and J. Pickavance [UKQCD Collaboration], Phys. Rev. D **74** (2006) 114504; H. Wada, T. Kunihiro, S. Muroya, A. Nakamura, C. Nonaka and M. Sekiguchi, Phys. Lett. B **652** (2007) 250; S. Prelovsek, C. Dawson, T. Izubuchi, K. Orginos and A. Soni, Phys. Rev. D **70** (2004) 094503; S. Prelovsek, T. Draper, C. B. Lang, M. Limmer, K. F. Liu, N. Mathur and D. Mohler, arXiv:1002.0193 [hep-ph].

Pion Elastic Form Factor in a Rather Broad Range of Momentum Transfers from Local-Duality QCD Sum Rule

Dmitri Melikhov[1,a,b,c], Irina Balakireva[c], and Wolfgang Lucha[a]
[a]*HEPHY, Austrian Academy of Sciences, Nikolsdorfergasse 18, A-1050 Vienna, Austria*
[b]*Faculty of Physics, University of Vienna, Boltzmanngasse 5, A-1090 Vienna, Austria*
[c]*SINP, Moscow State University, 119991 Moscow, Russia*

Revisiting the relevance of local duality for the pion elastic form factor gives rise to optimism.

Recently, several analyses of the pion form factor $F_\pi(Q^2)$ at momentum transfer Q^2 around $Q^2 \approx 4 - 50\,\mathrm{GeV}^2$ have appeared [1] which claim that $F_\pi(Q^2)$ remains much larger than the pQCD result even at $Q^2 \approx 50\,\mathrm{GeV}^2$ (see Fig. 1a). These studies obtain a much larger $F_\pi(Q^2)$ than our result from the local-duality sum rule [2]. They imply that the LD limit is strongly violated even at rather large Q^2. QCD sum rules utilizing nonlocal condensates [3] arrive at more moderate claims but also observe a large local-duality violation at $Q^2 = 10 - 20\,\mathrm{GeV}^2$. A careful inspection reveals that all these analyses involve explicit or implicit assumptions. Consequently, in a recent study [4] we scrutinized the LD model and its accuracy, by taking advantage of the case of quantum mechanics: there hadronic features, such as form factors, may be found independently of the sum-rule method by solving the Schrödinger equation.

1 Local-Duality Sum Rules

Local-duality (LD) sum rules [6] are nothing but dispersive N-point sum rules in the limit of infinitely large Borel-mass parameter $\widetilde{M}$, that is, for $\tau \equiv 1/\widetilde{M}^2 \to 0$. In this limit, all power corrections vanish. The *assumption* of *quark–hadron duality* claims that, above some effective continuum threshold s_{eff}, the contributions of excited and continuum states at hadron level are dual to the high-energy region of the perturbative diagrams arising from QCD. Under this assumption, in the chiral limit the LD sum rules of interest for the present analysis read

$$f_\pi^2 = \int_0^{\bar{s}_{\mathrm{eff}}} ds\, \rho_{\mathrm{pert}}(s)\,, \qquad F_\pi(Q^2)\, f_\pi^2 = \int_0^{s_{\mathrm{eff}}(Q)} \int_0^{s_{\mathrm{eff}}(Q)} ds_1\, ds_2\, \Delta_{\mathrm{pert}}(s_1, s_2, Q)\,. \tag{1}$$

The spectral densities $\rho_{\mathrm{pert}}(s)$ and $\Delta_{\mathrm{pert}}(s_1, s_2, Q)$ are given by QCD perturbation theory [7]. All details of nonperturbative dynamics are encoded in the effective continuum thresholds $\bar{s}_{\mathrm{eff}}$ and $s_{\mathrm{eff}}(Q)$. Fixing these, pion decay constant f_π and form factor $F_\pi(Q^2)$ can be derived.

[1] dmitri_melikhov@gmx.de

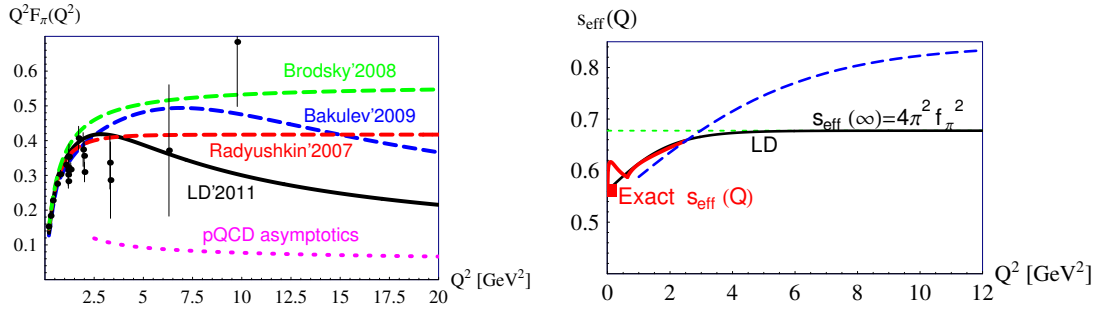

(a) (b)

Figure 1: Dependence of both pion elastic form factor $F_\pi(Q^2)$ (a) and effective continuum threshold $s_{\rm eff}(Q)$ (b) on the momentum transfer Q. In (b) the red line is the exact threshold $s_{\rm eff}(Q)$ as reconstructed from experimental $F_\pi(Q^2 \leqslant 2.5\ {\rm GeV}^2)$ data [5], the blue refers to a sum-rule study using nonlocal condensates [3], the black is our LD model (2) for $s_{\rm eff}(Q)$.

One should be aware that any effective continuum threshold is different from the physical continuum threshold: the latter is a constant determined by the masses of the lowest-lying hadronic excitations whereas the effective continuum threshold is just an ingredient of the sum-rule method related to a specific implementation of quark–hadron duality. Therefore, effective thresholds are not constant but depend on the external kinematic variables [8,9].

Taking into account the properties of the perturbative 2- and 3-point spectral functions, one may formulate an approximate *LD model for the effective threshold* $s_{\rm eff}(Q)$: our model is based on some smooth interpolation between the behaviour of $s_{\rm eff}(Q)$ for $Q \to 0$, determined by a Ward identity, and for $Q \to \infty$, determined by factorization properties of $\Delta_{\rm pert}(s_1, s_2, Q)$. Remembering the well-measured pion elastic form factor in the region near $Q^2 \approx 2.5\ {\rm GeV}^2$, we propose [4], in terms of the strong coupling constant $\alpha_s(Q^2)$, the simple parametrization

$$s_{\rm eff}(Q) = \frac{4\pi^2 f_\pi^2}{1+\alpha_s(0)/\pi}\left[1+\tanh\left(\frac{Q^2}{Q_0^2}\right)\frac{\alpha_s(0)}{\pi}\right], \qquad Q_0^2 = 2.02\ {\rm GeV}^2\ . \tag{2}$$

For small Q^2, following [2] we assume a freezing of $\alpha_s(Q^2)$. Note that $s_{\rm eff}(Q)$ approaches its LD limit, viz., $s_{\rm eff} = 4\pi^2 f_\pi^2$, already in the region $Q^2 > 4-5\ {\rm GeV}^2$ (Fig. 1b). Accordingly, the only essential nonperturbative input for the LD model (2) is the pion decay constant f_π.

Figure 1a depicts the corresponding prediction for the pion elastic form factor $F_\pi(Q^2)$. Our LD model provides a perfect description of all the available experimental data in the region $Q^2 = 1-2.5\ {\rm GeV}^2$. For $Q^2 \geqslant 3-4\ {\rm GeV}^2$, the LD model reproduces well all the data except for the single point $Q^2 = 10\ {\rm GeV}^2$; there our prediction is off the actual experimental value (which, in any case, is affected by a rather large error) by roughly two standard deviations. Interestingly enough, in the range $Q^2 \geqslant 3-4\ {\rm GeV}^2$ the LD model yields significantly lower predictions than the findings of the different theoretical approaches presented in Refs. [1,3].

A closer inspection of Fig. 1 easily reveals that it is virtually impossible to construct models compatible with all experimental findings in $Q^2 = 2.5 - 10\ \text{GeV}^2$: those approaches that hit the data at $Q^2 = 10\ \text{GeV}^2$ overestimate the data points of better quality at $Q^2 \approx 2 - 4\ \text{GeV}^2$.

By construction, the LD model (2) is but an approximate model which involves too few free parameters to be able to take into account some subtle details of the confinement dynamics. Nevertheless, we would like to estimate the uncertainties of hadron-parameter predictions we might expect for the momentum-transfer range $Q^2 \geqslant 3 - 4\ \text{GeV}^2$. The obvious place to study this and to get an idea of the order of magnitude of the errors is quantum mechanics: there solving Schrödinger's equation numerically [10] gives the exact bound-state features.

2 Local-Duality Effective-Threshold Model in Quantum Mechanics

The main ingredient that constrains the formulation of our LD model (2) is the factorization of hard form factors. Consequently, this model may be tested in quantum mechanics (QM) for potentials containing both Coulomb and confining interactions. For definiteness, we [4] consider a set of power-law confining potentials: $V_{\text{conf}}(r) \propto r^n$, $n = 2, 1, \frac{1}{2}$. We adopt model parameters suitable for hadron physics and fix the strengths of all our $V_{\text{conf}}(r)$ such that for each of them the Schrödinger equation yields the *same value* $\psi(0)$ of the configuration-space bound-state wave function $\psi(r)$ at the origin and hence the same QM LD threshold model.

We identified an important *universal* behaviour, which does not depend on the details of the confining interaction: the accuracy of the LD model for both effective continuum threshold and elastic form factor increases with Q in the range $Q \geqslant 2$ GeV. Accordingly, we may infer that, if in the region $Q^2 \approx 4 - 8\ \text{GeV}^2$ the LD setup provides a satisfactory description of the experimental data, the accuracy of our predictions will not be worse for larger values of Q^2.

3 Summary, Conclusions, and Outlook

We investigated the pion elastic form factor $F_\pi(Q^2)$ by means of an LD model, which can be formulated in any theory where hard exclusive amplitudes satisfy a factorization theorem (in essence, any theory where the interactions behave Coulomb-like at small distances and confining at large distances). Figure 1 and our QM studies lead us to our main conclusions:

1. For $Q^2 \leqslant 4\ \text{GeV}^2$, our exact effective threshold $s_{\text{eff}}(Q)$ exhibits a rapid variation with Q. This observation implies that the accuracy of the LD model for these momentum transfers depends on subtle details of the confining interactions and cannot be predicted in advance.

2. For $Q^2 \geqslant 4\ \text{GeV}^2$, irrespective of any details of the underlying confining interactions, the *maximum* deviations of the LD-model predictions from the exact elastic form factor occur in the range $Q^2 \approx 4 - 8\ \text{GeV}^2$. For Q^2 beyond this interval, our LD model's accuracy increases very fast. Our QM toy model with power-law potentials shows that, for arbitrary confining interactions, our LD model entails rather accurate numerical results for $Q^2 \geqslant 20 - 30\ \text{GeV}^2$.

3. Very precise data [5] on $F_\pi(Q^2)$ indicate that the LD limit $s_{\rm eff}(\infty) = 4\pi^2 f_\pi^2$ of the effective threshold is reached already at comparatively low values $Q^2 = 5 - 6$ GeV^2; therefore, large deviations from the LD limit at $Q^2 = 20 - 50$ GeV^2, as obtained in [1], appear to us unlikely. Moreover, we expect the pion form factor at $Q^2 = 10 - 20$ GeV^2 to be considerably lower than the prediction of an approach based on a sum rule involving nonlocal condensates [3].

Our analysis is not meant to constitute a proof of but rather to provide an argument for the *accuracy* of the LD model in QCD and the expected behaviour of the pion elastic form factor at large Q^2. Thus, the accurate measurement of F_π in the region $Q^2 = 4 - 10$ GeV^2 will have important implications for the behaviour of F_π at larger Q^2, up to asymptotically large Q^2.

Acknowledgments

DM is supported by the Austrian Science Fund (FWF), project no. P22843.

Bibliography

[1] H. R. Grigoryan and A. V. Radyushkin, Phys. Rev. D **76**, 115007 (2007); Phys. Rev. D **78**, 115008 (2008); S. J. Brodsky and G. F. de Téramond, Phys. Rev. D **77**, 056007 (2008); M. Bel̆ička *et al.*, Phys. Rev. C **83**, 028201 (2011).

[2] V. Braguta, W. Lucha, and D. Melikhov, Phys. Lett. B **661**, 354 (2008).

[3] A. P. Bakulev, A. V. Pimikov, and N. G. Stefanis, Phys. Rev. D **79**, 093010 (2009).

[4] I. Balakireva, W. Lucha, and D. Melikhov, arXiv:1103.3781 [hep-ph].

[5] C. J. Bebek *et al.*, Phys. Rev. D **17**, 1693 (1978); T. Horn *et al.*, Phys. Rev. Lett. **97**, 192001 (2006); V. Tadevosyan *et al.*, Phys. Rev. C **75**, 055205 (2007); G. M. Huber *et al.*, Phys. Rev. C **78**, 045203 (2008).

[6] A. V. Radyushkin, Acta Phys. Polon. B **26**, 2067 (1995).

[7] D. Melikhov, Phys. Rev. D **53**, 2460 (1996); Eur. Phys. J. direct **C2**, 1 (2002); V. Anisovich, D. Melikhov, and V. Nikonov, Phys. Rev. D **52**, 5295 (1995); Phys. Rev. D **55**, 2918 (1997).

[8] W. Lucha, D. Melikhov, and S. Simula, Phys. Rev. D **76**, 036002 (2007); Phys. Lett. B **657**, 148 (2007); Phys. Atom. Nucl. **71**, 1461 (2008); Phys. Lett. B **671**, 445 (2009); arXiv:1107.1848 [hep-ph]; D. Melikhov, Phys. Lett. B **671**, 450 (2009); W. Lucha and D. Melikhov, Phys. Rev. D **73**, 054009 (2006); Phys. Atom. Nucl. **70**, 891 (2007).

[9] W. Lucha, D. Melikhov, H. Sazdjian, and S. Simula, Phys. Rev. D **80**, 114028 (2009); W. Lucha, D. Melikhov, and S. Simula, Phys. Rev. D **79**, 096011 (2009); J. Phys. G **37**, 035003 (2010); Phys. Lett. B **687**, 48 (2010); Phys. Atom. Nucl. **73**, 1770 (2010); J. Phys. G **38**, 105002 (2011); Phys. Lett. B **701**, 82 (2011); in *QCD@Work2010*, eds. L. Angelini *et al.*, AIP Conf. Proc. **1317** (AIP, Melville, New York, 2010), p. 316, arXiv:1008.0167 [hep-ph]; arXiv:1108.0844 [hep-ph].

[10] W. Lucha and F. F. Schöberl, Int. J. Mod. Phys. C **10**, 607 (1999).

Calculation of the pion electromagnetic form factor from lattice QCD

Bastian B. Brandt[1,a], Andreas Jüttner[b], Hartmut Wittig[a,c]
[a]*Institut für Kernphysik, University of Mainz, Becher-Weg 45, D-55099*
[b]*CERN, Physics Department, TH Unit, CH-1211 Geneva 23*
[c]*Helmholtz Institute Mainz, University of Mainz, D-55099 Mainz*

We present a lattice calculation of the vector form factor of the pion for two flavours of non-perturbatively $O(a)$ improved Wilson fermions. For the measurements we utilise the CLS ensembles which include various lattice spacings and pion masses down to about 250 MeV. To obtain a fine momentum resolution near zero momentum transfer (q^2) partially twisted boundary conditions are employed using several twist angles. Due to the fine resolution around $q^2 = 0$ we are able to determine the slope of the form factor and, in turn, extract the charge radius of the pion without any model dependence. The results for the form factor and the charge radius are then compared to chiral perturbation theory and phenomenological models which are used to extrapolate the results to the physical point.

Over the last years Monte-Carlo simulations of lattice QCD started to produce accurate and reliable results for a number of quantities of phenomenological interest, such as e.g. the spectrum of the low lying hadrons and light quark masses (see e.g. [1] and [2]). Despite good agreement between theory and experiment for these quantities there are others where lattice QCD does not coincide with experiment. The origin of these discrepancies is not clear since a number of systematic effects have to be controlled both in experiment and simulations. A particular example where experiment and theory are not in satisfactory agreement are observables connected with structural properties of the nucleon, such as electric and magnetic form factors as well as the nucleon axial charge (see e.g. [3–6]). Another technically simpler observable where similar systematic effects enter is the pion electromagnetic form factor $f_{\pi\pi}(q^2)$, where q is the momentum transfer. The fact that $f_{\pi\pi}$ receives no contribution from quark-disconnected diagrams for two degenerate flavours makes it the ideal observable to perform a precision calculation in lattice QCD. Nevertheless, in the region of small momentum transfers the extraction of $f_{\pi\pi}(q^2)$ usually suffers from an intrinsic model dependence, since a direct calculation in that region has not been possible so far for both experiment and theory. Related to the pion form factor in that kinematical regime is the pion charge radius $\langle r_\pi^2 \rangle$ defined by the linear behavior of $f_{\pi\pi}(q^2)$ at $q^2 = 0$,

$$f_{\pi\pi}(q^2) = 1 + \frac{\langle r_\pi^2 \rangle}{6}\, q^2 + \ldots \quad \Rightarrow \quad \langle r_\pi^2 \rangle = 6\, \frac{d\, f_\pi(q^2)}{dq^2}\bigg|_{q^2=0} . \tag{1}$$

[1]brandt@kph.uni-mainz.de

β	a[fm]	lattice	# masses	$m_\pi L$	Labels	Statistic
5.20	0.08	64×32^3	3	6.0 – 4.0	A3 – A5	$\mathcal{O}(100)$
5.30	0.07	64×32^3	2	6.2, 4.7	E4, E5	$\mathcal{O}(100)$
5.30	0.07	96×48^3	1	5.0	F6	233
5.50	0.05	96×48^3	3	7.7 – 5.3	N3 – N5	$\mathcal{O}(100)$

Table 1: Compilation of simulation parameters.

The extraction of $\langle r_\pi^2 \rangle$ is thus mostly governed by the modeling of the q^2-dependence of $f_{\pi\pi}$ unless results are available around $q^2 \approx 0$. In lattice QCD the accessible momenta are usually obtained by Fourier transformation and thus constrained by finite lattice volume. This has changed recently by the introduction of partially twisted boundary conditions [8,9] that in principle allow arbitrary small momentum transfers in lattice simulations [10].

Our calculation of $f_{\pi\pi}$ employs ensembles generated in the context of the CLS project[2] and include three different lattice spacings with three different pion masses each. The main parameters of the ensembles used in the analysis are shown in table 1. To reduce the statistical noise we use stochastic $Z(2) \times Z(2)$ wall sources for the computation of the quark propagators, see e.g. [7]. The momenta are generated by five twist angles tuned so as to obtain as many as 30 values of q^2 below the lowest accessible q^2 from Fourier-momentum. We express our result in units of the Sommer scale r_0 [11] in the chiral limit, which has been measured for these ensembles in [12]. To compare our data to experimental results and results from other collaborations we use $r_0 = 0.471$ fm as obtained in [13]. To make optimal use of the generated data we extract $f_{\pi\pi}$ using a combination of the three different ratios of two- and three-point functions defined in [10]. The error bars are estimated with the bootstrap method using 1000 samples. For more details of the simulations see [14] and [6] as well as our upcoming publication.

The results for the pion form factor on our lightest ensemble for each lattice spacing are shown in figure 1, together with the results from [15–17] and the experimental results from [18]. Our points reach down to $(r_0\, q)^2 \lesssim -10^{-4}$ with small statistical uncertainties. This enables us to use a linear fit to $f_{\pi\pi}(q^2)$ in the region $(r_0\, q)^2 \leqslant -0.15$ to extract $\langle r_\pi^2 \rangle$ without any model dependence. The results from the linear fit are shown in figure 2 (left) for all ensembles, together with the other results quoted above. We see consistency with the results from other collaborations. Note that our results might show some residual cut-off dependence, investigated in our forthcoming publication.

Since our quark masses are bigger than the physical ones, we have to perform a chiral extrapolation to the physical point, guided by chiral perturbation theory (χPT). The χPT expressions for $f_{\pi\pi}$, and thus also for $\langle r_\pi^2 \rangle$, have been worked out to next-to-next-to leading order (NNLO) in [19]. As an intermediate step to compare to the NNLO formulae we start with the comparison to NLO, which was derived in [20]. In figure 2 (right) we show the results for the only free parameter $\bar{\ell}_6$ from the fit with $(r_0\, q)^2 \leqslant -0.15$ against $(m_\pi\, r_0)^2$.

[2] `https://twiki.cern.ch/twiki/bin/view/CLS/WebHome`

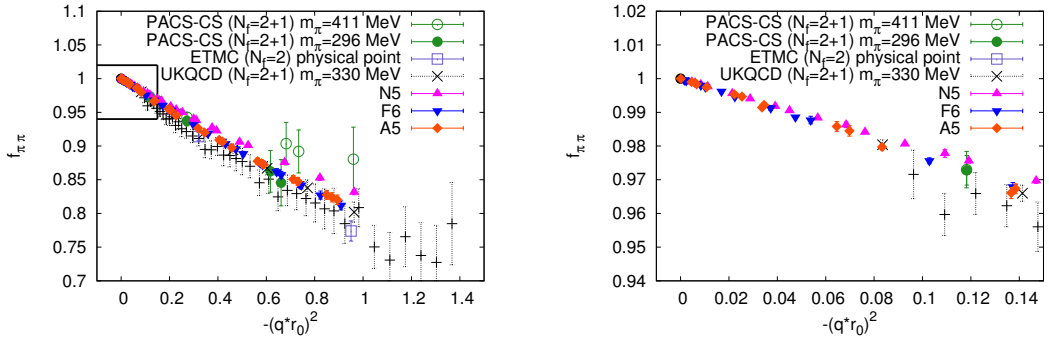

Figure 1: Results for the pion form factor for the lightest quark mass for each lattice spacing compared with the results from PACS-CS [15], ETMC [16] and UKQCD [17], as well as the experimental results from [18]. The right figure is the inset in the top left-hand corner.

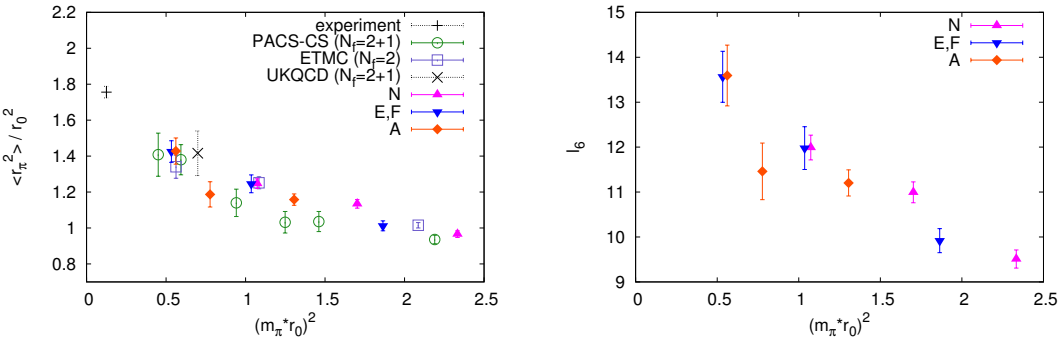

Figure 2: Left: Results for the pion charge radius extracted from linear fits to $f_{\pi\pi}(q^2)$ in the region $(r_0\,q)^2 \leqslant -0.15$ against $(m_\pi\,r_0)^2$ together with results from other collaborations. **Right:** Results for $\bar{\ell}_6$ against $(m_\pi\,r_0)^2$.

If χPT to NLO were a good description for the mass range of our simulations we would expect $\bar{\ell}_6$ to be constant, which is apparently not the case. This observation is consistent with the findings of earlier studies as e.g. in [15, 16]. To make a statement on $\langle r_\pi^2 \rangle$ at the physical point we thus envisage to use χPT to NNLO. In addition, finite volume effects as well as lattice artefacts, which might still be present in our analysis, are not taken into account so far. The discussion of the corresponding analysis of both, χPT to NNLO and finite volume effects and lattice artefacts, is postponed to a later publication.

Conclusions: In this proceedings article we have given an overview on our ongoing determination of the electromagnetic form factor of the pion in lattice QCD. We use twisted boundary conditions to attain a high density of measurements around $q^2 = 0$ which allows us to extract the charge radius without residual model dependence. We have compared our measurements to χPT at NLO and conclude that NLO is insufficient to describe the data in this mass range consistently. In the final analysis we are going to compare our measurements to χPT at NNLO and perform detailed studies on cut-off effects, finite volume effects and contributions to the form factor from excited states.

Acknowledgments

We like to thank our colleges from CLS for sharing ensembles. The simulations were done on the dedicated QCD cluster Wilson in Mainz. This work is funded in parts by SFB 443 of the DFG.

Bibliography

[1] S. Durr *et al.*, Science **322** (2008) 1224, [arXiv:0906.3599 [hep-lat]].

[2] G. Colangelo *et al.*, Eur. Phys. J. **C71** (2011) 1695, [arXiv:1011.4408 [hep-lat]].

[3] C. Alexandrou, PoS **LATTICE2010** (2010) 001, [arXiv:1011.3660 [hep-lat]].

[4] S. Collins *et al.*, [arXiv:1106.3580 [hep-lat]].

[5] S. Capitani, B. Knippschild, M. Della Morte, H. Wittig, PoS **LATTICE2010** (2010) 147, [arXiv:1011.1358 [hep-lat]].

[6] B. B. Brandt *et al.*, arXiv:1106.1554 [hep-lat].

[7] P. A. Boyle *et al.*, JHEP **0808** (2008) 086, [arXiv:0804.1501 [hep-lat]].

[8] P. F. Bedaque, Phys. Lett. **B593** (2004) 82, [nucl-th/0402051].

[9] G. M. de Divitiis, R. Petronzio, N. Tantalo, Phys. Lett. **B595** (2004) 408, [hep-lat/0405002].

[10] P. A. Boyle *et al.*, JHEP **0705** (2007) 016, [hep-lat/0703005 [HEP-LAT]].

[11] R. Sommer, Nucl. Phys. **B411** (1994) 839, [hep-lat/9310022].

[12] M. Donnellan *et al.*, Nucl. Phys. **B849** (2011) 45. [arXiv:1012.3037 [hep-lat]].

[13] G. von Hippel, Talk presented at the International Symposium on Lattice Field Theory, "Lattice 2011".

[14] B. B. Brandt *et al.*, PoS **LATTICE2010** (2010) 164, [arXiv:1010.2390 [hep-lat]].

[15] O. H. Nguyen, K. -I. Ishikawa, A. Ukawa, N. Ukita, JHEP **1104** (2011) 122, [arXiv:1102.3652 [hep-lat]].

[16] R. Frezzotti *et al.* [ETM Collaboration], Phys. Rev. **D79** (2009) 074506, [arXiv:0812.4042 [hep-lat]].

[17] P. A. Boyle *et al.*, JHEP **0807** (2008) 112, [arXiv:0804.3971 [hep-lat]].

[18] S. R. Amendolia *et al.* [NA7 Collaboration], Nucl. Phys. **B277** (1986) 168.

[19] J. Bijnens, G. Colangelo, P. Talavera, JHEP **9805** (1998) 014, [hep-ph/9805389].

[20] J. Gasser, H. Leutwyler, Annals Phys. **158** (1984) 142.

Hadron Physics at KLOE and KLOE-2

Camilla Di Donato[1] on behalf of KLOE and KLOE-2 Collaborations
I.N.F.N. Sezione di Napoli
Complesso Universitario M.S.A., Via Cintia ed.6
I-80126 Napoli, ITALY

The KLOE Collaboration completed the full data taking on March 2006, acquiring 2.5 fb^{-1} at the peak of the ϕ and other 240 pb^{-1} off-peak. A new Collaboration is working on a new project, called KLOE-2, to refine and extend the KLOE physics program.
We present here some preliminary and published results from the KLOE Collaboration on the pseudoscalar η meson and the study of $\gamma\gamma$ processes, that are among the main points of the KLOE-2 physics program.

1 Introduction

The KLOE experiment has collected 2.5 fb^{-1} at the peak of the ϕ resonance at the e^+e^- collider DAΦNE in Frascati. KLOE has performed several precision measurements, here we present the preliminary analysis of the $\eta \to \pi^+\pi^-\gamma$ decay channel to study box anomaly and the recently published branching ratio measurement of $\eta \to e^+e^-e^+e^-$ decay channel, never observed before. Pseudoscalar production at the ϕ-factory associated to internal conversion of the photon into a lepton pair allows the measurement of the form factor $F(q_1^2 = M(\phi)^2, q_2^2 > 0)$ of pseudoscalar mesons in the kinematical region of interest for the VMD model: a preliminary study of $\phi \to \eta e^+e^-$ is based on 739 pb^{-1}, using the $\eta \to \pi^+\pi^-\pi^0$ final state.
From a sample of 240 pb^{-1} taken off the ϕ resonance, a preliminary analysis of the $e^+e^- \to e^+e^-\eta$ process, without $e^\pm$ tagging in the final state has been performed. The same data set has been used to search for the $f_0(600)$ produced in $\gamma\gamma$ interactions via the reaction $e^+e^- \to e^+e^-\pi^0\pi^0$.
The KLOE detector is being upgraded with small angle tagging devices, to detect both high and low energy $e^\pm$ in $e^+e^- \to e^+e^-X$ events. The inner tracker and small angle calorimeters are scheduled to be installed in a subsequent step, providing wider acceptance for both charged particles and photons. This is the new KLOE-2 project [1]: the detector is successfully rolled in the new DAΦNE interaction region, with a new beam crossing scheme allowing for a reduced beam size and increased luminosity. The main goal of KLOE-2 is to collect an integrated luminosity of about 20 fb^{-1} in 2-3 years in order to refine and extend the KLOE physics programme.

[1] didonato@na.infn.it

2 The Pseudoscalar η meson

The decays $\eta, \eta' \to \pi^+\pi^-\gamma$ are supposed to get contribution from the anomaly accounted by the Wess Zumino Witten term into the Chiral Perturbation Theory Lagrangian [2]. Those anomalous processes, known as box anomalies, proceed via a vector meson resonant contribution (VDM) and maybe via a direct term. The presence of this direct term affects the partial width value in the case of the $\eta \to \pi^+\pi^-\gamma$ and the dipion invariant mass distribution, in the case of $\eta' \to \pi^+\pi^-\gamma$.
A comparison of the experimental $M_{\pi^+\pi^-}$ spectra and partial width for η, η' meson with theoretical predictions is mandatory to clarify the role of non-resonant contribution to the processes. The $\eta \to \pi^+\pi^-\gamma$ decay has been measured in 1970 by Gormley et al. (7250 events) [3] and in the 1973 by Layter et al. (18150 events) [4]. Theoretical papers trying to combine the two measurements found discrepancies in data treatment and problems in obtaining consistent results [2]. In 2007 CLEO Coll. has published the measurement $\Gamma_{\eta\to\pi^+\pi^-\gamma}/\Gamma_{\eta\to\pi^+\pi^-\pi^0} = 0.175 \pm 0.007 \pm 0.006$, based on 859 $\eta \to \pi^+\pi^-\gamma$ events [5], which is more then 3σ below the old measurements. KLOE result [6], obtained using 558 pb^{-1}, gives $\Gamma_{\eta\to\pi^+\pi^-\gamma}/\Gamma_{\eta\to\pi^+\pi^-\pi^0} = 0.1838 \pm 0.0005_{stat} \pm 0.0030_{syst}$, in agreement with the latest CLEO evaluation, providing strong evidence in favour of the box anomaly/direct term.

The knowledge of the η meson coupling to virtual photons is important for calculation of anomalous magnetic moment of the muon, because the pseudoscalar exchange is the major contribution to the hadron light-by-light scattering [1]. In the $\eta \to e^+e^-e^+e^-$ process we have conversion decays, which offer the possibility to precisely measure the virtual photon 4-momentum, via the e^+ and e^- 4-momenta and we are directly sensitive to the η meson transition form factor because there are no hadrons among the decay products. The first theoretical evaluation dates from 1967 [7] and predicts a branching ratio $BR(\eta \to e^+e^-e^+e^-) = 2.59 \times 10^{-5}$. Double lepton-antilepton η decays have been searched by CMD-2 and WASA, obtaining upper limits at level of the theoretical expectation. KLOE has published the first observation of the $\eta \to e^+e^-e^+e^-$ decay, analysing 1.7 fb^{-1} and identifing 362 ± 29 events which results in a branching ratio of $(2.4 \pm 0.2_{stat+bkg} \pm 0.1_{syst}) \times 10^{-5}$, in agreement with theoretical predictions [8].
Vector-meson-dominance assumption provides good description of photon coupling to hadrons, and, implementing systematic corrections to standard VMD, it correctly describes the $\omega \to \pi^0\mu^+\mu^-$ experimental results too. In this framework deviation from standard VMD for the $\phi \to \eta e^+e^-$ decay spectrum is predicted. The only existing data available come from SND experiment, which has measured the M_{ee} invariant mass distribution with 213 events [9]. KLOE has selected 7000 $\phi \to \eta e^+e^-$ with $\eta \to \pi^+\pi^-\pi^0$ using a sample of 739 pb^{-1}. Preliminary fit to the M_{ee} using decay parametrization from [10] and $F(q^2)$ as from [11], indicates the possibility to reach a 5% error on form factor slope.

2.1 Gamma-gamma Physics

The coupling of photons to scalar and pseudoscalar mesons brings information on meson's quark structure and can be measured directly in e^+e^- colliders via the reaction $e^+e^- \to e^+e^-\gamma^*\gamma^* \to e^+e^-X$. Using the Weizsäcker-Williams approximation [12] to understand main qualitative features of the process, when no cuts are applied to the final state leptons, it is possible to evaluate the event yields: $N_{eeX} = L_{ee}\int \frac{dF}{dW_{\gamma\gamma}}\sigma_{\gamma\gamma\to X}(W_{\gamma\gamma})dW_{\gamma\gamma}$ the L_{ee} is the integrated luminosity, $W_{\gamma\gamma}$ is the mass of the $\gamma^*\gamma^*$ and $dF/dW_{\gamma\gamma}$ the two photons flux function, defined as follows: $\frac{dF}{dW_{\gamma\gamma}} = \frac{1}{W_{\gamma\gamma}}(\frac{2\alpha}{\pi})^2(ln\frac{E_b}{m_e})^2 f(z)$ with E_b beam energy and $f(z)$ is a function of $z = \frac{W_{\gamma\gamma}}{2E_b}$.
Single π^0 or η production is accessible and this allows to improve determination of two photon decay width of these meson. In particular KLOE is looking for $e^+e^- \to e^+e^-\eta$ with $\eta \to \pi^+\pi^-\pi^0$ final state: in a preliminary analysis of 240 pb^{-1} off-peak data about 600 events from η meson, produced in $\gamma\gamma$ interactions have been disentangled, versus other processes, with a statistical accuracy on $\Gamma_{\gamma\gamma}$ comparable with existing measurements. The same off-peak data have been analysed to search for $e^+e^- \to e^+e^-\eta$ with $\eta \to \pi^0\pi^0\pi^0$ final state.
The question concerning $\sigma/f_0(600)$ meson has been debated for a long time. An indirect evidence comes from $\phi \to \pi^0\pi^0\gamma$ KLOE analysis [13]. The $e^+e^- \to e^+e^-\pi^0\pi^0$ process is a clean electromagnetic probe to investigate the question, because it is expected to be plainly affected by σ contribution. Our preliminary analysis on the off-peak data, shows a clear enhancement over estimated backgrounds at low $M_{4\gamma}$; see Fig.1. Background subtraction

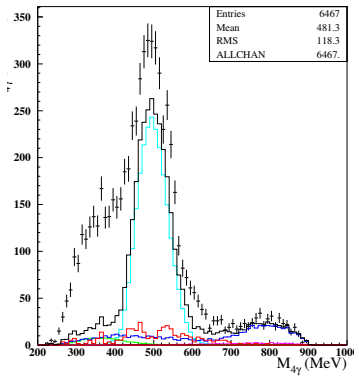

Figure 1: Preliminary spectrum of 4-photons invariant mass with KLOE: dots are data, black line is total MC background, lightblue is $K_S\,K_L$ decays, blue is $e^+e^- \to \omega\pi^0$ and magenta is $\phi \to f_0\gamma$; a clear evidence of $e^+e^- \to e^+e^-\pi^0\pi^0$ is given by the excess events at low $M_{4\gamma}$ invariant mass is visible

and study of differential cross section together with the understanding of the $\sigma \to \pi\pi$ contribution are in progress.

Due to large background from $e^+e^- \to \gamma\gamma(\gamma)$, information from $e^\pm$ taggers already installed at KLOE-2, will be crucial in the analysis of new data to look for the production of σ.

The KLOE experiment with 2.5 fb^{-1} integrated luminosity at the peak of the ϕ resonance at the e^+e^- collider DAΦNE, has published several interesting results. In the next future a new data-taking campaign will be realized by KLOE-2 at the upgraded DAΦNE, with the aim to collect about 20 fb^{-1} in order to refine and extend the KLOE physics program.

Bibliography

[1] G. Amelino-Camelia, F. Archilli, D. Babusci, D. Badoni, G. Bencivenni, J. Bernabeu, R. A. Bertlmann, D. R. Boito *et al.*, Eur. Phys. J. **C68** (2010) 619-681.

[2] M. Benayoun, P. David, L. DelBuono, P. Leruste, H. B. O'Connell, Eur. Phys. J. **C31** (2003) 525-547.

[3] M. Gormley, E. Hyman, W. -Y. Lee, T. Nash, J. Peoples, C. Schultz, S. Stein, Phys. Rev. **D2** (1970) 501-505.

[4] J. G. Layter, J. A. Appel, A. Kotlewski, W. -Y. Lee, S. Stein, J. J. Thaler, Phys. Rev. **D7** (1973) 2565-2568; J. J. Thaler, J. A. Appel, A. Kotlewski, J. G. Layter, W. -Y. Lee, S. Stein, Phys. Rev. **D7** (1973) 2569-2571.

[5] A. Lopez *et al.* [CLEO Collaboration], Phys. Rev. Lett. **99** (2007) 122001.

[6] F. Ambrosino, *et al.* [The KLOE and KLOE2 Collaborations], [arXiv:1107.5733 [hep-ex]].

[7] C. Jarlskog and H. Pilkuhn, Nucl. Phys. B **1** (1967) 264.

[8] F. Ambrosino, *et al.* [The KLOE and KLOE2 Collaborations], Phys. Lett. **B702** (2011) 324-328. [arXiv:1105.6067 [hep-ex]].

[9] M. N. Achasov, V. M. Aulchenko, K. I. Beloborodov, A. V. Berdyugin, A. G. Bogdanchikov, A. V. Bozhenok, A. D. Bukin, D. A. Bukin *et al.*, Phys. Lett. **B504** (2001) 275-281.

[10] L. G. Landsberg, Phys. Rept. **128** (1985) 301-376.

[11] N. N. Achasov, A. A. Kozhevnikov, Sov. J. Nucl. Phys. **55** (1992) 449-459.

[12] S. J. Brodsky, T. Kinoshita, H. Terazawa, Phys. Rev. **D4** (1971) 1532-1557.

[13] F. Ambrosino *et al.* [KLOE Collaboration], Eur. Phys. J. **C49** (2007) 473-488.

Analysis of diffractive dissociation of exclusive $K^-\pi^+\pi^-$ events in the high energetic hadron beam of the COMPASS-experiment

Prometeusz K. Jasinski[1] on behalf of the COMPASS Collaboration
Institut für Kernphysik Mainz
Johann-Joachim-Becher-Weg 45
D 55128 Mainz, Germany

In order to study the light-meson spectrum the COMPASS experiment at CERN was taking data with a 190 GeV/c hadron beam hitting a liquid hydrogen target in the years 2008 and 2009. The negative hadron beam contained mainly pions and a small fraction of about 2.5% of kaons. Kaons were identified using CEDAR PID detectors in the beamline. One of the channels of interest are diffractively produced resonances decaying into the $K^-\ \pi^+\ \pi^-$ final state. The presented data selection resulted in 270 000 events from 2008 hadron-beam data. The invariant mass spectra show already the well known resonances like the $K_1(1270)$, $K_1(1400)$ and the $K_2(1770)$. To disentangle all contributing resonances techniques of mass independent partial wave analysis were applied. A short review on the ongoing studies is presented. *Supported by BMBF under the contract 06MZ224.*

1 Introduction

A bound $q\bar{q}$ state in a potential with additional orbital angular momentum between the quarks has several eigenstates whose energy corresponds to the mass of the meson. A coupling of an s or $\bar{s}$ quark with lighter quarks creates isospin $I_3 = 1/2$ states. Those are classified by their total spin-parity J^P. No further eigenvalues like $C(G)$-parity are available as symmetry is broken due to the heavier strange quark.

Resonances decaying into $K^\mp\pi^\pm\pi^\mp$ final states were measured at several experiments [1–3] in the past. Most of them in the late 70s, like WA03 [4] at CERN, often quoted to be the "best" measurement so far in this channel. After 30 years still many unconfirmed resonances [5] as well as open questions about their interpretation exist, giving us the motivation to remeasure those states with the COMPASS high-precision spectrometer.

[1] jasinski@kph.uni-mainz.de

2 Measurement

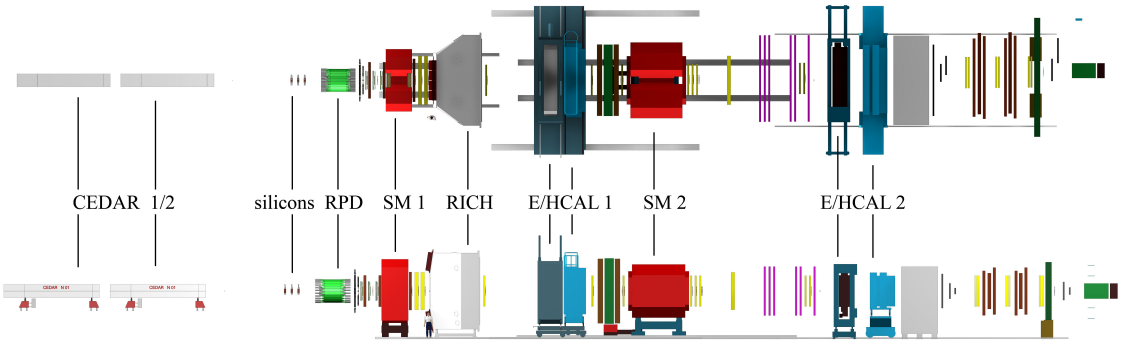

Figure 1: Illustration of the two-stage COMPASS Spectrometer (top/side view). For details see the text.

The production mechanism of choice was single-diffractive dissociation of a projectile on a proton target (see figure 2 left). A beam particle was excited via reggeon (pomeron) exchange to a higher state preserving charge, flavour, energy and G-parity. The target proton stayed intact, only four-momentum was transferred to the proton.

The COMPASS hadron runs in the years 2008 and 2009 were mainly dedicated to the study of meson or baryon excitations. The 60 m long two-stage spectrometer is sketched in figure 1. The negative hadron beam was consisting mainly of pions with a small kaon admixture of about 2.5%. These were tagged by CEDAR detectors 30 m upstream of the target [6]. In single-diffractive processes the target proton scatters elastically. A Recoil Proton Detector (RPD) measured the time of flight of the protons that were kicked out of the 40 cm long liquid hydrogen target using two barrels of scintillator slabs.

Momenta of charged final states were determined by two spectrometer stages, each initialized by a spectrometer magnet (SM), and more then 200 planes of tracking devices along the spectrometer. In addition the first stage featured a ring imaging Cherenkov detector (RICH) for final-state particle identification (PID). Kaons could be separated from pions with momenta up to 50 GeV/c. Neutral particles were identified by their energy deposit in electromagnetic calorimeters (ECAL) in both stages. A more detailed description of the spectrometer is found in [7].

The application of cuts as track multiplicity, charge conservation, planarity of the beam particle, recoil proton and resonance as well as the application of the RICH PID to the negatively charged tracks yielded in about 270 000 final-state events forming the invariant mass distribution in figure 2 (right). As RICH momentum acceptance effects played a bigger role in the smaller phase space of low invariant masses the mass distribution shows an enlarged contribution of higher masses in the K_2 region as compared to previous measurements [4]. The corresponding sub-mass spectra in figure 3 for $K^-\pi^+$ and $\pi^-\pi^+$ track combinations

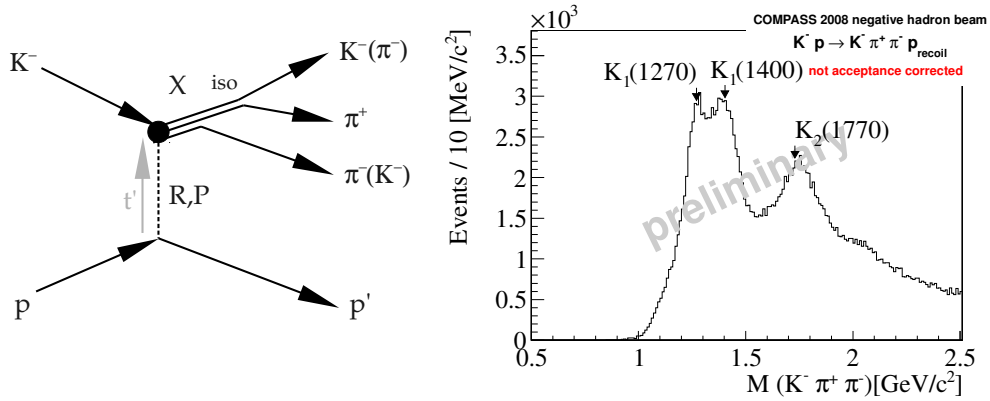

Figure 2: Left: Single diffractive excitation of kaons into $K^-\pi^+\pi^-$ final states via reggeon (pomeron) exchange with a target proton. The dissociation of the intermediate state X is described by a chain of successive two-body decays. Right: The invariant $K^-\pi^+\pi^-$ mass distribution for the 2008 COMPASS data after all cuts.

support the assumption of a decay chain with intermediate isobar states as $K^*(892)$ or $\rho(770)$.

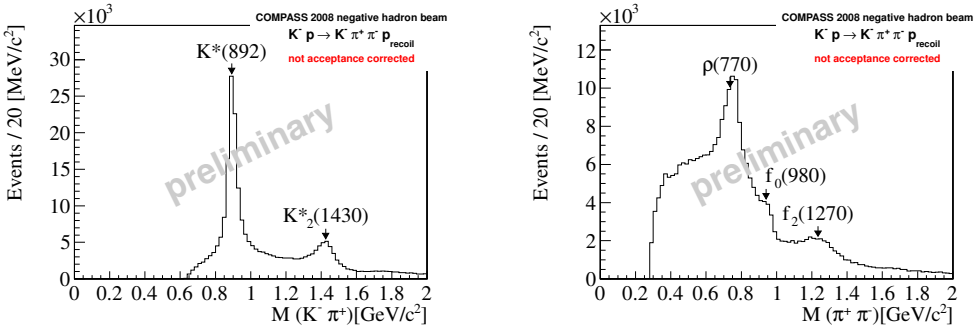

Figure 3: The invariant $K^-\pi^+$ (left) and $\pi^+\pi^-$ (right) mass distributions as contained in the $K^-\pi^+\pi^-$ final state.

3 Partial-wave analysis

The combination of known resonances in the isobar invariant mass spectra in figure 3 and the bachelor particle allows to compose a spin-parity basis for the observed angular distributions. The data sample was divided in invariant $K^-\pi^+\pi^-$ mass bins of 20 MeV/c^2

width. An acceptance-corrected maximum likelihood fit using a spin-density matrix of rank two was performed in each bin. In total 19 partial waves plus a flat wave were found to describe the data set the best. Results were at large parts in good agreement with previous measurements by WA03 [4], but also differences were observed.

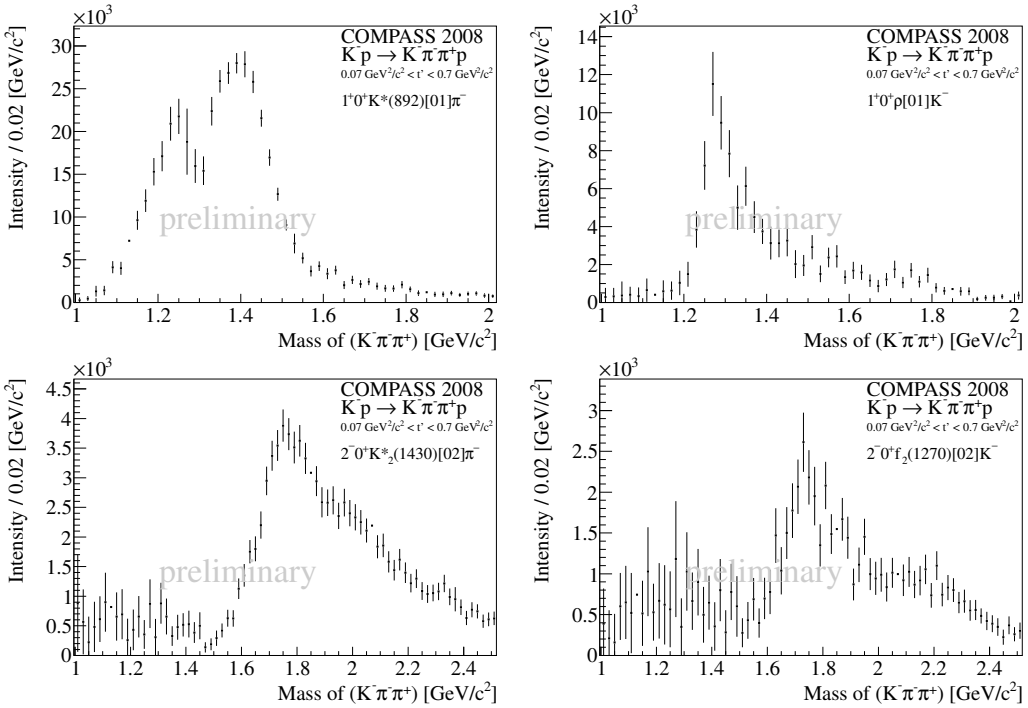

Figure 4: Intensity distributions of the four main partial waves from a mass-independent fit to the COMPASS data. The low-mass region is dominated by $J^P = 1^+$ states coupling to ρK^- and $K^*\pi^-$ channels. The high mass region consists of $J^P = 2^-$ states coupling mainly to $K_2^*\pi^-$ and f_2K^- channels. Both states are believed to be a mixture of spin-singlet and spin-triplet states.

Exemplary four intensities are shown in figure 4. The largest intensities were found in the $J^P = 1^+$ waves coupling mostly to the $K^*\pi^-$ and ρK^- channels. Two peaks were observed particularly in the $K^*\pi^-$ branch. Those are known to be the $K_1(1270)$ and the $K_1(1400)$, the spin singlet and triplet state in the constituent quark model. In contrast to results by WA03 the coupling of the $K_1(1400)$ to the $K^*\pi^-$ states seems to be resulting in a $J^P = 1^+$ spin total with nearly equal intensities for both resonances.

A similar mixing of two spin states is also expected in the $J^P = 2^-$ waves. Indeed broad resonant structures are present in the high-mass region coupling mainly to $K_2^*\pi^-$ and f_2K^- waves. A further decomposition needs a mass-dependent fit as those resonances are strongly overlapping. The mass dependent fit algorithm is work in progress.

Peaks in the $J^P = 2^+$ waves confirm once again the existence of the well known $K_2^*(1430)$

and strong intensities were observed in the low-mass region for $J^P = 0^-$ waves. For a clean identification of a possibly existing $K(1460)$ also here a mass-dependent fit must be applied. These waves are sensitive to Deck-like effects that cannot be separated by a mass-independent fit alone.

4 Conclusion and Outlook

COMPASS data of 2008 contain a clean sample of kaonic resonances decaying into $K^-\pi^+\pi^-$ final states. About 270 000 events were subjected to mass-independent partial-wave analysis showing a composition of $J^P = 0^-, 1^+, 2^+, 2^-$ states that needs further investigation as many resonances in the high-mass region are strongly overlapping. Well-known resonances were observed and the existence of at least one resonance in the $J^P = 0^-$ waves is likely. With the analysis of 2009 data we will probably double the number of events and a prospective mass-dependent partial-wave analysis will give us information about masses and widths of the contained resonances.

Acknowledgments

I thank the German *Federal Ministry of Education and Research* (BMBF) for financial support. Moreover the very good organization of the Hadron 2011 conference is acknowledged, too.

Bibliography

[1] G. W. Brandenburg *et al.*, Phys. Rev. Lett. **36**, 703, 706 (1976).

[2] Yu. M. Antipov *et al.*, Nucl. Phys. B **86**, 381, 402 (1975).

[3] H. Guler *et al.*, Phys. Rev. D **83**, 032005, (2011).

[4] C. Daum *et al.*, Nucl. Phys. B **187**, 1 (1981).

[5] C. Amsler *et al.*(Particle Data Group), Phys. Lett. B **667**, 1 (2010).

[6] C. Bovet *et al.*, IEEE Trans.Nucl.Sci. **25**, 572, 576 (1978).

[7] P. Abbon *et al.*, Nucl. Instrum. Methods A **577**, 455, 518 (2007).

Light Vector Meson Photoproduction off of ^{1}H at Jefferson Lab and ρ-ω Interference in the Leptonic Decay Channel

Chaden Djalali[1,a], Michael Paolone[a], Rakhsha Nasseripour[b], Michael Wood[c], Dennis Weygand[d], and the CLAS Collaboration
[a]*University of South Carolina, Columbia SC, USA*
[b]*George Washington University, Washington DC, USA*
[c]*Canisius College, Buffalo NY, USA*
[d]*Thomas Jefferson National Accelerator Facility, Newport News VA, USA*

Recent studies of light vector meson production in heavy nuclear targets has generated interest in ρ-ω interference in the leptonic e^+e^- decay channel. An experimental study of the elementary process provides valuable input for theoretical models and calculations. In experiment E04-005 (g12), high statistics photoproduction data has been taken in Jefferson Lab's Hall B with the Cebaf Large Acceptance Spectrometer (CLAS). The invariant mass spectrum is fitted with two interfering relativistic Breit-Wigner functions to determine the interference phase. Preliminary analysis indicate a measurable ρ-ω interference.

1 Introduction

Partial restoration of chiral symmetry in ordinary nuclear matter suggests the modification of properties of vector mesons, such as a shift in mass and/or a change of width. Recently, several experiments have studied the properties of the ρ, ω and ϕ mesons in the medium via their rare leptonic decay to e^+e^- pairs. The ρ meson has a very short lifetime leading to the largest probability of decaying in the medium, while the ω and ϕ mesons (with their longer lifetimes) will mostly decay outside the medium in which they are produced. In most experiments,the majority of the ω and ϕ mesons decay outside of the medium and therefore their mass spectra are consistent with their free-space properties. However the information on the in-medium widths of these mesons can be extracted from their interactions with the nucleons as the mesons escape the nucleus using transparency ratios. Reference [1] discusses and compares these studies. The JLab transparency ratios drop faster that the CBELSA-TAPS ratios indicating an even larger in-medium width ($\Gamma_\omega \geqslant 200$ MeV). The very large ω-meson absorption observed in the e^+e^- channel cannot be explained with the

[1]djalali@sc.edu

current theoretical calculations. One explanation could be a destructive ρ-ω interference in nuclei. Interference due to ρ-ω mixing was first suggested by Glashow [2] in 1961. In the seventies, several experiments on C and Be targets and strong ρ-ω interference were observed in γA$\rightarrow e^+e^-$(X) reactions. [3–6]. Further motivation for the current study was based on calculations by Lutz and Soyeur [7] that predict relatively large ρ-ω interference in the γN$\rightarrow e^+e^-$N reaction (constructive interference on p, destructive interference on n).

2 The g12 experiment at JLab

The JLab E04-005 experiment (a.k.a. CLAS experiment g12) main purpose was to study exotic meson production and excited cascade states through photoproduction. The study of the vector mesons and their decays in e^+e^- was conducted in parallel. A tagged photon beam of energies up to 5.5 GeV was used on a liquid hydrogen target cell 40 cm in length and 4 cm in diameter. The target cell was placed 90 cm upstream from the CLAS center to increase coverage of very forward angle particles. The Electromagnetic Calorimeter (EC) and the Cherenkov Counter (CC) are the critical component of CLAS which lead to an e/π rejection factor better than 10^{-6} for di-lepton pairs. The experimental procedure is described in detail in Ref. [9].

In addition to the channels of interest ($\rho, \omega, \phi \rightarrow e^+e^-$), two other physical channels (treated as "background" in this study) are the Dalitz decays of mesons and the Bethe-Heitler pair production. For either of these channels, a simple cut on the opening angle of the e^+e^- pair significantly reduces their contributions. It almost eliminates all Dalitz decay events and substantially reduces the Bethe-Heitler "background". The remaining Bethe-Heitler contribution can be easily estimated and subtracted. If one looks at the inclusive reaction $\gamma p \rightarrow e^+e^-X$, one has to take into account the combinatorial e^+e^- background which arises from leptons from uncorrelated events. The magnitude and shape of this background can be determined from the data by measuring the amount of like charge lepton pairs (e^+e^+ and e^-e^-). This procedure is described in Ref. [9].

Additionally, a cut is made on the missing mass squared off of the dilepton pair, $(\gamma + p_{targ} - e^+ - e^-)^2$ around the mass of the proton squared. This cut eliminates higher mass baryon states in the final state and puts restrictions on the production mechanism (varying t-channel ρ-ω production processes). An additional benefit of this cut is the complete elimination of the combinatorial background.

3 ρ-ω interference

To describe the photoproduction of the vector mesons on the proton, the total amplitude F can be written as a combination of the ρ and ω meson amplitudes with a complex phase

term: $F = f_\rho + ie^{i\phi_\rho} f_\omega$. f_ρ and f_ω are relativistic Breit-Wigner functions and ϕ_ρ is the interference phase. The cross section is obtained by squaring this amplitude.

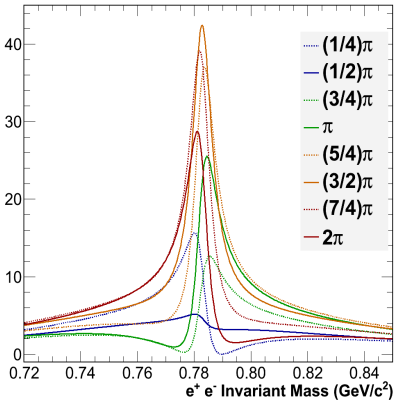

Figure 1: Predicted ρ-ω interference shape as a function of the phase ϕ_ρ

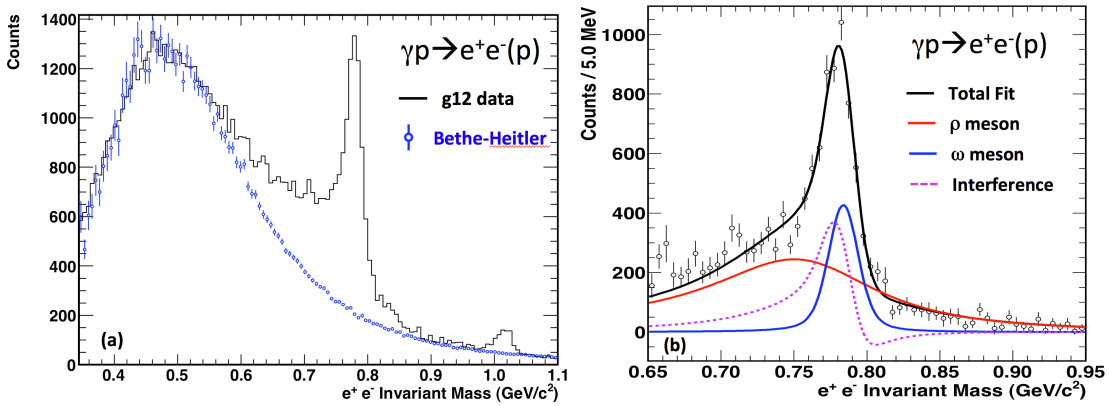

Figure 2: (a) Calculated Bethe-Heitler contribution (blue) compared to data (black); (b) Bethe-Heitler subtracted e^+e^- invariant mass spectrum fit showing the ρ, ω and interference term contributions

The ρ-ω interference as a function of the interference phase ϕ is shown in Figure 1. The Bethe-Heitler contribution is calculated and matches very well with the data (see Figure 2-(a)). Once the Bethe-Heitler contribution is subtracted, the e^+e^- invariant mass spectrum is fitted with two interfering relativistic Breit-Wigner functions. The ρ width in the Breit-Wigner function is set to be mass dependent [8]. Figure 2-(b) shows a typical fit with contributions from the ρ and ω mesons as well as the interference term. Different fits have been carried out with and without the interference. The interference term is required to substantially improve the chi-squared of the fit.

4 Summary and Conclusion

The g12 experiment at JLab has generated large statistics data in the e^+e^- decay channel. The ρ, ω and ϕ mesons are clearly observed. Selecting the γ N $\rightarrow$ e^+e^- (p) channel, the combinatorial background is suppressed. The Bethe-Heitler contribution has been calculated and subtracted from the e^+e^- invariant mass spectrum. Preliminary analysis show a ρ-ω interference. Further analysis is underway to estimate the uncertainties before extracting the final ρ-ω interference phase. The measured cross sections will be compared to Lutz and Soyeur predictions [7]. These studies will be extended to nuclei.

Acknowledgments

The authors are thankful to U. Mosel, J. Weil, M. Soyeur and E. Oset for their theoretical support. This work was supported by the U.S. Department of Energy and the National Science Foundation. The Jefferson Science Associates, LLC, operates the Thomas Jefferson National Accelerator Facility for the United States Department of Energy under contract No. DE-AC05-06OR23177.

Bibliography

[1] M. H. Wood *et al.*, Phys. Rev. Lett. **105**, 112301 (2010).

[2] S. L. Glashow, Phys. Rev. Lett. **7**, 469 (1961).

[3] P. J. Biggs *et al.*, Phys. Rev. Lett. **24**, 1197 (1970).

[4] P. J. Biggs *et al.*, Phys. Rev. Lett. **27**, 1157 (1971).

[5] H. Alvensleben *et al.*, Nucl. Phys. **B25**, 333 (1971).

[6] H. Alvensleben *et al.*, Phys. Rev. Lett. **25**, 1373 (1970).

[7] M. F. M. Lutz, M. Soyeur, Nucl. Phys. **A760**, 85 (2005).

[8] M. N. Achasov *et al.*, Phys. Rev. **D65**, 032002 (2002).

[9] M. H. Wood *et al.*, Phys. Rev. **C78**, 015201 (2008).

Exploration of resonance properties in chiral perturbation theory with explicit $U_A(1)$ anomaly

Zhi-Hui Guo[a,b] and J. A. Oller[b]
[a]*Department of Physics, Hebei Normal University, 050016 Shijiazhuang, China*
[b]*Departamento de Física, Universidad de Murcia, E-30071 Murcia, Spain*

We study the resonance properties within chiral perturbation theory by explicitly taking into account the $U_A(1)$ anomaly effect. This assures we have the appropriate degrees of freedom of low energy QCD in the large N_C limit. We calculate the various resonance properties, such as mass, width and residues, for the physical case, i.e. $N_C = 3$. Then we extrapolate the values of N_C to study the trajectories of resonance poles.

1 Introduction

The combination of chiral perturbation theory (χPT) and non-perturbative methods inspired from S- matrix theory, play an important role in the study of resonances nowadays [1]. A straightforward application of this approach is to determine the properties of the resonance, such as the mass and the width. A deeper understanding of the resonance structure can be obtained by combining the $1/N_C$ expansion of QCD in χPT [2]. A novel ingredient in our current study is the singlet η_1, which is massive even in the chiral limit due to the $U_A(1)$ anomaly effect. This ingredient has been commonly ignored in the previous works on the study of N_C trajectories of resonance poles [2]. Since it turns out to be the ninth pseudo Goldstone in the chiral and large N_C limit and becomes a relevant degree of freedom in the low energy QCD for large N_C, it is necessary to take this effect into account to study resonance properties at large N_C. In our study, this gap is filled by using the $U(3)$ χPT, which incorporates the massive singlet η_1 as its explicit degree of freedom.

2 Theoretical setup

The current study of resonance properties is based on the complete one-loop calculation of meson-meson scattering within $U(3)$ χPT by explicitly including the tree level exchanges of scalar and vector resonances. The perturbative calculation incorporates not only the genuine meson-meson scattering diagrams, including the loops and the resonance exchanges, but also the contributions from the wave function renormalizations, mass renormalizations,

pseudo-Goldstone weak decay constants and $\eta - \eta'$ mixing. The master formula to unitarize the perturbative $U(3)$ χPT results is from a simplified version of N/D method derived in [3]

$$T_J^I(s)^{-1} = N_J^I(s)^{-1} + g(s)\,, \tag{1}$$

where $T_J^I(s)$ denotes the unitarized partial wave amplitudes with well defined isospin I and angular momentum J. $N_J^I(s)$ collects the crossed channel cuts and can be constructed from the perturbative results

$$N_J^I(s) = T_J^I(s)^{(2)+\mathrm{Res}+\mathrm{Loop}} + T_J^I(s)^{(2)}\ g(s)\ T_J^I(s)^{(2)}\,, \tag{2}$$

where $T_J^I(s)^{(2)+\mathrm{Res}+\mathrm{Loop}}$ stands for the partial wave amplitude from the perturbative calculation, with the superscripts (2), Res and Loop denoting the leading order amplitudes, resonance exchanges and loop contributions, respectively. The explicit expressions from the perturbative calculation can be found in Ref. [4]. $g(s)$ contains the right hand cuts and its explicit expression can be also found in [4] and references therein.

3 Results and Discussions

From the unitarized meson-meson scattering amplitudes, one can construct the phase shift, modulus of the S-matrix and invariant mass distribution [4]. Then we fit the various quantities to the experimental data to get the unknown parameters in our model. The resonance poles are found on the unphysical Riemann sheets, which can be obtained from the extrapolation of T-matrix on the physical sheet (the first sheet) to the unphyscial ones. In our study, the pole positions of three kinds of vector resonances are obtained: $\rho(770)$ with $IJ = 1\,1$, $K^*(892)$ with $IJ = \frac{1}{2}\,1$ and $\phi(1020)$ with $IJ = 0\,1$. For the scalar resonances, we find σ, $f_0(980)$ and $f_0(1370)$ for the $IJ = 0\,0$ case, $a_0(980)$ and $a_0(1450)$ for $IJ = 1\,0$ case, κ and $K^*(1430)$ for $IJ = \frac{1}{2}\,0$. The masses and widths of the above mentioned resonances are consistent with the PDG values [5]. We have also calculated the couplings between the resonances and the pseudo-scalar mesons. For the detailed result, see Ref. [4].

Then we extrapolate the values of N_C from 3 to larger numbers to study the corresponding behaviors of resonance poles. In this way, one can learn whether the resonance is a standard $\bar{q}q$ resonance by plotting the N_C trajectories of its pole positions. The basic criteria is that in the framework of large N_C QCD the mass of a standard $\bar{q}q$ resonance is a constant, while its decay width decreases as $1/N_C$ when N_C approaches to infinity. For $\rho(770)$, $K^*(892)$, $f_0(980)$, $f_0(1370)$, $a_0(1450)$ and $K^*(1430)$, we plot the quantities of $\Gamma * N_C$ (Γ denotes the width) and mass of the resonances as functions of N_C in Figs. 1 and 2 respectively. It is clear that the resonances appearing in those two figures all behave as the standard $\bar{q}q$ resonances, since their masses are more or less stable when varying N_C and their decay widths decrease as $1/N_C$ for large values of N_C. However for the very broad resonances σ and κ, we find their pole positions in the complex s plane approach to the real and negative axis when

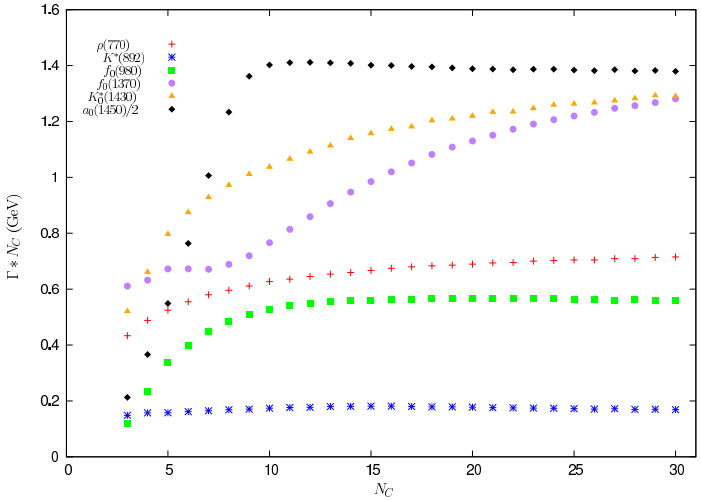

Figure 1: Decay widths of resonances as functions of N_C. For $a_0(1450)$, we plot the quantity of $\Gamma * N_C/2$. For the others, we plot the quantity of $\Gamma * N_C$ as functions of N_C.

increasing the values of N_C. In this case, it is not appropriate to interpret the imaginary part of $\sqrt{s}$ as the decay width. In Fig. 3, we plot the real and imaginary parts of s_σ and s_κ as functions of N_C, from where one can conclude that σ and κ resonances in our study do not correspond to the standard $\bar{q}q$ resonances for large N_C. For $a_0(980)$, both its width and mass increase when increasing N_C, indicating it does not seem to correspond to a standard $\bar{q}q$ resonance in our current study.

Acknowledgments

This work is partially funded by the DGICYT grant FPA2010-17806, the Fundación Séneca grant with Ref. 11871/PI/09, the EU-Research Infrastructure Integrating Activity "Study of Strongly Interacting Matter" (HadronPhysics2, grant No.227431) under the Seventh Framework Programme of EU, the Consolider-Ingenio 2010 Programme CPAN (CSD2007-00042), Natural Science Foundation of Hebei Province with contract No. A2011205093 and Doctor Foundation of Hebei Normal University with contract No. L2010B04.

Bibliography

[1] J. Oller and E. Oset, Nucl. Phys. **A620** (1997) 438; (E)−*ibid* A **652**(1999) 407; M. Albaladejo and J. A. Oller, Phys. Rev. Lett. **101** (2008) 252002; I. Caprini, G. Colangelo and H. Leutwyler, Phys. Rev. Lett. **96** (2006) 132001.

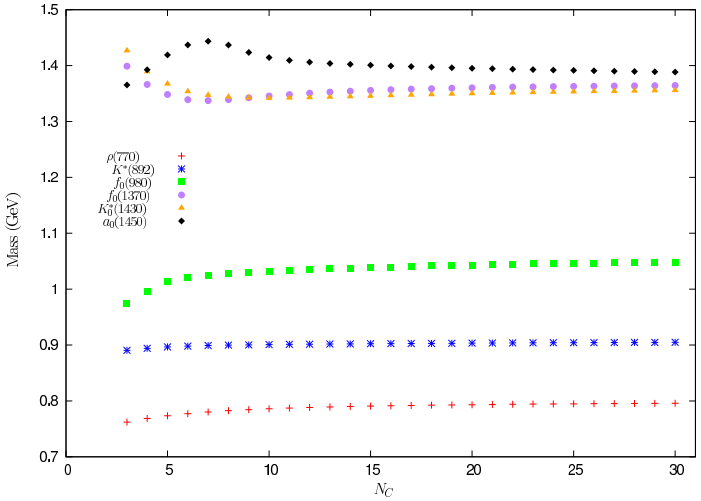

Figure 2: Masses of resonances as functions of N_C.

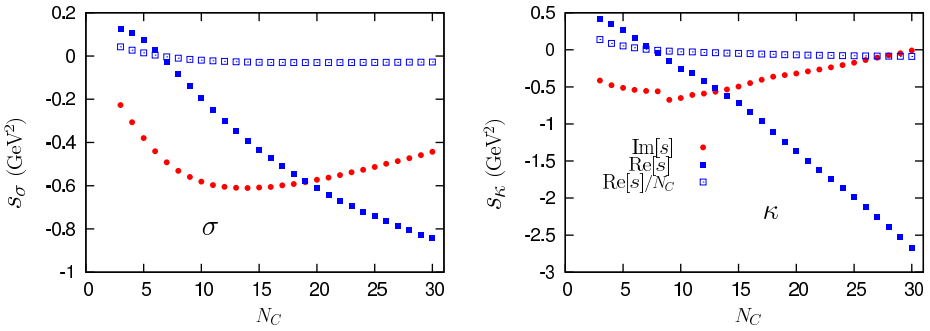

Figure 3: N_C trajectories for the imaginary and real parts of σ pole s_σ and κ pole s_κ.

[2] J. R. Peláez, Mod. Phys. Lett. **A19** (2004) 2879; Z. H. Guo, J. J. Sanz-Cillero and H.-Q. Zheng, JHEP **06** (2007) 030; J. Nieves, A. Pich and E. Ruiz Arriola, arXiv: 1107.3247 [hep-ph]; L. Y. Dai, X. G. Wang and H. Q. Zheng, arXiv: 1108.1451 [hep-ph].

[3] J. A. Oller and E. Oset, Phys. Rev. **D60** (1999) 074023; J. A. Oller, Phys. Lett. B **477** (2000) 187; J. A. Oller and U. G. Meissner, Phys. Lett. B **500** (2001) 263.

[4] Zhi-Hui Guo and J. A. Oller, Phys. Rev. **D84** (2011) 034005; Z. H. Guo, J. Prades and J. A. Oller, Nucl. Phys. Proc. Suppl. B **207-208** (2010) 184.

[5] K. Nakamura, *et al.*, (Particle Data Group), J. Phys. G 37 (2010) 075021.

Pion mass dependence of $\pi\pi$ phase shifts within standard and unitarized ChPT versus Lattice results

Jenifer Nebreda, José Ramón Peláez, and Guillermo Ríos
Departamento de Física Teórica II. Universidad Complutense de Madrid, 28040, Madrid, Spain

We report on our recent results in the study of the chiral extrapolation of the phase-shifts in elastic pion-pion scattering, using both standard and unitarized ChPT to one and two loops. In the standard ChPT approach, limited to low momenta, we study the S, P and D waves. Unitarization extends the analysis to energies of around 1 GeV, being compatible with standard ChPT at low energies for the S and P waves. We then compare with lattice results and find a good agreement of standard ChPT below 200 MeV for the I=2, J=0 and I=1, J=1 channels and up to 500 MeV for the I=2, J=2 channel. Unitarized ChPT improves the agreement in the scalar and vector channels at higher energies. We have also performed a Montecarlo analysis to provide an estimation of the uncertainties.

1 Introduction

Since the low-energy regime is beyond the reach of perturbative QCD, one may rely on lattice techniques in order to describe the hadronic processes in terms of quarks and gluons. However, Lattice QCD presents complications such as the implementation of chiral symmetry, the small physical values of the light quarks and the existence of quarkline disconnected diagrams. Thus, few lattice results on phase shifts are available, and those existing correspond to large pion masses. Fortunately, we can make use of Chiral Perturbation Theory (ChPT), which provides the quark mass dependence of the meson-meson scattering amplitudes in the low energy region, to compare its results to those of lattice studies by increasing the mass of the quarks up to the applicability limits of the theory.

Although in the conference we also commented on the resonance pole dependence on quark masses, here we only refer to the original reference [1] for such matters and prefer to concentrate on our recent study [2] of the phase shift dependence on the averaged u and d quark mass, $\hat{m}$, or, equivalently, on the pion mass, M_π. In particular, we include here novel calculations at $M_\pi = 266$ MeV in order to compare with very recent lattice results [3] on the I=1, J=1 phase shift, since this issue triggered some interesting discussions at this conference.

First, we will describe the standard one and two-loop SU(2) ChPT [4]. This approach has the advantage of being completely model independent but it is limited to the low energy region.

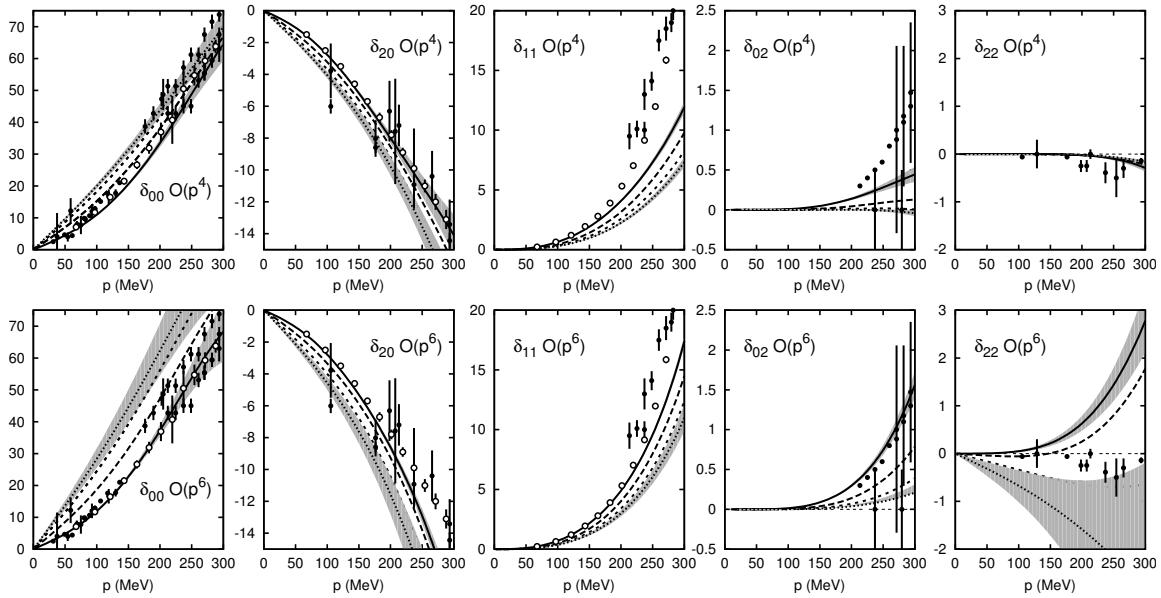

Figure 1: $\pi\pi$ phase shifts from standard ChPT up to one loop (first row) and to two loops (second row). Different lines stand for different pion masses: continuous, long dashed, short dashed and dotted for $M_\pi = 139.57$, 230, 300 and 350 MeV respectively. We only show error bands for the lightest and heaviest masses. Experimental data (circles) come from [7] (black circles) and the precise model independent dispersive data analysis from [8] (white circles).

This is the reason why we next extend our study to unitarized ChPT, using the well-known one-loop elastic Inverse Amplitude Method (IAM), which allows us to calculate the phase shift quark mass dependence up to higher values of M_π.

2 Quark mass dependence of $\pi\pi$ phase shifts

Standard ChPT We study the dependence of the $\pi\pi$ phase shifts on the pion mass M_π using the SU(2) scattering amplitudes in [4] and the LECs in [5], except for l_3^r that is taken from [6]. In Fig. 1 we show phases on different channels for different pion masses, to one and two loops (first and second row respectively). They are plotted as a function of the center of mass momentum -and not of the energy- in order to subtract the trivial effect of the threshold. A Montecarlo gaussian sampling based on the errors of the LECs has been used to calculate the error bands. We find that the dependence of the phase shifts on M_π is very soft at one loop and somehow stronger at two loops, specially for the I=2, J=2 channel.

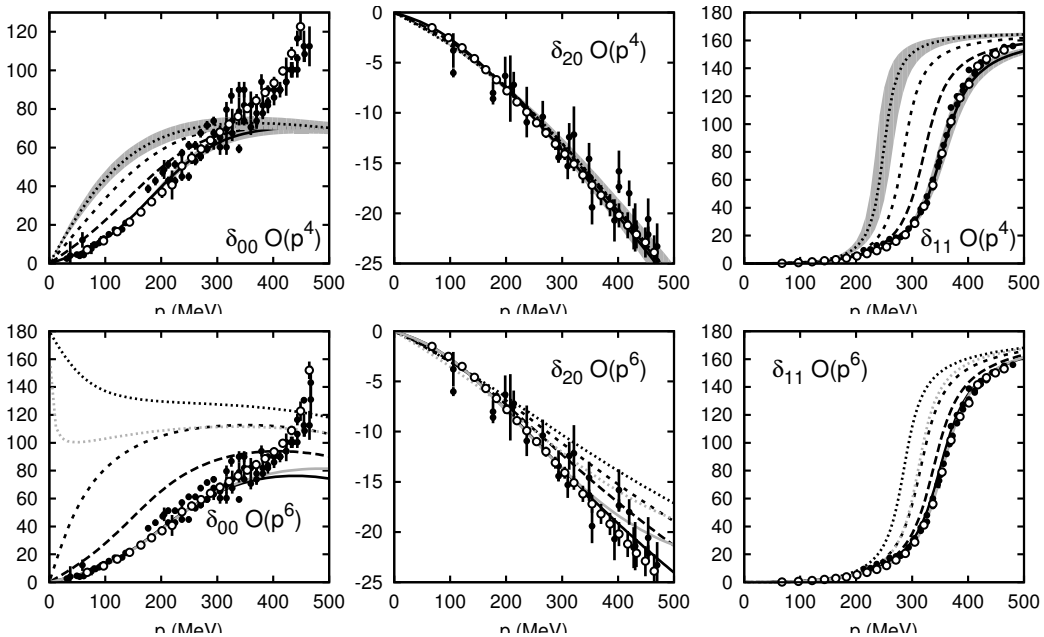

Figure 2: $\pi\pi$ phase shifts from unitarized ChPT up to one loop (upper row) and to two loops (lower row). Different lines stand for different pion masses: continuous, long dashed, short dashed and dotted for $M_\pi = 139.57$, 230, 300 and 350 MeV respectively. At one loop we show error bands only for the lightest and heaviest masses. At two loops no error analysis of the LECs has been carried out yet, thus we show results for the set of LECs called A in [9] and we add the results obtained with set D for the lightest and heaviest masses in light gray in order to give an idea of the size of the errors. Experimental data (rounded points) come from [7] (black circles) and the precise model independent dispersive data analysis from [8] (white circles).

Unitarized ChPT We use now the elastic IAM to unitarize our amplitudes, so that the applicability limit is extended to the elastic resonance region. In Fig. 2 we show $\pi\pi$ phase shifts (note that the one and two-loop IAM cannot be used for the D-waves) for different pion masses. For the one loop analysis (upper row) we used the LECs in [10] and for the two-loop analysis (lower row) we used the two sets A and D in [9]. We found that the dependence on the pion mass is again quite soft, specially for the I=2, J=0 channel and somewhat stronger at two loops than at one loop.

Comparison to lattice results In order to compare with lattice results [3, 11, 12], we show in Fig. 3 the $\pi\pi$ phase shifts in channels (I,J) = (2,0), (2,2) and (1,1) for higher pion masses, up to 444 MeV. Let us remark that this energy region is somewhat above the applicability limits of our method, which may provide precise results up to pion masses of, at most, 300-350 MeV. Therefore, our results at higher masses should be considered just qualitatively and, in fact, above $M_\pi = 450$ MeV we do not even show them here (see [2]). For these

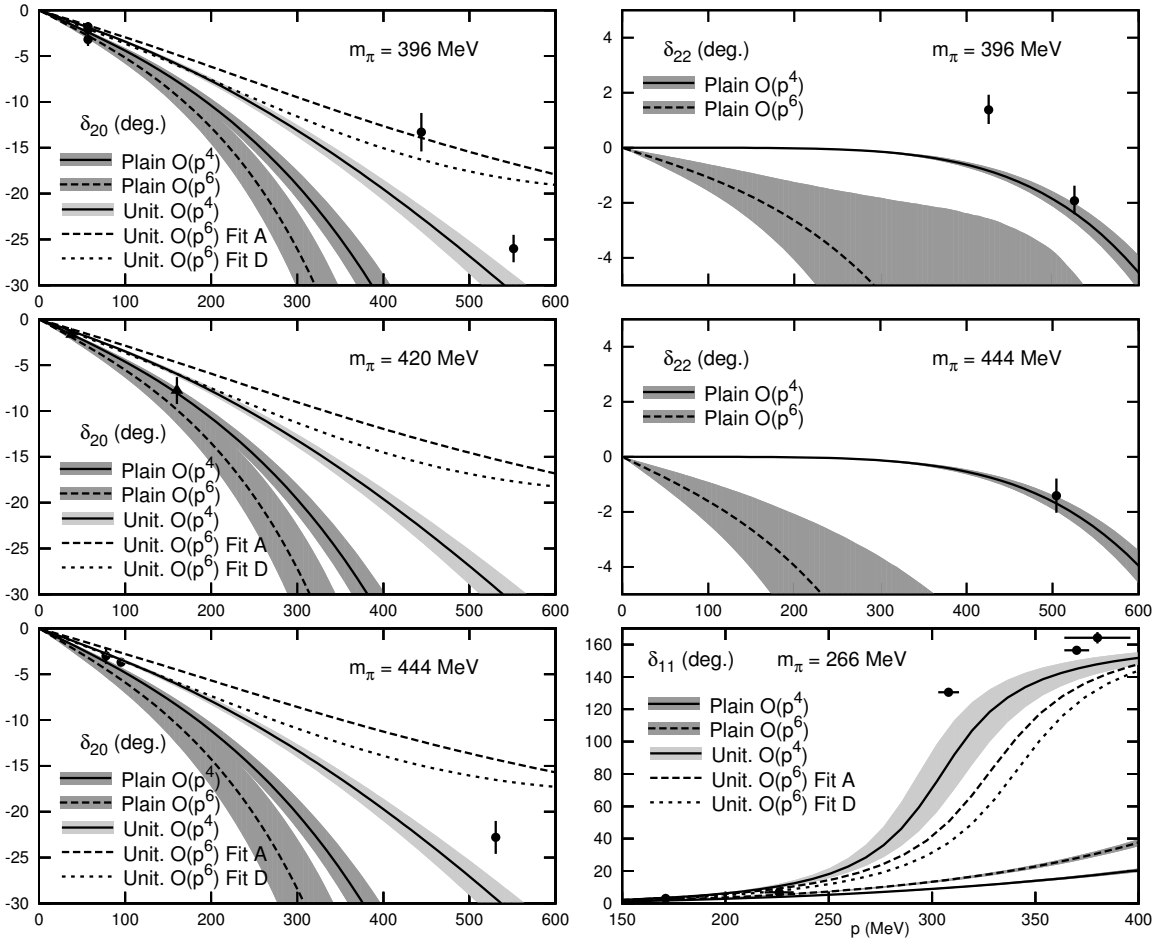

Figure 3: Left column: One and two-loop phase shifts from plain and unitarized ChPT for the I=2, J=0 channel compared to lattice results coming from [12] (circles) and [11] (triangles). **Right column, two upper panels:** One and two-loop phase shifts from plain ChPT for the I=2, J=2 channel compared to lattice results coming from [12] (circles). **Right column, lower panel:** One and two-loop phase shifts from plain and unitarized ChPT for the I=1, J=1 channel compared to lattice results coming from [3] (circles).

proceedings we have added a new calculation of the I=1, J=1 phase shift at $M_\pi = 266$ MeV in order to compare with the recent lattice results in [3] also presented at this conference. Standard ChPT shows a good agreement with lattice results below $p \simeq 200$ MeV up to pion masses of 400-450 MeV, while a nice improvement above 200 MeV is found when using unitarized ChPT for the scalar and vector channels.

Acknowledgments

We thank J. Dudek, D. Mohler and S. Prelovsek for lattice results and detailed explanations. Work partially supported by Spanish MICINN: FPA2007-29115-E, FPA2008-00592 and FIS2006-03438, U.Complutense/Banco Santander grant PR34/07-15875-BSCH and UCM-BSCH GR58/08 910309 and EU-Research Infrastructure Integrating Activity "Study of Strongly Interacting Matter" (HadronPhysics2, Grant 227431) under the EU Seventh Framework Programme.

Bibliography

[1] J. Nebreda and J. R. Pelaez., Phys. Rev. D **81**, 054035 (2010).

[2] J. Nebreda, J. R. Pelaez and G. Rios, Phys. Rev. D **83**, 094011 (2011).

[3] C. B. Lang, D. Mohler, S. Prelovsek and M. Vidmar, arXiv:1105.5636 [hep-lat].

[4] J. Bijnens *et al.*, Phys. Lett. B **374**, 210 (1996).

[5] G. Colangelo, J. Gasser and H. Leutwyler, Nucl. Phys. B **603**, 125 (2001).

[6] G. Colangelo *et al.*, Eur. Phys. J. C **71**, 1695 (2011).

[7] L. Rosselet *et al.*, Phys. Rev. D **15**, 574 (1977). S. Pislak *et al.* [BNL-E865 Collaboration], Phys. Rev. Lett. **87**, 221801 (2001) G. Grayer *et al.*, Nucl. Phys. B **75**, 189 (1974). S. D. Protopopescu *et al.*, Phys. Rev. D **7**, 1279 (1973). W. Hoogland *et al.*, Nucl. Phys. B **126**, 109 (1977). M. J. Losty *et al.*, Nucl. Phys. B **69**, 185 (1974). N. B. Durusoy *et al.*, Phys. Lett. B **45**, 517 (1973). P. Estabrooks and A. D. Martin, Nucl. Phys. B **79**, 301 (1974). B. Hyams *et al.*, Nucl. Phys. B **64**, 134 (1973). D. H. Cohen, T. Ferbel, P. Slattery and B. Werner, Phys. Rev. D **7**, 661 (1973). J. R. Batley *et al.* [NA48/2 Collaboration], Eur. Phys. J. C **54**, 411 (2008).

[8] R. Garcia-Martin *et al.*, Phys. Rev. D **83**, 074004 (2011).

[9] J. R. Pelaez and G. Rios, Phys. Rev. D **82**, 114002 (2010).

[10] C. Hanhart, J. R. Pelaez and G. Rios, Phys. Rev. Lett. **100**, 152001 (2008).

[11] K. Sasaki and N. Ishizuka, Phys. Rev. D **78**, 014511 (2008).

[12] J. J. Dudek *et al.*, Phys. Rev. D **83**, 071504 (2011).

The Search for Exotic Mesons in $\gamma p \to \pi^+\pi^+\pi^- n$ with CLAS at Jefferson Lab

Craig Bookwalter[1] on behalf of the CLAS Collaboration
Department of Physics
Florida State University
Tallahassee, FL 32306

The $\pi_1(1600)$, a $J^{PC} = 1^{-+}$ exotic meson has been observed by experiments using pion beams. Theorists predict that photon beams could produce gluonic hybrid mesons, of which the $\pi_1(1600)$ is a candidate, at enhanced levels relative to pion beams. The g12 rungroup at Jefferson Lab's CEBAF Large Acceptance Spectrometer (CLAS) has recently acquired a large photoproduction dataset, using a liquid hydrogen target and tagged photons from a 5.71 GeV electron beam. A partial-wave analysis of 502K $\gamma p \to \pi^+\pi^+\pi^- n$ events selected from the g12 dataset has been performed, and preliminary fit results show strong evidence for well-known states such as the $a_1(1260)$, $a_2(1320)$, and $\pi_2(1670)$. However, we observe no evidence for the production of the $\pi_1(1600)$ in either the partial-wave intensities or the relative complex phase between the 1^{-+} and the 2^{-+} (corresponding to the π_2) partial waves.

1 Introduction

Theoretical work indicates that photon beams may be able to abundantly produce gluonic hybrid mesons. The flux-tube model of Isgur and Paton [1] has been central in the theoretical study of gluonic hybrids, and the vector nature of the photon is optimal for promoting the flux-tube to an excited state, possibly producing hybrids in proportions equal to that of the $a_2(1320)$ [2]. Additionally, calculations on the lattice in the charmonium regime show a strong photocoupling for $c\bar{c}$ hybrids [3], which could bode well for the photoproduction of light exotics. Some of these states carry spin J, parity P, and C-parity that are inaccessible to ordinary $q\bar{q}$ matter. These exotic J^{PC} states are readily identified in experiment by means of partial-wave analysis. Light exotics have been searched for in pion production but photoproduction has remained largely unexplored until recently.

Members of the CLAS collaboration in Hall B at Jefferson Lab have completed two photoproduction experiments to look for light exotics. The first, completed in 2001 as part of the CLAS g6c rungroup, acquired 250K $\gamma p \to \pi^+\pi^+\pi^- n$ events in search of the $\pi_1(1600)$

[1] craigb@jlab.org

exotic, sighted first in pion production experiments [4], [5]. CLAS acceptance is optimized for baryon spectroscopy, so the partial-wave analysis was performed on a smaller set of 83K events where background from Δ and N^* decays had been removed by kinematic cuts. No evidence for a 1^{-+} exotic signal was found [6], a direct challenge to claims that gluonic hybrids could be produced on an equal footing with the $a_2(1320)$. However, statistics were insufficient to rule out a $\pi_1(1600)$ produced at the same level as it was observed in pion production, at a few percent of the a_2.

In order to look for $\pi_1(1600)$ photoproduction at lower levels, the HyCLAS experiment was proposed in 2004, with data taken in 2008 as a member of the CLAS g12 rungroup.

2 Features of the CLAS g12 Dataset

The g12 run of CLAS was completed in June of 2008, acquiring 26 billion events of various topologies. From these 26B triggers we have isolated 6 million exclusive $\gamma p \to \pi^+\pi^+\pi^-n$ events by vertex and timing cuts, with the neutron selected via missing mass. These events have either a mesonic topology, where $\gamma\ p \to\ Xn \to \pi^+\pi^+\pi^-n$, or a baryonic topology, where $\gamma\ p \to\ N^*\rho \to \pi^+\pi^+\pi^-n$, as can be seen by the light-shaded distributions in Figure 1. Our analysis depends on having a pure sample of mesonic events, so we selected events with the following criteria:

$$|t_{3\pi} - t_{min}| = |t'| < 0.105\ \mathrm{GeV}^2/c^4; \quad \theta_{lab}(\pi^+) < 25^\circ \text{ (both } \pi^+)$$

An example of the post-cut $n\pi$ mass distributions, as well as the resulting 3π mass distribution can also be found in Figure 1.

3 Partial-Wave Analysis of $\gamma\ p \to \pi^+\pi^+\pi^-n$ in CLAS g12 Data

We then subjected the final sample of 502K events to a partial-wave analysis based on the helicity formalism. Decay amplitudes are calculated in the reflectivity basis to ensure parity conservation, and then each is paired with a complex production amplitude. Those production amplitudes were then varied in a likelihood fit to find the most probable mixture of states given the set of input events. We then examine the norm of each production amplitude to look for peaks, as well as examining the phase difference between pairs of production amplitudes to look for movement corresponding to the interference of two Breit-Wigner distributions.

In particular, the fit presented contains 19 waves spread among four J^{PC}: 1^{++}, 2^{++}, 1^{-+}, and 2^{-+}. Since the helicity of the photon is constrained to be ± 1 and π exchange is the dominant production mechanism, we should not observe any spin-0 states, one of the most complicated features of pion-production analyses. Thus, most of the intensity is allocated

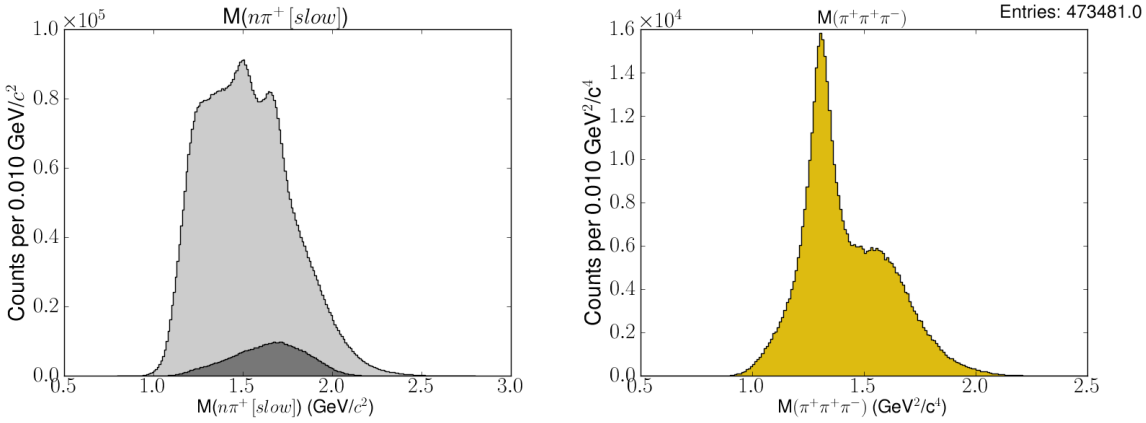

Figure 1: Left, the invariant mass of the neutron-π^+ system for the slow π^+, where the lighter pre-cut region shows N^* peaks and the darker region is what remains after kinematic cuts. **Right**, the 3π invariant mass distribution after the kinematic selections are applied. The prominent peak is in the region where one would expect an $a_2(1320)$, while a shoulder exists in the $\pi_2(1670)$ region.

to the M=1 waves. However, in the 1^{++} waves, shown in the first row of Figure 2, the M=0 makes a significant contribution. It is possible that these events are due to a $\rho\pi$ system produced in the S-wave via a Deck process. The M=1 waves of the 1^{++} show evidence for the $a_1(1260)$ in the S-wave $\rho\pi$ decay; interpretation of the 1^{++}D M=1 waves is not as clear presently.

The 2^{++} waves, illustrated in the middle row of Figure 2, show strong evidence for the presence of the $a_2(1320)$ in this data sample. The 2^{++}D M=0 wave was omitted because when included, it has zero intensity, as one would expect for an $a_2(1320)$ produced via pion exchange from a photon beam. We can test our resonant interpretation of the 1^{++}S and 2^{++}D intensities by examining their phase difference. The results, illustrated in the middle right plot of Figure 2, seem to indicate the presence of the $a_1(1260)$ and $a_2(1320)$ in our sample.

The 2^{-+} waves, illustrated in the bottom row of Figure 2, show strong evidence for the presence of the $\pi_2(1670)$ in our sample as well. Both the 2^{-+} $(f_2(1270)\pi)_S$ and 2^{-+} $(\rho\pi)_P$ show broad enhancements reminscent of Breit-Wigner shapes, with the $f_2\pi$ decay the dominant mode, as one would expect from branching ratios reported by the PDG. Also if the Deck effect is present in this channel, we should also observe it in the 2^{-+} M=0 waves. Only the $(f_2\pi)_S$ M=0 wave is included in this fit, but one can indeed see a small peak in its intensity.

Finally, the exotic 1^{-+} waves, as illustrated in Figure 3, do not show resonant structure in their intensities. Furthermore, examining the phase difference relative to the 2^{-+} M=1 $(f_2\pi)_S$ waves, one finds no motion indicative of a resonance. In fact, as also illustrated in

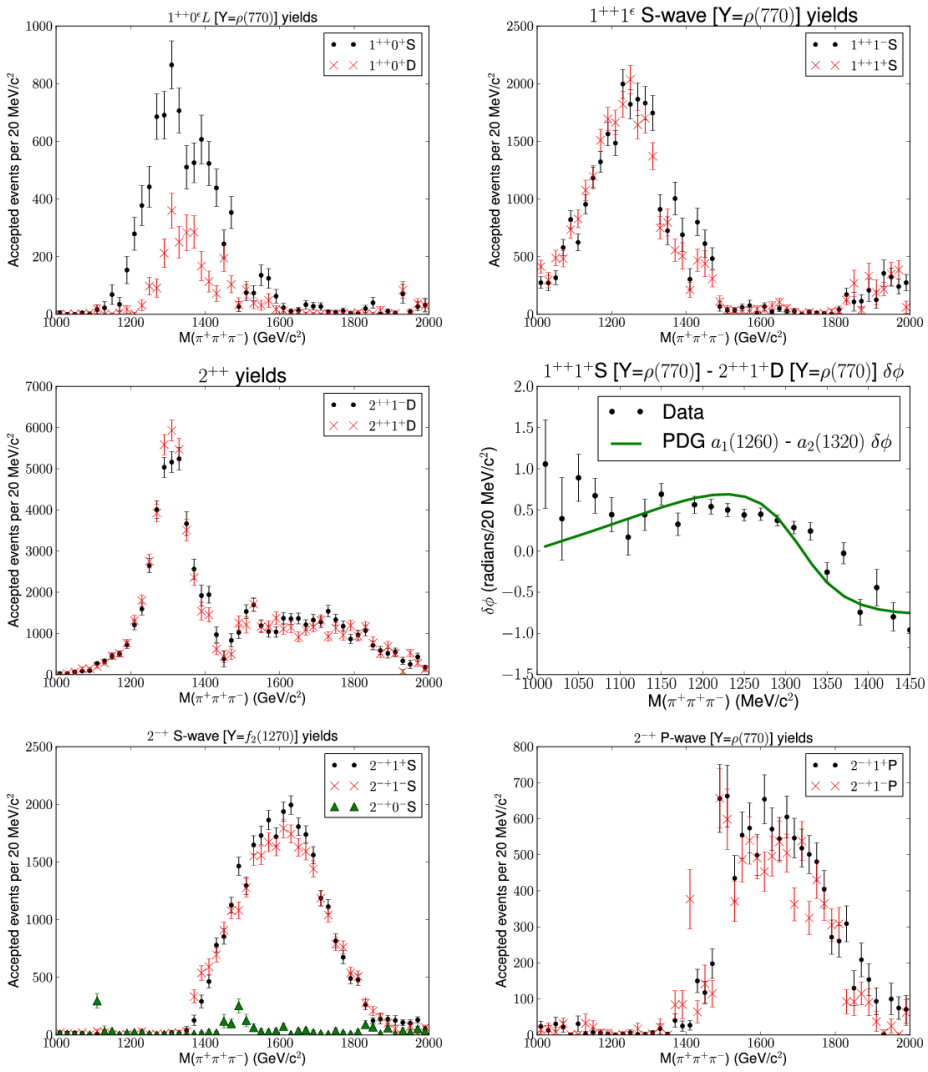

Figure 2: Top row: accepted yields for 1^{++} waves. The yields for the M=0 waves on the left are a possible signature for the Deck effect in photoproduction, as a photon beam exchanging a π forbids any states from being produced with M=0. On the right, the $(\rho\pi)_S$ decay of the 1^{++} shows strong evidence for the $a_1(1260)$. **Middle row**: on the left, the accepted yields of the 2^{++}, showing strong evidence for the presence of the $a_2(1320)$. The two reflectivities are populated equally because of the circular polarization of the photon beam used in the experiment. On the right, the phase difference between the $1^{++}1^+$S and $2^{++}1^+$D waves. Overlaid is the phase difference between two Breit-Wigner amplitudes constructed with the mass and width reported by the Particle Data Group. **Bottom row**: accepted yields for the largest 2^{-+} contributors. The intensity for the $(f_2\pi)_S$ decay on the left, along with the $(\rho\pi)_P$ decay on the right, shows good evidence for the presence of the $\pi_2(1670)$.

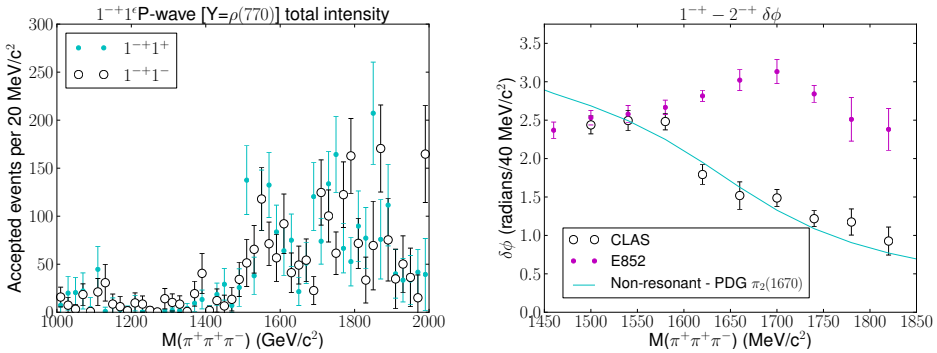

Figure 3: On the **left**, the intensities of the 1^{-+} M=1 waves are plotted, showing no clear evidence for resonant structure, as is true for the 1^{-+} M=0 wave (not shown). On the **right** is an overlay of the 1^{-+} - 2^{-+} phase motion for both the presented CLAS result and the results reported by E852 in [4]. One can see a clear turning-over of the E852 phase, indicative of interference between two Breit-Wigner forms. The CLAS phase has a steady decrease, indicative of a resonating π_2 being subtracted from a nonresonant 1^{-+}, as shown by the curve.

Figure 3, one can compare directly between the phase observed in [4] and the phase we observe, and where there is a clear turning-over in the E852 data, our data shows a clear downward trend, indicative of a resonant 2^{-+} subtracted from a nonresonant background.

Thus our preliminary conclusion is that there is no evidence for the presence of a 1^{-+} resonance in our data sample. These results are not necessarily in conflict with past pion-production results; the analyses in [4] and [5] examine diffractive processes while this analysis proceeds via charge exchange. Thus we can explain the discrepancy if we posit that the $\pi_1(1600)$ is produced via Pomeron exchange.

Bibliography

[1] N. Isgur and J. E. Paton, Phys. Lett. B **124**, 247 (1983).

[2] F. E. Close and P. R. Page, Phys. Rev. D **52**, 1706 (1995)

[3] J. J. Dudek, R. Edwards and C. E. Thomas, Phys. Rev. D **79**, 094504 (2009) [arXiv:0902.2241 [hep-ph]].

[4] S. U. Chung *et al.*, Phys. Rev. D **65**, 072001 (2002).

[5] A. Alekseev [The COMPASS Collaboration], arXiv:0910.5842 [hep-ex].

[6] M. Nozar *et al.* [CLAS Collaboration], Phys. Rev. Lett. **102**, 102002 (2009) [arXiv:0805.4438 [hep-ex]].

The exotic $\eta'\pi^-$ Wave in $190\,\mathrm{GeV}$ $\pi^- p \to \pi^-\eta' p$ at COMPASS

Tobias Schlüter[1] on behalf of the COMPASS Collaboration
Ludwig-Maximilians-Universität München, Department für Physik, 85748 Garching, GERMANY

A sample of 35 000 events of the type $\pi^- p \to \eta'\pi^- p_{\mathrm{slow}}$ ($\eta' \to \eta\pi^-\pi^+$, $\eta \to \gamma\gamma$) with $-t > 0.1\,\mathrm{GeV}^2/c^2$ was selected from COMPASS 2008 data for a partial-wave analysis. We study the broad P_+ structure known from previous experiments at lower energies, in particular its phase motion relative to the D_+-wave near the $a_2(1320)$ mass and relative to a broad D_+-wave structure at higher mass. We also find the $a_4(2040)$. We compare kinematic plots for the $\eta'\pi^-$ and $\eta\pi^-$ final states.

1 Introduction

The existence of strongly-bound, resonant states with quantum numbers not allowed for a fermion-antifermion system has long been expected. In the light-quark sector isospin symmetry also disallows such a state for charged $u\bar{d}$, $d\bar{u}$ mesons. On the other hand, a system decaying into the two pseudo-scalar mesons π, η (π, η') with orbital angular momentum $L = 1$ has quantum numbers $J^{PG} = 1^{-+}$, and thus any resonant contribution to such a system would have to be identified with a non-$q\bar{q}$ resonance.

Indeed, several collaborations claimed the observation of such a resonance in the $\eta\pi$ system at $m(\eta\pi) \approx 1.4\,\mathrm{GeV}/c^2$ [1–3]. Likewise a very strong P-wave contribution was observed in the $\eta'\pi^-$ system [1, 4] at $m(\eta'\pi) \approx 1.6\,\mathrm{GeV}/c^2$, but the resonant character of the structure observed in both systems has been questioned [5].

We report on the current status of the analysis of the $\eta'\pi^-$ and $\eta\pi^-$ final states as observed in the data from the 2008 run of the COMPASS experiment at CERN and compare our results to the above-quoted publications. The COMPASS experimental setup [6, 7] is a two-stage magnetic spectrometer attached to the SPS accelerator facility at CERN. During the bulk of the 2008/09 campaigns the experiment's goal was the study of the light meson spectrum. A $190\,\mathrm{GeV}/c$ secondary pion beam impinged on a liquid hydrogen target. The main trigger components were a beam definition trigger together with a recoil proton detector (RPD). The RPD ensured an unscathed proton emitted at large angles with momentum corresponding to momentum transfer $-t \gtrsim 0.1\,\mathrm{GeV}^2$. A veto counter near the spectrometer

[1] tobias.schlueter@cern.ch

entry further suppressed events with particles emitted at large angles, especially from target fragmentation [8, 9]. An additional veto suppressed events where the beam particle passed through the target undeflected. Both stages of the spectrometer are equipped with tracking detectors and particle identification and neutral detection by means of electromagnetic and hadronic calorimetry. In addition, the first spectrometer stage is equipped with a Ring-Imaging Cherenkov detector, allowing for particle identifcation.

2 Data Selection

Besides trigger requirements, the events considered were selected by the following topological criteria: a well-defined primary interaction vertex inside the target with three outgoing tracks (assumed to be pions) attached and two clusters in the electromagnetic calorimeters. In order to select the intended $\pi^-\eta'$ and $\pi^-\eta$ final states, the invariant mass obtained by attaching the pair of calorimeter clusters to the primary vertex was required to fall into the range of the η or π^0 mass, respectively. The so-identified neutral particle was then — after a 1C kinematic fit — combined with both possible $\pi^-\pi^+$ pairs. If the invariant mass of either combination was found to match the $\eta' \to \pi^-\pi^+\eta$ or, respectively, $\eta \to \pi^-\pi^+\pi^0$ hypothesis, the event was accepted after additional cuts on the total momentum. The procedure yielded 35 000 events for the $\pi^-\eta'$ final state and 110 000 events for the $\pi^-\eta$ final state. The intermediate steps are illustrated in Fig. 1 for the selection of the $\eta'\pi^-$ final state. The $\eta\pi^-$ selection is similar.

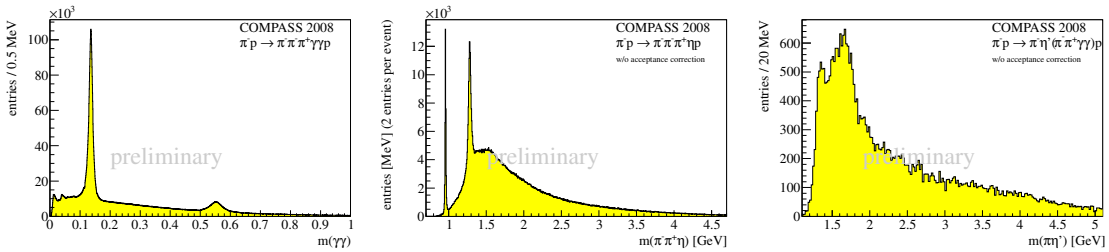

Figure 1: Data selection. Left: $\gamma\gamma$ mass spectrum for events with three charged tracks. The $\pi^0(135)$ and $\eta(548)$ peaks are clearly visible. Center: $\pi^-\pi^+\eta$ mass spectrum for kinematically complete events. Two peaks corresponding to $\eta'(958)$ and $f_1(1285)$ stand out. Right: Final $\pi^-\eta'$ mass spectrum. The peak of the $a_2(1320)$ is visible near threshold.

3 Final-State Kinematics

The data are expected to be dominated by natural parity exchange waves with $M = 1$, both from the favored pomeron exchange and from the results of previous analyses. This is easily verified by plotting the angle ϕ between decay and production plane in the

mass bin [GeV/c^2]	fit with $A\exp(-B\lvert t\rvert)$	fit with $A\lvert t\rvert\exp(-B\lvert t\rvert)$
$m < 1.5$	5.5	8.2
$1.5 < m < 1.9$	5.1	7.5
$1.9 < m < 2.2$	4.8	7.1
$2.2 < m < 3$	4.6	6.9

Table 1: Fit to the slope parameter B in units of GeV^{-2} for momentum transfer as function of mass. E852 found the much broader $B = 2.93\,\text{GeV}^{-2}$ when fitting with a single exponential.

Gottfried-Jackson frame [10] where the $\sin^2\phi$ contribution dominates (not shown). The remainder of the kinematical information is contained in the momentum transfer t, the polar angle of the η or η' meson in the GJ frame $\cos\theta_{\text{GJ}}$, and the invariant mass m of the two-body system under consideration. In Fig. 2 the distribution of $\cos\theta_{\text{GJ}}$ as function of m is shown for both the $\eta\pi^-$ and $\eta'\pi^-$ systems. Outstanding features are the occurence of the $a_2(1320)$ meson, a structure near 2 GeV/c^2 corresponding to the $a_4(2040)$ meson, whose intereference with a spin-2 background can be made out in the $\eta\pi^-$ data, and a strong forward-backward peaking for masses above 2 GeV/c^2, pointing towards non-resonant contributions. Especially in the $\eta'\pi^-$ data a strong forward backward asymmetry is observed in the data, with a fast turnover around the $a_2(1320)$ mass range, corresponding to relative phase motion of the odd (P_+) and even (D_+) contributions.

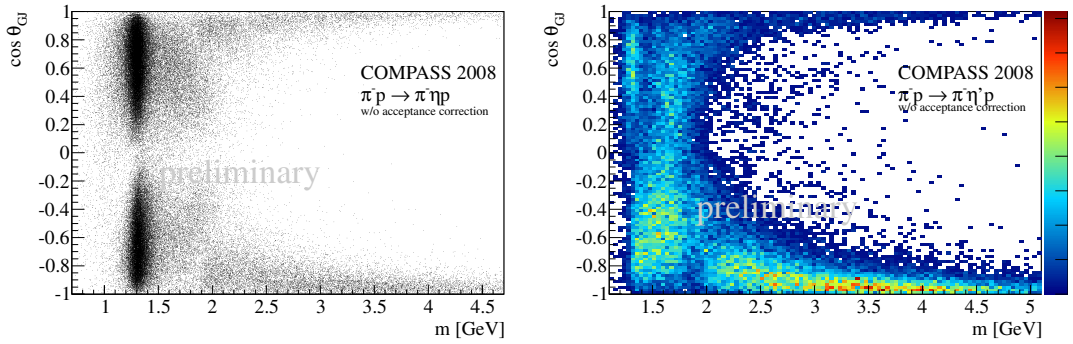

Figure 2: Kinematics. The distribution in $\cos\theta_{\text{GJ}}$ as function of invariant mass m (not acceptance corrected). Left for the $\eta\pi^-$ system, right for the $\eta'\pi^-$ system.

The E852 experiment claimed an unusual momentum transfer distribution in the production of the $\eta'\pi^-$ system [4]. We cannot confirm this observation, see Tab. 1.

4 Partial-Wave Analysis of the $\eta'\pi^-$ System

In this section we present the results of a partial-wave analysis in mass bins of the $\eta'\pi^-$ data. The analysis follows the lines of the previous analyses, allowing S, P, and D waves with $M \leqslant 1$ in both natural and unnatural exchange. Additionally, the spin-4, $M = 1$ G_+-wave was allowed. The η' was separated from the $\pi^-\pi^+\eta$ background by introducing its experimental shape as a pseudo-isobar and fitting in the complete 4-body phase-space where besides the $\pi^-\eta'$ waves an additional incoherent flat, phase-space-like contribution was allowed. From these ingredients an extended log-likelihood function is constructed and maximized, taking into account the detector acceptance via normalization integrals calculated from Monte-Carlo data. The results for the intensities of the positive-reflectivity wave are shown in Fig. 3. The relative phases are shown in Fig. 4.

We confirm the presence of a broad structure in the P_+-wave of the $\eta'\pi^-$. A fit to the intensity of this structure by a single-channel relativistic Breit-Wigner shape underestimates the high-mass side of the distribution. We confirm the presence of the $a_4(2040)$ resonance in this channel previously seen by E852 [4]. This resonance is also visible in the 3π data [11]. A resonant interpretation of the P_+-wave would have to be reconciled with the relative phase-motions compared to the other waves, and the apparent onset of double-Regge production or similar processes above $\approx 2\,\text{GeV}$ whose low-mass impact is not yet understood.

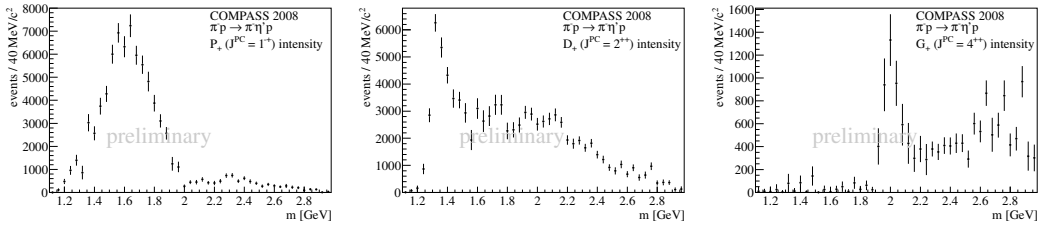

Figure 3: Intensities of the positive-reflectivity waves. From left to right: P_+, D_+, G_+.

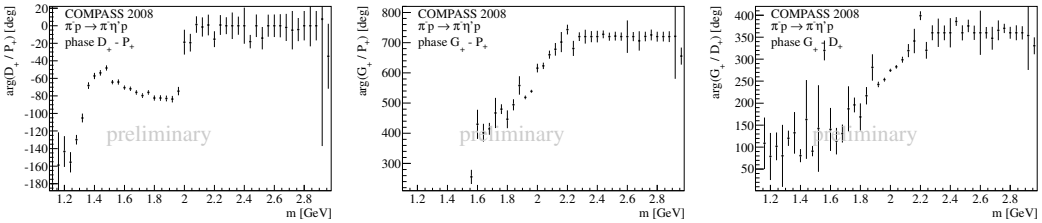

Figure 4: Relative phases of the positive-reflectivity waves. From left to right in obvious notation: $D_+ - P_+$, $G_+ - P_+$, $G_+ - D_+$.

Acknowledgments

We acknowledge financial support by the German Bundesministerium für Bildung und Forschung (BMBF), by the Maier-Leibnitz-Laboratorium der LMU und TU München, and by the DFG cluster of excellence "Origin and Structure of the Universe".

Bibliography

[1] **VES** Collaboration, G. Beladidze *et al.*, "Study of $\pi^- N \to \eta\pi^- N$ and $\pi^- N \to \eta'\pi^- N$ reactions at 37 GeV/c," *Phys. Lett.* **B313** (1993) 276–282.

[2] **E852** Collaboration, D. Thompson *et al.*, "Evidence for Exotic Meson Production in the Reaction $\pi^- p \to \eta\pi^- p$ at 18 GeV/c," *Phys. Rev. Lett.* **79** (1997) 1630–1633, arXiv:hep-ex/9705011.

[3] **Crystal Barrel** Collaboration, A. Abele *et al.*, "Exotic $\eta\pi$ state in $\overline{p}d$ annihilation at rest into $\pi^-\pi^0\eta p_{\text{spectator}}$," *Phys. Lett.* **B423** (1998) 175–184.

[4] **E852** Collaboration, E. I. Ivanov *et al.*, "Observation of exotic meson production in the reaction $\pi^- p \to \eta'\pi^- p$ at 18 GeV/c," *Phys. Rev. Lett.* **86** (2001) 3977–3980, arXiv:hep-ex/0101058.

[5] A. Szczepaniak, M. Swat, A. Dzierba, and S. Teige, "Study of the $\eta\pi$ and $\eta'\pi$ spectra and interpretation of possible exotic $J^{PC} = 1^{-+}$ mesons," *Phys. Rev. Lett.* **91** (2003) 092002, arXiv:hep-ph/0304095.

[6] **COMPASS** Collaboration, P. Abbon *et al.*, "The COMPASS Experiment at CERN," *Nucl. Instr. and Meth. A* **577** (2007) 455–518, arXiv:hep-ex/0703049.

[7] **COMPASS** Collaboration, M. Alekseev *et al.*, "The COMPASS Setup for Physics with Hadron Beams." In preparation.

[8] **COMPASS** Collaboration, T. Schlüter, "The COMPASS sandwich veto detector and a first look at kaonic final states from a π^-(190 GeV) beam on a proton target," *Eur. Phys. J.* **C** SPIN-Praha-2009, to be published, arXiv:1108.4295 [hep-ex].

[9] T. Schlüter *et al.*, "Large-Area Sandwich Veto Detector with WLS Fibre Readout for Hadron Spectroscopy at COMPASS," *Nucl. Instr. and Meth. A* (2011) In Press, Corrected Proof, arXiv:1108.4587 [physics.ins-det].

[10] K. Gottfried and J. D. Jackson, "On the Connection between Production Mechanism and Decay of Resonances at High Energies," *Nuovo Cim.* **33** (1964) 309–330.

[11] **COMPASS** Collaboration, F. Nerling, These proceedings, arXiv:1108.5969 [hep-ex].

Properties of light scalar mesons in the complex plane

Bachir Moussallam
Groupe de physique théorique, IPN, Université Paris-sud 11, 91406 Orsay, France

The flavour and glue structure of the light scalar mesons in QCD are probed by studying the couplings of the $\sigma(600)$ and $f_0(980)$ to the operators $\bar{q}q$, θ^μ_μ and to two photons.

1 Introduction

A precise identification of the exotic contents of the light scalar mesons is an old challenge for hadron physics. The idea of using the Roy dispersive representations in the complex plane [1] decisively clarified the status of the broad σ resonance and led to an accurate determination of its mass and width. The $I = 0$ scalars have the same quantum numbers as the expected lightest glueball. If all quark masses were heavy in QCD ($m_q \gtrsim 1GeV$) the glueball would be an extremely narrow meson (decaying only to two photons) with a mass slightly below two GeV [2]. Properties of the glueball in physical QCD, i.e. with three light quarks, are not yet computable in lattice simulations. A scenario suggested in [3] is that there could be two glueballs below 2 GeV, the lightest one could be the σ. Another question concerns the identification of a flavour multiplet: do the σ, κ, $a_0(980)$, $f_0(980)$ mesons belong to a nonet? This is far from obvious, e.g. several properties of the $a_0(980)$, $f_0(980)$ seem well explained by a $K\overline{K}$ molecule model [4]. I discuss below the evaluation of couplings of the σ and $f_0(980)$ to operators j_S using complex plane methods, which should provide quantitative inputs for answering some of these questions on the light scalars. Taking $j_S = \theta^\mu_\mu$ probes the gluon content, while $j_S = \overline{u}u + \overline{d}d$, $\overline{s}s$ probes the quark-antiquark content. The couplings to two photons will also be updated.

2 Poles and residues from an extended S-wave Roy solution:

Pion-pion partial-wave amplitudes obey a set of coupled integral representations as a consequence of analyticity and crossing symmetry [5]. On the real axis, at low energy, they combine with the unitarity relation into a set of non-linear equations which strongly constrain the S and the P-wave amplitudes. These equations were reconsidered recently in great detail [6]. Solutions were generated for given scattering lengths a_0^0, a_0^2 with a matching point $\sqrt{s_A} = 0.8$ GeV (i.e. using experimental inputs for $s > s_A$). The new experimental

results on K_{l4} decays, analyzed with these solutions lead to very precise determinations of the scattering lengths [7]

$$a_0^0 = 0.2196 \pm 0.0028_{\text{stat}} \pm 0.0020_{\text{sys}}, \tag{1}$$
$$a_0^2 = -0.0444 \pm 0.0007_{\text{stat}} \pm 0.0005_{\text{sys}} \pm 0.0008_{\text{ChPT}}$$

In order to improve the constraints on the $f_0(980)$ resonance, we begin by constructing a solution for the $I = 0$ S-wave over an extended region with a matching point $s_K = 4m_K^2$. Increasing the matching point from s_A to s_K leads to two differences: a) the matching point coincides with a two-particle threshold, the phase-shift has a cusp and one cannot use the continuity of the derivative argument to eliminate unphysical solutions, b) the multiplicity of the solutions (which depends on the phase-shift at the matching point [8]) increases by one unit. It turns out that unphysical solutions can still be identified provided the phase-shift is not too large ($\delta_K = \delta_0^0(s_K) \lesssim 225^\circ$). The solutions then depend on one arbitrary parameter which can be taken as the value of the phase at one energy, e.g. $\delta_A = \delta_0^0(s_A)$. It is then determined by fitting the experimental phase-shifts in the range $[s_A, s_K]$ with the Roy solutions. One, in fact, can fit not only δ_A but also δ_K which is not very accurately determined from the data above s_K.

η_0^0	δ_A	δ_K	$\hat{\chi}^2_{\text{Hyams}}$	$\hat{\chi}^2_{\text{Kaminski}}$
shallow	$(80.9 \pm 1.4)^\circ$	$\left(190^{+5}_{-10}\right)^\circ$	2.7	1.9
deep	$(82.9 \pm 1.7)^\circ$	$\left(200^{+5}_{-10}\right)^\circ$	2.2	1.3

Table 1: Fitted values of δ_A and δ_K corresponding to two different central values (shallow-dip, deep-dip) for η_0^0.

The shape of the inelasticity, which sets in effectively at $s \geqslant s_K$ affects the phase-shift below s_K via the Roy equation. The central value of η_0^0 fitted to the determination from $\pi\pi$ production experiments displays a deep dip structure [9]. The one based on the inelastic channels displays a shallower dip (while compatible within the errors). The recent analysis of ref. [11], using constraints from a variant of the Roy equations in the region $\sqrt{s} \leqslant 1.1$ GeV, favours a deep dip structure. Our fit leads to the same conclusion, see table 1.

	$\sqrt{z_S}$ (MeV)	$\dot{S}_0^0(z_S)$ (GeV^{-2})
$\sigma(600)$	$\left(442^{+5}_{-8}\right) - i\left(274^{+6}_{-5}\right)$	$-\left(0.75^{+0.10}_{-0.15}\right) - i\left(2.20^{+0.14}_{-0.10}\right)$
$f_0(980)$	$\left(996^{+4}_{-14}\right) - i\left(24^{+11}_{-3}\right)$	$-\left(1.1^{+3.0}_{-0.4}\right) - i\left(6.6^{+0.8}_{-1.0}\right)$

Table 2: Poles and S-matrix derivatives from the extended Roy solution.

Next, one can compute the amplitude for complex energies. The position of the poles on the second Riemann sheet correspond to the zeros of the S-matrix $S_0^0(z) = 1 - 2\sigma^\pi(z)t_0^0(z)$ (see e.g. [1]) with $\sigma^\pi(z) = \sqrt{4m_\pi^2/z - 1}$. The results for the zeros and for the corresponding derivatives of S_0^0 (needed for the determination of the residues) are shown in table 2.

3 Couplings to two photons

Couplings of the light scalars to two photons can be determined from the amplitudes $\gamma\gamma \to \pi^0\pi^0, \pi^+\pi^-$. As a consequence of analyticity and unitarity, the partial-wave amplitudes $h^I_{J,\lambda\lambda'}(s)$ satisfy Omnès-type dispersive representations. A two-channel representation for $h^0_{0,++}(s)$ was reconsidered recently [12]. It should be valid in a range $\sqrt{s} \lesssim 1.1 - 1.2$ GeV where it is a good approximation to retain just two channels ($\pi\pi$, $K\overline{K}$) in the unitarity relation and has the form

$$(2)\quad \begin{pmatrix} h^0_{0,++}(s) \\ k^0_{0,++}(s) \end{pmatrix} = \begin{pmatrix} \bar{h}^{0,Born}_{0,++}(s) \\ \bar{k}^{0,Born}_{0,++}(s) \end{pmatrix} + \overline{\overline{\Omega}}(s) \times \left[\begin{pmatrix} b^{(0)}s + b'^{(0)}s^2 \\ b^{(0)}_K s + b'^{(0)}_K s^2 \end{pmatrix} + \frac{s^3}{\pi}\int_{-\infty}^{-s_0} \frac{ds'}{(s')^3(s'-s)} \times \right.$$
$$\left. \overline{\overline{\Omega}}^{-1}(s')\mathrm{Im} \begin{pmatrix} \bar{h}^{0,Res}_{0,++}(s') \\ \bar{k}^{0,Res}_{0,++}(s') \end{pmatrix} - \frac{s^3}{\pi}\int_{4m_\pi^2}^{\infty} \frac{ds'}{(s')^3(s'-s)} \mathrm{Im}\,\overline{\overline{\Omega}}^{-1}(s') \begin{pmatrix} \bar{h}^{0,Born}_{0,++}(s') \\ \bar{k}^{0,Born}_{0,++}(s') \end{pmatrix} \right].$$

The key ingredient in this equation is the Omnès matrix $\overline{\overline{\Omega}}$ which must be computed numerically from the T-matrix. Eq. (2) involves integrals over the left-hand cut of the amplitude which is generated by cross-channel singularities: the pion pole ($\bar{h}^{I,Born}_{0,++}$) and multi-pion cuts which are approximated by resonance poles. It also involves four polynomial parameters which appear upon writing over-subtracted dispersion relations such as to cutoff contributions from higher energy regions. They were determined in ref. [12] from a chirally constrained fit of the Belle data [13]. The representation (2) then allows one to compute the amplitude $h^0_{0,++}(s)$ for complex values of s. Extension to the second Riemann sheet is performed from standard formulas [14] involving $S^0_0(s)$. The couplings $g_{S\pi\pi}$ and $g_{S\gamma\gamma}$ are identified from the residues and one then defines the 2γ decay width [14] in terms of $|g_{S\gamma\gamma}|$. We find the following results for the σ and $f_0(980)$ (in KeV)

$$(3)\qquad \Gamma_{\sigma(600)\to 2\gamma} = \left(2.08 \pm 0.20\,^{+0.07}_{-0.04}\right),\ \Gamma_{f_0(980)\to 2\gamma} = \left(0.29 \pm 0.21\,^{+0.02}_{-0.07}\right).$$

The result for the σ agrees with that presented by Hoferichter at this conference and is somewhat smaller than the one in ref. [14].

4 Couplings to gluonic and quark-antiquark operators

Let us introduce, formally at first, couplings of the scalar mesons to $\bar{q}q$ operators and to the trace of the energy-momentum tensor θ^μ_μ,

$$(4)\qquad \langle 0|\bar{u}u + \bar{d}d|S\rangle = \sqrt{2}B_0\, C^{uu}_S, \quad \langle 0|\bar{s}s|S\rangle = B_0\, C^{ss}_S, \quad \langle 0|\theta^\mu_\mu|S\rangle = m_S^2\, C^\theta_S\,.$$

In order to give precise meaning to these one considers the correlators

$$(5)\qquad \Pi_{jj}(p^2) = i\int d^4x\, e^{ipx}\langle 0|T j_S(x) j_S(0)|0\rangle$$

where $j_S(x)$ is one of the scalar operators considered above. The discontinuity along the cut in the elastic region $4m_\pi^2 \leqslant s \leqslant 16m_\pi^2$ follows from the Källen-Lehmann representation and allows one to deduce the expression for the second sheet extension of the correlator,

$$\Pi_{jj}^{II}(z) = \Pi_{jj}(z) + \frac{3}{16\pi}\frac{\sigma^\pi(z)\left(F_j(z)\right)^2}{1-2\sigma^\pi(z)t_0^0(z)} \,. \tag{6}$$

$F_j(s)$ is the pion form factor associated with j_S. $\Pi_{jj}^{II}(z)$ exhibits poles at $z = z_S$ corresponding to the scalar mesons. The coupling constants (4) are naturally identified from the residues and are thus determined in the terms of the value of the form-factor $F_j(z_S)$.

Analyticity properties of the form-factors allows them to be expressed in terms of the Omnès matrix. For this purpose, one considers the two component vector $\overline{F}(s)$ such that $\overline{F}_1(s) = F_j^\pi(s)$, $\overline{F}_2(s) = 2/\sqrt{3}F_j^K(s)$. Multiplying $\overline{F}(s)$ by the inverse of the Omnès matrix removes the right-hand cut up to a point s_2 where two-channel unitarity is no longer a good approximation. One then deduces that in the region $|s| \lesssim s_2$ the form-factors obey the following representation,

	$\sigma(600)$	$f_0(980)$
$\lvert C_S^{uu}\rvert$	$206 \pm 4^{+4}_{-6}$	$82 \pm 31^{+12}_{-7}$
$\lvert C_S^{ss}\rvert$	$17 \pm 5^{+1}_{-7}$	$146 \pm 44^{+14}_{-7}$
$\lvert C_S^{\theta}\rvert$	$197 \pm 15^{+21}_{-6}$	$114 \pm 44^{+22}_{-7}$

Table 3: *Absolute values (in MeV) of the couplings of the σ and $f_0(980)$ to operators.*

$$\begin{pmatrix} F_j^\pi(s) \\ \frac{2}{\sqrt{3}}F_j^K(s) \end{pmatrix} = \begin{pmatrix} \Omega_{11}(s) & \Omega_{12}(s) \\ \Omega_{21}(s) & \Omega_{22}(s) \end{pmatrix} \begin{pmatrix} \alpha + \alpha' s \\ \beta + \beta' s \end{pmatrix} \,. \tag{7}$$

The polynomial parameters in eq. (7) can be estimated from the chiral expansion at leading order [15]. The magnitudes of the resulting couplings are shown in table 3: the first and second error in the entries reflect the uncertainties in the polynomial parameters and in the Omnès matrix respectively .

In summary, one finds that both the σ and the $f_0(980)$ couple significantly to θ_μ^μ. The sum of the couplings is in qualitative agreement with the result of ref. [3]. The coupling of the σ to the $\overline{u}u + \overline{d}d$ operator can be compared to the coupling of the $a_0(980)$ to $\overline{u}d$. Converting the finite-energy sum rule result of Maltman [16] to the present normalisation gives $|C^{ud}_{a_0(980)}| = 197 \pm 37$ MeV. Thus, the σ and a_0 couplings are nearly equal, which is compatible with an assignment of both mesons into the same multiplet. We have also estimated the κ meson coupling $|C^{us}_{\kappa(800)}| \simeq 156$ MeV. The couplings of the light scalars σ, κ, $a_0(980)$, $f_0(980)$ to $\overline{q}q$ operators are therefore not unusually small, as one could expect in a naive tetraquark model, and their values are compatible with a nonet assignment.

Bibliography

[1] I. Caprini, G. Colangelo and H. Leutwyler, Phys. Rev. Lett. **96** (2006) 132001

[2] C. J. Morningstar and M. J. Peardon, Phys. Rev. D **60** (1999) 034509

[3] S. Narison and G. Veneziano, Int. J. Mod. Phys. A **4** (1989) 2751.

[4] J. D. Weinstein and N. Isgur, Phys. Rev. D **41** (1990) 2236.

[5] S. M. Roy, Phys. Lett. B **36** (1971) 353.

[6] B. Ananthanarayan, G. Colangelo, J. Gasser and H. Leutwyler, Phys. Rept. **353** (2001) 207

[7] J. R. Batley *et al.* [NA48-2 Collaboration], Eur. Phys. J. C **70** (2010) 635.

[8] C. Pomponiu and G. Wanders, Nucl. Phys. B **103** (1976) 172.

[9] B. Hyams *et al.*, Nucl. Phys. B **64** (1973) 134

[10] R. Kaminski, L. Lesniak and K. Rybicki, Z. Phys. C **74** (1997) 79

[11] R. Garcia-Martin, R. Kaminski, J. R. Pelaez, J. Ruiz de Elvira and F. J. Yndurain, Phys. Rev. D **83** (2011) 074004

[12] R. Garcia-Martin and B. Moussallam, Eur. Phys. J. C **70** (2010) 155

[13] T. Mori *et al.* [Belle Collaboration], J. Phys. Soc. Jap. **76** (2007) 074102, S. Uehara *et al.* [Belle Collaboration], Phys. Rev. D **78** (2008) 052004

[14] M. R. Pennington, Phys. Rev. Lett. **97** (2006) 011601.

[15] J. F. Donoghue, J. Gasser, H. Leutwyler, Nucl. Phys. **B343**, 341-368 (1990).

[16] K. Maltman, Phys. Lett. B **462** (1999) 14

Spectra of Light and Heavy Mesons, Glueball and QCD Effective Coupling

Gurjav Ganbold[1]
Bogoliubov Laboratory of Theoretical Physics
Joint Institute for Nuclear Research
141980 Dubna, Russia;
Institute of Physics and Technology
210651 Ulaanbaatar, Mongolia

The spectroscopy of conventional mesons as well as the glueball ground state are investigated within a relativistic quantum-field model based on analytical confinement. Ladder Bethe-Salpeter-type equations are derived to define the spectra of quark-antiquark and two-gluon bound states. We provide a new analytic estimate of the lowest-state glueball mass and calculate the spectrum of light, intermediate and heavy mesons in a wide range of energy scale $\sim 0.1 - 10$ GeV. The QCD effective coupling α_s is studied by exploiting the conventional meson spectrum. A new, independent and specific infrared-finite behavior of QCD running coupling is found below ~ 1 GeV. By introducing only a minimal set of model parameters, we obtain results in reasonable agreement with recent experimental data.

1 Introduction

Understanding of a number of phenomena such as quark confinement, hadronization and nonvanishing vacuum expectation values, etc. requires a correct description of hadron dynamics in the infrared (IR) region at low energies below 1 GeV. Particularly, many quantities in hadron physics are affected by the IR behavior of the the QCD effective coupling α_s in different amounts. QCD predicts the functional form of the energy dependence of α_s on energy scale Q, but its actual values are determined only at relatively high energies [1]. The long-distance behavior of α_s is not well defined, it needs to be more specified [2, 3] and remains one of the actual problems in particle physics. On the other hand, the calculations of hadron mass characteristics on the level of experimental data precision still remain among the unsolved problems in QCD.

It represents a certain interest to investigate some low-energy physics problems, such as hadronisation, glueball states, QCD effective (running) charge within a simple relativistic

[1]ganbold@theor.jinr.ru

model based on physically transparent hypotheses, which can be treated by simple analytic methods.

Below, we take into account the dependence of α_s on mass scale M and determine the QCD effective charge in the low-energy region by exploiting the hadron spectrum [4]. For the spectra of two-quark bound states we develop a relativistic quantum-field model based on analytic (or, IR) confinement and consider Lagrangian [5]:

$$\mathcal{L} = -\frac{1}{4}\left(\partial^\mu \mathcal{A}^A_\nu - \partial^\nu \mathcal{A}^A_\mu - g f^{ABC}\mathcal{A}^B_\mu \mathcal{A}^C_\nu\right)^2 + \sum_f \left(\overline{q}^a_f \left[\gamma_\alpha \partial^\alpha - m_f + g\Gamma^\alpha_C \mathcal{A}^C_\alpha\right]^{ab} q^b_f\right), \tag{1}$$

where $\mathcal{A}^C_\alpha$ is gluon adjoint representation, q^a_f - quark field and $\Gamma^\alpha_C = i\gamma_\alpha t^C$. The model parameters are the confinement scale Λ and the constituent quark masses m_f=$\{m_{ud}, m_s, m_c, m_b\}$.

Within the model the quark and gluon propagators $\tilde{S}(\hat{p})$ and $\tilde{D}(p)$ are entire analytic functions in the Euclidean space. The quark propagator reads:

$$\tilde{S}^{ab}_m(\hat{p}) = \delta^{ab}\frac{i\hat{p} + m_f[1 \pm \gamma_5\,(1 + (m_f/\Lambda)^2/4)^{-1}]}{\Lambda m_f}\exp\left\{-\frac{p^2 + m_f^2}{2\Lambda^2}\right\}. \tag{2}$$

Recent theoretical results predict an IR behavior of the gluon propagator [6,7]. We consider a gluon propagator exhibiting an IR-finite behavior in Feynman gauge as follows:

$$\tilde{D}^{AB}_{\mu\nu}(p) = \delta^{AB}\delta_{\mu\nu}\frac{1 - \exp\left(-p^2/\Lambda^2\right)}{p^2} = \delta^{AB}\delta_{\mu\nu}\int\limits_0^{1/\Lambda^2} ds\, e^{-sp^2}. \tag{3}$$

The leading-order contributions to the $(q\overline{q})$ and two-gluon bound states read:

$$Z_{q\overline{q}} = \iint \mathcal{D}\overline{q}\mathcal{D}q \exp\left\{-(\overline{q}S^{-1}q) + \frac{g^2}{2}\left\langle(\overline{q}\Gamma\mathcal{A}q)^2\right\rangle_D\right\},$$
$$Z_{\mathcal{A}\mathcal{A}} = \left\langle \exp\left\{-\frac{g}{2}\,(f\mathcal{A}\mathcal{A}F)\right\}\right\rangle_D, \qquad \langle(\bullet)\rangle_D \doteq \int \mathcal{D}\mathcal{A}\, e^{-\frac{1}{2}(\mathcal{A}D^{-1}\mathcal{A})}(\bullet).$$

First, we allocate the one-gluon exchange between colored biquark currents and isolate the color-singlet combinations. Then, perform a Fierz transformation and introduce a system of orthonormalized functions $\{U_Q(x)\}$, where $Q = \{n_r, l, \mu\}$ are quantum numbers. By involving a Gaussian path-integral representation defined on auxiliary fields $B_\mathcal{N}$ for the exponential in $Z_{q\overline{q}}$ we take explicit path integration over quark variables. Let us introduce a *Hadronization Ansatz* and identify $B_\mathcal{N}(x)$ with meson fields carrying quantum numbers $\mathcal{N} = \{Q, J, f_1, f_2\}$. We isolate all quadratic field configurations ($\sim B^2_\mathcal{N}$) in the 'kinetic' term and rewrite the partition function for mesons [4]:

$$Z_{q\overline{q}} \to Z = \int \prod_\mathcal{N} \mathcal{D}B_\mathcal{N} \exp\left\{-\frac{1}{2}\sum_{\mathcal{N}\mathcal{N}'}\left(B_\mathcal{N}\left[\delta^{\mathcal{N}\mathcal{N}'} + \alpha_s\lambda_{\mathcal{N}\mathcal{N}'}\right]B_{\mathcal{N}'}\right) - W_{res}[B_\mathcal{N}]\right\}, \tag{4}$$

$J^{PC}=0^{-+}$	$M_{\mathbf{P}}$	$J^{PC}=0^{-+}$	$M_{\mathbf{P}}$	$J^{PC}=1^{--}$	$M_{\mathbf{V}}$	$J^{PC}=1^{--}$	$M_{\mathbf{V}}$
$\pi(138)$	138	$\eta_c(2980)$	3039	$\rho(770)$	770	$D_s^*(2112)$	2112
$K(495)$	495	$B(5279)$	5339	$\omega(782)$	785	$J/\psi(3097)$	3097
$\eta(547)$	547	$B_s(5370)$	5439	$K^*(892)$	892	$B^*(5325)$	5357
$D(1870)$	1941	$B_c(6286)$	6489	$\Phi(1019)$	1022	$\Upsilon(9460)$	9460
$D_s(1970)$	2039	$\eta_b(9389)$	9442	$D^*(2010)$	2010		

Table 1: Estimated masses M of conventional mesons (in MeV) at $\Lambda = 345$ MeV [4].

where the residual part $W_{res}[B_{\mathcal{N}}] \sim 0(B^3_{\mathcal{N}})$ describes interaction between mesons.

The Fourier transform of the leading-order term of the polarization operator reads

$$\lambda_{JJ'}(p,x,y) = \frac{16\pi}{9}\sqrt{C_J\,C_{J'}D(x)D(y)}\int\frac{d^4k}{(2\pi)^4}\,e^{-ik(x-y)}\mathrm{Tr}\left[O_J\tilde{S}_{m_1}\Big(\hat{k}+\xi_1\hat{p}\Big)\,O_{J'}\tilde{S}_{m_2}\Big(\hat{k}-\xi_2\hat{p}\Big)\right].$$

We diagonalize the polarization kernel on the orthonormal basis $\{U_{\mathcal{N}}\}$:

$$\iint dxdy\,U_{\mathcal{N}}(x)\lambda_{JJ'}(p,x,y)U_{\mathcal{N}'}(y) = \delta^{\mathcal{N}\mathcal{N}'}\,\lambda_{\mathcal{N}}(-p^2)$$

that is equivalent to the solution of the corresponding ladder Bethe-Salpeter equation.

In relativistic quantum-field theory a stable bound state of n massive particles shows up as a pole in the S matrix with a center of mass energy. Accordingly, the meson masses may be derived from the equation [4]:

$$1+\hat{\alpha}_s\cdot\lambda_{\mathcal{N}}(M^2_{\mathcal{N}}) = 0\,,\qquad -p^2 = M^2_{\mathcal{N}}\,. \tag{5}$$

2 Meson Spectrum and QCD Effective Coupling

Further we exploit Eq. (5) in different ways, by solving either for $\hat{\alpha}_s$ at given masses, or for M_J at known values of $\hat{\alpha}_s$.

1) First, we adjust the model parameters by fitting heavy meson masses ($M \geqslant 2$ GeV) and newest data for α_s. Then, we fix model parameters as follows (in units of MeV) [4]:

$$\Lambda = 345\,,\quad m_{ud} = 192.56\,,\quad m_s = 293.45\,,\quad m_c = 1447.59\,,\quad m_b = 4692.51\,.$$

2) Having adjusted model parameters, we estimate $\hat{\alpha}_s(M)$ in the low-energy domain corresponding to light meson masses below ~ 1 GeV.

3) We calculate some meson masses in a wide range of energy $1 < M < 9.5$ GeV with relative error less than 3.5 percent (shown in Table 1). The estimated meson masses do not change considerably (less than 0.5 percent) under changes of $330 < \Lambda < 360$ MeV.

4) We perform global evaluation of $\hat{\alpha}_s(M)$ at the mass scale of conventional mesons by using formula $\hat{\alpha}_s(M_J) = -1/\lambda_J(M_J,\Lambda,m_1,m_2)$ and plot the resulting curves at different Λ in Figure 1 in comparison with recent low- and high-energy data of $\alpha_s(Q)$ [8].

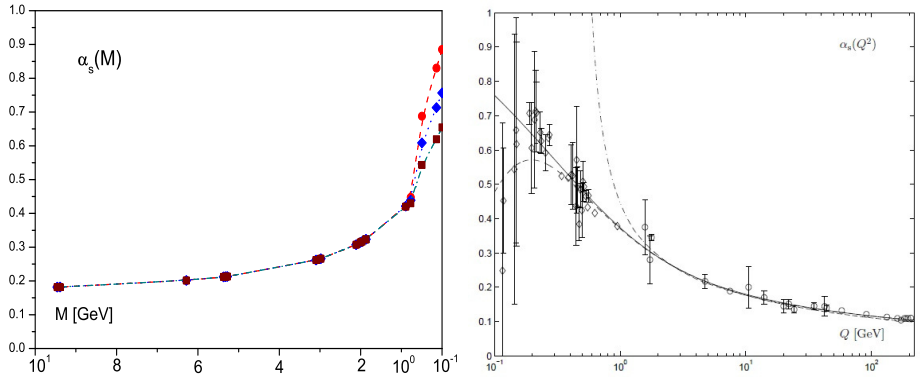

Figure 1: Our estimates of $\hat{\alpha}_s(M)$ in interval from 0 to 10 GeV at different values of confinement scale: $\Lambda = 330$ MeV (dots), $\Lambda = 345$ MeV (rhombs) and $\Lambda = 360$ MeV (squares) compared with $\alpha_s(Q)$ defined in low- (diamonds) and high-energy (circles) experiments. Also shown are the three-loop analytic coupling (solid curve), its perturbative counterpart (dot-dashed) and the massive one-loop analytic coupling (dashed) (see [8]).

3 IR-finite Behaviour of the QCD Running Coupling

The possibility that the QCD coupling features an IR-finite behavior has been extensively studied (e.g., [9]). By deriving the coupling at origin $\hat{\alpha}_s^0 \doteq \hat{\alpha}_s(0)$ for zero meson mass $M = 0$ and at particular values $m = m_{ud} = 192.56$ MeV and $\Lambda = 345$ MeV we estimate it

$$\hat{\alpha}_s^0 = 0.757\,, \qquad \text{or} \qquad \hat{\alpha}_s^0/\pi = 0.241\,. \tag{6}$$

Note, QCD running coupling behaves different in Euclidean and Minkowskian domains, but at origin they coincide $\alpha_s(0) = \hat{\alpha}_s(0)$ [4]. We may conclude that our result (6) is in a reasonable agreement with often quoted estimates

$$\begin{cases} \alpha_s^0/\pi \simeq 0.19 - 0.25 & [10]\,, \quad \alpha_s^0/\pi \simeq 0.265 \quad [11]\,, \\ \alpha_s^0/\pi \simeq 0.26 & [12]\,, \quad \left\langle \alpha_s^0/\pi \right\rangle_{1\,GeV} \simeq 0.2 \quad [13]\,. \end{cases} \tag{7}$$

4 Glueball Lowest State

Because of the confinement, gluons are not observed, they may only come in bound states called *glueballs*. Glueballs are the most unusual particles predicted by the QCD but not found experimentally yet [14]. There are predictions expecting non-$q\bar{q}$ scalar objects, like glueballs and multiquark states in the mass range $\sim 1500 \div 1800$ MeV [15–17].

The glueball spectrum has been studied by using effective approaches like the QCD sum rules [18], Coulomb gauge QCD [19], various potential [20] and string models [21] as well as lattice QCD simulations [22, 23].

Below we consider a two-gluon scalar bound state. First, we isolate the color-singlet term in the bi-gluon current in $Z_{\mathcal{A}\mathcal{A}}$. The second-order matrix element contains color-singlet two-gluon current and consists of spin-zero (scalar) and spin-two (tensor) components. We consider the scalar component. By omitting details of intermediate calculations (similar to those represented in the previous section) we define the Bethe-Salpeter kernel:

$$\Pi(z) \doteq \iint dtds\; U_n(t)\sqrt{W(t)}\; D\left(\frac{t+s}{2}+z\right)\cdot D\left(\frac{t+s}{2}-z\right)\sqrt{W(s)}\; U_n(s)\,.$$

Here we consider the gluon propagator (in Feynman gauge):

$$\tilde{D}^{AB}_{\mu\nu}(p) = \delta^{AB}\frac{\delta_{\mu\nu}}{p^2}\exp\left(-p^2/4\Lambda^2\right)\,.$$

The glueball mass M_G is defined from equation:

$$1-\frac{8\,g^2}{3}\int dz\, e^{izp}\,\Pi(z)=0\,,\qquad p^2=-M_G^2\,. \tag{8}$$

The final analytic result for the lowest-state glueball mass reads

$$M_G = 2\Lambda\left[\ln\left(\frac{\alpha_{crit}}{\alpha_s}\right)\right]^{1/2}\,,\qquad \alpha_{crit}\doteq\frac{3\pi(3+2\sqrt{2})^2}{4}\,. \tag{9}$$

Particularly, for $\Lambda_{QCD}\approx 360$ MeV and $\alpha_s(M_\tau)=0.343$ we estimate $M_G\approx 1710$ MeV.

Else, with values $\alpha_s = 1.5023$ and $\Lambda = 416.4$ MeV obtained by fitting the meson masses and weak decay constants we calculate the scalar glueball mass as follows [5]

$$M_G = 1661\ \text{MeV}\,. \tag{10}$$

Our estimate is in reasonable agreement with other predictions [15, 18, 22, 23]. The recent quenched lattice estimate favors a scalar glueball mass $M_G = 1710 \pm 50 \pm 58$ MeV [24].

To conclude, we demonstrated that global properties of some low-energy phenomena may be explained reasonably in the framework of a simple relativistic quantum-field model if one guesses correct symmetry structure of the quark-gluon interaction in the confinement region and uses simple forms of propagators in the hadronization regime. We do not aim to obtain the behavior of the coupling constant at all scales. At moderate $M^2 = -p^2$ we obtain α_s in coincidence with the QCD predictions. However, at large mass scale (above 10 GeV) $\hat{\alpha}_s$ decreases much faster than expected by QCD prediction. The reason is the use of confined propagators in the form of entire (exponential) functions. As an application, we performed estimates on conventional meson spectrum and the lowest glueball mass and, the result was in reasonable agreement with experimental data.

Bibliography

[1] S. Bethke, J. Phys. **G26**, R27 (2000).

[2] D.V. Shirkov, Theor. Math. Phys. **132**, 1309 (2002).

[3] O. Kaczmarek and F. Zantow, Phys. Rev. **D71**, 114510 (2005).

[4] G. Ganbold, Phys. Rev. **D81**, 094008 (2010).

[5] G. Ganbold, Phys. Rev. **D79**, 034034 (2009).

[6] C. S. Fischer, R. Alkofer and H. Reinhardt, Phys. Rev. **D65**, 094008 (2002).

[7] C. Lerche and L. von Smekal, Phys. Rev. **D65**, 125006 (2002).

[8] M. Baldicchi *et al.*, Phys. Rev. **D77**, 034013 (2008).

[9] D. V. Shirkov and I. L. Solovtsov, Phys. Rev. Lett. **79**, 1209 (1997);
D. V. Shirkov, Theor. Math. Phys. **136**, 893 (2003).

[10] S. Godfrey and N. Isgur, Phys. Rev. **D32**, 189 (1985).

[11] T. Zhang and R. Koniuk, Phys. Lett. **B261**, 311 (1991).

[12] F. Halzen, G. I. Krein and A. A. Natale, Phys. Rev. **D47**, 295 (1993).

[13] Yu. L. Dokshitzer, G. Marchesini and B. R. Webber, Nucl. Phys. **B469**, 93 (1996).

[14] E. Klempt and A. Zaitsev, Phys. Rep. **454**, 1 (2007).

[15] C. Amsler, N.A. Tornqvist, Phys. Rep. **389**, 61 (2004).

[16] D.V. Bugg, Phys. Lett. **C397**, 257 (2004).

[17] W.-M. Yao *et al.*, J. Phys. **G33**, 1 (2006).

[18] S. Narison, Nucl. Phys. **B509**, 312 (1998); Nucl. Phys. **A675**, 54 (2000).

[19] A.P. Szczepaniak and E.S. Swanson, Phys. Lett. **B577**, 61 (2003).

[20] A.B. Kaidalov and Yu.A. Simonov, Phys. Lett. **B636**, 101 (2006).

[21] F. Brau, C. Semay, and B. Silvestre-Brac, Phys. Rev. **D70**, 014017 (2004).

[22] C.J. Morningstar and M. Peardon, Phys. Rev. **D60**, 034509 (1999).

[23] H.B. Meyer and M.J. Teper, Phys. Lett. **B605**, 344 (2005).

[24] Y. Chen *et al.*, Phys. Rev. **D73**, 014516 (2006).

First results from the CMD3 Detector at the VEPP2000 Collider

Evgeny P. Solodov[1] on behalf of the CMD3 Collaboration
Budker Institute of Nuclear Physics
Novosibirsk, Russia

Regular data taking started at the VEPP2000 e^+e^- Collider with CMD3 and SND detectors. Energy scan for center-of-mass energy from 1 GeV to 2 GeV has been performed with about 20 pb^{-1} per detector. We present first preliminary results from the CMD3 detector.

1 Introduction

Production of low energy hadrons in e^+e^- collisions remains an interesting experimental area due to its important contribution to the Standard Model (SM) calculations of the muon anomalious magnetic moment and $\alpha(s)$.

An e^+e^- collider of the next generation, VEPP2000 [1], has been constructed and started regular data taking in BudkerINP, Novosibirsk, Russia. It is designed to cover a center-of-mass ($E_{c.m.}$) energy from hadron production threshold up to 2 GeV.

Two detectors [2], SND and CMD3, have been prepared for the rich physics program at the VEPP2000 collider. During next few years we plan to scan the available energy range to measure the hadron production cross sections with a percent or better accuracy level, as well as a study production dynamics for the multi-hadron channels.

In this paper we present preliminary results from the first energy scan of the 1-2 GeV center-of-mass energy region obtained with the CMD3 detector.

2 The VEPP2000 Collider

The VEPP2000 collider is described elsewere [1] and the layout is shown in Fig. 1. A special feature of the machine is the using of the solenoidal focusing for the interaction regions. This new approach allows to suppress beam-beam effects and store larger currents. During the energy scan, reported here, a luminosity up to $2{\cdot}10^{31}$ $cm^{-2}sec^{-1}$ has been demonstrated, limited by the positron current. With a new positron source, currently under construction, the designed luminosity is 10^{32} $cm^{-2}sec^{-1}$.

[1]solodov@inp.nsk.su

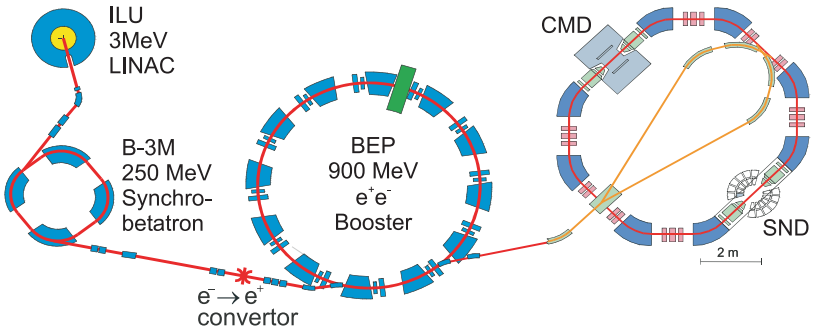

Figure 1: The layout of the VEPP2000 complex. The locations of the CMD3 and SND detectors are shown.

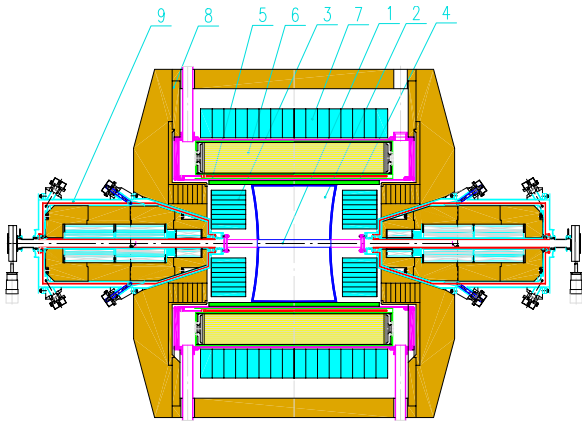

Figure 2: The CMD3 detector: 1-Interaction region; 2-Drift chamber; 3-BGO end cap calorimeter; 4-Z-proportional chamber; 5-SC magnet ; 6-LXe calorimeter; 7-CsI calorimeter; 8-Yoke; 9-Focusing solenoids.

3 The CMD3 Detector

The CMD3 detector is described elsewere [2] and detector elements are shown in Fig. 2. It is a general purpose magnetic detector, providing good spatial and momentum resolutions for the charged particles [3], and very good (about 1-2 mm) spatial resolution for photons in the LXe calorimeter [4], as well as good photon energy measurement. The detector performance is demonstrated in Fig. 3, where DC and calorimeter responses are shown for collinear events at $E_{c.m.}$=1.975 GeV. A relatively clean selection of the processes $e^+e^- \to e^+e^-$, $P\overline{P}$, K^+K^-, $\pi^+\pi^-$ can be performed using detector subsystems.

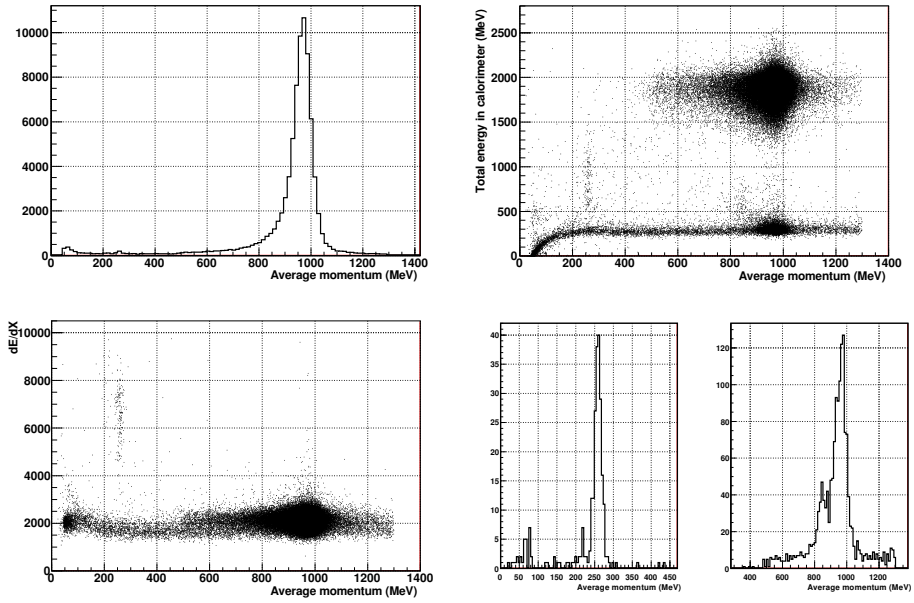

Figure 3: The CMD3 detector performance at $E_{c.m}$=1.975 GeV for collinear events: (top left) the average momentum ; (bottom left) the dedx DC measurement versus average momentum; (top right) the total energy deposition in the calorimeter versus average momentum; (bottom right) the $e^+e^- \to P\overline{P}$ signal from dedx>3000 selection and $e^+e^- \to K^+K^-$ and $e^+e^- \to \pi^+\pi^-$ signals from calorimeter energy deposition selection.

4 First Physics results

We perform the energy scan in the 1-2 GeV center-of-mass energy, collecting data at 40 energy points with about 0.5 pb^{-1} integrated luminosity. This luminosity corresponds to 200000 to 50000 events of Bhabha events (per point) used for the luminosity measurements and from a few hundred to a few thousand of multihadrons events like $\pi^+\pi^-\pi^0$, $2(\pi^+\pi^-)$, $2(\pi^+\pi^-)\pi^0$, $K^+K^-\pi^+\pi^-$, 6π etc.

As shown in Fig. 3(bottom), a simple requirement of dEdX>3000 gives a very clean signal of the $e^+e^- \to P\overline{P}$ process with about 200 events per energy point. We estimate the cross section for four energy points above the threshold and show in Fig. 4 a comparison of our preliminary results with other measurements.

In this paper we also show our preliminary measurement of the $e^+e^- \to 3(\pi^+\pi^-)$ cross section. We detect five and six charged tracks and using the total energy for six tracks and missing mass for five tracks select candidates for the $e^+e^- \to 3(\pi^+\pi^-)$ reaction with almost no background, as shown in Fig. 5(left). Our cross section measurement is shown in Fig. 5(right) in comparison with recent BaBar data.

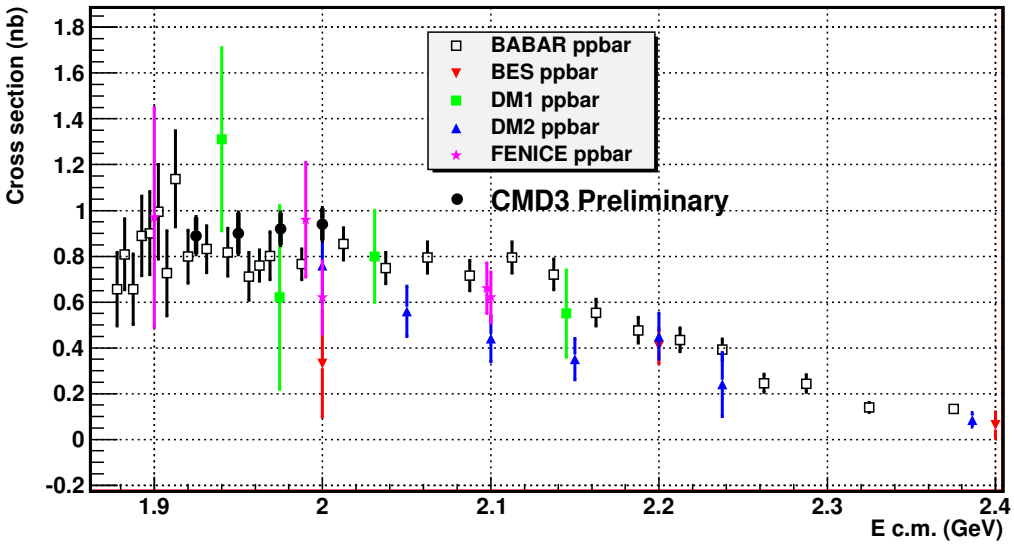

Figure 4: The CMD3 study of the $e^+e^- \to P\overline{P}$ process in comparison with other measurements.

Acknowledgments

We are grateful to VEPP2000 team for the excelent machine operation.

This work is supported in part by FEDERAL TARGET PROGRAM "Scientific and scientific-pedagogical personnel of innovative Russia in 2009-2013" and by the grants RFBR 09-02-01019, RFBR 09-02-00643, RFBR 09-02-00276, RFBR 10-02-00253, RFBR 10-02-00695, RFBR 11-02-00112.

Bibliography

[1] V.V. Danilov *et al.*, Proceedings EPAC'96, Barcelona, p1593, (1996). I.A.Koop, Nucl.Phys. B (Proc. Suppl.) 181-182 (2008) 371-375.

[2] B.I.Khazin, Nucl.Phys. B (Proc. Suppl.) 181-182 (2008) 376-380.

[3] Nucl. Instr. and Meth. A, Volume 623, Issue 1, 1 November 2010, Pages 114-116

[4] Nucl. Instr. and Meth. A, Volume 598, Issue 1, 1 January 2009, Pages 266-267.

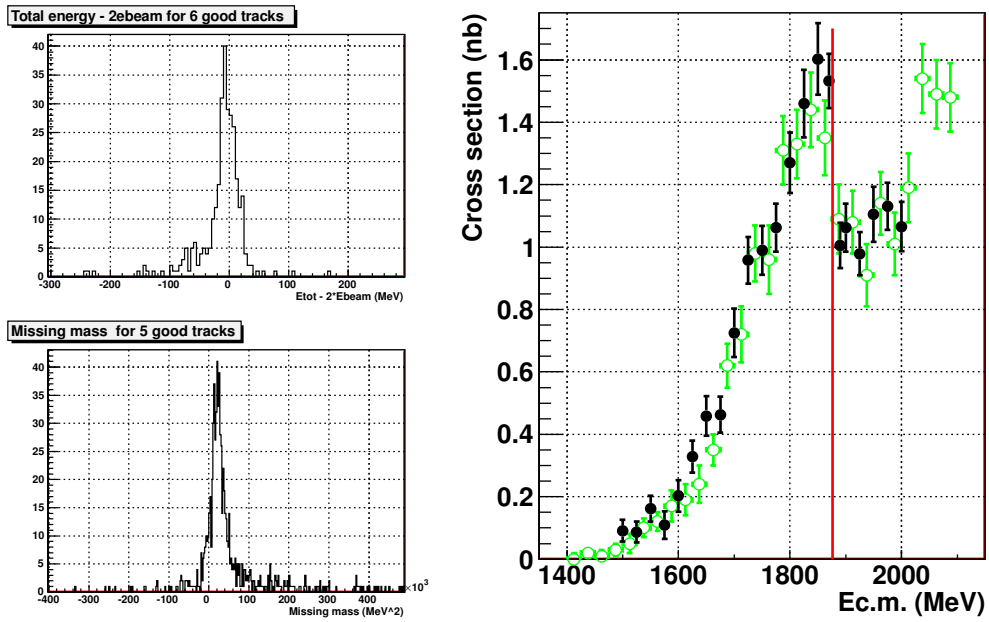

Figure 5: The CMD3 study of the $e^+e^- \to 3(\pi^+\pi^-)$ process: (left) the difference of the 6 pions total energy and $E_{c.m.}$ (top) and missing mass for 5 tracks (bottom); (right) the $e^+e^- \to 3(\pi^+\pi^-)$ cross section measured by CMD3 detector (dots) in comparison with the BaBar data (open circles). Line shows the $P\overline{P}$ threshold.

Diffractive Dissociation into $\pi^-\pi^-\pi^+$ Final State at COMPASS

Florian Haas[1] on behalf of the COMPASS Collaboration
Physik Department E18
Technische Universität München
D-85748 Garching, GERMANY

Diffractive dissociation reactions studied at the COMPASS experiment at CERN provide access to the light-meson spectrum. During a pilot run in 2004, using a negative pion beam and a Pb target, 420k $\pi^-\pi^-\pi^+$ final-state events with masses below 2.5 GeV/c^2 were recorded, yielding a significant spin-exotic signal for the controversial $\pi_1(1600)$ resonance. After a major upgrade of the spectrometer in 2007, the following two years were dedicated to hadron spectroscopy. Using again a pion beam, but now with a liquid hydrogen target, a unique statistics of ∼60M events of the 3π final state was gathered in 2008. During a short campaign in 2009, the H_2 target was replaced by several solid state targets in order to study the effect of the target material on the production. A partial-wave analysis (PWA) was performed on all these data sets and results are presented.

1 Introduction

In the quark model mesons are described as bound states of quarks and anti-quarks. They are characterized by a set of quantum numbers, which are isospin I, G-parity (for light unflavoured mesons), the total spin J, parity P and, for neutral mesons, charge conjugation parity C. Quantum Chromo Dynamics (QCD) predicts the existence of states beyond the quark model, like hybrids, i.e. systems consisting of a color octet $q\bar{q}$ pair neutralized in color by gluonic excitation, or glue balls, consisting only of glue. The experimental identification of such states, however, is difficult due to mixing with $q\bar{q}$ configurations with the same quantum numbers. The observation of meson states whose quantum numbers can not be explained within the quark model, e.g. $J^{PC} = 0^{--}, 0^{+-}, 1^{-+}, \ldots$, would be an evidence for quark-gluon configurations beyond the quark model.

The lightest hybrid, predicted in a mass region of 1.3 – 2.2 GeV/c^2, is expected to have exotic quantum numbers $J^{PC} = 1^{-+}$ [1], and therefore does not mix with pure $q\bar{q}$ states. There are three experimental candidates for a light 1^{-+} hybrid. The $\pi_1(1400)$ was observed

[1] florian.haas@tum.de

by E852 [2], VES [3], and Crystal Barrel [4]. Another 1^{-+} state, the $\pi_1(1600)$, decaying into $\rho\pi$ [5–7], $\eta'\pi$ [8,9], $f_1(1285)\pi$ [10,11] and $b_1(1235)\pi$ [11] was observed in peripheral $\pi^- p$ interactions in E852 and VES. The resonant nature of both states, however, is still heavily disputed in the community [3,11,12]. A third exotic state, $\pi_1(2000)$, decaying to $f_1\pi$ and $b_1\pi$ was seen in only one experiment [10]. The COMPASS experiment will contribute significantly to the search for exotic mesons and glue balls in the light-meson sector.

COMPASS, the **CO**mmon **M**uon and **P**roton **A**pparatus for **S**tructure and **S**pectroscopy [13] is located at the CERN SPS accelerator. It is a two-stage magnetic spectrometer which provides a large angular acceptance over a wide momentum range. In addition to calorimetry and particle identification, COMPASS is equipped with a very precise charged particle tracking system. For the beam tracking, Silicon detectors around the target, Scintillating Fibers and PixelGEMs are used. Close to the beam large-size GEM detectors and Micromegas are the backbone of the tracking system. The periphery is covered by Drift Chambers and MWPCs.

2 The $\pi^-\pi^-\pi^+$ Final State

Diffractive dissociation is a process where an incoming beam particle impinges on a target and is excited to an intermediate state X which finally decays into an n-body final state. Here we focus on the diffraction of a 190 GeV/c π^- beam into the $\pi^-\pi^-\pi^+$ final state. The target particle stays intact, taking away the recoil momentum. In Fig. 1a the distribution of the kinematic variable t' is shown, which is given by $|t| - |t|_{\text{min}}$ where t is the squared four-momentum transfer to the target nucleus and $|t|_{\text{min}}$ the minimum value of $|t|$ allowed by kinematics for a given mass m_X. This analysis focuses on events in the "high-t'" region between 0.1 and 1.0 GeV$^2/c^2$ (see Fig. 1a) where E852 [6] observed the production of the exotic $\pi_1(1600)$ with $J^{PC} = 1^{-+}$.

Figure 1b shows the invariant mass spectrum of $\sim 4.2 \cdot 10^5$ events of the 3π final state on a Pb target. In addition, the intensity of the isotropic background wave (triangles) is shown, as obtained from a partial-wave analysis, which will be described in the next section. Figure 1c shows the invariant mass distribution for $\sim 60 \cdot 10^6$ events taken with a liquid hydrogen target. Due to an upgrade of the spectrometer it is sensitive to higher masses than during 2004 data taking.

2.1 Partial-Wave Technique and Isobar Model

The present analysis is based on the isobar model, assuming that the intermediate state X decays first into an isobar and a bachelor pion, with relative orbital angular momentum L between the two. The isobar subsequently decays into a $\pi^-\pi^+$ pair. A partial-wave analysis (PWA), performed in two steps, was applied to the data. The first step is a fit in bins of the

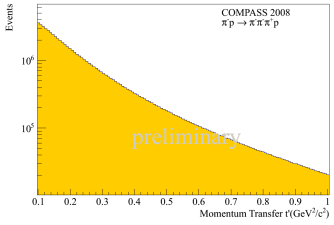

(a) Squared four-momentum transfer t', logarithmic scale.

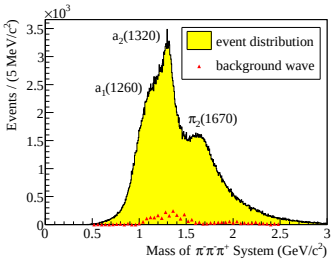

(b) 3π invariant mass spectrum for Pb target (from [14]).

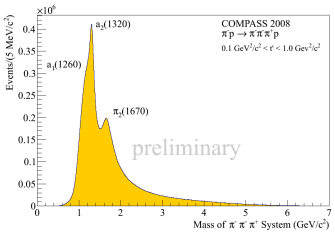

(c) 3π invariant mass spectrum for H_2 target.

Figure 1: Kinematic Distributions.

3π invariant mass m_X using the cross section parametrisation:

$$\sigma(\tau, m_X, t') = \sum_{\epsilon=\pm 1} \sum_{r=1}^{N_r} \left| \sum_i T^{\epsilon}_{ir}(m_X) f^{\epsilon}_i(t') \psi^{\epsilon}_i(\tau, m) \right|^2 \tag{1}$$

The transition amplitudes T^{ϵ}_{ir} are the fitting parameters. They are obtained by an extended maximum likelihood fit. The real functions $f^{\epsilon}_i(t')$ describe the t' dependence of the cross-section. The decay amplitudes $\psi^{\epsilon}_i(\tau, m)$ are described by Zemach tensors or D functions. τ represents the five phase-space variables of the three-body decay. The indices i and ϵ denote different partial waves, defined by a set of quantum numbers $J^{PC} M^{\epsilon}$[isobar π]L.

M is the absolute value of the spin projection onto the beam direction; ϵ is the reflectivity [15], which describes the symmetry under reflections through the production plane and corresponds to the naturality of the exchanged particle in the reaction. By incoherent summation over r different spin states of the target are taken into account.

In a second step the m_X dependence of the spin-density matrix, as obtained from the first step, is fit using a χ^2 minimization method and a model based on Breit-Wigner functions for the resonant parts plus coherent background terms (mass-dependent fit).

2.2 Fit Results

For a data sample obtained with a Pb target during the 2004 campaign, the model, on which the corresponding fit in 40 MeV mass bins is based on, consists of 42 partial waves: 34 waves with natural parity exchange ($\varepsilon = 1$) and 7 waves corresponding to unnatural parity exchange. An additional background wave is added incoherently to the cross-section. Except the latter, the waves are constructed with quantum numbers ranging from total spin $J = 0$ to $J = 4$, spin projection $M = 0$ and $M = 1$ and orbital angular momentum $L = S$ to $L = G$. Five isobars were used, four ($\rho(770)$, $f_0(980)$, $f_2(1270)$ and $\rho_3(1690)$) described by

Breit-Wigner functions and in addition a $\pi\pi_S$-wave parametrized with the "K_1"-solution [16] from which the complex amplitude of the $f_0(980)$ was subtracted. Exponential functions specify the t' dependence. Thresholds on the 3π mass were applied to most of the waves, in order to stabilize the fit. To the six most prominent waves a mass-dependent fit was applied. Breit-Wigner functions and a coherent background, where necessary, are characterizing the waves.

Figures 2a-c show the intensity of the three most prominent waves, $1^{++}0^+\rho\pi S$, $2^{++}1^+\rho\pi D$, and $2^{-+}0^+f_2\pi S$. Of peculiar interest are the fit results for the spin-exotic wave. The $1^{-+}1^+\rho\pi P$ intensity (Fig. 2d) features a broad bump, centered at 1.7 GeV/c^2, with a visible low-mass shoulder. A constant-width Breit-Wigner function (blue curve) and a non-resonant background (purple curve), possibly caused by Deck-like effects, describe the data well. To clarify the resonant nature of this exotic amplitude, its interferences with well established states have been studied. Figure 2e shows the phase difference to the $1^{++}0^+\rho\pi S$ wave (Fig. 2b), which clearly rises between 1.5 and 1.9 GeV/c^2. Figure 2f shows that the exotic wave is phase locked with the $\pi_2(1670)$ resonance in the $2^{-+}0^+f_2\pi S$ wave, which can be explained by the presence of a $\pi_1(1600)$ with mass and width similar to the $\pi_2(1670)$. Further details of this analysis can be found in [14].

A similar analysis was applied to the large data set with the liquid hydrogen target. The waveset, used for the 2004 analysis, was extended due to 150 times larger statistics. Additional waves, with $J = 5$ and $J = 6$, $M = 2$ and waves described by a sixth isobar ($f_0(1500)$ were implemented. No t' dependence was introduced. A mass-dependent fit was not performed yet. The result of a fit in 20 MeV mass bins can be seen in Fig. 3.

Again the intensity of the three major waves is plotted (Fig. 3a-c), while Fig. 3d shows the exotic wave, where in contrast to the previous results the signal-to-background ratio is much smaller. This effect can be observed in several $M = 1$ waves, which is discussed in more detail in Sec. 2.3. But nevertheless a peak centered at 1.65 GeV/c^2 and a respective phase motion (Fig. 3e) with respect to the $1^{++}0^+\rho\pi S$ wave (Fig. 3b) can be seen in the same mass region as in the 2004 analysis. Also the flat phase difference (Fig. 3f) between the spin-exotic and the $2^{-+}0^+f_2\pi S$ wave (Fig. 3c) is in good agreement with the fit results on a Pb target. The peak-like structure at 1.1 GeV/c^2 is not yet completely understood. The fact that no change of the phase difference can be seen in the corresponding mass region in Fig. 3e, suggests a non-resonant mechanism. Further studies are underway.

2.3 Dependence of $\pi^-\pi^-\pi^+$ Production on the Target Material

A striking finding is the target material dependence of the population of the M sub-states of the produced waves which becomes evident from the analysis of data taken with a Pb target (2004, 2009) and with the lH target (2008), and which is shown here for the 2008/2009 data sets. Due to different amounts of statistics both data samples are normalized to the integral of the narrow $2^{++}1^+\rho\pi D$ wave in the region between 1.1 and 1.6 GeV/c^2. A clear difference

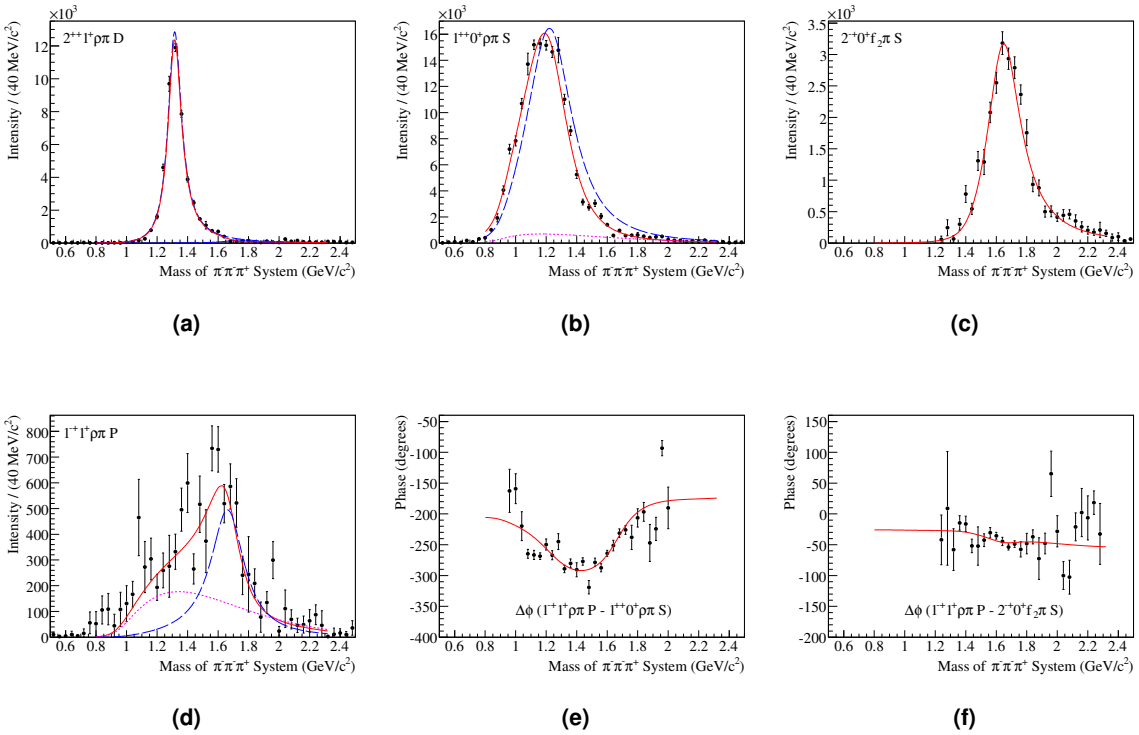

Figure 2: Intensities of major waves: (a) $2^{++}1^{+}\rho\pi D$, (b) $1^{++}0^{+}\rho\pi S$ and (c) $2^{-+}0^{+}f_2\pi S$, the red curve represents the mass-dependent fit of the $a_2(1320)$, the $a_1(1260)$ and the $\pi_2(1670)$ respectively. (d) Intensity of the spin-exotic wave $1^{-+}1^{+}\rho\pi P$, and phase differences of this wave with respect to the (e) $1^{++}0^{+}\rho\pi S$, and the (f) $2^{-+}0^{+}f_2\pi S$ waves (Pb target). All plots from (from [14])

in population of M sub-states can be seen in comparison of the two data samples. As an example the total intensities of $J^{PC} = 1^{++}$waves with different M projections are shown in Fig. 4. The population of $M = 1$ waves is significantly higher for the heavy nuclear target (Fig. 4e) than for hydrogen (Fig. 4b). At the same time, the population of $M = 0$ waves is reduced for Pb (Fig. 4d) as compared to hydrogen (Fig. 4a). With the applied normalization the total intensity for both projections, however, is rather similar (Fig. 4c and Fig. 4f). The origin of this dependence is yet unexplained.

3 Conclusions

The COMPASS spectrometer is a powerful tool to investigate the light meson spectrum. The 2004 pilot run data on a Pb target show a strong signal of the spin-exotic $\pi_1(1600)$, observed in the $1^{-+}1^{+}\rho\pi P$ wave.

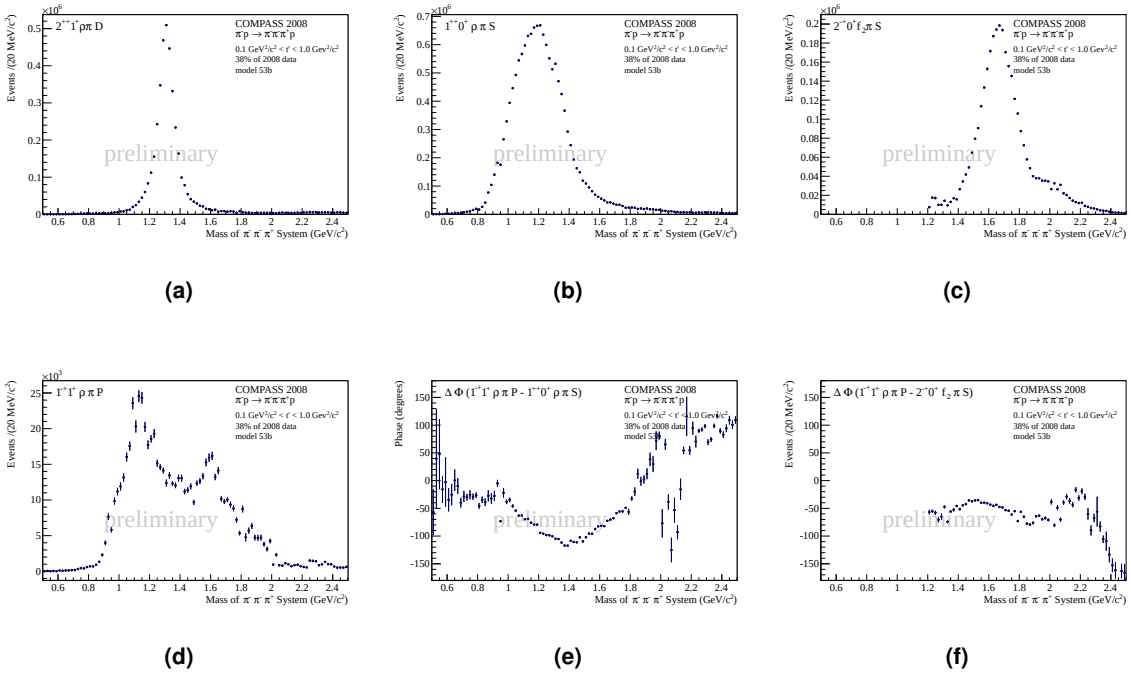

Figure 3: Intensities of major waves: (a) $2^{++}1^{+}\rho\pi D$, (b) $1^{++}0^{+}\rho\pi S$ and (c) $2^{-+}0^{+}f_2\pi S$, no mass-dependent fit applied yet. (d) Intensity of the spin-exotic wave $1^{-+}1^{+}\rho\pi P$, and phase differences of this wave with respect to the (e) $1^{++}0^{+}\rho\pi S$, and the (f) $2^{-+}0^{+}f_2\pi S$ waves, no mass-dependent fit applied yet (H_2 target).

During the hadron spectroscopy data taking campaign in 2008 COMPASS recorded a large diffractive data sample on a proton target which in the $\pi^-\pi^-\pi^+$ final state exceeds the available world statistics by a factor of 10. Preliminary fit results confirm the presence of the $\pi_1(1600)$ in good agreement with the 2004 analysis, also on the lH target. A striking difference, however, is the dependence of the production strength for different M sub-states of waves on the target material which indicates a suppression of $M = 1$ states for light targets. Fits in mass and t' bins are underway as well as leakage studies. Also Deck-like effects will be studied, in order to get a deeper insight into non-resonant contributions. This knowledge will lead to an improved mass-dependent fit to clarify the resonance nature of structures seen in the data, especially in the spin-exotic $J^{PC} = 1^{-+}$ wave.

Acknowledgments

This work is supported by the the German BMBF, the Maier-Leibnitz-Labor der LMU und TU München, and the DFG cluster of excellence *Origin and Structure of the Universe*.

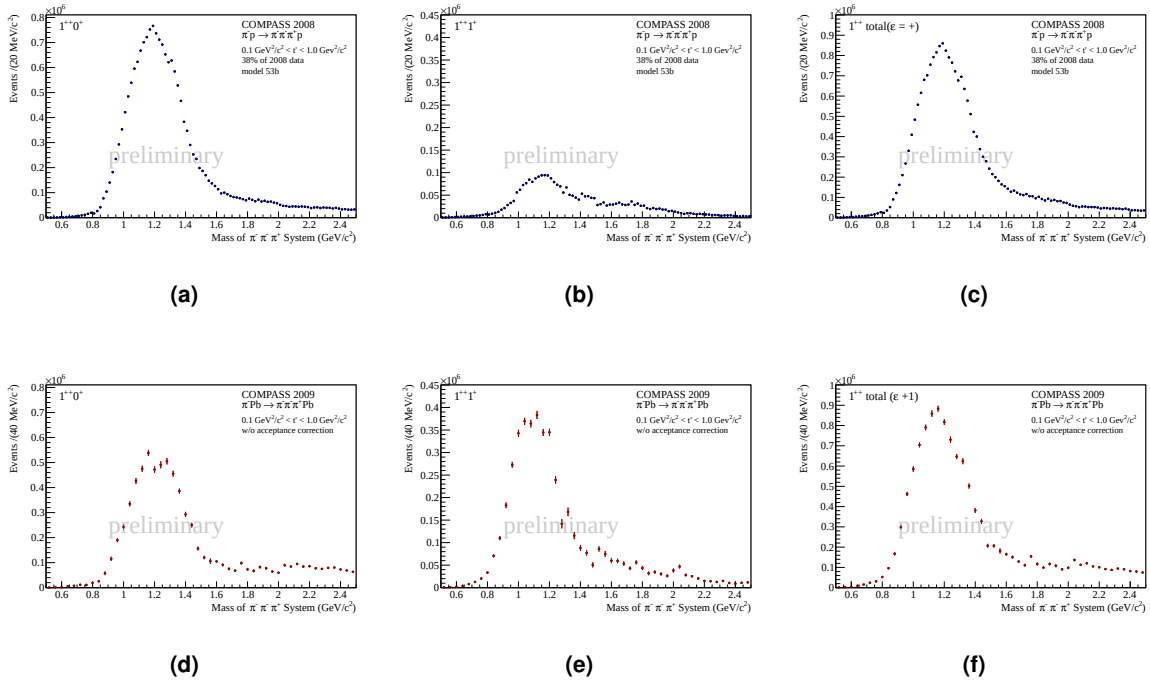

Figure 4: Intensity sum of $J^{PC} = 1^{++}$ waves with $M = 0$: (a) H_2, (d) Pb, $M = 1$: (b) H_2, (e) Pb, and for both M projections: (c) H_2, (f) Pb, same scaling, Pb data normalized to H_2 data.

Bibliography

[1] K. J. Juge, J. Kuti and C. Morningstar, AIP Conf. Proc. **688**, 193 (2004).

[2] D. R. Thompson *et al.*, Phys. Rev. Lett. **79**, 1630 (1997).

[3] V. Dorofeev *et al.*, AIP Conf. Proc. **619**, 143 (2002).

[4] A. Abele *et al.*, Phys. Lett. **B423**, 175 (1998); A. Abele *et al.*, Phys. Lett. **B446**, 349 (1999).

[5] G. S. Adams *et al.*, Phys. Rev. Lett. **81**, 5760 (1998).

[6] S. U. Chung *et al.*, Phys. Rev. **D65**, 072001 (2002).

[7] Y. Khokhlov *et al.*, Nucl. Phys. **A663**, 596 (2000).

[8] G. M. Beladidze *et al.*, Phys. Lett. **B313**, 276 (1993).

[9] E. I. Ivanov *et al.*, Phys. Rev. Lett. **86**, 3977 (2001).

[10] J. Kuhn *et al.*, Phys. Lett. **B595**, 109 (2004); M. Lu *et al.*, Phys. Rev. Lett. **94**, 032002 (2005).

[11] D. V. Amelin *et al.*, Phys. Atom. Nucl. **68**, 359 (2005).

[12] A. R. Dzerbia *et al.*, Phys. Rev. **D73**, 072001 (2006).

[13] P. Abbon *et al.*, Nucl. Instr. Meth. A **577**, 455 (2007).

[14] A. Alekseev *et al.*, COMPASS Collaboration, Phys. Rev. Lett. **104**, 241803 (2010).

[15] S. U. Chung and T. L. Trueman, Phys. Rev. **D11**, 633 (1975).

[16] K. L. Au, D. Morgan, M. R. Pennington, Phys. Rev. **D35**, 1633 (1987).

Spin-exotic search in the $\rho\pi$ decay channel: **New results on $\pi^-\pi^0\pi^0$ in comparison to $\pi^-\pi^+\pi^-$ final states** (diffractively produced on proton)

Frank Nerling[1] on behalf of the COMPASS Collaboration
Physikalisches Institut, Albert-Ludwigs-Universität Freiburg
79104 Freiburg, GERMANY

The COMPASS experiment at CERN SPS features charged particle tracking as well as good coverage by electromagnetic calorimetry, and our data provide an excellent opportunity for simultaneous observation of new states in different decay modes by the same experiment. The existence of the spin-exotic $\pi_1(1600)$ resonance in the $\rho\pi$ decay channel is studied for the first time at COMPASS in both decay modes of the diffractively produced $(3\pi)^-$ system: $\pi^- p \to \pi^-\pi^+\pi^- p$ and $\pi^-\ p \to \pi^-\pi^0\pi^0\ p$. A preliminary partial-wave analysis performed on the 2008 proton target data allows for a first conclusive comparison of both $(3\pi)^-$ decay modes not only for main waves but also for small ones. We find the neutral versus charged mode results in excellent agreement with expectations from isospin symmetry. Both, the intensities and the relative phases to well-known resonances, are consistent for the neutral and the charged decay modes of the $(3\pi)^-$ system. The status on the search for the spin-exotic $\pi_1(1600)$ resonance produced on a proton target is discussed.

1 Introduction

The existence of exotic states beyond the simple Constituent Quark Model (CQM) has been speculated about almost since the introduction of colour [1,2]. So-called hybrid mesons ($q\bar{q}$ states with excited gluonic degree of freedom) and glueballs (purely gluonic states without valence quarks) are allowed within Quantum Chromodynamics due to the self-coupling of gluons via the colour-charge, while they are forbidden within the CQM. Even though glueball candidates have been reported by the Crystal Barrel and the WA102 experiments, the mixing with ordinary isoscalar mesons makes the interpretation difficult. Several light hybrids on the other hand are predicted to have exotic J^{PC} quantum numbers and are thus promising candidates in the search for resonances beyond the CQM. The hybrid candidate lowest in mass is predicted [3] to have a mass between 1.3 and 2.2 GeV/c^2 and exotic quantum numbers $J^{PC} = 1^{-+}$, not attainable by ordinary $q\bar{q}$ states. Several experimentally

[1] nerling@cern.ch

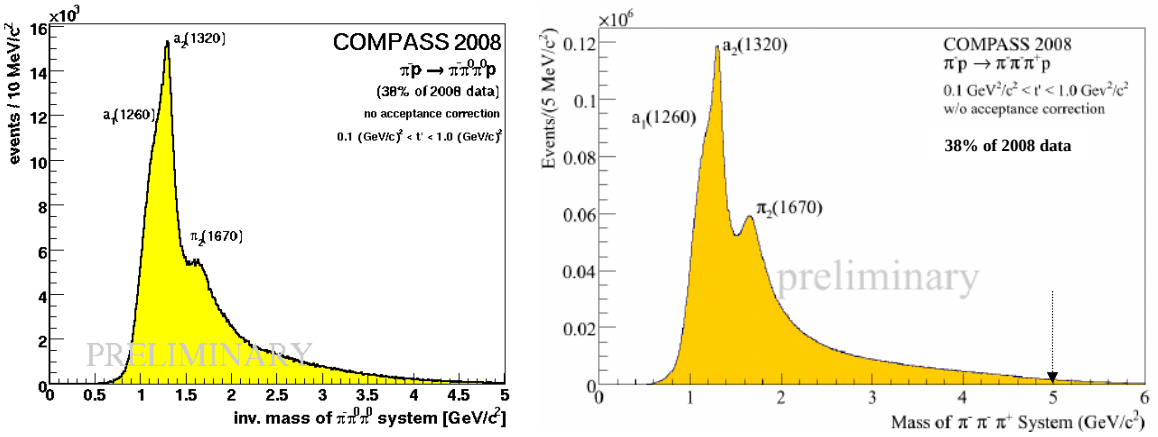

Figure 1: Total mass spectrum of the $(3\pi)^-$ systems – neutral *(left)* versus charged decay mode *(right)*. The spectra look similar as expected, showing both the most prominent, well-known resonances $a_1(1260)$, $a_2(1320)$ and $\pi_2(1670)$.

observed 1^{-+} hybrid candidates in the light-quark sector have been reported in different decay channels in the past, however, they are all still controversially discussed in the community, see e.g. [4]. In particular, the resonant nature of the $\pi_1(1600)$ observed by both E852 and VES in the $\rho\pi$ decay channel [5, 6] in 3π final states is questioned. In later publications, certain conclusions were withdrawn [7] and re-analyses of the $(3\pi)^-$ system in two different final states within the same collaboration lead to opposite conclusions [8], respectively. One may get a hint at this controversy looking at [9].

After a short pilot run in 2004 (190 GeV/c π^- beam, Pb target), we recorded high statistics using a 190 GeV/c negative pion beam scattered off a liquid hydrogen (proton) target. A similar amount of data with 190 GeV/c positive hadron beams has been taken in 2009, as well as some data (negative beam) with nuclear targets. As a first input to the puzzle, COMPASS observed a significant J^{PC} spin-exotic signal in the 2004 data (in three charged pion final states) consistent with the disputed $\pi_1(1600)$ that was accepted for publication last year [10]. The proton and nuclear target data taken in 2008/09 will enable COMPASS to further clarify the situation.

2 New results of $\pi^-\pi^0\pi^0$ in comparison to $\pi^-\pi^+\pi^-$ final states

The invariant mass of the $(3\,\pi)^-$ system is shown for the neutral and the charged $\rho\pi$ decay modes in Fig. 1. About half of the 2008 data with negative pion beam of 190 GeV/c have been analysed so far in the high momentum transfer t' region of $0.1\,\mathrm{GeV}^2/c^2 < t' < 1.0\,\mathrm{GeV}^2/c^2$. Due to the different detection efficiencies obtained for neutral and charged particles, this translates to ∼1 M events (neutral mode) and ∼24 M event (charged mode), respectively, being roughly in the range as expected in general.

The new mass-independent PWA results for neutral and charged mode data presented in

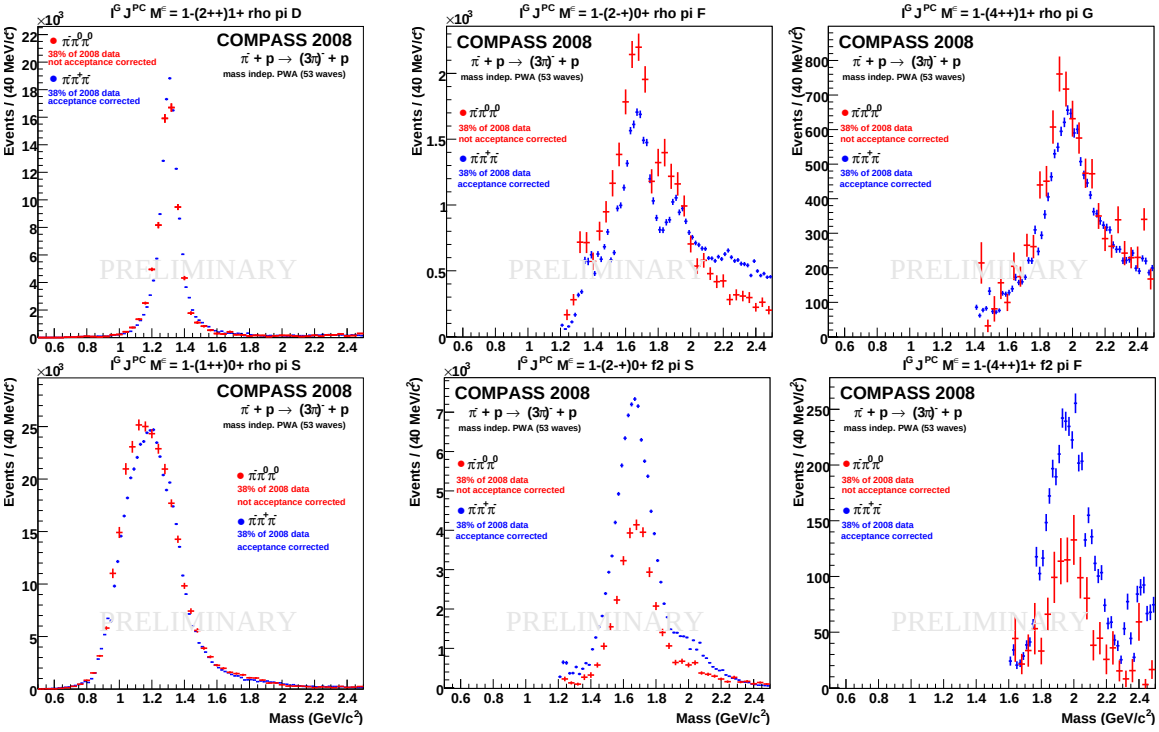

Figure 2: Comparison of PWA mass-independent fit result for neutral versus charged mode – exemplary main and small waves: *(Top, left)* $a_2(1320)$ used for normalisation, *(top & bottom, centre)* $\pi_2(1670)$, *(top & bottom, right)* $a_4(2040)$, and *(bottom, left)* $a_1(1260)$, respectively *(red = neutral, blue = charged)*. For discussion see text.

this paper, are normalised using the $a_2(1320)$ as a standard candle as shown in Fig. 2 (top, left) in order to compensate for the different detection efficiencies. This makes the fitted intensities for individual partial waves comparable between neutral and charged modes. With respect to [11], the wave-set has been extended from 42 to 53 waves, cf. also [12] giving further details on the analysis of the $\pi^-\pi^+\pi^-$ final states likewise, and the data analysed for the neutral mode has been increased by about a factor of five, allowing for a first conclusive comparison also for small waves. A detailed description of the applied PWA method can be found in [11, 12] and references therein.

Even though the neutral mode data have not yet been corrected for acceptance (which is rather flat for the charged mode), our data is in good agreement with expectations from isospin coupling considerations. If an isospin 1 resonance decays into $\rho\pi$, similar intensities are expected for neutral and charged mode, whereas decays into $f_2\pi$ should show a suppression factor of two for the neutral w.r.t. to the charged mode data, simply due to the Clebsch-Gordan coefficients determining the different isospin coupling for the different underlying isobar structure, i.e. decays into an isovector versus an isoscalar. This is shown for some exemplary main and small waves in Fig. 2. The $a_1(1260)$ decaying into $\rho\pi$ is observed with same width and intensity for both modes, similarly for the $\pi_1(1670)$

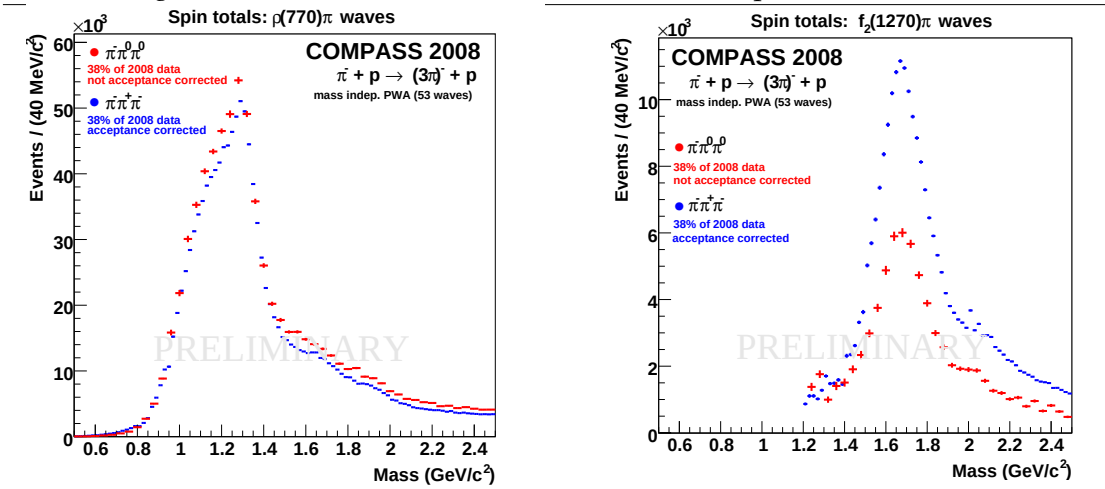

Figure 3: Intensity sums of all partial waves decaying into $\rho\pi$ *(left)* and $f_2\pi$ *(right)* intermediate states included in the fit are in good agreement with expectations from isospin symmetry. For discussion see text.

and $a_4(2040)$ decays into $\rho\pi$, whereas a suppression factor of about two is observed for the neutral mode intensities as compared to the charged mode data for the resonances decaying into $f_2\pi$ — as expected. That our data follows the expectation from isospin symmetry to a large extent throughout the whole wave-set is shown by Fig. 3, depicting the intensity sums of all $\rho\pi$ and $f_2\pi$ partial waves, respectively.

This simple isospin-symmetry holds only presumed the branchings are entirely determined by the isospin Clebsch-Gordan coefficients, which is not true in general for $f_{0,2}\pi$ decays, as Bose-Symmetrisation with the other π^- and π^0, respectively, is required and might change the observed ratio of intensities due to interference effects. There is no such effect, however, for $\rho\pi$ decays since whatever the effect might be, it is the same for both decay modes, and therefore cancels out. We checked by calculation using the wave function, that there is no such effect for $\pi_2(1670)$ decaying into $f_2\pi$, for which the pure suppression factor of two is indeed expected, as given in Table 1. Depending on the overlap of the isobars on the Dalitz plot, interference effects might change the factor of two, as for example in case of the $\pi(1800)$ decay into $f_0(980)\pi$, for which we expect to find an enlarged suppression factor (Tab. 1) in good agreement with our data, see Fig. 4 (top, centre). Apart of the fitted

BR = N($\pi^-\pi^0\pi^0$)/N($\pi^-\pi^-\pi^+$) – calculated from isobar model amplitudes
BR($0^{-+}f_0(980)\pi$ S) = 0.44 (at 1.8 GeV)
BR($1^{++}(\pi\pi)_s\pi$ P) = 0.80 (at 1.3 GeV)
BR($2^{-+}f_2(1270)\pi$ S) = 0.50 (at 1.67 GeV)

Table 1: Isospin symmetry and final state Bose-Symmetrisation: Calculation of the relative branching ratios (BR) of neutral to charged mode for decays via different isobars. The isospin Clebsch-Gordan coefficients have been applied inside the PWA normalisation integral calculator to calculate the BR for the different partial waves.

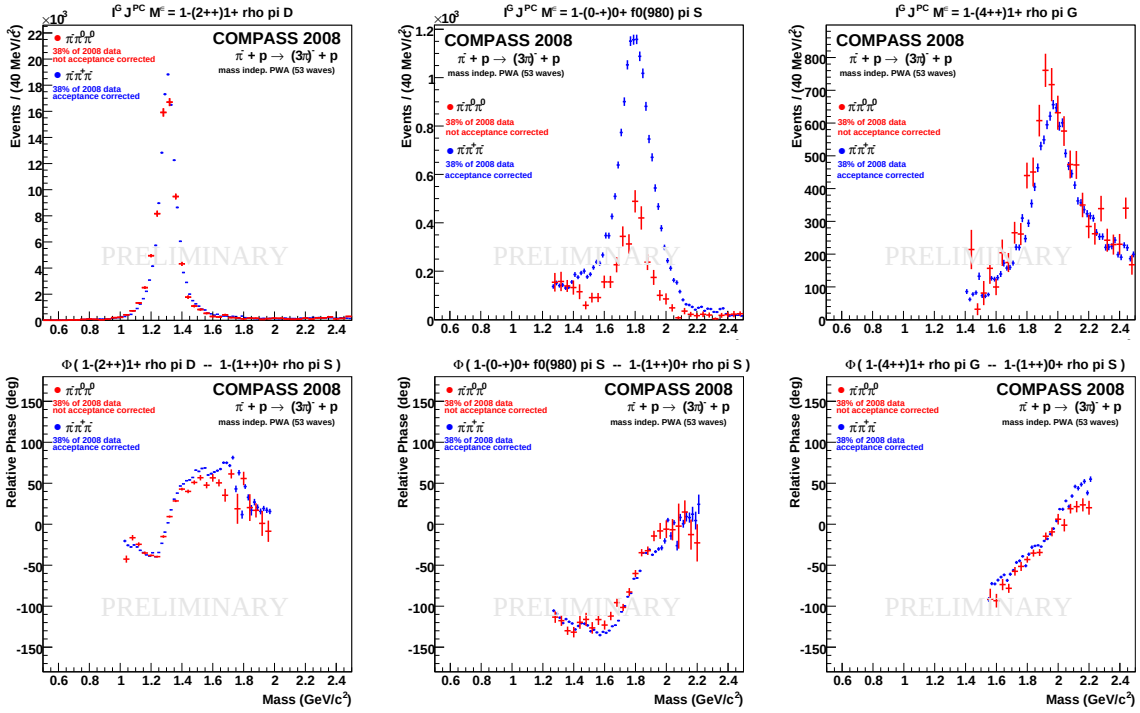

Figure 4: Relative phase difference Φ for main and small waves with respect to the prominent $a_1(1260)$ (see Fig.2, *left, bottom*): *(Left)* $a_2(1320) \rightarrow \rho\pi$, *(centre)* $\pi(1800) \rightarrow f_0(980)\pi$, and *(right)* $a_4(2040) \rightarrow \rho\pi$, respectively *(red = neutral, blue = charged)*. The well-known $a_2(1320)$ resonance as well as the smaller, less prominent ones show a clean, rapid phase motion relatively to the $a_1(1260)$. Not only the intensities but also the phases are consistent for both, neutral and charged mode, for discussion see text.

intensities it is conclusive to look at the phase difference of a possible resonance with respect to a well-know one. If the candidate is indeed a resonance, connected with the reference one (but not phase-locked), it should manifest in a clean phase motion between them, as it is shown for main and small waves in Fig. 4, using the prominent $a_1(1260)$ as reference. For the $a_2(1320)$, we find a rapid phase motion just in the range between the maxima of both objects, consistently coinciding for the neutral and the charged mode data. For the $\pi_2(1670)$ and the $a_4(2040)$, we observe a clean, rapid phase motion as well, again consistently coinciding for both modes. As they are more separated in mass from the reference, they are resonating against the tail of the $a_1(1260)$ resulting in observed phase motions limited to the mass range (about 1.7-1.9 and 1.7-2.0 GeV$/c^2$, respectively) of the given resonance under study.

3 Conclusions & summary

The hadron data taken in 2008/09 will allow COMPASS to contribute solving the puzzle of light spin-exotic mesons. The high statistics and the possibility of detecting final states involving neutral particles allows for simultaneous observation and confirmation of new states in different final states by the same experiment. The new results presented on the $\rho\pi$ decay channel in both, neutral and charged decay modes of the $(3\pi)^-$ system, appear very consistent and solid not only for main but also for small waves. There is presently no contradiction between both analysis results. In particular the coinciding relative phases of various resonances confirm already now the excellent potential to conclude on the existence of the spin-exotic $\pi_1(1600)$ resonance in the $\rho\pi$ decay channel, simultaneously observed in two different final states with the same experiment.

Acknowledgments

This work is supported by the BMBF (Germany), especially via the "Nutzungsinitiative CERN".

Bibliography

[1] R. Jaffe and K. Johnsons, *Phys. Lett. B* **60** (1976) 201.

[2] T. Barnes *et al.*, *Nucl. Phys. B* **224** (1983) 241.

[3] K.J. Juge, J. Kuti, C. Morningstar, *AIP Conf. Proc.* **688** (2004) 193.

[4] C.A. Meyer and Y.Van. Haarlem, *Phys. Rev. C* **82** (2010) 025208.

[5] G. S. Adams *et al.*, *Phys. Rev. Lett.* **81**, (1998) 5760.

[6] Y. Khokhlov, *Nucl. Phys.* **A663** (2000) 596.

[7] D. V. Amelin *et al.*, *Phys. Atom. Nucl.* **68** (2005) 359.

[8] A.R. Dzierba *et al.*, *Phys. Rev. D* **73** (2006) 072001.

[9] K. Nakamura *et al.* (Particle Data Group), J. Phys. G **37** (2010) 075021.

[10] M. Alekseev *et al.*, COMPASS collaboration, *Phys. Rev. Lett*, **104** (2010) 241803.

[11] F. Nerling, *AIP Conf. Proc.* **1257** (2010) 286; arXiv:1007.2951[hep-ex].

[12] F. Haas, *These proceedings* (2011).

Hadronic resonances made of multi-vector mesons

Luis Roca[a], Junko Yamagata-Sekihara[b], and Eulogio Oset[b]
[a]*Departamento de Física. Universidad de Murcia. E-30071, Murcia. SPAIN*
[b]*Departamento de Física Teórica and IFIC, Univ. de Valencia-CSIC, 22085, 46071 Valencia, SPAIN*

In previous works regarding the interaction of two vector mesons using the techniques of the chiral unitary approach, it was shown that the vector-vector interaction in s-wave with spins aligned is very strong both for $\rho-\rho$ and $K^*-\rho$ to the point to get dynamically the $f_2(1270)$ and $K_2^*(1430)$ resonances. In the work presented in this talk we use the rho-rho and $\rho-K^*$ interaction in spin 2 and isospin 0 channel to show that the resonances $\rho_3(1690)$, $f_4(2050)$, $\rho_5(2350)$ and $f_6(2510)$ and the strange $K_2^*(1430)$, $K_3^*(1780)$, $K_4^*(2045)$, $K_5^*(2380)$ and a not yet discovered K_6^* are basically molecules of increasing number of $\rho(770)$ mesons (with also a $K^*(892)$ in the case of the strange states). We use the fixed center approximation of the Faddeev equations to write the multi-body interaction in terms of the two-body scattering amplitudes. We find the masses of the states very close to the experimental values.

The chiral unitary approach has unraveled the molecular nature of many hadronic resonances [1–7]. As far as the interaction of vector mesons is concerned the $f_2(1270)$ and $K_2^*(1430)$ can be generated from the $\rho\rho$ and $K^*\rho$ unitarized interactions respectively in spin S=2, isospin I=0, with a very strong binding energy [8, 9]. In view of this strong $\rho\rho$ interaction, it is natural to ask whether is it possible to obtain bound systems with increasing number of ρ mesons as building blocks. Regarding this question, it is worth noting that in the PDG [10] there are intriguing mesons with large spin, of the ρ and f_0 type, whose quantum numbers match systems made with 3, 4, 5 and 6 ρ mesons with their spins aligned. These are the $\rho_3(1690)$ (3^{--}), $f_4(2050)$ (4^{++}), $\rho_5(2350)$ (5^{--}) and $f_6(2510)$ (6^{++}) resonances. Whether these systems with spin $J=2,3,4,5,6$ can be interpreted as few body systems made of an increasing numbers of $\rho(770)$ mesons is the main aim of the present work.

The basic ingredient for the calculation of the multi-ρ scattering is the two-ρ interaction [8]. From the hidden gauge symmetry Lagrangian [11–14] for vector mesons, the $\rho\rho$ potential can be obtained. The term of interest for the present work to which these Lagrangians lead are a four vector meson contact term and a four vector meson interaction through the exchange of an intermediate vector meson in the t and u channels. From these Lagrangians the potential V can be obtained, to which the contact and ρ-exchange terms contribute. For the present work only the spin $S=2$ and isospin $I=0$, $I=2$, are necessary. Actually, the $\rho\rho$ $S=2$, $I=0$ is strongly attractive. This is the most important reason to obtain a bound $\rho\rho$ state with these quantum numbers as we explain below.

With this potential the total $\rho\rho$ scattering amplitude can be obtained. In order to extend the range of applicability of the interaction to the resonance region, the implementation of exact unitarity is mandatory. In this case, we use the Bethe-Salpeter (BS) equation where the kernel is the potential V described above, $T = \frac{V}{1-VG}$, for each spin-isospin channel. In the BS equation, G is the $\rho\rho$ loop function [2, 3], which can be regularized by means of dimensional regularization or using a three-momentum cutoff, which is the only free parameter in the whole model and is chosen such as to produce the peak of $|T|^2$ at the experimental mass of the $f_2(1270)$.

For the multi-ρ systems we evaluate the scattering amplitudes for the interactions of two clusters made up of ρ-mesons. For the interaction of three ρ mesons we consider the interaction of one of the ρ mesons with the other two clustered in and $f_2(1270)$. To this purpose we use the fixed center approximation to the Faddeev equations (FCA), which are written in terms of two partition functions T_1, T_2, which sum up to the total scattering matrix, T, and read

$$T_1 = t_1 + t_1 G_0 T_2 \,, \quad T_2 = t_2 + t_2 G_0 T_1 \,, \quad T = T_1 + T_2 \tag{1}$$

where T is the total scattering amplitude we are looking for, T_i accounts for all the diagrams starting with the interaction of the external particle with particle i of the compound system and t_i represent the $\rho\rho$ unitarized scattering amplitude of a ρ^+ with any of the other ρ in the $I = 0$ $\rho\rho$ system.

In fig. 1 we show the modulus squared of the amplitudes for different number of ρ mesons considering only the single scattering mechanisms (dotted line) and the full model (solid and dashed lines). The difference between the solid and dashed lines is the value of a cutoff present in the form factor [15] needed in the evaluation of the 5ρ and 6ρ meson systems. The position of the maximum in the modulus squared of the amplitudes can be associated with the masses of the corresponding resonances. It is worth noting that the model has no free parameters once a cutoff is chosen in ref. [8] to obtain the experimental mass of the $f_2(1270)$ resonance.

The values of the masses that we obtain are in very good agreement with the experimental values of the masses of the resonances considered in the present work, the $\rho_3(1690)$, $f_4(2050)$, $\rho_5(2350)$ and $f_6(2510)$. This is a remarkable fact given the simplicity of the underlying idea.

An extension of the model to the strange sector including K^* vector mesons has been also done in ref. [16].

In Fig. 2 we show the modulus squared of the different multy-body scattering amplitudes with strangeness. The resonant structure of the amplitudes is clearly evident in the plot, which can be associated to the resonances labeled in the figures with masses given by the position of the maxima.

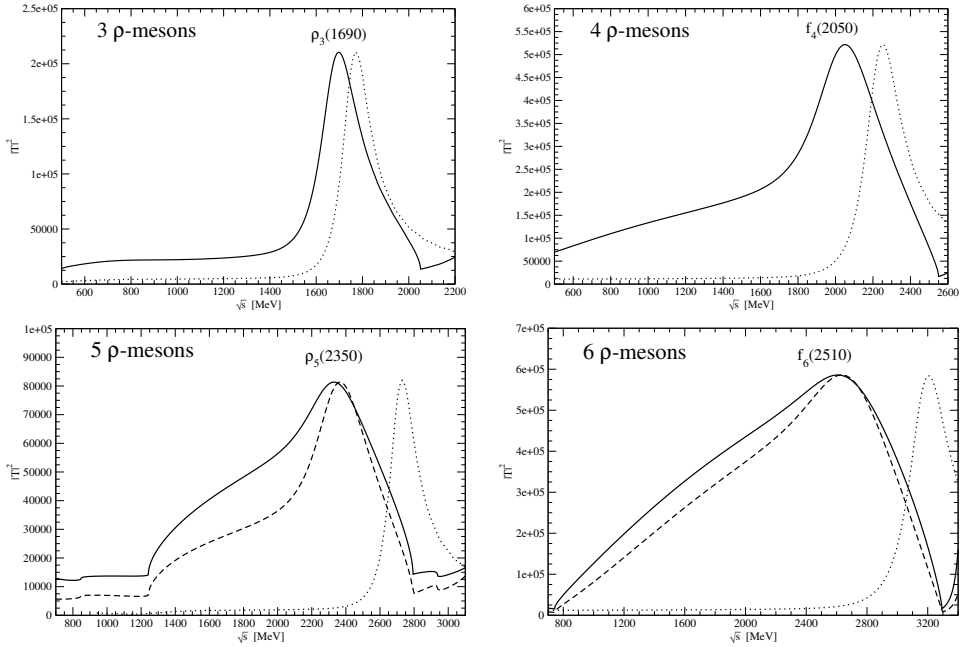

Figure 1: Modulus squared of the unitarized multi-ρ amplitudes. Solid line: full model with cutoff form factor = 1500 MeV; dashed line: full model with cutoff form factor = 875 MeV; dotted line: only single-scattering contribution.

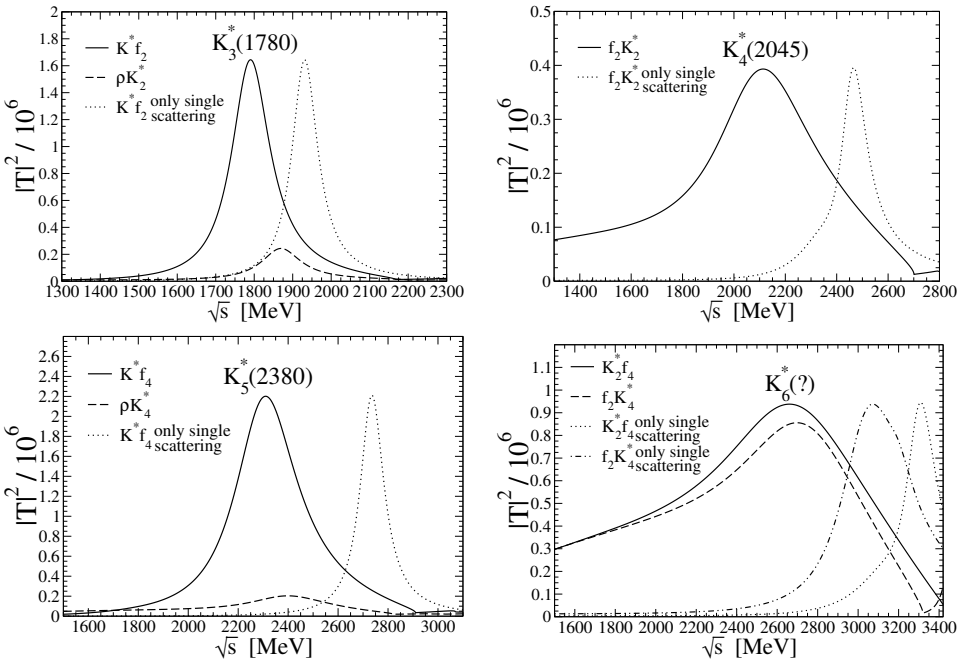

Figure 2: Modulus squared of the unitarized K^*–multi-ρ amplitudes.

The claims made here that the already observed states up to $J = 6$ correspond to multi ρ and/or K^* states is a novel idea worth consideration. New studies with different formalisms and different points of view would be most welcome, as well as possible experimental tests which could help unveil the real nature of these states.

Acknowledgments

This work is partly supported by DGICYT contracts FIS2006-03438, FPA2007-62777 and the EU Integrated Infrastructure Initiative Hadron Physics Project under Grant Agreement n.227431.

Bibliography

[1] N. Kaiser, P. B. Siegel and W. Weise,

[2] J. A. Oller and E. Oset, Nucl. Phys. A **620** (1997) 438 [Erratum-ibid. A **652** (1999) 407].

[3] J.A. Oller, E. Oset and J. R. Peláez, Phys. Rev. D 59 (1999) 74001.

[4] J. A. Oller and E. Oset, Phys. Rev. D **60** (1999) 074023.

[5] E. Oset and A. Ramos, Nucl. Phys. A **635** (1998) 99.

[6] J. Nieves and E. Ruiz Arriola, Nucl. Phys. A **679**, 57 (2000).

[7] J. A. Oller and U. G. Meissner, Phys. Lett. B **500**, 263 (2001).

[8] R. Molina, D. Nicmorus and E. Oset, Phys. Rev. D **78** (2008) 114018.

[9] L. S. Geng and E. Oset, Phys. Rev. D **79**, 074009 (2009).

[10] C. Amsler *et al.* [Particle Data Group], Phys. Lett. B **667** (2008) 1.

[11] M. Bando, T. Kugo, S. Uehara, K. Yamawaki and T. Yanagida, Phys. Rev. Lett. **54** (1985) 1215.

[12] M. Bando, T. Kugo and K. Yamawaki, Phys. Rept. **164** (1988) 217.

[13] M. Harada and K. Yamawaki, Phys. Rept. **381**, 1 (2003).

[14] U. G. Meissner, Phys. Rept. **161**, 213 (1988).

[15] L. Roca, E. Oset, Phys. Rev. **D82** (2010) 054013.

[16] J. Yamagata-Sekihara, L. Roca and E. Oset, Phys. Rev. D **82**, 094017 (2010).

Mixing properties of $a_1(1260)$ meson consisting of hadronic composite and quark composite

Hideko Nagahiro[1,ab], Kanabu Nawa[b], Sho Ozaki[c], Daisuke Jido[d], and Atsushi Hosaka[b]
[a]*Department of Physics, Nara Women's University, Nara 630-8506, Japan*
[b]*Research Center for Nuclear Physics, Osaka University, Osaka 567-0047, Japan*
[c]*Department of Physics, The University of Tokyo, Tokyo 113-0033, Japan*
[d]*Yukawa Institute for Theoretical Physics, Kyoto University, Kyoto 606-8502, Japan*

A practical method to analyze the mixing structure of hadrons consisting of two components of quark and hadronic composite is discussed. As an example we investigate the properties of the axial vector meson $a_1(1260)$ and discuss its mixing properties quantitatively.

One of recent interests in the hadron structure is whether hadrons are made up of quarks described in the conventional quark model, or rather develop subcomponents of quark-clusters inside hadrons. In fact, hadronic resonant states physically observed should be mixture of more than one component like hadronic and quark-composites, an important issue is to clarify how these components are mixed in a hadron. In this work, we focus on hadron structure having two components of quark and hadronic composite. We propose a method to disentangle their mixture, by taking the $a_1(1260)$ meson as an example. The a_1 is a candidate of the chiral partner of ρ described as a $q\bar{q}$ in many models, while, in coupled-channel approaches based on the chiral effective theory, the a_1 meson has been described as a dynamically generated resonance in the $\pi\rho$ scattering [1–3]. We first solve the $\pi\rho$ scattering amplitude to find the poles corresponding to the physical a_1, and then develop a method to clarify its mixing nature. The detailed discussions are given in Ref. [4].

By solving the Bethe-Salpeter equation, we can obtain the $\pi\rho$ scattering amplitude as

$$t = \frac{v}{1 - vG}\,, \tag{1}$$

where v is the four-point Weinberg-Tomozawa interaction and G $\pi\rho$ two-body propagator. If the potential v is sufficiently attractive, the amplitude develops a pole corresponding to the $\pi\rho$-composite a_1 meson [1] without $q\bar{q}$ quark-core [5, 6].

The elementary a_1 meson also contributes to the $\pi\rho$ scattering amplitude in the form of an effective $\pi\rho$ interaction: $v_{a_1} = g(s - m_{a_1}^2 + i\epsilon)^{-1} g$, where g is the coupling to $\pi\rho$ and m_{a_1}

[1]nagahiro@cc.nara-wu.ac.jp

the bare mass of the elementary a_1 meson. The full scattering amplitude T having both interactions v and v_{a_1} is then written by,

$$T = \frac{v + v_{a_1}}{1 - (v + v_{a_1})G} \,. \tag{2}$$

This amplitude generates poles corresponding to physical resonant states of the problem. To study the mixing nature, we express equivalently the amplitude t in Eq. (1) as,

$$t \equiv g_R(s) \frac{1}{s - s_p} g_R(s), \tag{3}$$

where s_p is the pole position of the amplitude t in Eq. (1). In this form, we can interpret $(s - s_p)^{-1}$ as the one-particle propagator of the composite a_1 meson by taking an analogy with the conventional discussion of bound state problem [5]. Having the form of Eq. (3), we now rewrite the scattering amplitude T in Eq. (2) as,

$$T = (g_R, g) \frac{1}{\hat{D}_0^{-1} - \hat{\Sigma}} \begin{pmatrix} g_R \\ g \end{pmatrix} \,, \tag{4}$$

where

$$\hat{D}_0^{-1} = \begin{pmatrix} s - s_p & \\ & s - m_{a_1}^2 \end{pmatrix}, \;\; \hat{\Sigma} = \begin{pmatrix} g_R G g & \\ g G g_R & g G g \end{pmatrix} \,. \tag{5}$$

The diagonal elements of the matrix $\hat{D}_0$ are the free propagators of the two a_1's, one for the composite and the other for the elementary ones having the proper normalization, and the matrix $\hat{\Sigma}$ expresses the self-energy and interactions for these modes.

The expression of Eq. (4) makes it possible to analyze the mixing nature of the physical a_1 in terms of the original two bases. Having the amplitude in this form, $\hat{D} \equiv (\hat{D}_0^{-1} - \hat{\Sigma})^{-1}$ is identified with the propagators of the physical states represented by the bases of the elementary and composite a_1's. The residues of the diagonal elements D^{ii} defined by,

$$D^{ii} = \frac{z_a^{ii}}{s - M_a^2} + \frac{z_b^{ii}}{s - M_b^2} + (\text{regular term}) \;\; (i = 1, 2) \,, \tag{6}$$

have the meaning of the wave function renormalization and then carry the information on the mixing rate of the physical resonant states. The concrete forms of the potentials used in Eq. (2) are given in Ref. [4].

We find two poles at (a) $\sqrt{s} = 1033 - 107i$ MeV and at (b) $1728 - 313i$ MeV, corresponding to the physical states in the present model. These pole positions are significantly different from those of the two basis states, $\sqrt{s_p} = 1012 - 221i$ MeV and $m_{a_1} = 1189$ MeV, because of the mixing effect. In Fig. 1(a), we show the resulting pole-flow in the complex-energy plane by changing the mixing parameter x introduced by $g_{a_1\pi\rho} \to x g_{a_1\pi\rho}$. When the mixing is turned on, the pole starting from the composite a_1 (we refer to it as "pole-a") approaches

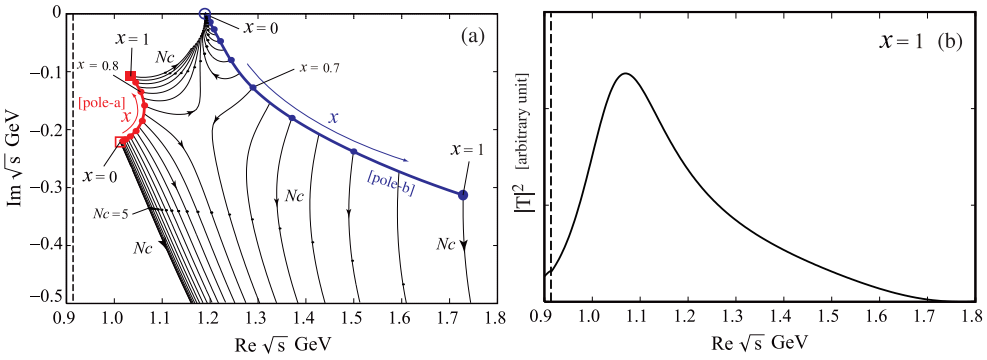

Figure 1: (a) Trajectories of the poles in the full scattering amplitude in Eq. (2) by changing the mixing parameter x (thick lines). The open square indicates the pole position of the composite a_1 and open circle indicates the elementary a_1 pole ($x = 0$). The other end points of solid circle and square correspond to the physical points ($x = 1$). Thin lines represent the pole-flows as N_c is increased from $N_c = 3$ for fixed x. (b) Squared amplitude $|T|^2$ of $\pi\rho \to \pi\rho$ process on the real energy axis for the mixing parameter $x = 1$.

the real axis, ending at $1033 - 107i$ MeV when $x = 1$ (solid square), while that from the elementary a_1 pole ("pole-b") goes far from the real axis and reaches $1728 - 313i$ MeV when $x = 1$ (solid circle). In Fig. 1(b), we show the squared amplitude $|T|^2$ in Eq. (2) (or (4)) at $x = 1$, and find that a peak structure is dominated by the pole-a. Therefore, the pole expected to be observed in experiments is the pole-a located at lower energy position that comes from the composite a_1 pole.

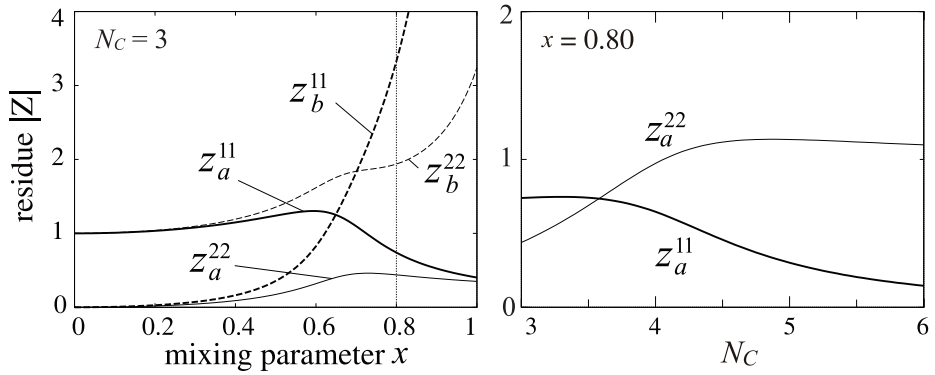

Figure 2: Absolute value of the residues defined in Eq. (6). The left panel shows the mixing parameter x dependence at $N_c = 3$ while the right panel is the N_c dependence at $x = 0.8$. The meaning of each line is indicated in the figure.

In Fig. 2(left panel) we show the absolute values of the residues as functions of the mixing parameter x. One of the most important messages can be read from the magnitude of z_a^{11} and z_a^{22} at $x = 1$, which are the residues of the possibly observed a_1 state. We can see that

the pole-a at $x = 1$, although its location is close to the composite a_1 pole, has a component of the elementary a_1 meson *comparable to* that of the composite a_1. The detailed discussions are given in Ref. [4].

Next, we test the large N_c dependence of the pole positions according to the scaling law of the pion decay constant f_π as $f_\pi \to f_\pi\sqrt{N_c/3}$. In Fig. 1, we also show the trajectories of the pole positions by changing the N_c value for fixed mixing strength. The fate of the large N_c depends strongly on the mixing parameter x, although the component of the composite a_1 is always larger than that of elementary ($z_a^{11} > z_a^{22}$) at $N_c = 3$ as shown in Fig. 2 (left panel). In Fig. 2 (right panel), we show the N_c dependence of the residues of pole-a at $x = 0.8$. There we find that the magnitudes of the residues of the pole-a, z_a^{11} and z_a^{22}, interchange at $N_c \sim 3.5$. This indicates that the nature of the resonance *changes as N_c is varied*. Thus, for the mixed system of elementary and composite components, the large N_c limit does not always reflect the world at $N_c = 3$.

We have developed a general method to analyze the mixing structure of hadrons consisting of two components of quark and hadronic composites by taking the $a_1(1260)$ axial-vector meson as an example. The present analysis points out theoretically that the a_1 meson has comparable amount of the elementary a_1 component to the $\pi\rho$ composite a_1. We also have shown explicitly that the mixing nature of hadrons in the large N_c limit could differ from that at finite $N_c = 3$. Quest for evidences of the mixing nature in physical observables is an interesting future work.

Acknowledgments

This work is in part supported by Grant-in-Aid for Scientific Research (Nos. 22105510, 22105509, 22105507 and E01:21105006). This work was done in part under the Yukawa International Program for Quark-hadron Sciences (YIPQS).

Bibliography

[1] L. Roca, E. Oset, and J. Singh. Phys. Rev. **D72**, 014002 (2005).

[2] M. F. M. Lutz and E. E. Kolomeitsev. Nucl. Phys. **A730**, 392–416 (2004).

[3] H. Nagahiro, L. Roca, A. Hosaka, and E. Oset. Phys. Rev. **D79**, 014015 (2009).

[4] H. Nagahiro, K. Nawa, S. Ozaki, D. Jido, A. Hosaka, Phys. Rev. **D83**, 111504 (2011).

[5] D. Lurie and A. J. Macfarlane. Phys. Rev. **136**, B816 (1964).

[6] T. Hyodo, D. Jido, and A. Hosaka. Phys. Rev. **C78**, 025203 (2008).

New observations on light hadron spectroscopy at BESIII

Hongwei Liu[1] on behalf of the BESIII Collaboration
Institute of High Energy Physics
100049 Beijing, P. R. China

With samples of 225 million J/ψ events and 106 million ψ' events collected in the BESIII detector, $p\overline{p}$ mass threshold enhancement is evident in J/ψ radiative decays, which is consistent with BESII result. No significant narrow enhancement is observed in ψ' radiative decays. For $J/\psi \to \gamma\pi^+\pi^-\eta'$ decay, the $X(1835)$, which was previously observed by BESII, is confirmed with a statistical significance that is larger than 20σ and the angular distribution of the radiative photon is consistent with expectations for a pseudoscalar. In addition, in the $\pi^+\pi^-\eta'$ invariant mass spectrum, the $X(2120)$ and the $X(2370)$, are observed with statistical significance larger than 7.2σ and 6.4σ , respectively. A new process $J/\psi \to \omega X(1870) \to \omega a_0\pi$ is also observed in $J/\psi \to \omega\pi^+\pi^-\eta$ decay.

1 Introduction

The Beijing Electron Positron Collider II (BEPCII) is a double ring collider, focusing on the τ-charm energy region, of which the designed luminosity is $1 \times 10^{33} cm^{-2}s^{-1}$ at the center of mass energy of 3770 MeV. The Beijing Spectrometer III (BESIII) is a general-purpose detector, which is the only experiment at BEPCII, and consists of four subdetectors: a main drift chamber, a time of flight system, a CsI(Tl) electromagnetic calorimeter, and a muon chamber. A superconducting solenoidal magnet locates between the calorimeter and the muon chamber and provides 1.0 T magnetic field. Up to now, BESIII has accumulated the word largest sample for J/ψ(225×10^6), $\psi^{'}$(106×10^6), $\psi(3770)$ ($2.9\ fb^{-1}$).

Multi-quark states, glueballs and hybrids have been searched for experimentally for a very long time, but none have been established. However, during the past three years, a lot of unexpected experimental evidence for hadrons cannot (easily) be explained by the conventional quark model. For example, at BESII:$p\overline{p}$ threshold enhancement was observed in $J/\psi \to \gamma p\overline{p}$,and X(1835) was observed in $J/\psi \to \gamma\pi^+\pi^-\eta'$. Taking advantage of the high luminosity provided by the BEPCII collider, BESIII collaboration has reported several new observations and many high precision measurements on light hadron spectroscopy such as the X(1835) resonance, $p\overline{p}$ mass threshold enhancement. In this talk, we will present the relative results of these new observations and measurements.

[1]liuhw@ihep.ac.cn

2 Observations

2.1 $p\overline{p}$ mass threshold study in J/ψ and $\psi^{'}$ radiative decays

A strong $p\overline{p}$ mass threshold enhancement was firstly observed by BESII experiment in the $J/\psi \to \gamma p\overline{p}$ [1]decay. One interesting feature of this enhancement is that no corresponding structure is reported in the relative channels, including B-meson decays [2], radiative decays of ψ' [3] and Υ [4], or the decay of $J/\psi \to \omega p\overline{p}$ [5].

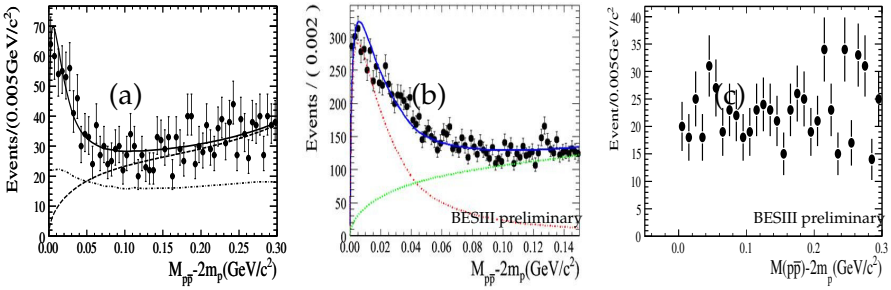

Figure 1: $p\overline{p}$ invariant mass distribution of :(a) $\psi' \to \pi^+\pi^- J/\psi(\gamma p\overline{p})$;(b) $J/\psi \to \gamma p\overline{p}$;(c) $\psi' \to \gamma p\overline{p}$. The dashed curve shows the fitted background polynomial. The dash-dotted curve in (a) represents how the acceptance varies with $M_{p\overline{p}}$.

FIG. 1 (a) and (b) show the $p\overline{p}$ invariant mass distribution of $\psi' \to \pi^+\pi^- J/\psi(\gamma p\overline{p})$ and direct $J/\psi \to \gamma p\overline{p}$. The strong threshold enhancement structure can be observed. The fitted resonance parameters are $M = 1861^{+6}_{-13}(\text{stat.})^{+7}_{-26}(\text{syst.})$ MeV/c^2 and $\Gamma < 38$ MeV/c^2 at the 90% C.L. for $\psi' \to \pi^+\pi^- J/\psi(\gamma p\overline{p})$. However, no significant threshold enhancement structure is found in $\psi' \to \gamma p\overline{p}$ decays, shown in FIG. 1 (c). The negative observations implies that the pure FSI effect alone cannot totally account for the strong threshold enhancement observed in the radiative decay of J/ψ.

2.2 Confirmation of X(1835) and observation of two new structures in $J/\psi \to \gamma\pi^+\pi^-\eta'$

The $X(1835)$ was firstly observed at BESII with a statistical significance of 7.7σ. Theoretical interpretations have been raised to settle the nature of this resonance, including the $p\overline{p}$ bound state [6], a glueball [7], a radial excitation of the η' meson [8], etc.

FIG. 2 Shown are the $\eta'\pi^+\pi^-$ invariant mass spectrum in $J/\psi \to \gamma\eta'\pi^+\pi^-$, where the η is detected in its (a) $\eta' \to \gamma\rho$ and (b)$\eta' \to \pi^+\pi^-\pi^0$ decay modes. The X(1835) resonance is clearly seen. Additional peaks are evident around 2.1 and 2.3 GeV/c^2, denoted as $X(2120)$ and $X(2370)$, as well as the $f_1(1510)$ and the distinct η_c. The fitting result of the combined mass spectrum is shown in FIG. 2 (c). The mass and width of $X(1835)$ are measured to be

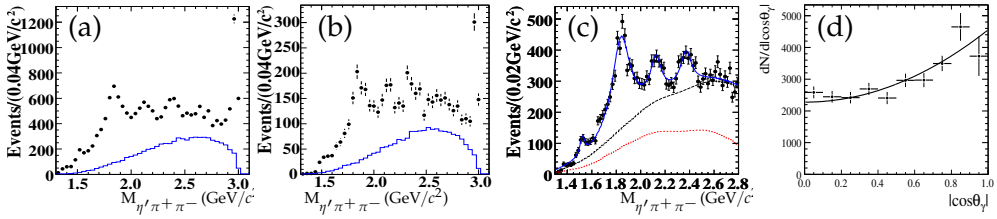

Figure 2: The invariant mass spectrum of $\eta'\pi^+\pi^-$ with (a) $\eta' \to \gamma\rho$, (b) $\eta' \to \eta\pi^+\pi^-$. (c) The fitting results of $\eta'\pi^+\pi^-$; (d) The $\cos^2\theta_\gamma$ distribution, where θ_γ is the polar angle of the photon in the J/ψ center of mass system. The solid circles are from data. The histograms are from $J/\psi \to \gamma\eta'\pi^+\pi^-$ phase space MC events.

$M = 1836.5 \pm 3.0(\text{stat.})^{+5.6}_{-2.1}(\text{syst.})$ MeV/c^2 and $\Gamma = 190 \pm 9(\text{stat.})^{+38}_{-36}(\text{syst.})$ MeV/c^2 with a significance of larger than 20σ. The statistical significance of the $X(2120)$ and $X(2370)$ are determined to be 7.2σ and 6.4σ respectively. For X(1835), the $\cos^2\theta_\gamma$ distribution is shown in FIG. 2 (d), where θ_γ is the polar angle of the photon in the J/ψ center of mass system. It agrees with $1 + \cos^2\theta_\gamma$, which is expected for a pseudoscalar.

2.3 Observation of $J/\psi \to \omega X(1870) \to \omega a_0(980)\pi$ in $J/\psi \to \omega\eta\pi^+\pi^-$

The $X(1860)$ in $J/\psi \to \gamma p\bar{p}$ and the X(1835) in $J/\psi \to \gamma\eta'\pi^+\pi^-$ stimulated the study of the decay patterns of these resonances. BESIII has finished the analysis of $J/\psi \to \omega\eta\pi^+\pi^-$ with J/ψ events.

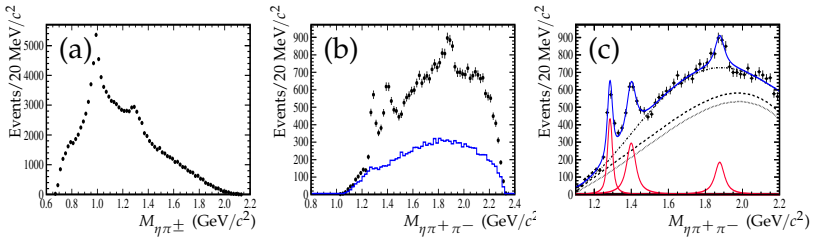

Figure 3: (a) The mass spectrum of $\eta\pi^\pm$; (b) The mass spectrum of $\eta\pi^+\pi^-$ in $a_0^\pm(980)$ mass window; (c) The $\eta\pi^+\pi^-$ mass spectrum fitting with $a_0^\pm(980)$. The dots are data. In (b), the histogram is from $J/\psi \to \omega\eta\pi^+\pi^-$ phase space MC events.

In the mass spectrum of $\eta\pi^\pm$, shown in FIG. 3 (a), the $a_0^\pm(980)$ peak is clearly seen. The mass spectrum of $\eta\pi^+\pi^-$ with $a_0^\pm(980)$ is shown in FIG. 3 (b). The $f_1(1285)$, $\eta(1405)$ and a clear peak around 1.8 GeV/c^2, denoted as $X(1870)$, can be seen. A fit with three resonances yields $M = 1877.3 \pm 6.3(\text{stat.})^{+6.3}_{-7.4}(\text{syst.})$ MeV/c^2 and $\Gamma = 57 \pm 12(\text{stat.})^{+19}_{-4}(\text{syst.})$ MeV/c^2 for $X(1870)$ with a statistical significance of 7.2σ. Additionally, the branching ratio of the

$\eta(1405)$ hadronic decay is measured to be smaller than the production in the radiative decays of J/ψ [9], which indicates $\eta(1405)$ may couple strongly to gluons.

3 Summary

In this talk, studies of $X(1860)$ in $J/\psi \to \gamma p\bar{p}$, $X(1835)$ and two new resonances in $J/\psi \to \gamma\eta'\pi^+\pi^-$, and $X(1870)$ in $J/\psi \to \omega\eta\pi^+\pi^-$ are reported. Whether these three peaks are from the same source still needs further experimental and theoretical studies. At BESIII, many precision measurements with high discovery potential have been possible and more physics results are expected.

Acknowledgments

We would like to thank the accelerator people at BEPCII for their hard work which makes our high luminosity possible. We would also like to thank the great computational and software support of the IHEP staff.

Bibliography

[1] J. Z. Bai *et al.* [BES Collaboration], Phys. Rev. Lett. **91**, 022001 (2003). [hep-ex/0303006].

[2] M. Z. Wang *et al.* [Belle Collaboration], Phys. Rev. Lett. **92**, 131801 (2004). [hep-ex/0310018].

[3] M. Ablikim *et al.* [BES Collaboration], Phys. Rev. Lett. **99**, 011802 (2007). [hep-ex/0612016].

[4] S. B. Athar *et al.* [CLEO Collaboration], Phys. Rev. **D73**, 032001 (2006). [hep-ex/0510015].

[5] M. Ablikim *et al.* [BES Collaboration], Eur. Phys. J. **C53**, 15-20 (2008). [arXiv:0710.5369 [hep-ex]].

[6] A. Datta, P. J. O'Donnell, Phys. Lett. **B567**, 273-276 (2003). [hep-ph/0306097].

[7] N. Kochelev, D. -P. Min, Phys. Lett. **B633**, 283-288 (2006). [hep-ph/0508288].

[8] T. Huang, S. -L. Zhu, Phys. Rev. **D73**, 014023 (2006). [hep-ph/0511153].

[9] K. Nakamura *et al.* (Particle Data Group), J. of Phys. G **37**, 075021 (2010).

Quarkonia

Quarkonia

Conveners

Bingsong	Zou	IHEP Beijing (*Chair*)
Mikihiko	Nakao	KEK
Ian	Shipsey	Purdue University
Yifang	Wang	IHEP Beijing
Nora	Brambilla	TU München
Bernhard	Ketzer	TU München

Session Chairs

Miriam	Fritsch	Universität Mainz
Nora	Brambilla	TU München
Simon	Eidelman	Budker Institute of Nuclear Physics
Mikihiko	Nakao	KEK
Bernhard	Ketzer	TU München

Contents

Measuring the phase between strong and EM J/ψ decay amplitudes

Marco Maggiora[1] on behalf of the BESIII Collaboration
Department of Physics - University of Turin and INFN - Turin
Via Pietro Giuria 1 I-109125 Torino, ITALY

A c.m. energy scan below the J/ψ peak foreseen in the next future at BESIII can probe the existence in all the exclusive possible final states of an interference pattern between the resonant $e^+e^- \to J/\psi \to hadrons$ and non-resonant $e^+e^- \to hadrons$ amplitudes. The relative phase of the strong J/ψ decay amplitude with respect to the electromagnetic one can hence be accessed for the first time in a model independent way.

1 Introduction

An interference pattern between the J/ψ decay and the non-resonant amplitudes has been observed in $e^+e^- \to \mu^+\mu^-$, the corresponding relative phase being in good agreement with what expected [1]. The 93 keV J/ψ decay width is often interpreted as a proof of a perturbative regime; in such a framework the J/ψ resonant strong A_{3g} and electromagnetic A_γ amplitudes (Fig. 1.a and 1.b) are predicted to be almost real [2–4], as expected for the non-resonant electromagnetic amplitude A_{em} (the non-resonant counterpart of A_γ shown in Fig. 1.c). On the contrary a wide experimental evidence ($J/\psi \to N\overline{N}, VP, PP, VV$ [5], where N, V and P stand respectively for nucleon, vector and pseudo-scalar meson) points toward an unexpected $\sim 90^\circ$ phase difference, consistent with no interference pattern in the case of hadronic amplitudes. These imaginary amplitudes have mostly been obtained comparing decay processes, belonging to the same category, modelling the amplitudes by means of SU_3 and SU_3 breaking; such additional theoretical hypotheses are questionable [6].

Asymptotically pQCD is supposed to hold, and the amplitudes relative to e^+e^- annihilations into hadrons at very high c.m. energies are expected to be real [3, 4]. It is possible that asymptotics is not yet fully reached at ~ 3 GeV for some channel, but anyhow presently QCD does not provide any explanation for so large imaginary amplitudes, i.e. such a huge phase difference $\sim 90^o$, although sub-dominant imaginary contributions are expected as a consequence of the time-like complex structure of $\alpha_{\rm QCD}$ [4].

[1] marco.maggiora@to.infn.it

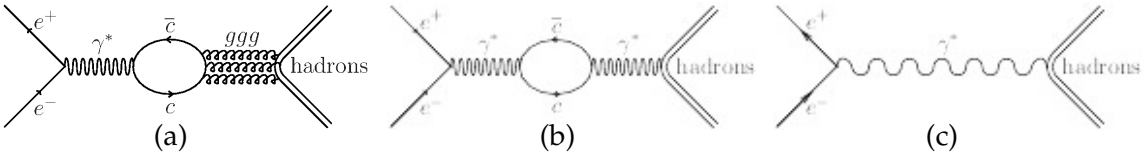

Figure 1: Diagrams for the process $e^+e^- \to$ hadrons: strong A_{3g} (a) and electromagnetic A_γ (b) contribution at ψ resonances; non-resonant electromagnetic A_{em} (c) contribution.

The interference term should vanish [7] once inclusively summing up on all the decay channels, as it is observed experimentally. This overall cancellation could be achieved because of real amplitudes with opposite sign, as expected for instance in the case of $p\overline{p}$ and $n\overline{n}$. BESIII Collaboration will soon probe the existence of a possible interference pattern between the amplitudes of Fig. 1 in all the possible exclusive channels by mean of a c.m. energy scan below the J/ψ peak (possibly in the future below the ψ' peak as well), giving access, in a model independent way, to their relative phases. A previous J/ψ scan by BESII shew no evidence for an interference pattern in the exclusive $\rho\pi$ channel [8]; exploiting the exceptional performances of BEPCII and BESIII, a final answer could be quickly achieved.

2 Measuring the phase between A_{3g} and A_γ

The BESIII Collaboration will search for an interference pattern in all the possible final states between the resonant and the non resonant amplitudes:

$$A_R = \alpha \left(\frac{x}{1+x^2} + i\frac{1}{1+x^2} \right) , \; x = \frac{M_{J/\psi} - \sqrt{s}}{\Gamma_{TOT}/2} \qquad ; \qquad A_{NR} = -\beta e^{i\Phi_p} \tag{1}$$

The resonant A_R amplitude for the process $e^+e^- \to J/\psi \to p\overline{p}$ can be factorised in a Breit-Wigner amplitude centred around the mass of the J/ψ, and a complex number α accounting for the two exclusive amplitudes A_{3g} and A_γ of Fig. 1.a and Fig. 1.b [5]. The non-resonant amplitude A_{NR} accounts for the diagram in Fig. 1.c, with $\beta^2 = \sigma\,(e^+e^- \Leftrightarrow p\overline{p})$.

Let us consider as a reference the phase $\Phi_{A_{3g}} = 0$. The phase Φ_{A_γ} is expected to be equal to the phase $\Phi_p = \Phi_{G_p^M}$ of the proton time-like form factor at $q^2 \sim M^2_{J/\psi}$, i.e. due to analyticity almost equal to that of the space-like form factor, and hence real. The same applies to $\Phi_{A_{NR}} \sim \Phi_p$ at $\sqrt{s} \sim M_{J/\psi}$. The α phase is not trivial:

$$\Phi_\alpha = \arctan \frac{|A_\gamma| \sin \Phi_p}{|A_{3g}| + |A_\gamma| \cos \Phi_p} \tag{2}$$

and depends on both the strong and e.m. resonant amplitudes moduli and on the phase Φ_p of A_γ. The overall phase of A_R is hence the sum of Φ_α and of the usual Breit-Wigner phase ($= 90^\circ$ at resonance). The interference term

$$I(x) = -\frac{2\beta\alpha}{1+x^2} \left(x \cos \Delta\Phi + \sin \Delta\Phi \right) \tag{3}$$

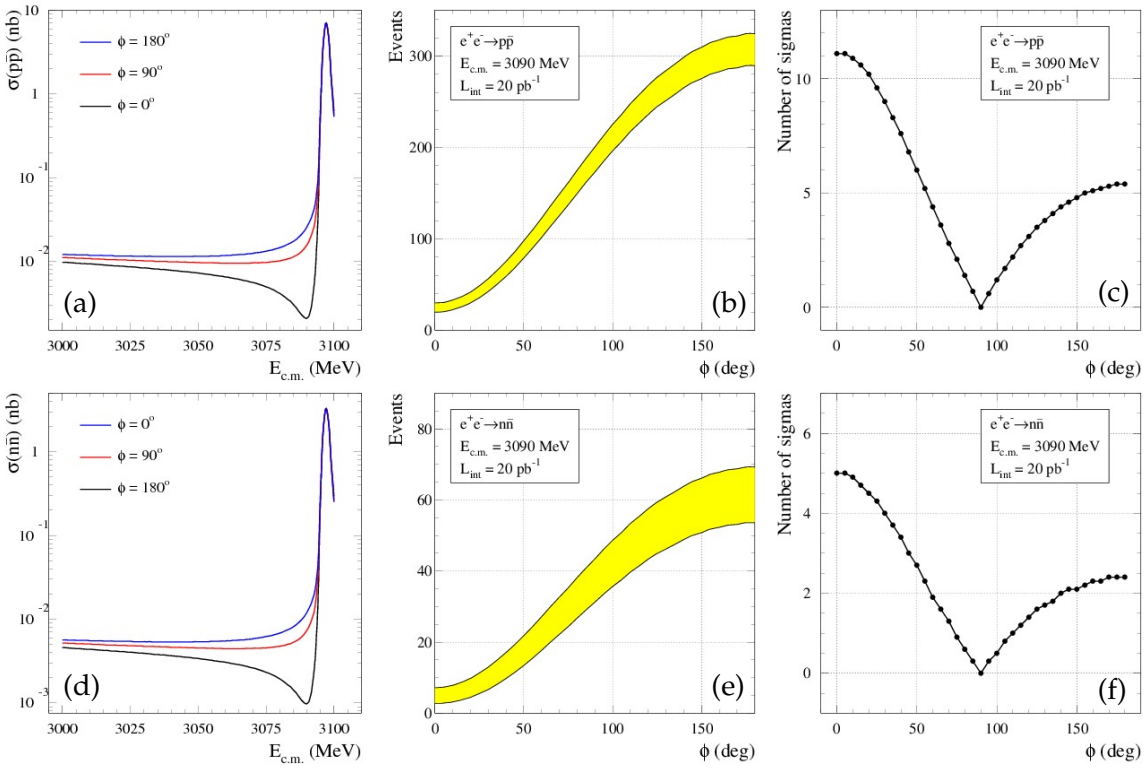

Figure 2: Left: expected interference patterns around the J/ψ peak; middle: number of events at the deep of the interference pattern; right: expected sensitivities w.r.t. the no interference scenario; for the $p\overline{p}$ and $n\overline{n}$ final states.

depends on the phase difference $\Delta\Phi = \Phi_p - \Phi_\alpha$, the physical quantity that can be directly determined through a resonance scan below the J/ψ peak. Such a scan allows to disentangle the different $\Delta\Phi$ values and to obtain through Eq. 2 the value of Φ_p with an accuracy depending on the number and on the statistics of the experimental points in the scan.

The left frames in Figures 2 and 3 show the expected interference patterns around the J/ψ peak for the $p\overline{p}$, $n\overline{n}$ and $\rho\pi$ final states in case of minimum and maximum interference. The radiative corrections and the beam energy spread proper of the BESIII scenario have been accounted for. The cross sections for a $\sqrt{s}$ roughly 100 MeV lower that $M_{J/\psi}$ are taken on as continuum references: $\sigma\left(e^+e^- \to p\overline{p}\right) \sim 11$ pb, $\sigma\left(e^+e^- \to n\overline{n}\right) \sim 5$ pb and $\sigma\left(e^+e^- \to \rho\pi\right) \sim 20$ pb [9, 10]. The $p\overline{p}$ and $n\overline{n}$ final states show opposite behaviours as expected due to the opposite signs of their magnetic moments. The central frames of Fig. 2 and 3 show, for the considered final states and under the assumption of an integrated luminosity $L_{int} = 20$ pb^{-1}, the expected dependencies on the phase Φ_p of the number of events at the deep of the interference pattern (different for each final state), while the right frames show with which sensitivity the interference patterns can be resolved from the $\Phi_P = 90^\circ$ scenarios.

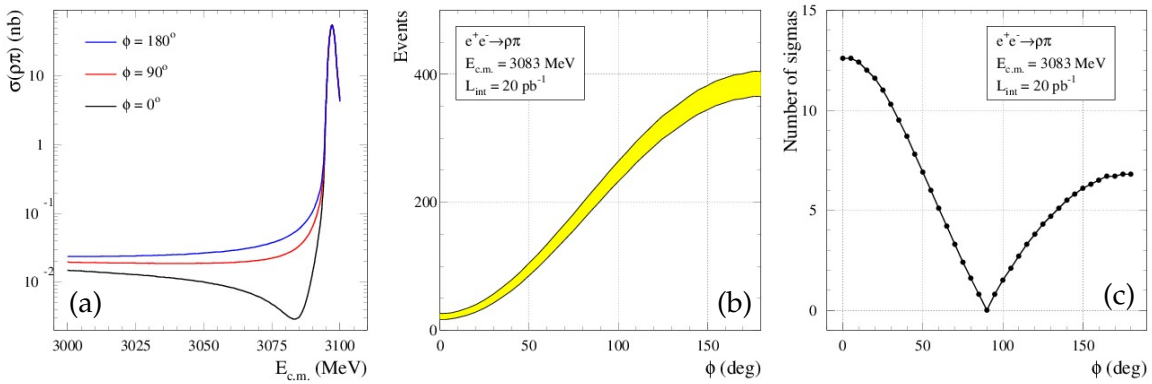

Figure 3: Left: expected interference patterns around the J/ψ peak; middle: number of events at the deep of the interference pattern; right: expected sensitivity w.r.t. the no interference scenario; for the $\rho\pi$ final state.

3 Conclusions

A c.m. energy scan below the J/ψ resonance will allow to probe at BESIII the existence of an interference pattern at the same time in all the possible exclusive final states, and to measure for the first time in a model independent way the relative phase of the strong and e.m. resonant amplitudes in the processes $e^+e^- \to J/\psi \to hadrons$.

Bibliography

[1] J. E. Augustin et al., Phys. Rev. Lett. **33**, 1406 (1974).

[2] V. L. Chernyak and I. R. Zhitnitski, Nucl. Phys. B **246**, 52 (1984).

[3] S. J. Brodsky and G. P. Lepage, Phys. Rev. D **24**, 2848 (1981).

[4] S. Pacetti and Y. Srivastava, arXiv:hep-ph/0007318 and references therein.

[5] R. Baldini, C. Bini, E. Luppi, Phys. Lett. B **404**, 362 (1997); R. Baldini et al., Phys. Lett. B **444**, 111 (1998); L. Kopke and N. Wermes, Phys. Rep. **174**, 67 (1989); J. Jousset et al., Phys. Rev. D **41**, 1389 (1990); M. Suzuki et al., Phys. Rev. D **60**, 051501 (1999).

[6] V. Chernyak, arXiv:hep-ph/9906387v2.

[7] J. M. Gerard and J. Weyers, Phys. Lett. B **462**, 324 (1999).

[8] J.Z. Bai et al., Phys. Rev. D **54**, 1221 (1996).

[9] B. Aubert et al., Phys. Rev. D **73**, 012005 (2006).

[10] R. Baldini, S. Pacetti and A. Zallo, arXiv:1008.0542v1 [hep-ph].

Study of charmonium spectroscopy at BESIII

Liangliang Wang[1] on behalf of the BESIII Collaboration
Institute of High Energy Physics, Chinese Academy of Sciences
Beijing, CHINA

In this talk, we will present the results on the charmonium spin singlet states below the open charm threshold, including h_c, η_c, and $\eta_c(2S)$. The masses, widthes, and production rates of these states will be reported. The results are based on a data sample of 106 million ψ' events collected with the BESIII experiments at the BEPCII collider.

1 Introduction

In 2009, $(106 \pm 4) \times 10^6$ ψ' events were collected with BESIII detector at the upgraded BEPC (BEPCII) [1]. All the resent results on charmonium spectroscopy reported in this proceeding are based on this set of data.

2 Observation of h_c

In 2010, the results on the production and decay of the h_c at the ψ' resonance was reported by BESIII [2], where the distributions of mass recoiling against a detected π^0 were studied to measure $\psi' \to \pi^0 h_c$ both inclusively (E1-untagged) and in events tagged as $h_c \to \gamma\eta_c$ (E1-tagged) by detection of the E1 transition photon. In 2011, 16 specific decay processes of η_c in the decay mode of $h_c \to \gamma\eta_c$ are studied to do the measurements of the h_c properties in addition. The simultaneous fit of the 16 π^0 recoil-mass spectra (Figure 1) yields $M(h_c) = 3525.31 \pm 0.11 \pm 0.15\text{MeV/c}^2$ and $\Gamma(h_c) = 0.70 \pm 0.28 \pm 0.25\text{MeV/c}^2$, where the first errors are statistical and the second systematic. These preliminary results are consistent with the previous BESIII inclusive results and CLEOc exclusive results ($M(h_c) = 3525.21 \pm 0.27 \pm 0.14\text{MeV/c}^2$) [3].

[1] llwang@ihep.ac.cn

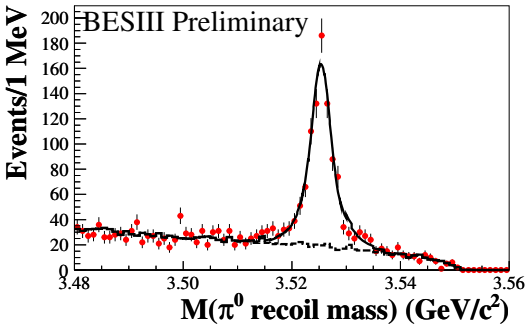

Figure 1: The summed π^0 recoil-mass spectrum of 16 specific decay processes of η_c in the decay mode of $h_c \to \gamma\eta_c$, where the line is the fit result.

3 Precision measurement of the η_c properties

With the largest ψ' sample collected by BESIII, the η_c mass and width are measured in the radiative transition $\psi' \to \gamma\eta_c$, where six decay modes of η_c are involved: $K^0_S K\pi$, $K^+K^-\pi^0$, $\pi^+\pi^-\eta$, $K^0_S K3\pi$, $K^+K^-\pi^+\pi^-\pi^0$ and $3(\pi^+\pi^-)$. A simultaneous fit with the unique η_c mass and width is performed on the η_c mass spectra, where the interference between η_c and non-η_c decays is considered and the quantum number of the non-η_c components are assumed to be 0^{-+}. The corresponding interference phase angles in different decay modes are found to be quite consistent and then set to the same one in final fit. The mass spectra and the simultaneous fit for different decay modes are shown in Figure 2. The obtained results are $M(\eta_c) = 2984.2 \pm 0.6 \pm 0.5\text{MeV/c2}$, $\Gamma(\eta_c) = 31.4 \pm 1.2 \pm 0.6\text{MeV}$, and $\phi = 2.41 \pm 0.06 \pm 0.04\text{rad}$, where the first errors are statistical and the second systematic. The BESIII preliminary results are consistent with those from two-photon production [4–6], as well as $J/\psi \to \gamma\eta_c$ by CLEOc [7]. And the precision of the measured mass and width are improved.

4 The first observation of the M1 transition $\psi' \to \gamma\eta_c(2S)$

BESIII observed this M1 transition $\psi' \to \gamma\eta_c(2S)$ with the decay mode $\eta_c(2S) \to K_S K\pi$ for the first time. Figure 3 shows the preliminary result for the invariant mass distribution of $K^0_S K\pi$ that the three-constraints kinematic fit has been applied (where the energy of the photon is allowed to be floating). The pure statistical significance is more than 6σ. The yielded events number is 50.6 ± 9.7 and $M(\eta_c(2S)) = 3638.5 \pm 2.3 \pm 1.0\text{MeV/c}^2$. With the detection efficiency from MC simulation, $B(\psi' \to \gamma\eta_c(2S) \to \gamma K^0_S K\pi) = (2.98 \pm 0.57 \pm 0.48) \times 10^{-6}$ is obtained. Combining the result $B(\eta_c(2S) \to K\overline{K}\pi) = (1.9 \pm 0.4 \pm 1.1)\%$

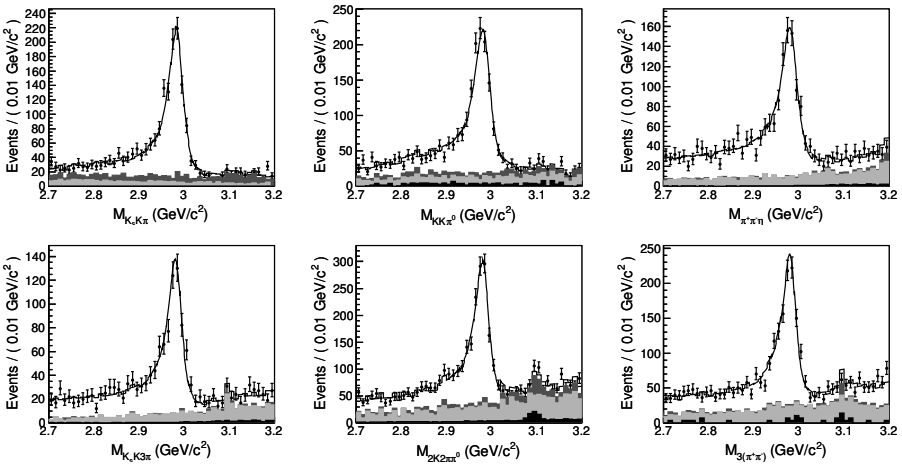

Figure 2: The mass spectra for different decay modes, where the line is the result of the simultaneous fit.

from Babar, it is first calculated that $B(\psi' \to \gamma\eta_c(2S)) = (4.7 \pm 0.9 \pm 3.0) \times 10^{-4}$ which is consistent with the CLEOc's upper limit [8] and prediction of potential model [9], where the first errors are statistical and the second systematic.

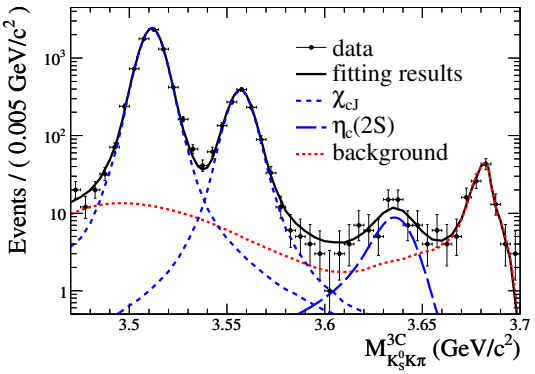

Figure 3: The invariant mass of $K_S^0 K\pi$ from $\psi' \to \gamma K_S^0 K\pi$.

5 Summary

With the largest ψ' data collected by BESIII, the following results on Charmonium spectroscopy are obtained: the properties of h_c are measured with inclusive and exclusive

methods respectively; the properties of η_c are precisely measured using the radiative decays of ψ', where the interference between η_c decays and non-η_c decays is taken into account; the M1 transition $\psi' \to \gamma\eta_c(2S)$ is observed for the first time.

Acknowledgments

We thank the BEPCII group for excellent operation of the accelerator, the IHEP computer group for valuable computing and network support, and all the colleagues contribute on the physical measurements.

Bibliography

[1] M. Ablikim *et al.* (BESIII Collaboration), *Phy. Rev. D* **81**, 052005 (2010).

[2] M. Ablikim *et al.* (BESIII Collaboration), *Phys. Rev. Lett.* **104**, 132002 (2010).

[3] S. Dobbs *et al.*(CLEO Collaboration), *Phys. Rev. Lett.* **101**, 182003 (2008).

[4] D. M. Asner *et al.*(CLEO Collaboration), *Phys. Rev. Lett.* **92**, 142001 (2004).

[5] B. Aubert *et al.*(BABAR Collaboration), *Phys. Rev. Lett.* **92**, 142002 (2004).

[6] S. Uehara *et al.*(Belle Collaboration), *Eur. Phys. J. C* **53**, 1 (2008).

[7] R. E. Mitchell *et al.*(CLEO Collaboration), *Phys. Rev. Lett.* **102**, 011801 (2009).

[8] D. Cronin-Hennessy, K. Y. Gao *et al.* (CLEO-c Collaboration), *Phys. Rev. D* **81**, 052002 (2010).

[9] Estia J. Eichten, Kenneth Lane, Chris Quigg, *Phys. Rev. Lett.* **89**, 162002 (2002).

Microscopic Model of Charmonium Strong Decays

Jorge Segovia[1], D.R. Entem, and F. Fernández
Departamento de Física Fundamental and IUFFyM
Universidad de Salamanca, E-37008 Salamanca, Spain

Although the spectra of heavy quarkonium systems has been successfully explained by certain QCD motivated potential models, their strong decays are difficult to deal with. We perform a microscopic calculation of charmonium strong decays using the same constituent quark model which successfully describes the $c\bar{c}$ meson spectrum. We compare the numerical results with the $^3P_0$ and the experimental data. Comparison with other predictions from similar models are included.

1 Introduction

Meson strong decay is a complex non-perturbative process that has not yet been described from QCD first principles. Instead, several phenomenological models have been developed to deal with this topic, like the $^3P_0$ model [1], the flux-tube model [2], or microscopic models (see Refs. [3–5]). The difference between the two approaches lies on the description of the $q\bar{q}$ creation vertex. While the $^3P_0$ model assumes that the $q\bar{q}$ pair is created from the vacuum, in the microscopic models the $q\bar{q}$ pair is created from the interquark interactions acting in the model.

The main ingredients in both calculations are the one-gluon exchange and the linear confinement. The differences lie in the Lorentz structure of the confinement being vector for Ref. [3, 4] and scalar for Ref. [5]. Phenomenology suggests that confinement has to be dominantly scalar in order to reproduce the hyperfine splitting observed in the charmonium sector. Strong decays may provide a new physics of information about the Lorentz structure.

In the present work, we generalize the schematic microscopic models of Refs. [3–5] using a more realistic constituent quark model which includes a linear screened confinement and studying the possible influence of the mixture of scalar and vector Lorentz structures.

[1] segonza@usal.es

2 Constituent quark model

Constituent quark masses, coming from the spontaneous chiral symmetry breaking of the QCD Lagrangian, together with the perturbative one-gluon exchange (OGE) and the non-perturbative confining interaction are the main pieces of potential models. In a pure gluon gauge theory the potential energy of the $q\bar{q}$ pair grows linearly with the interquark distance. However, the presence of sea quarks may soften the linear potential. Using this idea, Vijande *et al.* [6] developed a model which is able to describe meson phenomenology from the light to the heavy quark sector. This model incorporates a confinement potential $V_{\rm CON}^{\rm scalar}(\vec{r}_{ij}) = V_{\rm CON}^{\rm vector}(\vec{r}_{ij}) = \left[-a_c(1-e^{-\mu_c r_{ij}})+\Delta\right](\vec{\lambda}_i^c\cdot\vec{\lambda}_j^c)$, with a mixture of a scalar and vector Lorentz structures $V_{\rm CON}(\vec{r}_{ij}) = a_s V_{\rm CON}^{\rm scalar}(\vec{r}_{ij}) + (1-a_s)V_{\rm CON}^{\rm vector}(\vec{r}_{ij})$.

To evaluate the strong decay amplitudes, we solve the Schrödinger equation using the Gaussian Expansion Method [7]. The model parameters can be found in Ref. [8].

3 A microscopic decay model

In the microscopic decay models the interaction Hamiltonian can be written as [5]

$$H_I = \frac{1}{2}\int d^3x d^3y\, J^a(\vec{x})K(|\vec{x}-\vec{y}|)J^a(\vec{y}). \tag{1}$$

The current J^a in Eq. (1) is assumed to be a color octet. The currents J (with the color dependence $\lambda^a/2$ factored out) are $J(\vec{x}) = \overline{\psi}(\vec{x})\Gamma\psi(\vec{x})$ where $\Gamma = \mathcal{I}$, γ^0, $\vec{\gamma}$. The kernels associated with the currents described before are $K(r) = -4a_s\left[-a_c(1-e^{-\mu_c r})+\Delta\right]$, $+\frac{\alpha_s}{r}$ and $-\frac{\alpha_s}{r}$. For the vector Lorentz structure of the confinement we use as a kernel $K(r) = \pm(1-a_s)4\left[-a_c(1-e^{-\mu_c r})+\Delta\right]$, where $\pm$ refers to static and transverse vector terms, respectively.

4 Results and conclusions

The predictions for the total decay rates using the $^3P_0$ and the microscopic model are shown in Table 1. In general the total widths are lower in the microscopic model without improving the agreement with the experimental data.

It is difficult to compare our results with former calculations because either they are not fitted to the heavy quark sector [5] or does not include the same pieces of the current [3,4]. For the sake of the comparison we show in Table 2 the results of Ref. [4] together with our model prediction including only the static vector contribution and the full decay model. The basic difference between the two calculations is that in Ref. [4] the coupling with the meson-meson channels is treated nonperturbatively and this enhances the results when the threshold is close to the state. The predictions of the full decay model are clearly below the experimental data.

State	$^3P_0$	Mic.	Ref. [9]	Ref. [10]
$\psi(3770)$	26.4	19.0	27.6 ± 1.0	
$\psi(4040)$	111.0	39.1	80 ± 10	
$\psi(4160)$	115.7	32.7	103 ± 8	
$X(4360)$	113.7	102.2	$74 \pm 15 \pm 10$	
$\psi(4415)$	115.7	42.7	62 ± 20	119 ± 16
$X(4630)$	206.0	188.2	92^{+40+10}_{-24-21}	
$X(4660)$	134.8	142.2	$48 \pm 15 \pm 3$	

Table 1: Total decay rates, in MeV, predicted by the $^3P_0$ and the microscopic models.

Decay	Ref. [4]	j^0Kj^0	Mic.	Exp. [9]
$\psi(3770) \to DD$	20.1	29.8	19.0	27.6 ± 1
$\psi(4040) \to DD$	0.1	1.4	10.2	
$\psi(4040) \to DD^*$	33.0	25.2	18.7	
$\psi(4040) \to D^*D^*$	33.0	35.0	9.1	
$\psi(4040) \to D_sD_s$	8.0	0.3	1.1	
total	74.0	61.9	39.1	80 ± 10
$\psi(4160) \to DD$	3.2	25.0	17.0	
$\psi(4160) \to DD^*$	6.9	0.5	7.4	
$\psi(4160) \to D^*D^*$	41.9	21.3	5.3	
$\psi(4160) \to D_sD_s$	5.6	0.03	2.6	
$\psi(4160) \to D_sD_s^*$	11.0	0.6	0.4	
total	69.2	47.4	32.7	103 ± 8

Table 2: Decay rates, in MeV, reported in Ref. [4] and our decay rates taking into account only the static vector contribution and the full model.

Finally, in Table 3 we compare the experimental ratios of some charmonium decays with the prediction of the different models. None of them can explain the experimental data.

Therefore the full model has not solved the disagreement of the theoretical calculation with the data and more theoretical and experimental work is needed to solve the problem of the charmonium strong decay widths.

Acknowledgments

This work has been partially funded by Ministerio de Ciencia y Tecnología under Contract No. FPA2010-21750-C02-02, by the European Community-Research Infrastructure Integrating Activity 'Study of Strongly Interacting Matter' (HadronPhysics2 Grant No. 227431) and by the Spanish Ingenio-Consolider 2010 Program CPAN (CSD2007-00042).

State	Ratio	Cornell	j^0Kj^0	Mic.	$^3P_0$	Measured [9]
$\psi(4040)$	$D\overline{D}/D\overline{D}^*$	0.003	0.06	0.54	0.21	$0.24 \pm 0.05 \pm 0.12$
	$D^*\overline{D}^*/D\overline{D}^*$	1.00	1.39	0.48	3.70	$0.18 \pm 0.14 \pm 0.03$
$\psi(4160)$	$D\overline{D}/D^*\overline{D}^*$	0.08	1.17	3.23	0.27	$0.02 \pm 0.03 \pm 0.02$
	$D\overline{D}^*/D^*\overline{D}^*$	0.16	0.02	1.40	0.03	$0.34 \pm 0.14 \pm 0.05$
$X(4360)$	$D\overline{D}/D^*\overline{D}^*$	-	0.40	0.12	0.90	$0.14 \pm 0.12 \pm 0.03$
	$D\overline{D}^*/D^*\overline{D}^*$	-	0.08	0.64	0.92	$0.17 \pm 0.25 \pm 0.03$
$\psi(4415)$	$D\overline{D}/D^*\overline{D}^*$	-	1.54	1.10	0.46	$0.14 \pm 0.12 \pm 0.03$
	$D\overline{D}^*/D^*\overline{D}^*$	-	0.28	0.92	0.18	$0.17 \pm 0.25 \pm 0.03$

Table 3: Some ratios predicted theoretically by the $^3P_0$ and the microscopic models. The comparison with the experimental data is included.

Bibliography

[1] L. Micu, Nucl. Phys. B **10**, 521 (1969); A. Le Yaouanc, L. Oliver, O. Péne and J. Raynal, Phys. Rev. D **8**, 2223 (1973); **9**, 1415 (1974); **11**, 1272 (1975).

[2] R. Kokoski and N. Isgur, Phys. Rev. D **35**, 907 (1987).

[3] E. Eichten, K. Gottfried, T. Kinoshita, K.D. Lane and T. M. Yan, Phys. Rev. D **17**, 3090 (1978); **21**, 203 (1980).

[4] Estia. J. Eichten, Kenneth Lane, and Chris Quigg, Phys. Rev. D **73** 014014 (2006)

[5] E.S. Ackleh, T. Barnes and E.S. Swanson, Phys. Rev. D **54**, 6811 (1996).

[6] J. Vijande, F. Fernández, and A. Valcarce, J. Phys. G **31**, 481 (2005).

[7] E. Hiyama, Y. Kino, and M. Kamimura, Prog. Part. Nucl. Phys. **51**, 223 (2003).

[8] J. Segovia, A.M. Yasser, D.R. Entem and F. Fernández, Phys. Rev. D **78**, 114033 (2008).

[9] K. Nakamura *et al.* (Particle Data Group), J. Phys. G **37**, 075021.

[10] K. K. Seth, Phys. Rev. D **72**, 017501 (2005).

Does $I = 1$ Isospin State Exist in $c\bar{c}$ Meson?

Hiroshi Noya[1,a] and Hiroshi Nakamura[b]
[a]*Institute of Physics, Hosei University at Tama, Machida, Tokyo 194-0298, Japan*
[b]*Department of Physics and Mathematics, College of Science and Engineering, Aoyamagakuin University, Fuchinobe, Sagamihara, Kanagawa 229-8558, Japan*

We analyze for X series $c\bar{c}$ mesons with the Diquark Cluster Model except for X(3872) meson. The mass formula for the $q^k\bar{q}^h$ system, which consistens of u,d,s and c quark, is given by

$$\begin{aligned} M = m_q\, n_T + M(1p_{1/2})\, n(1p_{1/2}) + M(1p_{3/2})\, n(1p_{3/2}) + M(1d_{3/2})\, n(1d_{3/2}) \\ + M(1d_{5/2})\, n(1d_{5/2}) + M(2s_{1/2})\, n(2s_{1/2}) \\ + \Delta_0\, (n_{\phi_0} + n_{\bar{\phi}_0}) + \Delta_1\, (n_{\phi_1} + n_{\bar{\phi}_1}) + \Sigma\Delta_{TS}. \end{aligned}$$

The M is the meson mass and m_q is the quark mass and the total quark number n_T = k + h where k is a number of quark and h is a number of antiquark. The M(nlj) is the single excitation energy from the $1s_{1/2}$ shell with the principal quantum number n and orbital and total angular momentum l and j.
The n(nlj) is the total number of excited quarks and antiquarks in the shell. The u or d quark quark-quark interaction in the s state diquark cluster is the following.
The interaction energy of the diquark cluster in the s state are

Δ_0= a – 3/4b for the spin 0, Δ_1= a + 1/4b for the spin 1,
a = 187 MeV, b = 195 MeV.

When one s quark includes for the s state insted of u or d quark, the interaction parameter a is the same but $b_s = (m/m_s)b$ where m is the u or d quark mass and m_s is the mass of s quark. Relating to the u,d and s quark parameters were already published [1]. The charm quark mass m_c = 1646 MeV and the interacion parameter a_c = 38.4 MeV are oblained using the mass of Λ_c and X(3845) meson. The n-c quark interaction, b is $b_c = (m/m_c)\, b$. The s-c quark intraction case, a_{cs} = - 34.7MeV is obtained by the X(4140) meson mass.

[1]hiroshinoya@yahoo.com

The interaction energy of the diquark cluster in the p state are

$$\Delta_{00} = \Delta_{11} = \Delta_{01} = 0, \Delta_{10} = -60 \text{ MeV}.$$

for u or d quark.
And Δ^s_{60} = - 19 MeV, $\Delta^s_{3*0} = 0$ in the p state if s quark includes one. Δ^c_{60} = - 5.5 MeV, $\Delta^c_{3*0} = 0$ in the p state if c quark includes one. One of the c or s quark in the p shell and the other one is in the s shell, Δ^{cs}_{60} = - 3.4 MeV, $\Delta^c_{3*0} = 0$. The first suffix of Δ_{ts} presents an isospin or flavour and second one is a spin,respectivly.

There are no any free parameter remains in our calculations. We will discusses the calculated results in three part. The first part is an ordinary cn $\overline{\text{cn}}$ quark system except X(3872).

In our calculation, X(3945) is the ground state of cn $\overline{\text{cn}}$ system.
We fixed the interaction parameter a_c by this meson. The mass, isospin, and spin for X(3940), X(4160), X(4260), X(4360) and X(4660) mesons are calculated and results are shown in Table 1.

Meson	Exp.	Configuration/[TS][TS] : $I^g(J^{pc})$	Cal.
X(3945)	3916	$[(1s_{1/2})_c(1s_{1/2})]^2$	Input
	$0^+(?^{?+})$	$[1/2\ 0][1/2\ 0] : 0^+(0^{++})$	
X(3940)	3942	$[(1s_{1/2})_c(1s_{1/2})]^2$	3951
	$?^?(?^{??})$	$[1/2\ 0][1/2\ 1] : 0^+(0^{++}),0^-(1^{+-})$	
X(4050)$^{\pm}$	4051	$[(1p_{1/2})_c(1s_{1/2})][(1s_{1/2})_c(1s_{1/2})]$	4056
	$?^?(?^?)$	$[1/2\ 0][1/2\ 1] : 1^-(1^-)$	
X(4160)	4156	$[(1p_{1/2})_c(1s_{1/2})][(1s_{1/2})_c(1p_{1/2})]$	4161
	$?^?(?^{??})$	$[1/2\ 0][1/2\ 1] : 0^+(1^{++})$	
X(4250)$^{\pm}$	4248	$[(1s_{1/2})_c(1p_{1/2})][(2s_{1/2})_c(1s_{1/2})]$	4279
	$?^?(?^?)$	$[1/2\ 0][1/2\ 1] : 1^-(1^-)$	
X(4260)	4263	$[(2s_{1/2})_c(1s_{1/2})][(1s_{1/2})_c(1p_{1/2})]$	4264
	$?^?(1^{--})$	$[1/2\ 1][1/2\ 0] : 0^-(1^{--})$	
X(4360)	4361	$[(1p_{1/2})_c(1s_{1/2})][(1s_{1/2})_c(1d_{3/2})]$	4383
	$?^?(1^{--})$	$[1/2\ 1][1/2\ 1] : 0^-(1^{--})$	
X(4430)$^{\pm}$	4443	$[(1p_{1/2})_c(1s_{1/2})][(1s_{1/2})_c(1p_{3/2})]$	4413
	$?^?(?^?)$	$[1/2\ 1][1/2\ 1] : 1^+(1^+)$	
X(4660)	4664	$[(1p_{1/2})_c(1s_{1/2})][(1s_{1/2})_c(2s_{1/2})]$	4637
	$?^?(1^{--})$	$[1/2\ 0][1/2\ 1] : 0^-(1^{--})$	

Table 1 : cn $\overline{\text{cn}}$ meson (unit MeV)

The mass, spin and parity of X(3940), X(4160), X(4260) are very good reproduced the experimental results. According to the Belle experiment [2], X(4050)$^{\pm}$, X(4250)$^{\pm}$ are decaying to $\pi^{+}\chi_{c1}(1p)$ and the BaBar and the Belle [3] experiment shown X(4430)$^{\pm}$ goes to $\pi^{+}\psi(2s)$ decay instated of two π mesons decay for these mesons.

In the strong decay the isospin is conserved. These three X mesons must have the isospin 1 because their decay products. This is the strong evidence that these mesons are consisting of the four quark meson. Our calculated results are naturally explaining for this situation. X(4050)$^{\pm}$, X(4250)$^{\pm}$ mass are reproduced quite well. All chaged three mesons are also in Table 1.

X(4260) is very interesting meson. If cn $\overline{\text{cn}}$ configuratin is used, we obtained very good agreement with the experimental mass. But using the Maiani et al configuration [4], the result is the same as Maiani's even it is completely different calculation method but it is poor agreement with the experimental mass.

X(4140) and X(4350) mesons are the four quark charmed strange meson because of the decay mode. X(4140) is the ground state of cs $\overline{\text{cs}}$ system. We use this meson to determine the parameter a_{cs} . We calculate the mass, isospin and spin with no free parameters remaining. The result is shown in Table 2. The mass of X(4350) is excellent reproduced and also it is suggest that this is the exotic meson $J^{PC} = 1^{-+}$.

Meson	Exp.	Configuration/[TS][TS] : $I^{g}(J^{pc})$	Cal.
X(4140)	4143	$[(1s_{1/2})_c(1s_{1/2})_s]^2$	Input
	$0^{+}(?^{?+})$	$[0\ 0][0\ 0] : 0^{+}(0^{++})$	
X(4260)	4263	$[(1p_{1/2})_c(1s_{1/2})_s][(1s_{1/2})_c(1p_{1/2})_s]$	4336
	$?^{?}(1^{--})$	$[0\ 1][1\ 0] : 0^{-}(1^{--})$	
X(4350)	4351	$[(1p_{3/2})_c(1s_{1/2})_s][(1s_{1/2})_c(1s_{1/2})_s]$	4347
	$0^{?}(?^{?+})$	$[0\ 0][0\ 1] : 0^{+}(1^{-+})$	
?	?	$[(1d_{3/2})_c(1s_{1/2})_s][(1s_{1/2})_c(1s_{1/2})_s]$	4443
	?	$[0\ 1][0\ 0] : 0^{+}(1^{++})$	

Table 2 : cs $\overline{\text{cs}}$ meson (unit MeV)

Concluding remarks:

The interesting results are I = 1 state exists for c$\bar{\text{c}}$ meson. These states cannot be explained by the simple c$\bar{\text{c}}$ meson. This is the strong evidence of the existence of the four quark state.

X(4140) and X(4350) are cs $\overline{\text{cs}}$ the charmed strange four quark meson. Especially X(4350) is possible as the exotic meson $J^{PC} = 1^{-+}$ from our calculation.

Bibliography

[1] Y. Uehara, N. Konno, H. Nakamura and H. Noya, Nucl. Phys. **A606**, 357 (1996); H. Noya and H. Nakamura, AIP Conference **1257**, 277 (2010).

[2] R. Mizuk *et al.*, Phys. Rev. **D78**, 072004 (2008).

[3] B. Aubert *et al.*, Phys. Rev. **D79**, 112001 (2009); R. Mizuk *et al.*, Phys. Rev. **D80**, 0311004(R) (2009); S. K. Choi *et al.*, Phys. Rev. Lett. **100**, 142001 (2008).

[4] L. Maiani *et al.*, Phys. Rev. **D72**, 031502(R) (2005).

HEAVY QUARKONIA
Recent Results from CLEO

Kamal K. Seth[1]
Northwestern University
Evanston, IL, USA

1 Introduction

Before it stopped data taking in 2008, CLEO had accumulated a large amount of e^+e^- data in the bottomonium and charmonium regions, as shown in Table 1. These data have led to valuable contributions in the spectroscopy of both $|c\bar{c}\rangle$ and $|b\bar{b}\rangle$ quarkonia, and their continuing analysis is leading to new physics results. In this presentation I want to describe some of the results obtained since HADRON 2009 [1]. More than a dozen papers on spectroscopy have been published since then, and my choice for this time-limited presentation is necessarily a subjective one.

Charmonium region	**Bottomonium region**
$\psi(2S, 3686) : 54\ \text{pb}^{-1}, \sim 27$ million $\psi(2S)$	$\Upsilon(1S) : 1056\ \text{pb}^{-1}, 20.8$ million $\Upsilon(1S)$
$\psi(3770) : 818\ \text{pb}^{-1}, \sim 5$ million $\psi(3770)$	$\Upsilon(2S) : 1305\ \text{pb}^{-1}, 9.3$ million $\Upsilon(2S)$
$\psi(4170) : 586\ \text{pb}^{-1}, \sim 5$ million $\psi(4170)$	$\Upsilon(3S) : 1378\ \text{pb}^{-1}, 5.9$ million $\Upsilon(3S)$
$\sqrt{s} = 3670$ MeV : $21\ \text{pb}^{-1}$	$\Upsilon(4S) : 9400\ \text{pb}^{-1}, 15.4$ million $B\overline{B}$
$\sqrt{s} = 4040$ MeV : $20.7\ \text{pb}^{-1}$	$\sqrt{s} = 10,520$ MeV : $4500\ \text{pb}^{-1}$
$\sqrt{s} = 4260$ MeV : $13.2\ \text{pb}^{-1}$	Off $\Upsilon(nS) : 800\ \text{pb}^{-1}$

Table 1: CLEO data in the charmonium and bottomonium regions

2 Hyperfine Interaction in Quarkonia

One of our major interests at CLEO during the last five years has been in the study of the hyperfine interaction in quarkonia, and our investigations into it have continued to yield new insights into the subject.

[1] kseth@northwestern.edu

The hyperfine or spin-spin interaction in $|c\bar{c}\rangle$ and $|b\bar{b}\rangle$ quarkonia leads to the hyperfine splitting between spin-triplet and spin-singlet states, which is defined as

$$\Delta M_{hf}(nL) = M(n^3L) - M(n^1L)$$

where n and L are the principal and angular momentum quantum numbers.

For a purely Coulombic central potential, as for $|e^+e^-\rangle$ positronium, for $|q\bar{q}\rangle$ quarkonium the hyperfine interaction is a contact interaction, and leads to the predictions —

$$\Delta M_{hf}(nS) = M(n^3S_1) - M(n^1S_0) = \frac{32\pi\alpha_s(m_q)}{9}(\psi(0)/m_q)^2, \quad L = 0$$

$$\Delta M_{hf}(nL) = M(n^3L) - M(n^1L) = 0, \qquad L \neq 0$$

where $\alpha_s(m_q)$ is the strong coupling constant for quark mass m_q, and $\psi(0)$ is the wave function at the origin.

The interest for quarkonia is in determining the extent to which these predictions are valid, because for quarkonia the central potential has the confinement part in addition to the Coulombic part, and the charm and beauty quarks, which have different masses, bring in different relativistic and higher order effects.

As is well known, in e^+e^- annihilation the spin-triplet-S wave states, called ψ_c and Υ_b, $^3S_1(J^{PC} = 1^{--})$ are directly produced, and the spin-triplet P-wave states, $^3P_J(J^{PC} = 0^{++}, 1^{++}, 2^{++})$, called χ_{cJ},χ_{bJ}, are strongly excited by E1 radiative transitions from the triplet S states. In contrast, the M1 radiative transitions to the spin-singlet states, $^1S_0(J^{PC} = 0^{-+})$, called η_c and η_b, and $^1P_1(J^{PC} = 1^{+-})$, called h_c and h_b, are much weaker and much more difficult to identify because of their close proximity to the triplet states. As a result, for more than two decades after the discovery of $J/\psi(1^3S_1)_{c\bar{c}}$, $\psi(2^3S_1)_{c\bar{c}}$, and $\Upsilon(n^3S_1)_{b\bar{b}}(n = 1, 2, 3, 4)$, the only singlet state which was successfully identified was $\eta_c(1^1S_0)$, and the only hyperfine splitting which was known was $\Delta M_{hf}(1S)_{c\bar{c}} = 116.6 \pm 1.2$ MeV [2]. As a result, it was not known how the hyperfine interaction between quarks changes with greater exposure to the confinement potential with increasing redius (1S versus 2S), with increasing angular momentum (S-wave versus P-wave), and increasing quark mass (c-quarks versus b-quarks). Great progress in answering these questions has been recently made by B-factories and CLEO in challenging new measurements. Belle identified $\eta_c'(2^1S_0)$ in B-decays [3], and it was confirmed by CLEO [4] and BaBar [5] in two photon formation. CLEO [6] identified $h_c(1^1P_1)$ in $\psi(2S)$ decay. BaBar [7] identified $\eta_b(1^1S_0)$ in $\Upsilon(3S)$ decays, and it was confirmed by CLEO [8]. Identification of $\eta_c(3^1S_0)$ and $h_c(2^1P_1)$, which lie above the $D\overline{D}$ break-up threshold, and $\eta_b(2, 3^1S_0)$ and $h_b(1, 2^1P_1)$ remained as challenges[2].

[2]For the breaking news on the discovery of $h_b(1, 2^1P_1)$ see Ref [14].

3 New Results for P-wave Singlet State $h_c(1^1P_1)$

CLEO reported the discovery of h_c in 2005 [6], and the precision measurement of its mass in 2008 [9],

$$\text{CLEO [2008]}: \; M(h_c, 1^1P_1) = 3525.28 \pm 0.19(\text{stat}) \pm 0.12(\text{syst}) \text{ MeV}.$$

It is extremely gratifying that BES III [10] has now confirmed this, with the result:

$$\text{BES III [2010]}: \; M(h_c, 1^1P_1) = 3525.40 \pm 0.13(\text{stat}) \pm 0.18(\text{syst}) \text{ MeV}.$$

The centroid of the ^3P_J states ($\chi_{0,1,2}$) is known to be [2]

$$\langle M(^3P_J)\rangle = [5M(^3P_2) + 3M(^3P_1) + M(^3P_0)] = 3525.30 \pm 0.04 \text{ MeV}.$$

If the ^3P_J states centroid mass $\langle M(^3P_J)\rangle$ above is identified as the mass $M(^3P)$, then the hyperfine splittings are

$$\text{CLEO:} \quad \Delta M_{hf}(1P)_{c\bar{c}} = +0.02 \pm 0.23 \text{ MeV, and}$$

$$\text{BES III:} \quad \Delta M_{hf}(1P)_{c\bar{c}} = -0.10 \pm 0.22 \text{ MeV}.$$

However, it must be pointed out that the identification of the centroid is only valid if the spin-orbit splitting between the ^3P_J states in perturbatively small. This is hardly the case here with $M(^3P_2) - M(^3P_0) = 141.45 \pm 0.32$ MeV, and the perturbative prediction $M(^3P_1) - M(^3P_0) = (5/2) \times [M(^3P_2) - M(^3P_1)] = 114$ MeV is 20% larger than the experimental result = 96 MeV. Why then is $\Delta M_{hf}(1P)$ so very close to zero? It is a mystery.

3.1 Beyond the discovery of h_c [11]

In our h_c discovery and mass papers in the decay

$$\psi(2S) \to \pi^0 h_c, \; h_c \to \gamma\eta_c$$

we made inclusive analyses of the π^0 recoil spectrum by either constraining the γ energy or η_c mass. As a result we could only determine the product branching fraction $\mathcal{B}(\psi(2S) \to \pi^0 h_c) \times \mathcal{B}(h_c \to \gamma\eta_c)$.

BES III data for 100 million $\psi(2S)$ allowed them to observe h_c directly in the π^0 recoil spectrum. It occured to us at CLEO recently to also attempt to also identify h_c directly in the π^0 recoil spectrum despite our factor four smaller 25.9 million $\psi(2S)$ sample. By rejecting very asymmetric $\pi^0 \to 2\gamma$ decays, as shown in Fig. 1, we were successful in identifying h_c. Our result is in excellent agreement with the BES III result [10]

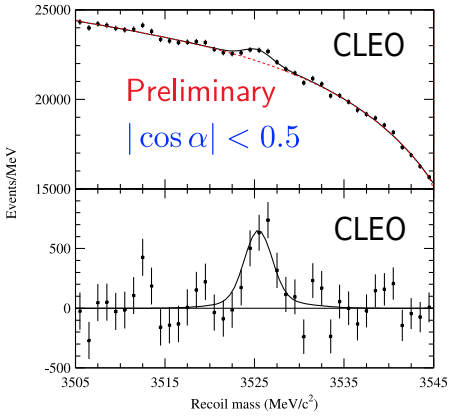

Figure 1: New CLEO result for the inclusive analysis of $\psi(2S) \to \pi^0 h_c$

CLEO: $\mathcal{B}[\psi(2S) \to \pi^0 h_c] = (9.0 \pm 1.5 \pm 1.2) \times 10^{-4}$ [11]

BES III: $\mathcal{B}[\psi(2S) \to \pi^0 h_c] = (8.4 \pm 1.3 \pm 1.0) \times 10^{-4}$ [10]

Average: $\mathcal{B}[\psi(2S) \to \pi^0 h_c] = (8.7 \pm 1.2) \times 10^{-4}$

3.2 Hadronic decays of h_c [12]

The CLEO result [9] $\mathcal{B}_1(\psi(2S) \to \pi^0 h_c) \times \mathcal{B}_2(h_c \to \gamma\eta_c) = (4.19 \pm 0.55) \times 10^{-4}$ has also been confirmed by BES III [10] with $\mathcal{B}_1(\psi(2S) \to \pi^0 h_c) \times \mathcal{B}_2(h_c \to \gamma\eta_c) = (4.58 \pm 0.64) \times 10^{-4}$, and the average is $\mathcal{B}_1(\psi(2S) \to \pi^0 h_c) \times \mathcal{B}_2(h_c \to \gamma\eta_c) = (4.39 \pm 0.42) \times 10^{-4}$. Combined with $\mathcal{B}_1(\psi(2S) \to \pi^0 h_c) = (8.7 \pm 1.2) \times 10^{-4}$, we obtain $B_2(h_c \to \gamma\eta_c) = (50.5 \pm 8.5)\%$. Therefore, we expect that the remaining 50% decays of h_c must be to hadrons. This suggests that decays to odd number of pions may be an important component of the hadronic decays. We have therefore measured [12]

$$\psi(2S) \to \pi^0 h_c,\ h_c \to (\pi^+\pi^-)\pi^0,\ n = 1, 2, 3$$

Unfortunately, no significant yield was found for 3 or 7 pion final states. Only a small 5 pion transition was observed with

$$\mathcal{B}(h_c \to 2(\pi^+\pi^-)\pi^0) = (1.9^{+0.7}_{-0.5}) \times 10^{-5}$$

This leaves us with the interesting question of what are the $\sim$ 50% unobserved hadronic decays of h_c.

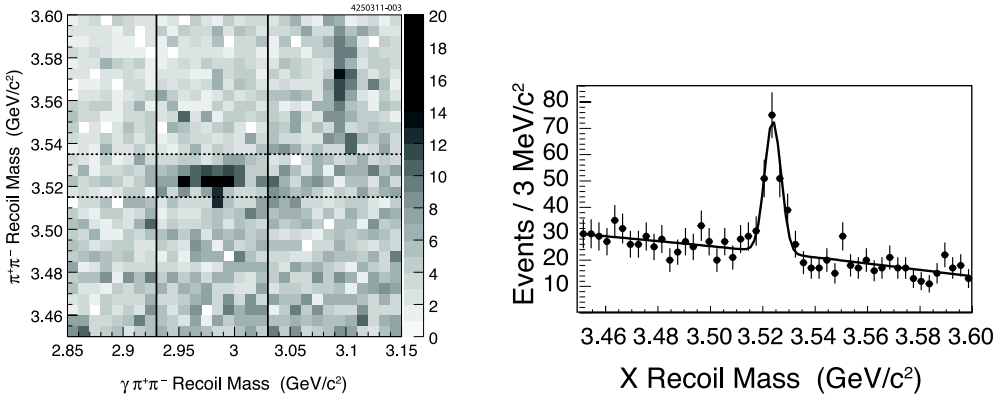

Figure 2: Illustrating the identification of h_c in $e^+e^-(4170) \to \pi^+\pi^- h_c$. Left: two dimensional plot showing h_c enhancement at the intersection of $M(\eta_c) \approx 2.98$ GeV and $M(h_c) \approx 3.52$ GeV. Right: distribution of events in the box marked in the two dimensional plot as function of $\pi^+\pi^-$ recoil mass.

3.3 Discovery of a new mode of h_c production [13]

CLEO has made an important discovery in identifying h_c formation in the $\pi^+\pi^-$ decay of $\psi(4170)$ above the $D\overline{D}$ threshold [13]. Using 586 pb^{-1} of e^+e^- annihilation data at $\sqrt{s} = 4170$ MeV we observe a 10σ signal for h_c in the decay

$$e^+e^-(4170) \to \pi^+\pi^- h_c(1P),$$

with $h_c \to \gamma\eta_c, \eta_c \to 12$ decay modes[3].

In the two dimensional plot shown in Fig. 2 the h_c signal is clearly seen in $\pi^+\pi^-$ recoil mass at the intersection of its radiative decay to η_c at 2.98 GeV. (The enhancement at 3.1 GeV is due to J/ψ.) In the projection h_c is seen as a strong enhancement over a featureless background. The production cross section is a very healthy 15.6 ± 4.2 pb. The paper has been accepted for publication in the PRL.

Our discovery of the population of $h_c(1P)$ in e^+e^- annihilations above the $D\overline{D}$ threshold of charmonium has led the Belle collaboration to search for $h_b(1P, 2P)$ in e^+e^- annihilations at $\sqrt{s} = 10.685$ GeV using the same technique of recoil against $\pi^+\pi^-$. They have achieved dramatic success, as you have already heard in their plenary presentation [14].

[3] $\eta_c \to 2(\pi^+\pi^-), 2(\pi^+\pi^-)2\pi^0, 3(\pi^+\pi^-), K^\pm K_S^0\pi^\mp, K^\pm K_S^0\pi^\mp\pi^+\pi^-, K^+K^-\pi^0, K^+K^-\pi^+\pi^-, K^+K^-\pi^+\pi^-\pi^0$, $K^+K^-2(\pi^+\pi^-), 2(K^+K^-), \eta\pi^+\pi^-$, and $\eta 2(\pi^+\pi^-)$.

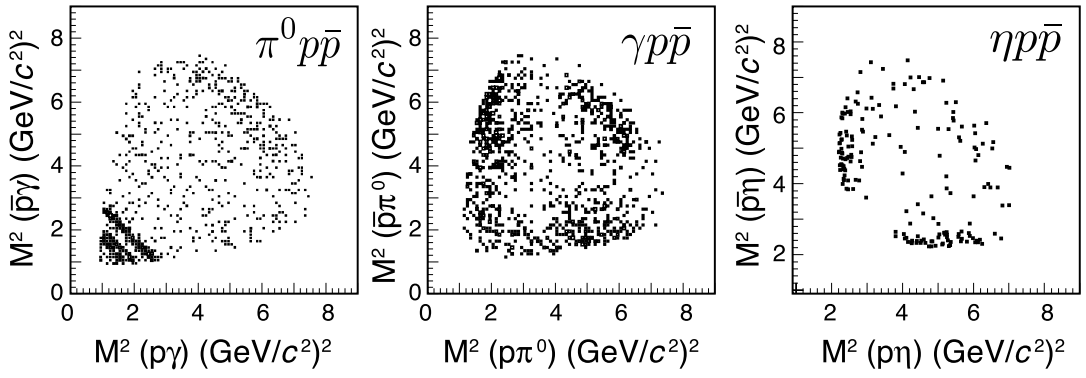

Figure 3: Dalitz plots for the three decays, $\psi(2S) \to \pi^0 p\overline{p}, \gamma p\overline{p}$, and $\eta p\overline{p}$.

4 Hadronic Decays of P-wave States of Bottomonium [16]

Compared to charmonium very few decays of bottomonium states have ever been measured. Earlier we reported on the first measurements of $\chi_{bJ}(1P, 2P), J = 0, 1, 2$, decays to fourteen exlusive hadronic final states [15].

$$\Upsilon(2S, 3S) \to \gamma\chi_{bJ}(1P, 2P), \quad \chi_{bJ}(1P, 2P) \to \text{hadrons}$$

We have now made the first measurements of

$$\Upsilon(2S, 3S) \to \gamma\chi_{bJ}(1P) \to \gamma\gamma\Upsilon(1S) \text{ [16]}$$

The results from $\Upsilon(2S) \to \gamma\chi_{bJ}(1P)$ are

$$\mathcal{B}[\chi_{bJ}(1P) \to \gamma\Upsilon(1S)] \text{ in } \% = 1.73 \pm 0.35(\chi_0),\ 33.0 \pm 2.6(\chi_1),\ 18.5 \pm 1.4(\chi_2)$$

These measurements lead to much improved determinations of

$$\mathcal{B}[\Upsilon(3S) \to \gamma\chi_{b1}(1P)] = (1.63 \pm 0.46) \times 10^{-3} \text{ (CLEO)}, \quad < 1.9 \times 10^{-3} \text{ [2,PDG]}$$

$$\mathcal{B}[\Upsilon(3S) \to \gamma\chi_{b2}(1P)] = (7.7 \pm 1.3) \times 10^{-3} \text{ (CLEO)}, \quad < 20.3 \times 10^{-3} \text{ [2,PDG]}$$

5 Decays of $\psi(2S)$ to $p\overline{p} + \gamma$, π^0 and η, and search for baryonium in $\psi(2S)$ and J/ψ decays [17]

This CLEO investigation [17] was motivated by the longstanding claim by BES for the interpretation of an observed near-threshold enhancement in the decay, $J/\psi \to \gamma(p\overline{p})$ as evidence for a weakly bound proton-antiproton resonance, R_{thr}, with $M(p\overline{p}) = 1859^{+6}_{-27}$ MeV, $\Gamma < 30$ MeV, and

$$\mathcal{B}(J/\psi \to \gamma R_{thr}) \times \mathcal{B}(R_{thr} \to p\overline{p}) = (7.0^{+1.9}_{-0.9}) \times 10^{-5}.$$

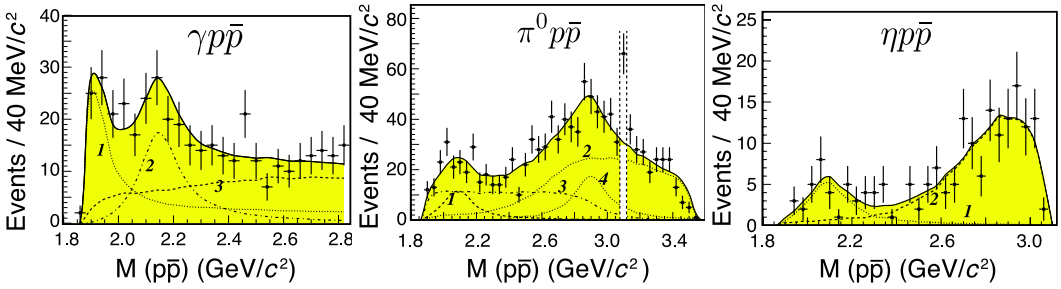

Figure 4: Event projections as function of $M(p\overline{p})$ in the decays $\psi(2S) \to \pi^0 p\overline{p}, \gamma p\overline{p}$, and $\eta p\overline{p}$. The curves show contributions of different intermediate resonances and their total.

Quantity	CLEO (10^{-5})	PDG10 (10^{-5})
$\mathcal{B}(\psi(2S) \to \gamma p\overline{p})$	4.18 ± 0.3	2.9 ± 0.6
$\mathcal{B}(\psi(2S) \to \pi^0 p\overline{p})$	15.4 ± 0.9	13.3 ± 1.7
$\mathcal{B}(\psi(2S) \to \eta p\overline{p})$	5.6 ± 0.7	6.0 ± 1.2
$\mathcal{B}(\psi(2S) \to \gamma f_2(1950)) \times \mathcal{B}(f_2(1950) \to p\overline{p})$	1.2 ± 0.2	
$\mathcal{B}(\psi(2S) \to \gamma f_2(2150)) \times \mathcal{B}(f_2(2150) \to p\overline{p})$	0.72 ± 0.18	
$\mathcal{B}(\psi(2S) \to \pi^0 R_1(2100)) \times \mathcal{B}(R_1(2100) \to p\overline{p})$	1.1 ± 0.4	
$\mathcal{B}(\psi(2S) \to \pi^0 R_2(2900)) \times \mathcal{B}(R_2(2900) \to p\overline{p})$	2.3 ± 0.7	
$\mathcal{B}(\psi(2S) \to \eta R_1(2100)) \times \mathcal{B}(R_1(2100) \to p\overline{p})$	1.2 ± 0.4	
$\mathcal{B}(\psi(2S) \to \overline{p} N_1^*(1440)) \times \mathcal{B}(N_1^*(1440) \to p\pi^0)$	8.1 ± 0.8	
$\mathcal{B}(\psi(2S) \to \overline{p} N_2^*(2300)) \times \mathcal{B}(N_2^*(2300) \to p\pi^0)$	4.0 ± 0.6	
$\mathcal{B}(\psi(2S) \to \overline{p} N^*(1535)) \times \mathcal{B}(N^*(1535) \to p\eta)$	4.4 ± 0.7	

Table 2: Branching fractions determined for $\psi(2S)$ decays into various intermediate N^* and meson states R_n which decay to $p\overline{p}$.

We argued that if the baryonium resonance was real, it should also be seen in $\psi(2S) \to \gamma(p\overline{p})$, and perhaps also in $\pi^0(p\overline{p})$ and $\eta(p\overline{p})$. Accordingly, we made a detailed analysis of our data set of 24.5 million $\psi(2S)$. The Dalitz plots in Fig. 3 show that a number of light quark resonances are excited in all three decays.

The structures observed in the Dalitz plots were analyzed via their projections as shown in Fig. 4. As listed in Table 2, branching fractions were determined for a number of baryon (N^*), and meson resonances (R) which decay into $p\overline{p}$. Most of these represent first such measurements. We note that among the intermediate states identified are $f_2(2150)$ and $N^*(2300)$ which have since been also observed by BES III [Hai-Bo Li at this conference].

We now turn to our results for the search for $p\overline{p}$ threshold enhancements. These are illus-

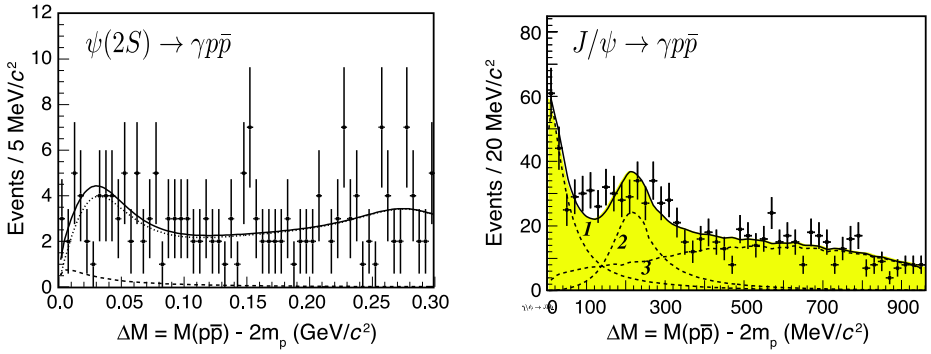

Figure 5: Event distributions as function of $\Delta M = M(p\overline{p}) - 2M_p$. left: $\psi(2S) \to \gamma p\overline{p}$; right: $J/\psi \to \gamma p\overline{p}$.

trated in Fig. 5 in terms of $\Delta M = M(p\overline{p}) - 2m_p$.

$\boldsymbol{\psi(2S) \to \gamma p\overline{p}}$: As shown in Fig. 5, we find no evidence for a threshold enhancement in $M(p\overline{p})$, and establish the upper limit for a resonance with BES parameters for $R_{\rm thr}$

$$\mathcal{B}(\psi(2S) \to \gamma \mathrm{R_{thr}}) \times \mathcal{B}(\mathrm{R_{thr}} \to p\overline{p}) < 1.6 \times 10^{-6}.$$

$\boldsymbol{J/\psi \to \gamma p\overline{p}}$: Using the data for 8.7 million J/ψ produced via $\psi(2S) \to \pi^+\pi^- J/\psi$, $\mathrm{R_{thr}}$ was also searched for in $J/\psi \to \gamma(p\overline{p})$.

As shown in Fig. 5, the observed threshold enhancement fitted in the region, $\Delta M = 0 - 900$ MeV leads to

$$M(\mathrm{R_{thr}}) = 1837 \pm 14 \text{ MeV}, \Gamma(\mathrm{R_{thr}}) = 0^{+44}_{-0} \text{ MeV, and}$$

$$\mathcal{B}(J/\psi \to \gamma \mathrm{R_{thr}}) \times \mathcal{B}(\mathrm{R_{thr}} \to p\overline{p}) = (11.4^{+6.0}_{-4.0}) \times 10^{-5}.$$

BES III has recently confirmed [18] the existence of a resonance decaying into $\pi^+\pi^-\eta'$ with $M = 1836.5^{+6.4}_{-3.7}$ MeV and $\Gamma = 190 \pm 39$ MeV. Such a wide resonance could very well decay into $p\overline{p}$ above threshold, and account for the observed threshold enhancement. BES II and we had earlier proposed this possibility, but BES III makes no comment about it in their latest paper [18].

6 Decays of χ_{cJ} to $p\overline{p} + \pi^0, \eta$ and ω [19]

The χ_{cJ} states are strongly populated by E1 radiative decays from $\psi(2S)$. CLEO has recently made measurements of χ_{cJ} decays to $p\overline{p} + \pi^0, \eta, \omega$ [19]. The results are presented in

$\mathcal{B}_\chi \times 10^4$	χ_0		χ_1		χ_2	
	CLEO	PDG [2]	CLEO	PDG [2]	CLEO	PDG [2]
$\mathcal{B}(\chi_J \to p\overline{p}\pi^0)$	7.8 ± 0.7	5.7 ± 1.2	1.8 ± 0.2	1.2 ± 0.5	4.8 ± 0.5	4.7 ± 1.0
$\mathcal{B}(\chi_J \to p\overline{p}\eta)$	3.7 ± 0.5	3.7 ± 1.1	1.6 ± 0.3	< 1.6	1.8 ± 0.3	2.0 ± 0.8
$\mathcal{B}(\chi_J \to p\overline{p}\omega)$	5.6 ± 0.7		2.3 ± 0.4		3.7 ± 0.5	

Table 3: Branching fractions determined for χ_J decays to $p\overline{p}\pi^0$, $p\overline{p}\eta$, and $p\overline{p}\omega$.

Table 3. The errors in these results are factor > 2 smaller than in the previous measurements.

Both sets of measurements, $\psi(2S) \to p\overline{p} + \gamma, \pi^0, \eta$ in Sec. 5 and $\chi_{cJ} \to p\overline{p} + \pi^0, \eta, \omega$ in Sec. 6, are potentially of great value to the future $p\overline{p}$ experimentation at PANDA(GSI).

7 Multipole Admixtures in Dipole Transitions [20]

If the radiative transitions $\chi_{c1}, \chi_{c2} \to \gamma J/\psi$ are attributed to a single quark, the E1 transitions can have small M2 components, with $a_2 = M2/\sqrt{E_1^2 + M_2^2}$. Simple predictions are that $a_2(\chi_1) = -(E_\gamma/4m_c)(1+\kappa_c)$, and $a_2(\chi_2) = (-3/\sqrt{5})(E_\gamma/4m_c)(1+\kappa_c)$, where κ_c is the anomalous magnetic moment of the charm quark.

Previous attempts at SLAC and Fermilab E760/E835 to measure $a_2(\chi_1, \chi_2)$ were limited mainly by statistics, and had large errors.

CLEO has recently made a high statistics measurement [20], with the results

$$a_2(\chi_{c1}) = (-6.26 \pm 0.67) \times 10^{-2}, \text{ and } \; a_2(\chi_{c2}) = (-9.3 \pm 1.6) \times 10^{-2}.$$

The ratio, $a_2(\chi_{c2})/a_2(\chi_{c1}) = 1.49 \pm 0.30$ is consistent with $3/\sqrt{5} = 1.34$, justifying the hypothesis of a **single quark transition**.

For assumed $m_c = 1.5$ GeV, we get

$$\chi_{c1} : (1+\kappa_c) = 0.88 \pm 0.20, \quad \chi_{c2} : (1+\kappa_c) = 1.10 \pm 0.19.$$

Both are consistent with **the anomalous magnetic moment of the charm quark,** $\kappa_c = 0$**.**

In a quenched lattice calculation the Jlab group predicts $a_2(\chi_{c1}) = (-20 \pm 6) \times 10^{-2}$, $a_2(\chi_{c2}) = (-39 \pm 7) \times 10^{-2}$, factors 3 to 4 larger than our measured values [21].

8 Interference in Strong and Electromagnetic Decays of $\psi(2S)$ to Pseudoscalar Pairs, $PP = \pi^+\pi^-, K^+K^-$ and K_SK_L [25]

Interest in final state interaction (FSI) phases originally arose from CP violation in K decays and B decays. However, it was discovered that large FSI phases are perhaps a general feature. Suzuki [22] and Rosner [23] have analyzed J/ψ decays into pseudoscalar-vector (PV) pairs, and pseudoscalar-pseudoscalar (PP) pairs, and find that the phase differences between strong and EM decay amplitudes in both PV and PP decays of J/ψ, measured as the interior angle δ of the triangle representing the amplitudes, is large

$$\delta(J/\psi, \psi(2S))_{PP} = \cos^{-1}\left(\frac{B(K^+K^-) - B(K_SK_L) - \rho B(\pi^+\pi^-)}{2\sqrt{B(K_SK_L) \times \rho \times B(\pi^+\pi^-)}}\right),$$

where ρ = phase space factor

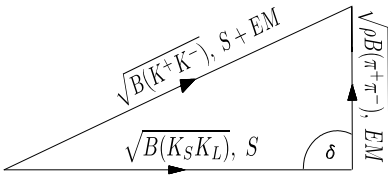

$$\delta(J/\psi)_{PP} = 89.6^\circ \pm 9.9^\circ(\text{Suzuki}),\ 89^\circ \pm 10^\circ(\text{Rosner}),\ 82^\circ \pm 9^\circ(\text{PDG2010})$$

Suzuki [24] raised the natural question if the $\sim \pi/2$ phase difference would also be found in the PP decays of $\psi(2S)$. If not, he wondered if it could perhaps explain the so called $\rho\pi$ (PV) problem: $\mathcal{B}(\psi(2S) \to \rho^0\pi^0)/\mathcal{B}(J/\psi \to \rho^0\pi^0) \approx 0.6\%$, instead of the pQCD expected value of $\sim 13\%$.

Previous measurements with small statistics $\psi(2S)$ data indicated large phase difference, $\delta(\psi(2S))_{PP}$, but with large errors, mainly due to the very small $\mathcal{B}(\psi(2S) \to \pi^+\pi^-)$, whose strong decay is forbidden by isospin conservation.

CLEO has now made a new measurement with 24.5 million $\psi(2S)$, and I present the preliminary results here [25]. The event distributions obtained for the three decays $\psi(2S) \to \pi^+\pi^-, K^+K^-$ and K_SK_L are shown in Fig. 6. The preliminary results for the measured branching fractions for the decays are listed in Table 4. These lead to a more precise result, $\delta(\psi(2S))_{PP} = 114^\circ \pm 11^\circ$.

In summary, both J/ψ and $\psi(2S)$ decays to pseudoscalar pairs give large phase difference between strong and EM amplitudes. The difference between $\delta(J/\psi) = 82^\circ \pm 9^\circ$ and $\delta(\psi(2S)) = 114^\circ \pm 11^\circ$ is 2.3σ. Question: Is this significant?

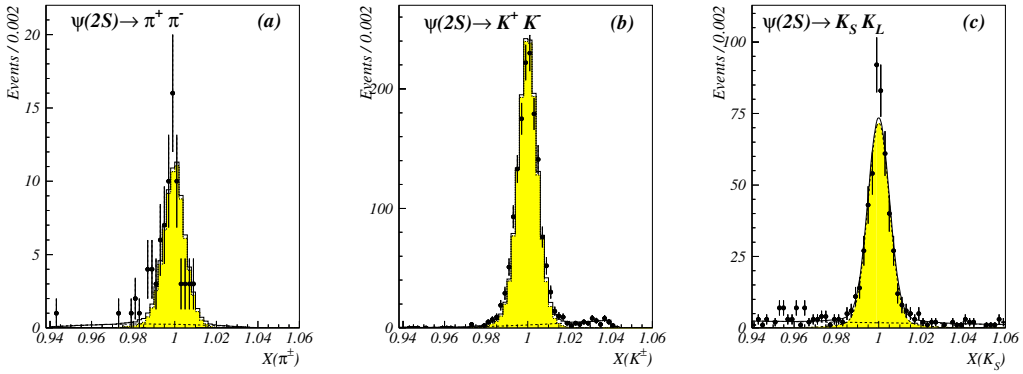

Figure 6: Event distributions as functions of $X(h) \equiv E(h)/E(\text{beam})$ for $h = \pi^{\pm}, K^{\pm}$, and K_S.

	DASP 1979	BES 2004	CLEO 2005	This analysis
$\mathcal{B}(\pi^+\pi^-) \times 10^5$	8 ± 5	0.84 ± 0.65	0.8 ± 0.8	0.72 ± 0.24
$\mathcal{B}(K^+K^-) \times 10^5$	10 ± 7	6.1 ± 2.1	6.3 ± 0.7	7.49 ± 0.43
$\mathcal{B}(K_SK_L) \times 10^5$	–	5.24 ± 0.67	5.8 ± 0.9	5.31 ± 0.43
$\delta(\psi(2S))_{PP}$	–	$(91 \pm 35)^{\circ}$*	$(87 \pm 20)^{\circ}$*	$(114 \pm 11)^{\circ}$

* Recalculated

Table 4: Branching fractions determined for $\psi(2S)$ decays into pseudoscalar pairs, $\pi^+\pi^-, K^+K^-$ and K_SK_L, and the resulting interference angle $\delta(\psi(2S))_{pp}$.

9 Summary

We have reported new results from the analysis of CLEO data for $\psi(2S)$, $\psi(4170)$, $\Upsilon(2S)$, and $\Upsilon(3S)$. These include:

1. Branching fractions for $\psi(2S) \to \pi^0 h_c(^1P_1)$.
2. Production of $h_c(^1P_1)$ in $e^+e^-(4170) \to \pi^+\pi^- h_c(^1P_1)$.
3. Branching fractions for $\Upsilon(3S) \to \gamma\chi_{b1,b2}(1P)$.
4. Decays of $\psi(2S)$ and $J/\psi \to p\overline{p} + \gamma$, π^0, and η, and search for $p\overline{p}$ threshold enhancements.
5. Multipole admixtures in $\psi(2S) \to \gamma\chi_J, \chi_J \to \gamma J/\psi$ dipole transitions.

6. Interference between strong and electromagnetic amplitudes in $\psi(2S)$ decays to pseudoscalar pairs, $\pi^+\pi^-$, K^+K^- and K_SK_L.

These results pose several interesting physics questions. Among these are:

- Why $\Delta M_{\rm hf}(1P) \equiv \langle M(^3P_J)\rangle - M(^1P_1) = 0$, if $\langle M(^3P_J)\rangle \neq M(^3P)$?
- What hadronic decays account for $\mathcal{B}(h_c \to \text{hadrons}) \approx 50\%$?
- Why is the $p\overline{p}$ threshold enhancement seen in J/ψ decay not seen in $\psi(2S)$ decay?
- What is the significance of the 2.3σ difference seen in the interference angle between strong and electromagnetic PP decays of J/ψ and $\psi(2S)$.

Bibliography

[1] A. Tomaradze, Proc. Hadron 2009, AIP Conf. Proc. 1257, 197 (2010).

[2] PDG 2010: Particle Data Group, “Review of Particle Physics", Journal of Physics G, 37, 075021 (2010).

[3] S. K. Choi et al. (Belle Collaboration), PRL 89, 102001 (2002).

[4] D. M. Asner et al. (CLEO Collaboration), PRL 92, 142001 (2004).

[5] B. Aubert et al. (BaBar Collaboration), PRL 92, 142002 (2004).

[6] J. L. Rosner et al. (CLEO Collaboration), PRL 95, 102003 (2005).

[7] B. Aubert et al. (BaBar Collaboration), PRL 101, 071801 (2008).

[8] G. Bonvicini et al. (CLEO Collaboration), PRD 81, 031104(R) (2010).

[9] S. Dobbs et al. (CLEO Collaboration), PRL 101, 182003 (2008).

[10] M. Ablikim et al. (BES III Collaboration), PRL 104, 132002 (2010).

[11] J. Y. Ge et al. (CLEO Collaboration), arXiv: 1106.3558 [hep-ex].

[12] G. S. Adams et al. (CLEO Collaboration), PRD 80, 051106(R) (2009).

[13] T. Pedlar et al. (CLEO Collaboration), arXiv: 1104.2025 [hep-ex], accepted by PRL.

[14] I. Adachi at al. (Belle Collaboration), arXiv: 1103.3419 [hep-ex].

[15] D. M. Asner et al. (CLEO Collaboration), PRD 78, 091103(R) (2008).

[16] M. Kornicer et al. (CLEO Collaboration), PRD 83, 054003 (2011).

[17] J. P. Alexander et al. (CLEO Collaboration), PRD 82, 092002 (2010).

[18] M. Ablikim et al. (BES III Collaboration), PRL 106, 072002 (2011).

[19] P. U. E. Onyisi et al. (CLEO Collaboration), PRD 82, 011103(R) (2010).

[20] M. Artuso et al. (CLEO Collaboration), PRD 80, 112003 (2009).

[21] J. J. Dudek et al., PRD 79, 094505 (2009).

[22] M. Suzuki, PRD 60, 051501(R) (1999).

[23] J. L. Rosner, PRD 60, 074029 (1999).

[24] M. Suzuki, PRD 63, 054021 (2001).

[25] K. K. Seth, for the CLEO Collaboration, this talk (preliminary results).

Electric dipole transitions of heavy quarkonium in pNRQCD

Piotr Pietrulewicz
Physik-Department, Technische Universität München
James-Franck-Str. 1, 85748 Garching, Germany

We propose a systematic, model-independent treatment of electric dipole transitions of heavy quarkonium. Within an effective field theory, concretely potential non-relativistic QCD, the relativistic corrections of relative order v^2 to the decay rate are derived. An existing formalism developed for M1 decays will be extended for our purpose. We scrutinize and complement former results from potential model calculations.

1 Introduction

Radiative transitions play an important role for our understanding of QCD, in particular of heavy quarkonium. They provide information about the wave functions describing the physical system and probe both the perturbative and non-perturbative regime. Especially E1 transitions give significant contributions to the total decay rate and are observed in the experimental facilities. Recently, decays of charmonium were measured at BES and CLEO, including the observation of the process $h_c \to \eta_c \gamma$ in 2010 [1]. Concerning bottomonium, CLEO, BaBar and Belle produced many data, e.g. for the determination of the branching fractions χ_b states [2,3]. A review about recent developments can be found in [4].

On the theory side, electric dipole transitions were treated in several potential models, a summary can be found in [5]. We will refer to [6] for comparison with the general results for χ-decays. A model-independent treatment to check and improve the calculations has been missing so far. However, in the last decade there has been significant progress using effective field theories (EFTs) to describe heavy quarkonium (see [7] and references therein). Since heavy quarkonium is assumed to be a non-relativistic system we may take advantage of the hierarchy of scales $m \gg mv \gg mv^2$, where $v \ll 1$ is the heavy quark velocity, m is the heavy quark mass ("hard scale"), $p \sim mv$ is the relative momentum of the bound state ("soft scale") $E \sim mv^2$ is the binding energy $E \sim mv^2$ ("ultrasoft scale"). The ultimate EFT living at the ultrasoft scale is potential non-relativistic QCD (pNRQCD). In 2005, for the first time radiative decays, concretely M1 transitions, were calculated in this theory [8]. Using the framework of that paper as a guideline we close the gap and compute the decay rates of the E1 processes $n^3P_J \to n'^3S_1 \gamma$ and $n^1P_1 \to n'^1S_0 \gamma$. The following is based on [9].

2 The Lagrangians in NRQCD and pNRQCD

By integrating out the hard scale $m \gg \Lambda_{QCD}$ from the fundamental theory, QCD, in perturbation theory ($\alpha_s(m) \ll 1$) one obtains non-relativistic QCD (NRQCD) [10, 11]. For the calculation of E1 transitions at NLO only the two-fermion Lagrangian $\mathcal{L}_{2-f}$ matters and the relevant part reads

$$\mathcal{L}_{2-f} = \psi^\dagger \left(iD_0 + \frac{\mathbf{D}^2}{2m} + \frac{\mathbf{D}^4}{8m^3} \right) \psi + ee_Q \psi^\dagger \left(\frac{c_F^{em}}{2m} \boldsymbol{\sigma} \cdot \mathbf{B}^{em} + i \frac{c_S^{em}}{8m^2} \boldsymbol{\sigma} \cdot [\mathbf{D}\times, \mathbf{E}^{em}] \right) \psi + c.c.. \tag{1}$$

with $iD_0 = i\partial_0 - gT^a A_0^a - ee_Q A_0^{em}$, $i\mathbf{D} = i\boldsymbol{\nabla} + gT^a \mathbf{A}^a + ee_Q \mathbf{A}^{em}$ and ψ denoting a Pauli spinor for the heavy quark. The matching coefficients are found to be $c_F^{em} = 1 + C_F \frac{\alpha_s}{2\pi} + \mathcal{O}(\alpha_s^2)$, $c_S^{em} = 2c_F^{em} - 1$.

For processes at the ultrasoft scale, NRQCD is not yet the appropriate theory, since there are still several scales entangled (p, E, Λ_{QCD}) and thus no homogeneous power counting can be established. Integrating out the soft scale mv we obtain a theory for ultrasoft modes, i.e. pNRQCD [12, 13]. The crucial step to disentangle the energy and momentum scale is the multipole expansion in the relative distance r. To be definite we will work in the weak-coupling regime, where $p \gg E \gtrsim \Lambda_{QCD}$. The power counting reads

$$r \sim 1/mv,\ \boldsymbol{\nabla}_r \equiv \partial/\partial\mathbf{r} \sim mv,\ \boldsymbol{\nabla} \equiv \partial/\partial\mathbf{R} \sim mv^2\,,\ \mathbf{E}, \mathbf{B} \sim (mv^2)^2,\ \mathbf{E}^{em}, \mathbf{B}^{em} \sim k_\gamma^2\,. \tag{2}$$

k_γ is the energy of the emitted photon, which scales like $k_\gamma \sim mv^2$ for transitions between states with different principal quantum numbers.

The pNRQCD-Lagrangian contributing at NLO in the decay rate, i.e. at order $k_\gamma^3 v^0/m^2$, reads

$$\begin{aligned} \mathcal{L}_{\text{pNRQCD}} = \int d^3r \text{Tr} \Bigg\{ & S^\dagger \left(i\partial_0 + \frac{\boldsymbol{\nabla}^2}{4m} + \frac{\boldsymbol{\nabla}_r^2}{m} + \frac{\boldsymbol{\nabla}_r^4}{4m^2} - V_S \right) S + O^\dagger \left(iD_0 + \frac{\mathbf{D}^2}{4m} + \frac{\boldsymbol{\nabla}_r^2}{m} - V_O \right) O \\ & + g V_A (O^\dagger \mathbf{r} \cdot \mathbf{E} S + S^\dagger \mathbf{r} \cdot \mathbf{E} O) \Bigg\} \\ & + \mathcal{L}_{\gamma\text{pNRQCD}} + \mathcal{L}_{\text{light}}\,, \end{aligned} \tag{3}$$

where the covariant derivatives are given by $iD_0 O = i\partial_0 O - g[T^a A_0^a, O]$ and $i\mathbf{D}O = i\boldsymbol{\nabla} O + g[T^a \mathbf{A}^a, O]$ and the trace goes over the color and spin indices. The singlet potential V_S has been calculated perturbatively and non-perturbatively to order $1/m^2$ ([14–16], for more original references see [7]), we display the structure of the relevant potentials for

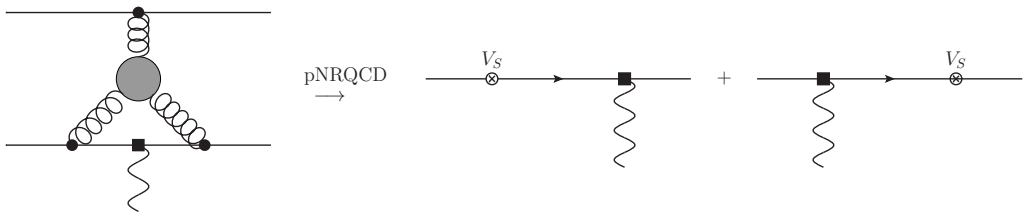

Figure 1: Example for a reducible diagram, if the electromagnetic operator commutes with the gluonic ones. It does not contribute to the matching coefficient of a single operator.

computations at NLO in the decay rate,

$$V_S(r) = V^{(0)}(r) + \frac{V_r^{(1)}(r)}{m} + \frac{V_{SI}^{(2)}(r)}{m^2} + \frac{V_{SD}^{(2)}(r)}{m^2}\,, \tag{4}$$

$$V_{SI}^{(2)}(r) = V_r^{(2)}(r) + \frac{1}{2}\{V_{p^2}^{(2)}(r), \mathbf{p}^2\} + \frac{V_{L^2}^{(2)}(r)}{r^2}\mathbf{L}^2\,, \tag{5}$$

$$V_{SD}^{(2)}(r) = V_{LS}^{(2)}(r)\mathbf{L}\cdot\mathbf{S} + V_{S^2}^{(2)}(r)\mathbf{S}^2 + V_{S_{12}}^{(2)}(r)\left[3(\hat{\mathbf{r}}\cdot\boldsymbol{\sigma}_1)(\hat{\mathbf{r}}\cdot\boldsymbol{\sigma}_2) - \boldsymbol{\sigma}_1\cdot\boldsymbol{\sigma}_2\right]\,. \tag{6}$$

The relevant part of $\mathcal{L}_{\gamma\text{pNRQCD}}$ for E1 transitions is

$$\begin{aligned}\mathcal{L}_{\gamma\text{pNRQCD}}^{E1} = ee_Q \int d^3r\,\mathrm{Tr}\Big\{ & V^{r\cdot E} S^\dagger \mathbf{r}\cdot\mathbf{E}^{em} S + V_O^{r\cdot E} O^\dagger \mathbf{r}\cdot\mathbf{E}^{em} O + \frac{1}{24} V^{(r\nabla)^2 r\cdot E} S^\dagger \mathbf{r}\cdot[(\mathbf{r}\boldsymbol{\nabla})^2\mathbf{E}^{em}] S \\ & + i\frac{1}{4m} V^{\nabla\cdot(r\times B)} S^\dagger \{\boldsymbol{\nabla}\cdot, \mathbf{r}\times\mathbf{B}^{em}\} S \\ & + i\frac{1}{12m} V^{\nabla_r\cdot(r\times(r\nabla)B)} S^\dagger \{\boldsymbol{\nabla}_r\cdot, \mathbf{r}\times[(\mathbf{r}\boldsymbol{\nabla})\mathbf{B}^{em}]\} S \\ & + \frac{1}{4m} V^{(r\nabla)\sigma\cdot B} [S^\dagger, \boldsymbol{\sigma}]\cdot[(\mathbf{r}\boldsymbol{\nabla})\mathbf{B}^{em}] S \\ & - i\frac{1}{4m^2} V^{\sigma\cdot(E\times\nabla_r)} [S^\dagger, \boldsymbol{\sigma}]\cdot(\mathbf{E}^{em}\times\boldsymbol{\nabla}_r) S \Big\}\,.\end{aligned} \tag{7}$$

In fact more terms are allowed according to the symmetries of pNRQCD. However, we can show that their matching coefficients vanish. The matching is done by equating Green's functions in NRQCD and pNRQCD at the energy scale mv order by order in the inverse mass and r. The crucial argument for several operators is that diagrams in NRQCD which can be cast into a reducible structure also give reducible diagrams in pNRQCD. Therefore they have to be subtracted to obtain irreducible operators in pNRQCD and do not play a role in the matching procedure. An example is the diagram in Fig. 1, where the gluonic contribution can be factorized out yielding just a potential. Using this argument we can fix all of the Wilson coefficients in (7), so that the exact QCD results reproduce the ones from tree level calculations, namely

$$V^{r\cdot E} = V_O^{r\cdot E} = V^{(r\nabla)^2 r\cdot E} = V^{\nabla\cdot(r\times B)} = V^{(r\nabla)\nabla_r\cdot(r\times B)} = 1,\; V^{(r\nabla)\sigma\cdot B} = c_F^{em},\; V^{\sigma\cdot(E\times\nabla_r)} = c_s^{em}\,. \tag{8}$$

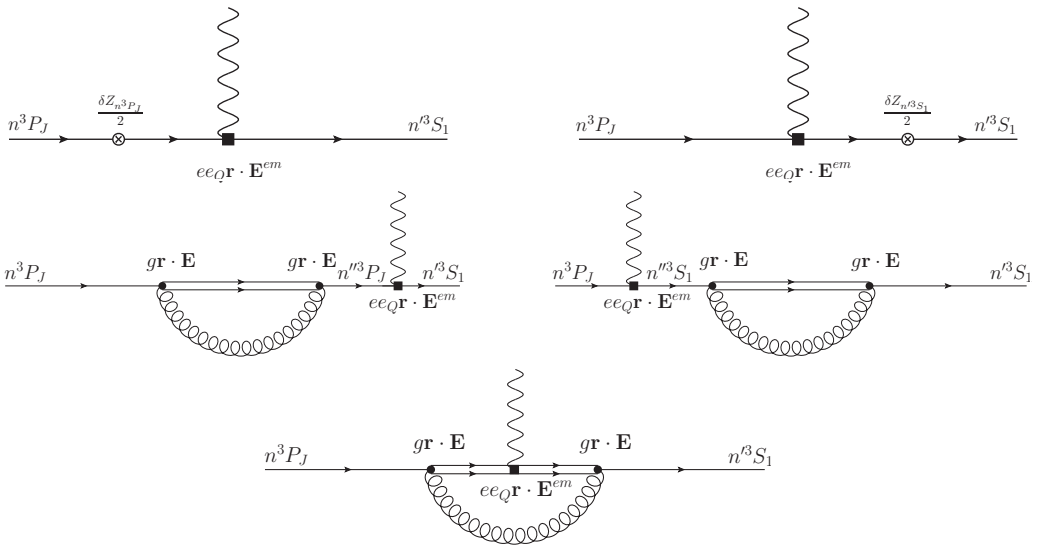

Figure 2: Color octet contributions to E1 transitions, the double line represents the intermediate octet state.

3 Results

With the help of the formalism developed in [8] we can describe the states in a quantum mechanical way using wave functions and compute the decay rate at NLO from the Lagrangian (7). We obtain

(9)

$$\Gamma_{n^3P_J\to n'^3S_1\gamma} = \frac{4}{9}\,\alpha_{em}e_Q^2k_\gamma^3 I_3^2(n1\to n'0)\left(1+R-\frac{k_\gamma^2}{60}\frac{I_5}{I_3}-\frac{k_\gamma}{6m}+\frac{k_\gamma(c_F^{em}-1)}{2m}\left[\frac{J(J+1)}{2}-2\right]\right),$$

where

(10)

$$I_N \equiv \int_0^\infty dr\, r^N R_{n'0}(r)R_{n1}(r)\,.$$

R contains all of the wave-function corrections due to the higher-order potentials mentioned in (4)-(6), the relativistic correction of the kinetic energy, $-\mathbf{p}^4/4m^3$, and higher-order Fock state contributions which are given by the diagrams in Fig. 2. In contrast to M1 transitions the latter ones do not vanish for E1 decays.

Compared to the results with the potential model calculation in [6] we find an equivalence between (9) and the corresponding formula there at the given order. However, we could give a range of validity, namely $p \gg \Lambda_{QCD}$, and include all relativistic corrections systematically, in particular the color-octet contributions in the weak-coupling regime and the one coming from $V_r^{(1)}$ [9]. Both were missing in former approaches. For $p \sim \Lambda_{QCD}$ new terms would enter yielding an extended expression.

Using these results as a basis one can extend the discussion to other processes like $n^1P_1 \to n'^1S_0\gamma$ and $n^3S_1 \to n'^3P_J\gamma$. Finally, also a phenomenological analysis is currently under way, which applies the theoretical results to charmonium and bottomonium decays.

Acknowledgments

I would like to thank Nora Brambilla and Antonio Vairo for the collaboration on this work.

Bibliography

[1] M. Ablikim *et al.* [The BESIII Collaboration], Phys. Rev. Lett. **104** (2010) 132002. [arXiv:1002.0501 [hep-ex]].

[2] M. Kornicer *et al.* [The CLEO Collaboration], Phys. Rev. **D83** (2011) 054003. [arXiv:1012.0589 [hep-ex]].

[3] J. P. Lees *et al.* [The BABAR Collaboration], [arXiv:1104.5254 [hep-ex]].

[4] N. Brambilla, S. Eidelman, B. K. Heltsley, R. Vogt, G. T. Bodwin, E. Eichten, A. D. Frawley, A. B. Meyer *et al.*, Eur. Phys. J. **C71** (2011) 1534. [arXiv:1010.5827 [hep-ph]].

[5] E. Eichten, S. Godfrey, H. Mahlke, J. L. Rosner, Rev. Mod. Phys. **80** (2008) 1161-1193. [hep-ph/0701208].

[6] H. Grotch, D. A. Owen, K. J. Sebastian, Phys. Rev. **D30** (1984) 1924.

[7] N. Brambilla, A. Pineda, J. Soto, A. Vairo, Rev. Mod. Phys. **77** (2005) 1423. [hep-ph/0410047].

[8] N. Brambilla, Y. Jia, A. Vairo, Phys. Rev. **D73** (2006) 054005. [hep-ph/0512369].

[9] P. Pietrulewicz, master thesis (Munich 2011).
N. Brambilla, P. Pietrulewicz, A. Vairo, TUM-EFT 25/11, in preparation.

[10] W. E. Caswell, G. P. Lepage, Phys. Lett. **B167** (1986) 437.

[11] G. T. Bodwin, E. Braaten, G. P. Lepage, Phys. Rev. **D51** (1995) 1125-1171. [hep-ph/9407339].

[12] A. Pineda, J. Soto, Nucl. Phys. Proc. Suppl. **64** (1998) 428-432. [hep-ph/9707481].

[13] N. Brambilla, A. Pineda, J. Soto, A. Vairo, Nucl. Phys. **B566** (2000) 275. [hep-ph/9907240].

[14] N. Brambilla, A. Pineda, J. Soto, A. Vairo, Phys. Lett. **B470** (1999) 215. [hep-ph/9910238].

[15] N. Brambilla, A. Pineda, J. Soto, A. Vairo, Phys. Rev. **D63** (2001) 014023. [hep-ph/0002250].

[16] A. Pineda, A. Vairo, Phys. Rev. **D63** (2001) 054007. [hep-ph/0009145].

Application of High Quality Antiproton Beam with Momentum Ranging from 1 GeV/c to 15 GeV/c to Study Charmonium and Charmed Hybrids

Mikhail Yu. Barabanov[1], A.S. Vodopyanov, V.Kh. Dodokhov and V.A. Babkin
Joint Institute for Nuclear Research,
Veksler and Baldin Laboratory of High Energy Physics
141980 Dubna, RUSSIA

The elaborate analysis of spectrum of charmonium states and charmed hybrids in the mass region over $D\overline{D}$-threshold is given. The combined approach based on the potential model and relativistic spherical symmetric top model for decay products has been proposed. The experimental data from different collaborations were analyzed. Especial attention was given to the new states with the hidden charm discovered recently. Eight of these states may be interpreted as higher laying radial excited charmonium states. But much more data on different decay modes are needed for deeper analysis. These data can be derived directly from the experiments using high quality antiproton beam with the momentum ranging from 1 GeV/c to 15 GeV/c (PANDA experiment at FAIR).

1 Introduction

The study of charmonium and charmed hybrids spectroscopy is one of the main domains of elementary particle physics. It seems to be a challenge nowadays. The research of charmonium (the system consisting of charmed quark-antiquark pair $c\bar{c}$) and charmed hybrids (the system consisting of charmed quark-antiquark pair strongly interacting with gluonic component $c\bar{c}$g) using the antiproton beam with momentum ranging from 1 GeV/c to 15 GeV/c in PANDA experiment at FAIR is perspective and interesting from the scientific point of view. Charmonium and charmed hybrids with different quantum numbers are copiously produced in antiproton-proton annihilation process. The accuracy of mass and width measurements depends only on the quality of antiproton beam (high luminosity, minimal beam momentum spread, small lateral beam dimension). It becomes possible to extract the information about excited states of charmonium which can be extremely useful for understanding the nature of strong interactions. The performed analysis of charmonium is promising to understand the dynamics of quark interactions at small distances [1].

[1]barabanov@sunhe.jinr.ru

2 Results of calculations

The charmonium system has been investigated in detail, first, in e^+e^--reactions, and afterwards — on a restricted scale but with high precision — in $\overline{p}p$-annihilations (the experiments R704 at CERN and E760/E835 at Fermilab). Nowadays the scalar $^1D_2$ and vector ^3D_J charmonium states are not established. The higher laying scalar $^1S_0$, $^1P_1$ and vector $^3S_1$, ^3P_J charmonium states are badly investigated [2]. The domain over $D\overline{D}$-threshold of 3.73 GeV/c^2 is poorly studied. According to the contemporary quark models (LQCD, flux tube model), namely in this domain, the existence of charmed hybrids with exotic ($J^{PC} = 0^{+-}, 1^{-+}, 2^{+-}$) as with non-exotic ($J^{PC} = 0^{-+}, 1^{+-}, 2^{-+}, 1^{++}, 1^{--}$) quantum numbers is expected [1,2].

The elaborated analysis of spectrum of the scalar ($^1S_0$,$^1P_1$,$^1D_2$), vector ($^3S_1$,^3P_J,^3D_J) charmonium states and charmed hybrids with exotic and non-exotic quantum numbers in the mass region mainly over $D\overline{D}$-threshold, has been fulfilled [3,4]. Different decay modes of charmonium such as decays into particle-antiparticle or $D\overline{D}$-pair, decays into light hadrons and decays with J/ψ in the final state were investigated. Concerning the charmed hybrids, the decays into charmonium and light mesons in the final state and decays into $D\overline{D}^*$-pair, were, in particular, analyzed. These modes possess small widths and significant branching ratios. This fact facilitates their experimental detection.

Using the combined approach based on the quarkonium potential model and relativistic top model for decay products, ten new radial excited states of charmonium were predicted in the mass region over $D\overline{D}$-threshold equal to 3.73 GeV/c^2. Sixteen charmed hybrids (lowest-laying hybrids and their radial excited states) are expected to exist in the discussed mass region. A special attention is given to the new states with the hidden charm discovered recently (XYZ-particles) [5,6]. The experimental data from different collaborations (Belle, BaBar, CLEO, CDF) were carefully analyzed. It has been found that eight of new recently discovered states may be interpreted as charmonium states (two scalar $^1S_0$, three vector $^3S_1$ and tree vector ^3P_J). But much more data on different decay channels (modes) are needed for deeper analysis. These data can be derived directly from PANDA experiment with its high quality antiproton beam. Hence, there is a possibility of measuring the masses, widths and branching ratios of different charmonium and charmed hybrid states with high accuracy.

Figure 1 illustrates the spectrum of scalar $^1S_0$ and vector $^3S_1$, ^3P_J states of charmonium. Black boxes correspond to the established charmonium states, black-white boxes — recently experimentally revealed states with the hidden charm (XYZ-particles) that may be interpreted as higher laying charmonium states. Possible existence of charmonium states marked by black-white boxes was predicted in our recent calculations. One can find that $X(3940)$ and $X(4160)$ can be interpreted as radial excited scalar $^1S_0$ states of charmonium; $Y(4260)$, $Y(4360)$ and $Y(4660)$ — as radial excited vector $^3S_1$ states of charmonium and $X(3915)$, $Y(3940)$, $Z(3930)$ — as radial excited vector ^3P_J states of charmonium. Finally, white boxes correspond to the states which are not found yet. But a possibility of existence

of these states is predicted in the framework of the combined approach. They may also be interpreted as higher laying radial excited states of charmonium.

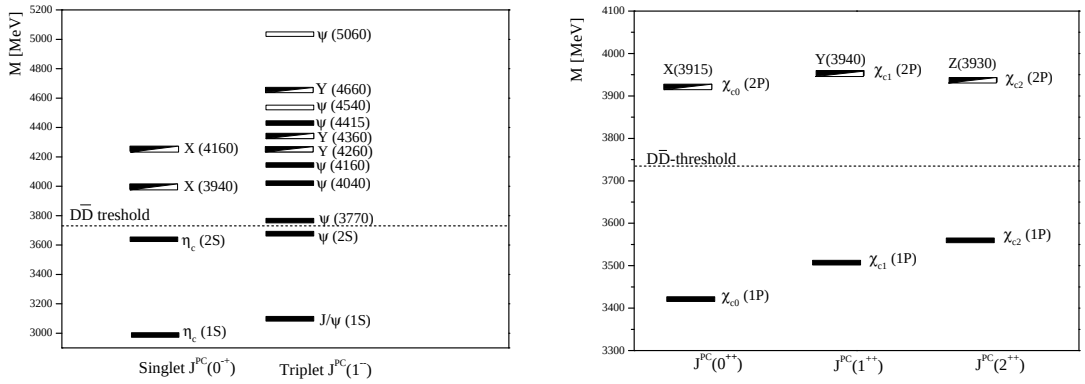

Figure 1: The spectrum of scalar ${}^1S_0$ and vector ${}^3S_1$ and ${}^3P_J$ states of charmonium.

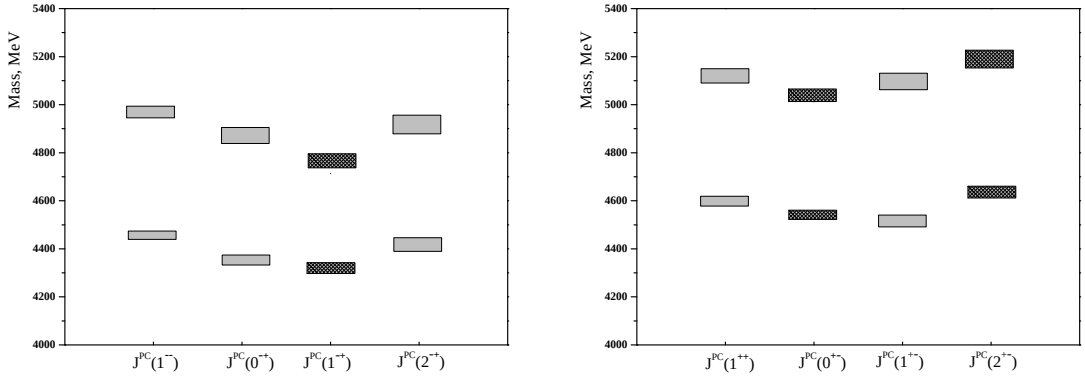

Figure 2: The spectrum of charmed hybrids with quantum numbers $J^{PC} = 2^{-+}, 1^{-+}, 1^{--}, 0^{-+}$ and $2^{+-}, 1^{+-}, 1^{++}, 0^{+-}$.

Figure 2 illustrates the spectrum of the lowest-laying charmonium hybrids and their radial excited states. Charmed hybrids with exotic quantum numbers are marked with dark colour and charmed hybrids with nonexotic quantum numbers — with light colour. One can find that the state with exotic quantum numbers $J^{PC} = 1^{-+}$ has the lowest mass equals to 4320 MeV/c^2. The results of calculations are in good agreement with the well accepted picture that the quartet $1^{--}, (0,1,2)^{-+}$ is lower in mass than $1^{++}, (0,1,2)^{+-}$. The expected splitting is about 150 – 250 MeV/c^2.

To be sure that the predicted charmonium and charmed hybrid states can really exist and can be found experimentally, their widths have been calculated [3,4]. The values of widths are of an order of several tens of MeV. This fact facilitates their experimental search.

3 Conclusions

Finally the progress of the future charmonium and charmed hybrids researches at FAIR is related to the results obtained below:

• A combined approach has been proposed to study charmonium and charmed hybrids on the basis of quarkonium potential model and relativistic top model for decay products.

• Several promising decay channels of charmonium like decays into light hadrons $\overline{p}p \to c\bar{c} \to \rho\pi$, decays into particle-antiparticle $\overline{p}p \to c\bar{c} \to \Sigma^0\overline{\Sigma}^0$, decays into $D\overline{D}$-pair and decays with J/ψ in the final state $\overline{p}p \to c\bar{c} \to J/\Psi + X$, were, in particular, analyzed.

• Ten radial excited states of charmonium (two scalar $^1S_0$, three vector $^3S_1$ and tree vector ^3P_J) above $D\overline{D}$-threshold have been predicted in the framework of the combined approach.

• Several promising decay channels of the charmed hybrids like decays into charmonium and light mesons in the final state $\overline{p}p \to c\bar{c}g \to \chi_{c0,1,2}(\eta, \pi\pi; ...)$, $\overline{p}p \to c\bar{c}g \to J/\Psi(\eta, \omega, \pi\pi; ...)$ and decays into $D\overline{D}^*$-pair $\overline{p}p \to c\bar{c}g \to D\overline{D}^*\eta$ were considered.

• Sixteen charmed hybrids with exotic and nonexotic quantum numbers are expected to exist in the framework of the combined approach.

• The recently discovered XYZ-particles have been analyzed. Some of these states can be interpreted as higher laying radial excited states of charmonium. The necessity of further studying the XYZ-particles and their main characteristics in PANDA experiment at FAIR has been demonstrated.

This work was supported by the FAIR- Russia Research Center (FRRC).

Bibliography

[1] PANDA Collaboration, Physics Perfomance Report, 63 (2009).

[2] Review of Particle Physics, Journal of Physics G: Nuclear and Particle Physics, **V. 37**, N. 7A, 1040 (2010).

[3] M.Yu. Barabanov et al., Hadronic Journal, **V. 32**, N. 2, 159 (2009).

[4] M.Yu. Barabanov et al., Proc. of the XX International Seminar on High Energy Physics Problems, Dubna, Russia, Oct 4-9, 137 (2010).

[5] E. Eichten, S. Godfrey, J. Rosner, Reviews of Modern Physics, **V. 80**, N. 3, 1161 (2008).

[6] N. Brambilla et al., European Physical Journal, C 71 :1534, 1 (2011).

Bottomonium results at Belle

Alexander Kuzmin[1] on behalf of the Belle Collaboration

BINP, 630090, Lavrentyeva 11, Novosibirsk, RUSSIA

Originally designed for CP violation studies in the B meson system, the B-Factories recently showed an exciting capability for improving our experimental knowledge in the field of hadron spectroscopy. We review results on bottomonium spectroscopy from the Belle experiment at the KEK-B e+e- collider and present exciting new results from the unique large data set taken at the Y(5S) resonance.

1 Introduction

The Belle Collaboration has collected a large sample of e^+e^- collisions at the energy of the $\Upsilon(5S)$ resonance, which lies above the threshold for production of B_s meson pairs, primarily for the purpose of studying decays of B_s. There have been a number of unexpected results on the non-$B_s\overline{B}_s$ decays of the $\Upsilon(5S)$. In particular, anomalously large rates for dipion transitions to lower bottomonium states $\Upsilon(5S) \to (\Upsilon(1S), \Upsilon(2S), \Upsilon(3S))\pi^+\pi^-$ have been observed [1]. If these signals are attributed entirely to the $\Upsilon(5S)$ decays, the measured partial decay widths $\Gamma[\Upsilon(5S) \to \Upsilon(nS)\pi^+\pi^-] \sim 0.5\,\text{MeV}$ are about two orders of magnitude larger than typical widths for dipion transitions among $\Upsilon(nS)$ states with $n \leqslant 4$.
Recently the CLEO-c Collaboration observed the process $e^+e^- \to h_c(1P)\pi^+\pi^-$ at a rate comparable to the process $e^+e^- \to J/\psi\pi^+\pi^-$ at $\sqrt{s} = 4170\,\text{MeV}$ and found an indication of an even higher transition rate at the $Y(4260)$ energy [2]. This implies that the $h_b(mP)$ production might be enhanced in the region of the Y_b and motivates a search for the $h_b(mP)$ in the $\Upsilon(5S)$ data.
We use the full $\Upsilon(5S)$ data sample with the integrated luminosity of $121.4\,\text{fb}^{-1}$ collected near the peak of the $\Upsilon(5S)$ resonance with the Belle detector [4] at the KEKB asymmetric-energy e^+e^- collider [3].

2 $\Upsilon(5S) \to h_b(mP)\pi^+\pi^-$ and $\Upsilon(nS)\pi^+\pi^-$ data analysis

We observe the $h_b(1P)$ and $h_b(2P)$ in the missing mass spectrum of $\pi^+\pi^-$ pairs. The $\pi^+\pi^-$ missing mass is defined as $MM(\pi^+\pi^-) \equiv \sqrt{(E_{c.m.} - E^*_{\pi^+\pi^-})^2 - p^{*2}_{\pi^+\pi^-}}$, where $E_{c.m.}$ is the

[1] a.s.kuzmin@inp.nsk.su

center-of-mass (c.m.) energy, $E^*_{\pi^+\pi^-}$ and $p^*_{\pi^+\pi^-}$ are the $\pi^+\pi^-$ energy and momentum measured in the c.m. frame. The details of the analysis can be founnd in [5]. The $MM(\pi^+\pi^-)$ distribution for the selected $\pi^+\pi^-$ pairs is shown in Fig. 1(a). In this figure only the $\Upsilon(5S) \to \Upsilon(1S)\pi^+\pi^-$ and $\Upsilon(5S) \to \Upsilon(2S)\pi^+\pi^-$ transitions are discernible.
To fit the $MM(\pi^+\pi^-)$ spectrum we separate it into three adjacent regions with boundaries at $MM(\pi^+\pi^-) = 9.3\,\mathrm{GeV}/c^2$, $9.8\,\mathrm{GeV}/c^2$, $10.1\,\mathrm{GeV}/c^2$ and $10.45\,\mathrm{GeV}/c^2$. We fit every region separately to better control the complicated shape of the combinatorial background, which is described by a Chebyshev polynomial of 6-7th order. In region 3 we subtract the K^0_S contribution bin-by-bin, while in other regions its shape is smooth and is absorbed into combinatorial background. The signal peaks are described by Gaussians with paramenters obtained from exclusive decays of the $\Upsilon(nS)$ to $\mu^+\mu^-$. The $MM(\pi^+\pi^-)$ spectrum with the combinatorial background and K^0_S contributions subtracted, and the signal function resulting from the fit overlaid, is shown in Fig. 1(b). The significance of the $h_b(1P)$ and

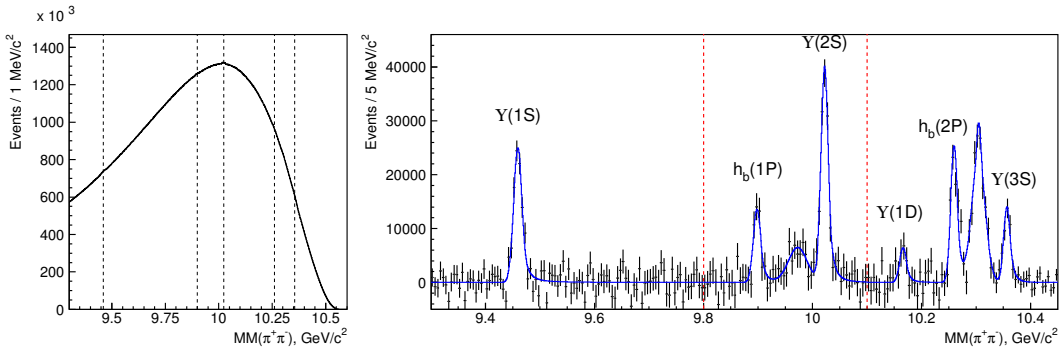

Figure 1: (a)The $MM(\pi^+\pi^-)$ distribution for the selected $\pi^+\pi^-$ pairs. Vertical lines indicate the locations of the $\Upsilon(1S)$, $h_b(1P)$, $\Upsilon(2S)$, $h_b(2P)$ and $\Upsilon(3S)$ signals. (b) The $MM(\pi^+\pi^-)$ spectrum with the combinatorial background contributions subtracted (dots with error bars) and signal component of the fit function (solid histogram).

$h_b(2P)$ signals which includes the systematic uncertainty is 5.5σ and 11.2σ, respectively.
This is the first observation of the $h_b(1P)$ and $h_b(2P)$ spin-singlet bottomonium states in the reaction $e^+e^- \to h_b(mP)\pi^+\pi^-$ at the $\Upsilon(5S)$ energy. We measure the masses and the cross sections relative to the $e^+e^- \to \Upsilon(2S)\pi^+\pi^-$ cross-section: $M = 9898.25 \pm 1.06^{+1.03}_{-1.07}\,\mathrm{MeV}/c^2$, $R = 0.407 \pm 0.079^{+0.043}_{-0.076}$ for the $h_b(1P)$ and $M = 10259.76 \pm 0.64^{+1.43}_{-1.03}\,\mathrm{MeV}/c^2$, $R = 0.78 \pm 0.09^{+0.22}_{-0.10}$ for the $h_b(2P)$. The masses do not differ significantly from the center-of-gravity of the corresponding χ_{bJ} states. For the hyperfine splitting we find $\Delta M_{\mathrm{HF}} = 1.62 \pm 1.52\,\mathrm{MeV}/c^2$ for the $h_b(1P)$ and $0.48^{+1.57}_{-1.22}\,\mathrm{MeV}/c^2$ for the $h_b(2P)$. The values of R are comparable with unity indicate that the $h_b(1P)$ and $h_b(2P)$ are produced via an exotic process that violates the suppression of heavy quark spin-flip.
For further study we investigate resonant structure of these decays [7]. Because of high background Dalitz plot analysis is impossible with current statistics, therefore we study the one-dimensional distributions in $M(h_b(mP)\pi)$. We define the $M(h_b(mP)\pi^+)$ as a missing

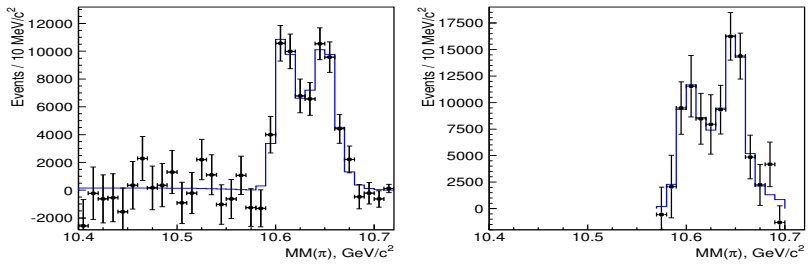

Figure 2: The yield of the $h_b(1P)$ (a) and $h_b(2P)$ (b) as a function of $MM(\pi)$ (points with error bars) and results of the fit (histogram).

mass of the opposite sign pion, $MM(\pi^-)$. We measure the yield of signal decays as a function of the $MM(\pi^\pm)$ by fitting the $MM(\pi^+\pi^-)$ spectra in the bins of $MM(\pi^\pm)$. We combine the $MM(\pi^+\pi^-)$ spectra for the corresponding $MM(\pi^+)$ and $MM(\pi^-)$ bins and we use half of the phase-space to avoid double counting. Results of fits for the $h_b(1P)$ yield as a function of $MM(\pi)$ are shown in Fig. 2. The $h_b(1P)$ yield exhibits a clear two-peak structure without any significant non-resonant contribution.

We perform a χ^2 fit to the $MM(\pi)$ distributions. We assume that spin-parity for both $Z_b(10610)$ and $Z_b(10650)$ is $J^P = 1^+$, therefore in the fit function we use a coherent sum of two P-wave Breit-Wigner amplitudes and a non-resonant contribution: $f = A\,|BW(s, M_1, \Gamma_1) + ae^{i\phi}BW(s, M_2, \Gamma_2) + be^{i\psi}|^2\,\frac{qp}{\sqrt{s}}$, where $\sqrt{s} \equiv MM(\pi)$; the variables A, M_k, Γ_k ($k = 1, 2$), a, ϕ, b and ψ are floating in the fit. The non-resonant amplitude is found to be consistent with zero. The results of the fit are shown in Fig. 2 and are summarized in Table 2. We find that the hypothesis of two resonances is favored over the hypothesis of a single resonance (no resonances) at the $7.4\,\sigma$ ($17.9\,\sigma$) level. The parameters of the $Z_b(10610)$ and $Z_b(10650)$ obtained in the fit of $h_b(1P)$ and $h_b(2P)$ are consistent with each other.

To select $\Upsilon(5S) \to \Upsilon(nS)\pi^+\pi^-$ candidate events, we require the presence of a pair of muon candidates with an invariant mass in the range of $8.0\ \mathrm{GeV}/c^2 < M(\mu^+\mu^-) < 11.0\ \mathrm{GeV}/c^2$ and two pion candidates of opposite charge. Candidate $\Upsilon(5S) \to \Upsilon(nS)\pi^+\pi^-$ events are identified by the invariant mass of the $\mu^+\mu^-$ combination and the missing mass associated with the $\pi^+\pi^-$ system calculated as $MM(\pi^+\pi^-) = \sqrt{(E_{c.m.} - E^*_{\pi^+\pi^-})^2 - p^{*2}_{\pi^+\pi^-}}$, where $E_{\mathrm{c.m.}}$ is the c.m. energy and $E^*_{\pi^+\pi^-}$ and $p^*_{\pi^+\pi^-}$ are the energy and momentum of the $\pi^+\pi^-$ system measured in the c.m. frame.

The amplitude analyses of the three-body $\Upsilon(5S) \to \Upsilon(nS)\pi^+\pi^-$ decays that are reported here are performed by means of unbinned maximum likelihood fits to two-dimensional Dalitz distributions. The logarithmic likelihood function $\mathcal{L}$ is then constructed as

$$\mathcal{L} = -2\sum \log(f_{\mathrm{sig}} S(s_1, s_2) + (1 - f_{\mathrm{sig}})B(s_1, s_2)), \quad (1)$$

where $S(s_1, s_2) = |M(s_1, s_2)|^2$ folded with the detector resolution function, $B(s_1, s_2) = 1$ and f_{sig} is a fraction of signal events in the data sample. Both $S(s_1, s_2)$ and $B(s_1, s_2)$ are corrected

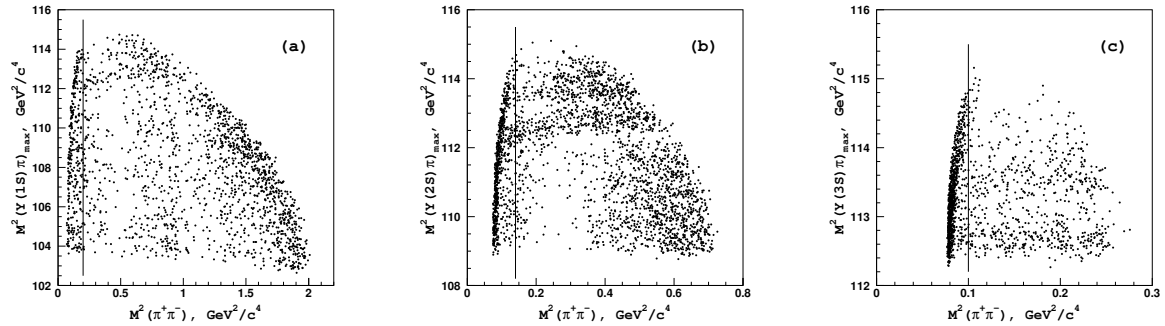

Figure 3: Dalitz plots for $\Upsilon(nS)\pi^+\pi^-$ events in the (a) $\Upsilon(1S)$; (b) $\Upsilon(2S)$; (c) $\Upsilon(3S)$ signal regions. The regions to the right of the vertical lines are included in the fit procedure.

for the reconstruction efficiency.

The background distribution functions were obtained from the $\Upsilon(nS)$ mass sidebands. There is a strong concentration of background events in the very low $\pi^+\pi^-$ invariant mass region; these are due to photon conversion on the innermost parts of the Belle detector. We exclude this region by applying the requirements on the $\pi^+\pi^-$ invariant mass. The background distribution for the remaining region is consistent with the uniform one.

The variation of reconstruction efficiency across the Dalitz plot is determined from MC simulation. The fraction of signal events in the signal region for each of the three $\Upsilon(nS)\pi^+\pi^-$ final states is determined from a fit to the corresponding $MM(\pi^+\pi^-)$ spectrum using a Crystal Ball function [6] for the Y signal and a linear function for the combinatorial background component.

Figure 3 shows Dalitz plots of the events in the signal regions for the three decay channels under study. In all cases, two horizontal bands are evident in the $\Upsilon(nS)\pi$ system near $10.61\,\mathrm{GeV}/c^2$ ($\sim 112.6\ \mathrm{GeV}^2/c^4$) and $10.65\,\mathrm{GeV}/c^2$ ($\sim 113.3\ \mathrm{GeV}^2/c^4$). In the following we refer to these structures as $Z_b(10610)$ and $Z_b(10650)$, respectively.

We use the following parameterization for the $\Upsilon(5S) \to \Upsilon(nS)\pi^+\pi^-$ three-body decay amplitude: $M(s_1, s_2) =$
$BW(s_1, M_2, \Gamma_2) + BW(s_2, M_2, \Gamma_2) + ae^{i\delta}(BW(s_1, M_2, \Gamma_2) + BW(s_2, M_2, \Gamma_2)) + A_{f_0} + A_{f_2} + A_{NR}$, where $s_{1\,2} = M^2(\Upsilon(nS)\pi^\pm)$. Here we assume that the dominant contributions come from the amplitudes that conserve the orientation of the spin of the heavy quarkonium state and, thus, both pions in the cascade decay $\Upsilon(5S) \to Z_b\pi \to \Upsilon(nS)\pi^+\pi^-$ are emitted in an S-wave with respect to the heavy quarkonium system. Consequently, we parameterize the observed $Z_b(10610)$ and $Z_b(10650)$ peaks with an S-wave Breit-Wigner function without $s-$dependence of the resonance width Γ. We also include amplitudes A_{f_0} and A_{f_2} to account for possible contributions in the $\pi^+\pi^-$ channel from $f_0(980)$ scalar and $f_2(1270)$ tensor states, respectively and non-resonant amplitude [8] $A_{\mathrm{NR}} = a_1^{\mathrm{nr}} \cdot e^{i\delta_1^{\mathrm{nr}}} + a_2^{\mathrm{nr}} \cdot e^{i\delta_2^{\mathrm{nr}}} \cdot s_3$, where $s_3 = M^2(\pi^+\pi^-)$ and a_1^{nr}, a_2^{nr}, δ_1^{nr} and δ_2^{nr} are free parameters of the fit.

Results of the fits are summarized in Table 2. The combined statistical significance of the two peaks exceeds 10 sigma for all tested models and for all $\Upsilon(nS)\pi^+\pi^-$ channels.

Table 1: The probabilities at which different J^P hypotheses are disfavored compared to the 1^+ hypothesis.

J^P	$Z_b(10610)$			$Z_b(10650)$		
	$\Upsilon(2S)\pi^+\pi^-$	$\Upsilon(3S)\pi^+\pi^-$	$h_b(1P)\pi^+\pi^-$	$\Upsilon(2S)\pi^+\pi^-$	$\Upsilon(3S)\pi^+\pi^-$	$h_b(1P)\pi^+\pi^-$
1^-	$3.6\,\sigma$	$0.3\,\sigma$	$0.3\,\sigma$	$3.7\,\sigma$	$2.6\,\sigma$	$2.7\,\sigma$
2^+	$4.3\,\sigma$	$3.5\,\sigma$	$4.3\,\sigma$	$4.4\,\sigma$	$2.7\,\sigma$	$2.1\,\sigma$
2^-	$2.7\,\sigma$	$2.8\,\sigma$		$2.9\,\sigma$	$2.6\,\sigma$	

We perform angular analyses to check consistency of the $J^P = 1^+$ assignment for the $Z_b(10610)$ and $Z_b(10650)$ states and to attempt to discriminate against other J^P hypotheses; we consider $J^P = 1^-, 2^+$ and 2^-. The 0^+ (0^-) assignment is forbidden by parity conservation in $Z_b \to \Upsilon(nS)\pi$ ($Z_b \to h_b(mP)\pi$) decays. We use the polar angles of the pions (denoted as θ_1 for a pion from the $Y(5S)$ decay and θ_2 for a pion from the Z_b decay), the spatial angle, $\theta_{\pi\pi}$, between the two pions and the angle, ϕ_p, between the plane defined by the pion from $Y(5S)$ decay and the beam direction and the plane defined by the two pions. Since the Z_b velocity is very small, $\beta < 0.02$, we neglect its recoil motion and measure all pion momenta in the c.m. frame. We assume that only the lowest wave contributes to the decay in the cases where more than one wave is possible.

We perform a binned maximum likelihood fit to these distributions. The fit function is a sum of the Z_b signal, non-resonant component and combinatorial background described by a properly normalized $MM(\pi^+\pi^-)$ sidebands. The non-resonant contribution varies with the $\cos\theta_{\pi\pi}$, therefore this variable is not used. The fit function is corrected for efficiency. The only floating parameter in the fit is the normalization of the Z_b signal component.The probabilities at which the 1^-, 2^+ and 2^- hypotheses are disfavored compared to the 1^+ hypothesis are calculated as $\sqrt{\Delta 2 \log \bar{L}}$ and given in Table 1. The presented numbers indicate that the 1^+ hypothesis for both $Z_b(10610)$ and $Z_b(10650)$ provides the best description of angular distributions among all other hypotheses with $J \leqslant 2$.

Table 2: Z_b and Z_b' parameters obtained from $\Upsilon(5S) \to \Upsilon(nS)\pi^+\pi^-$ and $\Upsilon(5S) \to h_b(mP)\pi^+\pi^-$ analyses. Quoted values are in MeV/c^2 for masses, in MeV for widths and in degrees for the relative phase. Relative amplitude is defined as $a_{Z_b}/a_{Z_b'}$.

Final state	$\Upsilon(1S)\pi^+\pi^-$	$\Upsilon(2S)\pi^+\pi^-$	$\Upsilon(3S)\pi^+\pi^-$	$h_b(1P)\pi^+\pi^-$	$h_b(2P)\pi^+\pi^-$
$M(Z_b(10610))$	$10609 \pm 3 \pm 2$	$10616 \pm 2^{+3}_{-4}$	$10608 \pm 2^{+5}_{-2}$	$10605.1 \pm 2.2^{+3.0}_{-1.0}$	$10596 \pm 7^{+5}_{-2}$
$\Gamma(Z_b(10610))$	$22.9 \pm 7.3 \pm 2$	$21.1 \pm 4^{+2}_{-3}$	$12.2 \pm 1.7 \pm 4$	$11.4^{+4.5\,+2.1}_{-3.9\,-1.2}$	$16^{+16\,+13}_{-10\,-4}$
$M(Z_b(10650))$	$10660 \pm 6 \pm 2$	$10653 \pm 2 \pm 2$	$10652 \pm 2 \pm 2$	$10654.5 \pm 2.5^{+1.0}_{-1.9}$	$10651 \pm 4 \pm 2$
$\Gamma(Z_b(10650))$	$12 \pm 10 \pm 3$	$16.4 \pm 3.6^{+4}_{-6}$	$10.9 \pm 2.6^{+4}_{-2}$	$20.9^{+5.4\,+2.1}_{-4.7\,-5.7}$	$12^{+11\,+8}_{-9\,-2}$
Rel. amplitude	$0.59 \pm 0.19^{+0.09}_{-0.03}$	$0.91 \pm 0.11^{+0.04}_{-0.03}$	$0.73 \pm 0.10^{+0.15}_{-0.05}$	$1.8^{+1.0\,+0.1}_{-0.7\,-0.5}$	$1.3^{+3.1\,+0.4}_{-1.1\,-0.7}$
Rel. phase,	$53 \pm 61^{+5}_{-50}$	$-20 \pm 18^{+14}_{-9}$	$6 \pm 24^{+23}_{-59}$	$188^{+44\,+4}_{-58\,-9}$	$255^{+56\,+12}_{-72\,-183}$

3 Discussion and Conclusions

In conclusion, we have observed two charged bottomonium-like resonances, the $Z_b(10610)$ and $Z_b(10650)$, with signals in five different decay channels, $\Upsilon(nS)\pi^\pm$ ($n = 1,2,3$) and $h_b(mP)\pi^\pm$ ($m = 1,2$). Parameters of the resonances as measured in different channels are summarized in Table 2. All channels yield consistent results. A simple weighted averages over all five channels give $M[Z_b(10610)] = 10608.4 \pm 2.0\,\mathrm{MeV}/c^2$, $\Gamma[Z_b(10610)] = 15.6 \pm 2.5\,\mathrm{MeV}$ and $M[Z_b(10650)] = 10653.2 \pm 1.5\,\mathrm{MeV}/c^2$, $\Gamma[Z_b(10650)] = 14.4 \pm 3.2\,\mathrm{MeV}$, where statistical and systematic errors are added in quadrature.
The measured masses of these states exceed by only a few MeV/c^2 the thresholds for the open beauty channels $B^*\overline{B}$ (10604.6 MeV) and $B^*\overline{B}^*$ (10650.2 MeV). This "coincidence" can be explained by a molecular-like type of new states, *i.e.*, their structure is determined by the strong interaction dynamics of the $B^*\overline{B}$ and $B^*\overline{B}^*$ meson pairs.
The widths of both states are similar and are of the order of $15\,\mathrm{MeV}/c^2$. The $Z_b(10610)$ production rate is similar to the $Z_b(10650)$ production rate for every decay channel. Their relative phase is consistent with zero for the final states with the $\Upsilon(nS)$ and consistent with 180 degree for the final states with the $h_b(mP)$.
The $\Upsilon(5S) \to h_b(mP)\pi^+\pi^-$ decays seem to be saturated by the $Z_b(10610)$ and $Z_b(10650)$ intermediate states; this decay mechanism is responsible for the high rate of the $\Upsilon(5S) \to h_b(mP)\pi^+\pi^-$ process measured recently by the Belle Collaboration.
Analysis of angular distributions for charged pions favors the $J^P = 1^+$ spin-parity assignment for both $Z_b(10610)$ and $Z_b(10650)$. Since the $\Upsilon(5S)$ has negative G-parity, Z_b states will have opposite G-parity due to emission of the pion.

Bibliography

[1] K.-F. Chen *et al.* (Belle Collaboration), Phys. Rev. Lett. **100**, 112001 (2008), K.-F. Chen *et al.* (Belle Collaboration), Phys. Rev. D **82**, 091106 (2010).

[2] T. K. Pedlar et al. (CLEO Collaboration), Phys. Rev. Lett. 107, 041803 (2011).

[3] S. Kurokawa and E. Kikutani, Nucl. Instrum. Methods Phys. Res. Sect., **A499**, 1 (2003).

[4] A. Abashian *et al.* (Belle Collaboration), Nucl. Instrum. Meth. A **479**, 117 (2002).

[5] D. M. Asner *et al.* (Belle Collaboration), arXiv:1103.3419 [hep-ex].

[6] T. Skwarnicki, Ph.D. Thesis, Institute for Nuclear Physics, Krakow 1986; DESY Internal Report, DESY F31-86-02 (1986).

[7] I.Adachi *et al.* (Belle Collaboration), arXiv:1105.4583 [hep-ex] .

[8] M.B. Voloshin, Prog. Part. Nucl. Phys. **61**, 455 (2008), Phys. Rev. D **74**, 054022 (2006).

Mass dependence of the heavy quark potential and its effects on quarkonium states

Alexander Laschka, Norbert Kaiser, and Wolfram Weise
Physik Department
Technische Universität München
D-85747 Garching, GERMANY

The heavy quark-antiquark potential is accessible in perturbative QCD and in lattice simulations. The perturbative short-distance part of the potential is contructed via a restricted Fourier transform, covering the momentum region where perturbative QCD is applicable. We show that for the leading order static term as well as for the mass dependent corrections, the perturbative part can be matched at intermediate distances with results from lattice QCD. From these matched potentials, quarkonium spectra with a single free parameter (the heavy quark mass) are derived and compared with empirical spectra. Furthermore, charm and bottom quark masses are deduced.

1 The static potential

The potential between two heavy quarks is a prime subject of interest since the early days of QCD. Nowadays it is defined in a non-relativistic effective theory framework. While the long distance part can be studied in lattice QCD simulations, perturbation theory should be expected to work at short distances. The potential can be organized in a power series of the inverse quark mass m:

$$V = V^{(0)} + \frac{V^{(1)}}{m/2} + \frac{V^{(2)}}{(m/2)^2} + \dots . \tag{1}$$

The leading term $V^{(0)}$ represents the static potential. It has the following form at two-loop order in momentum space:

$$\tilde{V}^{(0)}(|\vec{q}\,|) = -\frac{16\pi\alpha_s(|\vec{q}\,|)}{3\vec{q}^{\,2}} \left\{ 1 + \frac{\alpha_s(|\vec{q}\,|)}{4\pi}\, a_1 + \left(\frac{\alpha_s(|\vec{q}\,|)}{4\pi} \right)^2 a_2 + \dots \right\}, \tag{2}$$

where $\vec{q}$ is the three-momentum transfer. The constants a_1 and a_2 are [1–3]:

$$a_1 = 31/3 - 10/9\, n_f, \tag{3}$$

$$a_2 = 456.749 - 66.3542\, n_f + 1.23457\, n_f^2, \tag{4}$$

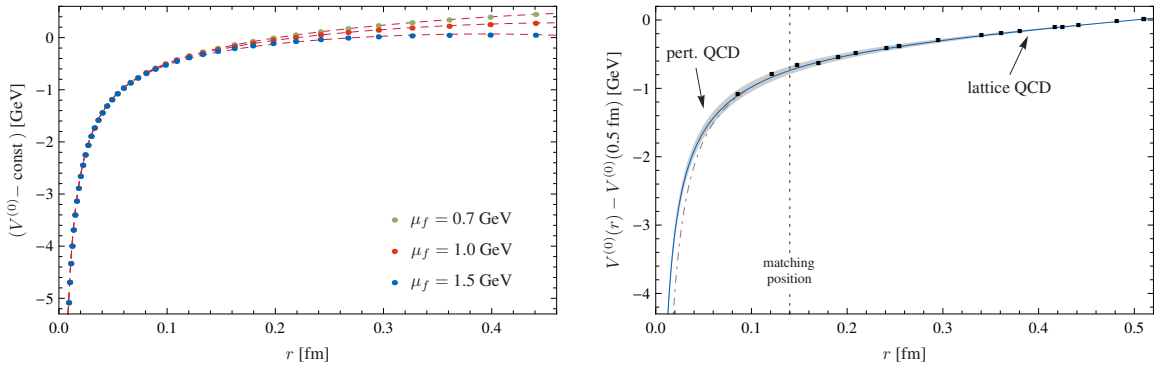

Figure 1: Static QCD potential (with $n_f = 3$) from the restricted numerical Fourier transform (6). Left: coordinate space potential at two-loop order for different values of μ_f. The curves have been shifted by a constant to match at small r values. Right: potential matched at $r = 0.14$ fm to a potential from lattice QCD [7]. Taken from Ref. [8].

where n_f is the number of light-quark flavors. Higher order terms have infrared contributions and are not considered at this level. Expressing $\alpha_s(|\vec{q}\,|)$ in a power series expansion about α_s at a fixed scale μ leads to the standard definition of the r-space static potential,

$$V^{(0)}(r) = -\frac{4}{3}\frac{\alpha_s(\mu)}{r}\left\{1 + \frac{\alpha_s(\mu)}{4\pi}\left[a_1 + 2\beta_0\, g_\mu(r)\right] + \left(\frac{\alpha_s(\mu)}{4\pi}\right)^2\left[a_2 + \beta_0^2\left(4g_\mu^2(r) + \pi^2/3\right) + 2g_\mu(r)(2a_1\beta_0 + \beta_1)\right] + \mathcal{O}(\alpha_s^3)\right\}, \tag{5}$$

with $g_\mu(r) = \ln(\mu r) + \gamma_E$. It is well known that this potential suffers from renormalon ambiguities [4,5] and shows a badly convergent behavior [6].

We work in the following in the potential subtracted (PS) scheme proposed by Beneke [4] and define the static r-space potential,

$$V^{(0)}(r, \mu_f) = \int\limits_{|\vec{q}\,|>\mu_f} \frac{d^3q}{(2\pi)^3}\, e^{i\vec{q}\cdot\vec{r}}\, \tilde{V}^{(0)}(|\vec{q}\,|)\,, \tag{6}$$

where $\tilde{V}^{(0)}(|\vec{q}\,|)$ is given in Eq. (2), but $\alpha_s(|\vec{q}\,|)$ is understood without resorting to a power series expansion. The momentum space cutoff μ_f is introduced in order to exclude the uncontrolled low momentum region. The potential $V^{(0)}(r, \mu_f)$ is evaluated numerically using four-loop RGE running for the strong coupling α_s. For distances $r \lesssim 0.2$ fm, this potential depends only marginally on μ_f as shown in the left plot of Fig. 1. The perturbative potential, valid at small distances, can be matched at intermediate distances to results from lattice QCD (see the rightmost plot in Fig. 1). For the matching point (dashed line) we choose $r = 0.14$ fm where both the perturbative and lattice potential are expected to be reliable.

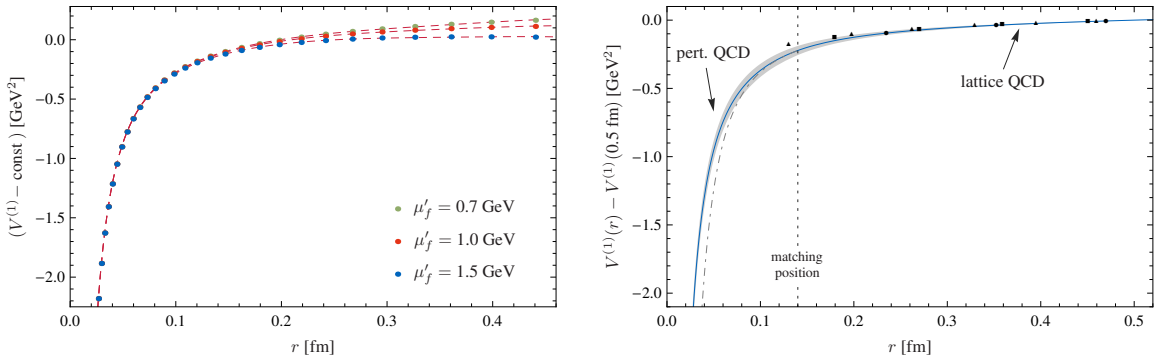

Figure 2: The order $1/m$ potential with $n_f = 3$, from the restricted Fourier transform. Left: perturbative potential for different cutoffs μ'_f. Right: perturbative potential matched at intermediate distances to a potential from lattice QCD. Taken from Ref. [8].

2 The order $1/m$ potential and quarkonium spectroscopy

$V^{(1)}$ in Eq. (1) is the first mass dependent correction to the static potential. It is spin independent and the leading term reads in momentum space [9]:

$$\tilde{V}^{(1)}(|\vec{q}\,|) = -\frac{2\pi^2\alpha_s^2(|\vec{q}\,|)}{|\vec{q}\,|}\{1 + \mathcal{O}(\alpha_s)\}\,. \tag{7}$$

It can be transformed analogously as in Eq. (6) to r-space with a low momentum cutoff μ'_f. The dependence of $V^{(1)}$ on the cutoff scale is again very weak for distances $r \lesssim 0.2$ fm. At long distances $V^{(1)}(r)$ is known from lattice QCD [10,11]. To fit the lattice data we use the form

$$V^{(1)}_{\text{fit}}(r) = -\frac{c'}{r^2} + d' \ln\left(\frac{r}{r_0}\right) + \text{const}, \tag{8}$$

motivated in [12]. As shown in Fig. 2 matching with the perturbative potential at intermediate distances is also possible at order $1/m$.

Using $V^{(0)}$ and $V^{(1)}$ as input in the Schrödinger equation, we can examine bottomonium and charmonium spectra. The overall constant of the potential is the only free parameter. This single parameter is related to the heavy quark mass in the PS scheme and can be translated in a second step to the bottom and charm quark masses in the $\overline{\text{MS}}$ scheme (see [8] for details). Our findings for the masses are summarized in Table 1 and compared to the values listed by the Particle Data Group (PDG) [13]. Results for the bottomonium and charmonium spectra are shown in Fig. 3. In both cases we find that the 1S states are the most strongly affected by $1/m$-effects. An additional effective one-gluon exchange spin dependent term with $\alpha_s^{\text{eff}} = 0.3$ (+h.f. in Fig. 3) would improve our predictions. Of course,

	$\overline{\text{MS}}$ masses [GeV]		
	Static	Static + $\mathcal{O}(1/m)$	PDG 2010
Bottom quark	4.20 ± 0.04	$4.18^{+0.05}_{-0.04}$	$4.19^{+0.18}_{-0.06}$
Charm quark	1.23 ± 0.04	$1.28^{+0.07}_{-0.06}$	$1.27^{+0.07}_{-0.09}$

Table 1: Comparison of quark masses obtained in our approach (leading order plus order $1/m$ corrections) with the values listed by the Particle Data Group (PDG) [13].

this step is purely ad hoc and needs to be substituted by the full potential of order $1/m^2$, to be investigated in forthcoming work.

Acknowledgments

Work supported in part by BMBF, GSI and the DFG Excellence Cluster "Origin and Structure of the Universe".

Bibliography

[1] M. Peter, *Phys. Rev. Lett.* **78**, 602 (1997).

[2] M. Peter, *Nucl. Phys.* **B501**, 471 (1997).

[3] Y. Schröder, *Phys. Lett.* **B447**, 321 (1999).

[4] M. Beneke, *Phys. Lett.* **B434**, 115 (1998).

[5] A. H. Hoang, M. C. Smith, T. Stelzer, S. Willenbrock, *Phys. Rev.* **D59**, 114014 (1999).

[6] A. Pineda, *J. Phys.* **G29**, 371 (2003).

[7] G. S. Bali, et al., *Phys. Rev.* **D62**, 054503 (2000).

[8] A. Laschka, N. Kaiser, W. Weise, *Phys. Rev.* **D83**, 094002 (2011).

[9] N. Brambilla, A. Pineda, J. Soto, A. Vairo, *Phys. Rev.* **D63**, 014023 (2000).

[10] Y. Koma, M. Koma, H. Wittig, *Phys. Rev. Lett.* **97**, 122003 (2006).

[11] M. Koma, Y. Koma, H. Wittig, *PoS* **Confinement8**, 105 (2008).

[12] G. Perez-Nadal, J. Soto, *Phys. Rev.* **D79**, 114002 (2009).

[13] K. Nakamura, et al., *J. Phys.* **G37**, 075021 (2010).

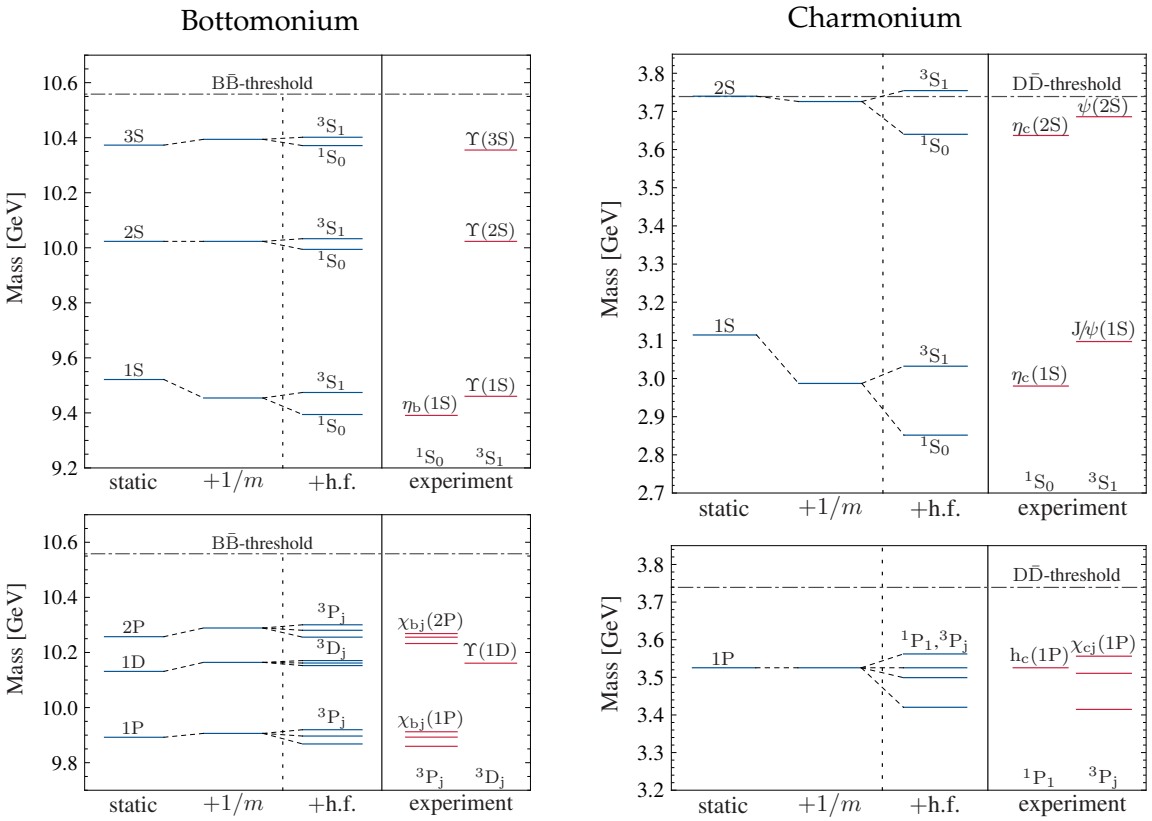

Figure 3: Bottomonium and charmonium spectrum in comparison with experiment. Static plus order $1/m$ results are shown, with additional hyperfine effects (h.f.) added phenomenologically. Taken from Ref. [8].

Quarkonia in dimuon final states and exclusive dimuon decays at LHCb

Giovanni Sabatino[1] on behalf of the LHCb Collaboration
Dipartimento di Fisica
Università degli Studi di Roma "Tor Vergata"
and INFN.

Quarkonia cross-sections in hadron collisions are fundamental observables for understanding the production mechanisms. Exploiting the dimuon decay mode, the cross-sections for J/ψ, double J/ψ, $\psi(2S)$ and $\Upsilon(1S)$ production have been measured at LHCb [1] with pp collisions at $\sqrt{s} = 7$ TeV. Moreover exclusive dimuon production, both resonant and non-resonant, has been studied and the cross-sections have been measured.

1 Introduction

Quarkonium production mechanisms in hadronic collisions are still subject of large interest and debate. It is well known that the Leading Order Color Singlet Model (CSM), leads to predictions of the cross-sections which are in disagreement with measurements [2], [3]. In recent years other models have been introduced like, for example, the Color Octet Model (COM), which in the framework of Non-Relativistic QCD (NRQCD) allows a better description of the observed cross-sections. The measurement of J/ψ, $\psi(2S)$ and Y production cross-sections at LHC energies is crucial for the understanding of the relative contributions of CSM and COM. Further hints can be given from double J/ψ production cross-section where higher order corrections are suppressed. Moreover measurements of exclusive dimuon events allow the behaviour of other states predicted by QCD, such as the pomeron and (so far unobserved) odderon, to be studied in a clean environment.

2 J/ψ cross-section

The J/ψ production cross-section has been measured at LHCb [4] with an integrated luminosity of 5.2 pb^{-1} in the fiducial region $2 < y < 4.5$ and $0 < p_{\mathrm{T}} < 14$ GeV/c. The

[1] giovanni.sabatino@roma2.infn.it

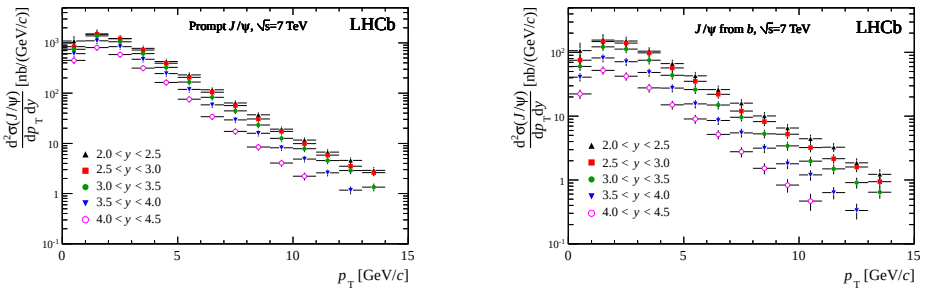

(a) **(b)**

Figure 1: Double differential cross-section in bins of $p_{\rm T}$ and y for promptly produced J/ψ (a) and for J/ψ from b-hadrons (b). Prompt J/ψ are assumed to be unpolarized.

J/ψ candidates have been reconstructed in the dimuon decay mode by fitting two tracks, identified as muons, to a common vertex. Prompt J/ψ, produced either directly in pp collisions or via feed-down from higher charmonium states, are separated from those produced in the decays of b-hadrons using the pseudo-propertime variable defined as $t_z = (z_{J/\psi} - z_{PV})M_{J/\psi}/p_z$, where the subscript $_{PV}$ stands for Primary Vertex, z is the coordinate along the beam axis and p_z is the component of the J/ψ momentum along the z direction. The cross-section has been measured in 14 bins of $p_{\rm T}$ and 5 bins of y. In each bin a simultaneous fit to the dimuon invariant mass and pseudo-propertime distributions has been performed in order to determine the number of prompt and non-prompt signal events. The number of events has then been corrected by the efficiency factors calculated from LHCb Monte Carlo simulation. The results are quoted in three different polarization scenarios: longitudinally polarized J/ψ, transversally polarized J/ψ and unpolarized J/ψ. Figure 1 shows the cross-section measured as a function of transverse momentum and rapidity. The cross-section integrated over the fiducial region is $\sigma = 10.52 \pm 0.04(\text{stat}) \pm 1.40(\text{syst})^{+1.64}_{-2.20}$ μb for prompt J/ψ and $\sigma = 1.14 \pm 0.01(\text{stat}) \pm 0.16(\text{syst})$ μb for J/ψ from b-hadrons. The asymmetric error on the prompt cross-section is due to the unknown polarization. Good agreement is found between data and theory predictions in particular with NLO NRQCD for prompt J/ψ and with FONLL model for J/ψ from b-hadrons.

3 Double J/ψ cross-section

Studies of double J/ψ production also allow the production mechanisms to be probed. Such production can be affected by the existence of charm tetra-quark states. At LHCb the double J/ψ production cross-section has been measured in the fiducial region $2 < y < 4.5$ and $0 < p_{\rm T} < 10$ GeV/c exploiting the dimuon decay mode [5]. The data sample used to perform the measurement corresponds to an integrated luminosity of 35.2 pb^{-1}. The strategy consists in reconstructing two muon pairs $(\mu^+,\mu^-)_1$ and $(\mu^+,\mu^-)_2$ in the same event.

In selecting candidates, particular care has been used to minimize the effect of duplicate tracks created by the reconstruction, while the pile-up effect (two J/ψ from consecutive collisions wrongly assigned to the same collision) has been demonstrated to be negligible. The distribution of $(\mu^+,\mu^-)_1$ invariant mass is fitted in bins of $(\mu^+,\mu^-)_2$ invariant mass in order to extract the total number of double J/ψ. The number of signal events is corrected by the efficiency factor to take into account the detector and selection effect. The cross-section measured is $\sigma_{J/\psi J/\psi} = 5.6 \pm 1.1 \pm 1.2$ nb where the first uncertainty is statistical and the second is systematic. The result can be compared with a LO QCD calculation [6] which predicts a value of 4.34 nb (4.15 nb) with (without) initial state gluon radiations.

4 $\psi(2S)$ cross-section

The $\psi(2S)$ meson, unlike J/ψ, has not appreciable feed-down from higher mass charmonium states, therefore the prompt cross-section is easier to interpret and it can be directly compared with the theory predictions. The inclusive $\psi(2S)$ cross-section has been measured at LHCb [7] with an integrated luminosity of 33.8 pb^{-1} exploiting the dimuon decay mode. The measurement has been performed in bins of $p_{\rm T}$ and y, in the fiducial region $0 < p_{\rm T} < 12$ GeV/c and $2 < y < 4.5$. The selection is similar to the $J/\psi \to \mu^+\mu^-$ one but with a harder cut on the muon $p_{\rm T}$: $p_{\rm T} > 1.2$ GeV/c instead of $p_{\rm T} > 0.7$ GeV/c. No division into prompt and non-prompt components has yet been performed: the fraction of $\psi(2S)$ from b is expected to be of the order of 10% at low $p_{\rm T}$ and 40% at large $p_{\rm T}$. Figure 2 (a) shows a comparison between the inclusive cross-section measured at LHCb and the predictions for prompt cross-section by different theoretical models [8]. The cross-section measured, integrated over the fiducial region, is $\sigma = 1.88 \pm 0.02({\rm stat}) \pm 0.31({\rm syst})^{+0.25}_{-0.48}$ μb, where the last asymmetric error is due to the unknown polarization.

5 $\Upsilon(1S)$ cross-section

At LHCb, the $\Upsilon(1S)$ production cross-section has been measured [9] with a data sample of 32.4 pb^{-1}. The measurement has been performed in bins of $p_{\rm T}$ and y, in the fiducial region $0 < p_{\rm T} < 15$ GeV/c and $2 < y < 4.5$. Thanks to the experimental resolution of about 50 MeV/c^2 it has been possible to separate fully the $\Upsilon(1S)$, $\Upsilon(2S)$ and $\Upsilon(3S)$ invariant mass peaks. The strategy for the cross-section measurement is the same already discussed above. The cross-section integrated over the fiducial region, assuming unpolarized $\Upsilon(1S)$, results to be $\sigma = 108.3 \pm 0.7^{+30.9}_{-25.8}$ nb, where the first uncertainty is statistical and the second is systematic. Figure 2 (b) shows a comparison between the cross-section measured and a theoretical prediction from NLO NRQCD.

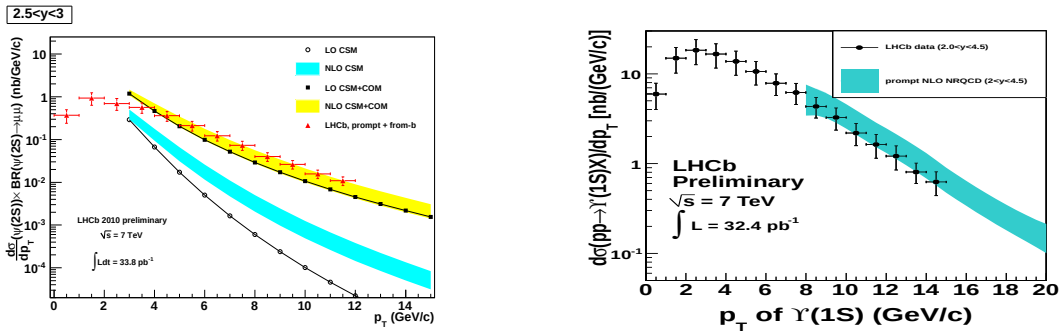

(a) (b)

Figure 2: (a) Differential cross-section in bins of p_{T} in the range $2.5 < y < 3$ for inclusive $\psi(2S)$ production. The predictions from theoretical models are made for prompt $\psi(2S)$ production. (b) Comparison between $\Upsilon(1S)$ cross-section measured at LHCb and NLO NRQCD predictions.

6 Exclusive dimuon production

Exclusive dimuon events, $pp \to p\mu^+\mu^- p$, are collisions in which an elastic interaction occurs between the two protons: they proceed undetected in the beam pipe and the event is characterized exclusively by only two muons. The two muons can be non-resonant, or resonant through intermediate production of a J/ψ, $\psi(2S)$ or χ_c state. Exclusive dimuon events allow to understand QCD in a clean environment, as they are unambiguous evidence for pomeron existence and allow to search for the odderon.

The selection requires no backward tracks (the Vertex Locator of LHCb allows some coverage for negative pseudorapidity: $-4 < \eta < -1.5$) and only two forward muons with $p_{\mathrm{T}}(\mu\mu) < 900$ MeV$/c$ to reduce the contamination from inelastic production. Moreover for χ_c, precisely one photon is required in addition. The measurement has been performed at LHCb with 36 pb^{-1} [10]. Table 1 reports the cross-sections measured for different dimuon productions. Theory predictions in this sector are rather uncertain and vary significantly. For example for exclusive J/ψ production there are predictions from 292 pb (Starlight), 330 pb (SuperChic) up to 710 pb [11].

7 Conclusions

Quarkonia production cross-section measurements, exploiting the dimuon decay mode, have been presented. The cross-sections are generally in good agreement with theory. Moreover a detailed study of the exclusive dimuon events has allowed the measurement of

Dimuon process	cross-section (pb)
$J/\psi \to \mu^+\mu^-$	$\sigma = 474 \pm 12 \pm 51 \pm 92$
$\psi(2S) \to \mu^+\mu^-$	$\sigma = 12.2 \pm 1.8 \pm 1.3 \pm 2.4$
$\chi_{c0} \to J/\psi(\mu^+\mu^-)\gamma$	$\sigma = 9.3 \pm 2.2 \pm 3.5 \pm 1.8$
$\chi_{c1} \to J/\psi(\mu^+\mu^-)\gamma$	$\sigma = 16.4 \pm 5.3 \pm 5.8 \pm 3.2$
$\chi_{c2} \to J/\psi(\mu^+\mu^-)\gamma$	$\sigma = 28.0 \pm 5.4 \pm 9.7 \pm 5.4$
non-resonant $\mu^+\mu^-$	$\sigma = 67 \pm 10 \pm 7 \pm 15$

Table 1: Cross-sections measured at LHCb for exclusive dimuon production. The pseudo-rapidity $\eta_\mu, \eta_\gamma \in [2, 4.5]$ and $m_{\mu^+\mu^-} > 2.5\ \mathrm{GeV}/c^2$ for the non-resonant cross-section.

the cross-sections for resonant and non-resonant production, providing important input for comparisons with theory.

Bibliography

[1] The LHCb Collaboration, A.A. Alves *et al.*, JINST 3, S08005 (2008).

[2] N. Brambilla *et al.*, HEP/PH 0412158 v2 CERN-2005-005.

[3] N. Brambilla *et al.*, arXiv:1010.5827v3 [hep-ph].

[4] The LHCb Collaboration, Aaij R. *et al.*, Eur. Phys. J. C 71 (2011) 1645.

[5] The LHCb Collaboration, Aaij R. *et al.*, CERN-LHCb-CONF-2011-009.

[6] A.V. Berezhnoy *et al.*, arXiv:1101.5881v1 [hep-ph].

[7] The LHCb Collaboration, CERN-LHCb-CONF-2011-026.

[8] M. Butenschoen and B. A. Kniehl, Phys. Rev. Lett. 106, 022003 (2011) and private communications.

[9] The LHCb Collaboration, CERN-LHCb-CONF-2011-016.

[10] The LHCb Collaboration, CERN-LHCb-CONF-2011-022.

[11] W. Schäfer *et al.*, PR D76 (2007) 094014.

Quarkonium production in pp collisions at 7 TeV with the CMS experiment

Bora Akgün[1] on behalf of the CMS Collaboration
Department of Physics
Carnegie Mellon University
5000 Forbes Avenue, Pittsburgh, PA 15213, USA

The production of J/ψ and Υ mesons is studied in pp collisions at $\sqrt{s} = 7$ TeV with the CMS experiment at the LHC. The J/ψ measurement is based on a dimuon sample corresponding to an integrated luminosity of 314 nb^{-1}. The J/ψ differential cross section is determined, as a function of the J/ψ transverse momentum, in three rapidity ranges. A fit to the decay length distribution is used to separate the prompt from the non-prompt (b hadron to J/ψ) component. Integrated over the J/ψ transverse momentum from 6.5 to 30 GeV/c and over rapidity in the range $|y| < 2.4$, the measured cross sections, times the dimuon decay branching fraction, are $70.9 \pm 2.1(\text{stat.}) \pm 3.0(\text{syst.}) \pm 7.8(\text{lumi.})$ nb for prompt J/ψ mesons, assuming unpolarized production, and $26.0 \pm 1.4(\text{stat.}) \pm 1.6(\text{syst.}) \pm 2.9(\text{lumi.})$ nb for J/ψ mesons from b-hadron decays. The Υ measurement is based on a dimuon sample corresponding to an integrated luminosity $3.1 \pm 0.3\,\text{pb}^{-1}$. Integrated over the rapidity range $|y| < 2$, we find the product of the $\Upsilon(1S)$ production cross section and branching fraction to dimuons to be $7.37 \pm 0.13(\text{stat.})^{+0.61}_{-0.42}(\text{syst.}) \pm 0.81(\text{lumi.})$ nb. This cross section is obtained assuming unpolarized $\Upsilon(1S)$ production. If the $\Upsilon(1S)$ production polarization is fully transverse or fully longitudinal, the cross section changes by about 20 %.

The hadroproduction of quarkonia is not understood since none of the existing theories successfully reproduces both the differential cross section and the polarization measurements of the J/ψ or Υ states [1]. It is expected that studying quarkonium hadroproduction at higher center-of-mass energies and over a wide rapidity range will facilitate significant improvements in our understanding. Measurements of quarkonium hadroproduction cross sections and production polarizations made at the Large Hadron Collider (LHC) will allow important tests of several alternative theoretical approaches, including non-relativistic QCD (NRQCD) factorization [2].

The data samples used in these analyses were recorded by the CMS detector [3] in pp collisions at a center-of-mass energy of 7 TeV. Many more details in these analyses are available in Refs. [4, 5]. The trigger requires the detection of two muons at the hardware level, without any further selection at the high-level trigger (HLT). The coincidence of two

[1]bora.akgun@cern.ch

muon signals without an explicit p_T requirement is sufficient to maintain the dimuon trigger without prescaling. All three detectors in the muon systems, drift tubes, cathode-strip and resistive-plate chambers, take part in the trigger decision.

Each muon is required to satisfy:

(1) $p_T^\mu > 3.5$ GeV/c if $|\eta^\mu| < 1.6$;
$p_T^\mu > 2.5$ GeV/c if $1.6 < |\eta^\mu| < 2.4$ (for Υ selection).

(2) $p_T^\mu > 3.3$ GeV/c if $|\eta^\mu| < 1.3$; $p^\mu > 2.9$ GeV/c if $1.3 < |\eta^\mu| < 2.2$;
$p_T^\mu > 2.4$ GeV/c if $2.2 < |\eta^\mu| < 2.4$ (for J/ψ selection).

The dimuon invariant-mass spectra in the J/ψ and $\Upsilon(nS)$ regions are shown in Fig. 1. The

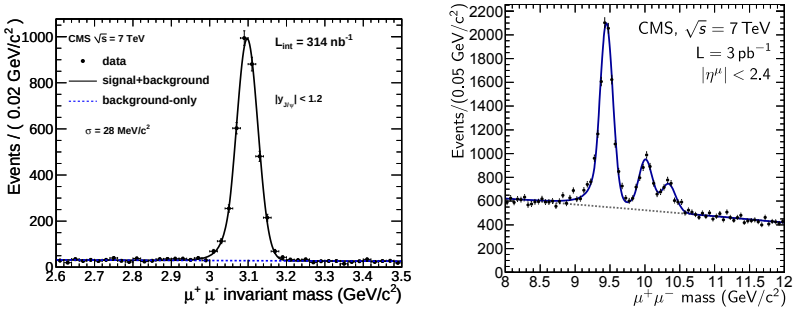

Figure 1: The dimuon invariant-mass distribution in the vicinity of the J/ψ resonance for $|y_{J/\psi}|$ <1.2 (left) and $\Upsilon(nS)$ resonances for $|\eta^\mu|$ <2.4 (right) .

acceptance A is defined as the fraction of detectable $J/\psi \to \mu^+\mu^-$ or $\Upsilon \to \mu^+\mu^-$ decays, as a function of the dimuon transverse momentum p_T and rapidity y,

$$A(p_T, y; \lambda_\theta) = \frac{N_{\rm det}(p_T, y; \lambda_\theta)}{N_{\rm gen}(p_T, y; \lambda_\theta)} \quad , \tag{3}$$

where $N_{\rm det}$ is the number of detectable J/ψ or Υ events in a given (p_T, y) bin, expressed in terms of the dimuon variables after detector smearing, and $N_{\rm gen}$ is the corresponding total number of generated J/ψ or Υ events in the Monte Carlo simulation. The parameter λ_θ reflects the fact that the acceptance is computed for various polarization scenarios.

The total muon efficiency can be factorized into three conditional terms,

$$\epsilon(\text{total}) = \epsilon(\text{trig}|\text{id}) \cdot \epsilon(\text{id}|\text{track}) \cdot \epsilon(\text{track}|\text{accepted}) \equiv \epsilon_{\rm trig} \cdot \epsilon_{\rm id} \cdot \epsilon_{\rm track} \,. \tag{4}$$

The tracking efficiency, $\epsilon_{\rm track}$, is the efficiency for a muon track from the quarkonium decay to be reconstructed in the presence of other activity in the silicon tracker, as determined with a track-embedding technique [6]. The muon identification efficiency, $\epsilon_{\rm id}$, is the probability

that the track in the silicon tracker is identified as a muon and is based on the tag-and-probe [7] method. The efficiency that an identified muon satisfies the trigger, ϵ_{trig}, is again measured with the same technique.

The differential cross section is determined from the signal yield, N_{fit}, obtained directly from a weighted fit to the dimuon invariant-mass spectrum, after correcting for the acceptance ($\mathcal{A}$) and the total efficiency (ϵ), through the equation:

$$\frac{d^2\sigma}{dp_T\,dy}\cdot\mathcal{B}\left(X\to\mu^+\mu^-\right)=\frac{N_{\text{fit}}\langle\frac{1}{\mathcal{A},\epsilon}\rangle}{\mathcal{L}\ \cdot\Delta p_T\cdot\Delta y}\,, \tag{5}$$

upon normalization by the integrated luminosity of the dataset, $\mathcal{L}$, and by the bin widths, Δp_T and Δy, of the dimuon transverse momentum and rapidity.

The yields are extracted via an unbinned maximum likelihood fit. The measured mass-lineshape of the J/ψ and each of the three Y states is parameterized by a "Crystal Ball" (CB) function. A second-degree polynomial is chosen to describe the background for the $\Upsilon(nS)$ states and an exponential function for the J/ψ background.

The $\Upsilon(nS)$ integrated production cross sections times branching fractions for the range $|y|<2$ are measured to be:

$$\begin{aligned}
&\sigma(pp\to\Upsilon(1S)X)\cdot\mathcal{B}(\Upsilon(1S)\to\mu^+\mu^-)=7.37\pm0.13(\text{stat.})^{+0.61}_{-0.42}(\text{syst.})\pm0.81(\text{lumi.})\,\text{nb}\,,\\
&\sigma(pp\to\Upsilon(2S)X)\cdot\mathcal{B}(\Upsilon(2S)\to\mu^+\mu^-)=1.90\pm0.09(\text{stat.})^{+0.20}_{-0.14}(\text{syst.})\pm0.24(\text{lumi.})\,\text{nb}\,,\\
&\sigma(pp\to\Upsilon(3S)X)\cdot\mathcal{B}(\Upsilon(3S)\to\mu^+\mu^-)=1.02\pm0.07(\text{stat.})^{+0.11}_{-0.08}(\text{syst.})\pm0.11(\text{lumi.})\,\text{nb}\,.
\end{aligned} \tag{6}$$

The $\Upsilon(1S)$ and $\Upsilon(2S)$ measurements include feed-down from higher-mass states, such as the χ_b family and the $\Upsilon(3S)$. These measurements assume unpolarized $\Upsilon(nS)$ production. Assumptions of fully-transverse or fully-longitudinal polarizations change the cross sections by about 20%. The $\Upsilon(nS)$ differential p_T cross sections are shown in Fig. 2 (left).

The total cross section times branching fraction for inclusive J/ψ production, obtained by integrating over p_T between 6.5 and 30 GeV/c and over rapidity $|y|<2.4$ in the unpolarized-production hypothesis, is:

$$\sigma(pp\to J/\psi+X)\cdot\text{BR}(J/\psi\to\mu^+\mu^-)=97.5\pm1.5(\text{stat.})\pm3.4(\text{syst.})\pm10.7(\text{lumi.})\,\text{nb}. \tag{7}$$

Fig. 2 (middle) shows the inclusive differential cross section in the three rapidity ranges, and Fig. 2 (right) shows the measured fraction of J/ψ from b-hadron decays (non-prompt) as a function of J/ψ p_T. It increases strongly with p_T. At low p_T, essentially all J/ψ mesons are promptly produced, whereas at $p_T\sim12$ GeV/c around one third come from beauty decays. This pattern does not show a significant change with rapidity (within the current uncertainties) over the range covered by the CMS detector. In Fig. 2 (right), the CMS results are compared to the measurements of CDF [8], obtained in $p\overline{p}$ collisions at $\sqrt{s}=1.96$ TeV. It is interesting to note that the increase of the b fraction with p_T is very similar between the

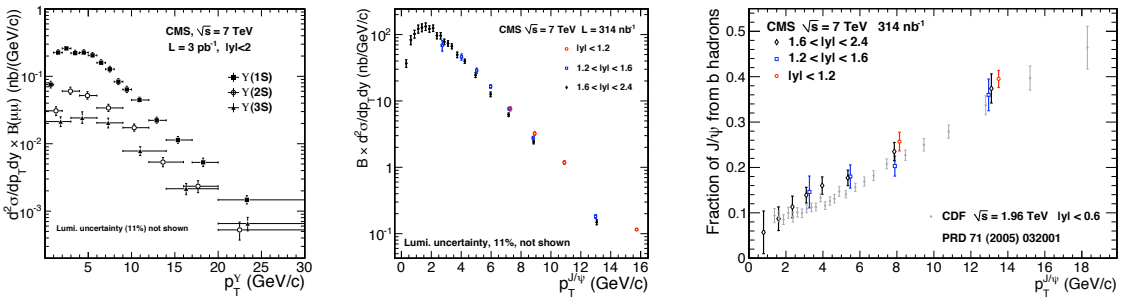

Figure 2: (left) $\Upsilon(nS)$ differential cross sections in the rapidity interval $|y| < 2$, (middle) fraction of the J/ψ production cross section originating from b-hadron decays, as a function of the J/ψ p_T, as measured by CMS in three rapidity bins and by CDF, at a lower collision energy, (right) differential inclusive J/ψ cross section as a function of p_T for the three different rapidity intervals and in the unpolarized-production scenario.

two experiments, the CMS points being only slightly higher, despite the different collision energies.

The J/ψ differential prompt and non-prompt measurements have been compared with theoretical calculations. A reasonable agreement is found between data and theory for the non-prompt case while the measured prompt J/ψ cross section exceeds the expectations at forward rapidity and low p_T.

Under the assumption that the cross section is uniform in rapidity for the measurement range of each experiment, the $\Upsilon(nS)$ cross sections measured at $\sqrt{s}$ =7 TeV are about three times larger than the cross sections measured at the Tevatron. This work provides new experimental results which will serve as input to ongoing theoretical investigations of the correct description of bottomonium production.

Bibliography

[1] Brambilla, N. *et al.*, "Heavy quarkonium physics", CERN-2005-005 (2004).

[2] Bodwin, G. T. and Braaten, E. and Lepage, G. P., "Rigorous QCD analysis of inclusive annihilation and production of heavy quarkonium", Phys. Rev., **D51**, 1125 (1995).

[3] CMS Collaboration, "The CMS experiment at the CERN LHC", JINST, **0803**, S08004 (2008).

[4] CMS Collaboration, "Measurement of the Inclusive Upsilon production cross section in pp collisions at $\sqrt{s} = 7$ TeV", Phys. Rev., **D83**, 112004 (2011).

[5] CMS Collaboration, "Prompt and non-prompt J/psi production in pp collisions at sqrt(s) = 7 TeV", Eur. Phys. J., **C71**, 1575 (2011).

[6] CMS Collaboration, "Measurement of tracking efficiency", CMS Physics Analysis Summary, CMS-PAS-TRK-10-002 (2010).

[7] CMS Collaboration, "Performance of muon identification in pp collisions at $\sqrt{s}$ = 7 TeV", CMS Physics Analysis Summary, CMS-PAS-MUO-10-002 (2010).

[8] CDF, "Measurement of the J/ψ meson and b-hadron production cross section in $p\overline{p}$ collisions at $\sqrt{s} = 1.96$ TeV", Phys. Rev., **D71**, 032001 (2005).

Results on Charmonium and Charmonium-like States at the Belle Experiment

Jens Sören Lange[1] on behalf of the Belle Collaboration
Justus-Liebig-Universität Giessen, II. Physikalisches Institut,
D-35392 Giessen, GERMANY

New results of the Belle experiment at the KEKB asymmetric e^+e^- collider are presented, in particular *(a)* measurement of the mass and width of the η_c and η_c' in B meson decays, *(b)* measurement of the mass, width and quantum numbers of the X(3872) and *(c)* observation of the χ_{c2} in B meson decays.

1 η_c and η_c' in B meson decays

The η_c is the 1^1S_0 ground state of charmonium with quantum numbers J^{PC}=0^{-+}. The η_c' represents the first radial excitation 2^1S_0. As a long-standing puzzle the width of the η_c has been determined with large discrepancies between experiments with different production mechanisms: in J/ψ and ψ' radiative decays $\Gamma_{\eta_c}\simeq$15 MeV, in B meson decays or $\gamma\gamma\to\eta_c$ $\Gamma_{\eta_c}\simeq$30 MeV [1]. One possible reason is the fact that in radiative decays the cross section is varying with the photon energy according to E_γ^a with an exponent $3\leqslant a\leqslant 7$, and thus leading to a distorted line shape of the observed η_c signal. However, in the case of the latter production mechanisms a Breit-Wigner lineshape is considered a valid parametrisation.

In a new analysis of $B^+\to K^+\eta_c(\to K_S K^\pm\pi^\mp)$ [2], the mass and the width of the η_c were determined by a 2-dimensional fit of the invariant mass $m(K_S K\pi)$ vs. the angle $\angle(K_S K)$. As the η_c is a pseudoscalar meson, the angular distribution should be flat. However, P-wave and D-wave components by non-resonant charmless B decays turned out to be non-negligible. By adding the angle into the fit, interference with the background is taken into account. The mass was determined as m=2985.4$\pm$1.5$^{+0.2}_{-2.0}$ MeV. The measured width in listed in Tab. 1, in comparison with other recent measurements.

The analysis was repeated for the η_c'. The measurement of the width of the η_c' is of high importance, as due to the vicinity to the $D^0\overline{D}^0$ threshold, potential model predictions are not reliable. In case of the η_c' the interference with the non-resonant background turned out to even have a higher impact for the fit and thus the determination of the width. The result is Γ=6.6$^{+8.4+2.6}_{-5.1-0.9}$ MeV for the fit with interference and Γ=41.1$\pm$12.0$^{+6.4}_{-10.9}$ MeV for a fit without

[1] soeren.lange@exp2.physik.uni-giessen.de

Γ_{η_c}	Production Mechanism	Reference
$35.1\pm3.1^{+1.0}_{-1.6}$ MeV	B decays	[2] and this paper
$30.5\pm1.0\pm0.9$ MeV	$\psi'\to\gamma\eta_c$	[3]
$28.1\pm3.2\pm2.2$ MeV	$\gamma\gamma\to\eta_c$	[4]
$31.7\pm1.2\pm0.8$ MeV	$\gamma\gamma\to\eta_c$	[5]
$36.3^{+3.7}_{-3.6}\pm4.4$ MeV	B decays	[6]

Table 1: Width measurements of the η_c.

interference (i.e. fit of only the invariant mass). The factor $\simeq$5 narrower width of the η_c' compared to the η_c can be explained by the wavefunctions of the states. The hadronic decay of both states proceeds by two gluons; three gluons are forbidden by parity. As the width scales with the wavefunction at the origin, i.e. $\Gamma(^1S_0\to gg)=(32\pi\alpha_S^2/m_c^2)|\psi(r=0)|^2$, and the wavefunction for the η_c' has one node (as it is n=1 radial excitation), the width at the origin must be narrower. With the new measurement, the error on the previous world average of the width of the η_c' was improved by factor $\simeq$2. For additional details of the analysis see [2].

2 Mass and Width of X(3872)

New results for the charmonium-like state X(3872) in the decays $B^+\to K^+$X(3872) and $B^0\to K^0(\to\pi^+\pi^-)$X(3872) are based upon the complete Belle data set of 711 fb^{-1} collected at the Y(4S) resonance [7]. For the determination of the mass and the width of the X(3872) in the decay X(3872)$\to J/\psi\pi^+\pi^-$, a 3-dimensional fit was performed using the three variables beam constraint mass $M_{\rm bc}=\sqrt{(E_{beam}^{cms})^2-(p_B^{cms})^2}$ (with the energy in the center-of-mass system E_{beam}^{cms} and the momentum of the B meson in the center-of-mass system p_B^{cms}), the invariant mass $m(J/\psi\pi^+\pi^-)$ and the energy difference $\Delta E=E_B^{cms}-E_{beam}^{cms}$ (with the energy of the B meson in the center-of-mass system E_B^{cms}). In a first step, the fit was performed for the reference channel $\psi'\to J/\psi\pi^+\pi^-$, and the resolution parameters (i.e. the widths of a core Gaussian and a tail Gaussian) were then fixed for the fit of the X(3872). Fig. 1 shows the data and the fits for the X(3872) (blue line: signal, dashed green line: background) in the projections of the three variables as defined above. The yield is 151$\pm$15 events for B^+ decays and 21.0$\pm$5.7 events for B^0 decays.

Mass of the X(3872). The mass, as determined by the fit, is listed in Tab. 2 in comparison to other precise measurements. As the X(3872) does not fit into any potential model prediction, it was discussed as a possible S-wave $D^{*0}\overline{D}^0$ molecular state. In this case, the binding energy E_b would be given by the mass difference m(X)$-m(D^{*0})-m(D^0)$. Including the new Belle result, the new world average mass of the X(3872) is m=3871.67$\pm$0.17 MeV. Using the current sum of the masses $m(D^0)+m(D^{*0})$=3871.79$\pm$0.30 MeV [1], a binding energy of $E_b=-0.12\pm0.35$ MeV can be calculated, which is surprisingly small. As E_b is

inverse proportional to the squared scattering length a, and the radius can in first order be approximated by $<r>=a/2$ [12], this would indicate a very large radius of the molecular state.

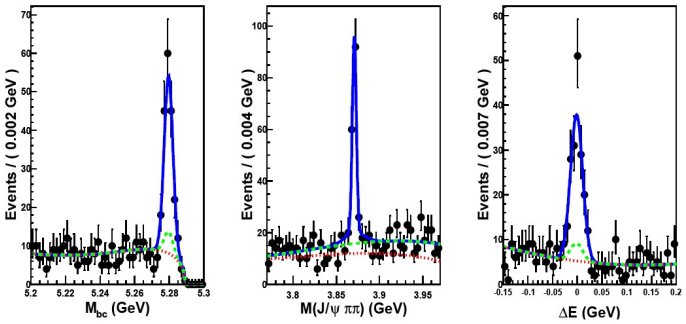

Figure 1: Beam constraint mass $M_{\rm bc}$ (left), invariant mass $m(J/\psi\pi^+\pi^-)$ (center) and ΔE (right) for $B^+\to K^+$X(3872)$(\to J/\psi\pi^+\pi^-)$.

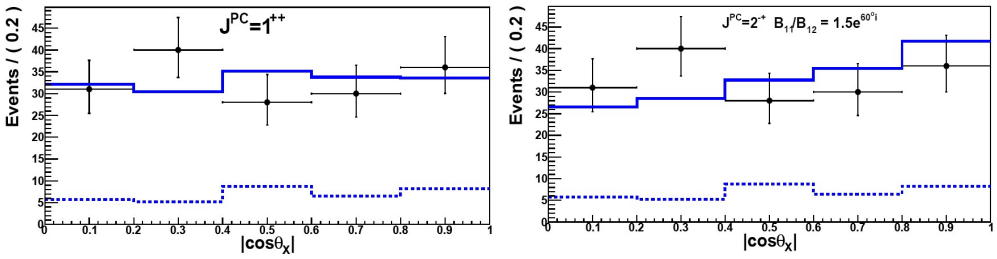

Figure 2: Distribution of $|\cos(\theta_X)|$ for $B^+\to K^+$X(3872)$(\to J/\psi\pi^+\pi^-)$. The blue line shows the fit for $J^{PC}=1^{++}$ (left) and $J^{PC}=2^{-+}$ (bottom). For details see text.

Width of the X(3872). With the 3-dimensional fit, also a new measurement of the width of the X(3872) was performed. Previously the best upper limit was $\Gamma_{X3872}<2.3$ MeV (90% C.L) [14]. The 3-dimensional fits are more sensitive to the natural width than the resolution provided by the detector $<\sigma>\simeq 4$ MeV because of the constraints which enter by $M_{\rm bc}$ and ΔE. As in case of the mass measurement above, the method of determining the width was validated using the ψ' as reference, providing a result of $\Gamma_{\psi'}^{measured}=0.52\pm0.11$ MeV. As the world average is $\Gamma_{\psi'}^{PDG}=0.304\pm0.009$ MeV, this indicates a bias in our measurement of $\Delta\Gamma=+0.23\pm0.11$ MeV. The procedure for the determination of the upper limit is as follows: for a given fixed width Γ the number of signal events and the number of peaking background events is kept floating in the 3-dim fit, and the likelihood is calculated. Then the 90% likelihood interval is determined by finding $w_{90\%}$ for an integral $\int_0^{w_{90\%}}\Gamma d\Gamma=0.9$. This procedure gives $w_{90\%}=0.95$ MeV, for which the bias has to be added, so that $\Gamma_{X(3872)}<1.2$ MeV at 90% C.L. is the final result. This upper limit is a factor of $\simeq 2$ narrower than the previous upper limit.

Experiment	Mass of X(3872)	
CDF2	3871.61±0.16±0.19 MeV	[8]
BaBar (B^+)	3871.4±0.6±0.1 MeV	[9]
BaBar (B^0)	3868.7±1.5±0.4 MeV	[9]
D0	3871.8±3.1±3.0 MeV	[10]
Belle	3871.84±0.27±0.19 MeV	[7] and this paper
LHCb	3871.96±0.46±0.10 MeV	[11]
New World Average	3871.67±0.17 MeV	

Table 2: Mass measurements of the X(3872).

Quantum numbers of the X(3872). If the X(3872) is a conventional charmonium state, there are two likely assignments. On the one hand there is the χ'_{c1}, a $^3P_1$ state with J^{PC}=1^{++}. The predicted mass by potential models is m=3953 MeV, thus $\simeq$70 MeV higher than the observed $X(3872)$ mass. This would be a n=2 radial excitation, and the quantum numbers are favoured by angular analyses [15] [16]. On the other hand there is the η_{c2}, a $^1D_2$ state with J^{PC}=2^{-+}. The predicted mass by potential models is m=3837 MeV, thus $\simeq$35 MeV lower than the observed $X(3872)$ mass. This would be a n=1 state, and the quantum numbers are favoured by the 3π mass distribution in the decay X(3872)$\rightarrow J/\psi\omega$ [17]. A new angular analysis was carried out with the new Belle data. For this purpose, it was assumed that the decay X(3872)$\rightarrow J/\psi\pi^+\pi^-$ proceeds via X(3872)$\rightarrow J/\psi\rho(\rightarrow\pi^+\pi^-)$ in the kinematic limit, i.e. both particles are at rest in the X(3872) rest frame. Due to $m_{X(3872)}\simeq m_\rho+m_{J/\psi}$ this is a valid assumption and it also implies that any higher partial waves can be neglected. For J^{PC}=1^{++}, there is only one amplitude with L=0 and S=1, where L and S are the total orbital angular momentum between and the total spin constructed from the ρ and the J/ψ. For J^{PC}=2^{-+}, there are two amplitudes with L=1 and S=1 or S=2. These two amplitudes can be mixed with a mixing parameter α, which is a complex number. The angular reference frame follows the definition of Rosner [18]. The angle θ_X is chosen as the angle between the J/ψ and the kaon direction in the $X(3872)$ rest frame. The angular distributions for θ_X for the different quantum numbers is given by:

$$
\begin{aligned}
(1) \qquad & J^{PC} = 1^{++}, && \frac{d\Gamma}{dcos\theta_X} \propto const. \\
& J^{PC} = 2^{-+}, \quad \alpha = 0, && \frac{d\Gamma}{dcos\theta_X} \propto \sin^2\theta_X \\
& J^{PC} = 2^{-+}, \quad \alpha = 1, && \frac{d\Gamma}{dcos\theta_X} \propto 1 + 3\cos^2\theta_X
\end{aligned}
$$

Two additional angles are defined as follows: the xy-plane is spanned by the kaon direction

Angle	χ^2/n.d.f.	C.L.	χ^2/n.d.f.	C.L.
	$J^{PC}=1^{++}$		$J^{PC}=2^{-+}$	
χ	1.76/4	0.78	4.60/4	0.33
θ_{lepton}	0.56/4	0.97	5.24/4	0.26
θ_X	3.82/4	0.51	4.72/4	0.32

Table 3: χ^2 values for the fit of the angular distributions. See text for the definitions of the angles.

and the π^+ and π^- (back-to-back) directions in the X(3872) rest frame. The x-axis is chosen to be along the kaon direction. The z-axis is constructed perpendicular to the xy-plane. The angle χ is chosen between the x-axis and the π^+ direction. The angle θ_μ is chosen between the μ^+ direction and the z-axis. A simultaneous fit for all three angles was performed, and the distributions and the fit results for θ_X are shown in Fig. 2. The χ^2 values are listed in Tab. 3. For the case of $J^{PC}=2^{-+}$, the values in Tab. 3 are given for $\alpha=0.69\cdot\exp(i23^o)$, which was found in a grid search and which is the only value which gives a confidence level >0.1 for all three angles. Although at the current level of statistical significance, it cannot be distinguished definitely between the two quantum numbers, however $J^{PC}=1^{++}$ seems to be slightly preferable in this analysis. For additional details see [7].

3 χ_{c2} in B Meson decays

In the decay $B^+\to K^+\chi_{c1,2}(\to J/\psi\gamma)$ for the first time a χ_{c2} signal could be observed with a statistical significance of 3.6σ (Fig. 3). This is the observation of a J=2 charmonium state with positive parity in B meson decays and thus very interesting for two reasons: on the one hand, due to the j_q=1/2 of the two charm quarks forming the charmonium state, and the J=0 in the initial state (i.e. $J^P=0^-$ for the B meson), J=0 and J=1 are preferred, and J=2 is difficult to be generated. One the other hand, this decay $0^-\to 0^-2^+$ is, because of the positive parity of the charmonium state, forbidden in naïve factorization [19]. This implies that at least one additional gluon is required to connect the charmonium and the K^+ sides. For additional details of the analysis see [20].

4 Summary

This paper covered three different topics. At first, the width of the η_c' was determined with a factor $\simeq$2 smaller error compared to the previous world average. Interference with non-resonant background turned out to be important and were taken into account. At second, new results on the X(3872) employed multi-dimensional fits, increasing by constraints the

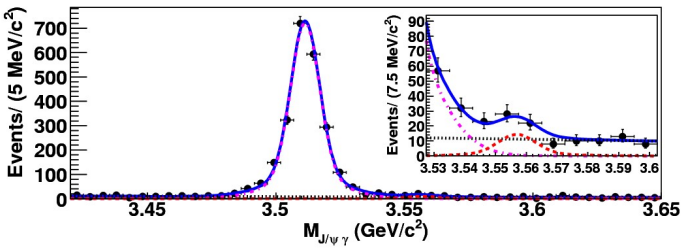

Figure 3: Invariant mass $m(J/\psi\gamma)$ for the decay $B^+ \to K^+ \chi_{c1,2}(\to J/\psi\gamma)$. The zoomed region shows the χ_{c2} signal. See text for details.

resolution to beyond the detector resolution. The new world average mass of the X(3872) is only 120±350 keV below the $D^{*0}\overline{D}^0$ threshold. At third, the production of a J^P=2^+ charmonium state was observed in B meson decays.

Bibliography

[1] K. Nakamura et al. (Particle Data Group), J. Phys. **G37**, 075021 (2010)

[2] Belle Collaboration, arXiv:1105.0978v2 [hep-ex], submitted to Phys. Lett. B

[3] Bes-III Collaboration, Proc. XIV International Conference on Hadron Spectroscopy (hadron2011), these proceedings

[4] Belle Collaboration, Eur. Phys. J. **C53**, 1 (2008)

[5] BaBar Collaboration, Phys. Rev. **D81**, 052010 (2010)

[6] BaBar Collaboration, Phys. Rev. **D78**, 012006 (2008)

[7] Belle Collaboration, arXiv:1107.0163 [hep-ex], to appear in Phys. Rev. D

[8] CDF2 Collaboration, Phys. Rev. Lett. **103**, 152001 (2009)

[9] BaBar Collaboration, Phys. Rev. **D77**, 111101R (2008)

[10] D0 Collaboration, Phys. Rev. Lett. **93**, 162002 (2004)

[11] LHCb Collaboration, Proc. XIX International Workshop on Deep-Inelastic Scattering and Related Subjects (DIS2011), LHCb-CONF-2011-021

[12] E. Braaten, M. Lu, Phys. Rev. **D76**, 094028 (2007)

[13] T. Barnes, S. Godfrey, E. S. Swanson, Phys. Rev. **D72**, 054026 (2005)

[14] Belle Collaboration, Phys. Rev. Lett. **91**, 262001 (2003)

[15] CDF-II Collaboration, Phys. Rev. Lett. **98**, 132002 (2007)

[16] Belle Collaboration, hep-ex/0505037

[17] The BaBar Collaboration, Phys. Rev. **D82**, 011101 (2010)

[18] J. L. Rosner, Phys. Rev. **D70**, 092023 (2004)

[19] M. Bauer, B. Stech, M. Wirbel, Z. Phys. **C34**, 103 (1987)

[20] Belle Collaboration, Phys. Rev. Lett. **107**, 091803 (2011)

Charmonium and Charmonium-like States with *BABAR*

Valentina Santoro[1] on behalf of the *BABAR* Collaboration
INFN Ferrara , via Saragat 1, Ferrara, 44122, ITALY

We review recent charmonium and charmonium-like state from the *BABAR* B-factory. A particular focus is given to the observation of the decay $X(3872) \to J/\psi\ \omega$ and to recent $\eta_c(1S)$ and $\eta_c(2S)$ results. The Observation of the $\chi_{c2}(2P)$ state will be also discussed.

1 Introduction

The charmonium spectrum consists of eight narrow states below the open charm threshold (3.73 GeV) and several tens of states above that. Below the threshold almost all states are well established. On the other hand, very little is known at higher energy. Only one state has been positively identified as a charmonium D state, the $\psi(3770)$, in addition there are several new "Charmonium-like" states that are very difficult to accommodate in the conventional charmonium spectrum.

2 Evidence for the decay $X(3872) \to J/\psi\ \omega$

The X(3872) it has been observed by several experiments in different decay modes and two production channels. Soon after its discovery [1] a great deal of effort has been expanded to understand the nature of the X(3872), especially its spin-parity assignment; so far, only $J^{PC} = 1^{++}$ or 2^{-+} can be assigned to the X(3872). In a previous *BABAR* analysis [2] of the decay $B \to J/\psi\omega K$ there was clear signal for the Y(3940) as reported by Belle [3] but there was no evidence for the X(3872). In this analysis were required for the ω candidates $0.765\ GeV/c^2 \leqslant m_{3\pi} \leqslant 0.7965\ GeV/c^2$. In a more recent *BABAR* analysis [4] the same decay mode has been studied using a slightly larger dataset and a lower ω mass limit: $0.74\ GeV/c^2 \leqslant m_{3\pi} \leqslant 0.7965\ GeV/c^2$. All other selection criteria are the same as in the previous analysis. The $J/\psi\ \omega$ mass distribution after background subtraction is shown in Fig. 1. There is clear signal for the $Y(3940)$, and evidence for the $X(3872)$. These signals are present in both B^+ and B^0 samples. The $m_{J/\psi\omega}$ distributions are fitted simultaneously with a function with three components: a Gaussian function for the X(3872), a relativistic S-wave Breit-Wigner for the Y(3940) and a broad Gaussian function multiplied by $m_{J/\psi\omega}$ for the nonresonant contribution. From the

[1] santoro@fe.infn.it

fit the following parameters are obtained: $m_{X(3872)} = 3873.0^{+1.8}_{-1.6}(stat) \pm 1.3(syst)\ MeV/c^2$, $m_{Y(3940)} = 3919.1^{+3.8}_{-3.4}(stat) \pm 2.0(syst)\ MeV/c^2$ and $\Gamma_{Y(3940)} = 31^{+10}_{-8} \pm 5\ MeV$. To investigate the parity of the X(3872) events with $3.8625\ GeV/c^2 \leqslant m_{J/\psi\omega} \leqslant 3.8825\ GeV/c^2$ are selected. For these events the $m_{3\pi}$ is shown on Fig. 2 and is compared with the Monte Carlo simulation for different spin assignment. The P-wave assignment is favored ($\chi^2 = 3.53/5$) over the S-wave ($\chi^2 = 1017/5$) hence $J^P = 2^-$ is favored over $J^P = 1^+$.

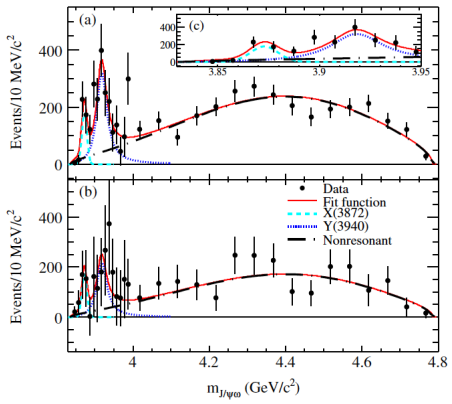

Figure 1: The $J/\psi\omega$ mass distribution for (a) $B^+ \to J/\psi\omega K^+$ and (b) $B^0 \to J/\psi\omega K^0_s$ decays; (c) shows the region $m_{J/\psi\omega} < 3.95\ GeV/c^2$ of (a). The curves show the fit results and the individual fit contributions.

3 Observation of the $\chi_{c2}(2P)$ meson in the reaction $\gamma\gamma \to D\overline{D}$

In 2006 the Belle collaboration observed the Z(3930) [5] in $\gamma\gamma$ production of the $D\overline{D}$ system and this is considered a strong candidate for the $\chi_{c2}(2P)$ state [5]. A recent *BABAR* analysis [6] confirmed this state, in the same production mechanism using a data sample of 384 fb^{-1}. After all the selection criteria applied the efficiency corrected $D\overline{D}$ mass distribution is shown in Fig. 3. There is clear signal for the Z(3930) with a significance of 5.8 σ. An unbinned maximum likelihood fit is performed to obtain the following parameters: $m_{Z(3930)} = 3926.7 \pm 2.7 \pm 1.1\ MeV/c^2$ and $\Gamma_{Z(3930)} = 21.3 \pm 6.8 \pm 3.6\ MeV$.
A decay angular analysis provides evidence that the Z(3930) is a tensor state with positive spin parity and C-parity ($J^{PC} = 2^{++}$) in agreement with the $\chi_{c2}(2P)$ interpretation. The value of the partial width $\Gamma_{\gamma\gamma} \times BF(Z(3930) \to D\overline{D})$ is found to be $(0.241 \pm 0.054 \pm 0.043)$ keV. All these measurements are in good agreement with the previous Belle measurements .

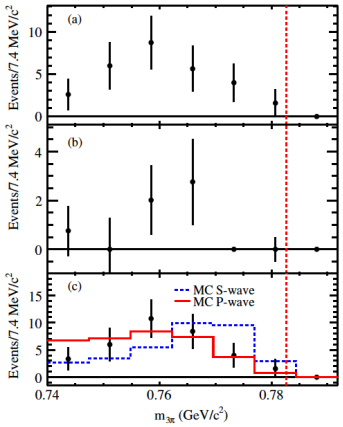

Figure 2: The $m_{3\pi}$ distribution for events 3.8625 $GeV/c^2 \leqslant m_{J/\psi\omega} \leqslant$ 3.8825 GeV/c^2 for (a) B^+, (b) B^0, and (c) combined. The vertical line shows the ω nominal mass. In (c), the solid (dashed) histogram shows the P-wave (S-wave) Monte Carlo events normalized to the number of data events.

4 Observation of the $\eta_c(1S)$ and $\eta_c(2S)$ decays to $K^+K^-\pi^+\pi^-\pi^0$

BABAR studied using 519.2 fb^{-1} collected at the $\Upsilon(4S)$, $\Upsilon(3S)$ and $\Upsilon(2S)$ the processes $e^+e^- \to e^+e^-\gamma\gamma \to e^+e^- f$ where f denotes $K^+K^-\pi^+\pi^-\pi^0$ or $K^0_S K^\pm\pi^\mp$ final states [7]. The allowed J^{PC} values of the initial state are $0^{\pm+}, 2^{\pm+}, 4^{\pm+}, ...; 3^{++}, 5^{++}$. Angular momentum, parity conservation, and charge conjugation invariance, then imply that these quantum numbers apply to the final states f also, except that the $K^0_S K^\pm\pi^\mp$ state cannot have $J^P = 0^+$. The $K^0_S K^\pm\pi^\mp$ and $K^+K^-\pi^+\pi^-\pi^0$ mass spectra are shown on Fig. 4. There are signals at the position of the $\eta_c(1S)$, J/ψ, $\chi_{c0}(1P)$, $\chi_{c2}(1P)$ and $\eta_c(2S)$ states. The mass and the width of the $\eta_c(1S)$ and $\eta_c(2S)$, extracted using a binned extended maximum likelihood fit, are respectively $m_{\eta_c(1S)} = 2982.5 \pm 0.4 \pm 1.4$ MeV/c^2, $m_{\eta_c(2S)} = 3638.5 \pm 1.5 \pm 0.8$ MeV/c^2 and $\Gamma_{\eta_c(1S)} = 32.1 \pm 1.1 \pm 1.3$ MeV, $\Gamma_{\eta_c(2S)} = 13.4 \pm 4.6 \pm 3.2$ MeV.

Bibliography

[1] S. K. Choi *et al.* [Belle Collaboration], Phys. Rev. Lett. **91**, 262001 (2003)

[2] B. Aubert *et al.* [BaBar Collaboration], Phys. Rev. Lett. **101**, 082001 (2008).

[3] K. Abe *et al.* [Belle Collaboration], Phys. Rev. Lett. **94**, 182002 (2005).

[4] P. del Amo Sanchez *et al.* [BaBar Collaboration], Phys. Rev. D **82**, 011101 (2010).

[5] S. Uehara *et al.* [Belle Collaboration], Phys. Rev. Lett. **96**, 082003 (2006).

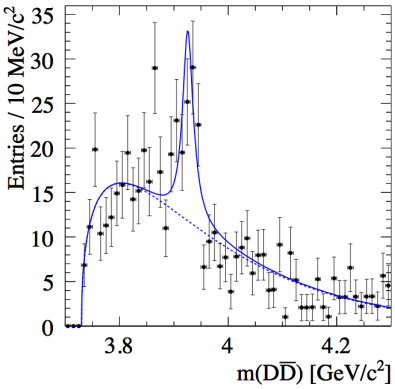

Figure 3: Efficiency corrected $D\overline{D}$ mass distribution with standard fit. The dotted line shows the background lineshape.

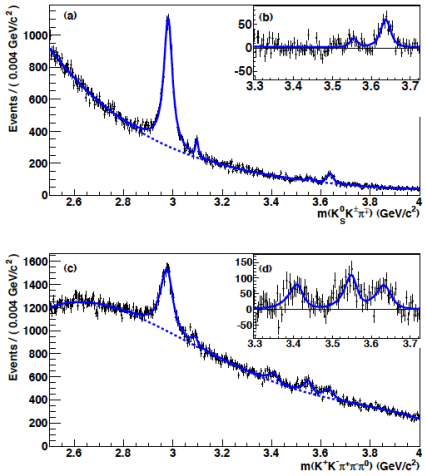

Figure 4: Fit to the $K^0_S K^{\pm}\pi^{\mp}$ (a) and $K^+K^-\pi^+\pi^-\pi^0$ (c) mass spectra. The solid curves represent the total fit functions and the dashed curves show the combinatorial background contributions. The background-subtracted distributions are shown in (b) and (d).

[6] B. Aubert *et al.* [BaBar Collaboration], Phys. Rev. D **81**, 092003 (2010).

[7] P. del Amo Sanchez *et al.* [BaBar collaboration], Phys. Rev. D **84**, 012004 (2011).

Molecular Effects in Charmonium Spectrum

David R. Entem[1,a], Pablo G. Ortega[a], and Francisco Fernández[a]
[a]*Departamento de Física Fundamental and IUFFyM*
Universidad de Salamanca, E-37008 Salamanca, Spain

We study the influence of possible molecular structures in the charmonium spectrum. We focus on the 0^{++} and 1^{--} sectors. In the first one we coupled the 2^3P_0 $q\bar{q}$ pair with DD, $J/\psi\omega$, D_sD_s and $J/\psi\phi$ channels and we obtain two states compatibles with the $X(3945)$ and the $Y(3940)$. In the second one we include the 3^3S_1 and 2^3D_1 charmonium states coupled to DD, DD^*, D^*D^*, D_sD_s, $D_sD_s^*$ and $D_s^*D_s^*$. In this calculation we obtain a new molecular state that could be the $G(3900)$ or the controversial $Y(4008)$ and two $c\bar{c}$ states dressed by the molecular components assigned to the $\psi(4040)$ and the $\psi(4160)$. The two $c\bar{c}$ states show interesting properties and in particular they solve the strong disagreement of the decay branching ratios measured by BABAR.

1 Introduction

The discovery of the J/ψ meson in 1974 was the experimental confirmation of the existence of the charm quark introduced theoretically in 1970 by Glashow, Iliopoulus and Maiani to explain the cancellation of loop diagrams in K^0 weak decays. Consisting of a charm c quark and a $\bar{c}$ antiquark, the J/ψ particle became the starting point of a whole family of bound states called charmonium. A further milestone in the knowledge of the charmonium structure began in 2002 with the new data coming from high luminosity experiments at B factories. Since then, many new states have been observed. A summary of these states can be found in Ref. [1]. Most of them are difficult to understand in a quark-antiquark framework and meson-antimeson molecular states may represent an alternative explanation to these states.

Probably the most popular of these new states is the $X(3872)$ which lies very close to the DD^* threshold and is the most accepted candidate to be a meson-antimeson bound state. In Ref. [2] we have performed a calculation of the $X(3872)$ state as a DD^* molecule in the framework of a constituent quark model [3]. There also the coupling to $q\bar{q}$ states is included and only when we mix the DD^* channel and the $\chi_{c1}(2P)$ state the $X(3872)$ appears as a bound state. The original $\chi_{c1}(2P)$ $q\bar{q}$ state acquires a significant DD^* component and can be identified with the $X(3940)$.

[1]entem@usal.es

Following these ideas we have started a program to study the influence of possible molecular structures in the charmonium spectrum. We have generalized our formalism to study resonance above thresholds. In this contribution we focus on the results found in the 0^{++} and 1^{--} sectors.

2 Theoretical framework

We work in the framework of a coupled channel calculation following Ref. [4] generalized to include several meson-antimeson channels and several $q\bar{q}$ states. The T-matrix is decomposed in a non-resonant and a resonant contribution. We look for poles of the T-matrix in the second Riemann sheet looking for zeros of the dressed propagator. Then we solve an eigenvalue problem to obtained the $c\bar{c}$ amplitudes and with them and the dressed vertex we obtained the meson-antimeson wave functions. Finally we define the partial widths evaluating the residues of the pole.

The $q\bar{q}$ states are found solving the Schrödinger equation with the $q\bar{q}$ interaction of Ref. [3]. The meson-antimeson interaction is consistently obtained using the Resonating Group Method with these wave functions and interaction. Finally we couple the $q\bar{q}$ states with the $q\bar{q}q\bar{q}$ states using the microscopic $^3P_0$ model.

3 The 0^{++} sector

We study the 3900 MeV energy region and we include in the calculation the $\chi_{c0}(2P)$ $c\bar{c}$ state and the DD, $J/\psi\omega$, D_sD_s and $J/\psi\phi$ meson-antimeson states. We found two states corresponding to the first two lines in Table 1. For comparison we show the result of the updated Cornell model (C^3) of Ref. [5]. Our second state corresponds to the $\chi_{c0}(2P)$ dressed by the meson-antimeson states and is similar to the one found in the C^3 model. In addition our framework also allows to study resonances due to the binding of meson-antimeson channels and we found and additional state.

The experimental situation is not clear. Two states were found in these energy region, namely the $X(3945)$ [6] and the $Y(3940)$ [7] and they could be the two states we find, although recently these two states have been summarize in one, the $X(3915)$, due to compatible properties.

4 The 1^{--} sector

We study the 4100 MeV energy region and we include the 3^3S_1 and 2^3D_1 $c\bar{c}$ states and the DD, DD^*, D^*D^*, D_sD_s, $D_sD_s^*$ and $D_s^*D_s^*$ meson-antimeson channels. Our results are summarized in Tables 2 and 3. We find two states corresponding to the dressing of

Mass(MeV)	2^3P_0	DD	$J/\psi\omega$	D_sD_s	$J/\psi\phi$	Γ_{DD}	$\Gamma_{J/\psi\omega}$	$\Gamma_{D_sD_s}$
$3896.05 - i2.10$	34.22	46.67	9.41	9.67	0.03	3.37	0.83	–
$3970.07 - i94.67$	57.27	35.32	0.15	5.72	1.54	38.69	2.89	147.76
$3881.4 - i\,30.75$	49	34.22	–	4.41	–			

Table 1: Pole position, probabilities and partial widths for the two states (in the first two lines) obtained in the 0^{++} sector. For comparison we show in the last line the result of the updated Cornell model (C^3) of Ref. [5] for the only state found in the 3900 MeV energy region.

$M\,(MeV)$	3^3S_1	2^3D_1	DD	DD^*	D^*D^*	D_sD_s	$D_sD_s^*$	$D_s^*D_s^*$
$3994.6 - i\,11.60$	31.56	3.00	2.49	36.44	17.75	7.53	0.52	0.71
$4048.4 - i\,7.54$	0.92	36.15	2.99	23.49	25.81	8.86	0.92	0.85
$4123.9 - i\,71.11$	59.01	0.98	2.13	6.84	19.19	0.75	3.37	7.73
$4038 - i\,37$	44.89	0.16	2.87	20.36	23.10	0.98	1.58	1.08
$(4160) - i\,24.6$	0.09	47.61	8.37	4.24	8.87	0.55	0.96	1.31

Table 2: Pole position and probabilities for the three states (in the first three lines) obtained in the 1^{--} sector. For comparison we show in the last line the result of the updated Cornell model (C^3) of Ref. [5] for the two states found in the 4100 MeV energy region.

the original $c\bar{c}$ states corresponding to the well established $\psi(4040)$ and $\psi(4160)$ and one additional state that could be the $G(3900)$ or the controversial $Y(4008)$.

The dressed states shows a peculiar feature. Although originally the 3^3S_1 state is below the 2^3D_1, when coupled to the meson-antimeson channels, the lowest state is predominantly 2^3D_1 and the highest 3^3S_1. This is due to the additional state which has a stronger coupling with the 3^3S_1 and push the dress state to higher energies. In order to test this new assignment we have calculated the branching ratios measured by BABAR [8]. We show the results for the original bare $q\bar{q}$ states and the states obtained in the coupled channel calculation in Table 4. There is a strong disagreement with the experimental data for the bare states, while the results for the coupled channel calculation are within three standard deviations.

M	Γ	$\Gamma(DD)$	$\Gamma(DD^*)$	$\Gamma(D^*D^*)$	$\Gamma(D_sD_s)$	$\Gamma(D_sD_s^*)$
3994.6	23.37	0.12	19.09	–	4.16	–
4048.4	15.09	0.51	7.24	4.42	2.92	–
4123.9	142.23	4.73	7.51	100.03	3.82	26.15

Table 3: Partial widths for the three states obtained in the 1^{--} sector.

Ratio	Experimental value	$q\bar{q}$ with $^3P_0$	Coupled channel
$\frac{\mathcal{B}(\psi(4040)\to D\overline{D})}{\mathcal{B}(\psi(4040)\to D\overline{D}^*)}$	$0.24 \pm 0.05 \pm 0.12$	0.21	0.07
$\frac{\mathcal{B}(\psi(4040)\to D^*\overline{D}^*)}{\mathcal{B}(\psi(4040)\to D\overline{D}^*)}$	$0.18 \pm 0.14 \pm 0.03$	3.7	0.61
$\frac{\mathcal{B}(\psi(4160)\to D\overline{D})}{\mathcal{B}(\psi(4160)\to D^*\overline{D}^*)}$	$0.02 \pm 0.03 \pm 0.02$	0.27	0.05
$\frac{\mathcal{B}(\psi(4160)\to D\overline{D}^*)}{\mathcal{B}(\psi(4160)\to D^*\overline{D}^*)}$	$0.34 \pm 0.14 \pm 0.05$	0.027	0.08

Table 4: Branching ratios measured by BABAR [8] for the $\psi(4040)$ and the $\psi(4160)$ (second column). The third column shows the result for the bare $c\bar{c}$ states and the fourth the results of the states of Table 2.

Acknowledgments

This work has been partially funded by Ministerio de Ciencia y Tecnología under Contract No. FPA2010-21750-C02-02, by the European Community-Research Infrastructure Integrating Activity 'Study of Strongly Interacting Matter' (HadronPhysics2 Grant No. 227431) and by the Spanish Ingenio-Consolider 2010 Program CPAN (CSD2007-00042).

Bibliography

[1] N. Brambilla *et al.*, Eur. Phys. J. C **71**, 1534 (2011).

[2] P.G. Ortega, J. Segovia, D.R. Entem, F. Fernández, Phys. Rev. D **81**, 054023 (2010).

[3] J. Vijande, F. Fernández, and A. Valcarce, J. Phys. G **31**, 481 (2005).

[4] V. Baru *et al.*, Eur. Phys. J. A **44**, 93 (2010).

[5] E.J. Eichten, K. Lane, and C. Quigg, Phys. Rev. D **73**, 014014 (2005).

[6] S. Uehara *et al.*, Phys. Rev. Lett. **104**, 092001 (2010).

[7] S.-K. Choi *et al.*, Phys. Rev. Lett. **94**, 182002 (2005).

[8] B. Aubert *et al.*, Phys. Rev. D **79**, 092001 (2009).

Exotic spectroscopy and quarkonia at LHCb

Bo Liu[1] on behalf of the LHCb Collaboration
Department of Engineering Physics, Tsinghua Unversity,
100084 Beijing, CHINA
and
Laboratoire de l'Accelerateur Lineaire, Universite Paris-Sud 11, CNRS/IN2P3 (UMR 8607),
91400 Orsay, FRANCE

Measurements of the X(3872) mass, $\psi(2S)$ production cross-section and χ_{c2}/χ_{c1} production ratio using around 35pb^{-1} of pp collision data at $\sqrt{s}$ = 7 TeV during the 2010 LHC running period with the LHCb detector are presented.

1 Introduction

The LHCb detector is a single-arm forward spectrometer designed to make precision measurements of CP violation and rare decays in the heavy flavour at the LHC [1]. It has a unique geometrical acceptance covering the pseudo-rapidity 1.9-4.9. This combined with excellent trigger, tracking and particle identification capabilities also makes it an ideal detector to study quarkonia.
This paper presents the measurements of the X(3872) mass, $\psi(2S)$ production cross-section and χ_c production ratio in pp collisions at $\sqrt{s}$ = 7 TeV with the data taken by the LHCb detector in 2010.

2 Measurement of X(3872) mass

The X(3872) meson is an exotic meson discovered in 2003 by the Belle collaboration [2]. Several properties of the X(3872) have been measured, but its nature is still uncertain and several models have been proposed. First, it is not excluded that the X(3872) is a conventional charmonium state with one candidate being the $\eta_{c2}(1D)$ meson [3]. However, the predicted mass of this state is far below the observed X(3872) mass. Given the proximity of the X(3872) mass to the $D^{*0}\overline{D}^0$ threshold, one possibility is that the X(3872) is a loosely bound deuteron-like $D^{*0}\overline{D}^0$ molecule, i.e. a $((u\bar{c}) - (c\overline{u}))$ system [3]. Another more exotic

[1]b-liu03@mails.thu.edu.cn

possibility is that the X(3872) is a tetraquark state [4]. A precise measurement of the mass is an important ingredient towards elucidating the nature of this state.

For accurate measurement of particle mass systematic uncertainties due to the momentum scale must be under control. The momentum scale [5] [6] is calibrated using a large sample of $J/\psi \to \mu^+\mu^-$ decays. This calibration accounts for a mixture of effects related to imperfect knowledge of the magnetic field map and of the alignment of the tracking system. The calibration is cross-checked using two-body decay of the $\Upsilon(1S)$, K^0_S and D^0. Based on comparisions of the values obtained for these masses and those quoted by the PDG [7] a systematic uncertainty of 0.1 per mille is assigned.

The X(3872) mass measurement is affected by the systematic uncertainties from the mass fitting (signal model (0.02 MeV/c^2), background model (0.02 MeV/c^2)), average momentum scale (0.05 MeV/c^2) , pseudo-rapidity dependence of momentum scale (0.03 MeV/c^2), energy loss correction of the detector description (0.05 MeV/c^2), alignment of tracking stations (0.05 MeV/c^2) and alignment of vertex detector (0.01 MeV/c^2). The total systematic uncertainty is 0.10 MeV/c^2.

Fig. 1 shows the the invariant $J/\psi\pi^+\pi^-$ mass distributions for opposite-sign (black points) and same-sign (blue filled histogram) candidates. Clear signals for both the $\psi(2S)$ and the X(3872) can be seen. The preliminary result is $M_{X(3872)} = 3871.96 \pm 0.46(\text{stat}) \pm 0.10(\text{syst})\text{MeV/c}^2$.

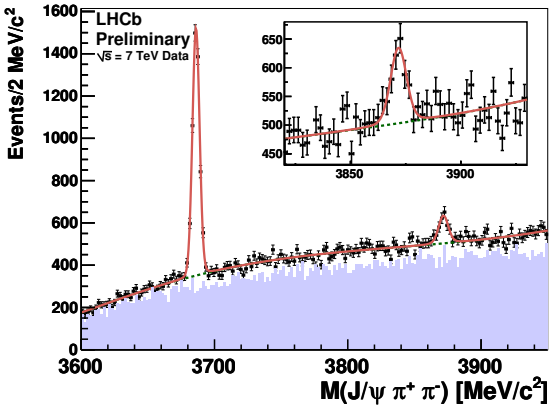

Figure 1: Invariant mass distribution of $J/\psi\pi^+\pi^-$ (black points with statistical error bars) and same-sign $J/\psi\pi^\pm\pi^\pm$ (blue filled histogram) candidates. The red curve is the result of the fit to the mass distribution. The insert shows a zoom of the region around the X(3872) mass.

3 Measurement of $\psi(2S)$ cross-section

Prompt heavy quarkonium production in hadron collisions is a subject of large interest [8]. In order to ensure an unambiguous comparison with theory, promptly produced quarkonia should be separated from those coming from b-hadron decays and from those cascading from higher mass states (feed-down): the $\psi(2S)$ meson has no appreciable feed-down from higher mass states and therefore the results can be directly compared with the theory, making it an ideal laboratory for QCD studies.

The differential cross-section [9] for the inclusive $\psi(2S)$ production is computed as

$$\frac{d^2\sigma}{dp_{\rm T}}(p_{\rm T}) = \frac{N_{\psi(2S)}(p_{\rm T})}{L_{\rm int}\epsilon(p_{\rm T})B(\psi(2S)\to e^+e^-)\Delta p_{\rm T}}$$

where $N_{\psi(2S)}(p_{\rm T})$ is the number of observed $\psi(2S)\to J/\psi\pi^+\pi^-$ decays, $L_{\rm int}$ is the integrated luminosity, $\epsilon(p_{\rm T})$ is the total detection efficiency, $B(\psi(2S)\to J/\psi\pi^+\pi^-)$ is the $\psi(2S)\to J/\psi\pi^+\pi^-$ branching ratio [7] and $\Delta p_{\rm T}$ is the bin size. In order to estimate the number of $\psi(2S)$ signal events, a fit to the $\psi(2S)$ mass distribution is performed independently in each $p_{\rm T}$ bin.

The total efficiency ϵ is the product of the geometric acceptance (A), the reconstruction efficiency ($\epsilon_{\rm rec}$) and the trigger efficiency ($\epsilon_{\rm tri}$). The factor $\epsilon_{\rm rec}$ includes the detection, reconstruction and selection efficiency. Monte Carlo simulations are used to estimate A, $\epsilon_{\rm rec}$ and $\epsilon_{\rm tri}$ for each bin.

The dominant systematic uncertainties are from the luminosity measurement 10%, the unknown polarization (bin-dependent), the trigger efficiency (bin-dependent) and the tracking efficiency (4% per track).

The integrated cross-section in the full range of $p_{\rm T}$ and rapidity (y) is found to be

$$\sigma(3<p_{\rm T}\leqslant 16{\rm GeV}/c, 2<y\leqslant 4.5) = 0.62\pm 0.04\pm 0.12^{+0.07}_{-0.14}\,{\rm nb}$$

where the first error is statistical, the second error is systematic and the third asymmetric error is related to the unknown polarization.

The double differential cross-sections for the $\psi(2S)\to J/\psi\pi^+\pi^-$ mode, another measurement of $\psi(2S)\to\mu^+\mu^-$ mode [9] and comparison with the prediction of prompt production by a NLO NRQCD model [10] are shown in Fig. 2. The results for the two decay modes and the theory are in good agreement.

4 Measurement of χ_c cross-section ratio

The study of P-wave charmonia χ_c(J=0,1,2) production is important for two reasons. First, the measurement of the production rates of χ_{c2} and χ_{c1} is sensitive to the Color-Singlet and

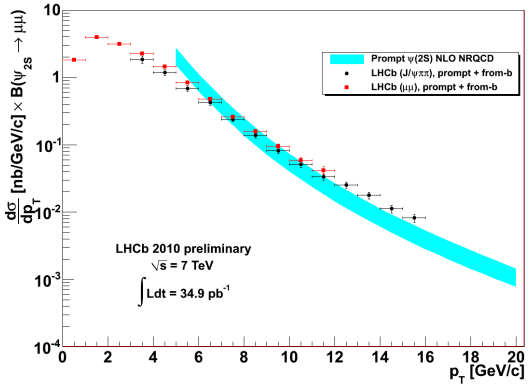

Figure 2: Comparison of the LHCb results for the differential production cross-section of $\psi(2S)$ with the predictions for prompt production by a NLO NRQCD model [14]. LHCb data include also $\psi(2S)$ from b: the fraction of $\psi(2S)$ from b is expected to be of the order of 10% at low $p_{\rm T}$ and to increase as function of $p_{\rm T}$ to about 40% [11].

Color-Octet production mechanisms. In addition, the feeddown contribution to prompt J/ψ production through radiative decays has important consequences for the J/ψ polarization measurement [12].

The production cross-section ratio of the χ_{c2} and χ_{c1} states is measured using

$$\frac{\sigma(\chi_{c2})}{\sigma(\chi_{c1})} = \frac{N_{\chi_{c2}}}{N_{\chi_{c1}}} \times \frac{\epsilon_{J/\psi}^{\chi_{c1}} \epsilon_{\gamma}^{\chi_{c1}} \epsilon_{\rm sel}^{\chi_{c1}}}{\epsilon_{J/\psi}^{\chi_{c2}} \epsilon_{\gamma}^{\chi_{c2}} \epsilon_{\rm sel}^{\chi_{c2}}} \times \frac{B(\chi_{c1} \to J/\psi\gamma)}{B(\chi_{c2} \to J/\psi\gamma)}$$

where $B(\chi_{c1} \to J/\psi\gamma)(B(\chi_{c2} \to J/\psi\gamma))$ are the $\chi_{c1}(\chi_{c2})$ branching ratios to the final state $J/\psi\gamma$. The event yield N_{χ_c} is from an unbinned maximum likelihood fit to the mass distribution. The efficiencies ϵ are extracted from the Monte Carlo simulation.

The main systematic uncertainties are from the fit (the fit model, fit range and fit method), the MC statistics, the unknown polarization and the $\chi_c \to J/\psi\gamma$ branching ratios.

The preliminary result for the ratio of the prompt χ_{c2} to χ_{c1} production cross-sections, $\frac{\sigma\chi_{c2}}{\sigma\chi_{c1}}$, as a function of $p_{\rm T}^{J/\psi}$ is shown in Figure 3. The preliminary result is broadly in agreement with the theorectical predictions at high $p_{\rm T}^{J/\psi}$. At low $p_{\rm T}^{J/\psi}$ there are indications of a discrepancy.

5 Summary

First results from studies of X(3872), χ_c and $\psi(2S)$ mesons using data collected by the LHCb detector have been presented. The results for the cross-sections are in reasonable agreement with theory. The larger data-set collected during the 2011 running period will

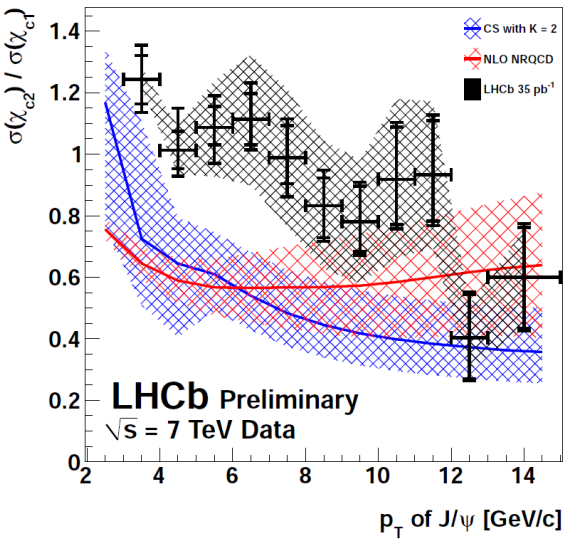

Figure 3: The ratio $\frac{\sigma\chi_{c2}}{\sigma\chi_{c1}}$ in bins of $p_{\mathrm{T}}^{J/\psi} \in [3; 15]$GeV/c. The internal error bars correspond to the statistical error on the χ_{c1} and χ_{c2} yields; the external error bars include the contribution from all the systematic uncertainties. The shaded area around the data points (black) shows the maximum effect of the unknown χ_c polarizations on the result. The upper limit corresponds to the spin state (χ_{c1}: $m_J = 1$; χ_{c2}: $m_J = 2$) and the lower limit corresponds to the spin state (χ_{c1}: $m_J = 0$; χ_{c2}: $m_J = 0$). The two other bands correspond to the ChiGen MC generator theoretical prediction [13](in blue) and NLO NRQCD (in red) [14].

allow the statistical uncertainties to be reduced and further studies (for example of the $\psi(2S)$ polarization) will be performed.

Bibliography

[1] The LHCb Collaboration, A. A. Alves et al., The LHCb detector at the LHC, JINST 3 (2008) S08005.

[2] The Belle collaboration, S.K. Choi et al., Observation of a new narrow charmonium state in exclusive $B^{\pm} \to K^{\pm}\pi^{+}\pi^{-}J/\psi$ decays, Phys. Rev. Lett. 91 (2003) 262001, arXiv:hep-ex/0309032.

[3] E. Swanson, The new heavy mesons: a status report, Physics Reports 429 (2006) 243, arXiv:hep-ph/0601110.

[4] L. Maiani, F. Piccinini, A. D. Polosa and V. Riquer, Diquark-antidiquarks with hidden or open charm and the nature of X(3872), Phys. Rev. D 71 (2005) 014028, arXiv:hep-ph/0412098

[5] The LHCb Collaboration, A. A. Alves et al., Measurment of the X(3872) mass with first LHCb data, CERN-LHCb-CONF-2011-030.

[6] The LHCb Collaboration, A. A. Alves et al., Measurement of b-hadron masses with exclusive J/ψX decays oss-section at $\sqrt{s}$ = 7 TeV in 2010 data, CERN-LHCb-CONF-2011-027.

[7] The Particle Data Group, K. Nakamura et al., Review of particle physics, J. Phys. G 37 (2010) 075021.

[8] N. Brambilla et al., Heavy quarkonium: progress, puzzles, and opportunities, Eur. Phys. 167 J. C 71 (2011) 1534.

[9] The LHCb Collaboration, A. A. Alves et al., Measurement of the $\psi(2S)$ production cross-section at $\sqrt{s}$ = 7 TeV in LHCb, CERN-LHCb-CONF-2011-026.

[10] Y.-Q.Ma et al., $J/\psi(\psi')$ production at the Tevatron and LHC at $O(\alpha_s^4 v^4)$ in non-relativistic QCD, Phys. Rev. Lett. 106, 042002, (2011) and private communication.

[11] The CDF collaboration, T. Aaltonen et al., Production of $\psi(2S)$ Mesons in $p\overline{p}$ Collisions 185 at 1.96 TeV, Phys. Rev. D80, 031103, (2009).

[12] The LHCb Collaboration, A. A. Alves et al., A measurement of the cross-section ratio σ_{c2}/σ_{c1} for prompt σ_c production at $\sqrt{s}$ = 7 TeV in LHCb, CERN-LHCb-CONF-2011-020.

[13] L. A. Harland-Lang and W. J. Stirling, private communication.

[14] Y. Ma, K. Wang, K. Chao, arXiv:1002.3987 (hep-ph).

Quarkonia Measurements with ALICE at the LHC

Frederick Kramer[1] on behalf of the ALICE Collaboration
Institut für Kernphysik
Johann Wolfgang Goethe–Universität
D 60438 Frankfurt, GERMANY

ALICE is the dedicated heavy-ion experiment at the Large Hadron Collider (LHC). It is designed to provide excellent capabilities to study the quark-gluon plasma (QGP) in the highest energy density regime opened up by the LHC. Quarkonia are crucial probes of the QGP. High-precision data from pp collisions are an essential baseline, and serve as a crucial test for competing models of quarkonium hadroproduction. ALICE measures quarkonia down to $p_{\mathrm{t}} = 0$ via their decay channels into $\mathrm{e}^+\mathrm{e}^-$ at central ($|y| < 0.9$) and into $\mu^+\mu^-$ at forward rapidity ($-4.0 < y < -2.5$). We present first results on the transverse momentum and rapidity distributions of the inclusive J/ψ production cross section in $\sqrt{s} = 7$ and 2.76 TeV pp collisions. The dependence of the J/ψ yield on the charged particle multiplicity in $\sqrt{s} = 7$ TeV pp collisions is discussed. Finally, results on the inclusive J/ψ production in $\sqrt{s_{\mathrm{NN}}} = 2.76$ TeV Pb–Pb collisions, the nuclear modification factor R_{AA} and the central-to-peripheral modification factor R_{CP} are shown.

Various models are describing the production of quarkonia in hadronic reactions such as proton-proton collisions. Three of the most popular ones are the Color Singlet Model, the nonrelativistic QCD approach (NRQCD) and the Color Evaporation Model [1–3]. So far their predictions do not fully reproduce the experimental observations such as differential cross sections or polarization, or many free parameters limit their predictive power. Precise measurements at a new energy regime will give new constraints to theory. Quarkonia, such as the J/ψ serve as a crucial probe to study the quark-gluon plasma (QGP) in heavy-ion collisions. The original prediction was a strong suppression of quarkonia yields [4] by color-screening of the $Q\overline{Q}$ pairs in the colored medium. This effect might depend on the binding radius of the different states and on the temperature of the fireball [5]; thus, a stronger suppression of higher excited states could even reflect the temperature of the medium. In central heavy-ion collisions at LHC energies J/ψ yields could also be affected in another way: charm quark pairs are abundant enough so that a statistical or kinetic J/ψ formation out of uncorrelated $c\bar{c}$ pairs might become dominant [6,7]. Furthermore, initial state effects such as shadowing – the modification of the parton distribution function of a nucleon inside a nucleus [3] – have to be taken into account. Final state effects like nuclear absorption are expected to be negligible at LHC energies. A measurement of such effects in

[1]kramer@ikf.uni-frankfurt.de

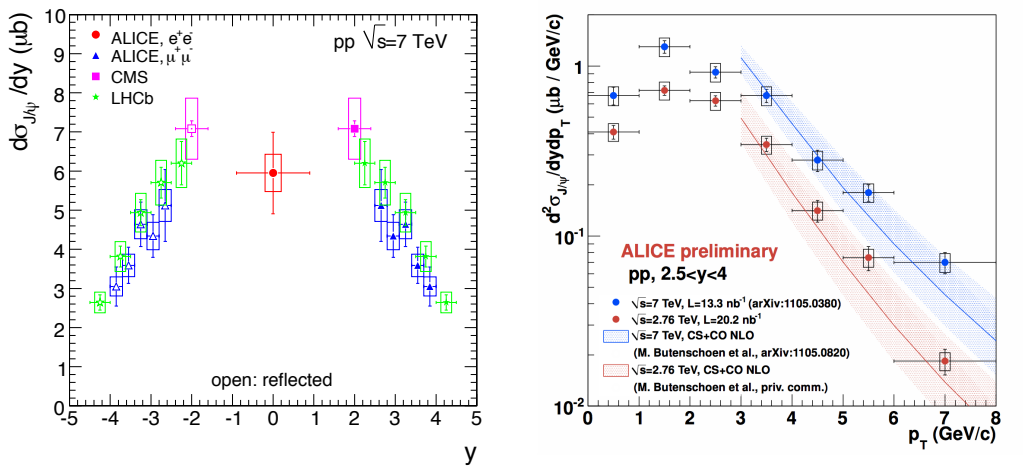

Figure 1: Differential J/ψ cross sections versus rapidity in 7 TeV pp collisions (left) and transverse momentum in 7 and 2.76 TeV pp collisions (right) [9, 11–13]

p–A collisions will be crucial for drawing final conclusions; any modification of the yields stronger than expected will provide insights into the created medium.

The ALICE [8] setup can be divided into two parts: the central rapidity detectors ($|\eta| < 0.9$) and the forward muon spectrometer ($-4.0 < \eta < -2.5$). For this analysis, in the central barrel, mainly two detectors are used: the Inner Tracking System (ITS) and the Time Projection Chamber (TPC). The large-volume TPC serves as the main tracking device. Furthermore it provides particle identification via the specific energy loss $\mathrm{d}E/\mathrm{d}x$ in the detector gas. Consisting of two layers each of silicon pixel, silicon strip and silicon drift detectors, the ITS provides high precision vertex reconstruction and tracking, improving the momentum resolution. The muon spectrometer consists of a 10 plane cathode pad chamber tracking system behind a frontal absorber and a 4 plane resistive plate chamber trigger system further downstream behind an iron filter wall. Muons with a momentum above 4 GeV/c are filtered and detected. In both channels, quarkonia are measured over a broad range of transverse momenta down to $p_\mathrm{t} = 0$. Finally, the VZERO detector, made of two scintillator arrays covering the pseudo rapidity ranges $-3.7 < \eta < -1.7$ and $2.8 < \eta < 5.1$, is used for triggering purposes and collision centrality determination.

Energy	System	Year	L(J/$\psi \to e^+e^-$)	L(J/$\psi \to \mu^+\mu^-$)
7 TeV	pp	2010	3.9 nb^{-1}	15.6 nb^{-1}
2.76 TeV	pp	2011	1.1 nb^{-1}	20.2 nb^{-1}
2.76 TeV	Pb–Pb	2010	2.7 μb^{-1}	2.7 μb^{-1}

Table 1: Integrated luminosities of the analyzed data samples

The J/ψ production was measured in $\sqrt{s} = 7$ and 2.76 TeV proton-proton collisions [9,10]. Table 1 shows the integrated luminosities of the two samples, both for the data recorded in the central barrel and the muon spectrometer. For the central barrel analysis, these are corresponding to the minimum bias trigger, defined as the logical OR between the requirement of at least one hit in the two ITS pixel layers, and a signal in one of the two VZERO detectors. For the muon analysis, also a coincidence with a track reconstructed by the muon trigger electronics is required. Differential cross sections have been obtained by the analysis of invariant mass spectra in different p_{t} and y bins [9]. Presented are inclusive results, containing contributions from direct J/ψ production and feed-down from higher mass quarkonia and B hadron decays. The left panel of Fig. 1 shows the obtained rapidity dependence of the J/ψ production at $\sqrt{s} = 7$ TeV. Red circles correspond to the measurement in the $\mathrm{e}^+\mathrm{e}^-$ ($|y| < 0.9$), blue triangles to the result in the $\mu^+\mu^-$ ($-4.0 < y < -2.5$) decay channels. While at forward rapidity results of other experiments (green: LHCb [11], magenta: CMS [12]) are in good agreement, ALICE is the only experiment at the LHC which is able to measure J/ψ down to $p_{\mathrm{t}} = 0$ and thus directly measure the p_{t} integrated cross section at midrapidity. The right panel of Fig. 1 shows the measured p_{t} spectra in the di-muon decay channel for the two different available beam energies. A Next to Leading Order (NLO) NRQCD prediction [13] is in good agreement with the data. For the first time, the dependence of the J/ψ production on the charged particle multiplicity has been measured in pp collisions. Figure 2 shows the results of the analyses in the $\mathrm{e}^+\mathrm{e}^-$ (red circles) and the $\mu^+\mu^-$ (blue triangles) decay channels. The multiplicity is normalized by the mean charged particle multiplicity [14] and has been determined in a pseudorapidity range of $|\eta| < 1.0$ by counting the number of tracklets found in the ITS pixel detector. The J/ψ yield per event in a given multiplicity bin is normalized to the inclusive yield per inelastic pp collision. An approximately linear increase with multiplicity is observed in both rapidity ranges. In the highest multiplicity bin, corresponding to approximately 5 times the minimum bias multiplicity, a J/ψ yield of around 6 times the minimum bias yield is found. The strong dependence of the J/ψ production on the event multiplicity is an intriguing result that needs a theoretical interpretation.

In fall 2010 the LHC collided Pb beams for the first time. Table 1 summarizes the integrated luminosity used for the analysis. The collision energy of $\sqrt{s_{\mathrm{NN}}} = 2.76$ TeV is almost 14 times higher than the energies reached at RHIC before. Having pp data recorded at the same energy allows to calculate the nuclear modification factor $R_{\mathrm{AA}} = Y_{\mathrm{Pb-Pb}} / \langle N_{\mathrm{coll}} \rangle Y_{\mathrm{pp}}$ for different Pb–Pb collision centralities. $\langle N_{\mathrm{coll}} \rangle$ corresponds to the average number of binary nucleon-nucleon collisions in a given centrality class. A R_{AA} equal to unity indicates no modification in heavy-ion collisions with respect to pp collisions. The left panel of Fig. 3 shows as red squares the result of this measurement as a function of $\langle N_{\mathrm{part}} \rangle$, the number of nucleons participating in the collision. To account for the bias due to the large centrality bins, $\langle N_{\mathrm{part}} \rangle$ has been weighted by N_{coll} [15]. Already for peripheral collisions ($\langle N_{\mathrm{part}} \rangle \simeq 70$), a suppression of the J/ψ yield is observed and R_{AA} is about 0.6. For more central collisions, the R_{AA} exhibits only a weak change. The data are compared

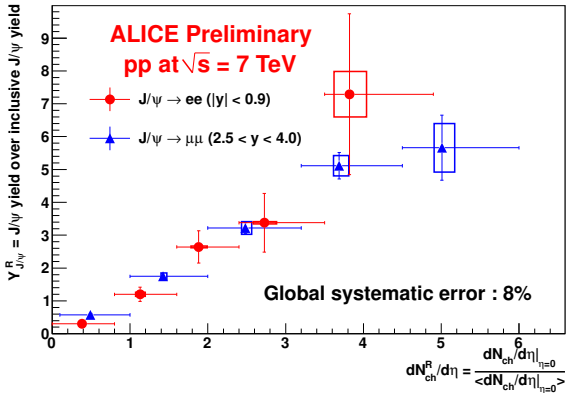

Figure 2: The measured multiplicity dependence of J/ψ production in 7 TeV pp collisions

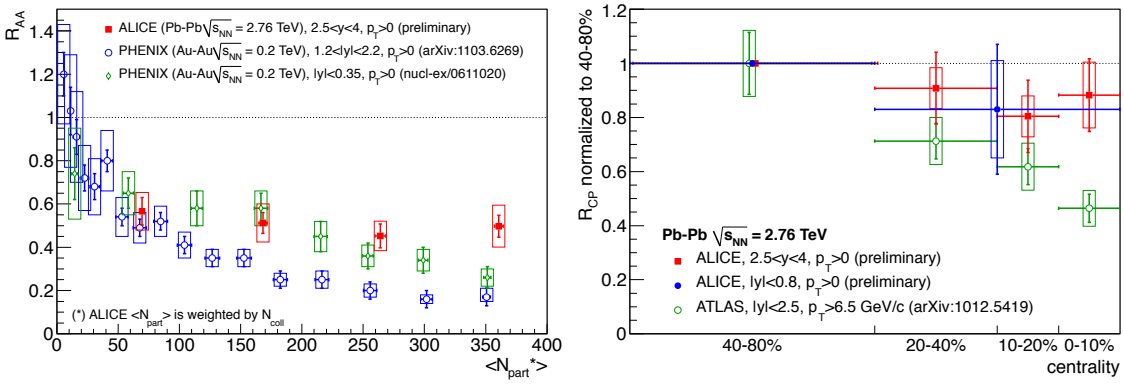

Figure 3: Left: $R_{\rm AA}$ at $\sqrt{s_{\rm NN}} = 2.76$ TeV compared to PHENIX results [16] at $\sqrt{s_{\rm NN}} = 0.2$ TeV, right: $R_{\rm CP}$ at $\sqrt{s_{\rm NN}} = 2.76$ TeV compared to the ATLAS result [17]

to results from the PHENIX experiment at RHIC [16] in green diamonds at central and in blue circles at forward rapidity. For central collisions the observed suppression is smaller than at RHIC, yet it has to be taken into account that shadowing and nuclear-absorption cross sections are expected to be different at the two energies. Also, the energy density at a given $N_{\rm part}$ presumably differs. A closer look into the difference of central and peripheral collisions can be obtained by calculating the central-to-peripheral modification factor $R_{\rm CP} = \left\langle N_{\rm coll}^{\rm per.} \right\rangle Y_{\rm Pb-Pb}^{\rm cent.} / \left\langle N_{\rm coll}^{\rm cent.} \right\rangle Y_{\rm Pb-Pb}^{\rm per.}$. There, the yields in the different centrality classes are divided by the corresponding average number of binary collisions. As reference, the most peripheral bin is used. Due to limitations in statistics it is currently set to a rather broad range of 40–80 %. An advantage of this variable is that many systematic uncertainties cancel out in the ratio. The right panel of Fig. 3 shows the measured $R_{\rm CP}$ as a function of the centrality. Red squares correspond to the ALICE result at forward rapidity. The challenging measurement in the di-electron channel at midrapidity (blue circles) agrees

within its errors; its precision will be improved in the next LHC Pb–Pb run. A similar conclusion can be drawn as from the R_{AA} result: compared to the most peripheral bin, a weak centrality dependence is observed. On the other hand, high p_{t} J/ψ, measured by ATLAS above 6.5 GeV/c, show a stronger suppression in central (0–10 %) events [17].

In summary, the inclusive J/ψ production has been measured both in pp and in Pb–Pb collisions. In pp, differential cross sections have been obtained for two different beam energies and rapidity ranges. An approximately linear increase of the J/ψ production with the charged particle multiplicity is observed both at central and forward rapidity, which calls for theoretical interpretation. In Pb–Pb, both nuclear modification factors R_{AA} and R_{CP} have been measured. A significant suppression of the J/ψ yield is observed, with a weak dependence on centrality. At central events, a smaller suppression has been found compared to PHENIX results at much lower collision energies.

Bibliography

[1] J. P. Lansberg, Int. J. Mod. Phys. **A21** (2006) 3857

[2] E. L. Berger and D. Jones, Phys. Rev. **D23** 7 (1981) 1521

[3] N. Brambilla et al., Eur. Phys. J. **C71** (2011) 1534

[4] T. Matsui and H. Satz, Phys. Lett. **B178** (1986) 416

[5] H. Satz, arXiv:hep-ph/0602245

[6] A. Andronic et al., Phys. Lett. **B571** (2003) 36

[7] R. L. Thews, Eur. Phys. J. **C34** (2005) 97

[8] The ALICE Collaboration, JINST 3 S08002 (2008)

[9] The ALICE Collaboration, arXiv:1105.0380, Submitted to Phys. Lett. B

[10] R. Arnaldi, arXiv:1107.0137, to appear in the proceedings of QM 2011

[11] The LHCb Collaboration, arXiv:1103.0423

[12] The CMS Collaboration, arXiv:1011.4193

[13] M. Butenschoen and B. A. Kniehl, arXiv:1105.0820

[14] The ALICE Collaboration, Eur. Phys. J. **C68** (2010) 345

[15] P. Pillot, arXiv:1108.3795, to appear in the proceedings of QM 2011

[16] The PHENIX Collaboration, arXiv:1103.6269, arXiv:nucl-ex/0611020

[17] The ATLAS Collaboration, Phys. Lett. **B697** (2011) 294

Heavy quarkonium spectrum and width in a weakly-coupled quark-gluon plasma

Jacopo Ghiglieri[1]
Physik-Department, Technische Universität München, James-Franck-Str. 1, 85748 Garching, Germany and Excellence Cluster Universe, Technische Universität München, Boltzmannstr. 2, 85748, Garching, Germany

We report a recent calculation of the heavy quarkonium energy levels and decay widths in a quark- gluon plasma whose temperature is much smaller than the inverse radius of the bound state, based on a Non-Relativistic Effective Field theory framework for heavy quarkonium at finite temperature. Relevance for the phenomenology of the $\Upsilon(1S)$ in heavy ion collisions is also discussed.

1 Introduction

The suppression of quarkonium has been hypothesized 25 years ago [1] to represent a signature of the formation of a deconfined medium and has been ever since intensely investigated, both theoretically and experimentally. Here we address the problem, central to these studies, of the behaviour of a quarkonium bound state in a deconfined thermal medium. To this end we shall illustrate the Effective Field Theory (EFT) framework that has been recently constructed in [2–4] (see also [5–7] for an analogous EFT of QED) by generalizing the successful zero-temperature framework of Non-Relativistic (NR) EFTs for heavy quarkonia to finite temperatures. These NR EFTs exploit the hierarchy $m \gg mv \gg mv^2$ that characterizes any NR binary bound state, m being in this case the heavy quark mass and v the relative velocity. mv is then the typical momentum transfer or inverse radius and $mv^2 \sim E$ the binding energy. The low-lying quarkonium states, especially the bottomonium ground states $\Upsilon(1S)$ and η_b, are believed to be approximately Coulombic. That corresponds to having $mv \sim m\alpha_s \gg \Lambda_{\rm QCD}$ and $mv^2 \sim m\alpha_s^2 \gtrsim \Lambda_{\rm QCD}$.
In a weakly-coupled plasma, which we consider in our study, the temperature T and the chromoelectric screening mass m_D are larger than $\Lambda_{\rm QCD}$ and, since $m_D^2 \sim g^2T^2$, $T \gg m_D$. Under these conditions one can then calculate observables relevant for the phenomenology of low-lying states to a large extent analytically in perturbation theory, which makes them extremely interesting, also in the light of the recent CMS measurements of the suppression of the Υ family [8].

[1] jacopo.ghiglieri@ph.tum.de

In [9] the perturbative $Q\overline{Q}$ static potential was computed in QCD for distances r such that $T \gg 1/r \gtrsim m_D$. The resulting potential surprisingly shows an imaginary part which is larger than the screened real part for $1/r \sim m_D$. This imaginary part can be traced back to the imaginary part of the gluon self-energy and is due to the Landau-damping phenomenon; it eventually leads to a thermal width for the bound state, which is in turn responsible for its dissociation, representing a change from the previous colour-screening paradigm. This change was further reinforced by the introduction of a *dissociation temperature* in [5, 10], defined as the temperature for which the imaginary part of the potentials becomes of the same size of its real part; parametrically it is of order $m\alpha_{\rm s}^{2/3}$ and hence smaller than the temperature at which screening sets in. A quantitative calculation of the dissociation temperature for the $\Upsilon(1S)$ can be found in [6] and a phenomenological analysis, based on these imaginary parts, of $b\bar{b}$ bound states at LHC energies can be found in [11].
In [2] the static $Q\overline{Q}$ was first studied in an EFT framework, systematically exploring the hierarchy of different energy scales in the problem. Many possibilities were considered, from temperature smaller than E to temperatures much larger than $1/r$, where the results of [9] were recovered in a rigorous EFT derivation. Furthermore a new dissociation mechanism, the colour-singlet to octet decay, was identified; it is the leading one when $E \gg m_D$. In [12] the relation between the proper real-time quarkonium potential and the correlator of two Polyakov loops, a quantity often measured on the lattice and used as input for potential models, was investigated. The breaking of Lorentz invariance induced by the preferred reference frame introduced by the medium was instead analyzed in [4] in the spin-orbit sector of the EFT. In the following we will report about the findings of [3], where in a specific range of temperatures the spectrum and width of quarkonia have been computed up to order $m\alpha_{\rm s}^5$. To this end, the specific global hierarchy that the NR and thermodynamical scales fulfill in the assumed range of parameters has been exploited by constructing a corresponding tower of EFTs.

2 Energy scales, the EFT formalism and the results

The aforementioned global hierarchy we assume is $m \gg m\alpha_{\rm s} \gg \pi T \gg m\alpha_{\rm s}^2 \gg m_D$, which implies a temperature below the dissociation temperature. We also remark that for the $\Upsilon(1S)$ at the LHC it may hold that $m_b \approx 5\ \text{GeV} > m_b\alpha_{\rm s} \approx 1.5\ \text{GeV} > \pi T \approx 1\ \text{GeV} > m\alpha_{\rm s}^2 \approx 0.5\ \text{GeV} \gtrsim m_D$.
Given this hierarchy, we now proceed to integrate out each scale in sequence. The integration of the mass scale m yields non-relativistic QCD (NRQCD) [13] and the further integration of the scale $m\alpha_{\rm s}$ from NRQCD gives potential non-relativistic QCD (pNRQCD) [14]. Since the temperature is much smaller than these two scales, it may be set to zero in the matching and the Lagrangians of NRQCD and pNRQCD are the same as at zero temperature.
Integrating out T from pNRQCD modifies it into its Hard Thermal Loop (HTL) version,

pNRQCD$_{\rm HTL}$ [2, 15], where the light degrees of freedom are described by the HTL effective Lagrangian [16] and the pNRQCD potentials receive a thermal part. Finally, within this EFT we can compute contribution to the spectrum and width from the scales E and m_D. Diagrams contributing to the calculation are shown in Fig. 1.

Figure 1: The diagrams contributing to our calculation. Single lines are colour-singlet $Q\overline{Q}$ states, double lines are colour octets, curly lines are gluons, vertices are chromoelectric dipoles and the blob is the gluon self-energy. The imaginary part of the first diagram yields the singlet-to-octet decay mechanism, whereas the second one gives the Landau damping contribution to the width.

Let us now show the final results for the thermal contribution to the spectrum and to the width up to order $m\alpha_{\rm s}^5$. We recall that for a Coulombic bound state the spectrum is at LO given by the Bohr levels $E_n = -mC_F^2\alpha_{\rm s}^2/(4n^2)$ and the Bohr radius is $a_0 = 2/(mC_F\alpha_{\rm s})$. The vacuum contribution to the spectrum up to order $m\alpha_{\rm s}^5$ can be read from [17].
The thermal contribution to the spectrum then reads

$$
\begin{aligned}
\delta E_{n,l}^{(\rm thermal)} \;=\;& \frac{\pi}{9} N_c C_F\, \alpha_{\rm s}^2\, T^2 \frac{a_0}{2}\left[3n^2 - l(l+1)\right] + \frac{\pi}{3} C_F^2\, \alpha_{\rm s}^2\, T^2\, a_0 \\
&+ \frac{E_n \alpha_{\rm s}^3}{3\pi}\left[\log\left(\frac{2\pi T}{E_1}\right)^2 - 2\gamma_E\right]\left\{\frac{4C_F^3\delta_{l0}}{n} + \frac{2N_c^2 C_F}{n(2l+1)} + \frac{N_c^3}{4}\right. \\
&\qquad \left. + N_c C_F^2\left[\frac{8}{n(2l+1)} - \frac{1}{n^2} - \frac{2\delta_{l0}}{n}\right]\right\} + \frac{2E_n C_F^3 \alpha_{\rm s}^3}{3\pi} L_{n,l} \\
&+ \frac{a_0^2 n^2}{2}\left[5n^2 + 1 - 3l(l+1)\right]\left\{-\left[\frac{3}{2\pi}\zeta(3) + \frac{\pi}{3}\right] C_F\, \alpha_{\rm s}\, T\, m_D^2\right. \\
&\qquad \left. + \frac{2}{3}\zeta(3)\, N_c C_F\, \alpha_{\rm s}^2\, T^3\right\}, \qquad (1)
\end{aligned}
$$

where $L_{n,l}$ is the QCD Bethe log [17]. The terms on the first line are the leading ones the power counting of the EFT and, being positive, lead to an increase in the mass of the bound state quadratic with the temperature.

For what concerns the thermal width, we have

$$\begin{aligned}\Gamma_{n,l}^{(\text{thermal})} &= \frac{1}{3}N_c^2 C_F \alpha_s^3 T + \frac{4}{3}\frac{C_F^2 \alpha_s^3 T}{n^2}(C_F + N_c) \\ &+ \frac{2E_n \alpha_s^3}{3}\left\{\frac{4C_F^3\delta_{l0}}{n} + N_c C_F^2\left[\frac{8}{n(2l+1)} - \frac{1}{n^2} - \frac{2\delta_{l0}}{n}\right] + \frac{2N_c^2 C_F}{n(2l+1)} + \frac{N_c^3}{4}\right\} \\ &- a_0^2 n^2\left[5n^2 + 1 - 3l(l+1)\right]\left[\left(\ln\frac{E_1^2}{T^2} + 2\gamma_E - 3 - \log 4 - 2\frac{\zeta'(2)}{\zeta(2)}\right)\right. \\ &\left.\times\frac{C_F}{6}\alpha_s T m_D^2 + \frac{4\pi}{9}\ln 2\; N_c C_F\,\alpha_s^2\,T^3\right] + \frac{8}{3}C_F\alpha_s\, T m_D^2\, a_0^2 n^4\, I_{n,l}\,, \end{aligned} \tag{2}$$

where $I_{n,l}$ is a new Bethe logarithm [3]. The terms in the first two lines are the leading ones and are caused by singlet-to-octet decay, whereas those on the last two lines are due to Landau damping. The width is at leading order linear in the temperature and much smaller than the binding energy. This small width is certainly not in contradiction with the recent CMS results [8] that point to a substantial survival of the $\Upsilon(1S)$ at the LHC.

Bibliography

[1] T. Matsui and H. Satz, Phys. Lett. B **178** (1986) 416.

[2] N. Brambilla, J. Ghiglieri, A. Vairo and P. Petreczky, Phys. Rev. D **78** (2008) 014017 [arXiv:0804.0993 [hep-ph]].

[3] N. Brambilla, M. A. Escobedo, J. Ghiglieri, J. Soto and A. Vairo, JHEP **1009** (2010) 038 [arXiv:1007.4156 [hep-ph]].

[4] N. Brambilla, M. A. Escobedo, J. Ghiglieri and A. Vairo, JHEP **1107** (2011) 096 [arXiv:1105.4807 [hep-ph]].

[5] M. A. Escobedo and J. Soto, Phys. Rev. A **78**, 032520 (2008), [arXiv:0804.0691 [hep-ph]].

[6] M. A. Escobedo and J. Soto, Phys. Rev. A **82**, 042506 (2010) [arXiv:1008.0254 [hep-ph]].

[7] M. A. Escobedo, J. Soto and M. Mannarelli, Phys. Rev. D **84** (2011) 016008 [arXiv:1105.1249 [hep-ph]].

[8] S. Chatrchyan *et al.* [CMS Collaboration], Phys. Rev. Lett. **107** (2011) 052302 [arXiv:1105.4894 [nucl-ex]], and CMS-PAS-HIN-10-006.

[9] M. Laine, O. Philipsen, P. Romatschke and M. Tassler, JHEP **0703** (2007) 054 [arXiv:hep-ph/0611300].

[10] M. Laine, Nucl. Phys. A **820** (2009) 25C [arXiv:0810.1112 [hep-ph]].

[11] M. Strickland, arXiv:1106.2571 [hep-ph].

[12] N. Brambilla, J. Ghiglieri, P. Petreczky and A. Vairo, Phys. Rev. D **82** (2010) 074019 [arXiv:1007.5172 [hep-ph]].

[13] W. E. Caswell and G. P. Lepage, Phys. Lett. B **167**, 437 (1986); G. T. Bodwin, E. Braaten and G. P. Lepage, Phys. Rev. D **51**, 1125 (1995) [Erratum-ibid. D **55**, 5853 (1997)] [hep-ph/9407339].

[14] A. Pineda and J. Soto, Nucl. Phys. Proc. Suppl. **64**, 428 (1998) [arXiv:hep-ph/9707481], N. Brambilla, A. Pineda, J. Soto and A. Vairo, Nucl. Phys. B **566**, 275 (2000) [arXiv:hep-ph/9907240].

[15] A. Vairo, PoS **CONFINEMENT8** (2008) 002 [arXiv:0901.3495 [hep-ph]].

[16] E. Braaten and R. D. Pisarski, Phys. Rev. D **45**, 1827 (1992).

[17] N. Brambilla, A. Pineda, J. Soto and A. Vairo, Phys. Lett. B **470**, 215 (1999) [arXiv:hep-ph/9910238], B. A. Kniehl, A. A. Penin, V. A. Smirnov and M. Steinhauser, Nucl. Phys. B **635**, 357 (2002) [arXiv:hep-ph/0203166].

Light Baryons

Light Baryons

Conveners

Gerhard	Mallot	CERN (*Chair*)
Volker	Burkert	JLab
Ulrike	Thoma	Universität Bonn
Boris	Grube	TU München

Session Chairs

Elke-Caroline	Aschenauer	BNL
Reinhard	Beck	Universität Bonn
Eva-Maria	Kabuss	Universität Mainz
Mauro	Anselmino	University of Torino, INFN
Ulrike	Thoma	Universität Bonn

Contents

Light Baryon Spectroscopy using the CLAS Spectrometer at Jefferson Laboratory

Volker Crede[1] on behalf of the CLAS Collaboration
Department of Physics
Florida State University
Tallahassee, FL 32306, USA

Baryons are complex systems of confined quarks and gluons and exhibit the characteristic spectra of excited states. The systematics of the baryon excitation spectrum is important to our understanding of the effective degrees of freedom underlying nucleon matter. High-energy electrons and photons are a remarkably clean probe of hadronic matter, providing a microscope for examining the nucleon and the strong nuclear force. Current experimental efforts with the CLAS spectrometer at Jefferson Laboratory utilize highly-polarized frozen-spin targets in combination with polarized photon beams. The status of the recent double-polarization experiments and some preliminary results are discussed in this contribution.

1 Introduction

It is widely accepted that models based on three constituent-quark degrees of freedom still provide the most comprehensive predictions of the nucleon excitation spectrum. While many predicted properties of the lower-mass (excited) states (< 1.8 GeV$/c^2$) agree fairly well with experimental findings, discrepancies concerning the number and ordering of states emerge above this threshold, mostly due to missing experimental information. In recent years, lattice-QCD has made significant progress toward understanding the spectra of baryons, despite the (still) large pion masses of about 420 MeV$/c^2$ used in these calculations. Since baryon resonances are broad and overlapping, individual excited states usually cannot be observed directly. To extract resonance parameters, the observed angular distributions need to be decomposed into partial waves in a partial wave analysis (PWA). Examples of PWA formalisms are described in [1,2]. Moreover, dynamical coupled channel models have been developed successfully in recent years from a more theoretical side. The EBAC group at Jefferson Laboratory (JLab) has demonstrated that the low physical mass of the Roper resonance can be explained by such coupled channel effects [3].

[1] crede@fsu.edu

The Search for new Excited Baryons

Differential cross sections alone result in ambiguous sets of resonances contributing to a particular photoproduction channel since almost all information on interference effects is lost. For this reason, the FROST experiment at JLab aims at performing so-called complete or nearly-complete experiments for reactions like $\gamma p \to N\pi$, $p\eta$, $p\omega$, K^+Y, and $p\pi^+\pi^-$, which will significantly reduce and eventually eliminate the ambiguities in the extraction of the scattering amplitude. The photoproduction of a single pseudoscalar meson off the nucleon is fully described by four complex parity-conserving amplitudes, which may be determined from eight well-chosen combinations of the unpolarized cross section, three single-spin, and four double-spin observables [4].

In the hyperon channels, precise cross section and polarization data have been measured in recent years, e.g. [5–8]. The weak decay of the hyperon provides additional access to the polarization of the recoiling hyperon rendering a complete experiment feasible. If all combinations of beam, target, and recoil polarization are measured, 16 observables can be extracted providing highly redundant information on the production amplitude. In reactions involving non-strange mesons (without measuring the recoil polarization), seven independent observables can be directly determined. The recoil polarization can then be inferred from beam-target double-polarization measurements. In recent years, very precise differential cross section data were obtained for single $p\pi^0$, $n\pi^+$, $p\eta$, $p\eta'$, and $p\omega$ production, e.g. [1,2,9]. Analyses on beam asymmetries for these reactions are currently being finalized. In $\gamma p \to p\omega$, the ω decay to $\pi^+\pi^-\pi^0$ provides additional polarization information, which further constrains the partial wave analysis for this reaction [2]. The high-spin resonance, $N(2190)G_{17}$, decaying to $p\omega$ could be identified and confirmed in photoproduction as well as the weakly established nucleon state, $N(1950)F_{15}$.

2 Experimental Setup

The results from the JLab double-polarization (FROST) measurements discussed at this conference were obtained with the CEBAF Large Acceptance Spectrometer (CLAS) [10] at the Thomas Jefferson National Accelerator Facility. Longitudinally polarized electrons with energies of 1.65 and 2.48 GeV were incident on the thin radiator of the Hall B Photon Tagger [11] and produced circularly-polarized tagged photons in the energy range between 0.35 and 2.35 GeV with a polarization value of $\approx 85\,\%$ for the initial electron. The photon helicity was flipped at a rate of 30 Hz. The frozen-spin butanol target had an average proton spin state polarization of $\approx 82\,\%$ parallel to the beam axis and $\approx 85\,\%$ anti-parallel to the beam axis. The average target temperature was 30 mK with beam on target. Degradation of target polarization occurred at rates of $\approx 0.9\,\%$ (parallel) and $\approx 1.5\,\%$ (anti-parallel) per day. The target was typically repolarized once a week, usually with flips of the polarization direction. Data were collected simultaneously for the butanol target at the center of the

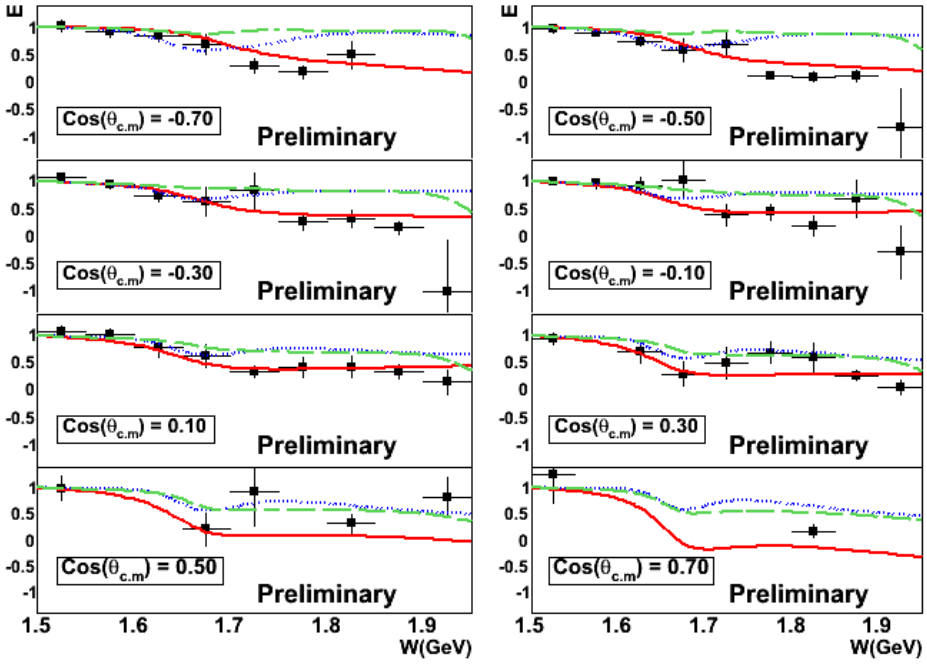

Figure 1: Preliminary results for E in $\vec{\gamma}\vec{p} \to p\eta$ for energies $W = 1.525 - 1.925$ GeV [12]. Curves: η-MAID (dotted line), Bonn-Gatchina PWA (dashed line), and SAID (solid line).

CLAS detector, and, slightly downstream for separate carbon and a polyethylene targets (to provide information on bound nucleon backgrounds in the butanol target).

3 The Helicity Asymmetry E for η Photoproduction on the Proton

Of particular importance are well-chosen decay channels that can help isolate contributions from individual excited states and clarify their importance. Photoproduction of η mesons offers the distinct advantage of serving as an *isospin filter* for the spectrum of nucleon resonances and, thus, simplifies data interpretations and theoretical efforts to predict the excited states contributing to these reactions. Since the η mesons have isospin $I = 0$, the $N\eta$ final states can only originate (in one-step processes) from intermediate $I = 1/2$ nucleon resonances.

The polarized cross section for the reaction $\vec{\gamma}\vec{p} \to p\eta$ of circularly-polarized photons on longitudinally-polarized protons is given by:

$$\frac{d\sigma}{d\Omega} = \frac{d\sigma}{d\Omega_0}\left(1 - \Lambda_z\,\delta_\odot\,E\right), \tag{1}$$

where $d\sigma/d\Omega_0$ is the unpolarized cross section. Λ_z and $\delta_\odot$ are the degrees of target and beam polarization, respectively. E denotes the helicity difference.

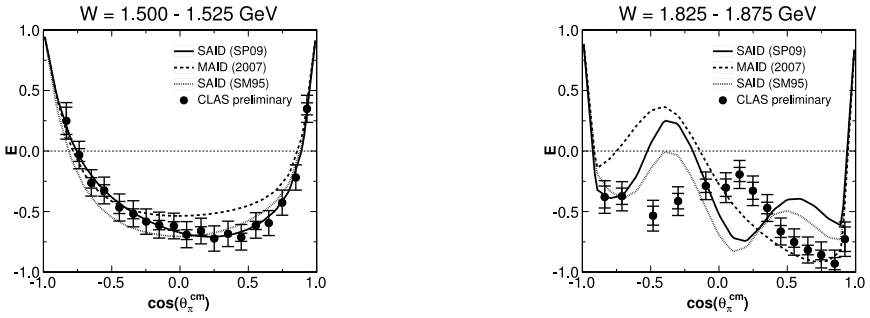

Figure 2: Preliminary results of the double-pololarization observable E (helicity difference) for $\vec{\gamma}\vec{p} \to n\pi^+$ [12]. The inner error bars indicate stat. uncertainties; the outer error bars include a 10 % sys. uncertainty, which is expected to be reduced in the final analysis. The curves show solutions of the SAID SP09 [1], MAID [13] and SAID SM95 PWA.

Preliminary results of the helicity difference E for $\vec{\gamma}\vec{p} \to p\eta$ are shown in Fig. 1. Since the η-threshold is dominated by the $N(1535)S_{11}$ resonance, the observable exhibits values close to unity for $W < 1.6\,\mathrm{GeV}/c^2$. The preliminary results indicate that the observable remains positive below about $W = 2$ GeV, shedding further light on contributing resonances.

4 The Helicity Asymmetry E for the Reaction $\vec{\gamma}\vec{p} \to n\pi^+$

Although many of the *unobserved* baryon resonances may have small couplings to πN, it is still important to study pion photoproduction. Polarization observables will help sift the several competing descriptions of the spectrum by more conclusively indicating which resonances are involved in elastic pion-nucleon scattering, as well as providing evidence for previously unidentified resonances. New resonances found in reactions like $\gamma N \to \pi N$ are expected to have masses larger than about $1.8\,\mathrm{GeV}/c^2$, although the higher-mass resonance contributions are expected to be more important in double-meson photoproduction.

The current database for pion photoproduction is mainly populated by unpolarized cross section data and single-spin observables. Fig. 2 shows preliminary results of the double-polarization E for $\vec{\gamma}\vec{p} \to n\pi^+$ (Eqn. 1). While the predictions shown in the figure agree nicely with the new data at low energies (left side), discrepancies emerge at higher energies (right side) for $W \geqslant 1.7\,\mathrm{GeV}/c^2$. Single-pion photoproduction appears less well understood than previously expected. For this reason, the present data will greatly reduce model-dependent uncertainties.

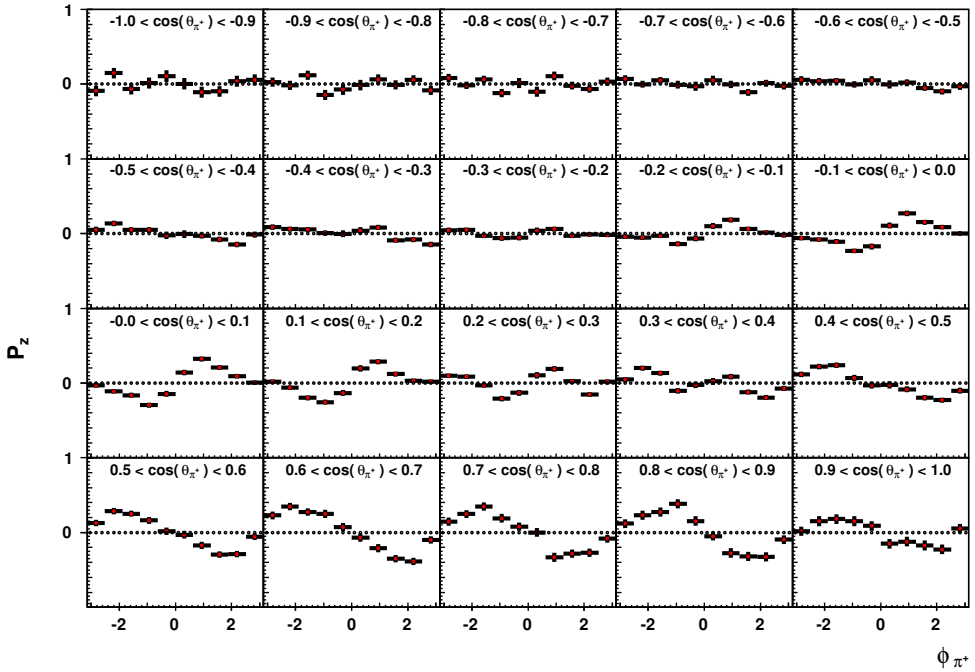

Figure 3: Preliminary target asymmetry, P_z, from FROST for the reaction $\gamma\vec{p} \to p\pi^+\pi^-$ for $E_\gamma \in [0.7, 0.8]$ GeV [12]. Error bars are statistical only.

5 Polarization Observables for $\pi^+\pi^-$ Production on the Proton

One of the key experiments in the search for yet unobserved states is the investigation of double-pion photoproduction. Quark models predict large couplings of those states to $\Delta\pi$, for instance. The five-dimensional cross section for the photoproduction of two pseudoscalar mesons using longitudinal target polarization and circularly-polarized (or unpolarized) beam can be written in the form [14]:

$$I \;=\; I_0 \{ (1 \,+\, \Lambda_z \cdot P_z) \,+\, \delta_\odot (I^\odot \,+\, \Lambda_z \cdot P_z^\odot) \},$$

where I_0 denotes the unpolarized cross section and $\delta_\odot$ and Λ_z denote the degree of beam and target polarization, respectively. The additional polarization observables, P_z and $I^\odot$, for the two-meson final state arise since the reaction is no longer restricted to a single plane. Fig. 3 shows an example for the observable P_z in $\gamma\vec{p} \to p\pi^+\pi^-$ [12]. The variables ϕ and θ denote the azimuthal and polar angle of the π^+ in the rest frame of the two mesons. The observable acquires surprisingly large values for $\cos\theta_{\pi^+} > 0$ with the statistical errors in some cases smaller than the symbol size. The expected odd behavior of the distribution is clearly visible.

6 Summary and Conclusion

The goal of measuring a sufficient number of polarization observables to unambiguously construct the scattering amplitude for a given channel is within reach. New resonance candidates have been proposed on the basis of recent high-quality photoproduction data, though a clear pattern of new states has not yet emerged. These efforts will soon shed light on the open questions concerning the spectrum of baryon resonances. A better understanding of QCD and the phenomenon of confinement appears on the horizon.

Acknowledgments

Work supported in parts by the U.S. Department of Energy: DE-FG02-92ER40735. Jefferson Science Associates operates the Thomas Jefferson National Accelerator Facility under DOE contract DE-AC05-06OR23177.

Bibliography

[1] M. Dugger *et al.* [CLAS Collaboration], Phys. Rev. **C79**, 065206 (2009);

[2] M. Williams *et al.* [CLAS Collaboration], Phys. Rev. **C80**, 065209 (2009).

[3] H. Kamano, S. X. Nakamura, T. -S. H. Lee, T. Sato, Phys. Rev. **C81**, 065207 (2010).

[4] W. -T. Chiang, F. Tabakin, Phys. Rev. **C55**, 2054-2066 (1997).

[5] R. Bradford et al., Phys. Rev. **C73**, 035202 (2006); Phys. Rev. **C75**, 035205 (2007).

[6] I. Hleiqawi *et al.* [CLAS Collaboration], Phys. Rev. **C75**, 042201 (2007); Erratum-ibid.C76:039905,2007.

[7] M. E. McCracken *et al.* [CLAS Collaboration], Phys. Rev. **C81**, 025201 (2010).

[8] S. A. Pereira *et al.* [CLAS Collaboration], Phys. Lett. **B688**, 289-293 (2010).

[9] W. Chen *et al.* [CLAS Collaboration], Phys. Rev. Lett. **103**, 012301 (2009).

[10] B. A. Mecking *et al.* [CLAS Collaboration], Nucl. Instrum. Meth. **A503**, 513-553 (2003).

[11] D. I. Sober *et al.*, Nucl. Instrum. Meth. **A440**, 263-284 (2000).

[12] B. Morrison, S. Park, NSTAR 2011, Jefferson Lab; S. Strauch, arXiv:1108.3050 [nucl-ex].

[13] D. Drechsel, O. Hanstein, S. S. Kamalov, L. Tiator, Nucl. Phys. **A645**, 145-174 (1999).

[14] W. Roberts, T. Oed, Phys. Rev. **C71**, 055201 (2005).

Measurement of the double polarisation observable G in the reactions $\vec{\gamma}\vec{p} \to p\pi^0$ and $\vec{\gamma}\vec{p} \to p\eta$

Marcus Grüner[1] for the CBELSA/TAPS collaboration
Helmholtz-Institut für Strahlen- und Kernphysik, University of Bonn, Germany

The excitation spectrum of the nucleon consists of several overlapping resonances. To identify these resonances and their contributions to the measured cross sections, a partial wave analysis is used. A set of at least eight, well chosen, single and double polarisation observables is needed to derive an unambiguous solution. With the Crystal Barrel/TAPS setup at ELSA, single and double polarisation observables can be measured in different reaction channels, by using the combination of a linearly or circularly polarised photon beam and a longitudinally or transversely polarised butanol frozen spin target.
Results of the G asymmetry measurement, using linearly polarised photons and longitudinally polarised protons, in the reactions $\vec{\gamma}\vec{p} \to p\pi^0$ and $\vec{\gamma}\vec{p} \to p\eta$ are presented.
This project is supported by the DFG (SFB/TR16).

1 Introduction

Photoproduction experiments can provide important contributions to the understanding of the excitation spectrum of the baryon. By using electromagnetic probes, the coupling of baryon resonances to different final states is accessable. As the total cross section is a quadratic sum of the contributing partial waves, small resonance structures are dominated by others and thus cannot be studied in the total cross section measurement. It is necessary to measure differential distributions of polarisation observables to resolve these weak resonance contributions. The single polarisation observable Σ can be accessed by scattering a linearly polarised photon beam on an unpolarised target. Its sensitivity to interferences of partial waves provides additional informations on small resonant structures, but does not lead to an unambiguous identification of all contributing partial waves. These ambiguouities can only be disentangled by double polarisation experiments, using a polarised photon beam on a polarised target. In the case of single scalar meson production, the experiment is complete if three single and four properly chosen double polarisation observables are measured in addition to the differential cross section [1]. In this case all amplitudes can be determined model-independently without descrete ambiguouities.
To access the double polarisation observable G, a linearly polarised photon beam was scattered on a longitudinally polarised target.

[1] gruener@hiskp.uni-bonn.de

2 Experimental Setup

The CBELSA/TAPS experiment is located at the ELSA accelerator facility in Bonn. The electron beam of up to 3.5 GeV can be used to produce linearly polarised photons via coherent bremsstrahlung on a diamond crystal. The energy of the beam photons is measured by a tagging spectrometer, which covers an energy range of 18% to 85% of the incident electron beam energy, with 96 plastic counters. A scintillating fibre hodoscope, consisting of 480 fibres, increases the energy resolution in the low energy regime to 0.2% - 2.2%. In the centre of the Crystal Barrel setup the frozen spin butanol target system provides longitudinally polarised protons with polarisation degrees of up to 80%. 1230 CsI(Tl) Crystals form the main calorimeter barrel and cover a polar angle range of 30° to 156° and 2π azimuthal angle. The main detector is equipped with a cylindrical scintillating fibre inner detector to allow charge identification. A forward detector covers the angular range down to 12°. It is composed of 90 CsI(Tl) crystals in combination with 180 plastic scintillator tiles for charge identification. The MiniTAPS calorimeter closes the detector front part down to 1°. Made up of 216 BaF_2 Crystals, and equipped with plastic scintillators, it provides a high granularity to account for the high count rates in the forward region.

3 Data Analysis

The datasets presented, were measured in 2008 and 2009, using coherent peak settings of 840 MeV, 1032 MeV, and 1250 MeV to produce maximal degrees of photon polarisation of 61%, 58%, and 55% respectively. An energy range of 580 MeV to 1380 MeV was divided into energybins of 33 MeV width in the π^0 photoproduction and 100 MeV width in the η photoproduction case. Events with one charged and two neutral particles in the final state were selected and cuts on the coplanarity, the collinearity, the missing mass of the proton, and a time cut were applied. The target material used in the polarised target system is butanol. Besides the reactions on free protons, mesons produced off protons bound in carbon contribute to the measured count rate, which therefore has to be written as:

$$(1) \qquad N(\theta,\phi) = (N_C + N_H)\left[1 - \frac{(N_C\Sigma_C + N_H\Sigma_H)}{(N_C + N_H)} p_\gamma^{lin} cos(2\phi) + \frac{N_H}{(N_C + N_H)} p_z p_\gamma^{lin} G sin(2\phi)\right]$$

whereas $N_C(N_H)$ is the pure count rate due to carbon(hydrogen), and $N(\theta,\phi)$ is the measured overall count rate. The differential count rate spectra were segmented into 12 θ bins and fitted by the following fit function:

$$(2) \qquad N(\theta,\phi) = A\,[1 - B\,cos(2\phi) + C\,sin(2\phi)]$$

Due to the carbon fraction in the target, it is not possible to determine Σ_H, the free proton beam asymmetry, in particular. The fitparameter B depends on a compound of the beam asymmetries of bound and free protons: $B = \frac{(N_C\Sigma_C + N_H\Sigma_H)}{(N_C + N_H)} p_\gamma^{lin}$. Assuming $\Sigma_C \approx \Sigma_H$, this simplifies to $B \approx \Sigma_H p_\gamma^{lin}$, so that the results can be compared to previous measurements.
The double polarisation observable G can be determined by analysing the fitparameter

$C = \frac{N_H}{(N_C + N_H)} p_z p_\gamma^{lin} G$. G is not affected by the carbon fraction in the target explicitly, because the protons bound in carbon are not polarised. For an absolute determination of the observable, the dilution factor $D = \frac{N_H}{(N_C + N_H)}$ is necessary. It was determined by measuring with a hydrogen and a carbon target separately, and scaling these datasets to match the data obtained with butanol [2]. In combination with the degrees of polarisation of the beam and the target this information was used to correct the fit results.

4 Preliminary Results

The measured beam asymmetry Σ for the reaction channels $\vec{\gamma}\vec{p} \rightarrow p\pi^0$ and $\vec{\gamma}\vec{p} \rightarrow p\eta$ is shown in figure 1. The results are in good agreement to data from the previous measurements of Graal [8] and D. Elsner [7]. The data sets are compared to different PWA solutions, BnGa [3], MAID [4] [5], and SAID [6].

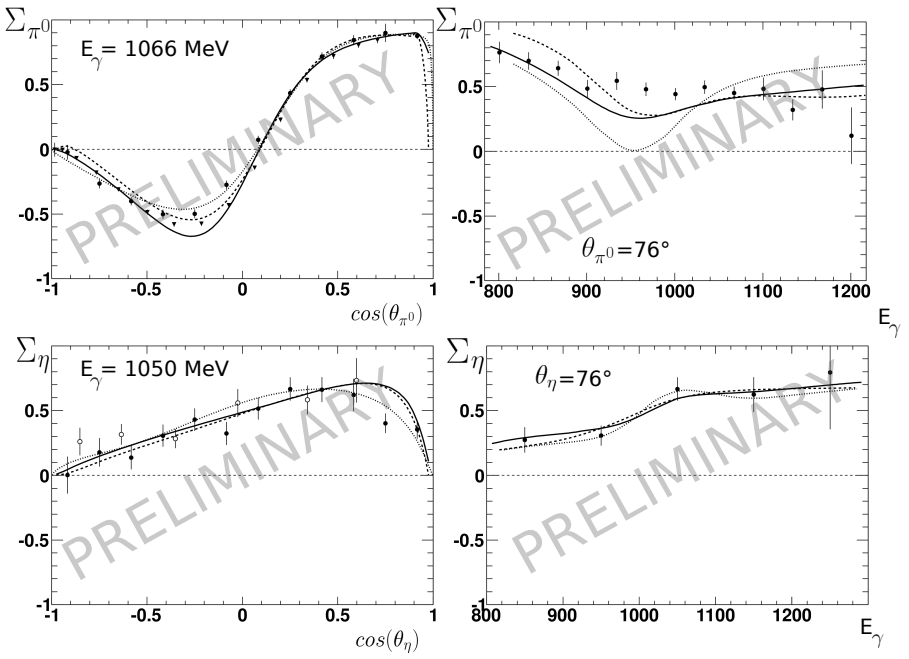

Figure 1: The single polarisation observable Σ. Top: $\gamma p \rightarrow p\pi^0$ The preliminary results (filled circles) are compared to results of the Graal collaboration [8] (triangles). Bottom: Preliminary results for the reaction $\gamma p \rightarrow p\eta$ (filled circles) in comparison to data measured by D.Elsner [7](open circles). The lines show different PWA solutions, BnGa (solid line), SAID (dashed line), MAID (dotted line).

Figure 2 shows the results of the G asymmetry measurement for the reactions $\vec{\gamma}\vec{p} \rightarrow p\pi^0$ and $\vec{\gamma}\vec{p} \rightarrow p\eta$. The PWA solutions roughly reflect the measured data, but differences are visible. Especially in the η photoproduction, the data cannot be discribed. These informations will provide new constraints for the prospective partial wave analysis.

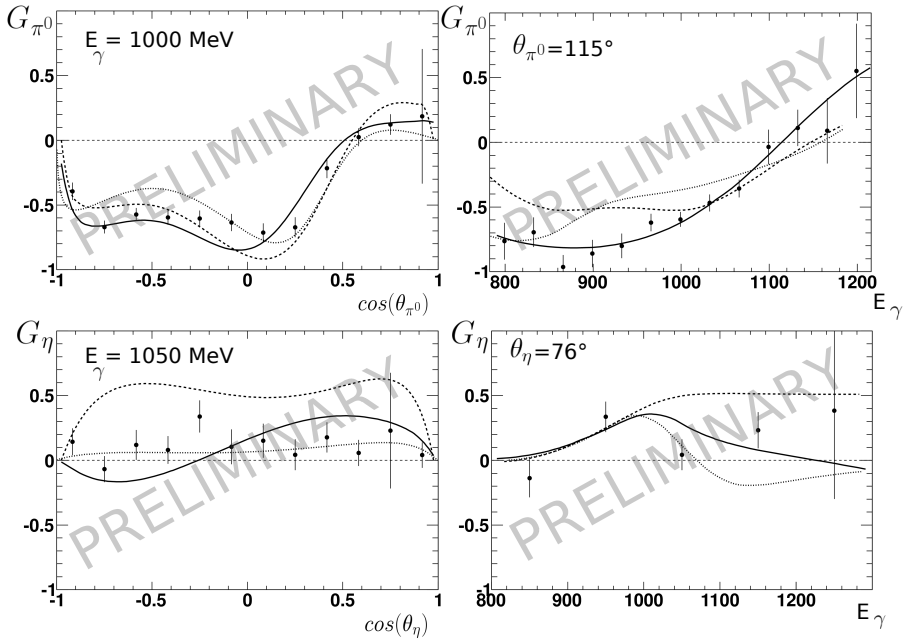

Figure 2: The double polarisation observable G. Top: $\gamma p \rightarrow p\pi^0$ bottom: $\gamma p \rightarrow p\eta$. The preliminary results (filled circles) are compared to PWA solutions, BnGa (solid line), SAID (dashed line), MAID (dotted line).

5 Summary

With the CBELSA/TAPS experiment single and double polarisation observables can be measured. The presented beam asymmetry Σ is in good agreement with the previous measurements. The obtained results of the double polarisation observable G show discrepancies to the current PWA predictions, which will have an impact to the prospective partial wave analysis.

Bibliography

[1] Chang W., Tabakin F., *Phys. Rev.* C **55**, 2054 (1997).

[2] Thiel A., *AIP Conf. Proc.* **1257**, 602 (2010).

[3] BnGa PWA solution BG2010-02, website: pwa.hiskp.uni-bonn.de

[4] Drechsel D., Komalov S.S. and Tiator L., *Eur. Phys.* J A **34**, 69 (2007).

[5] Chiang W.-T., Yang S.N., Tiator L., Vanderhaegen M., Drechsel D., *Phys. Rev.* C **68**, 045202 (2003).

[6] Dugger M. *et al.*, *Phys. Rev.* C **79**, 065206 (2009).

[7] Elsner D., *Eur. Phys.* J A **33**, 147 (2007).

[8] Bartalini O., *Eur. Phys.* J A **26**, 399 (2005).

Measurement of the double polarisation observable E in the reactions $\vec{\gamma}\vec{p} \to p\eta$ and $\vec{\gamma}\vec{p} \to p\pi^0$

Jonas Müller[1] and Manuela Gottschall for the CBELSA/TAPS Collaboration
Helmholtz-Institut für Strahlen- und Kernphysik, Nussallee 14-16, D-53115 Bonn, Germany

Polarisation observables are measured with the Crystal Barrel/TAPS experiment at ELSA for photoproduction reactions with various final states, using a circularly or linearly polarised photon beam and a longitudinally or transversely polarised frozen spin butanol target. The Crystal Barrel/TAPS setup provides a nearly 4π angular coverage, a good energy resolution and a high detection efficiency for photons, and is therefore ideally suited to study final states comprising neutral mesons. Results for the measurement of the double polarisation observable E for the reactions $\vec{\gamma}\,\vec{p} \to p\pi^0$ and $\vec{\gamma}\,\vec{p} \to p\eta$ are presented.

1 Introduction

One of the open challenges in subnuclear physics is to understand the non-perturbative regime of QCD, including the world of the nucleon and its excitations. In order to extract baryon resonances in photoproduction experiments, partial wave analyses need to be performed. A complete experiment is required to unambiguously determine the contributing amplitudes. This involves the measurement of carefully chosen single and double polarisation observables. Considering circular beam and longitudinal target polarisation, the cross section for the photoproduction of single pseudoscalar mesons can be written as

$$\frac{\mathrm{d}\sigma}{\mathrm{d}\Omega} = \left(\frac{\mathrm{d}\sigma}{\mathrm{d}\Omega}\right)_0 \left(1 - p_z p_\gamma^\circ E\right). \tag{1}$$

where $\left(\frac{\mathrm{d}\sigma}{\mathrm{d}\Omega}\right)_0$ is the unpolarised cross section, p_γ° the beam and p_z the target polarisation [1].

2 Experimental setup

The data presented has been taken with the Crystal Barrel/TAPS experiment at ELSA [2]. The setup consists of two electromagnetic calorimeters, the Crystal Barrel [3] and the

[1]jonas.mueller@hiskp.uni-bonn.de

MiniTAPS [4] detector, covering the polar angle from 1° to 156° and the full azimuthal angle. Plastic scintillator detectors and a three-layer plastic fibre detector [5] are used to obtain charge information. A tagged photon beam is produced from the electron beam impinging a radiator target. The Bonn Frozen Spin Target [6] uses butanol to provide polarised nucleons.

In order to extract the double polarisation observable E, data has been taken with a longitudinally polarised target and a circularly polarised photon beam produced via helicity transfer from a longitudinally polarised electron beam at an electron beam energy of 2.35 GeV. Mean polarisation values of $p_{e^-} \approx 64\%$ and $p_z \approx 73\%$ for beam and target were reached in the according beamtimes.

3 Data selection and preliminary results

The data sample was selected by choosing events with either three distinct hits in the calorimeters, two uncharged and one charged, or two uncharged hits in the calorimeters with an additional hit in a charge identification detector. The events were further selected by applying kinematic cuts on energy and momentum conservation and by cuts on the $\gamma\gamma$ invariant mass to separate the reactions $\vec{\gamma}\vec{p} \to p\pi^0$ and $\vec{\gamma}\vec{p} \to p\eta$.

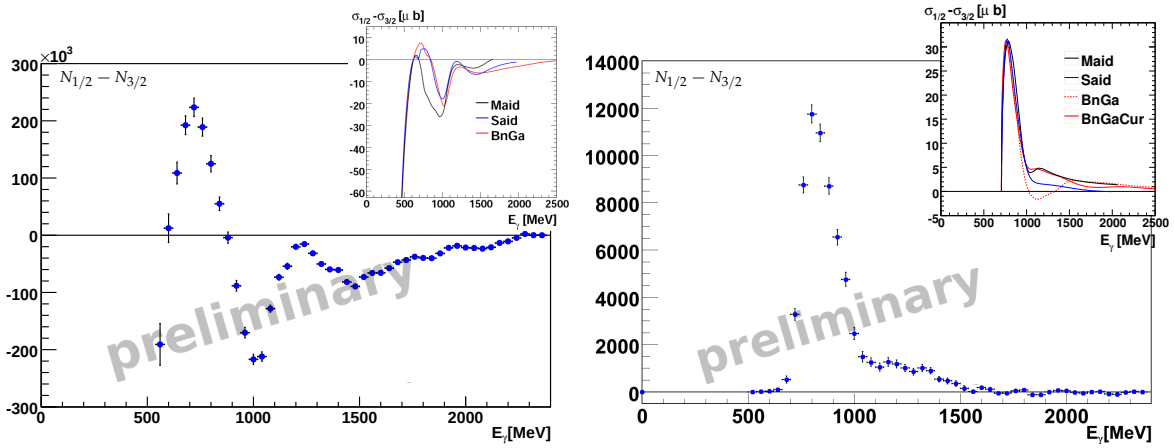

Figure 1: Polarisation weighted and acceptance corrected count rate difference for the reactions $\vec{\gamma}\vec{p} \to p\pi^0$ (left) and $\vec{\gamma}\vec{p} \to p\eta$ (right). The inlays show the predictions of the MAID [7], SAID [8], and BnGa [9] [10] analyses.

As not all protons in the butanol are polarised, two additional measurements on a carbon and a liquid hydrogen target were performed in order to determine an effective dilution factor f_{dil} which gives the ratio of polarisable protons to the total amount of nucleons in our data sample. The double polarisation observable E can then be extracted as

$$E = \frac{\sigma_{1/2} - \sigma_{3/2}}{\sigma_{1/2} + \sigma_{3/2}} = \frac{1}{p_\gamma^\circ \cdot p_z} \cdot \frac{1}{f_{\text{dil}}} \cdot \frac{N_{1/2} - N_{3/2}}{N_{1/2} + N_{3/2}} \tag{2}$$

with $\sigma_{1/2}$ and $\sigma_{3/2}$ being the cross sections and $N_{1/2}$ and $N_{3/2}$ the number of events with antiparallel and parallel spins of beam and target.

Fig. 1 shows the energy dependent count rate differences with antiparallel and parallel spin settings of target and beam in the reactions $\vec{\gamma}\vec{p} \to p\pi^0$ and $\vec{\gamma}\vec{p} \to p\eta$. One can clearly see the strong resonance peak due to the $S_{11}(1535)$ resonance in the $p\eta$ channel at photon energies below 1000 MeV and further to larger energies the highly debated region with possible contributions from a $P_{11}(1710)$ or a $P_{13}(1720)$. While the $P_{11}(1710)$ was not needed in the PWA solution named BnGa it contributes to BnGaCur, where also a reduced contribution of the $P_{13}(1720)$ was found compared to the earlier BnGa solution. The two different solutions lead to a significantly different prediction of $\sigma_{1/2} - \sigma_{3/2}$, BnGaCur showing a distribution with a higher similarity to the measured $N_{1/2} - N_{3/2}$ distribution. In the $p\pi^0$ channel, prominent structures over the whole energy range are visible, starting with an excess of $N_{3/2}$ events due to the $P_{33}(1232)$.

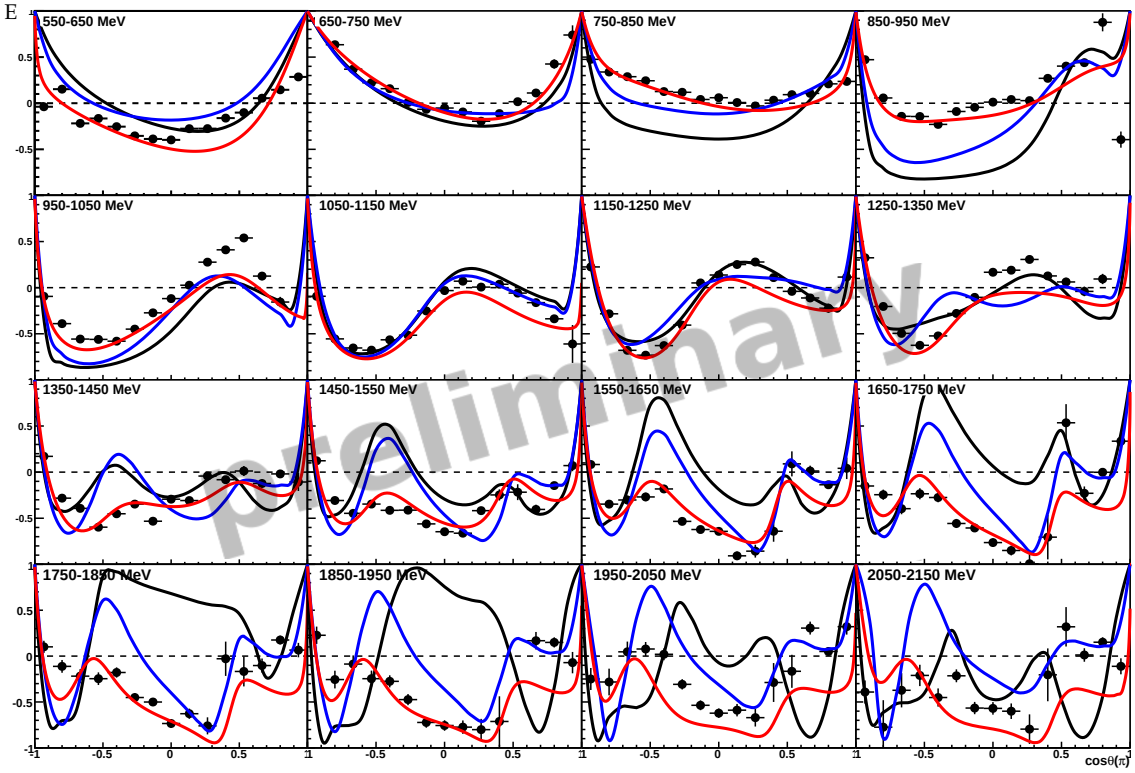

Figure 2: Observable E for the reaction $\vec{\gamma}\vec{p} \to p\pi^0$ as a function of $\cos(\theta^{\mathrm{CMS}}_{\pi^0})$ compared to the predictions of the MAID (black), SAID (blue), and BnGa (red) analyses.

Preliminary results for the double polarisation observable E in the reaction $\vec{\gamma}\vec{p} \to p\pi^0$ are shown in Fig. 2 as a function of $\cos(\theta^{\mathrm{CMS}}_{\pi^0})$. The shown error bars so far only include statistical uncertainties. Angular dependent structures appear up to the highest measured energies.

While data and predictions agree still well at lower energies, the analyses contradict each other for example between the second and third resonance region ($E_\gamma = 850 - 950$ MeV). In the third resonance region ($E_\gamma = 950 - 1050$ MeV), none of the predictions is able to describe the data and strong deviations appear at higher energies where also the predictions show significant differences.

4 Summary

The preliminary results for the measurement of the double polarisation observable E in the reactions $\vec{\gamma}\vec{p} \to p\pi^0$ and $\vec{\gamma}\vec{p} \to p\eta$ with the Crystal Barrel/TAPS experiment look very promising. Combined with the data obtained with a linearly polarised photon beam [11] and the transversely polarised target [12] this measurement is an important step towards a complete experiment and will provide further constraints for the PWA.

Acknowledgments

This work was supported by the *Deutsche Forschungsgemeinschaft* within SFB/TR-16.

Bibliography

[1] I. S. Barker, A. Donnachie, J. K. Storrow, *Nucl. Phys.* **B95**, 347–356 (1975).

[2] W. Hillert, *Eur. Phys. J. A* **28**, 139-148 (2006).

[3] E. Aker *et al.*, *Nucl. Instr. Methods A* **321**, 69-108 (1992).

[4] R. Novotny, *IEEE Trans. Nucl. Sci.* **NS-38**, 379-385 (1991).

[5] G. Suft *et al.*, *Nucl. Instr. Methods A* **531**, 416–424 (2005).

[6] Ch. Bradtke, H. Dutz, H. Peschel, *et al.*, *Nucl. Instr. Methods A* **436**, 430-442 (1999).

[7] D. Drechsel, S. S. Kamalov, L. Tiator, *Eur. Phys. J. A* **34**, 69-97 (2007).

[8] M. Dugger *et al.*, *Phys. Rev. C* **79**, 65206 (2009).

[9] Bonn-Gatchina partial wave analysis, solution BG2010-02, http://pwa.hiskp.uni-bonn.de (2010).

[10] A. Anisovich *et al.*, *Eur. Phys. J. A* **47**, 27 (2011).

[11] A. Thiel, *AIP Conf. Proc.* **1257**, 602–606 (2010).

[12] J. Hartmann, arXiv:1108.3459v3 [nucl-ex] (2011).

Baryon Spectroscopy at COMPASS

Alex Austregesilo[1] on behalf of the COMPASS Collaboration
Technische Universität München, Physik Department E18, D-85748 Garching

At the COMPASS experiment, diffractive dissociation of the beam proton is one of the dominant processes for the 190 GeV/c positive hadron beam impinging on a liquid hydrogen target. The status of the analysis of the reactions $p\,p \to p_f\,\pi^+\pi^-\,p_s$ and $p\,p \to p_f\,K^+K^-\,p_s$ is presented, where dominant features of the light-baryon spectrum become clearly visible. Furthermore, partial-wave analysis techniques to disentangle these spectra are discussed.

1 Introduction

COMPASS [1] is a fixed-target experiment at the CERN SPS for the investigation of structure and spectroscopy of hadrons. The experimental setup features a large-acceptance and high-resolution spectrometer including particle identification and calorimetry and is therefore ideal to address a broad range of different final states. The 190 GeV/c positive hadron beam impinging on a liquid hydrogen target gives the unique possibility to study proton diffractive dissociation. This peripheral scattering process is characterised by its four-momentum transfer distribution, the slope of which approximately reflects the size of the target particles. The prerequisite of coherent production translates into an upper limit for the mass of diffractively produced resonances of a few GeV/c^2 [2]. Exclusive events with three charged particles in the final state have been selected, this data set is the starting point for a dedicated partial-wave analysis.

2 Event Selection

The presented data correspond to 30% of the recorded proton-beam data set. The events were triggered by a coincidence between the incoming beam and the recoiling proton $p_{s(low)}$ from the reaction. The dedicated recoil-proton detector (RPD) around the target measured a pure proton signal. It can therefore be safely assumed that the target protons remain intact. On the other hand, the interaction is required to have a squared four-momentum transfer t' to the recoil proton larger than 0.07 GeV$^2/c^2$ in order to fall within the acceptance of the RPD trigger.

[1] aaust@tum.de

As the positive secondary hadron beam at 190 GeV/c consists of a mixture of 75% protons, 24% pions, and less than 1% kaons, the incoming beam particles were identified by two CEDAR detectors (ChErenkov Differential counter with Achromatic Ring focus) which achieved a nearly complete separation. In addition, particle identification was applied to distinguish between the fast proton p_f and the positive meson in the final state. As the COMPASS RICH (Ring Imaging CHerenkov) detector does not allow proton identification directly in a large part of the kinematic range, π^+ and K^+ signals were used, respectivly.

Only exclusive events were selected, where all particles in the reaction were detected and their energy as well as charge sum match the incident beam. In addition, the recoil proton and the forward going three-body system ($p_f\pi^+\pi^-$ or $p_fK^+K^-$) had to be back-to-back in the plane transverse to the beam. The resulting data sample includes merely a negligible contribution of non-exclusive background.

3 Diffractive dissociation of protons into $p_f\,\pi^+\pi^-$ final states

In Fig. 1 the invariant mass distribution of the $p_f\pi^+\pi^-$ system is shown. This excited proton spectrum is foreseen to be studied in detail by the means of partial-wave analysis. Few distinct structures can be observed at positions where there are several known N^* and Δ resonances with $N\pi\pi$ decay modes. Due to many ambiguities, it is not possible to assign resonances to these structures without a full partial-wave analysis of the data. For higher masses, the multitude of excited baryons creates a smooth curve which has a shoulder around 2.2 GeV/c^2.

Essential for the partial-wave analysis are resonances in the $p\pi^\pm$ and $\pi^+\pi^-$ subsystems which appear as intermediate states, the so-called isobars. The $\pi^+\pi^-$ invariant mass distribution in Fig. 2 shows clear signatures of $\rho^0(770)$, $f_0(980)$ and $f_2(1270)$. A similar set of resonances was observed in the diffractive dissociation of pions into $\pi^-\pi^+\pi^-$ [3].

The invariant mass spectrum of the $p_f\pi^-$ subsystem, depicted in Fig. 3, exhibits a distinct

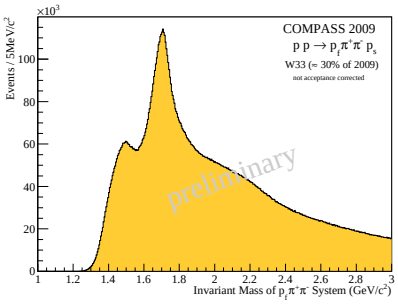

Figure 1: *Invariant mass distribution of $p_f\pi^+\pi^-$ system*

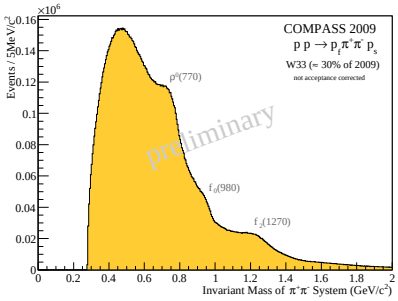

Figure 2: *Invariant mass distribution of $\pi^+\pi^-$ subsystem*

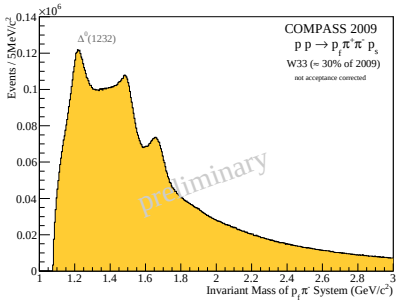

Figure 3: *Invariant mass distribution of $p_f\pi^-$ subsystem*

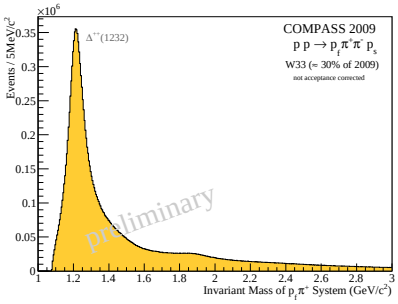

Figure 4: *Invariant mass distribution of $p_f\pi^+$ subsystem*

excited baryon spectrum, featuring a prominent $\Delta^0(1232)P_{33}$ together with additional structures that are probably related to the $N(1440)P_{11}$, $N(1650)S_{11}$ and $\Delta(1700)D_{33}$. However, also here assignments based on the mass alone are ambiguous. Naturally, the doubly charged $p_f\pi^+$ combination is less populated. In addition to the outstanding $\Delta^{++}(1232)P_{33}$, there seem to be higher excitations around $1.9\,\mathrm{GeV}/c^2$.

In Fig. 5, 6 and 7, the three-body invariant mass is presented versus the invariant masses of the three possible sub-systems in order to illustrate the quality of the data sample. The above described isobars appear clearly as vertical bands in this manner.

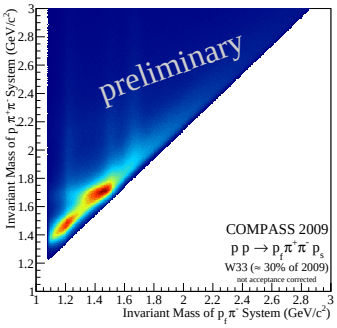

Figure 5: *Invariant mass of $p_f\pi^+\pi^-$ vs. $p_f\pi^-$ subsystem*

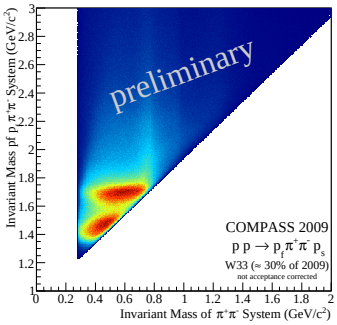

Figure 6: *Invariant mass of $p_f\pi^+\pi^-$ vs. $\pi^+\pi^-$ subsystem*

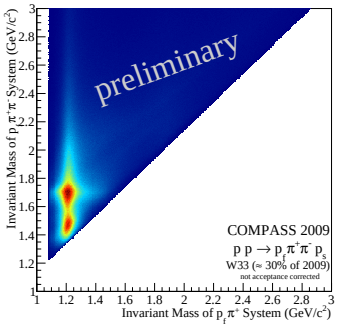

Figure 7: *Invariant mass of $p_f\pi^+\pi^-$ vs. $p_f\pi^+$ subsystem*

4 Diffractive dissociation of protons into $p_f K^+K^-$ final states

A different aspect of the baryon spectrum becomes accessible when the pions are replaced by kaons in the event selection described above. However, the number of events is considerably lower and therefore the unambiguous identification of resonances is more difficult.

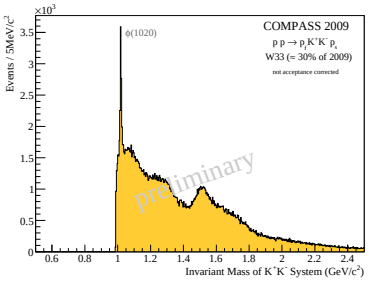

Figure 8: *Invariant mass distribution of K^+K^- subsystem*

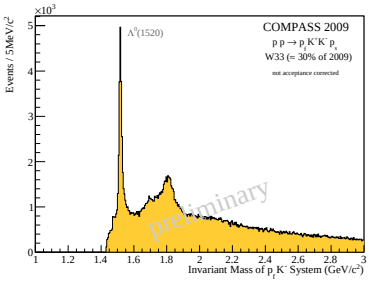

Figure 9: *Invariant mass distribution of $p_f K^-$ subsystem*

While no special features can be seen in the three-particle invariant mass spectrum, the subsystems do show interesting structures. Most prominent is the very narrow $\phi(1020)$ peak that appears as expected in the K^+K^- invariant mass as shown in Fig. 8. In addition the invariant mass distribution exhibits structures at masses of known resonances like the $a_2(1320)$ and the $f_0(1500)$.

A sharp baryon resonance, the $\Lambda(1520)D_{03}$, can be found in the invariant mass spectrum of the $p\,K^-$ combination (cf. Fig. 9). Higher baryon excitations with strangeness are visible for example around 1.7 and 1.8 GeV/c, although less pronounced.

5 Partial-Wave Analysis

The selected data set is the starting point for a dedicated partial-wave analysis. The incoming beam proton scattering off the target is excited into an intermediate state X, with quantum numbers which can differ from those of the initial state. This reaction can be assumed to proceed via t-channel Reggeon exchange, thus justifying the factorisation of the total cross section into a resonance and a recoil vertex without final state interaction. Considering only subsequent two-body decays of X (i.e. applying the isobar model) [3], three different decay topologies into the same final state $p_f\,\pi^+\pi^-$ are possible which are shown in Fig. 10.

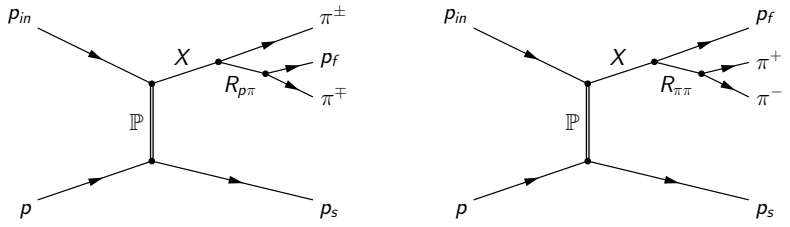

Figure 10: *Possible Decays of Resonance X*

Taking the observed invariant mass spectra into account (cf. Section 3), the isobar candidates can be either mesonic (e.g. $(\pi\pi)_S$, $\rho^0(770)$, $f_2(1270)$, ...) or baryonic (e.g. $\Delta(1232)P_{33}$, $N(1440)P_{11}$, $N(1650)S_{11}$, $\Delta(1700)D_{33}$, ...). The partial-wave analysis is carried out by a program developed at Brookhaven [4] and adapted for COMPASS [5]. D-functions and the canonical basis are used to evaluate the decay amplitudes.

6 Conclusions

In the years 2008 and 2009, the COMPASS experiment collected a unique data set with a proton beam impinging on a liquid hydrogen target. As the diffractive dissociation of the beam proton plays a dominant role, the high resolution spectrometer combined with the clean trigger makes COMPASS an ideal tool to explore the baryon spectrum.

Thorough event selection studies led to a clean exclusive data sample, where structures at positions of known resonances become already apparent in the invariant mass distributions. Profiting from partial-wave analysis techniques developed for the search of exotic mesons [3], COMPASS has great potential to contribute to the field of light-quark baryon spectroscopy.

Acknowledgments

This work is supported by the German Bundesministerium für Bildung und Forschung, the Maier-Leibnitz-Laboratorium der LMU und TU München, and the DFG Cluster of Excellence *Origin and Structure of the Universe*.

Bibliography

[1] COMPASS Collab. (P. Abbon *et al.*), *The COMPASS Experiment at CERN*, Nucl. Instr. Meth. **A577**, 455 (2007).

[2] U. Amaldi, M. Jacob and G. Matthiae, *Diffraction of Hadronic Waves*, Ann. Rev. Nucl. Part. Sci. **26**, 385 (1976).

[3] COMPASS Collab. (M. G. Alexeev *et al.*), *Observation of a $J^{PC} = 1^{-+}$ exotic resonance in diffractive dissociation of 190 GeV/c π^- into $\pi^-\pi^-\pi^+$*, Phys. Rev. Lett. **104**, 241803 (2010).

[4] J. P. Cummings and D. P. Weygand, *An Object-Oriented Approach to Partial Wave Analysis*, arXiv:physics/0309052v1

[5] S. Neubert et al, `http://sourceforge.net/projects/rootpwa`

Photoproduction of η-Mesons off ^{3}He

Lilian Witthauer[1] for the A2 Collaboration
Department of Physics
University of Basel
CH-4056 Basel, SWITZERLAND

Photoproduction of η-mesons off ^{3}He has been studied at the MAMI accelerator using the Crystal Ball/TAPS detector setup. The total cross section for the coherent η-photoproduction was measured with improved statistical quality. Both, the total and differential cross sections show evidence for dominant final state interaction. Additionally, the photoproduction of η-mesons off quasi-free protons and neutrons was studied. The preliminary cross section on the neutron confirms the narrow bump-like structure at $W \simeq 1.7$ GeV, which was already seen in different experiments on the deuterium target [1–3, 10, 11].

1 Introduction

Photoproduction of mesons is an ideal tool to investigate the meson-nucleon (-nucleus) interactions. An important question is whether the properties of the strong interaction allow the formation of meson-nucleus bound states. The best candidate for such a bound state is the η-meson. Already in the 1980s Bhalerao, Liu and Haider [4, 5] found that an attractive ηN s-wave interaction might lead to the formation of quasi-bound η-nucleus states, the so-called η-mesic nuclei. Such quasi-bound states should give rise to an enhancement at the threshold of the cross section relative to the expectation for phase space behavior. Such threshold behaviours have been previously studied in hadron and photon induced reactions for η-^{3}He [6,7] and η-^{4}He [8,9] systems. With the 4π-detector in Mainz, this experiment was able to improve the statistical quality of the coherent η-photoproduction off ^{3}He drastically. The results will be discussed below.
Besides the investigation of η-mesic nuclei, this experiment was used to study the excitation spectrum of the nucleon. In particular, total cross sections of η-photoproduction off quasi-free protons and neutrons have been measured. Previous experiments [1–3, 10, 11] have reported a narrow structure at $W \simeq 1.7$ GeV with a width of ~ 25 MeV in the cross section on the neutron which is not visible for the proton.
The experiment was carried out at the MAMI acceleration facility in Mainz. A circularly polarised tagged photon beam with energies up to 1.4 GeV and a typical energy resolution

[1] lilian.witthauer@unibas.ch

of 4 MeV was used. For a geometrical acceptance close to 4π steradian several detectors are needed. The Crystal Ball detector (CB) surrounds the target and is made of 720 NaI crystals. Inside the CB the Particle Identification Detector (PID) is placed. The PID is made of 24 plastic scintillators and is used to identify charged particles. The opening angle to the forward direction of the CB is covered using the photon spectrometer TAPS. The TAPS detector is made of BaF_2 and $PbWO_4$ crystals and is placed 1.475 m in front of the target. A plastic veto is mounted in front of every BaF_2 crystal. The cryogenic ^{3}He target is centered in CB and has a length of 5.3 cm and a density of 0.069 g/cm^3.

2 Results

To investigate the formation of a η-nucleus bound states, the cross section of the coherent η-photoproduction was measured. An invariant mass analysis for each energy and meson center-of-mass polar angle has been performed to identify the $\eta \rightarrow 2\gamma$ and $\eta \rightarrow 6\gamma$ decay. Due to the overdetermined kinematics the missing energy was used to separate the coherent from breakup reactions. The total cross section of the two decay channels are shown in Fig.1

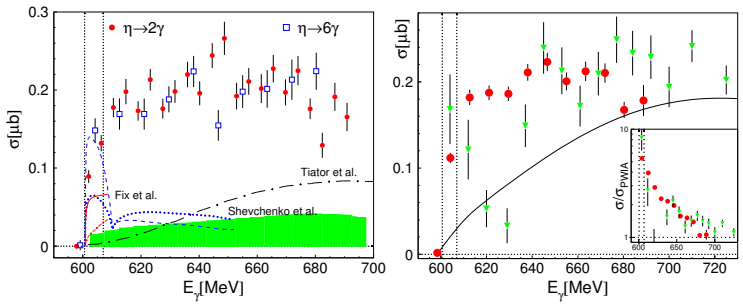

Figure 1: Left: Coherent η cross section for $\eta \rightarrow 2\gamma$ (red) and $\eta \rightarrow 6\gamma$ (blue). Several models are indicated. Right: The average of $\eta \rightarrow 2\gamma$ and $\eta \rightarrow 6\gamma$ is compared to a previous measurement by M. Pfeiffer et al. [6].

(left). Both results are in good agreement and show a steep increase between the coherent and the breakup threshold. All indicated models do not reproduce the data. On the right side the average of the two cross sections is compared to an earlier experiment [6]. The two measurements are in agreement if one takes into account the lower statistical quality of the older results.

The η-photoproduction off quasi-free protons and neutrons has been identified with an invariant mass analysis. The competing background, which mainly comes from $\eta\pi^0$ reactions, was eliminated by cutting on the missing mass and on the coplanarity of the η-nucleon pair. Additionally, the background was reduced by coincidence cuts and a random background subtraction. Monte-Carlo simulations with Geant4 were used for the angle and energy dependent detection efficiency correction. On the one hand the cross section was calculated

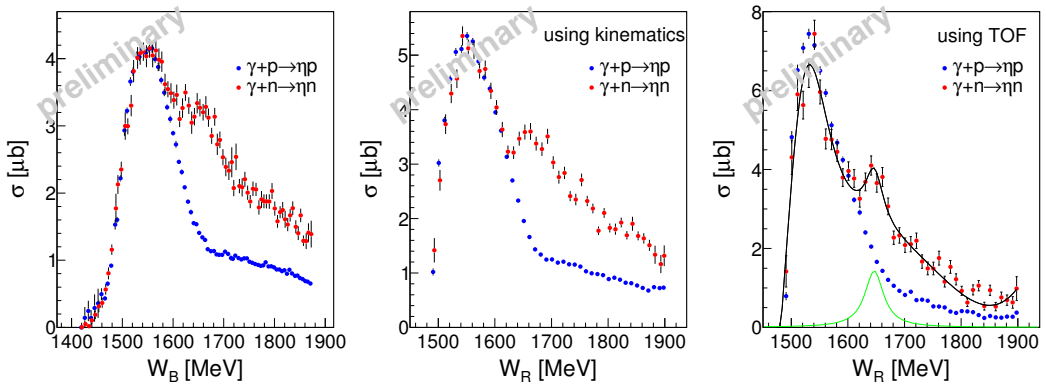

Figure 2: Total cross sections of quasi-free η-photoproduction on the proton (blue) and on the neutron (red). The proton cross section is scaled to the neutron. The cross section on the right-hand side is fitted with two Breit-Wigner functions and a background polynomial. The fit yields a width of 45 MeV for the structure, which is comparable to the experimental resolution.

as a function of the center of mass energy with the initial state particles:

$$W_B^2 = (P_\gamma + P_{N,i})^2 = 2E_\gamma m_N + m_N^2$$

Since the momentum of the initial state nucleon is not exactly known, the structures are smeared out due to the Fermi motion. On the other hand the center-of-mass energy has been calculated with the final state particles:

$$W_R^2 = (P_\eta + P_{N,f})^2$$

In this case no effects of Fermi motion are visible but the experimental resultion of the recoil nucleon is the limiting factor. The resulting cross sections as a function of W_B (left) and W_R (middle) are visible in Fig.2. In the central picture the structure around $W \simeq 1675$ MeV is quite narrow, whereas the structure on the left side is broadened by Fermi motion. The position of this structure is consistent with the deuterium data by I. Jaeglé et al. [1,2] but is somewhat broader. This is caused by the fact that the kinematical reconstruction of the recoil nucleon momentum is more approximate in ^{3}He than in deuterium. Since one has a three-body final state instead of a two-body final state one has to assume that the two spectator nucleons have no relative momentum. To overcome this problem the recoil nucleon momentum has been calculated for nucleons detected in TAPS using time-of-flight instead of kinematics, which results in the cross sections in Fig.2 (right). In this case the structure has a width of 45 MeV which is comparable to the experimental resolution.

3 Conclusions

The coherent η-photoproduction off ^{3}He was measured with improved statistical quality. The resulting total cross section rises extremely between the coherent and breakup threshold. The angular distributions at threshold (not shown) are almost isotropic or have even an angular dependence opposite to the expectation from the form factor behavior. All these effects are strong evidence for dominant final state interaction, which could be related to a resonant state at η-photoproduction threshold.
The cross section of quasi-free η-photoproduction on the neutron shows a bump-like structure. The position and width of this structure is consistent with the deuteron data. The existence of this structure in the cross section on ^{3}He, which has a different neutron-to-proton ratio and a bigger Fermi motion than deuterium, makes it very unlikely that this structure is caused by rescattering of mesons or final state interaction. Currently further experiments are running at MAMI in Mainz and ELSA in Bonn to measure single and double polarisation observables which then can be used to identify the responsible partial waves.

Acknowledgments

This work was supported by Schweizerischer Nationalfonds, DFG, and EU/FP6. The results on the η-mesic nuclei are part of the PhD-Thesis of F. Pheron.

Bibliography

[1] I. Jaeglé *et al.*, Phys. Rev. Lett. 100 (2008) 252002.

[2] I. Jaeglé *et al.*, Eur. Phys. J. A47 (2011) 89.

[3] D. Werthmüller, Chinese Physics C 2009 33(12): 1345-1348.

[4] R.S. Bhalerao and L.C. Liu, Phys. Rev. Lett. 54 (1985) 865.

[5] L.C. Liu and Q. Haider, Phys. Rev. C 34 (1986) 1845.

[6] M. Pfeiffer *et al.*, Phys. Rev. Lett. 92 (2004) 252001.

[7] T. Mersmann *et al.*, Phys. Rev. Lett. 98, (2007) 242301.

[8] V. Hejny *et al.*, Eur. Phys. J. A6 (1999) 83.

[9] V. Hejny *et al.*, Eur. Phys. J. A13 (2002) 493.

[10] V. Kuznetsov *et al.*, hep-ex 0606065.

[11] F. Miyahara *et al.*, Prog. Theor. Phys. Suppl.168:90-96, 2007.

Notes on New Narrow N*

Maxim V. Polyakov
Institute for Theoretical Physics II , Ruhr-University Bochum, D-44780 Bochum, GERMANY

We briefly discuss the most recent evidences for narrow nucleon excitation (N*) with mass around 1680 MeV. The data show that the N* should have much stronger photocoupling to the neutron than to the proton. That makes it a good candidate for the anti-decuplet member.

Theoretical predictions for anti-decuplet N*

In this short contribution we discuss fresh evidences for the nucleon from the anti-decuplet [1]. A detailed account for predictions and evidences for new narrow nucleon can be found in Ref. [2]. Main properties of N* from the anti-deculpet which were predicted theoretically in years 1997-2004 are the following:

- Quantum numbers are P_{11} ($J^P = \frac{1}{2}^+$, isospin=$\frac{1}{2}$) [1].
- Narrow width of $\Gamma \leqslant 40$ MeV [1,3,5].
- Mass of $M \sim 1650 - 1720$ MeV [4,5].
- Strong suppression of the proton photocopling relative to the neutron one [6]. This prediction was based on SU(3) flavour symmetry only. Therefore it can be used as a clear benchmark for a nucleon member of the anti-decuplet.
- The πN coupling is suppressed, N* prefers to decay into ηN, $K\Lambda$ and $\pi\Delta$ [1,3,5].

N* in γn collisions

In the γn collisions (with non-suppressed exit channels such as ηn, γn, $K_S\Lambda$, etc.) the signal of the anti-decuplet nucleon should be seen as a prominent narrow peak in the cross section [6]. However, the neutron is bound in a nucleus, hence the narrow resonance signal is hidden by nuclear effects (by the Fermi motion at the first place[1]). Four groups - GRAAL [9,10], CBELSA/TAPS [11], LNS [12], and Crystal Ball/TAPS [13] - managed to overcome this difficulty and reported evidence for a narrow structure at $W \sim 1680$ MeV in the η photoproduction on the neutron (neutron anomaly[2]).

In year 2011 more results on the neutron anomaly were obtained. In Ref. [14] the neutron anomaly was also observed in the Compton scattering – the study of quasi-free Compton scattering on the neutron revealed a narrow ($\Gamma = 28 \pm 12$ MeV) peak at ~ 1685 MeV with significance of $\sim 4.6\sigma$. Such peak is absent in the proton Compton scattering.

[1] Observation of the neutron anomaly in the η photoproduction off ^{3}He [7] excludes other nuclear effects.

[2] The name "neutron anomaly" was introduced in Ref. [8] to denote the bump in the quasi-free $\gamma n \to \eta n$ cross section around $W \sim 1680$ MeV and its apparent absence in the quasi-free $\gamma p \to \eta p$ cross section.

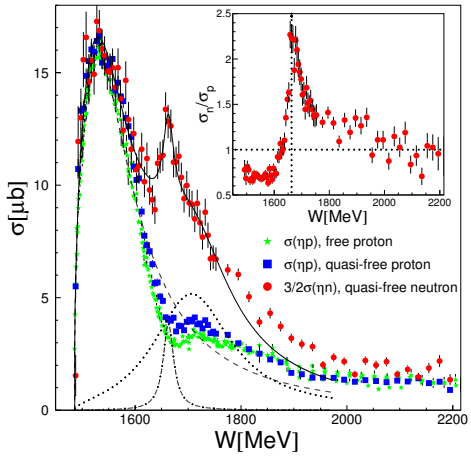

Figure 1: Figure from Ref. [15]. Total cross sections as function of final state invariant mass W with cut on spectator momentum $p_s \leqslant 100$ MeV. (Red) dots: quasi-free neutron, (blue) squares: quasi-free proton, (green) stars: free proton data. Insert: ratio of quasi-free neutron - proton data.

In Ref. [15] the de-folding of the Fermi motion in quasi-free η photoproduction off neutron has been performed. As a result the data exhibit pronounced narrow ($\Gamma = 25 \pm 12$ MeV) peak at $W \sim 1670$ MeV in the total cross section of $\gamma n \to \eta n$ shown in Fig. 1.

Looking at this figure, the first natural hypothesis is that the peak is due to contribution of a narrow nucleon resonance. However, due to the very negative attitude of the community to narrow pentaquarks (see e.g. [16]) one tries to find another explanation for the neutron anomaly first. Detailed discussion of the "conventional explanations" can be found in Ref. [2]. Some of them are refuted already by recent experimental data of Refs. [14,15]. Here we touch presently popular results of Ref. [17] only. Ref. [17] attributes the peak in the neutron channel (see e.g. Fig. 1) to the KY threshold cusp effects.

A dedicated experimental search of the KY threshold cusp effects was performed in Ref. [18]. A very small effect was found. Our studies (in preparation) showed that if the peak in Fig. 1 is due to the cusp effects it would imply that $S_{11}(1650)$ resonance must have extraordinarily large coupling to KY channels, in acute disagreement with flavour SU(3). Moreover several questions to cusp effects of Ref. [17] remain unanswered: 1) Why the neutron anomaly is absent in the pion photoproduction? 2) What is the physics reason for very fine cancelation (fine tuning) of the KY threshold cusp effects in the proton channel?

N* in γp collisions

The first search of the putative anti-decuplet nucleon in $\gamma p \to \eta p$ process was performed in Refs. [2,8]. It was found that the beam asymmetry Σ exhibits a sharp structure around $W \sim 1685$ MeV. That structure looks like a peak at forward angles which develops into an oscillating structure at larger scattering angles. Such a behaviour may occur by interference

observable	extracted value	refs. (neutron data)	refs. (proton data)
mass (MeV)	1680 ± 15	[9–15] [3]$^{\star)}$	[2,8,20,22] [3]$^{\star)}$
$\Gamma_{\rm tot}$ (MeV)	$\leqslant 40$	[9–15] [3]$^{\star)}$	[2,8,20,22] [3]$^{\star)}$
$\Gamma_{\pi N}$ (MeV)	$\leqslant 0.5$	[3]$^{\star)}$	[3]$^{\star)}$
$\sqrt{{\rm Br}_{\eta N}} A^n_{1/2}$ (10^{-3} GeV$^{-1/2}$)	12-18	[15,21]	
$\sqrt{{\rm Br}_{\eta N}} A^p_{1/2}$ (10^{-3} GeV$^{-1/2}$)	1-3		[2,8,20,22]

Table 1: *Our estimate* of properties of the putative narrow N* extracted from the data. $^{\star)}$In Ref. [3] the elastic πN scattering data were analyzed and the tolerance limits for N* parameters were obtained. The preferable quantum numbers in this analysis are P_{11}.

of a narrow resonance with a smooth background. The observed structure was identified in Refs. [2,8] with the contribution of a resonance with mass $M \sim 1685$ MeV, narrow width of $\Gamma \leqslant 25$ MeV, and small photo-coupling of $\sqrt{{\rm Br}_{\eta N}} A^p_{1/2} \sim (1-2) \cdot 10^{-3}$ GeV$^{-1/2}$.

About an year ago the Crystal Ball Collaboration at MAMI published high precision data on η photoproduction on the free proton [19]. The cross section was measured in fine steps in photon energy. The measured cross section exhibits an oscillating with energy structure around 1690 MeV. The best fit to the data was achieved with a new version of SAID (GE09) [19]. However, inspection of this fit reveals a systematic deviation of data from the fit curves in the $1650 - 1730$ MeV region. In [20] this deviation was interpreted as indication for a nucleon resonance with mass of $M \sim 1685$ MeV, a narrow width of $\Gamma \leqslant 50$ MeV, and a small resonance photo-coupling in the range of $\sqrt{{\rm Br}_{\eta N}} A^p_{1/2} \sim (0.3-3) \cdot 10^{-3}$ GeV$^{-1/2}$. In this case no PWA of the data was performed as needed to decide whether or not a resonance occurs in a certain partial wave.

Such PWA was performed in Ref. [22]. A fit using only known broad resonances and standard background amplitudes can not describe the relatively narrow oscillating structure in the cross section in the mass region of 1660-1750 MeV. An improved description of the data can be reached by either assuming the existence of a narrow resonance at a mass of about 1700 MeV with small photo-coupling or by a threshold effect. In the latter case the observed structure is explained by a strong (resonant or non-resonant) $\gamma p \to \omega p$ coupling in the S_{11} partial wave. When the beam asymmetry data of Refs. [2,8] are included in the fit, the solution with a narrow P_{11} state is preferred. In that fit, mass and width of the putative resonance converge to $M \sim$1694 MeV and $\Gamma \sim 40$ MeV, respectively, and the photo-coupling to $\sqrt{{\rm Br}_{\eta N}} A^p_{1/2} \sim 2.6 \cdot 10^{-3}$ GeV$^{-1/2}$.

In Table 1 we summarize *our estimates* of the properties of the narrow N* which can be extracted from the present data. The obtained values fit neatly to the predicted properties of the anti-decuplet N*. Future experiments, especially on double polarization neutron observables, will show whether an analogous Table will appear in PDG.

Bibliography

[1] D. Diakonov, V. Petrov and M. V. Polyakov, Z. Phys. A **359** (1997) 305.

[2] V. Kuznetsov *et al.*, Acta Phys. Polon. B **39**, 1949 (2008) [arXiv:0807.2316 [hep-ex]]; arXiv:hep-ex/0703003.

[3] R. A. Arndt *et al.*, Phys. Rev. C **69**, 035208 (2004) [arXiv:nucl-th/0312126].

[4] D. Diakonov and V. Petrov, Phys. Rev. D **69** (2004) 094011 [arXiv:hep-ph/0310212].

[5] J. R. Ellis, M. Karliner and M. Praszalowicz, JHEP **0405** (2004) 002; M. Praszalowicz, Acta Phys. Polon. B **35** (2004) 1625 [arXiv:hep-ph/0402038].

[6] M. V. Polyakov and A. Rathke, Eur. Phys. J. A **18**, 691 (2003) [arXiv:hep-ph/0303138].

[7] L. Witthauer, this proceedings, and http://jazz.physik.unibas.ch/site/theses.html

[8] V. Kuznetsov and M. V. Polyakov, JETP Lett. **88**, 347 (2008) [arXiv:0807.3217 [hep-ph]].

[9] V. Kuznetsov [GRAAL Collaboration], arXiv:hep-ex/0409032.

[10] V. Kuznetsov *et al.*, Phys. Lett. B **647**, 23 (2007) [arXiv:hep-ex/0606065].

[11] I. Jaegle *et al.* , Phys. Rev. Lett. **100** (2008) 252002 [arXiv:0804.4841 [nucl-ex]].

[12] F. Miyahara *et al.*, Prog. Theor. Phys. Suppl. **168**, 90 (2007).

[13] D. Werthmuller [for the Crystal Ball/TAPS collaborations], Chin. Phys. C **33**, 1345 (2009) [arXiv:1001.3840 [nucl-ex]].

[14] V. Kuznetsov *et al.*, Phys. Rev. C **83** (2011) 022201(R) [arXiv:1003.4585 [hep-ex]].

[15] I. Jaegle *et al.*, Eur. Phys. J. A **47** (2011) 89 [arXiv:1107.2046 [nucl-ex]].

[16] C.G. Wohl, in K. Nakamura *et al.* [Particle Data Group Collaboration], J. Phys. G **G37** (2010) 075021; F. Close, Nature **435** (2005) 287-288.

[17] M. Doring and K. Nakayama, Phys. Lett. B **683**, 145 (2010) [arXiv:0909.3538 [nucl-th]].

[18] T. M. Knasel *et al.*, Phys. Rev. **D11** (1975) 1-13; B. Nelson *et al.*, Phys. Rev. Lett. **31** (1973) 901-904.

[19] E. F. McNicoll *et al.*, Phys. Rev. C **82** (2010) 035208.

[20] V. Kuznetsov, M. V. Polyakov and M. Thurmann, arXiv:1102.5209 [hep-ph].

[21] Y. I. Azimov, *et al.*, Eur. Phys. J. A **25**, 325 (2005) [arXiv:hep-ph/0506236].

[22] A. V. Anisovich *et al.*, arXiv:1108.3010 [hep-ph].

Single and Double Pion Photoproduction off the Deuteron

Manuel Dieterle[1] for the A2 Collaboration
Department of Physics
University of Basel
CH-4056 Basel, SWITZERLAND

There is evidence that the photoproduction of single and double pions off bound nucleons inside a nucleus are not only affected by Fermi motion but also by other nuclear effects, such as final state interactions or meson rescattering. We will present preliminary results of a high statistics measurement of single and double pion photoproduction of quasi-free protons and neutrons off the deuteron carried out at the Mainzer Microtron.

1 Introduction

The following paragraphs present preliminary results about single and double π^0 photoproduction off the deuteron that both originate from the same experiment accomplished in December 2007 at the Mainzer Microtron (MAMI) in Mainz, Germany. The MAMI electron beam facility produces a continuous photon beam with energies up to 1.5 GeV. The photon beam was circularly polarized and the main detectors used in this experiments providing nearly full angular coverage are the *Crystal Ball* calorimeter (CB) surrounding the target and the TAPS-detector which is placed as a forward wall. The separation of neutral and charged particles is done with plastic scintillators, either as bars arranged in a cylindrical setup surrounding the target (CB) or as hexagonally shaped vetos (TAPS). Furthermore a χ^2-test is used to identify the photons stemming from the meson decay and to isolate the recoil neutron.
The single and double π^0 cross sections were measured throughout the second and third resonance region in coincidence with recoil protons (quasi-free exclusive reaction on the proton), in coincidence with recoil neutrons (quasi-free exclusive reaction on the neutron) and without a condition for the detection of recoil nucleons (quasi-free inclusive reaction). Both quasi-free exclusive reactions sum up to the quasi-free inclusive channel, since the contribution of the coherent process is negligible in the energy region of interest.

[1]manuel.dieterle@unibas.ch

2 Results

The left-hand side of figure 1 shows the preliminary single π^0 total cross section of the quasi-free exclusive reaction on the proton $\gamma + d \rightarrow \pi^0 + p(n)$ (filled blue circles) together with the quasi-free exclusive reaction on the neutron $\gamma + d \rightarrow \pi^0 + n(p)$ (filled red circles). The right-hand side of figure 1 shows the preliminary single π^0 total cross section of the quasi-free inclusive reaction $\gamma + d \rightarrow \pi^0 + (N)$ (filled black circles) together with the sum of the two quasi-free exclusive reactions (open magenta circles). As well shown are previous results [1] for the inclusive reaction (open green circles) and the predicted cross sections from the theoretical models MAID [2] (dashed lines) and SAID [3] (full lines) folded with Fermi motion.

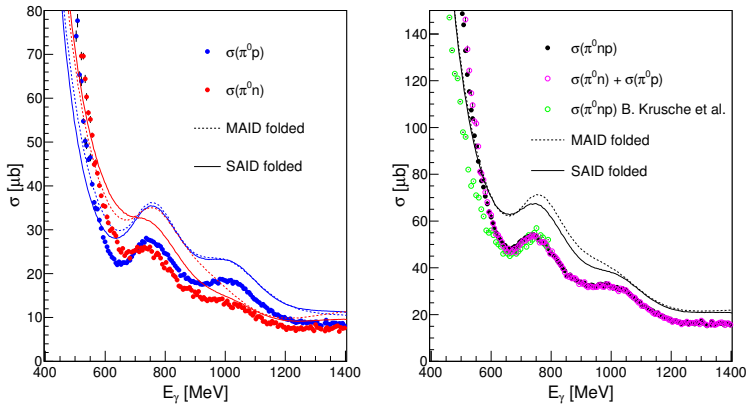

Figure 1: Preliminary single π^0 total cross sections of the quasi-free exclusive (left-hand side) and quasi-free inclusive (right-hand side) reaction. The labelling is explained in the text.

It can be seen in figure 1 that the shapes of the measured cross sections (full red, blue and black circles) are in nice agreement with the theoretical MAID [2] and SAID [3] models but there is a disagreement in magnitude. Furthermore, the sum of the quasi-free exclusive cross sections (open magenta circles) add up perfectly to the measured quasi-free inclusive cross section (full black circles). This indicates a very clean identification of the reaction channels. In addition, the measured quasi-free inclusive cross section (full black circles) is in good agreement with earlier results from MAMI B [1].

The left-hand side of figure 2 shows preliminary results for the $2\pi^0$ total cross sections of the quasi-free exclusive reaction on the proton $\gamma + d \rightarrow \pi^0\pi^0 + p(n)$ (filled blue triangles) together with the quasi-free exclusive reaction on the neutron $\gamma + d \rightarrow \pi^0\pi^0 + n(p)$ (filled red triangles) and the quasi-free inclusive reaction $\gamma + d \rightarrow \pi^0\pi^0 + (N)$ (filled black triangles).

The right-hand side of figure 2 illustrates the measured beam helicity asymmetries $I^{\odot}(\Phi) = 1/P_\gamma(d\sigma^+ - d\sigma^-)/(d\sigma^+ + d\sigma^-) = 1/P_\gamma(N^+ - N^-)/(N^+ + N^-)$ [4] of the quasi-free exclusive

reaction on the proton (full blue triangles) and on the neutron (full red triangles) for different regions of beam energy. The dashed lines correspond to a fit to the data.

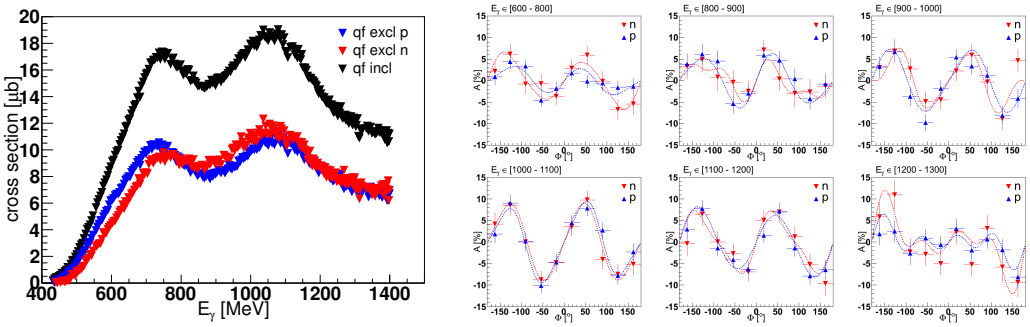

Figure 2: Very preliminary double π^0 total cross sections (left-hand side) and beam helicity asymmetries (right-hand side). The labelling is explained in the text.

3 Interpretation

The identical shape of the measured single π^0 total cross sections and the theoretical MAID [2] and SAID [3] models (see figure 1) demonstrates a correct understanding of the resonance contributions to the different reactions, i.e. mainly $D_{13}(1520)$, $F_{15}(1680)$ to single π^0 photoproduction on the proton and $D_{13}(1520)$, $D_{15}(1675)$ on the neutron. The discrepancy in absolute height between the measured single π^0 total cross sections and the theoretical models (see figure 1) can not be explained by nuclear Fermi motion. The fact that folding the theoretical models with Fermi motion does not overcome this problem reveals the importance of other nuclear effects, such as final state interactions, meson rescattering or others. This discrepancy was already earlier observed by B. Krusche *et al.* [1] and H. Shimizu [5]. H. Shimizu reported an overestimation of the data by models of $\sim 125\%$, as shown at the left-hand side of figure 3. The same level of overestimation was observed in this work, as depicted on the right-hand side in figure 3, where the models are scaled down by a factor of 0.8.

Double π^0 photoproduction is mainly used to study the properties of sequential decays since this is the dominated decay mechanism. Even though the MAID model [2] predicts a nearly identical total cross section for the production on the proton and on the neutron, the resoncance contribution to the two reactions is rather different. For example, the electromagnetic excitation of the $F_{15}(1680)$ ($D_{15}(1675)$) is predicted to be much stronger on the proton (neutron) than on the neutron (proton). For this reason one would suggest that sensitive quantities such as the beam helicity asymmetry would depend on such a coupling and hence will not be the same on the proton and on the neutron.
The measured $2\pi^0$ total cross sections on the proton and neutron (left-hand side of figure 2) show no big difference and hence confirm the predictions. However, it is rather astonishing

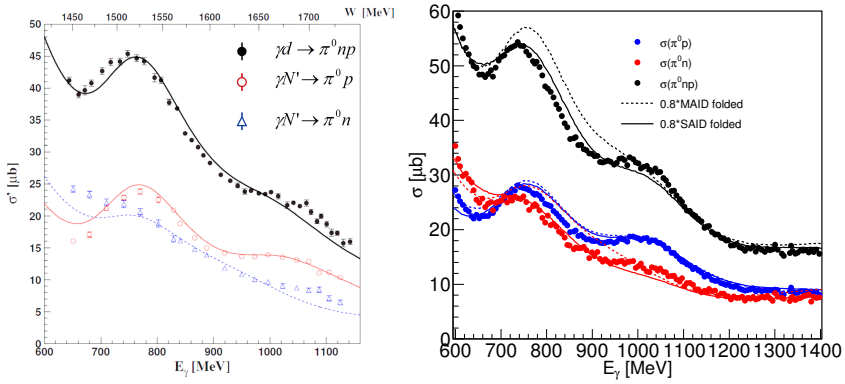

Figure 3: Quasi-free exclusive total cross sections compared to the MAID [2] and SAID [3] models scaled down by a factor 0.8. Left-hand side: H. Shimizu [5], right-hand side: This work. Note the reverted color coding on the left figure between red and blue.

that the measured beam helicity asymmetries for the proton and neutron are as well identical within the error bars. Additionally, the results on the quasi-free proton were defolded from Fermi motion and compared to published data on the free proton and are in good agreement with each other (not shown here) which indicates a correct reconstruction of the reaction. Yet, earlier works [4] also contradicted many model predictions concerning the asymmetries, therefore further input is needed in order to understand this behavior.

Acknowledgments

This work is supported by Schweizerischer Nationalfonds (SNF), Deutsche Forschungsgemeinschaft (DFG) and EU/FP6. All the work on the double π^0 channel is done by M. Oberle *et al.*.

Bibliography

[1] B. Krusche *et al.*, Eur. Phys. J. A 6 (1999) 309

[2] D. Drechsel, O. Hanstein, S.S. Kamalov and L. Tiator, Nucl. Phys. A **645** (1999) 145

[3] R. Arndt *et al.*, VPI and SU Scattering Analysis Interactive Dialin

[4] D. Krambrich, F. Zehr, A. Fix, L. Roca *et al.*, Phys. Rev. Lett. 103 (2009) 052002

[5] H. Shimizu, Slides presented at the NNR workshop 2009, June 8.-10., 2009, Edinburgh

Excited Nucleons Study at BESIII

Xiaotao Liao[1] on behalf of the BESIII Collaboration
Institute of High Energy Physics
Chinese Academy of Sciences
100049 Beijing, China

With the 106 million ψ' events collected at BESIII in 2009, the decay of $\psi' \to p\overline{p}\eta$ is studied. Partial wave analysis shows that N(1535) contributes a lot in the mass spectrum of $p\eta(\overline{p}\eta)$. The mass, width and spin-parity of N(1535) are determined to be $1.524^{+0.005+0.010}_{-0.005-0.005} GeV/c^2$, $0.130^{+0.027+0.061}_{-0.027-0.014} GeV/c^2$ and $\frac{1}{2}^-$. The decay of $\psi' \to p\overline{p}\pi^0$ is also studied.

1 Introduction

Although symmetric non-relativistic three-quark models of baryons are quite successful in interpreting low-lying excited baryon resonances, they tend to predict far more excited states than are found experimentally (missing resonance problem) [1, 2]. From the theoretical point of view, this could be due to a wrong choice of the degrees of freedom and models considering di-quarks have been proposed [3]. Experimentally, the situation is very complicated due to the large number of broad and overlapping states that are observed. Moreover, in traditional studies using tagged photons or pion beams, both isospin 1/2 and isospin 3/2 resonances are excited, further complicating the analysis.

An alternative method to investigate nucleon resonances is via decays of charmonium states such as J/ψ and ψ'. By selecting specific decay channels, such as $\psi' \to p\overline{p}\pi^0$, the N* intermediate resonance coupling to $p\pi^0$ or $\overline{p}\pi^0$ can be studied. Here, Δ resonances are excluded due to isospin conservation. As a consequence, the reduced number of states greatly facilitates the analysis [4].

N* production in $J/\psi \to p\overline{p}\eta$ was studied using partial wave analysis at BESI [5], in which two N* resonances were observed. In a recent analysis of $J/\psi \to p\overline{n}\pi^- + c.c.$ [6], a new N* resonance around $2GeV/c^2$ named $N_x(2065)$ was observed. This $N_x(2065)$ was also observed in the decay of $J/\psi \to p\overline{p}\pi^0$ [7]. The production of N(2065) in J/ψ decay is close to the edge of the phase space. Thus, a similar search for this resonance in the ψ' decays might be helpful. Here we report a study of N* resonances from $\psi' \to p\overline{p}\eta$ and $\psi' \to p\overline{p}\pi^0$ based on the 106M ψ' sample collected by the upgraded Beijing Spectrometer (BESIII), located at the Beijing Electron-Positron Collider(BEPCII) [8].

[1] liaoxt@ihep.ac.cn

2 Partial wave analysis of $\psi' \to p\overline{p}\eta$

In this analysis, only $\eta \to \gamma\gamma$ is used, which is about 40% [9] of the total statistics. In Figure 1, the left plot shows a clean η peak and the η mass cut(dashed line), and the right plot shows the dalitz plot of $M^2_{p\eta}$ versus $M^2_{\overline{p}\eta}$. The presence of N* resonance in $M_{p\eta}$ and $M_{\overline{p}\eta}$ is obvious.

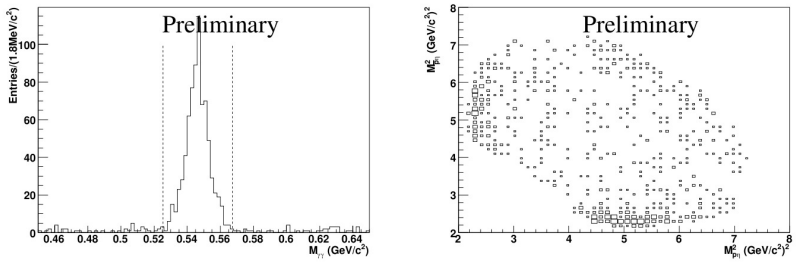

Figure 1: $M_{\gamma\gamma}$(left) and the dalitz plot of $M^2_{p\eta}$ versus $M^2_{\overline{p}\eta}$(right). Dashed lines in the left plot indicate the cut values used.

A partial wave analysis(PWA) has been done, in which the phase space decay, one 1^{--} $p\overline{p}$ resonance, and nine N* intermediate resonances: N(1440), N(1520), N(1535), N(1650), N(1700), N(1710), N(1720), N(1900), N(2080), are considered, and their mass, width, spin-parity and other parameters are taken from PDG [9]. The significance level of each resonance is studied and only N(1535) and the phase space decay are significant. Using N(1535) and the phase space decay, the PWA result agrees with the data well (Figure 2).

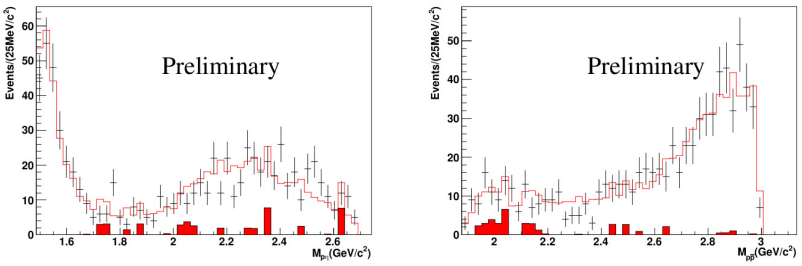

Figure 2: The invariant mass of $p\eta$(left) and $p\overline{p}$(right). The histogram is for PWA result, the error bar corresponds data, and the shaded histogram means the background from η sideband and the continuum data.

From the result of PWA, the mass and width of N(1535) are $1.524^{+0.005+0.010}_{-0.005-0.005} GeV/c^2$ and $0.130^{+0.027+0.061}_{-0.027-0.014} GeV/c^2$, where the first errors are statistical and the second are systematic. And the spin-parity is determined to be $\frac{1}{2}^-$. These are consistent with the PDG values [9]. The branching ratio of $\psi' \to p\overline{p}\eta$ is measured to be $(6.6 \pm 0.3 \pm 0.6) \times 10^{-5}$. This measure-

ment agrees with PDG value [9], but has a smaller error. The production branching ratio of ψ' to $p\overline{p}\eta$ via N(1535) is $(5.5^{+0.3+7.4}_{-0.3-1.0}) \times 10^{-5}$. This is the first measurement.

3 Study of $\psi' \to p\overline{p}\pi^0$

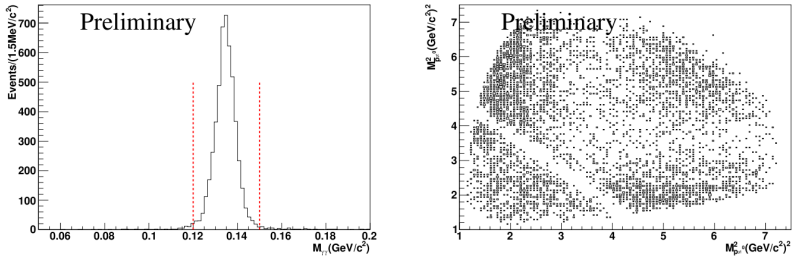

Figure 3: $M_{\gamma\gamma}$(left) and the dalitz plot of $M^2_{p\pi^0}$ versus $M^2_{\overline{p}\pi^0}$(right). Dashed lines in the left plot indicate the cut values used.The gap of the right plot is due to the cut of J/ψ decays.

This analysis has the same final states as the former decay. In Figure 3, the left plot shows the clean π^0 peak and the cut(dashed line) on its mass spectrum, and the right plot shows the dalitz plot of $M^2_{p\pi^0}$ versus $M^2_{\overline{p}\pi^0}$ which is obviously non-uniform. The mass spectra of $p\pi^0$ and $p\overline{p}$ are shown in Figure 4. Several N* peak can be seen below $1.7GeV/c^2$ from the $p\pi^0$ mass spectrum. In this analysis, $p\overline{p}$ production are excluded.

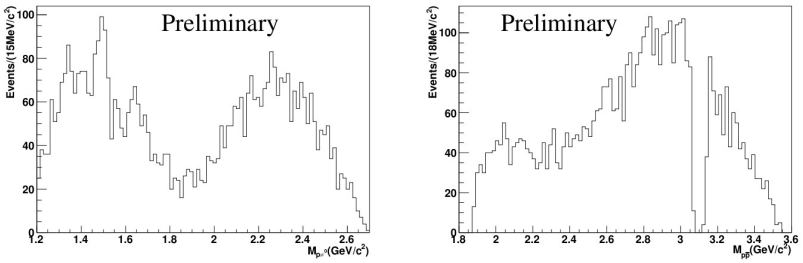

Figure 4: The invariant mass of $p\pi^0$(left) and $p\overline{p}$(right). The gap of the right plot is due to the cut of J/ψ decays.

In a recent analysis of the CLEO-c Collaboration [10], $\psi' \to p\overline{p}\pi^0$ are studied using 24.5×10^6 ψ' events. Without taking account of any possible interferences between resonances, they studied the contibution of two N* resonances N(1440) and N(2300) and two $p\overline{p}$ resonances $R_1(2100)$ and $R_2(2900)$ respect to the structures in $p\pi^0$ and $p\overline{p}$ mass spectra. In our present investigation, with almost four times of statistics than CLEO-c's analysis and also taking account of the interferences, more detailed information about intermediate states are expected. Now, the partial wave analysis of this work is ongoing.

4 Summary

In this analysis, two ψ' decay channels about excited nucleon states are reported. For these channels via charmonium decay, the reduced number of intermediate resonances due to the isospin conservation greatly facilitates the analysis. The purpose of this paper focuses on showing the way of N* study via charmonium decay at BESIII. Using this method, more analysis related to excited nucleon states could be performed with many other decay channels, such as $\psi' \to N\overline{N}$ by $N\pi\pi$(or $\overline{N}\pi\pi$) coupling. Beside of excited baryon study, this method could also be used to study excited hyperons, such as Λ^*, Σ^*, and Ξ^* states. With the accumulating of more charmonium data samples, BESIII will have a bright future at the excited nucleon study.

Acknowledgments

We would like to thank the accelerator people at BEPCII for their hard work which makes our high luminosity possible. We would also like to acknowledge the IHEP computing center for maintaining our excellent computing environment.

Bibliography

[1] S. Capstick and W. Roberts, Phys. Rev. **D 47**, 1994(1993).

[2] N. Isgur and G. Karl, Phys. Rev. **D 19**, 2653(1979).

[3] E. Santopinto et al., Phys.Rev. **C 72**, 022201(R)(2005).

[4] H. Li et al. (BES Collaboration), Nucl. Phys. **A 675**, 189c (2000).

[5] J. Z. Bai et al. (BES Collaboration), Phys. Lett. **B 510**, 75 (2001).

[6] M. Ablikim et al. (BES Collaboration), Phys. Rev. Lett. 97, 062001(2006).

[7] M. Ablikim et al. (BES Collaboration), Phys. Rev. **D 80**, 052004 (2009).

[8] M. Ablikim et al. (BES Collaboration), Nucl. Instrum. Meth. **A 614**, 345 (2010).

[9] K. Nakamura et al. (Particle Data Group), J. of Phys. **G 37**, 075021 (2010).

[10] J. P. Alexander et al. (CLEO Collaboration), Phys. Rev. **D 82**, 092002 (2010).

Process-dependent transverse momentum distributions from Lattice QCD

Bernhard U. Musch[1]
Jefferson Lab
12000 Jefferson Avenue
Newport News, VA 23606, USA

Certain single-spin asymmetries in semi-inclusive DIS (SIDIS) and the Drell-Yan process (DY) can be explained by transverse momentum dependent parton distribution functions (TMDs) that are predicted to differ in sign for SIDIS and DY. On the lattice, we can use non-local operators with U-shaped Wilson lines to study these TMDs, in particular the Sivers- and the Boer-Mulders function. We discuss the method, its limitations and preliminary results from an exploratory calculation using lattices generated by the MILC and LHP collaborations.

1 Introduction

Transverse momentum dependent parton distribution functions (TMDs) provide three-dimensional pictures of the momentum distribution of quarks inside a relativistic proton, see, e.g., chapter 2 of Ref. [1] for a recent review. TMDs enter as non-perturbative ingredients in the factorized cross section of processes like semi-inclusive deep inelastic scattering (SIDIS) or the Drell-Yan process (DY) at low transverse momentum. Due to initial state interactions (in DY) or final state interactions (in SIDIS) [2] whose theoretical explanation is deeply connected to the principle of gauge invariance, the operator definition of TMDs is to a certain extent process-dependent. This leads to the prediction that so-called naively time-reversal odd (T-odd) TMDs differ in sign for SIDIS and DY [3]. The T-odd distributions at leading twist are thought to be responsible for large single-spin asymmetries observed in experiment, see, e.g., [4]. Here we address them using lattice QCD.

In previous lattice studies of TMDs [5, 6], a simplified, "process-independent" operator geometry was chosen that does not strictly correspond to the definition of TMDs appearing in the description of SIDIS or DY, and that does not feature T-odd TMDs. Here we go beyond this simplification and show preliminary results obtained with a "process-dependent" operator geometry that may ultimately allow quantitative comparisons to experimental SIDIS or DY results.

[1] bmusch@jlab.org

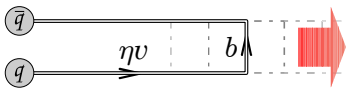

Figure 1: Geometry of the staple shaped gauge link. On the lattice, we compute the SIDIS/DY limits $\eta \to \pm\infty$ by increasing the extent of the staple step by step, as indicated by the dashed lines and the arrow.

The correlator that defines TMDs for SIDIS and DY can be written in general as

$$\Phi^{[\Gamma]} \equiv \frac{1}{2}\int \frac{d^4b}{(2\pi)^4}\, e^{ip\cdot b}\, \frac{\overbrace{\langle P,S|\ \bar{q}(0)\,\Gamma\,\mathcal{U}[0,\eta v,\eta v+b,b]\,q(b)\ |P,S\rangle}^{\equiv\, \widetilde{\Phi}^{[\Gamma]}_{\text{unsubtr.}}(b,P,S,\eta v,\mu)}}{\widetilde{\mathcal{S}}(b^2,\ldots)} \tag{1}$$

where P and S are momentum and spin of the nucleon, p is the quark momentum, Γ is a Dirac matrix and μ is a renormalization scale. Note that b corresponds to the variable l in the notation of Refs. [5,6]. The precise definition of the soft factor $\widetilde{\mathcal{S}}$ varies in different theory frameworks, see, e.g., [7–9]. However, it cancels explicitly in the quantities for which we show results.

We use light cone coordinates and consider a fast nucleon, $P_\perp = 0$, $P^+ \gg M$. Integrating over the suppressed component p^- of the intrinsic quark momentum, the decomposition of the correlator [10,11] yields

$$\int dp^-\, \Phi^{[\gamma^+]} = f_1(x,\boldsymbol{p}_T^2;\hat{\zeta},\eta,\ldots) - \frac{\boldsymbol{\epsilon}_{ij}\boldsymbol{p}_i\boldsymbol{S}_j}{m_N} f_{1T}^\perp(x,\boldsymbol{p}_T^2;\hat{\zeta},\eta,\ldots) \tag{2}$$

for a projection $\Gamma = \gamma^+$ on leading twist and for transverse nucleon polarization $\boldsymbol{S}_T$. Here f_1 and the Sivers function $f_{1T}^\perp$ [13] are the two TMDs that describe the corresponding distribution of quarks with respect to the longitudinal momentum fraction $x \equiv p^+/P^+$ and the transverse momentum $\boldsymbol{p}_T$ of the quark. The Wilson line $\mathcal{U}$ in Eq. (1) ensures gauge invariance and effectively represents gluon exchanges in initial or final state interactions. As illustrated in Fig. 1, it is composed of two parallel straight sections along the direction $v \approx \hat{n}_-$ and a gauge link bridging the (transverse) gap at the far ends. For SIDIS, the extent η of the staple is $+\infty$, while for DY the staple extends in the opposite direction, $\eta = -\infty$. The T-odd Sivers function $f_{1T}^\perp$ differs for SIDIS and DY, $f_{1T}^\perp(\eta=+\infty) = -f_{1T}^\perp(\eta=-\infty)$, while $f_1(\eta=+\infty) = f_1(\eta=-\infty)$ exhibits T-even behavior. Another leading-twist T-odd TMD is the Boer-Mulders function $h_1^\perp$ [14], which describes correlations in $\boldsymbol{p}\times\boldsymbol{s}$ of quarks polarized transversely along $\boldsymbol{s}_T$ in an unpolarized nucleon. Employing a direction v off the light cone $\hat{n}_-$ direction is one way to regularize rapidity divergences in the correlator, see, e.g., Refs. [7,15]. Taking v space-like [9,16,17] also opens up the possibility to perform lattice calculations. The TMDs obtained in this framework depend on an additional parameter, here introduced as a dimensionless quantity $\hat{\zeta} \equiv v\cdot P/\sqrt{|v^2|P^2}$. At large enough values of $\hat{\zeta}$, the $\hat{\zeta}$-dependence of TMDs can be obtained from evolution equations, see, e.g., Refs. [9,18].

Dependencies of the TMDs on further regularization or renormalization scales have been indicated by the dots and cancel in the quantities we consider.

2 Lattice calculations

In previous lattice studies of TMDs [5,6], a direct, straight gauge link $\mathcal{U}[0,b]$ was employed, corresponding to $\eta = 0$ in Eq. (1). We make use of the same lattice at $m_\pi \approx 500$ MeV [19] and the same techniques as in these earlier works, except that we now implement the staple-shaped operator geometry of Fig. 1. We also improve our statistics using the new arrangement of nucleon sources and coherent sinks of Ref. [20]. In essence, we calculate $\widetilde{\Phi}^{[\Gamma]}_{\text{unsubtr.}}(b,P,S,\eta v,\mu)$ directly for a large selection of lattice vectors $\boldsymbol{b}$, $\boldsymbol{P}$ and $\eta\boldsymbol{v}$. As before, we restrict the operator to have no extent in Euclidean time direction. Consequently, b and v can only have spatial components on the lattice. For a given lattice nucleon three-momentum $\boldsymbol{P}^{\text{lat}}$, the regularization parameter $\hat{\zeta}$ is thus limited by $\hat{\zeta} \leqslant |\boldsymbol{P}^{\text{lat}}|/M^2$. The translation of the results obtained in the lattice frame to the TMD language is established through a parametrization of $\widetilde{\Phi}^{[\Gamma]}_{\text{unsubtr.}}$ in terms of Lorentz-invariant amplitudes $\widetilde{A}_i$ and $\widetilde{B}_i$, analogously to Ref. [11] but in b-space. To be able to construct quantities where the soft factor cancels, we work with TMDs in Fourier space and their b-derivatives, see Ref. [12] for details. For a generic TMD f we define

$$\tilde{f}(x,\boldsymbol{b}_T^2) \equiv \int d^2\boldsymbol{p}_T\, e^{i\boldsymbol{b}_T\cdot\boldsymbol{p}_T}\, f(x,\boldsymbol{p}_T^2), \qquad \tilde{f}^{(n)}(x,\boldsymbol{b}_T^2) \equiv n!\left(-\frac{2}{M^2}\partial_{\boldsymbol{b}_T^2}\right)^n \tilde{f}(x,\boldsymbol{b}_T^2) \tag{3}$$

In the limit $\boldsymbol{b}_T^2 \to 0$, the latter correspond to the usual $\boldsymbol{p}_T$-moments:

$$\tilde{f}^{(n)}(x,0) = \int d^2\boldsymbol{p}_T\, (\boldsymbol{p}_T^2/2M^2)^n f(x,\boldsymbol{p}_T^2) \equiv f^{(n)}(x). \tag{4}$$

Consider the quantity $\langle \boldsymbol{p}_y\rangle_{TU}(x) \equiv M\, f_{1T}^{\perp(1)}(x)/f_1^{(0)}(x)$, which has an interpretation as the average transverse momentum in transverse y-direction carried by the quarks inside a nucleon polarized in transverse x-direction. We now show that similar quantities are accessible on the lattice. Here we restrict ourselves to x-integrated TMDs $\tilde{f}^{[1](n)}(\boldsymbol{b}_T^2) \equiv \int_{-1}^{1} dx\, \tilde{f}^{[1](n)}(x,\boldsymbol{b}_T^2)$, which can be obtained from the amplitudes at $b\cdot P = 0$:

$$\frac{1}{2}\widetilde{\Phi}^{[\gamma^+]}_{\text{unsubtr.}}\bigg|_{\substack{b\cdot P=0\\ S=0}} = P^+ \underbrace{\left(\widetilde{A}_2 + R(\hat{\zeta})\widetilde{B}_1\right)}_{\widetilde{\mathcal{S}}(b^2,\dots)\,\tilde{f}_1^{[1](0)}(\boldsymbol{b}_T^2)} - iMP^+\boldsymbol{\epsilon}_{ij}\boldsymbol{b}_i\boldsymbol{S}_j \underbrace{\left(\widetilde{A}_{12} - R(\hat{\zeta})\widetilde{B}_8\right)}_{\widetilde{\mathcal{S}}(b^2,\dots)\,\tilde{f}_{1T}^{\perp[1](1)}(\boldsymbol{b}_T^2)}, \tag{5}$$

where $R(\hat{\zeta}) \equiv 1 - (1+\hat{\zeta}^{-2})^{1/2}$. We thus can construct a ratio which looks similar to the average momentum $\langle \boldsymbol{p}_y\rangle_{TU}(x)$, but is formed from x-integrated distributions and generalized to non-zero $\boldsymbol{b}_T$, in the following called the (generalized) Sivers shift:

$$\langle \boldsymbol{p}_y\rangle_{TU}(|\boldsymbol{b}_T|) \equiv M\frac{\tilde{f}_{1T}^{\perp[1](1)}(\boldsymbol{b}_T^2)}{\tilde{f}_1^{[1](0)}(\boldsymbol{b}_T^2)} = -M\frac{\widetilde{A}_{12} - R(\hat{\zeta})\widetilde{B}_8}{\widetilde{A}_2 + R(\hat{\zeta})\widetilde{B}_1}\bigg|_{b\cdot P\,=\,0}. \tag{6}$$

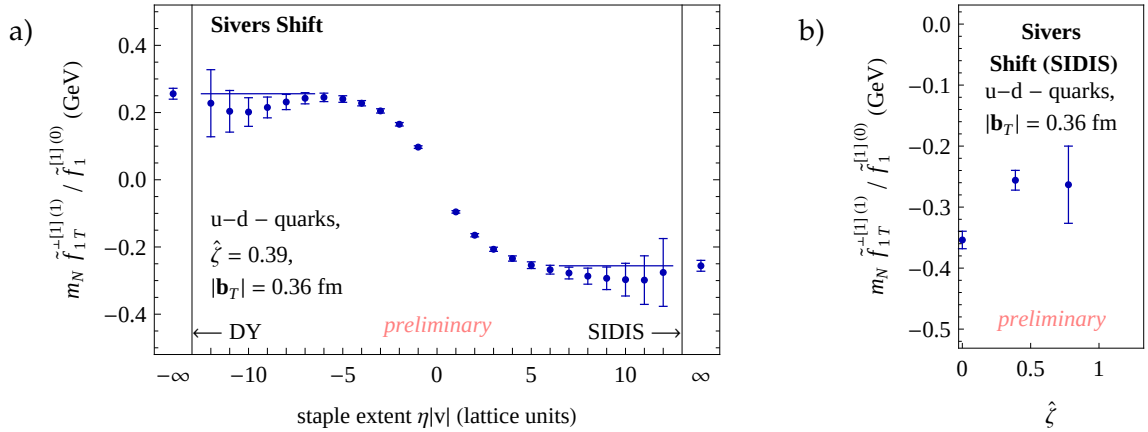

Figure 2: Generalized Sivers shift of up−down quarks (isovector) on the $20^3 \times 64$ lattice at a pion mass $m_\pi \approx 500$ MeV and a lattice spacing of $a \approx 0.12$ fm. a) results as a function of the staple extent η. A simple estimate of the SIDIS/DY values at $\eta \to \pm\infty$ is obtained from a fit of an odd but otherwise constant function to the data at $|\eta v| \geqslant 7a$. Potentially significant systematic uncertainties in this procedure have not been taken into account in this preliminary analysis. b) Extracted SIDIS results for several values of $\hat{\zeta}$.

Analogously, the "Boer-Mulders shift" can be constructed using $\tilde{h}_1^{\perp[1](1)}$ instead of $\tilde{f}_{1T}^{\perp[1](1)}$. The soft factor and multiplicative renormalization factors cancel in the above ratio. However, the dependence on the rapidity cutoff parameter $\hat{\zeta}$ (not shown in the arguments) survives. Figures 2 a) demonstrates how the SIDIS or DY Sivers shift can be read off from the plateau reached at large positive or negative η, respectively. The extraction of these asymptotic values is still preliminary and lacks an estimate of systematic errors. In Fig. 2 b), we plot the extracted SIDIS results as a function of $\hat{\zeta}$ and find indications of a strong $\hat{\zeta}$-dependence at the rather low values of $\hat{\zeta}$ presently accessible to us. A major future challenge is to generate statistically well-determined results at higher values of $\hat{\zeta}$ and to make contact with the $\hat{\zeta}$-evolution predicted by perturbative QCD.

Acknowledgments

Thanks are due to Philipp Hägler, John Negele, Andreas Schäfer and Alexei Prokudin for feedback and support, and to Harut Avakian, Vladimir Braun, John Collins, Markus Diehl, Leonard Gamberg and Dru Renner for helpful discussions. We are grateful to the LHP and MILC collaborations, for providing gauge configurations and propagators used in this work [19, 20]. Our software uses the `Chroma`-library [21], and we use USQCD computing resources at Jefferson Lab. Authored by Jefferson Science Associates, LLC under U.S. DOE Contract No. DE-AC05-06OR23177. The U.S. Government retains a non-exclusive, paid-up, irrevocable, world-wide license to publish or reproduce this manuscript for U.S. Government purposes.

Bibliography

[1] D. Boer, M. Diehl, R. Milner, R. Venugopalan, W. Vogelsang, D. Kaplan, H. Montgomery, S. Vigdor *et al.* [arXiv:1108.1713 [nucl-th]].

[2] S. J. Brodsky, D. S. Hwang and I. Schmidt, Phys. Lett. B **530**, 99 (2002)

[3] J. C. Collins, Phys. Lett. B **536**, 43 (2002)

[4] M. Anselmino *et al.*, Eur. Phys. J. A **39**, 89 (2009)

[5] Ph. Hägler, B. U. Musch, J. W. Negele and A. Schäfer, Europhys. Lett. **88**, 61001 (2009)

[6] B. U. Musch, P. Hägler, J. W. Negele and A. Schäfer, Phys. Rev. D **83**, 094507 (2011)

[7] X. d. Ji, J. p. Ma and F. Yuan, Phys. Rev. D **71**, 034005 (2005)

[8] I. O. Cherednikov and N. G. Stefanis, Nucl. Phys. B **802**, 146 (2008)

[9] S. M. Aybat and T. C. Rogers, Phys. Rev. D **83**, 114042 (2011)

[10] P. J. Mulders and R. D. Tangerman, Nucl. Phys. B **461**, 197 (1996) [Erratum-ibid. B **484**, 538 (1997)]

[11] K. Goeke, A. Metz and M. Schlegel, Phys. Lett. B **618**, 90 (2005)

[12] D. Boer, L. Gamberg, B. Musch and A. Prokudin, arXiv:1107.5294 [hep-ph].

[13] D. W. Sivers, Phys. Rev. D **41**, 83 (1990).

[14] D. Boer and P. J. Mulders, Phys. Rev. D **57**, 5780 (1998)

[15] J. C. Collins and D. E. Soper, Nucl. Phys. B **193**, 381 (1981) [Erratum-ibid. B **213**, 545 (1983)] [Nucl. Phys. B **213**, 545 (1983)].

[16] J. C. Collins and A. Metz, Phys. Rev. Lett. **93**, 252001 (2004)

[17] John C. Collins, *"Foundations of Perturbative QCD"*, Cambridge University Press (2011), ISBN 9780521855334

[18] A. Idilbi, X. d. Ji, J. P. Ma and F. Yuan, Phys. Rev. D **70**, 074021 (2004)

[19] C. Aubin *et al.*, Phys. Rev. D **70**, 094505 (2004)

[20] J. D. Bratt *et al.* [LHP Collaboration], Phys. Rev. D **82**, 094502 (2010)

[21] R. G. Edwards and B. Joo [SciDAC, LHP and UKQCD Collaborations], Nucl. Phys. Proc. Suppl. **140**, 832 (2005)

The light nuclei spin structure from hadronic channels at intermediate energies

Pavel K. Kurilkin[1,a], V.P. Ladygin[a], T. Uesaka[b], V.V. Glagolev[a], Yu.V. Gurchin[a], A.Yu. Isupov[a], K. Itoh[c], M. Janek[a,d], J.-T. Karachuk[a,e], T. Kawabata[b], A.N. Khrenov[a], A.S. Kiselev[a], V.A. Kizka[a], A.B. Kurepin[f], A.K. Kurilkin[a], V.A. Krasnov[a,f], N.B. Ladygina[a], D. Lipchinski[e], A.N. Livanov[a,f], Y. Maeda[g], A.I. Malakhov[a], G. Martinska[h], S. Nedev[i], S.M. Piyadin[a], E.B. Plekhanov[a], J. Popovichi[e], S. Rangelov[i], S.G. Reznikov[a], P.A. Rukoyatkin[a], S. Sakaguchi[j], H. Sakai[c,k], K. Sekiguchi[j], K. Suda[j], A.A. Terekhin[a,l], J. Urban[h], T.A. Vasiliev[a], and I.E. Vnukov[l]

[a] *Joint Institute for Nuclear Research, Dubna, Russia*
[b] *Center for Nuclear Study, University of Tokyo, Tokyo, Japan*
[c] *Department of Physics, Saitama University, Urawa, Japan*
[d] *Physics Department, University of Zilina, Zilina, Slovakia*
[e] *Advanced Research Institute for Electrical Engineering, Bucharest, Romania*
[f] *Institute for Nuclear Research, Moscow, Russia*
[g] *Kyushi University, Harozaki, Japan*
[h] *P.J.Safarik University, Kosice, Slovakia*
[i] *University of Chemical Technology and Metallurgy, Sofia, Bulgaria*
[j] *RIKEN (the Institute for Physical and Chemical Research), Saitama, Japan*
[k] *University of Tokyo, Tokyo, Japan*
[l] *Belgorod State University, Belgorod, Russia*

The investigation of the d, ^{3}H and ^{3}He spin structure has been performed at the RIKEN(Japan) accelerator research facility and VBLHEP(JINR) using both polarized and unpolarized deuteron beams. The experimental results on the analyzing powers studies in $dp-$ elastic scattering, d(d,^{3}H)p and d(d,^{3}He)n reactions are presented. The vector and tensor analyzing powers for $dp-$ elastic scattering at 880 and 2000 MeV are obtained at the Nuclotron(VBLHEP). The result on the analyzing powers A_y, A_{yy} of the deuteron at 2000 MeV are compared with relativistic multiple scattering model calculations. The data on the tensor analyzing powers for the d(d,^{3}H)p and d(d,^{3}He)n reactions obtained at $E_d = 200$ and 270 MeV demonstrate the sensitivity to the ^{3}H, ^{3}He and deuteron spin structure. The essential disagreements between the experimental results and the theoretical calculations within the one-nucleon exchange model framework are observed. The wide experimental program on the study of the polarization effects in $dp-$ elastic scattering, $dp-$nonmesonic breakup, d(d,^{3}He)n, d(d,^{3}H)p and d(^{3}He,^{4}He)p reactions using internal and extracted beam at Nuclotron is discussed.

[1] pkurilkin@jinr.ru

1 Introduction

The main goal of the investigation of the reaction induced by the polarized deuterons is to establish the nature of $2N$ and $3N$ forces, the role of the relativistic effects and nonucleon degrees of freedom. The last decades such investigation were performed at different experiments all over the world at RIKEN, KVI, IUCF and RCNP. This activity was stimulated by the discrepancy of 30% between the measured cross section for deuteron-proton($dp-$) elastic scattering at intermediate energies and the Faddeev calculations using modern potentials of nucleon-nucleon interaction.

2 Experimental results

The research program on the light nuclei structure investigation at the Nuclotron includes experiments using both internal and extracted polarized deuteron beams.
The study of the energy dependence of polarization observables for the $dp-$ elastic scattering and deuteron breakup reaction are conducted at internal target station(ITS) setup. A detailed description of the experiment can be found in [1].
The deuteron analyzing powers measurements in dp- elastic scattering have been performed at ITS using polarized beam from polarized ion source (PIS) POLARIS at the energies 880 and 2000 MeV. The beam polarization measurement has been performed at 270 MeV where the precise data on the tensor and vector analyzing powers exist.
The results on the angular dependence of the vector A_y and tensor A_{yy} analyzing powers in $dp-$ elastic scattering at 2000 MeV are shown in Figures 1 and 2, respectively. The data obtained at Argonne National Laboratory(ANL) are presented by the solid symbols. Open squares and circles are the data obtained at the ITS and at hydrogen bubble chamber at JINR, respectively. The dashed and solid lines are the results of the relativistic multiple scattering model calculations [2] with and without of the double scattering term. The full calculations are in a reasonable agreement with the data.

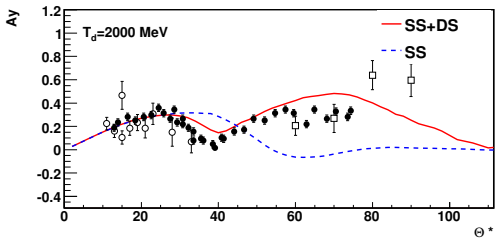

Figure 1: Vector A_y analyzing power in dp-elastic scattering at 2000 MeV. The symbols and curves are explained in the text.

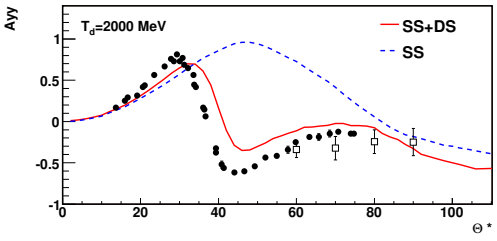

Figure 2: Tensor A_{yy} analyzing power in dp-elastic scattering at 2000 MeV. The symbols and curves are the same as in Figure 1.

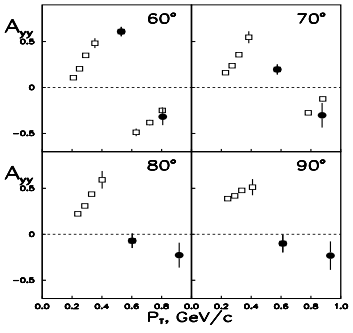

Figure 3: Tensor A_{yy} analyzing power in dp-elastic scattering obtained at the fixed angles of 60°, 70°, 80° and 90° in cms as a function of transverse momentum p_T. The symbols are explained in text.

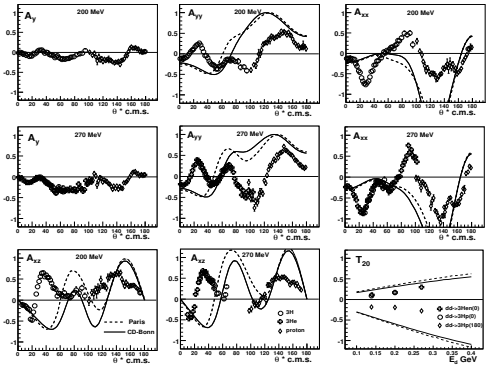

Figure 4: The analyzing powers data in d(d,^3He)n and d(d,^3H)p at 200 and 270 MeV. The curves are the calculation within one-nucleon-exchange approximation.

The dependencies of the tensor A_{yy} analyzing power in $dp-$ elastic scattering obtained at the fixed angles of 60°, 70°, 80° and 90° in the cms as a function of transverse momentum p_T are shown in Figure 3. The open and solid symbols represent the data obtained at RIKEN, Saclay, ANL and at the Nuclotron, respectively. It would be interesting to extend the range of the measurements to larger p_T, where the manifestation of non-nucleonic degrees of freedom is expected.

Figure 4 presents the analyzing powers results in the d(d,^{3}H)p and d(d,^{3}He)n reactions obtained at RARF(RIKEN, Japan) at 200 and 270 MeV. The details of the experiment can be found in [3]. The solid and long-dashed curves are the result of ONE calculations using CD-Bonn and Paris deuteron and ^{3}He wave function, respectively. One can see that ONE calculations are in the qualitative agreement with the data on the T_{20}. The analyzing powers behaviors are not reproduced by ONE model. The reason of this discrepancy can be in the inadequate description of the $3N$-bound state spin structure and/or more complicated reaction mechanism. The multiple scattering calculations are in progress now.

3 Future plans

Future plans of DSS (Deuteron spin structure) - collaborations in spin studies are related with the construction of new polarized deuteron source. The energy scan of the $dp-$elastic scattering observables and measurements of the analyzing powers in $dp-$ nonmesonic breakup will be done using internal target and polarized deuteron beam from new PIS. The $dp-$elastic scattering and $dp-$nonmesonic breakup cross section measurements can be done with the current unpolarized ion source as the first step. The $dp-$nonmesonic breakup reaction will be investigated at ITS at the Nuclotron using $\Delta E - E$ techniques for the de-

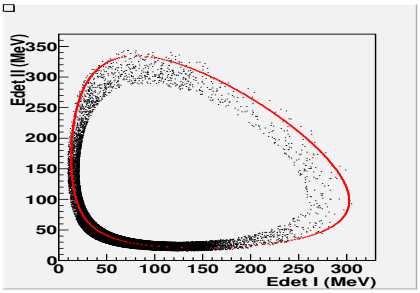

Figure 5: The correlation of the $\Delta E + E$ information from 2 proton detectors in case the dp-breakup reaction investigation at 500 MeV. $\Theta_1 = 34^\circ$, $\Theta_2 = 29.8^\circ$, $\phi_{12} = 180^\circ$

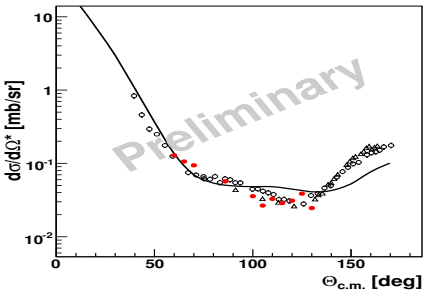

Figure 6: The results on the angular dependence of the dp-elastic cross section obtained at 880 MeV at Nuclotron in March 2011. World data at 850 MeV and 940 MeV are marked by the open triangles and circles, respectively.

tection of two final protons. Figure 5 presents the correlation of the $\Delta E - E$ information from 2 proton detectors. A kinematic relation are shown by the solid line. The preliminary results on the angular dependence of the $dp-$elastic scattering cross section obtained at 880 MeV at the Nuclotron in March 2011 are presented in Figure 6 by the solid symbols. They are compared with experimental data obtained at 850 MeV and 940 MeV given by the open triangles and circles, respectively. Solid line are the result multiple scattering model calculations [2].

The first line experiment with the extracted polarized deuteron beam for new PIS is the spin observables study for the $^3H(d,p)^4He$ reaction at the energies 1.0-1.75 GeV, where the contribution from the deuteron D-state is expected to reach the maximum.

New experimental data will ensure the important information about the light nuclei spin structure at short internucleonic distances, where the relativistic effects and 3N forces play an important role.

Acknowledgments

The work was supported in part by the RFBR under Grant $N^\circ 10-02-00087a$.

Bibliography

[1] T. Uesaka, V.P. Ladygin *et al.*, Phys. Part. Nucl. Lett., **3**, 305, (2006)

[2] N. B. Ladygina, Eur. Phys. J., **A44**, 91, (2009).

[3] M. Janek *et al.*, Eur. Phys. J. **A33**, 39, (2007).

A pivotal year for Generalized Parton Distributions

Hervé Moutarde[1,a], J. Ball[a], G. Charles[a], B. Moreno[a], F. Sabatié[a], and S. Procureur[a]
[a] *IRFU/Service de Physique Nucléaire, CEA, Centre de Saclay, F-91191 Gif-sur-Yvette, FRANCE*

The field of Generalized Parton Distribution (GPD) benefited from a wealth of exclusive reactions measurements since 2000. Extraction of GPDs from observables has begun with this first generation of experiments. In the short and mid-term future the programs of COMPASS-II and JLab at 12 GeV will enlarge the existing kinematic domain and open an era of high-precision measurements. Tools for phenomenological analysis are being developed at the same time and will be mature to handle these forthcoming measurements. In the long-term future the EIC project will allow an ambitious spin program in the small to intermediate x_B domain.

1 Introduction

The Deeply Virtual Compton Scattering (DVCS) process was early recognized as the cleanest way to access Generalised Parton Distributions (GPD) and has been so far a very active field of research. However a flavour separation of GPDs will require Deeply Virtual Meson Production (DVMP) measurements (see reviews [1–4] and references therein).

One of the goals of this program is imaging the nucleon in 3d. Present observables may already be fit, giving indications on the actual sensitivity of observables to GPDs and hints to elaborate robust extracting methods.

The first section is a brief reminder. The second part outlines some results of the extraction of GPDs as of 2011. The last section mentions promising future prospects.

2 DVCS at leading twist and leading order

Four GPDs H, E, $\tilde{H}$ and $\tilde{E}$ describe DVCS at leading twist and leading order, but the cross section depend on the Compton Form Factors (CFF) $\mathcal{H}$, $\mathcal{E}$, $\tilde{\mathcal{H}}$ and $\tilde{\mathcal{E}}$ (see ref. [5]). The GPDs depend on the generalised Bjorken variable [5] ξ (or equivalently on the standard Bjorken variable x_B), the virtuality of the initial photon Q^2 and the square momentum transfer between initial and final protons t. The CFFs are convolutions along the variable x of GPDs

[1] herve.moutarde@cea.fr

with known kernels. This integration kernel yields a real and an imaginary part to a CFF. They are related by fixed-t dispersion relations [6,7] involving a subtraction constant related to the D-term [8]. However the D-term is poorly known and most of DVCS measurements were made in the region $\xi \leqslant 0.5$. Using dispersion relations thus rely on models and may introduce biases in the extraction of GPDs from DVCS data. For that reason the real and imaginary parts of CFFs are taken as independent in some fitting procedures.

3 Status of GPD analysis

3.1 Counting degrees of freedom

The problem consists in extracting four functions H, E, $\tilde{H}$ and $\tilde{E}$ of three variables[2] x, ξ and t for each quark flavour (u, d and s). The knowledge of these functions should provide us Parton Distribution Functions (PDF) and Form Factors (FF). A naive counting quickly shows that building a flexible yet robust GPD parametrization is very involved because the number of free parameters has to remain low to keep the fit tractable and the numerics under control.

3.2 Local fits

This approach is detailed in ref. [9] and assumes the independence of the real and imaginary parts of CFFs. The mains assumptions are the validity of the twist-2 analysis of existing DVCS measurements and a negligible contribution of $\mathrm{Im}\,\tilde{\mathcal{E}}$. Each kinematic bin (x_B, t, Q^2) is taken independently of the others, and the seven values $\mathrm{Re}\,\mathcal{H}$, $\mathrm{Im}\,\mathcal{H}$, $\mathrm{Re}\,\mathcal{E}$, $\mathrm{Im}\,\mathcal{E}$, $\mathrm{Re}\,\tilde{\mathcal{H}}$, $\mathrm{Im}\,\tilde{\mathcal{H}}$ and $\mathrm{Re}\,\tilde{\mathcal{E}}$ are extracted simultaneously. Nothing prevents large fluctuations between two neighbouring kinematic bins. In the following we will refer to these fits as *local fits*.

The model-dependence is almost as low as possible but the problem is often ill-posed because the harmonic structure of a given observable (*e.g.* a BSA) at fixed kinematic usually depends on less than 7 parameters. Thus it is mandatory to combine different observables on the same kinematic bins (for example BSAs and Target Spin Asymmetries (TSA) or Beam Charge asymmetries (BCA)) and to assume boundaries for the values the CFFs may take.

3.3 Global fits

In the spirit of the work done on PDFs and FFs, *global fits* require a physically motivated parametrization of GPDs and deal with all observables on all kinematic bins at once.

The free coefficients entering the expressions for GPDs are determined either from PDFs and FFs or from DVCS data. Two such studies have been reported so far for DVCS. In the

[2] We omit the Q^2-dependence which is governed by the QCD evolution equations.

first case [10] all DVCS measurements on an unpolarized target are included in the fit in a (mostly) H-dominant framework. Fixed-t dispersion relations are used as a key ingredient. In the second case [11] CLAS and HERMES measurements are used in the fit, and JLab Hall A data are computed as a prediction of the fitting Ansatz ; all four GPDs H, E, $\tilde{H}$ and $\tilde{E}$ are described.

The extrapolation outside the physical region (for example the interesting limits $t \to 0$ or $\xi \to 0$) is possible but an assessment of the parametrization uncertainties is a complex task in itself.

3.4 Hydrid : Local / global fits

This *hydrid* fitting procedure [12] is a combination of the previous two methods and has been applied with the main assumption of H-dominance and twist-2 accuracy. It involves a parametrization with the minimal properties : smoothness, leading order Q^2 evolution and polynomial parametrization. Since the functional is otherwise arbitrary, it is *a posteriori* validated by the quality of the fit.

The model dependence is tested by a systematic comparison to local fits and an estimate of the systematic error induced by the H-dominance hypothesis. The good agreement of the two methods (local fits vs global fits) is a necessary consistency check of this approach. The treatment of systematic errors is however a weak point since there is no rigorous procedure to evaluate them and only estimates are given using joint models and fits.

3.5 Neural networks

Neural network fits had been successfully performed for PDFs but their use for GPD extraction is quite recent. First results are described in [13] within the H-dominance assumption. It is worth noting that it is a new development in the field of GPD extraction. It is hoped it will allow better estimates of errors when extrapolating outside the fitting domain.

3.6 Key results

To our knowledge, the first extraction of a combination of GPDs was made in [14] and the progress have been continuous so far. The different methods all agree on the following key results :

- Dominance of twist 2 and validity of a GPD analysis of DVCS data. This is no trivial result considering the low Q^2 range accessible in Hermes and JLab kinematics.
- $\mathrm{Im}\,\mathcal{H}$ is the best determined quantity with an overall fair agreement between all estimates. However large uncertainties subsist on $\mathrm{Re}\,\mathcal{H}$.

- There are already some indications about the invalidity of the H-dominance hypothesis even with the experimental statistical accuracy achieved so far.

3.7 A trivial universality check

Since GPDs have been modelled or extracted from DVCS and DVMP measurements, it is natural to check if these objects are identical. Although far from a satisfactory treatment of the universality question, as a first step we can take GPDs obtained in DVMP studies, predict DVCS observables and compare them to existing measurements. The predictions of the Kroll - Goloskokov model (see [15] and references therein) are depicted in Fig. 1 (left). In spite of the fair agreement between this model and the extracted values of $\mathcal{H}$, the resulting DVCS prediction tends to overshoot the data. This is reminiscent of the current version of the VGG GPD model [1].

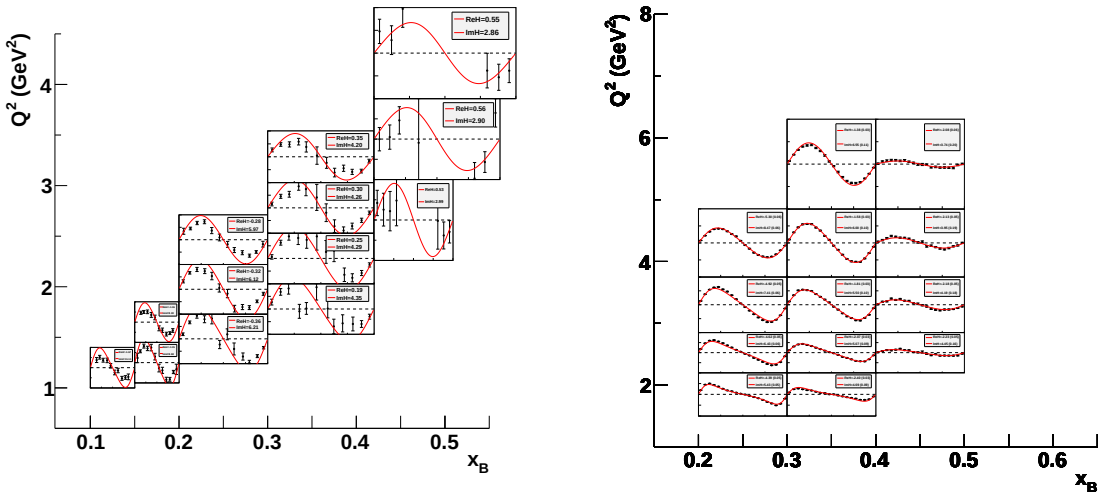

Figure 1: Measured CLAS BSAs for $-0.4 < t < -0.2$ GeV^2. The red lines correspond to the prediction of the Kroll - Goloskokov GPD model (left). Projected CLAS12 BSAs for $-0.35 < t < -0.25$ GeV^2. Statistical errors are smaller than data point bullets. The red lines correspond to a fit of the data. (right)

4 Prospects

4.1 Facilities and projects

In 2012 COMPASS-II will start running its GPD program, giving access to several observables with beam spin and charge differences, in between the kinematic domain of collider

and fixed-target experiments.

By 2015 JLab's 12 GeV upgrade will reach a time of high-precision measurements with an expected few percent accuracy. See Fig. 1 (right) for projected data and a tentative fit. Despite an apparent agreement, the high accuracy of the data does not allow a fit assuming H-dominance any more.

The science case for an electron-ion collider (EIC) has been developed since 2010 [16]. In the 2020 decade we expect to produce a wealth of GPD related spin observables (see projected data in Fig. 2) with the aim of imaging the sea quark and gluon content of the nucleon.

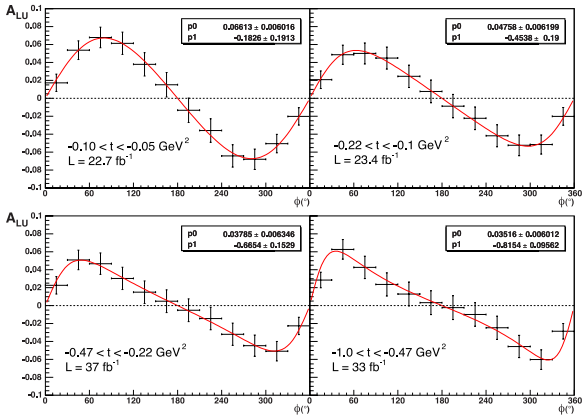

Figure 2: Photon electroproduction beam spin asymmetries for the 20 × 250 EIC configuration, in the typical kinematic bin: $1.58 \cdot 10^{-3} < x_B < 2.51 \cdot 10^{-3}$, $3.16 < Q^2 < 5.61$ GeV^2 for four different t-bins as shown on each plot. Up to about 3 months of beam time with 50% efficiency is necessary to achieve reasonable statistics in some of the bins.

4.2 Phenomenological tools for GPD analysis

A software platform is being developed to handle the phenomenological analysis of past and forthcoming data. It contains a database of experimental results, a database of theoretical predictions, a fitting engine and a visualizing software to compare measurements and model expectations. Modularity is a key-issue of the design : the same libraries are used to extract GPDs from measurements and to design new experiments connected to experimental descriptions and event generators.

5 Conclusions

During the 2000s GPD studies have made tremendous progress, with important measurements and encouraging first results on the extraction of GPDs. However a robust and efficient fitting strategy for DVCS and DVMP is still needed.

The 2010s will be very exciting times for GPDs : new facilities, high-precision measurements and bigger kinematic domains will constrain the phenomenology of GPDs. To this end a platform dedicated to global GPD analysis is currently under development.

Acknowledgments

The author would like to thank S. Goloskokov, P. Guichon, P. Kroll, K. Kumerički, D. Müller and K. Passek-Kumerički for many fruitful and stimulating discussions. The author also thanks the organizers of the 14th International Conference on Hadron Spectroscopy held in Munich (June 13 -June 17, 2011). This work was supported in part by the Commissariat à l'Energie Atomique and the GDR n° 3034 Physique du Nucleon.

Bibliography

[1] K. Goeke, M.V. Polyakov and M. Vanderhaeghen, Prog. Part. Nucl. Phys. **47**, 401 (2001).

[2] M. Diehl, Phys. Rept. **388**, 41 (2003).

[3] A.V. Belitsky and A.V. Radyushkin, Phys. Rept. **418**, 1 (2005).

[4] S. Boffi and B. Pasquini, Riv. Nuovo Cim. **30**, 387 (2007).

[5] A.V. Belitsky, D. Mueller and A. Kirchner, Nucl. Phys. B **629**, 323 (2002).

[6] I.V. Anikin and O.V. Teryaev, Phys. Rev. D **76**, 056007 (2007).

[7] M. Diehl and D.Yu. Ivanov, Eur. Phys. J. C **52**, 919 (2007).

[8] M.V. Polyakov and C. Weiss, Phys. Rev. D **60**, 114017 (1999).

[9] M. Guidal, Eur. Phys. J. A **37**, 319 (2008).

[10] K. Kumerički and D. Mueller, Nucl. Phys. B **841**, 1 (2010).

[11] G.R. Goldstein, J. Osvaldo Gonzalez Hernandez and S. Liuti, Phys. Rev. D **84** 034007 (2011).

[12] H. Moutarde, Phys. Rev D **79**, 094021 (2009).

[13] K. Kumerički, D. Müller and A. Schäfer, JHEP **1107**, 073 (2011).

[14] C. Muñoz Camacho *et al.*, Phys. Rev. Lett. **97**, 262002 (2006).

[15] S. Goloskokov and P. Kroll, Eur. Phys. J. C. **65**, 137 (2010).

[16] D. Boer *et al.*, Report of the joint BNL/INT/JLab program on the science case for an Electron-Ion Collider, Sept. 13 to Nov. 19, 2010, Institute for Nuclear Theory, Seattle.

COMPASS — a facility to study QCD

Eva-Maria Kabuß[1] on behalf of the COMPASS Collaboration
Institut für Kernphysik
Johannes-Gutenberg-Universität Mainz
D-55099 Mainz, Germany

An overview on the new COMPASS II experimental programme is presented. The main topics include a study of Primakoff reactions, generalised parton distributions via deeply virtual Compton scattering and transverse momentum dependent distributions in Drell-Yan processes in the pion scattering off polarised protons. Moreover, the studies of semi-inclusive deep inelastic scattering on unpolarised target will be continued.

1 Introduction

The COMPASS experiment [1] uses the unique CERN SPS M2 beamline that is able to deliver high-energy hadron and polarised muon beams. The COMPASS apparatus [2] consists of a high-resolution two stage forward spectrometer and a versatile target section allowing to use polarised and unpolarised targets for the various physics programmes. Up to now measurements were performed to study the longitudinal and transverse spin structure of the nucleon in polarised muon-nucleon scattering as well as meson spectroscopy and Primakoff reactions using negatively and positively charged hadron beams.

Recently, the COMPASS II proposal [3] was submitted to improve the knowledge of the momentum structure of the nucleon towards a three dimensional picture. For this a series of new measurements is planned. A study of generalised parton distributions (GPD) will be done in exclusive reactions like deeply virtual Compton scattering (DVCS) and deeply virtual meson production (DVMP) [4, 5]. In parallel the study of flavour separation and hadron fragmentation in semi-inclusive deep inelastic scattering (SIDIS) will be continued. Drell-Yan processes will be used for a complementary study of transverse momentum dependent distributions (TMD) using a transversely polarised target [6]. At very low momentum transfers Primakoff reactions can be used to extract pion and kaon polarisabilities. The COMPASS II proposal was approved on December 2010 for an initial data taking of three years.

[1] emk@kph.uni-mainz.de

2 Primakoff reactions

Chiral perturbation theory allows to predict the low energy behaviour of Compton scattering off pions and kaons [7]. The deviation from the response of a pointlike particle is parametrised in first order by the polarisabilities α and β in terms of $\alpha - \beta$ and $\alpha + \beta$. Although a number of measurements, mainly for $\alpha_\pi - \beta_\pi$, were performed no firm conclusion could be drawn on the comparison to the chiral prediction for $\alpha_\pi - \beta_\pi = 5.70 \pm 1.0 \cdot 10^{-4}$ fm^3 [8],

One of the unique features at COMPASS is the availability of pion and muons beams, where pointlike muons can be used for comparison and systematic studies. Switching between muon and pion beams is possible within few hours. Exploratory measurements were performed in 2004 and 2009 to establish the feasibility and to study the achievable systematic uncertainties in such measurements. With a total measurement time of about 120 d (90 d for π and 30 d for μ, planned in 2012) a statistical precision of $\alpha_\pi - \beta_\pi$ of $0.7 \cdot 10^{-4}$ fm^3 is expected. In addition, $\alpha_\pi + \beta_\pi$ as well as higher order terms will be accessible. The small kaon component in the negatively charged hadron beam will allow a first measurement of the kaon polarisability. Reactions with one or two neutral pions instead of a photon in the final state will allow to investigate the chiral anomaly and get further insight into chiral dynamics. [8].

3 GPD measurements

Generalised parton distributions provide a unified description of form factors and parton distributions and allow transverse imaging of the nucleon [9]. Two of them, GPD H and E, can be studied in DVCS using unpolarised and transversely polarised targets while all four GPDs, H, E, $\tilde{H}$ and $\tilde{E}$ can be accessed in DVMP. GPD H and E allow also to study the total angular momentum carried by quarks inside the nucleon [10].

The measurements will exploit the availability of 160 GeV $\mu^\pm$ beams with opposite polarisation scattering off a liquid hydrogen target in the initial phase. For a later stage also a transversely polarised NH_3 target is under consideration. The experiment will cover a unique kinematic range at intermediate values of the Bjorken scaling variable x_{Bj} ($0.01 < x_{\mathrm{Bj}} < 0.1$), a region not yet covered by any other experiment. In this kinematic range the Bethe-Heitler process is a competing process. Being well known it can serve as a reference process. GPDs will be studied measuring the so called "beam charge and spin" difference and sum which allow to extract the real and imaginary part of GPD H from the obtained Compton amplitudes. The t dependence of the DVCS cross section can be parametrised as $\frac{\mathrm{d}\sigma}{\mathrm{d}t} \sim \exp(-B(x_{\mathrm{Bj}})|t|)$. Figure 1 (left) shows the projected statistical accuracy using two years of data taking for a measurement of the x_{Bj} dependence of the t slope parameter B of the DVCS cross section for two values of the slope parameter α'

with $B(x_{\mathrm{Bj}}) = B_0 + 2\alpha' \log(x_0/x_{\mathrm{Bj}})$. At small x_{Bj}, B can be related to the transverse size of the nucleon $< r_\perp^2(x_{\mathrm{Bj}}) > \approx 2B(x_{\mathrm{Bj}})$.

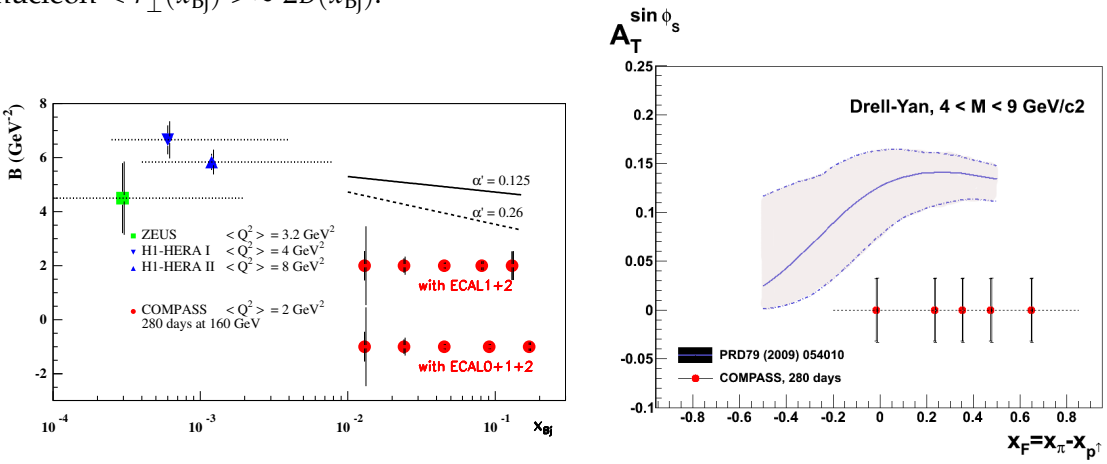

Figure 1: Projections for the statistical accuracy of (left) the slope parameter $B(x_{\mathrm{Bj}})$ of the DVCS cross section for $1 < Q^2/(\mathrm{GeV}/c)^2 < 8$; also shown are published data with a similar Q^2, (right) the Sivers asymmetry for two years of data taking compared to the prediction of [11] for the high mass region.

For these measurements the COMPASS spectrometer has to be upgraded with a 2.5 m long liquid hydrogen target, a 4 m long recoil proton detector and hermetic coverage with electromagnetic calorimetry. The feasibility of the measurement was studied in several test measurements, the latest in 2009 which showed a clear DVCS signal at high x_{Bj}. A first data taking with the full set-up is planned for the end of 2012.

In parallel to the DVCS and DVMP measurements the study of SIDIS will be continued. The main aim is to improve the knowledge on fragmentation functions, especially for strange quarks, and to constrain the strange quark distribution. Due to the large amount of data, detailed studies of the dependence on several kinematic variables like x_{Bj}, z, Q^2 and p_T for hadron multiplicities will be possible, which will also provide high precision inputs to NLO pQCD analyses. Moreover, the study of TMDs in unpolarised SIDIS off protons will complement the previous measurements with the COMPASS polarised ^{6}LiD target.

4 Drell-Yan measurements

Complementary aspects of the nucleon can be studied with TMDs. They provide a dynamic picture using the intrinsic transverse momentum of partons inside the nucleon. Previously COMPASS had access to e.g. the Sivers TMD and the Boer-Mulders TMD in SIDIS off transversely polarised targets. In these measurements TMDs are convoluted with fragmentation functions. An alternative approach is offered by Drell-Yan processes. Here a convolution of

two TMDs from the projectile and the target is studied. Such data will allow a test of the factorisation ansatz: the sign of the Sivers and Boer-Mulders functions are expected to be opposite in DY and SIDIS.

The measurements will be done using a 190 GeV pion beam impinging of the transversely polarised COMPASS NH_3 target. In the final state a pair of oppositely charged muons will be selected using a new dimuon trigger system. To reduce the high hadron background an absorber will be placed downstream of the target which also contains a tungsten plug to absorb the non-interacting beam. The dominant process is the annihilation of a valence anti-quark from the pion with an valence quark from the proton. The combinatorial background can be estimated using like-sign muon pairs. Muon pairs in the mass range of $(4 \leqslant M_{\mu\mu}/(\mathrm{MeV}/c^2) \leqslant 9)$ will be used to extract the signal as the estimated background is very small in this region. In two years of data taking 230000 high mass DY events are expected. In Fig. 1 (right) the achievable statistical accuracy for the Sivers asymmetry is compared to a recent theoretical prediction [11].

Acknowledgments

This work was supported by the Bundesministerium für Bildung und Forschung (Germany).

Bibliography

[1] COMPASS collaboration, Proposal, CERN-SPSLC 96-14, SPSC/P 297, March 1996.

[2] COMPASS, P. Abbon *et al.*, Nucl. Instr. Meth. A **577** (2007) 455.

[3] COMPASS collaboration, COMPASS II proposal, CERN-SPSC-2010-014, SPSC-P-340, May 2010.

[4] D. Mueller et al., Fortsch. Phys. **42** (1994) 101.

[5] A.V. Radyushkin, Phys. Lett. B **385** (1996) 333; Phys. Rev. D **56** (1997) 5524.

[6] S. Arnold *et al.*, Phys. Rev. D **79** (2009) 034005.

[7] J. Gasser *et al.*, Ann. Phys. **158** (2006) 84.

[8] N. Kaiser, J. Friedric, Eur. phys. J A36 (2008) 181.

[9] M. Burkardt, Phys. Rev. D **62** (2000) 071503, erratum-ibid. D **66** (2002) 119903

[10] X. Ji, Phys. Rev. Lett. **78** (1997) 610; Phys. Rev. D **55** (1997) 7114.

[11] M. Anselmino *et al.*, Phys. Rev. D **79** (2009) 054010.

The $K^- d \to \Lambda(1405) n$ reaction with the DAFNE set up and the $\overline{K}NN$ system revisited

Eulogio Oset[a], D. Jido[b], T. Sekihara[b], M. Bayar[a], and J. Yamagata-Sekihara[a]
[a]*Departamento de Física Teórica and IFIC, Centro Mixto Universidad de Valencia-CSIC, Institutos de Investigación de Paterna, Aptdo. 22085, 46071 Valencia, Spain*
[b]*Yukawa Institute for Theoretical Physics, Kyoto University, Kyoto 606-8502, Japan*

The K^- induced production of $\Lambda(1405)$ in the $K^- d \to \pi\Sigma n$ reaction is investigated having in mind the conditions of the DAFNE facility at Frascati. We find that the fastest kaons from the decay of the ϕ at DAFNE are well suited to see this resonance if one selects forward going neutrons in the center of mass, which reduce the contribution of single scattering and stress the contribution of the double scattering where the signal of the resonance appears clearer. We take advantage to report briefly on a recent work in which in addition to the $\overline{K}NN$ system with total spin S=0, we find a less bound state (although with equally large width) with S=1, like in the $K^- d$ reported in the first part.

1 Introduction

In a recent paper [1] we reported on the interest of the $K^- d \to \pi\Sigma n$ reaction, which was measured in [2]. The idea is that the K^- scatters with a neutron, loses energy and can interact with the proton to produce the $\Lambda(1405)$. In this way the production of the resonance is induced by a K^- and this guarantees that the state excited if mostly the one appearing at higher energy and narrow, out of the two $\Lambda(1405)$ states found in [3]. One of the conditions for the success of the experiment was to use kaons in flight. The reason is that the process that shows clearly the resonance peak is the double scattering. If the kaon is away from threshold, the dominant one body scattering is far away of the resonance region and peaks at higher energies. At lower energies of the kaon, the peak of the one body collision appears close to threshold and blurs the signal of the $\Lambda(1405)$ coming from double scattering. The DAFNE conditions, where the kaons come from the decay of the ϕ, produce low energy kaons. Yet, we have found in [4] that, in spite of the low momenta of the kaons, one can still see the good signal for the resonance, but on the condition that neutrons are detected simultaneously in the forward direction in the CM, which drastically reduces the background from single scattering. Since we are working with the $K^- d$ reaction, we also report on recent results from [5], where in addition to the $\overline{K}NN$ system with total spin S=0, reported in several theoretical works [6–8], we find a less bound state (although with equally large width) with S=1.

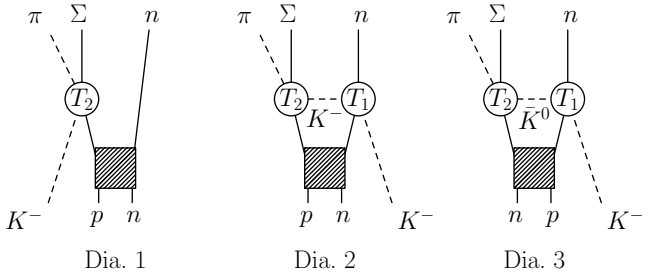

Figure 1: Diagrams for the calculation of the $K^- d \to \pi\Sigma n$ reaction. T_1 and T_2 denote the scattering amplitudes for $\overline{K}N \to \overline{K}N$ and $\overline{K}N \to \pi\Sigma$, respectively.

2 The formalism

The $\mathcal{T}$ matrix for the $K^- d \to \pi\Sigma n$ reaction is given by the sum of the contribution of the three diagrams of fig. 1, $\mathcal{T} = \mathcal{T}_1 + \mathcal{T}_2 + \mathcal{T}_3$, where the different amplitudes are given by

$$\mathcal{T}_1 = T_{K^- p \to \pi\Sigma}(M_{\pi\Sigma})\, \varphi(\vec{p}_n - \frac{\vec{p}_d}{2}). \tag{1}$$

$$\mathcal{T}_2 = T_{K^- p \to \pi\Sigma}(M_{\pi\Sigma}) \int \frac{d^3q}{(2\pi)^3} \frac{\tilde{\varphi}(\vec{q} + \vec{p}_n - \vec{k} - \frac{\vec{p}_d}{2})}{q^2 - m_K^2 + i\epsilon} T_{K^- n \to K^- n}(W_1)\,. \tag{2}$$

$$\mathcal{T}_3 = -T_{\overline{K}^0 n \to \pi\Sigma}(M_{\pi\Sigma}) \int \frac{d^3q}{(2\pi)^3} \frac{\tilde{\varphi}(\vec{q} + \vec{p}_n - \vec{k} - \frac{\vec{p}_d}{2})}{q^2 - m_K^2 + i\epsilon} T_{K^- p \to \overline{K}^0 n}(W_1)\,. \tag{3}$$

with $\varphi(\vec{p}_n - \frac{\vec{p}_d}{2})$ the deuteron wave function in momentum space and

$$q^0 = M_N + k^0 - p_n^0\,, \tag{4}$$

$$W_1 = \sqrt{(q^0 + p_n^0)^2 - (\vec{q} + \vec{p}_n)^2}\,. \tag{5}$$

For q^0 we have assumed that the deuteron at rest has energy $2M_N - B$, and we have taken half of it for one nucleon, neglecting the small binding energy. The variable W_1 depends, however, on the running $\vec{q}$ variable.

In fig. 2 we show the results for the cross sections for different intervals of neutron angle with respect to the original K^- in the center of mass frame. We find that when the angles are chosen small the signal of the resonance appears neatly, because the condition of the

neutron detection in coincidence has drastically reduced the contribution form the single collision. We have checked that even with the small signal that we find the cross sections are sufficiently large to be measure at DAFNE, collecting data for a few months while other experiments are running at the same time [9]

3 The $\overline{K}NN$ system in S=1

In several papers it has been reported that there is a bound state of $\overline{K}NN$ with S=0 [6–8]. They use different techniques to get the state, Faddeev equations in [6,7] and a variational calculation in [8]. In all cases they looked for the most bound state [8] or explicitly for the S=0 state, for which one has reasons that it is the most bound state. The S=1 system was not looked at. Ina recent paper [5], this system has been studied, together with the S=0 one, by means of the Fixed Center Approximation to the Faddeev equations, and it has been found that indeed, the S=0 state is the most bound. Upon changing the size of the NN system to agree with the results of [8], we find that the results for the S=0 system are very similar to those of [8], which uses the same input from the chiral Lagrangians, with a binding energy around 40 MeV, and a width without consideration of K^- absorption of 50 MeV. However, we also find a system bound with S=1, like one would have for $K^- d$ in s-wave, as we have studied in the first part. However, this state is less bound than the one for S=0, only about 27 MeV and a similar width. Interesting as these results re, we should keep in mind that the experimental finding of such states, is certainly difficult, since the width is larger than the binding energy, Our finding now that there is a lower sate with a different spin, can only complicate the experimental search further, c since in many possible experiments the contribution from the two states would produce overlapping states with also a large width, which could blur any signal of a possible bound state.

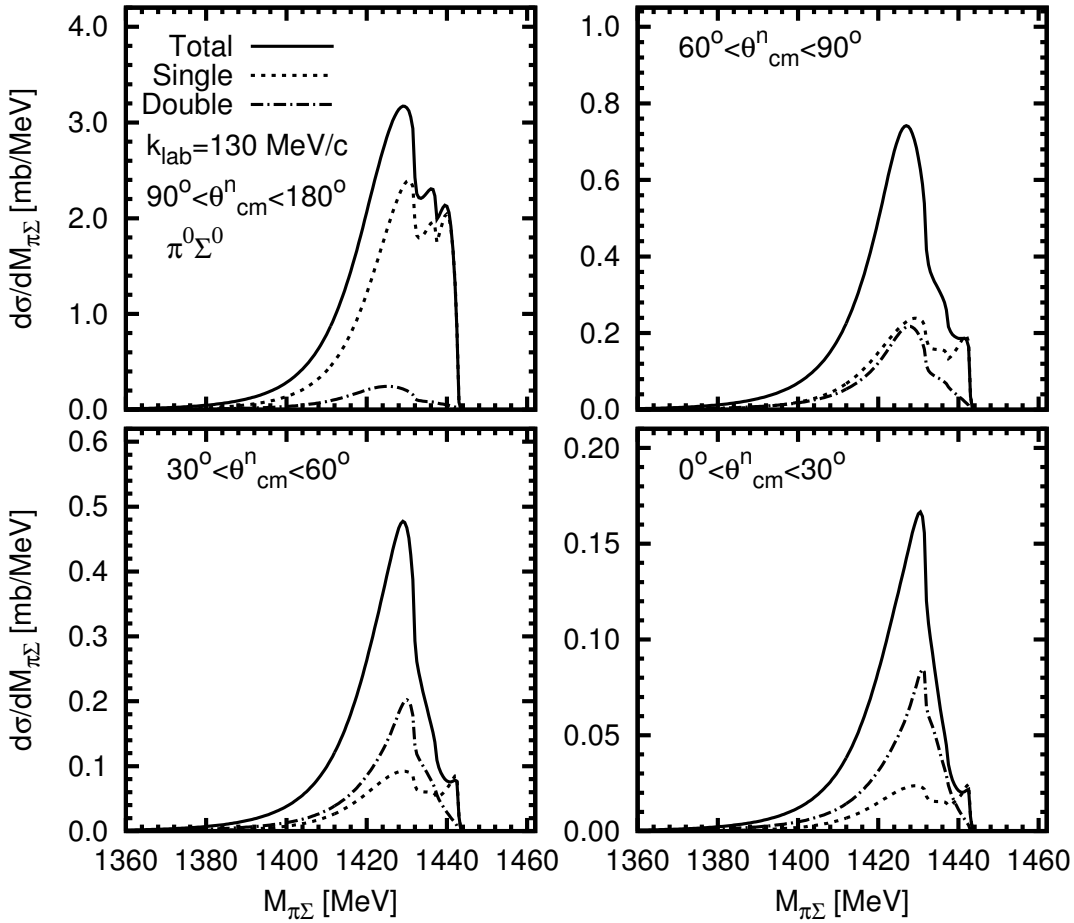

Figure 2: $\pi\Sigma$ invariant mass spectra of $K^- d \to \pi^0\Sigma^0 n$ with 130 MeV/c of incident K^- momentum imposing angular cuts for the emitted neutron with respect to the incident K^- in the CM frame, $90^\circ < \theta^n_{\rm c.m.} < 180^\circ$ (up-left), $60^\circ < \theta^n_{\rm c.m.} < 90^\circ$ (up-right), $30^\circ < \theta^n_{\rm c.m.} < 60^\circ$ (down-left) and $0^\circ < \theta^n_{\rm c.m.} < 30^\circ$ (down-right). In each panel, the solid line denotes the total contributions of the three diagrams, while the dotted and dash-dotted lines show the calculations from the single and double scatterings, respectively.

Bibliography

[1] D. Jido, E. Oset and T. Sekihara, Eur. Phys. J. A **47** (2011) 42 [arXiv:1008.4423 [nucl-th]].

[2] O. Braun *et al.*, Nucl. Phys. B **129**, 1 (1977).

[3] D. Jido, J. A. Oller, E. Oset, A. Ramos and U. G. Meissner, Nucl. Phys. A **725**, 181 (2003) [arXiv:nucl-th/0303062].

[4] D. Jido, E. Oset, T. Sekihara, Eur. Phys. J. **A47**, 42 (2011). [arXiv:1008.4423 [nucl-th]].

[5] M. Bayar, J. Yamagata-Sekihara, E. Oset, Phys. Rev. **C84**, 015209 (2011). [arXiv:1102.2854 [hep-ph]].

[6] N. V. Shevchenko, A. Gal, J. Mares, Phys. Rev. Lett. **98**, 082301 (2007). [nucl-th/0610022].

[7] Y. Ikeda, T. Sato, Phys. Rev. **C76**, 035203 (2007). [arXiv:0704.1978 [nucl-th]].

[8] A. Dote, T. Hyodo, W. Weise, Phys. Rev. **C79**, 014003 (2009). [arXiv:0806.4917 [nucl-th]].

[9] Nevio Grion, private communication.

Mesons and baryons in the holographic soft-wall model

Valery E. Lyubovitskij[1,a], Thomas Gutsche[a], Ivan Schmidt[b], Alfredo Vega[b]
[a] *Institut für Theoretische Physik, Universität Tübingen, Kepler Center for Astro, and Particle Physics, Auf der Morgenstelle 14, D-72076 Tübingen, Germany*
[b] *Departamento de Física y Centro Científico Tecnológico de Valparaíso (CCTVal), Universidad Técnica Federico Santa María, Casilla 110-V, Valparaíso, Chile*

Mesons and baryons are considered in soft-wall holographic approach based on the correspondence of string theory in AdS space and conformal field theory in physical space-time. The model generates Regge trajectories linear in n and $J(L)$ for the hadronic mass spectrum. Results obtained for heavy-light meson masses and decay constants are consistent with predictions of HQET. In the baryon sector applications to the nucleon electromagnetic form factors and generalized parton distributions are discussed.

Based on the gauge/gravity duality [1] a class of AdS/QCD approaches was recently successfully developed for describing the phenomenology of hadronic properties. In order to break conformal invariance and incorporate confinement in the infrared region two alternative AdS/QCD backgrounds have been suggested in the literature: the "hard-wall" approach [2], based on the introduction of an IR brane cutoff in the fifth dimension, and the "soft-wall" approach [3–12], based on using a soft cutoff. In series of papers [9–12] we developed the soft-wall approaches, which have been successfully applied for the study of meson and baryon properties. Here we present a summary of recent results: meson mass spectrum and decay constants of light and heavy mesons, nucleon electromagnetic form factors and generalized parton distributions. Our starting point are the effective $(d+1)$ dimensional actions formulated in AdS space in terms of boson or fermion bulk fields, which serve as holographic images of mesons and baryons. For illustration we consider the simplest actions — for scalar fields ($J = 0$) [10]

$$S_0 = \frac{1}{2}\int d^dx dz \sqrt{g} e^{-\varphi(z)} \left[g^{MN} \partial_M S(x,z) \partial_N S(x,z) - \Big(\mu_S^2 + \Delta V_0(z)\Big) S^2(x,z) \right].$$

and $J = 1/2$ fermions [7,11]:

$$\begin{aligned} S_{1/2} &= \int d^dx dz \, \sqrt{g}\, e^{-\varphi(z)} \left[\frac{i}{2} \overline{\Psi}(x,z) \epsilon_a^M \Gamma^a \mathcal{D}_M \Psi(x,z) - \frac{i}{2} (\mathcal{D}_M \Psi(x,z))^\dagger \Gamma^0 \epsilon_a^M \Gamma^a \Psi(x,z) \right. \\ &- \left. \overline{\Psi}(x,z) \Big(\mu_\Psi + \varphi(z)/R\Big) \Psi(x,z) \right], \end{aligned}$$

[1] On leave of absence from Department of Physics, Tomsk State University, 634050 Tomsk, Russia

where S and Ψ are the scalar and fermion bulk fields, $\mathcal{D}_M$ is the covariant derivative acting on the fermion field, $\Gamma^a = (\gamma^\mu, -i\gamma^5)$ are the Dirac matrices, $\varphi(z) = \kappa^2 z^2$ is the dilaton field, R is the AdS radius, $\Delta V_0(z)$ is the dilaton potential. μ_S and μ_Ψ are the masses of scalar and fermion bulk fields defined as $\mu_S^2 R^2 = \Delta_M(\Delta_M - d)$ and $\mu_\Psi R = \Delta_B - d/2$. Here $\Delta_M = \tau_M = 2 + L$ and $\Delta_B = \tau_B + 1/2 = 7/2 + L$ are the dimensions of scalar and fermion fields, which due to the QCD/gravity correspondence are related to the scaling dimensions (twists τ_M, τ_B) of the corresponding interpolating operators, where $L = \max |L_z|$ [4]. These actions give information about the propagation of bulk fields inside AdS space (bulk-to-bulk propagators), from inside to the boundary of the AdS space (bulk-to-boundary propagators) and bound state solutions - profiles of the Kaluza-Klein (KK) modes in extra-dimension, which correspond to the hadronic wave functions in impact space. We suppose a free propagation of the bulk field along the d Poincaré coordinates with four-momentum p, and a constrained propagation along the $(d+1)$-th coordinate z (due to confinement imposed by the dilaton field). In particular, it was shown [4] that the extra-dimensional coordinate z corresponds to the light-front impact variable. It was also shown [8] that in case of the scattering problem the sign of the dilaton profile is important to fulfill certain model-independent constraints. But we recently showed [12], that in case of the bound state problem the sign of the dilaton profile is irrelevant, if the action is properly set up. Moreover, in solving the bound-state problem, it is more convenient to move the dilaton field from the exponential prefactor to the effective potential [4, 12]. Then we use a KK expansion for the bulk fields factorizing the dependence on d Poincaré coordinates x and the holographic variable z. E.g. in case of scalar field it is given by $S(x,z) = \sum_n S_n(x)\, \Phi_n(z)$, where n is the radial quantum number, $S_n(x)$ is the tower of the KK modes dual to scalar mesons and Φ_n are their extra-dimensional profiles (wave-functions) satisfying the Schrödinger-type equation with the potential depending on dilaton field. Then using the obtained wave functions Φ_n we calculate matrix elements describing hadronic processes. Finally, we present the results of our calculations for mesonic decay constants (Table 1) and spectrum (Tables 2 and 3), nucleon helicity-independent generalized parton distributions (GPDs) in Fig.1. Note, by construction we reproduce the power scaling of nucleon electromagnetic (EM) form factors at large Q^2 and our predictions for the EM radii are compare well with data:

$$\langle r_E^2 \rangle^p = 0.91 \text{ fm}^2 \text{ (our)}, \ 0.77 \text{ fm}^2 \text{ (data)}; \ \langle r_E^2 \rangle^n = -0.12 \text{ fm}^2 \text{ (our)}, \ -0.12 \text{ fm}^2 \text{ (data)},$$
$$\langle r_M^2 \rangle^p = 0.85 \text{ fm}^2 \text{ (our)}, \ 0.73 \text{ fm}^2 \text{ (data)}; \ \langle r_M^2 \rangle^n = 0.88 \text{ fm}^2 \text{ (our)}, \ 0.76 \text{ fm}^2 \text{ (data)}.$$

Acknowledgments

The authors thank Stan Brodsky and Guy de Téramond for useful discussions and remarks. This work was supported by Federal Targeted Program "Scientific and scientific-pedagogical personnel of innovative Russia" Contract No. 02.740.11.0238, by FONDECYT (Chile) under

Meson	Data	Our
π^-	$130.4 \pm 0.03 \pm 0.2$	131
K^-	$156.1 \pm 0.2 \pm 0.8$	155
D^+	206.7 ± 8.9	167
D_s^+	257.5 ± 6.1	170
B^-	193 ± 11	139
B_s^0	$253 \pm 8 \pm 7$	144

Table 1: Decay constants f_P (MeV) of pseudoscalar mesons.

Meson	n	L	S	Mass [MeV]			
π	0	0,1,2,3	0	140	1355	1777	2099
π	0,1,2,3	0	0	140	1355	1777	2099
K	0	0,1,2,3	0	496	1505	1901	2207
$f_0[\bar{n}n]$	0,1,2,3	1	1	1114	1600	1952	2244
$f_0[\bar{s}s]$	0,1,2,3	1	1	1304	1762	2093	2372
$a_0(980)$	0,1,2,3	1	1	1114	1600	1952	2372
$\rho(770)$	0,1,2,3	0	1	804	1565	1942	2240
$\phi(1020)$	0,1,2,3	0	1	1019	1818	2170	2447
$a_1(1260)$	0,1,2,3	1	1	1358	1779	2101	2375

Table 2: Masses of light mesons

Meson	J^P	n	L	S	Mass [MeV]			
$D(1870)$	0^-	0	0,1,2,3	0	1857	2435	2696	2905
$D^*(2010)$	1^-	0	0,1,2,3	1	2015	2547	2797	3000
$D_s(1969)$	0^-	0	0,1,2,3	0	1963	2621	2883	3085
$D_s^*(2107)$	1^-	0	0,1,2,3	1	2113	2725	2977	3173
$B(5279)$	0^-	0	0,1,2,3	0	5279	5791	5964	6089
$B^*(5325)$	1^-	0	0,1,2,3	1	5336	5843	6015	6139
$B_s(5366)$	0^-	0	0,1,2,3	0	5360	5941	6124	6250
$B_s^*(5413)$	1^-	0	0,1,2,3	1	5416	5992	6173	6298

Table 3: Masses of heavy-light mesons

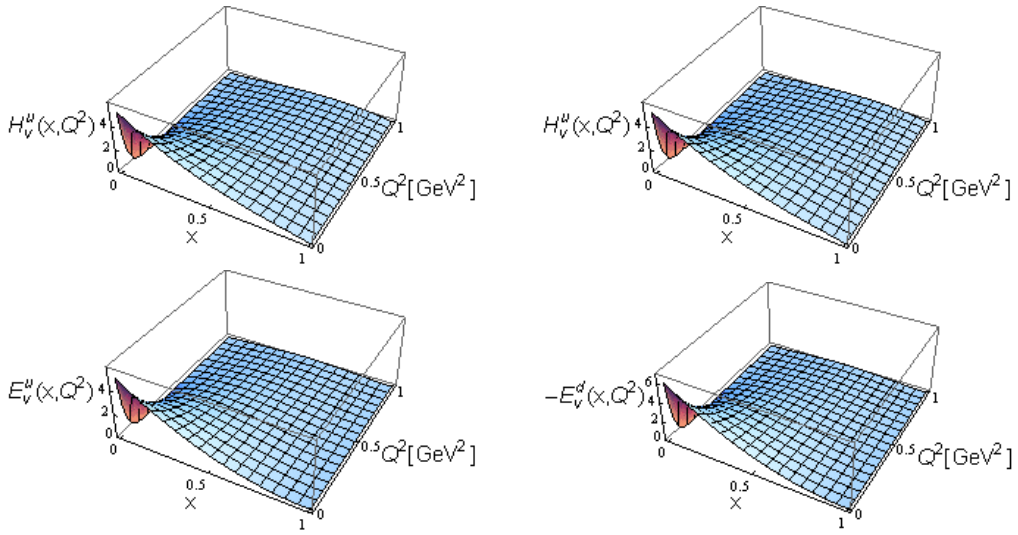

Figure 1: Nucleon helicity-independent GPDs in momentum space

Grant No. 1100287. A.V. acknowledges the financial support from FONDECYT (Chile) Grant No. 3100028. V.E.L. would like to thank Departamento de Física y Centro Científico Tecnológico de Valparaíso (CCTVal), Universidad Técnica Federico Santa María, Valparaíso, Chile for warm hospitality.

Bibliography

[1] J. M. Maldacena, Adv. Theor. Math. Phys. **2**, 231 (1998); S. S. Gubser, I. R. Klebanov and A. M. Polyakov, Phys. Lett. B **428**, 105 (1998); E. Witten, Adv. Theor. Math. Phys. **2**, 253 (1998).

[2] J. Polchinski, M. J. Strassler, Phys. Rev. Lett. **88**, 031601 (2002).

[3] A. Karch, E. Katz, D. T. Son and M. A. Stephanov, Phys. Rev. D **74**, 015005 (2006).

[4] S. J. Brodsky, G. F. de Teramond, Phys. Rev. Lett. **96**, 201601 (2006); Phys. Rev. D **77**, 056007 (2008); Nucl. Phys. Proc. Suppl. **199**, 89 (2010).

[5] O. Andreev, Phys. Rev. D **73**, 107901 (2006); H. Forkel, M. Beyer and T. Frederico, JHEP **0707**, 077 (2007).

[6] G. F. de Teramond and S. J. Brodsky, AIP Conf. Proc. **1257**, 59 (2010).

[7] Z. Abidin and C. E. Carlson, Phys. Rev. D **79**, 115003 (2009).

[8] A. Karch, E. Katz, D. T. Son, M. A. Stephanov, JHEP **1104**, 066 (2011).

[9] A. Vega and I. Schmidt, Phys. Rev. D **78**, 017703 (2008); A. Vega and I. Schmidt, Phys. Rev. D **79**, 055003 (2009); A. Vega, I. Schmidt, T. Branz, T. Gutsche and V. E. Lyubovitskij, Phys. Rev. D **80**, 055014 (2010); A. Vega, I. Schmidt, Phys. Rev. **D82**, 115023 (2010).

[10] T. Branz, T. Gutsche, V. E. Lyubovitskij, I. Schmidt, A. Vega, Phys. Rev. D **82**, 074022 (2010).

[11] A. Vega, I. Schmidt, T. Gutsche, V. E. Lyubovitskij, Phys. Rev. D **83**, 036001 (2011).

[12] T. Gutsche, V. E. Lyubovitskij, I. Schmidt and A. Vega, arXiv:1108.0346 [hep-ph].

A new perspective on the $\Delta_{5/2^+}(2000)$ puzzle

Pedro González[a,b], Ju-Jun Xie[b,c], A. Martínez Torres[d], and E. Oset[a,b]
[a]*Departamento de Física Teórica (Universidad de Valencia (UV)), Valencia, Spain*
[b]*Instituto de Física Corpuscular (IFIC), Centro Mixto CSIC-Universidad de Valencia, Institutos de Investigación de Paterna, Aptd. 22085, E-46071 Valencia, Spain*
[c]*Department of Physics, Zhengzhou University, Zhengzhou, Henan 450001, China*
[d]*Yukawa Institute for Theoretical Physics, Kyoto University, Kyoto 606-8502, Japan*

We argue that $\Delta_{5/2^+}(2000)(**)$, cataloged as a resonance in the Particle Data Book Review (PDG), should be interpreted instead as two distinctive resonances, $\Delta_{5/2^+}(\sim 1740)$ and $\Delta_{5/2^+}(\sim 2200)$. Our argument is based on a solution of the $\pi\Delta\rho$ problem in a Fixed Center Approximation (FCA) to the Fadeev equations. $\Delta_{5/2^+}(\sim 1740)$ can then be interpreted as a $\pi-(\Delta\rho)_{N(1675)}$ bound state. As a corollary $\Delta_{1/2^+}(1750)(*)$ can be understood as a $\pi N_{1/2^-}(1650)$ bound state.

1 Introduction

In the PDG [1] there is only a well established $\Delta_{5/2^+}$ resonance, $\Delta(1905)\ F_{35}\ (****)$, and fair evidence of the existence of another one, $\Delta(2000)\ F_{35}\ (**)$. However, a careful look at this last resonance shows that its nominal mass is in fact estimated from $\Delta(1724\pm 61)$, $\Delta(1752\pm 32)$ and $\Delta(2200\pm 125)$ respectively extracted from three independent analyses [2–4]. Moreover a recent new data analysis has reported a $\Delta_{5/2^+}$ with a pole position at 1738 MeV [5].

From a $3q$ description the $\Delta_{5/2^+}(1905)$ is naturally accommodated as the lowest $\Delta_{5/2^+}$ state in the second energy band [6]. Similarly, the reported $\Delta_{5/2^+}(2200)$ with a more uncertain mass (2200 ± 125 MeV) may be reasonably located in the fourth energy band. On the contrary $\Delta_{5/2^+}(1740)$ can not be accommodated as a $3q$ state without seriously spoiling the overall spectral description. The same kind of problem was tackled in [7] regarding the description of $\Delta_{5/2^-}(1930)$ with a mass much lower than the corresponding to the third energy band, the first available band for such a state. There the consideration of the $\rho\Delta$ channel, whose threshold (2002 MeV) lies close above the experimental mass of the resonance and far below the $3q$ mass (~ 2150 MeV), allowed for an explanation of $\Delta_{5/2^-}(1930)$ and its partners, $\Delta_{3/2^-}(1940)$ and $\Delta_{1/2^-}(1900)$, as $\rho\Delta$ bound states in the $I=3/2$ sector. In addition $N_{1/2^-}(1650)$, $N_{3/2^-}(1700)$ and $N_{5/2^-}(1675)$ were also well described as $\rho\Delta$ bound states in the $I=1/2$ sector although with a bigger sensitivity in this case to the cutoff (or subtraction constant) parameter employed in the chiral unitary approach.

For $\Delta_{5/2^+}(1740)$ one can easily identify a meson-baryon threshold, $\left[\pi N_{5/2^-}(1675)\right]_{threshold} =$ 1814 MeV, in between the $3q$ mass ($\sim$ 1910 MeV) and data. Then one can wonder about the possibility that the $\pi N_{5/2^-}(1675)$ system may give rise to a bound state which could provide theoretical support to the fair evidence of the existence of $\Delta_{5/2^+}(1740)$. Actually this bound state nature would provide an explanation to the extraction of this resonance in some data analyses and not in others. It turns out that only analyses reproducing the $\pi\pi N$ production cross section data extract it. Let us note that this would be a necessary condition to extract $\Delta_{5/2^+}(1740)$ if corresponding to a $\pi N_{5/2^-}(1675)$ state (let us recall that $N_{5/2^-}(1675)$ decays to πN and to $\pi\pi N$ with branching fractions of 40% and 55% respectively). To examine this possibility we have performed an analysis of the $\pi N_{5/2^-}(1675)$ system by assuming that $N_{5/2^-}(1675)$ is a $\rho\Delta$ bound state (we have fixed the subtraction constant $a_{\Delta\rho} = -2.28$ to get precisely the mass of $N(1675)$) [8].

2 Formalism

The interaction of a particle with a bound state of a pair of particles at very low energies or below threshold can be efficiently and accurately studied by means of the FCA to the Faddeev equations for the three-particle system [9]. For the Δ-ρ-π system the π is assumed to scatter one by one the fixed centers ρ and Δ. Then the total three-body scattering amplitude T is given in terms of two partition functions T_1 and T_2 accounting for the diagrams starting with the interaction of the π with particle i of the compound system:

$$T = T_1 + T_2, \tag{1}$$

$$T_1 = t_1 + t_1 G_0 T_2, \tag{2}$$

$$T_2 = t_2 + t_2 G_0 T_1 \tag{3}$$

where t_i represent the $\Delta\pi$ and $\rho\pi$ unitarized scattering amplitudes, see Refs. [10, 11] for details. G_0 is the loop function for the π meson propagating inside the $N_{5/2^-}(1675)$ resonance (see Ref. [8] for details).

3 Results and discussion

The dynamic generation of resonances from our formalism depends on two subtraction constants, $a_{\Delta\pi}$ and $a_{\rho\pi}$, respectively associated to the Δ-π and ρ-π unitarized $s-$wave interactions entering in our calculation. We assume that they are effective parameters, their values implicitly taking into account the effects of the $3q$ component of $N_{5/2^-}(1675)$. Therefore they could differ significantly from the values used in Refs. [10, 11].

Examples of results giving rise to a $\pi - N(1675)$ bound state are graphically shown in Fig. 1. The three peaks in the figures may be unambiguously assigned to $\Delta_{5/2^+}(1740)$, $\Delta_{5/2^+}(1905)$ and $\Delta_{5/2^+}(2200)$. Note that the location of the first peak varies from 1770 MeV to 1800 MeV,

a little bit higher than the masses of the existing candidates in [1]. Indeed we could force $a_{\Delta\pi} = -4.3$ to get an average mass of 1740 MeV. Therefore these results should mainly be interpreted as a fit to fix the parameters in our formalism. In order to gain confidence about the possible existence of $\Delta_{5/2^+}(1740)$ it becomes essential that further predictions from our formalism (with no free parameters) are successful in the interpretation of data. Let us examine some of these predictions in the $I = 3/2$ sector.

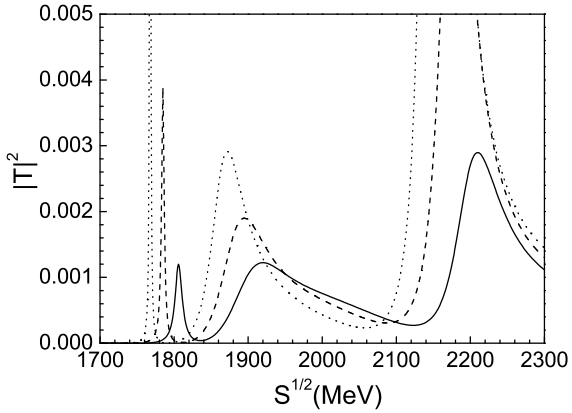

Figure 1: Modulus squared of the three-body scattering amplitude for $I = 3/2$. Results obtained with $a_{\rho\pi} = -2.0$ and $a_{\Delta\pi} = -2.6$ (solid line), -3.0 (dash line), -3.4 (dotted line).

Δ resonances generated from $\pi N_{3/2^-}(1700)$ and $\pi N_{1/2^-}(1650)$ are of particular interest since $N_{3/2^-}(1700)$ and $N_{1/2^-}(1650)$ are dynamically generated from $\Delta\rho$ as degenerate states to $N_{5/2^-}(1675)$. Hence we predict $I = 3/2$, $J^P = 1/2^+, 3/2^+$ states almost degenerate to $\Delta_{5/2^+}(1740)$. For $J^P = 1/2^+$ the state may be assigned to $\Delta_{1/2^+}(1750)(*)$, a resonance that can not be described by quark models [6]. It should be remarked that only analyses reproducing the $\pi\pi N$ production cross section data extract it as it was the case for $\Delta_{5/2^+}(1740)$. Therefore the mere existence of $\Delta_{1/2^+}(1750)(*)$ could be considered within our calculation framework as an argument in favor of the existence of $\Delta_{5/2^+}(1740)$. In what respects to $\Delta_{3/2^+}(\sim 1740)$ it is assigned to $\Delta_{3/2^+}(1600)$ which is also overpredicted by $3q$ models as the first radial excitation of the $\Delta(1232)$. However, other channels as $\sigma\Delta(1232)$ and $\pi N_{3/2^-}(1520)$ could be playing a more important role in the generation of this resonance [12].

Additional analyses have been done in the $I = 3/2, 1/2$ sectors [8]. The consistency of the whole scheme and the good agreement with data makes us confident that the approximations followed draw the essential dynamics. From our results we may conclude that there is a sound theoretical basis to support the data analyses extracting two distinctive resonances, $\Delta_{5/2^+}(1740)$ and $\Delta_{5/2^+}(2200)$, cataloged altogether as $\Delta_{5/2^+}(2000)$ in the PDG.

Acknowledgments

This work is partly supported by DGICYT Contract No. FIS2006-03438, the Generalitat Valenciana in the project PROMETEO and the EU Integrated Infrastructure Initiative Hadron Physics Project under contract RII3-CT-2004-506078. J.-J.X. acknowledges Ministerio de Educación Grant SAB2009-0116. The work of A.M.T. is supported by the Grant-in-Aid for the Global COE Program "The Next Generation of Physics, Spun from Universality and Emergence" from the Ministry of Education, Culture, Sports, Science and Technology (MEXT) of Japan. P.G. benefits from the funding by the Spanish Ministerio de Ciencia y Tecnología and UE FEDER under Contract No. FPA2007-65748, by the Spanish Consolider Ingenio 2010 Program CPAN (CSD2007-00042) and by the Prometeo Program (2009/129) of the Generalitat Valenciana. Partial funding is also provided by HadronPhisics2, a FP7-Integrating Activities and Infrastructure Program of the EU under Grant 227431.

Bibliography

[1] K. Nakamura *et al.* (Particle Data Group), J. Phys. G **37**, 075021 (2010).

[2] T. P. Vrana, S. A. Dytman and T.-S. H. Lee, Phys. Rep. **328**, 181 (2000).

[3] D.M. Manley and E.M. Saleski, Phys. Rev. D **45**, 4002 (1992).

[4] R.E. Cutkosky, C.P. Forsyth, J.B. Babcock, R.L. Kelly, and R.E. Hendrick, Proceedings of the IV International Conference on Baryon Resonances (Baryon 1980), edited by N. Isgur, Toronto 1980.

[5] N. Suzuki *et al.* (EBAC), Phys. Rev. Lett. **104**, 042302 (2010).

[6] S. Capstick and N. Isgur, Phys. Rev. D **34**, 2809 (1986); S. Capstick and W. Roberts, Prog. Part. Nucl. Phys. **45** S241 (2000).

[7] P. González, E. Oset and J. Vijande, Phys. Rev. C **79**, 025209 (2009).

[8] Ju-Jun Xie, A. Martínez Torres, E. Oset and P. González, Phys. Rev. C **83**, 055204 (2011).

[9] R. Chand and R. H. Dalitz, Annals Phys. **20**, 1 (1962); R. C. Barrett and A. Deloff, Phys. Rev. C **60**, 025201 (1999); R. C. Barrett and A. Deloff, Phys. Rev. C **60**, 025201 (1999); S. S. Kamalov, E. Oset and A. Ramos, Nucl. Phys. A **690**, 494 (2001).

[10] Sourav Sarkar, E. Oset, and M. J. Vicente Vacas, Nucl. Phys. A **750**, 294 (2005), Erratum-ibid. A **780**, 90 (2006), and references therein.

[11] L. Roca, E. Oset, and J. Singh, Phys. Rev. D **72**, 014002 (2005) and references therein.

[12] P. González, J. Vijande and A. Valcarce, Phys. Rev. C **77**, 065213 (2008).

Pion scattering and electro-production on nucleons in the resonance region in chiral quark models

Simon Širca[1,a,b], Bojan Golli[c,b], Manuel Fiolhais[d], and Pedro Alberto[d]
[a]*Faculty of Mathematics and Physics, University of Ljubljana, Slovenia*
[b]*Jožef Stefan Institute, Ljubljana, Slovenia*
[c]*Faculty of Education, University of Ljubljana, Slovenia*
[d]*Departamento de Fisica and Centro de Fisica Computacional, Universidade de Coimbra, Portugal*

Pion scattering and electro-production amplitudes have been computed in a coupled-channel framework incorporating quasi-bound quark-model states, based on the Cloudy Bag model. All relevant low-lying nucleon resonances in the P33, P11, and S11 partial waves have been covered, including the $\Delta(1232)$, the $N^*(1440)$, $N^*(1535)$, and $N^*(1650)$. Consistent results have been obtained for elastic and inelastic scattering (two-pion, eta-N, and K-Lambda channels), as well as for electro-production. The meson cloud has been shown to play a major role, in particular in electro-magnetic observables in the P33 and P11 channels.

The study of pion scattering and electro-production on nucleons in the region of low-lying resonances helps us establish meaningful connections between the data and resonance properties obtained in model calculations. One of the key aspects is the interplay of quark and meson degrees of freedom. The conceptual foundations of our approach in chiral quark models date back to the paper [1], in which we demonstrated the importance of the pion cloud in the electro-production of pions in the region of the $\Delta(1232)$. We found that the pion cloud contributes $\sim 45\,\%$ to the magnetic dipole amplitude, and strongly dominates the electric quadrupole amplitude, a result later confirmed by many related calculations.

In our previous work [2] we have shown that in models in which mesons couple linearly to the quark core, the elements of the K matrix for meson-baryon scattering $MB \to M'B'$ in the basis with good total angular momentum J, isospin T and parity take the form:

$$K^{JT}_{M'B'\,MB} = -\pi\mathcal{N}_{MB}\langle\Psi^{MB}_{JT}||V_{M'}(k)||\Psi_{B'}\rangle\,, \qquad \mathcal{N}_{MB} = \sqrt{\frac{\omega_M E_B}{k_M W}}\,. \tag{1}$$

Here $|\Psi^{MB}_{JT}\rangle$ is the principal value state:

$$|\Psi^{MB}_{JT}\rangle = \mathcal{N}_{MB}\left\{[a^\dagger(k_M)|\Psi_B\rangle]^{JT} + \sum_{\mathcal{R}} c^{MB}_{\mathcal{R}}|\Phi_{\mathcal{R}}\rangle + \sum_{M'B'}\int \frac{\mathrm{d}k\,\chi^{M'B'\,MB}(k)}{\omega_k + E_{B'}(k) - W}\,[a^\dagger(k)|\Psi_{B'}\rangle]^{JT}\right\}\,,$$

[1]simon.sirca@fmf.uni-lj.si

$\Psi_{B'}$ is the fully dressed outgoing baryon state, and $V_{M'}(k)$ is the quark-meson vertex determined in the underlying quark model. The first term represents the free meson (π, η, σ, ...) and the baryon (N, Δ, ...) and defines the channel, the next term is the sum over *bare* tree-quark states $\Phi_{\mathcal{R}}$ involving different excitations of the quark core, the third term introduces meson clouds around different isobars. In the case of two-pion decays, we assume that they proceed either through an unstable meson (e.g. ρ-meson, σ-meson) or through a baryon resonance (e.g. $\Delta(1232)$, $N^*(1440)$). The meson amplitudes $\chi^{M'B'\,MB}(k)$ are proportional to the (half) off-shell K-matrix elements (1), and obey a coupled set of equations of the Lippmann-Schwinger type. The resulting amplitudes take the form

$$\chi^{M'B'\,MB}(k) = -\sum_{\mathcal{R}} c_{\mathcal{R}}^{MB} \mathcal{V}_{B'\mathcal{R}}^{M'}(k) + \mathcal{D}^{M'B'\,MB}(k)\,,$$

where the first term represents the contribution of resonances, while $\mathcal{D}^{M'B'\,MB}(k)$ originates in non-resonant background processes. Here $c_{\mathcal{R}}^{MB} = \mathcal{V}_{B\mathcal{R}}^{M}/(Z_{\mathcal{R}}(W)(W - M_{\mathcal{R}}))$, $\mathcal{V}_{B\mathcal{R}}^{M}$ is the dressed matrix element of the quark-meson interaction between the resonant state and the baryon state in the channel MB, and $Z_{\mathcal{R}}$ is the wave-function normalization. The resulting physical resonant states $\mathcal{R}$ are superpositions of the bare 3-quark states $\Phi_{\mathcal{R}'}$. The T matrix is obtained by solving the Heitler's equation $T = K + \mathrm{i}TK$.

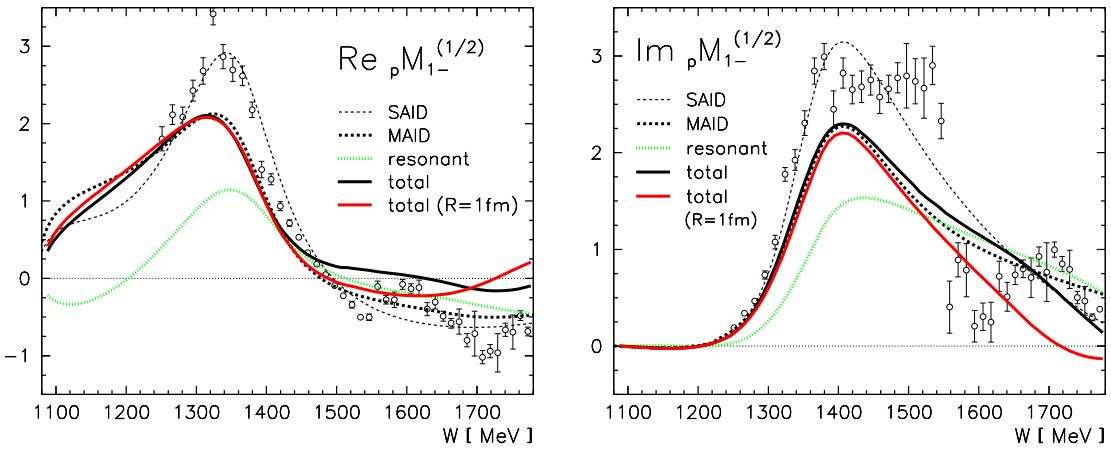

Figure 1: Real and imaginary parts of the magnetic electro-production multipole for the proton target, isospin-1/2 channel, in the P11 partial wave (the Roper resonance).

More recently, we have extended the method outlined above to the calculation of meson electro-production amplitudes by including the γN channel [3,4]. The electro-production amplitude in the vicinity of a chosen resonance $\mathcal{R} = N^*$ can be cast in the form

$$\mathcal{M}_{\gamma NMB} = \mathcal{M}_{\gamma NMB}^{(res)} + \mathcal{M}_{\gamma NMB}^{(bg)} = \sqrt{\frac{\omega_\gamma E_N^\gamma}{\omega_M E_B}} \frac{1}{\pi \mathcal{V}_{BN^*}} \langle \Psi_{N^*}^{(res)}(W) | V_\gamma | \Psi_N \rangle\, T_{MBMB} + \mathcal{M}_{\gamma NMB}^{(bg)}\,,$$

where T_{MBMB} is the meson-baryon scattering amplitude, and the electro-excitation of the resonance is described by the helicity amplitude $\langle \Psi_{N^*}^{(res)}(W) | V_\gamma | \Psi_N \rangle = A_{\gamma N \to N^*}$. Here

$V_\gamma(\mu,\vec{k}_\gamma)$ is the interaction of the photon with the electro-magnetic current, and contains quark and pion contributions as specified by the underlying quark model.

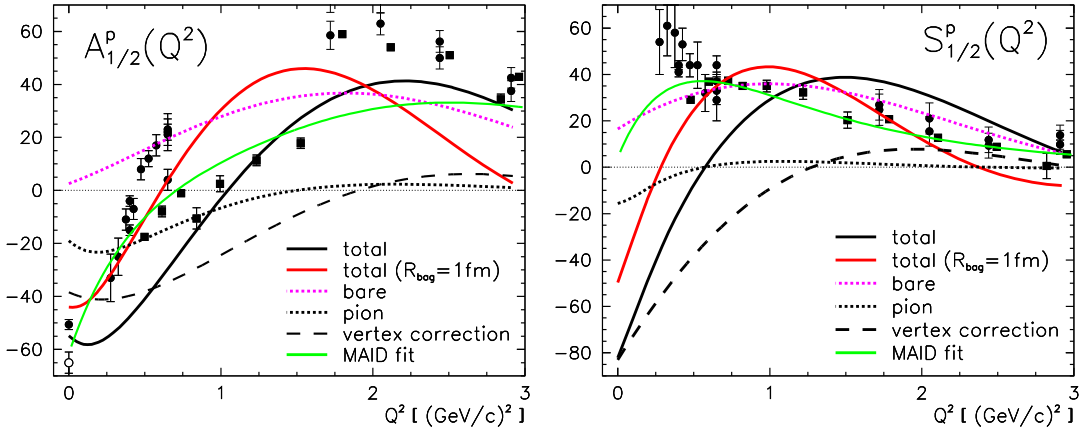

Figure 2: Different contributions to the transverse and scalar helicity amplitudes for the electro-excitation of the $N^\star(1440)$ (Roper) resonance in the P11 partial wave.

In the P11 case we have included the πN, $\pi\Delta$, $\pi N^*(1440)$ and σN channels, while the sum over $\mathcal{R}$ consists of the nucleon, $N^*(1440)$, and $N^*(1710)$ resonance; in the S11 case we have considered the πN, $\pi\Delta$, $\pi N^*(1440)$, ρN and $K\Lambda$ channels, as well as $N^*(1535)$ and $N^*(1650)$ resonances. We have used the quark-model wave-functions for the negative-parity states in the form $\Phi_\mathcal{R} = c^\mathcal{R}_A|(1s)^2(1p_{3/2})^1\rangle + c^\mathcal{R}_P|(1s)^2(1p_{1/2})^1\rangle_1 + c^\mathcal{R}_{P'}|(1s)^2(1p_{1/2})^1\rangle_2$, where the mixing coefficients of [5] have been adopted.

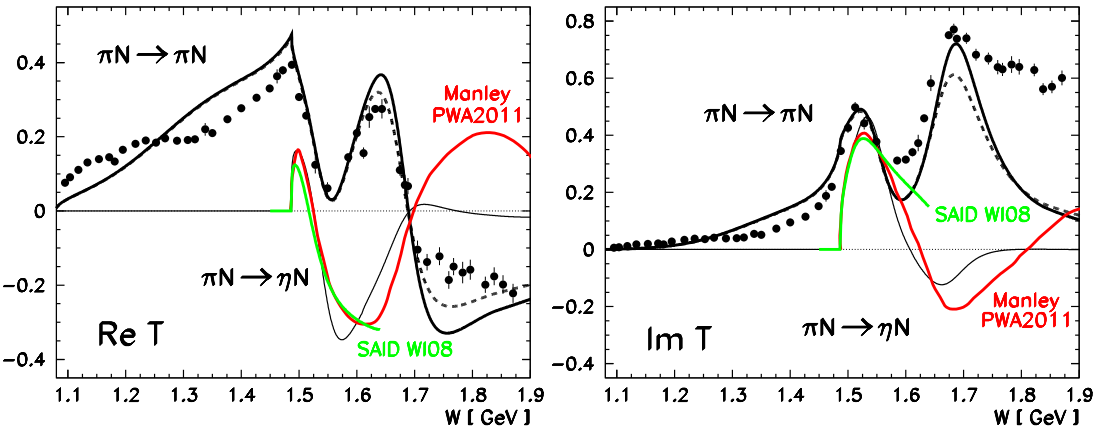

Figure 3: The real and imaginary part of the scattering T matrix for the S11 partial wave. Shown are the elastic results as well as those for the $\pi N \to \eta N$ channel. The solid lines were obtained by using the reduced value of the d-wave $\pi\Delta$ coupling while the dashed lines correspond to the unmodified quark-model values for the baryon-meson couplings.

The quark-meson vertices were computed in a SU(3)-extended Cloudy Bag Model with the quark-meson Lagrangian $\mathcal{L}^{(qM)}_{CBM} = -(\mathrm{i}/2f_M)\,\overline{q}\gamma_5\lambda_a q\phi_a\delta\left(r - R_{bag}\right)$, $a = 1, 2, \ldots, 8$. We used $R_{bag} = 0.83\,\mathrm{fm}$, the interaction parameter $f_\pi = 76\,\mathrm{MeV}$ which reproduces the experimental $g_{\pi NN}$ coupling, $f_K = 1.2\,f_\pi$, and either $f_\eta = 1.2\,f_\pi$ or $f_\eta = f_\pi$. The bare masses of $\Phi_{\mathcal{R}}$ were adjusted to reproduce the positions of the resonances.

We have reproduced reasonably well the main features of the M_{1-} electro-production amplitude from the threshold up to $W \sim 1700$ MeV (Figs. 1 and 3), as well as the transverse and scalar helicity amplitudes for Q^2 up to $\sim 3\,\mathrm{GeV}^2/\mathrm{c}^2$. Our calculations indicate that the pion cloud plays an important role, especially in the region of low Q^2 (long-range effects). In the case of the $N^*(1440)$ resonance (Fig. 2), the quark contribution to $A^p_{1/2}$ is positive, while the pion contribution and the vertex corrections due to meson loops are negative. These two effects are responsible for the zero crossing of the amplitude. At higher Q^2 (short-range physics) the quark core takes over, rendering $A^p_{1/2}$ positive.

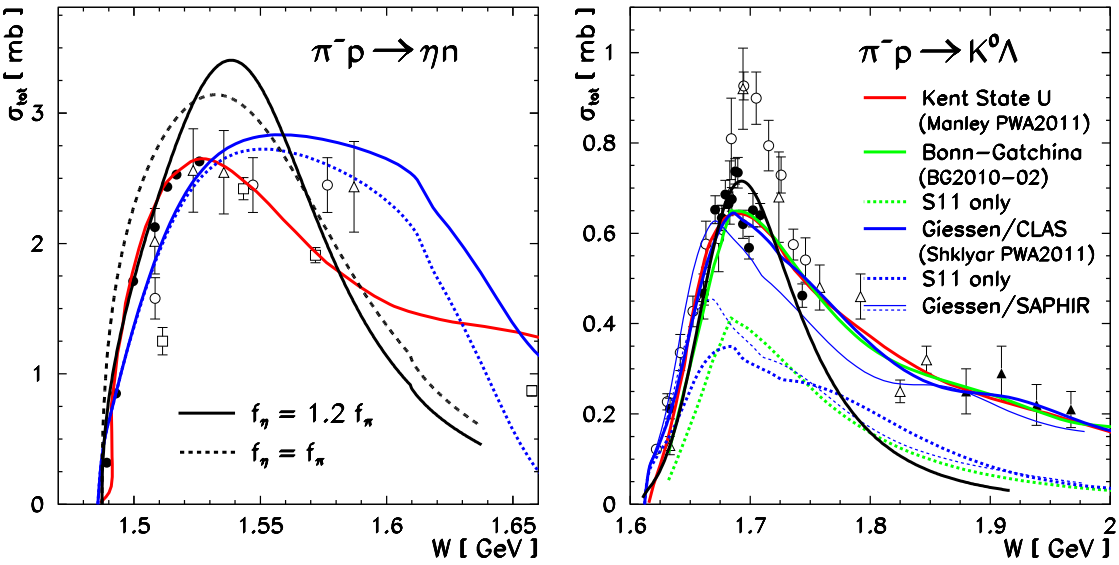

Figure 4: Left: the S11 contribution to the total cross-section for the $\pi^- p \to \eta n$ reaction. Right: total cross-section for the $\pi^- p \to K^0 \Lambda$ process. Our result: black solid and dashed lines; other analyses are color-coded in the figure legend.

The results for pion-induced meson production amplitudes in the S11 partial wave are shown in Fig. 3. Near the $N^*(1535)$ resonance, just above the η threshold, the elastic and inelastic amplitudes are strongly influenced by the s-wave ηN channel. Near the $N^*(1650)$ resonance, additional channels become more relevant, such as the $\pi\Delta$ with $l = 2$, the $K\Lambda$ with $l = 0$, two channels involving the ρ meson with $l = 0$ ($\rho_1 N$) and $l = 2$ ($\rho_3 N$), and the $\pi N^*(1440)$ channel with $l = 0$. The S11 contributions to the total cross-section for the $\pi^- p \to \eta n$ and $\pi^- p \to K^0 \Lambda$ processes are shown in Fig. 4 (left and right, respectively).

The results for η photoproduction are shown in Fig. 5 (left). The behavior is almost completely driven by the properties of the $N^*(1535)$ resonance and the threshold behavior of the ηN amplitude, but is almost insensitive to background processes. The good overall agreement with the data for η production strongly supports our conjecture about the dominance of the genuine three-quark configuration in the $N^*(1535)$ state. The absolute value of the E_{0+} amplitude in the $K\Lambda$ channel is shown in Fig. 5 (right). While the cross-section for pion-induced production of K^+ appears to be over-estimated in our model, the photo-production amplitude is smaller than predicted by phenomenological analyses. This discrepancy remains an open question and represents a challenge for further investigation.

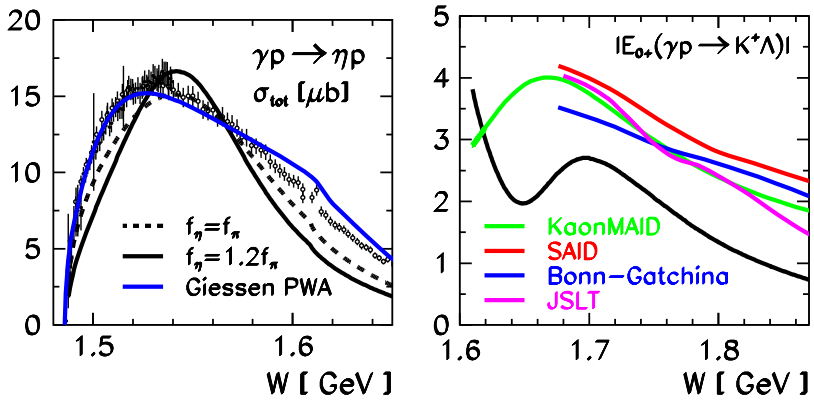

Figure 5: Left: total cross-section for eta photoproduction on the proton. Right: the absolute value of the transverse K^+ photo-production amplitude E_{0+}. Our result: black solid and dashed lines; other calculations are color-coded in the figure legend.

Acknowledgments

The Authors wish to thank Andrei Sarantsev and Vitaliy Shklyar for providing us with the most recent data files from their analyses.

Bibliography

[1] M. Fiolhais, B. Golli, S. Širca, Phys. Lett. B **373** (1996) 229.

[2] B. Golli, S. Širca, Eur. Phys. J. A **38** (2008) 271.

[3] B. Golli, S. Širca, M. Fiolhais, Eur. Phys. J. A **42** (2009) 185.

[4] B. Golli, S. Širca, Eur. Phys. J. A **47** (2011) 61.

[5] F. Myhrer, J. Wroldsen, Z. Phys. C **25** (1984) 281.

Nucleon Resonance Electrocouplings from the CLAS Data on Exclusive Meson Electroproduction off Protons

Victor I. Mokeev[1,a,b], Inna G. Aznauryan[c], and Volker D. Burkert[a]
[a]*Jefferson Lab, USA*
[b]*Skobeltsyn Nuclear Physics Institute at Moscow State University, Russia*
[c]*Yerevan Physics Institute, Armenia*

$\gamma_v NN^*$ transition helicity amplitudes (electrocouplings) of several prominent excited proton states are determined for the first time in independent analyses of $\pi^+ n$, $\pi^0 p$, and $\pi^+\pi^- p$ electroproduction off protons. Analysis of $\pi^+\pi^- p$ electroproduction has extended considerably information on electrocouplings of high lying N* states, which decay preferentially to the $N\pi\pi$ final states.

1 Introduction

The studies of nucleon resonance structure from the data on different exclusive meson electroproduction channels off nucleons represent an important direction in the N^* program with the CLAS detector with the primary objective of determining electrocouplings of all prominent excited proton states in a wide area of photon virtualities Q^2<5.0 GeV^2 [1]. In this paper we present the results on N^* electrocouplings obtained in independent analysis of $\pi^0 p$, $\pi^+ n$, and $\pi^+\pi^- p$ electroproduction off protons.

2 Evaluation of N^* electrocouplings from exclusive meson electroproduction data

The $\pi^+ n$, $\pi^0 p$, and $\pi^+\pi^- p$ exclusive channels are major contributors to meson electroproduction off protons in N^* excitation region. They are sensitive to N^* contributions and account for $\approx$ 90% of meson electroproduction cross section. Non-resonant contributions in these channels are different, while N^* electrocouplings remain the same, since resonance electroproduction and hadronic decay amplitudes are independent. Therefore, consistent values of N^* electrocouplings determined from different major meson electroproduction channels strongly support a reliable extraction of these fundamental quantities.

[1]mokeev@jlab.org

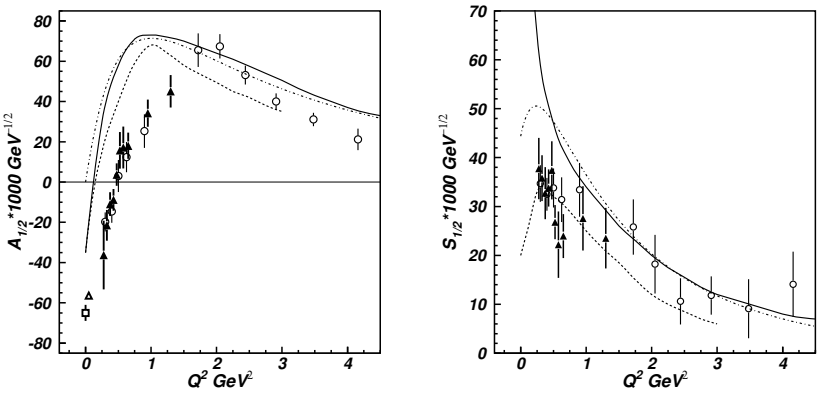

Figure 1: Electrocouplings of the $P_{11}(1440)$ resonance determined in independent analyses of the CLAS data on $N\pi$ (circles) and $\pi^+\pi^- p$ (triangles) electroproduction off protons. Square and triangle at Q^2=0 correspond to RPP [8] and the CLAS $N\pi$ [9] photoproduction results, respectively. The results of relativistic light-front quark models [10,11] are shown by solid and dashed lines, respectively. Results of the covariant valence quark-spectator diquark model [12] are shown by the dashed dotted line.

The CLAS data considerably extended information on $\pi^+ n$, $\pi^0 p$ electroproduction off protons. A total of nearly 120000 data points on unpolarized differential cross sections, longitudinally polarized beam asymmetries, and longitudinal target and beam-target asymmetries were obtained with almost complete coverage of the accessible phase space [2]. The data were analyzed within the framework of two conceptually different approaches: a) the unitary isobar model (UIM) and b) a model, employing dispersion relations [3,4]. The two approaches provide good description of the $N\pi$ data in the entire range covered by the CLAS measurements: $W < 1.7$ GeV and $Q^2 < 5.0$ GeV^2, resulting in χ^2/d.p. < 2.0.

Nine independent one-fold-differential and fully-integrated $\pi^+\pi^- p$ electroproduction cross sections of protons are determined from the CLAS measurements [5,6] in 131 bins of W and Q^2 in a mass range $W < 2.0$ GeV, and with photon virtualities of $0.25 < Q^2 < 1.5$ GeV^2. Analysis of these data within framework of the meson-baryon JM reaction model [7,14] allowed us to establish all essential contributing mechanisms from their manifestation in the measured cross sections. Reasonable data description makes it possible to provide a reliable separation between resonant and non-resonant contributions needed for extraction of N^* electrocouplings from $\pi^+\pi^- p$ electroproduction data.

3 Results and discussion

Electrocouplings of the $P_{11}(1440)$, $D_{13}(1520)$ states have become available from independent analyses of the CLAS data on $\pi^+ n$, $\pi^0 p$ ($Q^2 < 5.0$ GeV^2), and $\pi^+\pi^- p$ ($Q^2 < 1.5$ GeV^2)

electroproduction channels [2,14]. Their values obtained from these major meson electroproduction channels with different non-resonant mechanisms are in a good agreement. As an example, electrocouplings of the $P_{11}(1440)$ state are shown in Fig. 1. Consistent results on N^* electrocouplings demonstrate that the reaction models [4,7,10] mentioned in the Section 2 provide reliable evaluation of these fundamental quantities. It makes possible to determine electrocouplings of all resonances that decay preferentially to the either $N\pi$ or $N\pi\pi$ final states analyzing independently the $N\pi$ or $\pi^+\pi^- p$ electroproduction channels.

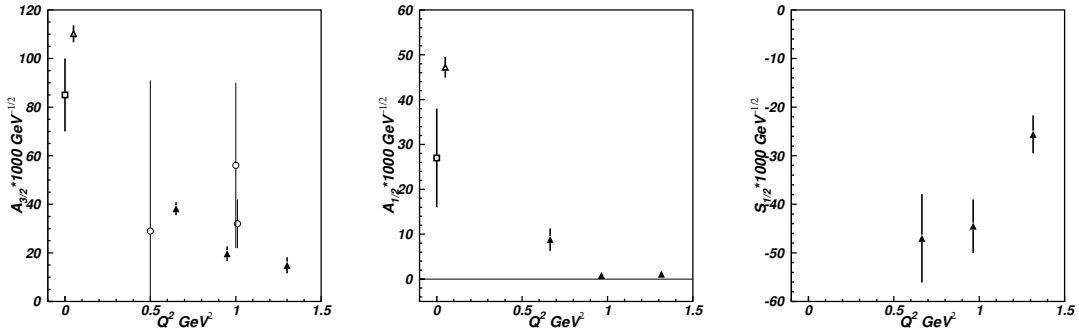

Figure 2: Electrocouplings of $D_{33}(1700)$ (left) and $S_{31}(1620)$ (middle and right) resonances from analyses of the CLAS data on $\pi^+\pi^- p$ [5,6] and world data [15] on $N\pi$ electroproduction off protons. Symbols are the same as in Fig. 1.

Preliminary results on electrocouplings of $S_{31}(1620)$, $S_{11}(1650)$, $F_{15}(1685)$, $D_{33}(1700)$ and $P_{13}(1720)$ states were obtained from the CLAS $\pi^+\pi^- p$ electroproduction data [5]. The CLAS results provide accurate data on the Q^2-evolution of the transverse electrocouplings and the first information on the longitudinal electrocouplings of all the above mentioned excited proton states. Several examples are shown in Fig. 2. A dominance of longitudinal $S_{1/2}$ electrocoupling is observed in electroexcitation of $S_{31}(1620)$ state at $Q^2 > 0.5$ GeV^2 (see Fig. 2).

The CLAS results on electrocouplings of prominent resonances stimulated the development of N^* structure models [16,17]. The analysis of resonance electrocouplings within the framework of light front [10,11] and quark-spectator diquark [12] models, complemented by the coupled channel approach [13] demonstrate that the structure of N^* states in a mass range $W < 1.6$ GeV is determined by a combined contribution of an internal core of three dressed quarks and an external meson-baryon cloud. The recent studies in the light-front quark model [18] revealed an important role of dynamical mass and structure of dressed quarks in Q^2-evolution of of N^* electrocouplings. Furthermore, two conceptually different approaches of QCD-Dyson-Schwinger equations [19,20] and Lattice QCD [21–23]-are making progress toward the description of N^* electrocouplings from the first principles of QCD.

Bibliography

[1] V. D. Burkert et al., J. Phys: Conf. Ser. **299**, 012008 (2011).

[2] I. G. Aznauryan et al., CLAS Collaboration, Phys. Rev. C **80**, 055203 (2009).

[3] I. G. Aznauryan, Phys. Rev. C **67**, 0152009 (2003).

[4] I. G. Aznauryan et al., Phys. Rev. C **71**, 015201 (2005).

[5] M. Ripani et al., CLAS Collaboration, Phys. Rev. Lett. **91**, 022002 (2003)

[6] G. V. Fedotov et al., CLAS Collaboration, Phys. Rev. C**79**, 015204 (2009).

[7] V. I. Mokeev et al., Phys. Rev.C **80**, 045212 (2009).

[8] Review of Particle Physics, J. Phys. G **37**, 075021 (2010).

[9] M. Dugger et al., CLAS Collaboration, Phys. Rev. C **79**, 065206 (2009).

[10] I. G. Aznauryan, Phys. Rev. C **76**, 025212 (2007).

[11] S. Capstick and B. D. Keister, Phys. Rev. D **51**, 3598 (1995).

[12] G. Ramalho and K. Tsushima, Phys. Rev. D **81**, 074020 (2010).

[13] B. Julia-Diaz, et al., Phys. Rev. C **77**, 045205 (2008).

[14] I. G.Aznauryan, V. D. Burkert, V. I. Mokeev, arXiv:1108.1125[nucl-ex].

[15] V. D. Burkert et al., Phys. Rev. C **67**, 035204 (2003).

[16] C. D. Roberts, arXiv:1108.1030 [nucl-th].

[17] I. G. Aznauryan, et al., arXiv:0907.1901 [nucl-th].

[18] I. G.Aznauryan, V. D. Burkert, private communication.

[19] C. D. Roberts, I. C. Cloet, L. Chang, and H. L. L. Roberts, arXiv:1108.1327 [nucl-th]

[20] H. L. L. Roberts et al., Few Body System **51**, 1 (2011).

[21] R. G. Edwards et al., arXiv:1104.5152 [hep-ph], accepted by Phys. Rev. D.

[22] H.-W. Lin, Chin. Phys. C **33**, 1238 (2009), H.-W. Lin and S. D Cohen, arXiv:1108.2528 [hep-lat].

[23] V. Braun, et al., Phys. Rev. Lett. **103**, 072001 (2009).

Covariant Electroweak Structure of Light and Strange Baryons

Ki-Seok Choi[1] and Willibald Plessas
Theoretical Physics, Institute of Physics
University of Graz
A–8010 Graz, Austria

We have investigated the electromagnetic and axial form factors of all light and strange baryon ground states within the relativistic constituent-quark model. The electromagnetic and axial current operators have been constructed along the spectator model in point-form relativistic dynamics. We have obtained covariant predictions for the electroweak form factors, for momentum transfers up to $Q^2 = 4$ GeV^2, as well as the electric radii, magnetic moments, and axial charges. The theoretical results in general agree very well with the existing phenomenological data. In cases, where no experimental information is yet available, the results are compatible with data from lattice quantum chromodynamics. While our results for the nucleon have already been published in the literature, we show here only the electromagnetic and axial form factors of the Δ. Corresponding results for the strange baryons are due to be published elsewhere.

1 Theory and Framework

Electromagnetic and weak form factors are decisive observables reflecting the finite extension of hadrons. There has been a long-lasting debate about which degrees of freedom govern the structure of baryons at low and intermediate momentum transfers. With the advent of new and more precise experimental data these questions might soon be settled. In addition, lattice-QCD results have by now become more and more helpful for the understanding of various model results.

We have carried out a full program of investigating the electroweak structures of baryons in the framework of the relativistic constituent-quark model (RCQM). Starting out from a relativistically invariant mass operator, yielding a correct description of baryon spectroscopy, we have proceeded to calculate the electromagnetic and axial form factors of all baryon ground states in the point-form approach. The latter has the big advantage of yielding covariant predictions for the observables, i.e. the matrix elements of the current operators sandwiched between the mass-operator eigenstates. In particular, the form factors cannot only be made to fulfill all symmetries of the Poincaré group but also to observe time

[1] ki.choi@uni-graz.at

reversal invariance and current conservation, even if a spectator-model construction is employed [1, 2]; in these references, like in the ones given in the next paragraph, one can also find a thorough description of our theoretical framework, while all details of the calculations are contained in ref. [3].

Regarding the nucleon all the relativistic predictions specifically by the RCQM based on Goldstone-boson exchange (GBE) [4, 5] have already been published in the literature. Refs. [6–8] contain the electromagnetic form factors of both the proton and the neutron, together with their electric radii and magnetic moments, as well as the nucleon axial form factors and the nucleon axial charge. Electric radii and magnetic moments of all baryon ground states are published in ref. [9], while in refs. [10, 11] the predictions of the axial charges have been reported for all baryon ground states and also their excitations up to a resonance energy of $E \sim 2$ GeV. In some of these references as well as in refs. [2, 12] comparisons to analogous predictions by the one-gluon-exchange (OGE) RCQM [13] have also been given.

Due to space limitations in this contribution, we have chosen to exemplify our results by considering only the Δ. The corresponding results for all the other strange baryon ground states are in the course of being published in forthcoming papers.

2 Results

Fig. 1 contains the covariant predictions of the GBE [4] and OGE [13] RCQMs for the electromagnetic form factors of the Δ's. Except for the the magnetic moments of the Δ^+ and Δ^{++}, for which experimental data exist (shown in Fig. 1 by the solid triangle and solid square, respectively), we can compare our results only to available lattice-QCD data [14]. From this, obviously, the RCQM predictions are found to be quite reasonable, where in particular the experimentally measured magnetic moments are reproduced within their uncertainties. Contrary to the case of the nucleon [2, 12], also no decisive differences are seen between the GBE and OGE RCQM results for the Δ electromagnetic form factors.

In Fig. 2 we show the covariant RCQM predictions for the Δ axial form factor $G_A^\Delta(Q^2)$. Our definition of this observable is given in ref. [11], where also the values of the Δ axial charges, g_A^Δ=-4.47 and g_A^Δ=-4.30 for the GBE and OGE RCQMs, respectively, were published. All of these results are again found in good agreement with most recent lattice-QCD results [17,18], and in addition the values for the axial charges are nicely compatible with results from chiral perturbation theory [19].

The overall behaviour of our RCQM results for all the other strange baryons turns out to be very similar to what is shown here for the Δ's and has been seen before for the nucleon. Whenever experimental data exist (beyond the nucleon specifically for the electric radii and magnetic moments) the theoretical predictions, especially of the GBE RCQM, are well compatible with them. In other cases, when lattice-QCD results are available, we usually find reasonable agreement too.

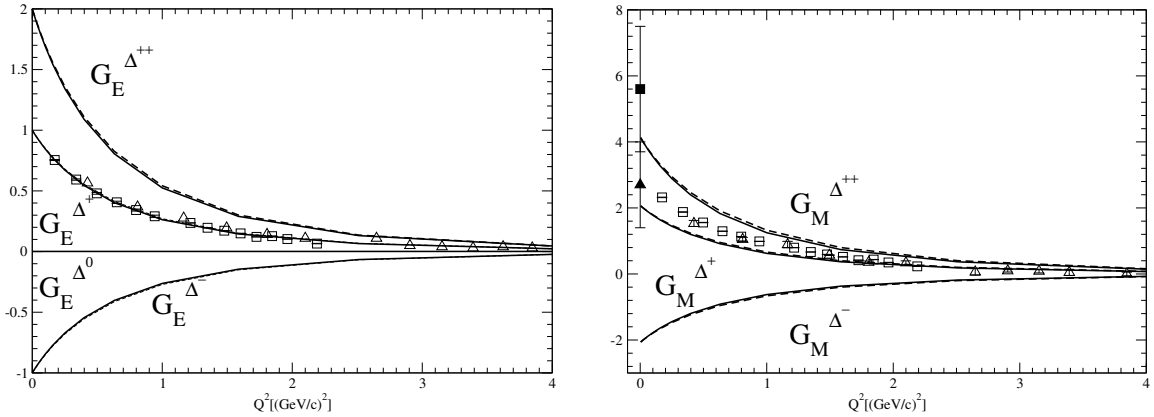

Figure 1: Electric (left panel) and magnetic (right panel) form factors of the Δ's as predicted by the GBE (solid lines) and OGE (dashed lines) RCQMs in comparison to lattice-QCD results for the Δ^+ from ref. [14] (open triangles and open squares) and experimental values for magnetic moments of the Δ^+ (solid triangle) and Δ^{++} (solid square) from refs. [15] and [16], respectively.

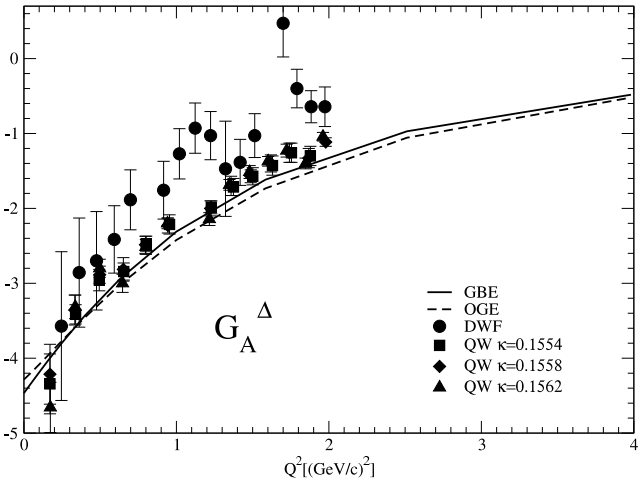

Figure 2: Δ axial form factor G_A^Δ as predicted by the GBE (solid lines) and OGE (dashed lines) RCQMs in comparison to lattice-QCD results from refs. [17,18].

Acknowledgments

This work was supported by the Austrian Science Fund, FWF, through the Doctoral Program on *Hadrons in Vacuum, Nuclei, and Stars* (FWF DK W1203-N08).

Bibliography

[1] T. Melde, L. Canton, W. Plessas, and R. F. Wagenbrunn, Eur. Phys. J. A **25**, 97 (2005).

[2] T. Melde, K. Berger, L. Canton, W. Plessas, and R. F. Wagenbrunn, Phys. Rev. D **76**, 074020 (2007).

[3] Ki-Seok Choi, PhD Thesis, University of Graz, 2011.

[4] L. Y. Glozman, W. Plessas, K. Varga, and R. F. Wagenbrunn, Phys. Rev. D **58**, 094030 (1998).

[5] L. Y. Glozman, Z. Papp, W. Plessas, K. Varga, and R. F. Wagenbrunn, Phys. Rev. C **57**, 3406 (1998).

[6] R. F. Wagenbrunn, S. Boffi, W. Klink, W. Plessas, and M. Radici, Phys. Lett. B **511**, 33 (2001).

[7] S. Boffi, L. Y. Glozman, W. Klink, W. Plessas, M. Radici, and R. F. Wagenbrunn, Eur. Phys. J. A **14**, 17 (2002).

[8] L. Y. Glozman, M. Radici, R. F. Wagenbrunn, S. Boffi, W. Klink, and W. Plessas, Phys. Lett. B **516**, 183 (2001).

[9] K. Berger, R. F. Wagenbrunn, and W. Plessas, Phys. Rev. D **70**, 094027 (2004).

[10] K.-S. Choi, W. Plessas, and R. F. Wagenbrunn, Phys. Rev. C **81**, 028201 (2010).

[11] K.-S. Choi, W. Plessas, and R. F. Wagenbrunn, Phys. Rev. D **82**, 014007 (2010).

[12] W. Plessas, PoS(LC2010)017; arXiv:1011.0156.

[13] L. Theussl, R. F. Wagenbrunn, B. Desplanques, and W. Plessas, Eur. Phys. J. A **12**, 91 (2001).

[14] C. Alexandrou et al., Phys. Rev. D **79**, 014507 (2009).

[15] M. Kotulla et al., Phys. Rev. Lett. **89**, 272001 (2002).

[16] K. Nakamura et al., J. Phys. G **37**, 075021 (2010).

[17] C. Alexandrou et al., PoS(LATTICE2010)141; arXiv:1011.0411.

[18] C. Alexandrou et al., arXiv:1106.6000.

[19] F. J. Jiang and B. C. Tiburzi, Phys. Rev. D **78**, 017504 (2008).

Strangeness magnetic moments of N and Δ

Harleen Dahiya[1] and Neetika Sharma
Department of Physics, Dr. B.R. Ambedkar National Institute of Technology, Jalandhar-144011, India

We have calculated the strangeness contribution to the magnetic moments of the nucleon and Δ decuplet baryons in the chiral constituent quark model with configuration mixing (χCQM$_{\rm config}$) which is known to provide a satisfactory explanation of the proton spin crisis and related issues. Our results are consistent with the recent experimental observations.

1 Introduction

The recent measurements by several groups SAMPLE at MIT-Bates [1], G0 at JLab [2], A4 at MAMI [3] and by HAPPEX at JLab [4] regarding the contribution of strangeness to the electromagnetic form factors of the nucleon have triggered a great deal of interest in finding the strangeness magnetic moment of the proton ($\mu(p)^s$). The SAMPLE experiment has observed $\mu(p)^s$ to be $0.37 \pm 0.26 \pm 0.20$ [1] whereas G0 [2], A4 [3] and HAPPEX [4] have observed the combination of electric and magnetic form factors. It is widely recognized that a knowledge about the strangeness content of the nucleon would undoubtedly provide vital clues to the non-perturbative aspects of QCD.

Chiral constituent quark model (χCQM) [6] can yield an adequate description of the quark sea generation through the chiral fluctuations and is also successful in giving a satisfactory explanation of proton spin crisis [7]. Recently, it has been shown chiral constituent quark model with configuration mixing (χCQM$_{\rm config}$) when coupled with the quark sea polarization and orbital angular momentum through the Cheng-Li mechansim [8] is able to give an excellent fit [9] to the octet and decuplet magnetic moments. It, therefore, becomes desirable to carry out the calculations of the strangeness contribution to the magnetic moments of nucleon in the χCQM$_{\rm config}$ in the light of some recent observations [1–5]. For the sake of completeness, we would also like to calculate the strangeness contribution to the magnetic moments of decuplet baryons $\mu(\Delta^{++})^s$, $\mu(\Delta^{+})^s$, $\mu(\Delta^{o})^s$ and $\mu(\Delta^{-})^s$ which have not been observed experimentally.

[1]dahiyah@nitj.ac.in

2 Chiral Constituent Quark Model

The basic process in the χCQM formalism is the emission of a Goldstone boson (GB) by a constituent quark which further splits into a $q\overline{q}$ pair [8, 10, 11], for example, $q_{\pm} \rightarrow \mathrm{GB}^0 + q'_{\mp} \rightarrow (q\overline{q}') + q'_{\mp}$, where $q\overline{q}' + q'$ constitute the quark sea [8] and the $\pm$ signs refer to the quark helicities. The effective Lagrangian describing interaction between quarks and a nonet of GBs, consisting of octet and a singlet, can be expressed as $\mathcal{L} = g_8\overline{\mathbf{q}}\left(\Phi + \zeta\frac{\eta'}{\sqrt{3}}I\right)\mathbf{q} = g_8\overline{\mathbf{q}}\left(\Phi'\right)\mathbf{q}$, where $\zeta = g_1/g_8$, g_1 and g_8 are the coupling constants for the singlet and octet GBs, respectively, I is the 3×3 identity matrix. The GB field which includes the octet and the singlet GBs is written as

$$(1)\ \Phi' = \begin{pmatrix} \frac{\pi^0}{\sqrt{2}} + \beta\frac{\eta}{\sqrt{6}} + \zeta\frac{\eta'}{\sqrt{3}} & \pi^+ & \alpha K^+ \\ \pi^- & -\frac{\pi^0}{\sqrt{2}} + \beta\frac{\eta}{\sqrt{6}} + \zeta\frac{\eta'}{\sqrt{3}} & \alpha K^0 \\ \alpha K^- & \alpha\overline{K}^0 & -\beta\frac{2\eta}{\sqrt{6}} + \zeta\frac{\eta'}{\sqrt{3}} \end{pmatrix} \text{and } q = \begin{pmatrix} u \\ d \\ s \end{pmatrix}.$$

SU(3) symmetry breaking is introduced by considering $M_s > M_{u,d}$ as well as by considering the masses of GBs to be nondegenerate ($M_{K,\eta} > M_\pi$ and $M_{\eta'} > M_{K,\eta}$) [8,10]. The parameter $a(=|g_8|^2)$ denotes the probability of chiral fluctuation $u(d) \rightarrow d(u) + \pi^{+(-)}$, $\alpha^2 a$, $\beta^2 a$ and $\zeta^2 a$ respectively denote the probabilities of fluctuations $u(d) \rightarrow s + K^{-(0)}$, $u(d,s) \rightarrow u(d,s) + \eta$ and $u(d,s) \rightarrow u(d,s) + \eta'$.

3 Magnetic moment

The magnetic moment of a given baryon in the χCQM can be expressed as $\mu(B)_{\text{total}} = \mu(B)_{\text{val}} + \mu(B)_{\text{sea}}$, where $\mu(B)_{\text{val}}$ represents the contribution of the valence quarks and $\mu(B)_{\text{sea}}$ corresponding to the quark sea. Further, $\mu(B)_{\text{sea}}$ can be written as $\mu(B)_{\text{sea}} = \mu(B)_{\text{spin}} + \mu(B)_{\text{orbit}}$, where the first term is the magnetic moment contribution of the q' coming from the spin polarization and the second term is due to the rotational motion of the two bodies, q' and GB and referred to as the orbital angular momentum by Cheng and Li [8].

The strangeness contribution to the magnetic moment of the proton $\mu(p)^s$ receives contributions only from the quark sea and is expressed as $\mu(p)^s = \mu(p)^s_{\text{spin}} + \mu(p)^s_{\text{orbit}}$ where $\mu(p)^s_{\text{spin}} = \sum_{q=u,d,s}\Delta q(p)^s_{\text{sea}}\mu_q$ and $\mu(p)^s_{\text{orbit}} = \frac{4}{3}[\mu(u_+ \rightarrow s_-)] - \frac{1}{3}[\mu(d_+ \rightarrow s_-)]$. Here, $\mu_q = \frac{e_q}{2M_q}$ $(q = u, d, s)$ is the quark magnetic moment, e_q and M_q are the electric charge and the mass respectively for the quark q and $\mu(q_+ \rightarrow s_-) = \frac{e_s}{2M_q}\langle l_q\rangle + \frac{e_q - e_s}{2M_{GB}}\langle l_{GB}\rangle$. The quantities (l_q, l_{GB}) and (M_q, M_{GB}) are the orbital angular momenta and masses of quark and GB, respectively. The strangeness contribution to the magnetic moments of the neutron $n(ddu)$ as well as the decuplet baryons $\Delta^{++}(uuu)$, $\Delta^+(uud)$, $\Delta^o(udd)$ and $\Delta^-(ddd)$ can be calculated similarly.

Baryon	Data	$\mu(B)^s_{\text{spin}}$	$\mu(B)^s_{\text{orbit}}$	$\mu(B)^s$
p	$0.37 \pm 0.26 \pm 0.20$ [1]	-0.09	0.06	-0.03
n	–	0.06	-0.09	-0.03
Δ^{++}	–	-0.29	0.18	-0.11
Δ^{+}	–	-0.14	0.11	-0.03
Δ^{o}	–	-0.04	-0.03	-0.07
Δ^{-}	–	-0.09	0.15	0.06

Table 1: The calculated values of the strangeness contribution to the magnetic moment of nucleon and Δ decuplet baryons in the χCQM$_{\text{config}}$.

4 Results and Discussion

In Table 1, we have presented the spin and orbital contributions pertaining to the strangeness magnetic moment of the nucleon and Δ baryons. From the Table one finds that the present result for the strangeness contribution to the magnetic moment of proton looks to be in agreement with the most recent results available for $\mu(p)^s$. On closer examination of the results, several interesting points emerge. The strangeness contribution to the magnetic moment is coming from spin and orbital angular momentum of the quark sea with opposite signs. These contributions are fairly significant and they cancel in the right direction to give the right magnitude to $\mu(p)^s$, For example, the spin contribution in this case is $-0.09\mu_N$ and the contribution coming from the orbital angular momentum is $0.05\mu_N$. These contributions cancel to give a small value for $\mu(p)^s$ $-0.03\mu_N$ which is consistent with the other observed results. Interestingly, in the case of $\mu(n)^s$, the magnetic moment is dominated by the orbital part as was observed in the case of the total magnetic moments [9] however, the total strangeness magnetic moment is same as that of the proton. Therefore, an experimental observation of this would not only justify the Cheng-Li mechanism [8] but would also suggest that the chiral fluctuations is able to generate the appropriate amount of strangeness in the nucleon. For the sake of completeness, we have also presented the results of $\mu(\Delta^{++})^s$, $\mu(\Delta^{+})^s$, $\mu(\Delta^{o})^s$, $\mu(\Delta^{-})^s$ and here also we find that there is a substantial contribution from spin and orbital angular momentum. In general, one can find that whenever there is an excess of d quarks the orbital part dominates, whereas when we have an excess of u quarks, the spin polarization dominates.

In conclusion, χCQM$_{\text{config}}$ is able to provide a fairly good description of the strangeness contribution to the magnetic moment $\mu(p)^s$ and our result is consistent with the latest experimental measurements as well as with the other calculations. The constituent quarks and the weakly interacting Goldstone bosons constitute the appropriate degrees of freedom in the nonperturbative regime of QCD and the quark sea generation through the chiral fluctuation is the key in understanding the strangeness content of the nucleon.

Acknowledgments

H.D. would like to thank the organizers of Hadron2011 and DAE-BRNS, Government of India, for financial support.

Bibliography

[1] SAMPLE Collaboration, D.T. Spayde *et al.*, Phys. Lett. **B 583**, 79 (2004).

[2] G0 Collaboration, D. Armstrong *et al.*, Phys. Rev. Lett. **95**, 092001 (2005).

[3] A4 Collaboration, F.E. Maas *et al.*, Phys. Rev. Lett. **94**, 152001 (2005).

[4] HAPPEX Collaboration, K.A. Aniol *et al.*, Phys. Rev. Lett. **98**, 032301 (2007); *ibid.* Eur. Phys. J. **A 31**, 597 (2007).

[5] K. Nakamura *et al.* (Particle Data Group), J. Phys. G **37**, 075021 (2010).

[6] S. Weinberg, Physica **A 96**, 327 (1979); A. Manohar and H. Georgi, Nucl. Phys. **B 234**, 189 (1984).

[7] E.J. Eichten, I. Hinchliffe and C. Quigg, Phys. Rev. **D 45**, 2269 (1992).

[8] T.P. Cheng and Ling Fong Li, Phys. Rev. Lett. **74**, 2872 (1995); *ibid.* Phys. Rev. **D 57**, 344 (1998); *ibid.* Phys. Rev. Lett. **80**, 2789 (1998); X. Song, Phys. Rev. **D 57**, 4114 (1998).

[9] H. Dahiya and M. Gupta, Phys. Rev. D **66**, 051501(R) (2002); **67**, 114015 (2003); **67**, 074001 (2003); N. Sharma, H. Dahiya, P.K. Chatley, and M. Gupta, Phys. Rev. D **81** , 073001 (2010).

[10] J. Linde, T. Ohlsson and Hakan Snellman, Phys. Rev. **D 57**, 452 (1998).

[11] H. Dahiya and M. Gupta, Phys. Rev. D **64**, 014013 (2001); **67**, 074001 (2003); Int. J. Mod. Phys. A **19**, 5027 (2004); **21**, 4255 (2006).

Heavy Hadrons

Heavy Hadrons

Conveners

Stefano	Bianco	INFN Frascati (*Chair*)
Harry	Lipkin	Weizmann Institute of Science
Alberto	Reis	CBPF Rio de Janeireo
Stephan	Paul	TU München

Session Chairs

Alberto	Correa dos Reis	CBPF Rio de Janeireo
Hal	Evans	Indiana University
Christophorus	Grab	ETH Zurich
Stefano	Bianco	INFN Frascati
Stephan	Paul	TU München

Contents

The role of final-state interactions in Dalitz plot studies

Bastian Kubis[1]
Helmholtz-Institut für Strahlen- und Kernphysik (Theorie) and
Bethe Center for Theoretical Physics, Universität Bonn, Germany

Dalitz plot studies for multi-hadron decays of heavy mesons are expected to become very important tools for precision investigations of CP violation. A thorough understanding of the hadronic final-state interactions is a prerequisite to achieve a highly sensitive, model-independent study of CP-violating phases in such processes. We illustrate the theoretical tools available, as well as still to be developed, from low-to-medium-energy hadron physics for this purpose, and the goals of the informal *Les Nabis* network studying these and related problems.

1 CP-violation in Dalitz plots

A precise study of final-state interactions is increasingly becoming of paramount importance for our understanding of the most diverse aspects of particle decays involving hadrons. Final-state interactions can be of significance for various reasons: if they are strong, they can significantly enhance decay probabilities; they can significantly *shape* the decay probabilities, most prominently through the occurrence of resonances; besides resonances, also new and non-trivial analytic structures can occur, such as threshold or cusp effects (for the prominent role cusp effects have played recently in studying pion–pion interactions, see Ref. [1] and references therein); and finally, they introduce strong or hadronic phases or imaginary parts, the existence of which is a prerequisite for the extraction of CP-violating phases in weak decays (see e.g. Ref. [2]). Dalitz plot studies of weak three-body decays of mesons with open heavy flavor (both D and B) are expected to acquire a key role in future precision investigations of CP violation, due to their much richer kinematic freedom compared to the (effective) two-body final states predominantly used to study CP violation at the B factories. In many cases, the branching fractions are significantly larger; furthermore, the resonance-rich environment of multi-meson final states may help to enlarge small CP phases in parts of the Dalitz plot, and differential observables may allow to obtain information on the operator structure that drives CP violation beyond the Standard Model, once it is observed. Since the results from the B factories have shown that the Cabibbo–Kobayashi–Maskawa theory [3] represents at least the dominant source of CP violation, our long-term goal will

[1] kubis@hiskp.uni-bonn.de

be to find other sources of CP violation that contribute additional, smaller effects. For this purpose, clearly extremely accurate measurements *and* means of theoretical interpretation are required. Strong evidence for CP violation in three-body final states has already been reported for $B^\pm \to K^\pm\pi^\mp\pi^\pm$ [4], e.g. with a 3.7σ signal in the effective $K\rho$ channel, while only negative results exist for D decays so far [5].

There are different possibilities how to analyze CP violation in Dalitz plots. One suggestion is a strictly model-independent extraction from the data directly [6,7], e.g. using the *significance* [7] variable defined as

$$(1) \qquad {}^{\mathrm{Dp}}S_{\mathrm{CP}}(i) \doteq \frac{N(i)-\overline{N}(i)}{\sqrt{N(i)+\overline{N}(i)}} \,,$$

where $N(i)$ and $\overline{N}(i)$ denote the event numbers of CP-conjugate decay modes in a specific Dalitz plot bin i. CP violation can then be identified in a deviation from a purely Gaussian distribution in the significance plots. The significance method allows to study *local* asymmetries and requires no theoretical input at all.

An alternative approach, in contrast, makes use of information on the strong amplitudes as input. To see why this may be advantageous, we consider the following toy model:[2] consider event number distributions given by a (Breit–Wigner) resonance signal (of mass M_{res} and width Γ_{res}) on a certain background, with a CP-violating phase δ_{CP}, according to

$$(2) \quad N,\, \overline{N} = \alpha + \beta\,\mathrm{Re}\left\{\frac{e^{\pm i\delta_{\mathrm{CP}}}}{s-M_{\mathrm{res}}^2+iM_{\mathrm{res}}\Gamma_{\mathrm{res}}}\right\} \quad \Rightarrow \quad N-\overline{N} = \frac{\sin\delta_{\mathrm{CP}}\times 2\beta M_{\mathrm{res}}\Gamma_{\mathrm{res}}}{(s-M_{\mathrm{res}}^2)^2+(M_{\mathrm{res}}\Gamma_{\mathrm{res}})^2} \,.$$

Figure 1 shows the count-rate difference and the corresponding significance distributions for two simulated cases of pseudo-data of different statistical weight: while in the high-statistics case, there indeed seems to be a deviation from Gaussian distribution in the significance, this is definitely lost in the case of less events. In contrast, fitting the data with the functional form (2) still allows to extract δ_{CP} with some (limited) accuracy even in the sparser sample. So while the theoretical assumptions and prejudices going into such an analysis clearly have to be very carefully judged, their benefit in terms of vastly increased sensitivity is also obvious.

In the following, we will therefore briefly sketch some of the tools available to analyze the hadronic amplitudes of the (light) final-state particles (such as pions and kaons).

2 Pion–pion scattering: Roy equations

Analyticity, unitarity, and crossing symmetry provide a high degree of constraint for the pion–pion scattering amplitude, which can be exploited using dispersion relations. Starting

[2] I am grateful to C. Hanhart for providing me with this example.

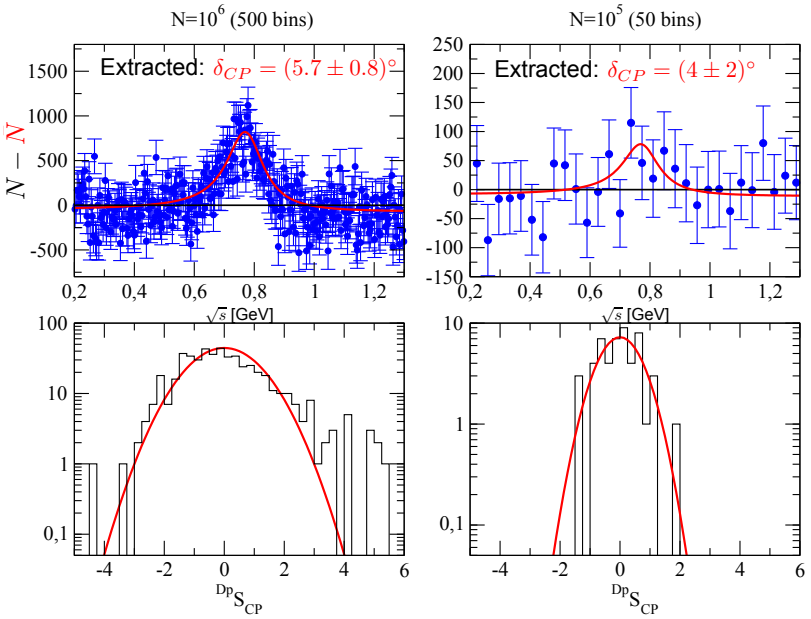

Figure 1: Toy example for extraction of a CP-violating phase, for high- (left) and low- (right) statistics samples, using the known Breit–Wigner shape (top) versus the significance variable (bottom). Input parameters used are $\delta_{\rm CP} = 5°$, $M_{\rm res} = 0.77\,\text{GeV}$, $\Gamma_{\rm res} = 0.15\,\text{GeV}$. Figure courtesy of C. Hanhart.

from a twice-subtracted dispersion relation at fixed Mandelstam variable t,

$$T(s,t) = c(t) + \frac{1}{\pi}\int_{4M_\pi^2}^{\infty} ds' \left\{ \frac{s^2}{s'^2(s'-s)} + \frac{u^2}{s'^2(s'-u)} \right\} \text{Im}\, T(s',t)\,, \tag{3}$$

the subtraction function $c(t)$ can be determined from crossing symmetry. Projecting onto partial waves t_J^I of definite angular momentum J and isospin I, one obtains a coupled system of partial-wave integral equations,

$$t_J^I(s) = k_J^I(s) + \sum_{I'=0}^{2}\sum_{J'=0}^{\infty}\int_{4M_\pi^2}^{\infty} ds' K_{JJ'}^{II'}(s,s')\text{Im}\, t_{J'}^{I'}(s')\,, \tag{4}$$

where the kernels $K_{JJ'}^{II'}(s,s')$ are kinematical functions known analytically. The subtraction polynomial $k_J^I(s)$ contains the $\pi\pi$ scattering lengths as the only free parameters; these may in turn be further constrained by matching to chiral perturbation theory [8]. Equation (4) can finally be turned into a coupled set of equations for the *phase shifts*, the Roy equations [9], by assuming elastic unitarity in the form

$$t_J^I(s) = \frac{e^{2i\delta_J^I(s)} - 1}{2i\sigma}\,, \quad \text{Im}\, t_J^I(s) = \sigma |t_J^I(s)|^2\,, \quad \sigma = \sqrt{1 - \frac{4M_\pi^2}{s}}\,. \tag{5}$$

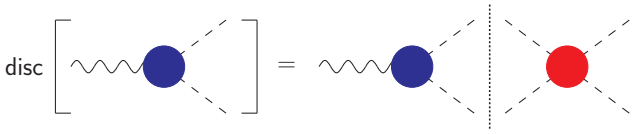

Figure 2: Graphical representation of the consequence of analyticity and unitarity for form factors.

Modern precision analyses of the Roy equations have been performed in Ref. [10], and similarly for pion–kaon scattering [11]; compare also the discussion of $\gamma\gamma \to \pi\pi$ at this conference [12]. These provide us with high-precision parameterizations of the most relevant scattering amplitudes for light mesons appearing in the final states of heavy-meson decays.

3 Analyticity and unitarity for form factors

Final-state interactions between *only two* strongly interacting particles can be described in terms of form factors, which in turn can be linked to the properties of scattering amplitudes using analyticity and unitarity. As illustrated in Fig. 2, the unitarity relation for a form factor $F_J^I(s)$ (here: of the pion) reads

$$\text{Im}\, F_J^I(s) = F_J^I(s) \times \theta\big(s - 4M_\pi^2\big) \times \sin\delta_J^I(s) e^{-i\delta_J^I(s)} \,, \tag{6}$$

from which one immediately deduces Watson's final-state theorem [13]: the form factor shares the phase $\delta_J^I(s)$ of the (elastic) scattering amplitude. The solution to Eq. (6) is obtained in terms of the Omnès function [14],

$$F_J^I(s) = P_J^I(s)\Omega_J^I(s) \,, \quad \Omega_J^I(s) = \exp\left\{\frac{s}{\pi}\int\limits_{4M_\pi^2}^{\infty} ds' \frac{\delta_J^I(s')}{s'(s'-s)}\right\} , \tag{7}$$

where $P_J^I(s)$ is a polynomial. Note that the Omnès function is completely given in terms of the phase shift. A classic application of such a form factor representation is the pion vector form factor $F_V^\pi(s)$, which rather than by Eq. (7) is written in a more refined way as

$$F_V^\pi(s) = \Omega_1^1(s) G_\omega(s) \Omega_{\text{inel}}(s) \,, \tag{8}$$

where $G_\omega(s)$ takes into account $\rho - \omega$ mixing, and $\Omega_{\text{inel}}(s)$ parameterizes inelasticities, effectively setting in above $s \gtrsim (M_\pi + M_\omega)^2$, using conformal mapping techniques [15]. Such form factor representations can be used for analyses of the $e^+e^- \to \pi^+\pi^-$ data to reduce the error of the hadronic contribution to the muon $g-2$, or to check the compatibility of the data with analyticity and unitarity [16]. Note that the effects of chiral dynamics

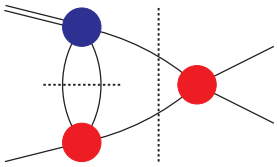

Figure 3: Example for the complication of the analytic structure of 4-point functions through crossed-channel effects, here for the decay of an η (double line) into three pions (single lines).

are particularly important for *scalar* form factors, where a parameterization in terms of Breit–Wigner resonances can lead to completely wrong phase motions (see e.g. Ref. [17] for the context of $B \to 3\pi$ decays).

4 Dispersion relations for three-body decays

The application of dispersion relations to three-body decays is more complicated than the treatment of form factors due to the more involved analytic structure, and the possibility of crossed-channel rescattering (compare also Ref. [18] reported at this conference); see Fig. 3 for a depiction of the complication of the unitarity relation. We discuss here the (low-energy) example of $\eta \to 3\pi$ decays, which has received much renewed attention recently [19,20] due to its importance for the extraction of the light quark mass ratios. One starts by decomposing the amplitude $\mathcal{M}(s,t,u) \propto \mathcal{A}(\eta \to \pi^+\pi^-\pi^0)$ into partial waves of isospin I according to [21,22]

$$\mathcal{M}(s,t,u) = \mathcal{M}_0(s) + (s-t)\mathcal{M}_1(u) + (s-u)\mathcal{M}_1(t) + \mathcal{M}_2(t) + \mathcal{M}_2(u) - \frac{2}{3}\mathcal{M}_2(s)\,, \tag{9}$$

where the $\mathcal{M}_I(s)$ are functions of one variable only, with only a right-hand cut. Equation (9) is exact as long as discontinuities of D- and higher partial waves are neglected. The unitarity relation for the $\mathcal{M}_I(s)$,

$$\mathrm{Im}\,\mathcal{M}_I(s) = \left\{\mathcal{M}_I(s) + \hat{\mathcal{M}}_I(s)\right\} \times \theta\left(s - 4M_\pi^2\right) \times \sin\delta_I(s) e^{-i\delta_I(s)} \tag{10}$$

(we now ignore the angular-momentum indices), is then complicated compared to Eq. (6) by *inhomogeneities* $\hat{\mathcal{M}}_I(s)$, which are given by angular averages over the $\mathcal{M}_I$ according to

$$\begin{aligned}
\hat{\mathcal{M}}_0(s) &= \frac{2}{3}\langle\mathcal{M}_0\rangle(s) + \frac{20}{9}\langle\mathcal{M}_2\rangle(s) + 2(s-s_0)\langle\mathcal{M}_1\rangle(s) + \frac{2}{3}\kappa(s)\langle z\mathcal{M}_1\rangle(s)\,, \\
\langle z^n f\rangle(s) &= \frac{1}{2}\int_{-1}^{1} dz\, z^n f\left(\tfrac{1}{2}(3s_0 - s + z\kappa(s))\right)\,, \quad s_0 = \frac{1}{3}\left(M_\eta^2 + 3M_\pi^2\right)\,, \\
\kappa(s) &= \sqrt{(s-(M_\eta+M_\pi)^2)(s-(M_\eta-M_\pi)^2)} \times \sqrt{1 - \frac{4\,M_\pi^2}{s}}\,,
\end{aligned} \tag{11}$$

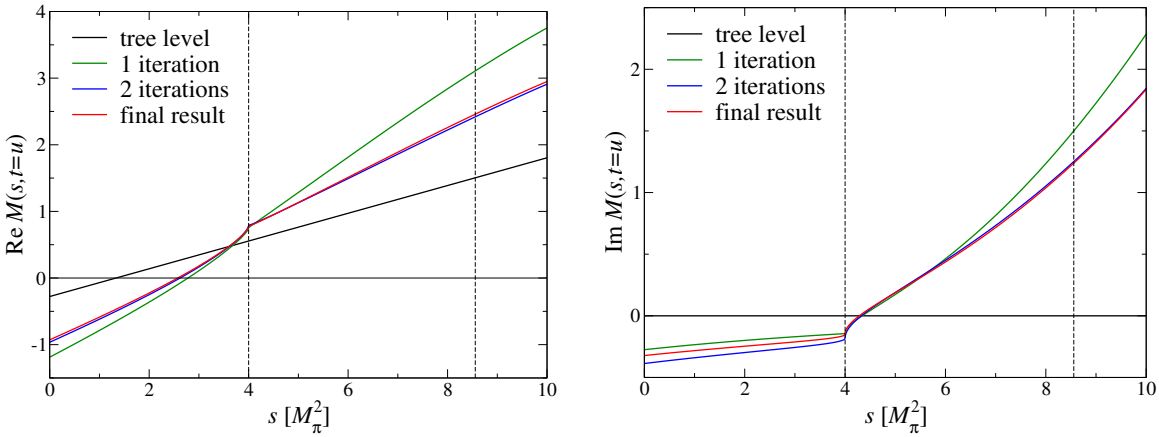

Figure 4: Real and imaginary part of the $\eta \to \pi^+\pi^-\pi^0$ amplitude $\mathcal{M}(s, t = u)$. Compare also Ref. [19].

and similarly for the other $\hat{\mathcal{M}}_I$. Note that the angular integration including the $\kappa(s)$ function is non-trivial and generates a complex analytic structure, including three-particle cuts due to the fact that the η is unstable and decays. The analog to the Omnès solution (7) are then integral equations involving the inhomogeneities [22]

$$\mathcal{M}_0(s) = \Omega_0(s)\left\{\alpha_0 + \beta_0\, s + \gamma_0\, s^2 + \frac{s^3}{\pi}\int_{4M_\pi^2}^{\infty}\frac{ds'}{s'^3}\,\frac{\sin\delta_0(s')\hat{\mathcal{M}}_0(s')}{|\Omega_0(s')|(s'-s-i\epsilon)}\right\}, \tag{12}$$

with subtraction constants α_0, β_0, γ_0, and similar forms for the other partial waves. (See Ref. [23] for earlier, related formulations.) Equations (11) and (12) can then be solved iteratively, e.g. matching the subtraction constants to chiral perturbation theory, see Fig. 4. The iteration converges fast, with the second iteration already very close to the final result.

The method sketched here is currently also applied to other light-meson decays such as $\eta' \to \eta\pi\pi$ or $\omega, \phi \to 3\pi$ [24]. Challenges to be faced when extending this formalism to heavy-meson decays include the necessity to treat systems of integral equations when coupled channels within one partial wave cannot be ignored, or inelasticities are not negligible. In particular when considering B-meson decays, elastic unitarity will surely not be sufficient. It will have to be checked when a purely perturbative treatment of crossed-channel effects is feasible (compare e.g. Ref. [25]), and when higher partial waves become important. To investigate these and related questions is part of the program of the informal *Les Nabis* network [26], which brings together physicists from theory and experiment in heavy- and light-quark physics and aims at optimizing future Dalitz plot studies along the lines sketched here—with the strong goal to better interpret the mechanism of CP violation in nature, yet at the same time teaching us important lessons on nonperturbative strong interactions.

Acknowledgments

I would like to thank the organizers of Hadron 2011 for inviting me to such an inspiring conference, C. Hanhart for stimulating discussions concerning the material presented here, and I. I. Bigi as well as M. Hoferichter for useful comments on this write-up. Partial financial support by DFG (SFB/TR 16, "Subnuclear Structure of Matter"), by the project "Study of Strongly Interacting Matter" (HadronPhysics2, grant 227431) under the 7th Framework Program of the EU, and by the Helmholtz Association providing funds to the virtual institute "Spin and strong QCD" (VH-VI-231) is gratefully acknowledged.

Bibliography

[1] J. Gasser, B. Kubis and A. Rusetsky, Nucl. Phys. B **850**, 96 (2011) [arXiv:1103.4273 [hep-ph]]; B. Kubis, EPJ Web Conf. **3**, 01008 (2010) [arXiv:0912.3440 [hep-ph]].

[2] I. I. Bigi and A. I. Sanda, *CP violation* (2nd ed.), Camb. Monogr. Part. Phys. Nucl. Phys. Cosmol. **28**, 1 (2009).

[3] N. Cabibbo, Phys. Rev. Lett. **10**, 531 (1963); M. Kobayashi and T. Maskawa, Prog. Theor. Phys. **49**, 652 (1973).

[4] A. Garmash *et al.* [Belle Collaboration], Phys. Rev. Lett. **96**, 251803 (2006) [arXiv:hep-ex/0512066]; B. Aubert *et al.* [BABAR Collaboration], Phys. Rev. D **78**, 012004 (2008) [arXiv:0803.4451 [hep-ex]].

[5] B. Aubert *et al.* [BABAR Collaboration], Phys. Rev. D **78**, 051102 (2008) [arXiv:0802.4035 [hep-ex]].

[6] S. Gardner, Phys. Lett. B **553**, 261 (2003) [arXiv:hep-ph/0203152]; S. Gardner and J. Tandean, Phys. Rev. D **69**, 034011 (2004) [arXiv:hep-ph/0308228].

[7] I. Bediaga, I. I. Bigi, A. Gomes, G. Guerrer, J. Miranda and A. C. d. Reis, Phys. Rev. D **80**, 096006 (2009) [arXiv:0905.4233 [hep-ph]].

[8] G. Colangelo, J. Gasser and H. Leutwyler, Nucl. Phys. B **603**, 125 (2001) [arXiv:hep-ph/0103088].

[9] S. M. Roy, Phys. Lett. B **36**, 353 (1971).

[10] B. Ananthanarayan, G. Colangelo, J. Gasser and H. Leutwyler, Phys. Rept. **353**, 207 (2001) [arXiv:hep-ph/0005297]; R. García-Martín, R. Kamiński, J. R. Peláez, J. Ruiz de Elvira and F. J. Ynduráin, Phys. Rev. D **83**, 074004 (2011) [arXiv:1102.2183 [hep-ph]].

[11] P. Büttiker, S. Descotes-Genon and B. Moussallam, Eur. Phys. J. C **33**, 409 (2004) [arXiv:hep-ph/0310283]

[12] M. Hoferichter, D. R. Phillips and C. Schat, arXiv:1106.4147 [hep-ph]; arXiv:1108.4776 [hep-ph], *these proceedings*.

[13] K. M. Watson, Phys. Rev. **95**, 228 (1954).

[14] R. Omnès, Nuovo Cim. **8**, 316 (1958).

[15] J. F. De Trocóniz and F. J. Ynduráin, Phys. Rev. D **65**, 093001 (2002) [arXiv:hep-ph/0106025].

[16] H. Leutwyler, arXiv:hep-ph/0212324; G. Colangelo, Nucl. Phys. Proc. Suppl. **131**, 185 (2004) [arXiv:hep-ph/0312017].

[17] S. Gardner and U.-G. Meißner, Phys. Rev. D **65**, 094004 (2002) [arXiv:hep-ph/0112281].

[18] P. C. Magalhães *et al.*, arXiv:1105.5120 [hep-ph]; P. C. Magalhães, *these proceedings*.

[19] G. Colangelo, S. Lanz and E. Passemar, PoS **CD09**, 047 (2009) [arXiv:0910.0765 [hep-ph]].

[20] S. P. Schneider, B. Kubis and C. Ditsche, JHEP **1102**, 028 (2011) [arXiv:1010.3946 [hep-ph]]; K. Kampf, M. Knecht, J. Novotný and M. Zdráhal, arXiv:1103.0982 [hep-ph].

[21] J. Stern, H. Sazdjian and N. H. Fuchs, Phys. Rev. D **47**, 3814 (1993) [arXiv:hep-ph/9301244].

[22] A. V. Anisovich and H. Leutwyler, Phys. Lett. B **375**, 335 (1996) [arXiv:hep-ph/9601237].

[23] N. N. Khuri and S. B. Treiman, Phys. Rev. **119**, 1115 (1960); I. J. R. Aitchison, J. Phys. G **3**, 121 (1977).

[24] S. P. Schneider, F. Niecknig and B. Kubis, *work in progress*.

[25] B. Liu, M. Büscher, F. K. Guo, C. Hanhart and U.-G. Meißner, Eur. Phys. J. C **63**, 93 (2009) [arXiv:0901.1185 [hep-ph]].

[26] I. I. Bigi, S. Gardner, C. Hanhart, B. Kubis, T. Mannel, U.-G. Meißner, W. Ochs, J. A. Oller, J.R. Peláez, M.R. Pennington, A. Sibirtsev (*theory*); I. Bediaga, A.E. Bondar, A. Denig, T. J. Gershon, W. Gradl, B. T. Meadows, K. Peters, U. Wiedner, G. Wilkinson (*experiment*) *et al.* [Les Nabis Collaboration].

Three-body final state interactions in $D^+ \to K^-\pi^+\pi^+$

Patrícia C. Magalhães[1,a], M. R. Robilotta[a], K. S. F. F. Guimarães[b], T. Frederico[b], W. de Paula[b], A. C. dos Reis[c], I. and Bediaga[c]

[a] *Instituto de Física, Universidade de São Paulo, São Paulo, SP, Brazil, 05315-970*

[b] *Instituto Tecnológico de Aeronáutica, São José dos Campos, SP, Brazil, 12.228-900*

[c] *Centro Brasileiro de Pesquisas Físicas, Rio de Janeiro, RJ, Brazil, 22290-180*

We stress the importance of three-body final state interactions in $D^+ \to K^-\pi^+\pi^+$. The basic building block is the $K\pi$ amplitude with parameters determined by a fit to elastic LASS data. Based on a vector weak vertex, we can describe the $K\pi$ phase production experimental in the elastic region.

1 Introduction

Decays of D mesons became an important source of information about light scalars mesons, especially in the reactions $D^+ \to K^-\pi^+\pi^+$and $D^+ \to \pi^+\pi^+\pi^-$. We calculate three-body effects in the decay $D^+ \to K^-\pi^+\pi^+$and our main motivation is the discrepancy between the projection of $K^-\pi^+$ S-wave amplitudes from E791 [1] and FOCUS [2] experiments, and the scattering $K^-\pi^+$ S-wave from LASS [3]. To calculate the $D^+ \to K^-\pi^+\pi^+$decay, we need to deal with two independent families of processes: the weak vertex, usually treated by quark factorization techniques in the literature [4], and the strong final state interactions (FSIs), which do take place after the weak decay. We concentrate on the three-body structure of FSIs and aim at identifying leading effects. Technical details of our calculation can be found in [5]. Among the simplifications made, we mention the absence in the $K\pi$ amplitude of both isospin $3/2$ and P waves, as well as couplings to vector mesons and to inelastic channels.

The $K\pi$ amplitude is an essential ingredient in the three-body FSIs. We employ an elastic amplitude inspired on chiral perturbation theory, eqs.(1, 2), supplemented by unitarization. The tuning to elastic LASS data [3] defines the three free parameters in (1, 2). This amplitude contains two poles, associated with the κ and the $K_0^*(1430)$.

$$\overline{T}_{1/2} = \frac{1}{F^2}\left[s + 3\,t/4 - (M_\pi^2 + M_K^2)\right] - \frac{\alpha(s)}{s - m_R^2}\,, \tag{1}$$

$$\alpha = \frac{3}{2F^4}\left[c_d\, s - (c_d - c_m)\,(M_\pi^2 + M_K^2)\,\right]^2\,. \tag{2}$$

[1] patricia@if.usp.br

In our exploratory work, we assume three simple topologies for the weak amplitude, indicated schematically in fig. 1. The strengths of these vertices are respectively W_a, W_b and W_c, taken as constants, and their strong evolution is studied independently.

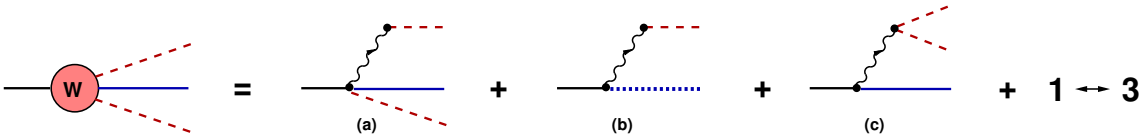

Figure 1: Topologies for the weak vertex: the dotted line is a scalar resonance and the wavy line is a W^+, which is contractile to a point in the calculation; in diagram c, one of the pions is neutral.

2 Three-body FSIs

Our treatment of FSIs departs from a Faddeev-like integral equation, represented in fig.2 top, which is subsequently expanded perturbatively, fig.2 bottom. Terms in the FSI series

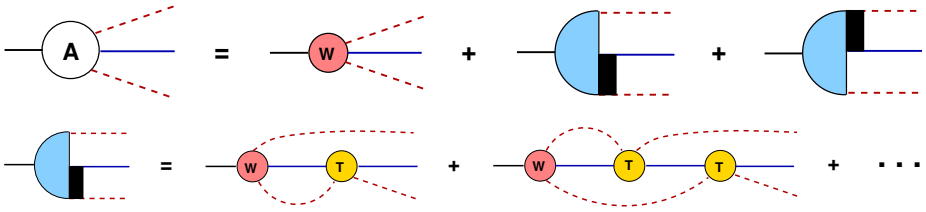

Figure 2: $D^+ \to K^-\pi^+\pi^+$decay: (top) partonic amplitude (red) and hadronic multiple scattering in the ladder approximation; (bottom) rescattering series implementing three-body unitary.

contain a recursive component, the $K\pi$ two-body amplitude. Each weak topology in fig.1 is coupled to this series, giving rise to the amplitudes A_a (fig. 3), A_b (fig. 4) and A_c (fig. 5). Processes arising from the weak vertex (a) in fig.1 involves a tree term, whereas the three-body rescattering series starting from the weak vertex b has to be treated properly in order to avoid double counting. The bottom line in fig. 4 represents the construction of resonance width. In the case of process associated with the weak vertex c in fig.5, the series is simplified, since the π_0 produced directly from the W^+ decay is not present in the final state and the tree diagram does not play a role.

For simplicity, we show here contributions from FSI series up to a single rescattering. This is a good approximation, since higher order terms tend to decrease. In the case of A_a, the leading contributions are given in the first line in fig.3, which include both tree and one loop diagrams. In A_b, only the first diagram in the upper line of fig. 4 is kept and, in A_c, the leading term is just the one loop diagram in the middle of fig. 5. In graph 6,

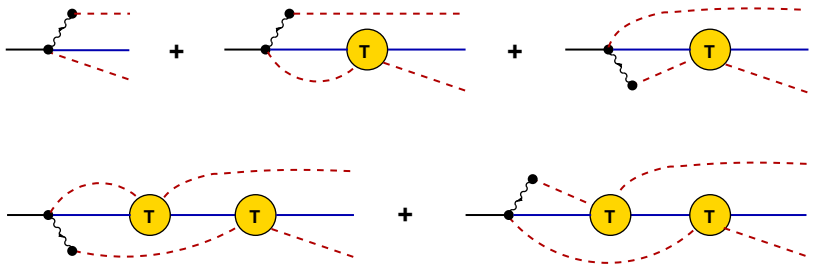

Figure 3: Diagrams involving the weak vertex W_a; the wavy line is a W^+, always plugged to a π^+; the π produced together with the $\overline{K}$ on the opposite side can be either positive or neutral.

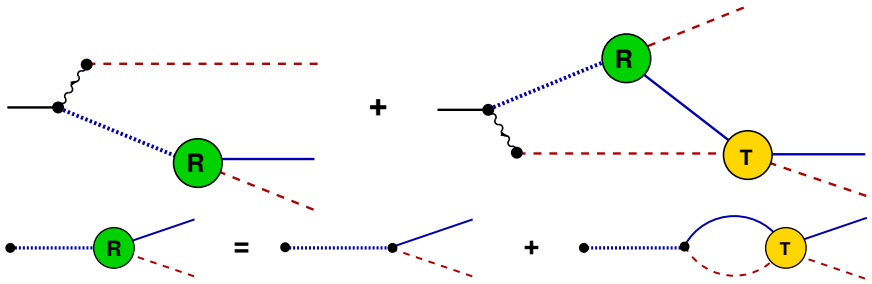

Figure 4: Diagrams involving the weak vertex W_b; the wavy line is a W^+, always plugged to a π^+ and the dotted line is a scalar resonance, which has a width given by the substructure R described at the bottom line.

we show these individual contributions for the phase, compared with the experimental scattering (LASS) [3] and production (FOCUS) [2] data. As we can see, while contributions from A_a and A_b fall exactly over the elastic $K\pi$ phase, the amplitude A_c coincides with FOCUS data [2] up to the region of the peak, when shifted by -163^0. The A_c topology is the only involving only a proper three-body interactions whereas A_a and A_b include tree contributions.

Thus, with a simple model of three-body final state interactions and a number of simplifying assumption we can reconcile experimental data between two-body interactions and weak decays, stressing the importance of proper three-body effects in the $D^+ \to K^-\pi^+\pi^+$decay

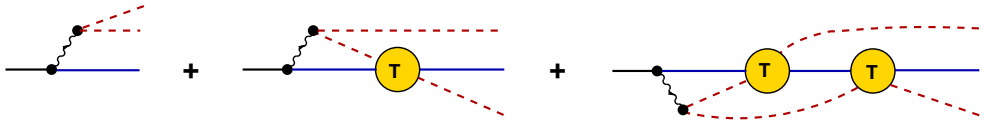

Figure 5: Diagrams involving W_c; one of the pions in the weak vertex is neutral.

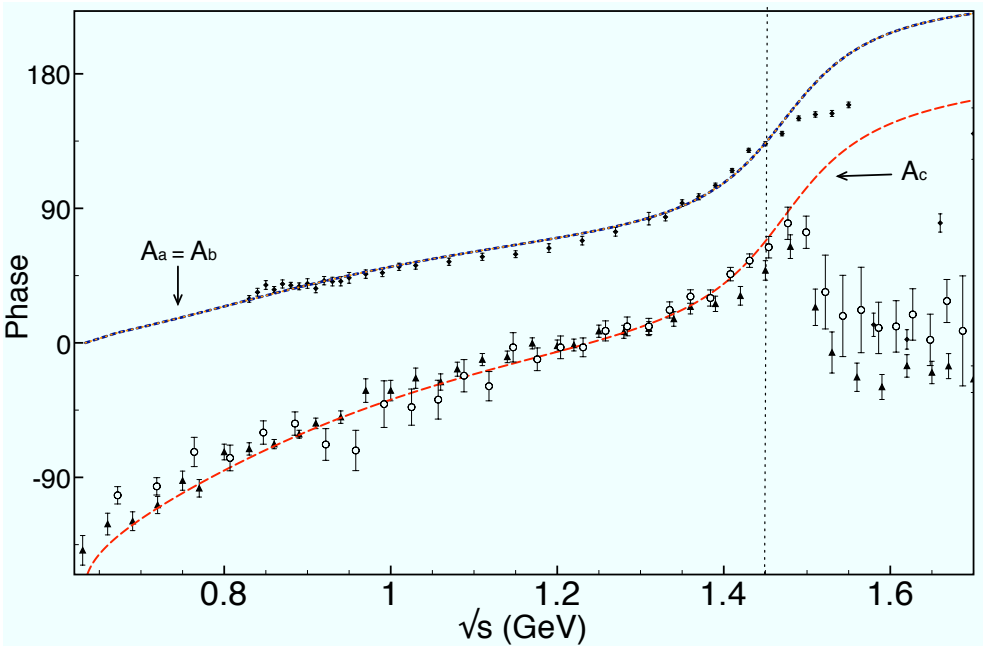

Figure 6: Leading contributions of the amplitudes A_a (blue doted), A_b (orange dashed) and A_c shifted by -163^0 (red long dashed), compared with FOCUS [2](triangle), E791 [1](circle), and elastic $K\pi$ results from LASS [3](diamond).

amplitude. More calculation details can be found in reference [5].

Acknowledgments

This work was supported by FAPESP. PCM would like to thanks the organizers of Hadron2011 for the local support.

Bibliography

[1] E.M. Aitala *et al.* (E791), Phys. Rev. Lett. **89**, 121801 (2002); E.M. Aitala *et al.* [E791 Collaboration], Phys. Rev. D**73**, 032004 (2006); Erratum-ibid. D **74**, 059901 (2006).

[2] J.M. Link *et al.* [FOCUS Collaboration], Phys. Lett. B **681**, 14 (2009).

[3] D. Aston et al., Nucl.Phys. B **296**, 493 (1988); P. Estabrooks et al., Nucl. Phys. B **133**, 490 (1978).

[4] D. R. Boito, R. Escribano, Phys. Rev. D **80**, 054007 (2009); M. Diakonou and F. Diakonos, Phys. Lett. B **216**, 436 (1989).

[5] P.C.Magalhães *et al.*, [ArXiv:1105.5120].

$\eta - \eta'$ Mixing – From Electromagnetic Transitions to Weak Decays of Charm and Beauty Hadrons

Camilla Di Donato[1,a], Giulia Ricciardi[a,b], and Ikaros Bigi[c]
[a] *I.N.F.N. Sezione di Napoli, Complesso M.S.A. — via Cintia, 80126 Napoli, Italy*
[b] *Dipartimento di Scienze Fisiche, Universitá di Napoli Federico II, Complesso M.S.A.*
[c] *Department of Physics, University of Notre Dame du Lac, Notre Dame, IN 46556, USA*

It has been realized for a long time that knowing the η and η' wave functions in terms of quark and gluon components probes our understanding of non-perturbative QCD dynamics. Great effort has been given to this challenge – yet no clear picture has emerged even with the most recent KLOE data. We point out which measurements would be most helpful in arriving at a more definite conclusion. A better knowledge of these wave functions will significantly help to disentangle the weight of different decay subprocesses in semi-leptonic decays of D^+, D_s^+ and B^+ mesons. The resulting insights will be instrumental in treating even non-leptonic B transitions involving η and η' and their CP asymmetries; thus they can sharpen the case for or against New Physics intervening there.

1 Introduction

The question of the $\eta - \eta'$ mixing go back to the beginning of the quark model era and with the advent of QCD it became even more involved, since QCD brought with it more dynamical degrees of freedom, the gluons, which can form a second class of $SU(3)$ singlet. Showing there is a pure gluonic component would establish for the first time that gluons play an independent role also in hadronic spectroscopy; we know that the presence of gluons as independent degree of freedom has been demonstrated as progenitors of jets in hard collisions. Knowing $\eta - \eta'$ mixing is essential also to disentangle SM hadronic uncertanties versus New Physics. Great effort has been given to this challenge, but yet not clear picture has emerged[2] [1].
In this paper we retrace the essential element to treat the $\eta - \eta'$ mixing, starting from the electromagnetic processes up to weak decays of charm and beauty hadrons to search for a thread for more definite conclusions.

[1] camilla.didonato@na.infn.it, giulia.ricciardi@na.infn.it, ibigi@nd.edu
[2] The complete bibliography can be found in reference [1]

1.1 The Pseudoscalar Mixing Angle

The mixing of the η and η' mesons can be described in two different bases: the $SU(3)_{fl}$ singlet and octet components, $|\eta_0\rangle$ and $|\eta_8\rangle$, respectively; the quark-flavor basis with $|\eta_q\rangle$ and $|\eta_s\rangle$:

$$\begin{pmatrix} |\eta\rangle \\ |\eta'\rangle \end{pmatrix} = \begin{pmatrix} \cos\theta_P & -\sin\theta_P \\ \sin\theta_P & \cos\theta_P \end{pmatrix} \begin{pmatrix} |\eta_8\rangle \\ |\eta_0\rangle \end{pmatrix} \rightarrow \begin{pmatrix} \cos\phi_P & -\sin\phi_P \\ \sin\phi_P & \cos\phi_P \end{pmatrix} \begin{pmatrix} s & |\eta_q\rangle \\ & |\eta_s\rangle \end{pmatrix}$$

Just for orientation: the quadratic [linear] Gell-Mann Okubo (GMO) mass formula points to $\theta_P \simeq -10^\circ$, $\phi_P \simeq 44.7^\circ$ [$\theta_P \simeq -23^\circ$, $\phi_P \simeq 31.7^\circ$].

In the nineties several papers [2] have been shown the mixing cannot be adequately described by a single angle and, due to $SU(3)_{fl}$ breaking, the mixing of decay constants does not necessarily follow the same pattern as state mixing. We have two mixing angle: θ_8 and θ_0 in the $SU(3)_{fl}$ and ϕ_q and ϕ_s in the flavour basis. The estimated difference $\theta_8 - \theta_0$ can be large as $-12^\circ/-19^\circ$. The quark-flavour basis play a key rule, indeed the mixing is large, order $\simeq 40^\circ$, but the difference between the two mixing angles is determined by OZI-rule violating contribution: the angles $\phi_q - \phi_s$ nearly coincide.

In QCD we can have a $SU(3)_{fl}$ singlet from quark-antiquark combinations and also from pure gluon configurations with the simplest one being a gluon-gluon (gg) combination. We take into account the possibility that the η and η' wave functions could contain such configuration, gluonium. We will ignore mixing with heavier pseudoscalar mesons, because the scale for gluonic excitations is presumably lower then the J/ψ mass. One would also expect the heavier η' to contain a higher dose of gluonic component then the η, which is also mainly a $SU(3)_{fl}$ octet. Present evaluations come from phenomenological analyses.

2 Electromagnetic and Strong Transitions

Several electromagnetic and strong transitions can provide information on the mixing angles and the gluonic content: radiative vector and pseudoscalar meson decays ψ', ψ, $\phi \rightarrow \gamma\eta'$ *vs.* $\gamma\eta$; ρ, $\omega \rightarrow \gamma\eta$ and $\eta' \rightarrow \gamma\omega$, $\gamma\rho$; decays into two photons or production in $\gamma\gamma$ collisions, $\eta' \rightarrow 2\gamma$ vs. $\eta \rightarrow 2\gamma$, $\gamma\gamma \rightarrow \eta$ vs. $\gamma\gamma \rightarrow \eta'$; decays of ψ into PV final states with the vector meson acting as a 'flavour filter', $\psi \rightarrow \rho/\omega/\phi + \eta$ vs. η'. The modern analyses [3–5] get consistent results, but their message, concerning the gluonium content of η', is ambivalent. The conclusion related to the discrepancy among those analyses is that the $\eta' \rightarrow \gamma\gamma$ seems to play a key role in the mixing parameters determination and the inverse process, $\gamma\gamma \rightarrow \eta'$, provides an important check of whether a resonance is a conventional $q\bar{q}$.

3 Weak Decays of Charm and Beauty Hadrons

Knowing reliably the η and η' wave functions is an important input for our understanding of several weak decays of beauty and charm hadrons. Most crucially we need it for predicting of CP asymmetries involving η and η' in the final states and to understand whether a deviation from SM predictions can be seen as a signal of New Physics. The approach in the analysis is the phenomenological one, but lattice QCD simulation have just entered the adult period and first calculation gives ϕ_P order 40°. Since one expects semi-leptonic transitions to be driven by SM dynamics only, their detailed studies teach us lessons on how non-perturbative hadronization transforms quark level transitions. The transitions $D_s^+ \to \eta^{(\prime)} l^+ \nu$, $D^+ \to \eta^{(\prime)} l^+ \nu$ and $B^+ \to \eta^{(\prime)} l^+ \nu$ proceed on greatly different time scales, since they are driven by weak interactions on the Cabibbo allowed, Cabibbo suppressed and KM suppressed levels, respectively. Yet they can provide us with highly complementary information in the sense that they produce the $\eta^{(\prime)}$ via their $s\bar{s}$, $d\bar{d}$ and $u\bar{u}$ components, respectively. The analyses of those processes again indicate a mixing angle ϕ_P order 40°. Considering also the fact that $\eta^{(\prime)}$ could be excited via a gg component the available data indicate, with a $\phi_P = 37.7^\circ$, an η' gluonium content at level of 12% [1]. The theoretical situation is more complex while spectator diagrams generate leading contributions. The so-called weak annihilation (WA) process contributes moderately to inclusive decay rates, but it could affect exclusive channel considerably. The strength of the effect depends on the size of the gluonic component in the η' wave function and on how much gg radiation one can expect in semileptonic D_s^+, D^+ and B^+ decays. Since the main effect might come from the interference with the spectator amplitude, it can a priori enhance or reduce those rates. Recent analyses [6], based on exclusive semileptonic D decays, which considers both the widths and the lepton energy moments, shows no clear evidence of WA effects. In $B^\pm$ semileptonic decays with $\eta - \eta'$ in the final states the situation is analogous to that for the $D^\pm$, except that their rates are suppressed by $|V_{us}/V_{cb}|^2$ rather than $|V_{cd}/V_{cs}|^2$ and that the range in q^2 is much large. CLEO [7] gives first evidence of $B^+ \to \eta l^+ \nu$, and later on also BaBar [8] has mesured the branching ratio, but the experimental situation is not yet satisfying: anyway the ratio $\mathcal{B}(B^+ \to \eta' l^+ \nu)/\mathcal{B}(B^+ \to \eta l^+ \nu) = 0.67 \pm 0.24_{stat} \pm 0.11_{syst}$ [9] seems to allow a large gluonic singlet contribution to the η' form factor. The corresponding ratio involving the B_s mesons, $\mathcal{B}(B_s \to \eta' l^+ l^-)/\mathcal{B}(B_s \to \eta l^+ l^-)$, is also potentially informative on the $\eta^{(\prime)}$ gluonic content, although experimentally much more challenging; they are within the reach of facilities like the Super-Flavour factories.

4 CP Violation

Within the SM many charmless non-leptonic B decays receive significant or even leading contributions from loop processes, which represent quantum corrections. Thus they provide fertile hunting grounds for New Physics, in particular in their CP asymmetries. Modes

like $B \to \eta^{(\prime)} K$ and $B_s \to \eta^{(\prime)} \phi$ seem particularly well-suited in this respect. The $B \to \eta^{(\prime)} K$ decays may proceed through tree diagrams $\bar{b} \to \bar{u} u \bar{s}$, but such contributions are color and CKM suppressed; then we have penguins $b \to s$. The same basic penguin mechanism is expected to drive both $B \to \eta^{(\prime)} K$ and $B \to \pi K$, but the rate of the former is measured to be much larger. A possible distinctive contribution are flavour singlet amplitudes, that are not allowed if the final state contains only flavour non singlet states such pions or kaons. In flavour singlet penguins two gluons couple to the η' violating the OZI rule and the amplitude can get contributions from the pure gluonic component of the η'.

5 Conclusions

In conclusion, after many and hard efforts to understand the $\eta - \eta'$ wave functions it is still intriguing to improve our understanding of the non perturbative effects in QCD, it will help to identify new physics in CP asymmetries in B and D decays.

Bibliography

[1] C. Di Donato, G. Ricciardi, I. Bigi, [arXiv:1105.3557 [hep-ph]].

[2] T. Feldmann, Int. J. Mod. Phys. **A15** (2000) 159-207. [hep-ph/9907491], and papers quoted therein

[3] F. Ambrosino *et al.* [KLOE Collaboration], Phys. Lett. **B648** (2007) 267-273; F. Ambrosino, A. Antonelli, M. Antonelli, F. Archilli, P. Beltrame, G. Bencivenni, S. Bertolucci, C. Bini *et al.*, JHEP **0907** (2009) 105.

[4] R. Escribano, J. Nadal, JHEP **0705** (2007) 006.

[5] C. E. Thomas, JHEP **0710** (2007) 026.

[6] P. Gambino, J. F. Kamenik, Nucl. Phys. **B840** (2010) 424-437.

[7] N. E. Adam *et al.* [CLEO Collaboration], Phys. Rev. Lett. **99** (2007) 041802.

[8] B. Aubert *et al.* [BABAR Collaboration], Phys. Rev. Lett. **101** (2008) 081801.

[9] P. del Amo Sanchez *et al.* [BABAR Collaboration], Phys. Rev. **D83** (2011) 052011.

Studies of the $X(3872)$ as a mixed molecule-charmonium state in QCD Sum Rules

Carina M. Zanetti[1]
Instituto de Física, Universidade de São Paulo, C.P. 66318, 05389-970 São Paulo, SP, Brazil

We use QCD sum rules to investigate the nature of the meson $X(3872)$, assumed to be a mixture between charmonium and exotic molecular $[c\bar{q}][q\bar{c}]$ states with $J^{PC} = 1^{++}$. We discuss the mass of the state, decay widths of the channels J/ψ+pions and $J/\psi\gamma$, and the branching ratio for the production of the state in the decay $B \to X(3872)K$.

The state $X(3872)$ has been first observed by the Belle collaboration in the decay $B^+ \to X(3872)K^+ \to J/\psi\pi^+\pi^-K^+$ [1], and was later confirmed by CDF, D0 and BaBar [2]. The current world average mass is $m_X = (3871.4 \pm 0.6)$ MeV, and the total decay width is $\Gamma < 2.3$ MeV at 90% confidence level. Further studies from Belle, Babar and CDF strongly favor the quantum numbers $J^{PC} = 1^{++}$ or 2^{-+} [3].

The $X(3872)$ was the first state of an increasing number of candidates for exotic hadrons discovered recently. The mass of this state is smaller than the one predicted by the constituent quark model predictions [7]. Moreover, the decay rates of processes $X(3872) \to J/\psi\,\pi^+\pi^-\pi^0$ and $X(3872) \to J/\psi\pi^+\pi^-$ are comparable [3]:

$$\frac{\Gamma(X \to J/\psi\,\pi^+\pi^-\pi^0)}{\Gamma(X \to J/\psi\pi^+\pi^-)} = 1.0 \pm 0.4 \pm 0.3, \tag{1}$$

which may indicate a strong isospin and G parity violation, which is incompatible with a $c\bar{c}$ structure for $X(3872)$. These are strong evidences that the $X(3872)$ is not a conventional $q\bar{q}$ state, and attempts to treat this state as a multiquark state are being pursued, e.g. molecules or tetraquarks states. The QCD sum rules (QCDSR) technique is an important tool in the study the structure of hadronic states. In Ref. [4] the QCDSR calculations were performed to study the tetraquark structure $[cq][\overline{cq}]$, and the mass obtained was $m_X = (3.92 \pm 0.13)$ GeV. With a current for the mesonic molecule of the type $(D^{*0}\overline{D}^0 - \overline{D}^{*0}D^0)$ the QCDSR calculation reported in [5] obtained the mass $m_X = (3.87 \pm 0.07)$ GeV in a better agreement with the experimental mass. Although the QCDSR results for the mass of the $X(3872)$ are good, it is not possible to describe the decays data with the same success [6].

There are also evidences that seem to indicate the existence of a $c\bar{c}$ component in the $X(3872)$ structure, as discussed in Refs. [8, 9]. Also, the recent observation, reported by BaBar [10],

[1] carina@if.usp.br

of the decay $X(3872) \to \psi(2S)\gamma$ at a rate: $\mathcal{B}(X \to \psi(2S)\,\gamma)/\mathcal{B}(X \to \psi\gamma) = 3.4 \pm 1.4$, is much bigger than the molecular prediction $\Gamma(X \to \psi(2S)\,\gamma)/\Gamma(X \to \psi\gamma) \sim 4 \times 10^{-3}$ [11].

In what follows we present some results of the QCD sum rules (QCDSR) calculations on the $X(3872)$, which we assume to be a mixed charmonium-molecular state. This is implemented following the prescription suggested in [12] for the light sector. The mixing is done at the level of the currents and is extended to the charm sector. In a different context (not in QCDSR), a similar mixing was suggested already some time ago by Suzuki [9]. Physically, this corresponds to a fluctuation of the $c\bar{c}$ state where a gluon is emitted and subsequently splits into a light quark-antiquark pair, which lives for some time and behaves like a molecule-like state

The the mass of a hadronic state can be calculated in QCDSR [13] from the two-point correlator using a current that creates the states with the quantum number of the hadron. Considering the X(3872) as a $J^{PC} = 1^{++}$ state we can construct a mixed charmonium-molecule current, following [12]. The $D^0\,D^{*0}$ molecule is interpolated by (with $q = u$):

$$J_\mu^{(4q)}(x) = \frac{1}{\sqrt{2}}\Big[\left(\overline{q}_a(x)\gamma_5 c_a(x)\overline{c}_b(x)\gamma_\mu q_b(x)\right) - \left(\overline{q}_a(x)\gamma_\mu c_a(x)\overline{c}_b(x)\gamma_5 q_b(x)\right)\Big]. \tag{2}$$

As in ref. [12] we define the normalized two-quark current as

$$J_\mu^{(2q)}(x) = \frac{1}{6\sqrt{2}}\langle\overline{u}u\rangle\,\overline{c}_a(x)\gamma_\mu\gamma_5 c_a(x), \tag{3}$$

and from these two currents we build the following mixed charmonium-molecular current for the $X(3872)$:

$$J_\mu^{q}(x) = \sin(\theta)J_\mu^{(4q)}(x) + \cos(\theta)J_\mu^{(2q)}(x)\,, \tag{4}$$

where θ is the mixing angle between the two-quarks and four-quarks states.

The mass of the $X(3872)$ was obtained in Ref. [14], using the current (4). Taking into account the variation of the mixing angle θ in the region $5^\circ \leqslant \theta \leqslant 13^\circ$, the QCDSR calculation of the mass gives:

$$m_X = (3.77 \pm 0.18)\ \text{GeV}\,, \tag{5}$$

which is in a good agreement with the experimental value. The value obtained for the mass grows with the value of the mixing angle θ, but for $\theta \geqslant 30^\circ$ it reaches a stable value being completely determined by the molecular part of the current.

In order to study the decays of the $X(3872)$ it is necessary to calculate the three-point function of the effective vertex for such decay. As a result of the calculation we can obtain the coupling constant that can be used to compute partial widths.

The width for the decay $X \to J/\psi V \to J/\psi F$ where $F = \pi^+\pi^-(\pi^+\pi^-\pi^0)$ for $V = \rho(\omega)$ is calculated in [14], introducing a small admixture of D^+D^{*-} and D^-D^{*+} components, then the X current is written as:

$$J^X_\mu(x) = \cos\alpha J^u_\mu(x) + \sin\alpha J^d_\mu(x), \tag{6}$$

with $J^u_\mu(x)$ and $J^d_\mu(x)$ given by Eq.(4). The mixing angle between the different light flavors are determined through the ratio (1) to be $\alpha \simeq 20^\circ$, which was obtained previously in [6, 15].

The QCDSR analysis of the three-point function of the vertex $X - J/\psi - V$ was performed with the same range of the mixing angle $5^\circ \leqslant \theta \leqslant 13^\circ$ used to determine the mass. The partial width obtained was:

$$\Gamma\left(X \to J/\psi\pi^+\pi^-\pi^0\right) = (9.3 \pm 6.9) \text{ MeV}. \tag{7}$$

in complete agreement with the experimental upper limit.

The work done in Ref. [14] showed the possibility of the description of the $X(3872)$ as a mixed state in QCDSR, fixing the mixing angles to be $5^\circ \leqslant \theta \leqslant 13^\circ$ and $\alpha \sim 20^\circ$. In Refs. [16] and [17] it was investigated further consequences of this analysis, calculating the radiative decay and the production in B decays, using the mixing angles determined in [14].

Belle Collaboration reported the radiative decay mode $X(3872) \to \gamma J/\psi$ [3] with the branching ratio: $\frac{\Gamma(X\to J/\psi\gamma)}{\Gamma(X\to J/\psi\,\pi^+\pi^-)} = 0.14 \pm 0.05$. The QCDSR analysis in [16] gives the ratio

$$\frac{\Gamma(X \to J/\psi\,\gamma)}{\Gamma(X \to J/\psi\,\pi^+\pi^-)} = 0.19 \pm 0.13\,, \tag{8}$$

which is in complete agreement with the experimental result.

The channel of production of the X from B decays, $B^\pm \to X(3872)K^\pm$, is studied in Ref. [17]. This was done in the factorization approach, where the process can be viewed as two subprocesses with two different couplings: the parameter λ_W in gives the coupling between the weak current and the X state, and the form factors $f_\pm(q^2)$ describe the weak transition $B \to K$. The branching ratio is therefore calculated was:

$$\mathcal{B}(B \to X(3872)K) = (1.00 \pm 0.68) \times 10^{-5}\,, \tag{9}$$

The result (9) is in agreement with the experimental upper limit $\mathcal{B}(B^\pm \to K^\pm X(3872)) < 3.2 \times 10^{-4}$ [18].

In summary, we present the QCDSR analysis of the $X(3872)$ state considering a mixed charmonium-molecular current. The analysis for the state mass, decays into J/ψ+pions and $J/\psi\gamma$, and the production from B decays are consistent using the mixing angles in Eq. (6) and (4) with the values $\alpha = 20^\circ$ and $5^\circ \leqslant \theta \leqslant 13^\circ$. The result presented here shows that in QCDSR is possible to explain the properties of the $X(3872)$ assuming that it is a mixture between a $c\bar{c}$ state and $D^0\overline{D}^{*0}$, $\overline{D}^0D^{*0}$, D^+D^{*-} and D^-D^{*+} molecular states.

Acknowledgments

This work supported by FAPESP (Brazil).

Bibliography

[1] S.-K. Choi *et al.* [Belle Collaboration], Phys. Rev. Lett. **91**, 262001 (2003).

[2] V. M. Abazov *et al.* [D0 Collaboration], Phys. Rev. Lett. **93**, 162002 (2004); D. Acosta *et al.* [CDF Collaboration], Phys. Rev. Lett. **93**, 072001 (2004); B. Aubert *et al.* [BaBar Collaboration], Phys. Rev. D **71**, 071103 (2005).

[3] K. Abe *et al.* [Belle Collaboration], hep-ex/0505037, hep-ex/0505038.

[4] R.D. Matheus, S. Narison, M. Nielsen and J.-M. Richard, Phys. Rev. D **75**, 014005 (2007).

[5] S.H. Lee, M. Nielsen and U. Wiedner, arXiv:0803.1168.

[6] F.S. Navarra, M. Nielsen, Phys. Lett. **B639**, 272 (2006).

[7] T. Barnes and S. Godfrey, Phys. Rev. D **69**, 054008 (2004).

[8] C. Bignamini, B. Grinstein, F. Piccinini, A. D. Polosa and C. Sabelli, Phys. Rev. Lett. **103**, 162001 (2009).

[9] M. Suzuki, Phys. Rev. D **72**, 114013 (2005).

[10] B. Aubert *et al.* [BaBar Collaboration], Phys. Rev. Lett. **102**, 132001 (2009).

[11] E.S. Swanson, Phys. Lett. B **588**, 189 (2004); Phys. Lett. B **598**, 197 (2004)

[12] J. Sugiyama, T. Nakamura, N. Ishii, T. Nishikawa and M. Oka, Phys. Rev. D **76**, 114010 (2007)

[13] M.A. Shifman, A.I. and Vainshtein and V.I. Zakharov, Nucl. Phys. B **147**, 385 (1979); L.J. Reinders, H. Rubinstein and S. Yazaki, Phys. Rept. **127**, 1 (1985).

[14] R. D. Matheus, F. S. Navarra, M. Nielsen and C. M. Zanetti, Phys. Rev. D **80**, 056002 (2009)

[15] L. Maiani, F. Piccinini, A.D. Polosa, V. Riquer, Phys. Rev. D **71**, 014028 (2005).

[16] M. Nielsen and C. M. Zanetti, Phys. Rev. D **82**, 116002 (2010)

[17] C. M. Zanetti, M. Nielsen, R. D. Matheus, Phys. Lett. **B702**, 359-363 (2011).

[18] B. Aubert *et al.* [BABAR Collaboration], Phys. Rev. Lett. **96**, 052002 (2006)

A Comprehensive Interpretation of the D_{sJ} states

Feng-Kun Guo[1,a] and Ulf-G. Meißner[b]
[a]*Helmholtz-Institut für Strahlen- und Kernphysik and Bethe Center for Theoretical Physics, Universität Bonn, D–53115 Bonn, Germany*
[b]*Institut für Kernphysik, Institute for Advanced Simulation and Jülich Center for Hadron Physics, Forschungszentrum Jülich, D–52425 Jülich, Germany*

We propose that the $D_{sJ}(2860)$ and $D_{sJ}(3040)$ are $D_1(2420)K$ and $D^*(2600)K$ bound states, respectively. Together with the famous $D_{s0}^*(2317)$ and $D_{s1}(2460)$, they belong to a family of kaonic bound states. With input only from the mass of the $D_{s0}^*(2317)$, both the predicted mass and decay pattern of the $D_{sJ}(2860)$ agree remarkably well with the measurements. The properties of the $D_{sJ}(3040)$ agree with the data as well. More kaonic bound states are also predicted awaiting experimental test. We suggest to search for a predicted $D_{s2}^*(2910)$ with a 10 MeV width in the D^*K channel and the $D_{sJ}(3040)$ in the $D_s\omega$ channel.

The constituent quark model has achieved a great success in the hadron spectroscopy until recent years when many new hadronic states were observed. The $D_{s0}^*(2317)$ and $D_{s1}(2460)$ are two outstanding examples. After their discovery, more charm-strange mesons were found, including the $D_{s1}^*(2700)$ [1, 2], $D_{sJ}(2860)$ [1] and $D_{sJ}(3040)$ [3]. The mass, decay patterns and angular distribution of the $D_{s1}^*(2700)$ were measured to be consistent with the expectation of a $2S$ $J^P = 1^-$ state. The information on the $D_{sJ}(3040)$ is not enough for identifying its nature. Among the three states, the $D_{sJ}(2860)$ is the most puzzling one.

The ratio of the different decay modes of the $D_{sJ}(2860)$ was measured to be [4]

$$R_{D_{sJ}(2860)} = \frac{\Gamma(D_{sJ}(2860) \to D^*K)}{\Gamma(D_{sJ}(2860) \to DK)} = 1.10 \pm 0.24. \tag{1}$$

Using heavy hadron chiral perturbation theory, one can calculate such a ratio without any parameter at leading order because the D^* and D are related to each other by heavy quark spin symmetry. The ratio was calculated for various possible quantum number assignments assuming a $c\bar{s}$ nature [5]. The result for $(2S, 1^-)$ is 1.23 and agrees with the data rather well. The other possibility is $(2P, 2^+)$, and the result 0.63 is not far from the data. However, the $(2S, 1^-)$ $c\bar{s}$ meson has already been identified as the $D_{s1}^*(2700)$, and the $(2P, 2^+)$ one would have a mass as large as 3.1 GeV [6]. Hence it is a challenge to understand the properties of the $D_{sJ}(2860)$ theoretically although some models exist (for references, see [7]). As will be shown in the following, both the mass and decay patterns can be nicely described were it a $D_1(2420)K$ bound state (for more details, see [7]).

[1]fkguo@hiskp.uni-bonn.de

	$D_1(2420)K$	$D_2(2460)K$	$D(2550)K$	$D^*(2600)K$	$\overline{B}_1(5720)K$	$\overline{B}_2(5747)K$
J^P	1^-	2^-	0^+	1^+	1^-	2^-
Results	2870 ± 9	2910 ± 9	2984 ± 10	3052 ± 11	6151 ± 33	6169 ± 33
Data	$2862 \pm 2^{+5}_{-2}$			$3044 \pm 8^{+30}_{-5}$		

Table 1: Predicted masses of heavy meson kaonic bound states. The experimental values are listed in the fourth row for comparison. All masses are given in MeV.

Among the models for the positive-parity charm-strange mesons $D^*_{s0}(2317)$ and $D_{s1}(2460)$, the hadronic molecular scenario (DK for $D^*_{s0}(2317)$ and D^*K for $D_{s1}(2460)$) [8–12] is very interesting because the experimental fact $M_{D_{s1}(2460)} - M_{D^*_{s0}(2317)} \simeq M_{D^*} - M_D$ emerges as its natural consequence [13]. One may ask whether there are other kaonic bound states of heavy mesons.

At low energies, the leading order interaction between the pseudo Goldstone bosons (including pions, kaons and eta for the SU(3) case) and matter fields is governed by chiral symmetry. Neglecting the Born term which is rather small, the scattering amplitude $V(s,t,u)$ is given by the so-called Weinberg-Tomozawa term. In order to obtain a bound state or a resonance, one has to perform a resummation. This can be done by using [14]

$$T(s) = V(s)[1 - G(s)V(s)]^{-1}, \tag{2}$$

where $V(s)$ is the S-wave projection of $V(s,t,u)$ and $G(s)$ consists of loop functions. In this way, the $D^*_{s0}(2317)$ and $D_{s1}(2460)$ are generated as the DK and D^*K bound states, respectively. By doing this, we have used the fact that the life time of the ground-state D and D^* is so long that their decays can be neglected in the calculations. But what is the meaning of a long life time? It should be contrasted to the range of forces which may be estimated as $1/m_\rho$ with m_ρ being the ρ-meson mass. Hence, it is natural to extend the above considerations to other heavy mesons whose width is much smaller than m_ρ (or more conservatively $2m_\pi$). There is one parameter is Eq. (2), the so-called subtraction constant $a(\mu)$ with μ being the dimensional regularization scale, which is introduced to regularize the divergent loop function. We fix the value of $a(\mu)$ to reproduce the mass of the $D^*_{s0}(2317)$ for each choice of μ. The scale μ is allowed to vary between 1 GeV and the mass of the scattered heavy meson, and in this way we estimate the uncertainties of the calculations. A family of heavy-flavor kaonic bound states can be produced. The $D^{(*)}K$ and $\overline{B}^{(*)}K$ bound states have been studied in the literature. In Table 1, results for some other states are shown in comparison with existent data. The agreement suggests that the $D_{sJ}(2860)$ and $D_{sJ}(3040)$ may be interpreted as the $D_1(2420)K$ and $D^*(2600)K$ bound states, respectively. Using the heavy quark–diquark symmetry, further predict a bound state of the kaon and the doubly-charmed baryon $\overline{\Xi}_{cc}(3520)$ with a mass of 3956 ± 20 MeV.

It is important for any identification of the nature of a hadron to reproduce not only its mass, but also its decay patterns. And it is the latter that can be used to distinguish various

models producing similar masses. The decays of $D_{sJ}(2860)$ and $D_{sJ}(3040)$ are dominated by the two-body decays occurring through the rescattering processes $D_1(2420)K \to D^{(*)}K$ and $D^*(2600)K \to D^*K$, respectively. Utilizing heavy quark spin symmetry, we get a parameter-free prediction for the ratio defined in Eq. (1),

$$R_{D_{sJ}(2860)} = 2\frac{M_{D^*}}{M_D}\left|\frac{\vec{k}_{D^*}}{\vec{k}_D}\right|^3 = 1.23. \tag{3}$$

The agreement with the measured value 1.10 ± 0.24 is remarkable. Furthermore, the helicity angular distribution for the sequential process $D_{sJ}(2860) \to D^*K \to D\pi K$ also agrees with the observation [3].

Assuming the decay widths of these kaonic bound states are exhausted by two-body decays, ratios of the total widths can be predicted based on spin symmetry. At leading order, we obtain $\Gamma_{D_{s2}^*(2910)}/\Gamma_{D_{sJ}(2860)} \simeq 0.2$ and $\Gamma_{D_{s0}^*(2985)}/\Gamma_{D_{sJ}(3040)} < 1$. Thus we have $\Gamma_{D_{s2}^*(2910)} \sim 10$ MeV.

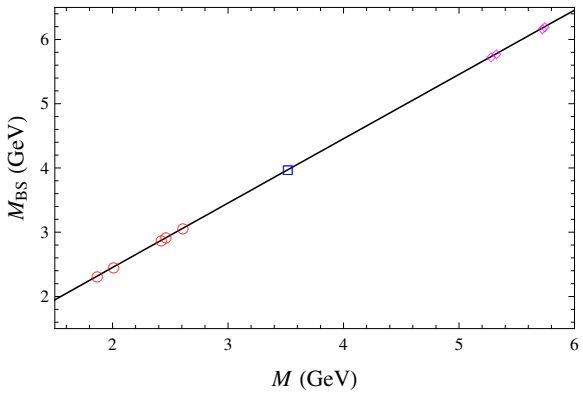

Figure 1: Trajectory of the masses of the generated kaonic bound states obtained with $\mu = 1$ GeV. The charmed, bottom mesons, and doubly charm baryon are labeled by circles, diamonds, and square, respectively.

For a potential use in the future, it might be useful to give a general expression for the masses of such kaonic bound states even approximately. For $\mu = 1$ GeV, a linear expression

$$M_{\rm BS} = 1.002M + 0.450\ \text{GeV}, \tag{4}$$

where M is the mass of the scattered heavy meson or doubly-heavy baryon, covers a range from the charmed mesons to the doubly bottom baryons, see Fig. 1 for the trajectory.

Given the small widths of the $D_1(2420)$ and $D_2(2460)$, the predictions for the $D_{sJ}(2860)$ and $D_{s2}^*(2910)$ should be rather robust. For the $D_{sJ}(2860)$, we expect that an inclusion of the inelastic channels $D^{(*)}K$ and $D_s^{(*)}\eta$ would not change the results much, because these channels are in a P-wave, and so is of higher order compared to the D_1K and $D_{s1}\eta$.

Similar discussion also applies for their bottom cousins. The results for the $D(2550)K$ and $D^*(2600)K$ are of more uncertainty because the $D(2550)$ and $D^*(2600)$ are larger, and also more inelastic channels can couple even in an S-wave. Nevertheless, the $D^*(2600)K$ bound state picture allows the decay of $D_{sJ}(3040)$ into $D_s\omega$ which is highly suppressed were it a $c\bar{s}$ meson due to the OZI rule. We therefore urge the experimentalists to search for the $D_{s2}^*(2910)$ in the D^*K channel and the $D_{sJ}(3040)$ in the $D_s\omega$ channel.

Acknowledgments

This works is partially supported by the HGF through funds provided to the virtual institute "Spin and strong QCD" (VH-VI-231), the DFG (SFB/TR 16), the EU I3HP "Study of Strongly Interacting Matter" under the Seventh Framework Program of the EU, and by BMBF (Grant No. 06BN9006).

Bibliography

[1] B. Aubert *et al.* [BABAR Collaboration], Phys. Rev. Lett. **97**, 222001 (2006).

[2] J. Brodzicka *et al.* [Belle Collaboration], Phys. Rev. Lett. **100**, 092001 (2008).

[3] B. Aubert *et al.* [BABAR Collaboration], Phys. Rev. D **80**, 092003 (2009).

[4] K. Nakamura *et al.* [Particle Data Group], J. Phys. G **37**, 075021 (2010).

[5] P. Colangelo, F. De Fazio, S. Nicotri, Phys. Lett. B **642**, 48 (2006).

[6] M. Di Pierro, E. Eichten, Phys. Rev. D **64**, 114004 (2001).

[7] F.-K. Guo and U.-G. Meißner, Phys. Rev. D **84**, 014013 (2011).

[8] T. Barnes, F. E. Close, H. J. Lipkin, Phys. Rev. D **68**, 054006 (2003).

[9] E. E. Kolomeitsev, M. F. M. Lutz, Phys. Lett. B **582**, 39 (2004).

[10] F.-K. Guo, P.-N. Shen, H.-C. Chiang *et al.*, Phys. Lett. B **641**, 278 (2006); F.-K. Guo, P.-N. Shen, H.-C. Chiang, Phys. Lett. B **647**, 133 (2007).

[11] F.-K. Guo, C. Hanhart, U.-G. Meißner, Eur. Phys. J. A **40**, 171 (2009).

[12] D. Gamermann, E. Oset, D. Strottman *et al.*, Phys. Rev. D **76**, 074016 (2007).

[13] F.-K. Guo, C. Hanhart, U.-G. Meißner, Phys. Rev. Lett. **102**, 242004 (2009).

[14] J. A. Oller, E. Oset, Nucl. Phys. A **620**, 438 (1997); J. A. Oller, U.-G. Meißner, Phys. Lett. B **500**, 263 (2001).

A molecular interpretation for the $D_{s2}^*(2573)$ and the prediction of novel exotic charmed mesons

Raquel Molina[1,a], T. Branz[b], and Eulogio Oset[a]
[a]*Instituto de Física Corpuscular (IFIC, centro mixto CSIC-UV), Valencia, Spain*
[b]*Institut für Theoretische Physik, Universität Tübingen, Tübingen, Germany*

We review the vector-vector interaction within the hidden gauge formalism in a coupled channel unitary approach. The study of the vector-vector interaction is extended to include all the sectors not studied before. This includes: $C = 0; S = 1$ (hidden-charm), $C = 1, S = 1$, and the flavor exotic sectors $C = 1; S = -1, 2$ and $C = 2; S = 0, 1, 2$. We find nine states. One of them can be identified with the $D_{s2}^*(2573)$ and is interpreted as a D^*K^* molecular state. The other eight resonances can be observed in future experiments at PANDA/FAIR. Some of them are found in the flavor exotic sectors, $C = 1; S = -1$, $C = 2; S = 0, 1$, and can be considered as $D^*\overline{K^*}$, D^*D^* and $D_s^*D^*$ molecular states.

1 Introduction

The interaction of vector mesons with themselves is done using the lagrangians of the hidden gauge formalism, which mix vector mesons with pseudoscalars and respect chiral symmetry [1]. For example, in [2], the authors found two poles in the $\rho\rho$ amplitude that can be clearly identified with the $f_0(1375)$ and the $f_2(1270)$ as $\rho\rho$ resonances states decaying in 2π or 4π by means of a box diagram mechanism. This work has been extended to the general case of two vectors of the 16-plet of SU(4) and many resonances have been obtained as a bound system of two vectors, such is the case of the $K_2^*(1430)$, the $D_2^*(2460)$ or the $Y(3940)$ (see [3–5] for more details).

In this talk we study all the sectors not studied before within the hidden gauge formalism, the $C = 0; S = 1$ (hidden-charm) sector, $C = 1, S = 1$, and the flavor exotic sectors $C = 1; S = -1, 2$ and $C = 2; S = 0, 1, 2$. Unlike other predicted states in the coupled channel unitary approach, these flavor exotic mesons cannot obviously be accomodated in the $q\bar{q}$ spectrum. Looking for these states is a new challenge for the experimentalist.

[1] rmolina@ific.uv.es

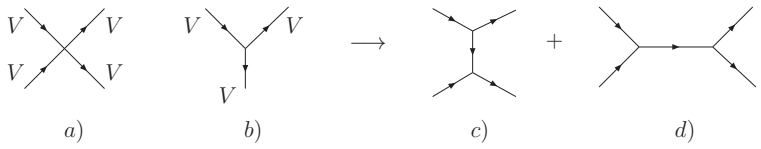

Figure 1: Terms of the $\mathcal{L}_{III}$ Lagrangian: a) four-vector contact term; b) three-vector interaction; c) t and u channels from vector exchange; d) s channel for vector exchange.

2 Formalism

We refer to [6] for a detailled explanation. The hidden-gauge formalism is applied in order to describe the interaction between vector mesons and vector mesons with pseudoscalars and photons [1]. The hidden-gauge Lagrangian, which is consistent with chiral symmetry, provides this former interaction from the term $\mathcal{L} = -\frac{1}{4}\langle \overline{V}_{\mu\nu}\overline{V}^{\mu\nu}\rangle$, from where we can get the four-vector and three-vector interaction depicted in Figs. 1 a) and b) respectively. The last one leads to the diagrams of Figs. 1 c) and d), where a vector meson is exchanged. However only the a) and c) diagrams are considered because those of Fig. 1 d) represent a minor component of s-wave (or p-wave repulsive for equal masses) and can be neglected [3]. We make the approximation of low momenta of the external vectors compared to the mass of the vector mesons, $\vec{k}/M_V \sim 0$, and the polarization vectors of the external vector mesons reduce to the spatial components.

The amplitudes of the diagrams in Fig. 1 a) and c) are projected in isospin, spin and s-wave, then, they are inserted into the Bethe-Salpeter equation, $T = (\hat{1} - VG)^{-1}\, V$, as the kernel V, being G a diagonal matrix where the matrix elements are the two meson loop functions for each channel, which are evaluated by means of dimensional regularization. In the complex plane of $\sqrt{s}$, bound states appear as poles over the real axis and below thresholds on the first Riemann sheet. In contrast, resonances are identified by poles on the second Riemann sheet above the thresholds of the channels which are open. The convolution of the G two-meson function loop is included to take into account the width of ρ and K^* mesons decaying in 2π and πK respectively. The use of the convoluted loop function provides larger widths of the states than without convolution, but the width obtained by means of this mechanism is small. Another way to consider the decay of the vector mesons into pairs of pseudoscalar is to include a box-type Feynman diagram where all the lines of the box are pseudoscalar mesons. This diagram takes into account the decay of these VV states into two pseudoscalars and has only $J^P = 0^+, 2^+$ quantum numbers. Therefore, the states with $J^P = 1^+$ are obtained in the model with a small width of a few KeV due to only the convolution of the G loop function. For the evaluation of this box diagram, two form factors are included in the PPV vertex, one is $F_1(q^2) = \frac{\Lambda_b^2 - m_1^2}{\Lambda_b^2 - (k_1^0 - q^0)^2 + |\vec{q}|^2}$ (Model A), and the other one is an exponential parametrization for an off-shell $\pi(K)$, $F(q^2) = e^{((q^0)^2 - |\vec{q}|^2)/\Lambda^2}$, together with this last form factor we use the experimental value of $g_D = 8.95$ (Model B).

C,S	$I[J^P]$	$\sqrt{s}$	$\Gamma_{\rm A}(\Lambda=1400)$	$\Gamma_{\rm B}(\Lambda=1000)$	State	$\sqrt{s}_{\rm exp}$	$\Gamma_{\rm exp}$
$1,-1$	$0[0^+]$	2848	23	25			
	$0[1^+]$	2839	3	3			
	$0[2^+]$	2733	11	22			
$1,1$	$0[0^+]$	2683	20	44			
	$0[1^+]$	2707	4×10^{-3}	4×10^{-3}			
	$0[2^+]$	2572	7	18	$D_{s2}(2573)$	2572.6 ± 0.9	20 ± 5
	$1[2^+]$	2786	8	9			
$2,0$	$0[1^+]$	3969	0	0			
$2,1$	$1/2[1^+]$	4101	0	0			

Table 1: Summary of the nine states obtained. The width is given for the model A, Γ_A, and B, Γ_B. All the quantities here are in MeV.

3 Results

3.1 Resonances from the VV interaction

We evaluate the pole positions in the sectors where we find attractive interaction and calculate the couplings to each channel from the residue of the amplitudes. In the sectors $C=1;S=-1;I=0$, $C=1;S=1;I=0,1$, $C=2;S=0;I=0$, $C=2;S=1;I=1/2$ the interaction is atractive enough to get bound states or resonances whereas the attraction is too small to bind the system or repulsive in the sectors $C=0;S=1;I=1/2$ (hidden charm), $C=1;S=-1;I=1$, $C=1;S=2;I=1/2$, $C=2;S=0;I=1$ and $C=2;S=2;I=0$. In Table 1 we give a summary of the states obtained for the models A and B with $\Lambda=1400$ and 1000 respectively, together with the only experimental counterpart observed so far. The evaluation of the coupling constants show that the three states found in the $C=1;S=-1;I=0$ sector couple strongly to $D^*\overline{K}^*$ (the only possible channel in this sector). This sector is flavor exotic and there is not any experimental counterpart observed yet. In the $C=1;S=1$ sector, three states are found for $I=0$ coupling mostly to D^*K^*, being the other two channels, $D_s^*\omega$ and $D_s^*\phi$, less dominant. For $I=1$ one state is found that couples to D^*K^* and $D_s^*\rho$, also in this case the D^*K^* contribution is dominant. In this sector, the state with $I=0$ and $J=2$ is assigned to the $D_{s2}(2572)$. In the sectors $C=2;S=0$ and $C=2;S=1$ only one state for $J=1$ is found for each sector, coupling to D^*D^* and $D^*D_s^*$ respectively. These two sectors are also flavor exotic and there is not any observation of such kind of states up to now.

4 Conclusions

We studied dynamically generated resonances from vector-vector interaction in the charm-strange and hidden-charm sectors and extended for the first time the formalism to flavor

exotic sectors. Our analysis of the T matrix resulted in nine bound states, with only one that has an experimental counterpart, the $D_{s2}^*(2573)$. We get new narrow structures with $C = 1$, $S = -1$ and $C = 2$, $S = 0, 1$ that cannot be accomodated in the $q\bar{q}$ spectrum. We encourage to the experimentalist to look for these new flavor exotic states at the PANDA/FAIR facility.

Bibliography

[1] M. Bando, T. Kugo, S. Uehara, K. Yamawaki and T. Yanagida, Phys. Rev. Lett. **54**, 1215 (1985). M. Bando, T. Kugo and K. Yamawaki, Phys. Rept. **164**, 217 (1988). M. Harada and K. Yamawaki, Phys. Rept. **381**, 1 (2003). U. G. Meissner, Phys. Rept. **161**, 213 (1988).

[2] R. Molina, D. Nicmorus and E. Oset, Phys. Rev. D **78**, 114018 (2008)

[3] L. S. Geng and E. Oset, Phys. Rev. D **79**, 074009 (2009)

[4] R. Molina, H. Nagahiro, A. Hosaka and E. Oset, Phys. Rev. D **80**, 014025 (2009)

[5] R. Molina and E. Oset, Phys. Rev. D **80**, 114013 (2009)

[6] R. Molina, T. Branz and E. Oset, Phys. Rev. D **82**, 014010 (2010)

D and D_s meson spectroscopy from lattice QCD

Daniel Mohler[1] and R. M. Woloshyn
TRIUMF
4004 Wesbrook Mall, Vancouver, BC
V6T 2A3, CANADA

We present results for the low-lying spectrum of D and D_s mesons from a lattice QCD calculation on 2+1 flavor Clover-Wilson configurations generated by the PACS-CS collaboration. In particular S- and P-wave states of charmed and charmed-strange mesons are explored for pion masses down to 156MeV. For the heavy quark, the Fermilab method is employed. In addition to ground states, some excited states are extracted using the variational method. To check our setup, calculations of the charmonium spectrum are also carried out. For charmonium, the low-lying spectrum agrees favorably with experiment. For heavy-strange and heavy-light systems substantial differences in comparison to experiment values remain in channels with nearby scattering states.

1 Introduction

The spectrum of charmed mesons contains states for which quark model expectations [1] did not hold. In particular, the charmed-strange mesons $D^{\star}_{s0}(2317)$ and $D_{s1}(2460)$, which in the limit of an infinitely heavy quark form a pair of mass-degenerate states with $j^P = \frac{1}{2}$(where j the total angular momentum of the light quark and P is parity) turn out to be narrow states with masses below the DK and $D^{\star}K$ thresholds. Due to their unanticipated properties, it has been conjectured that these states are not of a simple $\bar{q}q$ nature. Lattice QCD is ideally suited to calculate the properties of hadrons from first principles. In recent years conceptional and algorithmic improvements have enabled calculations with light dynamical quarks in boxes of size $\approx$2.5fm and with fine lattice spacings. We present results from a recent calculation of charmonium and charmed mesons using dynamical gauge configurations with light sea quarks corresponding to pion masses as low as 156MeV, which is a significant improvement over previous simulations which employed either the quenched approximation or very heavy sea quarks. The following section summarizes the technical aspects of our simulation and the last section presents selected results. For more details please refer to the full published results [2].

[1] mohler@triumf.ca

2 Technicalities

For this study 2+1 Clover-Wilson configurations generated by the PACS-CS collaboration [3] have been used. While the mass of the strange quark is kept close to its physical mass, pions made from light up and down quarks range from 702 MeV to 156 MeV. The number of lattice points is $32^3 \times 64$ and the lattice spacing has been determined [3] to be 0.907(13)fm. Table 1 shows some of the run parameters and the number of configurations used.

Ensemble	$c_{sw}^{(h)}$	$\kappa_{u/d}$	κ_s	#configs D/D_s
1	1.52617	0.13700	0.13640	200/200
2	1.52493	0.13727	0.13640	-/200
3	1.52381	0.13754	0.13640	200/200
4	1.52327	0.13754	0.13660	-/200
5	1.52326	0.13770	0.13640	200/348
6	1.52264	0.13781	0.13640	198/198

Table 1: Run parameters for the PACS-CS lattices [3]. All gauge configurations have been generated with the inverse gauge coupling $\beta = 1.90$ and the light quark clover coefficient $c_{sw}^{(l)} = 1.715$. The quantity $c_{sw}^{(h)}$ denotes the heavy quark clover coefficient.

For the charm quarks we use the *Fermilab method* [4–6]. In this approach the spin-averaged *kinetic mass* of the charmed-strange mesons is tuned to assume its physical value. Once the tuning has been done, differences in the rest masses are to be compared to experiment. The resulting charm quark hopping parameter κ_c is listed in Table 1.

The spectrum results are obtained using the variational method [7,8]. For a given set of quantum numbers a matrix $C(t)_{ij}$ of interpolating fields is constructed

$$C(t)_{ij} = \sum_n \mathrm{e}^{-tE_n} \langle 0|O_i|n\rangle \left\langle n|O_j^\dagger|0\right\rangle . \tag{1}$$

On each time slice the generalized eigenvalue problem (GEVP) is solved

$$\begin{aligned} C(t)\vec{\psi}^{(k)} &= \lambda^{(k)}(t)C(t_0)\vec{\psi}^{(k)}, \\ \lambda^{(k)}(t) &\propto \mathrm{e}^{-tE_k}\left(1+\mathcal{O}\left(\mathrm{e}^{-t\Delta E_k}\right)\right). \end{aligned} \tag{2}$$

Asymptotically only a single state contributes to each eigenvalue. For details of our quark sources, which contain Jacobi-smeared [9,10] and derivative sources [11,12] please refer to the published results [2].

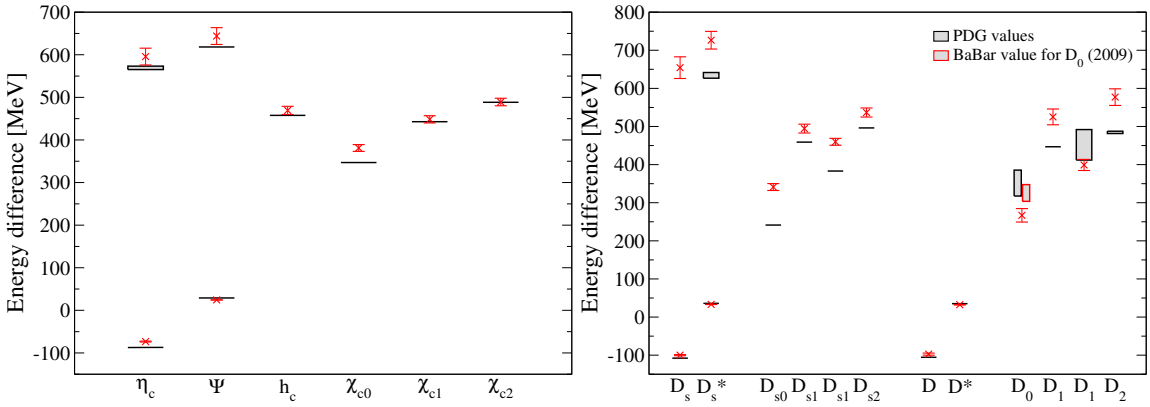

Figure 1: Left panel: Mass splittings in the charmonium spectrum compared to the spin-averaged ground state mass $(M_{\eta_c} + 3M_{J\Psi})/4$. Right panel: Same for charmed mesons.

3 Results

In this section we present a selection of results for charmed mesons and for charmonium. The charmonium spectrum below the DD and $D^\star D$ thresholds is a good test case for our setup[2], as it contains only well established and uncontroversial states that are all believed to be predominantly of a $\bar{q}q$ nature and as our tuning procedure uses no input from the charmonium spectrum. The results we obtain for the lightest sea quarks are plotted in the left panel of Figure 1. Some additional results are also shown in Table 2. In general our charmonium results agree qualitatively with the experimental spectrum. The Spin-dependent splittings displayed in Table 2 are expected to be sensitive to discretization effects and we expect that these are the dominant reason for underestimating the splittings compared to experiment.

Mass difference	Our results [MeV]	Experiment [MeV]
1S hyperfine	$97.8 \pm 0.5 \pm 1.4$	116.6 ± 1.2
1P spin-orbit	$37.5 \pm 2.4 \pm 0.5$	46.6 ± 0.1
1P tensor	$10.44 \pm 1.13 \pm 0.15$	16.25 ± 0.07
2S hyperfine	$48 \pm 18 \pm 1$	49 ± 4

Table 2: Spin dependent mass splitting in the Charmonium spectrum.

The right panel of Figure 1 shows the D and D_s spectrum as extracted from our simulation on the ensemble with the lightest sea quark mass. We obtain reasonable values for the hyperfine splittings and for the pairs of states corresponding to the multiplet with $j^P = \frac{3}{2}$ in

[2] in particular with regard to the discretization of the heavy charm quark

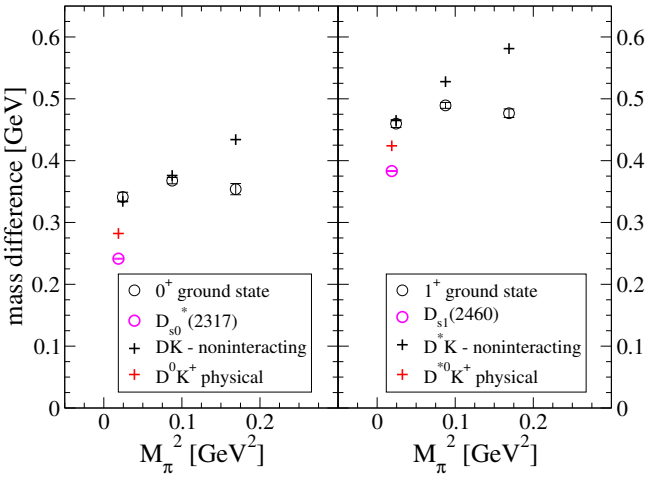

Figure 2: Measured energy levels for the $D^\star_{s0}$ (left panel) and D_{s1} (right panel) ground states (black circles) compared to experimental states (magenta circles). All masses are plotted with respect to the spin-averaged D_s ground state. The plus signs denote the DK and $D^\star K$ scattering levels on the lattice (black) and in nature (red). At our lowest pion mass the artificially heavy scattering states are very close to the measured ground state energy.

the heavy quark limit. While light sea quarks are important for several of the states, the doublets corresponding to $j^P = \frac{1}{2}$ in the heavy quark limit show a substantial difference compared to experiment, which is hard to explain by discretization effects alone. For these states the nearby DK and $D^\star K$ thresholds may play an important role. Figure 2 compares the measured energy levels in the lattice simulation with the experimental resonance and the relevant scattering threshold from experiment. It can be seen that the scattering threshold in our simulation is slightly unphysical. While the state we observe seems to coincide with the scattering threshold at the smallest pion mass, this is no longer the case for larger pion masses and the overlaps of the state with our interpolator basis (as encoded in the eigenvectors of the GEVP) suggests that we see the same state at all pion masses. In light of this, further studies should include the relevant multi-meson states in the variational basis, which is challenging from a computational point of view.

Acknowledgments

We thank the PACS-CS collaboration for access to their gauge configurations. The calculations were performed on computing clusters at TRIUMF and York University. We thank Sonia Bacca and Randy Lewis for making these resources available. This work is supported in part by the Natural Sciences and Engineering Research Council of Canada (NSERC).

Bibliography

[1] S. Godfrey and N. Isgur, *Phys. Rev.* **D32**, 189–231 (1985).

[2] D. Mohler and R. M. Woloshyn, arXiv:1103.5506.

[3] S. Aoki *et al.*, **PACS-CS** Collaboration, *Phys. Rev.* **D79**, 034503 (2009).

[4] A. X. El-Khadra, A. S. Kronfeld, and P. B. Mackenzie, *Phys. Rev.* **D55**, 3933–3957 (1997).

[5] M. B. Oktay and A. S. Kronfeld, *Phys. Rev.* **D78**, 014504 (2008).

[6] C. Bernard *et al.*, *Phys. Rev.* **D83**, 034503 (2011).

[7] M. Lüscher and U. Wolff, *Nucl. Phys.* **B339**, 222–252 (1990).

[8] C. Michael, *Nucl. Phys.* **B259**, 58 (1985).

[9] S. Güsken *et al.*, *Phys. Lett.* **B227**, 266 (1989).

[10] C. Best *et al.*, *Phys. Rev.* **D56**, 2743–2754 (1997).

[11] P. Lacock, C. Michael, P. Boyle, and P. Rowland, **UKQCD** Collaboration, *Phys. Rev.* **D54**, 6997–7009 (1996).

[12] C. Gattringer, L. Y. Glozman, C. B. Lang, D. Mohler, and S. Prelovsek, *Phys. Rev.* **D78**, 034501 (2008).

The Physics Potential of SuperB

Fergus F. Wilson[1] on behalf of the SuperB Collaboration
STFC Rutherford Appleton Laboratory, Chilton, Didcot, Oxon, OX11 0QX, UK

Super$B$ is a major new European e^+e^- collider facility to be built in Italy that will provide a precise study of the structure of New Physics beyond the Standard Model at energy scales above the LHC as well as a comprehensive program of Standard Model physics. In this article, I review the physics opportunities, the status of the accelerator and detector studies, and the future plans.

1 Introduction

The new Super$B$ facility will investigate the consequences for flavour physics of any discoveries at the LHC and search for New Physics (NP) signatures at energy scales that exceed the direct search capabilities of the LHC. A super-flavour factory will also be able to improve the precision and sensitivity of the previous generation of flavour factories by factors of five to ten. The sides and angles of the Unitarity Triangle will be determined to an accuracy of $\sim 1\%$. Limits on Lepton Flavour Violation (LFV) in τ decays will be improved by two orders of magnitude. It will become feasible to search for CP violation (CPV) in charm mixing. Extensive searches for new states in bottomium and charmonium spectroscopy will be achieved. New precision measurements of electroweak properties, such as the running of the weak mixing angle $\sin^2\theta_W$ with energy, should become possible.

Flavour physics is an ideal tool for indirect searches for NP. Both mixing and CPV in B and D mesons occur at the loop level in the Standard Model (SM) and therefore can be subject to NP corrections. New virtual particles occurring in the loops or tree diagrams can also change the predicted branching fractions or angular distributions of rare decays. Current experimental limits indicate NP with trivial flavour couplings has a scale in the 10-100 TeV range, which is much higher than the 1 TeV scale suggested by SM Higgs physics. This means that either the NP scale can not be seen in direct searches at the LHC or the NP scale is close to 1 TeV and therefore the flavour structure of the NP must be very complex. In either case, indirect searches provide a way of understanding the new phenomena in great detail.

Super$B$ is an asymmetric e^+e^- collider with a 1.3 km circumference. The design calls for 6.7 GeV positrons colliding with 4.18 GeV electrons at a centre of mass energy $\sqrt{s} =$

[1]Fergus.Wilson@stfc.ac.uk

10.58 GeV. The boost $\beta\gamma = 0.238$ is approximately half the value used at *BABAR* [1]. The electron beam can be 60%-80% polarized. The design luminosity is $10^{36}\,\mathrm{cm}^{-2}\mathrm{s}^{-1}$ and data taking is expected to start in the latter part of this decade with a delivered integrated luminosity of 75 ab^{-1} over five years. It should be possible to exceed the baseline luminosity specification, leading to the prospect of collecting 20-40 ab^{-1} per year in later years.

In the following sections, I discuss the physics potential of some of the key measurements to be made at the Super*B* factory with an integrated luminosity of 75 ab^{-1}. In addition, there is a comprehensive program for B_s at the $\Upsilon(5S)$ resonance, bottomium and charmonium spectroscopy, ISR physics, g-2 hadronic contributions, and two-photon interactions, to name just a few.

2 Physics Potential

Both *BABAR* and Belle [2] have successfully measured the CKM Unitarity Triangle angles α, β and γ [3]. Although there are discrepancies in some measurements, overall everything is consistent to a few sigma. Increasing the statistics will show if these tensions are real and possible signs of NP. It will be possible to measure the angles α and γ to $1-2\%$, and β to 0.1%. $|V_{cb}|$ and $|V_{ub}|$ can be measured to 1% and 2% accuracy, respectively, in both inclusive and exclusive semileptonic decays. The production of copious amounts of charm decays could lead to the measurement of the charm Unitarity Triangle parameters. Figure 1 shows the $\overline{\rho}$-$\overline{\eta}$ plane with current and predicted experimental measurements, assuming the current measurements maintain their central values.

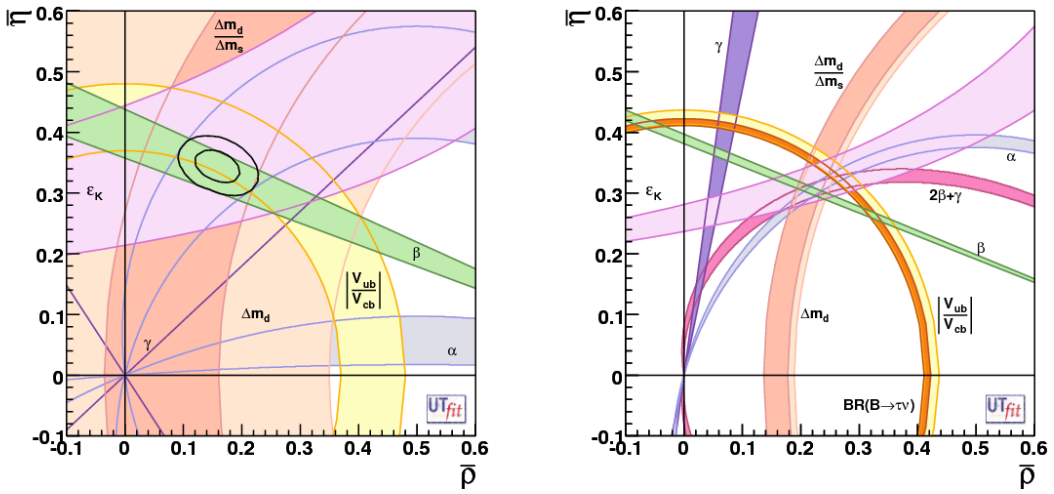

Figure 1: Regions corresponding to 95% probability for $\overline{\rho}$ and $\overline{\eta}$ with current measurements (left) and with Super*B* precision assuming the current central values (right).

	H^+	MFV	non-MFV	NP	Right-hand	LTH	SUSY models				
	high tanβ			Z-penguins	currents		AC	RVV2	AKM	δLL	FBMSSM
$\mathcal{B}(\tau \to \mu\gamma)$							L	L	M	L	L
$\mathcal{B}(\tau \to \mu\mu\mu)$						L					
$\mathcal{B}(B \to \tau\nu, \mu\nu)$	L-CKM										
$\mathcal{B}(B \to K^{(*)}\nu\bar{\nu})$			M	L			M	M	M	M	M
$S_{K^0_S\pi^0\gamma}$					L						
Angle β (ΔS)			L-CKM		L		L	M	M	L	L
$A_{CP}(B \to X_s\gamma)$			L		M		M	M	M	L	L
$\mathcal{B}(B \to X_s\gamma)$		L	M		M						
$\mathcal{B}(B \to X_s ll)$			M	M	M						
$A_{FB}(B \to K^{(*)}ll)$							M	M	M	L	L
Charm mixing							L	M	M	M	M
CPV in Charm	L									L	

Table 1: The golden matrix of observables versus a sample of NP scenarios. MFV is a representative Minimal Flavour Violation model; LTH is a Littlest Higgs Model with T Parity. A number of explicit SUSY models are included [6]. L denotes a large effect, M a measurable effect and L-CKM indicates a measurement that requires precise measurement of the CKM matrix. ΔS is the difference in the angle β between $b \to s$ penguin-dominated transitions and $b \to c\bar{c}s$ decays.

Super$B$ will make precision measurements of a series of "Golden Modes". The SM predictions for these modes are well calculated and they can be cleanly measured experimentally. NP scenarios can be differentiated by comparing the measured values with NP predictions. Table 1 shows just some of the key measurements and a sample of NP models.

In 2-Higgs-doublet (2HDM-II) and MSSM models, the decay $B \to \tau\nu$ is sensitive to the presence of a charged Higgs H^- replacing the SM W^-. Super$B$ will be able to exclude masses up to $\sim 2-3$ TeV for values of $\tan\beta$ up to 80. The region of charged Higgs mass versus $\tan\beta$ that can be excluded is shown in Figure 2 for both the 2HDM-II and MSSM models. This includes the current 20% uncertainty from f_b and $V_{\rm ub}$ that can be expected to be much reduced in the future.

Super$B$ can access the off-diagonal elements of generic squark mass matrices in the MSSM model using the mass insertion approximation. These can not be seen by the LHC general purpose detectors. As an example, Super$B$ is sensitive to non-zero values of the matrix element $(\delta^d_{23})_{LL,LR}$ for gluino masses in the 1-10 TeV range through decays such as $b \to s\gamma$ and $b \to sl^+l^-$ (Figure 3).

An almost equal number of $\tau^+\tau^-$ pairs are produced as $B\bar{B}$ pairs at the $\Upsilon(4S)$ resonance. Current experimental 90% confidence level upper limits on τ LFV are in the $10^{-8} - 10^{-7}$ range, depending on the decay. In the very clean environment of Super$B$, upper limits on τ LFV can be achieved down to a level of 2×10^{-10} for $\tau \to \mu\mu\mu$ and Super$B$ can measure the upper limits in ~ 50 other τ decay modes. Background-free modes should scale with the luminosity while other modes will scale with $\sqrt{\mathcal{L}}$ or better, thanks to re-optimized analysis techniques. In $\tau \to \mu\gamma$ for example, LFV is predicted at the level $10^{-10} - 10^{-7}$ depending

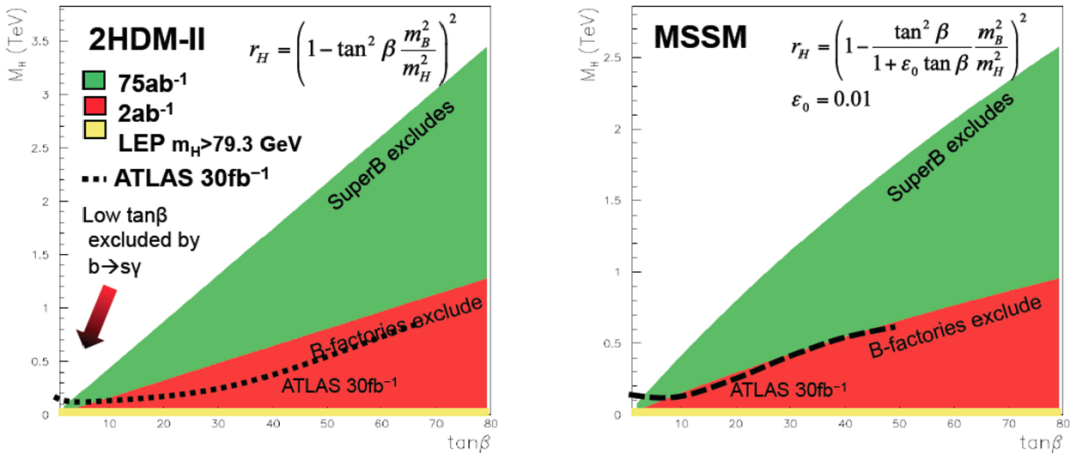

Figure 2: The mass of the charged Higgs versus $\tan\beta$ from $B \to \tau\nu$ decays for a 2HDM-II (left) and MSSM (right) model. The dark (red) region is excluded assuming the *BABAR* and Belle datasets are combined and the light (green) region shows the exclusion potential of Super*B*.

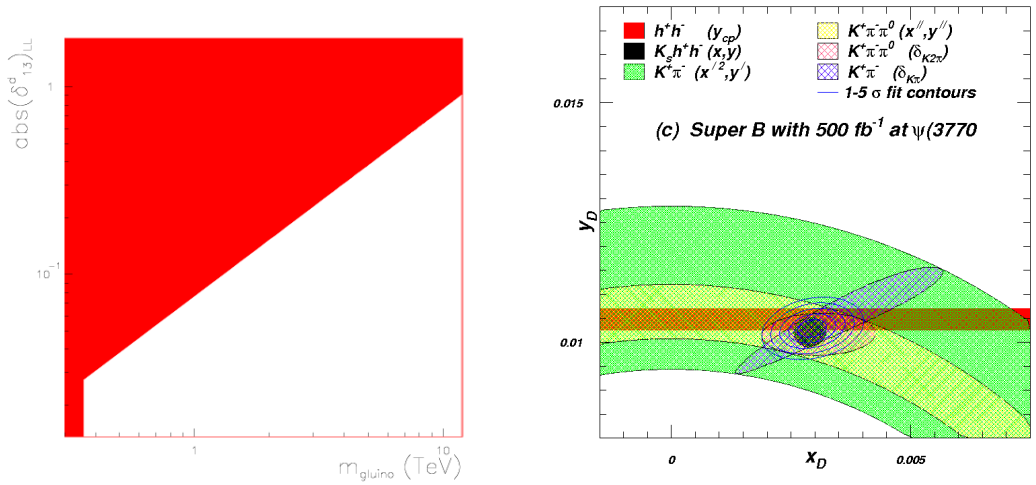

Figure 3: Left: The shaded (red) region shows where a measurement can be made (defined as a 3σ significance) of the matrix element $(\delta^d_{23})_{LL,LR}$ as a function of gluino mass in an MSSM model from measurements involving a $b \to s$ transition. Right: the expected precision on charm mixing parameters from combining BES-III and Super*B* $\psi(3770)$ and $\Upsilon(4S)$ data.

on the NP model. SU(5) SUSY GUT models predict $\tau \to \mu\gamma$ branching fractions between 10^{-7} and 10^{-9} depending on the NP phase, so the majority of the parameter space is within

the expected Super$B$ sensitivity of 2×10^{-9}.

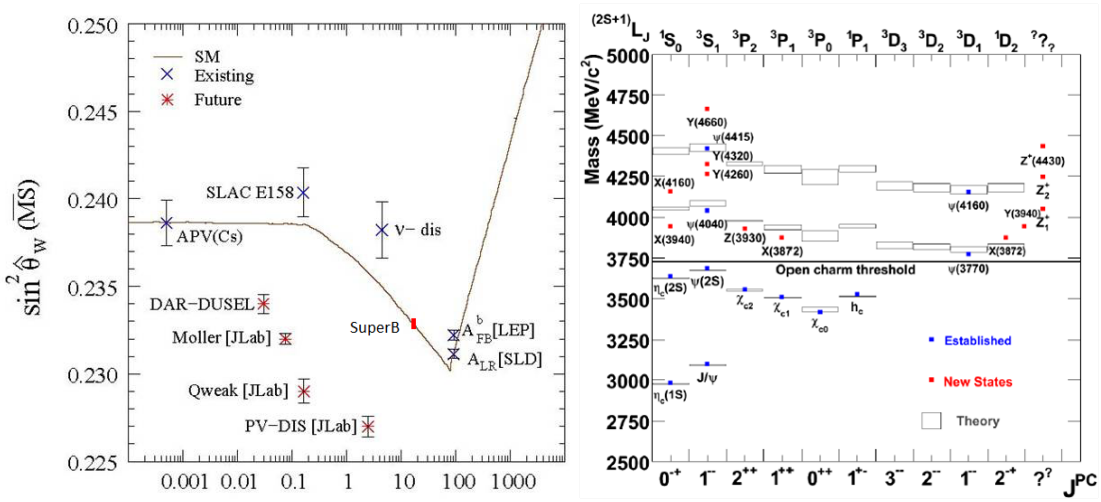

Figure 4: Left: Measurements of $\sin^2\theta_w$ as a function of energy (GeV). The size of the bar at an energy ~ 10.6 GeV representing the Super$B$ measurement is approximately the same size as the error. Right: Measured masses of newly observed states positioned according to their most likely quantum numbers.

CPV in charm decays is expected to be very low in the SM ($< 1\%$) so its detection would be a clear indicator of NP. Current values for the mixing parameters x and y from HFAG [3] fits give $(0.63 \pm 0.20)\%$ and $(0.75 \pm 0.12)\%$, respectively, allowing for CPV [4]. At Super$B$, the errors should reduce to 0.07% and 0.02%, respectively. If the results are combined with expected results from BES-III and a dedicated Super$B$ 500 fb^{-1} run ($\sim$ 4 months running) at the $D\,\overline{D}$ threshold, the BES-III/CLEO-c physics programme can be repeated leading to a further reduction in these errors to 0.02% and 0.01%, respectively. This is shown in the right-hand plot of Figure 3.

If a polarised electron beam is available, many of the upper limits on τ LFV modes can be improved by an additional factor of two. The polarisation also allows for the search for τ EDM at a level of $2 \times 10^{-19} e$ cm and measurement of the τ anomalous magnetic moment $\Delta\alpha_\tau$ with an error of 10^{-6}. The value of $\sin^2\theta_w$ can be measured with an accuracy $\pm 1.8 \times 10^{-4}$ at $Q = 10.58$ GeV and so help understand the discrepancy in the measurements from LEP, SLD and NuTev [5]. This is shown in the left-hand plot of Figure 4 where the size of the bar at $Q = 10.58$ GeV represents the expected error on the Super$B$ measurement. It may even be possible to measure $\sin^2\theta_w$ at the $\psi(3770)$ mass if polarisation can be achieved.

The B-Factories and the Tevatron have discovered heavy bound states that do not fit into the conventional meson interpretation. However, apart from some exceptions like the $X(3872)$, they have only been observed in a single decay channel with a significance only just above 5σ. The right-hand plot of Figure 4 shows some of the newly discovered states. Possible

explanations include hybrids, molecules, tetraquarks and threshold effects. Super$B$'s ability to run at the $\Upsilon(nS)$ resonances and charm threshold provides a unique opportunity for testing low- and high-energy QCD predictions. Predicting the expected rates for poorly measured resonances is of course hard and work is on-going to improve the extrapolations. The $B \to X(3872)K$ decays should produce $\sim 2k - 10k$ events in each of their main decay channels. $\Upsilon(4260) \to J/\psi\,\pi^+\pi^-$ will have $\sim 45k$ events, while $\sim 4.5k$ events can be expected for both $\Upsilon(4350)$ and $\Upsilon(4660)$ decaying to $\psi(2S)\pi^+\pi^-$. It should be possible to confirm the existence of the $Z_1^+(4050)$, $Z^+(4430)$ and $Z_2^+(4430)$ as Super$B$ will collect between $150k - 2M$ events of the relevant fully reconstructed final states $J/\psi\,\pi^+K$, $\psi(2S)\pi^+K$, and $\chi_{cJ}\pi^+K$.

3 Status of the project

The physics potential [6], and the detector [7] and accelerator [8] plans have been extensively documented. The accelerator parameters are close to final for operating in the $\psi(3770)$ to $\Upsilon(5S)$ energy range and the accelerator will reuse large parts of the SLAC PEP-II hardware. The campus of Tor Vergata University, Rome, was chosen as the site at the end of May 2011. Data taking should begin five to six years after construction begins.

Bibliography

[1] B. Aubert et al., (*BABAR* Collaboration), Nucl. Instrum. Methods Phys. Res., Sect. A **479**, 1 (2002).

[2] A. Abashian et al., (Belle Collaboration), Nucl. Instrum. Methods Phys. Res., Sect. A **479**, 1 (2002).

[3] Heavy Flavor Averaging Group (HFAG), www.slac.stanford.edu/xorg/hfag.

[4] C. Amsler et al., J. Phys. **G37**, (2010) 075021.

[5] EW Working Groups, *Precision Electroweak measurements on the Z Resonance*, Phys. Rept. **427**, 257 (2006).

[6] D.G. Hitlin et al., *New Physics at the Super Flavor Factory*, [arXiv:0810.1312.1541]; M. Bona et al., *SuperB Conceptual Design Report*, [arXiv:0709.0451]; B. O'Leary et al., *SuperB Progress Report – Physics*, [arXiv:1008.1541].

[7] E. Grauges et al., *SuperB Progress Report – Detector*, [arXiv:1007.4241].

[8] M.E. Biagini et al., *SuperB Progress Report – Accelerator*, [arXiv:1009.6178].

Heavy-Quark Masses and Heavy-Meson Decay Constants from Borel Sum Rules in QCD

Dmitri Melikhov[1,a,b,c], Wolfgang Lucha[a], and Silvano Simula[d]
[a]*HEPHY, Austrian Academy of Sciences, Nikolsdorfergasse 18, A-1050 Vienna, Austria*
[b]*Faculty of Physics, University of Vienna, Boltzmanngasse 5, A-1090 Vienna, Austria*
[c]*SINP, Moscow State University, 119991 Moscow, Russia*
[d]*INFN, Sezione di Roma Tre, Via della Vasca Navale 84, I-00146 Roma, Italy*

Slight sophistications of the QCD sum-rule formalism may have great impact on the reliability of predicted hadron observables, as exemplified for the case of heavy-meson decay constants.

Quark–Hadron Duality. The extraction of the decay constant f_P of any ground-state heavy pseudoscalar meson P from QCD sum rules [1–3] is a two-phase process: First, the operator product expansion (OPE) for the Borel-transformed correlation function of the two relevant pseudoscalar heavy-light currents has to be derived. Second, even if all parameters of this OPE were known exactly, the knowledge of merely *truncated* OPEs for correlators allows to extract bound-state features with only a limited accuracy, reflecting an intrinsic uncertainty of the QCD sum-rule formalism. Controlling this uncertainty poses a delicate challenge [4]. We consider mesons $P \equiv (Q\,\overline{q})$ of mass M_P composed of heavy quarks Q and light quarks $\overline{q}$. The *assumption* of *quark–hadron duality* entails a relation between the hadronic ground-state contribution and the QCD correlator truncated at a certain *effective continuum threshold* s_{eff}:

$$(1) \qquad f_P^2\, M_P^4 \exp(-M_P^2\,\tau) = \Pi_{\text{dual}}(\tau, s_{\text{eff}}) \equiv \int_{(m_Q+m_q)^2}^{s_{\text{eff}}} \mathrm{d}s \exp(-s\,\tau)\,\rho_{\text{pert}}(s) + \Pi_{\text{power}}(\tau)\ .$$

Obviously, in order to be able to extract f_P one has to develop a procedure determining s_{eff}. Borel transformations introduce a mass parameter $\widetilde{M}$, included here in the form $\tau \equiv 1/\widetilde{M}^2$. A crucial, albeit rather trivial, observation is that s_{eff} must be a function of τ. Otherwise, the two members of (1) exhibit different τ-behaviour. The *exact* effective continuum threshold, which would reproduce the *true* values of hadron mass and decay constant on the left-hand side of (1), is, clearly, not known. Therefore, our ideas of *extracting* hadron parameters from sum rules consist in attempting to obtain a reliable approximation to the exact threshold s_{eff} and to control the accuracy of this approximation. In a recent series of publications [5], we have constructed all procedures, techniques, and algorithms required to achieve this goal: With our concept of $s_{\text{eff}}(\tau)$, we define dual mass M_{dual} and dual decay constant f_{dual} of P by

$$M_{\text{dual}}^2(\tau) \equiv -\frac{\mathrm{d}}{\mathrm{d}\tau} \log \Pi_{\text{dual}}(\tau, s_{\text{eff}}(\tau))\ , \qquad f_{\text{dual}}^2(\tau) \equiv M_P^{-4} \exp(M_P^2\,\tau)\,\Pi_{\text{dual}}(\tau, s_{\text{eff}}(\tau))\ .$$

[1]dmitri_melikhov@gmx.de

If the ground-state mass' actual value M_P is known, the deviation of our dual ground-state mass $M_{\rm dual}$ from this M_P indicates the amount of excited-state contributions picked up by our dual correlator $\Pi_{\rm dual}(\tau, s_{\rm eff}(\tau))$. Assuming specific Ansätze for our function $s_{\rm eff}(\tau)$ and requiring least deviation of our $M_{\rm dual}$ from the true M_P in the range of admissible values of the Borel parameter τ leads to a variational solution for the effective threshold. With $s_{\rm eff}(\tau)$ at hand, we find the P-meson's decay constant from the second of the above dual relations. The traditional *assumption* for the effective threshold is that it is a (τ-independent) constant. In addition to this very crude approximation, we consider for $s_{\rm eff}(\tau)$ also polynomials in τ. It is easy to imagine that a τ-dependent threshold greatly facilitates reproducing the true mass value M_P. This implies that a dual correlator with τ-dependent threshold isolates the ground state to much higher extent and is less plagued by excited-state contamination than a dual correlator with the conventional, but naïve, τ-independent threshold. Consequently, the accuracies of extracted hadron observables are drastically improved. Recent experience from various quantum-mechanical test grounds reveals that the band of results computed from linear, quadratic, and cubic Ansätze for $s_{\rm eff}(\tau)$ encompasses the exact f_P value [5] and that the extraction procedures in quantum mechanics and in QCD are (even quantitatively) very similar [6]. For all the details of our improved sum-rule approach, consult Refs. [2–7].

OPE and Heavy-Quark Mass Scheme. A close inspection shows that for both heavy-light correlators and resulting decay constants the choice of the precise mass scheme adopted for defining the heavy-quark mass is crucial. The OPE for the correlator (1) to three-loop order was derived in terms of the heavy-quark *pole mass* in [8]. An alternative is to reorganize the perturbative expansions in terms of the heavy-quark *running* $\overline{MS}$ *mass* [9]. Figure 1 presents the B-meson decay constant f_B resulting from both choices. In each case, a *constant* effective threshold [differing, of course, for pole (s_0) and $\overline{\rm MS}$ ($\overline{s_0}$) mass scheme] is fixed by requiring maximum stability of the f_B value obtained. From this exercise we gain important insights:

(a) In the pole-mass scheme, the perturbative series for the decay constant shows no sign of convergence. The separate contributions of LO, NLO, and NNLO terms are of similar size. Accordingly, the pole-mass-scheme result for f_B significantly underestimates its true value.

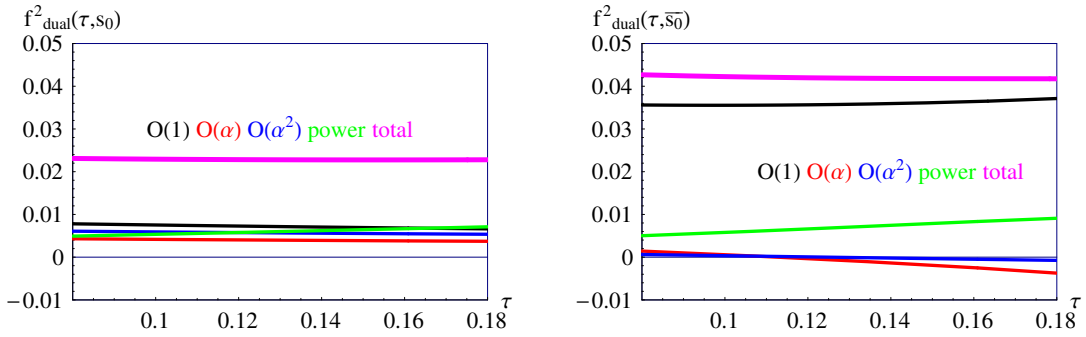

Figure 1: Dual decay constants $f_{\rm dual}$ of the B meson extracted, for constant thresholds $\overline{(s_0)}$, from the correlator (1) expressed in terms of the b-quark's pole (left) and $\overline{\rm MS}$ (right) mass.

(b) Reorganizing the perturbative series in terms of the heavy-quark $\overline{\rm MS}$ mass generates an impressively distinct *hierarchy of the perturbative contributions*. Our dual decay constant $f_{\rm dual}$ obtained using the $\overline{\rm MS}$ scheme proves to be some 40% larger than in the pole-mass scheme.

(c) Interestingly, in *both* mass schemes the decay constant exhibits perfect stability in a wide range of the Borel parameter τ. This clearly tells us that mere Borel stability is not sufficient to ensure the reliability of a sum-rule extraction of bound-state features. Repeatedly [4], we tried to draw the attention of sum-rule practitioners to this observation; nevertheless, some authors seem to be content with Borel stability as a proof of the trustability of their findings.

In view of the above, we adopt the OPE expressed in terms of running $\overline{\rm MS}$ quark masses [9].

Decay Constants of D and D_s [2,3]. Straightforward application of our sum-rule algorithm yields, as our predictions for the decay constants of the charmed pseudoscalar mesons $D_{(s)}$,

$$f_D = (206.2 \pm 7.3_{\rm (OPE)} \pm 5.1_{\rm (syst)})\ {\rm MeV}\ ,$$
$$f_{D_s} = (245.3 \pm 15.7_{\rm (OPE)} \pm 4.5_{\rm (syst)})\ {\rm MeV}\ .$$

Herein, the OPE-related errors are computed by bootstrap studies allowing the parameters induced by QCD (i.e., quark masses, $\alpha_{\rm s}$, and condensates) to vary in their respective ranges. We observe perfect agreement of our results with the corresponding lattice QCD outcomes. Let us emphasize that the τ-dependent effective threshold constitutes *the* crucial ingredient for a successful prediction of decay constants of charmed heavy mesons by the sum rule (1). Standard τ-independent approximations entail a much lower value for the D-meson decay constant, f_D, that resides rather far from both the experimental data *and* the lattice findings.

Decay Constants of B and B_s [2]. Our QCD sum-rule results for the decay constants $f_{B_{(s)}}$ of the pseudoscalar beauty mesons $B_{(s)}$ turn out to be extremely sensitive to the input value of the b-quark mass; for instance, the b-quark's $\overline{\rm MS}$-mass range $\overline{m}_b(\overline{m}_b) = (4.163 \pm 0.016)$ GeV [10] gives results that are barely compatible with recent lattice computations of these decay constants. However, inverting the logic by requiring our sum-rule result for f_B to match the average of these lattice calculations provides the very precise value of the b-quark $\overline{\rm MS}$ mass

$$\overline{m}_b(\overline{m}_b) = (4.245 \pm 0.025)\ {\rm GeV}\ .$$

The corresponding estimates for f_B and f_{B_s} emerging within our sum-rule prescriptions are

$$f_B = (193.4 \pm 12.3_{\rm (OPE)} \pm 4.3_{\rm (syst)})\ {\rm MeV}\ ,$$
$$f_{B_s} = (232.5 \pm 18.6_{\rm (OPE)} \pm 2.4_{\rm (syst)})\ {\rm MeV}\ .$$

Summary and Conclusions.

1. The τ-dependence of effective thresholds emerges naturally when one attempts to render the duality relation exact. Let us emphasize two facts: (a) In principle, this τ-dependence is *not* in conflict with the properties of quantum field theories. (b) Our analysis of $D_{(s)}$ mesons indicates that it will indeed raise the quality of the resulting sum-rule predictions *decisively*.

2. Our study of *charmed mesons* clearly demonstrates that using Borel-parameter-dependent thresholds leads to lots of essential improvements: (i) The accuracy of sum-rule predictions for decay constants is significantly increased. (ii) It has become possible to extract a realistic systematic error and to diminish it to the level of a few percent. (iii) Our prescription brings the QCD sum-rule approach into perfect agreement with both lattice QCD and experiment.

3. The *beauty-meson* decay constants $f_{B_{(s)}}$ are extremely sensitive to the choice of the b-quark mass: Regarding this as a kind of serendipity and matching our QCD sum-rule outcome for f_B to the corresponding average of lattice evaluations enables us to arrive at a rather precise estimate of $\overline{m}_b(\overline{m}_b)$ in good agreement with several lattice results but which, unfortunately, has no overlap with a recent, rather accurate determination [10]; for details, consult Ref. [2].

Acknowledgments

DM is supported by the Austrian Science Fund (FWF), project no. P22843.

Bibliography

[1] M. A. Shifman, A. I. Vainshtein, and V. I. Zakharov, Nucl. Phys. B **147**, 385 (1979).

[2] W. Lucha, D. Melikhov, and S. Simula, J. Phys. G: Nucl. Part. Phys. **38**, 105002 (2011).

[3] W. Lucha, D. Melikhov, and S. Simula, Phys. Lett. B **701**, 82 (2011); arXiv:1108.0844 [hep-ph].

[4] W. Lucha, D. Melikhov, and S. Simula, Phys. Rev. D **76**, 036002 (2007); Phys. Lett. B **657**, 148 (2007); Phys. Atom. Nucl. **71**, 1461 (2008); Phys. Lett. B **671**, 445 (2009); arXiv:1107.1848 [hep-ph]; D. Melikhov, Phys. Lett. B **671**, 450 (2009).

[5] W. Lucha, D. Melikhov, and S. Simula, Phys. Rev. D **79**, 096011 (2009); J. Phys. G: Nucl. Part. Phys. **37**, 035003 (2010); W. Lucha, D. Melikhov, H. Sazdjian, and S. Simula, Phys. Rev. D **80**, 114028 (2009).

[6] W. Lucha, D. Melikhov, and S. Simula, Phys. Lett. B **687**, 48 (2010); Phys. Atom. Nucl. **73**, 1770 (2010); in *QCD@Work 2010*, eds. L. Angelini *et al.*, AIP Conf. Proc. **1317** (AIP, Melville, New York, 2010), p. 316, arXiv:1008.0167 [hep-ph].

[7] W. Lucha, D. Melikhov, and S. Simula, in *QCD@Work 2010*, eds. L. Angelini *et al.*, AIP Conf. Proc. **1317** (AIP, Melville, New York, 2010), p. 310, arXiv:1008.3129 [hep-ph]; PoS (ICHEP 2010) 210; PoS (QFTHEP2010) 058.

[8] K. G. Chetyrkin and M. Steinhauser, Phys. Lett. B **502**, 104 (2001); Eur. Phys. J. C **21**, 319 (2001).

[9] M. Jamin and B. O. Lange, Phys. Rev. D **65**, 056005 (2002).

[10] K. G. Chetyrkin *et al.*, Phys. Rev. D **80**, 074010 (2009).

First mass measurements at LHCb

Roberta Cardinale[1] on behalf of the LHCb Collaboration
Department of Physics
University of Genova and INFN Genova,
I-16146 Genova, ITALY

At LHCb the first preliminary mass measurements of fully reconstructed b-hadron states in modes decaying to a J/ψ have been performed using $\sim 35\,\mathrm{pb}^{-1}$ of data collected during 2010. The systematics on the alignment of the tracking system and the momentum scale calibration are addressed. In this note precise mass measurements for B^0, B^+, B_s, B_c and Λ_b are presented.

1 Introduction

Hadrons are made of quarks and gluons bound together by the strong interaction described by QCD. The hadron mass is a simple property that can be used to test QCD.

The LHCb experiment is dedicated to explore CP violation and rare decays of b- and c-hadrons at the LHC [1]. The mass measurement relies both on the tracking system that combined with the dipole magnet, gives a good momentum resolution, and on the capability to identify muons of the muon detector.

2 Selection

Mass measurements have been performed using six exclusive decay modes (and charge-conjugate) with a J/ψ in the final state: $B^+ \to J/\psi K^+$, $B^0 \to J/\psi K^{*0}$, $B^0 \to J/\psi K^0_s$, $B^0_s \to J/\psi\phi$ and $\Lambda_b \to J/\psi\Lambda$, $B^+_c \to J/\psi\pi^+$ with $J/\psi \to \mu^+\mu^-$, $\phi \to K^+K^-$, $K^{*0} \to K^-\pi^+$, $K^0_s \to \pi^+\pi^-$ and $\Lambda \to p\pi^-$. The selection [2, 3] is based on kinematic and topological variables such as goodness of the vertex fit, transverse momentum, impact parameter, b-hadron lifetime and Particle Identification (PID). A mass constrained vertex fit for J/ψ, K^0_s and Λ has been performed to improve the b-hadron mass resolution.

[1] roberta.cardinale@ge.infn.it

3 Selected Events Mass Distributions

The mass distributions of the selected candidates for two of the different considered channels are reported in Figure 1 together with the results of an unbinned maximum likelihood fit (gaussian plus an exponential for the background).

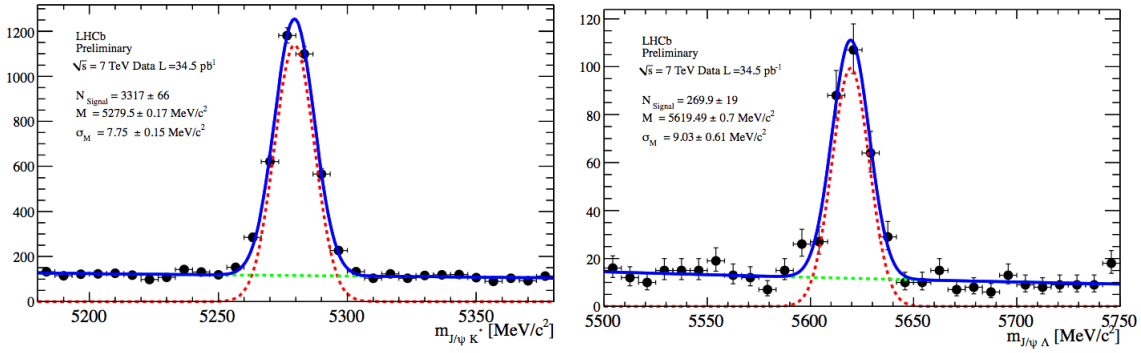

Figure 1: Mass distribution of the selected events for $B^0 \to J/\psi K^{*0}$ and $\Lambda_b \to J/\psi\Lambda$ channels.

4 Detector Alignment and Momentum Scale Calibration

A good alignment of the detector is essential to perform precise mass measurements. Both $J/\psi \to \mu^+\mu^-$ decay high momentum tracks and $D^0 \to K\pi$ decays have been used. A shift in the J/ψ mass across 2010 data taking period has been detected and has been correlated to temperature variations of the Trigger Tracker during 2010 data taking period (Figure 2). Since Trigger Tracker modules are mounted on aluminium cooling plate, the variation of temperature gives a contraction of the modules of 400 μm that is not negligible compared with the intrinsic resolution of the detector (50 μm). Therefore a run dependent alignment has been performed.

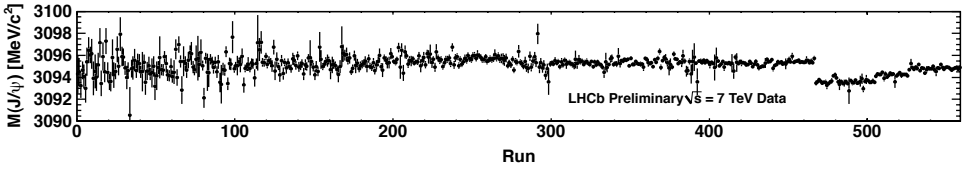

Figure 2: J/ψ mass across 2010 data taking period: three shifts corresponding to the three operating temperature changes are observed around run number 470, 510 and 530.

Decay	Measured mass [MeV/c^2]	PDG average [MeV/c^2]
$\Upsilon(1S) \to \mu^+\mu^-$	9459.90 ± 0.54	9460.30 ± 0.26
$J/\psi \to \mu^+\mu^-$	3096.97 ± 0.01	3096.916 ± 0.011
$D^0 \to K^-\pi^+$	1864.75 ± 0.07	1864.83 ± 0.14
$K^0_S \to \pi^+\pi^-$	497.62 ± 0.01	497.61 ± 0.02
$\psi(2S) \to J/\psi\pi^+\pi^-$	3686.12 ± 0.06	3686.09 ± 0.04

Table 1: Validation of the momentum scale using two body decays (Υ, D^0, K^0_s) and $\psi(2S) \to J/\psi\pi^+\pi^-$.

Another important step for mass measurements is the calibration of the momentum scale obtained using the $J/\psi \to \mu^+\mu^-$ decays. The momentum measurement has to be corrected with a precision better than 10^{-3}. After the run dependent alignment and the momentum scale calibration the variation of the J/ψ mass over time is at the level of $\Delta m/m = 10^{-5}$.The momentum scale calibration procedure has been validated using other two body resonance decay modes (Υ, D^0, K^0_s) and $\psi(2S) \to J/\psi\pi^+\pi^-$ decay. The agreement of the measured masses with the PDG values [4] is good (Table 1). The momentum scale factor from those decays has been evaluated to be known at the level of 10^{-4}.

5 Results and Systematic Uncertainties

Several systematics have been evaluated. Signal and background have been modeled using different functions. Systematic uncertainties are assigned associated with the precision of the momentum scale knowledge, of the detector description (energy loss correction) and of the detector alignment.

The measured mass at LHCb are reported below and compared with the other available measurements in Figure 3. If mass differences are considered the systematic error related to

$$\begin{aligned}
M(B^+ \to J/\psi K^+) &= 5279.27 \pm 0.11\ (\text{stat}) \pm 0.20\ (\text{syst})\ \text{MeV/c}^2 \\
M(B^0 \to J/\psi K^{*0}) &= 5279.54 \pm 0.15\ (\text{stat}) \pm 0.16\ (\text{syst})\ \text{MeV/c}^2 \\
M(B^0 \to J/\psi K^0_s) &= 5279.61 \pm 0.29\ (\text{stat}) \pm 0.20\ (\text{syst})\ \text{MeV/c}^2 \\
M(B^0_s \to J/\psi\phi) &= 5366.60 \pm 0.28(\text{stat}) \pm 0.21(\text{syst})\ \text{MeV/c}^2 \\
M(\Lambda_b \to J/\psi\Lambda) &= 5619.49 \pm 0.70\ (\text{stat}) \pm 0.19\ (\text{syst})\ \text{MeV/c}^2 \\
M(B^+_c \to J/\psi\pi^+) &= 6268.0 \pm 4.0\ (\text{stat}) \pm 0.6\ (\text{syst})\ \text{MeV/c}^2
\end{aligned}$$

the determination of the average momentum scale largely cancels.

$$
\begin{aligned}
M(B^0 \to J/\psi K^*) - M(B^+ \to J/\psi K^+) &= 0.27 \pm 0.19\,(\text{stat}) \pm 0.12\,(\text{syst}) \\
M(B^0 \to J/\psi K^0_S) - M(B^+ \to J/\psi K^+) &= 0.34 \pm 0.31\,(\text{stat}) \pm 0.10\,(\text{syst}) \\
M(B^0_s \to J/\psi \phi) - M(B^+ \to J/\psi K^+) &= 87.33 \pm 0.30\,(\text{stat}) \pm 0.19\,(\text{syst}) \\
M(\Lambda_b \to J/\psi \Lambda) - M(B^+ \to J/\psi K^+) &= 340.22 \pm 0.71\,(\text{stat}) \pm 0.08\,(\text{syst}) \\
M(B^+_c \to J/\psi \pi^+) - M(B^+ \to J/\psi K^+) &= 988.7 \pm 4.0\,(\text{stat}) \pm 0.5\,(\text{syst})
\end{aligned}
$$

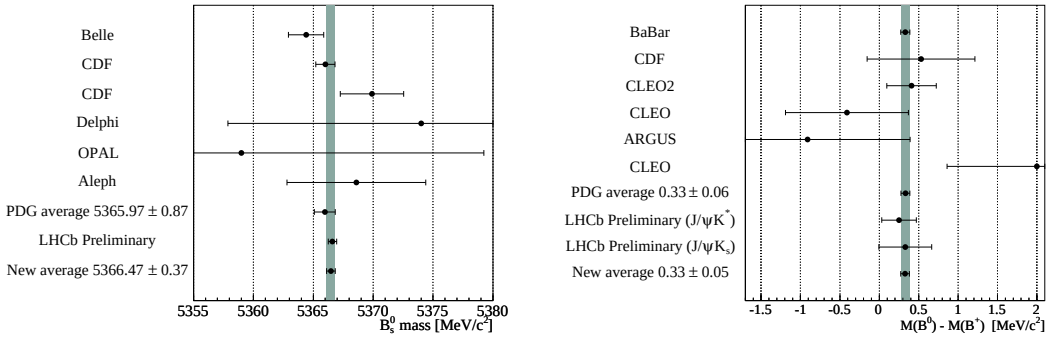

Figure 3: LHCb measurements for B^0_s and mass difference $M(B^0) - M(B^+)$ compared with current values from other experiments.

6 Conclusions

LHCb mass measurements of the b-hadrons $B^+, B^0, B^0_s, \Lambda_b$ and B^+_c agree with previous values and significantly improve the world average precision on these quantities. In particular, the measurements of the masses of B^+, B^0, B^0_s and Λ_b are the most precise results so far obtained. These measurements will be improved with more data, and measurements will also be performed of other hadrons such as the Ω_b and the excited B hadron states.

Bibliography

[1] LHCb collaboration, JINST **3** (2008) S08005, and references therein

[2] LHCb collaboration, *Selections and lifetime measurements for exclusive $b \to J/\psi X$ decays with $J/\psi \to \mu^+\mu^-$ with 2010 data*, CERN-LHCb-CONF-2011-001 (2011).

[3] LHCb collaboration, *Measurement of the B^+ to B^+ production cross-section ratio at $\sqrt{s} = 7$ TeV in LHCb*, CERN-LHCb-CONF-2011-017 (2011).

[4] K. Nakamura et al. [Particle Data Group], *Review of particle physics*, J. Phys. G **37** (2010) 075021.

P-wave spin-spin splitting and meson loops

Timothy J. Burns[1]
INFN Roma
Piazzale A. Moro 2
Roma, 00185
ITALY

In quark potential models the hyperfine splitting of P-wave mesons is zero in the nonrelativistic limit, a prediction strikingly confirmed by experiment in both charmonia and bottomonia. The result, however, ignores the coupling of bare quarkonia to meson-meson pairs. This coupling causes mass shifts among the states and so could potentially spoil the quark model prediction. This turns out not to be the case: in a variety of models the hyperfine splitting remains small despite large mass shifts. This is shown to be a generic feature of models in which the coupling involves the creation of a light quark pair with spin-one and the quark spin wavefunctions are conserved. This talk reports on the results of ref. [1].

In quark potential models the mass M_{SLJ} of a meson of spin S, orbital angular momentum L and total angular momentum J can be expressed in perturbation theory,

$$M_{SLJ} = M + \Delta_s \langle \tfrac{1}{2}\tfrac{1}{2} \rangle_S + \Delta_t \langle \mathbf{T} \rangle_{SLJ} + \Delta_o \langle \mathbf{L}\cdot\mathbf{S} \rangle_{SLJ}, \tag{1}$$

in terms of expectations values M, Δ_s, Δ_t and Δ_o of the spin-independent, spin-spin, tensor and spin-orbit terms. For P-wave mesons the hyperfine splitting Δ_s, which can be expressed in terms of the meson masses by taking the appropriate linear combination of the above,

$$\frac{1}{9}\left(M_{^3\mathrm{P}_0} + 3M_{^3\mathrm{P}_1} + 5M_{^3\mathrm{P}_2}\right) - M_{^1\mathrm{P}_1} = \Delta_s, \tag{2}$$

is zero in the nonrelativistic limit. The experimental charmonia [2] and bottomonia [3, 4] masses are in excellent agreement with this prediction :

$$\begin{aligned}
\overline{M}_{\chi_c(1\mathrm{P})} - M_{h_c(1\mathrm{P})} &= +0.02 \pm 0.19 \pm 0.13 \text{ MeV(CLEO)}, \\
\overline{M}_{\chi_b(1\mathrm{P})} - M_{h_b(1\mathrm{P})} &= +2 \pm 4 \pm 1 \text{ MeV(BaBar)}, \\
\overline{M}_{\chi_b(1\mathrm{P})} - M_{h_b(1\mathrm{P})} &= +1.62 \pm 1.52 \text{ MeV(Belle)}, \\
\overline{M}_{\chi_b(2\mathrm{P})} - M_{h_b(2\mathrm{P})} &= +0.48^{+1.57}_{-1.22} \text{ MeV(Belle)}.
\end{aligned}$$

The quark model result ignores the effect of the coupling of bare quarkonia to meson-meson pairs. This "unquenching" causes mass shifts, and since the χ_0, χ_1, χ_2 and h have different

[1]Timothy.Burns@roma1.infn.it

Ref.		$\Delta M_{^3\mathrm{P}_0}$	$\Delta M_{^3\mathrm{P}_1}$	$\Delta M_{^3\mathrm{P}_2}$	$\Delta M_{^1\mathrm{P}_1}$	Ind.
[5]	1P, $c\bar{c}$	459	496	521	504	-1.8
[6]	1P, $c\bar{c}$	198	215	228	219	-1.3
[7]	1P, $c\bar{c}$	35	38	63	52	-2.9
[8]	1P, $c\bar{c}$	131	152	175	162	-0.4
[9]	1P, $c\bar{c}$	173	180	185	182	0.0
[9]	1P, $b\bar{b}$	43	44	45	44	-0.4
[9]	2P, $b\bar{b}$	55	56	58	57	0.0
[10]	1P, $b\bar{b}$	80.777	84.823	87.388	85.785	-0.013
[10]	2P, $b\bar{b}$	73.578	77.608	80.146	78.522	-0.048

Table 1: The magnitudes of the mass shifts computed in various models. The final column "Ind." shows the induced hyperfine splitting due to loop effects.

spin and total angular momenta, their couplings and therefore mass shifts differ. This leads to deviations from the quenched mass formula (1), which one might expect could spoil the quark model result.

Remarkably, this is not the case. Table 1 shows the mass shifts ΔM_{SLJ} of P-wave $c\bar{c}$ and $b\bar{b}$ due to coupling to pseudoscalar and vector mesons, computed in a variety of different approaches [2]. Although the mass shifts can be large, the relative shift between any two states is much smaller, which to some extent explains the empirical success of quenched quark models [5,9]. The relative shifts are, however, still large compared to the experimental hyperfine splittings. It is therefore striking to note that their linear combination

$$-\frac{1}{9}\left(\Delta M_{^3\mathrm{P}_0} + 3\Delta M_{^3\mathrm{P}_1} + 5\Delta M_{^3\mathrm{P}_2}\right) + \Delta M_{^1\mathrm{P}_1}, \tag{3}$$

which is the correction to equation (2) due to unquenching, is much smaller still: these induced hyperfine splittings are presented in the final column "Ind." of the table. It thus appears that there is some mechanism in place protecting the smallness of the hyperfine splitting. This is particularly interesting given that the various models differ in several respects.

A feature common to all of the models is that the coupling involves the creation of a light quark pair in spin triplet. The quark spin and spatial degrees of freedom factorise so that the amplitude for the coupling can be expressed as a linear combination of spatial matrix elements weighted by angular momentum recoupling factors. For the coupling to a pair of S-wave mesons there is a single spatial matrix element A_l for each partial wave l [11]. The corresponding recoupling coefficients $C_{SLJ}^{s_1 s_2 l}$, for the coupling of a state with S, L and J quantum numbers to a pair of S-wave mesons with spins s_1, s_2, can be deduced from the general expression of ref. [12].

[2] The values quoted for ref. [10] correct a factor of 2 in the coupling of χ_{b0} to bottom-strange meson pairs.

For a channel described by binding energy $\epsilon_{SLJ}^{s_1s_2}$ and reduced mass $\mu_{s_1s_2}$, the (downward) mass shift and meson-meson probability are, respectively,

$$\Delta M_{SLJ}^{s_1s_2l} = C_{SLJ}^{s_1s_2l} \int dp \frac{p^2|A_l(p)|^2}{\epsilon_{SLJ}^{s_1s_2} + p^2/2\mu_{s_1s_2}}, \qquad P_{SLJ}^{s_1s_2l} = C_{SLJ}^{s_1s_2l} \int dp \frac{p^2|A_l(p)|^2}{\left(\epsilon_{SLJ}^{s_1s_2} + p^2/2\mu_{s_1s_2}\right)^2}. \tag{4}$$

Introducing a quantity $X_{SLJ}^{s_1s_2}$, which parameterizes the reduced mass and binding energy of a given channel in terms of the spin-averaged values μ and ϵ (those corresponding to setting all spin splittings to zero),

$$\mu_{s_1s_2}\epsilon_{SLJ}^{s_1s_2} = \mu\epsilon(1 + X_{SLJ}^{s_1s_2}), \tag{5}$$

the mass shift can be expressed in a power series expansion,

$$\Delta M_{SLJ}^{s_1s_2l} = C_{SLJ}^{s_1s_2l} \frac{\mu_{s_1s_2}}{\mu} \frac{1}{\epsilon} \sum_{n=0}^{\infty} (-X_{SLJ}^{s_1s_2})^n \int dp \frac{p^2|A_l(p)|^2}{(1 + p^2/2\mu\epsilon)^{n+1}}. \tag{6}$$

The first two terms in the series involve the integrals in the two equations (4), but with μ and ϵ in place of $\mu_{s_1s_2}$ and $\epsilon_{SLJ}^{s_1s_2}$. These terms can be thought of as the the spin-averaged mass shift and meson-meson probability. Calling these ΔM^l and P^l, the approximate formula for the mass shift due to a given channel is

$$\Delta M_{SLJ}^{s_1s_2l} \approx C_{SLJ}^{s_1s_2l} \frac{\mu_{s_1s_2}}{\mu} \left(\Delta M^l - X_{SLJ}^{s_1s_2}\epsilon P^l\right), \tag{7}$$

which turns out to be a reasonable approximation for $c\bar{c}$ and an excellent approximation for $b\bar{b}$. The total mass shift is the sum over those of the different channels, which is straightforward using the properties of the coefficients $C_{SLJ}^{s_1s_2l}$. The correction (3) to the hyperfine splitting due to channel coupling follows immediately; everything cancels except a term proportional to Δ_s,

$$-\frac{1}{9}\left(\Delta M_{^3\mathrm{P}_0} + 3\Delta M_{^3\mathrm{P}_1} + 5\Delta M_{^3\mathrm{P}_2}\right) + \Delta M_{^1\mathrm{P}_1} = -\Delta_s \sum_l P^l. \tag{8}$$

Thus to this order, in the nonrelativistic limit ($\Delta_s = 0$) the result of zero hyperfine splitting survives corrections due to unquenching. The small hyperfine splittings in Table 1 are indicative of the magnitude of quadratic corrections to the expansion (7), and the smallness of $X_{SLJ}^{s_1s_2}$ explains why the mechanism works even better for $b\bar{b}$ than $c\bar{c}$.

The mechanism relies on the factorisation of quark spin and spatial degrees of freedom and the assumption that the coupling involves the creation of a quark pair with spin one. The observed small hyperfine splittings thus supports this picture, which is also consistent with lattice QCD [13].

The same mechanism protects the hyperfine splitting of D-wave and higher L mesons; thus one can predict the mass of the $^1\mathrm{D}_2$ bottomonium in terms of the $^3\mathrm{D}_{1,2,3}$, as in ref. [14].

Notice in Table 1 that in each model the induced hyperfine splitting is less than (or equal to) zero. If the physical hyperfine splitting is positive, as is favoured by the bulk of experimental and lattice data, then in the absence of some other effect the bare potential model splitting Δ_s must be positive. This may help to distinguish among different models, which disagree on the sign of Δ_s [15].

Another common feature is the hierarchy of mass splittings,

$$\Delta M_{^3\mathrm{P}_2} > \Delta M_{^1\mathrm{P}_1} > \Delta M_{^3\mathrm{P}_1} > \Delta M_{^3\mathrm{P}_0}, \tag{9}$$

which implies that unquenching brings meson masses closer together with respect to their bare values. Comparison of quenched and unquenched lattice QCD calculations would be an interesting test of this effect.

Bibliography

[1] T. J. Burns, Phys. Rev. **D84**, 034021 (2011), 1105.2533.

[2] S. Dobbs et al. (CLEO), Phys. Rev. Lett. **101**, 182003 (2008), 0805.4599.

[3] J. P. Lees et al. (BABAR) (2011), 1102.4565.

[4] I. Adachi et al. (Belle) (2011), 1103.3419.

[5] T. Barnes and E. S. Swanson, Phys. Rev. **C77**, 055206 (2008), 0711.2080.

[6] Y. S. Kalashnikova, Phys. Rev. **D72**, 034010 (2005), hep-ph/0506270.

[7] B.-Q. Li, C. Meng, and K.-T. Chao, Phys. Rev. **D80**, 014012 (2009), 0904.4068.

[8] C. Yang, B.-F. Li, X.-L. Chen, and W.-Z. Deng (2010), 1011.6124.

[9] S. Ono and N. A. Törnqvist, Z. Phys. **C23**, 59 (1984).

[10] J.-F. Liu and G.-J. Ding (2011), 1105.0855.

[11] T. J. Burns, F. E. Close, and C. E. Thomas, Phys. Rev. **D77**, 034008 (2008), 0709.1816.

[12] T. J. Burns (2006), hep-ph/0611132.

[13] T. J. Burns and F. E. Close, Phys. Rev. **D74**, 034003 (2006), hep-ph/0604161.

[14] T. J. Burns, F. Piccinini, A. D. Polosa, and C. Sabelli, Phys. Rev. **D82**, 074003 (2010), 1008.0018.

[15] S. Godfrey and J. L. Rosner, Phys. Rev. **D66**, 014012 (2002), hep-ph/0205255.

Heavy-flavor production in pp and Pb–Pb collisions at LHC with ALICE

Kai Schweda[1] on behalf of the ALICE Collaboration
Physikalisches Institut der Universität Heidelberg, Philosophenweg 12, D-69120 Heidelberg, Germany

We report recent results from the ALICE experiment the Large Hadron Collider on open charmed hadron production in pp collisions at $\sqrt{s} = 2.76$ and 7 TeV, and Pb–Pb collisions at $\sqrt{s_{NN}} = 2.76$ TeV. Open charmed hadrons are kinematically fully reconstructed in the hadronic decay channels $D^0 \to K^-\pi^+$, $D^+ \to K^-\pi^+\pi^+$, and $D^{*+}(2010) \to D^0\pi^+$ and identified through their invariant mass. Combinatorial background is minimized by selecting a displaced vertex topology. Inclusive charm and beauty production is measured by detecting electrons (muons) from semi-leptonic decays of open charmed and beauty hadrons in the central (forward) region. Comparison to results from state-of-the-art QCD calculations is given. First results on nuclear modifications factors in Pb–Pb collisions from hadronic and semi-leptonic decays are presented.

1 Introduction

The ALICE experiment [1] was designed to study strongly interacting matter at the highest temperatures and energy densities available in the laboratory, in high-energy nucleus-nucleus collisions at the Large Hadron Collider. Heavy quarks (charm and bottom) are unique probes for studies of bulk phenomena, due to their large mass relative to the temperature of the medium, and are abundantly produced at LHC energies. Here, heavy-quark production rates in pp collisions provide the essential baseline for such studies in heavy ion collisions. In addition, quantitative understanding of heavy-quark production is crucial in the search for new physics phenomena at the LHC, where heavy-quark production often comprises an important and irreducible background [2].

For hard processes in nucleus-nucleus (AA) collisions, in the absence of any nuclear medium effects their production rates are expected to scale with the number $\langle N_{\rm coll}\rangle$ of binary nucleon-nucleon collisions when compared to pp rates. The nuclear modification factor to quantify this relationship is defined as:

$$R_{AA}(p_T) = \frac{1}{\langle N_{\rm coll}\rangle} \cdot \frac{{\rm d}N_{AA}/{\rm d}p_T}{{\rm d}N_{pp}/{\rm d}p_T} = \frac{1}{\langle T_{AA}\rangle} \cdot \frac{{\rm d}N_{AA}/{\rm d}p_T}{{\rm d}\sigma_{pp}/{\rm d}p_T} \quad (1)$$

[1] kschweda@cern.ch

which equals unity in case of no nuclear effects. Here, $\langle T_{AA} \rangle$ is the average nuclear overlap function calculated in a Glauber model of the nucleus-nucleus collision geometry.

The heavy-quark detection performance of ALICE is described in detail in [3]. The main components for these measurements in the central region of ALICE are the Inner Tracking System (ITS) covering a radial distance of 3.9 cm to 43.0 cm from the collision vertex and based on high-granularity silicon technology, surrounded by a Time Projection Chamber (TPC) embedded in a magnetic field of 0.5 T. Both components provide high-precision tracking of charged particles in the pseudo-rapidity range $|\eta| < 0.9$, with a relative momentum resolution of better than 4% at $p_T < 20$ GeV/c and a pointing resolution to the collision vertex of better than 75(20) μm at $p_T > 1(20)$ GeV/c in the plane transverse to the beam direction. Particle identification is provided by the specific energy deposit dE/dx in the TPC gas, and time-of–flight. Electrons at transverse momenta below 6 GeV/c are identified by a combination of dE/dx and time-of–flight, and above 2 GeV/c by the Transition Radiation Detector and in the Electromagnetic Calorimeter. Muons are identified utilizing a frontal absorber with a thickness of ten interaction lengths λ_I, and a muon filter of thickness $7\lambda_I$ covering the pseudo-rapidity range $-4 < \eta < -2.5$. Data were recorded using a minimum bias trigger selection which was defined by a signal present in either of two scintillator hodoscopes positioned at forward and backward direction, or in the ITS of the central barrel.

2 Calibrating the probe in pp collisions at $\sqrt{s}$ = 7 TeV

Open charmed hadrons within $|y| < 0.5$ are fully reconstructed in the channels $D^0 \to K^-\pi^+$, $D^+ \to K^-\pi^+\pi^+$, and $D^{*+}(2010) \to D^0\pi^+$ and their charge conjugates and identified through

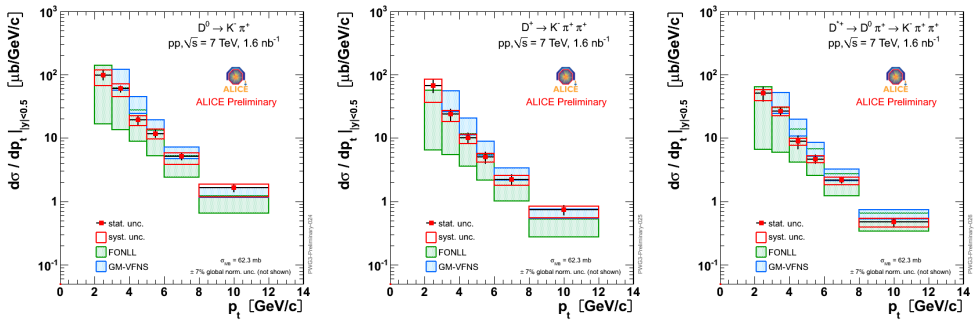

Figure 1: Differential production cross section of prompt D^0, D^+, and D^{*+}mesons and their charge conjugates within the rapidity interval $|y| < 0.5$ in pp collisions at $\sqrt{s} = 7$ TeV and predictions from pQCD calculations [4,5].

their invariant mass. Combinatorial background is minimized by selecting a displaced vertex topology, i.e. the separation of tracks stemming from the secondary vertex of the

weakly decaying D meson that is displaced from the primary collision vertex. Particle identification, especially of charged kaons, further reduces the background. The contribution of secondary D mesons from the decay of B mesons is corrected for, and amounts to about 15% estimated from production cross sections using FONLL [4] and applying reconstruction efficiencies obtained from detailed detector simulations. The prompt D meson production cross section is shown in Fig. 1.

The measured spectrum covers the transverse momentum range from 2 - 12 GeV/c with an integrated luminosity of $\mathcal{L}_{\rm int} = 1.6\ {\rm nb}^{-1}$. With four times more statistics on tape from the year 2010 data taking, we expect to extend the momentum range down to 1 GeV/c and up to at least 20 GeV/c. Results from calculations based on perturbative QCD [4,5] are in agreement with measurement within uncertainties.

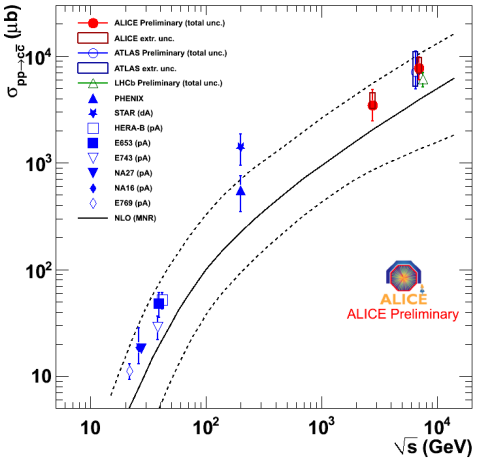

Figure 2: Open charm production cross section extrapolated to full phase space at various center-of-mass energies [8–12].

The measured cross sections were extrapolated to full phase space by scaling the measured cross section by the ratio of the total cross section over the cross section in the experimentally covered phase space calculated with FONLL. Systematic uncertainties of the calculation were estimated as follows: the renormalization and factorization scale variables μ_R and μ_F were varied up and down by a factor of two with the additional constraint $0.5 < \mu_R/\mu_F < 2.0$, the charm quark mass was varied independently within 0.20 GeV/c^2 around the central value at $m_c = 1.5\ {\rm GeV}/c^2$, uncertainties in the parton distribution functions were estimated using the CTEQ6.6 PDF error eigenvectors. The total charm production cross section was estimated for each species of D meson separately by dividing the total D meson production cross section by the relative production yield for a charm quark hadronizing to a particular species of D meson. The relative production yields have been measured at LEP at the Z-resonance [6,7] and have been applied to our results. We then calculated the weighted

average of the total charm production cross section from the extrapolated values for D^0, D^+, and D^{*+}. The dependence of the total charm production cross section [8–12] on the collision energy is shown in Fig. 2. The error boxes around the ATLAS and ALICE points denote the extrapolation uncertainties alone, whilst the error bars are the overall uncertainties. The black curves show results from next-to-leading-order predictions from the MNR calculation framework, together with its uncertainties. Note that all data points populate the upper band of the theoretical prediction.

Electrons from semi-leptonic decays of heavy quarks were extracted from the inclusive electron spectrum by subtracting a cocktail of background electrons with the dominant contributions from π^0 and η Dalitz decays and decays of the vector mesons ρ, ω, and ϕ as well as photon conversions to electron-positron pairs in the detector material [13]. The yields for neutral mesons were taken from the measured neutral pion cross section and the assumption of m_T scaling [14]. The inclusive raw electron spectrum has a residual contamination from mis-identified charged pions of up to 15% at high p_T, which has been determined experimentally and then subtracted . Muons were measured at forward rapidity in the muon spectrometer [13]. The inclusive muon spectrum contains three major background contributions: muons from the decay in-flight of light hadrons, muons from the decay of hadrons produced through interactions in the absorber, and hadrons punching through the front absorber. The latter background is efficiently rejected by requiring matching of tracks in the spectrometer with tracks in the trigger system. The other two background sources are highly momentum dependent and were subtracted using results from detailed simulations. Our muon measurement covers the transverse momentum range from 2 - 10 GeV/c. Results from FONLL calculations are in good agreement with our data.

The collision energy for Pb–Pb was $\sqrt{s_{NN}}$= 2.76 TeV. To obtain the p+p reference cross section at this energy, the measured pp cross section was scaled by the momentum dependent ratio of cross sections from FONLL calculations at $\sqrt{s}$ = 2.76 over 7 TeV [15]. The resulting cross section reference for D^0 and D^+ was experimentally checked, though with limited precision, during a brief data taking run with pp collisions at $\sqrt{s}$ = 2.76 TeV and good agreement was found.

3 Medium modifications in Pb–Pb collisions at $\sqrt{s_{NN}}$= 2.76 TeV

In the analysis of 17 million minimum bias triggered Pb–Pb collisions, we followed an identical analysis strategy as outlined above for pp collisions. The collision centrality was defined by the sum of the signal amplitudes in the scintillator hodoscopes [16]. The contribution of feed-down from B meson decays has been estimated from FONLL calculations to be 10%–15%, depending on p_T, and was subtracted. The as-yet unknown nuclear modification of B mesons has been accounted for by varying the B meson yield up and down by a factor of 3, resulting in a variation of the D meson nuclear modification factor of less than 15%. Systematic uncertainties due to tracking, particle identification and topological selection of

D mesons amount to about 35%. The nuclear modification factor of D^0 (filled triangles) and D^+ (filled squares) mesons is shown on the left side of Fig. 3 for 0 - 20% most central Pb–Pb collisions. We observe a strong suppression of a factor 4-5 for $p_T > 5$ GeV/c, comparable with values for charged pions (filled circles). Electrons (filled circles) from semi-leptonic

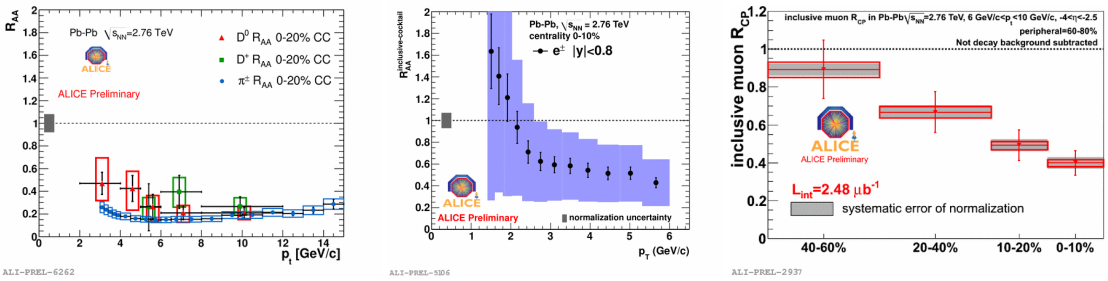

Figure 3: Left: Nuclear modification factor for D^0, D^+, and π^+ in central Pb–Pb collisions at $\sqrt{s_{NN}}$= 2.76 TeV. Statistical (bars), systematic (open boxes) normalization (filled boxes) uncertainties are shown. Middle: Nuclear modification factor for electrons (filled circles) from semi-leptonic decays of heavy quarks. Right: Nuclear modification factor for inclusive muons (filled triangles).

decays of heavy quarks show a suppression of a factor 1.5 - 4 above a transverse momentum of 4 GeV/c, as shown in the middle of Fig. 3. The systematic uncertainty is dominated by the correction for the electron identification. Inclusive muons (filled triangles), integrated over the transverse momentum range from $p_T > 6$ to 10 GeV/c, are shown on the right side of Fig. 3 and exhibit a suppression of a factor of larger than two in most central collisions. In this momentum range decays from B mesons should significantly contribute to the spectrum. We estimate the contamination from light-quark decays in the inclusive muon spectrum from detailed simulations to be less than 15%. The centrality dependence of the nuclear modification factor for D mesons, electrons from semi-leptonic decays of heavy quarks and inclusive muons shows a strong decrease towards more central collisions and is compatible with unity for most peripheral collisions.

4 Conclusions

ALICE has measured D mesons, and electrons and muons from semi-leptonic decays of heavy quarks in pp and Pb–Pb collisions at LHC. We observe a strong yield suppression in Pb–Pb collisions of a factor 4-5 for D mesons when compared to scaled results from pp collisions, comparable with the measured suppression for charged pions. Electrons from semi-leptonic decays of heavy quarks and inclusive muons also show strong suppression of a factor up to 3 at momenta $p_T > 5$ GeV/c where decays from B mesons are expected as the dominant contribution. The upcoming high luminosity Pb–Pb run at the end of 2011

and a possible p–Pb run the year after will enable ALICE to precisely measure heavy-quark production, disentangle bottom from charm production and quantify initial-state nuclear effects.

Bibliography

[1] K. Aamodt *et al.* (ALICE collaboration), J. Instrum. 3 (2008) S08002.

[2] H. E. Haber, G. L. Kane, S. Dawson, Front. Phys. 80:1-448, 2000.

[3] B.Allesandro *et al.* (ALICE collaboration), J. Phys. G 32 (2006) 1295.

[4] M. Cacciari, M. Greco, and P. Nason, JHEP 9805 (1998) 007; idem, private communication (2011).

[5] B. A. Kniehl, G. Kramer, I. Schienbein, and H. Spiesberger, Phys. Rev. Lett. 96 (2006) 012001; idem, private communication (2011).

[6] B. A. Kniehl, and G. Kramer, Phys.Rev. D74 037502 (2006).

[7] K. Ackerstaff *et al.* (OPAL collaboration), Eur. Phys. J. C1 (1997), 439.

[8] C. Lourenço, and H.K. Wöhri, Phys. Rept. 433 (2006) 127.

[9] ATLAS collaboration, internal note: ATLAS-CONF-2011-017 (2011).

[10] LHCb collaboration, internal note: LHCb-CONF-2010-013 (2010).

[11] J. Adams *et al.* (STAR collaboration), Phys. Rev. Lett. 94 (2005) 62301.

[12] A. Adare *et al.* (PHENIX collaboration), arXiv:1005.1627v2 (2010).

[13] A. Dainese (ALICE collaboration), *proceedings of the Quark Matter 2011 conference* (ed. Y. Schutz and U. Wiedemann), J. Phys. G, to be published.

[14] G. Gatoff and C. Y. Wong, Phys. Rev. D46 (1992) 997.

[15] R. Averbeck, N. Bastid, Z. Conesa del Valle, P. Crochet, A. Dainese, and X. Zhang, arXiv:1107.3243 [hep-ph] (2011).

[16] A. Toia (ALICE collaboration), *proceedings of the Quark Matter 2011 conference* (ed. Y. Schutz and U. Wiedemann), J. Phys. G, to be published.

Measurements of Inclusive b–Quark Production at 7 TeV with the CMS Experiment

Paolo Bellan on behalf of the CMS Collaboration
Padova University and INFN – 35131 Padova, Italy

Measurements performed by the CMS experiment of the cross section for inclusive b-quark production in proton-proton collisions at $\sqrt{s} = 7$ TeV are presented. The measurements are based on different methods, such as inclusive jet measurements with secondary vertex tagging or selecting a sample of events containing jets and at least one muon, where the transverse momentum of the muon with respect to the closest jet axis discriminates b events from the background. The results are compared with predictions based on perturbative QCD calculations at leading and next-to-leading order.

1 Introduction

The study of heavy-quark production in high-energy hadronic interactions plays a key role in testing next-to-leading order (NLO) Quantum Chromodynamics (QCD) calculations. In the past, discrepancies were observed between experimental data and theoretical predictions, e.g. at Tevatron [1–4] and HERA [5–8]. Substantial progress has been achieved in the understanding of heavy-quark production at Tevatron energies [9], but large theoretical uncertainties still remain, mainly due to the dependence of the calculations on the renormalization and factorization scales. The observed large scale dependence of the NLO calculations is considered to be a symptom of large contributions from higher orders: small-x effects [10, 11], where $x \sim m_{\mathrm{b}}/\sqrt{s}$, are possibly relevant in the low transverse momentum (p_{T}) domain, while multiple-gluon radiation leads to large logarithms of $p_{\mathrm{T}}/m_{\mathrm{b}}$ and may be important at high p_{T} [12]. The resummed logarithms of $p_{\mathrm{T}}/m_{\mathrm{b}}$ at next-to-leading-logarithmic accuracy have been matched to the fixed-order NLO calculation for massive quarks [13]. At the non-perturbative level, the b–hadron p_{T} spectrum depends strongly on the parametrization of the fragmentation function [14]. The b-quark production cross section has also been studied in the general-mass variable-flavor-number scheme [15] and the k_{T} factorization QCD approach [16, 17].

Measurements of b–hadron production at higher energies than before, provided by the Large Hadron Collider (LHC), represent an important test of the new theoretical calculations

just mentioned. Measurements of inclusive b–quark production cross section require identification of inclusive events in which a b-quark has been produced in pp collisions. In results reported here, the discrimination of the heavy quark events has been achieved either exclusively, reconstructing the whole decay channel of a B meson, or inclusively, considering hard jets. In this context, two different tagging techniques have been applied: reconstruction of a displaced secondary vertex, and analysis of the transverse momentum spectrum of an energetic muon with respect to the closest jet.

2 The CMS detector

A detailed description of the CMS detector can be found elsewhere [18]. Some of the most relevant features for heavy flavor physics are summarized here.

The core CMS apparatus is a superconducting solenoid, of 6 m internal diameter, providing a magnetic field of 3.8 T. Within the field volume there are the silicon pixel and strip tracker, the crystal electromagnetic calorimeter and the brass/scintillator hadron calorimeter. Muons are detected by three types of gas-ionization detectors embedded in the steel return yoke: Drift Tubes (DT), Cathode Strip Chambers (CSC), and Resistive Plate Chambers (RPC). The muon detectors cover a pseudorapidity window $|\eta| < 2.4$, where $\eta = -\ln[\tan(\theta/2)]$, where the polar angle θ is measured from the z-axis, which points along the counterclockwise beam direction. The silicon tracker is composed of pixel detectors (three barrel layers and two forward disks on each side of the detector, made of 66 million 100×150 μm^2 pixels) followed by microstrip detectors (ten barrel layers plus three inner disks and nine forward disks on each side of the detector, with 10 million strips of pitch between 80 and 184 μm). Thanks to the strong magnetic field and the high granularity of the silicon tracker, the transverse momentum, p_{T}, of the muons matched to reconstructed tracks is measured with a resolution of about 1 % for the typical muons used in this analysis. The silicon tracker also provides the primary vertex position, with ~ 20 μm accuracy.

The first level (L1) of the CMS trigger system, composed of custom hardware processors, uses information from the calorimeters and muon detectors to select the most interesting events. The High Level Trigger (HLT) further decreases the rate before data storage.

3 Open beauty

b–jets play a key role in searches for new physics beyond the Standard Model. It took a while to fully establish a consistency between the Tevatron data and pQCD predictions for b–jet production cross section. Generally speaking, b–jets cross section measurements are highly non-trivial, and sizable uncertainties affect both theory and experiment: on one side, one has to deal with a typical multi–scale problem, in which the center–of–mass collision energy, mass of the b–quark and the factorization and re–normalization scales

are entangled in a subtle way; on the other hand, excellent performance of the tracking is required, challenging the detector full potential.

The CMS Collaboration has published results, reviewed in the next sections, concerning two complementary measurements of b–jet production cross section. These results have made use of two different b–tagging techniques, were performed over 85 nb^{-1} and 60 nb^{-1} of 2010 data, respectively [19, 20], and were obtained using track or particle–flow jets. Typical values achieved by the CMS detector of the jet resolution and the energy scale uncertainty, at the time of these results were reported, were about $10 - 15\%$, and below 3%, respectively.

3.1 b–jets with muons

The measurement of the integrated and differential cross section of the reaction $pp \rightarrow b + X \rightarrow \mu + X$ has been performed on jets coming from b–quarks. The production of a b–quark decaying semi–leptonically is deduced by the identification of a rather energetic muon inside a jet, where the transverse momentum relative to the jet axis is quite sizable. For a muon from a b–decay, the transverse momentum relative to the jet axis is on average larger than when the muon comes from light quarks; through this property it is hence possible to discriminate events in which b–quarks were produced.

A binned log-likelihood fit is performed on the spectrum of such a quantity, called "p_{T}^{rel}", using template distributions provided by the simulation for b and c quarks, and derived from the data for gluons and lighter quarks. This latter distribution is dominated by hadrons misidentified as muons (mainly decay-in-flight), so they are reweighted by the misidentification rate measured in the data. Considering that the fit is not able to distinguish between light quark, gluon and charm components, these are merged together. The b–jet tag efficiency achieved with this technique is about 74% at $p_{\text{T}}^{\mu} \simeq 6$ GeV, and close to 100% above 20 GeV, whereas the contamination is $\sim 7\%$ in lowest p_{T} bin, asymptotically decreasing towards 2% at high p_{T}.

The result of the inclusive production cross section for b quarks decaying into muons within the kinematic range $p_{\text{T}}^{\mu} > 6$ GeV and $|\eta^{\mu}| < 2.1$ is:

$$\sigma = 1.32 \pm 0.01(\text{stat}) \pm 0.30(\text{syst}) \pm 0.15(\text{lumi})\ \mu b$$

where the first uncertainty is statistical, the second is systematic, and the third is associated with the estimation of the integrated luminosity. Fig. 1 shows the measured value of the cross section for the reaction $pp \rightarrow b + X \rightarrow \mu + X$, as a function of the muon's p_{T} and y. The result includes efficiency of trigger $(88 \pm 5)\%$, of muon reconstruction $(94 \pm 3)\%$ and muon-jet association $(77 \pm 8)\%$.

The fit stability was tested against variation of the binning, repeating the fits on many simulated pseudo–experiments, cross–checking the results using jets from particle flow and performing the fits on the impact parameter distribution.

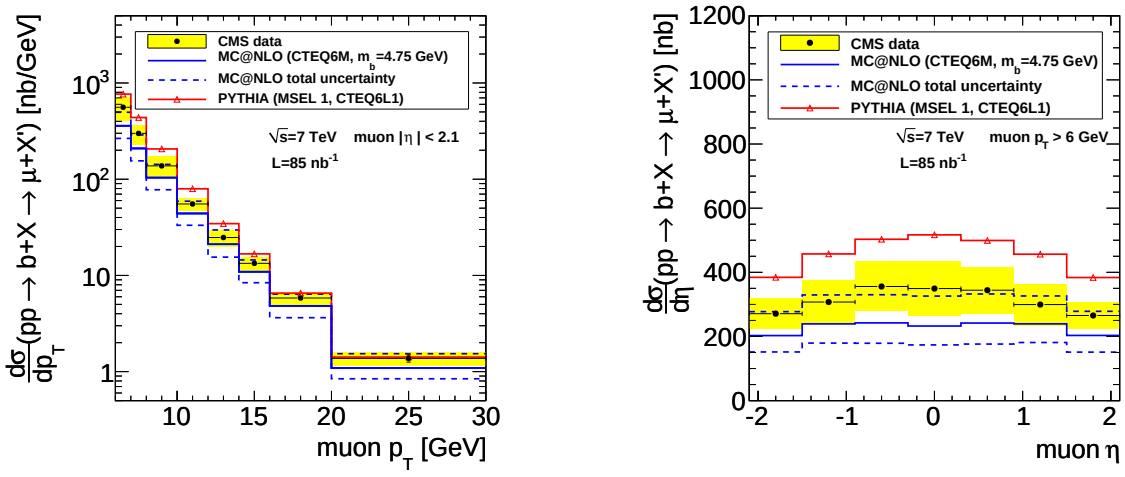

Figure 1: Differential cross section (left) $\frac{d\sigma}{dp_{\mathrm{T}}^{\mu}}(pp \to b + X \to \mu + X', |\eta^{\mu}| < 2.1)$, and (right) $\frac{d\sigma}{d\eta^{\mu}}(pp \to \pm X \to \mu + X', p_{\mathrm{T}}^{\mu} > 6$ GeV). The two possible muon charges are not distinguished and the process $pp \to \overline{b} + X \to \mu + X'$ is included. The black points are the CMS measurements. Vertical error bars showing the statistical error are smaller than the point size in most bins, the horizontal bars indicate the bin width. The yellow band shows the quadratic sum of statistical and systematic uncertainties. The systematic uncertainty (11%) of the luminosity measurement is not included. The solid blue line shows the MC@NLO result and the dashed blue lines illustrate the theoretical uncertainty as described in the text. The solid red line with dots shows the PYTHIA result.

Table 1 summarizes the systematic uncertainties entailed in this measurement. The uncertainties dominating the measurement are those coming from the approximate knowledge of the signal and the background p_{T}^{rel} shape.

Fig. 2 shows the ratio of the measured differential production cross sections in p_{T} and η over the predictions of the MC@NLO computation, as well as those provided by the Pythia [21], CASCADE MC [22] and the FONLL [23] calculations.

3.2 b–tagging with secondary vertices

The identification of jets coming from the hadronization of b–quarks is possible also through the reconstruction of secondary vertices (SV). Once a displaced SV is reconstructed, different discriminators can be used to tag the jet as originating from a b–quark. In the analysis presented here, the discriminator adopted is a monotonic function of the 3D decay length. The decay length significance cut is chosen so that the corresponding tagging efficiency is about 60% at $p_{\mathrm{T}}^{jet} = 100$ GeV, with a contamination of $\sim 0.1\%$. The b–tagging efficiency and

Table 1: Summary of systematic cross section uncertainties. The systematic uncertainty can vary depending on the muon transverse momentum and pseudorapidity as indicated by the range.

source	cross section uncertainty (%)
Trigger efficiency	5
Muon reconstruction efficiency	3
Hadron tracking efficiency	2
b p_{T}^{rel} shape uncertainty	$\leqslant 21$
Background p_{T}^{rel} shape uncertainty	2–14
Background composition	3–6
Production mechanism	2–5
Fragmentation	1–4
Decay	3
Underlying event	10
Luminosity	11

the mistag rates from *c* or light jets are evaluated from simulated events and constrained by a data/MC scale factor. The b–tagging efficiency with the selections used in this analysis is between 6% and 60% at $p_{\mathrm{T}} > 18$ GeV and $|y| < 2.0$. The efficiency rises at higher p_{T} as the b–hadron proper-time increases. In order to evaluate the purity of the selected sample, a fit to the SV mass distribution is performed, taking the shapes from simulated events, and letting free the relative normalizations for c and b jets, with the (small) contribution from light quarks fixed to the Monte Carlo expectations ("template fit"). The efficiencies estimated from MC, and the estimates of b-tagged sample purity resulting from fits to secondary-vertex mass from data are shown in Fig. 3.

The data sample was collected using hadronic triggers with different thresholds of the jet p_{T}. To merge them, the individual p_{T} spectra of jets have been normalized with the luminosity of their data taking periods, and then combined into a single spectrum with the jet p_{T} bins corresponding to intervals where the triggers were fully efficient. The overall transverse jet energy range goes from 18 to 300 GeV, and the measurements have been performed in four η intervals. The jet energy corrections applied for rapidity dependence, and those for absolute scale and p_{T} dependence, come from real data and simulated events, respectively.

The leading systematic uncertainties affecting the measurements are:

- the jet energy scale of b–jets relatively to the inclusive ones ($4 - 5\%$);
- data-driven constraints on b-tagging efficiency (20%);
- mistag rate for charm ($3 - 4$ %) and for light jets (1 – 10%).

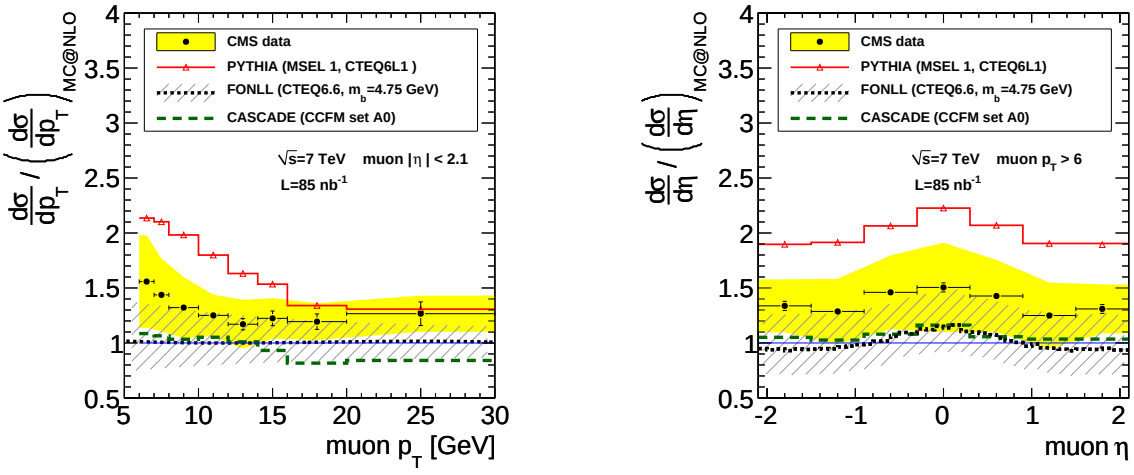

Figure 2: Differential cross section (left) $\frac{d\sigma}{dp_{\mathrm{T}}^{\mu}}(pp \to b + X \to \mu + X', |\eta^{\mu}| < 2.1)$, and (right) $\frac{d\sigma}{d\eta^{\mu}}(pp \to b + X \to \mu + X', p_{\mathrm{T}}^{\mu} > 6$ GeV), divided by their MC@NLO predictions. The two possible muon charges are not distinguished; the cross section includes the process $pp \to \bar{b} + X \to \mu + X$. The black points are the CMS measurements. Vertical error bars showing the statistical error are smaller than the point size in most bins, the horizontal bars indicate the bin width. The yellow band shows the quadratic sum of statistical and systematic uncertainties. The systematic uncertainty (11%) of the luminosity measurement is not included. Superimposed are the FONLL result (black dotted line) with uncertainties (hatched band), the CASCADE result (green, dashed line) and the pythia result (red line with markers), divided by the MC@NLO cross section.

Fig. 4 shows the results for the production cross section measurements for b–jets as a function of the b–jet transverse momentum, compared with the MC@NLO predictions, and the ratio with the inclusive jets cross-section. While the agreement with Pythia and MC@NLO is reasonable, significant differences in shape are evident, the simulations predicting more b–jets at high p_{T} than what is observed.

4 Conclusions

Recent results published by the CMS Collaboration on open beauty production have been summarized, all of them obtained analyzing the pp collision data at 7 TeV collected in the year 2010. The studies made with two different techniques for b–tagging have been shown, together with the comparisons of the production cross section measured in the data with the predictions from the available theoretical models.

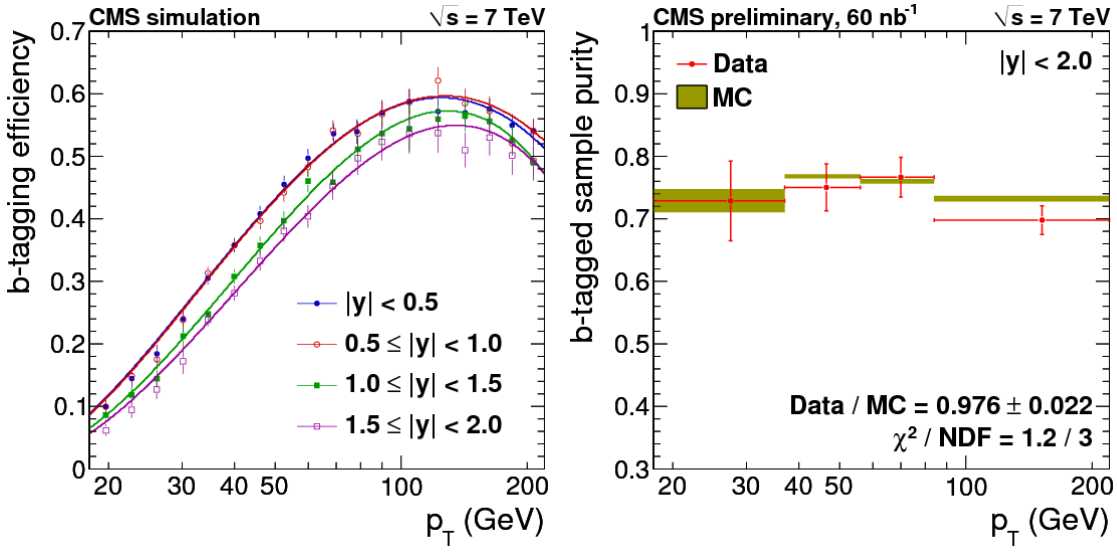

Figure 3: b–tagging efficiency in different rapidity bins, as estimated on simulated events (left). The b–tagged sample purity obtained using fits to secondary vertex mass (right)

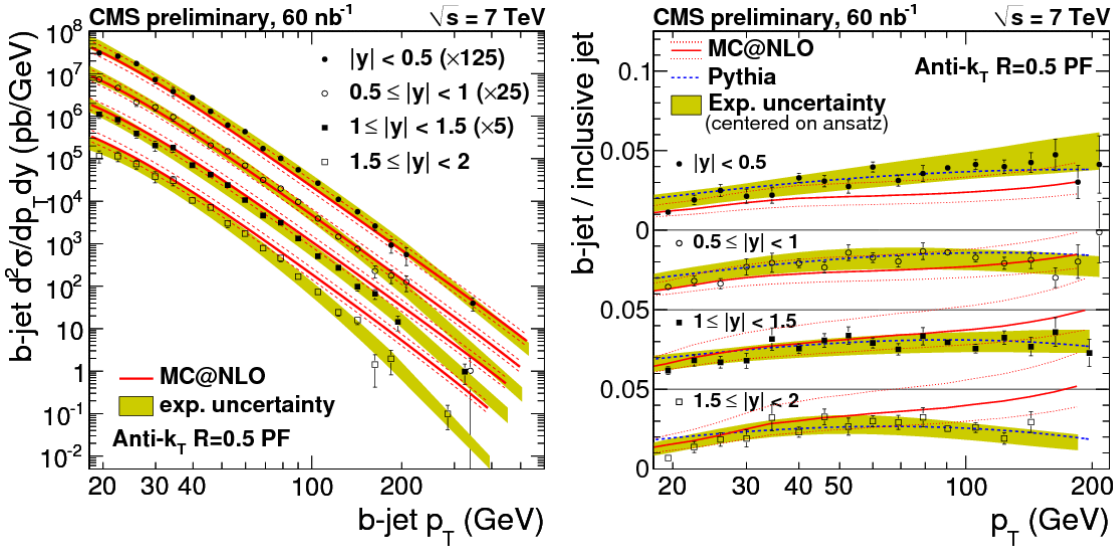

Figure 4: Production cross section measurement for b–jet as a function of the b–jet transverse momentum compared with the MC@NLO predictions (left) and the ratio of the b–jet cross section over the inclusive jets (right).

Acknowledgments

The involvement in this work was made possible by the founding of the INFN, sezione di Padova. I am grateful to Prof. U. Gasparini for all the sustaining and encouraging, and to

the entire CMS Padova group for the fruitful collaboration.

Bibliography

[1] D0 Collaboration, "Inclusive μ and b quark production cross-sections in $p\overline{p}$collisions at $\sqrt{s} = 1.8$ TeV", Phys. Rev. Lett. 74 (1995) 3548-3552.

[2] D0 Collaboration, "The $b\overline{b}$production cross section and angular correlations in $p\overline{p}$collisions at $\sqrt{s} = 1.8$ TeV", Phys. Lett. B487 (2000) 264-272.

[3] CDF Collaboration, "Measurement of the bottom quark production cross section using semileptonic decay electrons in $p\overline{p}$collisions at $\sqrt{s} = 1.8$ TeV", Phys. Rev. Lett. 71 (1993) 500-504.

[4] CDF Collaboration,"Measurement of the b-Hadron Production Cross Section Using Decays to $\mu D_0 X$ Final States in $p\overline{p}$Collisions at $\sqrt{s} = 1.96$ TeV", Phys. Rev. D79 (2009) 092003.

[5] H1 Collaboration, "Measurement of open beauty production at HERA", Phys. Lett. B467 (1999) 156-164.

[6] H1 Collaboration, "Measurement of beauty production at HERA using events with muons and jets", Eur. Phys. J. C41 (2005) 453-467.

[7] ZEUS Collaboration, "Measurement of beauty photoproduction using decays into muons in dijet events at HERA", JHEP 04 (2009) 133.

[8] ZEUS Collaboration, "Measurement of charm and beauty production in deep inelastic ep scattering from decays into muons at HERA", Eur. Phys. J. C65 (2010) 65-79.

[9] M. Cacciari, S. Frixione, M. L. Mangano et al., "QCD analysis of first b cross-section data at 1.96 TeV", JHEP 0407 (2004) 033.

[10] J.C. Collins and R.K. Ellis, "Heavy quark production in very high-energy hadron collisions", Nucl. Phys. B 360 (1991) 3.

[11] S. Catani, M. Ciafaloni and F. Hautmann, "High-energy factorization and small x heavy flavor production", Nucl. Phys. B 366 (1991) 135.

[12] M. Cacciari and M. Greco, "Large p_{T} hadroproduction of heavy quarks", Nucl. Phys. B 421 (1994) 530.

[13] M. Cacciari, M. Greco and P. Nason, "The p_{T} spectrum in heavy- avour hadroproduction", JHEP 05 (1998) 007.

[14] S. Frixione et al., "Heavy quark production", Adv. Ser. Direct. High Energy Phys. 15 (1998) 609.

[15] B.A. Kniehl, G. Kramer, I. Schienbein and H. Spiesberger, "Finite-mass effects on inclusive B–meson hadroproduction", Phys. Rev. D 77 (2008) 014011.

[16] M.G. Ryskin, A.G. Shuvaev and Y.M. Shabelski, "Comparison of k_{T} factorization approach and QCD parton model for charm and beauty hadroproduction", Phys. Atom. Nucl. 64 (2001) 1995.

[17] H. Jung, "Heavy quark production at the Tevatron and HERA using k_{T} factorization with CCFM evolution", Phys. Rev. D 65 (2002) 034015.

[18] CMS Collaboration, "The CMS experiment at the CERN LHC", JINST 0803 (2008) S08004.

[19] CMS Collaboration, "Inclusive b-hadron production cross section with muons in pp collisions at $\sqrt{s} = 7$ TeV", Journal of High Energy Physics Volume 2011, Number 3, 90.

[20] CMS Collaboration, "Inclusive b-jet production in pp collisions at $\sqrt{s} = 7$ TeV", CMS-PAS-BPH-10-009.

[21] T. Sjöstrand, S. Mrenna, P.Z. Skands, "PYTHIA 6.4 physics and manual", J. High Energy Phys. 0605, 026 (2006).

[22] H. Jung et al., "The CCFM Monte Carlo generator CASCADE", Comput. Phys. Commun. 143 (2002) 100-111.

[23] M. Cacciari, S. Frixione, P. Nason, "The p_{T} spectrum in heavy flavor photoproduction", J. High Energy Phys. 0103, 006 (2001).

Measurement of $B\overline{B}$ Angular Correlations at $\sqrt{s} = 7$ TeV with the CMS Experiment

Christoph Grab on behalf of the CMS Collaboration
Institute for Particle Physics, ETH Zurich,
CH-8093 Zurich, Switzerland

Measurements of the angular correlations between beauty and anti-beauty hadrons produced in LHC pp collisions at $\sqrt{s} = 7$ TeV are presented. These results probe for the first time the small angular separation region and show sensitivity to collinear particle emission. The results are compared with predictions based on perturbative QCD calculations at leading and next-to-leading order.

1 Introduction

Studies of production properties of beauty quarks (b) at the CERN LHC collider are of twofold interest. Firstly, the b production process provides an excellent opportunity to study details of perturbative Quantum Chromodynamics (pQCD). Over the years, the various tensions between the predictions and the measurements, that existed in data at lower energies such as the HERA or the Tevatron collider, have been reduced, however not completely resolved. Studies at the LHC collider with higher centre-of-mass energies complement the previous data, but also expand the reach and provide tests at precisions below the present theoretical uncertainties.

Secondly, b quark production constitutes one of the major backgrounds in many of the searches for new physics. Any production channel of exotic states, that produces top quarks or W-bosons, will inherently have a large b production rate. It is of importance not only to understand the absolute production rates, but also to be able to describe the details of the b production dynamics. Thus, a solid understanding of the topology of the final states will be crucial to constitute efficient criteria to distinguish possible signal signatures from b-induced background configurations.

Within the leading-order (LO) QCD picture, the production of $b\overline{b}$ in pp collisions at LHC can be attributed to three parton level production subprocesses, commonly denoted by flavour creation (FCR), flavour excitation (FEX) and gluon splitting (GSP) (see Fig. 1). At higher orders, the distinction becomes scale dependent, and is thus less well defined. Due to the different dynamics of these components, the final state topologies differ substantially from each other. FCR pertains to the $2 \rightarrow 2$ processes gluon-fusion and $q\overline{q}$ annihilation, where the

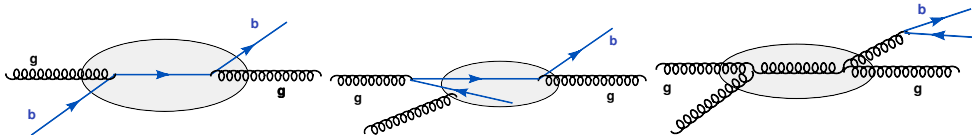

Figure 1: Examples of schematic Feynman diagrams for the three subprocesses: flavour creation (FCR, top), flavour excitation (FCR, middle) and gluon splitting (GSP, bottom).

b and $\overline{\text{b}}$ are emitted in a back-to-back configuration. FEX refers to the $2 \rightarrow 3$ process, where one b quark of a b$\overline{\text{b}}$ pair from the proton sea participates in the hard scattering, thereby producing an asymmetry in the momentum and angular distribution of the final state. The GSP contribution on the other hand describes gluons from either initial or final state, that split into a b$\overline{\text{b}}$ pair, which in turn are emitted preferentially at small opening angles and low p_{T}. Furthermore, the relative production rates themselves vary also as a function of the energy scale. It is expected, that at higher energies the gluon splitting contributions dominate, ie. processes with a collinear branching of gluons into B$\overline{\text{B}}$ pairs will become the major source of b quark production.

2 Measurements of B$\overline{\text{B}}$ Angular Correlations

CMS has performed the first measurement [1] of the angular correlations between beauty and anti-beauty hadrons (B$\overline{\text{B}}$) produced in pp collisions at $\sqrt{s} = 7$ TeV, thereby probing for the first time the region of small angular separation. The analysis is based on a data sample corresponding to an integrated luminosity of $3.1 \pm 0.3\,\text{pb}^{-1}$. A detailed description of the CMS detector can be found in Ref. [2].

The measurements are done differentially as a function of the opening angle for different event scales, which are characterised by the leading jet transverse momentum in the event (independently of b hadrons). The leading jet of the event is used to trigger. The trigger thresholds are chosen such as to reach an efficiency over 99% for all three energy scale bins, which correspond to a leading jet p_{T} in excess of 56, 84 and 120 GeV, respectively, when using corrected jet energies.

The cross sections are determined by applying efficiency corrections and normalising to the total integrated luminosity. The angular correlations between the two B hadrons are measured in terms of the difference in azimuthal angles ($\Delta\phi$) in radians and the combined separation variable $\Delta R = \sqrt{(\Delta\eta)^2 + (\Delta\phi)^2}$, where $\Delta\eta$ is the pseudorapidity. The analysis results are quoted for the visible kinematic range defined by the phase space at the B hadron level by the requirements $|\eta(\text{B})| < 2.0$ and $p_{\text{T}}(\text{B}) > 15$ GeV for both of the B hadrons. The leading jet used to define the minimum energy scale is required to be within a pseudorapidity of $|\eta(\text{jet})| < 3.0$.

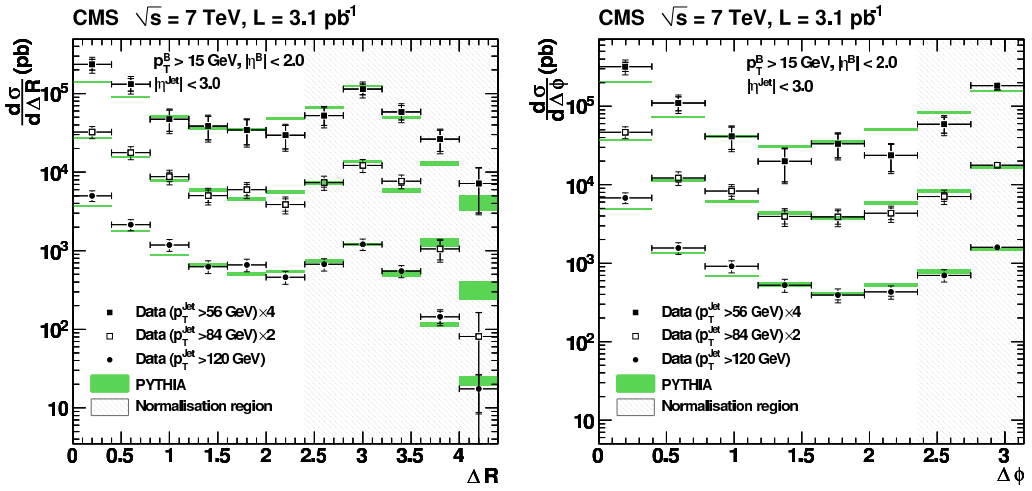

Figure 2: Differential B$\overline{\text{B}}$ production cross sections as a function of ΔR (left) and $\Delta\phi$ (rad) (right) for the three leading jet p_{T} regions. For clarity, the $p_{\text{T}} > 56$ and 84 GeV bins are offset by a factor 4 and 2, respectively. The error bars of the data show the statistical (inner) and the total (outer bars) uncertainties. A common uncertainty of 47% due to the absolute normalisation on the data points is not included. The PYTHIA prediction is normalised to the region $\Delta R > 2.4$ or $\Delta\phi > 2.4$. The widths of the shaded bands indicate the statistical uncertainties of the predictions.

In order to measure the angular correlations also in the collinear regime, the reconstruction of the B hadrons is done independently of jet algorithms. The method uses the B hadron decays and is based on an iterative inclusive secondary vertex finder that exploits the excellent CMS tracking information [3]. This allowed to approximate the flight direction of the original B hadron by the vector between the primary (PV) and the secondary vertices (SV). A resolution of 0.02 rad in ΔR could be achieved that way. The average overall event reconstruction efficiencies (for both B hadrons) are found to be of order 10% at an average purity of 84%. Detailed studies were performed to ensure high accuracy in the B-hadron kinematics description. In addition, the angular dependence of the efficiency description was verified by a special event mixing technique, both in data and the simulation.

The measured cross sections are presented in Fig.2. Overlaid are the predictions by the PYTHIA calculations, which are normalised to the $\Delta R > 2.4$ or $\Delta\phi > 2.4$ (rad) regions, where the calculations are expected to be more reliable. Note, that an overall common uncertainty of 47% due to the absolute normalisation is not shown in the figures.

We find that the cross sections at small ΔR or $\Delta\phi$ are substantial and even exceed the values observed at large angular separation values. Hence, the configurations where the two B hadrons are emitted in opposite directions are much less likely than the collinear configuration.

The measurements are compared to various predictions, based on LO and next-to-leading

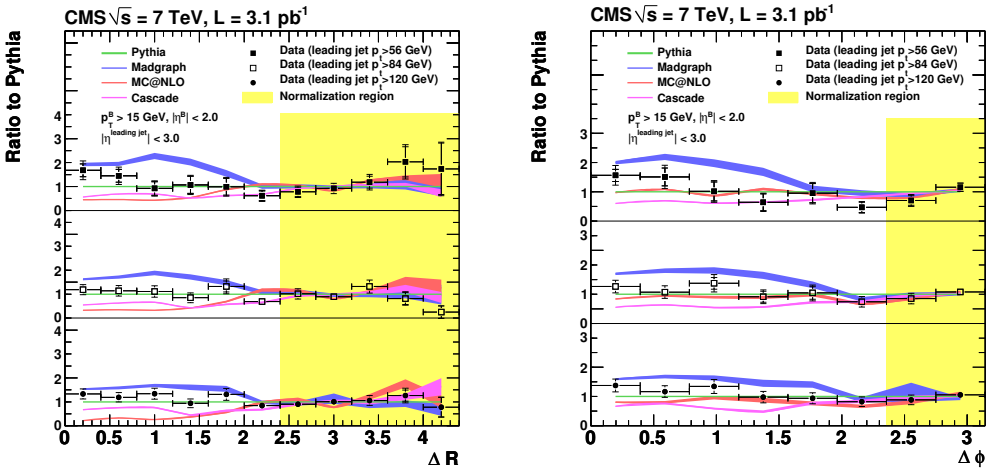

Figure 3: Ratio of the differential $B\overline{B}$ production cross sections, as a function of ΔR (left) and $\Delta\phi$ (rad) (right), for data, MADGRAPH, MC@NLO and CASCADE, with respect to the PYTHIA predictions, shown also for the three leading jet p_T bins. The simulation is normalised to the region $\Delta R > 2.4$ and $\Delta\phi > 2.4$ (rad) (FCR region), as indicated by the shaded normalisation region. The widths of the theory bands indicate the statistical uncertainties of the simulation.

(NLO) pQCD calculations. Figure 3 illustrates the shape sensitivity by showing the ratio of the different ΔR distributions to the PYTHIA Monte Carlo predictions. It is found, that the overall tendency in shape is in general reasonably described by the predictions, however the normalizations and the details in shape, in particular at small opening angles are not described well by any of the calculations. Apart from MADGRAPH program, all predictions underestimate the amount of gluon splitting contributions in the collinear region.

Perturbative QCD predicts a back-to-back configuration for the production of the $B\overline{B}$ pair (i.e. large values of ΔR and/or $\Delta\phi$) for the LO processes. In contrast, the region of phase space with small opening angles between the B and $\overline{B}$ hadrons provides strong sensitivity to collinear emission processes, such as the ones present in higher-order processes. Gluon radiation which splits into $b\overline{b}$ pairs is anticipated to have a smaller angular separation between the b quarks.

The measurements show that the $B\overline{B}$ production cross section ratio $\rho_{\Delta R} = \sigma_{\Delta R<0.8} \,/\, \sigma_{\Delta R>2.4}$ increases as a function of the leading jet p_T in the event (see Fig. 4). Larger p_T values lead to more gluon radiation and, hence, are expected to produce more gluon splitting into $B\overline{B}$ pairs. This general trend is described reasonably by the theoretical calculations.

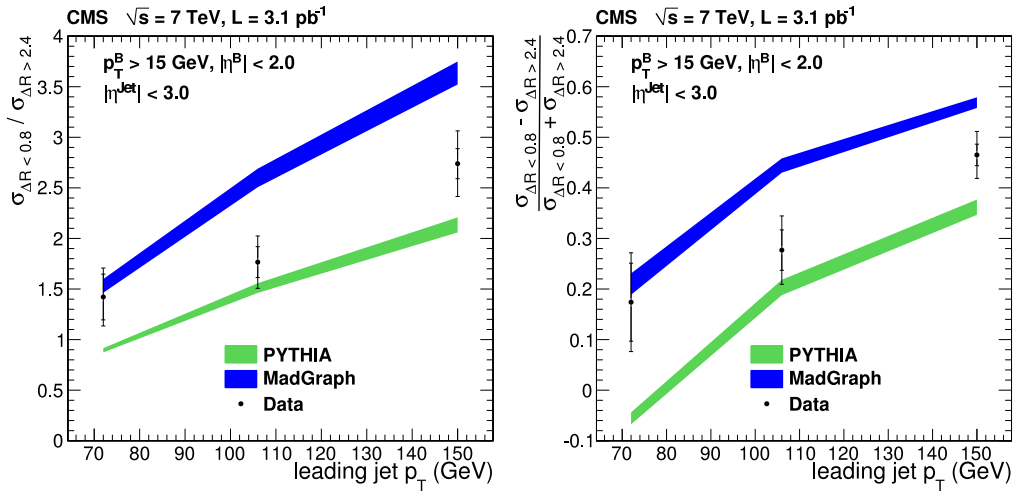

Figure 4: Left: ratio between the B$\overline{\text{B}}$ production cross sections in $\Delta R < 0.8$ and $\Delta R > 2.4$, $\rho_{\Delta R} = \sigma_{\Delta R<0.8} \,/\, \sigma_{\Delta R>2.4}$, as a function of the leading jet p_{T}. Right: asymmetry between the two regions, $(\sigma_{\Delta R<0.8} - \sigma_{\Delta R>2.4}) \,/\, (\sigma_{\Delta R<0.8} + \sigma_{\Delta R>2.4})$. The symbols denote the data averaged over the bins and are plotted at the mean leading jet p_{T} of the bins. For the data points, the error bars show the statistical (inner bars) and the total (outer bars) errors. Also shown are the predictions from the PYTHIA and MADGRAPH simulations, where the widths of the bands indicate the uncertainties arising from the limited number of simulated events.

3 Conclusions

The first measurements of inclusive beauty production have been performed at the LHC by the CMS experiment over a large range from very low transverse momenta up to 300 GeV in the central rapidity region. Comparisons with theoretical predictions, based on pQCD calculations have confirmed the large production cross section. The calculations in general describe the overall features of beauty production fairly well. However, the predictions do not yet adequately describe the differential measurements, neither in the B transverse momentum, nor the rapidity nor the B$\overline{\text{B}}$ opening angle distributions.

Bibliography

[1] CMS Collaboration, "Measurement of B anti-B Angular Correlations based on Secondary Vertex Reconstruction at $\sqrt{s} = 7$ TeV", JHEP **03** (2011) 136.

[2] CMS Collaboration, "The CMS experiment at the CERN LHC", JINST **3** (2008) S08004.

[3] CMS Collaboration, "CMS Tracking Performance Results from Early LHC Operation", Eur. Phys. J. **C70** (2010) 1165.

Studies of open heavy flavour production at LHCb

Artur Ukleja on behalf of the LHCb Collaboration
Soltan Institute for Nuclear Studies, Warsaw, Poland

The data collected by LHCb in 2010 have been used to study the production of beauty hadrons in pp collisions at $\sqrt{s} = 7$ TeV. Differential cross-sections are measured and compared with theoretical predictions. Results are also shown on relative fractions of B_s and Λ_b production.

1 Introduction

The LHCb is one of the four LHC experiments which started data-taking in 2010 at a centre-of-mass energy of 7 TeV. The LHCb detector [1] is a forward spectrometer dedicated to measure CP violating and rare decays of hadrons containing b and c quarks. Knowledge of the b yield is critical in ascertaining the sensitivity of experiments that aim to measure fundamental parameters of interest involving, for example, CP violation. It is useful for normalising backgrounds for measurements of higher mass objects that decay into $b\bar{b}$, such as the Higgs boson. The first data taken with the LHCb detector allows for the measurements of the production cross-section for the average of b- and $\bar{b}$-flavoured hadrons in pp collisions which also can be compared to QCD predictions. The LHCb detector explores a unique kinematic region. It detects b hadrons produced in a cone centered around the beam axis covering a region of pseudo-rapidity η, ranging approximately between 2 and 5, and with transverse momenta ranging from 0 to about 15 GeV. The $b\bar{b}$ quark production cross-section is related with the fragmentation fractions which are needed to determine any B_s^0 branching ratio at the LHC. The fragmentation fractions f_u, f_d, f_s and f_Λ describe the probability that a b quark will fragment into a B_q meson (where $q = u, d, s$), or Λ_b baryon, respectively. The measurement of branching ratio of the rare decay $B_s^0 \to \mu^+\mu^-$ is the prime example where knowledge on ratio of f_s/f_d is crucial to reach the highest sensitivity in the search for New Physics [2].

2 The b-flavoured hadrons cross-section measurements

Two independent data samples are used to measure the cross-section for $b\bar{b}$ quark production and the results are subsequently combined (Figure 1). The decay channel $b \to D^0\mu^-\overline{\nu}X$ is used, as it has a large branching fraction of $(6.84 \pm 0.35)\%$, and is advantageous from

the point of view of signal to background. For the earliest period of data taking the number of colliding bunches was sufficiently low that the high-level trigger could process all crossing and accept events when at least one track was reconstructed in either the VELO [1] or the tracking stations. This data set, called as "microbias", has an integrated luminosity $\mathcal{L} = 2.9$ nb^{-1}. The second sample, referred to as "triggered", uses triggers designed to select a single muon. Here $\mathcal{L} = 12.2$ nb^{-1}. The cross-section to produce b-flavoured hadrons is measured to be $\sigma(b\bar{b}X) = (75.3 \pm 5.4 \pm 13.0)$ μb in the pseudo-rapidity interval $2 < \eta < 6$ over the entire range of p_T assuming the LEP fraction for fragmentation into b-flavoured hadrons [3]. The measured cross-section is consistent with theoretical predictions. For extrapolation to the full η region using PYTHIA 6.4 total $b\bar{b}$ cross-section of $\sigma(b\bar{b}X) = (284 \pm 20 \pm 49)$ μb based on LEP fragmentation results; using the Tevatron fragmentation fractions the result increases by 19 %.

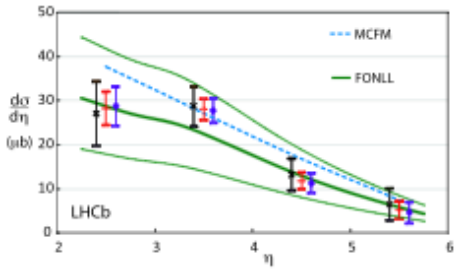

Figure 1: The $\sigma(pp \to b\bar{b}X)$ as a function of η for the microbias ($\times$) and triggered ($\bullet$) samples, shown displaced from the bin center and the average ($+$). The data are shown as points with statistics error bars only, the MCFM [4] prediction as a dashed line, and the FONLL [5] prediction as a thick solid line. The thin upper and lower lines indicate the theoretical uncertainties on the FONLL prediction.

The cross-section to produce b-flavoured hadrons also was determined from the measurements of double-differential cross-section for J/ψ from b in the various (y, p_T) bins [6] which are shown in Figure 2. The analysis is based on a data sample corresponding to the $\mathcal{L} = 5.2$ pb^{-1}. The measured cross-section for the production of J/ψ from b integrated over the fiducial region $p_T \in [0; 14]$ GeV and $y \in [2.0; 4.5]$ is $\sigma(J/\psi\ from\ b) = 1.14 \pm 0.01 \pm 0.16$ μb, where the first uncertainty is statistical and the second systematic. Using this measurement and the LHCb Monte Carlo simulation based on PYTHIA 6.4, the cross-section to produce b-flavoured hadrons extrapolated to the full polar angle range is $\sigma(b\bar{b}X) = (288 \pm 4 \pm 48)$ μb. This result is in excellent agreement with $\sigma(b\bar{b}X) = (284 \pm 20 \pm 49)$ μb obtained from b decays into $D^0\mu^-\bar{\nu}X$.

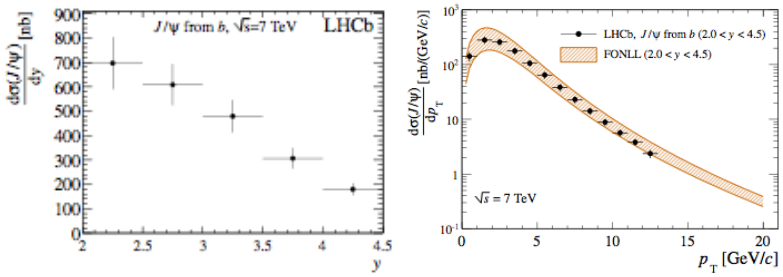

Figure 2: Left: Differential production cross-section as a function of y integrated over p_T, for unpolarised J/ψ from b. The errors are the quadratic sums of the statistical and systematic uncertainties. **Right:** Comparison of the LHCb results for the differential J/ψ from b production for unpolarised J/ψ (circles with error bars) with J/ψ from b production as predicted by FONLL (hatched orange uncertainty band).

3 Fragmentation fraction measurements

Knowledge of the fragmentation fractions allows to relate theoretical predictions of the $b\bar{b}$ quark production cross-section, derived from perturbative QCD, to the observed hadrons. It suffices to measure the ratio of B_s production to either B^- or $\overline{B}^0$ production to perform precise absolute B_s branching fraction measurements. The first data taken with the LHCb detector allows for the measurements of two ratios of fragmentation fractions: strange B meson to light B meson production $[f_s/(f_u + f_d)]$ and Λ_b baryon to light B meson production $[f_{\Lambda_b}/(f_u + f_d)]$, where $f_q \equiv \mathcal{B}(b \to B_q)$ and $f_{\Lambda_b} \equiv \mathcal{B}(b \to \Lambda_b)$ [7]. The results are shown in Figure 3 as a function of the charmed hadron-muon system transverse momentum p_T and of the b-hadron pseudo-rapidity η. This analysis follows previous analysis of $b \to D^0\mu^-\overline{\nu}X$ [3]. Charmed hadrons and muons are combined to form a partially reconstructed b-hadron by requiring that they come from a common vertex. Details of the event selection are described in [7]. Perturbative QCD calculations lead to expect the ratios $[f_s/(f_u + f_d)]$ and $[f_{\Lambda_b}/(f_u + f_d)]$ to be fairly independent of the pseudo-rapidity η, while a possible dependence upon the b-hadron transverse momentum p_T is not ruled out, especially for the ratios involving baryon species. The measured ratio $[f_s/(f_u + f_d)]$ is fairly constant over the whole $\eta - p_T$ domain. By fitting all the data to a single constant, we obtain $[f_s/(f_u + f_d)] = 0.134 \pm 0.004^{+0.011}_{-0.010}$ in the interval $\eta = (2, 5)$, where the first error is statistical and the second is systematic. The corresponding ratio $[f_{\Lambda_b}/(f_u + f_d)]$ is found to be dependent upon the transverse momentum of the charm hadron-μ pair. Assuming the linear dependence, we get $[f_{\Lambda_b}/(f_u + f_d)] = (0.404 \pm 0.017 \pm 0.027 \pm 0.105) \times [1 - (0.031 \pm 0.004 \pm 0.003) \times p_T(\text{GeV})]$, where the errors on the absolute scale are statistical, systematic and absolute scale uncertainty due to the error in $\mathcal{B}(\Lambda_c \to pK\pi)$ respectively. No η dependence is found.

The relative abundances of the three decay modes $B^0 \to D^-(K^+\pi^-\pi^-)\pi^+$, $B^0 \to D^-(K^+\pi^-\pi^-)K^+$ and $B_s^0 \to D_s^-(K^+K^-\pi^-)\pi^+$ are used to determine the ratio of

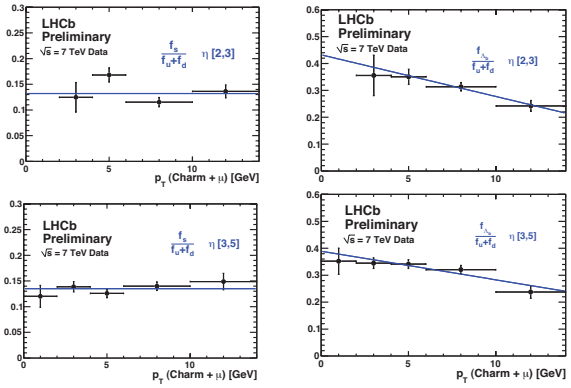

Figure 3: The ratio between $\overline{B_s^0}$ and light B meson production fractions as a function of the transverse momentum of the $D_s\mu$ pair (left) and fragmentation ratio $[f_{\Lambda_b}/(f_u + f_d)]$ dependence upon $p_T(\mu\Lambda_c)$ (right) in two bins of η. The errors shown are statistical only [7].

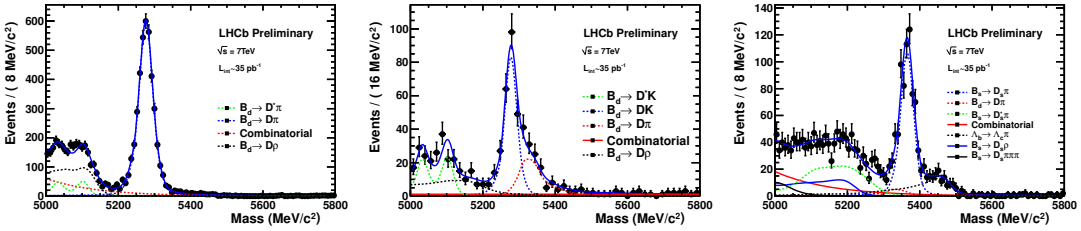

Figure 4: Results of the fits to $B^0 \to D^-\pi^+$, $B^0 \to D^-K^+$ and $B_s^0 \to D_s^-\pi^+$ candidates (left to right). The curves are as summarised in the legends and described in the text [8].

fragmentation fractions f_s/f_d. Details of event selection are described in [8]. The $B^0 \to D^-\pi^+$, $B^0 \to D^-K^+$ and $B_s^0 \to D_s^-\pi^+$ event yields are 4109 ± 75, 253 ± 21 and 670 ± 34, respectively, and the fit results are shown in Figure 4. This analysis is based on $\mathcal{L} = 35\ \text{pb}^{-1}$ of data collected using the LHCb detector during the 2010 LHC running. The theoretically cleaner extraction f_s/f_d is performed using the decays $B^0 \to D^-K^+$ and $B_s^0 \to D_s^-\pi^+$ as $f_s/f_d = 0.242 \pm 0.024 \pm 0.018 \pm 0.016$, where the first error is the statistical, the second the systematic uncertainty, and the third the theoretical uncertainty dominated by the uncertainty on the form factor ratio. The ratio f_s/f_d extracted from the modes $B^0 \to D^-\pi^+$ and $B_s^0 \to D_s^-\pi^+$ is found to be $f_s/f_d = 0.249 \pm 0.013 \pm 0.020 \pm 0.025$, where the theoretical uncertainty increases by an additional uncertainty from the W-exchange diagrams [9]. The two values for f_s/f_d can be combined into a single value, by taking all correlated uncertainties into account. The average values is $f_s/f_d = 0.245 \pm 0.017 \pm 0.018 \pm 0.018$. These values of f_s/f_d are in good agreement with the values determined at LEP and at the Tevatron.

Bibliography

[1] LHCb Collaboration, A. Augusto Alves Jr. *et al.*, JINST 3,S08005 (2008).

[2] LHCb Collaboration, R. Aaij *et al.*, Phys.Lett. B699,330-340 (2011).

[3] LHCb Collaboration, R. Aaij *et al.*, Phys.Lett. B694,209 (2010).

[4] Monte Carlo for FeMtobarn processes, http://mcfm.fnal.gov/.

[5] M. Cacciari, P. Nason, S. Frixione, M. Mangano, G. Ridolfi, private communication.

[6] LHCb Collaboration, R. Aaij *et al.*, Eur.Phys.J C71,1645 (2011).

[7] LHCb Collaboration, R. Aaij *et al.*, LHCb-CONF-2011-028 (2011).

[8] LHCb Collaboration, R. Aaij *et al.*, LHCb-CONF-2011-013 (2011).

[9] R. Fleisher, N. Serra, N. Tuning, Phys. Rev. D83, 014017 (2011).

Weak B Decays into Orbitally Excited Charmed Mesons

Jorge Segovia[1], C. Albertus, D. R. Entem, F. Fernández, E. Hernández, and M. A. Pérez-García
Departamento de Física Fundamental and IUFFyM
Universidad de Salamanca, E-37008 Salamanca, Spain

The BaBar Collaboration has recently reported branching fractions for semileptonic decays of the B meson into final states with charged and neutral $D_1(2420)$ and $D_2^*(2460)$, two narrow orbitally excited charmed mesons. We evaluate these branching fractions within the framework of a constituent quark model in two steps, one which involves a semileptonic decay and the other one mediated by a strong process. Our results are in agreement with the experimental data.

1 Introduction

Different collaborations have recently reported semileptonic B decays into orbitally excited charmed mesons providing detailed results of branching fractions [1,2]. These data offer new theoretical possibilities to test meson models as far as they include a weak decay followed by a strong one.

All these magnitudes can be consistently calculated in the framework of constituent quark models because they can simultaneously account for the hadronic part of the weak process and the strong meson decays. In this context meson strong decay has been described successfully in phenomenological models, like the $^3P_0$ model [3] or in microscopic models (see Refs. [4,5]). The matrix element for the weak process factorizes into a leptonic and a hadronic part. It is the hadronic part that contains the non-perturbative strong interaction effects and we shall evaluate it within the constituent quark model (CQM) of Ref. [6] which successfully describes hadron phenomenology and reactions. Details of the calculation can be found in Ref. [7].

2 Theoretical framework

2.1 Constituent quark model

Spontaneous chiral symmetry breaking of the QCD Lagrangian together with the perturbative one-gluon exchange (OGE) and the non-perturbative confining interaction are the

[1]segonza@usal.es

main pieces of potential models. Using this idea, Vijande *et al.* [6] developed a model of the quark-quark interaction which is able to describe meson phenomenology from the light to the heavy quark sector. Further details can be found in Ref. [6].

In order to find the quark-antiquark bound states, we solve the Schrödinger equation by Rayleigh-Ritz variational principle. We use the Gaussian Expansion Method [8] that provides enough accuracy and makes the subsequent evaluation of the decay amplitude matrix elements easier.

Model parameters are given in Ref [9].

2.2 Weak and strong decays

In the weak decay we have a $\overline{b} \to \overline{c}$ transition at the quark level and we need to evaluate the hadronic matrix elements of the weak current

$$J_{\mu}^{bc}(0) = \overline{\psi}_b(0)\gamma_{\mu}(I-\gamma_5)\psi_c(0). \tag{1}$$

The hadronic matrix elements involved in these processes can be parametrized in terms of form factors. The expression of the hadron tensor in the helicity formalism [10] has been calculated following Ref. [11].

To describe the meson decay process $A \to B + C$, the $^3P_0$ decay model assumes that a quark and an antiquark are created with vacuum quantum numbers. The created $q\overline{q}$ pair together with the $q\overline{q}$ pair from the initial meson regroups in the two outgoing mesons via a quark rearrangement process. For the $^3P_0$ decay model, the interaction Hamiltonian is given by

$$H_I = g\int d^3x\overline{\psi}(\vec{x})\psi(\vec{x}) \tag{2}$$

where g is related to the dimensionless constant giving the strength of the $q\overline{q}$ pair creation from the vacuum as $\gamma = \frac{g}{2m_q}$.

In the microscopic decay models, the strong decays are driven by the interquark Hamiltonian which determines the spectrum. In our case we have the one-gluon exchange and a mixture of scalar and vector Lorentz confining interactions appearing as the kernels. These interactions and their associated decay amplitudes are undoubtedly all present and should be added coherently. The Hamiltonian of the interaction can be written as

$$H_I = \frac{1}{2}\int d^3x d^3y\, J^a(\vec{x})K(|\vec{x}-\vec{y}|)J^a(\vec{y}), \tag{3}$$

where current $J^a(\vec{x})$ in Eq. (3) is assumed to be a color octet. Calculation details referred to the microscopic model can be found in Ref. [12].

	Belle [1] ($\times 10^{-3}$)	BaBar [2] ($\times 10^{-3}$)	$^3P_0$ ($\times 10^{-3}$)	Mic. ($\times 10^{-3}$)
$D_1(2420)$				
$\mathcal{B}(B^+ \to \overline{D}_1^0 l^+ \nu_l)\mathcal{B}(\overline{D}_1^0 \to D^{*-}\pi^+)$	$4.2 \pm 0.7 \pm 0.7$	$2.97 \pm 0.17 \pm 0.17$	2.57	2.57
$\mathcal{B}(B^0 \to D_1^- l^+ \nu_l)\mathcal{B}(D_1^- \to \overline{D}^{*0}\pi^-)$	$5.4 \pm 1.9 \pm 0.9$	$2.78 \pm 0.24 \pm 0.25$	2.39	2.39
$D_2^*(2460)$				
$\mathcal{B}(B^+ \to \overline{D}_2^{*0} l^+ \nu_l)\mathcal{B}(\overline{D}_2^{*0} \to D^-\pi^+)$	$2.2 \pm 0.3 \pm 0.4$	$1.4 \pm 0.2 \pm 0.2^{(*)}$	1.43	1.47
$\mathcal{B}(B^+ \to \overline{D}_2^{*0} l^+ \nu_l)\mathcal{B}(\overline{D}_2^{*0} \to D^{*-}\pi^+)$	$1.8 \pm 0.6 \pm 0.3$	$0.9 \pm 0.2 \pm 0.2^{(*)}$	0.79	0.75
$\mathcal{B}(B^+ \to \overline{D}_2^{*0} l^+ \nu_l)\mathcal{B}(\overline{D}_2^{*0} \to D^{(*)-}\pi^+)$	$4.0 \pm 0.7 \pm 0.5$	$2.3 \pm 0.2 \pm 0.2$	2.22	2.22
$\mathcal{B}(B^0 \to D_2^{*-} l^+ \nu_l)\mathcal{B}(D_2^{*-} \to \overline{D}^0\pi^-)$	$2.2 \pm 0.4 \pm 0.4$	$1.1 \pm 0.2 \pm 0.1^{(*)}$	1.34	1.38
$\mathcal{B}(B^0 \to D_2^{*-} l^+ \nu_l)\mathcal{B}(D_2^{*-} \to \overline{D}^{*0}\pi^-)$	< 3	$0.7 \pm 0.2 \pm 0.1^{(*)}$	0.74	0.70
$\mathcal{B}(B^0 \to D_2^{*-} l^+ \nu_l)\mathcal{B}(D_2^{*-} \to \overline{D}^{(*)0}\pi^-)$	< 5.2	$1.8 \pm 0.3 \pm 0.1$	2.08	2.08
$\mathcal{B}_{D/D^{(*)}}$	0.55 ± 0.03	$0.62 \pm 0.03 \pm 0.02$	0.65	0.66

Table 1: Most recent experimental measurements reported by Belle and BaBar Collaborations and their comparison with our results. The symbol $(*)$ indicates the estimated results from the original data using $B_{D/D^{(*)}}$.

3 Results

The final results and their comparison with the experimental data are given in Table 1. Both $^3P_0$ and microscopic models predict similar branching ratios. The predictions for the $B \to D_1 l\nu_l$ and $B \to D_2^* l\nu_l$ are in good agreement with the latest experimental measurements by the BaBar Collaboration. They are significantly smaller than the Belle data, though.

4 Conclusions

We have performed a calculation of the branching fractions for the semileptonic decays of B meson into final states containing the narrow orbitally excited charmed mesons.

We worked in the framework of the constituent quark model of Ref. [6]. We have calculated the semileptonic decay rates within the helicity formalism of Ref. [10] and following the work in Ref. [11]. The strong decay widths have been calculated using two models, the $^3P_0$ model and a microscopic model based on the quark-antiquark interactions present in the CQM model of Ref. [6].

From the experimental point of view, Belle and BaBar Collaborations provide their most recent measurements for the B meson in Refs. [1] and [2], respectively.

Our results for B semileptonic decays into $D_1(2420)$ and $D_2(2460)$ are in good agreement with the latest experimental measurements by the BaBar Collaboration.

Acknowledgments

This work has been partially funded by the Spanish Ministerio de Ciencia y Tecnología under Contracts Nos. FIS2006-03438, FIS2009-07238 and FPA2010-21750-C02-02, by the Spanish Ingenio-Consolider 2010 Programs CPAN CSD2007-00042 and MultiDark CSD2009-0064, and by the European Community-Research Infrastructure Integrating Activity 'Study of Strongly Interacting Matter' (HadronPhysics2 Grant No. 227431). C. A. thanks a Juan de la Cierva contract from the Spanish Ministerio de Educación y Ciencia.

Bibliography

[1] D. Liventsev *et al.* (Belle Collaboration), Phys. Rev. D **77**, 091503 (2008).

[2] B. Aubert *et al.* (BaBar Collaboration), Phys. Rev. Lett. **103**, 051803 (2009).

[3] L. Micu, Nucl. Phys. B **10**, 521 (1969).

[4] E. Eichten, K. Gottfried, T. Kinoshita, K.D. Lane and T. M. Yan, Phys. Rev. D **17**, 3090 (1978); E. Eichten and J. Goldman, *ibid.* **23**, 203 (1981); see also W.S. Jaronski and D. Robson, *ibid.* **32**, 1198 (1985).

[5] E.S. Ackleh, T. Barnes and E.S. Swanson, Phys. Rev. D **54**, 6811 (1996).

[6] J. Vijande, F. Fernández and A. Valcarce, J. Phys. G **31**, 481 (2005).

[7] J. Segovia, C. Albertus, D.R. Entem, F. Fernández, E. Hernández and M.A. Pérez-García, arXiv:1107.4248 [hep-ph].

[8] E. Hiyama, Y. Kino, and M. Kamimura, Prog. Part. Nucl. Phys. **51**, 223 (2003).

[9] J. Segovia, A.M. Yasser, D.R. Entem and F. Fernández, Phys. Rev. D **78**, 114033 (2008).

[10] M.A. Ivanov, J.G. Körner and P. Santorelli, Phys. Rev. D **73**, 054024 (2006).

[11] E. Hernández, J. Nieves and J.M. Verde-Velasco, Phys. Rev. D **74**, 074008 (2006).

[12] J. Segovia, D.R. Entem and F. Fernández, in Proceedings of Hadron2011, eConf C110613 (2011).

Heavy Baryon Spectrum and New Heavy Exotics

Marek Karliner[1,a], Harry J. Lipkin[b,c], and Nils A. Törnqvist[d]
[a]Raymond and Beverly Sackler School of Physics and Astronomy, Tel Aviv University, Israel
[b]Department of Particle Physics, Weizmann Institute of Science, Rehovot 76100, Israel
[c]High Energy Physics Division, Argonne National Laboratory Argonne, IL 60439-4815, USA
[d]Department of Physical Sciences, University of Helsinki, POB 64, FIN-0014 Finland

We discuss several highly accurate theoretical predictions for masses of baryons containing the b quark which have been recently confirmed by experimental data. Several predictions are given for additional properties of heavy baryons. We also discuss the two charged exotic resonances Z_b with quantum numbers of a $(b\bar{b}u\bar{d})$ tetraquark, very recently reported by Belle in the channel $[\Upsilon(nS)\pi^+,\ n=1,2,3]$. Among possible implications are deeply bound $I=0$ counterparts of the Z_b-s and existence of a $\Sigma_b^+\Sigma_b^-$ dibaryon, a *beauteron*.

1 Introduction

QCD describes hadrons as valence quarks in a sea of gluons and $\bar{q}q$ pairs. At distances above $\sim$ 1 GeV^{-1} quarks acquire an effective *constituent mass* due to chiral symmetry breaking. A hadron can then be thought of as a bound state of constituent quarks. In the zeroth-order approximation the hadron mass M is then given by the sum of the masses of its constituent quarks m_i, $M=\sum_i m_i$. The binding and kinetic energies are "swallowed" by the constituent quarks masses. The first and most important correction comes from the color hyper-fine (HF) chromo-magnetic interaction,

$$(1)\quad M=\sum_i m_i+\sum_{i<j} V_{ij}^{HF(QCD)}\,; \qquad V_{ij}^{HF(QCD)}=v_0\,(\vec{\lambda}_i\cdot\vec{\lambda}_j)\,\frac{\vec{\sigma}_i\cdot\vec{\sigma}_j}{m_i m_j}\,\langle\psi|\delta(r_i-r_j)|\psi\rangle$$

where v_0 gives the overall strength of the HF interaction, $\vec{\lambda}_{i,j}$ are the $SU(3)$ color matrices, $\sigma_{i,j}$ are the quark spin operators and $|\psi\rangle$ is the hadron wave function. This is a contact spin-spin interaction, analogous to the EM hyperfine interaction, which is a product of the magnetic moments, $V_{ij}^{HF(QED)}\propto\vec{\mu}_i\cdot\vec{\mu}_j=e^2\,\vec{\sigma}_i\cdot\vec{\sigma}_j/(m_i m_j)$. In QCD, the $SU(3)_c$ generators take place of the electric charge. From eq. (1) many very accurate results have been obtained for the masses of the ground-state hadrons. Nevertheless, several caveats are in order. First, this is a low-energy phenomenological model, still awaiting a rigorous derivation

[1]marek@proton.tau.ac.il

from QCD. It is far from providing a complete description of the hadronic spectrum, but it provides excellent predictions for mass splittings and magnetic moments. The crucial assumptions of the model are: (a) HF interaction is considered as a perturbation which does not change the wave function; (b) effective masses of quarks are the same inside mesons and baryons; (c) there are no 3-body effects.

2 Effective masses of quarks

Constituent quark mass differences depend strongly on the flavor of the spectator or "neighbor" quark [1]. For example, $m_s - m_d \approx 180$ MeV when the spectator is a light quark but the same mass difference is only about 90 MeV when the spectator is a b quark. Since these are *effective masses*, we should not be surprised that their difference is affected by the environment, but the large size of the shift is quite surprising and its quantitative derivation from QCD is an outstanding challenge for theory. We can extract the ratio of the constituent quark masses from the ratio of the the hyperfine splittings in the corresponding mesons. The hyperfine splitting between K^* and K mesons is given by

$$M(K^*)-M(K)=v_0\frac{\vec{\lambda}_u\cdot\vec{\lambda}_s}{m_u m_s}\left[(\vec{\sigma}_u\cdot\vec{\sigma}_s)_{K^*}-(\vec{\sigma}_u\cdot\vec{\sigma}_s)_K\right]\langle\psi|\delta(r)|\psi\rangle=4v_0\frac{\vec{\lambda}_u\cdot\vec{\lambda}_s}{m_u m_s}\langle\psi|\delta(r)|\psi\rangle, \tag{2}$$

and similarly for hyperfine splitting between D^* and D with $s\to c$ everywhere. From (2) and its D analogue we then immediately obtain

$$\frac{M(K^*)-M(K)}{M(D^*)-M(D)}\approx\frac{m_c}{m_s} \tag{3}$$

2.1 Color hyperfine splitting in baryons

As an example of hyperfine splitting in baryons, let us now discuss the HF splitting in the Σ (uds) baryons. Σ^* has spin $\frac{3}{2}$, so the u and d quarks must be in a state of relative spin 1. The Σ has isospin 1, so the wave function of u and d is symmetric in flavor. It is also symmetric in space, since in the ground state the quarks are in a relative S-wave. On the other hand, the u-d wave function is antisymmetric in color, since the two quarks must couple to a $\mathbf{3}^*$ of color to neutralize the color of the third quark. The u-d wave function must be antisymmetric in flavor $\times$ spin $\times$ space $\times$ color, so it follows it must be symmetric in spin, i.e. u and d are coupled to spin one. Since u and d are in spin 1 state in both Σ^* and Σ their HF interaction with each other cancels between the two and thus the u-d pair does not contribute to the $\Sigma^*-\Sigma$ HF splitting,

$$M(\Sigma^*)-M(\Sigma)=6v_0\frac{\vec{\lambda}_u\cdot\vec{\lambda}_s}{m_u m_s}\langle\psi|\delta(r_{rs})|\psi\rangle \tag{4}$$

we can then use eqs. (2) and (4) to compare the quark mass ratio obtained from mesons and baryons:

$$\left(\frac{m_c}{m_s}\right)_{Bar} = \frac{M_{\Sigma^*} - M_\Sigma}{M_{\Sigma_c^*} - M_{\Sigma_c}} = 2.84; \qquad \left(\frac{m_c}{m_s}\right)_{Mes} = \frac{M_{K^*} - M_K}{M_{D^*} - M_D} = 2.81 \tag{5}$$

$$\left(\frac{m_c}{m_u}\right)_{Bar} = \frac{M_\Delta - M_p}{M_{\Sigma_c^*} - M_{\Sigma_c}} = 4.36; \qquad \left(\frac{m_c}{m_u}\right)_{Mes} = \frac{M_\rho - M_\pi}{M_{D^*} - M_D} = 4.46 \tag{6}$$

We find the same value from mesons and baryons $\pm 2\%$.

The presence of a fourth flavor gives us the possibility of obtaining a new type of mass relation between mesons and baryons. The $\Sigma - \Lambda$ mass difference is believed to be due to the difference between the $u - d$ and $u - s$ hyperfine interactions. Similarly, the $\Sigma_c - \Lambda_c$ mass difference is believed to be due to the difference between the $u - d$ and $u - c$ hyperfine interactions. We therefore obtain the relation

$$\left(\frac{\frac{1}{m_u^2} - \frac{1}{m_u m_c}}{\frac{1}{m_u^2} - \frac{1}{m_u m_s}}\right)_{Bar/Mes} = \frac{M_{\Sigma_c} - M_{\Lambda_c}}{M_\Sigma - M_\Lambda} = 2.16 \quad \approx \quad \frac{(M_\rho - M_\pi) - (M_{D^*} - M_D)}{(M_\rho - M_\pi) - (M_{K^*} - M_K)} = 2.10 \tag{7}$$

The meson and baryon relations agree to $\pm 3\%$.We can write down an analogous relation for hadrons containing the b quark instead of the s quark, obtaining the prediction for splitting between Σ_b and Λ_b:

$$\frac{M_{\Sigma_b} - M_{\Lambda_b}}{M_\Sigma - M_\Lambda} = \frac{(M_\rho - M_\pi) - (M_{B^*} - M_B)}{(M_\rho - M_\pi) - (M_{K^*} - M_K)} = 2.51 \tag{8}$$

yielding $M(\Sigma_b) - M(\Lambda_b) = 194\,\mathrm{MeV}$ [1, 2]. This splitting was measured by CDF [3], with isospin-averaged mass difference $M(\Sigma_b) - M(\Lambda_b) = 192$ MeV. There is also the prediction for the spin splittings, good to 5%

$$M(\Sigma_b^*) - M(\Sigma_b) = \frac{M(B^*) - M(B)}{M(K^*) - M(K)} \cdot [M(\Sigma^*) - M(\Sigma)] = 22\,\mathrm{MeV} \tag{9}$$

to be compared with 21 MeV from the isospin-average of CDF measurements [3]. The challenge is to understand how and under what assumptions one can derive from QCD the very simple model of hadronic structure at low energies which leads to such accurate predictions.

3 Magnetic Moments of Heavy Quark Baryons

In Λ, Λ_c and Λ_b baryons the light quarks are coupled to spin zero. Therefore the magnetic moments of these baryons are determined by the magnetic moments of the s, c and b quarks,

respectively. The latter are proportional to the chromomagnetic moments which determine the hyperfine splitting in baryon spectra. We can use this fact to predict the Λ_c and Λ_b baryon magnetic moments by relating them to the hyperfine splittings in the same way as given in the original prediction [5] of the Λ magnetic moment. We obtain

$$\mu_{\Lambda_c} = -2\mu_\Lambda \cdot \frac{M_{\Sigma_c^*} - M_{\Sigma_c}}{M_{\Sigma^*} - M_\Sigma} = 0.43 \ \text{ n.m.}; \qquad \mu_{\Lambda_b} = \ \mu_\Lambda \cdot \frac{M_{\Sigma_b^*} - M_{\Sigma_b}}{M_{\Sigma^*} - M_\Sigma} = -0.067\,\text{n.m.} \tag{10}$$

We hope these observables can be measured in foreseeable future and view the predictions (10) as a challenge for the experimental community.

4 Predicting the Masses of b-Baryons

On top of the already discussed Σ_b with quark content bqq, $q = u, d$. there are two additional ground-state b-baryons, Ξ_b and Ω_b:

Ξ_b: the quark content is bsq. Ξ_b can be obtained from an "ordinary" Ξ (ssd or ssu) by replacing one of the s quarks by a b, with one important difference. In the ordinary Ξ, Fermi statistics dictates that two s quarks must couple to spin-1, while in the ground state of Ξ_b the (sq) diquarks have spin zero. Consequently, the Ξ_b mass is given by the expression: $\Xi_b = m_b + m_s + m_u - 3v\langle\delta(r_{us})\rangle/m_u m_s$. The Ξ_b mass can thus be predicted using the known Ξ_c baryon mass as a starting point and adding the corrections due to mass differences and HF interactions:

$$\Xi_b = \Xi_c + (m_b - m_c) - 3v\left(\langle\delta(r_{us})\rangle_{\Xi_b} - \langle\delta(r_{us})\rangle_{\Xi_c}\right)/(m_u m_s) \tag{11}$$

Since the Ξ_b and Ξ_c baryons contain a strange quark, and the effective constituent quark masses depend on the spectator quark, the optimal way to estimate the mass difference $(m_b - m_c)$ is from mesons which contain both s and b or c quarks:

$$m_b - m_c = \tfrac{1}{4}(3B_s^* + B_s) - \tfrac{1}{4}(3D_s^* + D_s) = 3324.6 \pm 1.4\ . \tag{12}$$

On this basis we predicted [7] $M(\Xi_b) = 5795 \pm 5$ MeV. Our paper was submitted on June 14, 2007. The next day CDF announced the result [9], $M(\Xi_b) = 5792.9 \pm 2.5 \pm 1.7$ MeV, following up on an earlier D0 measurement, $M(\Xi_b) = 5774 \pm 11 \pm 15$ MeV [8].

Ω_b: for the spin-averaged Ω_b mass we have

$$\tfrac{1}{3}(2M(\Omega_b^*) + M(\Omega_b)) = \tfrac{1}{3}(2M(\Omega_c^*) + M(\Omega_c)) + (m_b - m_c)_{B_s - D_s} = 6068.9 \pm 2.4\ \text{MeV} \tag{13}$$

For the HF splitting we obtain

$$M(\Omega_b^*) - M(\Omega_b) = (M(\Omega_c^*) - M(\Omega_c))\frac{m_c}{m_b}\frac{\langle\delta(r_{bs})\rangle_{\Omega_b}}{\langle\delta(r_{cs})\rangle_{\Omega_c}} = 30.7 \pm 1.3\ \text{MeV} \tag{14}$$

leading to the following predictions:

$$M(\Omega_b) = 6052.1 \pm 5.6\ \text{MeV}; \qquad M(\Omega_b^*) = 6082.8 \pm 5.6\ \text{MeV} \tag{15}$$

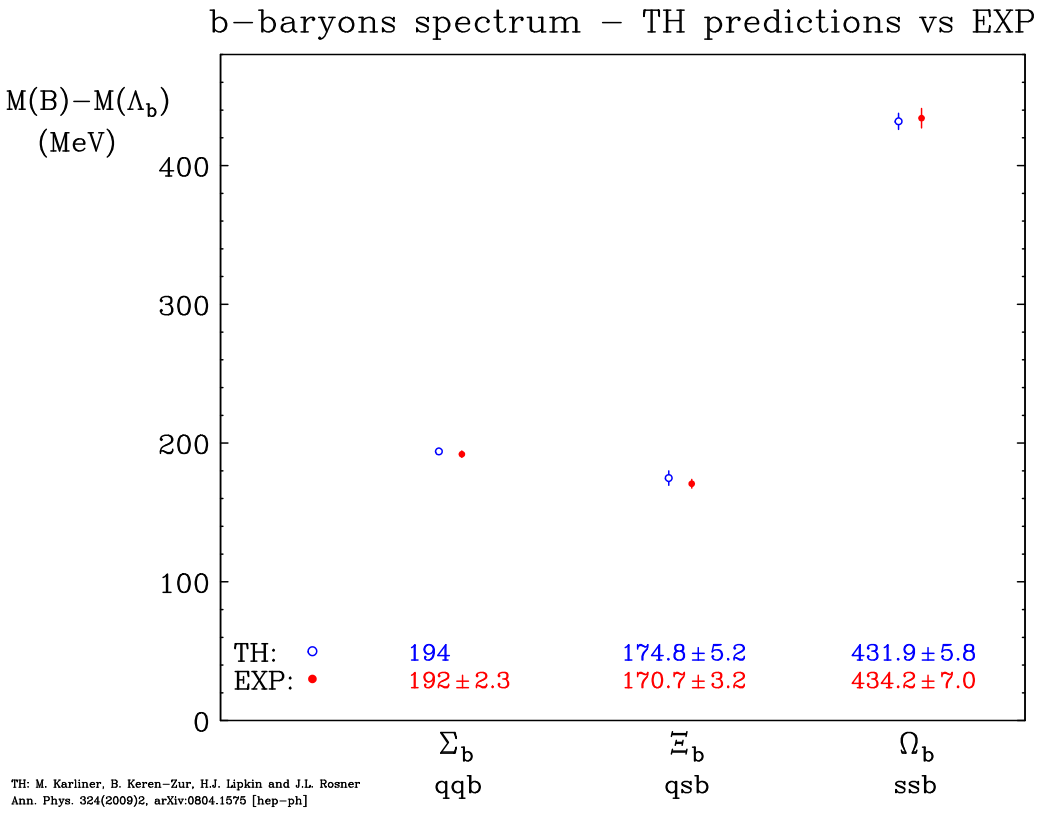

Figure 1: Masses of b-baryons – theoretical predictions [7, 10] vs. experiment.

About four months after our prediction (15) for Ω_b mass [10], D0 collaboration published the first measurement of Ω_b mass [11]: $M(\Omega_b)_{D0} = 6165 \pm 10(stat.) \pm 13(syst.)$ MeV . The deviation from the central value of our prediction was huge, 113 MeV. Understandably, we were very eager to see the CDF result. CDF published their result about nine months later, in May 2009 [12]: $M(\Omega_b)_{CDF} = 6054 \pm 6.8(stat.) \pm 0.9(syst.)$ MeV . Fig. 1 shows a comparison of our predictions for the masses of Σ_b, Ξ_b and Ω_b baryons with the CDF experimental data. We have made additional predictions [7, 10] for some excited states of b-baryons. Our results are summarized in Table 10 of Ref. [10].

The sign in our prediction $M(\Sigma_b^*) - M(\Sigma_b) < M(\Omega_b^*) - M(\Omega_b)$, appears to be counterintuitive, since the color hyperfine interaction is inversely proportional to the quark mass. This reversed inequality is not predicted by other recent approaches [13–15], but it is also seen in the charm data, $M(\Sigma_c^*) - M(\Sigma_c) = 64.3 \pm 0.5\,\text{MeV} < M(\Omega_c^*) - M(\Omega_c) = 70.8 \pm 1.5\,\text{MeV}$. This suggests that the sign of the $SU(3)$ symmetry breaking gives information about the form of the potential. It is of interest to follow this clue theoretically and experimentally.

5 Heavy exotics

Ordinary hadrons contain either a $q\bar{q}$ pair or 3 quarks. The possible color representations of quark combinations are then completely determined by confinement. In a meson the $q\bar{q}$ pair *must* couple to a color singlet and in a baryon any two quarks *must* couple to an anti-triplet of color, to neutralize the color charge of the third quark. The situation is very different in exotic hadrons which contain both qq and $q\bar{q}$ pairs, eg. a tetraquark with two heavy quarks Q and two light quarks q, $Q\overline{Q}q\bar{q}$. Such states have important color-space correlations that are completely absent in ordinary mesons and baryons [16]. One also needs to keep in mind that the q-$\bar{q}$ interaction is much stronger than q-q interaction. The result is emergence of color structures that are totally different from those in normal hadrons. In turn, this leads to some very unusual experimental properties of such states. Until May 2011 the leading candidate has been the $X(3872)$, which is most likely either a $c\bar{c}q\bar{q}$ or a threshold bound state of D and $\overline{D}^*$. Given that $X(3872)$ exists, it is fascinating to explore possible analogues containing b quarks. General considerations suggest that such states should be more strongly bound, since the attraction due to color forces is the roughly same, but the repulsion due to kinetic energy is smaller, as $E_k \sim p^2/m_Q$. Using a simple model, we have suggested that $b\bar{b}q\bar{q}$ might be below the $B\overline{B}$ threshold and $b\bar{c}q\bar{q}$ might be below the $B\overline{D}$ threshold. A crucial difference vs. ordinary mesons is that $(Qq)(\overline{Q}\overline{q})$ can form a $\overline{\mathbf{6}}\mathbf{6}$ color configuration which has much stronger binding than $\overline{\mathbf{3}}\mathbf{3}$. Some of these states have exotic electric charge, e.g. $bd\bar{c}\bar{u} \to J/\psi\pi^-\pi^-$. Their decays have striking experimental signatures: monoenergetic photons and/or pions, e.g. $bq\bar{c}\bar{q}$ with $I{=}0$ above $B_c\pi$ threshold can decay into $B_c\pi$ via isospin violation, or electromagnetically into $B_c\gamma$, both very narrow.

Hadrons containing two b quarks, such as double-bottom baryons bbq or $b\bar{b}q\bar{q}$ and $bb\overline{q}\overline{q}$ tetraquarks have a unique and a spectacular decay mode with two J/ψ-s in the final state. To see this, recall that a b quark can decay via the hadronic mode $b \to \bar{c}cs \to J/\psi s$. If both b quarks in a double-bottom hadron decay this way, for a bb baryon we get $(bbq) \to J/\psi J/\psi(ssq) \to J/\psi J/\psi\,\Xi$, and similarly for a tetraquark: $(b\bar{b}q\bar{q}) \to J/\psi\, J/\psi(\bar{s}s\bar{q}q) \to J/\psi\, J/\psi\, K\, K$, etc., with all final state hadrons coming from the same vertex. This unique signature is however hampered by a very low rate expected for such a process, especially if one uses dimuons to identify the J/ψ-s. It is both challenge and a opportunity for LHCb [16].

Exotic double-bottom hadrons Z_b: theoretical prediction and discovery by Belle

In 2008 Belle reported [17] anomalously large (by two orders of magnitude) branching ratios for the decays $\Upsilon(5S) \to \Upsilon(mS)\pi^+\pi^-$, $m = 1, 2$. In [18] we suggested that the enhancement is due to an intermediate state of a tetraquark $T_{\bar{b}b} = (\bar{b}bu\bar{d})$ and a pion, mediating the two-step process

$$\Upsilon(5S) \;\to\; T^{\pm}_{\bar{b}b}\,\pi^{\mp} \;\to\; \Upsilon(mS)\,\pi^+\pi^-$$

We proposed looking for the $(\bar{b}bu\bar{d})$ tetraquark in these decays as peaks in the invariant mass of $\Upsilon(1S)\pi^+$ or $\Upsilon(2S)\pi^+$ systems.

Very recently Belle collaboration confirmed this prediction, announcing [19] the observation of two charged bottomonium-like resonances Z_b as narrow structures in $\pi^\pm\Upsilon(nS)$ $(n = 1, 2, 3)$ and $\pi^\pm h_b(mP)$ $(m = 1, 2)$ mass spectra that are produced in association with a single charged pion in $\Upsilon(5S)$ decays.

The measured masses of the two structures averaged over the five final states are $M_1 = 10608.4 \pm 2.0$ MeV, $M_2 = 10653.2 \pm 1.5$ MeV, both with a width of about 15 MeV.

Interestingly enough, the two masses M_1 and M_2 are about 3 MeV above the respective $B^*\overline{B}$ and $B^*\overline{B^*}$ thresholds. This strongly suggests a parallel with $X(3872)$, whose mass is almost exactly at the $D^*\overline{D}$ threshold. It also raises the possibility that such states might have a complementary description as deuteron-like "molecule" of two heavy mesons quasi-bound by pion exchange [20, 21].

The attraction due to π exchange is 3 times weaker in the I=1 channel than in the I=0 channel. This is because for I=1 only π^0 contributes, whereas for I=0 both π^0 and $\pi^\pm$ contribute. Consequently, in the charm system the I=1 state is far above the $D^*\overline{D}$ threshold and only the I=0 $X(3872)$ is bound 2 MeV below the average of the isospin-related D^+D^{*-} and $D^0\overline{D^0}$ thresholds. The situation is likely to be different in the bottom system. This is because the attraction due to π exchange is essentially the same, but the B mesons are much heavier than D mesons, so the kinetic energy is much smaller by a factor of $\sim m(B)/m(D) \approx 2.8$. Therefore the net binding is much stronger than in the charm system. This raises two very interesting possibilities:

(a) the Z_b states are almost bound (or quasi bound) $B^*\overline{B}$ and $B^*\overline{B^*}$ I=1 , $J^P = 1^+$ states near threshold; the neutral members of their isomultiplets have C=−1, G=+1 ;

(b) since the binding in the I=0 channel is much stronger than in the I=1 channel, if we neglect effects other than π exchange *we expect the corresponding* I^G=0^+ , $J^{PC} = 1^{++}$ *states to be up to 40-50 MeV below the thresholds* [22]. The I=0 states would then be expected close in mass to the $\Upsilon(4S)$. Their expected decay modes are

$$Z_b(I{=}0) \to \Upsilon(mS)\pi^+\pi^- \qquad \text{and} \qquad Z_b(I{=}0) \to \Upsilon(mS)\gamma\,,$$

as well as

$$Z_b(I{=}0) \to B\overline{B}\gamma \quad \text{via} \quad B^* \to B\gamma, \;\; E_\gamma = 46 \text{ MeV};$$

which might well be within the reach of LHCb.

A $(\Sigma_b^+\Sigma_b^-)$ *beauteron* dibaryon?

The discovery of the Z_b states and their probable interpretation as $B^*\overline{B}$ and $B^*\overline{B^*}$ bound by pion exchange raises an interesting possibility that a strongly bound $\Sigma_b^+\,\Sigma_b^-$ deuteron-like state might exist, a *beauteron*. This is because Σ_b is about 500 MeV heavier than B^* and having I=1, it couples more strongly to pions than B and B^* which have $I = \frac{1}{2}$. The opposite

electric charges of Σ_b^+ and Σ_b^- provide an additional attraction. A possible decay mode of the beauteron is

$$(\Sigma_b^+ \Sigma_b^-) \to \Lambda_b \, \Lambda_b \, \pi^+ \pi^-$$

which might be observable in LHCb. If the beauteron exists, it should also be seen in lattice QCD.

Acknowledgments

The work on heavy baryons described here was done in collaboration with B. Keren-Zur and J. Rosner. It was supported in part by a grant from the Israel Science Foundation. The research of H.J.L. was supported in part by the U.S. Department of Energy, Division of High Energy Physics, Contract DE-AC02-06CH11357.

Bibliography

[1] M. Karliner and H.J. Lipkin,hep-ph/0307243, Phys. Lett. **B575** (2003) 249.

[2] M. Karliner and H. J. Lipkin, Phys. Lett. B **660**, 539 (2008) [arXiv:hep-ph/0611306].

[3] T. Aaltonen *et al.* [CDF Collaboration], Phys. Rev. Lett. **99** (2007) 202001.

[4] M. Karliner and H. J. Lipkin, Phys. Lett. B **650**, 185 (2007) [arXiv:hep-ph/0608004].

[5] A. De Rujula, H. Georgi and S.L. Glashow, Phys. Rev. D12 (1975) 147

[6] B. Keren-Zur, Annals Phys. **323**, 631 (2008) [arXiv:hep-ph/0703011].

[7] M. Karliner, B. Keren-Zur, H. J. Lipkin and J. L. Rosner, arXiv:0706.2163v1 [hep-ph].

[8] V. M. Abazov *et al.* [D0 Collaboration], Phys. Rev. Lett. 99 (2007) 052001.

[9] T. Aaltonen *et al.* [CDF Collaboration], Phys. Rev. Lett. 99 (2007) 052002.

[10] M. Karliner, B. Keren-Zur, H. J. Lipkin and J. L. Rosner, arXiv:0708.4027 [hep-ph] (unpublished) and arXiv:0804.1575 [hep-ph], Annals Phys **324**,2 (2009).

[11] V. M. Abazov *et al.* [D0 Collaboration], Phys. Rev. Lett. **101**, 232002 (2008) [arXiv:0808.4142 [hep-ex]].

[12] T. Aaltonen *et al.* [CDF Collaboration], Phys. Rev. D **80**, 072003 (2009) [arXiv:0905.3123 [hep-ex]].

[13] D. Ebert *et al.*, Phys. Rev. D 72 (2005) 034026; Phys. Lett. B **659** (2008) 612.

[14] W. Roberts and M. Pervin, arXiv:0711.2492 [nucl-th].

[15] E. E. Jenkins, Phys. Rev. D 77 (2008) 034012.

[16] M. Karliner and H. J. Lipkin, Phys. Lett. B **638**, 221 (2006) [arXiv:hep-ph/0601193].

[17] K. F. Chen *et al.* [Belle Collaboration], Phys. Rev. Lett. **100**, 112001 (2008) [arXiv:0710.2577 [hep-ex]].

[18] M. Karliner and H. J. Lipkin, arXiv:0802.0649 [hep-ph].

[19] I. Adachi *et al.* [Belle Collaboration], arXiv:1105.4583 [hep-ex].

[20] N. A. Törnqvist, Z. Phys. C **61**, 525 (1994) [arXiv:hep-ph/9310247]; Phys. Lett. B **590**, 209 (2004) [arXiv:hep-ph/0402237].

[21] C. E. Thomas, F. E. Close, Phys. Rev. **D78**, 034007 (2008). [arXiv:0805.3653 [hep-ph]].

[22] M. Karliner, H.J. Lipkin and N. A. Törnqvist, unpublished.

Baryon bound states of three hadrons with charm and hidden charm

Chu-Wen Xiao[1,a], Melahat Bayar[a,b], and Eulogio Oset[a]
[a]*Departamento de Física Teórica and IFIC, Centro Mixto Universidad de Valencia-CSIC, Institutos de Investigación de Paterna, Aptdo. 22085, 46071 Valencia, Spain*
[b]*Department of Physics, Kocaeli University, 41380 Izmit, Turkey*

In this talk, we show our recent theoretical results for three-body systems in the charm sector which are made of three hadrons and contain one nucleon, one D meson and in addition another meson, $\overline{D}$, K or $\overline{K}$.

1 Introduction

While the three baryon system has been a subject of intense theoretical study, it has only been recently that attention was brought to systems with two mesons and one baryon. The low lying excited $J^P = 1/2^+$ Λ and Σ states were described in [1], and N^* states in [2], combining Faddeev equations and chiral dynamics. A N^* state around 1920 MeV was predicted in [3] as a molecule of $NK\overline{K}$, corroborated in [4] and [5] by Faddeev equations. For three mesons systems, the X(2175) (now $\phi(2170)$) was explained as a resonant $K\overline{K}\phi$ system in [6]. Similarly the $K(1460)$ is explained as a $KK\overline{K}$ state in [7].

In a recent work we study the three body systems in the charm sector, and use the Fixed Center Approximation to the Faddeev equations (FCA), which has been proved to be reliable in [8,9] and has been applied to the study of the $NK\overline{K}$ system [10] and the results compare favorably with those of the Faddeev approach in [4] and those of the variational approach in [3]. There are some well known two body states in this sector, such as $\Lambda_c(2595)$ in DN with its coupled channels interaction [11,12], $D_{s0}^*(2317)$ in KD interaction [13–15], and the hypothetical $X(3700)$ generated in isospin I=0 $D\overline{D}$ interaction [13]. These states are the clusters in the FCA in our study.

2 Formalism

Following [9,10,16], we will apply the FCA to study the charm sector. The FCA approximation to Faddeev equations is depicted in Figure 1.

[1]chuwen.xiao@ific.uv.es

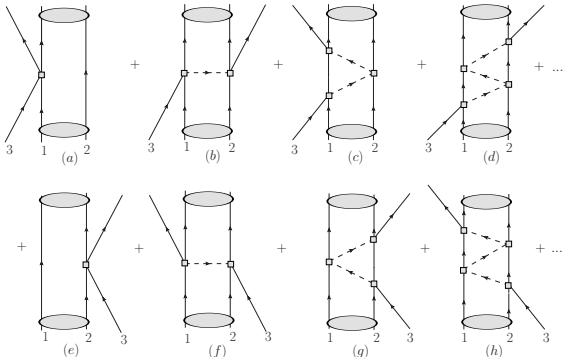

Figure 1: Diagrammatic representation of the FCA to Faddeev equations.

With this meaning of the FCA, the equations can be written by two partition functions T_1, T_2 which sum all diagrams of the series of Fig. 1,

$$T_1 = t_1 + t_1 G_0 T_2, \tag{1}$$

$$T_2 = t_2 + t_2 G_0 T_1, \tag{2}$$

$$T = T_1 + T_2, \tag{3}$$

where T is the total three-body scattering amplitude. The amplitudes t_1 and t_2 represent the unitary scattering amplitudes respectively. And G_0 is the propagator of particle 3.

3 Results

In this part we show the results of our investigation in that systems $\overline{K}DN$, NDK and $ND\overline{D}$. In Figure 2 (left) we show the results of $|T|^2$ for the $\overline{K}\Lambda_c(2595)$ scattering in the $\overline{K}DN$ system. We find a peak around 3150 MeV, slightly above the threshold of the $\Lambda_c(2595) + \overline{K}$ mass (3088 MeV) and below the threshold of the $\overline{K}DN$ system (3298 MeV), of which the width is about 50 MeV. For the system $\overline{K}DN$, its quantum numbers are $C = +1, S = -1$ and $J^P = \frac{1}{2}^+$ since we only consider the interaction among the components in $L = 0$.

In the NDK system, we obtain $|T|^2$ for the $ND^*_{s0}(2317)$ scattering shown in Fig. 2 (right). We found a peak around 3050 MeV which is about 200 MeV below the $N + D^*_{s0}(2317)$ threshold and the width less than 10 MeV. We also do not find a counterpart in the PDG and the quantum numbers, with positive strangeness, correspond to an exotic state.

Finally we obtain the T matrix, for the $ND\overline{D}$ interaction by means Eq. (3), and show the results of $|T|^2$ in Figure 3. From this figure we can see that there is a clear peak of $|T|^2$ around 4400 MeV and the width is very small, less than 10 MeV. The peak appears below the $ND\overline{D}$ and $NX(3700)$ thresholds and corresponds to a bound state of $NX(3700)$. This

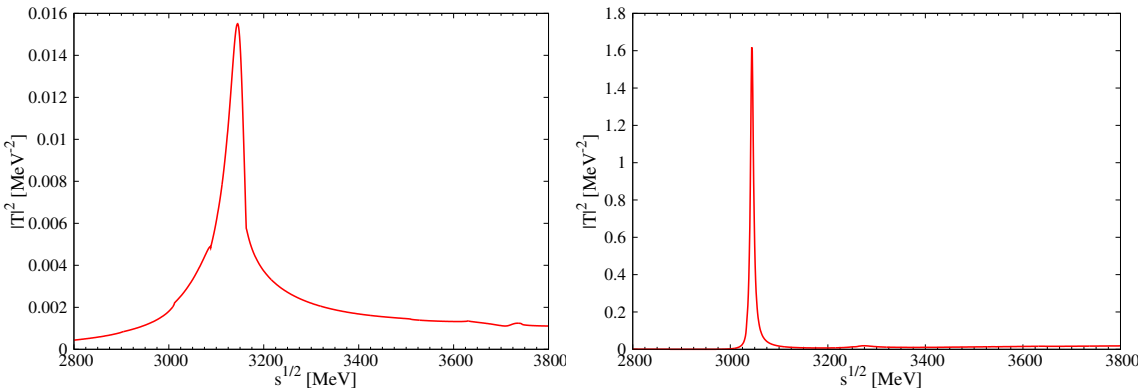

Figure 2: Modulus squared of the scattering amplitude for $\overline{K}\Lambda_c(2595)$ (left) and $ND^*_{s0}(2317)$ (right).

would be a hidden charm baryon state of $J^P = \frac{1}{2}^+$ which appears in the same region of energies as other hidden charm states of $J^P = \frac{1}{2}^-$ obtained in [17,18].

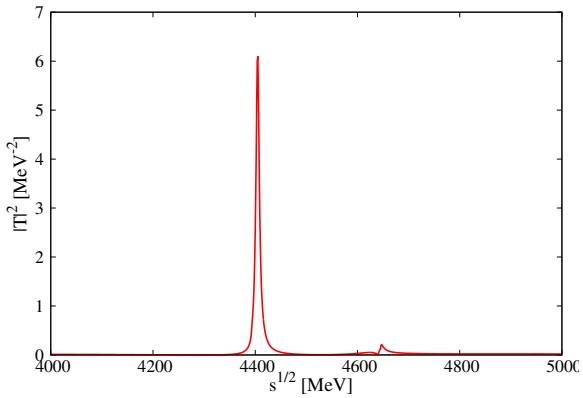

Figure 3: Modulus squared of the the $NX(3700)$ scattering amplitude.

4 Conclusion

In all cases we find bound or quasibound states, relatively narrow, with energies 3150 MeV, 3050 MeV and 4400 MeV, respectively. All these states have $J^P = 1/2^+$ and isospin $I = 1/2$ and differ by their charm or strangeness content, $S = -1, C = 1$, $S = 1, C = 1$, $S = 0, C = 0$, respectively. We hope that the work stimulates other theory calculations and future experiments in Facilities of FAIR or BELLE upgrade to prove our findings.

Acknowledgments

This work is partly supported by DGICYT contract FIS2006-03438, the Generalitat Valenciana in the program Prometeo and the EU Integrated Infrastructure Initiative Hadron Physics Project under Grant Agreement n.227431. M. Bayar acknowledges support of the Scientific and Technical Research Council (TUBITAK) BIDEP-2219 grant.

Bibliography

[1] A. Martinez Torres, K. P. Khemchandani, E. Oset, Phys. Rev. **C77**, 042203 (2008).

[2] K. P. Khemchandani, A. Martinez Torres, E. Oset, Eur. Phys. J. **A37**, 233-243 (2008).

[3] D. Jido, Y. Kanada-En'yo, Phys. Rev. **C78**, 035203 (2008).

[4] A. Martinez Torres, K. P. Khemchandani, E. Oset, Phys. Rev. **C79**, 065207 (2009).

[5] A. Martinez Torres, D. Jido, Phys. Rev. **C82**, 038202 (2010).

[6] A. Martinez Torres, K. P. Khemchandani, L. S. Geng, M. Napsuciale, E. Oset, Phys. Rev. **D78**, 074031 (2008).

[7] A. M. Torres, D. Jido, Y. Kanada-En'yo, [arXiv:1102.1505 [nucl-th]].

[8] A. Gal, Int. J. Mod. Phys. **A22**, 226-233 (2007).

[9] M. Bayar, J. Yamagata-Sekihara, E. Oset, Phys. Rev. C **84**, 015209 (2011).

[10] J. J. Xie, A. Martinez Torres and E. Oset, Phys. Rev. C **83**, 065207 (2011).

[11] J. Hofmann, M. F. M. Lutz, Nucl. Phys. **A763**, 90-139 (2005).

[12] T. Mizutani, A. Ramos, Phys. Rev. **C74**, 065201 (2006).

[13] D. Gamermann, E. Oset, D. Strottman, M. J. Vicente Vacas, Phys. Rev. **D76**, 074016 (2007).

[14] J. Hofmann, M. F. M. Lutz, Nucl. Phys. **A733**, 142-152 (2004).

[15] F. -K. Guo, P. -N. Shen, H. -C. Chiang, R. -G. Ping, Phys. Lett. **B641**, 278-285 (2006).

[16] L. Roca and E. Oset, Phys. Rev. D **82**, 054013 (2010).

[17] J. -J. Wu, R. Molina, E. Oset, B. S. Zou, Phys. Rev. Lett. **105**, 232001 (2010).

[18] J. -J. Wu, R. Molina, E. Oset, B. S. Zou, [arXiv:1011.2399 [nucl-th]].

Heavy Hadron Production and Spectroscopy at ATLAS

Carlo Schiavi[1] on behalf of the ATLAS Collaboration
INFN Sezione di Genova

ATLAS has studied heavy flavor production and measured the production cross sections of heavy quarkonium, open bottom and charm in $\sqrt{s}$=7 TeV proton-proton collisions at the Large Hadron Collider. Differential cross sections as a function of transverse momentum and pseudo-rapidity are hereby discussed. ATLAS capabilities to reconstruct heavy quarkonium states, D-mesons and B-hadrons in exclusive decay modes are demonstrated.

1 Introduction

ATLAS (A Toroidal LHC ApparatuS) is a general purpose experiment operating at the Large Hadron Collider at CERN. Its research program is mainly focused on the investigation of processes beyond the Standard Model, but includes also a wide set of flavor physics studies with early data. Heavy flavor processes provide valuable samples to measure detector performance, based on the reconstruction of known particles with c and b quark content. Once this is established, measurements of production cross sections for open beauty and charm and heavy quarkonium states allow to test QCD predictions for proton-proton collisions at $\sqrt{s}$ = 7 TeV.
After a brief description of the relevant ATLAS detector and reconstruction components, results on inclusive $J/\psi \to \mu^+\mu^-$ production and on the study of exclusive B and D hadron decays are reported.

2 ATLAS tracking and trigger systems

The main ingredients for flavor physics studies are the reconstruction of charged particles and the identification of muons produced in the pp collisions. For this purpose, the ATLAS detector [1] is equipped with two main tracking systems.
The Inner Detector (ID), placed in the immediate proximity of the beam line and surrounded by a solenoidal magnet providing a 2 T field, measures charged particle tracks in a pseudo-rapidity range of $|\eta| < 2.5$. Adopting three different detector technologies (pixel sensors, silicon strips and straw tubes) it reaches an overall design momentum precision of $\sigma_{p_T}/p_T =$

[1]Carlo.Schiavi@cern.ch

$3.4\times10^{-4}\cdot p_T/\text{GeV}\oplus 0.015$.
The Muon Spectrometer (MS), the outermost ATLAS detector, covers a range of $|\eta|<2.7$, adopting four detector technologies suitable for both triggering and tracking purposes (monitored drift tubes, cathode strip chambers, thin-gap chambers and resistive plate chambers). Exploiting the field generated by an air-core toroidal magnet, it is designed to measure transverse momenta with ∼3% precision over most of the p_T range and below 10% up to 1 TeV.
The muon reconstruction is performed matching tracks or track segments in the MS and ID, combining them to form a full muon track and refitting its track parameters.
Another crucial ingredient for any physics study is the trigger system, selecting a few relevant events out of a vast majority of uninteresting pp collisions. The ATLAS trigger consists of a first hardware level, mainly based on MS and calorimeters, and two subsequent software levels, accessing data from the entire detector to refine the first level selection.
The results presented in the following use two different trigger selections. Studies based on the reconstruction of $J/\psi\to\mu^+\mu^-$ decays rely on single muon triggers, with different p_T thresholds for different luminosities. The D meson studies are instead performed on events selected by minimum bias triggers, based on scintillators mounted at each end of the ID or on the measurement of tracking activity in randomly triggered events.

3 Inclusive J/ψ cross section measurement

Charmonium states decaying into muon pairs have been studied both to evaluate the ATLAS detector performance and to measure their production properties.
The analysis of $J/\psi\to\mu^+\mu^-$ decays [2], based on an integrated luminosity of 2.3 pb^{-1}, measures the inclusive J/ψ production cross section and the fractions of prompt and non-prompt components. Pairs of reconstructed muons passing standard quality and kinematical cuts are used to identify J/ψ candidates with p_T between 1 and 70 GeV. These are grouped in four rapidity bins, covering $|y|<2.4$, and their number is extracted fitting the $\mu^+\mu^-$ invariant mass spectrum. In order to estimate the true number of J/ψ decays in each bin, corrections for detector and reconstruction efficiency, bin migration and acceptance are applied with the corresponding uncertainties. For the kinematic acceptance, which strongly depends on the J/ψ polarization, not yet measured at LHC, different spin alignment scenarios are studied. Five extreme cases, including isotropic, fully longitudinal and transverse polarization, are identified; acceptance factors are evaluated for each case and the envelope of the resulting values is taken as an additional uncertainty. Figure 1 shows the resulting inclusive J/ψ production cross section, as a function of J/ψ transverse momentum, in the four rapidity bins analyzed. A comparison with CMS results [3] is performed for those rapidity bins close enough to permit it, showing good agreement within experimental uncertainties.

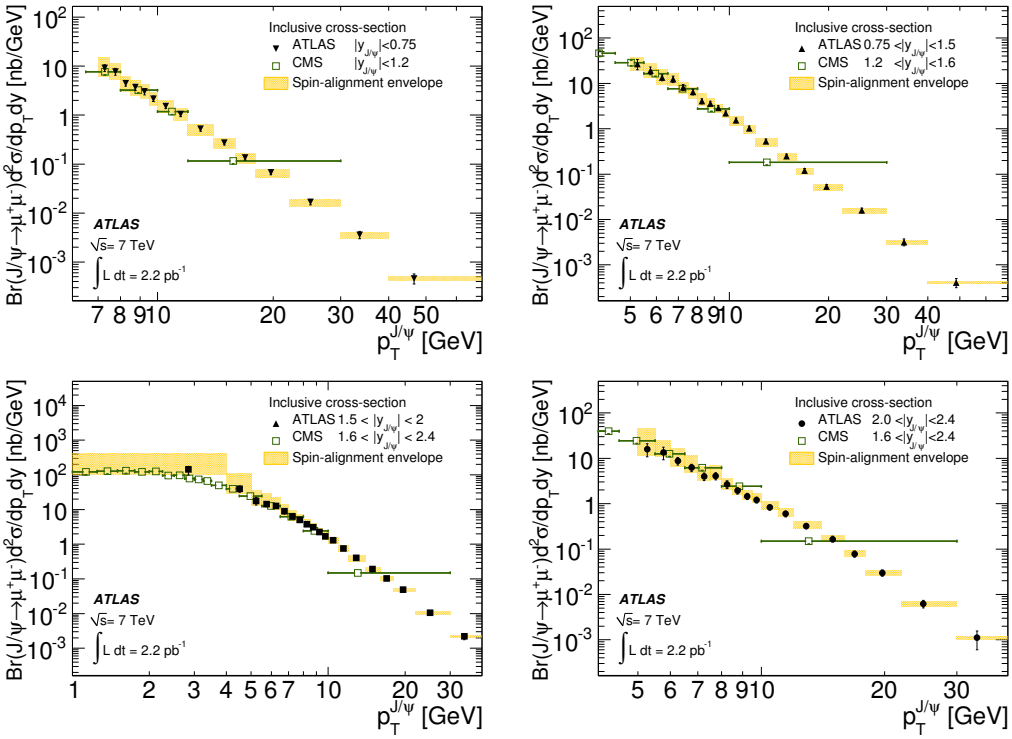

Figure 1: Inclusive J/ψ production cross section as a function of J/ψ transverse momentum in the four rapidity bins studied. Overlaid are a band representing the variation of the result under various spin-alignment scenarios and the equivalent results from CMS. The luminosity uncertainty (3.4%) is not shown.

4 Exclusive B and D hadron reconstruction

The reconstruction and identification of open beauty is a necessary prerequisite for the investigation of CP violation processes and rare decays. As a first step, the reconstruction of various exclusive B hadron decay modes, in which a J/ψ is produced and decays to opposite sign muons, is studied. Event selection and reconstruction proceed very similarly to what described for the inclusive J/ψ case, with additional constraints specific to each exclusive decay chain. In particular, the capability to identify $B^{\pm} \to J/\psi\, K^{\pm}$, $B_d^0 \to J/\psi\, K^0$ and $B_s^0 \to J/\psi\, \phi$ decays [4] [5] is demonstrated. Figure 2 shows the invariant mass distributions of B_d^0 and B_s^0 candidates reconstructed in an integrated luminosity of 40 pb^{-1}.

In the open charm sector, several exclusive D meson decay modes are observed and the corresponding production cross sections are measured [6], with an integrated luminosity of 1.1 nb^{-1}. The limitation on the data sample size comes from the use of minimum bias triggers, which were active only in the earliest data-taking phase, due to their high rate, incompatible with running at higher luminosities. The D meson candidates are

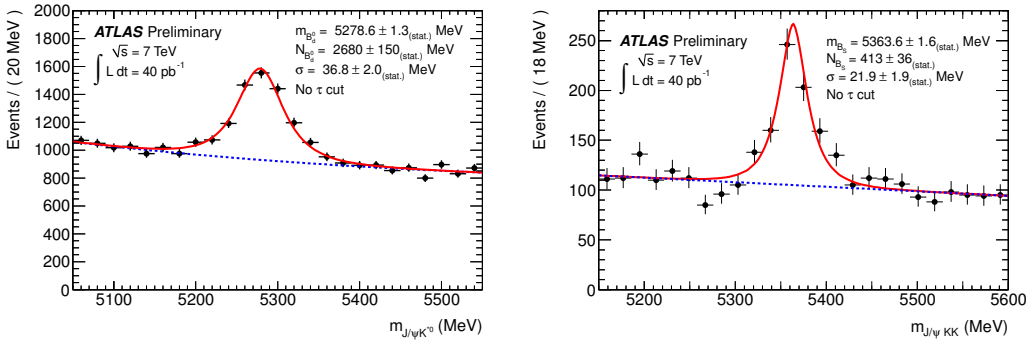

Figure 2: Invariant mass distributions of reconstructed candidates of $B_d^0 \to J/\psi\, K^0$ (left) and $B_s^0 \to J/\psi\, \phi$ (right). The points with error bars are data. The solid line is the projection of the result of the unbinned maximum likelihood fit. The dashed line is the projection for the background component of the same fit.

identified starting from charged tracks reconstructed in the ID and applying different tracking, vertexing, lifetime and invariant mass cuts, depending on the exclusive decay chain under study. Similarly to what done for the $J/\psi \to \mu^+\mu^-$ case, the true number of D mesons is estimated applying efficiency, bin migration and acceptance corrections. For $D^{\star\pm}$ studies, the decay chain $D^{\star+} \to D^0\pi^+$ with $D^0 \to K^-\pi^+$ is analyzed; the resulting $D^{\star\pm}$ production cross section, as a function of $D^{\star\pm}$ transverse momentum and absolute pseudo-rapidity, are shown in Figure 3, where a comparison with different theoretical predictions is overlaid, showing good agreement within experimental and theoretical uncertainties.

5 Conclusions

During its first year of data taking, the ATLAS experiment produced many heavy flavor measurements at an unprecedented proton-proton collision energy. As part of the rich ATLAS physics programme, the inclusive J/ψ and exclusive D meson production cross sections were measured. In the open bottom sector, the capability of reconstructing and identifying exclusive decay modes was demonstrated, paving the way for precise measurements of B meson properties and searches for the new physics phenomena in rare decays.

Bibliography

[1] ATLAS Collaboration, The ATLAS Experiment at the CERN Large Hadron Collider, JINST **3** (2008) S08003

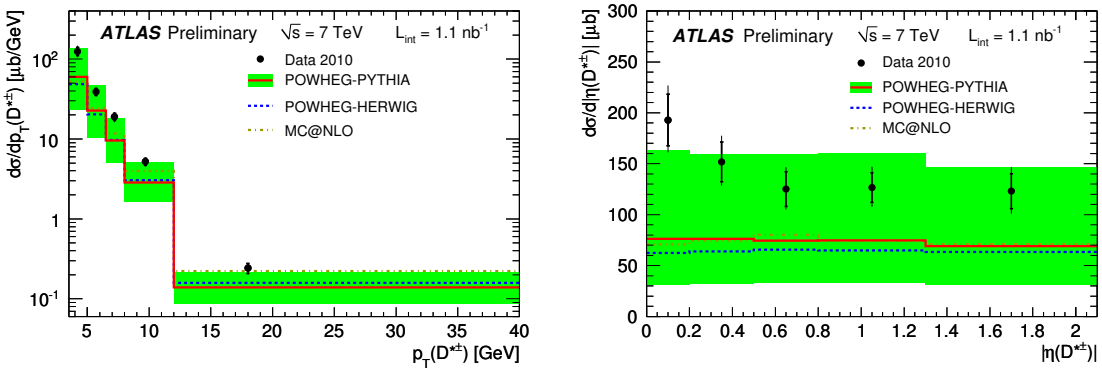

Figure 3: Differential cross section for $D^{\star\pm}$ mesons as a function of p_T (left) and $|\eta|$ (right) for data (points) compared to the NLO QCD calculations of POWHEG-PYTHIA, POWHEG-HERWIG and MC@NLO (histograms). The inner error bars show the statistical uncertainties and the outer error bars show the statistical and systematic uncertainties added in quadrature. The band shows the estimated theoretical uncertainty of the POWHEG-PYTHIA calculation.

[2] ATLAS Collaboration, Measurement of the differential cross-sections of inclusive, prompt and non-prompt J/ψ production in proton-proton collisions at $\sqrt{s}$=7 TeV, Nucl. Phys. B **850** (2011) 387-444

[3] CMS Collaboration, Prompt and non-prompt J/ψ production in pp collisions at $\sqrt{s}$=7 TeV, Eur.Phys.J. **C71** (2011) 1575

[4] ATLAS Collaboration, Observation of the $B^{\pm}$ meson in the decay $B^{\pm} \to J/\psi(\mu^+\mu^-)\, K^{\pm}$, ATLAS-CONF-2010-098 (2010)

[5] ATLAS Collaboration, Observation of the B_d^0 and B_s^0 mesons in the decays $B_d^0 \to J/\psi K^0$ and $B_s^0 \to J/\psi\phi$ in ATLAS, ATLAS-CONF-2011-050 (2011)

[6] ATLAS Collaboration, Measurement of $D^{(\star)}$ meson production cross-sections in pp collisions at $\sqrt{s}$=7 TeV with the ATLAS detector, ATLAS-CONF-2011-017 (2011)

Effective Quark-Quark Interaction in Heavy Baryons

Joseph P. Day[1], Ki-Seok Choi, and Willibald Plessas
Theoretical Physics, Institute of Physics, University of Graz, A–8010 Graz, Austria

We report results from a study of heavy-baryon spectroscopy within a relativistic constituent-quark model, whose hyperfine interaction is based on Goldstone-boson-exchange dynamics. While for light-flavor constituent quarks it is now commonly accepted that the effective quark-quark interaction is (predominantly) furnished by Goldstone-boson exchange – due to spontaneous chiral-symmetry breaking of quantum chromodynamics at low energies – there is currently still much speculation about the light-heavy and heavy-heavy quark-quark interactions. With the increasing amount of experimental data on heavy-baryon spectroscopy these issues might soon be settled. Here, we show, how the relativistic constituent-quark model with Goldstone-boson-exchange hyperfine interactions can be extended to charm and bottom baryons. It is found that the same model that has previously been successful in reproducing the light and strange baryon spectra is also in line with the existing phenomenological data on heavy-baryon spectroscopy. An analogous model with one-gluon-exchange hyperfine interactions for light-heavy flavors does not achieve a similarly good performance.

1 Framework

We view hadrons as relativistic bound states of constituent quarks Q. Baryons are are thus considered as $\{QQQ\}$ systems. Even if heavy-flavor quarks are involved, it is mandatory to work in a relativistic framework in order to prevent pathologies and/or severe shortcomings. Our relativistic constituent-quark model (RCQM) is based on a relativistically invariant mass operator $\hat{M} = \hat{M}_{\text{free}} + \hat{M}_{\text{int}}$ that includes the Q-Q interaction according to the Bakamijian-Thomas construction [1]. In the rest frame of the baryon, $\vec{P} = \sum_i^3 \vec{k}_i^2 = 0$, the free and interacting parts of the mass operator thus read

$$\hat{M}_{\text{free}} = \sum_{i=1}^{3} \sqrt{\hat{m}_i^2 + \hat{\vec{k}}_i^2}\,, \qquad \hat{M}_{\text{int}} = \sum_{i<j}^{3} \hat{V}_{ij} = \sum_{i<j}^{3} (\hat{V}_{ij}^{\text{conf}} + \hat{V}_{ij}^{\text{hf}})\,, \tag{1}$$

where the $\vec{k}_i$ correspond to the three-momenta of the individual quarks with rest masses m_i and the mutual Q-Q potentials $\hat{V}_{ij}$ are composed of confinement and hyperfine interactions.

[1]joseph.day@uni-graz.at

By employing such a mass operator $\hat{M}^2 = \hat{P}^\mu \hat{P}_\mu$, with baryon four-momentum $\hat{P}_\mu = (\hat{H}, \hat{P}_1, \hat{P}_2, \hat{P}_3)$, one satisfies the Poincaré algebra involving all ten generators $\{\hat{H}, \hat{P}_i, \hat{J}_i, \hat{K}_i\}$ of time and space translations, spatial rotations as well as Lorentz boosts, respectively:

$$\begin{array}{lll} [\hat{P}_i, \hat{P}_j] = 0\,, & [\hat{J}_i\,, \hat{H}] = 0\,, & [\hat{P}_i, \hat{H}] = 0\,, \\ [\hat{K}_i, \hat{H}] = i\hat{P}_i\,, & [\hat{J}_i, \hat{J}_j] = i\epsilon_{ijk}\hat{J}_k\,, & [\hat{J}_i, \hat{K}_j] = i\epsilon_{ijk}\hat{K}_k\,, \\ [\hat{J}_i, \hat{P}_j] = i\epsilon_{ijk}\hat{P}_k\,, & [\hat{K}_i, \hat{K}_j] = -i\epsilon_{ijk}\hat{J}_k\,, & [\hat{K}_i, \hat{P}_j] = i\delta_{ij}\hat{H}\,. \end{array}$$

The solution of the eigenvalue equation of the mass operator $\hat{M}$ yields the relativistically invariant mass spectra as well as the baryon eigenstates (in the standard rest frame) [2].

2 Goldstone-Boson Exchange in the $SU(3)_F$ Sector

In order to incorporate the property of spontaneous breaking of chiral symmetry of low-energy QCD, the Graz group has proposed a RCQM with Goldstone-boson-exchange (GBE) hyperfine interactions between constituent quarks [3]. In addition to a linearly rising confinement potential, as following from lattice QCD, the model comes with a spin-spin hyperfine interaction of the form

$$V_{ij}^{\mathrm{hf}} = \left[V_\pi \sum_{a=1}^{3} \lambda_i^a \lambda_j^a + V_K \sum_{a=4}^{7} \lambda_i^a \lambda_j^a + V_\eta \lambda_i^8 \lambda_j^8 + V_{\eta'} \lambda_i^0 \lambda_j^0 \right] \vec{\sigma}_i \cdot \vec{\sigma}_j\,, \tag{2}$$

where the λ_i^a are the $SU(3)_F$ Gell-Mann matrices and $\vec{\sigma}_i$ the $SU(2)_S$ Pauli matrices of quark i. The GBE is cast into the exchange of pseudoscalar mesons π, K, and η, including the singlet η' due to the $U(1)_A$ anomaly. The corresponding meson-exchange potentials as a function of the relative Q-Q distance $\vec{r}_{ij}$ read

$$V_\gamma(\vec{r}_{ij}) = \frac{g_\gamma^2}{2\pi} \frac{1}{12 m_i m_j} \left[\mu_\gamma^2 \frac{e^{-\mu_\gamma r_{ij}}}{r_{ij}} - \Lambda_\gamma^2 \frac{e^{-\Lambda_\gamma r_{ij}}}{r_{ij}} \right], \quad \gamma = \pi, K, \eta, \eta'\,, \tag{3}$$

where g_γ is the meson-quark coupling constant, μ_γ the mass of the exchanged meson, and Λ_γ an adjusted cut-off parameter. As immediately evident, the GBE RCQM produces a spin- and flavor-dependent hyperfine interaction. It has hitherto been quite successful not only in describing the spectroscopy of all baryons with flavors u, d, and s in a unified framework but also in a number of baryon reactions [4].

3 Extension of the GBE RCQM to Heavy Baryons

We have investigated, if the same model can be extended to include also baryons with flavors c and b in a consistent manner. Thus we have generalized the hyperfine interaction

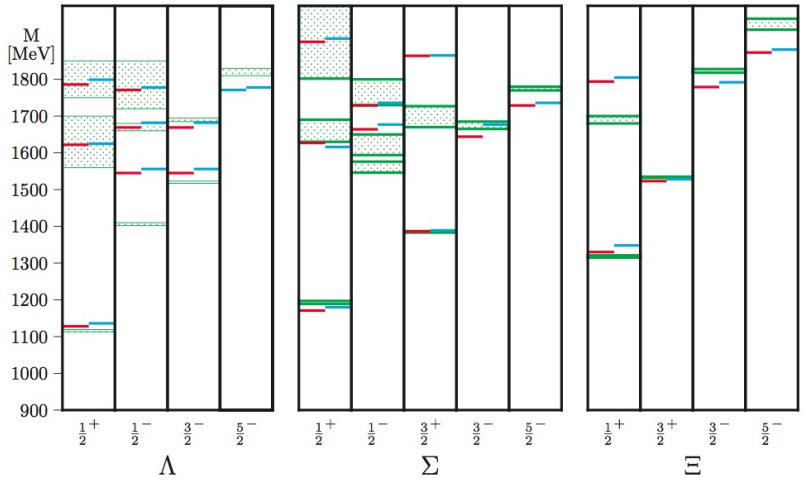

Figure 1: Comparison of $SU(5)_F$ (left/red levels) and $SU(3)_F$ (right/blue levels) hyperfine interactions in the GBE RCQM for the examples of the Λ, Σ, and Ξ baryons with definite spin and parity J^P in each column. The green boxes represent the experimental data with their uncertainties as given by the PDG [6].

of eq. (2) to $SU(5)_F$ in the following manner

$$
\begin{aligned}
(4) \qquad V_{ij}^{\mathrm{hf}} \;=\; & \Bigg[V_\pi \sum_{a=1}^{3} \lambda_i^a \lambda_j^a + V_K \sum_{a=4}^{7} \lambda_i^a \lambda_j^a + V_{\eta_8} \lambda_i^8 \lambda_j^8 + V_{\eta_0} \lambda_i^0 \lambda_j^0 \\
& + V_D \sum_{a=9}^{12} \lambda_i^a \lambda_j^a + V_{D_s} \sum_{a=13}^{14} \lambda_i^a \lambda_j^a + V_{\eta_{15}} \lambda_i^{15} \lambda_j^{15} \\
& + V_B \sum_{a=16}^{19} \lambda_i^a \lambda_j^a + V_{B_s} \sum_{a=20}^{21} \lambda_i^a \lambda_j^a + V_{B_c} \sum_{a=22}^{23} \lambda_i^a \lambda_j^a + V_{\eta_{24}} \lambda_i^{24} \lambda_j^{24} \Bigg] \vec{\sigma}_i \cdot \vec{\sigma}_j \,,
\end{aligned}
$$

where the various meson-exchange potentials are assumed in the same form as in eq. (3). The complete parametrization of the $SU(5)_F$ GBE RCQM can be found in ref. [5].

Obviously, this new construction also influences the Q-Q interaction in the $SU(3)_F$ sector (specifically through the diagonal elements in the flavor matrices λ_{15} as well as λ_{24}). Therefore our first concern is to maintain the good performance regarding the baryon spectroscopy with u, d, and s flavors. In Fig. 1 we give a selective comparison of the $SU(3)_F$ and $SU(5)_F$ models vis-à-vis the experimental data.

It is found that the quality of light and strange baryon spectroscopy is comparable for both the $SU(3)_F$ and $SU(5)_F$ models. In the latter, some of the levels, such as the $J^P = \frac{1}{2}^+$ Λ ground state, are even closer to experiment. A similar agreement occurs for the N, Δ, and Ω states. In particular, due to its specific flavor dependence, also the $SU(5)_F$ model produces

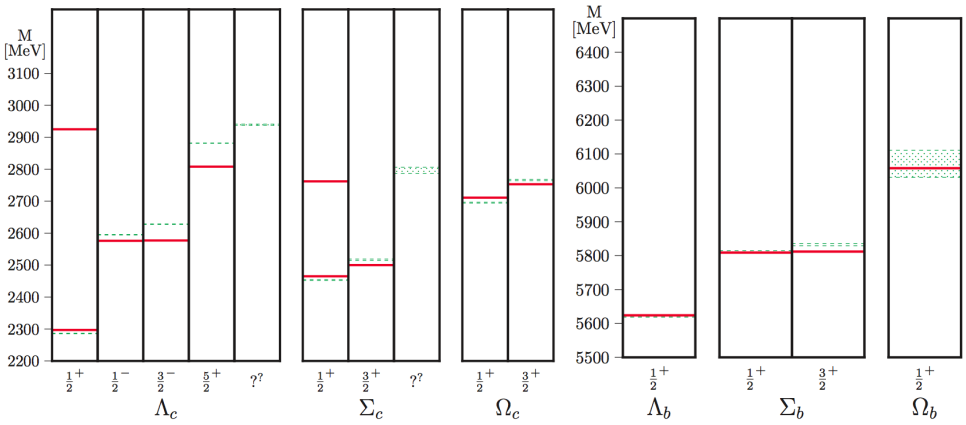

Figure 2: Heavy-baryon spectra as produced by the $SU(5)_F$ GBE RCQM (solid/red levels) in comparison to experimental data with their uncertainties, as quoted by the PDG [6] (dotted/green levels resp. boxes).

the correct orderings of positive- and negative-parity excitations simultaneously in the N and Λ spectra.

In Fig. 2 we show the results of the extended $SU(5)_F$ GBE RCQM for some heavy-baryon spectra. It appears that all levels can be reproduced satisfactorily. The same is true for the other cases not shown here because of space limitations.

At this stage we have succeeded in constructing a universal RCQM based on GBE dynamics that works in the whole baryon spectroscopy within $SU(5)_F$. For heavy baryons, additional experimental data are highly desirable in order to better determine the model parameters and put the theory to more stringent tests. Similarly, applications to describing reactions with heavy baryons (e.g., form factors and decays) will be most interesting to study.

Acknowledgments

This work was supported by the Austrian Science Fund, FWF, through the Doctoral Program on *Hadrons in Vacuum, Nuclei, and Stars* (FWF DK W1203-N08).

Bibliography

[1] B. Bakamijian and L.H. Thomas, Phys. Rev. **92**, 1300 (1953).

[2] T. Melde, W. Plessas, and B. Sengl, Phys. Rev. D **77**, 114002 (2008).

[3] L.Y. Glozman *et al.*, Phys. Rev. D **58**, 094030 (1998).

[4] W. Plessas, PoS(LC2010)017; arXiv:1011.0156.

[5] J.P. Day, Ki-Seok Choi, and W. Plessas, in preparation.

[6] K. Nakamura *et al.*(Particle Data Group), J. Phys. G **37**, 075021 (2010).

Heavy Hadron Spectroscopy and Production at the Tevatron

Igor V. Gorelov[1] on behalf of the CDF and DØ Collaborations
Department of Physics and Astronomy,
University of New Mexico, MSC07 4220,
1919 Lomas Blvd. NE,
Albuquerque, NM 87131-0001, USA

Using data from $p\bar{p}$ collisions at $\sqrt{s} = 1.96\,\text{TeV}$ recorded by the CDF II and DØ detectors at the Fermilab Tevatron, we present recent results on charm and bottom hadrons. We the most recent CDF results on properties of the four bottom baryon resonant states $\Sigma_b^{(*)-}$, $\Sigma_b^{(*)+}$. New results on exotic $Y(4140)$ state observed by CDF are also reported. A precise measurement of production rates of the lowest lying bottom baryon, Λ_b^0, produced in the DØ detector is presented.

1 Measurement of the Masses and Widths of the Bottom Baryons $\Sigma_b^{(*)-}$ and $\Sigma_b^{(*)+}$ with the CDF II Detector

Baryons with a heavy quark Q as the "nucleus" and a light diquark q_1q_2 as the two orbiting "electrons" are the helium atoms of QCD. The heavy quark in the baryon may be used as a probe of confinement which allows the study of non-perturbative QCD in a different regime from that of the light baryons.

A recent comprehensive review of the experimental and theoretical status of baryon spectroscopy with many useful references can be found in Ref. [1]. The resonant $\Sigma_b^{(*)}$ states have been discovered by CDF [2], and this study follows that first observation.

The $\Sigma_b^{(*)\pm}$ candidates are reconstructed in their exclusive decay modes to $\Lambda_b^0\pi_{soft}^{\pm}$. The base state Λ_b^0 is reconstructed in its weak decay $\Lambda_b^0 \to \Lambda_c^+\pi_b^-$ with the Λ_c^+ candidates found in the $\Lambda_c^+ \to pK^-\pi^+$ decay by fitting three tracks to a common vertex. The Λ_b^0 vertex is formed by a Λ_c^+ candidate combined with a fourth pion track, the π_b^-, having a transverse momentum above $1.5\,\text{GeV}/c$. Then the vertex is subjected to a three-dimensional kinematic fit. The Λ_b^0 signal in the invariant mass distribution $M(\Lambda_c^+\pi_b^-)$ amounts to approximately 16 300 candidates at the expected Λ_b^0 mass, with a signal to background ratio

[1] gorelov@fnal.gov

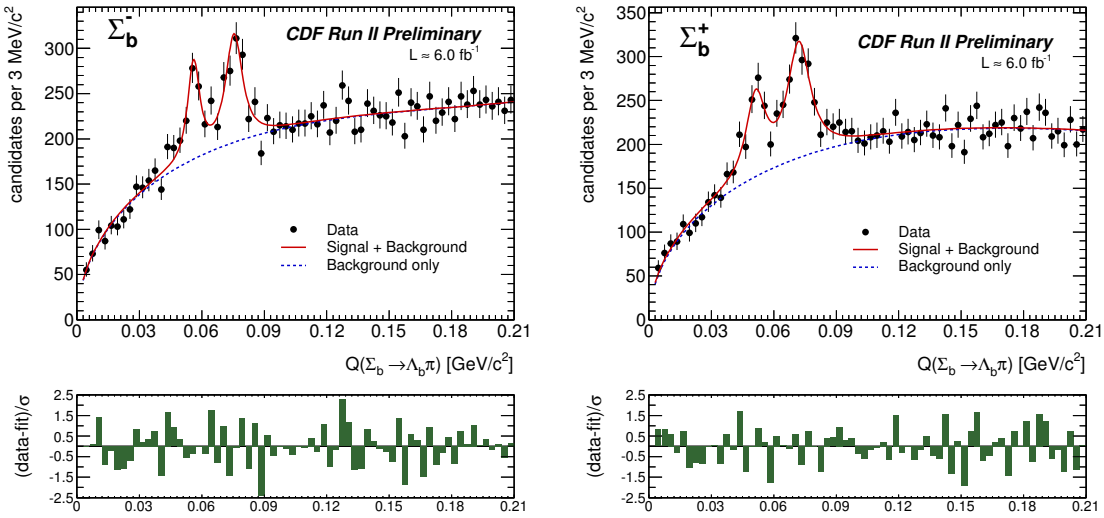

Figure 1: The Q-value spectra for $\Sigma_b^{(*)-}$ (left plot) and $\Sigma_b^{(*)+}$ (right plot) candidates, where $Q = M(\Lambda_b^0\pi^\pm) - M(\Lambda_b^0) - m_{\pi^\pm}$, are shown with the projection of the corresponding unbinned ML fit superimposed on the binned distribution. The pull distributions of the fit (bottom plots) are evenly distributed around zero with fluctuations of about a $\pm 2\sigma$ range.

around 1.8. To produce the spectra of $\Sigma_b^{(*)\pm} \to \Lambda_b^0\pi^\pm_{soft}$ candidates, each $\Lambda_c^+\pi_b^-$ candidate from the Λ_b^0 signal region of $m(\Lambda_b^0) \in (5.561, 5.677)\,\mathrm{GeV}/c^2$ is combined with one of the tracks remaining in the event with transverse momentum above $200\,\mathrm{MeV}/c^2$ and with a pion mass hypothesis assigned. The analysis of the $\Sigma_b^{(*)\pm}$ signals is performed using the mass difference distributions $Q = m(\Lambda_b^0\pi^\pm_{soft}) - m(\Lambda_b^0) - m(\pi^\pm)$, where $m(\pi^\pm)$ is set to its world-average value [3]. The mass resolution of the $m(\Lambda_b^0 \to \Lambda_c^+\pi_b^-)$ signal and most of the systematic uncertainties cancel in the mass difference spectrum, yielding fine detector resolution in the Q-value scale. The experimental $\Sigma_b^{(*)-}$ and $\Sigma_b^{(*)+}$ Q-value distributions, each fitted with an individual unbinned maximum likelihood (ML) functions, are shown in Fig. 1. The projection of the corresponding unbinned ML fit is superimposed on each graph. The shape of the signal is modeled with a non-relativistic Breit-Wigner function convoluted with a Gaussian detector resolution. As the soft pion $\pi^\pm_{soft}$ is emitted in a P-wave, the Breit-Wigner width parameter is modified by the P-wave factor [4] $\Gamma = \Gamma_0 \cdot \left(p^*_{\pi_{soft}}/p^{*0}_{\pi_{soft}}\right)^3$. The background is described by an ordinary second order polynomial modulated by a kinematically motivated threshold factor, specifically $\sqrt{(Q+m_\pi)^2 - m_T{}^2} \cdot \mathcal{P}^2(Q; C, b_1, b_2)$. The left and right plots in Fig. 1 show clear signals of Σ_b^-, Σ_b^{*-} and Σ_b^+, Σ_b^{*+}, respectively. The significance of every peak is well above $6 \cdot \sigma$. The analysis results are arranged in Table 1.

In conclusion, the first observation [2] of the $\Sigma_b^{(*)\pm}$ bottom baryons has been confirmed.

State	Q-value, MeV/c^2	Absolute mass m, MeV/c^2	Width Γ, MeV/c^2
Σ_b^-	$56.2\,^{+0.6\,+0.1}_{-0.5\,-0.4}$	$5815.5\,^{+0.6}_{-0.5} \pm 1.7$	$4.3\,^{+3.1+1.0}_{-2.1-1.1}$
Σ_b^{*-}	$75.7 \pm 0.6\,^{+0.1}_{-0.6}$	$5835.0 \pm 0.6 \pm 1.8$	$6.4\,^{+2.2\,+0.7}_{-1.8\,-1.1}$
Σ_b^+	$52.0\,^{+0.9\,+0.1}_{-0.8\,-0.4}$	$5811.2\,^{+0.9}_{-0.8} \pm 1.7$	$9.2\,^{+3.8\,+1.0}_{-2.9\,-1.1}$
Σ_b^{*+}	$72.7 \pm 0.7\,^{+0.1}_{-0.6}$	$5832.0 \pm 0.7 \pm 1.8$	$10.4\,^{+2.7\,+0.8}_{-2.2\,-1.2}$
	Isospin mass splitting, MeV/c^2		
$m(\Sigma_b^+) - m(\Sigma_b^-)$		$-4.2\,^{+1.1}_{-0.9} \pm 0.1$	
$m(\Sigma_b^{*+}) - m(\Sigma_b^{*-})$		$-3.0 \pm 0.9 \pm 0.1$	

Table 1: Summary of the final results. For all the entries, the first uncertainty is the statistical one and the second is systematic. To extract the absolute masses, the best CDF mass measurement for Λ_b^0 [5] has been used.

The direct mass difference measurements have statistical precision a factor of $\gtrsim 2.3$ better than was previously reported [2] due to the larger dataset. The measurements are in good agreement with the previous results. The isospin mass splittings within the $I = 1$ triplets of Σ_b and Σ_b^* states have been extracted for the first time. The $\Sigma_b^{(*)-}$ states have higher mass values than their $\Sigma_b^{(*)+}$ partners following a pattern [6] common to most of the known isospin multiplets. These measurements favor the phenomenological explanation of this ordering due to higher masses of d-quarks than u-quarks and a larger electromagnetic contribution due to electrostatic Coulomb forces between quarks in $\Sigma_b^{(*)-}$ states than in the $\Sigma_b^{(*)+}$ ones. The natural widths of the $\Sigma_b^{\pm}$ and $\Sigma_b^{*\pm}$ states have been measured for the first time. The measurements are in agreement with theoretical expectations [7], within their experimental uncertainties. For further details on this analysis, please see [8].

2 Update on the $\Upsilon(4140)$ Near-Threshold Structure in $J/\Psi\phi$ Mass Spectrum of the $B^+ \to J/\Psi\phi K^+$ Decays

Recently, evidence has been reported by the CDF Collaboration for a narrow structure near the $J/\psi\phi$ threshold in exclusive $B^+ \to J/\psi\phi K^+$ decays produced in $p\overline{p}$ collisions at $\sqrt{s} = 1.96$ TeV [9]. A latest update [10] reports a preliminary confirmation of the signal in $M(J/\psi\phi)$ spectrum. The analysis is based on a larger sample of data comprising an integrated luminosity of $\sim 6\,\mathrm{pb}^{-1}$ accumulated by the CDF II detector. The specific data sample is collected by a dedicated three-level dimuon trigger recording $J/\psi \to \mu^+\mu^-$ events.

The $B^+ \to J/\psi\phi K^+$ candidates are reconstructed from $J/\psi \to \mu^+\mu^-$ candidates taken within $\pm 50\,\mathrm{MeV}/c^2$ around the mass of the J/ψ and $\phi \to K^-K^+$ candidates within a $\pm 7\,\mathrm{MeV}/c^2$ window at the ϕ mass combined further with the K^+ positive track. All five tracks are subjected to a $3D$ kinematic fit to a common vertex with $M(J/\psi)$ constrained to its PDG value.

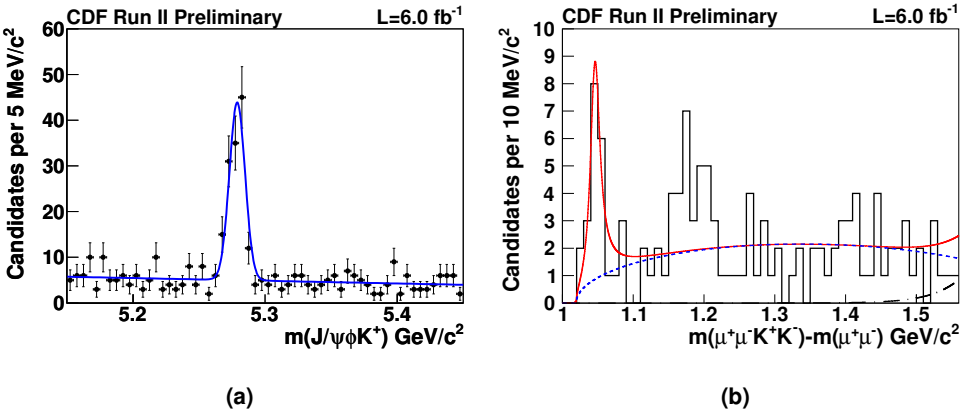

Figure 2: (a): The B^+ meson mass distribution $M(J/\psi\phi K^+)$ is shown with a fit to the data made with a Gaussian signal function and a linear background function. (b): The mass difference spectrum $\Delta M = M(\mu^+\mu^-K^-K^+) - M(\mu^+\mu^-)$ with the $\mu^+\mu^-K^-K^+$ combinations contained within $B^+ \to J/\psi\phi K^+$ candidates at $\pm 3\sigma$ around nominal $M(B^+)$ [3]; the background is predicted by the sum of the pure three-body phase space background contribution (dotted curve) and the B_s^0 meson contamination (fixed to 3.3, dash-dotted curve); the solid red curve is the total unbinned ML fit where the signal PDF is an S-wave Breit-Wigner convoluted with the resolution of $\sigma = 1.7\,\mathrm{MeV}/c^2$.

dE/dx and ToF measurements are used to identify three kaons contributing to the final state to further suppress the combinatorial background. The total transverse momentum p_T of the final candidate is required to be above $4\,\mathrm{GeV}/c$. The plot in Fig. 2a shows a prominent B^+ meson signal of 115 ± 12 (stat) events in the invariant mass spectrum $M(J/\psi\phi K^+)$. Selecting the B^+ candidates in $\pm 3\sigma$ mass range around its nominal mass the mass difference spectrum $\Delta M = M(\mu^+\mu^-K^-K^+) - M(\mu^+\mu^-)$ within final states of those B^+ candidates is examined. An enhancement near a threshold is seen at the Fig. 2b. The unbinned ML fit shown at the plot returns the signal position, width and its yield arranged in a Table 2. The fitted parameters are consistent with the previous results [9] on the $Y(4140)$ state. The p-value of the observed signal with respect to the background is determined using a statistical trials generation. It has been found to be $p \approx 2.3 \cdot 10^{-7}$ or $\approx 5.0 \cdot \sigma$ in Gaussian terms. In conclusion, the increased $B^+ \to J/\psi\phi K^+$ sample at CDF allows further investigation of the $Y(4140)$ structure and a preliminary observation of the signal is reported [10]. The mass and width are found to be consistent with the previous report [9].

Other experimental groups [11] [12] [13] do not confirm the observation of the $Y(4140)$ structure. Further investigation is needed and work is ongoing at CDF Collaboration to update the whole analysis on the full Run II data sample.

State	ΔM, MeV/c^2	M, MeV/c^2	Γ, MeV/c^2	N_{cands}	N_σ
$Y(4140)$	$1046.7^{+2.9}_{-3.0}$	$4143.4^{+2.9}_{-3.0} \pm 0.6$	$15.3^{+10.4}_{-6.1} \pm 2.5$	19 ± 6	$\approx 5.0 \cdot \sigma$
$\mathcal{B}(B^+ \to Y(4140)K^+) \cdot \mathcal{B}(Y(4140) \to J/\psi\phi)/\mathcal{B}(B^+ \to J/\psi\phi K^+) = 0.149 \pm 0.039 \pm 0.024$					

Table 2: Summary of the results found for the $Y(4140)$. On all the entries, the first uncertainty is the statistical one and the second is systematic. The absolute masses are extracted from the fitted ΔM and the world average $M(J/\psi)$ [3]. The measured relative branching ratio for $Y(4140)$ is presented in row 2.

3 Measurement of the Λ_b^0 Production Fraction $f(b \to \Lambda_b^0) \cdot \mathcal{B}(\Lambda_b^0 \to J/\Psi\Lambda^0)$ with the DØ Detector

For the Λ_b^0, the lightest bottom baryon, only a few decay channels have been studied, and the uncertainties on its branching fractions are large, $\sim (30-60)\%$. Increasingly precise measurements of $f(b \to \Lambda_b^0) \cdot \mathcal{B}(\Lambda_b^0 \to J/\psi\Lambda^0)$ (where $f(b \to \Lambda_b)$ is the fraction of b quarks which hadronize to Λ_b^0 baryons) will allow better tests of models including PQCD and relativistic and nonrelativistic quark models which predict heavy baryon decays. Moreover, these measurements could help in the study of $b \to s$ transitions such as $\Lambda_b^0 \to \mu^+\mu^-\Lambda^0$ [14] [15], which are topologically similar to $\Lambda_b^0 \to J/\psi\Lambda^0$ where $J/\psi \to \mu^+\mu^-$.

DØ reports an improved measurement (relative to Ref. [16]) on the relative production fraction, specifically

$$\sigma_{\text{rel}} = \frac{f(b \to \Lambda_b^0) \cdot \mathcal{B}(\Lambda_b^0 \to J/\psi\Lambda^0)}{f(b \to B^0) \cdot \mathcal{B}(B^0 \to J/\psi K_S^0)} = \frac{N(\Lambda_b^0)}{N(B^0)} \cdot \frac{\mathcal{B}(\Lambda_b^0 \to J/\psi\Lambda^0)}{\mathcal{B}(B^0 \to J/\psi K_S^0)} \cdot \frac{\mathcal{B}(K_S^0 \to \pi^+\pi^-)}{\mathcal{B}(\Lambda^0 \to p\pi^-)} \cdot \epsilon\,,$$

where $\epsilon = 2.37 \pm 0.05$ (MC stat.) is the relative detection efficiency of the well-measured $B^0 \to J/\psi K_S^0$ reference signal in denominator with respect to the $\Lambda_b^0 \to J/\psi\Lambda^0$ in the numerator. From this measurement one can extract $f(b \to \Lambda_b^0) \cdot \mathcal{B}(\Lambda_b^0 \to J/\psi\Lambda^0)$ with a significantly improved precision compared to the current world average [3]. The study is based on $\int \mathcal{L}\,dt \approx 6.1\,\text{fb}^{-1}$ of $p\overline{p}$ collisions collected with the DØ detector between 2002 and 2009. The invariant mass distributions of the Λ_b^0 and B^0 candidates passing the analysis criteria are shown in Fig. 3a and Fig. 3b correspondingly. To extract the yields of the observed Λ_b^0 and B^0 hadrons, an unbinned ML fit is applied to each mass distribution assuming a double Gaussian function for each signal and a second order polynomial distribution for their backgrounds. The fits yield $N(\Lambda_b^0 \to J/\psi\Lambda^0) = 314 \pm 29$ events and $N(B^0 \to J/\psi K_S^0) = 2335 \pm 73$ events. In summary, the DØ Collaboration has obtained the production fraction multiplied by the branching fraction for the decay $\Lambda_b^0 \to J/\psi\Lambda^0$ relative to that for the decay $B^0 \to J/\psi K_S^0$ to be

$$\sigma_{\text{rel}} = 0.345 \pm 0.034(\text{stat}) \pm 0.033(\text{syst}) \pm 0.003\,(\text{PDG})\,.$$

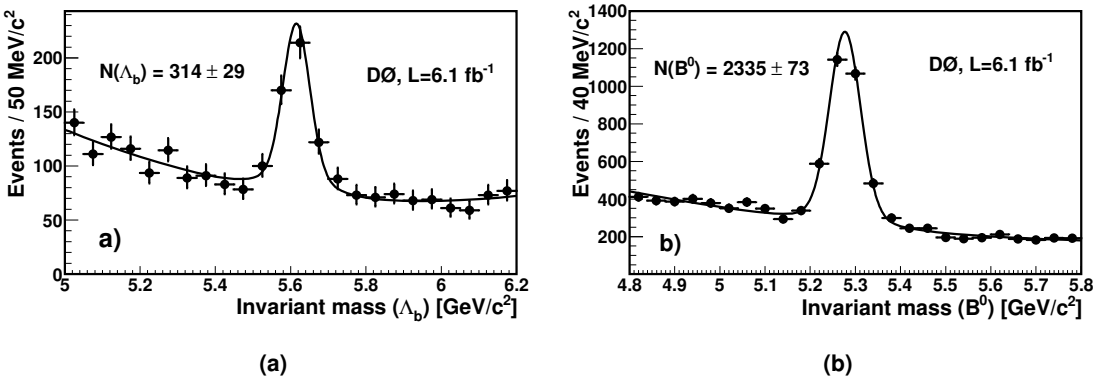

Figure 3: Invariant mass distribution in data for (a) $\Lambda_b^0 \to J/\psi\Lambda^0$ and (b) $B^0 \to J/\psi K_S^0$ decays. Fit results are superimposed.

The measurement is the most precise to date and exceeds the precision of the current value reported as the world average, 0.27 ± 0.13 [3]. Using the PDG value [3], $f(b \to B^0) \cdot \mathcal{B}(B^0 \to J/\psi K_S^0) = (1.74 \pm 0.08) \times 10^{-4}$, one extracts

$$f(b \to \Lambda_b^0) \cdot \mathcal{B}(\Lambda_b^0 \to J/\psi\Lambda^0) = [6.01 \pm 0.60(\text{stat}) \pm 0.58(\text{syst}) \pm 0.28\,(\text{PDG})] \times 10^{-5}$$

which can be compared directly to the world average value of $(4.7 \pm 2.3) \times 10^{-5}$ [3]. This result represents a reduction by a factor of ~ 3 of the uncertainty with respect to the previous measurement [16]. For further details on this analysis, please see [17].

Acknowledgments

The author is grateful to his colleagues from the CDF and DØ *B*-Physics Working Groups for useful suggestions and comments made during preparation of this talk. The author thanks the US Department of Energy for support of this work.

Bibliography

[1] E. Klempt and J. M. Richard, Rev. Mod. Phys. **82**, 1095 (2010). [arXiv:0901.2055 [hep-ph]].

[2] T. Aaltonen *et al.* (CDF Collaboration), Phys. Rev. Lett. **99**, 202001 (2007). [arXiv:0706.3868 [hep-ex]].

[3] K. Nakamura *et al.* (Particle Data Group), J. Phys. G **37**, 075021 (2010).

[4] J. D. Jackson, Nuovo Cim. **34**, 1644 (1964). J. D. Jackson, private communication, 11.06.07.

[5] D. E. Acosta *et al.* (CDF Collaboration), Phys. Rev. Lett. **96**, 202001 (2006). [arXiv:hep-ex/0508022].

[6] F. K. Guo, C. Hanhart and U. G. Meissner, J. High Energy Phys. 09 (2008) 136. [arXiv:0809.2359 [hep-ph]].

[7] J. G. Korner, M. Kramer and D. Pirjol, Prog. Part. Nucl. Phys. **33**, 787 (1994); X. H. Guo, K. W. Wei and X. H. Wu, Phys. Rev. D **77**, 036003 (2008); [arXiv:0710.1474 [hep-ph]]. C. W. Hwang, Eur. Phys. J. C **50**, 793 (2007). [arXiv:hep-ph/0611221].

[8] C. Calancha, I. Gorelov (on behalf of the CDF Collaboration), PoS **ICHEP2010**, 203 (2010). [arXiv:1011.5236 [hep-ex]].

[9] T. Aaltonen *et al.* (CDF Collaboration), Phys. Rev. Lett. **102**, 242002 (2009). [arXiv:0903.2229 [hep-ex]].

[10] T. Aaltonen *et al.* (The CDF Collaboration), [arXiv:1101.6058 [hep-ex]].

[11] C. P. Shen *et al.* (Belle Collaboration), Phys. Rev. Lett. **104**, 112004 (2010). [arXiv:0912.2383 [hep-ex]].

[12] The LHCb Collaboration, "Search for $X(4140)$ in $B^+ \to J/\psi\phi K^+$", report CERN-LHCb-CONF-2011-045.

[13] S. Stone, "Heavy Flavor Physics", to appear in Proceedings of the DPF-2011 Conference, Providence, RI, August 8-13, 2011. [arXiv:1109.3361 [hep-ph]].

[14] C. -H. Chen, C. Q. Geng, Phys. Rev. D **64**, 074001 (2001).

[15] T. M. Aliev, A. Ozpineci and M. Savci, Phys. Rev. D **65**, 115002 (2002).

[16] F. Abe *et al.* (CDF collaboration), Phys. Rev. D **55**, 1142 (1997).

[17] V. M. Abazov *et al.* (DØ Collaboration), Phys. Rev. **D84**, 031102 (2011). [arXiv:1105.0690 [hep-ex]].

Hadrons in Hot and Cold Medium

Hadrons in Hot and Cold Medium

Conveners

Tullio	Bressani	INFN Torino (*Chair*)
Tomofumi	Nagae	Kyoto University
Laura	Fabbietti	TU München

Session Chairs

Laura	Fabbietti	TU München
Tullio	Bressani	Istituto Nazionale di Fisica Nucleare
Wolfram	Weise	TU München
Tomofumi	Nagae	Kyoto University

Contents

Recent results on the weak decay of Λ hypernuclei

Stefania Bufalino[1]
Istituto Nazionale di Fisica Nucleare
Sezione di Torino, Via P. Giuria 1
I-10125 Torino, ITALY

The latest results from the FINUDA experiment on the Weak Decay of p-shell Λ-hypernuclei are presented and discussed. π^- spectra from mesonic decay were measured with magnetic analysis for the first time for ${}^{7}_{\Lambda}Li$, ${}^{9}_{\Lambda}Be$, ${}^{11}_{\Lambda}B$ and ${}^{15}_{\Lambda}N$. Branching ratio $\Gamma_{\pi^-}/\Gamma_{tot}$ were derived from the measured spectra. In addition spectra of protons from NMWD were obtained for ${}^{5}_{\Lambda}He$, ${}^{7}_{\Lambda}Li$, ${}^{9}_{\Lambda}Be$, ${}^{11}_{\Lambda}B$, ${}^{12}_{\Lambda}C$, ${}^{13}_{\Lambda}C$, ${}^{15}_{\Lambda}N$ and ${}^{16}_{\Lambda}O$. An estimation of the contributions of both Final State Interactions (FSI) and two-nucleon induced (2N) decay processes was performed, following a model independent approach. These results are confirmed by a new analysis of the triple coincidence (π^-, p, n) events.

1 Analysis method and results

The information coming from the study of the Λ-hypernuclei weak decay channels completes the knowledge on strange nuclear systems by spectroscopy, gained both by missing mass analyses and γ-ray measurements. Λ-hypernuclei decay through both mesonic (MWD) and non-mesonic weak decay (NMWD) processes. In MWD the Λ hyperon decays to a nucleon and a pion in the nuclear medium, similarly to the weak decay mode in free space:

$$\Lambda_{free} \rightarrow p + \pi^- + 37.8\ \text{MeV} \quad (64.2\%) \tag{1}$$

$$n + \pi^0 + 41.1\ \text{MeV} \quad (35.8\%) \tag{2}$$

in which the emitted nucleon (pion) carries a momentum $q \approx 100$ MeV/c. The theory of hypernuclear MWD was initiated by Dalitz [1, 2], and motivated by the observation of MWD reactions in the pioneering hypernuclear physics experiments with photographic emulsions. Following the development of counter techniques for use in (K^-, π^-) and (π^+, K^+) reactions on nuclei in the 1970s and 1980s, a considerable body of experimental data on Γ_{π^-} and/or Γ_{π^0} is now available on light Λ-hypernuclei up to ${}^{12}_{\Lambda}$C ([3] and references therein). As far as the NMWD is concerned, there are three decay channels:

[1] bufalino@to.infn.it

$$(3) \qquad {}^{A}_{\Lambda}\mathrm{Z} \rightarrow {}^{A-2}(\mathrm{Z}-1) + p + n \qquad (\Gamma_p)$$

$$(4) \qquad {}^{A}_{\Lambda}\mathrm{Z} \rightarrow {}^{A-2}\mathrm{Z} + n + n \qquad (\Gamma_n)$$

$$(5) \qquad {}^{A}_{\Lambda}\mathrm{Z} \rightarrow {}^{A-3}\mathrm{Z}' + N + N + N \qquad (\Gamma_2)$$

The channel (5) is known as two-nucleon induced (2N) decay and is due to the interaction of the Λ with a pair of strongly correlated nucleons; Z' stands for Z, $Z-1$ or $Z-2$ depending on the particular nucleons combination. The total NMWD rate of a Λ–hypernucleus is given by their sum: $\Gamma_{\mathrm{NMWD}} = \Gamma_p + \Gamma_n + \Gamma_2$. Several important experimental progresses in NMWD study have been made in the latest years but no experimental evidence has been obtained so far for the 2N induced decay. In the present work I report on measurements by the FINUDA experiment of MWD of hypernuclei in the p-shell comparing the measured π^- spectra and decay rates with the calculations by [4]. Furthermore I will describe two independent analyses of the NMWD of ${}^{7}_{\Lambda}Li$, ${}^{9}_{\Lambda}Be$, ${}^{11}_{\Lambda}B$, ${}^{12}_{\Lambda}C$, ${}^{13}_{\Lambda}C$, ${}^{15}_{\Lambda}N$ and ${}^{16}_{\Lambda}O$ hypernuclei which provided values for the 2N decay. The complete analysis and discussion of the results was already published in Ref. [5–7].

The results reported in the present paper have been obtained by analyzing the data collected by the FINUDA experiment, from 2003 to 2007 and correspond to an integrated luminosity of ~ 1.2 fb^{-1}. FINUDA is a fixed target experiment installed at one of the two interaction points of the DAΦNE e^+e^- ϕ–factory of Laboratori Nazionali di Frascati (INFN–Italy). Λ-hypernuclei are produced by means of the (K^-, π^-) reaction with K^-'s at rest by stopping in very thin targets the low energy ($\sim$ 16 MeV) K^-'s coming from the $\Phi \rightarrow K^-K^+$ decay channel. The analysis was performed on events collected out of ${}^{6}Li$, ${}^{7}Li$, ${}^{9}Be$, ${}^{12}C$, ${}^{13}C$ and (D_2O) targets. The experimental method is briefly described here, while full details are reported in [5–7]. To investigate the MWD process (1) all the events characterized by the presence of two π^-'s detected in coincidence were selected. One π^-, with a momentum as high as $260 - 290$ MeV/c, gives the signature of the formation of the ground-state of the hypernuclear system or of a low lying excited state decaying to it by electromagnetic emission. The second π^-, with a momentum lower than 115 MeV/c, gives the signature of the decay. The lower threshold for the detection momentum of these π^-'s is $\sim$ 80 MeV/c and their momentum resolution is Δp / p $\sim$ 6% FWHM at 110 MeV/c. The analysis of the NMWD was performed by selecting all the events with two particles emitted in coincidence: a π^- carrying the information of the hypernucleus formation and a proton coming from the same K^- interaction vertex, which gives the signature of the NMWD. Protons were identified with an efficiency of 90% and the proton energy resolution was ΔE/E$\sim$ 2% FWHM at 80 MeV. A further requirement was made asking for the detection of a neutron. The outer FINUDA detector, called TOFONE [7], a barrel of 72 scintillator slabs was used for trigger and P.I.D. (by Time Of Flight) of the charged particles and to detect even neutral ones with an efficiency of the order of 10% for neutrons in the range 15-150 MeV. The energy resolution on the neutron is $\sim$13% at 10 MeV and $\sim$10% at 100 MeV.

As far as the MWD is concerned, the π^- spectra allow to have a more careful confirmation of the elementary mechanism that is supposed to underlie the decay process, as well as to have information on the spin-parity of the initial hypernuclear ground state. In this respect the study of pion spectra from MWD can be regarded as an indirect spectroscopic investigation tool. Due to the π^- momentum detection threshold of the apparatus ($\sim$ 80 MeV/c), only MWD spectra of ${}^{7}_{\Lambda}Li$, ${}^{9}_{\Lambda}Be$, ${}^{11}_{\Lambda}B$ (${}^{12}C$ targets) and ${}^{15}_{\Lambda}N$ (${}^{16}O$ target) were investigated. Spectra from ${}^{12}_{\Lambda}$C and ${}^{16}_{\Lambda}$O could not be observed. The decay π^- momentum spectra show interesting structures whose meaning can be better understood by considering the corresponding kinetic energy spectra that are directly related to the excitation function of the daugther nucleus. Kinetic energy spectra, background subtracted and acceptance corrected, were evaluated for MWD of ${}^{7}_{\Lambda}$Li, ${}^{9}_{\Lambda}$Be, ${}^{11}_{\Lambda}$B and ${}^{15}_{\Lambda}$N. Based on these measurements, the spin-parity assignment $1/2^+$ for ${}^{7}_{\Lambda}$Li and $5/2^+$ for ${}^{11}_{\Lambda}$B ground-state were confirmed. The ground-state spin of ${}^{15}_{\Lambda}$N has not been determined experimentally and the most recent theoretical study of Λ-hypernuclear spin dependence predicts $J^{\pi}({}^{15}_{\Lambda}\mathrm{N}_{g.s.}) = 3/2^+$. The shape of the measured spectrum slightly favors $J^{\pi}({}^{15}_{\Lambda}\mathrm{N}_{g.s.}) = 3/2^+$ with respect of $1/2^+$ and considering the total MWD rate it was possible to determine for the first time the ${}^{15}_{\Lambda}\mathrm{N}_{g.s.}$ spin parity. For the full discussion of the interpretation of the ${}^{15}_{\Lambda}$N spectrum see [5]. The values of the branching ratios of the MWD reaction was also evaluated for the studied hypernuclei and they are reported in Fig. 1. It is remarkable that a very good agreement holds among the present results and previous measurements, when existing, and among the present results and theoretical calculations. Very strong nuclear structure effects are also evident.

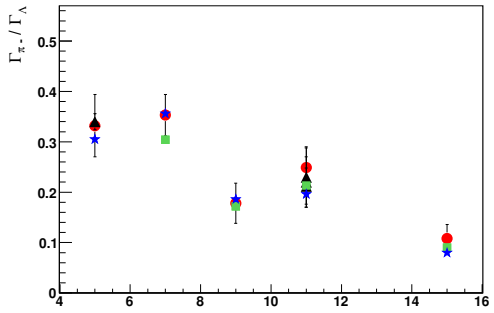

Figure 1: Total π^- decay rate Γ_{π^-} in units of Γ_Λ as a function of the hypernuclear mass number A. Open circles: ${}^{7}_{\Lambda}$Li, ${}^{9}_{\Lambda}$Be, ${}^{11}_{\Lambda}$B and ${}^{15}_{\Lambda}$N values measured by FINUDA [5]; ${}^{5}_{\Lambda}$He is also reported for sake of completeness. Full triangles: previous measurements; open squares: theoretical calculations from [8]; full stars: theoretical calculation from [4].

With regard to the NMWD study, in Fig. 2 the kinetic energy spectra of protons coming from the NMWD of ${}^{5}_{\Lambda}He$, ${}^{7}_{\Lambda}Li$, ${}^{9}_{\Lambda}Be$, ${}^{11}_{\Lambda}B$, ${}^{12}_{\Lambda}C$, ${}^{13}_{\Lambda}C$, ${}^{15}_{\Lambda}N$ and ${}^{16}_{\Lambda}O$ are shown. All the spectra are background subtracted and acceptance corrected; the errors in the spectra are statistical only and include both the contributions from background subtraction and acceptance correction. We estimated a systematic error of less than 5%. Even though affected by considerable errors, in particular in the low energy region, the proton kinetic energy spectra show a clear trend as a function of the hypernuclear mass number A (from 5 to 16): a peak around 80

MeV (which corresponds to about half of the Q–value for the free $\Lambda p \to np$ reaction) is broadened by the Fermi motion of nucleons and more and more blurred as A increases. The peak is smeared, on its low energy side, by a rise that can be ascribed to FSI and two–nucleon induced weak decays.
To estimate the contribution of this last channel each proton spectrum from 80 MeV onwards was fitted by a Gaussian function. It was assumed that the proton spectrum beyond the peak mean value is due to protons coming from the $\Lambda p \to np$ reaction and that the 2N channel can be neglected in this region (A_{high}). On the contrary, the spectrum below the peak mean value is fed by protons from both $\Lambda p \to np$ and 2N decays and is also affected by FSI (A_{low}). The determination of the 2N decay was based on two assumptions: the first one is that the two–nucleon induced NMWD is dominated by the $\Lambda np \to nnp$ channel ($\Gamma_2 = \Gamma(\Lambda np \to nnp) + \Gamma(\Lambda pp \to npp) + \Gamma(\Lambda nn \to nnn) \equiv \Gamma_{np} + \Gamma_{pp} + \Gamma_{nn} \simeq \Gamma_{np}$) since the recent microscopical calculation of Ref. [12] quote $\Gamma_{np} : \Gamma_{pp} : \Gamma_{nn} = 0.83 : 0.12 : 0.04$ and the second one stands on a constant Γ_2/Γ_p ratio for the considered hypernuclear mass range.

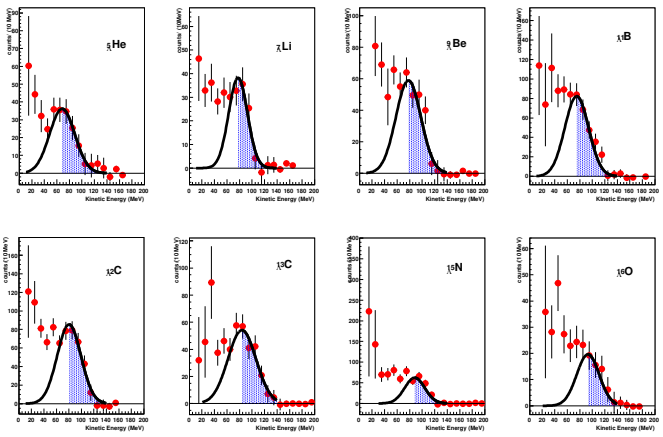

Figure 2: Proton kinetic energy spectra from the NMWD of (from left to right): ${}^{5}_{\Lambda}He$, ${}^{7}_{\Lambda}Li$, ${}^{9}_{\Lambda}Be$, ${}^{11}_{\Lambda}B$, ${}^{12}_{\Lambda}C$, ${}^{13}_{\Lambda}C$, ${}^{15}_{\Lambda}N$ and ${}^{16}_{\Lambda}O$. The blue filled area is the spectrum area in which the two–nucleon induced NMWD is negligible.

Consider now the ratio:

$$R \equiv \frac{A_{\rm low}}{A_{\rm low} + A_{\rm high}} = \frac{0.5 + \dfrac{\Gamma_2}{\Gamma_p}}{1 + \dfrac{\Gamma_2}{\Gamma_p}} + bA \; . \tag{6}$$

In Fig. 3 the experimental values of this ratio are plotted as a function of A.

Following a model independent analysis, fully described in [6] a value of $\Gamma_2/\Gamma_p = 0.43 \pm 0.25$ was determined. As discussed in [6], to determine $\Gamma_2/\Gamma_{\rm NMWD}$ the Γ_n/Γ_p ratio needs to be

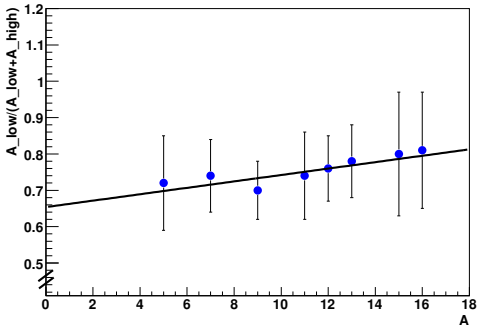

Figure 3: The ratio $A_{\rm low}/(A_{\rm low}+A_{\rm high})$ as a function of the hypernuclear mass number.

known. Using recent experimental results [9] for ${}^{5}_{\Lambda}H$ and for ${}^{12}_{\Lambda}C$ together with the above determination of Γ_2/Γ_p one obtains $\Gamma_2/\Gamma_{\rm NMWD} = 0.24 \pm 0.10$.

In a following analysis of the events with a triple (π^-, n, p) coincidences a neutron was required in addition. We also fixed for each hypernucleus a proton energy threshold E_p=20 MeV below the Gaussian mean value μ found in [6]. We verified that this value was the best compromise on the signal/background ratio and furthermore we chose a threshold for the angular correlation between the neutron and the proton of cosθ(np)=-0.8.
We analized then the triple coincidence (π^-, n, p) selecting alla the events with E_p lower than the threshold and cosθ(np)>-0.8. These events correspond mainly to the $\Lambda np \rightarrow nnp$ process with a small contribution of FSI. Fig. 4 shows the dependence on the mass number A of the selected events divided by the number of protons with $E_p \geqslant \mu$; the above number should be proportional to Γ_{np} and Γ_p respectively.

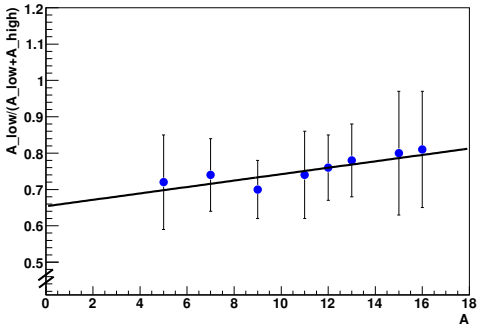

Figure 4: The ratio $N_{\rm n}/N_{\rm p}$ as a function of the hypernuclear mass number A.

Following the same assumpion of [6] we found $\Gamma_{np}/\Gamma_p = 0.39 \pm 0.16_{stat}{}^{+0.04_{sys}}_{-0.03_{sys}}$. Using the experimental value of Γ_n/Γ_p reported in [9] for ${}^{5}_{\Lambda}He$ and ${}^{12}_{\Lambda}C$ and our determination

of Γ_{np}/Γ_p we obtain $\Gamma_{2N}/\Gamma_{\rm NMWD} = 0.21 \pm 0.07_{stat}{}^{+0.03_{sys}}_{-0.02_{sys}}$. This value supports the latest theoretical predictions [14] ($\Gamma_2/\Gamma_{\rm NMWD}$=0.26), the recent experimental results of [11] (0.29 ± 0.13) and the previous FINUDA result [6], but bears a smaller error. Calculating the mean of the experimental determinations [7, 11] of $\Gamma_{2N}/\Gamma_{\rm NMWD}$ at our disposal one found that the contribution of the two–nucleon induced decay is 0.25 ± 0.15.

2 Conclusions

The FINUDA experiment has performed a systematic study of MWD and NMWD charged particles spectra of Λ–hypernuclei in the $A = 5 \div 16$ mass range. From the study of the kinetic energy spetra of π^- the spin-parity assignment $J^\pi(^{15}_{\Lambda}{\rm N}_{g.s.}) = 3/2^+$ was made. The proton spectra from the NMWD were also analyzed and an evaluation of the nucleon FSI effects and of the 2N decay contribution to the NMWD process was performed: an experimental value of $\Gamma_2/\Gamma_{NMWD} = 0.24 \pm 0.10$ was obtained. This result was confirmed in the analysis of the triple (π^-, n, p) coincidence, with a reduction of the error and leading to an estimate of Γ_2/Γ_{NMWD}=$0.21 \pm 0.07_{stat}{}^{+0.03_{sys}}_{-0.02_{sys}}$

Bibliography

[1] R.H. Dalitz, L. Liu, *Phys. Rev.* **116** (1959) 1312.

[2] D. Kiełczewska, D. Ziemińska, R.H. Dalitz, *Nucl. Phys.* **A 333** (1980) 367.

[3] Y. Sato, *et al., Phys. Rev.* **C 71** (2005) 025203.

[4] A. Gal, *Nucl. Phys.* **A 828** (2009) 72.

[5] M. Agnello *et al.*, *Phys. Lett.* **B 681** (2009) 139.

[6] Agnello M *et al.*, (2010) *Phys. Lett.* B **685** 247.

[7] Agnello M *et al.*, (2011) *Phys. Lett.* B **701** 556.

[8] T. Motoba, K. Itonaga, *Progr. Theor. Phys. Suppl.* **117** (1994) 477.

[9] Bhang H *et al.*, (2007) *Eur. Phys. J.* A **33** 259.

[10] Parker J D *et al.*, (2007) *Phys. Rev.* C **76** 035501.

[11] Kim M *et al.*, (2009) *Phys. Rev. Lett.* **103** 182502.

[12] Bauer E and Garbarino G, (2009) *Nucl. Phys.* A **828** 29.

[13] Agnello M *et al.*, (2008) *Nucl. Phys.* A **804** 151.

[14] E. Bauer and G. Garbarino, *Phys. Rev* **C 81** (2010) 064315.

First observation of ${}^{6}_{\Lambda}$H

Elena Botta[1,a,b], M. Agnello[c], L. Benussi[d], M. Bertani[d], H.C. Bhang[e], G. Bonomi[f,g], M. Bregant[h,i], T. Bressani[a,b], S. Bufalino[a], L. Busso[a,j], D. Calvo[a], P. Camerini[h,i], B. Dalena[k,l], F. De Mori[a,b], G. D' Erasmo[k,l], F.L. Fabbri[d], A. Feliciello[a], A. Filippi[a], E.M. Fiore[k,l], A. Fontana[g], H. Fujioka[m], P. Genova[g], P. Gianotti[d], N. Grion[i], V. Lucherini[d], S. Marcello[a,b], N. Mirfakhrai[n], F. Moia[f,g], O. Morra[a,o], T. Nagae[m], H. Outa[p], A. Pantaleo[l], V. Paticchio[l], S. Piano[i], R. Rui[h,i], G. Simonetti[k,l], R. Wheadon[a], and A. Zenoni[f,g]

[a] *Istituto Nazionale di Fisica Nucleare - Sezione di Torino, Torino, ITALY*
[b] *Università degli Studi di Torino, Dipartimento di Fisica Sperimentale, Torino, ITALY*
[c] *Politecnico di Torino, Dipartimento di Fisica, Torino, ITALY*
[d] *Istituto Nazionale di Fisica Nucleare - Laboratori Nazionali di Frascati, Frascati, ITALY*
[e] *Seoul National University, Department of Physics, Seoul, SOUTH KOREA*
[f] *Università di Brescia, Dipartimento di Meccanica, Brescia, ITALY*
[g] *Istituto Nazionale di Fisica Nucleare - Sezione di Pavia, Pavia, ITALY*
[h] *Università di Trieste, Dipartimento di Fisica, Trieste, ITALY*
[i] *Istituto Nazionale di Fisica Nucleare - Sezione di Trieste, Trieste, ITALY*
[j] *Università degli Studi di Torino, Dipartimento di Fisica Generale, Torino, ITALY*
[k] *Università degli Studi di Bari, Dipartimento di Fisica, Bari, ITALY*
[l] *Istituto Nazionale di Fisica Nucleare - Sezione di Bari, Bari, ITALY*
[m] *Kyoto University, Department of Physics, Kyoto, JAPAN*
[n] *Shahid Behesty University, Department of Physics, Teheran, IRAN*
[o] *INAF-IFSI - Sezione di Torino, Torino, ITALY*
[p] *RIKEN, Wako, JAPAN*

The FINUDA experiment has observed for the first time the hyper superheavy hydrogen ${}^{6}_{\Lambda}$H by means of the (K^{-}_{stop}, π^{+}) reaction on ^{6}Li targets. Preliminary results are presented concerning the binding energy of this exotic nuclear system and its production rate.

1 Introduction

In 1995 Majling [1] pointed out the possible existence of bound light Λ-hypernuclei with a large neutron excess: the so called "glue-like" rôle of the Λ hyperon could produce neutron rich Λ-hypernuclei beyond the neutron stability drip line for ordinary nuclei. In particular, for systems as light as ${}^{6}_{\Lambda}$H and ${}^{7}_{\Lambda}$H, binding energies similar to those of normal

[1] botta@to.infn.it

Λ-hypernuclei in the same mass number range and production rates $\leqslant 10^{-5}/K^{-}_{stop}$ were predicted for the (K^{-}_{stop}, π^{+}) reaction. Akaishi and collaborators [2] evaluated the binding energy of the ${}^{6}_{\Lambda}$H system by introducing an additional binding contribution due to the three body ΛNN force resulting from the coherent part of the ΛN-ΣN coupling.

From the experimental side, upper limits for the production of ${}^{9}_{\Lambda}$He, ${}^{12}_{\Lambda}$Be and ${}^{16}_{\Lambda}$C have been obtained [3] exploiting the (K^{-}_{stop}, π^{+}) reaction, while the production of ${}^{10}_{\Lambda}$Li has been reported [4] analysing the (π^{-}, K^{+}) reaction in flight. The most recent attempt to observe neutron rich Λ-hypernuclei through the (K^{-}_{stop}, π^{+}) reaction was performed by the FINUDA experiment [5] on ^{6}Li, ^{7}Li and ^{12}C targets; upper limits were assessed for the production rates of ${}^{6}_{\Lambda}$H ($(2.5 \pm 0.4_{stat\ -0.1syst}^{+0.4}) \cdot 10^{-5}/K^{-}_{stop}$), ${}^{7}_{\Lambda}$H and ${}^{12}_{\Lambda}$Be.

2 Experimental and analysis technique

FINUDA [6] was an experiment installed at one of the two interaction regions of the DAΦNE $e^{+}e^{-}$ collider, the INFN-LNF Φ(1020)-factory; it was mainly dedicated to hypernuclear physics. The structure of the apparatus allowed to study at the same time the formation and the decay of Λ-hypernuclei by means of a high resolution magnetic spectroscopy of the emitted charged particles. In particular, for reactions occurring in the apparatus sector where ^{6}Li targets were located, for π^{+} with momentum $\sim$ 250 MeV/c the resolution of the tracker is σ_p = (1.1±0.1) MeV/c [7] and the precision on the absolute momentum calibration is better than 0.12 MeV/c; for π^{-} with momentum $\sim$ 130 MeV/c the resolution is $\sigma_p = (1.2 \pm 0.1)$ MeV/c and the absolute calibration is 0.2 MeV/c.

Preliminary results of the analysis of ${}^{6}_{\Lambda}$H production from the complete FINUDA statistics are presented here. To identify the neutron rich system production and to reduce the background, the complete production and decay reaction chain was investigated:

$$(1) \qquad \begin{aligned} K^{-} + {}^{6}Li \ &\rightarrow \ {}^{6}_{\Lambda}H + \pi^{+} \quad (\mathrm{p}(\pi^{+}) \sim 252\ \mathrm{MeV/c}) \\ &\hookrightarrow {}^{6}He + \pi^{-} \quad (\mathrm{p}(\pi^{-}) \sim 136.5\ \mathrm{MeV/c}). \end{aligned}$$

For the two reactions, occurring at rest, we can write:

$$\begin{aligned} M(K^{-}) + 3M(p) \ &+ \ 3M(n) - B({}^{6}Li) = M({}^{6}_{\Lambda}H) + T({}^{6}_{\Lambda}H) + M(\pi^{+}) + T(\pi^{+}), \\ M({}^{6}_{\Lambda}H) \ &= \ 2M(p) + 4M(n) - B({}^{6}He) + T({}^{6}He) + M(\pi^{-}) + T(\pi^{-}), \end{aligned}$$

where M are the masses, T the kinetic energies and B the binding energies. By eliminating M(${}^{6}_{\Lambda}$H):

$$(2) \qquad \begin{aligned} T(\pi^{+}) + T(\pi^{-}) \ &= \ M(K^{-}) + M(p) - M(n) - 2M(\pi) \\ &\quad -B({}^{6}Li) + B({}^{6}He) - T({}^{6}He) - T({}^{6}_{\Lambda}H); \end{aligned}$$

the right hand term is independent on the ${}^{6}_{\Lambda}$H binding energy, within the FINUDA energy resolution, and $T(\pi^{+}) + T(\pi^{-})$ = 203.0±1.3 MeV. Events were selected in the distribution

of the sum of the energy in the region (202÷204) MeV. The p(π^+) and p(π^-) momentum distributions of the selected events show a smooth shape compatible with the background due to, respectively, decay and formation of the Σ^+ hyperon in the interaction of the stopped K^- with a proton of the target ^{6}Li nucleus. These distributions fall to zero, respectively, at p(π^+)= 245 MeV/c and p(π^-)=145 MeV/c. These limit values correspond to ${}^{6}_{\Lambda}$H masses higher than the total mass of the ($\Lambda + {}^3\mathrm{H} + 2n$) and ($\Lambda + {}^5\mathrm{H}$) unbound systems. A further cut on p(π^+)=(249÷255) MeV/c and p(π^-)=(130÷138) MeV/c was thus applied to select bound ${}^{6}_{\Lambda}$H. Three events fulfilled such selections: they are candidate to be ${}^{6}_{\Lambda}$H.

3 Results and interpretation

For each of the three selected events the ${}^{6}_{\Lambda}$H mass and binding energy, B_Λ, with respect to both the ($\Lambda + {}^3\mathrm{H} + 2n$) and the ($\Lambda + {}^5\mathrm{H}$) systems, have been evaluated; the values are reported in Table 1. The mean value of the ${}^{6}_{\Lambda}$H mass is M(${}^{6}_{\Lambda}$H)=5801.43±0.74; the error is statistical only.

T_{tot} (MeV)	p(π^+) (MeV/c)	p(π^-) (MeV/c)	M (MeV)	B^5_Λ (MeV)	B^3_Λ (MeV)	M (MeV)	B^5_Λ (MeV)	B^3_Λ (MeV)
202.5	251.3	135.1	5802.33	3.11	1.41	5801.41	4.03	2.33
202.7	250.0	136.9	5803.45	1.99	0.29	5802.73	2.71	1.01
202.1	253.8	131.2	5799.97	5.47	3.77	5798.66	6.78	5.08

Table 1: Kinematic features, ${}^{6}_{\Lambda}$H mass, M, and binding energy with respect to ($\Lambda + {}^5\mathrm{H}$), B^5_Λ, and ($\Lambda + {}^3\mathrm{H} + 2n$), B^3_Λ, from production (col. 4, 5, 6) and decay (col. 7, 8, 9) reactions of the three ${}^{6}_{\Lambda}$H candidate events. T_{tot} =T(π^+)+T(π^-). The errors are $\sigma(T_{tot})$=1.3 MeV, $\sigma(p_{\pi^+})$=1.1 MeV/c, $\sigma(p_{\pi^-})$=1.2 MeV/c, σ(M)=$\sigma(B_\Lambda)$=0.96 MeV for production reaction, =0.84 MeV for decay reaction.

Before discussing the physical interpretation of the above results, it is mandatory to examine carefully whether the above three events could be due to physical or instrumental backgrounds that could affect the data.

The main source of instrumental background is the presence of fake tracks, misidentified as true events by the track reconstruction algorithms. To evaluate this background events relative to target nuclei other than ^{6}Li (^{7}Li, ^{9}Be, ^{13}C, ^{16}O) were selected with the same selection criteria applied for ^{6}Li. The instrumental background (BGD1) contribution was evaluated as 0.27±0.27 fake events from ^{6}Li targets.

Concerning the physical backgrounds, the reaction chains that could contribute to the (π^+, π^-) coincidences with the same conditions applied to identify the production and mesonic

decay of a bound ${}^{6}_{\Lambda}$H are:

$$K^- + {}^6Li \rightarrow \Sigma^+ + {}^4He + n + \pi^- \quad (\mathrm{p}(\pi^-) \leqslant 190\ \mathrm{MeV/c}), \\ \hookrightarrow n + \pi^+ \quad (\mathrm{p}(\pi^+) \leqslant 282\ \mathrm{MeV/c}) \tag{3}$$

$$K^- + {}^6Li \rightarrow {}^{4}_{\Lambda}H + n + n + \pi^+ \quad (\mathrm{p}(\pi^+) \leqslant 252\ \mathrm{MeV/c}), \\ \hookrightarrow {}^4He + \pi^- \quad (\mathrm{p}(\pi^-) \sim 132.8\ \mathrm{MeV/c}). \tag{4}$$

Both reaction chains have been studied with the FINUDA simulation program fully reproducing the apparatus geometry, detection and trigger efficiency. For the chain (3) the interaction of K^- with a proton of the target nucleus has been simulated in the quasi-free approximation ($K^- + p \rightarrow \Sigma^+ + \pi^-$); the chain (4) has been described through the four-body phase space kinematics. The simulated events were then reconstructed and submitted to the same quality cuts and same selections criteria applied in the data analysis.

Taking into account the branching fraction for the $K^-_{stop} + p \rightarrow \Sigma^+ + \pi^-$ reaction on nuclei, the $\Sigma^+ + p \rightarrow \Lambda + p$ conversion probability and the $\Sigma^+ \rightarrow n + \pi^+$ decay branching ratio, a background of 0.12±0.07 events on ^{6}Li targets is obtained (BGD2) from chain (3). The contribution of chain (4) was evaluated by taking into account the formation probability of ${}^{4}_{\Lambda}$H stopping a K^- in a ^{6}Li target [8], the probability of two charge-exchange reactions in sequence, (π^-, π^0) and (π^0, π^+), on the two remaining protons of the ^{6}Li nucleus and the branching ratio for the ${}^{4}_{\Lambda}$H→^{4}He+π^- [8] ; a background of 0.0008±0.0004 events on the ^{6}Li targets is obtained, fully negligible with respect to both the instrumental, BGD1, and chain(3), BGD2, contributions.

The described method allows to determine the product $R \cdot BR(\pi^-)$, where R is the ${}^{6}_{\Lambda}$H production rate per stopped K^- and $BR(\pi^-)$ the branching ratio for the mesonic decay ${}^{6}_{\Lambda}H \rightarrow {}^6He + \pi^-$:

$$R \cdot BR(\pi^-) = \frac{N - BGD1 - BGD2}{\epsilon(\pi^+)\,\epsilon(\pi^-)\,K^-_{stop}({}^6Li)} = (1.3 \pm 0.9) \cdot 10^{-6}/K^-_{stop}. \tag{5}$$

where N indicates the three candidate events, $\epsilon(\pi^+)$ and $\epsilon(\pi^-)$ indicate the global efficiency for the detection of π^+ and π^- evaluated by means of the full FINUDA simulation code, $K^-_{stop}({}^6Li)$ is the number of K^- stopped in ^{6}Li targets, $K^-_{stop}({}^6Li) \sim 2.7 \cdot 10^7$. The value (5) has to be corrected for the purity of the bulk used to manufact the ^{6}Li targets used, 90%, and for the statistical reduction due to the cut on T(π^+)+T(π^-), giving $R \cdot BR(\pi^-) = (2.6 \pm 1.8) \cdot 10^{-6}/K^-_{stop}$. By assuming $BR(\pi^-)$=49%, considering the analogous decay ${}^{4}_{\Lambda}H \rightarrow {}^4He + \pi^-$ [8], we find $R = (5.2 \pm 3.6) \cdot 10^{-6}/K^-_{stop}$, fully consistent with the previous upper limit obtained by FINUDA [5].

4 Conclusions

The FINUDA experiment has observed for the first time the formation and decay of the hyper superheavy hydrogen ${}^{6}_{\Lambda}$H through the (K^-, π^+) reaction on ^{6}Li targets. The mass of the system has been determined as M(${}^{6}_{\Lambda}$H)=5801.43$\pm$0.74, while the production rate is assessed as $R = (5.2 \pm 3.6) \cdot 10^{-6}/K^-_{stop}$.

Bibliography

[1] L. Majling, Nucl. Phys. **A585** (1995) 211c.

[2] Y. Akaishi *et al.*,, *Frascati Physics Series*, **XVI** (1999) 59.

[3] K. Kubota *et al.*, *Nucl.Phys.* **A602** (1996) 327.

[4] P.K. Saha *et al.*, *Phys. Rev. Lett.* **94** (2005) 05202.

[5] M. Agnello *et al.*, *Phys. Lett.* **B640** (2006) 145.

[6] M. Agnello *et al.*, *Phys. Lett.* **B685** (2010) 247.

[7] M. Agnello *et al.*, *Phys. Lett.* **B698** (2011) 219.

[8] H. Tamura *et al.*, *Phys. Rev.* **C40** (1989) R479.

Kaonic ^{3}He and ^{4}He X-ray measurements in SIDDHARTA

Tomoichi Ishiwatari[1,a], M. Bazzi[b], G. Beer[c], C. Berucci[b], L. Bombelli[d], A.M. Bragadireanu[b,e], M. Cargnelli[a], A. Clozza[b], G. Corradi[b], C. Curceanu (Petrascu)[b], A. d'Uffizi[b], C. Fiorini[d], F. Ghio[f], B. Girolami[f], C. Guaraldo[b], R.S. Hayano[g], M. Iliescu[b,e], M. Iwasaki[h], P. Kienle[i], P. Levi Sandri[b], V. Lucherini[b], J. Marton[a], S. Okada[b], D. Pietreanu[b], K. Piscicchia[b], M. Poli Lener[b], T. Ponta[e], R. Quaglia[d], A. Rizzo[b], A. Romero Vidal[b], A. Scordo[b], H. Shi[g], D.L. Sirghi[b,e], F. Sirghi[b,e], H. Tatsuno[b], A. Tudorache[e], V. Tudorache[e], O. Vazquez Doce[b], E. Widmann[a], B. Wünschek[a], and J. Zmeskal[a]

[a] *Stefan-Meyer-Institut für subatomare Physik, Vienna, AUSTRIA*
[b] *INFN, Laboratori di Frascati, Frascati (Roma), ITALY*
[c] *Dep. of Phys. and Astro., Univ. of Victoria, Victoria B.C., CANADA*
[d] *Politecnico di Milano, Sez. di Elettronica, Milano, ITALY*
[e] *IFIN-HH, Magurele, Bucharest, ROMANIA*
[f] *INFN, Sez. di Roma I and Inst. Superiore di Sanita, Roma, ITALY*
[g] *Univ. of Tokyo, Tokyo, JAPAN*
[h] *RIKEN, The Inst. of Phys. and Chem. Research, Saitama, JAPAN*
[i] *Tech. Univ. München, Physik Dep., Garching, GERMANY*

The strong-interaction shift of kaonic ^{3}He and ^{4}He $2p$ states was measured using gaseous targets for the first time in the SIDDHARTA experiment. The determined shift of kaonic ^{4}He is much smaller than the values obtained in the experiments performed in 70's and 80's. Thus, the problems in kaonic helium (the "kaonic helium puzzle") was definitely solved by our measurements. The first observation of the kaonic ^{3}He X-rays was also achieved. The shift both of kaonic ^{3}He and ^{4}He was found to be as small as a few eV.

1 Introduction

There was a serious problem in the strong-interaction shift of the kaonic ^{4}He $2p$ level. The experimentally determined shift of the kaonic ^{4}He $3d \rightarrow 2p$ X-ray transition gave a large shift (about -40 eV) [1], while a predicted value deduced from optical models using the kaonic atom data of $Z \geqslant 3$ was about 0 eV [2]. Recently this abnormal $2p$ level shift was focused on theoretical studies related to kaonic nuclear states, where a shift as large as 10

[1] tomoichi.ishiwatari@assoc.oeaw.ac.at

eV was estimated [3]. However, no theory could obtain such a large measured shift of -40 eV. Therefore, confirmation measurements were awaited for a long time.

The experiment by the KEK E570 collaboration determined the shift of $+2 \pm 2$ (stat) ± 2 (syst) eV [4], which disagreed with the previously measured value of -43 ± 8 eV.

Therefore, the SIDDHARTA experiment measured the kaonic ^{4}He X-rays to confirm the new result obtained by E570 [5]. In addition, the kaonic ^{3}He X-rays were measured using the same experimental apparatus, by replacing the target gas [6]. The latter was the world first's observation. This experiment provided new results on the kaon-helium interaction.

2 Experiment

The kaonic helium X-rays were measured in the SIDDHARTA experiment, which was performed in the DAΦNE e^+e^- collider at LNF (Italy). Charged kaon pairs produced by the annihilation of e^+e^- beams were detected by two scintillators installed in the interaction point. X-rays were detected using large area silicon drift detectors (SDDs) with a total area of 144 cm^2 [7]. Background events associated with the accelerator were rejected using the timing between the X-ray hits on the SDDs and the coincidence of K^+K^- pairs. A gaseous target was used in the measurement. The advantage was the negligible effect of Compton scattering in helium, where the contribution of the Compton tail was one of the difficulties in the analysis in the previous experiments [1, 4].

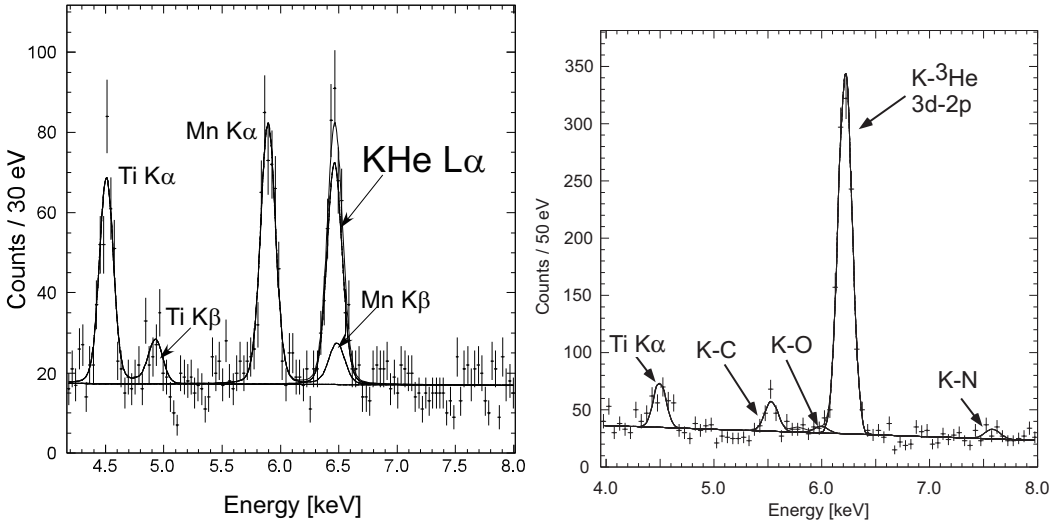

Figure 1: X-ray energy spectra of the $3d \rightarrow 2p$ transition of kaonic ^{4}He (left) and ^{3}He (right). The energy of these transitions were determined within an accuracy of a few eV.

The data of kaonic helium were taken during the beam time in 2009. The X-ray energy data of each SDD were calibrated using the X-ray tube installed in the setup. The background

events uncorrelated to the timing of production of kaonic atoms were rejected by the analysis. A detailed description of the analysis can be found in [5–7].

Figure 1(left) shows the X-ray energy spectrum of kaonic ^{4}He [5]. The position of the kaonic helium X-rays are indicated in the figure. The Mn Kα and Kβ lines were originated from an ^{55}Fe source installed in the setup. These lines were used for calibration purpose and stability check of the SDDs [7]. The right figure shows the X-ray energy spectrum of kaonic ^{3}He. In addition to the kaonic ^{3}He X-ray line, some kaonic atom X-ray lines were seen, which were originated from the material (Kapton Polyimide) of the target cell window [6].

The strong interaction shift of the kaonic He 2p states was obtained from the fit of the kaonic He X-ray peaks. The determined shifts are shown in Fig. 2.

3 Conclusions

The SIDDHARTA experiment measured the strong-interaction shift both of the kaonic ^{3}He and ^{4}He 2p levels with an accuracy of several eV. They were measured using gaseous targets for the first time, and the world first's observation of kaonic ^{3}He X-rays was achieved.

A large shift of the order of -40 eV determined by the experiments performed in 70's and 80's was not obtained neither in kaonic ^{3}He nor kaonic ^{4}He. Both are consistent with 0 eV within the errors. The results agree with theoretical predictions determined from other kaonic atoms with $Z \geqslant 3$ using optical model approaches [2]. However, the SIDDHARTA results may indicate a possible isotope shift between kaonic ^{3}He and kaonic ^{4}He. Also, the theoretical prediction by [3] cannot be excluded within our accuracy.

More precise measurements are very important to understand the kaon-helium interaction. Such precision measurements can be performed in the J-PARC E17 experiment [8].

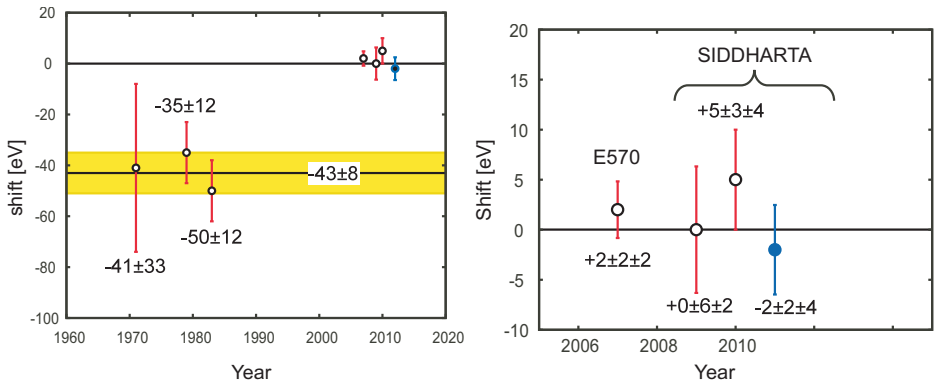

Figure 2: Comparison of experimental results. Open circle: K-^{4}He 2p state, Closed circle: K-^{3}He 2p state. A negative (positive) value of the shift shows a repulsive (attractive) shift.

Acknowledgments

We thank C. Capoccia, B. Dulach, and D. Tagnani from LNF-INFN; and H. Schneider, L. Stohwasser, and D. Stückler from Stefan-Meyer-Institut, for their fundamental contribution in designing and building the SIDDHARTA setup. We thank as well the DAΦNE staff for the excellent working conditions and permanent support. Part of this work was supported by HadronPhysics I3 FP6 European Community program, Contract No. RII3-CT-2004-506078; the European Community Research Infrastructure Integrating Activity "Study of Strongly Interacting Matter" (HadronPhysics2, Grant Agreement No. 227431) under the Seventh Framework Programme of EU; Austrian Federal Ministry of Science and Research BMBWK 650962/0001 VI/2/2009; Romanian National Authority for Scientific Research, Contract No. 2-CeX 06-11-11/2006; Grant-in-Aid for Specially Promoted Research (20002003), MEXT, Japan; and the Austrian Science Fund (FWF): [P20651-N20].

Bibliography

[1] S. Baird *et al.*, Nucl. Phys. A **392**, 297 (1983).

[2] C.J. Batty, Nucl. Phys. A **508**, 89c (1990).

[3] Y. Akaishi, *Proc. Inter. Conf. on Exotic Atoms (EXA05)*, Austrian Academy of Sciences Press, Vienna (2005), p. 45; `http://dx.doi.org/10.1553/exa05s45`.

[4] S. Okada *et al.*, Phys. Lett. B **653**, 387 (2007).

[5] SIDDHARTA Collaboration, Phys. Lett. B **681**, 310 (2009).

[6] SIDDHARTA Collaboration, Phys. Lett. B **697**, 199 (2011).

[7] M. Bazzi *et al.*, Nucl. Instr. and Meth. A **628**, 264 (2011).

[8] R. S. Hayano *et al.*, Proposal of J-PARC 50-GeV PS, *"Precision spectroscopy of Kaonic Helium 3 $3d \rightarrow 2p$ X-rays"*, (2006).

A new measurement of kaonic hydrogen atom X-rays at DAΦNE

Shinji Okada[1,a], M. Bazzi[a], G. Beer[b], C. Berucci[a], L. Bombelli[c], A.M. Bragadireanu[a,d], M. Cargnelli[e], A. Clozza[a], G. Corradi[a], C. Curceanu (Petrascu)[a], A. d'Uffizi[a], C. Fiorini[c], F. Ghio[f], B. Girolami[f], C. Guaraldo[a], R.S. Hayano[g], M. Iliescu[a,d], T. Ishiwatari[e], M. Iwasaki[h], P. Kienle[i], P. Levi Sandri[a], V. Lucherini[a], J. Marton[e], D. Pietreanu[d], K. Piscicchia[a], M. Poli Lener[a], T. Ponta[d], R. Quaglia[c], A. Rizzo[a], A. Romero Vidal[a], E. Sbardella[a], A. Scordo[a], H. Shi[g], D.L. Sirghi[a,d], F. Sirghi[a,d], H. Tatsuno[a], A. Tudorache[d], V. Tudorache[d], O. Vazquez Doce[a], E. Widmann[e], and J. Zmeskal[e] (SIDDHARTA collaboration)

[a] *INFN, Laboratori Nazionali di Frascati, Frascati (Roma), Italy*
[b] *Dep. of Phys. and Astro., Univ. of Victoria, Victoria B.C., Canada*
[c] *Politechno di Milano, Sez. di Elettronica, Milano, Italy*
[d] *IFIN-HH, Magurele, Bucharest, Romania*
[e] *Stefan-Meyer-Institut für subatomare Physik, Vienna, Austria*
[f] *INFN Sez. di Roma I and Inst. Superiore di Sanita, Roma, Italy*
[g] *Univ. of Tokyo, Tokyo, Japan*
[h] *RIKEN, The Inst. of Phys. and Chem. Research, Saitama, Japan*
[i] *Tech. Univ. München, Physik Dep., Garching, Germany*

Kaonic hydrogen atom provides a unique laboratory for studying the kaon-nucleon strong interaction at the threshold energy. The SIDDHARTA collaboration has measured the K-series x rays of kaonic hydrogen atoms at the DAΦNE electron-positron collider of Laboratori Nazionali di Frascati, and has determined the strong-interaction shift and width of the 1s atomic energy level with the best accuracy up to now. The measured shift and width result in the most precise value of the $\overline{K}N$ scattering lengths which will provide vital constraints on the theoretical description of the low-energy $\overline{K}N$ interaction.

1 Introduction

Kaonic hydrogen atom is a Coulomb bound system formed by a K^- and a proton, but is affected by the strong interaction at short range. The influence appears as a shifting of the 1s atomic energy level from its pure electromagnetic (EM) value and a broadening due to reducing the lifetime of the state by the absorption. The shift and width can be deduced

[1] shinji.okada@lnf.infn.it

by the spectroscopy of kaonic-hydrogen x-ray transitions feeding the 1*s* states, namely the *K*-series x rays.

It is well known that the measured strong-interaction shift and width are directly related to the real and imaginary parts of the complex $K^- p$ *S*-wave scattering length [1]. The kaonic-hydrogen x-ray data are therefore crucial for theories of the $\overline{K}N$ system together with the low-energy $\overline{K}N$ data.

The low-energy $\overline{K}N$ system has attracted attention as a testing ground for chiral SU(3) dynamics in low-energy QCD and the role of explicit chiral symmetry-breaking due to the relatively large strange quark mass. The data are also strongly related to recent hot topics – the structure of the $\Lambda(1405)$ resonance and the deeply bound kaonic systems. Recent progress of this field is summarized in [2].

In the current experiment, called SIDDHARTA, we have measured the *K*-series x rays of kaonic hydrogen atoms and determined the most precise values of the strong-interaction shift and width of the 1*s* energy level. Recently, the final result is submitted for publication [3]. In this paper, we present an overview of the kaonic hydrogen measurement.

2 Experiment

The SIDDHARTA experiment was performed at the DAΦNE positron-electron collider. The collider produces the ϕ-resonances of which 49 % decay into back-to-back K^+K^- pairs. Resulting monochromatic low-energy kaons were degraded and stopped in a cryogenic hydrogen gaseous target. A coincidence of two plastic scintillation counters mounted above and below the e^+e^- interaction point was used as a kaon trigger. X rays emitted from the kaonic atoms were detected by 144 silicon drift detectors (SDDs), each having an effective area of 1 cm^2, developed within a European research project devoted to this experiment. The SDD has an excellent energy resolution of $\sim$ 180 eV (FWHM) at 6 keV and a good timing resolution of $\sim$ 800 ns (FWHM). A detailed description of our experimental setup is given in [3, 4].

3 Result

Figure 1 (a) shows a kaonic-hydrogen x-ray spectrum. We have also measured x-ray spectrum with a deuterium target (for the first-ever exploratory measurement of kaonic-deuterium x rays), as shown in Fig. 1 (b). The kaonic-hydrogen x-ray transitions were clearly observed while those for kaonic deuterium were not visible. This appears to be consistent with the theoretical expectation that kaonic deuterium x rays have one order lower yield per stopped K^- and greater width than those of kaonic hydrogen x rays (*e.g.*, [5]).

A dot-dashed line in Fig. 1 (a) indicates the EM value of the kaonic-hydrogen $K\alpha$. Comparing the kaonic-hydrogen $K\alpha$ peak and the EM value, there is no room for doubt about a

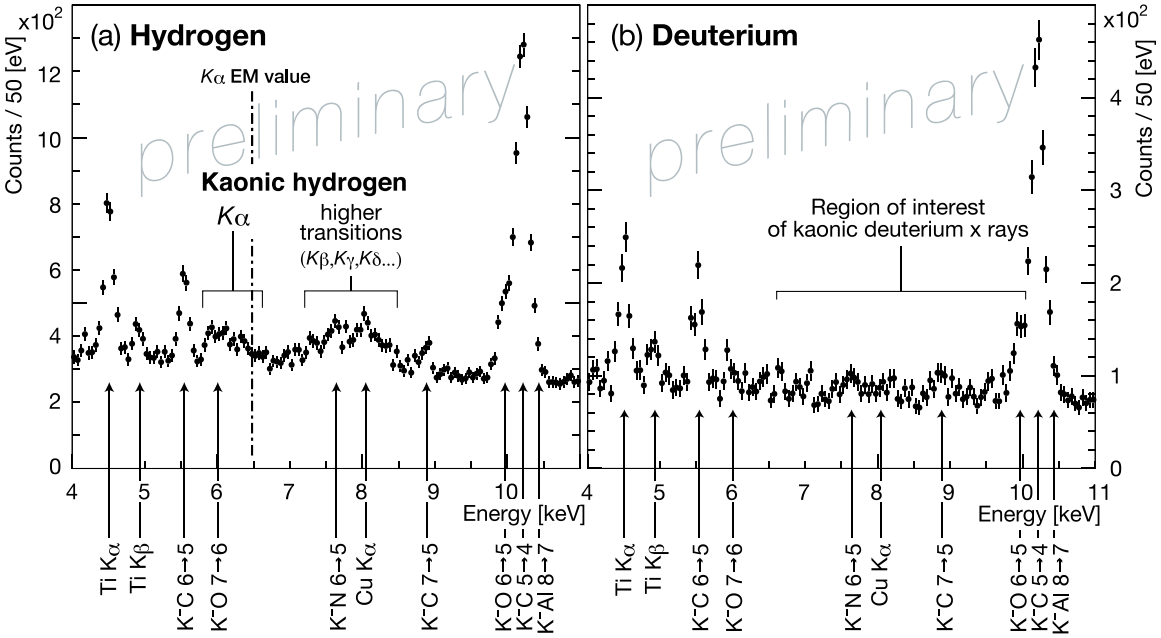

Figure 1: The measured x-ray spectra taken (a) with hydrogen target and (b) with deuterium target. The dot-dashed vertical line indicates the EM value of the kaonic-hydrogen $K\alpha$.

repulsive-type shift of the kaonic-hydrogen 1s-energy level, which is consistent with the analysis of the low energy $\overline{K}N$ scattering data.

The continuous background is related to the following two type of particles: the charged kaon secondaries (synchronous background) and lost beam particles (asynchronous background). In the most recent measurement of the kaonic hydrogen x-ray (DEAR) [6] performed at DAΦNE as well, the kaonic-hydrogen spectrum suffered from the huge asynchronous background due to lack of the timing capability of x-ray detectors (CCDs) used. The event selection using time difference between kaon arrival (with kaon detectors) and x-ray detection (with SDDs) significantly reduced the asynchronous background and improved the signal-to-background ratio by more than a factor of 10 with respect to the corresponding DEAR ratio of about 1/100.

Many other kaonic-atom x rays and characteristic x rays were detected in both spectra as indicated with arrows in the figures. Those kaonic-atom lines are attributable to the target-cell wall made of Kapton polyimide film ($C_{22}H_{10}O_5N_2$) and its support frames made of aluminum. The characteristic x rays come from high-purity titanium and copper foils installed for *in-situ* x-ray energy calibration.

There are three background x-ray lines overlapping with the kaonic-hydrogen signals : kaonic oxygen 7-6 (6.0 keV), kaonic nitrogen 6-5 (7.6 keV) and fluorescence x ray of copper

$K\alpha$ (8.0 keV). In the fitting procedure of the kaonic-hydrogen spectrum, it turned out to be essential to use the kaonic-deuterium spectrum to quantify the kaonic background x-ray lines. We have therefore performed a global simultaneous fit of the hydrogen and deuterium spectra, where the background intensities were determined using both spectra and a normalization factor defined by the ratio of the high-statistics kaonic-carbon 5-4 peak in both spectra.

As a result, we have determined the most precise values of the strong-interaction energy-level shift and width of the kaonic-hydrogen atom 1s state [3]. Our determination of the shift and width allows more precise evaluation of $\overline{K}N$ scattering lengths which will yield vital constraints on the theoretical description of the low-energy $\overline{K}N$ interaction.

Acknowledgments

We thank C. Capoccia, B. Dulach, and D. Tagnani from LNF-INFN; and H. Schneider, L. Stohwasser, and D. Stückler from Stefan-Meyer-Institut, for their fundamental contribution in designing and building the SIDDHARTA setup. We thank as well the DAΦNE staff for the excellent working conditions and permanent support. Part of this work was supported by HadronPhysics I3 FP6 European Community program, Contract No. RII3-CT-2004-506078; the European Community-Research Infrastructure Integrating Activity "Study of Strongly Interacting Matter" (HadronPhysics2, Grant Agreement No. 227431) under the Seventh Framework Programme of EU; Austrian Federal Ministry of Science and Research BMBWK 650962/0001 VI/2/2009; Romanian National Authority for Scientific Research, Contract No. 2-CeX 06-11-11/2006; and the Grant-in-Aid for Specially Promoted Research (20002003), MEXT, Japan.

Bibliography

[1] S. Deser et al., Phys. Rev. 96 (1954) 774; T. L. Trueman, Nucl. Phys. 26 (1961) 57; A. Deloff, Phys. Rev. C 13 (1976) 730.

[2] C. Curceanu, J. Zmeskal, Mini-Proceedings of ECT Workshop "Strangeness in Nuclei", arXiv:1104.1926, and references therein.

[3] SIDDHARTA Collaboration, arXiv:1105.3090, Phys. Lett. B, submitted for publication.

[4] SIDDHARTA Collaboration, Phys. Lett. B 681 (2009) 310; Phys. Lett. B 693 (2011) 199.

[5] T. Koike, T. Harada, Y. Akaishi, Phys. Rev. C 53 (1996) 79.

[6] G. Beer *et al.*, Phys. Rev. Lett. 94 (2005) 212302.

Photoproduction of η' Mesons from Nuclei

Mariana Nanova[1] on behalf of the CBELSA/TAPS Collaboration
II. Physikalisches Institut
Universität Giessen,
D-35392 Giessen, GERMANY

The photoproduction of η'-mesons from different nuclei has been measured using the Crystal Barrel(CB)/TAPS detector system at the ELSA accelerator facility in Bonn. Recent results on the in-medium properties of the η'-meson, derived from the transparency ratio measurements, are presented. The absorption of the η'-meson in nuclear matter is compared to the properties of the other mesons (η and ω).

1 Introduction

As we know from hadron physics, the light pseudoscalar mesons (π, K, η) are the Nambu-Goldstone bosons associated with the spontaneous breaking of the QCD chiral symmetry. Introducing the current quark masses these mesons together with the heavier $\eta'(958)$ meson show a mass spectrum which is believed to be explained by the explicit flavor $SU(3)$ breaking and the axial $U_A(1)$ anomaly. Recently, there have been several important developments in the study of the spontaneous breaking of chiral symmetry and its partial restoration at finite density. Theoretical studies predict a possible mass shift of the η'-meson at finite density and the formation of bound states [1]. Up to the last two years η' photoproduction was not much explored, but with new generation experiments results on differential and total cross sections of η' photoproduction on the proton [2] and the deuteron [3] have now become available.
The investigation of η'-meson production in photon induced reactions on solid target provides information on in-medium properties of the meson. The in-medium width of the η'-meson can be extracted from the attenuation of the meson flux deduced from a transparency ratio measurement. However, η'-meson will decay outside of the nucleus because of their long lifetime and thus their in-medium mass is not directly accessible experimentally. Consequently, an experimental observation of a possible mass shift of the η'-meson in-medium is extremly difficult. In the present work, we concentrate on the transparency ratio measurement of the η'-meson and disccuss its absorption properties.

[1]Mariana.Nanova@physik.uni-giessen.de

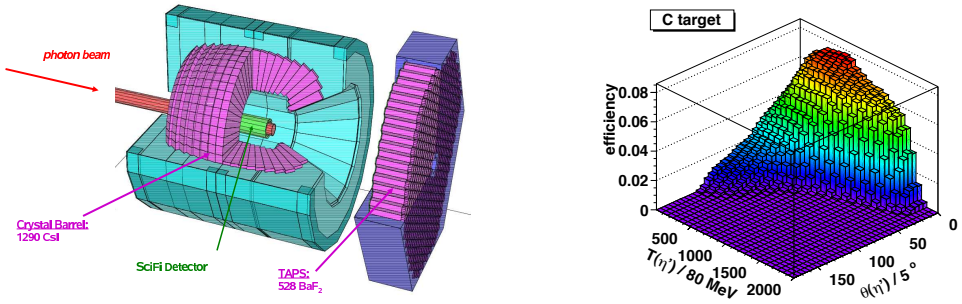

Figure 1: (Color online) Left: Sketch of the CB/TAPS setup. The tagged photons impinge on the nuclear target in the center of the Crystal Barrel detector. The TAPS detector at a distance of 1.18 m from the target serves as a forward wall of the Crystal Barrel. The combined detector system provides photon detection capability over almost the full solid angle. Charged particles leaving the target are identified in the inner scintillating-fiber detector and in the plastic scintillators in front of each BaF_2 crystal in TAPS. Right: Detector acceptance for the $\eta' \rightarrow \pi^0\pi^0\eta$ decay as a function of the kinetic energy (T) and the polar angle (θ) for an incident photon energy range of 1200 to 2200 MeV. The simulation is for a carbon (C) target, taking the trigger conditions into account.

2 Data Analysis

The experiment has been performed at the ELSA facility in Bonn [4, 5] using the Crystal Barrel(CB) [6] and TAPS [7] detector system (Fig. 1 left). The combined Crystal Barrel/TAPS detector covered 99% of the full 4π solid angle. The high granularity of the system makes it very well suited for the detection of multi-photon final states. Tagged photon beams of energy up to 2.6 GeV were produced via bremsstrahlung and impinged on a solid target. For the measurements targets of C, Ca, Nb and Pb were used. A more detailed description of the detector setup and the running conditions have been given in [8, 9].

The detector acceptance was determined by Monte Carlo simulations using the GEANT3 package, including all features of the detector system, trigger conditions and all cuts for particle indentification. To avoid further uncertainties due to reaction kinematics and final state interactions, the η'-meson detection efficiency was simulated as a function of the kinetic energy and the polar angle - $\epsilon(T_{\eta'}, \theta_{\eta'})$. Typical efficiencies are 7% and slighly different for the different targets. The detection efficiency for η' on the C target, taking the trigger conditions into account, is shown in Fig. 1 (right). Experimental data are efficiency corrected event-by-event with this acceptance as described in [3].

The η'-mesons were identified via the $\eta' \rightarrow \pi^0\pi^0\eta \rightarrow 6\gamma$ decay channel, which has a branching ratio of 8%. For the reconstruction of the η'-mesons only events with at least 6 or 7 neutral hits have been selected. The competing channel with the same final state,

namely $\eta \rightarrow \pi^0\pi^0\pi^0 \rightarrow 6\gamma$, has been reconstructed and the corresponding events have been rejected from the further analysis. In addition only events were kept with at least one combination of the 6 photons to two photon pairs with invariant masses between 110 and 160 MeV (π^0) and one pair between 500 and 600 MeV (η). The $\pi^0\pi^0\eta$ invariant mass distributions for the different solid targets are shown in Fig. 2. The resulting cross sections are used to calculate the transparency ratio of the η'-meson for a given nucleus A from the formula (1), normalized to the carbon data:

$$T_A = \frac{12 \cdot \sigma_{\gamma A \rightarrow \eta' A'}}{A \cdot \sigma_{\gamma C \rightarrow \eta' C}} \,. \tag{1}$$

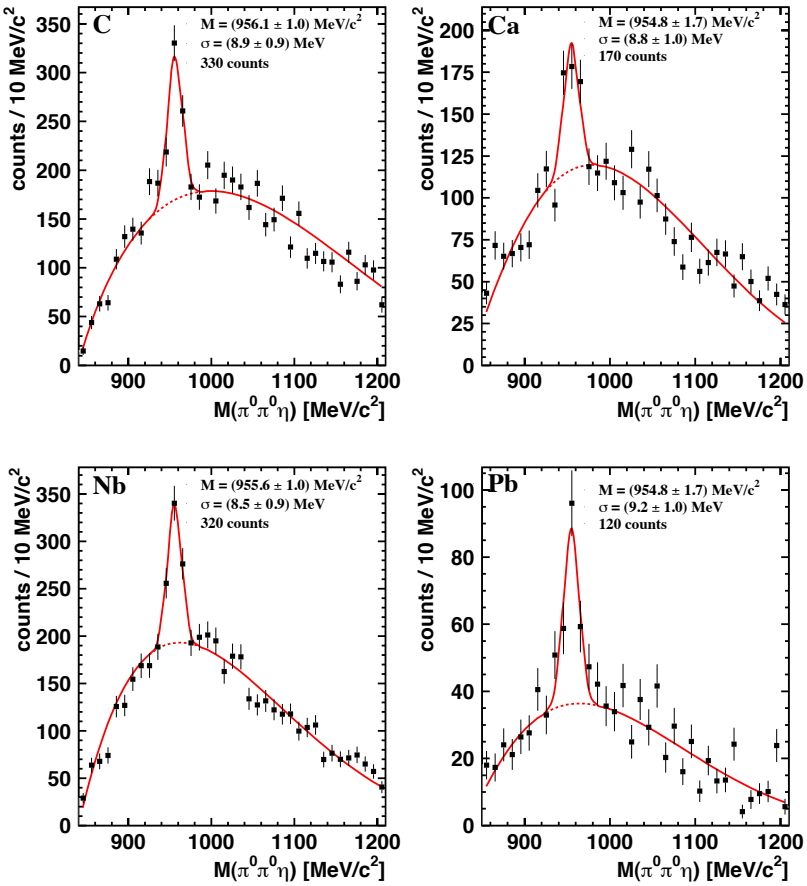

Figure 2: Invariant mass spectrum of $\pi^0\pi^0\eta$ for ^{12}C, ^{40}Ca, ^{93}Nb and ^{208}Pb targets in incident photon energy range 1200 - 2200 MeV. The distributions have not been corrected for the detector acceptance. The solid curve is a fit to the spectrum. See text for more details.

T_A describes the loss of flux of η'-mesons in nuclei via inelastic processes like: $\eta' N \rightarrow \pi^0 N$.

To avoid systematic uncertainties due to unknown secondary production processes, the transparency ratio has been normalized to a light target with equal numbers of protons and neutrons (C) and not to the cross section on the nucleon.

3 Results and Discussion

The transparency ratio has been extracted as defined in Eq. 1 and is shown in Fig. 3 as full (red) triangles. The data are compared to the transparency ratio of the ω-meson measured by [10]. The solid lines are fits to the data points, yielding slope parameters of -0.14 and -0.33 for $\eta^{'}$ and ω, respectively. As it can be seen from the figure, $\eta^{'}$-mesons are only weakly absorbed via inelastic channels like $\eta^{'}N \rightarrow \pi N$ as compared to the ω-meson. Information on the in-medium width of the $\eta^{'}$ is still not available since theoretical calculations are needed. It is important to study also the contribution of secondary production processes like $\pi N \rightarrow \eta^{'}N$, which could increase the number of observed η'-mesons and thus distort the transparency ratio.

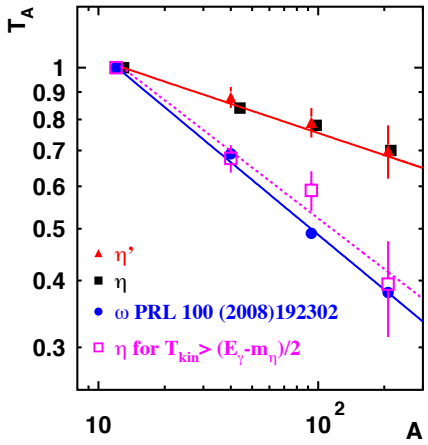

Figure 3: Transparency ratio for the η'-meson (full red triangles) in the incident photon energy range 1200 - 2200 MeV compared to the transparency ratio for the ω-meson (full blue circles) [10] and for the η-meson without (full black sqares) and with (empty magenta squares) a cut on the kinetic energy. The solid curve is a fit to the spectrum. See text for more details.

At least for η photoproduction this effect has been studied and has been found to have a significant contribution [11]. As it can be seen in Fig. 3, after applying the condition to select η-mesons with higher kinetic energy as suggested in [11] the transparency ratio has

changed dramatically and shows a slope of -0.33 which is quite different from the previous one - the empty (magenta) squares in Fig. 3. For this reason a new analysis of the data has been started with a condition to select only $\eta^{'}$-mesons with a higher kinetic energy to suppress the contribution from $\pi N \rightarrow \eta^{'} N$ channels. The results will be prepared for publication very soon.

Acknowledgments

We thank the scientific and technical staff at ELSA and the collaborating institutions for their important contribution to the experiment. This work is supported by DFG through SFB/TR 16 "subnuclear structure of matter" and by the Schweizerischer Nationalfond.

Bibliography

[1] H. Nagahiro, M. Takizawa, S. Hirenzaki, Phys. Rev. C, **74**, 045203 (2006).

[2] V. Crede *et al.*, CBELSA/TAPS Collaboration, Phys. Rev. C, **80**, 055202 (2009).

[3] I. Jaegle *et al.*, CBELSA/TAPS Collaboration, Eur. Phys. J. A **47**, 11 (2011).

[4] D. Husmann, and W. J. Schwille, Phys. Bl. **44**, 40 (1988).

[5] W. Hillert, Eur. Phys. J. A **28**, 139 (2006).

[6] E. Aker *et al.*, Nucl. Instr. and Methods A **321**, 69 (1992).

[7] R. Novotny *et al.*, IEEE Trans. Nucl. Sci. **38**, 392 (1991).

[8] M. Nanova *et al.*, CBELSA/TAPS Collaboration, Phys. Rev. C **82**, 035209 (2010).

[9] D. Elsner *et al.*, Eur. Phys. J. A **33**, 147 (2007).

[10] M. Kotulla *et al.*, Phys. Rev. Lett. **100**, 192302 (2008).

[11] T. Mertens *et al.*, CBELSA/TAPS Collaboration, Eur. Phys. J. A **38**, 195 (2008).

$\overline{K}^*$ mesons in matter

Raquel Molina[1,a], Laura Tolós[b], Ángels Ramos[c], and Eulogio Oset[a]
[a]*Instituto de Física Corpuscular (IFIC, centro mixto CSIC-UV), Valencia, Spain*
[b]*Instituto de Ciencias del Espacio (ICE, CSIC), Barcelona, Spain*
[c]*Universidad de Barcelona, Barcelona, Spain*

We study the properties of $\overline{K}^*$ mesons in nuclear matter. The $\overline{K}^*$ self-energy is evaluated in dense matter, which consists of two components: The interaction of $\overline{K}^*$ mesons with nucleons, and the renormalization of its decay channel, $\overline{K}\pi$, in nuclear matter. For the first part of the selfenergy, a unitary approach in coupled channels within the framework of the local hidden gauge formalism is used. The in-medium $\overline{K}^*N$ interaction accounts for Pauli blocking effects and the inclusion of the $\overline{K}^*$ selfenergy in a self-consistent manner. In addition, the ratio of the $\gamma A \to K^+ K^{*-} A'$ reaction is calculated, which will be useful for future observations. The results are rather spectacular since the $\overline{K}^*$ develops an in-medium width of 260 MeV, five times larger than in free space and much bigger than for the ρ meson.

1 Introduction

The investigation of the interaction of vector mesons with nuclear matter has been a matter of debate for a long time. In contrast to the model derived by Hatsuda and Lee [1], which predicts a 20% decrease in the ρ mass at ρ_0, $m = m_0(1 - 0.16\,\frac{\rho}{\rho_0})$, the Nambu Jona Lasinio model [2] tell us there is no shift of the vector masses. Moreover, detailed calculations show a broadening of the ρ, ω and ϕ mesons in nuclear matter and small changes in the masses [3–5]. However, no discussion has been made about the properties of strange vector mesons ($\overline{K}^*$) in the medium, which is the focus of attention of this work. The $\overline{K}^*$ selfenergy have two components, the in-medium $\overline{K}^*$ interaction with nucleons that accounts for Pauli-blocking and is incorporated in a selfconsistent way and the $\overline{K}\pi$ decay channel in matter. In this paper we evaluate the $\overline{K}^*N$ spectral function and analyze the $\gamma A \to K^+ K^{*-} A'$ ratio, which can give us valuable information for future experiments involving $\overline{K}^*$ in matter.

2 Formalism: The $\overline{K}^*$ selfenergy

In this section we briefly summarize the procedure in order to evaluate the $\overline{K}^*$ selfenergy. We refer to [6] for a detailed explanation. The two sources of modification of the $\overline{K}^*$ selfenergy in nuclear matter are:

[1]rmolina@ific.uv.es

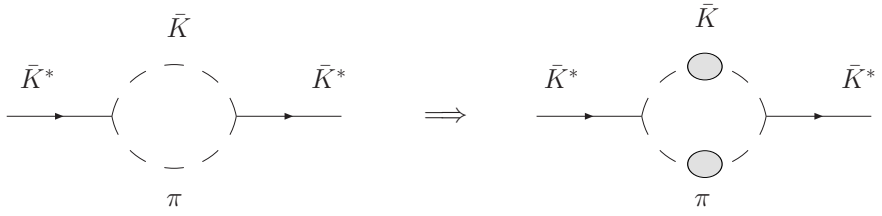

Figure 1: The $\overline{K}$ propagator renormalized to allow its decay into $\overline{K}\pi$, in the free space (left), and in the medium (right), including the self-energies of the $\overline{K}$ and π mesons.

a) **The contribution of the decay mode $\overline{K}\pi$ in dense matter**. In order to evaluate this part, we need to include the selfenergies of the $\overline{K}$ and π in the loop, as shown in Fig. 1. In the free space, for the first diagram in Fig. 1, we have

$$\Pi^0_{\overline{K}^*}(q^0,\vec{q}\,) = 2g^2\vec{\epsilon}\cdot\vec{\epsilon}\,' \int \frac{d^4k}{(2\pi)^4}\frac{\vec{k}^{\,2}}{k^2-m_\pi^2}\frac{1}{(q-k)^2-m_{\overline{K}}^2+i\epsilon}\,. \tag{1}$$

The imaginary part of the $\overline{K}^*$ selfenergy at rest provides the theoretical value of the $\overline{K}^*$ width, $\Gamma_{K^{*-}} = -\mathrm{Im}\Pi^0_{\overline{K}^*}/m_{\overline{K}^*} = 42$ MeV, which is quite close to the experimental value of $\Gamma^{\mathbf{exp}}_{K^{*-}} = 50.8 \pm 0.9$ MeV. In the medium, we have, on one hand, the contribution of the $\overline{K}$ selfenergy that considers interactions of the type $\overline{K}N \to \pi\Sigma$, $\pi\Lambda$, $\overline{K}N$ ..., in s-wave and $\overline{K}N \to \Lambda$, Σ or Σ^* in p-wave. On the other hand, the pion selfenergy (mostly p-wave) includes particle(p)-hole(h), Δ-h and 2p-2h excitation. This is done through the Lehman representation of the propagators:

$$\begin{aligned} -i\Pi^{\rho,(\mathrm{a})}_{\overline{K}^*}(q^0,\vec{q}\,) = \quad & 2\,g^2\vec{\epsilon}\cdot\vec{\epsilon}\,' \int \frac{d^4k}{(2\pi)^4}\vec{k}^{\,2}\int_0^\infty \frac{d\omega}{\pi}(-2\omega)\frac{\mathrm{Im}D_\pi(\omega,\vec{k}\,)}{(k^0)^2-\omega^2+i\epsilon} \\ \times \quad & \int_0^\infty \frac{d\omega'}{\pi}(-)\left\{\frac{\mathrm{Im}D_{\overline{K}}(\omega',\vec{q}-\vec{k}\,)}{q^0-k^0-\omega'+i\eta} - \frac{\mathrm{Im}D_K(\omega',\vec{q}-\vec{k}\,)}{q^0-k^0+\omega'-i\eta}\right\}\,, \end{aligned} \tag{2}$$

where the real part of the free $\overline{K}^*$ selfenergy has been subtracted since we use the physical mass of the $\overline{K}^*$. Moreover, one has to implement the vertex corrections to guarantee the gauge invariance of the model, to which, one simply replaces the p-wave pion selfenergy with:

$$\Pi^{(p)}_\pi \Longrightarrow \frac{\Pi^{(p)}_\pi}{\vec{k}^{\,2}}\left(\vec{k}^{\,2} + \left[D^0_\pi(k)\right]^{-1} + \frac{3}{4}\frac{\left[D^0_\pi(k)\right]^{-2}}{\vec{k}^{\,2}}\right)\,, \tag{3}$$

with $\left[D^0_\pi(k)\right]^{-1} = (k^0)^2 - \vec{k}^{\,2} - m_\pi^2$.

b) $\overline{K}^*$ **self-energy from the s-wave $\overline{K}^*N$ interaction.** This includes quasi-elastic process, $\overline{K}^*N \to \overline{K}^*N$, and absorption channels, $\overline{K}^*N \to \rho Y, \omega Y, \phi Y, \ldots$ with $Y = \Lambda, \Sigma$. We

follow the work of [7] for the interaction of a $\overline{K}^*$ with nucleons. In this framework the antikaon interacts with a nucleon by means of the exchange of a vector meson. The Lagrangian for the three-vector vertex is provided by the hidden gauge formalism and the constructed $VB \to VB$ transition potential is used as the kernel of the Bethe Salpeter equation, $T = [1 - V * 40 * G]^{-1} V$.

The medium modifications are incorporated in the loop function of the two vector mesons, G. One of the sources of density dependence comes from the Pauli principle acting on the nucleons and another source is the $\overline{K}^*$ self-energy incorporated in the $\overline{K}^* N$ intermediate states self-consistently. The in-medium $\overline{K}^*$ self-energy is then obtained by integrating $T^{\rho}_{\overline{K}^* N}$ over the nucleon Fermi sea,

$$\Pi^{\rho,(b)}_{\overline{K}^*}(q^0, \vec{q}\,) = \int \frac{d^3p}{(2\pi)^3}\, n(\vec{p}\,) \left[T^{\rho\,(I=0)}_{\overline{K}^* N}(P^0, \vec{P}) + 3T^{\rho\,(I=1)}_{\overline{K}^* N}(P^0, \vec{P}) \right] . \tag{4}$$

The self-energy $\Pi^{\rho,(b)}_{\overline{K}^*}$ is determined self-consistently since the in-medium amplitude $T^{\rho}_{\overline{K}^* N}$ depends also on $\Pi^{\rho,(a)}_{\overline{K}^*}$ and $\Pi^{\rho,(b)}_{\overline{K}^*}$.

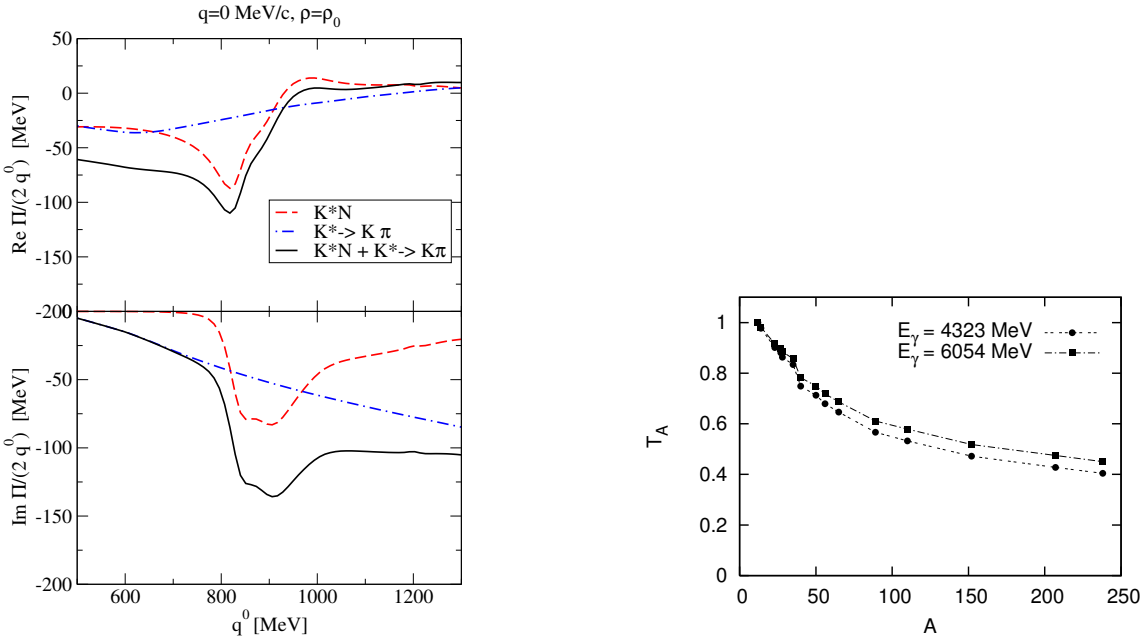

Figure 2: Left: real and imaginary parts of the $\overline{K}^*$ self-energy as functions of the meson energy q^0 for zero momentum and normal density ρ_0 showing the different contributions: (i) self-consistent calculation of the $\overline{K}^* N$ interaction (dashed lines), (ii) self-energy coming from $\overline{K}^* \to \overline{K}\pi$ decay (dot-dashed lines), and (iii) combined self-energy from both previous sources (solid lines). Right: transparency ratio

3 Results

We show in Fig. 2(left) the $\overline{K}^*$ self-energy at ρ_0 (solid line) due to the different processes, $\overline{K}^* \to \overline{K}\pi$ in the medium (dot-dashed lines), and $\overline{K}^* N$ interaction (dashed line). For $\overline{K}^*$ energies around 800-900 MeV we observe an enhancement of the width together with some structures in the real part of the self-energy. This comes from the coupling of the $\overline{K}^*$ to the dynamically generated $\Lambda(1783)N^{-1}$ and $\Sigma(1830)N^{-1}$ excitations. At low energies, the width of the $\overline{K}^*$ is governed by the $\overline{K}\pi$ decay mechanism in dense matter. At the $\overline{K}^*$ mass, the $\overline{K}^*$ feels a moderately attractive optical potential and acquires a width of 260 MeV, which is about 5 times its width in vacuum.

In Fig. 2(right), the transparency ratio is plotted for two different energies. We observe a very strong attenuation of the $\overline{K}^*$ production process due to the decay or absorption channels $\overline{K}^* \to \overline{K}\pi$ and $\overline{K}^* N \to VY$ with increasing nuclear-mass number A. This is due to the larger path that the $\overline{K}^*$ has to follow before it leaves the nucleus, having more chances to decay or get absorbed. The analysis of the transparency ratio is a very efficient experimental tool to study changes in the width of hadrons in dense matter.

Bibliography

[1] G. E. Brown and M. Rho, Phys. Rev. Lett. **66**, 2720 (1991)

[2] V. Bernard and U. G. Meissner, Nucl. Phys. A **489**, 647 (1988)

[3] W. Peters, M. Post, H. Lenske, S. Leupold and U. Mosel, Nucl. Phys. A **632**, 109 (1998). D. Cabrera, E. Oset and M. J. Vicente Vacas, Nucl. Phys. A **705**, 90 (2002)

[4] M. Kaskulov, E. Hernandez and E. Oset, Eur. Phys. J. A **31**, 245 (2007)

[5] D. Cabrera and M. J. Vicente Vacas, Phys. Rev. C **67**, 045203 (2003)

[6] L. Tolos, R. Molina, E. Oset, A. Ramos, Phys. Rev. **C82**, 045210 (2010).

[7] E. Oset and A. Ramos, Eur. Phys. J. A **44**, 445 (2010)

Determination of the in-medium ϕ-meson width from proton-nucleus collisions

Andrey Polyanskiy[1,a,b], M. Hartmann[a], B. Kämpfer[c], Yu. T. Kiselev[b], V. K. Magas[d]
E. Ya. Paryev[e], L. Roca[f], H. Schade[c], and C. Wilkin[g]
[a] *Institut für Kernphysik and Jülich Centre for Hadron Physics, Forschungszentrum Jülich, D-52425 Jülich, Germany*
[b] *Institute for Theoretical and Experimental Physics, RU-117312 Moscow, Russia*
[c] *Forschungszentrum Dresden Rossendorf, D-01314 Dresden, Germany*
[d] *Departament d'Estructura i Constituents de la Materia and Institut de Ciencies del Cosmos, Universitat de Barcelona, 08028 Barcelona, Spain*
[e] *Institute for Nuclear Research, Russian Academy of Science, RU-117312 Moscow, Russia*
[f] *Departamento de Física, Universidad de Murcia, E-30071 Murcia, Spain*
[g] *Physics and Astronomy Department, UCL, London WC1E 6BT, United Kingdom*

The production of ϕ mesons on C, Cu, Ag, and Au targets has been measured via the $\phi \to K^+K^-$ decay at an incident proton energy of 2.83 GeV with the ANKE spectrometer at COSY. From an analysis of the target mass dependence of the production cross section the in-medium ϕ width have been extracted in the momentum region of 0.6–1.6 GeV/c for normal nuclear density and compared with results of other experiments.

1 Introduction

The study of the effective masses and widths of light vector mesons in nuclear medium, through their production with hadron, heavy–ion and photon beams incident on nuclear targets, has received considerable attention in recent years [1,2]. The vacuum width of the $\phi(1020)$ meson is narrow compared to other nearby resonances. It is therefore the best place to test for medium modifications because small effects should be experimentally observable. The main modification of the ϕ in nuclear matter is expected to be a broadening of its spectral function, whereas its mass should be hardly changed.

Dileptons from $\phi \to e^+e^-/\mu^+\mu^-$ decays experience no strong final-state interactions in a nucleus. Broadening of the ϕ in the nucleus should be directly testable by examining $\ell^+\ell^-$ mass spectra. However, such a measurement is difficult due to the low branching ratios.

[1] a.polyanskiy@fz-juelich.de

The KEK-PS-E325 collaboration measured e^+e^- invariant mass distributions in the ϕ region in proton-induced reactions on carbon and copper at 12 GeV and deduced a mass shift of 3.4% and a width increase by a factor of 3.6 at normal nuclear density ρ_0 for ϕ momenta around 1 GeV/c [3]. This corresponds to an in-medium ϕ width of about 11 MeV in the nuclear rest frame for the average measured ϕ momentum.

An alternative way to determine the in-medium broadening of the ϕ meson has been adopted in [4, 5]. The variation of the ϕ production cross section (or nuclear transparency ratio) with atomic number A has been studied both experimentally and theoretically. This A-variation depends on the attenuation of the ϕ flux in the nuclear target which, in turn, is governed by the imaginary part of the in-medium ϕ self-energy or width. In the low-density approximation, this width is related to an effective ϕN total cross section $\sigma_{\phi N}$ [2].

A large in-medium ϕN total cross section of about 35 mb was inferred by the LEPS collaboration from measurements of K^+K^- pairs photoproduced on Li, C, Al and Cu targets at SPring-8 for average ϕ momenta $\approx$ 1.8 GeV/c [4]. In the low-density approximation, this implies an in-medium ϕ width of about 97 MeV/c^2 in the nuclear rest frame at density ρ_0. The value of $\sigma_{\phi N}$ is significantly larger than the cross section in free space, viz. $\approx$ 10 mb.

The CLAS collaboration studied ϕ photoproduction on ^{2}H, C, Ti, Fe, Pb targets by measuring the e^+e^- decay [5]. From an analysis of the transparency ratios normalised to carbon within the Glauber model, values of $\sigma_{\phi N}$ in the range of 16–70 mb were extracted for an average ϕ momentum of $\approx$ 2 GeV/c, which is not inconsistent with the LEPS result.

Both the LEPS and CLAS results are larger than that obtained at KEK. One possible reason for the discrepancy could be the different ϕ momenta. A study of momentum dependence of the in-medium width could therefore provide useful information about the properties of the ϕ meson in a nucleus.

2 Experiment and Results

We have measured the production of ϕ mesons at small angles in the collisions of 2.83 GeV protons with C, Cu, Ag, and Au targets via the $\phi \to K^+K^-$ decay, using the ANKE-COSY magnetic spectrometer. The 2.83 GeV proton beam energy corresponds to an excess energy of about 76 MeV above the free NN threshold where few production channels are open. Secondary ϕ production processes are also expected to be less important at small angles.

As a first step, we have studied the nuclear transparency ratio normalised to carbon, $R = (12/A)(\sigma^A/\sigma^C)$, averaged over the ϕ momentum range 0.6–1.6 GeV/c [6, 7]. Here σ^A and σ^C are inclusive cross sections for ϕ production in pA (A = Cu, Ag, Au) and pC collisions in the angular cone $\theta_\phi < 8^\circ$. The comparison of the ratio with model calculations [8, 9] yields an in-medium ϕ width of $33 - 50$ MeV/c^2 in the nuclear rest frame for an average ϕ momentum of 1.1 GeV/c for normal nuclear density ρ_0=0.16 fm^{-3}.

The large number of reconstructed ϕ mesons for each target (7000–10000) allows the data to be put into six bins of approximately equal statistics in order to carry out more detailed studies. In Fig. 1 the preliminary results on the momentum dependence of the measured transparency ratios is shown for different nuclei. A decrease of the ratios with p_ϕ could be a signal of contributions of secondary ϕ production processes, especially for the lower momentum.

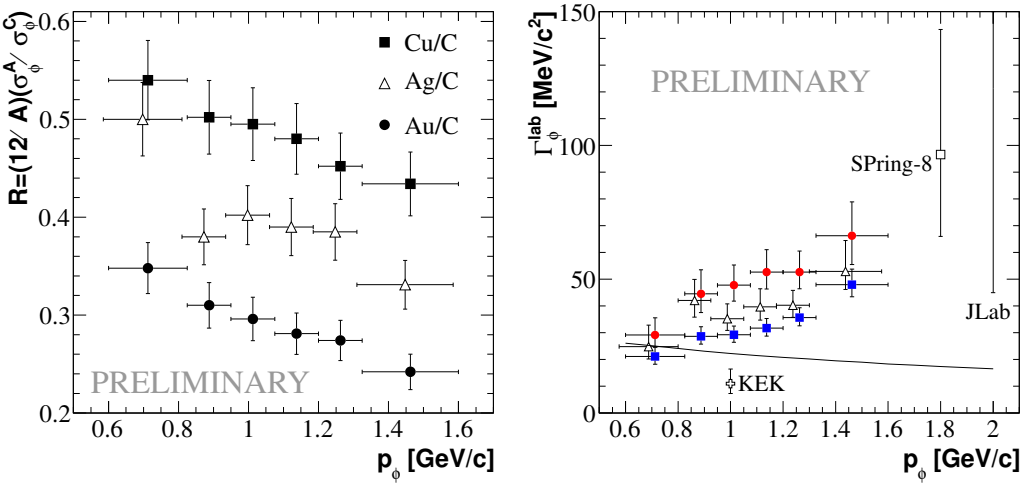

Figure 1: Left: Momentum dependence of the transparency ratios for the four nuclei studied. Right: Momentum dependence of the ϕ in-medium width for normal nuclear density exctracted using different models: Model 1 (blue squares), Model 2 (red circles) and Model 3 (open triangles). Experimental results by KEK-PS-E325 [3], Spring-8 [4] and JLab [5] are also plotted. The theoretical prediction of [10, 11] is shown by the solid line.

Any extraction of in-medium ϕ widths is model dependent; we consider three approaches.
Model 1: The eikonal approximation of the Valencia group [8] uses the predicted ϕ self-energy in nuclear medium [10, 11] both for the one-step ($pN \to pN\phi$) and for the two-step ϕ production processes, with nucleon and Δ intermediate states.
Model 2: Paryev [9] developed the spectral function approach for ϕ production in both the primary proton-nucleon and secondary pion-nucleon channels.
Model 3: The Rossendorf BUU transport calculation [12] includes a variety of secondary ϕ production processes. In contrast to Models 1 and 2, where ϕ absorption is governed by its width, Γ_ϕ, Model 3 describes it in terms of an effective in-medium ϕN cross section $\sigma_{\phi N}$ that can be related to the ϕ width Γ_ϕ within the low-density approximation (LDA).

The in-medium ϕ width in the nuclear rest frame at normal nuclear density obtained in these models is presented in Fig. 1. Similar behaviour is seen for all three approaches and the differences come mainly from the divergent descriptions of the secondary production processes. The ϕ width extracted is in agreement with the Spring-8 [4] and JLab [5] results that have been measured for slightly higher momentum and exceeds the Valencia

prediction [10, 11].

In order to understand further the model calculations, the double differential cross sections for ϕ production have been evaluated within the ANKE acceptance window for different momentum bins. The major systematic uncertainty arises from the evaluation of the integrated luminosity L_{int}^{A} for target A. For this purpose the flux of π^+ mesons with momentum ≈ 500 MeV/c produced at small angles was measured. In order to estimate the double differential cross section for forward π^+ production at 2.83 GeV, the available experimental data [13, 14] have been combined (for details see Appendix A).

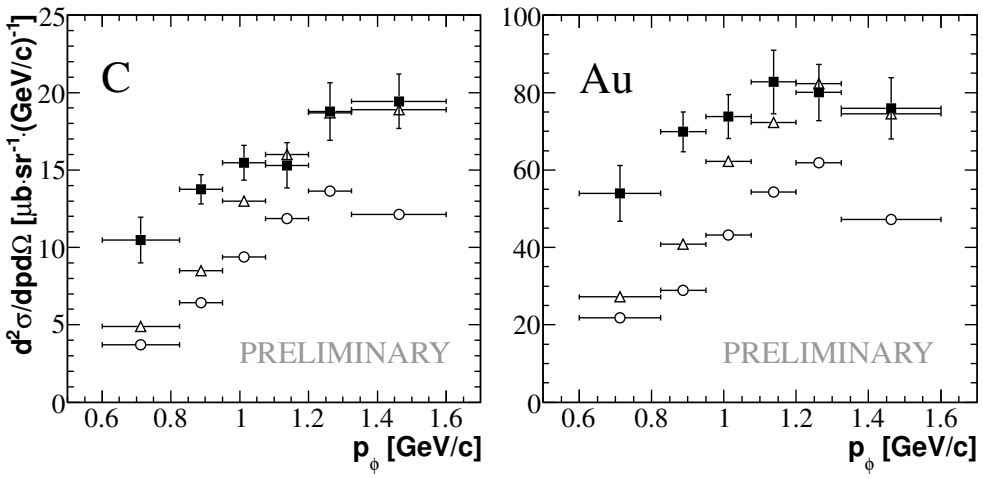

Figure 2: Comparison of the measured double differential cross section for ϕ production at small angles (full squares) for carbon (left) and gold (right) nuclei with the predictions of Models 2 (open circles) and 3 (open triangles).

The double differential cross sections for ϕ production were estimated in the Paryev and BUU calculations and in Fig. 2 the measured cross sections for carbon and gold nuclei are compared with the predictions in these models. The extracted values of the in-medium ϕ width or $\sigma_{\phi N}$ cross section have been used to estimate the ϕ production cross section within these models. The BUU calculation describes rather well the high momenta, where direct ϕ production dominates. Both models strongly underestimate ϕ production at low momenta. This suggests that some process, whose contribution to the ϕ production cross sections increases for low ϕ momenta and with the size of the nucleus, is not included in the models. Further theoretical studies of secondary production processes is therefore clearly needed to extract the maximum information from these experiments.

The results presented here would not have been possible without the efforts of the COSY machine crew and other members of the ANKE collaboration. The work was supported in part by the BMBF, DFG, COSY-FFE, RFBR and VI-QCD.

1 Cross section for π^+ production at small angles at 2.83 GeV

There are no experimental data for π^+ production in pA collisions at 2.83 GeV and so estimates have been made on the basis of the available differential cross sections for forward π^+ and π^- production measured under closely related kinematic conditions [13, 14].

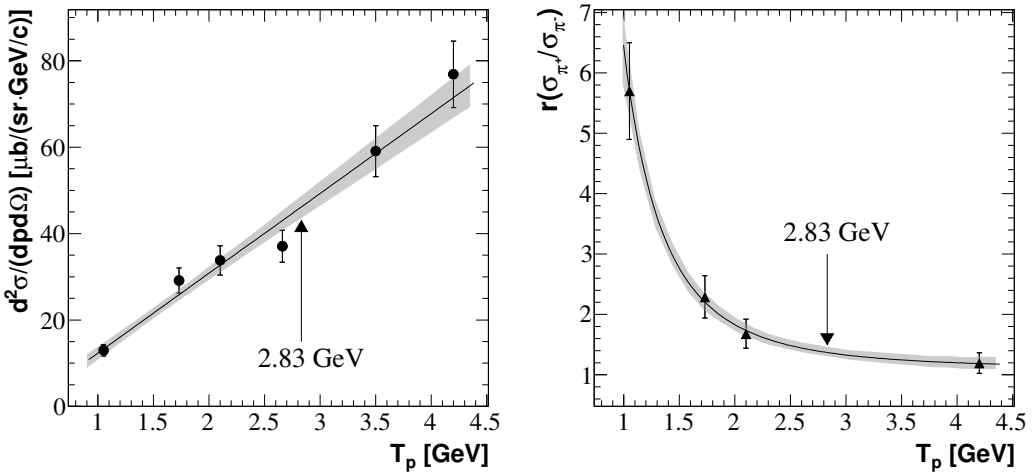

Figure 3: Left: Corrected double differential cross section for π^- production on carbon [14]. Right: Ratio of the double differential cross sections for π^+ and π^- production [14]. Errors of the fits are shown by the shaded bands ($cl = 67\%$). For explanations, see the text.

In Ref [13] a total systematic uncertainty of 6% was quoted, though the maximal beam energy used was only 1 GeV. Momentum spectra of π^+ and π^- at six higher energies were measured in the range 1–4.2 GeV [14] with an overall systematic uncertainty of 20% and a relative error between points of 10%.

A	$d^2\sigma^A_{\pi^+}/(dp\,d\Omega)$ mb/(sr GeV/c)
C	59.8 ± 7.2
Cu	113 ± 15
Ag	138 ± 19
Au	174 ± 24

Table 1: Cross sections assumed for the forward production of 500 MeV/c π^+ in the collision of 2.83 GeV protons with C, Cu, Ag, and Au targets. The errors include all statistical and systematic effects, as explained in the text.

A weighted average of the cross sections for the production of 500 MeV/c π^- from carbon at 1 GeV [13] and 1.05 GeV [14] was first determined and the π^- values obtained in [14]

scaled to match this average at 1 GeV. The linear fit to the energy dependence of the scaled cross sections shown in Fig. 3 allows us to estimate the cross section at 2.83 GeV.

The dependence with beam energy of the ratio r(C) of the cross sections for 500 MeV/c π^+ and π^- production was then fitted by an exponential function to obtain a result at 2.83 GeV (Fig. 3). Finally, the differential cross section for forward π^+ production was derived from the values of $\sigma^{\mathrm{C}}(\pi^-)$ and r(C). The cross sections for the other targets (Cu, Ag and Au) were determined assuming a $A^{\alpha_{\pi^+}}$ dependence with the exponent $\alpha_{\pi^+} = 0.38 \pm 0.02$ [6]. They are listed in Table 1.

To check this methodology, a similar procedure was carried out for the data from Cu and Pb targets [13, 14]. The results obtained agree with the values for Cu and Au listed in Table 1 within 2–3%. Since the statistical errors are small, the main contributions to the total uncertainties of the π^+ production cross sections are systematic. The resulting uncertainty for different nuclei is $\approx$ 12–14%.

Bibliography

[1] R. S. Hayano and T. Hatsuda, Rev. Mod. Phys. **82**, 2949 (2010).

[2] S. Leupold, V. Metag, and U. Mosel, Int. J. Mod. Phys. E **19**, 147 (2010).

[3] R. Muto *et al.*, Phys. Rev. Lett. **98**, 042501 (2007).

[4] T. Ishikawa *et al.*, Phys. Lett. B **608**, 215 (2005).

[5] M. H. Wood *et al.*, Phys. Rev. Lett. **105**, 112301 (2010).

[6] A. Polyanskiy *et al.*, Phys. Lett. B **695**, 74 (2011).

[7] M. Hartmann *et al.*, AIP Conf. Proc. **1322**, 349 (2010).

[8] V. K. Magas, L. Roca and E. Oset, Phys. Rev. C **71**, 065202 (2005).

[9] E. Ya. Paryev, J. Phys. G **36**, 015103 (2009).

[10] D. Cabrera and M. J. Vicente Vacas, Phys. Rev. C **67**, 045203 (2003).

[11] D. Cabrera, L. Roca, E. Oset, H. Toki, and M. J. Vicente Vacas, Nucl. Phys. A **733**, 130 (2004).

[12] H. Schade, University of Dresden PhD thesis (2010).

[13] V. V. Abaev *et al.*, J. Phys. G **14**, 903 (1988).

[14] J. Papp *et al.*, Phys. Rev. Lett. **34**, 601 (1975); J. Papp, Report LBL-**3633** (1975).

Measuring the J/ψ-Nucleon dissociation cross section with PANDA

Paul Bühler[1]
Stephan Meyer Institute for Subatomic Physics
Austrian Academy of Sciences
Boltzmanngasse 3
AT - 1090 Vienna, Austria

With the PANDA detector at the HESR at FAIR it will be possible to study the production and absorption of charmed hadrons in nuclear targets. Of special interest in this context is the determination of the J/ψ-nucleon dissociation cross section. This can be determined with measurements of the J/ψ yield in $\overline{\mathrm{p}}$A reactions using different target materials. The experiment is described and numerical simulations are presented.

1 Introduction

The inelastic J/ψ-nucleon cross section $\sigma_{J/\psi \mathrm{N}}$ is important in understanding the role of the formation of a Quark-Gluon-Plasma, QGP in the J/ψ suppression observed in high energy nuclear collisions. For an interpretation of these data the quantitative understanding of the nuclear effects - those which are not related to QGP formation - that also affect J/ψ production in nucleus-nucleus reactions is crucial. The inelastic scattering of the J/ψ state in cold nuclear matter is expected to be the dominant contribution of this kind. Its strength is described by the J/ψ-nucleon inelastic cross section, $\sigma_{J/\psi \mathrm{N}}$.

$\sigma_{J/\psi \mathrm{N}}$ can be determined with reactions, in which J/ψ are produced in nuclear medium. It is from the comparison of the expected number of produced J/ψ and the actually measured number of J/ψ escaping from the nuclear medium that the dissociation cross section is derived.

Current experimental values of $\sigma_{J/\psi \mathrm{N}}$ have mainly been obtained from inclusive hadro- and leptoproduction of J/ψ on nuclear targets [1]. In these experiments the determination of $\sigma_{J/\psi \mathrm{N}}$ is hampered by co-acting effects (co-movers, feed down, ...) which affect the number of escaping J/ψs. Thus the various contributions have to be disentangled to extract the effect of the J/ψ-Nucleon dissociation on the observed suppression of the J/ψ yield.

In $\overline{\mathrm{p}}$A reactions the momentum of the incident $\overline{\mathrm{p}}$ can be tuned such that J/ψs are produced exclusively at a relatively well defined momentum. This will facilitate the analysis of the data significantly.

[1] paul.buehler@oeaw.ac.at

2 The experiment

The idea for this experiment for measuring $\sigma_{J/\psi N}$ can be traced back to a paper by Brodsky & Mueller [2]. The principle of the measurement is illustrated in figure 1a). J/ψs are formed in $\bar{p}$A reactions, when an incident $\bar{p}$ annihilates with a nucleon within a target nucleus. The momentum of the incident antiproton is tuned such that the center-of-mass energy E_{cm} of the antiproton-nucleon system is close to the resonance energy of the J/ψ of 3.097 GeV/c^2 and J/ψ is formed exclusively. The formed J/ψ has an initial velocity and sets off to escape from the nucleus. There are two possible fates for the J/ψ - either it will decay due to its finite lifetime or it will be absorbed in an inelastic reaction with a nucleon.

The number of J/ψ formed in the nucleus N_{form} and the number of J/ψ escaping the Nucleus N_{esc} are related through

$$N_{esc} = N_{form}\left(1 - \sigma_{J/\psi N}\left\langle\int \rho \cdot dl\right\rangle\right) \tag{1}$$

$\left\langle\int \rho \cdot dl\right\rangle$ is the average integrated nucleon density along the path of the J/ψ through the nucleus, where the average is to be taken over all formations.

Equation (1) represents a recipe for the measurement of $\sigma_{J/\psi N}$. It contains a few quantities which either need to be determined experimentally (N_{esc}) or by simulation/calculation (N_{form}, $\left\langle\int \rho \cdot dl\right\rangle$). The success of the measurement thus depends on the exact determination of the absolute values of these quantities.

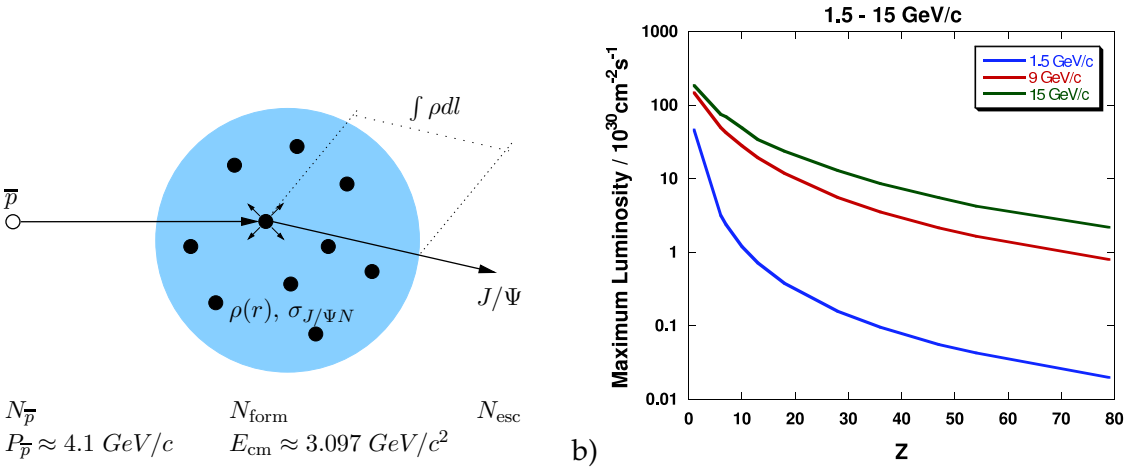

Figure 1: a) Illustration of the $\bar{p}A$ reaction which is used to measure the J/ψ-Nucleon dissociation cross section $\sigma_{J/\psi N}$. b) Luminosity of the HESR with a nuclear target as function of the atomic number of the target material [3].

3 Measurement with PANDA

J/ψs are experimentally best identified by their decay into lepton pairs $e^+e^-/\mu^+\mu^-$. The corresponding branching ratio is 5.9 % for either of these two decay channels [4]. The simple topology in this reaction allows to efficiently identify J/ψs decaying into lepton pairs with a detector like PANDA and also can be exploited to reduce the background to an acceptable level. The cross section for formation of J/ψ in $\overline{\mathrm{p}}$A is by a factor of a few times 10^9 smaller than the total inelastic cross section of typically 1 b. Thus a background suppression of at least 10^{-10} has to be and can be achieved with PANDA (see [3] for further details). The reconstruction efficiency for the decay channel $J/\psi \to e^+e^-$ was estimated to be around 70% and somewhat less for $J/\psi \to \mu^+\mu^-$.

The number of formed J/ψ, $\mathrm{N_{form}}$ is given by

$$\mathrm{N_{form}} = \int L\ dt \cdot \langle \sigma_{\mathrm{form}} \rangle \tag{2}$$

$\int L\ dt$ is the luminosity integrated over the measurement time. $\langle \sigma_{\mathrm{form}} \rangle$ is the average formation cross section.

The measurement of the luminosity will have to be carried out instantaneously with a dedicated luminosity monitor. The achievable luminosity at the High Energy Storage Ring, HESR at the future FAIR with a nuclear target is shown in figure 1b) [3]. Due to the enhanced absorption and scattering in heavier targets, the luminosity decreases with increasing atomic number of the target material. At the J/ψ resonance momentum the achievable luminosity will range from $\approx 5\ \frac{pb^{-1}}{d}$ at $Z \leqslant 10$ to $\approx 10^{-2}\ \frac{pb^{-1}}{d}$ at $Z \geqslant 40$.

The formation probability in a single $\overline{\mathrm{p}}$p is well described by the Breit-Wigner formula and is a function of the available center-of-mass energy $\mathrm{E_{cm}}$ (corrections for initial-state radiation can be applied [5]). The formation cross section at resonance in a $\overline{\mathrm{p}}$p reaction and final decay into a e^+e^- pair is 275.7 nb (relevant parameters have been determined by [6]). The effective formation cross section $\langle \sigma_{\mathrm{form}} \rangle$ in $\overline{p}A$ reactions however is considerably smaller than this peak value. Due to the Fermi motion of the nucleons in the nucleus, the available $\mathrm{E_{cm}}$ is determined not only by the energy of the beam particle but also depends on the Fermi momentum of the involved nucleon. Thus $\langle \sigma_{\mathrm{form}} \rangle$ is the formation probability averaged over all particular formations.

The value of $\langle \sigma_{\mathrm{form}} \rangle$ was determined by Monte Carlo simulations using a Glauber type model. The nucleus is described by a radial nucleon density profile $\rho(r)$ which is taken from [7,8]. The distribution of the Fermi-motion is modeled using a local Thomas-Fermi approximation in which the Fermi momentum $\mathrm{P_F}$ depends on the local nucleon density $\rho(r)$ as $\mathrm{P_F} = \hbar c(3\pi^2\rho(r))^{1/3}$. It is assumed, as has been pointed out by Farrar et al. [9] that the formation time of J/ψ is short enough such that color transparency effects can be neglected.

In this model the formation points are not homogeneously distributed in the nucleus. The number of antiprotons decreases with increasing depth s due to the absorption in the nuclear matter. With the total $\overline{p}p$ cross section of $\approx$ 7 fm^2 at 4 GeV/c [10] and a typical nuclear density of 0.1 fm^{-3} the penetration depth is typically in the order of a few fm only. For the Monte Carlo simulation thus first a location within the nucleus is selected according to the survival probability of the antiprotons ($\propto e^{-\sigma_{tot}\int_{-\infty}^{s}\rho(x,b)dx}$). Then the momentum of the nucleon is selected according to the local distribution of the Fermi-momentum. Together with the momentum of the beam particle, which is distributed according to a Gaussian function with a relative width of typically 10^{-4} (this corresponds to the High Intensity mode of the HESR), and under consideration of the nuclear binding energy, the E_{cm} is computed. This is finally inserted into the Breit-Wigner formula to compute the formation probability. In order to compute the dissociation probability the nucleon density along the path of the J/ψ is integrated up to the point where the J/ψ decays. Figure 2 shows results of these simulations.

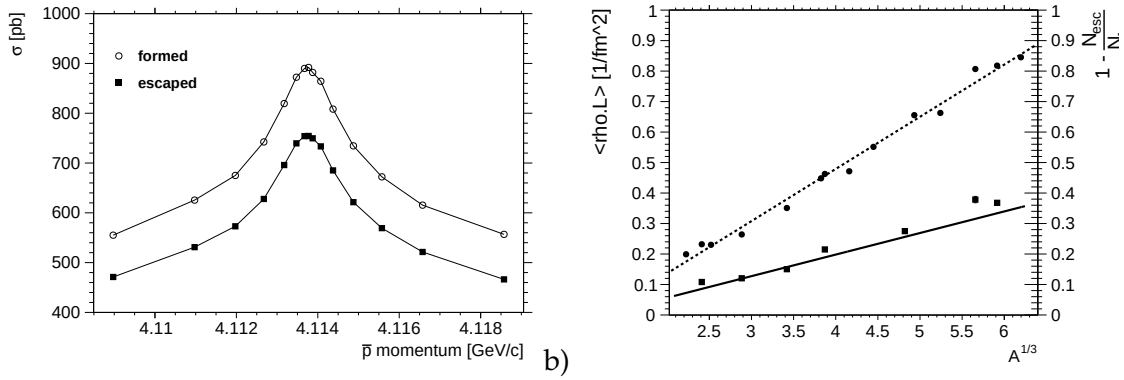

a) b)

Figure 2: a) $\langle\sigma_{\text{form}}\rangle$ and $\langle\sigma_{esc}\rangle$ as function of the $\overline{p}$ momentum in a ^{40}Ca target b) $(1 - N_{esc}/N_{form})$ (square symbols) and $\left\langle\int\rho\cdot dl\right\rangle$ as function of nuclear mass of the target material.

In the left panel the expected cross section for formation $\langle\sigma_{\text{form}}\rangle$ and the cross section for escaping and decaying into an electron-positron pair $\langle\sigma_{esc}\rangle$ is plotted as function of the beam momentum. The peak value of $\langle\sigma_{esc}\rangle$ is in the order of 700 pb in this case. With a total reconstruction efficiency of 50% and an average luminosity of 10^{31} cm^{-2}s^{-1} the number of J/ψ per day would be around 300.

According to equation (1) $\sigma_{J/\psi N}$ is obtained by the quotient of $(1 - N_{esc}/N_{form})$ and $\left\langle\int\rho\cdot dl\right\rangle$. For consistency checks, measurements of N_{esc} should be carried out for several beam momenta which allow to reconstruct the broadened resonance and should also be repeated with different target materials.

The square symbols plotted in the right panel of figure 2 represent the quantity $(1 - N_{esc}/N_{form})$ and the circular symbols show the quantity $\left\langle\int\rho\cdot dl\right\rangle$ for different target materi-

als. The dotted line is the best linear fit to the $\left\langle \int \rho \cdot dl \right\rangle$ points, whereas the bold line is the dotted line scaled to match the $(1 - \mathrm{N_{esc}}/\mathrm{N_{form}})$ data points best. The scaling factor is the measurement of $\sigma_{J/\psi \mathrm{N}}$ and in these simulations its value is found to be very close to the value which was used as input.

4 Conclusions

Measurements of the J/ψ yield in $\overline{\mathrm{p}}$A reactions close to resonance in different target materials allow to determine the J/ψ-nucleon dissociation cross section. The experiment depends on an accurate measurement of the number of J/ψ escaping the nucleus and an accurate prediction of the number of J/ψ formed in the nuclear medium. The presented simulations suggest, that in light target materials with this reaction up to a few hundred J/ψ will be formed and detected with the PANDA detector per day. Measurements on different target materials will allow to check results for consistency.

Acknowledgments

I would like to thank Albert Gillitzer for helpful comments and discussions.

Bibliography

[1] F. Arleo & V.-N. Tram, European Physical Journal C **55** (2008) 449.

[2] S. J. Brodsky & A. H. Mueller, Physics Letter B **206** (1988) 685.

[3] PANDA collaboration, Physics Performance Report for PANDA, arXiv:0903.3905v1 [hep-ex].

[4] K. Nakamura *et al.*(Particle Data Group), Journal of Physics G **37** (2010) 075021 (URL: http:pdg.lbl.gov).

[5] D. C. Kennedy, Physical Review D **46** (1992) 461.

[6] T. A. Armstrong *et al.*, Physical Review D **47** (1993) 772.

[7] H. De Vries *et al.*, Atomic Data and Nuclear Data Tables **36** (1987) 495.

[8] W. Reuter *et al.*, Physical Review C **26** (1982) 806.

[9] G. R. Farrar *et al.*, Nuclear Physics B **345** (1990) 125.

[10] V. Flaminio *et al.*, CERN-HER 79-03, CERN libraries Geneva, CM-P00048064 (1979).

Precision Spectroscopy of Pionic Atom at RIKEN-RIBF

Satoshi Itoh[1,a], G.P.A. Berg[b], H. Geissel[c], R.S. Hayano[a], N. Inabe[d], K. Itahashi[d], D. Kameda[d], T. Kubo[d], H. Matsubara[e], H. Michimasa[e], K. Miki[e], H. Miya[e], M. Nakamura[f], T. Nishi[a], S. Noji[e], S. Ota[d], K. Suzuki[g], H. Takeda[d], K. Todoroki[a], K. Tsukada[d], T. Uesaka[e], H. Weick[c], and K. Yoshida[d]

[a] *Department of Physics, University of Tokyo, Tokyo, JAPAN*
[b] *JINA and Department of Physics, University of Notre Dame, Indiana, USA*
[c] *GSI, Darmstadt, GERMANY*
[d] *RIKEN Nishina Center, RIKEN, Saitama, JAPAN*
[e] *Center of Nuclear Study, University of Tokyo, Tokyo, JAPAN*
[f] *Department of Physics, Tokyo Institute of Technology, Tokyo, JAPAN*
[g] *Stefan-Meyer-Institut für subatomare Physik, Vienna, AUSTRIA*

We performed a precision spectroscopy experiment of the pionic atom at the RIKEN RI beam factory (RIBF) in October 2010. A new ion-optical setup was developed for both the beam transfer (BT) line to the target and the spectrometer in order to accomplish the dispersion matching which eliminates the effect of the momentum spread of the primary beam. We measured the first data of the deeply bound states of the pionic ^{121}Sn atom and observed the angular dependence of the bound states.

1 Introduction

The order parameter of the chiral symmetry breaking, the quark condensate $\langle\bar{q}q\rangle$, is expected to change in nuclear medium. At normal nuclear densities, the quark condensate is reduced by 30% compared the vacuum value. The experimental determination of this in-medium change is one of the important themes in contemporary hadron physics. However, the quark condensate is not physically observable. Therefore, we combine two relations, the in-medium Glashow-Weinberg relation [1] and the in-medium Tomozawa-Weinberg relation [2], to formulate the in-medium change of the quark condensate in terms of the physical observable b_1, which is the isovector pion-nucleus scattering length.

A precise spectroscopic experiment at GSI for the pionic ^{115}Sn, ^{119}Sn and ^{123}Sn atoms yielded the first accurate measurement of the b_1 enhancement at normal nuclear density

[1] itoh@nucl.phys.s.u-tokyo.ac.jp

with the result $b_1^{\text{free}}/b_1 = 0.78$ [3], where the b_1^{free} was very precisely determined by the pionic hydrogen x-ray spectroscopy at PSI [4]. However, the values of b_1 where not as accurately determined as the b_1^{free} parameter. Therefore, the objective of the present project is to improve the in-medium b_1 accuracy. This requires a better energy resolution.

We plan systematic measurements of the pionic atoms for several stable isotope and isotone targets at RIBF [5]. Especially, we expect that the measurement for isotones will help reduce the uncertainty due to the neutron distributions. We call this project the pionic Atom Factory (piAF) project [6]. In October 2010, we performed a pilot experiment of the piAF project in order to develop the method of precision spectroscopy at RIBF. We chose ^{122}Sn as the first target of the piAF project because ^{122}Sn located at the intersection of two chains of isotopes and isotones.

2 Experiment

We used the (d,^{3}He) reaction to produce the pionic atom. The deuteron beam energy of $T_d = 500$ MeV was chosen to satisfy the recoilless condition. We measured the momentum of the helium using the BigRIPS spectrometer [7] to analyze the Q-value of the (d,^{3}He) reaction. At the dispersive focal plane F5, we installed two sets of multi-wire drift chambers and one set of segmented scintillation counters. At the achromatic focal plane F7, we installed a scintillation counter. The particle identification was performed by the measurement of the energy loss in the scintillation counters and the time of flight between F5 and F7.

One advantage of using the RIKEN facility is the high beam intensity, which is higher by a factor of ten compared to the beam that was used in the GSI experiment. Hence, we can use thinner target allowing for better resolution. On the other hand, the momentum spread of the primary beam of the RIKEN is larger by a factor of three compared to the momentum spread at GSI. Therefore, we use the dispersion matching [8] which eliminates the effect of the large momentum spread in order to achieve a resolution better by a factor of about two, i.e. about 200 keV (FWHM).

The dispersion matching condition is described as

$$b_{16}s_{11} + b_{26}s_{12} + Cs_{16} = 0, \tag{1}$$

where b_{ij} and s_{ij} denote the R-matrix elements of the BT line and the BigRIPS spectrometer, respectively, and C is the kinematic factor of the (d,^{3}He) reaction at the target. The kinematic factor is 1.3 for the pionic atom production. The elements s_{ij} were selected to achieve a resolving power of 3500, such that $s_{11} = -1.8$, $s_{12} = 0.0$ mm/mrad, and $s_{16} = 64$ mm/%. The elements b_{ij} were selected to satisfy the matching condition specified in equation (1), namely $b_{16} = 46$ mm/% and $b_{26} = 0.0$ mrad/%. The momentum dispersion s_{16} and b_{16} were measured by scaling beam line magnets with the results 61.8 mm/% and 43.8 mm/%, respectively. The measured values were in sufficient agreement with the design values.

3 Results

The panel on the left side of Figure 1 shows measured counts as a function of the horizontal position at the dispersive focal plane F5. The x-axis is proportional to the momentum increases from left to right. The panel on the right side of Figure 1 shows the 2-dimentional scatter plot of the vertical angle of F5 versus the horizontal position. This is the first data of the deeply bound states of the pionic ^{121}Sn atom and the first observation of the angular dependence of the deeply bound states.

The panel on the left side of Figure 2 shows position spectrum at F5 with the condition $\theta < 15$ mrad, where θ is the beam angle at the target. The right-side panel of Figure 2 shows the calculated spectra for the formation of the pionic bound states [9]. In this calculation, the experimental energy resolution is assumed to be 150 keV (FWHM).

Our result at forward angles is consistent with the theoretical calculation and we identify the peak at the right as the 1s pionic state. A more detailed analysis to deduce the binding energy and the width of each peak and to identify the configuration of each peak is ongoing.

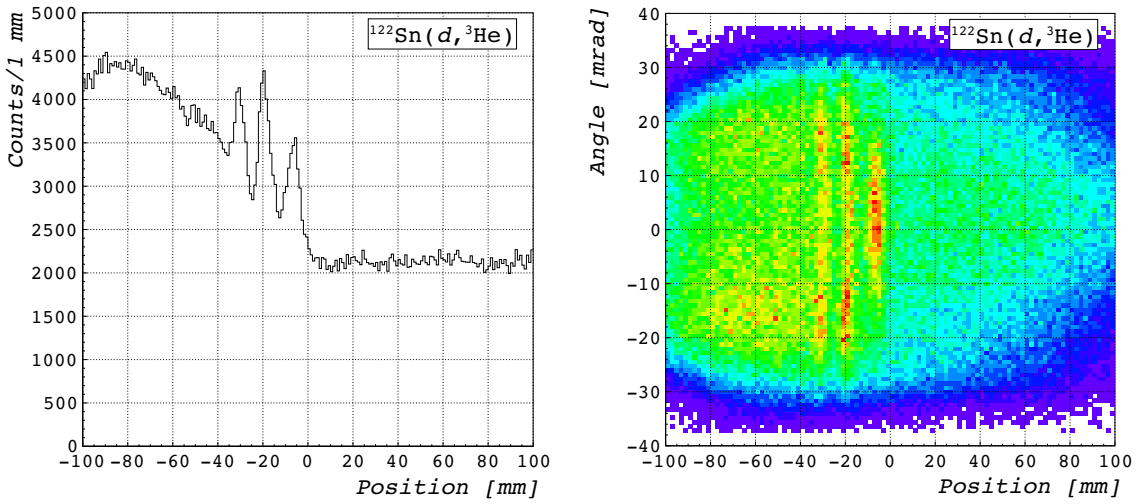

Figure 1: A position spectrum at the dispersive focal plane F5 (left) and a 2-dimentional scatter plot of the vertical angle versus the horizontal position at F5 (right) are shown.

Acknowledgments

This work is supported by a Grant-in-Aid for Scientific Research on Innovative Areas (No. 22105517).

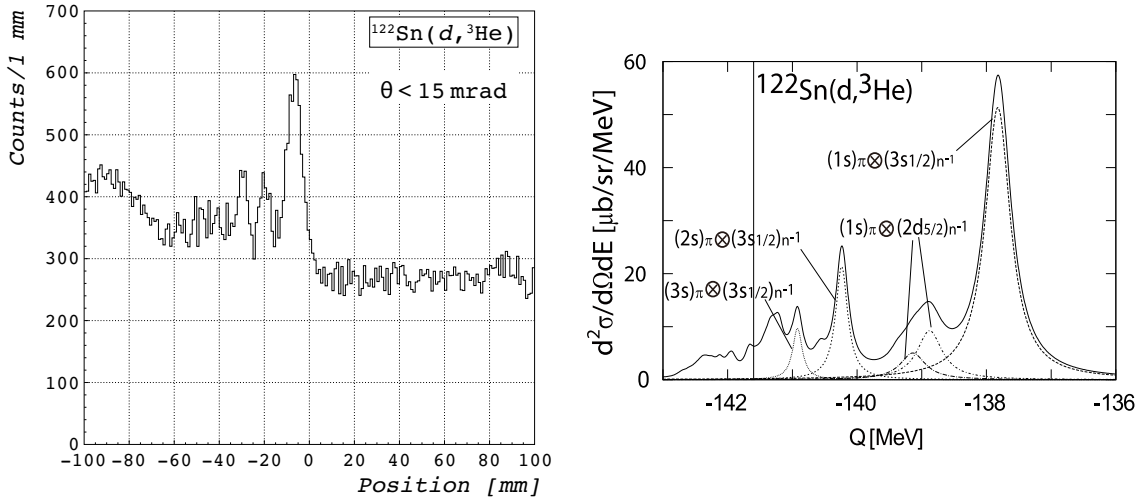

Figure 2: A position spectrum at forward angles ($\theta < 15$ mrad (left) and the theoretical calculation of the Q-value spectrum [9] (right) are displayed.

Bibliography

[1] D. Jido, T. Hatsuda and T. Kunihiro, Phys. Lett. B **670**, 109 (2008).

[2] E.E. Kolomeitsev, N. Kaiser and W. Weise, Phys. Rev. Lett. **90**, 092501 (2003).

[3] K. Suzuki *et al.*, Phys. Rev. Lett. **92**, 072302 (2004).

[4] D. Gotta *et al.*, Lect. Notes Phys. **745**, 165 (2008).

[5] Y. Yano, Nucl. Inst. Meth. B **261**, 1009 (2007).

[6] K. Itahashi *et al.*, RIBF proposal No.054 (2008).

[7] T. Kubo, Nucl. Inst. Meth. B **204**, 97 (2003).

[8] T. Wakasa *et al.*, Nucl. Inst. Meth. A **482**, 79 (2002).

[9] N. Ikeno *et al.*, Prog. Theor. Phys.(in press), arXiv:1107.5918[nucl-th].

Partial restoration of chiral symmetry and pion in nuclear medium

Daisuke Jido[1,a] and Soichiro Goda[b]
[a]*Yukawa Institute for Theoretical Physics, Kyoto University, Kyoto 606-8502, JAPAN*
[b]*Department of Physics, Graduate School of Science, Kyoto University, Kyoto, 606-8502, JAPAN*

We discuss partial restoration of chiral symmetry in nuclear medium, which is realized as an effective reduction of the quark condensate in nuclear medium. We derive the in-medium Weinberg-Tomozawa relation. We also give a brief calculation of the in-medium quark condensate based on chiral perturbation theory. We conclude that the density dependence of the quark condensate beyond the linear density comes from the vertex correction of the chiral field insertion and nucleon correlations.

1 Introduction

One of the goals of the contemporary nuclear physics is to figure out the QCD vacuum structure at finite density and/or temperature. Especially, the fate of dynamical breaking of chiral symmetry in finite baryonic density is phenomenologically interesting, because we could obtain experimental evidence of partial restoration of chiral symmetry in the nuclear medium by investigating in-medium properties of meson in nuclei. Recently, precise measurements of the spectra of deeply bound pionic atoms were performed [1,2], and with these data the pion optical potential parameters were determination in detail. Especially, the repulsive enhancement of the isovector π^--nucleus interaction was accurately extracted as $b_1^{\rm free}/b_1 = 0.78 \pm 0.05$ at around $\rho \sim 0.6\rho$ [2]. The b_1 repulsive enhancement was also seen in low-energy pion-nucleus scatterings [3]. With help of the theoretical discussion [4,5], the b_1 parameter is converted to the in-medium pion decay constant F_t, and we concluded that the experimental finding of the b_1 enhancement is to be a signal of the reduction of the pion decay constant in nuclear matter. Further, the exact relation between the in-medium pion decay constant and quark condensate was also found at the linear density approximation in Ref. [5]. Now we have arrived at the qualitative confirmation of the partial restoration of chiral symmetry in nuclear medium and should go a step further to make the argument more quantitative [7,8]. In this paper we briefly discuss the sum rule for the in-medium quark condensate and the in-medium Weinber-Tomozawa relation. We also show a calculation of the in-medium quark condensate based on chiral perturbation theory beyond the linear density.

[1]jido@yukawa.kyoto-u.ac.jp

2 Sum rule for the in-medium quark condensate

To connect the phenomenological consequences extracted from experimental observation to the quark condensate, we need theoretical consideration which makes bridge between hadronic description and quark language. In Ref. [5], an exact sum rule for a symmetric nuclear matter was derived in the chiral limit:

$$\sum_{\alpha} \mathrm{Re}\left[F_{t,\alpha} G_{\alpha}^{*1/2}\right] = -\langle\bar{q}q\rangle^{*} \tag{1}$$

where the summation is taken over all of pionic zero modes in nuclear matter which have the same quantum number with the pion in nuclear matter and whose energy is zero measured from the nuclear matter ground state, and the matrix elements of $F_{t,\alpha}$ and $G_{\alpha}^{1/2}$ are given in the nuclear matter rest frame by

$$\langle\Omega|A_0^a|\Omega_\alpha^b(k)\rangle = i\delta^{ab}\omega_\alpha F_{t,\alpha} \tag{2}$$

$$\langle\Omega_\alpha^b|\phi_5^a|\Omega\rangle = \delta^{ab} G_\alpha^{*1/2} \tag{3}$$

with the axial current A_μ^a, the pseudoscalar density ϕ_5^a, the ground state of the symmetric nuclear matter $|\Omega\rangle$ and the pionic zero mode state $|\Omega_\alpha\rangle$.

One of the most important consequence of this sum rule is that to obtain the in-medium chiral condensate one has to sum up all of the pionic zero modes. This means that one should not have to separate out the in-medium pion properties from complicated dynamics of pion and nuclear matter. This sum rule is valid for all densities and derived by current algebra as a low energy theorem. Instead, we need description of dynamics of in-medium pion and nuclear matter for actual calculation of matrix elements. This sum rule is also available for experimental confirmation of partial restoration of chiral symmetry, once the matrix elements are extracted from experimental observation.

In the linear density approximation, the sum rule can be simplified to $F_t G_\pi^{*1/2} = -\langle\bar{q}q\rangle^*$. By taking its ratio to the in-vacuum Glashow-Weinberg relation $F_\pi G_\pi^{1/2} = -\langle\bar{q}q\rangle$ [9], we obtain the scaling law

$$\frac{F_t}{F_\pi} Z_\pi^{1/2} = \frac{\langle\bar{q}q\rangle^*}{\langle\bar{q}q\rangle} \,. \tag{4}$$

where $Z_\pi^{1/2}$ is the in-medium wavefunction renormalization, which can be extracted at the linear density from the πN scattering data. The in-medium reduction of the pion decay constant was obtained in the pionic atom.

3 In-medium Weinberg-Tomozawa relation

As discussed in Ref. [5], the in-medium Weinberg-Tomozawa relation can be derived by considering the chiral-limit correlation function of the axial current A_μ^a in the asymmetric

nuclear matter: $\Pi_\nu^{ab}(q) = \int d^4x e^{iq\cdot x}\partial^\mu \langle \Omega'|T[A_\mu^a(x)A_\nu^b(0)]|\Omega'\rangle$, where $|\Omega'\rangle$ is the ground state of the asymmetric nuclear matter normalized as $\langle\Omega'|\Omega'\rangle = 1$ and specified by the isoscalar density $\rho = \rho_p + \rho_n$ and the isovector density $\delta\rho = \rho_p - \rho_n$. In the soft limit, using the axial current conservation $\partial \cdot A = 0$, we obtain

$$\Pi_{\nu=0}^{ab}(0) = \int d^3x [A_0^a(x), A_0^b(0)] = i\epsilon^{ab3}\langle\Omega'|V_0^3|\Omega'\rangle, \tag{5}$$

where we have used the commutation relation $[Q_5^a, A_\nu^b] = i\epsilon^{abc}V_\nu^c$. The matrix element in the right hand side of Eq. (5) implies a spacial average of the isospin density in the nuclear matter and counts the z component of the isospin of the nuclear matter state. For the ground state of nuclear matter, at the linear $\delta\rho$, the matrix element is written as

$$\Pi_0^{ab}(0) \simeq i\epsilon^{ab3}\frac{1}{2}\delta\rho. \tag{6}$$

On the other hand, inserting the hadronic complete set into the correlation function, we obtain the hadronic description of the correlation function in the soft limit where we take $\vec{q} \to 0$ first as

$$\Pi_0^{ab}(0) = \lim_{\omega\to 0} i\omega(\omega F_t^{a\alpha})\frac{1}{\omega^2\delta^{\alpha\beta} - \Sigma^{\alpha\beta}}(\omega F_t^{\beta b}), \tag{7}$$

where $\Sigma^{\alpha\beta}$ is the self-energy of the zero mode and F_t^{ab} is the matrix element of the axial current for the ground state $|\Omega'\rangle$ and the pionic zero modes in the asymmetric nuclear matter $|\Omega'_\alpha\rangle$ given by $\langle\Omega'|A_0^a|\Omega'_\alpha\rangle = i\omega F_t^{a\alpha}$. Thus we obtain a sum rule

$$\sum_{\alpha,\beta}\lim_{\omega\to 0}\omega F_t^{a\alpha}\left(\delta^{\alpha\beta} - \frac{1}{2\omega}\frac{\partial\Sigma^{\alpha\beta}}{\partial\omega}\right)^{-1}F_t^{\beta b} = \epsilon^{ab3}\frac{1}{2}\delta\rho. \tag{8}$$

The explicit expression of the $F_t^{a\alpha}$ and $\Sigma^{\alpha\beta}$ depends on the description of the complete set, but the sum is not dependent on the description. Now we expand $F_t^{\alpha\beta}$ and $\Sigma^{\alpha\beta}$ in terms of the isovector density $\delta\rho$, and find

$$\Sigma^{\alpha\beta} = \epsilon^{\alpha\beta3}\frac{\omega}{F_t^2}\delta\rho, \tag{9}$$

where F_t is the decay constant in the symmetric nuclear matter given in Eq. (2). This is just a consequence of the isospin symmetry

4 A model calculation of the quark condensate

The sum rule (1) was derived by considering the correlation function of the axial current and pseudoscalar density in symmetric nuclear matter at the chiral limit: $\Pi_5^{ab}(q) =$

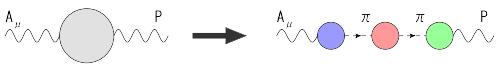

Figure 1: Separation of $\langle A^a_\mu(q)P^b(0)\rangle^*$.

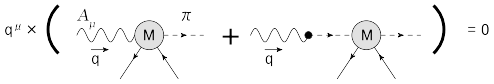

Figure 2: Conservation of axial current

$\int d^4x e^{iq\cdot x}\partial^\mu\langle\Omega|T[A^a_\mu(x)\phi^b_5(0)]|\Omega\rangle$. Taking the soft limit and using the Ward-Takahashi identity, we obtain

$$\lim_{q\to 0}\int d^4x e^{iq\cdot x}\partial^\mu\langle\Omega|T[A^a_\mu(x)\phi^b_5(0)]|\Omega\rangle = -i\delta^{ab}\langle\bar{q}q\rangle^* \tag{10}$$

In this section, we directly calculate the left hand side based on in-medium chiral perturbation theory. Here we take, for example, the formulation developed in Refs. [10], in which the generating functional of the SU(2) chiral Lagrangian in non-interacting nucleon gas environment is calculated in expansions of Fermi-see insertion and chiral order counting. The Fermi momentum k_f is also regarded as a small expansion parameter as well as the pion momentum and mass in the in-vacuum chiral perturbation theory.

We calculate the in-medium Green function $\langle A^a_\mu(q)P^b(0)\rangle^*$ in the chiral limit [12]. First of all, it is possible to separate the Green function into the three parts, the medium corrections of the decay constant, pion wavefunction and the pseudo-scalar coupling (Fig. 1), which are connected with the in-vacuum pion propagators. Among three parts, there is cancellation between the corrections for the decay constant and wavefunction at the soft limit $q_\mu \to 0$ thanks to the axial vector current conservation in the chiral limit, $\partial^\mu A^a_\mu(x) = 0$. This is a generalized Goldberger-Treiman relation (Fig. 2). Therefore, only the density dependence of the pseudo-scalar coupling contributes to the in-medium quark condensate.

The medium correction for the quark condensate starts from $O(p^4)$ of the chiral expansion, but the contribution of this order vanishes at the chiral limit due to the cancelation mentioned above. The leading order correction is given by the diagram shown in Fig. 3(a) with the $O(p^2)$ πPNN vertex. This contribution reproduces the well-known result of the linear density approximation [11]:

$$\langle\bar{u}u+\bar{d}d\rangle^* = \langle\bar{u}u+\bar{d}d\rangle_0(1+\frac{8c_1\rho}{f_\pi^2}), \tag{11}$$

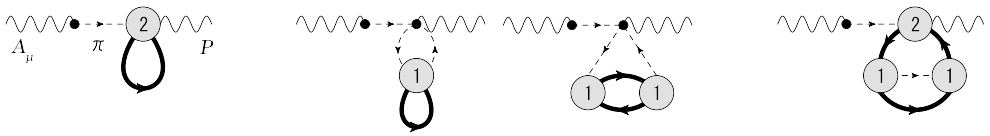

(a) $O(p^5)$ (b) $O(p^6)$ (c) $O(p^7)$

Figure 3: Diagrams for the medium corrections of the quark condensate in the chiral limit. $O(p^n)$ means the order of the chiral expansion.

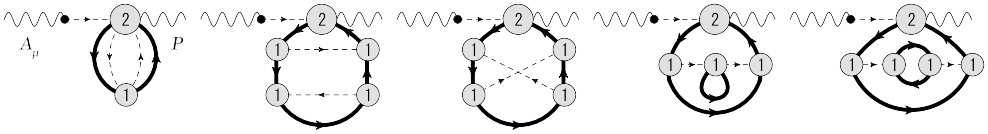

Figure 4: Further higher order contributions. These diagrams represent the two-pion exchange and nucleon-nucleon correlations.

where $\langle\bar{u}u + \bar{d}d\rangle_0$ is the quark condensate in vacuum, ρ is the nuclear matter density and c_1 is one of the low energy constants (LEC) in the πN chiral Lagrangian at $O(p^2)$, which is related to the πN sigma term. With $C_1 = -0.58\ \mathrm{GeV}^{-1}$, $f_\pi = 92.4$ MeV and the normal nuclear density $\rho_0 = 0.17\ \mathrm{fm}^{-3}$, we have $\langle\bar{u}u + \bar{d}d\rangle^* = \langle\bar{u}u + \bar{d}d\rangle_0(1 - 0.35\rho/\rho_0)$. This suggests 30 percent reduction of the quark condensate at the nuclear density.

Further density corrections beyond the linear density can be calculated with the diagrams shown in Fig. 3(b) and(c). They are counted as $O(p^6)$ and $O(p^7)$ of the chiral expansion and give k_f^4 and higher power contributions. In this way, one can perform the systematic expansion in terms of the chiral counting with this formulation. Since, as discussed above, the finite density contribution to the quark condensate comes only from the medium corrections of the pseudo-scalar coupling, further higher order corrections come from diagrams shown in Fig. 4. This means that the density corrections of the quark condensate are given by multi-pion exchanges between nucleons and multi-nucleon correlations in the nuclear matter. Therefore, in order to perform the realistic calculation of the in-medium quark condensate, one has to first formulate realistic nuclear matter. Indeed, the in-medium chiral perturbation theory has the systematic scheme for counting the order of the chiral expansion and this is good for theoretical analyses. Nevertheless, only the pion-nucleon dynamics described by the chiral perturbation theory may not describe realistic nuclear matter, and more phenomenological descriptions are necessary to obtain realistic nuclear matter having the saturation properties. Thus, we may have to go beyond the chiral counting scheme in order to calculate the quark condensate in nuclear matter.

5 Conclusion

The deeply bound pionic atoms are the most successful systems to investigate the in-medium pion properties, because we have certainly the bound states with so narrow widths that we can perform detailed spectroscopy. From the observed spectra we can extract in-medium pion properties. With these quantities we have concluded that partial restoration of chiral symmetry takes place in nucleus with help of theoretical arguments, which complete the story from the observation to QCD. Now we are going to the next stage to determine the in-medium quark condensate quantitatively. We have also performed brief calculation of the in-medium quark condensate based on chiral perturbation theory. This calculation

shows that to obtain the realistic quark condensate in a nuclear medium one needs realistic description of nuclear matter.

Acknowledgments

This work was partially supported by the Grant-in-Aid for Scientific Research from JSPS (Nos. 22740161, 22105507). This work was done in part under the Yukawa International Program for Quark-hadron Sciences (YIPQS). The Feynman diagrams in this paper were drawn using jaxodraw [13].

Bibliography

[1] H. Geissel *et al.*, Phys. Rev. Lett. **88**, 122301 (2002); K. Itahashi *et al.*, Phys. Rev. C **62** 025202 (2000).

[2] K. Suzuki *et al.*, Phys. Rev. Lett. **92** 072302 (2004); P. Kienle and T. Yamazaki, Prog. Part. Nucl. Phys. **52** 85 (2004).

[3] E. Friedman *et al.*, Phys. Rev. Lett. **93** (2004) 122302; E. Friedman *et al.*, Phys. Rev. C **72** (2005) 034609.

[4] E.E. Kolomeitsev, N. Kaiser, and W. Weise, Phys. Rev. Lett. **90**, 092501 (2003).

[5] D. Jido, T. Hatsuda and T. Kunihiro, Phys. Lett. B **670** (2008) 109; Prog. Theor. Phys. Suppl. **168** (2007) 478.

[6] D. Jido, T. Hatsuda, and T. Kunihiro, Phys. Rev. **D63**, 011901 (2001).

[7] N. Kaiser, P. de Homont, and W. Weise, Phys. Rev. **C77**, 025204 (2008).

[8] N. Ikeno *et al.*, Prog. Theor. Phys. (in press), arXiv:1107.5918 [nucl-th].

[9] S. L. Glashow and S. Weinberg, Phys. Rev. Lett. **20** (1968) 224.

[10] J. A. Oller, Phys. Rev. **C65** (2002) 025204; U. G. Meissner, J. A. Oller and A. Wirzba, Annals Phys. **297** (2002) 27.

[11] E. G. Drukarev and E. M. Levin, Prog. Part. Nucl. Phys. **27** (1991) 77.

[12] S. Goda and D. Jido, in preparation.

[13] D. Binosi and L. Theussl, Comput. Phys. Commun. **161** (2004) 76.

η' bound states in nuclei and partial restoration of chiral symmetry

Satoru Hirenzaki[1,a], Daisuke Jido[b], and Hideko Nagahiro[a]
[a]*Department of Physics, Nara Women's University, Nara 630-8506, Japan*
[b]*Yukawa Institute for Theoretical Physics, Kyoto University, Kyoto 606-8502, Japan*

We discuss the in-medium mass of the η' meson under partial restoration of chiral symmetry. The chiral SU(3)⊗SU(3) symmetry tells us the flavor singlet pseudoscalar meson η' should degenerate with the octet η meson in the SU(3) flavor limit, when chiral symmetry is restored in spite of $U(1)_A$ anomaly in the flavor single axial current. The suppression of the anomaly effect induces an order of 100 MeV reduction for the η' mass at the saturation density without introducing a large absorption width. We show the formation spectrum of the η' mesonic bound state in a nucleus as a possible observation of the η' mass reduction.

1 Introduction

Dynamical chiral symmetry breaking and its partial restoration in finite density systems is one of the important subjects of hadron physics. Recently, spectroscopy of deeply bound pionic atom of Sn [1] and low-energy pion-nucleus scattering [2], with helps of theoretical analyses [3], have suggested that the partial restoration does take place in nuclei with order of 30% reduction of the quark condensate. The reduction of the quark condensate in nuclear medium also leads to various phenomena, for instance, attractive enhancement of scalar-isoscalar $\pi\pi$ correlation in nuclei and the suppression of the mass difference between the chiral partners. Mass reduction of the η' meson is also induced by partial restoration of chiral symmetry [4]. The experimental observations of these phenomena, such as the reduction of the N-$N(1535)$ mass difference in the η mesonic nuclei formation [5], can be further confirmation of partial restoration of chiral symmetry in nucleus.

2 η' mass under chiral symmetry restoration

Experimentally, a strong mass reduction of η' ($\gtrsim$ 200 MeV) has been reported in Ref. [6] at RHIC. On the other hand, a small scattering length ($\sim$ 0.1 fm) has been suggested

[1]zaki@cc.nara-wu.ac.jp

in Ref. [7] which indicates small mass reduction around 10 MeV at normal saturation density in the linear density approximation. The transparency ratio of the η' meson in nuclei has suggested the absorption width of the η' meson in nuclei is around 30 MeV [8]. Theoretically, NJL model calculations suggested around 200 MeV mass reduction at the saturation density [9,10]. In the instanton picture, rapid decrease of the effects of instantons in finite energy density hadronic matter induces a reduction of the η' mass [11]. An effective model which is consistent to the $\eta' p$ scattering length data [7] was also proposed recently [12].

The basic idea of the present work is that, if density dependence of the $U(1)_A$ anomaly is moderate, a relatively large mass reduction of the η' meson is expected at nuclear density due to the partial restoration of chiral symmetry [4]. This is based on the following symmetry argument. Both the flavor single and octet pseudoscalar mesons composed of a $\bar{q}$-q pair belong to the same $(\mathbf{3},\bar{\mathbf{3}})\oplus(\bar{\mathbf{3}},\mathbf{3})$ chiral multiplet of the $SU(3)_L\otimes SU(3)_R$ group. Therefore, when the $SU(3)_L\otimes SU(3)_R$ chiral symmetry is manifest, the flavor singlet and octet mesons should degenerate, no matter how the $U(1)_A$ anomaly effect depends on the density. In other words, the chiral singlet gluonic current, which makes the η' mass lift up, cannot couple to the chiral pseudoscalar state without breaking chiral symmetry. Hence, the η and η' mass splitting can take place only with (dynamical and/or explicit) chiral symmetry breaking, meaning that the $U(1)_A$ anomaly effect does push the η' mass up but necessarily with the chiral symmetry breaking. In this way the mass splitting of the η-η' mesons is a consequence of the interplay of the $U(1)_A$ anomaly effect and the chiral symmetry breaking. Assuming 30% reduction of the quark condensate in nuclear medium, for instance, and that the mass difference of η and η' comes from the quark condensate linearly, one could expect an order of 100 MeV attraction for the η' meson coming from partial restoration of chiral symmetry in nuclear medium.

The present mechanism of the η' mass reduction in finite density has a unique feature. Although some many-body effects introduce an absorptive potential for the η' meson in medium, the mass reduction mechanism does not involve hadronic intermediate states and, thus, the attraction dose not accompany an additional imaginary part. Furthermore, in the present case, since the suppression of the $U(1)_A$ anomaly effect in nuclear medium induces the attractive interaction, the influence acts selectively on the η' meson and, thus, it does not induce inelastic transitions of the η' meson into lighter mesons in nuclear medium. Consequently the η' meson bound state may have a smaller width than the binding energy.

3 Formation spectrum of the η' mesonic nuclei

Now we discuss the η' bound states in a nucleus based on the above observation and show expected spectra of the η' mesonic nucleus formation in a $^{12}C(\pi^+,p)^{11}C\otimes\eta'$ reaction [4,13]. We perform a simple estimation of the η' bound states and, thus, assume a phenomenological optical potential of the η' meson in nuclei as $V_{\eta'}(r)=V_0\rho(r)/\rho_0$, with the Woods-Saxon

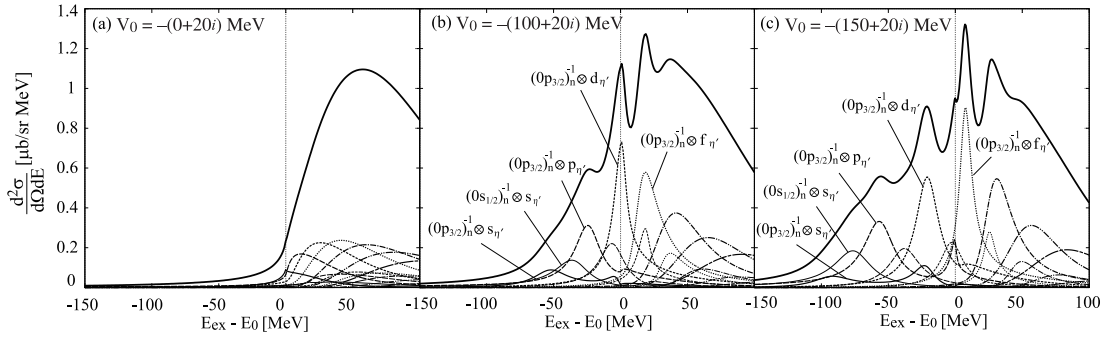

Figure 1: Calculated spectra of the $^{12}\mathrm{C}(\pi^+, p)^{11}\mathrm{C}\otimes\eta'$ at $p_\pi = 1.8$ GeV as functions of the exitation energy E_{ex} with (a) $V_0 = -(0 + 20i)$ MeV, (b) $V_0 = -(100 + 20i)$ MeV and (c) $V_0 = -(150 + 20i)$ MeV. The thick solid lines show the total spectra, and the dominant subcomponents are labeled by the neutron-hole state $(n\ell_j)_n^{-1}$ and the η' state $\ell_{\eta'}$.

type density distribution $\rho(r)$ for nucleus and the saturation density $\rho_0 = 0.17$ fm^{-3}. The depth of the attractive potential is an order of 100 MeV at the normal nuclear density as discussed above and the absorption width is expected to be less than 40 MeV [8] which corresponds to the 20 MeV imaginary part of the optical potential. The formation spectrum is calculated in the approach developed in Ref. [5, 14] using the impulse approximation and the Green's function method.

In Fig. 1, we show the calculated $^{12}\mathrm{C}(\pi^+, p)^{11}\mathrm{C}\otimes\eta'$ cross sections with three different potential parameters. In the figure, the vertical line indicates the η' production threshold in vacuum. In the case of no attractive potential, there is no structure in the η'-binding region but some bump in the quasi-free region. Finding so prominent peaks in the η'-binding region as to be possibly observed in future experiments, we conclude that with an order of 100 MeV mass reduction and a 40 MeV absorption width at the saturation density we have a chance to observe the η'-nucleus bound states in the $^{12}\mathrm{C}(\pi^+, p)$ reaction. We see also clear peaks around the η' production threshold, for instance $(0p_{3/2})_n^{-1}\otimes d_{\eta'}$ in plot (b) and $(0p_{3/2})_n^{-1}\otimes f_{\eta'}$ in plot (c). They are not signals of the bound states, however, these are remnants of the bound states which could be formed if the attraction would be stronger. Therefore, such peak structure also can be signals of the strong attractive potential.

4 Conclusion

We point out that partial restoration of chiral symmetry in a nuclear medium induces suppression of the $\mathrm{U}(1)_A$ anomaly effect to the η' mass. Consequently, we expect a large mass reduction of the η' meson in nuclear matter with a relatively smaller absorption width. The mass reduction could be observed as η'-nucleus bound states in the formation reactions. The interplay between the chiral symmetry restoration and the $\mathrm{U}(1)_A$ anomaly effect can be a clue to understand the η' mass generation mechanism. Therefore, experimental observations

of the deeply η'-nucleus bound states, or even confirmation of nonexistence of such deeply bound states, is important to solve the $U(1)_A$ problem.

Acknowledgments

This work was partially supported by the Grants-in-Aid for Scientific Research (No. 22740161, No. 20540273, and No. 22105510). This work was done in part under the Yukawa International Program for Quark- hadron Sciences (YIPQS).

Bibliography

[1] K. Suzuki *et al.*, Phys. Rev. Lett. **92** 072302 (2004).

[2] E. Friedman *et al.*, Phys. Rev. Lett. **93** (2004) 122302; E. Friedman *et al.*, Phys. Rev. C **72** (2005) 034609.

[3] E.E. Kolomeitsev, N. Kaiser, and W. Weise, Phys. Rev. Lett. **90**, 092501 (2003); D. Jido, T. Hatsuda and T. Kunihiro, Phys. Lett. B **670** (2008) 109; Prog. Theor. Phys. Suppl. **168** (2007) 478.

[4] D. Jido, H. Nagahiro, and S. Hirenzaki, arXiv:1109.0394[nucl-th].

[5] D. Jido, H. Nagahiro, and S. Hirenzaki, Phys. Rev. **C66** (2002) 045202; H. Nagahiro, D. Jido, and S. Hirenzaki, Phys. Rev. **C68** (2003) 035205; D. Jido, E.E. Kolomeitsev, H. Nagahiro, and S. Hirenzaki, Nucl. Phys. **A811** (2008) 158.

[6] T. Csorgo, R. Vertesi and J. Sziklai, Phys. Rev. Lett. **105** (2010) 182301; R. Vertesi, T. Csorgo and J. Sziklai, Phys. Rev. C **83** (2011) 054903.

[7] P. Moskal *et al.*, Phys. Lett. B **482** (2000) 356.

[8] M. Nanova, talk given at Baryons10, Osaka, Japan, (2010).

[9] P. Costa, M. C. Ruivo and Yu. L. Kalinovsky, Phys. Lett. B **560** (2003) 171.

[10] H. Nagahiro, M. Takizawa, and S. Hirenzaki, Phys. Rev. **C74** (2006) 045203.

[11] J. I. Kapusta, D. Kharzeev and L. D. McLerran, Phys. Rev. D **53** (1996) 5028.

[12] E. Oset, A. Ramos, Phys. Lett. **B**, in print, [arXiv:1010.5603 [nucl-th]].

[13] H. Nagahiro, Prog. Theor. Phys. Suppl. **186** (2010) 316-324.

[14] H. Nagahiro, D. Jido, and S. Hirenzaki, Nucl. Phys. **A761** (2005) 92; H. Nagahiro and S. Hirenzaki, Phys. Rev. Lett. **94** (2005) 232503; H. Nagahiro, D. Jido, and S. Hirenzaki, Phys.Rev. **C80** (2009) 025205.

Production and study of baryons with beauty at the Italian heavy-flavor factory (Super*B*)

Alessandro Feliciello[1,a], Tullio Bressani[a], and Vincenzo Lucherini[b]
[a]*INFN - Sezione di Torino, I-10125 Torino, ITALY*
[b]*Laboratori Nazionali di Frascati dell'INFN, I-00044 Frascati (RM), ITALY*

Super*B* is an INFN flagship project for a new high-luminosity heavy-flavor factory. Along with its companion detector, it is dedicated to the search for CP violation effects in the B meson sector with the aim of looking for direct and indirect signals of new physics, beyond the Standard Model. However it could offer as well the opportunity for a systematic, high-statistics study of b baryon properties and for a search for super-nuclei, that is bound nuclear systems with an explicit content of beauty.

1 Introduction

Following a long and successful tradition in building and operating lepton colliders, INFN launched a plan to construct the new Super*B* e^+e^- complex accelerator [1]. The selected site is the Tor Vergata University Campus, near Rome and close to the INFN-LNF historical research center. Super*B* will be an asymmetric, double-ring accelerator designed to run at the $\Upsilon(4S)$ resonance center-mass (c.m.) energy with a baseline luminosity in excess of 10^{36} cm^{-2} s^{-1}, that is about two orders of magnitude larger than the peak luminosity of the existing B-factories. The nominal beam energies will be $E_{e^+} \approx 6700$ MeV and $E_{e^-} \approx 4200$ MeV but Super*B* will have the capability of running in the c.m. energy range between $\psi(3770)$ (the charm threshold) and $\Upsilon(5S)$ resonance as well. Finally, it will be possible to have a $\sim$70% polarized electron beam [2], that also has significant impact on the physics potential of this project.
This next generation flavor-factory, along with its companion detector [3], will be mainly dedicated to the measurements of CP violating processes in the B meson sector, looking for deviation from the Standard Model predictions that can be interpreted as signals for new physics. At the same time the experiment will perform high-precision tests of the Standard Model. In addition Super*B* should be considered within a synergic strategy with LHCb, the flavor physics experiment recently started at the CERN LHC hadron collider. On one hand, if new physics phenomena will be observed at LHC, data from very sensitive heavy-flavor experiments will be necessary to constrain such results and to better understand their

[1] Alessandro.Feliciello@to.infn.it

nature. In this respect a high-luminosity, asymmetric flavor factory can then provide a set of complementary information. Moreover this alternative approach offers the additional advantage of cleanly extracting the signal, typical situation experienced at electromagnetic machines where the environment is much cleaner. On the other hand, if no evidence for physics beyond Standard Model will be found at the energy frontier experiments, then measurements that will be performed at Super*B* would allow for an alternative way to explore an energy range up to 10 TeV. The complete, wide spectrum of Super*B* physics reach is described in [4].

However Super*B* might offer a playground for a systematic study of the properties of b baryons and for an investigation of their interactions with nucleons in nuclei.

2 Bottom baryon production

Information on b baryons is scarce. It is sufficient to browse the last edition of The Review of Particle Physics [5] to realize how different is the level of knowledge about, for instance, B mesons and b baryons. In some cases the existence itself of such particles still ranges from very likely to certain and then a confirmation is highly desirable as long as the assessment of their quantum numbers and their branching fractions. One of the reasons of this lack of data is purely experimental: it is not so easy to abundantly produce heavy-flavor baryons and it is very challenging to extract signals from a huge background. A significant contribution to this field is being provided by the Tevatron Collider experiments [6] and very likely many data will soon flow from LHC. However flavor factories can play an important role as well.

The idea of creating heavy-flavor baryons at an e^+e^- collider is not brand new. About 20 years ago it was suggested [7] to exploit the charm and the beauty exchange reaction on nuclei in order to produce charmed and bottom baryons at the ARES facility, a proposed high-luminosity, single-pass, e^+e^- machine. The same method was recently used at DAΦNE, by the FINUDA experiment [8], in order to produce Λ and Σ hyperons via the strangeness exchange reaction induced by K^- following the ϕ resonance decay. Now Super*B* offers again the opportunity to have a unique source of b baryons.

At first glance it may be objected that the available c.m. energy ($\sim$10600 MeV) is not enough to produce even the lightest b baryon-antibaryon pair (m($\Lambda_b^0\overline{\Lambda_b^0}$) $\approx$ 11240 MeV). However the leading idea of the proposed experimental method is to put a thin target on the flight path of B^- mesons, emitted in the $\Upsilon(4S)$ resonance decay, in order to produce b baryons via the beauty exchange reactions

(1) $$B^-_{stop} + \mathcal{N}_{bound} \rightarrow \Lambda_b^0 + \pi^{-0},$$

(2) $$B^-_{stop} + \mathcal{N}_{bound} \rightarrow \Sigma_b^{\pm} + \pi^{-0+},$$

(3) $$B^-_{stop} + \mathcal{N}_{bound} \rightarrow \Sigma_b^{*\pm} + \pi^{-0+},$$

(4) $$B^-_{flight} + \mathcal{N}_{bound} \rightarrow \Xi_b^{-0} + K^{+0},$$

where $\mathcal{N}_{bound}$ indicates either a proton or a neutron bound in a nucleus. While processes (1–3) occur even with stopped particles, it has to be checked whether reaction (4) can be induced by B^- mesons in flight. Unfortunately the possibility of generating Ω_b^- by this method is completely out of discussion. The properties of the produced Λ_b^0, $\Sigma_b^{\pm}$, $\Sigma_b^{*\pm}$ and, possibly, Ξ_b^{-0} hadrons will be then studied, with unprecedented accuracy, through the measurement of their decay products in the Super*B* companion apparatus. Such a systematic observation of b baryons will offer the opportunity to get information on non-perturbative QCD and the potential models. The large mass difference between b quark and the other constituent quarks could in fact allow a significant simplification in the theoretical description of a system where a light quark pair (diquark) orbits around the "nucleus" b quark.

3 The experimental setup

In the innovative collision scheme designed in order to reach the highest possible luminosity [9], e^+ and e^- beams will have extremely reduced dimensions at the interaction point: 7.211 μm in the horizontal plane and 0.036 μm in the vertical one. These numbers make Super*B* particularly suitable for the installation of a thin target as close as possible to the $\Upsilon(4S)$ formation point, capable of intercepting the maximum fraction of the B^- mesons following the resonance decay. Actually this is the crucial point of the project, since the choice of the distance from the interaction point and the target entrance surface is constrained by the very small B^- meson $c\tau$ value (492.0 μm) and by the requirement of avoiding any interference with the circulating beams.

Another favorable condition is represented by the fact that e^+ and e^- beams will not collide head-on. This means that, besides the 2.519 GeV/c longitudinal (i.e. along the beam pipe axis) boost, $\Upsilon(4S)$ has a sizeable transverse momentum component (0.359 GeV/c) as well. Moreover preliminary Monte Carlo calculation shows that the angular distribution of the generated B^- mesons is such that they are preferentially emitted in the horizontal plane. An interesting solution could be then that of putting the target only in the hemisphere where the B^- mesons are produced with higher energy. The advantage is twofold: the target could be placed a little bit far away from the interaction point and the B^+ mesons traveling in the opposite, free hemisphere can be exploited in order to tag the event. The option currently under evaluation is that of using a half hollow cylinder, 1 mm long and with an internal radius of 0.2 mm and an external one of 0.5 mm. It will be placed with its axis coincident with the beam pipe one and, keeping in mind that Super*B* is an asymmetric machine, completely shifted in the $z > 0$ halfspace, i.e. beyond the interaction point, along the e^+ flight direction. The arguments to be taken into account in order to choose the proper target material are its mechanical stability, its electrical conductibility, the heating during accelerator normal operation and the power deposition in case of beam loss. Gold or Platinum seem to be the best candidates to fulfill these technical requirements. Very likely the target will be efficiently cooled and should be (re)movable during the beam injection

and machine tuning phase. However this does not represent an issue since it is possible to conceive a mechanism very similar to that routinely used to operate the beam scraper system.

The $e^+ + e^- \rightarrow \Upsilon(4S)$ production cross section is $\sim$1.1 nb. This means that at the design luminosity value of 10^{36} cm^{-2} s^{-1} $\Upsilon(4S)$ resonance will be generated at a rate of 1.1 kHz. By keeping in mind that it decays in a B^+B^- meson pair with a branching fraction of 51.6% we may expect to have a B^- meson flow of $\sim$550 Hz. By taking into account the fraction of surviving B^- with $\beta\gamma \approx 0.2$ (0.7%) and by making an educated guess about target acceptance and stopping efficiency (10%), reconstruction efficiency of the apparatus (10%) and accelerator daily duty cycle (70%) we estimate a b baryon production rate in excess of 2000 events per day.

4 From hyper- to super-nuclear physics

Another topic of fundamental interest that could be addressed is the investigation of b baryons interaction with nucleons in nuclei. It is indeed worth to remind that this experimental approach is the unique method to infer information about b baryon-nucleon interaction at low energies. This is a completely unexplored field and the challenge is to see whether a b baryon can become part of the target nucleus and can then form a nuclear bound system, called super-nucleus. The possible existence of such objects was suggested several years ago by Tyapkin [10], in complete analogy to what happens with s baryon Λ which can replace one nucleon in a nucleus to form nuclear bound systems, known as hyper-nuclei [11]. This is a very natural extension based on the expectation that the entire family of baryons experiences exchange forces which are similar to the corresponding interaction potentials. This statement is endorsed by the close similarity of the quark structure of the lightest flavored baryons Λ(uds), Λ_c^+(udc) and Λ_b^0(udb).

From the experimental point of view the main issue is the energy distribution of the b baryons generated in the processes (1–4). Preliminary calculations indicate that, when produced on free nucleons, their momentum spectrum typically ranges from $\sim$0.2 to $\sim$1.3 GeV/c. This fact could then reduce the fraction of b baryons with a sizeable probability of sticking to the target nucleus. To this purpose a careful study of how the nuclear medium affects the energy distribution of the produced b baryons must be performed in order to get a realistic estimation of the super-nuclei formation rate. As far as the identification of the produced super-fragment is concerned, a possible strategy could be based on the measurement of the generally high-energy decay products.

5 Conclusions

The construction of the Super*B* collider will allow to shed light on many fundamental aspects of the flavor physics thanks to the capability of collecting in a reasonable amount of time large data samples corresponding to an integrated luminosity ranging from 50 to 100 ab^{-1}.

However this new facility may offer the opportunity for carrying on a nuclear physics experiment, dedicated to a high-statistics study of *b* baryons properties and of their interactions with nucleons in nuclei, a subject absolutely unknown at present. This way it will be possible to look for super-nuclei as well, a definitively hard experimental task but of fundamental interest. Such an experiment may be integrated in the Super*B* companion apparatus.

Acknowledgments

The authors acknowledge the Super*B* Collaboration for the kind permission of using the fast simulation code in doing the preliminary calculations described in this paper.

Bibliography

[1] M. E. Biagini *et al.* [Super*B* Collaboration], arXiv:1009.6178 [physics.acc-ph].

[2] U. Wienands *et al.*, *In the Proceedings of 1st International Particle Accelerator Conference: IPAC'10, Kyoto, Japan, 23-28 May 2010, pp. TUPEB029*.

[3] E. Grauges *et al.* [Super*B* Collaboration], arXiv:1007.4241 [physics.ins-det].

[4] D. G. Hitlin *et al.*, arXiv:0810.1312 [hep-ph];
B. O'Leary *et al.* [Super*B* Collaboration], arXiv:1008.1541 [hep-ex].

[5] K. Nakamura *et al.* [Particle Data Group], J. Phys. G **37** (2010) 075021.

[6] S. Donati [CDF and D0 Collaborations], PoS **FPCP2010** (2010) 019.

[7] T. Bressani and F. Iazzi, Nuovo Cim. A **102** (1989) 597.

[8] A. Feliciello, Riv. Nuovo Cim. **32** (2009) 147.

[9] M. Bona *et al.* [Super*B* Collaboration], arXiv:0709.0451 [hep-ex].

[10] A. A. Tyapkin, Yad. Fiz. **22** (1975) 181.

[11] M. Danysz and J. Pniewsky, Philos. Mag. 44 (1953) 348.

In-medium properties of the ω meson near the production threshold

Michaela Thiel[1] on behalf of the A2 Collaboration
II. Physikalisches Institut, JLU Gießen, D-35392 Gießen, GERMANY

Using the CrystalBall/TAPS photon spectrometer at MAMI Mainz the ω photoproduction off nuclei (C, Nb) and off the proton (LH_2) were studied via the hadronic decay channel $\omega \to \pi^0\gamma$. The aim of this work is to investigate whether the properties of the ω meson are modified within normal nuclear matter. Two different experimental approaches have been used: the measurement of the ω lineshape and of the ω momentum distribution. Differences are expected to be most pronounced close to the production threshold ($E_{\gamma,thresh} = 1108$ MeV). Thus, the analyses were performed in the energy range 900 to 1300 MeV. Here we present the experimental results in comparison to GiBUU transport code calculations [1].

1 Introduction

The aim of this experiment is to study whether the well known vacuum mass and width of the ω meson changes in a strongly interacting environment. Possible modifications of these properties can help to understand the strong interaction in the non-perturbative sector of QCD. Hence, considerable attention has been given to this field in the last years, both from the theoretical and experimental side (e.g. [2]). The focus of this analysis is on the sector of light vector mesons where different model calculations predict relatively large changes in the mass or width. Due to the strong broadening of the ω meson in a nuclear medium [3] the sensitivity of the lineshape to in-medium modifications is reduced [4]. Whereas GiBUU calculations predict only small differences in the ω lineshape, the analysis of the momentum distribution is predicted to be more sensitive to in-medium modifications.

2 Experimental Setup

The data have been taken at the Mainz Mikrotron MAMI, using the combined detector system Crystal Ball [5] and TAPS [6]. When electrons from the accelerator with a maximum energy of $E_{e^-} = 1508$ MeV hit a radiation target of 10 μm copper Bremsstrahlung photons are produced. For these anaysis energy marked photons in the range of 900 to 1300 MeV

[1]michaela.thiel@exp2.physik.uni-giessen.de

have been used. The Crystal Ball calorimeter comprises 672 NaI(Tl) crystals with 15.7 radiation lengths. The detector covers polar angles from 20° to 160° and the full azimuthal angle. The polar angle up to 20° in forward direction is covered by the TAPS calorimeter in a forward wall configuration. It consists of 378 BaF_2 ($\approx$ 12 X_0) and 24 $PbWO_4$ ($\approx$ 12 X_0) crystals, covering the full azimuthal angle. For charged particle identification the PID, consisting of 24 plastic scintillator bars, in the center of the Crystal Ball as well as the 5 mm thick Veto plastic scintillators, placed in front of each TAPS crystal, have been used. The three different targets LH_2, C, Nb with 30 mm in diameter and 49 mm, 15 mm, 1 mm in length, respectively, were placed directly in the center of the Crystal Ball.

3 Experimental Approach

The channel of interest is the hadronic decay mode of the ω meson into three photons in the final state:

$$\gamma A \rightarrow (A-1)\omega p \rightarrow (A-1)\pi^0\gamma p \rightarrow (A-1)\gamma\gamma\gamma p \quad (1)$$

The invariant mass of the ω meson is reconstructed using the three photon final state invariant mass, where two of the photons have to come from a π^0 decay. Since the π^0 meson can rescatter in the nuclear medium its 4-momentum can change, leading to a distortion of the ω invariant mass. To suppress these final state interactions down to the percent level a cut on the kinetic energy $T_{\pi^0} > 150$ MeV is applied (for details see [7]).
For the analyses strict time cuts ($\pm 3\sigma$) have been applied to the detector systems (CB, TAPS, Tagger) and only events are used where exactly three photons are detected within the prompt peak. A cluster threshold of 50 MeV is required to reduce the amount of split-offs. For the lineshape analysis the proton is identified using time of flight and $\Delta E/E$ techniques. For this proton a cut on the missing mass between 800 and 950 MeV is applied.
Because of the relatively long lifetime of the omega meson (τ = 22 fm/c), the lineshape of the resulting $\pi^0\gamma$ invariant mass spectrum is always a superposition of vacuum and in-medium decays. Thus, to increase the amount of decays inside the nuclear medium the data have been taken close to the ω production threshold $E_{\gamma,thresh} = 1108$ MeV in the energy range 900 to 1300 MeV.

3.1 Lineshape Analysis

To extract the ω meson lineshape, the shape of the background has to be determined and subtracted. In Figure 1 (left) the $\pi^0\gamma$ invariant mass spectrum is shown. The background can be parametrized (dashed blue line) using the following equation:

$$b(x) = exp(p_0 + p_1 \cdot x + p_2 \cdot x^2 + p_3 \cdot x^3 + p_4 \cdot x^4). \quad (2)$$

In a second independent method the background is directly determined from the data. One of the main background sources comes from events with four photons in the final state ($\pi^0\pi^0$ or $\pi^0\eta$ events) where one photon is lost due to cluster overlapping or detection inefficiencies. Details can be found in [4]. Figure 1 (middle) shows the background determined from the data in magenta together with a fit through this contribution (dashed line). The good agreement of both methods can be seen in the right panel of Figure 1.

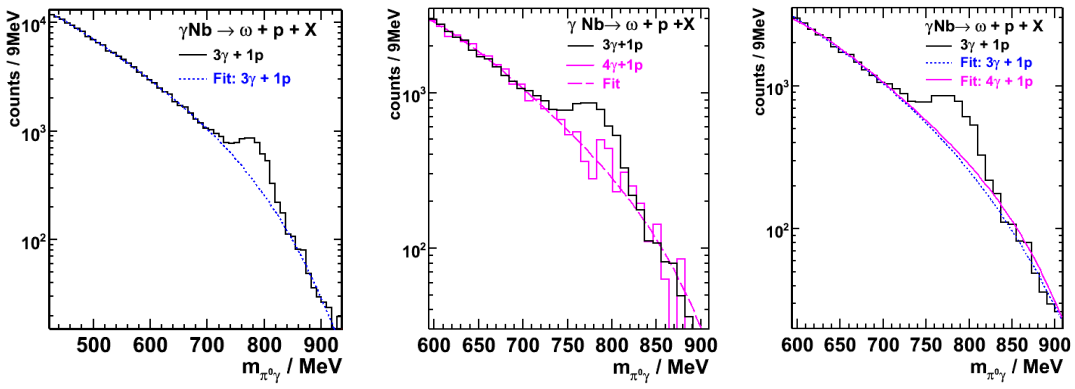

Figure 1: $\pi^0\gamma$ invariant mass spectrum for the Nb target (black). Left: The dashed blue line shows a fit of the background. Middle: The background determined directly from data (magenta) and a fit to the background contribution (dashed magenta). Right: Comparison of both background determination.

This can be verified by looking at the obtained lineshapes in Figure 2 (left). For the Nb data the background determined with the different methods is subtracted and within the error bars no significant deviations are observed.
The lineshape comparison of the three different targets provides good agreement between niobium and carbon, with a width slightly broader compared to LH_2 (see Figure 2 (middle)). In Figure 2 (right) the $\pi^0\gamma$ invariant mass spectrum is compared to different in-medium scenarios calculated with the GiBUU transport code [8]. Here the in-medium ω pole mass is modified as a function of the probed density according to:

$$m_\omega = m_\omega^0 \cdot \left(1 - 0.16 \cdot \frac{\rho_N}{\rho_0}\right) \tag{3}$$

For the scenarios including collisional broadening an in-medium width of $\Gamma_{med} = 150$ MeV has been assumed. Only small differences in the four scenarios are observed. The limited sensitivity arises from the strong broadening of the ω meson, resulting in a suppression of contributions from higher densities by order $1/\rho^2$ near the peak.

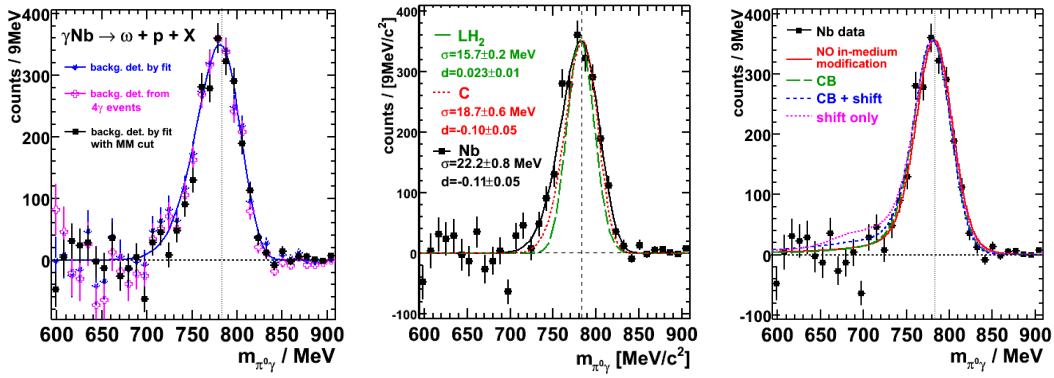

Figure 2: Left: Preliminary background subtracted $\pi^0\gamma$ invariant mass spectrum for the Nb target, applying the different background determination methods. Middle: Lineshape comparison for the three targets LH_2 (green), C (red) and Nb (black). The distortion of the lineshape due to different target thicknesses has been corrected for. Right: Background subtracted $\pi^0\gamma$ invariant mass spectrum on Nb target compared to GiBUU calculations: no modification (solid red line), collisional broadening (dashed green line), collisional broadening plus mass shift (dashed blue line) and mass shift only (dotted magenta line).

3.2 Momentum Distribution

The analysis of the momentum distribution implies information on in-medium properties at the nuclear density of the production point. Here the advantage is to be independent of any meson lifetime. For this analysis the ω yield is determined in different 50 MeV wide momentum bins from 150 MeV/c up to 1000 MeV/c. To have sufficient statistics over the full momentum range, the analysis is performed semi-exclusively without requiring the proton. In Figure 3 the experimentally observed momentum distributions (acceptance corrected) for C and Nb are compared to recent GiBUU transport calculations [9]. For comparison, the data points and the theory curves are normalized to the same area.

4 Conclusion

Although the statistics is good and improved to former experiments in this energy regime by a factor 3 (see [8]) only the "mass shift only" scenario seems to be disfavoured by the lineshape analysis. This result is confirmed by the analysis of the momentum distribution of the ω meson, which also disfavours the scenarios including a mass shift.

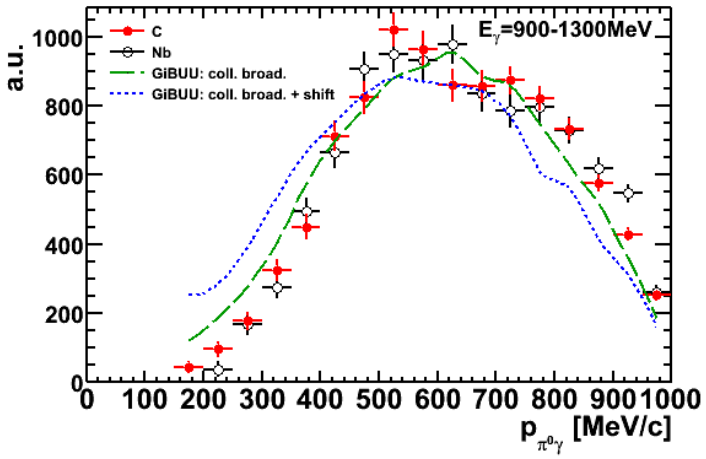

Figure 3: Momentum distribution for the two targets carbon (red points) and niobium (open circles), compared to GiBUU calculations: collisional broadening (dashed green line) and collisional broadening plus mass shift (dashed blue line).

Acknowledgments

This work was supported by DFG through SFB/TR16.

Bibliography

[1] http://gibuu.physik.uni-giessen.de

[2] S. Leupold, V. Metag, U.Mosel, Int. J. Mod. Phys. **1**9, 147 (2010).

[3] M. Kotulla *et al.*, Phys. Rev. Lett. **1**00, 192302 (2008).

[4] M. Nanova *et al.*, Phys. Rev. C **82**, 035209 (2010).

[5] A. Starostin *et al.*, Phys. Rev. C **64**, 055205 (2001).

[6] R. Novotny, IEEE Trans. Nucl. Sci. **38**, 379 (1991) .

[7] J.G. Messchendorp *et al.*, Eur. Phys. A **11**, 95 (2001).

[8] M. Nanova *et al.*, Eur. Phys. J. A **4**7, 16 (2011).

[9] J. Weil, private communication (2011).

Internal structure of the $\Lambda(1405)$ resonance probed in chiral unitary amplitude

Takayasu Sekihara[a], T. Hyodo[a], and D. Jido[b]
[a]*Department of Physics, Tokyo Institute of Technology, Tokyo 152-8551, Japan*
[b]*Yukawa Institute for Theoretical Physics, Kyoto University, Kyoto 606-8502, Japan*

The internal structure of the resonant $\Lambda(1405)$ state is investigated based on meson-baryon coupled-channels chiral dynamics. We evaluate $\Lambda(1405)$ form factors which are extracted from current-coupled scattering amplitudes in meson-baryon degrees of freedom. Using several probe currents and channel decomposition, we find that the resonant $\Lambda(1405)$ state is dominantly composed of widely spread $\overline{K}$ around N, with escaping $\pi\Sigma$ component.

1 Introduction

There are hadrons which are expected to have exotic structures, *e.g.*, hadronic molecules, and it is one of the important issues in hadron physics to clarify their structures. A classical example is the excited baryon $\Lambda(1405)$, which has been considered as an s-wave $\overline{K}N$ quasibound state [1]. It is also suggested by the modern theoretical approach based on the chiral dynamics within the unitary framework (the chiral unitary approach) [2–7] that $\Lambda(1405)$ is dynamically generated in the meson-baryon scattering, in addition to the good reproduction of the low-energy $K^- p$ cross sections and the $\Lambda(1405)$ peak in $\pi\Sigma$ mass spectrum. Moreover, the chiral unitary approach predicts double-pole structure for $\Lambda(1405)$ [4, 6] and one of the poles is expected to originate from the $\overline{K}N$ bound state [8, 9]. Some approaches for the survey on the $\Lambda(1405)$ structure in experiments have been proposed, e.g., in Refs. [10, 11].

If $\Lambda(1405)$ is dominated by the $\overline{K}N$ quasibound state with a small binding energy, one can expect that $\Lambda(1405)$ has a larger size than typical ground state baryons dominated by genuine qqq components. Motivated by this expectation, in Ref. [12] we have investigated the internal structure of the resonant $\Lambda(1405)$ state by evaluating density distributions obtained from the form factors on the $\Lambda(1405)$ pole originating from the $\overline{K}N$ bound state. In our study the $\Lambda(1405)$ form factors are directly extracted from the current-coupled scattering amplitude, which involves a response of $\Lambda(1405)$ to the external current. The current-coupled scattering amplitude is evaluated in a charge conserved way by considering current couplings to the constituent hadrons inside $\Lambda(1405)$. Here we note that the wave functions and form factors of $\Lambda(1405)$ were studied also in Ref. [13] in a cut-off scheme

within chiral unitary approach, which results were not significantly different from ours, except for the high momentum region compared to the cut-off.

2 Internal structure of $\Lambda(1405)$

In the chiral unitary approach, the meson-baryon scattering amplitude T_{ij} with channel indices i and j is obtained by a coupled-channels equation,

$$T_{ij}(\sqrt{s}) = V_{ij}(\sqrt{s}) + \sum_k V_{ik}(\sqrt{s}) G_k(\sqrt{s}) T_{kj}(\sqrt{s}), \tag{1}$$

with the interaction kernel V_{ij} given by chiral perturbation theory, a meson-baryon loop integral G_k, and the center-of-mass energy $\sqrt{s}$. The obtained amplitude contains dynamically generated $\Lambda(1405)$ in s wave. Next, in order to observe response of $\Lambda(1405)$ to the conserved probe current in the chiral unitary approach, we evaluate current-coupled scattering amplitude $T^\mu_{\gamma ij}$ in a charge conserved way, considering current couplings to the constituent hadrons as [12, 14]:

$$T^\mu_{\gamma ij}(\sqrt{s'}, \sqrt{s}; Q^2) = T^\mu_{\gamma(1)ij} + T^\mu_{\gamma(2)ij} + T^\mu_{\gamma(3)ij}, \tag{2}$$

with the squared current momentum Q^2 and

$$T^\mu_{\gamma(1)ij} = \sum_k T_{ik} D^\mu_{\mathrm{M}_k} T_{kj}, \quad T^\mu_{\gamma(2)ij} = \sum_k T_{ik} D^\mu_{\mathrm{B}_k} T_{kj}, \quad T^\mu_{\gamma(3)ij} = \sum_{k,l} T_{ik} G_k \Gamma^\mu_{kl} G_l T_{lj}, \tag{3}$$

where D_{M_k} and D_{B_k} are respectively loop integrals with the current couplings to the meson and baryon and Γ_{ij} represents $MBM'B'\gamma$ vertex. Then the $\Lambda(1405)$ form factor, $F^\mu(Q^2)$, can be extracted by [12, 15],

$$F^\mu(Q^2) = -\frac{(\sqrt{s'} - Z_{\mathrm{R}}) T^\mu_{\gamma ij}(\sqrt{s'}, \sqrt{s}; Q^2)}{T_{ij}(\sqrt{s})}\bigg|_{\sqrt{s}\to Z_{\mathrm{R}}}\bigg|_{\sqrt{s'}\to Z_{\mathrm{R}}}, \tag{4}$$

where Z_{R} is the $\Lambda(1405)$ pole position. Here we note that we have following relations:

$$\hat{Q}\frac{dG_k}{d\sqrt{s}} = (D^0_{\mathrm{M}_k} + D^0_{\mathrm{B}_k})|_{Q^2=0}, \quad \hat{Q}\frac{dV_{ij}}{d\sqrt{s}} = \Gamma^0_{ij}|_{Q^2=0}, \tag{5}$$

with $\hat{Q}$ being the charge of $\Lambda(1405)$ with respect to the probe current. These are the Ward-Takahashi identity for the two-body free propagator G_k and the elementary vertex V_{ij}.

Now let us show our results for the internal structure of the resonant $\Lambda(1405)$. First, we write a normalization relation for the baryonic [$F_{\mathrm{B}}(Q^2)$] and strangeness [$F_{\mathrm{S}}(Q^2)$] form factors of $\Lambda(1405)$ proved in Ref. [12],

$$F_{\mathrm{B}}(Q^2 = 0) = -F_{\mathrm{S}}(Q^2 = 0) = -\sum_{i,j} g_i g_j \left(\frac{dG_i}{d\sqrt{s}}\delta_{ij} + G_i \frac{dV_{ij}}{d\sqrt{s}} G_j\right)\bigg|_{\sqrt{s}\to Z_{\mathrm{R}}} = 1, \tag{6}$$

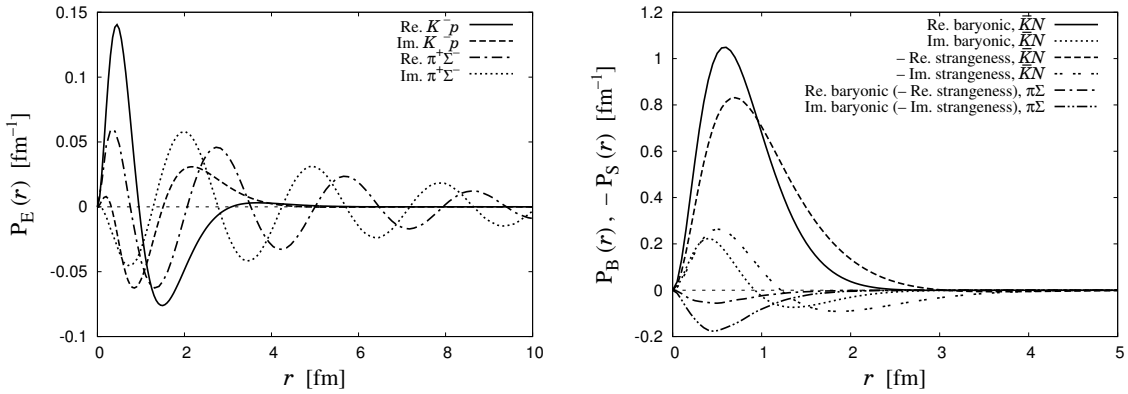

Figure 1: Electric (P_E, left), baryonic and strangeness (P_B and P_S, right) density distributions of $\Lambda(1405)$ in each component. Here P_E is shown in particle basis whereas P_B and P_S are in isospin basis [12].

where $g_i g_j$ is a residue of T_{ij} at the $\Lambda(1405)$ pole position and $dG_i/d\sqrt{s}$ ($dV_{ij}/d\sqrt{s}$) term comes from $D^0_{M_i} + D^0_{B_i}$ (Γ^0_{ij}) at $Q^2 = 0$. This relation corresponds to the Ward identity for the vertex and wave-function renormalization factors, and this originates from that we evaluate $T^{\mu}_{\gamma ij}$ in a charge conserved way with current couplings satisfying Ward-Takahashi identity (5). With this relation, we can pin down the dominant component of the $\Lambda(1405)$ structure by decomposing the summation in Eq. (6). As a result, we find that contribution from the $\bar{K}N(I = 0)$ channel ($= -g^2_{\bar{K}N} dG_{\bar{K}N}/d\sqrt{s}$) is $0.994 + 0.048i$ whereas contributions from other channels and the vertex term ($= -\sum_{i,j} g_i G_i dV_{ij}/d\sqrt{s} G_j g_j$) are negligibly small [12]. Therefore, this result indicates that the $\bar{K}N(I = 0)$ channel generates more than 99% of the $\Lambda(1405)$ charge, which is consistent with the $\bar{K}N$ quasibound state picture for $\Lambda(1405)$.

Next we show the electric, baryonic, and opposite-sign strangeness density distributions (P_E, P_B, and $-P_S$, respectively) of $\Lambda(1405)$ in each component in Fig. 1. From P_E, we can see that the negative (positive) charge distribution appears in $\Lambda(1405)$ due to the existence of lighter K^- (heavier p) in the outside (inside) region, bearing in mind the $\bar{K}N$ dominance for $\Lambda(1405)$. Also it is interesting to see the dumping oscillation in $\pi^+\Sigma^-$ (equivalently $\pi^-\Sigma^+$ with the opposite sign) component in P_E as the decay of the system, although this is not observed in the total P_E due to the cancellation of $\pi^+\Sigma^-$ and $\pi^-\Sigma^+$ components. On the other hand, P_B and P_S indicate that inside $\Lambda(1405)$ the $\bar{K}$ component has longer tail than the N component and $\bar{K}$ distribution largely exceeds typical hadronic size $\lesssim 1$ fm, bearing in mind that the baryonic (strangeness) current probes the N ($\bar{K}$) distribution inside $\Lambda(1405)$.

3 Summary

We have investigated the internal structure of the resonant $\Lambda(1405)$ state in the chiral unitary approach, in which $\Lambda(1405)$ is dynamically generated in meson-baryon coupled-channels chiral dynamics. Probing $\Lambda(1405)$ with conserved current in a charge conserved way, we have observed that $\overline{K}N$ component gives more than 99% of the total $\Lambda(1405)$ charge. The electric density distribution indicates that inside $\Lambda(1405)$ lighter K^- (heavier p) exists in the outside (inside) region and the escaping $\pi\Sigma$ component appears as the decay mode of $\Lambda(1405)$. Also from the baryonic and strangeness density distributions we have found that inside $\Lambda(1405)$ the $\overline{K}$ component has longer tail than the N component and $\overline{K}$ distribution largely exceeds typical hadronic size $\lesssim 1$ fm.

This work is partly supported by the Grand-in-Aid for Scientific Research from MEXT and JSPS (No. 21840026, 22105507, 22740161, and 22-3389).

Bibliography

[1] R. H. Dalitz and S. F. Tuan, Annals Phys. **10**, 307 (1960).

[2] N. Kaiser, P. B. Siegel and W. Weise, Nucl. Phys. A **594**, 325 (1995).

[3] E. Oset and A. Ramos, Nucl. Phys. A **635**, 99 (1998).

[4] J. A. Oller and U. G. Meissner, Phys. Lett. B **500**, 263 (2001).

[5] M. F. M. Lutz and E. E. Kolomeitsev, Nucl. Phys. A **700**, 193 (2002).

[6] D. Jido, J. A. Oller, E. Oset, A. Ramos and U. G. Meissner, Nucl. Phys. A **725**, 181 (2003).

[7] T. Hyodo and D. Jido, Prog. Part. Nucl. Phys. (2011), doi:10.1016/j.ppnp.2011.07.002.

[8] T. Hyodo and W. Weise, Phys. Rev. C **77**, 035204 (2008).

[9] T. Hyodo, D. Jido and A. Hosaka, Phys. Rev. C **78**, 025203 (2008).

[10] D. Jido, E. Oset and T. Sekihara, Eur. Phys. J. A **42**, 257 (2009); *ibid.* **47**, 42 (2011).

[11] S. Cho *et al.* [ExHIC Collaboration], Phys. Rev. Lett. **106**, 212001 (2011); arXiv:1107.1302 [nucl-th].

[12] T. Sekihara, T. Hyodo and D. Jido, Phys. Lett. B **669**, 133 (2008); Phys. Rev. C **83**, 055202 (2011).

[13] J. Yamagata-Sekihara, J. Nieves and E. Oset, Phys. Rev. D **83**, 014003 (2011).

[14] B. Borasoy, P. C. Bruns, U. G. Meissner and R. Nissler, Phys. Rev. C **72**, 065201 (2005).

[15] D. Jido, A. Hosaka, J. C. Nacher, E. Oset and A. Ramos, Phys. Rev. C **66**, 025203 (2002).

Hypernuclei Production by K^- at rest

Germano Bonomi[1]
Department of Mechanical and Industrial Engineering
via Branze 38, Brescia, ITALY
& INFN Pavia
via Bassi 6, Pavia, ITALY

The creation of a hypernucleus requires the injection of *strangeness* into the nucleus. This is possible in different ways, mainly using π^+ or K^- beams on fixed targets. A review of hypernuclei production by K^- at rest is here presented. When a K^- stops inside a nucleus it can undergo the so called "strangeness-exchange reaction", in which a neutron is replaced by a Λ with the emission of a pion. By precisely studying the outgoing pions both the binding energy and the formation probability of the hypernuclei can be measured. New measurements from the FINUDA experiment on ^{7}Li, ^{9}Be, ^{13}C and ^{16}O, coupled with previous measurements on ^{12}C and ^{16}O, allowed for the first time the study of the formation of hypernuclei as a function of the atomic mass number A. The new measurements also offered the possibility of disentangling the effects due to atomic wave-function of the captured K^- from those due to the pion optical nuclear potential and from those due to the specific hypernuclear states. These new results on the study of the hypernuclei production by K^- at rest are here presented and discussed.

1 Introduction

Hypernuclei are nuclear systems in which one or more nucleons are replaced by one (or more) hyperons [1]. The more known and studied for a long time (almost 60 years) are Λ-hypernuclei, in which one Λ-hyperon replaces a nucleon of the nucleus. In Fig. 1a) a simplified representation of the single-particle states of the nucleons for a ^{12}C nucleus is shown. When the Λ replaces a neutron [Fig. 1b)] it can occupy different states [see Fig. 1 c) to f)]. When it has the same quantum numbers of the neutron it has replaced, the state is called "*substitutional*".

Hypernuclei provide a unique laboratory suitable not only for studying nuclear structure in presence of a strange quark but also for probing weak interactions between baryons. Indeed hyperons-nucleons (YN) scattering experiments are difficult to perform and data are very limited. On the other hand from hypernuclear energy levels and theoretical models

[1]germano.bonomi@ing.unibs.it

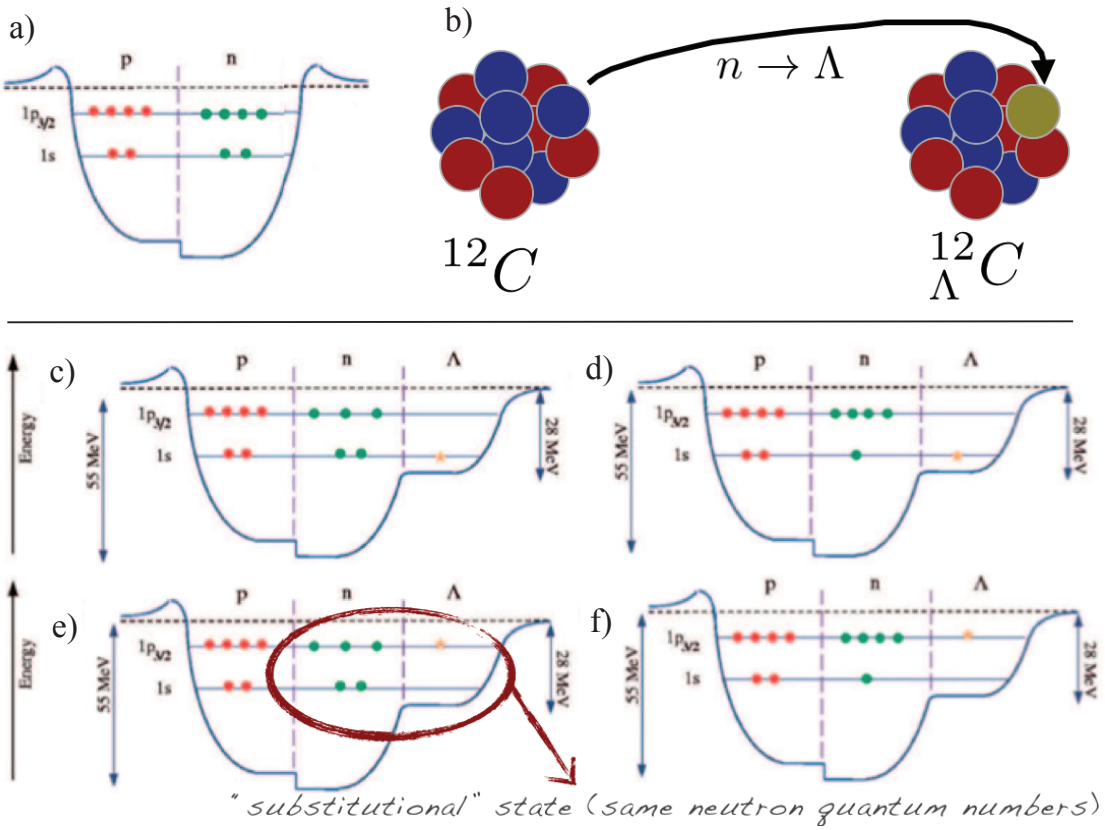

Figure 1: a) - Simplified representation of the single-particle states of the nucleons for a ^{12}C nucleus. c) to f) - Same as a) when a Λ replaced a neutron. State shown in e), when the Λ has the same quantum numbers of the neutron it replaced, it is called *substitutional* state. Representations taken from [2].

information about YN interaction can be extracted. Hypernuclei are also important to investigate dynamical changes of the nuclear structure induced by the added hyperon. In fact the Λ, reaching deep inside levels, it can attract the surrounding nucleons toward the interior ("*glue-like*" or "*core contraction*" effect), especially in light nuclei. Indeed the Λ-hyperon, since it does not suffer from Pauli blocking by other nucleons, it can penetrate into the nuclear interior and form deeply bound hypernuclear states.

2 Hypernuclei production

There are different ways to bring the *strangeness* inside a nucleus. Up to now three different reactions have been used:

1a)	$K^-_{inflight/stop} + n \rightarrow \Lambda + \pi^-$	*strangeness exchange reaction*
1b)	$K^-_{inflight/stop} + p \rightarrow \Lambda + \pi^o$	
2)	$\pi^+ + n \rightarrow \Lambda + K^+$	*associated production*
3)	$e + p \rightarrow e' + \Lambda + K^+$	*electroproduction*

Each reaction has its own advantages and plays its role in a complete program of hypernuclear spectroscopy. Reaction 1a) at rest was the first to be used [4]; reaction 2) then followed at BNL [5] and at KEK [6], while reaction 3) is relatively new [7]. The most important parameter in determining the differences of the distinct reactions is the momentum transfer. In Fig. 3 the relation between the beam momentum and the recoil/transfer momentum and between the momentum transfer and the hypernuclear cross section are shown. Low recoil momentum, like for the ($K^-_{inflight}$, π^-) reaction populates substitutional states, in which a nucleon is converted to a Λ hyperon in the same orbit with no orbital angular momentum transfer. In this way it is difficult to populate the ground state. A large recoil momentum on the other hand can excite high-spin hypernuclear states with a nucleon-hole having large angular momentum and a Λ hyperon having a small angular momentum, with the advantage to access more states.

The pros of the (K^-_{stop},π^-) reaction, if compared with the others, is the fact that it populates many states and it has a *high* formation probability compared to the associate production. On the other hand the kaon beam suffer energy struggling in the slowing down by *thick* absorbers and thus also the target must be relatively *thick* (some g/cm^2). This determines the principal drawbacks, like a large background and a limit on the energy resolution (the out-coming pions suffer multiple scattering inside the targets).

A complete list of experiments on Λ hypernuclear spectroscopy is shown in Fig. 2 [3]. It can be seen that the K^-_{stop} reaction was not so commonly used. Before the FINUDA experiment, which results will be presented in the following, the only other experiments that produced hypernuclei with the $K^-_{stop} + n \rightarrow \Lambda + \pi^-$ reaction were two [4, 8]. Recently another experiment used the $K^-_{stop} + p \rightarrow \Lambda + \pi^o$ reaction [9]. All these experiments used spectrometers designed for other purposes and modified to fit the needs of a hypernuclear apparatus. The FINUDA experiment on the other hand was specifically planned to produce and study hypernuclei.

3 FINUDA hypernuclear spectroscopy

FINUDA took data for few months in between 2003 and 2004 and 2006 and 2007 at the DAΦNE e^+-e^- collider machine at the national laboratory of the Italian Institute of Nuclear Physics (INFN) in Frascati. The e^+-e^- collisions create the Φ meson at rest that decays, about 50 % of the times, into two kaons with low kinetic energy ($\sim$ 16 MeV). The basic

Lab.	Year	Reaction p_{beam} (GeV/c)	Studied hypernuclei	Beam line/apparatus etc.
CERN	1972	$(K^-_{\text{stop}}, \pi^-)$	${}^{12}_{\Lambda}$C	
CERN	1975	(K^-, π^-) 0.90	${}^{9}_{\Lambda}$Be, ${}^{12}_{\Lambda}$C, ${}^{16}_{\Lambda}$O, ${}^{32}_{\Lambda}$S, ${}^{40}_{\Lambda}$Ca	Double Spectrometer
CERN	1978	(K^-, π^-) 0.79	${}^{6}_{\Lambda}$Li, ${}^{7}_{\Lambda}$Li, ${}^{9}_{\Lambda}$Be, ${}^{12}_{\Lambda}$C, ${}^{16}_{\Lambda}$O, ${}^{27}_{\Lambda}$Al,	SPESII
		−0.64	${}^{32}_{\Lambda}$S, ${}^{40}_{\Lambda}$Ca, ${}^{51}_{\Lambda}$V, ${}^{89}_{\Lambda}$Y, ${}^{209}_{\Lambda}$Bi	
BNL	1979	(K^-, π^-) 0.80	${}^{12}_{\Lambda}$C	LESB-I/Moby-Dick (E646)
BNL	1981	(K^-, π^-) 0.80	${}^{13}_{\Lambda}$C, ${}^{14}_{\Lambda}$N, ${}^{18}_{\Lambda}$O	LESB-I/Moby-Dick (E746)
BNL	1985	(π^+, K^+) 1.05	${}^{12}_{\Lambda}$C	LESB-I/Moby-Dick (E758)
BNL	1991	(π^+, K^+) 1.05	${}^{9}_{\Lambda}$Be, ${}^{12}_{\Lambda}$C, ${}^{16}_{\Lambda}$O, ${}^{28}_{\Lambda}$Si, ${}^{40}_{\Lambda}$Ca, ${}^{51}_{\Lambda}$V, ${}^{89}_{\Lambda}$Y	LESB-I/Moby-Dick (E798)
KEK	1990	$(K^-_{\text{stop}}, \pi^-)$	${}^{4}_{\Lambda}$He, ${}^{7}_{\Lambda}$Li, ${}^{9}_{\Lambda}$Be, ${}^{12}_{\Lambda}$C, ${}^{16}_{\Lambda}$O, ${}^{40}_{\Lambda}$Ca	K3/SKY (E117,166,167)
KEK	1991	(π^+, K^+) 1.05	${}^{12}_{\Lambda}$C, ${}^{56}_{\Lambda}$Fe	K2/PIK (E150)
KEK	1995	(π^+, K^+) 1.05	${}^{10}_{\Lambda}$B, ${}^{12}_{\Lambda}$C, ${}^{28}_{\Lambda}$Si, ${}^{89}_{\Lambda}$Y, ${}^{139}_{\Lambda}$La, ${}^{208}_{\Lambda}$Pb	K6/SKS (E140A)
KEK	1998	(π^+, K^+) 1.05	${}^{7}_{\Lambda}$Li, ${}^{9}_{\Lambda}$Be, ${}^{12}_{\Lambda}$C, ${}^{13}_{\Lambda}$C, ${}^{16}_{\Lambda}$O	K6/SKS (E336)
KEK	2001	(π^+, K^+) 1.05	${}^{12}_{\Lambda}$C, ${}^{51}_{\Lambda}$V, ${}^{89}_{\Lambda}$Y	K6/SKS (E369)
BNL	2000	$(K^-_{\text{stop}}, \pi^0)$	${}^{12}_{\Lambda}$B	LESB-II/NMS (E907)
JLab	2003	$(e, e'K^+)$ 1.8	${}^{3}_{\Lambda}$H, ${}^{4}_{\Lambda}$H	Hall-C (E91-016)
JLab	2002	$(e, e'K^+)$ 1.8	${}^{7}_{\Lambda}$He, ${}^{12}_{\Lambda}$B	Hall-C/HNSS (E89-009)
KEK	2004	(π^-, K^+) 1.20	${}^{10}_{\Lambda}$Li	K6/SKS (E519)
LNF	**2003**	$(\mathbf{K^-_{\text{stop}}}, \pi^-)$	${}^{7}_{\Lambda}$Li, ${}^{9}_{\Lambda}$Be, ${}^{12}_{\Lambda}$C, ${}^{13}_{\Lambda}$C, ${}^{16}_{\Lambda}$O	DAΦNE/FINUDA

Figure 2: Experiments on Λ hypernuclear spectroscopy (from [3] with the addition of FINUDA).

principle of FINDUA [10] was to use such monochromatic source of low energy K$^-$'s for the production of hypernuclei. Since it is impossible to obtain such low energy beams in other ways (for example with fixed target experiments as done previously), FINUDA represented a real breakthrough for stopped kaons experiments. FINUDA in particular was characterized by important features, in particular it could: mount very thin targets (few tens of g/cm^2 compared to some g/cm^2 of previous experiments), install up to 8 different targets in the same data taking (thus minimizing the systematics in comparing results from different nuclei), completely reconstruct an event with large acceptance (studying both the production and the decay of hypernuclei), simultaneously track also the μ^+ from the decay of the K$^+$ (which is generated in pair with the K$^-$) calibrating in this way the apparatus both for energy and rate measurements. Details about the FINUDA experimental setup can be found in [11–13] and references therein.

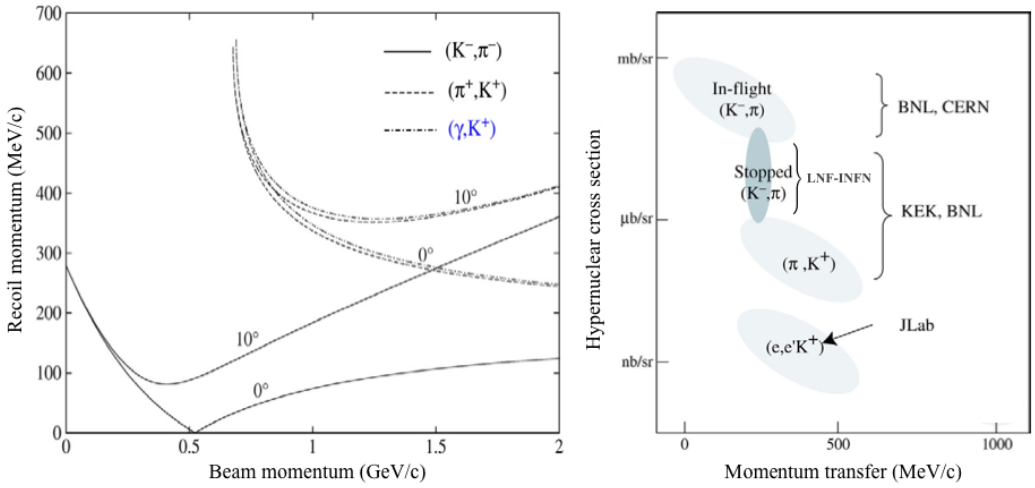

Figure 3: a) Recoil momentum as a function of the beam momentum (from [3]). When the momentum transfer is 0 (*magic (beam) momentum*), the hypernucleus production is called recoilless. b) Hypernuclear cross section as a function of the momentum transfer (from [2]). The production of hypernuclei by particles at rest is in reality defined by a capture rate (or formation probability) and not by cross section. Suitable normalization has been used.

The FINUDA apparatus was able to reconstruct charged particles coming out of the targets. Hypernuclear candidate events were selected by requiring the simultaneous presence of a K^- stopped inside a target and of a π^- originating from the same target. Details about the event selection and data analysis can be found elsewhere [11, 14]. Imposing the conservation of the energy and of the momentum, the tracking of the emerging π^- permits to calculate the hypernucleus binding energy, defined as the difference between the mass of the hypernucleus and the sum of the masses of the core nucleus (original nucleus without a neutron) and of the neutron. For what concerns the background, some other reactions between the K^- and the target can produce an emerging negative pion [$K^-(np) \rightarrow \Sigma^- p$ (followed by $\Sigma^- \rightarrow n\pi^-$ decay), $K^- n \rightarrow \Lambda\pi^-$ (so called Λ-*Quasi Free*), $K^- p \rightarrow \Sigma^-\pi^+$ (followed by $\Sigma^- \rightarrow n\pi^-$ decay)]. Another process that proved to be able to generate a π^- momentum distribution that can overlap with the one of hypernuclear formation is the in-flight K^- decay. All these reactions have been simulated with the FINUDA Monte Carlo in order to account for the background of our hypernuclear signal. A sum of the distributions of the background reactions and of Gaussians, for the signal, was used to reproduced the overall data behaviour (see [14] for details). The output of the fit was the weight of the various contributions, the number of events and the mean of the Gaussians. The position of the peaks gives directly the binding energy value of the hypernuclear states created, with a total error of 0.3 MeV. A more important information can be extracted from the number of events in the peaks. Taking into account all the efficiencies involved in the detection and reconstruction, the formation probability per stopped K^- can be calculated.

4 Results and discussions

The values of formation probabilities measured by the FINUDA experiments for ${}^{7}_{\Lambda}$Li, ${}^{9}_{\Lambda}$Be and ${}^{13}_{\Lambda}$C and ${}^{16}_{\Lambda}$O are reported in a recent publication [14]. Only few measurements of formation probability have been performed previously. Following the first experiment on a ^{12}C stopping target [4], measurement on some other nuclei (^{4}He, ^{12}C and ^{16}O) were subsequently performed [8]. A low statistics measurement on the (K^-_{stop}, π^o) reaction on ^{12}C was later published [9]. FINUDA also reported a first result on a ^{12}C target [11]. Based on these measurements the formation probability was a decreasing function of the atomic mass number A, but some discrepancy appeared for example between the ground state formation probabilities measured by [8,11] and [9]. The new FINUDA results [14], along with the one reported previously by FINUDA [11], offer a complete set of measurements that can be compared one each other to extract the formation probability as a function of the atomic mass number A. Since they were measured in the same experiment and using the same experimental and reconstruction techniques, the effect of systematic errors is thus minimized.

Since each target has more than one hypernuclear state (the ground plus some excited), it is not easy to extract the A dependence from the results. The ground state formation probability, as shown in Fig. 4 d), can be used, but for some hypernuclei (namely ${}^{7}_{\Lambda}$Li and ${}^{12}_{\Lambda}$C) the first excited state is too close to be isolated. In order to consider only well defined hypernuclides, hypernuclear states below the threshold for the decay by proton emission have been selected. The results are summarized in Fig. 4 a). A smoothly decreasing behaviour appears, with the exception of a strong enhancement corresponding to the formation of ${}^{12}_{\Lambda}$C. For comparison, in Fig. 4 b) the cross section measurement for the (π^+, K^+) production reaction [3] is also shown. The ratio between such values and the (K^-_{stop}, π^-) formation probability ones (Fig. 4 c) changes by a factor of 5 from ^{7}Li to ^{16}O. Two conclusions can be then drawn. First of all, the two production reactions (K^-_{stop}, π^-) and (π^+, K^+) show a distinct A dependence. Secondly, hypernuclei production on ^{12}C deviates from the overall behaviour, being higher than all other neighbour nuclei.

The new results [14] triggered a new study [15] to reproduce experimental data to extract information on the K^- nuclear potential V_K, important for kaon condensation in neutron-star matter, quasibound K-nuclear clusters, self-bound strange hadronic matter, etc. etc. The authors used the Distorted-Wave Impulse Approximation (DWIA) to calculate the formation probability for the target nuclei reported in [14]. Two different potentials were tested, namely a shallow (SH) and a deep (DD) ones with respectively $Re\ V_K \sim 50$ MeV and $Re\ V_K \sim 180$ MeV. The dependence on the nuclear density has also been taken into account. Although the calculated rates were about 15 % of the measured rates, the overall behaviour could be reproduced, the comparison slightly preferring the deep K^- nuclear potential over the shallow one.

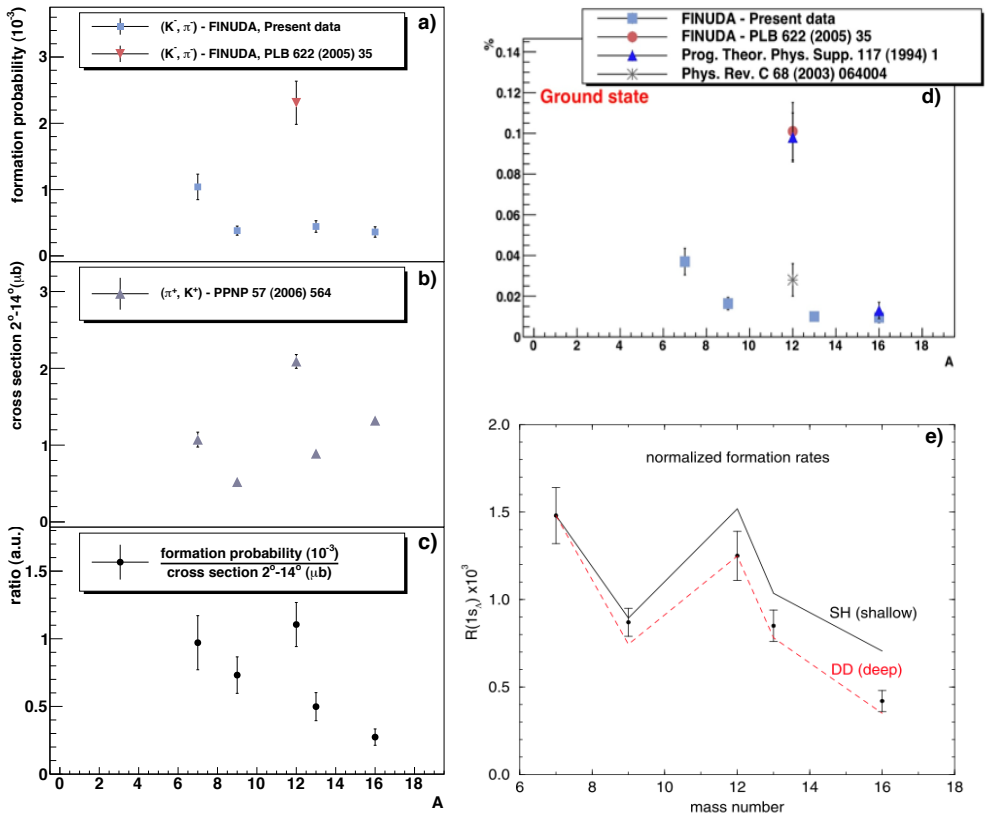

Figure 4: Formation probabilities from FINUDA [14] (a) and cross section from E336 [3] (b) for bound states (see text for details) as a function of A. Ratio between the two c). Theoretical prediction by [15] (e). Formation probabilities for the ground states (d).

5 Conclusions

The $K^-_{stop} + n \rightarrow \Lambda + \pi^-$ strangeness exchange reaction was the first [4] to be used for the creation of hypernuclei in *modern* (post emulsion/bubble chambers era). After having being used at BNL [5] and KEK [6], it found its *best configuration* at the INFN-LNF with the FINUDA experiment. Hypernuclei formation probabilities for stopped kaons has been measured for p-shell nuclei and for the first time a study as a function of A has been performed [14]. The new results gave new inputs to the theory to extract useful information about the K^- nuclear potential. No new experiment using the (K^-_{stop}, π^-) reaction is foreseen at the moment since future programs of hypernuclear physics, at JParc in Japan and at GSI in Germany, will be using different production methods. Complete reviews of hypernuclear physics can be found in [2,3,16,17].

Bibliography

[1] M. Danysz, J. Pniewski, Philos. Mag. **44** (1953) 348.

[2] T. Bressani, Proceedings of the International School of Physics "Enrico Fermi", IOP Press (2008), 3.

[3] O. Hashimoto and H. Tamura, *Spectroscopy of* Λ *hypernuclei*, Prog. Part. and Nucl. Phys. **57** (2006) 564-653.

[4] A. M. Faessler *et al.*, Phys. Lett. B **46** (1973) 468.

[5] R.E. Chrien et al., Phys. Lett. B 89 (1979) 31.

[6] M. Akei et al., Nuclear Phys. A 534 (1991) 478.

[7] F. Dohrmann et al., Phys. Rev. Lett. 93 (2004) 242501.

[8] H. Tamura, R. S. Hayano, H. Outa and T. Yamazaki, Prog. Theor. Phys. Suppl. **117** (1994) 1.

[9] M. W. Ahmed *et al.*, Phys. Rev. C **68** (2003) 064004

[10] T. Bressani, in Proceedings of the Workshop on Physics and Detectors for DAΦNE, Frascati, 1991, edited by G. Pancheri (Laboratori Nazionali di Frascati, Frascati, 1991), p. 475.

[11] M. Agnello *et al.*, Phys. Lett. B **622** (2005) 35.

[12] M. Agnello *et al.*, Phys. Lett. B **681** (2009) 139.

[13] M. Agnello *et al.*, Phys. Lett. B **685** (2010) 247.

[14] M. Agnello *et al.*, Phys. Lett. B **698** (2011) 219.

[15] A. Cieplý, E. Friedman, A. Gal and V. Krejčiřík, Phys. Lett. B **698** (2011) 226.

[16] R. E. Chrien and C. B. Dover, Ann. Rev. Nucl. Part. Sci **39** (1989) 113.

[17] H. Bando, T. Motoba and J. Zofka, Int. J. Mod. Phys. **5** (1990) 4021) 468.

Experimental studies of mesic nuclei at J-PARC

Hiroyuki Fujioka[1]
Department of Physics, Kyoto University
Kitashirakawa-Oiwakecho, Sakyo-ku, Kyoto 606-8502, Japan

The property of a pseudoscalar meson at finite density may be extracted by investigating mesic nuclei in detail. The existence of mesic nuclei is predicted theoretically, based on the understanding of the meson-nucleon interaction. Experimental programs to search for mesic nuclei at J-PARC are reviewed.

1 Introduction

Meson-nucleus bound states, a new kind of bound systems in strong interaction, will provide us unique information on hadron properties at finite density. In particular, $\overline{K}$-nuclear bound states (kaonic nuclei) and η-nuclear bound states (η mesic nuclei) attract a lot of attention from both experimentalists and theorists nowadays.

In this article, I would like to review related experimental programs at J-PARC briefly. Figure 1 is a schematic view of the J-PARC hadron experimental facility. Proton beam, accerelated to 30 GeV by the main ring, is delivered from the lower left to the production target. There are two beamlines for charged particles (K1.8 and K1.1) and one beamline for neutral kaons. The experiments described below will be performed in either the K1.8 beamline or the K1.8BR beamline (branch line of K1.8).

2 Kaonic nuclei

Because of the strong attraction between $I = 0$ $\overline{K}N$ pairs, an antikaon-nucleus system may exist as a quasi-bound state. For example, the existence of $\Lambda(1405)$ below the $\overline{K}N$ threshold can be regarded as a consequence of such a strong attractive interaction. It is a natural extension to consider $\overline{K}NN$ systems.

Theoretically, a variety of calculations of the $\overline{K}NN$ system have been carried out [1], supporting the existence of a bound state. The binding energy varies from ~ 10 MeV to ~ 100 MeV, and the decay width is moderately large. The difference mainly comes from the calculation method (Faddeev approach or variational approach) and the treatment of $\pi\Sigma N$ channel.

[1] fujioka@scphys.kyoto-u.ac.jp

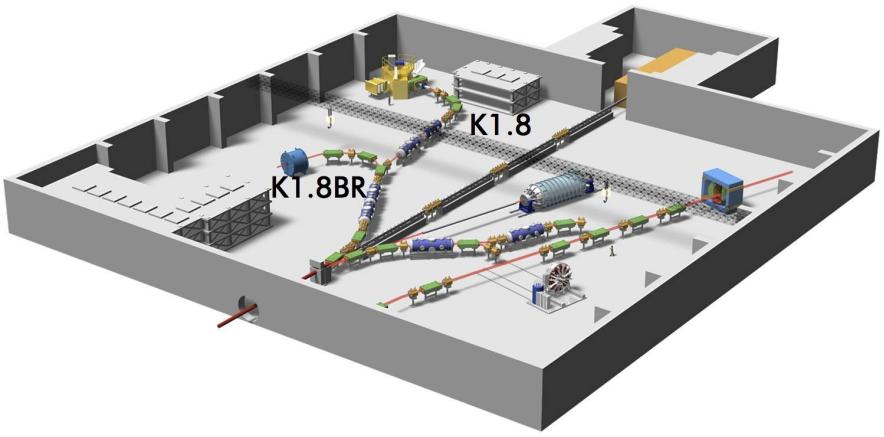

Figure 1: Layout of J-PARC hadron experimental facility.

From an experimental point of view, non-mesonic decay of K^-pp states into $\Lambda + p$ is a clean signal in searching for such an exotic state. Many experiments in the past and in the near future make use of this channel.

The first observation was reported by the FINUDA collaboration [2]. They detected a pair of Λ and proton in back-to-back from K^- absorption at rest. A slow K^- beam was supplied by the ϕ-factory DAΦNE. The invariant mass of the Λp pairs was far below the $K^- + 2p$ threshold, which is in contradiction with an assumption that they originated from a two-nucleon absorption process $K^- + "pp" \to \Lambda + p$. They interpreted Λp pairs may be originated from non-mesonic decay of K^-pp states, whose binding energy from the $K^- + 2p$ threshold is ~ 115 MeV and decay width is ~ 67 MeV. However, this interpretation is criticized by Magas *et al.* [3] and Pandejee *et al.* [4], both of which stress the importance of final state interaction after two-nucleon absorption.

Another indication was obtained by a reanalysis of the DISTO experiment, which performed an exclusive measurement of the $p + p \to p + \Lambda + K^+$ reaction [5]. A broad distinct peak was found in the K^+ missing-mass spectrum and the $p\Lambda$ invariant-mass spectrum, when they select events with a large-p_T proton and K^+. If the peak corresponds to a K^-pp state, its binding energy and decay width are ~ 105 MeV and ~ 118 MeV, respectively.

At present, the existence of K^-pp bound states whose binding energy is as large as 100 MeV is not established. Accordingly, it is vitally important to search for K^-pp states with various reactions. The $p + p \to p + \Lambda + K^+$ reaction with higher incident energy was measured at GSI in 2009, and the analysis is in progress [6]. The stopped K^- absorption reaction in ^{3}He and ^{4}He will be studied by the AMADEUS experiment at DAΦNE [7]. In J-PARC, two experiments with the ^{3}He(K^-, n) reaction (J-PARC E15 experiment) and the D(π^+, K^+) reaction (J-PARC E27 experiment) have been approved, and the preparation is in progress.

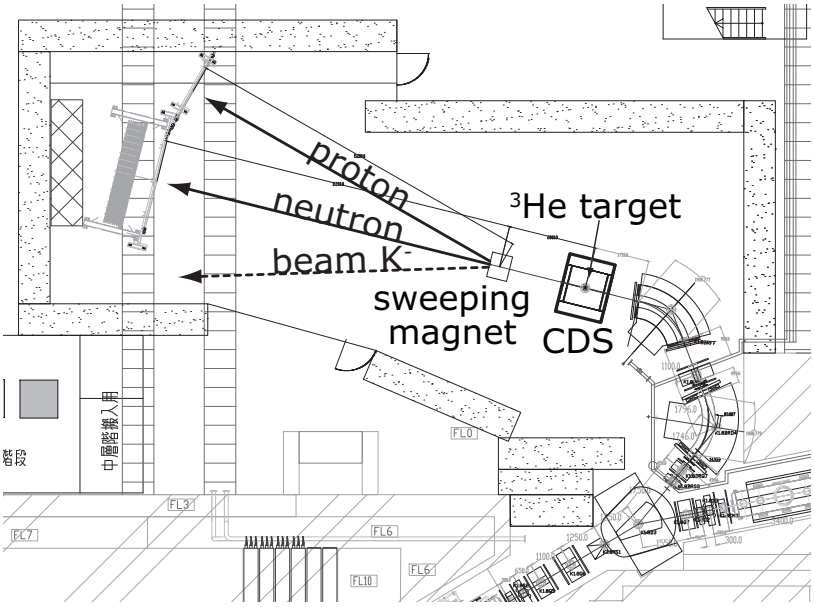

Figure 2: Setup for the J-PARC E15 experiment.

2.1 J-PARC E15 experiment

The J-PARC E15 experiment [8] will be performed at the K1.8BR beamline. 1.0 GeV/c K^- beam will be injected into liquid ^{3}He target. Figure 2 shows the experimental setup. Outgoing neutrons by the (K^-, n) reactions will be detected by a neutron counter about 15 m downstream of the target. The beam K^- will be swept away by a sweeping magnet in order not to hit the neutron counter, and as a by-product, scattered protons by the (K^-, p) reaction can be detected by installing an additional proton counter. The decay particles of K^-pp states into $\Lambda + p$ or $\Sigma^0 + p$ can be detected by a cylindrical detector system (CDS) which consist of a GEM-TPC tracker, a cylindrical drift chamber, and hodoscopes inside a solenoid magnet. Thereby, both missing-mass spectroscopy and invariant-mass spectroscopy will be enabled.

A CDS commissioning run with π^+ and K^- beam was carried out last autumn, and distinct peaks of Λ and K_S were observed by reconstructing the invariant mass of $p\pi^-$ and $\pi^+\pi^-$ pairs, respectively. The analysis for improving the resolution and the particle identification is under way.

2.2 J-PARC E27 experiment

The J-PARC E27 experiment will make use of the D(π^+, K^+) reaction [9]. K^-pp states will be produced by sticking a $\Lambda(1405)$, produced by the $n(\pi^+, K^+)$ reaction, on the spectator

proton. The experiment will use 1.5–1.6 GeV/c π^+ beam at the K1.8 beamline, and the scattered K^+ will be detected by the Superconducting Kaon Spectrometer (SKS).

It is essentially important to reduce background from quasi-free processes ($\pi^+ + "N" \to Y^{(*)} + K^+$). Tagging two protons from $K^- pp$ decay will help to eliminate these contributions; a proton from $Y^{(*)}$ decay tends to have a small emission angle, and the spectator proton is too slow to be detected experimentally. Thus, two sets of range counter arrays will be installed on the left and right sides of the deuterium target for detection of fast protons.

A test experiment with a prototype of the range counter arrays was done during the beam time for the E19 experiment, which searched for the Θ^+ pentaquark. Part of the range counter arrays were installed near hydrogen target, and scattered $\pi^\pm$'s and protons were stopped inside the arrays. A preliminary analysis revealed that clear p/π separation is possible by combining the energy loss in each counter, the time-of-flight between the start counter and the first layer of the array, and the range of the particle.

We plan to take the first data for the E27 experiment in early 2012, and the preparation of the detectors in the beamline and the SKS spectrometer as well as the range counter arrays is going on.

3 η mesic nuclei

The ηN interaction is weakly attractive, because the $N(1535)$ resonance, which strongly couples to ηN, lies above the ηN threshold. However the scattering length has a large ambiguity between $(0.270\text{–}1.050) + (0.190\text{–}0.399)i$ fm [10].

The first calculation by Haider and Liu [11] showed η mesic nuclei with the mass number $A \geqslant 12$ can be bound when the scattering length is set to $0.28 + 0.29i$ fm or $0.27 + 0.22i$ fm. If the real part of the scattering length is larger, there may be a possibility that an η meson is bound in a lighter nucleus such as ^{3}He and ^{4}He [10, 12].

Recently the COSY-GEM collaboration investigated the ^{27}Al(p, ^{3}He) reaction [13] at recoilless kinematics. By detecting back-to-back $\pi^- p$ pairs, which may originate from the decay of η mesic nuclei, they found an indication of η mesic nuclei with the binding energy of ~ 12 MeV.

Itahashi *et al.* propose to study the (π^-, n) reaction on ^{7}Li and ^{12}C target at J-PARC [14]. The advantage over a prior experiment at BNL [17] is the detection of back-to-back $\pi^- p$ pairs like the COSY-GEM experiment, and the recoilless condition by adjusting π^- momenta around 0.8–1.0 GeV/c and detecting zero-degree neutrons[2]. To achieve these conditions, the use of the E15 experimental setup is desirable. According to Ref. [15], the formation spectrum is sensitive to the in-medium property of $N(1535)$, which affects the η-nucleus

[2]The BNL experiment measured protons at scattering angle 15° from the (π^+, p) reaction, and the momentum transfer is larger than 200 MeV/c.

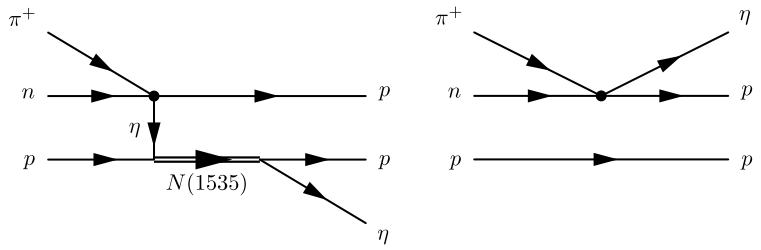

(a) double-scattering reaction **(b)** quasi-free reaction

Figure 3: Diagrams for the $\pi^+ d \to pp\eta$ reaction.

optical potential. While the mass difference of $N(1535)$ and N will not change largely in the chiral unitary model, the chiral doublet model leads to a decrease of the mass difference due to the partial restoration of chiral symmetry.

A pilot experiment with deuteron target is also under consideration [16] . The $\pi^+ d \to pp\eta$ reaction can be studied by detecting two protons. The dominant quasi-free process (Fig. 3b) can be eliminated because the spectator proton has a very small momentum, and we can select the double-scattering reaction (Fig. 3a). The differential cross section is sensitive to the low-energy ηN scattering amplitude because the elastic scattering $\eta N \to \eta N$ takes place near the threshold energy [18].

Lastly, the $(p, {}^3\mathrm{He})$ reaction, which was investigated by the COSY-GEM collaboration [18], may be studied at the K1.8 beamline together with the SKS spectrometer. The coincidence of decay particles will be mandatory to reduce huge background.

4 Summary

Intense $\pi^{\pm}$, K^-, and proton beams will allow us to investigate kaonic nuclei and η mesic nuclei. As well as the forward spectrometer, the detectors for decay particles of mesic nuclei are important to make the background level as small as possible. The preparation of the E15 and E27 experiments, both of which will search for $K^- pp$ bound states, is in progress. Moreover, search for η mesic nuclei will be feasible in future.

Acknowledgments

This work was partly supported by the Grants-in-Aid for Scientific Research from MEXT and JSPS (No. 20840047, 22105506).

Bibliography

[1] T. Hyodo and D. Jido, arXiv:1104.4474 [nucl-th].

[2] M. Agnello *et al.* [FINUDA Collaboration], Phys. Rev. Lett. **94**, 212303 (2005).

[3] V. K. Magas, E. Oset, A. Ramos, H. Toki, Phys. Rev. **C74**, 025206 (2006).

[4] G. Pandejee, N. J. Upadhyay, B. K. Jain, Phys. Rev. **C82**, 034608 (2010).

[5] T. Yamazaki, M. Maggiora, P. Kienle, K. Suzuki, A. Amoroso, M. Alexeev, F. Balestra, Y. Bedfer *et al.*, Phys. Rev. Lett. **104**, 132502 (2010).

[6] K. Suzuki *et al.* [FOPI Collaboration], Prog. Theor. Phys. Suppl. **186**, 351-356 (2010).

[7] J. Zmeskal [AMADEUS Collaboration], Int. J. Mod. Phys. **A26**, 414-419 (2011).

[8] M. Iwasaki, T. Nagae *et al.*, J-PARC E15 proposal.
`http://j-parc.jp/NuclPart/pac_0606/pdf/p15-Iwasaki.pdf`

[9] T. Nagae *et al.*, J-PARC E27 proposal.
`http://www.j-parc.jp/NuclPart/pac_0907/pdf/Nagae.pdf`

[10] Q. Haider, L. C. Liu, Phys. Rev. **C66**, 045208 (2002).

[11] Q. Haider, L. C. Liu, Phys. Lett. **B172**, 257-260 (1986); *ibid.* **174**, 465(E) (1986).

[12] A. Khoukaz, Acta Phys. Polon. **B41**, 2271-2280 (2010). [arXiv:1011.0882 [nucl-ex]].

[13] A. Budzanowski *et al.* [COSY-GEM Collaboration], Phys. Rev. **C79**, 012201 (2009).

[14] K. Itahashi *et al.*, J-PARC Letter of Intent.
`http://www.j-parc.jp/NuclPart/pac_0707/pdf/LoI-itahashi.pdf`

[15] H. Nagahiro, D. Jido, S. Hirenzaki, Phys. Rev. **C80**, 025205 (2009).

[16] H. Fujioka, Acta Phys. Polon. **B41**, 2261-2270 (2010).

[17] R. E. Chrien, S. Bart, P. Pile, R. Sutter, N. Tsoupas, H. O. Funsten, J. M. Finn, C. Lyndon *et al.*, Phys. Rev. Lett. **60**, 2595-2598 (1988).

[18] H. Garcilazo, M. T. Pena, Phys. Lett. **B696**, 386-389 (2011).

Probing cold nuclear matter with virtual photons

Michael Weber[1,a,b] and Manuel Lorenz[c] for the HADES Collaboration
[a]*Physik Department E12, Technische Universität München, 85748 Garching, Germany*
[b]*now at University of Houston, Houston, TX, USA*
[c]*Institut für Kernphysik, Goethe-Universität, 60438 Frankfurt, Germany*

We report data on e^+e^- pair emission in p + Nb collisions at energies above the light vector meson production threshold. Invariant mass distributions for the proton beam energy of $E_{kin} = 3.5$ GeV are compared to data from elementary p+p reactions at the same beam energy. The collected statistics and high acceptance for pair momenta from $\approx$ 50-2000 MeV/c allow for a comparison of fast and slow ω mesons. According to hadronic models, the latter ones should show the strongest modification in the line shape due to the nuclear medium.

1 Introduction

The study of hadron properties inside a strongly interacting medium has attracted plenty of attention both in theoretical and experimental nuclear physics. On the theory side, hadronic models predict already at twice nuclear ground state density strong modifications in the spectral function of the light vector mesons ρ and ω, which are most pronounced at low momenta relative to the surrounding medium [1].
Experimentally, such effects can be tested in proton -, pion - or photon - induced reactions on heavy nuclei. While the modifications are expected to be stronger in heavy ion collisions, cold nuclear matter experiments have the advantage of relative controlled conditions, since the system does not undergo a density evolution during the reaction. We want to put our focus on these reactions. e^+e^- pair spectroscopy is a promising probe for such studies due to the fact that electrons and positrons interact only electromagnetically and their kinematics stays almost undistorted while propagating through the ambient nuclear matter. One has two different observables at hand: the spectral shape in the e^+e^- invariant mass and/or the total yield for different nuclei. A sensible measurement of the shape requires the decay taking place inside the nucleus, which can be studied by requiring low vector meson momenta, in particular for ω and ϕ. The measurement of the yield or production cross section can be connected to the total width of the hadron via double transparency ratios [2,3].
So far, shape measurements in elementary reactions were done for the ρ meson by the

[1]michael.weber@ph.tum.de

CLAS experiment at JLab [4] and the E325 experiment at KEK [5]. However, the results are not conclusive so far. For the ω and ϕ meson several experiments [6–9] reported a sizable broadening of the total decay width inside the medium using double transparency ratios. To contribute to this still unresolved issue the HADES collaboration measured the inclusive e^+e^- pair production in proton induced reactions at $E_{kin} = 3.5$ GeV. The reference spectrum was obtained in p + p reactions and the in-medium effects were extracted from reactions utilizing the heavy nucleus Nb.

2 Experimental setup and measured e^+e^- spectra

The High Acceptance Di-Electron Spectrometer (HADES [10]) is installed at the GSI Helmholtzzentrum für Schwerionenforschung in Darmstadt and is provided with a proton or heavy-ion beam by the synchrotron SIS18. For the $e^\pm$ identification a hadron blind Ring Imaging CHerenkov detector (RICH) is used. Particle identification is supplemented by a time-of-flight measurement in a plastic scintillator wall (ToF) and an electromagnetic shower pattern in the Pre-Shower detector. Additional particle identification power can be gained by the inclusion of the energy loss information of the drift chambers and the scintillator wall.
A proton beam with a kinetic energy of $E_{kin} = 3.5$ GeV was incident on a liquid hydrogen target for the p + p run in 2007 [11] and on a 12-fold Nb target for the p + Nb run in 2008. The event selection was done in two steps. In the first trigger stage (LVL1), events with a charged particle multiplicity in the ToF wall of $M_{ch} \geqslant 3$ were selected. The second trigger stage (LVL2) selected events with at least one lepton candidate indicated by a ring in the RICH detector.

For the offline identification of electrons two independent methods were used. A multivariate analysis based on a neural network algorithm, where all relevant cut criteria are fed into the algorithm delivering a single scalar response value. Secondly, a standard method was used, where the cuts are applied directly on the relevant criteria (hardcuts). For the final spectra the average between the two methods was calculated. The difference between the two methods as well as the differences due to systematic variation of the cuts and self-consistency checks were taken as an estimate of the systematic errors.

All possible combinations of identified $e^{+/-}$ tracks were formed event by event and corrected for detector and reconstruction efficiencies. The latter ones were deduced using Monte-Carlo simulations embedded into real events. Invariant mass spectra of the unlike-sign pairs were then constructed from single $e^{+/-}$ tracks. To increase the purity of the $e^{+/-}$ sample a cut on the single track momentum $0.08 < p_e/(\mathrm{GeV/c}) < 2.00$ was applied. The combinatorial background (CB) was extracted from all like-sign pair combinations inside the same event. Since the CB stems predominantly from external γ-conversion it was reduced by cutting on the pair opening angle ($\alpha_{ee} > 9^\circ$) and on the track fitting quality. By subtracting the CB from the unlike-sign pairs the signal spectrum was obtained.

The measured invariant mass distributions of e^+e^- pairs for p+Nb and p+p reactions, together with a cocktail of several e^+e^- pair sources for the elementary case [11], are shown in the left panel of Fig. 1. Differential cross sections were obtained by normalizingg to elastic collisions for p+p reactions and negative pion production in p+Nb reactions. While the shape of the distributions shows no obvious differences, already in p+p collisions the cocktail fails to describe the data in the intermediate mass region.

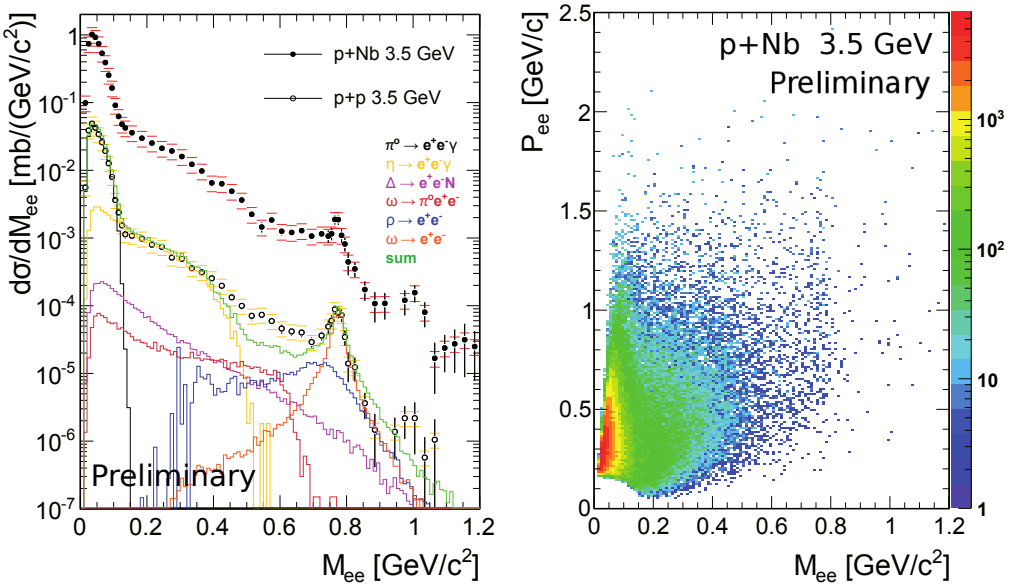

Figure 1: Invariant mass spectra (left) and the momentum dependence (right).

3 Low momentum pairs

The big advantage of the HADES setup compared to previous measurements of dielectrons from cold nuclear matter is the good coverage for low momentum pairs, as depicted in the right panel of Fig. 1. The collected statistics allows to compare a high and low momentum sample for different invariant mass regions as well as for identified ω mesons to the elementary pp data. While it is expected to see hardly any differences in the high momentum sample the low momentum pair should show effects related to the surrounding medium.

It should be stated here that these effects, if any, are not necessarily related to modification of the spectral function since also the production via secondary reactions might play an important role. These reactions then take place at lower average $\sqrt{s}$ and might run into the region were isospin effects become important [12].

4 Summary

We have measured inclusive e^+e^- pair production in p+p and p+Nb collisions at $E_{kin} = 3.5$ GeV. Already in p+p a e^+e^- cocktail based on model predictions fails to describe the data satisfactorily in the intermediate invariant mass region. Also the ω meson line shapes of the two spectra show no strong deviations. Further hints for in-medium changes of vector mesons in matter might be gained by a separate comparison of fast and slow pairs, which will be published soon in a forthcoming paper.

Acknowledgments

The collaboration acknowledges support by BMBF through grants 06DR9059D, 06FY9100I, 06MT9156 TP5 (Germany), by GSI (TKrue1012, TMFABI 1012, F&E), by the Helmholtz Alliance HA216/EMMI, by HIC for FAIR (LOEWE), by the DFG Excellence Cluster 153 "Universe" (Germany), by the Helmholtz young researcher group VH-NG-330, by MLL München, by grants MSMT LC07050, GAASCR IAA100480803 (Czech Republic), NN202 286038, NN202198639 (Poland), PTDC/FIS/113339/2009 (Portugal), CPAN:CSD2007-00042 (Spain), by CNRS/IN2P3 (France) and by INFN (Italy).

Bibliography

[1] M. Post, S. Leupold and U. Mosel, Nucl. Phys. **A 741** 81-148 (2004).

[2] M. Kaskulov, E. Hernandez and E. Oset, Eur. Phys. J. **A 31**, 245 (2007).

[3] P. Mühlich and U. Mosel, Nucl. Phys. **A 773**, 156 (2006).

[4] R. Nasseripour et al. (CLAS Collaboration), Phys. Rev. Lett. **99**, 262302 (2007).

[5] M. Naruki et al., Phys. Rev. Lett. **96**, 092301 (2006).

[6] M. Kotulla et al., Phys. Rev. Lett. **100**, 192302 (2008).

[7] T. Ishikawa et al. (SPring-8 Collaboration), Phys. Lett. **B 608**, 215-222 (2005).

[8] A. Polyanskiy et al. (ANKE Collaboration), Phys. Lett. **B 695**, 74 (2011).

[9] M. H. Wood et al. (CLAS Collaboration), Phys. Rev. Lett **105**, 112301 (2010).

[10] G. Agakishiev et al. (HADES Collaboration), Eur. Phys. J. **A 41**, 243 (2009).

[11] A. Rustamov et al. (HADES Collaboration), AIP Conf. Proc. **1257**, 736 (2010).

[12] W. K. Wilson et al. (DLS Collaboration), Phys. Rev. C **57**, 1865 (1998).

Study of neutral kaon production in $p + p$ and $p +$ Nb reactions

Kirill Lapidus[1,h], G. Agakishiev[f], D. Belver[o], A. Belyaev[f], A. Blanco[b], M. Böhmer[i], P. Cabanelas[o], S. Chernenko[f], J. C. Chen[h], A. Dybczak[c], E. Epple[h], L. Fabbietti[h], O. Fateev[f], P. Finocchiaro[a], P. Fonte[b,q], J. Friese[i], I. Fröhlich[g], T. Galatyuk[g,s], J. A. Garzón[o], M. Golubeva[k], D. González-Díaz[s], F. Guber[k], M. Gumberidze[m], T. Hennino[m], R. Holzmann[d], P. Huck[i], A. Ierusalimov[f], A. Ivashkin[k], M. Jurkovic[i], B. Kämpfer[e,t], T. Karavicheva[k], I. Koenig[d], W. Koenig[d], B. W. Kolb[d], G. Korcyl[c], G. Kornakov[o], R. Kotte[e], A. Kozuch[c,u], A. Krasa[n], F. Krizek[n], R. Krücken[i], H. Kuc[c,m], W. Kühn[j], A. Kugler[n], A. Kurepin[l], A. Kurilkin[f], P. Kurilkin[f], V. Ladygin[f], R. Lalik[h], S. Lang[d], T. Liu[m], L. Lopes[b], M. Lorenz[g], L. Maier[i], A. Mangiarotti[b], J. Markert[g], V. Metag[j], B. Michalska[c], J. Michel[g], C. Müntz[g], R. Münzer[h], L. Naumann[e], Y. C. Pachmayer[g], M. Palka[g], Y. Parpottas[l], V. Pechenov[d], O. Pechenova[g], J. Pietraszko[g], W. Przygoda[c], B. Ramstein[m], A. Reshetin[k], A. Rustamov[d], A. Sadovsky[l], P. Salabura[c], A. Schmah[p], J. Siebenson[h], Yu.G. Sobolev[n], S. Spataro[j,v], H. Ströbele[g], J. Stroth[g], C. Sturm[d], A. Tarantola[g], K. Teilab[g], P. Tlusty[n], M. Traxler[d], R. Trebacz[c], H. Tsertos[l], T. Vasiliev[f], V. Wagner[n], M. Weber[i], J. Wüstenfeld[e], S. Yurevich[d], and Y. Zanevsky[f]
(HADES collaboration)

[a] *Istituto Nazionale di Fisica Nucleare - Laboratori Nazionali del Sud, 95125 Catania, Italy*
[b] *LIP-Laboratório de Instrumentação e Física Experimental de Partículas, 3004-516 Coimbra, Portugal*
[c] *Smoluchowski Institute of Physics, Jagiellonian University of Cracow, 30-059 Kraków, Poland*
[d] *GSI Helmholtzzentrum für Schwerionenforschung GmbH, 64291 Darmstadt, Germany*
[e] *Institut für Strahlenphysik, Helmholtz-Zentrum Dresden-Rossendorf, 01314 Dresden, Germany*
[f] *Joint Institute of Nuclear Research, 141980 Dubna, Russia*
[g] *Institut für Kernphysik, Goethe-Universität, 60438 Frankfurt, Germany*
[h] *Excellence Cluster 'Origin and Structure of the Universe', 85748 Garching, Germany*
[i] *Physik Department E12, Technische Universität München, 85748 Garching, Germany*
[j] *II.Physikalisches Institut, Justus Liebig Universität Giessen, 35392 Giessen, Germany*
[k] *Institute for Nuclear Research, Russian Academy of Science, 117312 Moscow, Russia*
[l] *Department of Physics, University of Cyprus, 1678 Nicosia, Cyprus*
[m] *Institut de Physique Nucléaire (UMR 8608), CNRS/IN2P3 - Université Paris Sud F-91406 Orsay Cedex, France*
[n] *Nuclear Physics Institute, Academy of Sciences of Czech Republic, 25068 Rez, Czech Republic*
[o] *Departamento de Física de Partículas, Univ. de Santiago de Compostela, 15706 Santiago de Compostela, Spain*
[p] *also at Lawrence Berkeley National Laboratory, Berkeley, USA*
[q] *also at ISEC Coimbra, Coimbra, Portugal*

[1] kirill.lapidus@ph.tum.de

[r] *also at ExtreMe Matter Institute EMMI, 64291 Darmstadt, Germany*
[s] *also at Technische Universität Darmstadt, Darmstadt, Germany*
[t] *also at Technische Universität Dresden, 01062 Dresden, Germany*
[u] *also at Panstwowa Wyzsza Szkola Zawodowa, 33-300 Nowy Sacz, Poland*
[v] *also at Dipartimento di Fisica Generale, Università di Torino, 10125 Torino, Italy*

We report on the on-going analysis of the K^0 production in p+p and p+Nb collisions at $E_{kin} = 3.5$ GeV, aimed on the extraction of the in-medium kaon-nucleon potential at normal nuclear matter density.

1 Introduction

Modification of the kaon (antikaon) properties in the nuclear environment is a subject of permanent theoretical and experimental interest. Such an environment can be produced in heavy-ion collisions, where—at 1–2 AGeV kinetic beam energy—densities of up to 3 times normal nuclear matter density can be achieved. However, theory expects modifications of the kaon spectral function already at normal nuclear matter density [1], which can be explored with the production at nuclei, employing γ-, π- or proton-induced reactions.

It is predicted, that the kaon interaction with the nuclear environment is characterized by a repulsive potential, whereas for antikaons an attractive potential is favoured. The results of the flow analyses [2,3] support these expectations.

Resulting yields and phase space distributions of kaons in the final state reflect different aspects of kaon production and propagation, so it is challenging to find an observable that would be sensitive exclusively to the in-medium KN potential. As stressed in [4], one of the most promising observables to learn about the in-medium kaon-nucleon potential is the momentum distribution, in particular in the region of low momenta. Since a kaon is "repelled" from the ambient nucleus, the measured momentum distribution will be shifted to higher values as compared to the case where no sizeable effects of the potential are expected. Neutral kaons are particularly promising probes, since their kinematics is not distorted by the Coulomb interaction.

A number of experiments measured this observable. The ANKE collaboration studied K^+ production in proton-induced reactions at different nuclear targets in a small phase space at forward rapidities [6]; K^0 production in pion-induced reactions was explored by the FOPI collaboration [7]. Both collaborations presented the ratio of momentum distributions measured with heavy (silver, gold or lead) and light (carbon) targets: $\sigma_{Ag,Au,*124*Pb}(p_K)/\sigma_C(p_K)$. A characteristic depletion of the low momenta kaons ($p_K \leqslant 200$ MeV/c) and a peak-like structure at $p_K \approx 200$ MeV/c was observed in these ratio plots, in agreement with the

theory-driven expectations. From a comparison with transport model calculations, an in-medium potential of $+20 \pm 5$ MeV (the value at normal nuclear matter density, for low kaon momenta) was extracted.

The HADES collaboration contributed with a K^0 measurement in a medium-sized colliding system Ar+KCl at a kinetic beam energy of 1.756 AGeV [8]. The obtained p_t-distribution at mid-rapidity was compared with the IQMD transport calculations. A larger value of the potential of $+40$ MeV was extracted from this analysis.

The difference between the results, obtained in p(π)+A and A+A experiments, supports our intention to continue the HADES studies of K^0's with a new measurement in p+^{93}Nb reactions. As a reference system, free of the effects of the finite nuclear matter density, we employ p+p reactions. As compared to the previous p+A experiments, the main feature of our study is the high acceptance of the HADES detector for the low-p_t kaons in a broad range of rapidities.

2 The Experiment

The **H**igh-**A**cceptance **D**i-**E**lectron **S**pectrometer (HADES) is a modern multi-purpose detector currently operating at the SIS18 heavy-ion synchrotron (GSI Helmholtzzentrum, Darmstadt) in the region of kinetic beam energies of 1–2 AGeV (A+A), up to 3.5 GeV in proton-induced reactions. The main components of the experimental set-up are a superconducting magnet, four planes of Multiwire Drift Chambers used for the tracking of charged particles, a Time-of-Flight wall and a hadron blind RICH detector, cf. [5] for details.

In 2007 a measurement of proton-proton collisions at a kinetic beam energy of 3.5 GeV was performed. The beam with an average intensity $\sim 1 \times 10^6$ particles/s was incident on a liquid hydrogen target with a columnar density of 0.35 g/cm^2 and a total interaction probability of $\sim 2\%$. In total, 1.2×10^9 events were collected. In 2008 the same beam was employed with a ^{93}Nb target. Overall 4×10^9 events had been taken. In both runs, the first level trigger (LVL1) required at least 3 hits in the Time-of-Flight wall in order to suppress the contribution from elastic p+p scattering.

3 K^0_S analysis in proton-proton and proton-niobium collisions

A K^0 is identified by its short-lived component K^0_S that decays weakly into a $\pi^+\pi^-$-pair. Charged pions are identified with help of measured energy losses in the HADES subdetectors. In order to suppress the background, a set of additional cuts is applied to the reconstructed event topology: a) a cut on the distance from the secondary to the primary vertex $d_1 > 25$ mm; b) a cut on the distance of closest approach between the pion tracks $d_2 < 7$ mm and c) a cut on the distance of closest approach between a pion track and the primary vertex $d_3 < 7$ mm.

The resulting $\pi^+\pi^-$ invariant mass spectra are presented in Fig. 1 for p+p (left) and p+Nb (right) collisions. For both reactions, a clear signal corresponding to the K^0_S is visible on top of a combinatorial background.

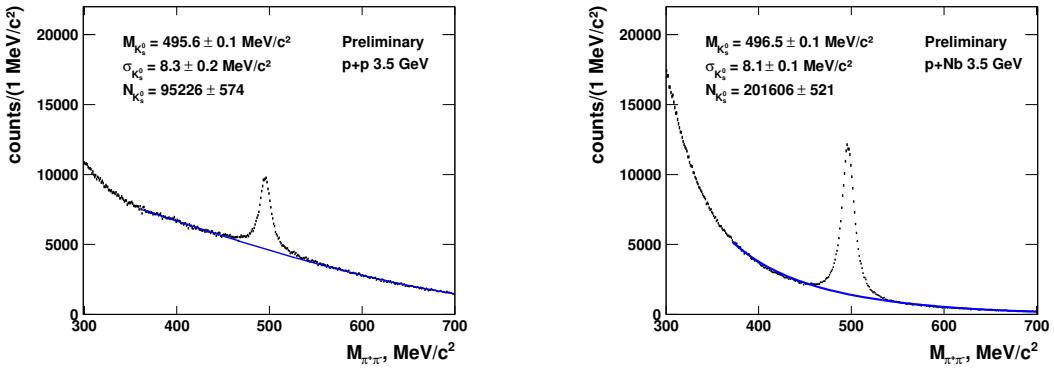

Figure 1: Black dots — data points of the invariant mass distribution of $\pi^+\pi^-$ pairs in p+p (left) collisions and p+Nb (right) collisions after applying event topology cuts; blue curves — combinatorial background (see text for details).

Several background reconstruction techniques were considered. In the p+p case the event mixing technique was found to be inapplicable. Instead, a simultaneous signal+background fit is performed, where the background is modeled as a sum of Landau and polynomial functions, and the signal as a sum of two Gaussians. The same method is applied to the p+Nb data, but in this case it was shown that the mixing event technique gives results consistent with the fitting procedure.

The large accumulated statistics of about 10^5 and 2×10^5 reconstructed K^0_S for the p+p and p+Nb runs, respectively, allows to perform a differential analysis of the K^0 production. The signal was extracted for a set of rapidity ($\Delta y = 0.1$) and transverse momentum ($\Delta p_t = 75$ MeV/c) bins. The measured p_t-spectra at mid-rapidity are presented in Fig. 2. It can be seen that for both reactions our results reach the most interesting low-p_t region.

4 Summary

We reported on the ongoing study of the K^0 production in p+p and p+Nb collisions at a kinetic beam energy of 3.5 GeV. The obtained high-statistics sample of reconstructed kaons allows to analyze the low-p_t region, where the sensitivity to the in-medium kaon-nucleon potential is expected to be maximal. A comparison of the efficiency corrected p_t-distributions and their ratios with transport model calculations will give information about the KN potential.

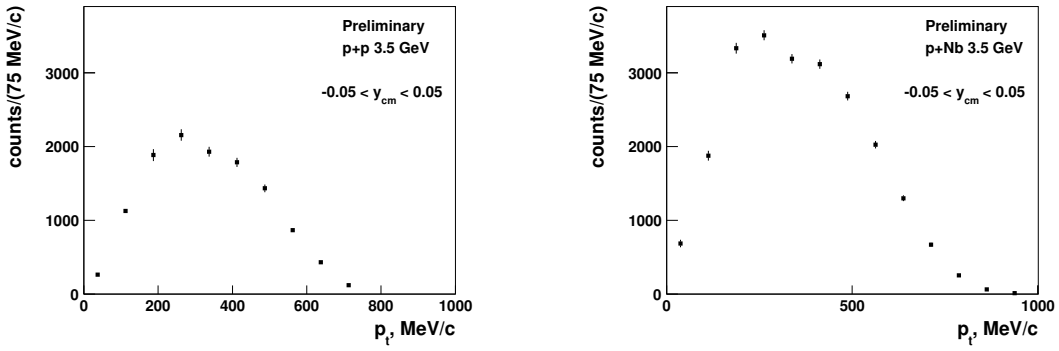

Figure 2: p_t-distributions of K^0_S's reconstructed in p+p (left) and p+Nb (right) collisions at mid-rapidity. No efficiency corrections were applied.

Acknowledgments

The collaboration acknowledges support by BMBF through grants 06DR9059D, 06FY9100I, 06MT9156 TP5 (Germany), by GSI (TKrue1012, TMFABI 1012, F&E), by the Helmholtz Alliance HA216/EMMI, by HIC for FAIR (LOEWE), by the DFG Excellence Cluster 153 "Universe" (Germany), by the Helmholtz young researcher group VH-NG-330, by MLL München, by grants MSMT LC07050, GAASCR IAA100480803 (Czech Republic), NN202286038, NN202198639 (Poland), PTDC/FIS/113339/2009 (Portugal), CPAN:CSD2007-00042 (Spain), by CNRS/IN2P3 (France) and by INFN (Italy).

Bibliography

[1] C. L. Korpa, M. F. M. Lutz, Acta Phys. Hung. **A22** (2005) 21-28.

[2] P. Crochet *et al.* [FOPI Collaboration], Phys. Lett. **B486** (2000) 6-12.

[3] F. Uhlig *et al.* [KaoS Collaboration], Phys. Rev. Lett. **95** (2005) 012301.

[4] C. Hartnack, H. Oeschler, Y. Leifels, E. L. Bratkovskaya, J. Aichelin, arXiv:1106.2083.

[5] G. Agakishiev *et al.* [HADES Collaboration], Eur. Phys. J. A **41** (2009) 243.

[6] M. Büscher *et al.*, Eur. Phys. J. **A22** (2004) 301-317.

[7] M. L. Benabderrahmane *et al.* [FOPI Collaboration], Phys. Rev. Lett. **102** (2009) 182501.

[8] G. Agakishiev *et al.* [HADES Collaboration], Phys. Rev. **C82** (2010) 044907.

Low-Energy Processes

Low-Energy Processes

Conveners

Eulogio	Oset	University of Valencia (*Chair*)
Achim	Denig	Universität Mainz
Jan	Friedrich	TU München

Session Chairs

Achim	Denig	Universität Mainz
Jan	Friedrich	TU München

Contents

Relativistic chiral representation of the πN scattering amplitude

Jose M. Alarcón[1,a], J. Martín Camalich[b,c], J. A. Oller[a], and L. Alvarez-Ruso[b]
[a]*Departamento de Física. Universidad de Murcia. E-30071, Murcia. Spain*
[b]*Departamento de Física Teórica and IFIC, Universidad de Valencia-CSIC, E-46071. Spain*
[c]*Department of Physics and Astronomy, University of Sussex, BN1 9QH, Brighton. UK*

We have analyzed pion-nucleon scattering using the manifestly relativistic covariant frameworks of *Infrared Regularization* (IR) and *Extended-On-Mass-Shell* (EOMS) up to $\mathcal{O}(q^3)$ in the chiral expansion, where q is a generic small momentum. We describe the low-energy phase shifts with a similar quality as previously achieved with Heavy Baryon Chiral Perturbation Theory, being the EOMS description better than the IR one. The Goldberger-Treiman discrepancy is extracted from data of partial wave analyses using both schemes, obtaining an unacceptable large value for the case of IR due to the loop contribution. On the other hand, EOMS gives small values compatible with other phenomenological approaches. Finally, we have unitarized the amplitudes provided by both schemes to extend the range of our description obtaining a good agreement with the data up to energies of $\sqrt{s} \approx 1.3$ GeV for the EOMS scheme while IR can not go beyond energies of $\sqrt{s} \approx 1.25$ GeV due to the unphysical cut that this scheme introduces.

1 Introduction

The πN scattering is a well known process at low energies, and there has been many attempts to use ChPT theory to describe it. The first one was the full covariant approach of [1], where they found problems with the power counting due to the non-vanishing mass of the nucleon in the chiral limit. Later, Heavy Baryon ChPT (HBChPT) was invented in order to solve the problem of power counting, but at the price of losing manifest Lorentz invariance [2]. This formalism describes well the physical region [3], but has problems of convergence in the subthreshold region [4] so it can not check some chiral symmetry predictions for QCD (low energy theorems). With this aim of checking the low energies theorems the Infrared Regularization (IR) [5] was proposed. This scheme keeps manifestly Lorentz invariance and satisfies the standard power counting of ChPT. The authors of Ref. [5] focused on the subthreshold region, and they used this new scheme for the first time to check low energy theorems [6]. The main conclusion of this work was that the one-loop

[1]e-mail: jmas1@um.es

representation is not precise enough to allow an accurate extrapolation of the physical data to the Cheng-Dashen point. The first attempt to describe the phase shifts employing IR was performed in [7] with the surprising result that the description of IR is worse than the one of HBChPT. They also obtained a huge violation of the Goldberger-Treiman (GT) relation ($20-30\%$). As we show in this work, the IR description is of the similar quality than the one provided by HBChPT, although a large violation of the GT relation remains. Importantly, the latter can be avoided by using the covariant renormalization scheme of Extended-On-Mass-Shell (EOMS) [8].

2 Perturbative Calculations

In order to obtain the LECs, we consider the phase shift analyses of the Karlsruhe group (KA85) [9] and the current solution of the GWU group (WI08) [10]. To fit the data of KA85 and WI08 we followed two strategies based on a different treatment of the P_{33} phase shifts: the first strategy (KA85-1 and WI08-1) consist of using the standard χ^2,[2] and the second one (KA85-2 and WI08-2) is based on fitting the function $\frac{\tan\delta_{P_{33}}}{|\vec{p}|^{2\ell+1}}$ around the threshold region. This function comes form the effective range expansion (ERE) of the P_{33} phase shifts. We also use this second strategy because we consider that the higher energy region for that partial wave is influenced by the $\Delta(1232)$. The results of these fits are shown in Figure 1. These perturbative fits reproduce the experimental data up to energies of 1.14 GeV for most of the partial waves. One can see that the results are very similar for both strategies, except for the P_{33} and P_{11} partial waves. For the latter, IR up to $\mathcal{O}(p^3)$ seems not to be able to reproduce the low energy region for the points provided by the GWU group (WI08-1 and WI08-2 fits). Instead of reproducing them, the curves accidentally fit better the points of the Karlsruhe group. This will translate into a result for the scattering volume, closer to the value of KA85 than the one of WI08. Results for the LECs and threshold parameters are given in [11]. Our averaged values are compatible with previous determinations of HBChPT [3].

With the value of d_{18} one can check the Goldberger-Treiman relation deviation considering that this deviation, up to $\mathcal{O}(M_\pi^3)$, is given by $\Delta_{GT} = -\frac{2M_\pi^2 d_{18}}{g_A}$ [5], where $g_{\pi N} = \frac{g_A m}{F_\pi}(1+\Delta_{GT})$. So that, for our averaged value of d_{18}, we obtain $\Delta_{GT} = 0.015 \pm 0.018$, that means $g_{\pi N} = 13.07 \pm 0.23$ or $f^2 = \frac{(g_{\pi N} M_\pi/4m)^2}{\pi} = 0.077 \pm 0.003$. Which is compatible with the values around $2-3\%$ obtained from πN and NN partial wave analyses of [12]. But when we implement the loop contributions, we obtain a huge GT relation violation due to the relativistic resummation performed by IR. For instance, for the fit KA85-1 one has a

[2] $\chi^2 = \sum_i \frac{(\delta-\delta_{th})^2}{err(\delta)^2}$, where δ is the experimental phase shift, δ_{th} is the theoretical one and $err(\delta)$ is an error that we assign as $err(\delta) = \sqrt{e_s^2 + e_r^2\delta^2}$. With $e_r = 0.2\%$ and $e_s = 0.1$ degrees. For more details about the designation of these values see [11].

22% of violation for the renormalization scale $\mu = 1$ GeV while for $\mu = 0.5$ GeV a 15% was observed.

3 Unitarized Calculations

We are interested now in extending the range of the description of the phase shifts. For that, we take care of the analyticity properties associated with the right-hand cut and implement unitarity to the πN amplitude. The partial wave amplitude $T_{IJ\ell}$ is written in terms of an interaction kernel $\mathcal{T}_{IJ\ell}$ and the unitary pion-nucleon loop function $g(s)$: $T_{IJ\ell} = (\mathcal{T}_{IJ\ell}^{-1} + g(s))^{-1}$ [13]. Written in this form, our amplitude satisfies unitarity **exactly**. The only undetermined parts of this definition are the interaction kernel $\mathcal{T}_{IJ\ell}$ and the subtraction constant a_1 contained in $g(s)$. The interaction kernel can be obtained by matching order by order with the perturbative result of ChPT [13, 14], and the subtraction constant a_1 is fixed by requiring $g(m^2) = 0$ in order to have the P_{11} nucleon pole in its right position. For the description of these higher energies we have to take into account the influence of the $\Delta(1232)$ in the P_{33} partial wave, so we decided to introduce a Castillejo-Dalitz-Dyson pole (CDD) in order to do so [13]. When studying that higher energy region, we noticed that IR gives rise to an unphysical cut for energies that can make $u = 0$ (Mandelstam variable), that corresponds to $s = 2(m^2 + M_\pi^2) \gtrsim 1.34^2$ GeV^2. This gives rise to a strong violation of unitarity for $s \gtrsim 1.34^2$ GeV^2 and fast rising of phase shifts for energies $\sqrt{s} \gtrsim 1.26$ GeV, so we decided to redo the fits up to energies of $\sqrt{s}_{max} = 1.25$ GeV for all the partial waves because it seems that up to this energy our amplitude is not affected by the unphysical cut introduced by IR. The result of our unitarized fit is shown in Figure 2, where one observes a drastic increase in the range of energies respect to the perturbative approach with a good description of the data. We could describe the contribution of the $\Delta(1232)$ thanks to the CDD while the problem with the points of the GWU for the P_{11} still remains. In [11] one can see that the values for the LECs and threshold parameters obtained with this unitarization technique are compatible with the perturbative one. Although this method does not constitute an alternative way to determine them and can be only employed in Unitary ChPT studies.

4 EOMS

Due to the problems we encounter in the IR scheme (scale dependence, huge GT deviation and unphysical cuts), we decided to redo our study in the so-called EOMS scheme [8]. In this relativistic scheme one removes explicitly the power counting breaking terms appearing in the loop integrals by absorbing them in the LECs of the most general Lagrangian. The proof that this can be done comes from IR, because Becher and Leutwyler proved that the power counting breaking terms are contained in what they called the regular part of the integral and this part is analytical in the quark masses and momenta [5]. As preliminary

results we checked that our calculation in this scheme is **scale independent** and provides a **better** perturbative description of the phase shifts for both experimental analyses (Figure 1), and a **small GT deviation** compatible with the values around $2-3\%$ of [12] when the full $\mathcal{O}(p^3)$ calculation is implemented.

Since this scheme is **free of unphysical cuts**, unitarization techniques give much better results, as we can see in Figure 2. Results for LECs and threshold parameters as well as the value of the Goldberger-Treiman discrepancy will be soon available in our next paper.

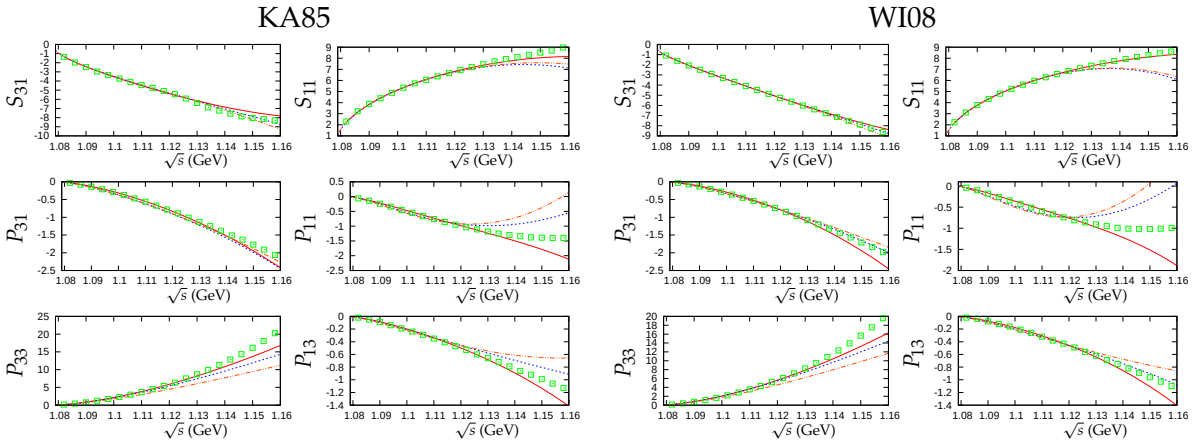

Figure 1: Perturbative fits to KA85 and WI08 data up to $\sqrt{s}_{max} = 1.13$ GeV. Solid line: EOMS (standard χ^2). Dashed line: IR (strategy 1). Dash-dotted line: IR (strategy 2).

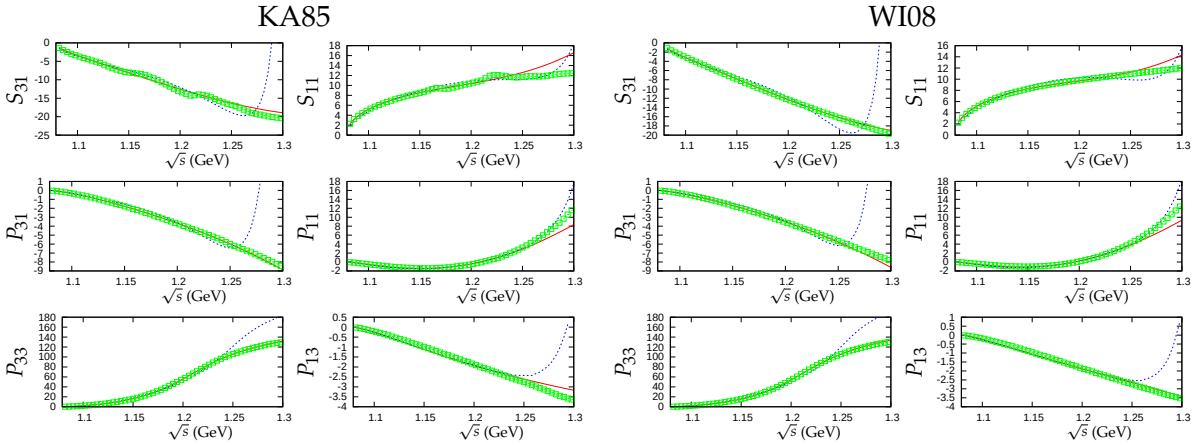

Figure 2: Unitarized fits to KA85 and WI08 data up to $\sqrt{s}_{max} = 1.25$ GeV. Solid line: EOMS. Dashed line: IR.

5 Summary and Conclusions

We studied πN scattering employing ChPT in the relativistic schemes of IR and EOMS up to $\mathcal{O}(p^3)$ using the data from the experimental analysis of the Karlsruhe and GWU groups to fit our theoretical results. We obtained an accurate reproduction of the phase shifts up to energies of 1.14 GeV for both schemes, though the EOMS description is better. These description are similar in quality to that obtained previously with $\mathcal{O}(p^3)$ HBChPT. This constitutes an **improvement** compared with previous works of IR [7]. We considered the Goldberger-Treiman relation in both schemes and obtained a huge deviation (20-30%) for IR when we implemented the loop contribution, while EOMS gives results compatible with the experimental analyses. We included non-perturbative methods of UChPT to resum the right-hand cut of the πN partial waves in order to extend the range of validity of our calculations and introduced a CDD pole to take into account the contribution of the $\Delta(1232)$ in the P_{33} partial wave. For the IR scheme we obtained a good reproduction of the phase shifts up to $\sqrt{s} \approx 1.25$ GeV, but we could not go beyond this energy due to the unphysical cut introduced by IR. While EOMS, that is free form that unphysical cut, could go beyond that limit and describe accurately the phase shifts up to $\sqrt{s} \approx 1.3$ GeV.

Bibliography

[1] J. Gasser, M. E. Sainio and A. Svarc, NPB 307:779 (1988)

[2] E. E. Jenkins and A. V. Manohar, Phys. Lett. B 255 (1991) 558.

[3] N. Fettes, U. G. Meißner and S. Steininger, Nucl. Phys. A 640 (1998) 199.

[4] V. Bernard, N. Kaiser, Ulf-G. Meissner, Int.J.Mod.Phys.E4:193-346,1995.

[5] T. Becher and H. Leutwyler, Eur. Phys. J. C 9 (1999) 643

[6] T. Becher and H. Leutwyler, JHEP 0106 (2001) 017.

[7] K. Torikoshi and P. J. Ellis, Phys. Rev. C 67 (2003) 015208.

[8] T. Fuchs, J. Gegelia, G. Japaridze and S. Scherer, Phys. Rev. D 68, 056005 (2003).

[9] R. Koch, Nucl. Phys. A 448 (1986) 707; R. Koch and E. Pietarinen, Nucl. Phys. A 336 (1980) 331.

[10] Computer code SAID, online program at http://gwdac.phys.gwu.edu/ , solution WI08. R. A. Arndt et al., Phys. Rev. C 74 (2006) 045205. solution SM01.

[11] J. M. Alarcón, J. Martín Camalich, J. A. Oller, L. Alvarez-Ruso, Phys. Rev. C 83 (2011) 055205.

[12] R. A. Arndt, R. L. Workman and M. M. Pavan, Phys. Rev. C 49 (1994) 2729.

[13] J. A. Oller and E. Oset, Phys. Rev. D 60 (1999) 074023.

[14] J. A. Oller and U. G. Meißner,Phys.Lett.B 500:263-272,2001.

Roy–Steiner equations for $\gamma\gamma \to \pi\pi$

Martin Hoferichter[1,a,b], Daniel R. Phillips[b], and Carlos Schat[b,c]
[a] *Helmholtz-Institut für Strahlen- und Kernphysik (Theorie) and Bethe Center for Theoretical Physics, Universität Bonn, Germany*
[b] *Institute of Nuclear and Particle Physics and Department of Physics and Astronomy, Ohio University, Athens, USA*
[c] *Instituto de Física de Buenos Aires, CONICET - Departamento de Física, FCEyN, Universidad de Buenos Aires, Argentina*

Starting from hyperbolic dispersion relations, we present a system of Roy–Steiner equations for pion Compton scattering that respects analyticity and unitarity requirements, gauge invariance, as well as crossing symmetry, and thus all symmetries of the underlying quantum field theory. To suppress the dependence on the high-energy region, we also consider once- and twice-subtracted versions of the equations, where the subtraction constants are identified with dipole and quadrupole pion polarizabilities. We consider the resolution of the $\gamma\gamma \to \pi\pi$ partial waves by a Muskhelishvili-Omnès representation with finite matching point, and discuss the consequences for the two-photon coupling of the σ resonance as well as its relation to pion polarizabilities.

1 Introduction

The Roy equations for $\pi\pi$ scattering [1] are a coupled system of partial wave dispersion relations that respects analyticity, unitarity, and crossing symmetry of the scattering amplitude. In recent years, partial wave dispersion relations in combination with unitarity (and chiral symmetry) have been used for high-precision studies of low-energy processes, both in $\pi\pi$ [2,3] and πK [4] scattering. An important application of $\pi\pi$ Roy equations in combination with Chiral Perturbation Theory (ChPT) was the precise prediction of the pole parameters of the σ resonance [5]

$$M_\sigma = 441^{+16}_{-8}\,\text{MeV}, \qquad \Gamma_\sigma = 544^{+18}_{-25}\,\text{MeV}. \tag{1}$$

The reaction $\gamma\gamma \to \pi\pi$ provides an alternative to $\pi\pi$ scattering for the excitation of the σ. In particular, as discussed in detail in [6], Roy-equation techniques in $\gamma\gamma \to \pi\pi$ allow us to constrain the σ's two-photon width $\Gamma_{\sigma\gamma\gamma}$ at a similar level of rigor as M_σ and Γ_σ based on $\pi\pi$ Roy equations.

[1] hoferichter@hiskp.uni-bonn.de

2 Roy equations for $\pi\pi$ scattering

Roy equations for $\pi\pi$ scattering are obtained by starting from a twice-subtracted dispersion relation at fixed Mandelstam t, determining the t-dependent subtraction constants by means of crossing symmetry, and finally performing a partial wave expansion. This leads to a coupled system of integral equations for the $\pi\pi$ partial waves $t_J^I(s)$ with isospin I and angular momentum J

$$t_J^I(s) = k_J^I(s) + \sum_{I'=0}^{2}\sum_{J'=0}^{\infty}\int_{4M_\pi^2}^{\infty} \mathrm{d}s' K_{JJ'}^{II'}(s,s')\,\mathrm{Im}\, t_{J'}^{I'}(s') \tag{2}$$

where $K_{JJ'}^{II'}$ are known kinematical kernel functions and the $\pi\pi$ scattering lengths—the only free parameters—appear in the subtraction term k_J^I. Assuming elastic unitarity

$$\mathrm{Im}\, t_J^I(s) = \sigma(s)|t_J^I(s)|^2, \quad t_J^I(s) = \frac{e^{2i\delta_J^I(s)}-1}{2i\sigma(s)}, \quad \sigma(s) = \sqrt{1-\frac{4M_\pi^2}{s}}, \tag{3}$$

(2) translates into a coupled integral equation for the phase shifts δ_J^I themselves.

3 Roy–Steiner equations for $\gamma\gamma \to \pi\pi$

Crossing symmetry in this case is less restrictive than for $\pi\pi$ scattering, as it couples $\gamma\gamma \to \pi\pi$ to pion Compton scattering $\gamma\pi \to \gamma\pi$, which we will consider as the s-channel process. Roy–Steiner equations are then most conveniently constructed based on hyperbolic dispersion relations [7]. The resulting system of integral equations couples the $\gamma\gamma \to \pi\pi$ partial waves $h_{J,\pm}^I(t)$ to the $\gamma\pi \to \gamma\pi$ partial waves $f_{J,\pm}^I(s)$ (with photon helicities $\pm$), e.g.

$$h_{J,-}^I(t) = \tilde{N}_J^-(t) + \frac{1}{\pi}\int_{M_\pi^2}^{\infty}\mathrm{d}s' \sum_{J'=1}^{\infty}\tilde{G}_{JJ'}^{-+}(t,s')\,\mathrm{Im}\, f_{J',+}^I(s') + \frac{1}{\pi}\int_{4M_\pi^2}^{\infty}\mathrm{d}t' \sum_{J'}\tilde{K}_{JJ'}^{--}(t,t')\,\mathrm{Im}\, h_{J',-}^I(t'), \tag{4}$$

where $\tilde{N}_J^-(t)$ includes the QED Born terms. Subtracting at $t = 0$, $s = M_\pi^2$, the subtraction constants directly correspond to pion polarizabilities. In the once-subtracted case, one needs the dipole polarizabilities $\alpha_1 \pm \beta_1$, while a second subtraction requires in addition knowledge of the quadrupole polarizabilities $\alpha_2 \pm \beta_2$.

Elastic unitarity is also less restrictive than for $\pi\pi$ scattering, since the unitarity relation is linear in $h_{J,\pm}^I$

$$\mathrm{Im}\, h_{J,\pm}^I(t) = \sigma(t) h_{J,\pm}^I(t) t_J^I(t)^*. \tag{5}$$

Below inelastic thresholds the phase of $h_{J,\pm}^I$ coincides with δ_J^I ("Watson's theorem"). Assuming this phase to be known, the equations thus reduce to a Muskhelishvili–Omnès problem for $h_{J,\pm}^I$ [8].

4 Muskhelishvili–Omnès solution and results for $\Gamma_{\sigma\gamma\gamma}$

To solve the equations for $h^I_{J,\pm}$, we truncate the system at $J = 2$. Furthermore, we assume the amplitudes to be known above the matching point $t_\mathrm{m} = (0.98\,\mathrm{GeV})^2$. The solution can then be written down in terms of Omnès functions

$$\Omega^I_J(t) = \exp\left\{\frac{t}{\pi}\int\limits_{4M_\pi^2}^{t_\mathrm{m}} \mathrm{d}t' \frac{\delta^I_J(t')}{t'(t'-t)}\right\}. \tag{6}$$

We find that the solutions for different partial waves in general do not decouple, e.g. the equation for the S-wave involves spectral integrals over the D-waves as well [6]. This is a new result of our dispersive treatment of $\gamma\gamma \to \pi\pi$ based on Roy–Steiner equations.

We approximate $\mathrm{Im}\, f^I_{J,\pm}(s)$, which at low energies is dominated by multi-pion states, by a sum of resonances [9]. Above the matching point we use a Breit–Wigner description of the $f_2(1270)$, which dominates the cross section at higher energies. Within our formalism [6] we derive a sum rule for the $I = 2$ polarizabilities, which—in combination with ChPT results for dipole and neutral-pion quadrupole polarizabilities [10]— produces an improved prediction

$$(\alpha_2 - \beta_2)^{\pi^\pm} = (15.3 \pm 3.7) \cdot 10^{-4}\mathrm{fm}^5 \tag{7}$$

for the charged-pion quadrupole polarizability. This sum-rule result together with the ChPT values for the other polarizabilities [10] leads to the "ChPT" prediction for the total cross section of $\gamma\gamma \to \pi^0\pi^0$ depicted in the left panel of Fig. 1. The result labeled "GMM" is found when we adopt the polarizability values of a recent fit of a two-channel Muskhelishvili–Omnès representation to $\gamma\gamma \to \pi\pi$ cross section data [9]. The uncertainty due to the $\pi\pi$ phases represented by the grey band is estimated by varying between two recent state-of-the-art analyses based on Roy and Roy-like equations [3,11]. We see that especially for the twice-subtracted version the agreement with experiment in the low-energy region is very good. Since we have shown that the σ lies within the domain of validity of our Roy–Steiner equations [6], this formalism allows for a reliable analytic continuation to the σ pole.

The main result of our analysis is shown in the right panel of Fig. 1: there is a correlation between $\Gamma_{\sigma\gamma\gamma}$ and the $I = 0$ pion polarizabilities that follows from Roy–Steiner equations and input for the $\pi\pi$ phases alone. In combination with the ChPT-plus-sum-rule input for the polarizabilities, we obtain

$$\Gamma_{\sigma\gamma\gamma} = (1.7 \pm 0.4)\,\mathrm{keV}. \tag{8}$$

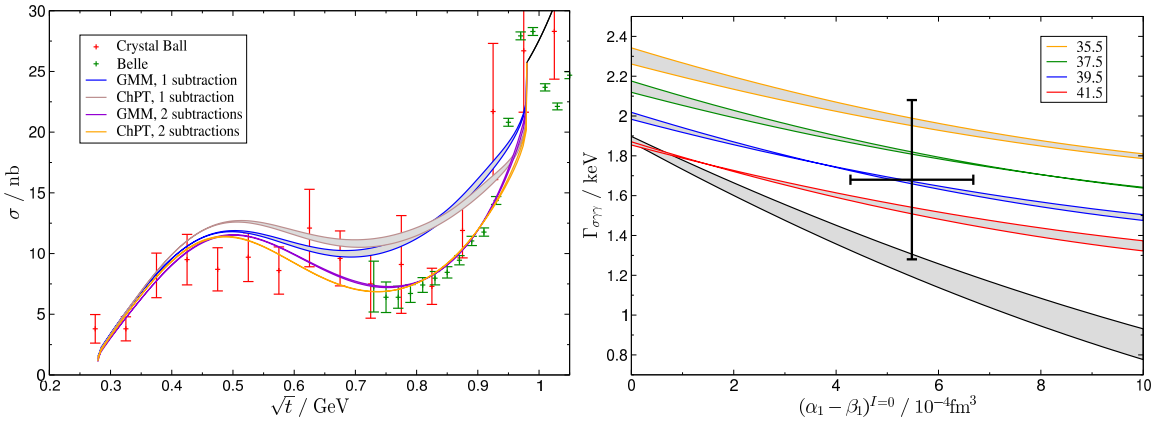

Figure 1: Total cross section for $\gamma\gamma \to \pi^0\pi^0$ for $|\cos\theta| \leqslant 0.8|$ (left) and $\Gamma_{\sigma\gamma\gamma}$ as a function of the $I = 0$ pion polarizabilities (right). The black line refers to the unsubtracted case and the colored lines to the twice-subtracted version with $(\alpha_2 - \beta_2)^{I=0}$ as indicated (in units of 10^{-4}fm^5). The grey bands represent the uncertainty due to the $\pi\pi$ input. The cross corresponds to the twice-subtracted case plus ChPT input.

Acknowledgments

This research was supported by the DFG (SFB/TR 16), the program "Kurzstipendien für DoktorandInnen" of the DAAD, the Bonn-Cologne Graduate School of Physics and Astronomy, the US Department of Energy (Office of Nuclear Physics), and CONICET.

Bibliography

[1] S. M. Roy, Phys. Lett. B **36** (1971) 353.

[2] B. Ananthanarayan, G. Colangelo, J. Gasser and H. Leutwyler, Phys. Rept. **353** (2001) 207.

[3] R. García-Martín, R. Kamiński, J. R. Peláez, J. Ruiz de Elvira and F. J. Ynduráin, Phys. Rev. D **83** (2011) 074004.

[4] P. Büttiker, S. Descotes-Genon and B. Moussallam, Eur. Phys. J. C **33** (2004) 409.

[5] I. Caprini, G. Colangelo and H. Leutwyler, Phys. Rev. Lett. **96** (2006) 132001.

[6] M. Hoferichter, D. R. Phillips and C. Schat, arXiv:1106.4147 [hep-ph].

[7] G. E. Hite and F. Steiner, Nuovo Cim. A **18** (1973) 237.

[8] N. Muskhelishvili, *Singular Integral Equations*, P. Noordhof, Groningen, 1953; R. Omnès, Nuovo Cim. **8** (1958) 316.

[9] R. García-Martín and B. Moussallam, Eur. Phys. J. C **70** (2010) 155.

[10] J. Gasser, M. A. Ivanov and M. E. Sainio, Nucl. Phys. B **728** (2005) 31; **745** (2006) 84.

[11] I. Caprini, G. Colangelo, H. Leutwyler, in preparation.

Chiral dynamical aspects of reactions recently measured at ELSA, MAMI, GRAAL, and other labs

Michael Döring
Helmholtz-Institut für Strahlen- und Kernphysik (Theorie) and Bethe Center for Theoretical Physics, Universität Bonn, Nußallee 14-16, D-53115 Bonn, Germany

Meson photoproduction is extensively studied in experimental facilities to gain insight into the hadron structure and their interaction. The measurements provide a testing ground for low- and intermediate-energy hadronic physics in form of, e.g., chiral effective theories, unitarized chiral approaches, or partial wave analyses. In these proceedings, two particular aspects are considered: The recently discovered enhancement of η photoproduction on the quasi-free neutron at energies around $\sqrt{s} \sim 1.67$ GeV is addressed within an SU(3) coupled-channel model. The $K\Sigma$ threshold plays a significant role. For the reaction $\vec{\gamma}p \to \pi^0\eta p$, the polarization observables I^S and I^C are evaluated from a chiral unitary amplitude developed earlier, showing the significance of the $\Delta(1700)\,D_{33}$ resonance and its S-wave decay into $\eta\Delta(1232)$ which indicates the dynamical nature of this resonance.

1 η photoproduction on the neutron

Extracting the resonance spectrum from photon-induced reactions is one of the main goals of current and past experimental programs at ELSA, GRAAL, JLab, MAMI, and other labs.

Recently, the reaction $\gamma n \to \eta n$ has become accessible in photoproduction experiments on the deuteron or nuclei [1–5]. At energies around $\sqrt{s} \sim 1.67$ GeV, an excess of η production on the neutron compared to the proton case has been reported. On the theoretical side, this excess has been interpreted as a potential signal for a non-strange member of an anti-decuplet of pentaquarks [6,7], however, there are also other explanations mostly in terms of different interfering partial waves [8–12].

In the presented work, the phenomenon is addressed within the chiral unitary framework developed in Ref. [13]. Details on the results presented in these proceedings can be found in Ref. [14], in particular a thorough discussion on the stability of the results. The hadronic interaction in the present framework [13, 14] is mediated by the Weinberg-Tomozawa interaction in the coupled channels πN, ηN, $K\Lambda$, and $K\Sigma$, unitarized in a Bethe-Salpeter equation. The model also contains explicit resonance states which account for the $N^*(1650)$ and a phenomenological background. The gauge invariant implementation of the photon

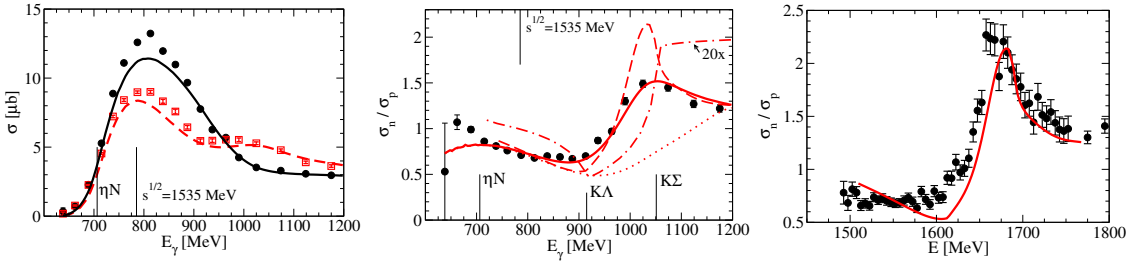

Figure 1: Left: Cross sections for the photoproduction on the quasi-free proton (solid line) and neutron (dotted line). Data: Ref. [4]. Center: Cross section ratio $\sigma(\gamma n \to \eta n)/\sigma(\gamma p \to \eta p)$. Data: Ref. [4]. Solid (dashed) line: Result, Fermi motion included (excluded). For the other curves, see text. Right: Prediction from Ref. [14] (smearing from Fermi motion removed). Data: Ref. [5].

interaction follows Refs. [15] (see also Refs. [16]). For the results on the quasi-free p and n in the deuteron, we use the impulse approximation.

In the presented work [14], *223*a global fit of E_{0+} multipoles, S-wave cross sections and partial waves has been performed for the reactions $\gamma N \to \pi N$, $\pi N \to \pi N$, $\gamma p \to \eta p$, $\gamma n \to \eta n$, $\pi N \to \eta N$, $\gamma N \to KY$, and $\pi N \to KY$ where $Y = \Lambda, \Sigma$, but we concentrate here on the results for $\gamma N \to \eta N$. In Fig. 1 to the left, the present result is compared with the recent cross section data on the quasi-free n and p from Ref. [4]. In the center, the ratio of these cross sections is shown (solid line). The appearance of the sharp peak in σ_n/σ_p is obviously due to the intermediate states $K\Lambda$ and $K\Sigma$ in the model. Indeed, both in $\gamma n \to \eta n$ and $\gamma p \to \eta p$, the photon can couple to charged pions and kaons in the intermediate πN and $K\Sigma$ states; however, in $\gamma p \to \eta p$ the photon coupling to the K^+ in the $K^+\Lambda$ state is possible, while this is not possible in $\gamma n \to \eta n$, because the corresponding intermediate state is given by $K^0\Lambda$ [14]. For the ratio σ_n/σ_p, this difference manifests itself in the observed peak structure in Fig. 1, center panel. Indeed, removing the photon coupling to the $K^+\Lambda$ state in the $\gamma p \to \eta p$ reaction, one obtains the ratio given by the dotted line; the peak has disappeared.

To check for the model dependence of the presented results, we have replaced the hadronic final state interaction (FSI) with the Weinberg-Tomozawa (WT) term. The photoproduction is then given by the triangle graph which contributes at next-to-leading order (NLO) in the chiral expansion of the amplitude [17]. The resulting ratio σ_n/σ_p, shown as the dash-dotted line in the center panel of Fig. 1 (multiplied by an arbitrary factor of 20), is, of course, very different in magnitude from the full result (dashed line) — replacing the strong, non-perturbative FSI by the tree-level WT term is certainly an oversimplification. However, the energy dependence shows the same pronounced KY cusps as the full result. In the future, the present explanation of the peak in terms of an S-wave threshold cusp could be tested within the chiral unitary framework of Ref. [18] or the hadron exchange framework of Ref. [19] where KY states have been included recently. In this context, it should be also mentioned that the narrow structure observed in photoproduction on the proton [20] has

recently been analyzed [21], and both a resonance hypothesis and a cusp from the ωN channel could explain the data.

Finally, one can overlay the published theoretical results of Ref. [14] for the case without Fermi motion (dashed curve in the center panel) with the very recent measurement of Ref. [5]. This is shown in the right panel. The prediction is quite quantitative; in particular, a cusp can indeed generate the extremely narrow structure seen in experiment. As an outlook, the presented approach could be extended to Compton scattering to test it with the recent data from Ref. [22].

Summarizing, the experimentally determined η photoproduction cross sections on quasi-free neutron and proton can be explained quantitatively within the present model which accounts for the S wave contribution only. The chiral coupled-channel SU(3) dynamics and its interplay with the photon lead to the occurrence of the observed spike-like structure in σ_n/σ_p.

2 The observables I^S and I^C in the reaction $\vec{\gamma}p \to \pi^0\eta p$

The photoproduction of meson pairs is proving to be a rich field allowing us to widen our understanding of hadron dynamics and hadron structure. Following much work devoted to the photoproduction of two pions in the last decade, $\pi^0\eta$ photoproduction has attracted attention recently [23–26]. Polarization observables are reported in Refs. [24, 27–29]. The reaction was studied theoretically in Refs. [30, 31] and partial waves analyses of the reaction have been also performed [32, 33], finding the $\Delta(1700)$ partial wave to be important. In the chiral unitary approach of Ref. [31], the process turned out to be dominated at low energies by the excitation of the $\Delta(1700)$, which then decays into $\eta\Delta$, with the Δ subsequently decaying into πN. In that approach, predictions of the cross section are possible because the $\Delta(1700)\Delta(1232)\eta$ and $\Delta(1700)\Sigma(1385)K$ couplings are known from the chiral unitary framework [34, 35] in which the $\Delta(1700)$ appears dynamically generated. In Ref. [36] the radiative decay width of the $\Delta(1700) \to \gamma N$ could be predicted, because the photon coupling to the mesons and baryons that constitute this resonance are all well known. The result is in agreement with the phenomenologically known values [37] from data analyses which are used in Refs. [24, 31, 38] for the $\gamma p \to \pi^0\eta p$ reaction. The theoretical framework from Refs. [31, 35] is quite predictive since another coupling of the $\Delta(1700)$ resonance is to the $K\Sigma(1385)$ state and the evaluated (differential) cross sections for the reaction $\gamma p \to K^0\pi^0\Sigma^+$ [31] agree with the measurements published in Ref. [39]. In Ref. [38], the chiral unitary amplitude from Ref. [31] has been used to relate eleven different pion- and photon-induced reactions.

From the list of the underlying processes included in Ref. [31], we show here only those in Fig. 2, which involve the $\Delta(1700)\eta\Delta$ and $\Delta(1700)K\Sigma(1385)$ vertices predicted from the chiral unitary amplitudes [35]. These processes give the largest contributions to the $\eta\Delta$ and $\pi^0 S_{11}(\eta p)$ final states. All free constants that appear in the model have been fixed from

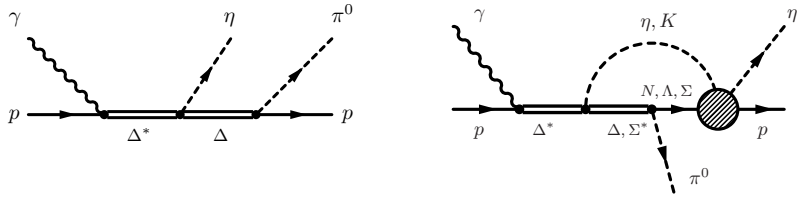

Figure 2: Left: Tree level process from the decay of the $\Delta(1700)$ to $\eta\Delta(1232)$. This is the dominant process. The complex $\Delta(1700) \to \eta\Delta(1232)$ coupling is a prediction within the chiral unitary framework. Right: Other processes with $\Delta(1700)\eta\Delta$ and $\Delta(1700)K\Sigma(1385)$ couplings and $\pi^0\, S_{11}(\eta p)$ final states. For the full list of processes, see Ref. [31].

other processes, thus the results of Ref. [31] can be regarded as predictions. The diagrams from Fig. 2 are gauge invariant. This is so since the $\gamma N\Delta(1700)$ coupling is obtained from the experimental data through an expression which is manifestly gauge invariant.

The recent work of Ref. [28] presents another challenge since new observables are measured, i.e, the I^S and I^C polarizations as a function of the ϕ^* angle between the decay plane and the reaction plane (for the precise definition of the reaction geometry, see e.g. Ref. [40]). In the work presented here [40], the chiral unitary amplitude developed in Refs. [31,38] is used to straightforwardly evaluate I^S and I^C and compare to the data. The predictions are shown in Fig. 3 with the (red) solid lines, together with the data from Ref. [28]. Note the symmetries $I^S(\phi^*) = -I^S(2\pi - \phi^*)$ and $I^C(\phi^*) = I^C(2\pi - \phi^*)$ [28]. The present results reproduce well the complex shapes of the angular distributions, while at the highest energies deviations start to become noticeable. The dotted lines show the results without using the diagrams from Fig. 2 which demonstrates that the $\Delta(1700)\Delta(1232)\eta$ and $\Delta(1700)\Sigma(1385)K$ couplings provide the essential dynamics. Indeed, using only the tree level diagram to the left of Fig. 2, the main features of the full results are already obtained (dash-dotted line in Fig. 3). Summarizing, the theoretical predictions of I^S, I^C, and I^θ in the reaction $\gamma p \to \pi^0\eta p$ agree well with the data recently measured at CBELSA/TAPS, providing support to a chiral unitary model, in which the $\Delta(1700)$ appears dynamically generated.

Bibliography

[1] V. Kuznetsov *et al.* [GRAAL Collaboration], Phys. Lett. B **647**, 23 (2007).

[2] F. Miyahara *et al.*, Prog. Theor. Phys. Suppl. **168**, 90 (2007).

[3] T. Mertens *et al.* [CBELSA and TAPS Collaboration], Eur. Phys. J. A **38**, 195 (2008).

[4] I. Jaegle *et al.* [CBELSA and TAPS Collaboration], Phys. Rev. Lett. **100**, 252002 (2008).

[5] I. Jaegle, B. Krusche *et al.*, Eur. Phys. J. **A47**, 89 (2011).

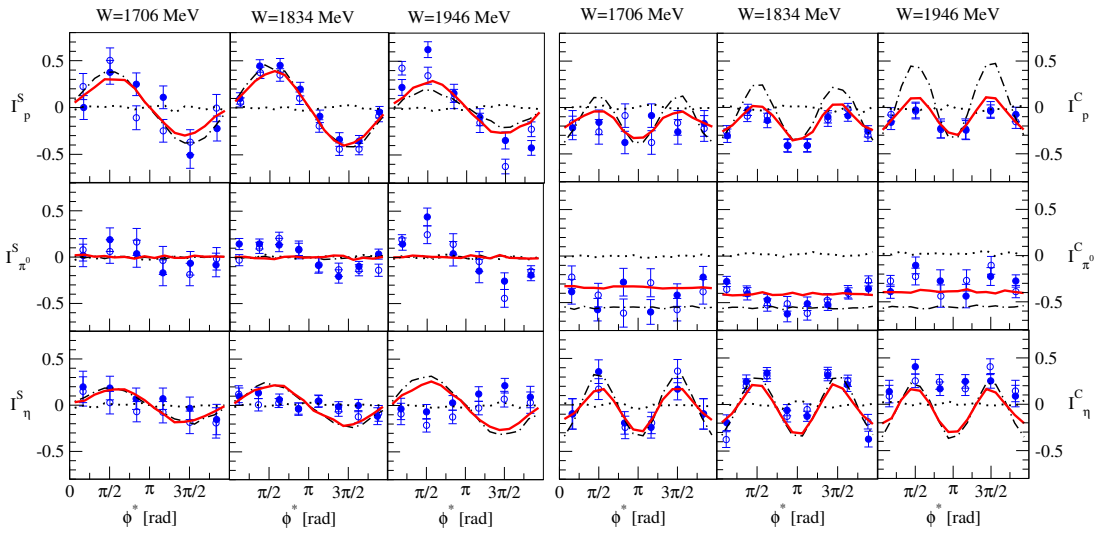

Figure 3: Left: Polarization observable $I^S(\phi^*)$, Right: Polarization observable $I^C(\phi^*)$. Shown are the three cases of p, π^0, and η spectators. Data: Ref. [28] (full circles). Empty circles: $-I^S(2\pi - \phi^*)$ and $I^C(2\pi - \phi^*)$, respectively. (Red) solid lines: Presented results [40], predicted from the model of Refs. [31,38]. (Black) dotted lines: Without the processes from Fig. 2. (Black) dash-dotted lines: Only contribution from the tree level diagram of Fig. 2, left.

[6] D. Diakonov, V. Petrov and M. V. Polyakov, Z. Phys. A **359**, 305 (1997).

[7] A. Fix, L. Tiator and M. V. Polyakov, Eur. Phys. J. A **32**, 311 (2007).

[8] R. A. Arndt *et al.*, Phys. Rev. C **69**, 035208 (2004).

[9] V. Shklyar, H. Lenske and U. Mosel, Phys. Lett. B **650**, 172 (2007).

[10] R. Shyam and O. Scholten, Phys. Rev. C **78**, 065201 (2008).

[11] W. T. Chiang, S. N. Yang, L. Tiator and D. Drechsel, Nucl. Phys. A **700**, 429 (2002).

[12] A. V. Anisovich *et al.*, Eur. Phys. J. A **41**, 13 (2009).

[13] M. Döring and K. Nakayama, Eur. Phys. J. A **43**, 83 (2010).

[14] M. Döring and K. Nakayama, Phys. Lett. B **683**, 145 (2010).

[15] H. Haberzettl, K. Nakayama and S. Krewald, Phys. Rev. C **74**, 045202 (2006).

[16] B. Borasoy, P. C. Bruns, U.-G. Meißner and R. Nissler, Eur. Phys. J. A **34**, 161 (2007).

[17] V. Bernard, N. Kaiser and U.-G. Meißner, Z. Phys. C **70**, 483 (1996).

[18] D. Ruic, M. Mai and U.-G. Meißner, arXiv:1108.4825 [nucl-th].

[19] M. Döring, C. Hanhart, F. Huang, S. Krewald, U.-G. Meißner, D. Rönchen, Nucl. Phys. **A851** , 58 (2011).

[20] E. F. McNicoll *et al.* [Crystal Ball Collaboration at MAMI], Phys. Rev. C **82** (2010) 035208 [Erratum-ibid. C **84** (2011) 029901].

[21] A. V. Anisovich, E. Klempt, V. Kuznetsov, V. A. Nikonov, M. V. Polyakov, A. V. Sarantsev and U. Thoma, arXiv:1108.3010 [hep-ph].

[22] V. Kuznetsov, M. V. Polyakov, V. Bellini, T. Boiko, S. Chebotaryov, H. -S. Dho, G. Gervino, F. Ghio *et al.*, Phys. Rev. **C83** , 022201 (2011).

[23] T. Nakabayashi *et al.*, Phys. Rev. C **74**, 035202 (2006).

[24] J. Ajaka *et al.*, Phys. Rev. Lett. **100**, 052003 (2008).

[25] I. Horn *et al.* [CB-ELSA Collaboration], Eur. Phys. J. A **38**, 173 (2008).

[26] V. L. Kashevarov, Eur. Phys. J. A **42**, 141 (2009).

[27] E. Gutz *et al.* [CBELSA/TAPS Collaboration], Eur. Phys. J. A **35**, 291 (2008).

[28] E. Gutz *et al.* [CBELSA/TAPS Collaboration], Phys. Lett. B **687**, 11 (2010).

[29] V. L. Kashevarov *et al.* [Crystal Ball at MAMI, TAPS, and A2 Collaborations], Phys. Lett. B **693**, 551 (2010).

[30] D. Jido, M. Oka and A. Hosaka, Prog. Theor. Phys. **106**, 873 (2001).

[31] M. Döring, E. Oset and D. Strottman, Phys. Rev. C **73**, 045209 (2006).

[32] A. Anisovich, E. Klempt, A. Sarantsev and U. Thoma, Eur. Phys. J. A **24**, 111 (2005).

[33] A. Fix, V. L. Kashevarov, A. Lee and M. Ostrick, Phys. Rev. C **82**, 035207 (2010).

[34] E. E. Kolomeitsev and M. F. M. Lutz, Phys. Lett. B **585**, 243 (2004).

[35] S. Sarkar, E. Oset and M. J. Vicente Vacas, Nucl. Phys. A **750**, 294 (2005).

[36] M. Döring, Nucl. Phys. A **786**, 164 (2007).

[37] K. Nakamura *et al.* [Particle Data Group Collaboration], J. Phys. G **G37** , 075021 (2010).

[38] M. Döring, E. Oset and D. Strottman, Phys. Lett. B **639**, 59 (2006).

[39] M. Nanova *et al.* [CBELSA/TAPS Collaboration], Eur. Phys. J. A **35**, 333 (2008).

[40] M. Döring, E. Oset and U.-G. Meißner, Eur. Phys. J. **A46** (2010) 315.

Spin-Flavor van der Waals Forces and NN interaction

Alvaro Calle Cordon[1,a] and E. Ruiz Arriola[b]
[a]*Thomas Jefferson National Accelerator Facility, Newport News, Virginia 23606, USA.*
[b]*Departamento de Física Atómica, Molecular y Nuclear, Universidad de Granada, E-18071 Granada, Spain.*

We study the Nucleon-Nucleon interaction in the Born-Oppenheimer approximation at second order in perturbation theory including the Δ resonance as an intermediate state. The potential resembles strongly chiral potentials computed either via soliton models or chiral perturbation theory and has a van der Waals like singularity at short distances which is handled by means of renormalization techniques. Results for the deuteron are discussed.

1 Introduction

A major goal of Nuclear Physics is the derivation of the Nucleon-Nucleon (NN) interaction from Quantum Chromodynamics (QCD). In QCD the fundamental degrees of freedom are colored quarks and gluons which are *confined* to form colorless strongly interacting hadrons. Because of this the resulting nuclear forces at sufficiently large distances correspond to spin-flavor excitations, very much like the dipole excitations generating the van der Waals (vdW) forces acting between atoms (for a review see e.g. [1]). In the Born-Oppenheimer (BO) approximation and assuming no retardation and no electron cloud overlap at large distances, the atom-atom energy at a separation distance r can be calculated at second order perturbation theory as,

$$V_{AA} = \langle AA|V_{\rm dip}|AA\rangle + \sum_{AA\neq A^*A^*} \frac{|\langle AA|V_{\rm dip}|A^*A^*\rangle|^2}{E_{AA}-E_{A^*A^*}} + \cdots = -\frac{C_6}{r^6} + \ldots , \quad (1)$$

where $|AA\rangle$ and $|A^*A^*\rangle$ is the electron wave function corresponding to a pair of well separated clusters in their atomic ground state and excited states respectively and where we assume a system with no permanent electric dipole. Driven by this compelling molecular analogy we want to analyze the NN interaction under similar dynamical assumptions.

The generalization to the NN system is straightforward, by just replacing $V_{\rm dip}$ by the One-Pion-Exchange (OPE) potential $V_{1\pi}$ and was already discussed in Ref. [2] within the context of chiral soliton models and the associated long-range spin-flavor universality. One

[1]cordon@jlab.org

considers the colorless nucleons as two quark clusters which in the chiral quark model exchange a colorless pion at large distances. The mutual (chiral) polarizability causes attraction between the nucleons, exactly in the same way as for atom-atom interactions and equivalently, using Eq. (1), one can obtain an optical potential where the effect of excited states as the Δ is included perturbatively,

$$V_{2N}(\boldsymbol{r}) = V^{1\pi}_{NN,NN}(\boldsymbol{r}) + 2\,\frac{|V^{1\pi}_{NN,N\Delta}(\boldsymbol{r})|^2}{M_N - M_\Delta} + \frac{1}{2}\,\frac{|V^{1\pi}_{NN,\Delta\Delta}(\boldsymbol{r})|^2}{M_N - M_\Delta} + \mathcal{O}(V^3)\,, \tag{2}$$

where $V^{1\pi}_{NN,NN}$ is the NN OPE potential and $V^{1\pi}_{NN,N\Delta}$ and $V^{1\pi}_{NN,\Delta\Delta}$ are OPE transition potentials [2]. Eq. (2) reproduces exactly the Skyrme soliton model result of Refs. [4,5]. At very short distances Eq. (2) behaves like a vdW potential $\sim -g_A^4/(\Delta f_\pi^4 r^6)$ and in fact it reduces to the Chiral Two-Pion-Exchange (ChTPE) potential at NLO-Δ [6,7] with the identification $h_A/g_A = f_{\pi N\Delta}/(2f_{\pi NN})$. Moreover, although both potentials are not completely equivalent they are very similar even at intermediate distances which explain why we achieve results for most of NN observables looking very much like those of more sophisticate chiral potentials.

2 Results

The BO-vdw potential, Eq. (2), presents a short distance singularity and to deal with it we use the method of renormalization with boundary conditions [8]. In [2] we showed satisfactory results for $^1S_0$ and $^3S_1 - ^3D_1$ phase shifts. Here and for the sake of brevity, we concentrate on deuteron properties. A more detailed study will be presented elsewhere. The deuteron is solved by fixing its binding energy $B_d = 2.224575$ MeV, the D/S ratio $\eta = 0.0256$ and the $^3S_1$ scattering length $a_{^3S_1} = 5.419$ fm from which we obtain the properties, $A_S = 0.873(8)\text{fm}^{-1/2}$, $r_m = 1.945(14)$fm, $Q_d = 0.2712(1)\text{fm}^2$, $P_D = 7.3(1.2)\%$, $\langle r^{-1}\rangle = 0.468(8)$, $a_{^3D_1} = 6.56(5)\text{fm}^5$, $a_{E_1} = 1.549(1)\text{fm}^3$ in the case in which we use the $SU(N_c)$ quark model relation with $N_c = 3$ and, $A_S = 0.886(9)\text{fm}^{-1/2}$, $r_m = 1.973(18)$fm, $Q_d = 0.2789(12)\text{fm}^2$, $P_D = 6.8(1.4)\%$, $\langle r^{-1}\rangle = 0.44(1)$, $a_{^3D_1} = 6.471(9)\text{fm}^5$, $a_{E_1} = 1.689(3)\text{fm}^3$ in the case $N_c \to \infty$. The estimate error corresponds to taking the extreme values $g_A = 1.26$ and $g_A = 1.29$. The renormalized $^1S_0$ and coupled $^3S_1$, E_1 and $^3D_1$ waves were already shown in Ref. [2]. The deuteron electromagnetic form factors in the IA using our renormalized wave functions are displayed in Fig. 1, which within uncertainties are reproduced rather well.

[2]This potential depends on the coupling constants $f_{\pi NN}$ and $f_{\pi N\Delta}$. We can use the relation $f_{\pi NN} = g_A m_\pi/(2f_\pi)$ and the $SU(N_c)$ relation [3] $f_{\pi N\Delta}/f_{\pi NN} = 3\sqrt{(N_c-1)(N_c+5)}/(\sqrt{2}(N_c+2))$ such that the only *free* parameter is actually g_A having an admissible value in between 1.26 and 1.29.

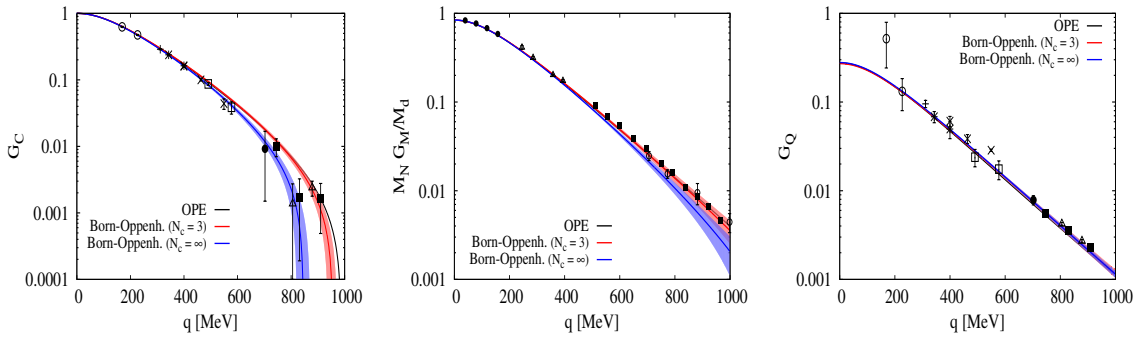

Figure 1: Deuteron charge G_C (left), magnetic G_M (middle) and quadrupole G_Q (right) form factors in the IA. The dependence with g_A is shown by light bands.

.

3 Three-body force

The extension to the three nucleon force (3NF) follows from the generalization of Eq. (2) for the 3N case, at 2nd order perturbation theory, being,

$$V_{3N} = \langle NNN|V_{OPE}|NNN\rangle + \sum_{NNN\neq HH'H''} \frac{|\langle NNN|V_{OPE}|HH'H''\rangle|^2}{E_{NNN} - E_{HH'H''}} + \mathcal{O}(V^3)\,, \tag{3}$$

where H, H' and H'' represent intermediate excited states and V_{OPE} is the sum of pairwise interactions between nucleons with the exchange of a pion, *i.e.*, $V_{OPE}(\mathbf{r}_1, \mathbf{r}_2, \mathbf{r}_3) = V_{OPE}(\mathbf{r}_{12}) + V_{OPE}(\mathbf{r}_{13}) + V_{OPE}(\mathbf{r}_{23})$ and $\mathbf{r}_{ij} = \mathbf{r}_i - \mathbf{r}_j$. Evaluating the matrix elements we obtain,

$$V_{3N} = \sum_{i\neq j} V^{1\pi}_{NN,NN}(\mathbf{r}_{ij}) + \frac{1}{M_N - M_\Delta} \sum_{i\neq j} |V^{1\pi}_{NN,N\Delta}(\mathbf{r}_{ij})|^2 + V^{FM}_{ijk}\,, \tag{4}$$

where V^{FM}_{ijk} is the old Fujita-Miyazawa 3NF [9]. So, in the BO the 3NF decomposes into a sum of One-Pion-Exchange Two-Nucleon (1PE-2N) pair interaction, a Two-Pion-Exchange Two-Nucleon (2PE-2N) with intermediate Δ pair interaction and a genuine Two-Pion-Exchange Three-Nucleon (2PE-3N) interaction. The emergence of short distance vdW singularities in given channels is evident. Unfortunately the renormalization of singular three-body problems, even within this simplified BO approach, has not yet been achieved. We note that similar interactions have proven to be essential, after introducing cut-offs, which modify the original interaction below 2fm, to describe the binding energies of light nuclei $A \leqslant 8$ [10]. This suggests that the BO approximation may be a workable scheme for multi-nucleon forces.

4 Conclusions

We have seen how the NN interaction can be faithfully represented as a vdW force that emerges as in atomic physics where one usually uses the Born-Oppenheimer approximation. We have calculated the two- and three-body force at second order in perturbation theory although higher order may in principle be included. The two nucleon potential reproduces exactly the Skyrme model result within the same approximation and its short distances behavior is identical to ChTPE at NLO-Δ. We have shown results for the deuteron properties and EM form factors having a very good agreement with experimental data. In the 3N sector, the BO potential contains the old Fujita-Miyazawa force as well as a residual 1PE-2N and a 2PE-2N with Δ.

Acknowledgments

ACC thanks Ch. Weiss and R. Schiavilla for discussions. Work supported by the Spanish DGI and FEDER funds with grant FIS2008-01143/FIS, Junta de Andalucía grant FQM225-05. Authored by a Jefferson Science Associate, LLC under U.S. DOE Contract No. DE-AC05-06OR23177.

Bibliography

[1] G. Feinberg, J. Sucher and C. K. Au, Phys. Rept. **180**, 83 (1989).

[2] E. Ruiz Arriola and A. Calle Cordon, arXiv:0910.1333 [hep-ph].

[3] G. Karl and J. E. Paton, Phys. Rev. D **30**, 238 (1984).

[4] N. R. Walet, R. D. Amado and A. Hosaka, Phys. Rev. Lett. **68**, 3849 (1992).

[5] N. R. Walet and R. D. Amado, Phys. Rev. C **47**, 498 (1993) [arXiv:nucl-th/9210015].

[6] N. Kaiser, S. Gerstendorfer and W. Weise, Nucl. Phys. A **637** (1998) 395 [arXiv:nucl-th/9802071].

[7] H. Krebs, E. Epelbaum and U. G. Meissner, Eur. Phys. J. A **32**, 127 (2007) [arXiv:nucl-th/0703087].

[8] M. Pavon Valderrama and E. R. Arriola, Phys. Rev. C **74**, 054001 (2006) [arXiv:nucl-th/0506047].

[9] J. Fujita and H. Miyazawa, Prog. Theor. Phys. **17**, 360 (1957).

[10] S. C. Pieper, V. R. Pandharipande, R. B. Wiringa and J. Carlson, Phys. Rev. C **64** (2001) 014001 [arXiv:nucl-th/0102004].

The $pp \to p\Lambda K^+$ and $pp \to p\Sigma^0 K^+$ Reactions in the Chiral Unitary Approach

Hua-Xing Chen[1,a,b], Ju-Jun Xie[a,c], and E .Oset[a]
[a]*Departamento de Física Teórica and IFIC, Centro Mixto Universidad de Valencia-CSIC, Institutos de Investigación de Paterna, Aptdo. 22085, 46071 Valencia, Spain*
[b]*School of Physics and Nuclear Energy Engineering, Beihang University, Beijing 100191, China*
[c]*Department of Physics, Zhengzhou University, Zhengzhou, Henan 450001, China*

We study the $pp \to p\Lambda K^+$ and $pp \to p\Sigma^0 K^+$ reactions near threshold by using a chiral unitary approach. We consider the single-pion and single-kaon exchange as well as the final state interactions of nucleon-hyperon, K-hyperon and K-nucleon systems. Our results on the total cross section of the $pp \to p\Lambda K^+$ reaction is consistent with the experimental data, and the experimental observed strong suppression of Σ^0 production compared to Λ production at the same excess energy can also be explained in our model.

1 Introduction

By using the chiral unitary approach, we study the $pp \to p\Lambda K^+$ and $pp \to p\Sigma^0 K^+$ reactions near threshold considering pion and kaon exchanges [1], where the $p\Lambda$ final state interaction (FSI) is very important [2,3]. The $\pi N \to K\Lambda$ amplitude also appears in this scheme, and the unitarization of this amplitude produces naturally the $N^*(1535)$ resonance [4], such that we can make a quantitative statement on its relevance in the $pp \to p\Lambda K^+$ reaction. We find that the $p\Lambda$ interaction close to threshold is very strong [5], and the FSI due to this source is unavoidable in an accurate calculation and we also take it into account.

We use a dynamical model similar to the one in Ref. [3] but we allow all pairs in the final state to undergo FSI, as a consequence of which we obtain a contribution from the $N^*(1535)$ using chiral unitary amplitudes. Our approach also differs from the other approaches on how the FSI is implemented, and for this we follow the steps of Ref. [6]. Furthermore, the experimental total cross section for the $pp \to p\Sigma^0 K^+$ reaction is strongly suppressed compared to that of the $pp \to p\Lambda K^+$ reaction at the same excess energy. This was explained by a destructive interference between π and K exchange in the reaction $pp \to p\Sigma^0 K^+$ [3].

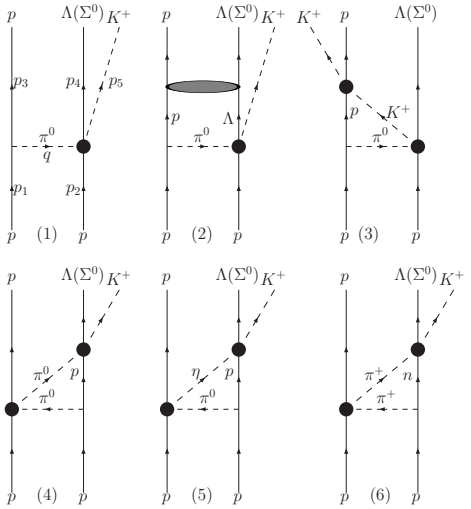

Figure 1: The π exchange mechanism of the $pp \to p\Lambda(\Sigma^0)K^+$ reactions including the final state interactions.

2 Formalism and ingredients

At the reaction threshold, the processes involving the exchange of π and K mesons are the dominant contributions, as in Ref. [3] and other works of the Juelich group. Accordingly we show the dominant diagrams exchanging π mesons in Fig. 1, where the definitions of the kinematics (p_1, p_2, p_3, p_4, p_5, and q) are shown in the first diagram. Those exchanging K mesons can be similarly obtained. First we write out the amplitudes for elementary production processes. For the first diagram of Fig. 1, we have

$$\mathcal{A}^1_\pi = -F_{\pi NN}(q^2) f_{\pi^0 pp} \sigma_z(1) q_z \frac{i}{q^2 - m_\pi^2} T_{\pi^0 p \to K^+ \Lambda}, \quad (1)$$

where $F_{\pi NN}(q^2)$ is the form factor containing a cutoff parameter Λ_π:

$$F_{\pi NN}(q^2) = \frac{\Lambda_\pi^2 - m_\pi^2}{\Lambda_\pi^2 - q^2}, \quad (2)$$

We can similarly obtain the "elementary production amplitudes" for the other diagrams, and the total production amplitude $\mathcal{M}$ can be written into two parts:

$$\mathcal{M} = \mathcal{M}_\pi + \mathcal{M}_K, \quad (3)$$

where $\mathcal{M}_\pi$ is for those diagrams involving π exchange ($\mathcal{M}_K$ for K exchange):

$$\mathcal{M}_\pi = \mathcal{A}^1_\pi + \sum_{i=2}^{6} \mathcal{A}^i_\pi G^i_\pi T^i_\pi, \quad (4)$$

[1] hxchen@ific.uv.es

where $\mathcal{A}^i_{\pi/K}$ are the elementary production processes which can be obtained similarly to Eq. (1) and G^i_π the loop functions of one meson and a baryon propagators, or two baryon propagators. Together with the final state interactions for meson-baryon cases (such as $T^3_\pi = T_{K^+p\to K^+p}$, etc.) and for baryon-baryon cases ($T^2_\pi = T_{\Lambda p\to\Lambda p}$, etc.), we can obtain the full total production amplitude $\mathcal{M}$.

The meson-baryon G-functions and T-matrices have been calculated in Refs. [7], and we only need to calculate the baryon-baryon ones which are done using the experimental data [8]. We also consider the transition between $pp \to p\Lambda K^+$ and $pp \to p\Sigma^0 K^+$, which is discussed in Ref. [1] in detail.

3 Numerical results and Discussion

The total cross section versus the excess energy (ε) for the $pp \to p\Lambda K^+$ and $pp \to p\Sigma^0 K^+$ reactions are calculated by using a Monte Carlo multi-particle phase space integration program. The results for ε from 0 MeV to 14 MeV is shown in Fig. 2 for the $pp \to p\Lambda K^+$ reaction with the cutoff $\Lambda_\pi = 1300$ MeV, together with the experimental data [8] for comparison. The solid and dashed lines show the results from our model with and without

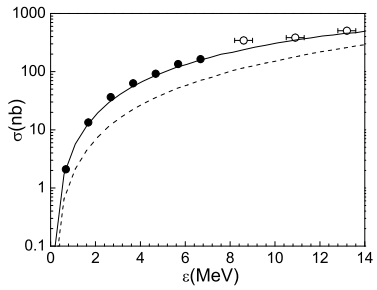

Figure 2: Total cross section vs excess energy ε for the $pp \to p\Lambda K^+$ reaction compared with experimental data from Refs. [8] (filled and open circles).

including the $p\Lambda$ FSI, respectively.

We can see that we can reproduce the experimental data quite well for the excess energy ε lower than 14 MeV. The dashed line is about two and a half times smaller than the experimental data at threshold but less than a factor of two smaller than experimental data at $\epsilon \sim 14$ MeV. This indicates that the $p\Lambda$ FSI is very important in the $pp \to p\Lambda K^+$ reaction close to threshold. This energy dependence of the FSI is what allows the determination of the ΛN interaction in other approaches which do not try to get absolute cross sections [9].

Acknowledgments

This work is partly supported by DGICYT contracts No. FIS2006-03438, FPA2007-62777, the Generalitat Valenciana in the program PROMETEO and the EU Integrated Infrastructure Initiative Hadron Physics Project under Grant Agreement No. 227431. Ju-Jun Xie acknowledges Ministerio de Educación Grant SAB2009-0116.

Bibliography

[1] J. J. Xie, H. X. Chen and E. Oset, arXiv:1105.4791 [nucl-th].

[2] R. Siebert *et al.*, Nucl. Phys. A **567**, 819 (1994); A. Sibirtsev, J. Haidenbauer, H. W. Hammer and S. Krewald, Eur. Phys. J. A **27**, 269 (2006); F. Hinterberger, A. Sibirtsev, Eur. Phys. J. A **21**, 313-321 (2004); A. Gasparyan, J. Haidenbauer, C. Hanhart, J. Speth, Phys. Rev. C **69**, 034006 (2004); T. Rozek *et al.*, Phys. Lett. B **643**, 251 (2006); A. Sibirtsev, J. Haidenbauer, H. W. Hammer and U. G. Meissner, Eur. Phys. J. A **29**, 363 (2006); B. C. Liu, B. S. Zou, Phys. Rev. Lett. **96**, 042002 (2006); K. Tsushima, A. Sibirtsev, A. W. Thomas, Phys. Lett. B **390**, 29 (1997); A. Sibirtsev, J. Haidenbauer, U. -G. Meissner, Phys. Rev. Lett. **98**, 039101 (2007); S. Abdel-Samad *et al.* [COSY-TOF Collaboration], Phys. Lett. B **632**, 27 (2006); B. -S. Zou, J. -J. Xie, Int. J. Mod. Phys. E **17**, 1753-1764 (2008); H. X. Yang *et al.* [BES COllaboration], Int. J. Mod. Phys. A **20**, 1985 (2005); R. Shyam, Phys. Rev. C **73**, 035211 (2006).

[3] A. Gasparian, J. Haidenbauer, C. Hanhart, L. Kondratyuk, J. Speth, Phys. Lett. B **480**, 273 (2000).

[4] N. Kaiser, P. B. Siegel, W. Weise, Phys. Lett. B **362**, 23 (1995); N. Kaiser, T. Waas, W. Weise, Nucl. Phys. A **612**, 297 (1997); J. Nieves, E. Ruiz Arriola, Phys. Rev. D **64**, 116008 (2001).

[5] C. B. Dover, A. Gal, Prog. Part. Nucl. Phys. **12**, 171 (1985); P. M. M. Maessen, T. A. Rijken, J. J. de Swart, Phys. Rev. C **40**, 2226 (1989).

[6] J. Yamagata-Sekihara, J. Nieves, E. Oset, Phys. Rev. D **83**, 014003 (2011).

[7] E. Oset and A. Ramos, Nucl. Phys. A **635**, 99 (1998); E. Oset, A. Ramos, and C. Bennhold, Phys. Lett. B **527**, 99 (2002); T. Inoue, E. Oset, M. J. Vicente Vacas, Phys. Rev. C **65**, 035204 (2002).

[8] J. T. Balewski et al., Phys. Lett. B **4**20, 211 (1998); S. Sewerin et al., Phys. Rev. Lett. **8**3, 682 (1999).

[9] A. Budzanowski *et al.*, Phys. Lett. B **687**, 31 (2010); F. Hinterberger, S. N. Nedev and R. Siudak, Int. J. Mod. Phys. A **20** (2005) 291.

Measurement of $\pi^-\gamma \to \pi^-\pi^-\pi^+$ at Low Masses, and Comparison to ChPT Prediction, at COMPASS

Stefanie Grabmüller[1,a], Dmitry Ryabchikov[b], and Jan M. Friedrich[a]
on behalf of the COMPASS Collaboration
[a] *Technische Universität München, Physik-Department, 85748 Garching, GERMANY*
[b] *State Research Center of the Russian Federation, IHEP, 142281 Protvino, RUSSIA*

This paper presents an analysis of $\pi^-\mathrm{Pb} \to X^-\mathrm{Pb} \to \pi^-\pi^-\pi^+\mathrm{Pb}$ events at 190 GeV/c beam momentum and very low four-momentum transfer $t' < 0.001\,\mathrm{GeV}^2/c^2$. Coherent scattering off the nucleus as a whole dominates with contributions from Reggeon, Pomeron and photon exchange. The latter originates from Primakoff reactions and is identified by the sharp Coulomb peak of intensities at $t' \approx 0$. The partial-wave analysis of these data focusses on new techniques for the extraction of the Primakoff contribution at low masses. Its measured absolute cross-section at $\sqrt{s} < 5m_\pi$ is well in agreement with the prediction from chiral perturbation theory.

1 Meson Spectroscopy at Low Momentum Transfer

Dissociation of pions on nuclear or hydrogen targets provides clean access to the light meson spectrum. In case of heavy target nuclei and low momentum transfer, mesons can be produced by two interaction mechanisms: diffractive production by Reggeon t'-channel exchange and Primakoff (or Coulomb) production via the exchange of quasi-real photons. The latter has its dominant contribution at vanishing momentum transfer and introduces spin-projection $M = \pm 1$ to the produced system. At low masses, *i.e.*at the threshold of the investigated final state, the only involved hadrons are pions scattering with each other and the photon. Thus predictions from chiral perturbation theory (ChPT), which take into account coupling to a real photon simultaneously, are supposed to be applicable. At higher masses, resonances can be produced, so that the radiative coupling of the $a_2(1320)$, and potentially also of heavier mesons, can be investigated. Also the interference between the Coulomb and diffractive production of these resonances can be studied.

COMPASS is a multi-purpose fixed-target experiment at the CERN SPS, that investigates the structure and spectroscopy of hadrons. The two-stage high-precision spectrometer [1] can detect outgoing particles within a large range of scattering angles and particle momenta, and provides a uniform acceptance, especially for reactions featuring low to intermediate momentum transfer from the beam to the target. For a short run with a 190 GeV/c hadron

[1] stefanie.grabmueller@tum.de

beam (composed of 96.8 % π^-, 2.4 % K^- and 0.8 % $\overline{p}$) on thin lead disk targets in 2004, additional silicon micro-strip detectors were installed downstream of the target to resolve also smallest scattering angles. With this setup, about 4 million exclusive $\pi^-\pi^-\pi^+$ events have been collected with a dedicated multiplicity trigger for charged-particle final states. About 1 million of these feature very low momentum transfer $t' < 0.001\,\mathrm{GeV}^2/c^2$, with $t' = |t| - |t|_{\mathrm{min}}$ constituted of the squared four-momentum transfer t from the beam to the produced system, and $|t|_{\mathrm{min}}$ the minimum value of $|t|$ allowed by kinematics. In this region, referred to as "Primakoff t'", photon exchange appears to be relevant in the data.

Partial-wave analysis (PWA) strives for determining all resonances present in a given data set and their properties by fitting angular distributions and taking into account interference effects. The PWA presented here is based on the commonly-known isobar model, that was adapted to the specific needs of the analysis. According to this model, the produced resonances decay via intermediate two-particle decays into the particles observed in the spectrometer. For 3π events, a partial wave in the reflectivity basis is written as $J^{PC}M^{\epsilon}[isobar\ \pi]L$, defining the quantum numbers of the resonance, J^{PC}, spin projection M, reflectivity ϵ, the isobar, and the angular momentum L between the di-pion resonance and the unpaired pion. The PWA method and its basic assumptions are described in more detail in Ref. [2] and the references therein.

2 Diagrams from ChPT

In the Primakoff t' region, decay amplitudes with $M = 1$ can be attributed to Primakoff production, *i.e.*effectively $\pi^-\gamma \to X^- \to \pi^-\pi^-\pi^+$ scattering when observing $\pi^-\mathrm{Pb} \to X^-\mathrm{Pb} \to \pi^-\pi^-\pi^+\mathrm{Pb}$. In addition the low mass region, i.e. $m_{3\pi} < 0.72\,\mathrm{GeV}/c^2$, is governed by pion-scattering instead of resonance production so that ChPT calculations are applicable. The leading order processes in ChPT are calculated in [3] and depicted in Fig. 1, including also the lead nucleus which is not part of the calculation. As it has been shown in [4] that for low masses the next order in ChPT (i.e. loops) does not change the cross-section of $\pi\gamma$-

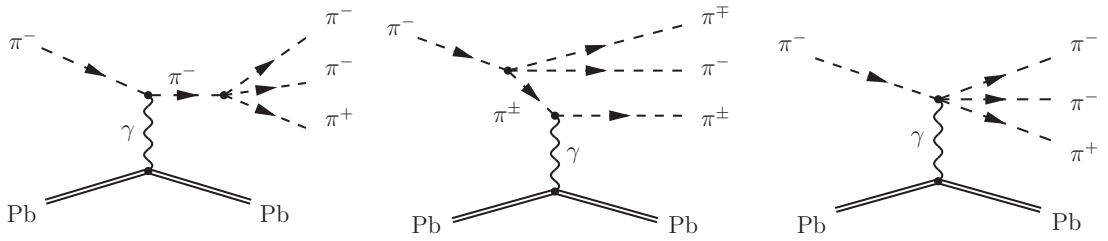

Figure 1: Leading order processes in ChPT [3] for the reaction $\pi^-\gamma \to \pi^-\pi^-\pi^+$, embedded in the Primakoff reaction contribution to $\pi^-\mathrm{Pb} \to \pi^-\pi^-\pi^+\mathrm{Pb}$.

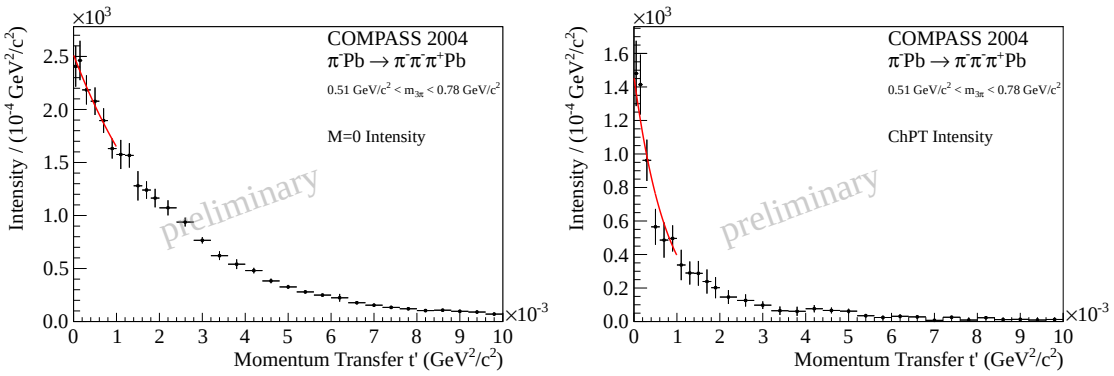

Figure 2: t' dependences of the $M = 0$ total intensity (left) and the intensity of the chiral amplitude (right) confirm the diffractive production of the $M = 0$ states as well as the Primakoff nature of the intensity picked up by the chiral amplitude.

scattering, σ_γ, appreciably, it is sufficient to introduce the leading order calculations for σ_γ into the PWA, multiplied with the quasi-real photon density provided by a nucleus of charge Z as given by Weizsäcker and Williams [5]. The experimentally observed cross-section is given by

$$\frac{d\sigma_{\mathrm{Pb}}}{ds\,dt'\,d\Phi_n} = \frac{\alpha \cdot Z^2}{\pi(s - m_\pi^2)} \cdot \frac{t' \cdot F_{\mathrm{eff}}^2(t')}{(t' + t_{\mathrm{min}})^2} \cdot \frac{d\sigma_\gamma}{d\Phi_n} \tag{1}$$

with $d\Phi_n$ the phase-space element for the final state system X^- and $F_{\mathrm{eff}}^2(t')$ the effective lead form factor, and is introduced in its fully differential form as an additional decay amplitude with $M = 1$ to the PWA fit. This special partial wave, called "chiral amplitude", is mathematically not orthogonal to the $M = 1$ waves of the isobar model, so that these have in fact to be replaced by the chiral amplitude in the low mass region. The resulting fit quality is compatible with the quality of a previous fit that used up to 6 waves with the $(\pi\pi)_s$ wave or the $\rho(770)$ as isobars, but the chiral-amplitude fit works with much less fitting parameters. At masses above $m_{3\pi} > 0.72\,\mathrm{GeV}/c^2$ isobaric decays that compete with the chiral amplitude have to be taken into account again.

In order to get a confirmation of the production mechanism that is attributed to the chiral amplitude, a dedicated set of PWA fits was carried out in several bins of t' in the low-mass region without taking into account any t' dependence of the decay amplitudes. The resulting intensity spectra of the total intensity of the chiral amplitude and the total $M = 0$ intensity in this mass region, dependent on t', are shown in Fig. 2. Both spectra are fitted by an exponential $\propto \exp(-bt')$ for $t' < 0.001\,\mathrm{GeV}^2/c^2$. The $M = 0$ intensity features a slope $b \approx 400\,\mathrm{GeV}^{-2}/c^{-2}$ which is compatible with diffractive production off lead nuclei. The ChPT intensity is much steeper with $b \approx 1600\,\mathrm{GeV}^{-2}/c^{-2}$ which is consistent with the expected effective slope of Primakoff production if the t' dependence from Eq. 1 is smeared with the experimental resolution.

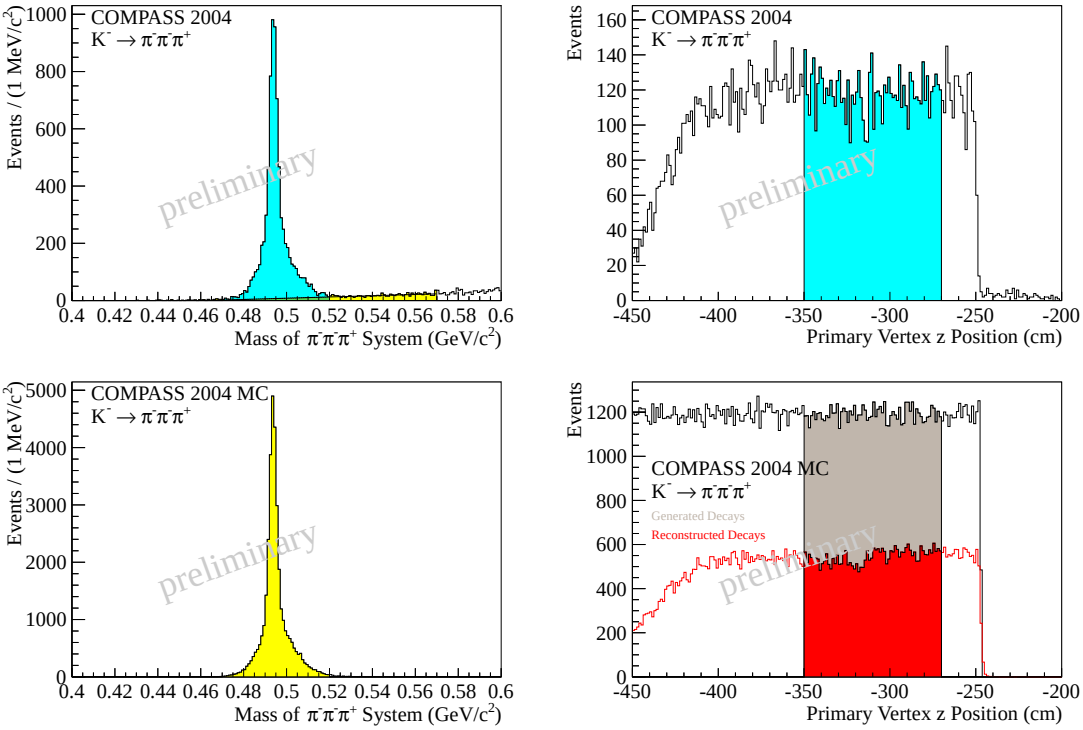

Figure 3: Luminosity determination from the free decay of beam kaons: Reconstructed invariant mass spectra (left) and decay vertex positions (right) for both COMPASS data (top row) and simulated kaon decays in the COMPASS target region (bottom row).

3 Absolute Cross-Section and ChPT Prediction

For the comparison with the ChPT prediction from [3], PWA fits for $0.44 < m_{3\pi} < 0.72\,\mathrm{GeV}/c^2$ were performed in $40\,\mathrm{MeV}/c^2$ mass bins for $t' < 0.001\,\mathrm{GeV}^2/c^2$, that use only the chiral amplitude associated with Primakoff production as $M = 1$ contribution.

The total intensity of the chiral amplitude, fitted from the experimental data and corrected for acceptance effects, is converted into its absolute cross-section via the well-known thickness of the lead target and the incoming beam flux. The absolute beam intensity was not monitored reliably, but the effective beam flux can be obtained with good precision from the observed $K^- \to \pi^-\pi^-\pi^+$ decays in the COMPASS target region, which originate from the kaon component present in the negative hadron beam. Thus the normalization is available from the same data-taking set (*i.e.*in the same final state, but with broader cut on the decay vertex position) featuring the same systematics concerning the relevant trigger and detector efficiencies. Fig. 3 presents the invariant 3π mass spectrum, obtained with broad vertex cut, showing the clean kaon signal (top left), from which the observed number of kaons is obtained after subtraction of the small background that is estimated

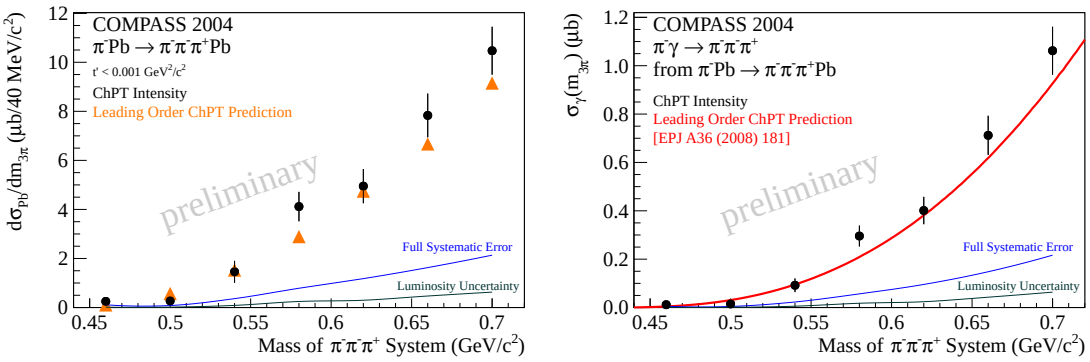

Figure 4: Measured cross-section of $\pi^-\text{Pb} \to \pi^-\pi^-\pi^+\text{Pb}$ induced by photon exchange (left) and absolute cross-section of $\pi^-\gamma \to \pi^-\pi^-\pi^+$ derived from it (right), both compared to the respective illustration of the ChPT prediction.

by a linear fit. The corresponding decay vertex distribution (Fig. 3 top right) shows that these decay vertices are reconstructed in free space, at the downstream end of the spectrum sharply limited by the position of the respective charged-particle multiplicity trigger, and upstream limited by the positions of the beam telescope detectors defining the vertex reconstruction efficiency. The background from pion interactions in the lead target is obtained from the vertex distribution in the neighboring mass region, scaled accordingly and subtracted statistically. The selected region of reconstructed vertex positions, that proceeds to the mass spectrum discussed before, is selected as indicated to assure uniform reconstruction efficiency inside the considered region. These two distributions were also confirmed by a dedicated full Monte Carlo (MC) simulation of kaon decays in the relevant region of the COMPASS spectrometer. Fig. 3 (bottom left) shows the mass distribution of the reconstructed MC kaon decays. The contribution from pion interactions present in the real data as smoothly rising background is now completely absent. The shape of the reconstructed kaon mass is precisely modeled. The broad part at the base of the kaon peak is traced back to kaons decaying upstream of the lead target. In that case all three decay pions undergo multiple scattering in the lead, which leads to the observed distortion. Fig. 3 (bottom right) presents the distributions for both simulated and reconstructed kaon decay vertices, confirming the indicated cuts on the reconstructed vertices in real data to be reasonably chosen.

The black points in Fig. 4 (left) show the cross-section of the Primakoff contribution to $\pi^-\text{Pb} \to \pi^-\pi^-\pi^+\text{Pb}$, *i.e.*the total intensity of the chiral amplitude in the respective mass bins converted by the kaon normalization, with their statistical uncertainties from the PWA. The triangles picture the ChPT prediction as given by Eq. 1 which is integrated in the same mass bins as used in the analysis of the data. The full systematic uncertainties include the uncertainty of the luminosity determination from the kaon decays, results from different fitting models, and estimations for the radiative corrections to be applied [6], so that the

total uncertainties sum up to about 20%.

From this measured cross-section the quasi-real photon density is divided out to get the cross-section of $\pi^-\gamma \to \pi^-\pi^-\pi^+$ presented in Fig. 4 (right). The ChPT calculation from [3] is depicted here as a continuous line, while the data points are still placed at the center of the respective bin in which they have been obtained, showing good agreement with the theoretical prediction.

4 Conclusion and Outlook

The result presented in this paper confirms the ChPT leading order calculation for $\pi^-\gamma \to \pi^-\pi^-\pi^+$ with an experimental uncertainty of about 20%, both in its integrated strength and its shape in the 5 dimensional three-body phase space for $m_{3\pi} < 0.72\,\mathrm{GeV}/c^2$, for the first time.

For the adjacent region of higher masses, both loop effects and explicit ρ contributions have additionally to be taken into account for the chiral amplitude. The need to include isobaric decays with $M = 1$ becomes obvious for masses approaching the $a_2(1320)$ resonances at latest. These extensions of the presented analysis are subject of work currently being carried out.

Acknowledgments

This work is supported by the German BMBF, the Maier-Leibnitz-Labor München, the DFG Cluster of Excellence Exc153, and CERN-RFBR grant 08-02-91009.

Bibliography

[1] COMPASS Collaboration, P. Abbon *et al.*, Nucl. Instrum. Meth. **A577**, 455 (2007), arXiv:0703049 [hep-ex].

[2] COMPASS Collaboration, M. G. Alekseev *et al.*, *Phys. Rev. Lett.* **104**, 241803 (2010), arXiv:0910.5842 [hep-ex].

[3] N. Kaiser, J. Friedrich, Eur. Phys. J. **A36**, 181 (2008), arXiv:0803.0995 [nucl-th].

[4] N. Kaiser, Nucl. Phys. **A848**, 198 (2010), arXiv:1007.5277 [hep-ph].

[5] I. Y. Pomeranchuk and I. M. Shmushkevich, Nucl. Phys. **23**, 452 (1961).

[6] N. Kaiser, `nkaiser@ph.tum.de`, *private communication* (2011).

Future Experiments

Future Experiments

Conveners

Andrey	Golutvin	Imperial College London (*Chair*)
Ulrich	Wiedner	Ruhr-Universität Bochum
Bernhard	Ketzer	TU München

Session Chair

Bernhard Ketzer	TU München

Contents

Future experiments

Peter Križan[1]
Faculty of Mathematics and Physics
University of Ljubljana
Ljubljana, Slovenia

The contribution discusses future experiments in hadron spectroscopy. It presents the physics motivation and the tools, i.e. the accelerators and the detectors. A review of the status of the relevant projects, Belle-II/SuperKEKB at KEK, SuperB in Italy, PANDA at FAIR, and CLAS12 and GlueX at JLAB, is also given.

1 Introduction

A substantial increase in the size of data samples available for searches of exotic hadronic states is expected in the next ten years. In what follows we shall discuss these future experiments in hadron spectroscopy. We will present the physics motivation and the tools, i.e. the accelerators and the detectors, and we will review the status of the relevant projects, Belle-II and SuperKEKB at KEK, SuperB in Italy, PANDA at FAIR, and CLAS12 and GlueX at JLAB.

2 Super B factories: Belle-II/SuperKEKB and SuperB

The two B factories, PEP-II with BaBar and KEKB with Belle, have been a real success story. They were built with the primary goal of measuring CP violation in the B system. From the discovery of large CP violation in 2001, the B factory results evolved into a precision measurement of the CP violation parameter $\sin 2\phi_1$ [1–3]. The constraints from measurements of angles and sides of the unitarity triangle show a remarkable agreement [4], which significantly contributed to the 2008 Nobel prize awarded to Kobayashi and Maskawa. The two B factories also studied numerous new phenomena, and, last but not least, observed a long list of new hadrons, some of which do not seem to fit into the standard meson and baryon schemes. All this was only possible because of the fantastic performance of the accelerators, much beyond their design values. In the KEKB case, the peak luminosity reached a world record value of $2.1 \times 10^{34}\mathrm{cm}^{-2}\mathrm{s}^{-1}$, exceeding the design value by a factor

[1]peter.krizan@ijs.si

of more than two. The two collaborations have accumulated data samples corresponding to integrated luminosities of 0.557 ab^{-1} (BaBar) and 1.041 ab^{-1} (Belle).

While B factories were built to check whether the SM with the CKM matrix is correct, the next generation of B factories (so called Super B factories) will search for departures from the Standard model. For this task, a $\approx$50 times larger data sample is needed [5], corresponding to an integrated luminosity of 50-75 ab^{-1}. Two recent publications summarize the physics potential of a super B factory, one prepared by Belle-II authors and guests [6], and the other by SuperB collaborators and guests [7]. To summarize, there is a good chance to see new phenomena, such as CP violation in B decays from new physics sources, or lepton flavor violation in τ decays. Needless to say that with such a large data sample there are many more topics to explore, including searches for new and exotic hadrons, and investigation of their properties.

Accelerators

To arrive at a $\approx$50 times larger data sample, a substantial upgrade of the B factory accelerator complex is required, leading to a 40 times larger peak luminosity. There are two super B factory projects under way. The first one, Belle II at SuperKEKB, foresees a substantial redesign of elements of the existing KEKB accelerator complex while retaining the same tunnel and related infrastructure. To increase the luminosity by a factor of 40, the plan is to modestly increase the current (by a factor of 2) with respect to the KEKB values, and dramatically shrink the beam size at the collision point, while the beam beam parameter is kept at the KEKB value (Table 1). In this 'nano-beam' scheme which was invented by Pantaleo Raimondi for the Italian SuperB project [8], the beams collide at a rather large angle of 83 mrad (compared to 22 mrad in KEKB). In addition, a lower beam asymmetry of 7 GeV and 4 GeV instead of 8 GeV and 3.5 GeV is needed to reduce the beam losses due to Touschek scattering in the lower energy beam. The modifications of the KEKB complex include: improvements in electron injection, a new positron target and damping ring, redesign of the lattices of the low energy (LER) and high energy (HER) rings, replacing short dipoles with longer ones (LER), installing TiN-coated beam pipe with ante-chambers, modifications of the RF system, and a completely redesigned interaction region [9].

Another approach to the design of a super B factory will be exploited in the Italian SuperB project [10]. Here it is foreseen that a new tunnel will be built (Fig. 1) at the campus of the Tor Vergata University, a few kilometers northwest of Frascati. Parts of the beam elements of PEP-II will be reused in the accelerator construction. In addition to the nano-beam scheme (Table 1), an essential feature of the SuperB accelerator is the crab waist collision of two beams in which special sextupoles will be used close to the interaction region to maximize the overlap of the two beams. This scheme was successfully tested at the DAΦNE ring by Pantaleo Raimondi and his team [11]. The SuperB accelerator is designed in such a way that it can be modified to run at the $\psi(3770)$ resonance close to charm threshold, where pairs of D^0 mesons are produced in a coherent $L = 1$ state [7].

	SuperKEKB		SuperB		
	LER (e^+)	HER (e^-)	LER (e^-)	HER (e^+)	
Energy	4.0	7.0	4.18	6.7	GeV
Half crossing angle	41.5		33		mrad
Horizontal emittance	3.2	4.3	1.82	1.97	nm
Emittance ratio	0.27	0.25	0.34	0.25	%
Beta functions at IP (x/y)	32 / 0.27	25 / 0.31	32 / 0.205	26 / 0.253	mm
Beam currents	3.6	2.6	1.82	1.97	A
Beam-beam parameter	0.0886	0.0830	0.0970	0.0971	
Luminosity	8×10^{35}		1×10^{36}		$\mathrm{cm}^{-2}\mathrm{s}^{-1}$

Table 1: SuperKEKB and SuperB: parameters of the low energy (LER) and high energy (HER) accelerator rings.

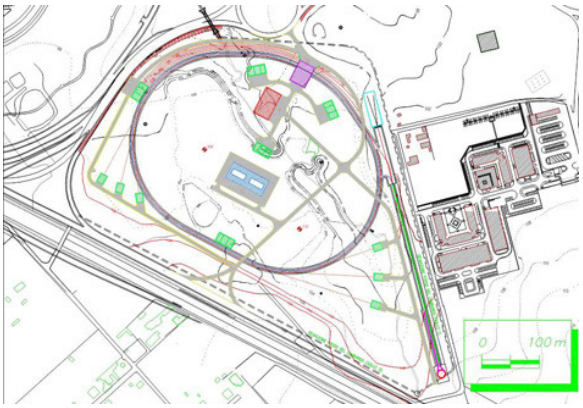

Figure 1: The new SuperB accelerator complex at Tor Vergata University site.

Detectors

The planned substantial increase in luminosity requires a careful design of the detectors. To maintain the excellent performance of the spectrometers, the critical issues will be to mitigate the effects of higher backgrounds (by a factor of 10 to 20), leading to an increase in occupancy and radiation damage, as well as fake hits and pile-up noise in the electromagnetic calorimeter. Higher event rates will require substantial modifications in the trigger scheme, DAQ and computing relative to the current experiments. In addition, improved hadron identification is needed, and similarly good (or better) hermeticity is required [9].

For the Belle-II detector (Fig. 2), the following solutions will be adopted [9]. The inner layers of the vertex detector will be replaced with a DEPFET pixel detector [12], the inner part of the main tracker (CDC, central drift chamber) will be replaced with a silicon strip detector, a better particle identification device will be used, the CsI(Tl) crystals of the end-

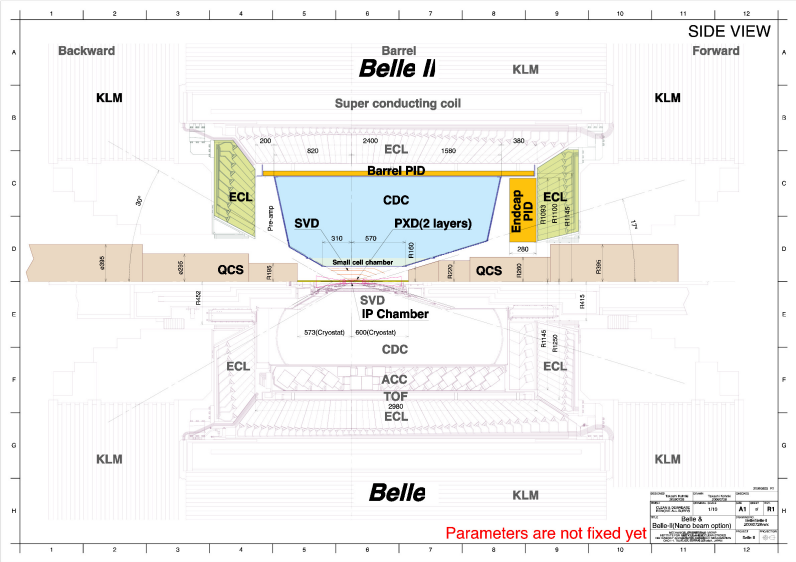

Figure 2: Upgraded Belle II spectrometer (top half) as compared to the present Belle detector (bottom half).

cap calorimeter will be replaced by pure CsI, the resistive plate chambers of the end-cap muon and K_L^0 detection system will be replaced by scintillator strips read out by SiPMs, and all components will be read-out by fast readout electronics and an improved computing system.

The hadron particle identification will be provided by a time-of-propagation (TOP) counter in the barrel part, and a RICH with a focusing aerogel radiator in the forward region of the spectrometer. The TOP counter [13] is a kind of DIRC counter [14] with quartz radiator bars in which the two dimensional information from a Cherenkov ring image is represented by the time of arrival and impact position of the Cherenkov photons at the photon detector. At a given momentum, the slower kaons (dotted in Fig. 3) emit Cherenkov photons at a smaller angle than pions; as a result, also their Cherenkov photons propagate longer along the quartz bar. Compared to the DIRC, the TOP counter construction is more compact, but requires photon detectors with single photon time resolution below 100 ps [13]. For the end-cap region a proximity focusing RICH with aerogel as radiator is being designed. The key issue in the performance of this type of RICH counter is to improve the Cherenkov angle resolution per track by increasing the number of detected photons. With a thicker radiator, the number of detected photons increases, but in a proximity focusing RICH the single photon resolution degrades because of the emission point uncertainty. However, this limitation can be overcome in a proximity focusing RICH with a non-homogeneous radiator [15], where one may achieve overlapping of the corresponding Cherenkov rings on the photon detector (Fig. 3). Both detectors are expected to considerably improve the

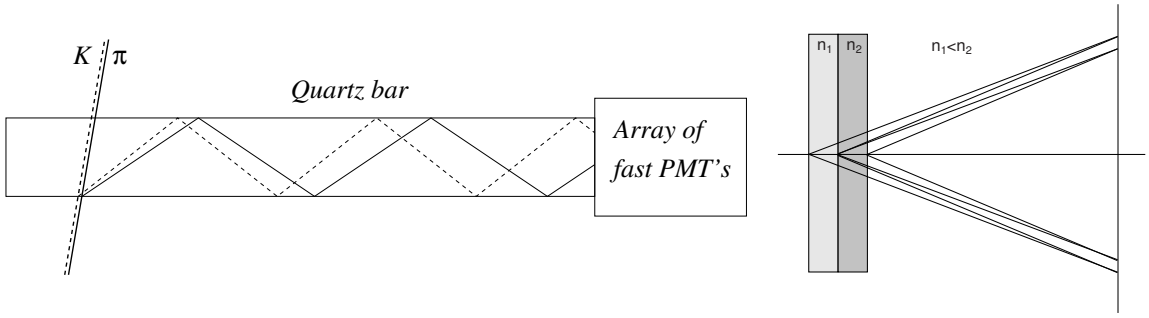

Figure 3: Belle-II PID systems: principle of operation of the TOP counter (left) and of the proximity focusing RICH with a nonhomogeneous aerogel radiator in the focusing configuration (right).

particle identification efficiency if compared to Belle; the end-cap RICH will provide a 4 σ π/K separation up to kinematic limits, and the barrel TOP counter will identify kaons with an efficiency exceeding 90% at a few percent pion fake probability.

The SuperB detector [16] will reuse several components of the BaBar spectrometer. In the baseline version two major changes are foreseen, replacing CsI(Tl) crystals in the forward calorimeter with LSO crystals, and a modification of the particle identification device, the DIRC counter. Options include a pixel detector layer, a RICH as the forward PID device and a veto electromagnetic calorimeter in the backward region to improve the hermeticity of the spectrometer.

In the new DIRC counter, the large stand-off box with single channel PMTs will be replaced by a compact focusing quartz block and multi-anode PMTs as photon sensors. By measuring the time of arrival of Cherenkov photons, the fast photon detectors will allow to correct for the chromatic error, i.e., variation of Cherenkov angle with wavelength [17]. The focusing DIRC counter is expected to extend the π/K separation range by improving the angular resolution by about 10%. At the same time, the order-of-magnitude lower mass of the expansion volume will considerably reduce the level of beam induced backgrounds.

Status of the projects

The SuperKEKB/Belle-II project has received initial construction funding in 2010 for the positron damping ring, and with the Japanese 'Very Advanced Research Support Program' a sizable fraction of funds for the main ring upgrade (exceeding 100 MUSD) for the period 2010-2012. KEK also managed to secure additional funds to complete the construction as scheduled, i.e., start the SuperKEKB commissioning in the autumn of 2014, and start data taking in 2015. It is expected that by 2017 the first 5 ab^{-1} of data will be collected, and the full data sample of 50 ab^{-1} will be reached in 2020/2021.

The SuperB project is the first in the list of 'flagship projects' of the new Italian national research plan over the next few years. The Italian government has delivered an initial

funding for 2010 as a part of a multi-annual funding program. The site has been chosen at the Tor Vergata University campus, a few kilometers northwest of the Frascati lab. The aim of the project is to accumulate 75 ab^{-1} on a time scale similar to SuperKEKB/Belle-II.

3 PANDA at FAIR

At the High-Energy Storage Ring (HESR) of the FAIR facility at GSI, the PANDA experiment is being prepared with the aim to study meson spectroscopy (excited D mesons, charmonia and charmonium like states, search for hybrids, tetraquarks, molecular states), charmed and multi-strange baryon spectroscopy, electromagnetic processes ($p\overline{p} \to e^+e^-$, $p\overline{p} \to \gamma\gamma$, Drell-Yan processes), properties of single and double hypernuclei, and properties of hadrons in nuclear matter [18]. Anti-protons as a probe are interesting because their interactions are rich with gluons, and the system allows to reach all states with fermion-antifermion quantum numbers, including states with high orbital angular momenta. Another feature of the experiment is a very high mass resolution in formation reactions.

The detector (Fig. 4) is required to cover the full solid angle, operate at high rates ($2 \cdot 10^7$ annihilations/s), allow for good particle identification ($\gamma, e, \mu, \pi, K, p$) and momentum resolution ($\approx 1\%$), vertexing (reconstruction of D, K^0_S, Λ), have an efficient software trigger (for e, μ, K, D, Λ) and stand a raw data rate exceeding 200 GB/s.

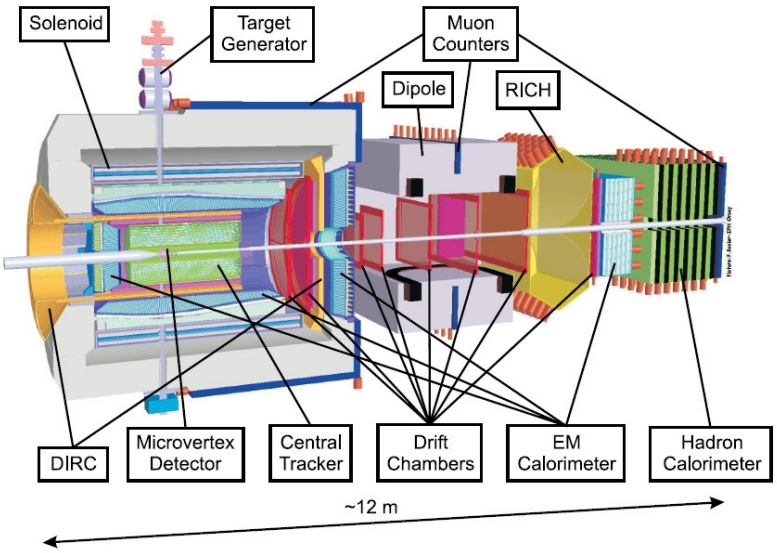

Figure 4: The PANDA spectrometer.

Antiprotons will impinge onto an internal target, which can be either in form of pellets (frozen droplets) or as a cluster jet (nanoparticles). The vertex detector will be a combination of a pixel detector with 10 million channels and a micro-strip detector with 70,000 strips.

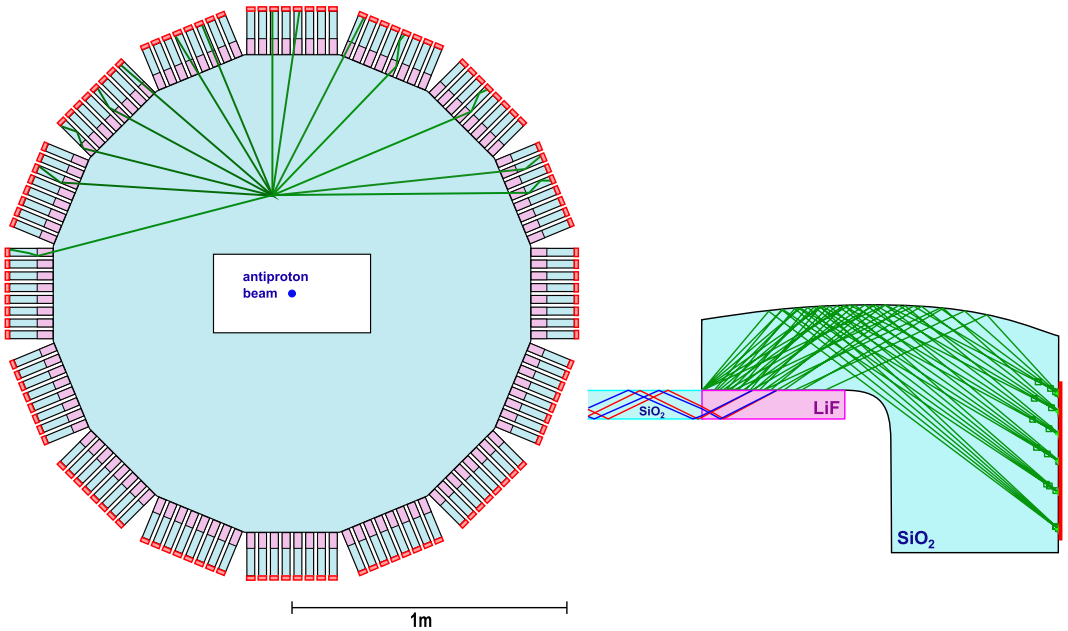

Figure 5: The forward DIRC counter of the PANDA experiment, a polygonal quartz disk read out through an array of focusing elements [20].

For charged hadron identification, two DIRC-like counters are considered [19]. For the barrel part, a focusing version will be used with a lens as a focusing element at the exit of the bar. In the forward direction, a novel type of DIRC device is being designed [20] with a 2 cm thick polygonal disc radiator made of quartz (Fig. 5). In this case Cherenkov photons are propagated to the sides of the disc, where they are focused with specially formed quartz pieces onto the photon detectors. An intermediate LiF piece is used to correct for the dispersion.

For an efficient high rate detection of gamma rays and neutral pions, a fast $PbWO_4$ based calorimeter will be used [21]. The counter will employ the second generation $PbWO_4$ crystals with a two times higher yield if compared to the $PbWO_4$ calorimeter of the CMS experiment. A further considerable increase in yield is expected from running the calorimeter at -25^0 C. As photosensors, large area APDs (14 x 7 mm^2) will be employed.

4 CLAS12 and GlueX

Considerable upgrade of the accelerator and of the detectors is underway at the Jefferson Lab. The CLAS detector [22] in Hall B is being upgraded to work at a higher luminosity (10^{35} $cm^{-2}s^{-1}$) and with an increased solid angle and momentum coverage, with the aim to study nucleon structure via generalized parton distributions [23]. Among the new features of the CLAS12 detector are an upgraded PID system (for separation of e/π, $\pi/K/p$, γ/π^0)

and an improved vertex detector for identification of weakly decaying strange baryons. The forward PID system upgrade involves a new high threshold Cherenkov counter, an improved TOF system, a higher granularity calorimeter and possibly a RICH counter [24]. The construction of the new CLAS12 detector is on schedule for the installation starting in October 2012.

The GlueX experiment is being constructed in the new experimental Hall D with the aim to search for exotic hybrids in the interaction of 9 GeV tagged polarized photons [25]. The detector construction is well underway, it is on-track for the first beam to be delivered in 2014.

5 Summary

Several new projects are under preparation with a potential to considerably improve our understanding of hadron physics. A major upgrade has started at KEK to construct the SuperKEKB accelerator and the Belle-II detector, and be ready for data taking by 2015. The SuperB project in Italy foresees building a new tunnel, reusing and upgrading the PEP-II accelerator and the BaBar detector. For the PANDA detector, a technical design report is expectd by the end of 2011, and installation in 2016/17. At JLAB, CLAS12 is on schedule for the installation in fall of 2012, and the GlueX experiment is on-track for the first beam in 2014. We can therefore expect a new, exciting era of discoveries in hadron physics.

Bibliography

[1] K. F. Chen *et al.* [Belle Collaboration], Phys. Rev. Lett. **98**, 031802 (2007).

[2] B. Aubert *et al.* [BABAR Collaboration], Phys. Rev. D **79**, 072009 (2009).

[3] Heavy Flavor Averaging Group, http://www.slac.stanford.edu/xorg/hfag/triangle/summer2010/index.shtml#sin2b

[4] CKMfitter Group (J. Charles et al.), Eur. Phys. J. C41, 1-131 (2005) [hep-ph/0406184], updated results and plots available at: http://ckmfitter.in2p3.fr; UTfit Collaboration, http://www.utfit.org/UTfit/

[5] K. Abe *et al.* (edited by S. Hashimoto, M. Hazumi, J. Haba, J. W. Flanagan and Y. Ohnishi), "Letter of Intent for KEK Super B Factory", KEK report 2004-04, http://superb.kek.jp/documents/loi/; M. Bona *et al.* [SuperB Collaboration], "SuperB: A High-Luminosity Asymmetric e^+e^- Super Flavor Factory. Conceptual Design Report," arXiv:0709.0451 [hep-ex].

[6] T. Aushev *et al.*, arXiv:1002.5012 [hep-ex].

[7] B. O'Leary *et al.* [SuperB Collaboration], arXiv:1008.1541 [hep-ex].

[8] P. Raimondi, Status of the SuperB Effort, presentation at the 2nd Workshop on Super B Factory, LNF-INFN, Frascati, March 2006, http://www.lnf.infn.it/conference/superb06/talks/raimondi1.ppt (2006).

[9] T. Abe *et al.*, arXiv:1011.0352 [physics.ins-det].

[10] M. Biagini *et al.*, arXiv:1009.6178 [physics.acc-ph].

[11] Section 3 of [10]; M. Zobov *et al.*, Phys. Rev. Lett. **104**, 174801 (2010).

[12] See for example J. Kemmer, G. Lutz, Nucl. Instr. Meth. A **253** 356 (1987); I. Peric, Nucl. Instr. Meth. A **579**, 658 (2007).

[13] K. Inami, Nucl. Instr. and Meth. A **595**, 96 (2008).

[14] I. Adam *et al.*, Nucl. Instr. and Meth. A **538** (2005) 281.

[15] T. Iijima, S. Korpar *et al.*, Nucl. Instr. and Meth. A **548**, 383 (2005).

[16] E. Grauges *et al.*, arXiv:1007.4241 [physics.inst-det].

[17] J. Benitez *et al.*, Nucl. Instrum. Meth. A **595**, 104 (2008).

[18] M. F. M. Lutz *et al.* [PANDA Collaboration], arXiv:0903.3905 [hep-ex].

[19] K. Föhl *et al.*, Nucl. Instr. and Meth. A **595** (2008) 88.

[20] P. Schönmeier *et al.*, Nucl. Instr. and Meth. A **595** (2008) 108.

[21] PANDA Collaboration, arXiv:0810.1216 [physics.ins-det].

[22] B. A. Mecking *et al.* [CLAS Collaboration], Nucl. Instrum. Meth. A **503** (2003) 513.

[23] S. Stepanyan, AIP Conf. Proc. **1257** (2010) 121 [arXiv:1004.0168 [hep-ph]].

[24] M. Contalbrigo, E. Cisbani and P. Rossi, Nucl. Instrum. Meth. A **639** (2011) 302.

[25] M. R. Shepherd [GLUEX Collaboration], AIP Conf. Proc. **1182** (2009) 816; D. Lawrence [GlueX Collaboration], AIP Conf. Proc. **1182** (2009) 811; I. Senderovich, these proceedings

LEPS II GeV photons at SPring-8

Masayuki Niiyama[1] for the LEPS II Collaboration
Department of Physics,
Kyoto University,
Kyoto, JAPAN

The construction of a new GeV photon beam line, LEPS II, has started at SPring-8 in Japan. The photon beam of LEPS II is produced by backward Compton scattering of laser photons on 8 GeV electrons. The beam intensity will be improved one order of magnitude compared to the current LEPS. The development of a full-acceptance detector which can detect both photons and charged particles is underway. The design and current status of the development of the beam line and the detector system is presented.

1 Introduction

The GeV photon beam line at SPring-8 (LEPS) started physics data taking in 2000. The photon beam of LEPS is produced by backward Compton scattering (BCS) of laser photons on 8 GeV electrons of SPring-8. The LEPS detector is optimized to detect particles produced at the forward angles, and the acceptance in the large scattering angle region is limited. The LEPS has reported various interesting data on the hadron photoproduction measured in the forward region [1]. However, a large-acceptance detector is indispensable to measure the production reaction in wide kinematical region, and to detect particles produced both in the primary reaction and the decay of a resonance state, simultaneously.

In the year 2010, the construction of a new GeV photon beam line, LEPS II, has started. At the LEPS II, the beam intensity will be ten times higher, and a full-acceptance detector system which can detect both charged and neutral particles will be constructed. One of the features of the BCS photon is the high polarization degree more than 90 %. The design and the current status of the development of LEPS II are described in following sections.

2 LEPS II beam line

SPring-8 is a third generation synchrotron radiation facility with 61 beam lines in Japan. Figure 1 shows a top view of the LEPS II beam line. The laser photons are injected from the

[1] niiyama@scphys.kyoto-u.ac.jp

laser hutch toward the straight section where backward Compton scattering takes place. The scattered photon beam is irradiated to the target at 150 m downstream from the BCS collision point. We use one of four long straight section of SPring-8, BL31LEP, for our new experiment, LEPS II. This beam line has a 30 m-long straight section between the bending magnets. The major contribution to the angular divergence of BCS photon beam is the angular divergence of the electron beam which collide with the laser beam. Thanks to the small angular divergence of the electron beam in the long straight section, a very narrow BCS photon beam is formed at LEPS II. The beam spot size at the target is about a few millimeters in RMS.

The maximum energy of BCS photons is 3 GeV when a 266-nm laser is used. In order to increase the intensity of BCS photon beam, photons from four laser modules are injected simultaneously. The long straight section of BL31LEP is advantageous to avoid the interference of lasers by changing the focus points of lasers along with the electron beam. In addition, further improvement of the luminosity of BCS photon beam is achieved by increasing the collision probability of a laser photon with a 8 GeV electron. The electron beam has ellipsoidal cross section due to the bending magnets of SPring-8 storage ring. The cylindrical lenses are used to shape the cross section of the laser beam to be ellipse, and to gain collision rate between a laser photon and a electron. Thus, the BCS photon intensity increases twice. The beam intensity is 10^6 cps for 1.5-3.0 GeV with the 266-nm Ar laser and 10^7 cps for 1.5-2.4 GeV with the 351-nm solid state laser, respectively. These are ten times higher than those of the LEPS I. The energy of a BCS photon is obtained by measuring the momentum of the recoiled electron. The scattered electron are bended in the bending magnet of the storage ring more strongly than circulating 8-GeV electrons. Thus, the momentum of the scattered electron is measured from the position of the electron after the magnet, from which the energy of the corresponding BCS photon is obtained.

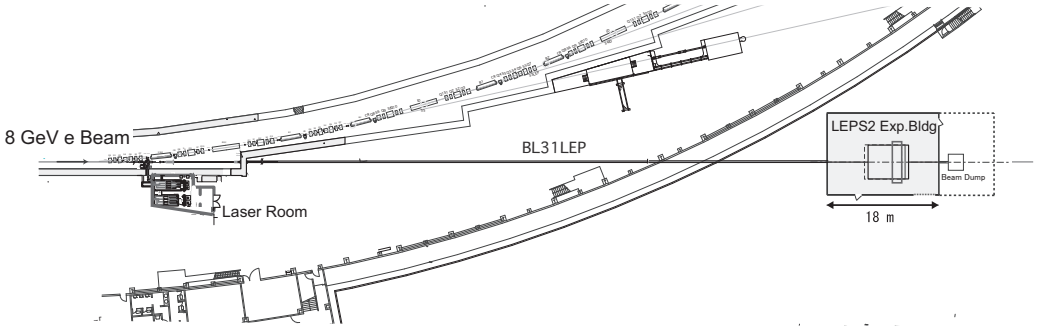

Figure 1: Top view of the LEPS II beam line.

3 LEPS II detector

Figure 2 shows a schematic view of the LEPS II detector. The LEPS II detector is designed to detect both of charged particles and photons. A solenoid magnet is shipped from USA to Japan in 2011, which was used for the kaon rare-decay experiment at BNL-AGS, E787/E949 [2]. The inner volume is 2.22-m long and 2.96-m in diameter. The LEPS II detector will be immersed in the solenoidal magnetic field of 1 T, which consists of double-sided silicon strip detectors (DSSD), forward drift chambers (FDC), a time projection chamber (TPC), time of propagation counter (TOP), range stack counter, resistive plate chamber (RPC-TOF), barrel electromagnetic calorimeter (EMCAL), and aerogel Čerenkov counter (AC). Charged particles are momentum-analyzed by the magnetic field of 1 T, and their trajectories are reconstructed by the DSSD, FDCs and TPC. The charged particles scattered at forward angles are detected by the DSSD and FDCs. On the other hand, the TPC measures the momentum in the large angle region. The momentum resolution of $\sim$1 % is achieved for 1 GeV kaons in the range of polar angle $\theta > 10^\circ$. The energy and direction of photons are measured with EMCAL, which is moved from BNL-AGS E949. The EMCAL is a sampling lead/plastic scintillator calorimeter with the total radiation length of $14.3X_0$ [2]. The polar angle coverage of the EMCAL is from 30° to 110°. The range stack counter can be used to detect neutrons with the detection efficiency up to 20 %.

The identification of momentum analyzed particles is performed by measuring a time of flight (TOF) from the target to the RPC-TOF in the low momentum region. A start signal for the TOF measurement is provided by the RF signal from the SPring-8 storage ring, which has a time resolution of 12 ps. Since the speeds of a laser photon and a 8 GeV electron are same, the arrival time of the BCS photon at the target is synchronized with the RF signal. A stop signal is provided by the RPC-TOF counters located at the barrel part where the radial distance is about 1 m. On the other hand, in the momentum region more than 1.2 GeV/c, Čerenkov counters are employed to distinguish kaons from pions. The high momentum particles up to 3 GeV/c are scattered at the forward region. The TOP counters are used to separate kaons from pions with 3σ in the end-cap region. The TOP counter is made of a quartz bar, which reconstruct the Čerenkov angle using the timing and position information of the Čerenkov photons traveling in the quartz bar [3]. In addition, the AC's are used at the barrel part for the K/π separation. The e^+e^- pair production is vetoed at the trigger level using the ultra low index AC with $n = 1.008$. The trigger rate of hadron production is estimated to be $\sim$5 kcps. A high rate dead-timeless readout system will be used for the data acquisition.

4 Summary

The construction of a new GeV photon beam line at SPring-8, LEPS II, has started in 2010. The beam intensity will be improved one order of magnitude compared to the current LEPS.

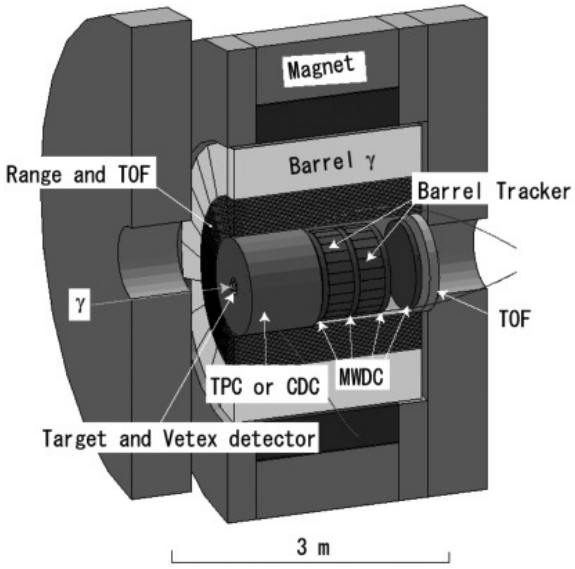

Figure 2: Schematic view of the LEPS II detector.

The development of a 4π detector which can detect both photons and charged particles is underway. The beam commissioning is planned to start in this year, and the physics data taking will start from 2013.

Bibliography

[1] T. Mibe *et al.*, Phys. Rev. Lett. **95**, 182001 (2005)
M. Niiyama *et al.*, Phys. Rev. C **78**, 035202 (2008)
T. Nakano *et al.*, Phys. Rev. C **79**, 025210 (2009)
M. Sumihama *et al.*, Phys. Rev. C **80**, 052201 (2009).

[2] M. S. Atiya *et al.*, Nucl. Instrum. Meth. A **321**, 129 (1992).

[3] M. Akatsu *et al.*, Nucl. Instrum. Meth. A **440**, 124 (2000).

Search for Gluonic Excitations in Hadrons with GlueX

Igor Senderovich[1] on behalf of the GlueX Collaboration
Department of Physics
University of Connecticut
2152 Hillside Rd. U-3046 Storrs, CT, U.S.A.

The GlueX experiment will employ a linearly polarized 9 GeV tagged photon beam incident on a liquid hydrogen target to search for exotic states in the light meson spectrum. Optimized for this purpose, the detector has a highly uniform acceptance over nearly 4π solid angle, with high efficiency for both neutral and charged final state particles. An overview of the physics motivation and detector design will be given.

1 Introduction

The firmly established states in the light meson spectrum have J^{PC} quantum numbers compatible solely with quark degrees of freedom. However, lattice QCD calculations have shown [1] [2] that the theory allows for *exotic states*: quantum numbers like 1^{-+} with mass near 2.0 GeV/c^2. Such quantum numbers and others like 0^{--}, 0^{+-}, 2^{+-} are impossible with quark degrees of freedom alone and may require excitation of the "glue" between the quarks. Identification of these "hybrid mesons" allows direct investigation of the field's dynamics and would provide a novel test of QCD. So far, most of the searches for hybrid mesons have been carried out with pion beams [3] [4], accumulating evidence of a state around 1.6 GeV/c^2.

It can be shown that hybrid mesons with spin-aligned quarks have exotic quantum numbers compared to the anti-aligned configuration. This suggests that a pion probe requires a spin flip to access exotic states, something that would not be necessary for a photon. Lattice calculations of radiative decays of $c\bar{c}$ states [1] appear to support the flux-tube model in suggesting that photo-production of exotic hybrid mesons may have a relatively large cross-section. However, suppression of spin flip may be a feature of the heavy charm quark: current efforts at calculations with lighter quarks may be able to put these suggestions on firmer ground. A separate advantage of a photo-production lies in being able to resolve the exchange mechanism (naturality) through linear polarization [5] [6]. To date, polarized, sufficiently high energy photo-production data is insufficient for a proper search for these novel meson states.

[1] senderovich@phys.uconn.edu

2 The GlueX Experiment

Hall D, a new facility dedicated to photon beam experiments on a fixed target is under construction in Jefferson Lab as part of the 12 GeV upgrade of the CEBAF accelerator. Photons will be produced from Coherent Bremsstrahlung (CB) of 12 GeV electrons in a diamond radiator and collimated 75 m downstream for effective filtering of the photon angular distribution and consequent polarization fraction improvement. The coherent enhancements in the spectrum are tuned via radiator orientation. The primary peak of (9 GeV, 40% polarization fraction) was selected as the optimal balance between these parameters (the latter vanishes at the end point.) CB on 20 μm thin diamond will yield a flux of $10^8\,\gamma$/s at $\sim 2\,\mu$A beam current tagged with 8 MeV/counter at the primary peak. A pair spectrometer will be utilized for tagger calibration and online polarimetry.

A 30 cm liquid hydrogen target will be used for the primary program of the experiment. Around the target, a hermetic "GlueX" detector has been designed optimally for meson spectroscopy with efficient partial wave analysis. This requires a nearly 4π, highly uniform acceptance and good tracking and calorimetry to handle neutral and charged final state particles. Figure 1 shows the basic GlueX detector components. Most of the detector is inside a 2.2 T solenoid with coverage in the polar angle split into the barrel and forward areas.

2.1 Tracking

The Central Drift Chamber (CDC) consists of 12 axial and 16, 6° stereo straw layers. Tests with cosmic rays have demonstrated resolution of $\sigma_r = 150\,\mu$m, $\sigma_z = 1.5$ mm and $\sigma_p/p = 1.5 - 3\%$. dE/dx information will be provided by this system to separate π, K and protons with momenta below 450 MeV/c.

Four Forward Drift Chambers (FDC) will be installed downstream. Each consists of 6 planes of 96 wires with a 1 cm pitch interleaved with cathode strips: 12 planes with 216 strips in each. Ghosting is minimized by reading out all of these electrodes and employing angular offsets between each plane. Spacial resolution of 200 μm is expected.

2.2 Calorimetry

The Barrel Calorimeter (BCAL) is of a 10% sampling "spaghetti" design with corrugated lead sheets interleaving 1 mm diameter scintillating fibers, read out by silicon photomultipliers (SiPMs). Resolutions $\sigma_E/E = 5.54/\sqrt{E} \oplus 1.6\%$, $\sigma_{\Delta t/2} = 70\,ps/\sqrt{E}$ have been demonstrated in a beam test [7]. dE/dx and time of flight information will be provided by this detector with a calculated 3σ time of flight-based separation of pions from protons below 0.75 GeV and kaon separation from pions and protons below 0.40 GeV and 0.55 GeV respectively.

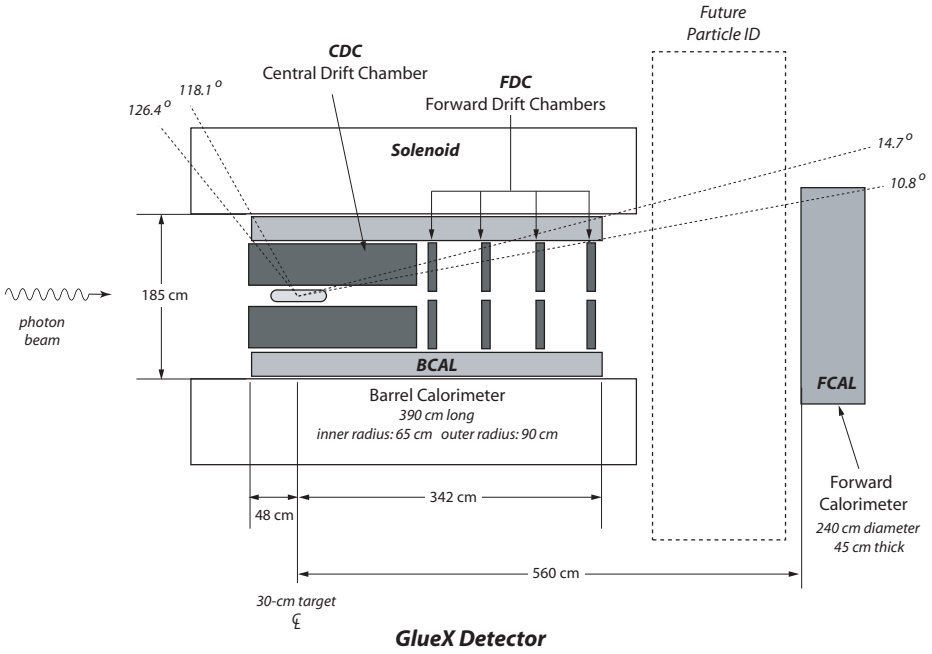

Figure 1: Simplified view of the GlueX detector: vertical cross-section along beam line. The tracking system: CDC and FDC are darkly shaded. Lightly shaded are the calorimeters: BCAL and FCAL. Not shown is the Start Counter around the target and the Time of Flight wall in front of the FCAL. Additional PID systems maybe be added later.

The FCAL is composed of 2800 F8-00 lead glass blocks with spacial segmentation of 4 cm. Used in the Brookhaven experiment E852 and RADPHI at JLab, this detector will be outfitted with light-guides to improve light collection. The resolutions are: $\sigma_E/E = 5.7/\sqrt{E} \oplus 1.6\%$ $\sigma_r = 5 - 6\,mm$ and $\sigma_t < 150\,ps$.

2.3 Time of Flight

Time of flight in the barrel region by the BCAL was described above. In the forward angles, a dedicated Time of Flight wall will be mounted in front of the FCAL. This device should achieve excellent separation between pions and protons at all energies relevant to the reactions of interest. A three sigma separation of kaons will be possible below 2-3 GeV. The prototype is close to achieving the required 100 ps resolution.

The complete time of flight system is assembled using a Start Counter around the target to identify the event with the beam bunch, information from the tagger and bunch timing from the accelerator. Additional particle identification detector components may be added between barrel and forward regions in the future.

3 Trigger, Electronics and Reconstruction

The limit of 20 kHz event rate to tape will be met with a minimum-bias trigger using track multiplicity and a minimum energy cut. The eventual full beam rate of 10^8 γ/s or photoproduction rate of 360 kHz will be addressed with an L3 computer farm. Simulations show effective reduction of low-energy events, 92% trigger rate above $\sim$ 6 GeV and a minimal effect on the important channels.

The readout needs of the detector are met with VMEx64/VXS, fully pipelined electronics such as the 250 MSPS flash ADC 16 channel module with 12 bit dynamic range and an 8 μs buffer, and the 32 channel F1TDC of better than 60 ps resolution and a 3.9 μs buffer (trigger latency: 3 μs.)

This high statistics experiment with the intensive Partial Wave Analysis (PWA) requires massive computing resources and efficient algorithms. Parallelization has been pursued at all levels: vectorized operations on CPUs, PWA on GPUs, and on-demand, fully threaded reconstruction and analysis. The computing resources of the collaboration are being integrated with the Open Science Grid (OSG) for opportunistic access to high-throughput resources.

4 Outlook

The civil construction of the new facility is almost finished, with detector installation beginning within months. Construction of major detector components is well underway. First beam is expected in 2014.

Bibliography

[1] J. J. Dudek, R. G. Edwards, M. J. Peardon, D. G. Richards and C. E. Thomas, Phys. Rev. Lett. **103** (2009) 262001 [arXiv:0909.0200 [hep-ph]].

[2] J. J. Dudek, R. G. Edwards, M. J. Peardon, D. G. Richards and C. E. Thomas, Phys. Rev. D **82** (2010) 034508 [arXiv:1004.4930 [hep-ph]].

[3] W. M. Yao *et al.* [Particle Data Group], ("Note on non-$q\bar{q}$ mesons") J. Phys. G **33** (2006) 1.

[4] B. Grube and f. t. C. Collaboration, arXiv:1002.1272 [hep-ex].

[5] F. Cooper, Phys. Rev. **170** (1968) 1602.

[6] R. L. Thews, Phys. Rev. **175** (1968) 1749.

[7] B. D. Leverington *et al.*, Nucl. Instrum. Meth. A **596**, 327 (2008).

Analysis Technologies

Analysis Technologies

Conveners

Klaus Peters GSI (*Chair*)
Boris Grube TU München

Session Chair

Boris Grube TU München

Contents

Partial Wave Analysis using Graphics Cards

Niklaus Berger[1]
Institute of High Energy Physics
Chinese Academy of Sciences
19B Yuquan Lu
100049 Beijing, CHINA

Partial wave analysis is a key technique in hadron spectroscopy. The use of unbinned likelihood fits on large statistics data samples and ever more complex physics models makes this analysis technique computationally very expensive. Parallel computing techniques, in particular the use of graphics processing units, are a powerful means to speed up analyses; in the contexts of the BES III, Compass and GlueX experiments, parallel analysis frameworks have been created. They provide both fits that are faster by more than two orders of magnitude than legacy code and environments to quickly program and run an analysis. This in turn allows the physicists to focus on the many difficult open problems pertaining to partial wave analysis.

1 Introduction

The advent of precise lattice calculations of hadron spectra (e.g. [1]) together with very high statistics data samples from experiments like BES III and Compass and, in the near future, GlueX and Panda, opens inroads to a deeper understanding of the bound states and resonances of quantum chromodynamics (QCD). Extracting resonance properties from experimental data is however far from straightforward; resonances tend to be broad and plentiful, leading to intricate interference patterns. In such an environment, simple fitting of mass spectra is usually not sufficient and a *partial wave analysis* (PWA) is required to extract resonance properties. In such an analysis, the full kinematic information is used and fitted to a model of the amplitude in a partial wave decomposition. In the cases discussed here, the model parameters are determined by an unbinned likelihood fit to the data. As models become ever more involved and huge data samples are (becoming) available, these likelihood fits are computationally very expensive. As it is exponentially hard to determine whether the fit (usually with a large number of free parameters) has found the searched for global minimum of the likelihood or one (of usually many) local minima and as there tends to be a lot of freedom in the model, many fits are required to obtain a certain degree of certainty on the stability and adequacy of the result. As most of these fits are performed

[1]nberger@ihep.ac.cn; now at Physics Institute, University of Heidelberg

sequentially, the turnaround time for a single fit, together with the effort required to code the amplitude model, determines the total analysis time.

In the context of the BES III, Compass and GlueX experiments, software frameworks for partial wave analysis addressing both the amplitude code and speed issues have been devised. Large speed-ups were obtained by parallelizing computations, particularly by the use of *graphics processing units* (GPUs). At the same time, the use of a common software base allows for a quick creation of analysis code for new channels. This in turn allows the physicists to focus on the difficult open problems, both of technical (large number of free parameters, correlations, detector resolution etc.) and physical (adequacy of models) nature.

2 Partial Wave Analysis as a computational problem

In a typical PWA (we use the simple radiative decay $J/\psi \longrightarrow \gamma X, X \longrightarrow K^+K^-$ [2] as an example), the decay is modelled by coherently summing the contributions from a variety of intermediate resonances X. The relative magnitudes and phases of these resonances are determined from a fit and the fit result is compared to the data. The set of resonances and their properties are changed until a sufficient agreement with the data is found.

The intensity I (relative number of events) at a particular point Ω in phase space can be expressed as

$$I(\Omega) = \left| \sum_{\alpha} V_\alpha A_\alpha(\Omega) \right|^2, \tag{1}$$

where the sum runs over all intermediate resonances α, V_α is the complex production amplitude for α (and the main free parameter in the fit) and $A_\alpha(\Omega)$ the complex decay amplitude at a particular point in phase space. The likelihood for a particular model is

$$\mathcal{L} \propto \prod_{i=1}^{N_{Data}} \frac{I(\Omega_i)}{\int \epsilon(\Omega) I(\Omega) d\Omega}, \tag{2}$$

where the product runs over all N_{Data} events in the sample and the integral is proportional to the total cross section, corrected for the detector efficiency $\epsilon(\Omega)$. The integral is usually performed numerically by summing over a large number N_{MC}^{Gen} of simulated events (Monte Carlo, MC) generated evenly in phase space[2]. The limited acceptance and efficiency of the detector can be taken into account by summing only over simulated events that pass the

[2]In case of a very uneven phase-space population, e.g. due to the presence of narrow resonances, it is advisable to generate a non-equidistributed MC sample and weight events to a flat distribution in order to reduce the sampling error caused by the strongly varying amplitude

reconstruction and analysis cuts. In a fit, a maximum of the logarithm of the likelihood, corresponding to the best set of parameters for the used model is searched for[3];

$$\ln \mathcal{L} \propto \sum_{i=1}^{N_{Data}} \ln \left(\sum_{\alpha} \sum_{\alpha'} V_\alpha V_{\alpha'}^* A_\alpha(\Omega_i) A_{\alpha'}^*(\Omega_i) \right) - \sum_{\alpha} \sum_{\alpha'} V_\alpha V_{\alpha'}^* \left(\frac{1}{N_{MC}^{Gen}} \sum_{j=1}^{N_{MC}^{Acc}} A_\alpha(\Omega_j) A_{\alpha'}^*(\Omega_j) \right).$$

The first sum runs over all data events, the second over all MC events. If the widths and masses of resonances are kept constant in the fit (i.e. the V_α's are the only free parameters), the last (inner) bracket and the $A_\alpha(\Omega_i)A_{\alpha'}^*(\Omega_i)$ term for each data event can be pre-calculated.

The number of floating point operations required is dominated by the sum over the data events and scales with $N_{iterations} \times N_{data} \times N_{waves}^2$, whilst the lookup table takes up storage space scaling with $N_{data} \times N_{waves}^2$. The storage space problem can be addressed by increasing the memory of the relevant machine ($\approx$1.5 GB are required per million events for a model with 20 partial waves), or with appropriate caching and staging mechanisms for data samples with several million events. If the required floating point operations are performed sequentially, the time required can however become prohibitively long.

Floating point precision can be an issue — the minimizing programs tend to fail if the delivered precision does not correspond to the expected one. For large amounts of data and simulated events however, the precision of the individual amplitude is not decisive, it can safely be computed in single precision. The final sum however has to be computed in double precision and the numerical result is strongly dependent on the summing algorithm; tree sums as usually implemented on GPUs perform much better here than accumulating loop summing employed in traditional CPU based programs.

There is no way of knowing whether the fit found just a local or the searched for global maximum of the likelihood. To gain confidence in the result, the fits are usually repeated with various sets of starting parameters. In addition, various models have to be tried out, especially in the study of possible new resonances and systematic effects. The thousands of fits needed in a typical partial wave analysis should thus be as fast as possible, especially as feedback from the physicist is required between the fits and they thus have to be run in sequence.

3 Parallel partial wave analysis

Most computing problems in particle physics are trivially parallel, as data consists of independent events. The traditional approach to parallelism is thus to treat different subsets of events on different cores/machines/in different locations and then have a relatively lightweight piece of code perform a synthesis. For PWA, this synthesis (namely the likelihood sum) has to be performed very frequently (for every fit iteration) and thus network

[3] As most fit programs search for a minimum as opposed to a maximum, $-\ln \mathcal{L}$ is fed to the minimizer.

latency quickly dominates for distributed architectures. As the calculations per event are relatively simple and exactly the same for all events, it is desirable to have a very large number of (simple) cores available in a single machine. This kind of architecture is provided by graphics processing units (GPUs). These devices were originally developed for the use in 3D games, calculating realistic colour shades of pixels. The large and performance-hungry game market has produced single chips with 1600 individual floating point units, which are available at prices of a few hundred Euros.

The potential of GPUs for scientific computing was quickly discovered, early efforts were however hampered by the lack of a suitable interface and most work was done via the *OpenGL* graphics interface. The two major GPU vendors, Nvidia and ATI then started their own GPU computing frameworks, named *CUDA* [3] and *ATI Stream* [4–6] respectively[4]. In recent years, a platform independent standard called *OpenCL* [7,8] has emerged. The successive choices of GPU interface for the BES III PWA framework and the final transition to *OpenCL* are described in [9].

In 2007 we started tests of GPUs for partial wave analysis at the BES III experiment; it quickly turned out that their architecture was very well suited to the task at hand — in fact, custom PWA hardware would very much look like a GPU, minus the display port — and that speed-ups with regards to a reference FORTRAN implementation of more than two orders of magnitude were obtainable [10]. The framework now provides facilities for amplitude calculation, minimization and plotting and is widely used for analyses at BES III. It continues to be developed and is available at [11].

The group at Indiana University at around the same time started creating a framework for PWA on multi-core machines and clusters, using *OpenMP* for inter-process communication. This framework, aimed at the CLEO-c, BES III and GlueX experiments shows beautiful scaling behaviour and now also harnesses GPUs using *CUDA*. It is available at [12].

Yet another framework, tightly integrated with the *root* data analysis toolset [13], was developed in Munich for use in the COMPASS experiment and now also incorporates GPU assisted fitting. It is available at [14].

A more ambitious effort for a very general framework for the PANDA experiment was started in Bochum and is still in its early stages, is however also aimed at an eventual parallel implementation.

The multitude of available frameworks demonstrate the great interest in the field, allow for cross checks and show that speed is indeed an important issue in PWA, but one that can be tackled with an appropriate combination of hard- and software.

[4]The ATI stream framework encompassed at various times different interfaces with different levels of abstraction and is nowadays also used for the ATI *Open CL* implementation.

4 Open technical problems in partial wave analysis

Probably the most difficult problem in PWA is the appropriate modelling of the physics processes, taking into account the unitarity of the S-matrix. There is currently a lot of theoretical work done in this area (see e.g. [15]); a completely satisfying treatment has however only been achieved for low energy $\pi\pi$ scattering. There is in addition a large range of technical/experimental problems as yet unsolved; they shall be discussed in the following.

Resolution Detectors have a finite resolution and the reconstructed kinematics of an event are thus different from the true ones. The unbinned approach to PWA precludes the use of unfolding techniques. For resonances with a large width, this is not particularly problematic; in cases however where resolution and width are of comparable size (a good example for most detectors is the ϕ meson), it is impossible to describe interference with other resonances and the reconstructed mass distribution with the same functional form. The only (and rather unsatisfactory) remedy is excluding the mass regions around narrow resonances from the fit, in the hope that the effects in the tails are not to severe.

Goodness of fit For unbinned distributions in a multi-dimensional variable space, there are is no effective goodness of fit test such as a χ^2 test; of course it is possible to perform tests on all sorts of binned projections — if these look bad, the fit is indeed bad, but unfortunately the opposite is not necessarily true.

Choice of waveset The choice of intermediate resonances is somewhat arbitrary; not dissimilar to the goodness of fit issue it is easy to tell if the waveset is insufficient, but a priori not knowable whether it is complete.

Fits with large numbers of parameters PWA fits have at least three (more often four, in more advanced models also more) free parameters per resonance, leading to fits with a very large number of parameters. In such fits it is impossible to know whether a minimum identified by the minimizer is just a local minimum or the searched for global one. Many heuristic methods (such as repeating fits with randomly chosen initial values) have been developed to gain confidence in a particular minimum; they however become excessively time consuming for large parameter spaces and will never provide certainty.

Fits with complex parameters PWA fits usually have complex parameters. As minimizers only deal with real numbers, some representation has to be chosen; however, both the Cartesian and the polar representations have issues. The Cartesian representation has the disadvantage of being disconnected from the physical parameters of magnitude and phase

and leads to large correlations (and thus bad fit convergence) in cases where the phase of a resonance is weakly constrained. The polar representation avoids these problems at the cost of introducing a lower boundary on the magnitude and a periodic phase parameter - both of which have their separate issues in the minimizers. A proper treatment of complex numbers and their derivatives inside the minimizers would be extremely helpful.

More control over the fitters The standard interfaces to fitters like *Minuit* [16] and *Fumili* [17] give the user relatively few control over the amount of additional checks and error calculations performed by the minimizers. In many cases however, most of the computing time is spent on just these. Options to perform only what is really needed at the current state of analysis would be very helpful.

Less control over the GPUs The two most widely used GPU frameworks today, *CUDA* and *OpenCL*, both have a fairly low level interface, giving the user a lot of control over how exactly the parallelism is to be implemented — for most particle physics applications it is however completely irrelevant which events are processed simultaneously, as long as all of them are processed fast. This could be achieved through a more comfortable high level interface.

Impact of results The last issue is sociological rather than technical in nature, but tightly linked with many of the technical issues. In very generalized terms, "standard" results, where PWA is used to determine quantum numbers of a bump visible in the mass spectrum and these turn out to be in accordance with expectations are easily accepted by the community (more or less independently of the sophistication of the analysis), "surprising" results, where resonances not directly visible in the mass spectrum are exposed by PWA and turn out to have unexpected (exotic) quantum numbers are usually not believed (again more or less independently of the sophistication of the analysis). As long as the issues listed above remain, PWA has a very hard time to provide the required *extraordinary evidence for extraordinary claims*.

5 Conclusions

Partial wave analysis is a key tool in hadron spectroscopy, of great importance to current and future experiments such as BES III, Compass, GlueX and Panda. PWA is computationally expensive and thus potentially slow — this can be overcome by applying parallel programming techniques and running the analyses on massively parallel devices such as GPUs. The success in this area gives us both the tools and the hope that we can solve or mitigate many of the other technical problems facing PWA, thus laying a foundation for a new golden age of hadron spectroscopy.

Acknowledgments

I am grateful to Matthew Shepherd, Ryan Mitchell and Sebastian Neubert for many insightful discussions about PWA fitting, hadron spectroscopy and fast code. The many users of the GPUPWA code in BES III have helped to move the project in the right direction by providing feedback, feature requests and bug reports.

This work has been financed by the Chinese Academy of Sciences and the Swiss National Science Foundation.

Bibliography

[1] J. J. Dudek, R. G. Edwards, B. Joo, M. J. Peardon, D. G. Richards, C. E. Thomas, Phys. Rev. **D83** (2011) 111502. [arXiv:1102.4299 [hep-lat]].

[2] J. Z. Bai *et al.* [BES Collaboration], Phys. Rev. **D68** (2003) 052003. [hep-ex/0307058].

[3] T. R. Halfhill, *Microprocessor Report* **01/28/08**, 1–6 (2008).

[4] Advanced Micro Devices, AMD stream computing, software stack, AMD white paper (2007), `http://ati.amd.com/technology/streamcomputing/firestream-sdk-whitepaper.pdf`.

[5] I. Buck, Data Parallel Computing on Graphics Hardware, Presentation at Graphics Hardware (2003), `http://graphics.stanford.edu/projects/brookgpu/GH03-Brook.ppt`.

[6] Advanced Micro Devices, AMD Stream Computing, Software Stack, AMD White Paper (2007).

[7] A. Munshi, The OpenCL specification, version 1.0, Tech. rep., The Khronos Group (2008), `http://www.khronos.org/registry/cl/specs/opencl-1.0.33.pdf`.

[8] A. Munshi, The OpenCL specification, version 1.1, Tech. rep., The Khronos Group (2010), `http://www.khronos.org/registry/cl/specs/opencl-1.1.pdf`.

[9] N. Berger, Partial wave analysis at BES III harnessing the power of GPUs, to appear in JPCS, proceedings of CHEP 2010, arXiv:1108.5673v1 [physics.data-an].

[10] N. Berger, B.J. Liu, and J.K. Wang, *J. Phys. Conf. Ser.* **219**, 042031 (2010).

[11] GPUPWA package, available at `http://sourceforge.net/projects/gpupwa/`.

[12] AMPTOOLS package, available at `http://sourceforge.net/projects/amptools/`.

[13] R. Brun, and F. Rademakers, *Nucl. Instrum. Meth.* **A389**, 81–86 (1997).

[14] ROOTPWA package, available at `http://sourceforge.net/projects/rootpwa/`.

[15] Amplitude Analysis in Hadron Spectroscopy, workshop at *European Centre for Theoretical Studies in Nuclear Physics and Related Areas*, Trento (2011), `http://www.ect.it/`.

[16] F. James, M. Roos, Comput. Phys. Commun. **10**, 343-367 (1975).

[17] S. N. Dymov, V. S. Kurbatov, I. N. Silin, S. V. Yaschenko, Nucl. Instrum. Meth. **A440**, 431-437 (2000).

Poster Session

Poster Session

Contents

Study of Deuteron-Proton and Deuteron-Deuteron Collisions at Intermediate Energies

Nadezhda Ladygina
Laboratory of High Energy Physics
Joint Institute for Nuclear Researches
141980 Dubna, RUSSIA

During a few decades hadronic reactions with a participation of the light nuclei were extensively investigated at the energies of few hundred MeV. These processes are the simplest examples of the hadron nucleus collision that is why the interest to this reaction is justified. A number of experiments is aimed at getting some information about the deuteron or helium wave functions as well as nucleon-nucleon amplitudes from the scattering observables.

In this paper I consider two reactions. The first of them is the dp-elastic scattering in the deuteron energy range between 500 MeV and 2 GeV. The second reaction is the $dd \to {}^3He\ n$ at the energies from 200 MeV up to 520 MeV. At these energies the methods based on the solution of the Faddeev equations are unusable. I start from the AGS-equations [1], [2] and iterate their over nucleon-nucleon t-matrix. The plane-wave-impulse-approximations (PWIA), single scattering (SS) and double scattering (DS) contributions are taken into consideration for the $dp \to dp$ process. For the $dd \to {}^3He\ n$ reaction I consider the one-nucleon-exchange (ONE) and single scattering terms. The applied approach was presented in details in refs. [3], [4].

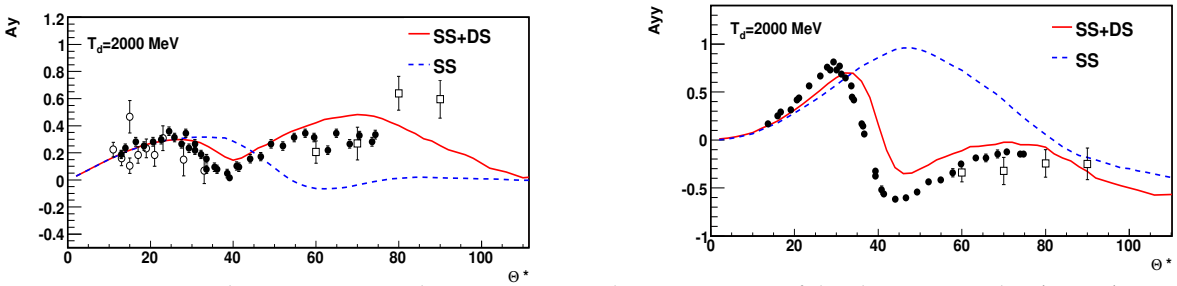

Figure 1: The vector,A_y, and tensor, A_{yy}, analyzing powers of the deuteron in the $dp \to dp$. The data are taken from: • [5]; ○ LHE JINR, hydrogen bubble chamber experiment, and ▫ LHE JINR Nuclotron, talk by P.Kurilkin given at this conference.

The results of the calculations for the dp- elastic scattering are given in Fig.1. The angular dependencies of the vector and tensor analyzing powers are presented at the deuteron energy of 2 GeV. Here, the solid curves correspond to the results of calculations including both the single scattering and double scattering terms. The dashed curves are the results

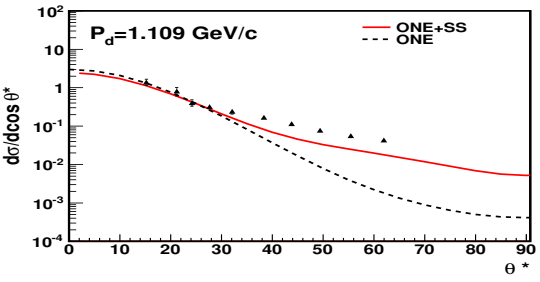

Figure 2: The differential cross section of the $dd \rightarrow {}^3He\, n$. The data are taken from [6].

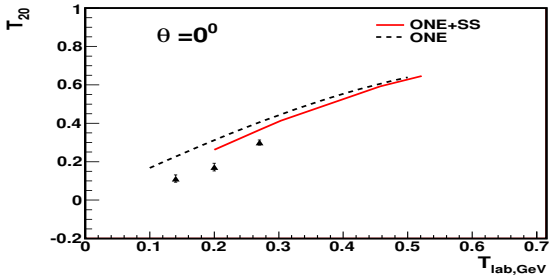

Figure 3: The tensor analyzing power in the $dd \rightarrow {}^3He\, n$. The data are taken from [7].

taking of account only SS-contribution. One can see the inclusion of the DS-term significantly improves the agreement between the theoretical predictions and experimental data, especially, for the tensor analyzing power.

The differential cross section of the $dd \rightarrow {}^3He\, n$ reaction is presented in Fig.2 at laboratory momentum of 1.109 GeV/c [6]. Also the energy dependence of the T_{20} has been obtained at zero scattering angle in the energy range between 200 MeV and 520 MeV (Fig.3). The results demonstrate the significant improvement an agreement of the data and theory predictions, especially, for non forward angles, when the single scattering term is included. It allows us to regard this approach as a next step towards a solution of the four-nucleon problem.

Acknowledgments

This work has been supported by the Russian Foundation for Basic Research under grant $N^{\underline{0}}$ 10-02-00087a.

Bibliography

[1] E.O.Alt, P.Grassberger, W.Sandhas, Nucl.Phys. **B2**, 167 (1967)

[2] P.Grassberger, W.Sandhas, Nucl.Phys.**B2**, 181 (1967)

[3] N.B.Ladygina, Phys.Atom.Nucl., **71**, 2039 (2008)

[4] N.B.Ladygina, Eur.J.Phys. **A42**, 91 (2009)

[5] M.Haji-Saied et al, Phys.Rev.**C36**, 2010 (1987)

[6] G.Bizard et al.,Phys.Rev. **C22**, 1632 (1980)

[7] V.P. Ladygin et al., Phys. Lett. **B598**, 47 (2004)

Properties of Σ_c and Λ_c baryons in quark-diquark model

Ajay Majethiya[1], Kaushal Thakkar, and P. C. Vinodkumar
Department of Physics, Sardar Patel University, Vallabh vidhyanagar-388120, India

Study of the heavy flavour hadrons containing either a charm quark or a beauty quark has become a subject of recent interest due to the observations reported by the experimental groups at Belle, BABAR, DELPHI, CLEO, CDF etc;. Most of the new states observed in these experimental facilities are within the heavy flavour sector with one or more heavy flavour quark composition.

In the quark-diquark model, the Hamiltonian of the baryon is expressed in terms of a diquark Hamiltonian (H_{jk}) plus qurk-diquark Hamiltonian ($H_{i,jk}$) as [1]

$$H = H_{jk} + H_{i,jk} \tag{1}$$

The diquark(jk) Hamiltonian and Hamiltonian of the relative motion of the diquark(jk) and the third quark(i) is described by $H_d = H_{jk} = \frac{p^2}{2m_{jk}} + V_{jk}(r_{jk})$ and $H_{i,d} = H_{i,jk} = \frac{q^2}{2m_{i,jk}} + V_{i,jk}(r_{i,jk})$ respectively. Where, p and q are the relative momenta of the quarks within the diquark and within the quark-diquark systems respectively. Here, the inter-quark potential (V_{jk}) and the quark-diquark potential ($V_{i,jk}$) are taken as $V_{jk} = -\frac{2}{3}\alpha_s \frac{1}{r_{jk}} + b\ r_{jk}^{\nu}$ and $V_{i,jk} = -\frac{4}{3}\alpha_s \frac{1}{r_{i,jk}} + b\ r_{i,jk}^{\nu}$ respectively. Employing the numerical method using mathematica notebook, we get the spin average mass of the system (ie. without spin contribution) as $M_{Qqq} = \Sigma m_i + E(\overline{\mu})$ where, $E(\mu)$ is the total binding energy obtained from Eqn.1. The spin dependent interactions among the diquark and among the quark-diquark structure have been included perturbatively by considering the spin dependent potential provided by [2]. The potential parameters of the model are fixed to yield the spin average mass of the ground state of $\Sigma_c^*(2518) - \Sigma_c(2454)$ baryon. The mass spiltting has been studied for different choices of the quark mass parameters, m_c for each case of the potential exponent (ν) with the different choice of the running strong coupling constant α_s. It is found that the choices of heavy quark mass parameter, m_c and α_s plays a decisive role in the mass splitting of the ground state baryons. The model parameters thus extracted here for the choices of $\alpha_s = 0.20$, $\alpha_s = 0.25$ and $\alpha_s = 0.30$ are listed in Table 1. With these sets of input values we have predicted the ground state mass of Λ_c. The three parameter sets deduced from the spectroscopy are being used to compute the magnetic moments, radiative decay and strong decay widths of Σ_c and Λ_c baryons with no additional parameters. The magnetic moments are computed by considering spin-flavor wave function of the baryonic state as well as by defining an effective bound state mass for the constituting quarks. Our results for the

[1]ajay.phy@gmail.com

Table 1: Mass, Magnetic moment and Decay width of Charm baryons

α_s	ν	m_c GeV	M_{Λ_c} GeV	$\mu_{\Sigma_c^+}$ μ_N	$\mu_{\Lambda_c^+}$ μ_N	$\Gamma_{\Sigma_c^+\to\Lambda_c^+\gamma}$ keV	$\Gamma_{\Sigma_c\to\Lambda_c\pi}$ MeV
0.20	0.4	1.100	2.346	0.312	0.429	10.15	< 0.01
	0.6	1.220	2.330	0.348	0.416	18.24	< 0.01
	0.8	1.280	2.323	0.365	0.410	24.39	<0.01
	1.0	1.320	2.317	0.377	0.407	27.96	< 0.01
0.25	0.4	1.360	2.310	0.389	0.404	34.17	< 0.01
	0.6	1.435	2.300	0.410	0.399	45.57	0.33
	0.8	1.480	2.298	0.422	0.396	49.54	0.61
	1.0	1.500	2.293	0.428	0.395	55.82	1.54
0.30	0.4	1.570	2.285	0.448	0.391	69.40	3.62
	0.6	1.615	2.280	0.460	0.388	79.21	5.26
	0.8	1.640	2.278	0.466	0.387	83.93	6.18
	1.0	1.650	2.275	0.470	0.386	89.31	7.14

choice of $\nu = 1.0$ and $\alpha_s = 0.25$ led to the fixing of charm mass parameter, m_c= 1.5 GeV to have the experimental $\Delta M_{(\Sigma_c^*(2518)-\Sigma_c(2454)}$= 64 MeV [3]. With the same model parameters, we have computed the mass of Λ_c as M_{Λ_c} = 2.293 GeV, as against the PDG2010 value of 2.286 GeV, the magnetic moment, $\mu_{\Lambda_c^+}$ = 0.395 μ_N, as against the value of 0.380 μ_N predicted in a relativistic quark model [4]. Our results for the transition decay width, $\Gamma_{\Sigma_c^+\to\Lambda_c^+\gamma}$ = 56.00 MeV is close to 60.00 MeV predicted by relativistic three quark model [5]. The overall agreement obtained in the present study indicates the success of the present model and the choice of the inter-quark potential for the description of the charm baryons.

Bibliography

[1] W. S. Carvalho *et al.*, arXiv:hep-ph **9404298v1**,(1994).

[2] S. S. Gershtein *et al.*, Heavy Ion Physics **9** , 133-144 (1999); Phys. Atom. Nucl., **63**; 274-286,(2000).

[3] K. Nakamura *et al.*, PDG, J. Phy. G: Nucl Part. Phy. **37**, 075021 (2010).

[4] Amand Faessler *et al.*, Phys. Rev. D **73**, 094013 (2006). Phys. **35**, 065001 (2008).

[5] M. A. Ivanov *et al.*, Phys. Rev.D **56** 348 (1998).

Nonet meson properties in Nambu Jona-Lasinio model with dimensional regularization

Hiroaki Kohyama[a], T. Inagaki[b], D. Kimura[c], and A. Kvinikhidze[d]
[a]*Department of Physics, Chung Yuan Christian University, Chung Li, TAIWAN*
[b]*Information Media Center, Hiroshima University, Hiroshima, Japan*
[c]*Learning Support Center, Hiroshima Shudo University, Hiroshima, Japan*
[d]*A. Razmadze Mathematical Institute of Georgian Academy of Sciences, Tbilisi, Georgia*

The Nambu Jona-Lasinio (NJL) model is one of the useful models of quantum chromodynamics, and it describes observed meson properties nicely. In this article, we study the nonet meson properties by using the NJL model with dimensional regularization at finite temperature and chemical potential. We find that the results show reasonable behaviors, which are similar to the ones seen in the model with the frequently used cutoff regularization. This may indicate that the model predictions are not drastically affected by the difference between the regularization procedures in the NJL model.

1 Introduction

The investigation of the meson properties has attracted a lot of attention in particle physics. To study them, we employ the Nambu Jona-Lasinio model [1] which is an useful effective model of QCD. The Lagrangian of our 3 flavor NJL model is written by

$$\begin{aligned}\mathcal{L}_{\rm NJL} = &\sum_{i,j}\overline{q}_i\left(i\partial\!\!\!/ - \hat{m}\right)_{ij} q_j + G\sum_a\Big[\big(\sum_{i,j}\overline{q}_i\lambda_a q_j\big)^2 + \big(\sum_{i,j}\overline{q}_i\, i\gamma_5\lambda_a q_j\big)^2\Big] \\ &- K\left[\det\overline{q}_i(1-\gamma_5)q_j + \text{h.c.}\,\right].\end{aligned}$$

Here the subscripts i, j represent the flavor indices, $\hat{m}$ is the current quark mass matrix $\mathrm{diag}(m_u, m_d, m_s)$, and λ_a are the Gell-Mann matrices in flavor space. G and K are the effective coupling constants for 4- and 6-fermion interactions.

Since the model is not renormalizable, the physical predictions depend on the regularization procedures. The most frequently used one is the three momentum cutoff method, and the model predicts the meson properties well (for reviews, see [2]). To test the other possible regularization method, we shall use the dimensional regularization here.

2 Nonet meson properties

Before performing the calculation for the meson properties, we have to set the model parameters. The model has 7 free parameters: current quark masses m_u, m_d, m_s, 4- and 6-point couplings G, K, dimension D, and the renormalization scale M_0 which are fixes so as to reproduce the meson properties. Here we use the following parameter set [3],

$$m_{u,d} = 5.5\text{MeV}, \quad m_s = 148\text{MeV}, \quad G = 0.023, \quad K = 8.4 \times 10^{-9}, \quad D = 2.78, \quad M_0 = 62.4\text{MeV}.$$

Having fixed the parameters, we are ready to study the nonet meson properties. Fig. 1

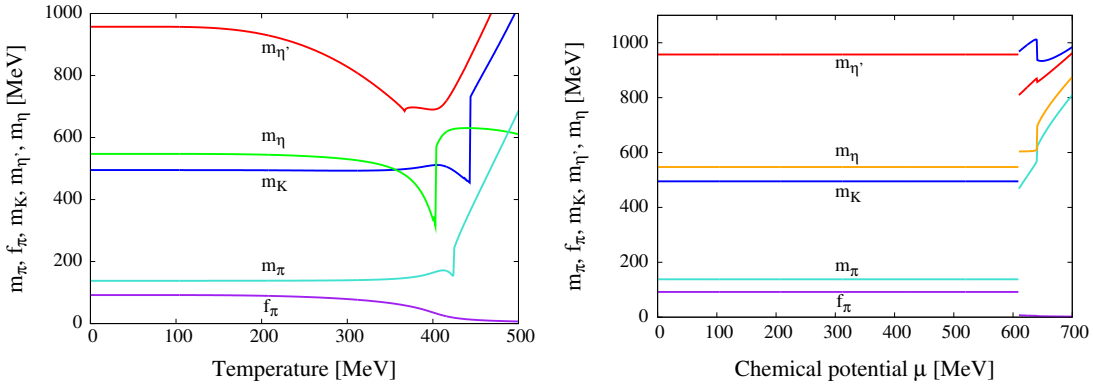

Figure 1: Meson properties. Left: finite T and $\mu = 0$. Right: $T = 10$MeV and finite μ.

shows the numerical results of the meson properties for finite temperature T and zero chemical potential μ (left), and low temperature $T = 10$MeV and finite μ (right). As we can see from the figure, the resulting meson properties show the similar behavior with the frequently used cutoff case. Thus the NJL model predicts the nonet meson properties nicely within the cutoff and dimensional regularizations. This may indicate that the model has regularization independent aspects, which is intriguing to study.

Bibliography

[1] Y. Nambu and G. Jona-Lasinio, Phys. Rev. **122**, 345 (1961); *ibid.* **124**, 246 (1961).

[2] S. P. Klevansky, Rev. Mod. Phys. **64**, 649 (1992); T. Hatsuda and T. Kunihiro, Phys. Rept. **247**, 221 (1994); M. Buballa, Phys. Rept. **407**, 205 (2005).

[3] T. Inagaki, D. Kimura, H. Kohyama and A. Kvinikhidze, Phys. Rev. D **83**, 034005 (2011).

Hadron Resonances Within a Constituent-Quark Model

Regina Kleinhappel[1,a] and Wolfgang Schweiger[a]
[a] *Physics Institute, University of Graz*

In order to get a more realistic description of the hadron spectrum we extend a constituent-quark model by explicit mesonic degrees of freedom. The resulting system of constituent (anti)quarks, which are subject to an instantaneous confining force, and mesons, which couple directly to the quarks, is treated by means of a relativistic coupled-channel framework. It can be formally shown that the mass-eigenvalue problem for such a system is equivalent to a hadronic eigenvalue problem in which the eigenstates of the pure confinement potential (bare hadrons) are coupled via meson loops. Following this kind of approach we have calculated hadron masses and decay widths for a simple toy model.

The resonance character of hadron excitations is usually not taken into account in constituent quark models. As a consequence most of the (perturbatively) calculated partial decay widths come out too small as compared to experiment [1]. This suggests that physical hadron resonances are not just simple bound states of valence (anti)quarks, but should also contain higher Fock components. We propose to model the additional quark-antiquark pairs by means of mesons which can couple directly to the valence (anti)quarks.

A natural starting point for this kind of description is the chiral constituent quark model [2]. Within this model it is assumed that the effective degrees of freedom emerging from the spontaneous breaking of chiral symmetry are (confined) constituent (anti)quarks and Goldstone bosons, i.e. the lightest pseudoscalar mesons. We use the point form of relativistic quantum mechanics in connection with the Bakamjian-Thomas construction to calculate mass spectra and decay widths. This kind of approach is Poincaré invariant and one only has to deal with an eigenvalue problem for an appropriately defined mass operator [3].

In order to allow for the decay of hadron excitations into a lower lying state by emission of a Goldstone boson we adopt a 2-channel mass operator. A general mass eigenstate has then a valence-(anti)quark component $|\psi_{\mathrm{val}}\rangle$ and a valence-(anti)quark + Goldstone-boson component $|\psi_{\mathrm{val+GB}}\rangle$. These components are coupled via vertex operators $\hat{K}$ and $\hat{K}^\dagger$ that describe the emission and absorption of the Goldstone boson by the (anti)quark, respectively. If $|\psi_{\mathrm{val+GB}}\rangle$ is eliminated by means of a Feshbach reduction one ends up with a mass-eigenvalue equation for $|\psi_{\mathrm{val}}\rangle$ which takes on the form:

$$(1) \qquad \big(\hat{M}_{\mathrm{val}} + \underbrace{\hat{K}^\dagger (m - \hat{M}_{\mathrm{val}+GB} + i0)^{-1} \hat{K}}_{\hat{V}_{\mathrm{opt}}(m)}\big)|\psi_{\mathrm{val}}\rangle = m|\psi_{\mathrm{val}}\rangle .$$

[1] regina.kleinhappel@uni-graz.at

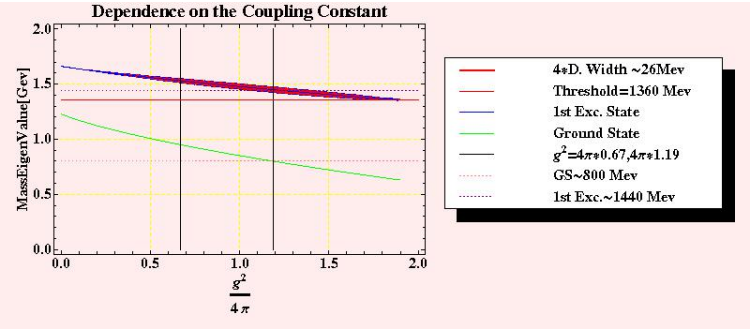

Figure 1: Predictions of our toy model. The mass of the ground state (green line) and the first excited state (blue line) as functions of the Goldstone-boson-quark coupling. The red band between the dashed blue lines indicates the decay width of the first excited state (multiplied by a factor 4 for better visibility). The range of couplings allowed by the Goldberger-Treiman relation is indicated by the black vertical lines.

The channel mass operators $\hat{M}_{\text{val}}$ and $\hat{M}_{\text{val}+GB}$ consist of a kinetic-energy term and an instantaneous confining potential. By expanding $|\psi_{\text{val}}\rangle$ in terms of eigenstates of $\hat{M}_{\text{val}}$ (which we call "bare hadrons") Eq. (1) can be converted into a system of algebraic equations for the expansion coefficients. Physically speaking, this system represents again a (non-linear) mass-eigenvalue problem, but on the hadronic level rather than on the quark level. It describes the coupling of bare hadrons via Goldstone-boson loops and has to be solved self-consistently (for details, see Ref. [4]).

As a first test we have applied these ideas to a simple toy model in which spin and isospin are completely neglected and the bare hadrons are just quark-antiquark pairs confined by a harmonic oscillator potential. In order to give the model some physical meaning we have adjusted the parameters such that the masses of the ground state and the first excited state of the ω are approximately reproduced. As can be seen in Fig. 1 the decay width of the first excited state exhibits a maximum of about 26 MeV as a function of the Goldstone-boson-(anti)quark coupling strength and vanishes as soon as the real part of the mass eigenvalue approaches the lowest threshold. We observe a considerable increase of the decay width as compared to perturbative calculations. This gives some hope that typical decay widths of 0.1 GeV or even more can be achieved for baryon resonances within the full chiral constituent-quark model.

Acknowledgments

R. Kleinhappel acknowledges the support of the "Fonds zur Förderung der wissenschaftlichen Forschung in Österreich" (FWF DK W1203-N16)

Bibliography

[1] T. Melde, W. Plessas and B. Sengl, Phys. Rev. C **76** (2007) 025204.

[2] L. Y. Glozman and D. O. Riska, Phys. Rept. **268** (1996) 263.

[3] E. P. Biernat, W. H. Klink and W. Schweiger, Few Body Syst. **49** (2011) 149.

[4] E. Kleinhappel, Master's thesis, Karl-Franzens-Universität Graz (2010).

Possible molecular bound states: $\Lambda_c N$ and $\Lambda_c \Lambda_c$

Yan-Rui Liu, W. Meguro, and Makoto Oka
Department of Physics, H-27, Tokyo Institute of Technology, Meguro, Tokyo 152-8551, Japan

The $\Lambda_c N$ and $\Lambda_c \Lambda_c$ bound state problems are explored in the coupled channel one-boson-exchange approach. The model involves a free cutoff parameter and several coupling constants which are determined by various methods. The coupled channel effects may finally result in $\Lambda_c N$ and $\Lambda_c \Lambda_c$ molecular bound states for a reasonable cutoff parameter.

Study of possible bound states may help us to understand the strong interaction in the non-perturbative region, which is always an interesting topic. In the heavy quark sector, molecule-like bound states are more likely to exist due to two reasons. The first one is the larger reduced mass of the system which renders the relatively smaller kinetic energy and is advantageous for the formation of hadronic molecules. The other one is the degeneracy of hadrons in the heavy quark limit which accounts for the coupled channel effects. As the lowest heavy quark baryon, Λ_c is interesting in that possible low-lying hadronic bound states containing it are stable. The channel couplings of Σ_c and Σ_c^* may give important contributions. Here we consider two charmed systems: $\Lambda_c N$ and $\Lambda_c \Lambda_c$. Frameworks to study them are similar. We construct effective Lagrangian, determine the coupling constants from various symmetries, derive one-meson-exchange potentials, and get binding energies by solving the coupled channel equations with the variational method [1]. We introduce a phenomenological cutoff parameter in the final potential to compensate the extended structure of the hadrons. Details of the formulations and results are given in Refs. [2,3].

For the $\Lambda_c N$ system, an early study using the SU(4) symmetry [4] concluded that whether there is a bound state needs further detailed coupled channel calculation. It is interesting to give the system a serious study with the modern effective theory and couplings to $\Sigma_c N$ and $\Sigma_c^* N$. We consider three coupled channels for the spin-singlet case: $\Lambda_c N(^1S_0)$, $\Sigma_c N(^1S_0)$, and $\Sigma_c^* N(^5D_0)$. For the spin-triplet case, we consider seven channels: $\Lambda_c N(^3S_1)$, $\Sigma_c N(^3S_1)$, $\Sigma_c^* N(^3S_1)$, $\Lambda_c N(^3D_1)$, $\Sigma_c N(^3D_1)$, $\Sigma_c^* N(^3D_1)$, and $\Sigma_c^* N(^5D_1)$. For comparison, we use both the one-pion-exchange potential (OPEP) model and the one-boson-exchange potential (OBEP) model in our study. A key feature is that one pion exchange is forbidden in the dominant channel $\Lambda_c N$ because of the isospin conservation. In the OPEP model, it is the coupled channel effect that one can get binding solutions with a reasonable cutoff parameter. By inspecting contributions of individual channel, one observes that the tensor interaction plays a key role. In the OBEP model, additional scalar and vector meson exchanges contribute significantly. It is more possible to have bound states in this model. In brief, one

expects the existence of $\Lambda_c N$ hadronic molecules.

For the $\Lambda_c \Lambda_c$ system, the allowed S-wave state is only spin-singlet because of Pauli principle. Channels which can couple with it are $\Sigma_c \Sigma_c ({}^1S_0)$, $\Sigma_c^* \Sigma_c^* ({}^1S_0)$, $\Sigma_c^* \Sigma_c^* ({}^5D_0)$, and $\Sigma_c \Sigma_c^* ({}^5D_0)$. Although Λ_c does not decay through strong interaction, $\Lambda_c \Lambda_c$ may mix with $\Xi_{cc} N$ by the exchange of charmed mesons. Since we consider the possible loosely bound molecular state, the mixing occurring at short distance may be unimportant and we neglect this channel. In addition, Ξ_{cc} has not been well established yet. For a study of possible bound states in the $\Xi_{cc} N$ system, one may consult Ref. [5]. We use only the long-range OPEP model in our study. Numerically, we can get a loosely bound $\Lambda_c \Lambda_c$ hadronic state with a reasonable cutoff parameter. Although the diagonal potentials are all repulsive, the channel coupling may result in binding solutions. The tensor force between S-wave channel and D-wave channel again plays a key role.

To summarize, we find that bound states in both $\Lambda_c N$ and $\Lambda_c \Lambda_c$ systems are possible although the binding energies depend on a phenomenological cutoff parameter. One expects that these hadronic molecular states may be looked for at experimental facilities.

Acknowledgments

This project was supported by JSPS under Contract No. P09027; KAKENHI under Contract Nos. 19540275, 20540281, 22105503, and 21.09027.

Bibliography

[1] E. Hiyama, Y. Kino and M. Kamimura, Prog. Part. Nucl. Phys. 51, 223 (2003).

[2] Y.R. Liu and M. Oka, arXiv: 1103.4624 [hep-ph].

[3] W. Meguro, Y.R. Liu, M. Oka, arXiv: 1105.3693 [hep-ph].

[4] C.B. Dover and S.H. Kahana, Phys. Rev. Lett. **39**, 1506 (1977).

[5] F. Frömel, B.Juliá-Díaz, D. O. Riska, Nucl. Phys. A **750**, 337 (2005); B.Juliá-Díaz, D. O. Riska, Nucl. Phys. A **755**, 431c (2005).

The $\omega\rho\pi$ coupling in the VMD model revisited

David García Gudiño[1] and G. Toledo Sánchez
Instituto de Física, Universidad Nacional Autónoma de México
AP 20-364, México D.F. 01000, México

We determine the value of the $\omega - \rho - \pi$ mesons coupling ($g_{\omega\rho\pi}$), in the context of the vector meson dominance model, from radiative decays, the $\omega \to 3\pi$ decay width and the $e^+e^- \to 3\pi$ cross section. For the last two observables we consider the presence of a contact term as mimic by a heavier resonance and find its magnitude to be close to other approaches. Our global average is $g_{\omega\rho\pi} = 13.8 \pm 0.1$ ($g_{\omega\rho\pi} = 11.3 \pm 1$) without (with) contact term. Although the value obtained is sensitive to the inclusion of the contact term, the current precision allows to accommodate its effects within the error bars.

1 Introduction

The coupling between the ω, ρ and π mesons ($g_{\omega\rho\pi}$) encodes the strength of the strong interaction between them. It is required in processes where the vertex appear as a subdiagram; some of these processes have an increasing experimental accuracy because of their implications in observables like the muon magnetic moment [1]. The direct determination of its magnitude would require the observation of the ω decaying into the others, but since there is not enough phase space to allow for the three particles to be on the mass shell, it must be extracted by indirect means. In the vector meson dominance (VMD) model it can be obtained from a set of different vectorial radiative decays, or in processes containing this vertex, for example the decay of the ω meson into three pions, which is well known to be dominated by the $\rho\pi \to 3\pi$ channel [2]. In this process the presence of a possible contact term contributing to the decay may strongly influence the determination of $g_{\omega\rho\pi}$ coupling. In this work we determine the value of $g_{\omega\rho\pi}$ in the context of the VMD model from radiative processes, from the $\omega \to 3\pi$ decay and from the $e^+e^- \to 3\pi$ cross section. These last two processes allow the presence of a contact term. A contact term and a pinched diagram due to the presence of a heavier meson in the intermediate state have the same Lorentz structure; in fact, it has been suggested this last one as the origin of the contact term itself. Here we explore at which extent the vector meson $\rho'(1450)$ can mimic a truly contact term under the VMD idea in the low energy regime. We also examine the effects of this term in the $g_{\omega\rho\pi}$ determination.

[1]davidgarcia@fisica.unam.mx

2 The $g_{\omega\rho\pi}$ coupling from different processes.

- In the VMD scheme $g_{\omega\rho\pi}$ can be obtained from several radiative processes such as $\rho^- \to \pi^-\gamma$, $\rho^0 \to \pi^0\gamma$, $\omega \to \pi^0\gamma$ and $\pi^0 \to \gamma\gamma$ from which we can directly obtain the $g_{\rho\pi\gamma}$ or $g_{\omega\pi\gamma}$ coupling and then relate them to the $g_{\omega\rho\pi}$ through the VMD relations

  (1) $$g_{\omega\rho\pi} = g_{\rho\pi\gamma}g_\omega/e \qquad g_{\omega\rho\pi} = g_{\omega\pi\gamma}g_\rho/e,$$

  where g_V is the VMD coupling, accounting for the probability of the photon transmutation into V, and can be determined from the $V \to e^+e^-$ decay. The results from these processes have been averaged and the final result is shown in the Table 1 as the $\text{VMD}_{radiative}$ prediction.

- Consider the $\omega(q) \to \pi^+(p_1)\pi^-(p_2)\pi^0(p_3)$ decay, whose amplitude is given by:

  (2) $$\mathcal{M}_D = \imath\epsilon_{\mu\alpha\beta\gamma}\eta^\mu p_1^\alpha p_2^\beta p_3^\gamma \left(6g_{3\pi} + 2g_{\omega\rho\pi}g_{\rho\pi\pi}\sum_{a=\{+,-,0\}} D^{-1}\left[\rho^a, p_i + p_j\right]\right)$$

  where, $D[\rho, Q] = Q^2 - m_\rho^2 + im_\rho\Gamma_\rho$ and $g_{3\pi}$ is the contact term; the heavier mass of the ρ' allows us to make the approximation $|g_{3\pi}| \approx \frac{g_{\omega\rho'\pi}g_{\rho'\pi\pi}}{m_{\rho'}^2} (= 49 \pm 24\ GeV^{-3})$. It is remarkable that this simple approach can mimic the contact term in the same magnitude as predicted in other approaches [3]. To obtain the $g_{\omega\rho\pi}$ from this decay we require to reproduce the experimental value of the total width by adjusting the coupling in both cases: with and without a contact term. Our results for these adjustments are presented in Table 1.

- Finally, we consider the $e^+e^- \to \omega \to 3\pi$ process, which has an expression closely related to Eqn. 2. To obtain the $g_{\omega\rho\pi}$ coupling, we have computed the cross section for this process ensuring the reproduction of the experimental data [4] by adjusting the coupling constant in both cases with and without the contact term. Our results are presented in Table 1.

	Without contact	With Contact (ρ')
$\text{VMD}_{radiative}$	11.6 ± 0.2	$--$
$\Gamma(\omega \to 3\pi)$	15.7 ± 0.1	12.6 ± 1.3
$\sigma(e^+e^- \to 3\pi)$	13.1 ± 0.1	9.8 ± 1.4
Weighted Average	13.8 ± 0.1	11.3 ± 1

Table 1: Final values for the $\omega\rho\pi$ coupling (GeV^{-1}).

3 Discussion

Table 1 shows the different values for the $g_{\omega\rho\pi}$ coupling obtained from the processes discussed above. The $\text{VMD}_{radiative}$ prediction do not posses information about a contact term and for this reason it is only considered without this contribution. As it can be seen, the value obtained for $g_{\omega\rho\pi}$ is sensitive to the inclusion of the contact term. Our final results are the weighted average. A more detailed version of this work can be found in [5].

Acknowledgments

We acknowledge the support of CONACyT, Mexico.

Bibliography

[1] M. Benayoun, P. David, L. DelBuono, O. Leitner Eur. Phys. Jour C **65** 211(2010) ; ibid **68** 355(2010).

[2] M. Gell-Mann, D. Sharp, W. G. Wagner, Phys. Rev. Lett. 8 (1962) 460.

[3] S. Rudaz, Phys. Lett. B 145 281(1984).

[4] R.R. Akhmetshin et al. Phys. Lett. B **578** 285(2004).

[5] D. García Gudiño and G. Toledo Sánchez, arXiv:1106.1467v1 [hep-ph]

Weak decays of doubly charmed baryons

Eliecer Hernández[1,a], Conrado Albertus[a], and Juan Nieves[b]
[a]*Departamento de Física Fundamental e IUFFyM*
Universidad de Salamanca, E-37008 Salamanca, SPAIN
[b]*Instituto de Física Corpuscular (IFIC), Centro Mixto CSIC-Universidad de Valencia*
Institutos de Investigación de Paterna, Aptd. 22085, E-46071 Valencia, SPAIN

Within a nonrelativistic quark model, we evaluate exclusive semileptonic decays of ground-state spin-1/2 doubly heavy charmed baryons driven by a quark $c \to s, d$ transition.

We shall only present final results for the decay widths. For the interested reader, Ref. [1] gives a full account of our work. In particular, a discussion on heavy quark spin symmetry constraints on form factors and the level to which those constraints are satisfied for the actual c-quark mass can be found there.

The quantum numbers of the baryons involved in our study are shown in Table 1. Quark model masses have been taken from our previous works in Refs. [2, 3]. Experimental masses are the ones given by the PDG [4] and in the table we quote the average over the different charge states. With the exception of the Ξ_{cc}, the agreement is fairly good. In the calculation we use experimental masses. For the Ξ_{cc} which is not well established, and for the Ω_{cc}, for which there is no experimental information, we take our model predictions of $M_{\Xi_{cc}} = 3613\,\text{MeV}$ and $M_{\Omega_{cc}} = 3712\,\text{MeV}$.

In Table 2 we give our results. To the best of our knowledge there are just a few other calculations of exclusive semileptonic decays of ground-state spin-1/2 doubly charmed baryons. Those are also shown in Table 2 for comparison. In Ref. [5] only the $\Xi_{cc} \to \Xi_c' e^+ \nu_e$ decay was evaluated using the relativistic three-quark model. In Ref. [6], the authors use heavy quark effective theory and non-relativistic QCD sum rules to evaluate both the lifetime of the Ξ_{cc} baryon and the branching ratio for the combined decay $\Xi_{cc} \to \Xi_c e^+ \nu_e + \Xi_c' e^+ \nu_e + \Xi_c^* e^+ \nu_e$ from which we have obtained the semileptonic decay widths shown in the table. We find a fair agreement of our predictions with both calculations. We also give results for exclusive semileptonic $c \to s$ decays of the Ω_{cc}^+ baryon and for sub dominant $c \to d$ decays of both the Ξ_{cc}^{++}, Ξ_{cc}^+ and Ω_{cc} baryons.

[1] gajatee@usal.es

Baryon	J^π	S^π	Quark content	Mass [MeV]	
				Quark model [2,3]	Experiment [4]
Ξ_{cc}	$\frac{1}{2}^+$	1^+	ccn	3613	3518.9
Ω_{cc}	$\frac{1}{2}^+$	1^+	ccs	3712	–
Λ_c	$\frac{1}{2}^+$	0^+	udc	2295	2286.5
Σ_c	$\frac{1}{2}^+$	1^+	nnc	2469	2453.6
Σ_c^*	$\frac{3}{2}^+$	1^+	nnc	2548	2518.0
Ξ_c	$\frac{1}{2}^+$	0^+	nsc	2474	2469.3
Ξ_c'	$\frac{1}{2}^+$	1^+	nsc	2578	2576.8
Ξ_c^*	$\frac{3}{2}^+$	1^+	nsc	2655	2645.9
Ω_c	$\frac{1}{2}^+$	1^+	ssc	2681	2695.2
Ω_c^*	$\frac{3}{2}^+$	1^+	ssc	2755	2765.9

Table 1: Quantum numbers of the baryons involved in this study. J^π is the spin-parity of the baryon, while S^π is the spin-parity of the two heavy or the two light quark subsystem. n denotes a u or d quark.

		This work	[5]	[6]
$\Gamma(\Xi_{cc}^{++} \to \Xi_c^+ e^+ \nu_e)$	$(c \to s)$	8.75×10^{-2}		
$\Gamma(\Xi_{cc}^{+} \to \Xi_c^0 e^+ \nu_e)$	$(c \to s)$	8.68×10^{-2}		
$\Gamma(\Xi_{cc}^{++} \to \Xi_c'^+ e^+ \nu_e)$	$(c \to s)$	0.146	$0.208 \div 0.258$	
$\Gamma(\Xi_{cc}^{+} \to \Xi_c'^0 e^+ \nu_e)$	$(c \to s)$	0.145	$0.208 \div 0.258$	
$\Gamma(\Xi_{cc}^{++} \to \Xi_c^{*+} e^+ \nu_e)$	$(c \to s)$	3.20×10^{-2}		
$\Gamma(\Xi_{cc}^{+} \to \Xi_c^{*0} e^+ \nu_e)$	$(c \to s)$	3.20×10^{-2}		
$\Gamma(\Xi_{cc}^{++} \to (\Xi_c^+ + \Xi_c'^+ + \Xi^{*+}) e^+ \nu_e)$	$(c \to s)$	0.266		$0.37 \pm 0.04^{(*)}$
$\Gamma(\Xi_{cc}^{+} \to (\Xi_c^0 + \Xi_c'^0 + \Xi_c^{*0}) e^+ \nu_e)$	$(c \to s)$	0.264		$0.47 \pm 0.15^{(*)}$
$\Gamma(\Xi_{cc}^{++} \to \Lambda_c^+ e^+ \nu_e)$	$(c \to d)$	4.86×10^{-3}		
$\Gamma(\Xi_{cc}^{++} \to \Sigma_c^+ e^+ \nu_e)$	$(c \to d)$	7.94×10^{-3}		
$\Gamma(\Xi_{cc}^{+} \to \Sigma_c^0 e^+ \nu_e)$	$(c \to d)$	1.58×10^{-2}		
$\Gamma(\Xi_{cc}^{++} \to \Sigma_c^{*+} e^+ \nu_e)$	$(c \to d)$	1.77×10^{-3}		
$\Gamma(\Xi_{cc}^{+} \to \Sigma_c^{*0} e^+ \nu_e)$	$(c \to d)$	3.54×10^{-3}		
$\Gamma(\Omega_{cc}^{+} \to \Omega_c^0 e^+ \nu_e)$	$(c \to s)$	0.282		
$\Gamma(\Omega_{cc}^{+} \to \Omega_c^{*0} e^+ \nu_e)$	$(c \to s)$	5.77×10^{-2}		
$\Gamma(\Omega_{cc}^{+} \to \Xi_c^0 e^+ \nu_e)$	$(c \to d)$	4.11×10^{-3}		
$\Gamma(\Omega_{cc}^{+} \to \Xi_c'^0 e^+ \nu_e)$	$(c \to d)$	7.44×10^{-3}		
$\Gamma(\Omega_{cc}^{+} \to \Xi_c^{*0} e^+ \nu_e)$	$(c \to d)$	1.72×10^{-3}		

Table 2: Decay widths in units of ps^{-1}. We use $|V_{cs}| = 0.97345$ and $|V_{cd}| = 0.2252$ taken from Ref. [4]. Results with an $(*)$, our estimates from the total decay widths and branching ratios in [6]. Similar results are obtained for $\mu^+ \nu_\mu$ leptons in the final state.

Acknowledgments

Research supported by contracts FIS2006-03438, FIS2008-01143/FIS, FPA2010-21750-C02-02, CSD2007-00042, PROMETEO/20090090 and by the EU HadronPhysics2 project, grant agreement no. 227431. C. A. thanks a Juan de la Cierva contract from the Spanish Ministerio de Educación y Ciencia.

Bibliography

[1] C. Albertus, E. Hernandez and J. Nieves, Phys. Lett. B **704**, 499 (2011).

[2] C. Albertus, J. E. Amaro, E. Hernandez and J. Nieves, Nucl. Phys. A **740**, 333 (2004).

[3] C. Albertus, E. Hernandez and J. Nieves, Phys. Lett. B **683**, 21 (2010).

[4] K. Nakamura et al. (Particle Data Group), J. Phys. G 37, 075021 (2010).

[5] A. Faessler, T. Gutsche, M. A. Ivanov, J. G. Korner and V. E. Lyubovitskij, Phys. Lett. B **518**, 55 (2001).

[6] V. V. Kiselev and A. K. Likhoded, Phys. Usp. **45**, 455 (2002) [Usp. Fiz. Nauk **172**, 497 (2002)] [arXiv:hep-ph/0103169]. See also A.I. Onishchenko, hep-ph/9912425; A.I. Onishchenko, hep-ph/0006271; A.I. Onishchenko, hep-ph/0006295.

Unprejudiced Look at Effective Continuum Thresholds in Borel Dispersive Sum Rules

Wolfgang Lucha[1,a], Dmitri Melikhov[a,b,c], and Silvano Simula[d]
[a]*HEPHY, Austrian Academy of Sciences, Nikolsdorfergasse 18, A-1050 Vienna, Austria*
[b]*Faculty of Physics, University of Vienna, Boltzmanngasse 5, A-1090 Vienna, Austria*
[c]*SINP, Moscow State University, 119991 Moscow, Russia*
[d]*INFN, Sezione di Roma Tre, Via della Vasca Navale 84, I-00146 Roma, Italy*

Dispersive sum rules represent long-standing tools for extracting hadron features from QCD; they are constructed by evaluating matrix elements of suitable operators (e.g. time-ordered products of quark currents) at the level of both hadron and QCD degrees of freedom. One's ignorance of hadronic excitations and continuum is circumvented by *'quark–hadron duality'*: beyond an *'effective threshold'* hadron and QCD contributions are *assumed* to cancel. We [1,2] estimate the error induced by such approximation and improve the accuracy of predictions by elevating our thresholds from constants to functions of momenta and a parameter T or τ entering upon *Borel transformation* [3]. This move enables us to define *dual correlators*, where the QCD member, truncated at effective threshold s_{eff}, *exactly* counterbalances the hadronic ground-state member; the form of s_{eff} can be determined by fitting known hadron features.

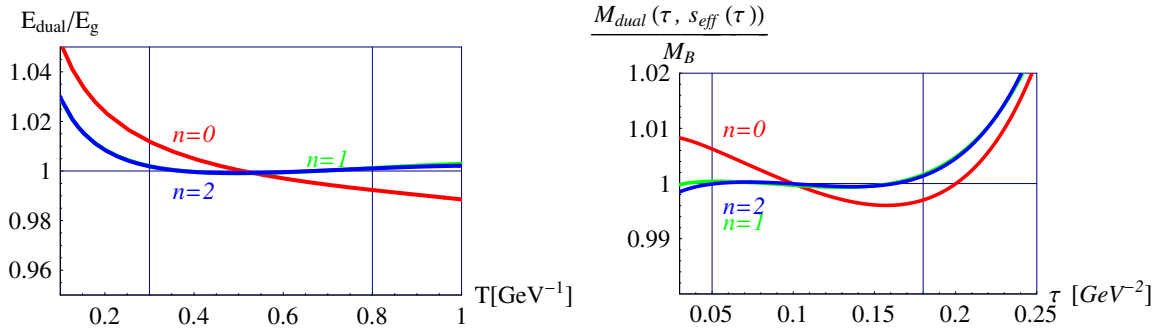

[1]Wolfgang.Lucha@oeaw.ac.at

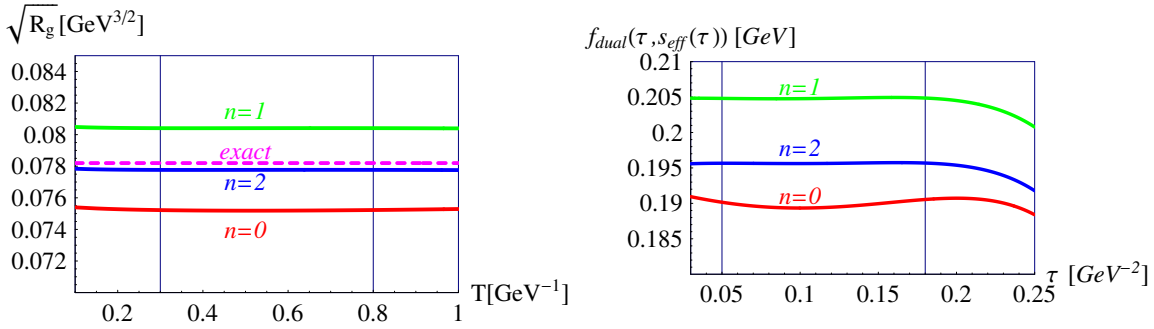

To scrutinize the applicability of our proposed modified sum-rule algorithm to QCD [4] we confront extractions of ground-state decay constants $\sqrt{R_g} \equiv |\Psi(\mathbf{0})|$ in quantum mechanics in terms of related wave functions $\Psi(\mathbf{x})$ with like extractions of heavy pseudoscalar-meson decay constants in QCD. The plots depict *dual* energy E_{dual} over true E_g and decay constant $\sqrt{R_g}$ resulting from the funnel potential describing heavy-quark bound states [5] (left), and B-meson mass M_{dual} over its experimental value M_B and decay constant f_{dual}, predicted by QCD (right), vs. the associated Borel parameter: Adopting polynomial Ansätze of degree n for the effective continuum thresholds, the band delimited by our $n = 1$ and $n = 2$ findings will provide an 'educated guess' of the intrinsic errors of bound-state features such as $\sqrt{R_g}$. The similarity of the procedures in quantum mechanics and QCD gives us great confidence that our sum-rule alterations will prove to be successful also in hadron phenomenology [6].

Acknowledgments

D.M. acknowledges support by the Austrian Science Fund (FWF) under Project No. P22843.

Bibliography

[1] W. Lucha, D. Melikhov, and S. Simula, Phys. Rev. D **76**, 036002 (2007); in *QCD@Work 2007*, eds. P. Colangelo *et al.*, AIP Conf. Proc. **964** (AIP, Melville, New York, 2007), p. 296; Phys. Atom. Nucl. **71**, 1461 (2008); Phys. Lett. B **657**, 148 (2007); in *Hadron 07*, eds. L. Benussi *et al.*, Frascati Phys. Ser. **46** (INFN, Laboratori Nazionali di Frascati, 2007), p. 1109; PoS Confinement8, 180 (2009).

[2] W. Lucha, D. Melikhov, and S. Simula, Phys. Lett. B **671**, 445 (2009); PoS Confinement8, 106 (2009); D. Melikhov, Phys. Lett. B **671**, 450 (2009).

[3] W. Lucha, D. Melikhov, and S. Simula, Phys. Rev. D **79**, 096011 (2009); J. Phys. G **37**, 035003 (2010); W. Lucha, D. Melikhov, H. Sazdjian, and S. Simula, Phys. Rev. D **80**, 114028 (2009).

[4] W. Lucha, D. Melikhov, and S. Simula, Phys. Lett. B **687**, 48 (2010); Phys. Atom. Nucl. **73**, 1770 (2010); in *QCD@Work 2010*, eds. L. Angelini *et al.*, AIP Conf. Proc. **1317** (AIP, Melville, New York, 2010), p. 316; in *QCHS IX*, eds. F. J. Llanes-Estrada and J. R. Peláez, AIP Conf. Proc. **1343** (AIP, Melville, New York, 2011), p. 624.

[5] W. Lucha, F. F. Schöberl, and D. Gromes, Phys. Rep. **200**, 127 (1991); W. Lucha and F. F. Schöberl, Int. J. Mod. Phys. A **7**, 6431 (1992).

[6] W. Lucha, D. Melikhov, and S. Simula, in *QCD@Work 2010*, eds. L. Angelini *et al.*, AIP Conf. Proc. **1317** (AIP, Melville, New York, 2010), p. 310; PoS ICHEP 2010, 210 (2010); J. Phys. G **38**, 105002 (2011); in *QCHS IX*, eds. F. J. Llanes-Estrada and J. R. Peláez, AIP Conf. Proc. **1343** (AIP, Melville, New York, 2011), p. 379; PoS QFTHEP2010, 058 (2010); Phys. Lett. B **701**, 82 (2011).

On lepton pair production in proton-antiproton collisions at intermediate energies and the main backgrounds.

Anna Skachkova[1] on behalf of the PANDA Collaboration
Joint Institute for Nuclear Research
Joliot-Curie 6, 141980 Dubna, Moscow region, Russia

The lepton pair production via the quark-antiquark annihilation subprocess in collisions of beam antiproton with the proton target at E_{beam} = 14 GeV (which corresponds to the center-of-mass energy of the $p\overline{p}$ system E_{cm} = 5.3 GeV) is studied on the basis of the event sample simulated by PYTHIA6 generator and PandaRoot package. Different kinematical variables which may be useful for design of the muon system and the electromagnetic calorimeter of the detector of PANDA experiment at FAIR, as well as for the study of proton structure functions in the available $x - Q^2$ kinematical region, are considered. The problems due to the presence of fake leptons that appear from meson decays, as well as due to the contribution of background QCD processes and minimum bias events, are also discussed. The set of cuts which allows one to separate the events with the signal lepton pairs from different kind of background events are proposed.

1 Introduction

This intermediate energy experiment ($E_{beam} < 15$ GeV) may play an important role because it allows to study the energy range where the perturbative methods of QCD (pQCD) come into interplay with a rich physics of bound states and resonances. A detailed and high-precision experimental study at PANDA may allow to discriminate between a large variety of existing nonperturbative approaches and models that already exist or are under development now. Dilepton events may serve as a powerful tool to get out the information about the parton distribution functions (PDFs) in hadrons [1]. The plans to study this process are included into the LoI and TPR of PANDA experiment at HESR. This study may provide an interesting information about quark dynamics inside the nucleon [2]. The results of study of leptons angle and energy spectra distributions, based on this Monte-Carlo simulation, was used for a proper geometrical design of PANDA muon system.

[1]Anna.Skachkova@cern.ch

2 Observations and Interpretation

The work presents the distributions of the most essential kinematical variables of individual leptons from $\overline{p}p \rightarrow l^+l^- + X$ (MMT-DY) and benchmark $\overline{p}p \rightarrow J/\psi + X$ ($J/\psi \rightarrow l^+l^-$) processes. These distributions allow one to estimate the energy, transverse momentum and angle ranges that may be covered by leptons produced in quark-antiquark annihilation process. The PYTHIA6 simulation has shown that one may expect to gain about $7 \cdot 10^7$ MMT-DY events per year for the luminosity $L = 2 \cdot 10^5$ mb^{-1}s^{-1}.

The study of kinematical characteristics of lepton pair as a whole system was also done. The analysis of distributions allowed to determine the region in x-Q^2-plane which can be available for measuring the proton structure function at PANDA: $0.05 \leqslant x \leqslant 0.7$ and $Q^2 \leqslant 6.25$ GeV.

An important problem of background suppresion is also considered. The histograms which demonstrate the relative contribution of different parents and grandparents of produced leptons are presented. According to PYTHIA, the fraction of signal dimuon events which include fake muons is about 16.6%. In a case of electrons the number of signal events fraction containing fake electrons is about 2%. The set of three cuts is proposed which allows to reduce the fraction of the signal events containig fake decay leptons to the values $fr_\mu = 0001\%$ in a case of $\mu^+\mu^-$ production and $fr_e = 0.008\%$ in e^+e^-. Much more dangerous background is caused by minimum-bias and QCD events. The proposed set of five cuts allows to get rid completely of minimum-bias and QCD background contribution in the $\mu^+\mu^-$ case and to reach the value of $S/B = 3.8$ for the e^+e^- case.

It was also noted that the study of events with two (and even three) lepton pairs would allow to improve the precision of the parameters of multiple quark interactions, which measurement will extend the region of QCD studies.

Acknowledgments

I am grateful to my coauthors for useful discussions and proposed topics for investigation. Additional thanks to FAIR-Russia Research Center (together with Federal Agency for Atomic Energy (Rosatom) and Helmholtz Association) for finantial support.

Bibliography

[1] A.N.Skachkova, N.B.Skachkov, G.D.Alexeev, arXiv: hep-ph/0506139v2;

[2] A.N.Skachkova, N.B.Skachkov, Phys.Part.Nucl.Lett, 2009, v.6, N4(153), p.504-518.

Pion-exchange tensor forces in nuclear excitations

Sergey I. Sukhoruchkin[1]
Petersburg Nuclear Physics Institute 188300 Gatchina, RUSSIA

Tensor nuclear forces are result of the pion-exchange and we consider these forces in connection with the origin of the systematic character of excitations and spacing in many nuclei: the observed frequent appearance of stable energy intervals with values rationally connected with the nucleon and the lepton (m_e) mass differences. This tuning effect includes pion mass, its mass difference ($9m_e$), residual interaction of nucleon quarks and nucleon masses.

The pion plays an important role in nuclear physics. Nucleon interactions in nuclei are considered as a result of the meson exchange. The role of tensor forces connected with the pion exchange in descriptions of nuclear binding energies and excitations was discussed in [1-3]. A combinations of spin/orbit values (parallel spin, orbital motions in opposite directions) are conditions for a manifestation of the pion exchange. We performed an analysis of excitations (E^*) in nuclei at different nuclear shells where tensor forces are important.

In sum E^* distributions of all nuclei (A$\leqslant$70, A$\leqslant$150) maxima corresponding to frequently appeared excitations are found at E^*=1022 keV=$2m_e$ and E^*=646-1293-1942 keV connected as 1/2-1-3/2 with the nucleon mass differences δm_N=1293.3 keV. This correlation was named "tuning effect" and some of coincidences observed in near-magic light nuclei are shown in Table 1 (top). The interval D=ε_o=1022.0 keV=$2m_e$ in ^{10}B (close to 2/9 of the pion mass difference [2,3]) corresponds to the spin-flip effect of nucleons in 1p shell.

The observed exact relation 3:1 in E^* of ^{41}Ca and ^{37}S (Table 1 right, valence neutron and pairs of protons in $1d_{3/2}$ shell, number of pairs 3 and 1) and the exact 1:2 relation in E^* of ^{37}S and ^{38} (N=21-22, one-two valence neutrons and a pair of protons above the subshell Z=14) correspond to a stable character of the interaction between nucleons with opposite orbital motions (tensor forces due to pion exchange dynamics). Stable intervals D=1293 keV were noticed also in sum spacing distribution in levels of ^{32,33}S. The first excitation in ^{32}Si (E^*=1941.5 keV, two holes in $1d_{3/2}$ subshell) coincides with (3/2)δm_N. We use analyses of D-distributions to check the observed regularities in low-lying excitations. Stable intervals close or rational to parameters ε_o and δm_N were observed in spacing of near-magic ^{18}F (Fig.1, D=162 keV, other D=480-642-1288 keV, n=1,3,4,8), in ^{23}Na (D=337-428-514 keV), ^{57}Ni (D=341 keV), ^{55}Co (D=324-512-682 keV) and ^{89,90}Y (D=482, 511-1024 keV).

[1]sergeis@pnpi.spb.ru

Table 1: *Top:* Comparison of excitations (in keV) of near-magic nuclei with spin-flipp effect in ^{10}B (ε_o=1022 keV) and δm_N=1293.3 keV. *Bottom:* The same for ^{101,103}Sn, $^{123-133}$Sb.

^AZ	^{10}B	^{10}B	^{12}C	^{18}Ne		^{41}Ca	^{37}S	^{38}S
J^π	0^+-1^+	2^-	0^+ (T=2)	0^+	0_2^+	3/2-	3/2-	2+
E^*	1021.8(2)	5110.3	27595(2)	3576.2	4590(8)	1942.8	646.2	1292.0
n(ε_o)	1	5	27	7/2	9/2	(3/2)δm_N	(1/2)δm_N	δm_N
Diff.	0.2(2)	0.3	1(2)	1(2)	9(8)	2(1)		1
^AZ	^{101}Sn	^{103}Sn	^{123}Sb	^{125}Sb	^{127}Sb	^{129}Sb	^{131}Sb	^{133}Sb
J^π	$7/2^+$	$7/2^+$	$5/2^+$	$5/2^+$	$5/2^+$	$5/2^+$	$5/2^+$	$5/2^+$
E^*	171.7(6)	168.0(1)	160.3(1)	332.1	491.2	645.2(1)	798.5	962.3(1)
n(ε_o)	1/3	1/3	(1/8)δm_N	δm_N/4	(3/8)δm_N	(4/8)δm_N	(5/8)δm_N	(6/8)δm_N
n·ε_o	170	170	161	323	484	646	808	969

In ^{101,103}Sn with valence neutrons above Z=N=50 core a stable character of excitations 170 keV=(1/6)ε_o=m_e/3 is shown in Table 1. Intervals D=512-3×170 keV and D=648-1293 keV in ^{97,98}Pd, stable E^*=644 keV in nuclei around the tin, E_1^*=1293.6 keV in ^{116}Sn and the interval D=1292.0 keV from it to the 1^+ state (D=δm_N) correspond to the tuning effect.

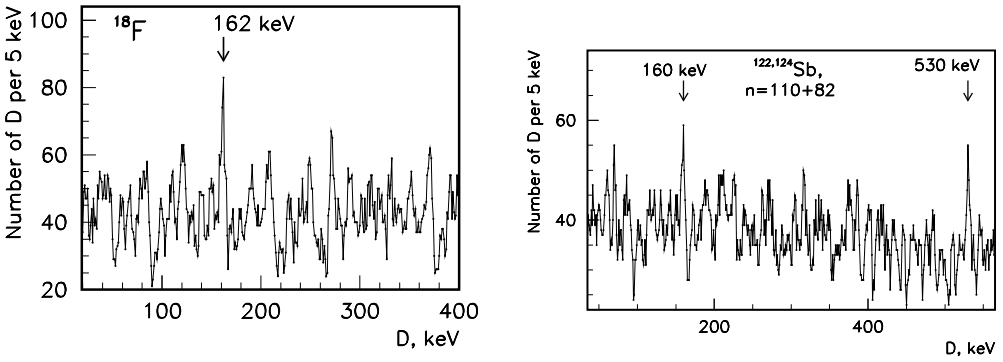

Figure 1: Maxima in spacing distributions in levels of ^{18}F and ^{122,124}Sb (right).

T.Otsuka [1] explained a linear trend of E^* in $^{123-133}$Sb (found by J.Schiffer et al.) as an action of tensor forces. The case in Sb isotopes ($\pi\ 2g_{7/2}$, $\nu\ 1h_{11/2}$) is similar to the discussed case of Ca-S-Si isotopes ($1d_{3/2}$, $1f_{7/2}$). The effect in Sb (constant slope 160 keV) is supported by the stable D=160 keV in neighbour ^{122,124}Sb (maximum in D-distribution, Fig.1 right).

The interval 3×161 keV=483 keV appears frequently together with D=492 keV and is substituted with it in ^{127}Sb. Stable D=492-984-3936 keV (n=1-2-4 of 492 keV=2×161 keV+170 keV) were found in many nuclei. In ^{38}Ar two stable intervals are D=1021 keV=2×511keV and

D=1476 keV=3×492 keV. Stable nucleon interaction was checked with data for all nuclei. Intervals (or periods) D=161 keV, 170 keV and 492 keV were found in many nuclei. Z-distribution of nuclei with such effects is shown in Fig.2. Maxima in regions Z=50-51 (ν $1h_{11/2}$) and Z=72-78 (π $1h_{11/2}$) are clearly seen. Stable interaction between nucleons was observed also as a linear dependence of proton separation energies (upon N, parameters ε_{p2n}=$S_p(N)$-$S_p(N-2)$=(2/3)ε_o and ε_{2n2p}=(4/3)ε_o for Z=51, 78 and 84).

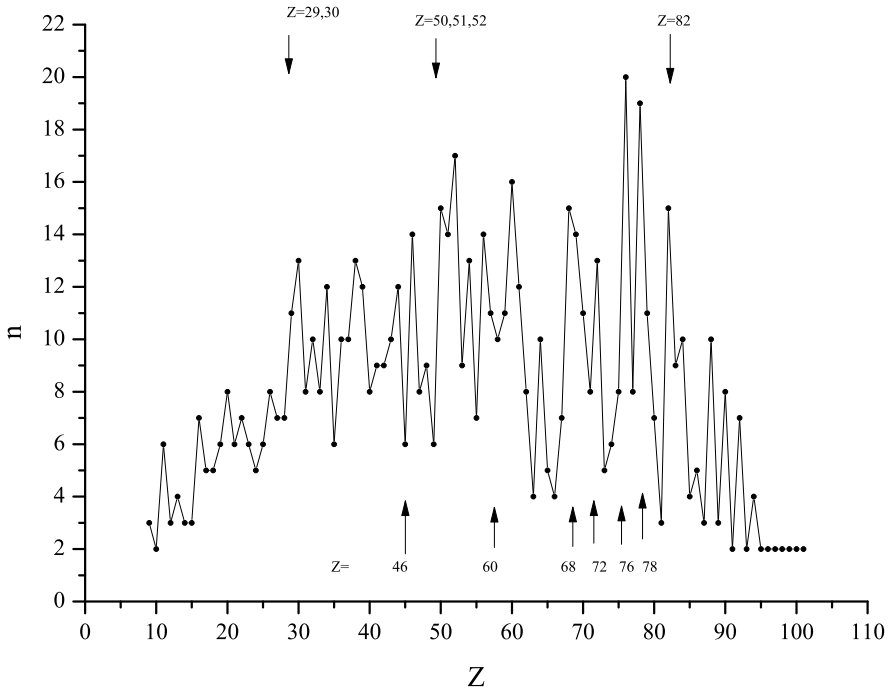

Figure 2: Distribution of Z-numbers of nuclei with stable intervals (arrows mark shells).

We considered nonstatistical effects in neutron resonances of the same nuclei. Maxima at D=373-745-1501 eV and 570 eV in D-distribution of resonances in ^{124}Sb are close to D=572 and 749-1496 eV in ^{105}Pd, ^{104}Rh, Th, ^{80}Br, Hf. One of exactly measured small splitting in low-lying levels of near-magic nuclei is D=1.078 keV between E^*=1022.394 and E^*=1021.326 in ^{82}Br corresponding to the grouping effect at E^*=ε_o. The relative values of this splitting 1.08/1022=1.06·10^{-3} and ratios between Sb intervals 373 eV/323 keV=1.15·10^{-3}, 570 eV/490 keV=1.16·10^{-3} are close to the QED radiative correction $\alpha/2\pi$=1.16·10^{-3}.

Long-range correlations in differences of nuclear binding energies ΔE_B connected with nucleon cluster effects were considered in [3] where the similar tuning effect was discussed.

Nucleons have a complex structure consisting (in the first approximation) of three con-

Table 2: Presentation of parameters of tuning effects in particle masses and nuclear binding energies ΔE_B (upper parts marked X = -1, 0, 1 at left) and in nuclear data (X = 1, 2 bottom) by expression $n \cdot 16 m_e (\alpha/2\pi)^X M$ with QED radiative correction $\alpha/2\pi$ (α=137^{-1}). Boxed values m_π-m_e, $m_e/3$ and neutron mass shift $N\delta - m_n - m_e$ relate to $(2/3)m_t = M_H$ with parameters α_Z=129^{-1} and α=137^{-1}. Stable intervals in E*, D_{ij} (X=1) and in neutron resonances (X=2) are considered as confirmation of intervals in particle masses (X=-1), namely, the mass grouping in TEVATRON experiment Δ°=4 GeV, 3:2:1 ratio between masses of top quark, Higgs boson and mass grouping effect in LEP experiment (M^{L3}) [3].

X	M	n = 1	n = 13	n = 14	n = 16	n = 17	n = 18
-1	$\frac{3}{2}$,$\frac{1}{2}$				m_t=171, M^{L3}=58		
GeV	1	$2\Delta^\circ$ - $2M_q$	M_Z=91.2		$\boxed{M_H=115}$		
0	1	$16m_e=\delta$	m_μ = 105.7		(f_π=131)	$\boxed{m_\pi\text{-}m_e}$	m_Δ-$m_n/2$=147
MeV	1	2Δ-ε_0	106 = ΔE_B		130 = ΔE_B	140 = ΔE_B	147.2 = ΔE_B
	3				$M''_q = m_\rho/2$	M'_q = 420	M_q = 441 = ΔE_B
1	1					$\boxed{N\delta - m_n\text{-}m_e = 161.6}$	$\boxed{170 = m_e/3}$
keV	1,3	9.5 = δ'	123	134	152, 455	162 (^{18}F), 160 (Sb)	172, 512 (Co)
	4,6		492	530		648 (^{97,98}Pd)	682(Co), ε_0
	8		984	1060	1212	1293 (Pd), ΣE^*	1360 (Te)
2	1,2,4	δ'',22,44	143		176	187, 373 (Sb), 749 (Br)	D in neutron
eV	8	88	570 (Sb)			1500 (Sb,Pd,Rh,Hf)	resonances

stituent quarks with the initial mass $M_q \approx$440 MeV originated from gluon quark-dressing effect. The residual quark interaction (nucleon Δ-excitation) and the effect of nearly constant binding energy of nucleons in nuclei correspond to strong interaction. Relations between particle masses, nuclear excitations and ΔE_B are given in Table 2 [3].

It was suggested by Y.Nambu that empirical relations in particle masses should be used for the development of the Standard Model. The appearance of the SM-parameter m_e and nucleon mass difference δm_N in nuclear data confirms this suggestion. For construction of Table 2 a proximity of QED factor $\alpha/2\pi$ to ratios between lepton masses (m_e, m_μ) and well-known parameters (Δ-excitation, Z-boson mass) were used. We use also exactly known experimental ratio between proton and electron masses to obtain relation between them (boxed in the central part of the Table). Both discussed intervals in nuclear excitations are related to the pion mass with QED factors $\alpha/2\pi$ and $\alpha_Z/2\pi$ (α_Z=1/129).

Bibliography

[1] T. Otsuka, T. Suzuki, Y. Utsuno : Nucl. Phys. A **805**, 127c (2008).

[2] Landoldt-Boernstein New Series, **vol. I/25A**, H. Schopper, ed. (Springer, 2012).

[3] Sukhoruchkin, S., Sukhoruchkin, D. : Int. J. Mod. Phys. E **20**, 906 (2011).

Hadronization in Nuclei – Multidimensional Study

Inti Lehmann[1] on behalf of the HERMES Collaboration
Department of Physics and Astronomy
University of Glasgow
Glasgow, G12 8QQ, Scotland/UK

Hadron multiplicities in semi-inclusive deep-inelastic scattering were measured on neon, krypton and xenon targets relative to deuterium at an electron-beam energy of 27.6 GeV at HERMES. These ratios were determined as a function of the virtual-photon energy ν, its virtuality Q^2, the fractional hadron energy z and the transverse hadron momentum with respect to the virtual-photon direction p_t. Dependences were analysed separately for positively and negatively charged pions and kaons as well as protons and antiprotons in a two-dimensional representation. These results will help to constrain mechanisms and models of hadronization much more decisively than by the use of integrated results as traditionally done. A few features particular to the two-dimensional representation are highlighted in this contribution.

Semi-inclusive production of hadrons in deep-inelastic lepton nucleus scattering (SIDIS) provides a way to study quark fragmentation or hadronization. Lepto-production of hadrons has the virtue that the energy and momentum transfered to the hit parton are well determined, as it is "tagged" by the scattered lepton. In these studies the nucleus is basically used as a scale probe of the underlying hadronization mechanism: by using nuclei of increasing size one can investigate the the space(time) development of hadronization.

The ratio of normalised yields Y_A^h on neon (Ne), krypton (Kr) and xenon (Xe) targets, denoted by A, compared to the same quantity on a deuterium D target: $R_A^h = Y_{\mathrm{A}}^h / Y_{\mathrm{D}}^h$ was measured with the HERMES spectrometer [1] at DESY, where h indicates positively and negatively charged pions ($\pi^{+/-}$) and kaons ($\mathrm{K}^{+/-}$), protons (p) and antiprotons ($\overline{\mathrm{p}}$). For the first time a two-dimensional representation is chosen for all hadrons separately. This allows to observe features that are hidden when integrating over large kinematic ranges. Details, references to previous measurements and theoretical studies can be found in Ref. [2].

The results show, for example (see Fig. 1), that π^+ and π^- behave similarly. However, their dependences with the virtual-photon energy ν change with the fraction carried by the hadron z. K^+ show different features compared to K^- which could be due to their different quark content. Particularly striking is the behaviour of protons, which show completely different trends in different ranges of z. Presumably, this is due to a sizable contribution of final-state interactions, such as knock-out processes, in addition to the fragmentation process.

[1] inti.lehmann@glasgow.ac.uk

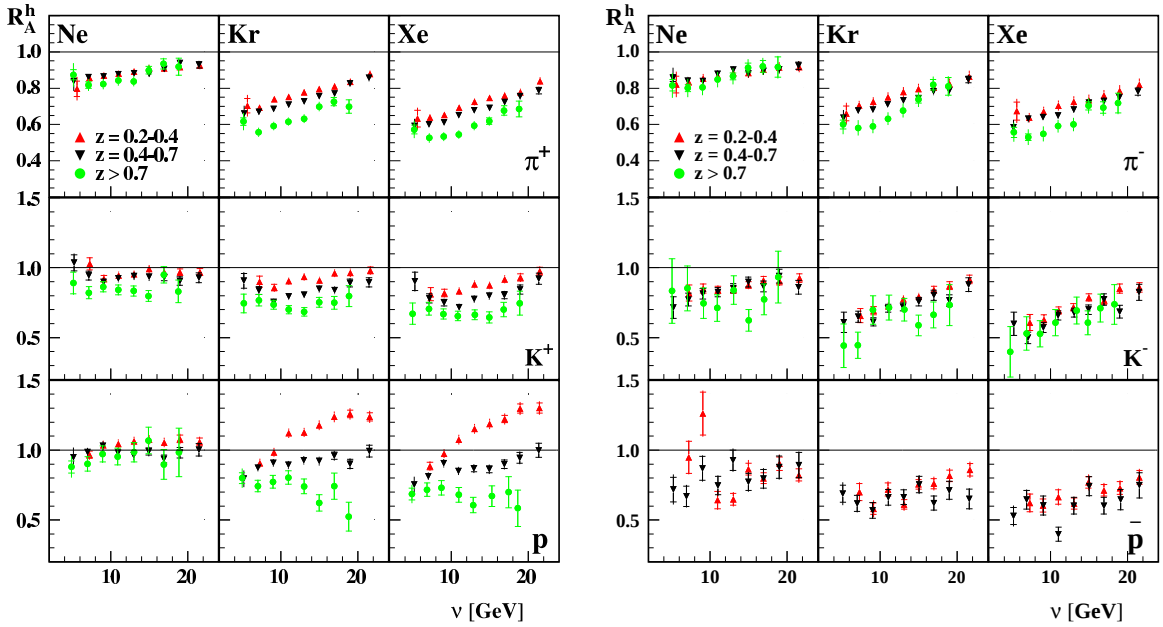

Figure 1: Dependence of R_A^h on ν for positively and negatively charged hadrons for three slices in z as indicated in the legend. The inner and outer error bars indicate the statistical and total uncertainties, respectively. For the latter the statistical and systematic bin-to-bin uncertainties were added in quadrature. In addition, scale uncertainties of 3%, 5%, 4%, and 10% are to be considered for pions, kaons, protons and antiprotons, respectively.

In conclusion, the two-dimensional distributions of R_A^h for identified π^+, π^-, K^+, K^-, protons and antiprotons, measured at HERMES [2], provide detailed information which is generally not accessible in the one-dimensional distributions (in which all kinematic variables except one are integrated over, as has been traditionally done). These new detailed data are expected to be an essential ingredient for constraining models of hadronization and, hence, improving our understanding of hadron formation.

We gratefully acknowledge the DESY management for its support, the staff at DESY and the collaborating institutions for their significant effort, and our national funding agencies for financial support.

Bibliography

[1] K. Ackerstaff *et al.* [HERMES], NIM A417 (1998) 230.

[2] A. Airapetian *et al.* [HERMES], Eur. Phys. J. A 47 (2011) 113.

Charmonium spectra at finite temperature from a Bayesian analysis of QCD sum rules

Philipp Gubler[1,a], Kenji Morita[b], and Makoto Oka[a]
[a]*Department of Physics, Tokyo Institute of Technology, Meguro, Tokyo 152-8551, Japan*
[b]*Yukawa Institute for Theoretical Physics, Kyoto University, Kyoto 606-8502, Japan*

Charmonium spectral functions at finite temperature are studied, making use of a recently developed method of analyzing QCD sum rules. Employing the Maximum Entropy Method enables us to directly obtain the spectral function from the sum rules, without having to introduce any specific assumption about its functional form. QCD sum rules incorporate finite temperature effects in form of changing values of the various gluonic condensates that appear in the operator product expansion. These changes depend on the energy density and pressure at finite temperature, which we extract from lattice QCD. As a result, J/ψ, η_c, χ_0 and χ_1 dissolve into the continuum already at temperatures around or slightly above the critical temperature T_c.

1 Introduction

The method of QCD sum rules [1] provides a powerful tool for investigating the properties of hadrons at finite temperature directly from QCD [2]. Using this approach the charmonium system was studied recently [3], and evidence for a considerable change just above T_c in the spectral functions of various channels was found. To specify the nature of this change is the major goal of the present study. For this task we employ the Maximum Entropy Method (MEM), which is applicable to QCD sum rules [4] and has the advantage that one does not have to introduce any strong assumption about the functional form of the spectral function, such as the "pole + continuum" ansatz, which is often used in QCD sum rule studies. This approach is especially suitable for the investigation of spectral functions at finite temperature, whose behavior can change drastically above the deconfinement temperature T_c. In these proceedings, we can only show the most important results of our investigation, while more details can be found in [5].

[1]phil@th.phys.titech.ac.jp

2 Results

Obtained spectral functions of the vector and pseudoscalar channels at several temperatures are shown in Fig. 1. The lowest peaks corresponding to the J/ψ and η_c are observed to disappear ("melt") just above the critical temperature T_c. The peaks appearing in the scalar and axial-vector channels, which represent the χ_0 and χ_1 resonances, exhibit a similar behavior. This melting effect is caused by a sudden change of the gluonic condensates around T_c. As was shown in [3], this change can be related to the behavior of the energy density and pressure of gluonic matter in this temperature region. A more thorough discussion on all important details of this study will be given in [6].

Furthermore, we note that the same calculation can be done also for bottomonium channels. Such an investigation is presently in progress.

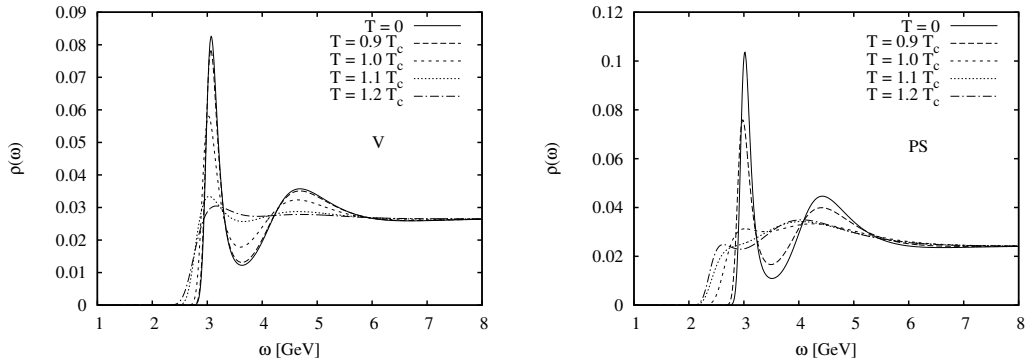

Figure 1: Spectral functions in the vector (left) and pseudosclalar channel (right). For obtaining these curves the default model was chosen to be a constant with a value adjusted to the perturbatively calculated spectral function at large energy.

Bibliography

[1] M.A. Shifman, A.I. Vainshtein, and V.I. Zakharov, Nucl. Phys. **B147**, 385 (1979); **B147**, 448 (1979).

[2] T. Hatsuda, Y. Koike and S.H. Lee, Nucl. Phys. **B394**, 221 (1993).

[3] K. Morita and S.H. Lee, Phys. Rev. Lett. **100**, 022301 (2008).

[4] P. Gubler and M. Oka, Prog. Theor. Phys. **124**, 995 (2010).

[5] P. Gubler, K. Morita and M. Oka, Phys. Rev. Lett. **107**, 092003 (2011).

[6] P. Gubler, K. Morita and M. Oka, in preparation.

$I = 1/2$ scalar meson in lattice QCD

Motoo Sekiguchi[1,a], Teiji Kunihiro[b], Shin Muroya[c], Atsushi Nakamura[d], Chiho Nonaka[e], and Hiroaki Wada[a]
[a]*Kokushikan University,* [b]*Kyoto University,* [c]*Matsumoto University,* [d]*Hiroshima University,* [e]*Nagoya University*

We present our recent study of I=1/2 scalar meson (κ meson) by the lattice QCD simulation.

1 Introduction

The I=0 scalar meson (σ) and I=1/2 meson (κ) are still a source of debated. The σ meson is now listed in the table of the Particle Data Group (PDG) [1]. Recent experimental candidates for the neutral κ are reported to have a mass about 800 MeV [2,3]. Moreover the charged κ is observed to be about 800 MeV by BES II collaboration [4,5]. However, the κ meson is not currently included in the table of the PDG summary [1]. These mesons can not be usual $q\bar{q}$ mesons as described in the non-relativistic costituent quark model since in such a quark model, J^{PC}=0^{++} meson is realized in the $^3P_0$ state, which implies that the mass of the these mesons must be as high as $1.2 \sim 1.6$ GeV. Several approches based on QCD have been performed the understanding of the structure of these mesons have not been setled yet [6–8].

There have been several attempts at lattice study of I=1/2 scalar meson. The first such calculation was carried out our (Scalar) collaboration [9]. All the lattice results for I=1/2 scalar meson with the used $\bar{s}q$ (where q is u and d) operator are consistent with mass of the K_0^*, but inconsistent the κ meson [9,10,12–14]. Recently , Prelovsek *et al.* presented the I=1/2 light scalar meson using the tetra quark type interpolating operators with the dynamical simulations and quenched simulations [15]. However they omitted the disconnected contributions.

2 Method and simulation

We perform dynamical simulations on I=1/2 scalar meson with much higher statistics and lager lattice volume than the previous simulations. We report the current status of our new data.

[1]motoo@kokushikan.ac.jp

We use gauge configurations from CP-PACS collaboration [16]. These configurations were generated with renormalization group improved gauge action and the Wilson-clover quark action. Our calculation is based upon the variational method. This method is to use several interpolating operators. The following interpolating operators were adopted the $\bar{s}_i \Gamma q_j$, (i, j =p, n, w). These operators are constructed from Jacobi smeared quarks of Gaussian type sources and sinks [11]. The subscript p denotes the point source. And the subscripts n, w denote the type of smearing used. Γ is gamma matrix.

We use 70 gauge configurations for our analysis of I=1 channel. We work on $16^3 \times 32$ lattice at β=1.95 and C_{sw}=1.5300 with a=0.1555(17) fm. The vale of the hopping parameter for $h_{u/d}$ for u/d quark is $h_{u/d}$=0.1390. Our mass ratio form_π/m_ρ = 0.741(5) is consistent with m_π/m_ρ =0.752(1) by CP-PACS with hopping parameter h=0 .1390.

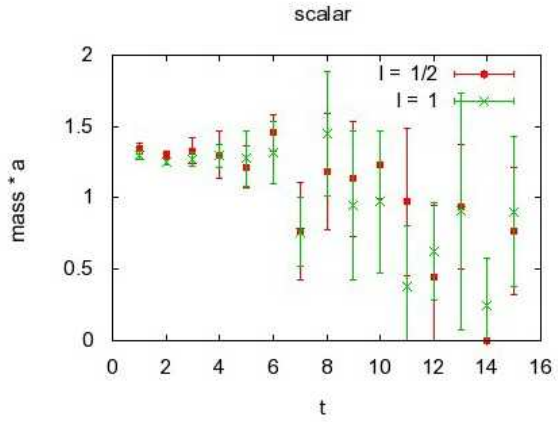

Figure 1: Effective mass of a_0 (I=1) and κ (I=1/2).

For our analysis of I=1/2 channel, we use 50 gauge configurations. We work on $16^3 \times 32$ lattice at β=1.95 and C_{sw}=1.5300 with a=0.1555(17) fm. The value of the hopping parameter for $h_{u/d}$ for u/d quark is $h_{u/d}$=0.1390 and the value of hopping parameter for s quark is h_s=0.1375. The s quark is valence approximation. Figure 1 shows the results for the effective mass a_0 (I=1) and κ meson. We have presented tentative results for mass ratio m_{a_0}/m_ρ=1.30(6) and m_κ/m_ρ=1.29(5).

3 Summary

Our simulations are the preliminary stage. The mass for scalar meson is more noisy than for π meson and ρ meson. It is necessary to generate much more gauge configurations and improve the statistical precision of the estimation of the κ meson.

The calculation was carried out on SX-9 at RCNP, Osaka University.

Bibliography

[1] Particle Data Group Collaboration, K. Nakamura *et al.*, J. Phys. **G37** 075021 (2011).

[2] E791 Collaboration, M. Aitala *et al.*, Phys. Rev. Lett. **89**, 121801 (2002).

[3] BES Collaboration, M. Ablikim *et al.*, Phys. Lett. **B633**, 681 (2006).

[4] BES Collaboration, M. Ablikim *et al.*, Phys. Lett. **B693**, 88 (2010).

[5] BES Collaboration, M. Ablikim *et al.*, Phys. Lett. **B698**, 183 (2011).

[6] S. Narison, Nucl. Phys. **B186** (Proc. Suppl.), 306 (2009), and references therein.

[7] T. Hyodo, D. Jido and T. Kunihiro, Nucl. Phys **848**, 341 (2010), and references therein.

[8] J. Nebreda and J.R. Peláez, Phys Rev **D81**, 054035 (2010), and references therein.

[9] SCALAR Collaboration, Phys. Rev. **D70**, 034504 (2004).

[10] SCALAR Collaboration, Phys. Lett. **B652**, 250 (2007).

[11] C. Gattringer *et al.*, Phys. Rev. **D78**, 034501 (2008).

[12] S. Prelovsek, C. Dawson, T. Izubuchi K. Orginos and A. Soni, Phys. Rev. **D70**, 094503 (2004).

[13] UKQCD Collaboration, C. McNeile and C. Michael, Phys. Rev. **D74**, 014508 (2006).

[14] N. Mathur *et al.*, Phys. Rev. **D76**, 114505 (2007).

[15] S. Prelovsek *et al.*, Phys Rev. **D82**, 094507 (2010).

[16] CP-PACS Collaboration, S. Aoki *et al.*, Phys. Rev. **D67**, 034503 (2003).

$\rho\rho N$ and $\rho\rho\Delta$ systems in the fixed center approximation of Faddeev equations

Bao-Xi Sun[1]
Institute of Theoretical Physics, Beijing University of Technology, Beijing 100124, China and IFIC, Universidad de Valencia, 46071 Valencia, Spain

The $\rho\rho N$ and $\rho\rho\Delta$ three-body systems have been studied within the framework of the fixed center approximation of Faddeev equation. The $\rho\rho$ interaction in isospin $I = 0$, spin $S = 2$ is strongly attractive, and so are the $N\rho$, $\Delta\rho$ interactions. This leads to bound states of both $\rho\rho N$ and $\rho\rho\Delta$. We find peaks of the modulus squared of the scattering matrix around 2227 MeV for $\rho\rho N$, and 2372 MeV for $\rho\rho\Delta$.

In Fig. 1, we show the results of $|T|^2$ for the $N\rho\rho$ system with $\Lambda = 875$ MeV, which is suited to obtain the $f_2(1270)$ resonance. We observe a peak around 2227 MeV with a width of 100 MeV. The peak does not have a standard Breit-Wigner form. The sharp peak could be indicative of a cusp effect but the threshold for $Nf_2(1270)$ is at 2210 MeV, about 17 MeV below the peak in Fig. 1. In fact, a small cusp peak at threshold is also visible in the figure

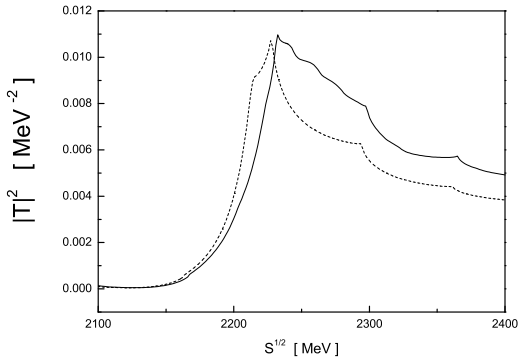

Figure 1: Modulus squared of the unitarized $N - \rho - \rho$ amplitude with $\Lambda = 875$ MeV. The solid line denotes the case with the $f_2(1270)$ decay width, and the dashed line is for the case without the $f_2(1270)$ decay width.

at this energy. On the other hand, when the convolution for the mass distribution of the

[1]sunbx@bjut.edu.cn

$f_2(1270)$ due to its width is considered, the peak of the cusp disappears, but a peak in $|T|^2$, slightly shifted to higher energies, still remains with a similar or slightly larger width.

In Fig. 2, we show the results of $|T|^2$ for the $\Delta\rho\rho$ system with $\Lambda = 875$ MeV. We observe a peak around 2372 MeV. Two features can be observed from Fig. 2. The peak has now an approximate Breit-Wigner shape and the strength of $|T|^2$ at the peak is about 200 times bigger than in Fig. 1 for the $N\rho\rho$ state, although the peak is now narrower than in Fig. 1. Yet, the integrated strength of the peak is still about 40 times bigger. The large value of T in the $\Delta\rho\rho$ case indicates that in a production of the resonance in one reaction, the magnitude of the resonance excitation would be large through the consideration of the intermediate $\Delta\rho\rho$ state and its coupling to the resonance. The consideration of the width of the $f_2(1270)$ reduces the strength of the peak and increases the width of the resonance. The width is still relatively small, about 25 MeV. In our approach, once the convolution for the width of the $f_2(1270)$ is done, the main decay channel would be $\Delta\pi\pi$. This is interesting to know from the experimental point of view.

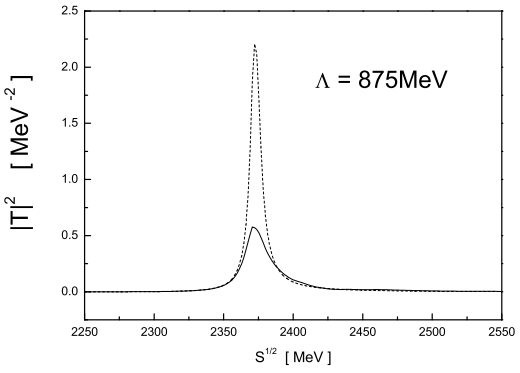

Figure 2: Modulus squared of the unitarized $\Delta - \rho - \rho$ amplitude with $\Lambda = 875$ MeV. The solid line denotes the case with the $f_2(1270)$ decay width, and the dashed line is for the case without the $f_2(1270)$ decay width.

Bibliography

[1] B. X. Sun,H. X. Chen and E. Oset, to be published in Eur. Phys. J. **A**, arXiv:1107.0209 [nucl-th] and references therein.

The $Y(3940)$, $Z(3930)$ and the $X(4160)$ as dynamically generated resonances from the vector-vector interaction

Raquel Molina[1] and Eulogio Oset
Instituto de Física Corpuscular (IFIC, centro mixto CSIC-UV), Valencia, Spain

We apply a unitary approach together with a set of hidden-gauge Lagrangians to study the vector-vector interaction. Concretely, we focus on the sector with quantum numbers charm $C = 0$ and strangeness $S = 0$ in the region around 4000 MeV. We get five poles, three of which could be identified with the Y(3940), Z(3930) and X(4160). These poles appear with quantum numbers $I = 0$ and $J^{PC} = 0^{++}, 2^{++}$ and 2^{++}, respectively, and can be considered as hadronic molecules made of $D^*\overline{D}^*$, $D_s^*\overline{D}_s^*$.

1 Introduction

The B-factories at SLAC, KEK and CESR, which were originally constructed to test matter-antimatter asymmetries or CP violation, have discovered new hidden-charm states around the energy region of 4000 MeV. Generally speaking, these states cannot be accomodated in the $c\bar{c}$ spectrum. They are naively called as XYZ particles.

In this talk we study the case of a system of two vector meson with charm $C = 0$ and strangeness $S = 0$ around 4000 MeV (hidden charm sector).

2 Formalism

Within the theorical framework, there are two main ingredients: first, we take the Lagrangians for the interaction of vector mesons among themselves, that come from the hidden gauge formalism of Bando-Kugo-Yamawaki [1]. Second, we introduce the potential V obtained from these Lagrangians (projected in s-wave, spin and isospin) in the Bethe Salpeter equation, $T = (\hat{1} - VG)^{-1}V$, where G is the loop function. Finally, we look for poles of the unitary T matrix in the second Riemann sheet. All this procedure is well explained in [2,3].

[1] rmolina@ific.uv.es

$I^G[J^{PC}]$	Theory		Experiment		
	(Mass, Width)	Name	Mass	Width	J^{PC}
$0^+[0^{++}]$	(3943, 17)	$Y(3940)$	3943 ± 17	87 ± 34	J^{P+}
			$3914.3^{+4.1}_{-3.8}$	33^{+12}_{-8}	
$0^-[1^{+-}]$	(3945, 0)	"$Y_p(3945)$"			
$0^+[2^{++}]$	(3922, 55)	$Z(3930)$	3929 ± 5	29 ± 10	2^{++}
$0^+[2^{++}]$	(4157, 102)	$X(4160)$	4156 ± 29	139^{+113}_{-65}	J^{P+}
$1^-[2^{++}]$	(3912, 120)	"$Y_p(3912)$"			

Table 1: Comparison of the mass, width and quantum numbers with the experiment. All the quantities are in units of MeV.

The results for the pole position obtained together with a possible assignment with some of the XYZ particles observed in the energy region of 4000 MeV is given in Table 1. While the Y(3940) and Z(3930) couple more to $D^*\overline{D}^*$ in the model, the X(4160) couples to $D_s^*\overline{D}_s^*$ mostly. The other two states, one with $I = 1$ and $J = 2$ and the other with $I = 0$ and $J = 1$ are predictions of the model.

3 Conclusions

We find five states with quantum numbers $I^G[J^{PC}] = 0^+[0^{++}], 0^-[1^{+-}], 0^+[2^{++}], 0^+[2^{++}]$ and $1^-[2^{++}]$ that are bound states or resonances made of $D^*\overline{D}^*$ and $D_s^*\overline{D}_s^*$ mostly. The states with $I^G[J^{PC}] = 0^-[1^{+-}]$ and $1^-[2^{++}]$ are predictions of the model whereas the others can be associated to the Z(3930), Y(4140) and X(4160). The region around 3940 MeV is very interesting and there could be more resonances not yet seen in this region.

Bibliography

[1] M. Bando, T. Kugo, S. Uehara, K. Yamawaki and T. Yanagida, Phys. Rev. Lett. **54**, 1215 (1985). M. Bando, T. Kugo and K. Yamawaki, Phys. Rept. **164**, 217 (1988). M. Harada and K. Yamawaki, Phys. Rept. **381**, 1 (2003)

[2] R. Molina, D. Nicmorus and E. Oset, Phys. Rev. D **78**, 114018 (2008)

[3] L. S. Geng and E. Oset, Phys. Rev. D **79**, 074009 (2009).

[4] R. Molina and E. Oset, Phys. Rev. D **80**, 114013 (2009)

[5] S. L. Olsen, ArXiv: 0901.2371 [hep-ex], 0909.2713 [hep-ex]

Test of OZI violation in vector meson production with COMPASS

Johannes Bernhard[1,a] and Karin Schönning[b] on behalf of the COMPASS Collaboration
[a]*Institut für Kernphysik, Johannes-Gutenberg-Universität Mainz*
[b]*CERN, Geneva*

The COMPASS experiment at CERN SPS completed its data taking with hadron beams (p, π, K) in the years 2008 and 2009 by collecting a large set of data using different targets (H_2, Pb, Ni, W). These data are dedicated to hadron spectroscopy, where the focus is directed to the search for exotic bound states of quarks and gluons (*hybrids, glueballs*). The production of such states is known to be favoured in glue-rich environments, *e.g.* so-called OZI-forbidden processes. The OZI rule postulates that processes with disconnected quark line diagrams are forbidden. On the one hand, the study of the degree of OZI violation in vector meson production yields the possibilty to learn more about the involved production mechanisms. On the other hand it helps to understand the nucleon's structure itself. Contrary to former experiments, the large data sample allows for detailed studies in respect to Feynman's variable x_F. We present results from the ongoing analysis on the comparison of ω and ϕ vector mesons production in $p\,p \longrightarrow p\,(\omega/\phi)\,p$, where the possibilty of measuring the spin alignment of both vector mesons at the same time makes COMPASS unique.

1 Introduction

The OZI rule [1] declares that processes with disconnected quark line diagrams are forbidden. Though being phenomenological when first formulated, it could later be explained by QCD. It has been helpful in explaining a multitude of phenomena, for example the large branching fraction of ϕ decays into $K\overline{K}$ final states and the suppressed production of mesons with an $s\bar{s}$ component. The production of ϕ mesons in reactions with only non-strange hadrons in the initial state is, according to OZI, only allowed due to the deviation $\delta_V = 3.7^o$ from ideal mixing of ω and ϕ. This gives a prediction of the cross section ratio $R = \sigma(AB \to \phi X)/\sigma(AB \to \omega X)$ of $4.2 \cdot *146 * 10^{-3}$ [2], where A, B and X are non-strange hadrons. Though based on a very simplified picture, the predicted value is in most reactions surprisingly well fulfilled [3]. However, violations have been observed in $p\overline{p}$ annihilations at rest and NN collisions as well as NN and $N\pi$ collisions near the kinematic threshold [4]. These violations have been interpreted as i) intermediate gluonic states [5], ii) a polarised

[1]johannes.bernhard@cern.ch

strangeness component in the nucleon [6] or, near the kinematic threshold, iii) differences in the production mechanism and the nature of the meson-nucleon interaction. The COMPASS experiment is well suited for precise tests of the OZI rule and can provide data in a new energy range. In the following, the COMPASS experiment and the recent results of the ongoing analysis will be presented.

COMPASS is a two-stage magnetic spectrometer [7] at the CERN SPS dedicated to structure studies and spectroscopy. It features large angular acceptance over a wide momentum range and is capable of particle identification with the means of a RICH detector. Neutral particles are detected with electromagnetic (ECAL1+2) and hadronic (HCAL1+2) calorimeters in both stages of the spectrometer. To confine data taking to the relevant processes of diffractive scattering and central production, a scintillator barrel detector (RPD) was surrounding the target and used to measure and trigger on recoiling protons.

2 Analysis and discussion

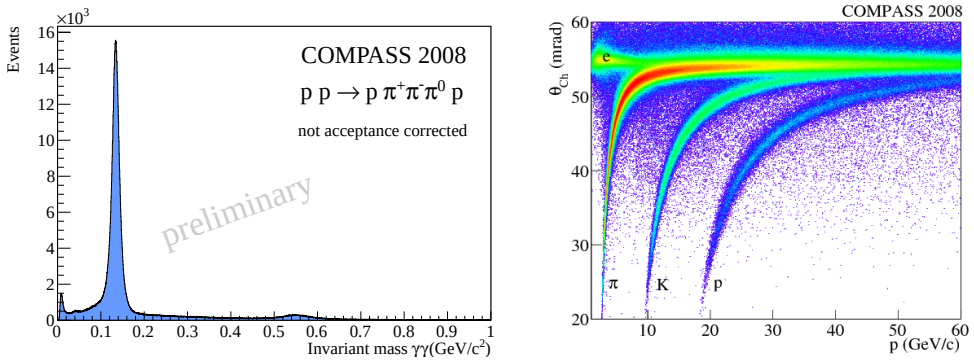

Figure 1: Left: Invariant mass distribution of $\gamma\gamma$ before cuts in the $p\,p \rightarrow p\,\pi^0\,\pi^+\,\pi^-\,p$ channel. Right: Cherenkov angle (RICH detector) vs. momentum of charged particles.

The analysis presented here concentrates on the 2008 $p\,p$ data set, *i.e.* one week of data of 190 GeV proton beams impinging on a liquid hydrogen target. The two channels $p\,p \rightarrow p\,\omega\,p, \omega \rightarrow \pi^+\,\pi^-\,\pi^0$ and $p\,p \rightarrow p\,\phi\,p, \phi \rightarrow K^+\,K^-$ were compared. For both channels, events were selected with one tagged incoming proton, one recoil proton in the RPD and three outgoing charged tracks from the primary vertex. Furthermore, in the ω case, a π^0 candidate reconstructed from two photons (see the left panel of Fig. 1) and a positive RICH identification of the π^+ were required. In the ϕ case, positive RICH identification of the K^+ was required (for the RICH separation, see the right panel of Fig. 1).

For both decay channels, the total momentum of the final state was required to be within $\pm\,6\,\mathrm{GeV}/c$ of the beam momentum and in addition, the recoiling proton and the forward $p\,\phi/p\,\omega$ system must be coplanar within $\pm\,2\,\sigma$ of the RPD's experimental resolution, *i.e.* 0.28 rad. The data are binned in terms of x_F of the forward proton. Fig. 2 shows the

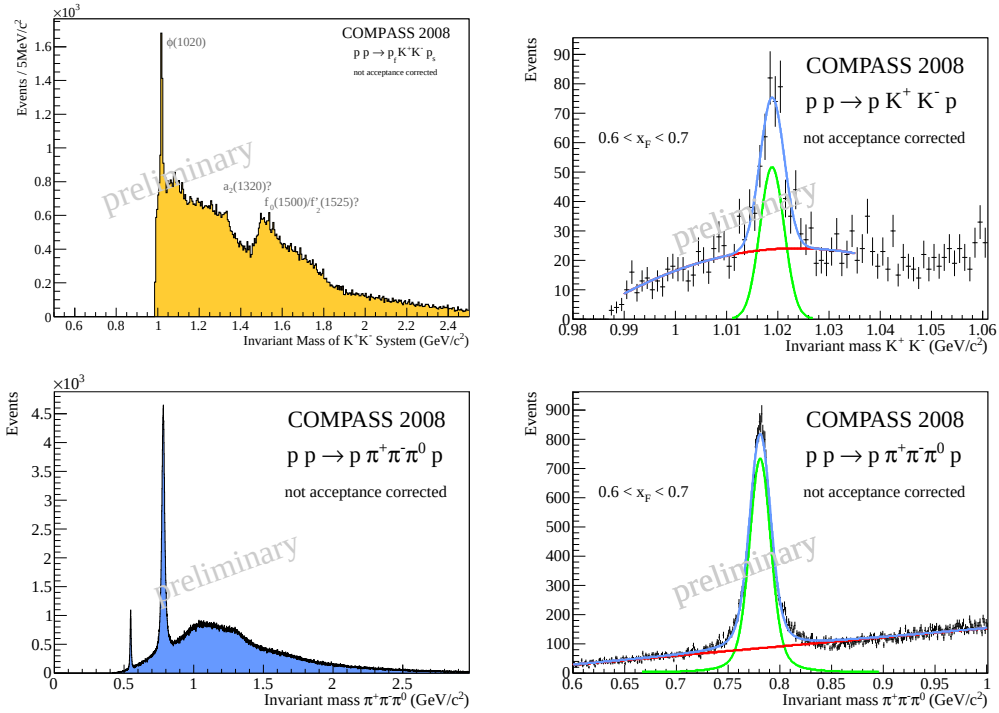

Figure 2: Invariant mass distributions of the $K^+\,K^-$ and $\pi^0\,\pi^+\,\pi^-$ subsystems. Left: Full data sample. Right: x_F of forward proton limited to $(0.6 < x_F < 0.7)$, with fitted curves as explained in the text.

invariant mass distributions of both the $K^+\,K^-$ and $\pi^0\,\pi^+\,\pi^-$ subsystems, respectively, for the total data sample presented here (upper left and lower left panel) and for the subinterval $0.6 < x_F < 0.7$. A Breit-Wigner curve, convoluted with a Gaussian on top of a polynomial background was fitted to the data and the background was subtracted in order to obtain the yield of each vector meson. The yields were corrected for the branching ratio (89.2% for $\omega \rightarrow \pi^+\,\pi^-\,\pi^0$ and 48.9% for $\phi \rightarrow K^+\,K^-$) and acceptance, which was obtained by MC simulations. There is a systematic uncertainty in the photon reconstruction efficiency of 10%, obtained by comparing the acceptance corrected yields of $\omega \rightarrow \pi^+\pi^-\pi^0$ and $\omega \rightarrow \gamma\pi^0$. The preliminary results are presented in Fig. 3. The systematics shown include

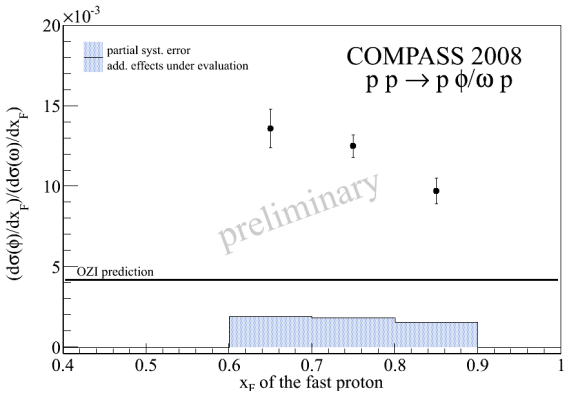

Figure 3: Acceptance corrected ratio R of ϕ and ω yields as a function of x_F of the forward proton.

the photon reconstruction efficiency and the error of the BW fit, the latter being smaller than 1.5%. Additional sources of systematic uncertainties like the RICH efficiency and the model dependence of the acceptance may also contribute non-negligibly but need further study and are therefore not quoted here. The COMPASS data show an OZI violation of approximately a factor of three.

3 Outlook

The 2009 proton data set will increase the statistics by a factor of ≈ 10 and will allow for finer binning. Furthermore, a dedicated comparative study of the vector meson spin alignment with respect to different quantisation axes, *e.g.* as performed in [8] or suggested in [9] is planned. This will give deeper insight into the underlying physics of diffractive and central processes at COMPASS energies. In particular, the studies of central systems will benefit from more knowledge of the production processes [10], but also the search for exotic states in multi-particle final states will profit due to better understanding of backgrounds, *e.g.* in $\pi^- p \rightarrow K_s K^{\pm} \pi^{\mp} \pi^{\mp} p$ [11].

Acknowledgments

This work was supported by the Bundesministerium für Bildung und Forschung (Germany).

Bibliography

[1] S. Okubo, Phys. Lett. **5** (1963) 165, G. Zweig; CERN report **TH-401** (1964);
J. Iizuka, Prog. Theor. Suppl. **38** (1966) 21.

[2] H.J. Lipkin, Phys. Lett. **B 60** (1976) 371.

[3] V.P. Nomokonov and M.G. Sapozhnikov, Particles and Nuclei **24** (2003) 184 and references therein.

[4] A. Sibirtsev and W. Cassing, Eur. Phys. J. **A 7** (2000) 407 and references therein.

[5] S.J. Lindenbaum, Nouvo Cim. **65 A** (1981) 222.

[6] J. Ellis *et al.* Phys. Lett. **B 353** (1995) 319;
J. Ellis *et al.*, Nucl. Phys. **A 673** (2000) 256.

[7] COMPASS collaboration, P.Abbon *et al.*, Nucl. Instr. and Meth. **A 577** (2007) 455-518;
COMPASS collaboration, M.Alekseev *et al.*, in prep. for Nucl. Instr. and Meth. **A**.

[8] K. Schönning *et al.*, Phys. Lett. **B 668**, (2008) 258;
F. Belleman *et al.*, Phys. Rev. **C 75** (2007) 015204.

[9] X. Quing-hua and L. Zuo-tang, Phys. Rev. **D 68** (2003) 034023.

[10] J.Bernhard, AIP Conf. Proc. **1257** (2010) 482-486.

[11] J.Bernhard and F.Nerling, *these proceedings*.

Diffractive dissociation into $K_s K^{\pm}\pi^{\mp}\pi^{-}$ final states

Johannes Bernhard[a] and Frank Nerling[1,b] on behalf of the COMPASS Collaboration
[a] *Institut für Kernphysik, Universität Mainz, 55099 Mainz, GERMANY*
[b] *Physikalisches Institut, Albert-Ludwigs-Universität Freiburg 79104 Freiburg, GERMANY*

The COMPASS fixed-target experiment at CERN/SPS is dedicated to the study of hadron structure and spectroscopy, especially the search for spin-exotic states. After having started to study the existence of the spin-exotic $\pi_1(1600)$ resonance in the 2004 pilot-run data, the new 2008/09 data will enable us to further clarify the situation. Apart from the $\pi_1(1600)$ resonance, also a spin-exotic $\pi_1(2000)$ was reported in the past in the $f_1(1285)\pi$ decay channel by the E852/BNL experiment, however, this state still lacks confirmation. We present a first event selection of the diffractively produced $(K\overline{K}\pi\pi)^-$ system showing clean $f_1(1285)$ and $f_1(1420)$ resonances at competing statistics. A partial-wave analysis started on $f_1(1285)\pi$ and $f_1(1420)\pi$ decay channels will further complete the search for spin-exotics in the 2008/09 COMPASS data.

1 Introduction

One important part of the COMPASS physics programme is the search for new states, in particular the search for spin-exotic states and glueballs. COMPASS has started to contribute to the puzzle of the existence of spin-exotic mesons with the published 2004 pilot-run data, showing a significant production strength for an exotic $J^{PC} = 1^{-+}$ state at $1.66\,\mathrm{GeV}/c^2$ [1]. The high-statistics 2008/09 data sets, covering almost all decay channels reported in the past, will further clarify the situation. Apart from the spin-exotic $\pi_1(1600)$ resonance observed in various decay channels and experiments, also a spin-exotic $\pi_1(2000)$ candidate was reported in the past by the E852 experiment at BNL in the $f_1(1285)\pi$ decay channel [2,3]. This state, however, still requires confirmation.

In this paper, we present the event selection of the diffractively produced $(K\overline{K}\pi\pi)^-$ system showing clean $f_1(1285)$ and $f_1(1420)$ signals competitive with the BNL/E852 data. The accessible mass range is extended beyond $2\,\mathrm{GeV}/c^2$. The started partial-wave analysis (PWA) of the $f_1(1285)\pi$ and $f_1(1420)\pi$ systems will further complete the search for spin-exotics in the 2008/09 COMPASS data. A PWA of the $(K\overline{K}\pi\pi)^-$ system will on the one hand complement previous searches in the $f_1\pi$-channel, on the other hand it will be the first PWA of the $f_1(1420)\pi$ system.

[1] nerling@cern.ch

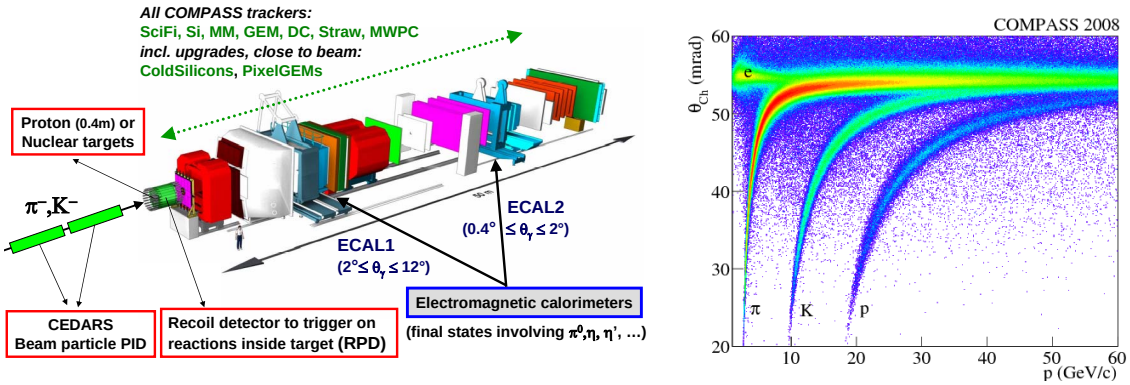

Figure 1: *(Left)* Sketch of the two-stage COMPASS spectrometer. *(Right)* Measured Cherenkov angle using RICH-1 versus particle momentum. Three bands appear corresponding to the different masses of pions, kaons, and (anti-)protons; some additional contribution from δ-electrons is present at low masses and angles.

The COMPASS two-stage spectrometer [4] at the CERN SPS features charged particle tracking and good coverage by electromagnetic calorimetry for both stages (Fig. 1). The fixed liquid hydrogen target is surrounded by a recoil proton detector (RPD) included in the trigger. Moreover, a Ring Imaging Cherenkov (RICH) detector in the first stage allows for final state particle identification (PID). A good separation of pions from kaons allows for final state PID and hence the study of kaonic final states. Two Cherenkov Differential counters with Achromatic Ring focus (CEDAR) upstream of the target are used to identify the incoming beam particle. Not only kaon diffraction, tagging the kaon contribution in the negative hadron beam (96.8 % π^-, 2.4 % K^-, 0.8 % $\bar{p}$) can thus be studied, cf. [5], but also production of strangeness with the pion beam, see also [6, 7]. The COMPASS data recorded with 190 GeV/c hadron beams in 2008/09 provide excellent opportunity for simultaneous observation of new states in various decay modes within the same experiment, see also [8–10].

2 First glimpse on the diffractively produced $(K\overline{K}\pi)^0$ system

The $(K\overline{K}\pi\pi)^-$ events are selected from the full 2008 data set taken with negatively charged pion beam. Exactly one reconstructed primary vertex inside the target volume is required for each event. Further, three outgoing charged tracks (two negative, one positive) were required, resulting in two types of final states: *(a)* $K_s K^+\pi^-\pi^-$ and *(b)* $K_s K^-\pi^+\pi^-$. The K^0s are identified by requiring the invariant mass of the pion pair from the reconstructed V^0 decay (after anticut on Λ and $\overline{\Lambda}$) to be within $\pm 20\,\mathrm{MeV}/c^2$ with respect to the PDG mass. Only events with exactly one K^0 candidate are accepted. By PID of the $K^{\pm}$ with the RICH detector (using the likelihood ratio of the Kaon assumption over others), the two types are separated, remaining particles are assumed to be pions. The beam energy is determined by the total momentum of the outgoing system. In order to select exclusive

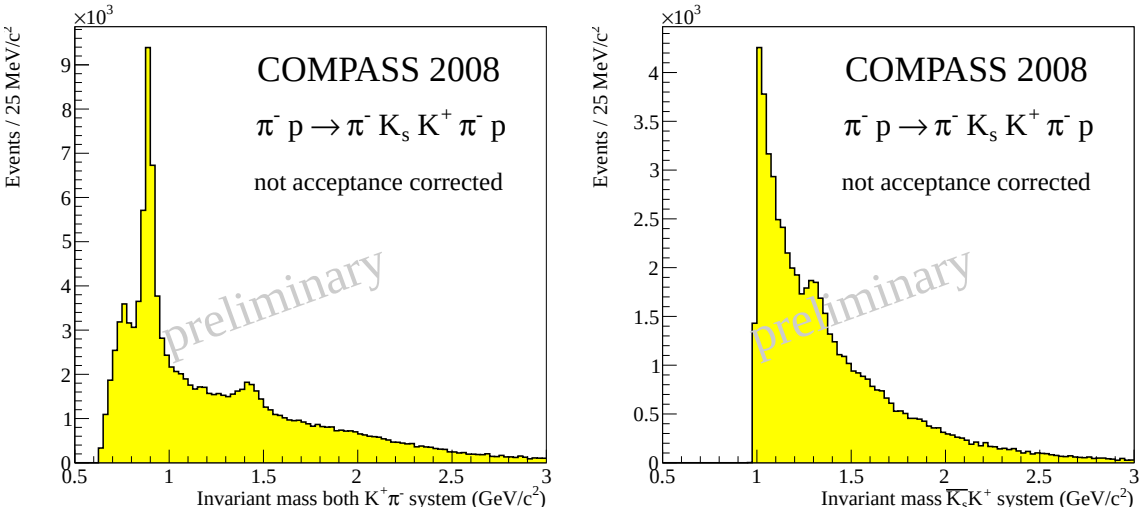

Figure 2: Exemplary sub mass spectra shown for event type (a) (similar for (b)). *Left:* The $(K\pi)^0$ subsystem features a clean $K^*(892)$ peak and some contribution from $K^*_{0,2}(1430)$. *Right:* The $(K\overline{K})$ subsystem shows a clean $a_0(980)$ peak at threshold and some $a_2(1320)$ contribution.

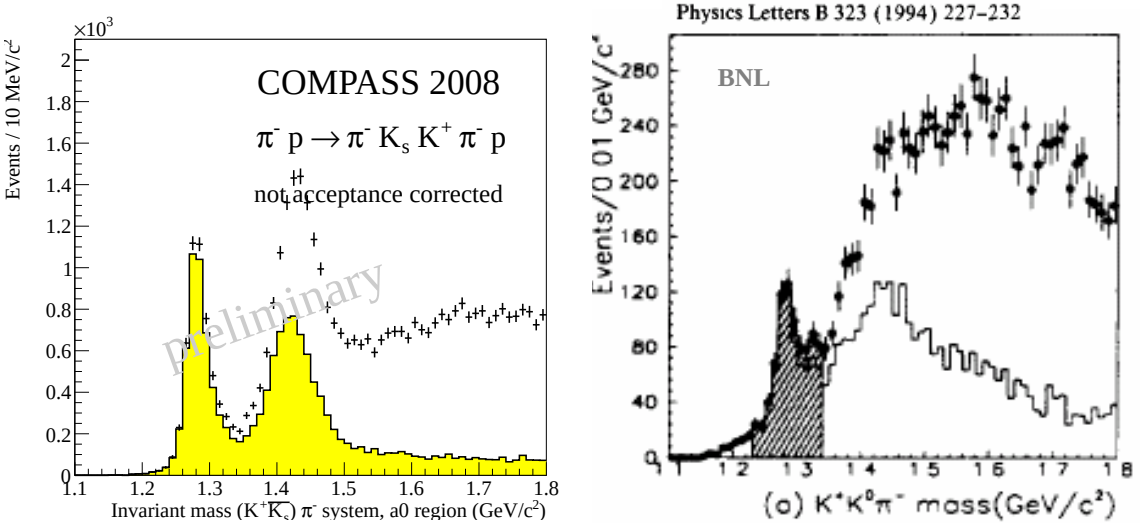

Figure 3: *Left:* The $(K\overline{K}\pi)^0$ subsystem, showing clean $f_1(1285)$ and $f_1(1420)$ peaks before (dots) and after (line) an additional restriction of the $K\overline{K}$ mass to the $a_0(980)$ region. *Right:* Comparing the similar plot published by BNL/E852 [2], the COMPASS statistics exceeds the one analysed by E852 by a factor of 10 (or a factor of about 20, taking into account also the 2009 data with negative pion beam). Not only the observed $f_1(1285)$ but also the $f_1(1420)$ are nearly background free as compared to BNL/E852 [2].

events, two main cuts are applied consistently in terms of $\pm 2\,\sigma$ of each distribution: On the calculated beam energy ($\pm 2\,\mathrm{GeV}/c^2$), and on the azimuthal angle anti-correlation (± 0.3 rad) of the recoil proton (measured with the RPD) and the outgoing system (measured with the spectrometer). To get a first glimpse on the isobars to be included for the PWA, the mass spectra of the different subsystems have been studied. In Fig. 2, the $(K\pi)^0$ and the $(K\overline{K})$ subsystems are exemplary shown, featuring clean $K^*(892)$ and $a_0(980)$ peaks, also contributions from $K^*_{0,2}(1430)$ and $a_2(1320)$ are present. The $(K\overline{K}\pi)^0$ subsystem (Fig. 3) is of particular interest, as a spin-exotic 1^{-+} resonance was reported in the $f_1(1285)\pi$ decay channel. It features clean $f_1(1285)$ and $f_1(1420)$ peaks. Even though an η contribution cannot be excluded, a first mass-independent PWA indicate contributions from $\eta(1405)$ and $\eta(1295)$ to be minor, consistent with the observation by E852 [3]. Further isobars obviously to be included are: $K\pi$ and KK s-wave contributions and, for event type *(b)* only, $\rho(770)$, $f_1(1270)$, and $f_0(600)$ or σ (corresponding mass spectra not shown).

3 Conclusions and summary

The COMPASS hadron data taken in 2008/09 will allow us to contribute solving the puzzle of light spin-exotic mesons, even extending the region to higher masses beyond $2\,\mathrm{GeV}/c^2$. We presented a first selection of $K_s K^{\pm}\pi^{\mp}\pi^{-}$ events, verifying our feasibility to study not only the diffractively produced $f_1(1285)\pi$ at competing statistics but also the $f_1(1420)\pi$ system. In the former decay mode, apart from the $\pi_1(1600)$, a second spin-exotic $J^{PC} = 1^{-+}$ resonance at $2\,\mathrm{GeV}/c^2$, the $\pi_1(2000)$, was reported in the past by one experiment [3], whereas the latter has never been studied before.

Acknowledgments

This work is supported by the BMBF (Germany), especially via the "Nutzungsinitiative CERN".

Bibliography

[1] M. Alekseev *et al.*, COMPASS collaboration, *Phys. Rev. Lett.*, **104** (2010) 241803.

[2] J.H. Lee *et al.*, *Phys. Lett. B* **323** (1994) 227.

[3] J. Kuhn *et al.*, *Phys. Lett. B* **595** (2004) 109.

[4] P. Abbon *et al.*, COMPASS collaboration, *Nucl. Instrum. Meth. A* **577** (2007) 455.

[5] P. Jasinski, *These proceedings* (2011).

[6] T. Schlüter, *AIP Conf. Proc.* **1257** (2010) 462.

[7] F. Nerling, *PoS ICHEP2010* (2010) 163; arXiv:1012.4993[hep-ex]

[8] F. Nerling, *AIP Conf. Proc.* **1257** (2010) 286; arXiv:1007.2951[hep-ex], also *these proceedings* (2011).

[9] F. Haas, *These proceedings* (2011).

[10] T. Schlüter, *These proceedings* (2011); arXiv:1108.6191[hep-ex].

Study of $a_0^0(980) - f_0(980)$ mixing at BESIII

Chunyan Liu on behalf of the BESIII Collaboration
Institute of High Energy Physics, Chinese Academy of Sciences, China, 100049

In this talk,we present direct measurements of $a_0^0(980) - f_0(980)$ mixing in the processes $J/\psi \to \phi f_0(980) \to \phi a_0^0(980) \to \phi\eta\pi^0$ and $\psi' \to \gamma\chi_{c1}, \chi_{c1} \to \pi^0 a_0^0(980) \to \pi^0 f_0(980) \to \pi^0\pi^+\pi^-$ with 2.25×10^8 J/ψ data and 1.06×10^8 ψ' data at BESIII.

1 Introduction

BESIII/BEPCII [1] is a major upgrade of the BESII detector and BEPC accelerator. The primary physics purposes are aimed at the study of hadron spectroscopy and τ-charm physics.
The nature of the scalar mesons $a_0^0(980)$ and $f_0(980)$ has been a hot topic in light hadron physics for many years. The mixing between $a_0^0(980)$ and $f_0(980)$ is expected to shed light on the nature of these two resonances. In this talk,we present the recent result from the study of $a_0^0(980) - f_0(980)$ mixing at BESIII [2].

2 Study of $a_0^0(980) - f_0(980)$ mixing at BESIII

The leading contribution to the isospin-violating mixing transition amplitudes for $f_0(980) \to a_0^0(980)$ and $a_0^0(980) \to f_0(980)$ are shown to be dominated by the difference of the unitarity cut which arises from the mass difference between the charged and neutral kaons. As a consequence, a narrow peak of about 8 MeV/c^2 is predicted between the charged and neutral kaon thresholds. Using the samples of 2.25×10^8 J/ψ and 1.06×10^8 ψ' events,we perform direct measurements of $a_0^0(980) - f_0(980)$ mixing in the processes $J/\psi \to \phi\eta\pi^0$ and $\psi' \to \gamma\chi_{c1}, \chi_{c1} \to \pi^0 a_0^0(980) \to \pi^0 f_0(980) \to \pi^0\pi^+\pi^-$.

FIG.(a) shows the fitting results of $\eta\pi^0$ mass spectrum recoiling against ϕ signal in $J/\psi \to \phi f_0(980) \to \phi a_0^0(980) \to \phi\eta\pi^0$.The dotted line shows the mixing signal. The dash-dotted line denotes the $a_0^0(980)$ from virtual photon or $K^*\overline{K}$ loop. The dashed line is a polynomial background constrained to the ϕ sideband. The significance of $f_0(980) \to a_0^0(980)$ mixing signals is 3.3 σ. The mixing branching ratio is determined to be $\mathcal{B}(J/\psi \to \phi f_0(980) \to \phi a_0^0(980) \to \phi\eta\pi^0)(< 5.4 \times 10^{-6}$ at the 90% C.L.).

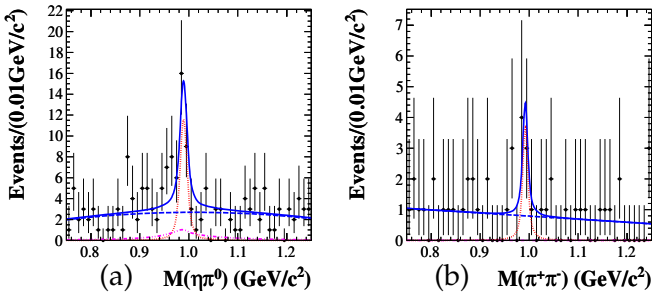

For $a_0^0(980) \to f_0(980)$ transition, the mass spectrum of $\pi^+\pi^-$ in the χ_{c1} mass window is fitted in a similar style, shown in FIG. (b).The significance of $a_0^0(980) \to f_0(980)$ mixing signals is 1.9 σ. The mixing branching ratio is determined to be $\mathcal{B}(\psi' \to \gamma\chi_{c1} \to \gamma\pi^0 a_0^0(980) \to \gamma\pi^0 f_0(980) \to \gamma\pi^0\pi^+\pi^-)(< 6.0 \times 10^{-7}$ at the 90% C.L.).The mixing intensities ξ_{fa} for $f_0(980) \to a_0^0(980)$ transition and ξ_{af} for $a_0^0(980) \to f_0(980)$ transition are defined and calculated as:

$\xi_{fa} = \frac{\mathcal{B}(J/\psi \to \phi f_0(980) \to \phi a_0^0(980) \to \phi\eta\pi^0)}{\mathcal{B}(J/\psi \to \phi f_0(980) \to \phi\pi^+\pi^-)}$ ($< 1.1\%$ at the 90% C.L.),

$\xi_{af} = \frac{\mathcal{B}(\psi' \to \gamma\chi_{c1} \to \gamma\pi^0 a_0^0(980) \to \gamma\pi^0 f_0(980) \to \gamma\pi^0\pi^+\pi^-)}{\mathcal{B}(\psi' \to \gamma\chi_{c1} \to \gamma\pi^0 a_0^0(980) \to \gamma\pi^0\pi^0\eta)}$ ($< 1.0\%$ at the 90% C.L.).

3 Summary

A new facility for physics in the charm-τ region BEPCII/BESIII has become operational. With the world¡¯s largest samples of J/ψ and ψ' collected at BESIII, the direct measurement of a_0 and f_0 mixing is performed for the first time.The measurements will be very helpful for pinning down the natures of $a_0^0(980)$ and $f_0(980)$.

Bibliography

[1] "Physics at BESIII", Edited by K. T. Chao and Y. F. Wang, Int. J. Mod. Phys. A **24**, No.1 (2009) supp.

[2] M. Ablikim *et al.* [BESIII Collaboration], Phys. Rev. D **83**, 032003 (2011).

[3] J. J. Wu, Q. Zhao, and B. S. Zou, Phys. Rev. D **75**, 114012 (2007).

[4] C. Hanhart, B. Kubis, and J. R. Pelaez, Phys. Rev. D **76**, 070428 (2007)

[5] J. J. Wu and B. S. Zou, Phys. Rev. D **78**, 074017 (2008).

N_c dependence of light resonances properties

Jenifer Nebreda, José Ramón Peláez, and Guillermo Ríos
Departamento de Física Teórica II. Universidad Complutense de Madrid, 28040, Madrid, Spain

We review our recent study of the N_c dependence of the parameters of the lightest scalar and vector mesons and other highly $1/N_c$ suppressed observables in a model independent way, showing that the expansions need unnaturally large coefficients for the scalars. We also study their mass and width N_c evolution by means of Unitarized Chiral Perturbation Theory to compare with the $\bar{q}q$ scaling $M \sim 1$, $\Gamma \sim 1/N_c$. We see that the vectors follow the $\bar{q}q$ scaling whereas the scalars do not, although we might be seeing a subdominant $\bar{q}q$ component in the $f_0(600)$ with a mass around 1 GeV in the two-loop analysis.

The nature of the scalar mesons is still the object of an intense debate and different models suggest that they may not be ordinary quark-antiquark mesons, but tetraquarks, meson molecules, glueballs, or a complicated mixture of all these. The problem, of course, is that we do not know how to solve QCD at low energies. However, since the QCD $1/N_c$ expansion is applicable at all energies, and the mass and width of $\bar{q}q$ mesons scale as $O(1)$ and $O(1/N_c)$, respectively, the N_c dependence of resonances becomes a powerful tool to study the nature of these resonances. Another useful approach is to extrapolate the pion mass up to the region where Lattice results are available. Results on this matter were shown in the poster, but due to space limitations here we prefer to focus on the more recent results on N_c extrapolation and particularly on the study of highly $1/N_c$ suppressed observables and refer the reader to the original publications on chiral extrapolation [1,2].

Mass and width dependence on N_c We first study the mass and width behavior of light resonances using ChPT—which is the QCD low energy effective Lagrangian—and unitarization with a dispersion relation. The poles of the $\rho(770)$ and $K^*(982)$ vectors behave predominantly as expected for $\bar{q}q$ states whereas those of the $f_0(600)$, also called σ, and $K(800)$ scalars do not. Still, a possible subdominant $\bar{q}q$ component for the $f_0(600)$ may arise naturally at two loops [3] within ChPT (less so at one loop), but with a mass around 1 GeV or more. We refer the reader to papers [3,4] for a more detailed discussion.

Highly $1/N_c$ suppressed observables In this section we provide adimensional observables with corrections suppressed further than $1/N_c$, that can also be applied directly to real data at $N_c = 3$, without the need to extrapolate to larger N_c using unitarized ChPT.

	$\rho(770)$	$K^*(892)$	$f_0(600)$	$K(800)$
a	-0.06 ± 0.01	0.02	-252^{+119}_{-156}	-2527
b	$0.37^{+0.04}_{-0.05}$	0.16	77^{+28}_{-24}	162

Table 1: Normalized coefficients of the $1/N_c$ expansion for different resonances. For $\bar{q}q$ resonances, all them are expected to be of order one or less.

Let $s_R = m_R^2 - im_R\Gamma_R$ be the pole position of a resonance that behaves as a $\bar{q}q$. Making use of the scaling behavior found in [5] for $\delta(m_R)$ and $\delta'(m_R)$, we can write down the following adimensional observables whose corrections are suppressed further than just $1/N_c$:

$$\left.\frac{\frac{\pi}{2} - \mathrm{Re}\, t^{-1}/\sigma}{\delta}\right|_{m_R^2} \equiv \Delta_1 = 1 + \frac{a}{N_c^3}, \tag{1}$$

$$\left. -\frac{[\mathrm{Re}\, t^{-1}]'}{\delta'\sigma}\right|_{m_R^2} \equiv \Delta_2 = 1 + \frac{b}{N_c^2}, \tag{2}$$

where $t(s)$ is the partial wave, $\sigma = 2k/\sqrt{s}$, k is the meson center of mass momentum and derivatives are taken with respect to s. The coefficients a and b should naturally be $O(1)$ or less. It is relatively simple to make a and b much smaller than one with cancellations with natural higher order $1/N_c$ contributions, but very unnatural to make them much larger. In Table 1 we show the resulting a and b for the lightest resonances found in $\pi\pi$ and πK elastic scattering. We observe that for the $\rho(770)$ and $K^*(892)$ vector resonances all parameters are of order one or less, as expected for $\bar{q}q$ states. In contrast, for the $f_0(600)$ and $K(800)$ scalar resonances we find that all parameters are larger, by two orders of magnitude, than expected for $\bar{q}q$ states, which makes the $\bar{q}q$ interpretation of both scalars extremely unnatural. Furthermore, unitarized ChPT can be used to calculate the $\Delta_i - 1$ observables, in order to show that, for scalars, what really happens is that they do not even follow the $1/N_c$ expansion of $\bar{q}q$ states given in Eqs. (1) and (2). For this analysis we refer the reader to [6]

Acknowledgments

J. Nebreda thanks the organizers for granting her the *best theory poster* prize, as well as for offering such a lively and interesting conference.

Bibliography

[1] J. R. Pelaez and G. Rios, Phys. Rev. D **82**, 114002 (2010).

[2] J. Nebreda and J. R. Pelaez., Phys. Rev. D **81**, 054035 (2010).

[3] J. R. Pelaez and G. Rios, Phys. Rev. Lett. **97**, 242002 (2006).

[4] J. R. Pelaez, Phys. Rev. Lett. **92**, 102001 (2004).

[5] J. Nieves and E. Ruiz Arriola, Phys. Lett. B **679**, 449 (2009).

[6] J. Nebreda, J. R. Pelaez and G. Rios, arXiv:1107.4200 [hep-ph].

Preliminary results on $e^+e^- \to$ hadrons from SND detector at VEPP-2000 collider

Alexander E. Obrazovsky[1] on behalf of the SND collaboration
Budker Institute of Nuclear Physics
11 Academician Lavrentiev ave.
630090 Novosibirsk, Russia

Preliminary results on $e^+e^- \to 3\pi, 4\pi, \omega\pi^0, \eta\pi^+\pi^-, n\overline{n}$ cross sections measured with SND detector at VEPP-2000 collider are reported. The data were collected in 2010–2011 in the energy range $2E$ = 1.0–2.0 GeV, the total integrated luminosity used is about 7 pb^{-1}.

Spherical Neutral Detector (SND) [1] is a general purpose non-magnetic detector for experiments at electron-positron collider VEPP-2000 [2] in Novosibirsk in the c.m. energy range $2E$ = 0.4–2.0 GeV. Experiments at VEPP-2000 with SND and Cryogenic Magnetic Detector (CMD) begun in 2010. In 2010 and 2011 two scans of the energy range $2E$ = 1.0–2.0 GeV (MHAD2010 and MHAD2011) were performed with the integrated luminosity of 5 and 25 pb^{-1}, respectively.

Preliminary results on some $e^+e^- \to$ *hadrons* cross sections are presented in Fig. 1. Cross sections of $e^+e^- \to \pi^+\pi^-\pi^0$, $\pi^+\pi^-\pi^0\pi^0$, $\omega\pi^0 \to \pi^0\pi^0\gamma$ and $\eta\pi^+\pi^-$ are measured using the data of MHAD2010 experiment. In the $e^+e^- \to \pi^+\pi^-\pi^0$ cross section, the $\omega(1420)$ and $\omega(1650)$ resonances are seen. The cross section of $e^+e^- \to \pi^+\pi^-\pi^0\pi^0$ is dominated by the $\rho(1450)$ and $\rho(1700)$ decays. The fit to the $e^+e^- \to \omega\pi^0$ cross section data takes into account contributions from the $\omega(782)$ and $\omega(1450)$ resonances. The cross section of $e^+e^- \to \eta\pi^+\pi^-$ is dominated by the $\rho(1450) \to \eta\pi^+\pi^-$ decay.

The $e^+e^- \to n\overline{n}$ cross section is measured on the part of MHAD2011 statistics, about 2.5 pb^{-1}. The detection efficiency is about 30 %. The $e^+e^- \to p\overline{p}$ and $\gamma\gamma$ background contributions are subtracted. Fitting the cross section with a step function yields $\sigma = 0.1 \pm 0.2$ nb below the threshold and $\sigma = 0.8 \pm 0.2$ nb above the threshold. All quoted errors are statistical. The sources of systematic uncertainties are being analyzed.

Future SND plans at VEPP-2000 include a scan of the full energy range $2E$ =0.4–2.0 GeV and the analysis of other $e^+e^- \to$ *hadrons* processes such as $e^+e^- \to K_SK_L, KK\pi, p\overline{p}$.

[1] obrazov@inp.nsk.su

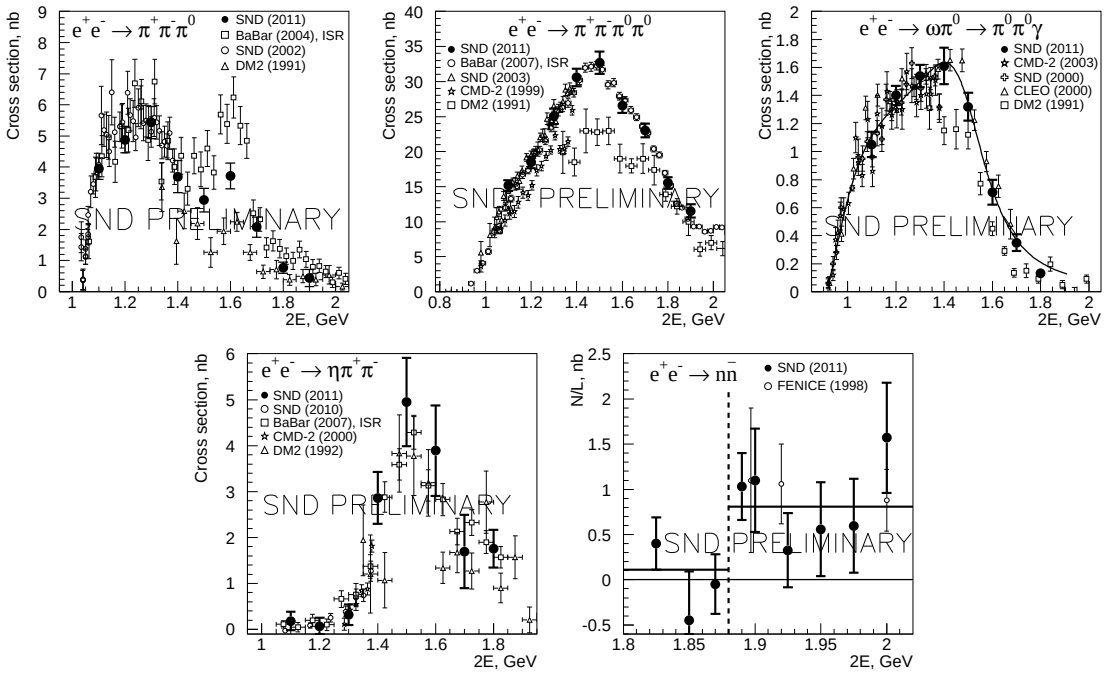

Figure 1: Cross sections measured with SND at VEPP-2000, in comparison with previous measurements.

Acknowledgments

This work is partially supported by the Russian Federation Presidental Grant for Scientific Schools NSh-6943.2010.2, Russian Fund for Basic Research Grant 11-02-00276-a and the Grant 14.740.11.1167 of Federal Program "Scientific and Pedagogical Personnel of Innovational Russia".

Bibliography

[1] M.N. Achasov *et al.*, Nucl. Instrum. Meth. A **598**, 31 (2009).
V.M. Aulchenko *et al.*, Nucl. Instrum. Meth. A **598**, 102 (2009).
A.Yu. Barnyakov *et al.*, Nucl. Instrum. Meth. A **598**, 163 (2009).
V.M. Aulchenko *et al.*, Nucl. Instrum. Meth. A **598**, 340 (2009).

[2] Yu.M. Shatunov *et al.*, in Proceedings of the 7th European Particle Accelerator Conference, Vienna, 2000, p. 439.

Scientific Program

Monday, June 13, 2011

Plenary Session 1 Chair: *Suh-Urk Chung*

08:50	Stephan Paul	Opening Remarks
09:00	Norbert Kaiser	Summary of Recent Progress in Chiral Perturbation Theory
09:30	Sebastian Neubert	Light-Meson Spectroscopy
10:00	Sinead Ryan	Meson Spectroscopy and Resonances
10:30	Claudia Patrignani	Heavy-Flavor Mesons
11:00		*Coffee Break*

Plenary Session 2 Chair: *Martin Faessler*

11:30	Fulvia De Fazio	Latest Developments in the Spectroscopy of Heavy Hadrons
12:00	Randolf Pohl	The Proton Size
12:30	Antonio Pineda	The Puzzle About the Protons Size
13:00		*Lunch Break*

Light Mesons 1 Chair: *Wolfgang Ochs*

14:30	Jose R. Pelaez	The nature of the lightest scalar meson, its N_c behavior and semi-local duality
15:00	Nikolay Achasov	Study of Light Scalars, the learned Lessons
15:20	Evgeny Solodov	Measurement of meson-photon transition form factors with the BABAR detector
15:40	Evgeny Solodov	Recent results on hadrons via Initial State radiation at BABAR

Light Baryons 1 Chair: *Elke-Caroline Aschenauer*

14:30	Volker Crede	Overview on CLAS baryon results
15:00	Marcus Grüner	Measurement of the double polarisation observable G in the reactions $\vec{\gamma}\vec{p} \to p\pi^0$ and $\vec{\gamma}\vec{p} \to p\eta$
15:25	Jonas Müller	Measurement of the double polarisation observable E in π^0 and η photoproduction

Heavy Hadrons 1

Chair: *Alberto Correa dos Reis*

14:30	Bastian Kubis	The role of final-state interactions in Dalitz plot studies
14:55	Patrícia C. Magalhães	Three-body Final State Interaction in $D^+ \to K^-\pi^+\pi^+$ and Its Effect on the $K\pi$ Phase Shift
15:15	Camilla Di Donato	$\eta - \eta'$ Mixing — From electromagnetic transitions to weak decays of charm and beauty hadrons
15:35	Carina M. Zanetti	Studies of the $X(3872)$ as a mixed molecule-charmonium state in QCD Sum Rules

Hadrons in Hot and Cold Medium 1

Chair: *Laura Fabbietti*

14:30	Stefania Bufalino	Weak Decay of Lambda Hypernuclei
14:55	Elena Botta	First Observation of the Heavy Hyper-Hydrogen isotope ${}^{6}_{\Lambda}\mathrm{H}$
15:15	Tomoichi Ishiwatari	Kaonic ^{3}He and ^{4}He X-ray measurements in SIDDHARTA
15:35	Shinji Okada	A new measurement of kaonic hydrogen X-rays
16:00		*Coffee Break*

Light Mesons 2

Chair: *Wolfgang Dünnweber*

16:30	Rainer Schicker	Central Meson Production in ALICE
17:00	Wolfgang Ochs	Glueballs from gluon jets at the LHC
17:20	Martin Schumacher	Structure of scalar mesons and the Higgs sector of strong interaction
17:40	Eulogio Oset	Finite volume effects in the meson scalar sector and generalization of Luescher approach to two coupled channels

Quarkonia 1

Chair: *Miriam Fritsch*

16:30	Marco Maggiora	Measuring the phase between strong and EM J/ψ decay amplitudes
16:50	Jifeng Hu	Study of charmonium decays at BESIII
17:10	Liangliang Wang	Study of charmonium spectroscopy at BESIII
17:30	Jorge Segovia	Microscopic Model of Charmonium Strong Decays
17:50	Hiroshi Noya	Does the $I = 1$ State exist in $c\bar{c}$ meson?

Light Baryons 2

Chair: *Reinhard Beck*

16:30	Alexander Austregesilo	Baryon Spectroscopy at COMPASS
16:50	Lilian Witthauer	Photoproduction of η-Mesons off Light Nuclei
17:10	Maxim Polyakov	A case for new narrow nucleon resonance
17:30	Manuel Dieterle	Single and Double Pion Photoproduction off the Deuteron
17:50	Xiaotao Liao	Study of $\psi' \to p\bar{p}\eta$ at BESIII

Heavy Hadrons 2 Chair: *Hal Evans*

16:50	Feng-Kun Guo	A comprehensive interpretation of the D_{sJ} states
17:10	Raquel Molina	A new interpretation for the $D_{s2}^{*}(2573)$ and the prediction of novel exotic charmed mesons
17:30	Daniel Mohler	D and D_s meson spectroscopy from lattice QCD
17:50	Fergus Wilson	The physics potential of SuperB
18:10		*Welcome Reception*

Tuesday, June 14, 2011

Plenary Session 3 Chair: *Marek Karliner*

09:00	Mauro Anselmino	Baryon structure and parton distribution functions
09:30	Jörg Pretz	Nucleon spin and parton distribution functions
10:00	Reinhard Beck	Light-baryon spectroscopy
10:30	James Zanotti	Hadron structure, baryon and meson form factors, $g-2$
11:00		*Coffee Break*

Plenary Session 4 Chair: *Claude Amsler*

11:30	Elke-Caroline Aschenauer	Highlights from the RHIC hadron physics programme
12:00	Mathias Butenschön	Recent developments in quarkonium production and open flavour production calculations
12:30	Yuanning Gao	Results on charmonium and charmmonium-like production from the LHC
13:00		*Lunch Break*

Quarkonia 2 Chair: *Nora Brambilla*

14:30	Kamal K. Seth	Heavy Quarkonia: Recent Results from CLEO
14:55	Piotr Pietrulewicz	Electric dipole transitions of heavy quarkonium
15:15	Simon Eidelman	Recent Results from the KEDR Detector
15:35	Mikhail Barabanov	Application of high-quality antiproton beam with momentum ranging from 1 GeV/c to 15 GeV/c to study charmonium and exotics

Light Baryons 3

Chair: *Eva-Maria Kabuss*

14:30	Bernhard Musch	Process-dependent transverse momentum distributions from lattice QCD
14:50	Pavel Kurilkin	The light nuclei spin structure from the hadronic interactions at intermediate energies
15:10	Christian Höppner	Cross section for quasi-real photo-production of charged hadrons with high transverse momenta in muon-deuteron scattering
15:30	Hervé Moutarde	Generalized Parton Distributions

Heavy Hadrons 3

Chair: *Christophorus Grab*

14:30	Dmitri Melikhov	Heavy-quark masses and heavy-meson decay constants from Borel sum rules in QCD
14:50	Roberta Cardinale	First mass measurements at LHCb
15:10	Timothy Burns	Spin-spin splittings and meson loops
15:30	Kai Schweda	Measurement of heavy flavour production in pp and Pb-Pb collisions at the LHC with ALICE

Low-Energy Processes 1

Chair: *Achim Denig*

14:30	Fabio Ambrosino	Chiral dynamics at KLOE, MAINZ, ELSA and other labs
14:55	Jose Manuel Alarcón	πN scattering in relativistic baryon chiral perturbation theory revisited
15:15	Manuel Pavón Valderrama	Perturbative Treatment of Chiral Two Pion Exchange in Nucleon-Nucleon Scattering
15:35	Martin Hoferichter	Roy-Steiner equations for $\gamma\gamma \to \pi\pi$
16:00		*Coffee Break*

Light Mesons 3

Chair: *Dennis Weygand*

16:30	Dmitri Melikhov	Pion form factor in a broad range of momentum transfers from local-duality QCD sum rule
16:50	Bastian Brandt	Precision calculation of the pion electromagnetic form factor from lattice QCD
17:10	Volker Metag	Determination of the η transition form-factor from the $\eta \to e^+e^-\gamma$ decay
17:30	Camilla Di Donato	Hadron Physics at KLOE and KLOE-2
17:50	Prometeusz Jasinski	Analysis of diffractive dissociation of exclusive $K^-\pi^+\pi^-$ events in the high energetic hadron beam of the COMPASS-experiment

Quarkonia 3

Chair: *Simon Eidelman*

16:30	Claudia Patrignani	Recent BABAR Studies of Bottomonium States
16:50	Alexander Kuzmin	Bottomonium results at Belle
17:10	Alexander Laschka	Mass dependence of the heavy quark potential and its effects on quarkonium states
17:30	Giovanni Sabatino	Quarkonia measurements in dimuon final states at LHCb
17:50	Bora Akgun	Quarkonium production in pp collisions at 7 TeV with the CMS experiment

Light Baryons 4

Chair: *Mauro Anselmino*

16:30	Eva-Maria Kabuss	Spin physics at COMPASS
16:50	Nour Makke	Quark fragmentation functions from SIDIS hadron multiplicities in COMPASS
17:10	Eulogio Oset	The $K^- d \to \Lambda(1405) n$ reaction with the DAΦNE set up and the two $\Lambda(1405)$ states
17:30	Valery Lyubovitskij	Mesons and baryons in holographic soft-wall model
17:50	Pedro González	A plausible explanation of the $\Delta_{5/2^+}(2000)$ puzzle

Hadrons in Hot and Cold Medium 2

Chair: *Tullio Bressani*

16:30	Mariana Nanova	Photoproduction of η' Mesons from Nuclei
16:50	Raquel Molina	K^* mesons in matter
17:10	Andrey Polyanskiy	Measurement of the in-medium ϕ-meson width in proton-nucleus collisions
17:30	Paul Bühler	Measuring the J/ψ-Nucleon dissociation cross section with PANDA
17:50	Satoshi Itoh	Precision Spectroscopy of Pionic Atom at RIKEN-RIBF

Poster Session

Michael Kunkel	Dalitz Decay of Pseudoscalar Mesons from Photoproduction on Hydrogen Target with CLAS
Nadezhda Ladygina	Study of deuteron-proton and deuteron-deuteron collisions at intermediate energies
Ajay Majethiya	Properties of charm baryons in quark-diquark model
Hiroaki Kohyama	Nonet meson properties in Nambu Jona-Lasinio model with dimensional regularization
Melahat Bayar	The $\overline{K}NN$ system with chiral dynamics
Monika Grothe	Measurements of Bose-Einstein correlations at LHC with CMS
Kazem Azizi	Strong coupling constants of heavy baryons to pseudoscalar and vector mesons
Ju Jun Xie	Faddeev fixed center approximation to the $N\overline{K}K$ system and the signature of a $N(1920)(1/2^+)$ state
Regina Kleinhappel	Hadron Resonances within a Constituent-Quark Model
Yanrui Liu	Possible hadronic molecules: $\Lambda_c N$ and $\Lambda_c - \Lambda_c$
David Garcia	About the contact term in the $\omega \to 3$pion process from the Vector Dominance point of view
Ricardo Torres-Andres	Chiral and isospin symmetry breaking: order parameters and susceptibilities
Eliecer Hernandez-Gajate	Weak decays of doubly-charmed baryons
Javier Vijande	Stability of many quark systems
Wolfgang Lucha	Unprejudiced look at effective continuum thresholds in Borel dispersive sum rules
Anna Skachkova	On lepton pair production in proton-antiproton collisions at intermediate energies and the main backgrounds
Andrea Lavagno	Hadron production at finite temperature and density within an effective relativistic mean field model
Sergey Sukhoruchkin	The role of pion-exchange tensor forces in nuclear excitations
Inti Lehmann	Hadronization in Nuclei — Multidimensional Study
Philipp Gubler	Charmonium spectra at finite temperature from a Bayesian analysis of QCD sum rules
Motoo Sekiguchi	$I = 1/2$ scalar meson in the lattice QCD
Bao-Xi Sun	A bound state of $N\rho\rho$ in the fixed center approximation of Faddeev equation
Raquel Molina	Prediction of Narrow N^* and Λ^* Resonances with Hidden Charm above 4 GeV
Raquel Molina	The $Y(3940)$, $Z(3930)$, and the $X(4160)$ as dynamically generated resonances from the vector-vector interaction
Johannes Bernhard	Test of OZI violation in vector meson production with COMPASS
Frank Nerling and Johannes Bernhard	Diffractive pion dissociation into $(K_s K^{\pm}\pi^{\mp}\pi^-)$ final states
Thiemo Nagel	Measurement of the Pion Polarizabilities at COMPASS
Chunyan Liu	Study of $a_0 - f_0$ mixing at BESIII
Jacobo Ruiz De Elvira	Precise dispersive analysis of the $f_0(600)$ and $f_0(980)$ resonances from pion-pion scattering
Guillermo Ríos	Properties of rho and sigma mesons from unitarized Chiral Perturbation Theory
Alexander Obrazovskiy	Preliminary results on $e^+e^- \to$ hadrons processes from SND detector at VEPP-2000 collider
Miguel Albaladejo	Dynamical generation of pseudoscalar resonances
Miguel Albaladejo	The scalar form factor and the radius of the sigma meson
Alexander Glushkov	Discharge of metastable nuclei during negative muon capture: Energy approach
Olga Khetselius	Spectroscopy of the hadronic atoms and superheavy atoms: Energy shifts and widths and strong interaction corrections
Jürgen Diefenbach	The OLYMPUS experiment at DORIS/DESY

Wednesday, June 15, 2011

Plenary Session 5 Chair: *Hartmut Wittig*

09:00	Mikko Laine	News from hadrons in hot medium
09:30	Ilya Selyuzhenkov	News from heavy-ion collisions (LHC and RHIC)
10:00	Andreas Jüttner	Review on results by the FLAG working group
10:30	Antonio Vairo	Recent progress on effective field theories for hadron states
11:00		*Coffee Break*

Plenary Session 6 Chair: *Volker Metag*

11:30	Nuno Leonardo	Results on bottomonium and bottommonium-like production from the LHC
12:00	Hai-Bo Li	Highlights from BESIII Experiment
12:30	Burkhard Kämpfer	Hadrons in cold medium
13:00	Toshiyuki Takahashi	Highlights from J-PARC Hadron Facility
13:30		*Lunch Break*

Thursday, June 16, 2011

Plenary Session 7 Chair: *Kamal K. Seth*

09:00	Simon Eidelman	Status of X, Y, Z states
09:30	Roxanne Springer	Theory of X, Y, Z states
10:00	Hal Evans	Results on production and spectroscopy of heavy mesons and baryons from LHC
10:30	Tetsuo Hyodo	Meson-baryon interactions and baryon resonances
11:00		*Coffee Break*

Plenary Session 8 Chair: *Eulogio Oset*

11:30	Kenneth H. Hicks	Highlights on hadron physics at CLAS
12:00	Thomas Kuhr	Heavy-flavor baryons
12:30	Robert Edwards	Baryon spectroscopy and resonances
13:00		*Lunch Break*

Light Mesons 4

Chair: *Volker Crede*

14:30	Dennis Weygand	Hadron Spectroscopy at CLAS
15:00	Chaden Djalali	Light Vector Meson Photoproduction off of H at Jefferson Lab and $\rho - \omega$ Interference in the Leptonic Decay Channel
15:20	Zhi-Hui Guo	Resonances and their N_c fates in $U(3)$ chiral perturbation theory
15:40	Jenifer Nebreda	Quark mass dependence of meson-meson resonances and phase shifts within standard and unitarized ChPT

Quarkonia 4

Chair: *Mikihiko Nakao*

14:30	Javier Vijande	Exotic gifts of nature
14:55	Sören Lange	New results on charmonium and charmonium-like systems at Belle
15:15	Valentina Santoro	Charmonium and Charmonium-like States with BABAR
15:35	David Rodriguez Entem	Molecular Effects in Charmonium Spectrum

Light Baryons 5

Chair: *Ulrike Thoma*

14:30	Simon Širca	Pion scattering and electro-production on nucleons in the resonance region in chiral quark models
14:55	Victor Mokeev	Nucleon resonance electrocouplings from CLAS data on pion electro-production
15:20	Ki-Seok Choi	Covariant electroweak structure of light and strange baryons

Future Experiments

Chair: *Bernhard Ketzer*

14:30	Peter Križan	Future experiments
14:55	J. H. Lee	The Electron-Ion Collider at BNL
15:15	Masayuki Niiyama	LEPS2 GeV photon at SPring-8
15:35	Igor Senderovich	Search for Hadrons with Gluonic Excitations with GlueX
16:00		*Coffee Break*

Light Mesons 5

Chair: *Paul Eugenio*

16:30	Craig Bookwalter	The Search for Exotic Mesons in $\gamma p \to \pi^+\pi^+\pi^- n$ with CLAS at Jefferson Lab
16:50	Dmitry Ryabchikov	Study of the reaction $\pi^-\mathrm{Be} \to \pi^-\pi^-\pi^+\eta\mathrm{Be}$ in the VES experiment
17:10	Tobias Schlüter	The Exotic $\eta'\pi^-$ Wave in 190 GeV $\pi^- + p \to \eta' + \pi^- + p$
17:30	Bachir Moussallam	Some properties of light scalar mesons in the complex plane
17:50	Gurjav Ganbold	Spectra of Light and Heavy Mesons, Glueball and QCD Effective Coupling

Quarkonia 5 Chair: *Bernhard Ketzer*

16:30	Bo Liu	Exotic spectroscopy and quarkonia at LHCb
16:55	Jian Wang	Observation of the $X(3872)$ state with the CMS experiment
17:20	Frederick Kramer	Quarkonia Measurements with ALICE at the LHC
17:45	Jacopo Ghiglieri	Heavy quarkonium spectrum and width in a weakly-coupled quark-gluon plasma

Heavy Hadrons 4 Chair: *Stefano Bianco*

16:30	Paolo Bellan	Measurements of inclusive B-quark production at 7 TeV with the CMS experiment
16:50	Hans-Christian Kästli	Measurement of exclusive B-hadron production at 7 TeV with the CMS experiment
17:10	Christophorus Grab	Measurement on B-hadron angular correlations at 7 TeV with the CMS experiment
17:30	Artur Ukleja	Studies of open heavy flavour production at LHCb
17:50	Jorge Segovia	Weak B Decays into Orbitally Excited Charmed Mesons

Hadrons in Hot and Cold Medium 3 Chair: *Wolfram Weise*

16:30	Daisuke Jido	Pseudoscalar mesons in nuclei and partial restoration of chiral symmetry
16:50	Satoru Hirenzaki	$\eta'(958)$ Bound States in Nuclei and Partial Restoration of Chiral Symmetry
17:10	Alessandro Feliciello	Production and study of baryons with beauty at the Italian heavy flavour factory (SuperB)
17:30	Michaela Thiel	In-medium properties of the ω meson near the production threshold
17:50	Takayasu Sekihara	Internal structure of resonant $\Lambda(1405)$ state in chiral dynamics

Friday, June 17, 2011

Light Mesons 6 Chair: *Claude Marchand*

09:00	Evgeny Solodov	First results from VEPP2000 collider in Novosibirsk
09:20	Florian Haas	Diffractive Dissociation into 3-Pion Final States at COMPASS
09:40	Frank Nerling	Spin-exotic search in the $\rho\pi$ decay channel: First results on $\pi^-\pi^0\pi^0$ in comparison to $\pi^-\pi^+\pi^-$ final states (diffractively produced on proton)
10:00	Luis Roca	Hadronic resonances made of multi-vector mesons
10:20	Hideko Nagahiro	Mixing properties of $a_1(1260)$ meson consisting of hadronic composite and quark composite
10:40	Hongwei Liu	New observations on hadron spectroscopy at BESIII

Heavy Hadrons 5 Chair: *Stephan Paul*

09:00	Marek Karliner	Heavy baryon spectrum, new heavy exotics and isospin breaking
09:30	Chu-Wen Xiao	Baryon bound states of three hadrons with charm and hidden charm
09:50	Carlo Schiavi	Heavy hadron spectroscopy and production at ATLAS
10:15	Joseph Day	Effective Quark-Quark Interaction in Heavy Baryons
10:35	Igor Gorelov	Heavy Hadron Spectroscopy and Production at Tevatron

Hadrons in Hot and Cold Medium 4 Chair: *Tomofumi Nagae*

09:00	Germano Bonomi	Hypernuclei Production by K^- at rest
09:25	Hiroyuki Fujioka	Experimental studies of mesic nuclei at J-PARC
09:50	Michael Weber	Probing cold nuclear matter with virtual photons
10:10	Kirill Lapidus	Neutral kaon production in $p + p$ and $p +$ Nb collisions

Low-Energy Processes 2 Chair: *Jan Friedrich*

09:00	Michael Döring	Chiral dynamical aspects of recent low energy reactions measured at MAMI, ELSA, GRAAL, and other labs
09:25	Álvaro Calle Cordón	Renormalization of Spin-Flavor Van der Waals Forces
09:45	Hua-Xing Chen	The $pp \to p\Lambda K^+$ and $pp \to p\Sigma^0 K^+$ reactions with chiral dynamics
10:05	Stefanie Grabmüller	$\pi^-\gamma \to \pi^-\pi^-\pi^+$ at low masses compared to ChPT prediction at COMPASS
10:25	Dmitry Ryabchikov	Study of interference of Coulomb and strong diffractive production of $\pi^-\pi^-\pi^+$ systems produced off Pb target at COMPASS
10:40	Mauro Piccini	Study of Ke4 decays at NA48 and ChPT tests
11:00		*Coffee Break*

Plenary Session 9 Chair: *Aleksander M. Zaitsev*

11:30	Hirokazu Tamura	Hyperons in nuclei - review
12:00	Piotr Salabura	In-medium modifications of hadrons
12:30	Thierry Lasserre	Neutrinos: recent results and developments
13:00		*Lunch Break*

Plenary Session 10 Chair: *Harry Lipkin*

14:30	Lars Schmitt	Hadron physics at FAIR
14:55	Boris Shwartz	The BELLE II project
15:20	Stefano Bianco	Summary Experiment
16:00	Chris Quigg	The future of hadrons (theory summary)
17:00		*End of Conference*

List of Participants

A

Prof. Nikolay	Achasov	Sobolev Institute for Mathematics
Mr. Bora	Akgun	Carnegie Mellon University
Prof. Ahmet T.	Alan	Hakkari University
Mr. Jose Manuel	Alarcón	Universidad de Murcia
Mr. Miguel	Albaladejo	Universidad de Murcia
Dr. Conrado	Albertus Torres	Universidad de Salamanca
Prof. Fabio	Ambrosino	Università degli Studi di Napoli and Sezione INFN, Napoli
Prof. Claude	Amsler	Universität Zürich
Prof. Mauro	Anselmino	University of Torino, INFN
Dr. Elke-Caroline	Aschenauer	BNL
Mr. Alex	Austregesilo	TU München
Dr. Kazem	Azizi	Dogus University

B

Dr. Mikhail	Barabanov	Joint Institute for Nuclear Research
Dr. Melahat	Bayar	Instituto de Fisica Corpuscular
Prof. Reinhard	Beck	Universität Bonn
Ms. Evgeniia	Beliaeva	GmbH PROFKOM
Dr. Paolo	Bellan	Padova University and INFN
Mr. Martin	Berger	TU München
Dr. Niklaus	Berger	IHEP Beijing
Mr. Johannes	Bernhard	Institut für Kernphysik, JGU Mainz
Dr. Stefano	Bianco	INFN Laboratori Nazionali di Frascati
Mr. Karl	Bicker	CERN
Dr. Germano	Bonomi	University of Brescia and INFN Pavia
Mr. Craig	Bookwalter	Florida State University
Prof. Elena	Botta	INFN-Sezione di Torino and Torino University
Prof. Nora	Brambilla	TU München
Mr. Bastian	Brandt	Universität Mainz
Prof. Tullio	Bressani	Istituto Nazionale di Fisica Nucleare
Dr. Paul	Bühler	Stefan Meyer Institute
Dr. Stefania	Bufalino	INFN - Sezione di Torino
Dr. Timothy	Burns	INFN, Roma
Dr. Mathias	Butenschön	Universität Hamburg

C

Dr. Álvaro	Calle Cordón	Jefferson Lab
Mrs. Roberta	Cardinale	University of Genova/ INFN Genova
Dr. Hua-Xing	Chen	IFIC, Valencia University
Ms. Jia-Chii	Chen	TU München, Excellence Cluster Universe
Mr. Ki-Seok	Choi	Graz Univ
Dr. Suh-Urk	Chung	TU München

Prof. Frank	Close	Oxford University
Prof. Guillermo	Contreras	Cinvestav
Mr. Alberto	Correa dos Reis	CBPF Rio de Janeireo
Prof. Volker	Crede	Florida State University
Dr. Francesco	Cusanno	TU München

D

Dr. Harleen	Dahiya	Dr. B.R. Ambedkar National Instituite of Technology
Mr. Joseph	Day	Universität Graz
Dr. Fulvia	De Fazio	INFN - Sezione di Bari
Prof. Achim	Denig	Universität Mainz
Dr. Camilla	Di Donato	INFN - Sezione di Napoli
Dr. Jürgen	Diefenbach	Hampton University
Mr. Manuel	Dieterle	Universität Basel
Prof. Chaden	Djalali	University of South Carolina
Prof. Antonio	Dobado	Complutense University
Dr. Michael	Döring	Helmholtz-Institut für Strahlen- und Kernphysik, Universität Bonn
Prof. Wolfgang	Dünnweber	LMU München

E

Dr. Robert	Edwards	Jefferson Lab
Dr. Simon	Eidelman	Budker Institute of Nuclear Physics
Ms. Eliane	Epple	Excellence Cluster Universe
Prof. Paul	Eugenio	Florida State University
Prof. Hal	Evans	Indiana University

F

Prof. Laura	Fabbietti	TU München
Prof. Martin	Faessler	LMU München
Dr. Alessandro	Feliciello	INFN - Sezione di Torino
Mrs. Karin	Frank	TU München
Dr. Jan	Friedrich	TU München
Dr. Miriam	Fritsch	Universität Mainz
Dr. Hiroyuki	Fujioka	Kyoto University

G

Prof. Yuanning	Gao	Tsinghua University
Mr. David	Garcia	Institute of Physics-UNAM
Mr. Jacopo	Ghiglieri	TU München
Prof. Alexander	Glushkov	Odessa University and Troitsl ISAN Russian Acad. Sci.
Dr. Pedro	González	Universitat de Valencia
Dr. Igor	Gorelov	University of New Mexico
Prof. Christophorus	Grab	ETH Zurich
Ms. Stefanie	Grabmüller	TU München
Prof. Wolfgang	Gradl	Universität Mainz

Dr. Boris	Grube	TU München
Mr. Marcus	Grüner	HISKP
Mr. Philipp	Gubler	Tokyo Institute of Technology
Dr. Feng-Kun	Guo	Universität Bonn
Dr. Zhi-Hui	Guo	Universidad de Murcia
Dr. Ganbold	Gurjav	Bogolubov Lab.Theor. Phys., JINR, Dubna

H

Mr. Florian	Haas	TU München
Dr. Eliecer	Hernandez-Gajate	University of Salamanca
Prof. Kenneth	Hicks	Ohio University
Prof. Satoru	Hirenzaki	Nara Women's University
Mr. Martin	Hoferichter	Universität Bonn
Mr. Stefan	Huber	TU München
Dr. Jifeng	Hu	Graduate University of Chinese Academy of Science
Dr. Tetsuo	Hyodo	Tokyo Institute of Technology
Mr. Christian	Höppner	TU München

I

Dr. Jaegle	Igal	University of Hawaii
Dr. Tomoichi	Ishiwatari	Stefan-Meyer-Institut für subatomare Physik
Mr. Satoshi	Itoh	University of Tokyo

J

Dr. Daisuke	Jido	Yukawa Institute for Theoretical Physics
Dr. Andreas	Jüttner	CERN

K

Prof. Eva-Maria	Kabuss	Institut für Kernphysik, Universität Mainz
Dr. Hans-Christian	Kästli	Paul Scherrer Institut
Prof. Burkhard	Kämpfer	Helmholtz-Zenrum Dresden-Rossendorf
Prof. Marek	Karliner	Tel Aviv University
Dr. Bernhard	Ketzer	TU München
Dr. Olga	Khetselius	Odessa University
Ms. Regina	Kleinhappel	Universität Graz
Dr. Hiroaki	Kohyama	Chung Yuan Christian University
Mr. Frederick	Kramer	IKF, Universität Frankfurt
Prof. Peter	Križan	University of Ljubljana and JSI
Prof. Bernd	Krusche	Universität Basel
Dr. Bastian	Kubis	Universität Bonn
Dr. Thomas	Kuhr	KIT
Mr. Michael	Kunkel	Old Dominion University
Dr. Pavel	Kurilkin	JINR
Dr. Aleksandr	Kuzmin	Budker Institute of Nuclear Physics SB RAN

L

Dr. Nadezhda	Ladygina	JINR
Prof. Mikko	Laine	Universität Bielefeld
Mr. Rafał	Lalik	Excellence Cluster Universe, TU München
Dr. Sören	Lange	Universität Giessen, II. Physikalisches Institut
Mr. Kirill	Lapidus	Excellence Cluster "Universe"
Mr. Alexander	Laschka	TU München
Dr. Thierry	Lasserre	Saclay
Dr. Andrea	Lavagno	Politecnico di Torino
Mr. Michael	Leeb	TU München
Dr. J.H.	Lee	BNL
Dr. Nuno	Leonardo	Purdue
Mr. Xiaotao	Liao	Institute of High Energy Physics, Chinese Academy of Sciences
Prof. Hai-Bo	Li	Institute of High Energy Physics
Prof. Harry	Lipkin	Weizmann Institute of Science
Mr. Bo	Liu	LAL/Tsinghua University
Ms. Chunyan	Liu	Institute of High Energy Physics
Ms. Hongwei	Liu	Institute of High Energy Physics
Dr. Yanrui	Liu	Tokyo Institute of Technology
Prof. Mario Luiz	Lopes da silva	Universidade Federal do Pampa
Dr. Wolfgang	Lucha	Austrian Academy of Sciences
Dr. Valery	Lyubovitskij	Institute of Theoretical Physics, Universität Tübingen

M

Mrs. Patrícia	Magalhães	Physics Institut of São Paulo University
Prof. Marco	Maggiora	University of Turin and INFN
Mr. Ajay	Majethiya	Department of Physics, Sardar Patel University,
Ms. Nour	Makke	CEA/Saclay
Dr. Gerhard	Mallot	CERN
Dr. Claude	Marchand	CEA IRFU/SPhN Saclay
Dr. Dmitri	Melikhov	HEPHY Vienna Austria and SINP Moscow Russia
Prof. Volker	Metag	II. Physikalisches Institut, Universität Giessen
Dr. Daniel	Mohler	TRIUMF
Dr. Victor	Mokeev	Jefferson Lab
Mrs. Raquel	Molina	IFIC
Dr. Bachir	Moussallam	IPN Orsay
Dr. Hervé	Moutarde	Irfu, CEA-Saclay
Mr. Jonas	Müller	HISKP, Universität Bonn
Dr. Bernhard	Musch	Jefferson Lab
Mr. Robert	Münzer	Excellence Cluster Universe, TU München

N

Prof. Tomofumi	Nagae	Kyoto University
Prof. Hideko	Nagahiro	Nara Women's University

Mr. Thiemo	Nagel	TU München
Prof. Mikihiko	Nakao	KEK
Dr. Mariana	Nanova	II. Physikalisches Institut, Universität Giessen
Ms. Jenifer	Nebreda	Universidad Complutense de Madrid
Mr. Sebastian	Neubert	TU München
Prof. Juan	Nieves	IFIC (CSIC-UV)
Dr. Masayuki	Niiyama	Nuclear and Hadronic Lab, Dept. of Physics, Facility of Science, Kyoto University
Dr. Hiroshi	Noya	Institute of Physics, Hosei University at Tama

O

Mr. Alexander	Obrazovsky	Budker Institute of Nuclear Physics
Dr. Wolfgang	Ochs	MPI für Physik
Dr. Shinji	Okada	LNF-INFN
Prof. Eulogio	Oset	IFIC, University of Valencia Spain

P

Dr. Claudia	Patrignani	Università and INFN Genova
Prof. Stephan	Paul	TU München
Dr. Manuel	Pavón Valderrama	Instituto de Física Corpuscular Valencia
Dr. Jose R.	Pelaez	Universidad Complutense
Prof. Klaus	Peters	GSI Darmstadt
Dr. Mauro	Piccini	INFN - Sezione di Perugia
Mr. Piotr	Pietrulewicz	TU München
Dr. Antonio Miguel	Pineda ruiz	Universitat Autònoma de Barcelona
Mr. Dominik	Pleiner	Excellence Cluster Universe, TU München
Dr. Randolf	Pohl	Max-Planck-Institut für Quantenoptik
Prof. Maxim	Polyakov	Ruhr Universität Bochum
Mr. Andrey	Polyanskiy	Institut für Kernphysik, FZ Jülich
Mr. Joerg	Pretz	Physikalisches Institut, Universität Bonn

Q

Prof. Chris	Quigg	Fermilab

R

Dr. Luis	Roca	University of Murcia
Dr. David	Rodriguez entem	University of Salamanca
Mr. Jacobo	Ruiz de elvira	Universidad Complutense
Dr. Dmitry	Ryabchikov	Institute for High Energy Physics, TU München
Dr. Sinead	Ryan	Trinity College Dublin
Mr. Guillermo	Ríos	Universidad Complutense de Madrid

S

Dr. Giovanni	Sabatino	Università di Roma "Tor Vergata" and INFN
Prof. Piotr	Salabura	Jagiellonian University
Mrs. Valentina	Santoro	INFN Ferrara
Dr. Carlo	Schiavi	INFN Genova
Dr. Rainer	Schicker	Universität Heidelberg

Mr. Tobias	Schlüter	LMU München
Dr. Lars	Schmitt	GSI
Prof. Martin	Schumacher	Zweites Physikalisches Institut der Universität Göttingen
Mr. Jorge	Segovia	University of Salamanca
Prof. Motoo	Sekiguchi	Kokushikan University
Dr. Takayasu	Sekihara	Tokyo Inst. Tech.
Dr. Ilya	Selyuzhenkov	EMMI/GSI
Mr. Igor	Senderovich	University of Connecticut
Mr. Satya	Seshavatharam.uv	Lanco Industries
Prof. Kamal K.	Seth	Northwestern University
Dr. Olga	Shekhovtsova	IFIC and University of Valencia
Prof. Xiaoyan	Shen	Institute of High Energy Physics
Prof. Boris	Shwartz	Budker Institute of Nuclear Physics
Mr. Johannes	Siebenson	TU München
Dr. Simon	Širca	Faculty of Mathematics and Physics, University of Ljubljana
Ms. Anna	Skachkova	JINR
Prof. Roxanne	Springer	Duke University
Prof. Evgeny	Solodov	Budker Institute of Nuclear Physics
Dr. Sergey	Sukhoruchkin	Petersburg Nuclear Physics Institute
Dr. Bao-Xi	Sun	Beijing University of Technology

T

Prof. Toshiyuki	Takahashi	KEK/J-PARC
Prof. Hirokazu	Tamura	Department of Physics, Tohoku University
Dr. Michaela	Thiel	II. Physikalisches Institut, Universität Giessen
Prof. Ulrike	Thoma	HISKP, Universität Bonn
Mr. Ricardo	Torres	Universidad Complutense

U

Mr. Sebastian	Uhl	TU München
Dr. Artur	Ukleja	Institute for Nuclear Studies
Dr. Alka	Upadhyay	Thapar University, Patiala

V

Dr. Antonio	Vairo	TU München
Dr. Alfredo	Valcarce	University Salamanca
Dr. Luigi	Vannucci	Laboratori Nazionali di Legnaro (INFN)
Prof. Javier	Vijande	University of Valencia

W

Mr. Jian	Wang	Institute of High Energy Physics
Dr. Liangliang	Wang	Institute of High Energy Physics
Ms. Qian	Wang	Institute of High Energy Physics, Chines Academy Sicenecs
Dr. Michael	Weber	University of Houston
Prof. Wolfram	Weise	TU München

Dr. Dennis	Weygand	Jefferson Lab
Prof. Ulrich	Wiedner	Ruhr-Universität Bochum
Ms. Lilian	Witthauer	Universität Basel
Prof. Hartmut	Wittig	Universität Mainz

X

Mr. Chu-Wen	Xiao	Departamento de Fisica Teorica and IFIC, Universidad de Valencia
Dr. Ju-Jun	Xie	IFIC, University of Valencia

Y

Mr. Hao	Yang	LMU München

Z

Prof. Alexander M.	Zaitsev	Institute for High Energy Physics
Dr. Carina Maria	Zanetti	Instituto de Física, USP
Dr. James	Zanotti	The University of Edinburgh

Taking time out from the poster session in the courtyard: participants of hadron2011.

After Dinner . . .

Kamal K. Seth

This morning Stephan Paul asked me to say a few words at the banquet, or give what is traditionally called the "after banquet" talk. I was intrigued — "why me"? With so many distinguished physicists around, "why me"? I first thought it was to punish me for asking too many questions in the talks. But that couldn't be the reason. If it were true, he could have asked Mark Karliner, or Eulogio Oset, or Nora Brambilla. So what could be the reason? And then I had the "eureka" moment. I realized it was part of a pattern —

At HADRON 2005 in Rio, I was asked to give a plenary review talk,

At HADRON 2007 in Frascati, I was asked to give a conference summary talk,

At HADRON 2011 in Munich, I was being asked to tell jokes.

Was that a pattern, perhaps a message. So I had to respond and agree to talk.

Since I mentioned the asking of questions, let me elaborate. There are three kinds of questions:

1. You ask about something because you do not know the answer.
2. You ask about something because you know the answer. It is to show that you are smarter than the speaker.
3. The third is not a question at all. It is an uninvited talk. It is generally to point out that the speaker did not refer to your earlier work. This is fine, except that I think there should be a statute of limitations about this. If you have to point out something you did, say more than five years ago, and it is not being referred to, perhaps there is a good reason for it.

I realize that I am stepping into some serious territory here, and all I was supposed to do was to tell some jokes. So let me try telling you a few, but with a message.

This first story is borrowed from a great after-dinner speaker, Dennis Wilkinson, well-known to those of you who have a nuclear physics background.

One day a priest and a taxi driver died. And then both of them went upstairs hoping to be admitted to Heaven. At the entrance hall sat St. Peter with an Apple Mac computer, looking into the life record of the candidates, and deciding whether they deserved entering

into Heaven, or whether they should be sent elsewhere. Both the priest and the taxi driver waited as St. Peter worked on the computer. After a long wait, he looked up, and told the taxi driver that he could go in. The priest continued to wait and got angrier and angrier as the time went on, and he was not told to go in. Finally, he just couldn't take it any more, and angrily asked St. Peter how a taxi driver was let in, and *he*, who had spent his life in the service of the Lord, was being kept out, cooling his heels. St. Peter said he would take a careful look at the record and tell him what the reason was. He worked on his Mac and said "Aha! There is a clear reason, my friend! You see, when you were preaching for the Lord your audience was mostly sleeping, but when he was driving the taxi, his passengers were praying."

So what is the message in this story. The message is for my theorist friends. It is: "Your place in the physics heaven will not depend on the excellence of your sermon, but on how many of your audience you put to sleep."

Now I realize that I am being unfair — giving advice to the theorists, and sparing the experimentalists. So here is some advice for my experimentalist friends.

A very well-known theorist was put on the PAC for experiments at CERN. He realized that he knew little about the nitty-gritty of experiments and did not know what to ask in order to make a good impression. So, he asked his wife, who is a well-known experimentalist, "What should I ask?", and she told him.

Here are the two questions he henceforth asked, and you can do the same.

1. The first question to always ask is: "What about your background?" I mean not your ethnic background, but the "background" in your data. We all realize how important this question is, particularly after the story of the "pentaquark," and perhaps some of the other "exotics."

2. The second question to ask is: "Have you done a Monte Carlo simulation, and what does it have to say about your data?"

If you learn to ask these two questions with a serious frown on your face, you will have established yourself as an astute physicist.

Finally, I have one other important advice for the experimentalists. It was given to me by my boss when I was a fresh post-doc at Duke University, and it is indeed the best advice I can pass on to my experimentalist friends. He said, "Kam, if you discover something really great in your measurement, don't ever make the mistake of repeating the measurement."

Well, I have now passed on some of the wisdom I have acquired doing research in particle and nuclear physics for more than forty years, and I hope you have as much fun doing it as I have had, and that you remember to make proper apologies to your "significant other," for making his/her life difficult!

And now, on to some more serious beer-drinking! We are in Munich.

Author Index

http://www.slac.stanford.edu/econf/C110613/